ISSN 0003-2654
VOL. 120 NO. 2 FEBRUARY 1995

The Analyst

An international analytical science journal

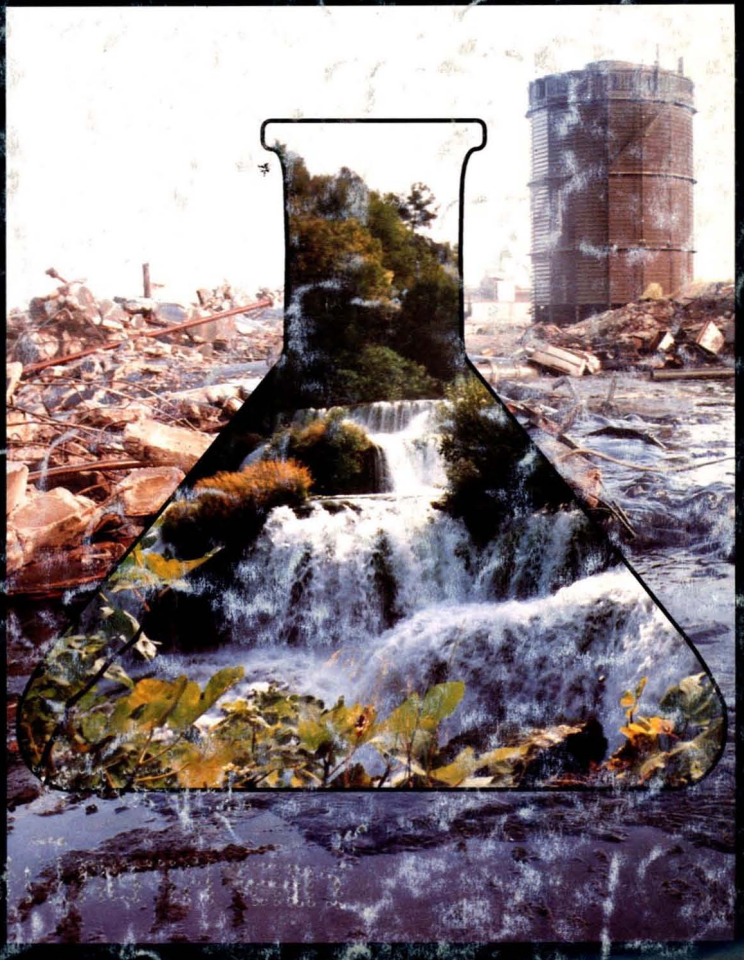

The Analyst

The Analytical Journal of The Royal Society of Chemistry

Analytical Editorial Board

Chairman: J. N. Miller (*Loughborough, UK*)

M. Cooke (*Sheffield, UK*)
C. S. Creaser (*Nottingham, UK*)
A. G. Davies (*London, UK*)
A. G. Fogg (*Loughborough, UK*)
J. M. Gordon (*Cambridge, UK*)
G. M. Greenway (*Hull, UK*)
S. J. Hill (*Plymouth, UK*)
D. L. Miles (*Keyworth, UK*)
R. M. Miller (*Gouda, The Netherlands*)
B. L. Sharp (*Loughborough, UK*)
M. R. Smyth (*Dublin, Ireland*)
Y. Thomassen (*Oslo, Norway*)
P. Vadgama (*Manchester, UK*)

Advisory Board

J. F. Alder (*Manchester, UK*)
A. M. Bond (*Victoria, Australia*)
J. G. Dorsey (*Cincinnati, OH, USA*)
L. Ebdon (*Plymouth, UK*)
A. F. Fell (*Bradford, UK*)
J. P. Foley (*Villanova, PA, USA*)
M. F. Giné (*Sao Paulo, Brazil*)
T. P. Hadjiioannou (*Athens, Greece*)
W. R. Heineman (*Cincinnati, OH, USA*)
A. Hulanicki (*Warsaw, Poland*)
I. Karube (*Yokohama, Japan*)
E. J. Newman (*Poole, UK*)
J. Pawliszyn (*Waterloo, Canada*)
T. B. Pierce (*Harwell, UK*)
E. Pungor (*Budapest, Hungary*)
J. Růžička (*Seattle, WA, USA*)
R. M. Smith (*Loughborough, UK*)
K. Štulík (*Prague, Czechoslovakia*)
J. D. R. Thomas (*Cardiff, UK*)
J. M. Thompson (*Birmingham, UK*)
K. C. Thompson (*Sheffield, UK*)
P. C. Uden (*Amherst, MA, USA*)
A. M. Ure (*Aberdeen, UK*)
C. M. G. van den Berg (*Liverpool, UK*)
A. Walsh, KB (*Melbourne, Australia*)
J. Wang (*Las Cruces, NM, USA*)
T. S. West (*Aberdeen, UK*)

Regional Advisory Editors

For advice and help to authors outside the UK

Professor Dr. U. A. Th. Brinkman, Free University of Amsterdam, 1083 de Boelelaan, **1081 HV Amsterdam,** THE NETHERLANDS.
Professor P. R. Coulet, Laboratoire de Génie Enzymatique, EP 19 CNRS-Université Claude Bernard Lyon 1, 43 Boulevard du 11 Novembre 1918, **69622 Villeurbanne Cedex,** FRANCE.
Professor O. Osibanjo, Department of Chemistry, University of Ibadan, **Ibadan,** NIGERIA.
Professor F. Palmisano, Universitá Degli Studi-Bari, Departimento di Chimica Campus Universitario, 4 Trav. 200 Re David—**70126 Bari,** ITALY.
Professor K. Saito, Coordination Chemistry Laboratories, Institute for Molecular Science, Myodaiji, **Okazaki 444,** JAPAN.
Professor M. Thompson, Department of Chemistry, University of Toronto, 80 St. George Street, **Toronto,** Ontario, CANADA M5S 1A1.
Professor Dr. M. Valcárcel, Departamento de Química Analítica, Facultad de Ciencias, Universidad de Córdoba, **14005 Córdoba,** SPAIN.
Professor J. F. van Staden, Department of Chemistry, University of Pretoria, **Pretoria 0002,** SOUTH AFRICA.
Professor Yu Ru-Qin, Department of Chemistry and Chemical Engineering, Hunan University, **Changsha,** PEOPLES REPUBLIC OF CHINA.
Professor Yu. A. Zolotov, Kurnakov Institute of General and Inorganic Chemistry, 31 Lenin Avenue, 117907, **Moscow V-71,** RUSSIA.

Editorial Manager, Analytical Journals: Janice M. Gordon

Editor, *The Analyst*
Harpal S. Minhas
The Royal Society of Chemistry,
Thomas Graham House, Science Park,
Milton Road, Cambridge, UK CB4 4WF
Telephone +44(0)1223 420066.
Fax +44(0)1223 420247.
E-Mail:Analyst@RSC.ORG(Internet)

US Associate Editor, *The Analyst*
Dr Julian F. Tyson
Department of Chemistry,
University of Massachusetts,
Box 34510 Amherst MA
01003-4510, USA
Telephone +1 413 545 0195
Fax +1 413 545 4846

Assistant Editors

Sarah Williams Caroline Seeley Yasmin Khan

Editorial Secretary: Claire Harris

Advertisements: Advertisement Department, The Royal Society of Chemistry, Burlington House, Piccadilly, London, UK W1V 0BN. Telephone +44(0)171-287 3091. Fax +44(0)171-494 1134.

Information for Authors

Full details of how to submit material for publication in *The Analyst* are given in the Instructions to Authors in the January issue. Separate copies are available on request.

The Analyst publishes original research papers, critical reviews, tutorial reviews, perspectives, news articles, book reviews and a conference diary.

Original research papers. The Analyst publishes full papers on all aspects of the theory and practice of analytical chemistry, fundamental and applied, inorganic and organic, including chemical, physical, biochemical, clinical, pharmaceutical, biological, environmental, automatic and computer-based methods. Papers on new approaches to existing methods, new techniques and instrumentation, detectors and sensors, and new areas of application with due attention to overcoming limitations and to underlying principles are all equally welcome.

Full critical reviews. These must be a critical evaluation of the existing state of knowledge on a particular facet of analytical chemistry.

Tutorial reviews. These should be informally written although they should still be a critical evaluation of a *specific* topic area. Some history and possible future developments should be given. Potential authors should contact the Editor before writing reviews.

Perspectives. These articles should provide either a personal view or a philosophical look at a topic relevant to analytical science. Alternatively, they may be relevant historical articles. Perspectives are included at the discretion of the Editor.

Particular attention should be paid to the use of standard methods of literature citation, including the journal abbreviations defined in Chemical Abstracts Service Source Index. Wherever possible, the nomenclature employed should follow IUPAC recommendations, and units and symbols should be those associated with SI.

Every paper will be submitted to at least two referees, by whose advice the Editorial Board of *The Analyst* will be guided as to its acceptance or rejection. Papers that are accepted must not be published elsewhere except by permission. Submission of a manuscript will be regarded as an undertaking that the same material is not being considered for publication by another journal.

Regional Advisory Editors. For the benefit of potential contributors outside the UK and N. America, a Group of Regional Advisory Editors exists. Requests for help or advice on matters related to the preparation of papers and their submission for publication in *The Analyst* can be sent to the nearest member of the Group. Currently serving Regional Advisory Editors are listed in each issue of *The Analyst.*

Manuscripts (four copies typed in double spacing) should be addressed to:

H. S. Minhas, Editor, *or*
J. F. Tyson, US Associate Editor

All queries relating to the presentation and submission of papers, and any correspondence regarding accepted papers and proofs, should be directed either to the Editor, or Associate Editor, *The Analyst.* Members of the Analytical Editorial Board (who may be contacted directly or *via* the Editorial Office) would welcome comments, suggestions and advice on general policy matters concerning *The Analyst.*

There is no page charge.

Fifty reprints are supplied free of charge.

The Analyst (ISSN 0003–2654) is published monthly by The Royal Society of Chemistry, Thomas Graham House, Science Park, Milton Road, Cambridge, UK CB4 4WF. All orders, accompanied with payment by cheque in sterling, payable on a UK clearing bank or in US dollars payable on a US clearing bank, should be sent directly to The Royal Society of Chemistry, Turpin Distribution Services Ltd., Blackhorse Road, Letchworth, Herts, UK SG6 1HN. Turpin Distribution Services Ltd., is wholly owned by the Royal Society of Chemistry. 1995 Annual subscription rate EC £408.00, USA $749.00, Canada £428.00 (excl. GST), Rest of World £428.00. Purchased with *Analytical Abstracts* EC £807.00, USA $1472.00, Canada £841.00 (excl. GST), Rest of World £841.00. Purchased with *Analytical Abstracts* plus *Analytical Proceedings* EC £925.00, USA $1699.00, Canada £971.00 (excl. GST), Rest of World £971.00. Purchased with *Analytical Proceedings* EC £492.00, USA $905.00, Canada £517.00 (excl. GST), Rest of World £517.00. Air freight and mailing in the USA by Publications Expediting Inc., 200 Meacham Avenue, Elmont, NY 11003.

USA Postmaster: Send address changes to: *The Analyst,* Publications Expediting Inc., 200 Meacham Avenue, Elmont, NY 11003. Second class postage paid at Jamaica, NY 11431. All other despatches outside the UK by Bulk Airmail within Europe, Accelerated Surface Post outside Europe. PRINTED IN THE UK.

© The Royal Society of Chemistry, 1995. All rights reserved. No part of this publication may be reproduced, stored in a retrieval system, or transmitted in any form, or by any means, electronic, mechanical, photographic, recording, or otherwise, without the prior permission of the publishers.

Guest Editorial

Towards Environmentally Conscientious Analytical Chemistry Through Miniaturization, Containment and Reagent Replacement

The present state of the art in chemistry is immersed in an ecological period. After the development of the ancient chemical practices (the archaeological and alchemical periods) and from the foundation of chemistry as a science, chemistry progressed from chemology, chemurgy and iatrochemistry to a scientific discipline. Thus, the evolution of chemistry has been introverted; through the search for new chemical principles and through technological developments with applications to other areas, chemistry has focused on itself. However, further development of science and technology needs now also to pay attention to the interaction between man and the biosphere, and resulting environmental implications.

Therefore, analytical chemistry is moving from its former interest in inorganic analysis and organic analytical chemistry to bioanalysis and environmental studies. The traditional interest in the qualitative, quantitative and structural composition of matter needs to be supplemented by yet another aspect, which will include the impact of its own activities on the environment.

Although environmental analysis in itself is an important step in the direction of ecological chemistry, the present focus on measurement of the influence of human activities does not address the negative aspect of current practices in analytical and research laboratories. This problem is likely to increase in the future, since the growing demand on analytical services increases the amount of chemical waste generated. Indeed, already requirements for the quality control of chemical and pharmaceutical production are expanding due to novel control activities, such as GMP (good manufacturing practices) and requirements of ISO 9000. In addition, tighter regulations on chemical waste disposal create an unprecedented demand on additional assays to be carried out. As a result, large numbers of assays produce a considerable volume of highly diversified, often very toxic, chemical waste. As a majority of chemical assays are, and will remain, reagent-based, and since many reagents are toxic and/or carcinogenic, corrective action needs to be taken. It might be tempting to propose that alternative, more environmentally acceptable, reagentless chemistries ought to be developed. Yet, considering the past efforts of generations of chemists that were needed to develop present assays, it is not realistic to hope that such a replacement can be made within the immediate future. Also, the majority of EPA- and FDA-certified analytical methods use corrosive and toxic chemicals, with no currently available alternatives. Owing to the diversity of analytical methods, waste from the analytical laboratory is often complex, composed of relatively small individual volumes, but of a large variety of chemicals, the mixtures of which are expensive to dispose of. In contrast to large-scale industrial chemical processes (such as dry cleaning, paint formulation or the synthesis of bulk chemicals), the volume of waste is not substantially reduced when only a single method of processing is improved upon. Therefore, reagent replacement is not the most effective approach.

A solution to this problem is to redesign existing reagent chemistries in such a way that the consumption of reagents, of sample material and waste production is minimized through miniaturization and that all solution handling tasks are fully contained and automated. This process will be driven not only by our environmental consciousness, but also by economy, since the costs of reagents and waste disposal are steadily increasing.

The redesign of reagent-based assays will be carried out in many ways, through the use of (*a*) robotics, (*b*) miniaturized chromatographies, (*c*) flow techniques, such as flow injection and sequential injection, and (*d*) advances in sensor technology. Of these techniques, flow-based methodologies (*e.g.*, chromatography, electrospray mass spectroscopy and stopped-flow injection) have the most significant potential, since in flow techniques, in contrast to batch methods, containment and washout is inherent and their miniaturization is not hindered by the difficulty of reproducibly dispensing microlitre volumes.

Though the ideal goal should indeed be replacement of toxic chemicals by harmless ones, an initial goal is to reduce the use of toxic chemicals by a factor of ten. This realistic target will have a considerable positive impact, not only on the environment and the economy of performing millions of assays daily, but also on the education of future generations of (analytical) chemists. As analytical chemistry progressively turns into what might be viewed as Chemical Instrumental Science, through redesign of its tools, it will have a considerable impact on how environmentally responsible the entirety of chemical research will become.

Pollution prevention, as conceptualized in the US by the EPA, may take many routes. Although the main focus has been on the (petro)chemical industry and on manufacturing, where alternative chemistries are being sought, the approach must be different for the analytical and research laboratory. In the US Dr. Joe Breen from the EPA had the vision to propose that there is much that analytical chemists can do. In Europe, it was the Scientific Committee of the Flow Analysis Conference in Toledo that made an award to the contribution focused on clean methods of analytical chemistry. There are, however, large differences between an ideal and real situation both in the USA and in Europe, where analytical and research laboratories remain a source of pollution. Because of this, it is important to turn the tide so that analytical chemists will contribute to the development of a 'clean analytical chemistry', which will avoid the unwanted effects of our activities.

The term 'conscientious analytical method' could become a term to describing the efforts taken to reduce the undesirable side effects of the tools of the trade. Indeed, it is time to enhance the role of analytical chemistry to take a lead towards the preserving of our environment rather than to measure its deterioration. Such an approach will be yet another reasonable compromise between science and society, based on the co-operation of analytical chemists working on both sides of the Atlantic.

Miguel de la Guardia and *Jaromir Ruzicka*

ห้องสมุดกลาง - 2 ... 2538

In-line, Titanium Dioxide-catalysed, Ultraviolet Mineralization of Toxic Aromatic Compounds in the Waste Stream from a Flow Injection-based Resorcinol Analyser*

Miguel de la Guardia, Karim D. Khalaf, Berween A. Hasan, Angel Morales-Rubio and Vicente Carbonell

Department of Analytical Chemistry, University of Valencia, 50 Dr. Moliner St., 46100 Burjassot, Valencia, Spain

A clean method was developed for the spectrophotometric determination of resorcinol. The method, based on the reaction between resorcinol and *p*-aminophenol (PAP), carried out in a flow system, involves an additional detoxification step based on the in-line TiO_2-catalysed photodegradation of the indophenol dye formed and the remaining unreacted PAP. For this, after the measurement step the waste stream is merged with a TiO_2 slurry (0.5 g l^{-1} in 0.22 mol l^{-1} HCl) and then passed through a UV photochemical reactor consisting of a PTFE tube (6 m × 0.8 mm i.d.) rolled on a UV lamp with a maximum irradiation wavelength of 254 nm. Under these conditions, the waste can be completely detoxified thus, providing a non-polluting method of analysis.

Keywords: Flow analysis; resorcinol determination; spectrophotometry; photolysis; titanium dioxide

Introduction

Large amounts of phenolic compounds are produced as raw materials, providing different sources of environmental contamination. Other sources are refinery plants and the common use of a series of compounds, such as pesticides, which degrade to phenols, hence the determination of phenols in water is a priority task in order to control environmental pollution.

Resorcinol is a phenolic compound used in tanning, manufacturing resins and dyes and in pharmaceutical formulations. It has many biological effects and can cause irritation of the skin and mucous membranes. The absorption of resorcinol can also cause methaemoglobinaemia, cyanosis, convulsions and death.[1]

Resorcinol can be determined by different chromatographic techniques and many spectrophotometric methods have been reported for the determination of resorcinol in water samples. Among these methods, several reagents have been employed for the determination of resorcinol and other phenolic compounds, such as 4-aminoantipyrine (4-AAP), 3-methyl-2-benzothiothiazoline hydrochloride (MBTH) and *p*-aminophenol (PAP), which produce coloured complex species which absorb at 410, 510 and 540 nm, respectively.[2,3]

In general, the analytical procedures developed have not taken into consideration that in addition to resorcinol, several of the reagents employed for its determination and the reaction products can be pollutants. However, it is essential to control the wastes from this kind of measurement in order to prevent laboratories engaged in this field of analysis from being additional sources of contamination. Hence, detoxification of the waste must be taken into consideration as an additional step in analyses of hazardous products that involve the use of toxic reagents.

To decompose toxic products, different chemical, thermal, photochemical and microbiological methods, which have been proposed for the degradation of pollutants, could be incorporated in the analytical measurements in order to develop clean analytical procedures.

A variety of dangerous compounds can be destroyed by photodegradation processes carried out in the presence of TiO_2 as a catalyst, providing photo-assisted catalytic procedures, which are very efficient for the destruction of organic compounds. The formation of electron–hole pairs, under illumination with UV or visible radiation, effects the successful oxidation of several organic compounds on the TiO_2 surface.[4–10]

Most photodegradation studies require the use of batch treatments which are tedious and difficult to automate. However, the development of flow injection (FI), now commonly applied in analytical chemistry,[11,12] offers many possibilities for the automation of photodegradation processes.

Previous studies carried out on in-line photochemical reactions demonstrated that PTFE tubing, instead of the typical quartz tubing, is very appropriate for providing sample irradiation[13] and based on this post-column UV photochemical reactions have been employed in liquid chromatography[13,14] and for the determination of nitrogen in water by using an air-segmented flow system.[15]

In the photochemical degradation of pesticides using TiO_2 as a catalyst, our earlier studies[16–18] indicated the possibility of using FI to carry out this kind of process in-line and faster than using the batch approach. This strategy could also be very useful in order to incorporate photodegradation reactors for the in-line detoxification of analytical wastes in order to provide cleaner analytical chemistry operations.

Recently, we have developed a flow analysis spectrophotometric method for the determination of resorcinol in waters[3] by means of its reaction with *p*-aminophenol (PAP) to produce a complex compound that shows maximum absorption at 540 nm. The method provides a limit of detection of 6.6 ng ml^{-1} (ppb) and a sample throughput of 300 h^{-1}, and is a fast and convenient method for the determination of resorcinol in waters.

In spite of all the advantages of the aforementioned method with regard to low limits of detection, reproducibility, economy and speed, it also has some disadvantages, which concern the final waste that certainly contains unreacted PAP and also the complex formed by the reaction between resorcinol and PAP. This mixture of phenolic compounds could be dangerous and hence detoxification of the final waste, by incorporating a photo-assisted catalytic unit after

* Submitted as a paper on Clean Analytical Methods.

the measurement cell, could prevent harmful environmental side-effects in laboratories that employ this spectrophotometric method.

The aim of this work was to develop a clean analytical procedure for the spectrophotometric determination of resorcinol by reaction with PAP, based on the in-line decomposition of analytical wastes, and a series of studies were carried out in order to establish the optimum experimental conditions for the in-line degradation of resorcinol, PAP and the complex resulting from the reaction between resorcinol and PAP.

Experimental

Apparatus and Reagents

A Hewett-Packard Model 8452A diode-array spectrophotometer, with HP 89530A MS-DOS UV/VIS software, was used for the spectrophotometric measurements. A flow cell of 50 μl internal volume and 1 cm pathlength was employed for carrying out the FI absorbance measurements and to control the degradation of the organic molecules as a function of time.

An ultraviolet lamp from Vilver Lourmet (Lyon, France), which provides UV radiation of 254 nm (220 V and 50 Hz), was employed as a light source to carry out the photo-assisted degradation.

Two four-channel manifolds (see Fig. 1) were used. The first manifold [Fig. 1(*a*)] was employed to study the heterogeneous photocatalytic degradation of PAP, resorcinol and the reaction product between resorcinol and PAP. The other [Fig. 1(*b*)], was used to carry out the spectrophotometric determination of resorcinol and the degradation of the waste simultaneously.

In both manifolds, a Gilson Minipuls P2 peristaltic pump was used to transport the carrier streams, and a Rheodyne Type 50 rotary injection valve was incorporated in the flow injection system in order to inject standards and samples. In all instances, channel A was used to transport PAP and channel B to transport potassium metaperiodate. Channel C was employed to introduce standard solutions of resorcinol prepared in NaOH [Fig. 1(*a*)], or to inject samples and standards into a sodium hydroxide carrier stream [Fig. 1(*b*)]. Channel D was used to introduce a titanium dioxide slurry. Connections between any two channels were made with Y-shaped merging zones in order to ensure good mixing between reagents.

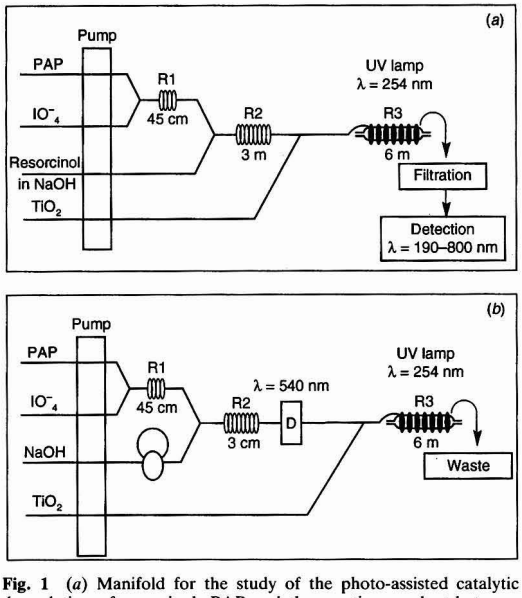

Fig. 1 (*a*) Manifold for the study of the photo-assisted catalytic degradation of resorcinol, PAP and the reaction product between resorcinol and PAP. (*b*) Manifold for the flow–spectrophotometric determination of resorcinol with PAP. D, detector; R_1 and R_2, reaction coils; and R_3, photo-assisted catalytic degradation coil.

Flexible vinyl tubing of 1.52 mm i.d. were used for the peristaltic pump, which allowed carrier flow rates from 0.5 to 4 ml min^{-1} in each channel to be obtained. The reaction coils were made of PTFE with an i.d. of 0.8 mm.

All reagents were of analytical-reagent grade. Resorcinol was supplied by Aldrich (Steinheim, Germany), *p*-aminophenol (PAP) by Fluka (Buchs, Switzerland), potassium metaperiodate and sodium hydroxide by Probus (Badalona, Spain) and titanium dioxide (anatase) powder, type P_{25}, by Degussa (Frankfurt, Germany). From these reagents, appropriate stock and working standard solutions were prepared as indicated in a previous paper.[3] Titanium dioxide suspensions were prepared in distilled water or in acidified distilled water.

General Procedure

Using the manifold shown in Fig. 1(*b*), a 50 μg ml^{-1} PAP solution is continuously fed by channel A, while channel B is used to transport 0.0002 mol l^{-1} KIO_4 solution, in order to obtain the benzoquinoneimine form of PAP, by its oxidation, which is carried out in the reaction coil R_1 (45 cm). A 0.006 mol l^{-1} NaOH solution is introduced by channel C in order to provide an appropriate alkaline medium for the reaction between resorcinol and PAP and also as a carrier for samples and standard solutions which are introduced by using a rotary valve with a loop of 500 μl. The reaction coil R_2 (60 cm) provides the formation of the complex between the benzoquinoneimine form of PAP and resorcinol. A TiO_2 slurry is continuously introduced by channel D and mixed with the final waste obtained after the detector. The reaction coil R_3 (600 cm), rolled on the UV lamp allows complete photodegration of all the remaining toxic products, thus effecting detoxification of the waste.

The carrier flow employed in all the channels is 0.8 ml min^{-1}, which provides a sample throughput of 60 h^{-1} for an injection volume of 500 μl.

Results and Discussion

Photocatalytic Degradation of Resorcinol

All the literature data indicate that photodegradation of organic compounds can occur in aqueous media owing to the presence of dissolved oxygen, which is necessary for the complete mineralization of the molecules. Therefore, a 40 μg ml^{-1} solution of resorcinol prepared in distilled water was subjected to photodegradation using the closed flow system indicated in Fig. 2(*a*), in which a 12 m PTFE coil was rolled around a UV lamp emitting at 254 nm in order to obtain a radial distribution of resorcinol and to be under the direct effect of the UV radiation. Fig. 2(*b*) shows that the absorption bands of resorcinol decrease gradually to zero when the solution is irradiated in the aforementioned manifold, the degradation yield of resorcinol being dependent on the irradiation time and hence complete mineralization of the high concentration of resorcinol assayed can be achieved in 17 min.

The degradation or resorcinol normally produces carbon dioxide and water according to the following equation:

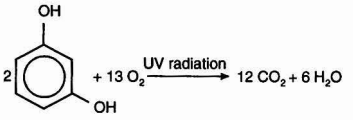

The complete mineralization of resorcinol is evidenced by the absence of the absorption bands after the irradiation time. However, a full degradation time of 17 min seems to be excessively long and not appropriate for use in flow systems, hence the decomposition of resorcinol was studied by using heterogeneous photo-assisted catalytic degradation in the presence of a TiO_2 slurry in order to shorten the degradation time to be more suitable for the FI methodology, using the manifold indicated in Fig. 1(*a*). The effects of several parameters on the degradation of resorcinol, such as TiO_2 slurry concentration (from 0.5 to 2 g l^{-1}) prepared in different concentrations of HCl (from 0 to 7 mol l^{-1}), flow rate of the streams (from 0.2 to 2 ml min^{-1}) and length of the degradation coil R_3 (from 6 to 18 m) were studied in the presence of potassium metaperiodate (0.0002 mol l^{-1}) and sodium hydroxide (0.006 mol l^{-1}) in order to carry out the degradation under the same experimental conditions as used for the FI spectrophotometric determination of resorcinol with PAP.

The results obtained show that resorcinol can be degraded very rapidly under all conditions and it was confirmed, from the spectra of a solution of 20 μg ml^{-1} of resorcinol, before and after irradiation in the presence of TiO_2 (0.5 g l^{-1}, prepared in 0.22 mol l^{-1} HCl) at different flow rates, that quantitative degradation of this phenolic compound can be achieved using carrier flow values of the order of 0.4 ml min^{-1}.

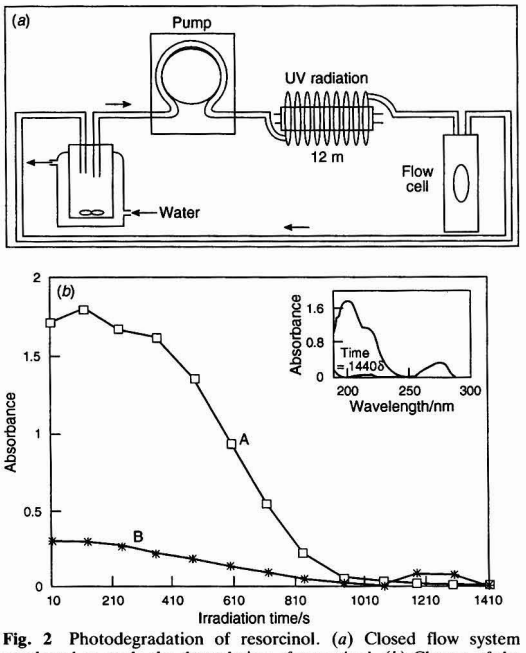

Fig. 2 Photodegradation of resorcinol. (*a*) Closed flow system employed to study the degradation of resorcinol. (*b*) Change of the absorbance of a 40 mg l^{-1} resorcinol solution as a function of irradiation time. A, 200 nm; B, 274 nm.

The final spectra obtained for resorcinol solutions after photo-assisted catalytic degradation have absorption bands at 195 and 224 nm, which correspond to the absorption of sodium hydroxide and potassium metaperiodate solution. The absorption band at 224 nm, which appeared during the degradation of resorcinol in the presence of KIO_4, does not correspond to the benzene ring,[19] but to the potassium iodate produced during the oxidation process in the acidic medium. These aspects were confirmed experimentally by further investigation of mixtures of potassium metaperiodate (0.0002 mol l^{-1}), NaOH (0.006 mol l^{-1}) and 0.5 g l^{-1} solutions of TiO_2 prepared in HCl of different concentrations. After UV irradiation, the band at 224 nm began to appear and increased as the acidity of TiO_2 slurry increased. Further evidence about the nature of this band (224 nm) was obtained by studying the degradation of 20 μg ml^{-1} of resorcinol prepared in 0.006 mol l^{-1} NaOH, without KIO_4, in the presence of TiO_2 (0.5 g l^{-1}, prepared in 0.22 mol l^{-1} HCl); the spectrum obtained did not show the band at 224 nm, which indicates that this band appeared as a result of the reduction of KIO_4 to KIO_3. Spectra obtained without KIO_4 showed a broad absorption band between 250 to 290 nm, which could correspond to the presence of undegraded resorcinol, whereas in the presence of KIO_4 this broad band disappeared owing to the effect of KIO_4 on enhancing the complete degradation of resorcinol.

Heterogeneous Photo-assisted Catalytic Degradation of p-*Aminophenol*

The problems found in the photodegradation of PAP by means of simple UV irradiation agree with those reported previously for different procedures of degradation. Photolysis of PAP was studied at 77 K in an ethanolic solution and in an alkaline alcohol medium[19] and it was confirmed that it gave compounds with different spectra assigned to $p\text{-}H_2NC_6H_4O^{\bullet}$ and $^{\bullet}HNC_6H_4O^{-}$ radicals. On the other hand, PAP was photolysed[20] in ethanol, diethylacetone–isopentane–ethanol and an aqueous alkaline solution at 77 K and electronic absorption spectra of the free radicals formed were measured. The UV irradiation of PAP in the mixture of organic solvents produced predominantly their cationic radical $[H_2NC_6H_4OH]^{+\bullet}$ and the irradiation of the phenolate-type compound $H_2NC_6H_4O^{-}$, which exists in alkaline solutions of $H_2NC_6H_4OH$, produced the neutral radical $H_2NC_6H_4O^{\bullet}$.

A study carried out on the ozonization of PAP[21] took into consideration the rate and the mechanism of the reaction

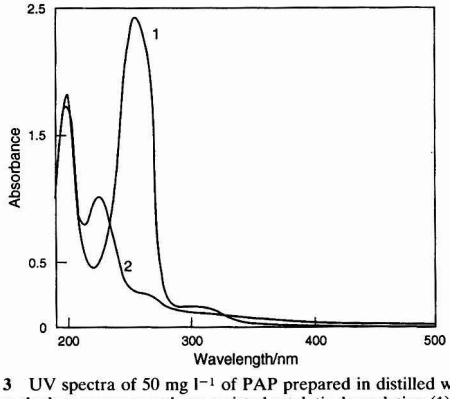

Fig. 3 UV spectra of 50 mg l^{-1} of PAP prepared in distilled water before the heterogeneous photo-assisted catalytic degradation (1) and after degradation process (2) with 0.5 g l^{-1} TiO_2 prepared in 0.22 mol l^{-1} HCl.

leading to the opening of the aromatic ring. In a dilute solution, the opening of the aromatic ring was achieved with an O_3-to-phenol ratio of approximately 5 and the reaction rate depended on the amount of O_3. Also, the degradation of PAP was influenced by pH.

It has also been reported that organics containing nitrogen, such as amine or ammonium groups, are relatively difficult to oxidize because they exhibit a complex mechanism in which the degradation to inorganic compounds occurs very slowly in several steps, initially as ammonia and finally as nitrate.[22]

The heterogeneous photo-assisted catalytic degradation of PAP with a TiO_2 slurry was subjected to an extensive study in the same way as for resorcinol. The results obtained showed that complete degradation of PAP, including the cleavage of the benzene ring, is a function of the irradiation time; Fig. 3 shows the absorption spectra of 50 μg ml^{-1} PAP before and after irradiation in the presence of a TiO_2 slurry in 0.22 mol l^{-1} HCl.

The results obtained indicate that 0.5 g l^{-1} of TiO_2 prepared in 0.22 mol l^{-1} HCl, using a flow rate of 0.8 ml min^{-1}, an R_3 coil length of 12 m and room temperature give the best degradation results; 50 μg ml^{-1} of PAP can be completely mineralized, as can be concluded from the disappearance of the band at 252 nm (see Fig. 3).

Heterogeneous Photo-assisted Catalytic Degradation of the Indophenol Dye Formed Between Resorcinol and PAP

The reaction of resorcinol (**3**) with PAP (**1**) takes place according to the following mechanism:

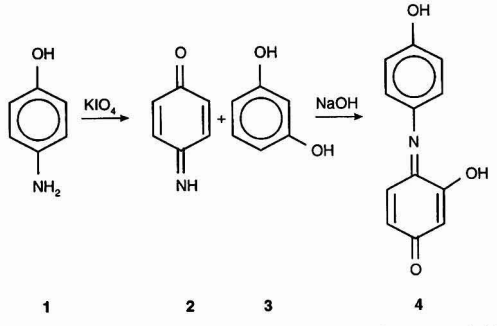

1 **2** **3** **4**

where PAP is oxidized by potassium metaperiodate to yield a very reactive benzoquinoneimine (**2**). The latter reacts very rapidly with resorcinol (**3**) in an alkaline medium through the electrophilic attack on C-4 of **3** to produce the corresponding indophenol dye (**4**), which shows an absorption maximum at 540 nm.

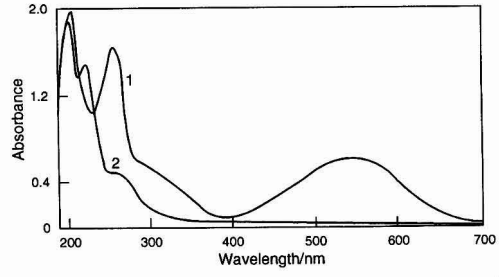

Fig. 4 UV/VIS spectra of the indophenol formed after the reaction of 20 mg l^{-1} of resorcinol with 50 mg l^{-1} of PAP in 0.006 mol l^{-1} NaOH and in the presence of 0.0002 mol l^{-1} KIO_4 before degradation (1) and after degradation (2) in the presence of TiO_2.

The final waste from the above method contains a mixture of the indophenol dye formed between resorcinol and PAP and an excess of PAP. The heterogeneous photo-assisted catalytic degradation of the reaction product was studied in the same way as for resorcinol and PAP. The results obtained show that the use of UV irradiation without TiO_2 has no effect on the mineralization of the indophenol dye, or on PAP, but on using the optimum conditions recommended for PAP degradation it can achieve complete destruction of all the compounds present in the final waste.

Fig. 4 shows the absorption spectra of the indophenol dye produced from the reaction of 20 μg ml^{-1} of resorcinol and 50 μg ml^{-1} of PAP in the presence of 0.006 mol l^{-1} NaOH and 0.0002 mol l^{-1} KIO_4, before and after UV irradiation at 254 nm in the presence of TiO_2 (0.5 g l^{-1} in 0.22 mol l^{-1} HCl) and, as can be seen, the latter spectrum shows that the complete degradation of the indophenol dye, and also that of the excess of PAP, takes place under the previously indicated conditions.

Method for the Determination of Resorcinol

As mentioned before, the maximum flow rate that can be used is 0.8 ml min^{-1}, when the photoreactor has an i.d. of 0.8 mm and a length of 6 m, which provides a very good degradation yield of the indophenol dye and the remaining PAP, and therefore the experimental conditions for the determination of resorcinol were modified to work at this flow rate; hence an R_2 coil length of 60 cm was employed instead of the 300 cm employed previously.[3]

A series of standard solutions containing 2–8 μm ml^{-1} of resorcinol were prepared in 0.006 mol l^{-1} NaOH. The absorption measurements were carried out by using the manifold shown in Fig. 1(*b*), which was constructed in such a way as to permit the measurement of the absorption of the reaction product with PAP and also the complete mineralization of all the organic compounds that are present in the final waste from this method. The results obtained for calibration provided the regression line $A = 0.007 + 0.0364\,c$, where A is the peak height of the FI recording, expressed in absorbance units, and c is the concentration of resorcinol in μg ml^{-1}. The regression coefficient, r, corresponding to the above calibration is 0.9993 and the limit of detection found under these conditions is 16 ng ml^{-1} of resorcinol, the relative standard deviation of four replicate analyses of a sample containing 4 μg ml^{-1} of resorcinol being 0.6% and the sample throughput 60 h^{-1}. The above limit of detection is about double that found without incorporating the detoxification step, and the method provides a five times poorer sample throughput than that obtained under the optimum experimental conditions for the FI–spectrophotometric determination of resorcinol.[3] However, the procedure developed provides a completely detoxified waste.

Conclusion

From these studies it can be concluded that the procedure developed, although is slightly less sensitive and slower than the previous method,[3] is clearly more environmentally acceptable, avoiding problems related to the toxicity of the laboratory wastes. It has been clearly established that the use of TiO_2-catalysed UV mineralization of toxic aromatic compounds can be achieved in a flow stream, providing a simple means for the *in situ* detoxification of analytical wastes.

References

1 *The Merck Index*, Merck, Rahway, NJ, 10th edn., NJ, 1983.
2 Frenzel, W., and Oleksy-Frenzel, J., *Anal. Chim. Acta*, 1992, **261**, 253.

3 Khalaf, K. D., Hasan, B. A., Morales-Rubio, A., and de la Guardia, M., *Talanta*, 1994, **41**, 547.
4 Bard, J. A., *Science*, 1980, **207**, 139.
5 Bard, J. A., *J. Phys. Chem.*, 1982, **86**, 172.
6 Gratzel, M., *Energy Resources Through Photochemistry and Catalysis*, Academic Press, New York, 1983.
7 Izumi, I., Dunn, A. M., Wilbourn, O. K., Fan, R. F., and Bard, J. A., *J. Phys. Chem.*, 1980, **84**, 3207.
8 Barbeni, M., Pramauro, E., Pelizzetti, E., Barfarelb, E., Gratzel, M., and Serpone, N., *Nouv. J. Chem.*, 1984, **8**, 547.
9 Barbeni, M., Marello, M., Pramauro, E., Pelizzetti, E., Vinceti, M., Borgarello, E., and Serpone, N., *Chemosphere*, 1987, **16**, 1165.
10 Serpone, N., Borgarello, E., Barbeni, M., Pelizzetti, E., Pichat, P., Hermann, M. J., and Fox, M. A., *J. Photochem.*, 1987, **36**, 373.
11 Růžička, J., and Hansen, E., *Flow Injection Analysis*, Wiley, New York, 2nd edn., 1988.
12 Valcarcel, M., and Luque de Castro, M. D., *Flow Injection Analysis: Principles and Applications*, Ellis Horwood, Chichester, 1987.
13 Scholten, A. H. M. T., Welling, P. L. M., Brinkman, U. A. Th., and Frei, R. N., *J. Chromatogr.*, 1980, **199**, 239.
14 Vihlein, M., and Schwab, E., *Chromatographia*, 1982, **15**, 140.
15 Kroon, H., *Anal. Chim. Acta*, 1993, **276**, 287.
16 Pramauro, E., and de la Guardia, M., *Richmac*, 1991, **IV** (3) 63.
17 Peris-Cardells, E., Terol, J., Mauri, A. R., Pramauro, E., and de la Guardia, M., *J. Environ. Sci. Health*, 1993, **28**, 431.
18 Parreño, R., Morales-Rubio, A., and de la Guardia, M., *J. Flow Anal.*, 1994, **11**, 79.
19 Tsubomura, H., Kimura, K., Yamada, H., and Kato, M., *Tetrahedron Lett.*, 1965, **47**, 4217.
20 Kimura, K., Yoshinaga, K., and Tsubomura, H., *J. Phys. Chem.*, 1976, **71**, 4485.
21 Dore, M., Langlais, B., and Legube, B., *Water Res.*, 1978, **12**, 413.
22 Low, G. K., McEvoy, S. R., and Matthews, R. W., *Environ. Sci. Technol.*, 1990, **25**, 460.

Paper 4/04261A
Received July 12, 1994
Accepted October 4, 1994

Photocatalytic Treatment of Laboratory Wastes Containing Aromatic Amines*

Edmondo Pramauro and Alessandra Bianco Prevot
Dipartimento di Chimica Analitica, Università di Torino, Via P. Giuria 5, 10125 Torino, Italy

Vincenzo Augugliaro and Leonardo Palmisano
Dipartimento di Ingegneria Chimica dei Processi e dei Materiali, Università di Palermo, Viale delle Scienze, 90128 Palermo, Italy

The photocatalytic degradation of several aniline derivatives present in aqueous solutions containing TiO_2 suspensions was investigated. The process leads to the complete and fast decomposition (within about 1 h) of the pollutant molecules, promoted by oxidizing radical species formed at the irradiated semiconductor/water interface. The stoichiometric formation of CO_2 from the organic carbon was assessed, whereas other inorganic end-products were detected depending on the nature of the aniline substituents. Unstable hydroxyaromatic intermediates were also identified during the initial steps of the treatment. The primary degradation, which follows pseudo-first-order kinetics, changes with the aniline substituents and is strongly dependent on pH.

Keywords: Photocatalysis; laboratory waste; degradation; pollutant; aromatic amine; aniline

Introduction

The problems related to the destruction of hazardous wastes are of actual interest, not only for people involved in industrial or agricultural activities, but also for those who operate in control laboratories, where more or less abundant stocks of contaminated solutions are usually produced and accumulated.

Among the analytes and reagents of environmental concern, aromatic amines constitute a very important class, as they have been recognized as high priority pollutants. The presence of these compounds, generally at very low concentration levels, is often investigated in a large amount of environmental and waste samples.

Aromatic amines can be also introduced as chemical reagents in analytical methods, usually as chelating ligands or coupling components in some spectrophotometric determinations. For example, the use of *o*-phenylenediamine and *p*-nitrosodiphenylamine (analysis of Pt metals), 2-aminobenzenethiol (determination of Mo^{VI}), benzidine (analysis of Cu and other metals) is mentioned in the literature.[1] Compounds such as 2,3-diaminonaphthalene (determination of selenium), *N*,*N*-diethyl-*p*-phenylenediamine (analysis of chlorine dioxide), or *N*-(1-naphthyl)-ethylenediamine (analysis of nitrite), are reported in current spectrophotometric methods applied to water and waste water analysis.[2] When used as analytical reagents, the concentration of these compounds in the corresponding laboratory wastes may be relevant.

The storage and successive destruction of such dangerous pollutants in authorized decontamination plants are usually expensive as they involve the meeting of very strict safety requirements. For this reason, the availability of suitable procedures able to destroy the contaminants present in collected waste solutions immediately after the analytical determination steps, could offer a useful alternative. In this light, the photocatalytic method based on the use of suspended semiconductor particles can be proposed as a relatively simple and low-cost procedure.[3]

When this approach is applied, either the complete decomposition of the target hazardous molecule or the absence of any toxic end-product must be assessed. Moreover, the identification of transient intermediates is also important as the possible formation of other toxic compounds during the process, even more dangerous than the initial substrate, cannot be excluded. For the above reasons, a very accurate analytical control of the reaction system becomes an essential requirement for a safe destruction of the pollutants.

Here we report on the photocatalytic transformation of aniline and some *para*-derivatives, present at the mg l^{-1} concentration level in aqueous solutions. The complete decomposition of such compounds was achieved in the presence of suspended TiO_2 (anatase) particles, under simulated AM1 solar light. Sampling and analysis of the reaction system showed that a typical mechanism based on hydroxylation and opening of the aromatic ring, with oxidation of the organic carbon to CO_2, can be proposed. The nitrogen of the amino group is mainly transformed into nitrate and ammonium ion, whereas nitrite and cyanate anions were also identified during the treatment of 4-nitro- and 4-cyanoaniline, respectively. Moreover, halide ions were detected as typical end-products of haloanilines.

Experimental

Reagents and Materials

The following high-purity aromatic amines were used as received: aniline, 4-methylaniline, 4-nitroaniline, 4-hydroxyaniline (from Carlo Erba, Milan, Italy); 4-fluoroaniline, 4-bromoaniline, 4-cyanoaniline (from Fluka, Milan, Italy); 4-ethylaniline and 4-chloroaniline (from Aldrich, Milwaukee, WI, USA).

Analytical-reagent-grade benzoic acid, sodium carbonate, sodium hydrogencarbonate, nitric acid, ammonium chloride, sodium nitrite and sodium hydroxide, were from Carlo Erba. Sodium *p*-hydroxybenzoate was purchased from Aldrich. Pure standards of the following compounds (Aldrich) were also used in the high-performance liquid chromatography (HPLC) experiments: 1,4-dihydroxybenzene (hydroquinone), 1,2-dihydroxybenzene (catechol), 1,3-dihydroxybenzene (resorcine), 1,2,4-trihydroxybenzene (hydroxyhydroquinone) and 4-aminophenol. All solvents used were chromatographic grade (Lichrosolv, Merck, Elmsford, NY, USA). Doubly distilled water was filtered through 0.45 μm cellulose

* Submitted as a paper on Clean Analytical Methods.

acetate membranes (HA, Millipore-waters, Milford, MA, USA) before use.

Powdered TiO_2 P25 Degussa (about 80% anatase form), having a surface area of 44 $m^2\ g^{-1}$, was used in the photodegradation experiments. The powder was first irradiated for several hours in aerated aqueous dispersions in order to eliminate adsorbed organic matter and thoroughly washed with doubly distilled water to remove the inorganic ions. Subsequently, the filtered suspension was dried (at temperatures below approximately 75 °C) and resuspended by stirring before use.

Stock solutions of each aniline derivative with concentrations ranging between 1×10^{-3} and 2×10^{-2} mol l^{-1} (depending upon their solubilities) were prepared by dissolving the required amount of the compound in water. These solutions, protected from light, were stored at 5 °C.

Irradiation Experiments

Irradiations were performed in cylindrical Pyrex glass cells (4 cm id × 2.5 cm height) of 5 ml of aquous suspensions containing 2×10^{-4} mol l^{-1} of each amine and the required amount of TiO_2 powder (500 mg l^{-1}), using a 1500 W Xe lamp (Solarbox, from CO.FO.MEGRA, Milan, Italy) equipped with a 315 nm cutoff filter and simulating the AM1 solar radiation. The experiments were carried out under aerobic conditions, and the mean temperature within the cell was 60 °C. A simple scheme of the employed device is shown in Fig. 1.

Analytical Determinations

The concentrations of unreacted anilines were determined as follows: the cell irradiation was stopped at fixed times, the dispersion was filtered through 0.45 μm cellulose membranes (HA, Millipore), and the filtrate was immediately analysed by HPLC. Typically 50–100 μl of the filtered samples were injected into the chromatograph composed of an L6200 pump (Hitachi, Tokyo, Japan), an L4200 ultraviolet (UV) detector, and an RP-C_{18} 5 μm Lichrospher (Merck) 250 mm × 4 mm id column. Isocratic elution with acetonitrile–water (different solvent: water ratios were used depending on the analyte) was performed at 1 ml min^{-1}. The amines were monitored at the wavelength of their maximum absorbance (in the range 225–270 nm), previously determined using a Uvikon 930 (Kontron, Zurich, Switzerland) spectrophotometer.

The formation of CO_2 (one of the mineralization end-products) was followed by headspace gas chromatography (GC), according to a procedure described elsewhere.[4] A Carlo Erba 4600 GC apparatus, equipped with a Hayesep Q 80/100 mesh (2 m × 6 mm id) packed column and a thermal conductivity detector, was used. The following working conditions were employed: flow rate, 30 ml min^{-1} (He carrier); detector temperature, 150 °C (block) and 250 °C (filament); injector temperature, 130 °C; and column temperature, 110 °C. Blank runs, performed after long-term irradiation experiments indicated a very low CO_2 contribution of about 0.6 mmol l^{-1}, were used to correct the obtained data.

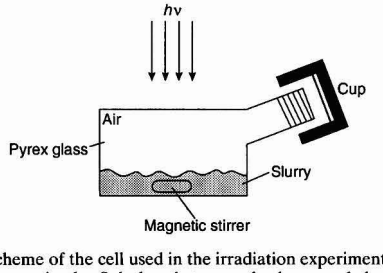

Fig. 1 Scheme of the cell used in the irradiation experiments (cutoff filters, present in the Solarbox between the lamp and the cell not shown).

The formation of halide anions (arising from the mineralization of haloanilines) was followed by suppressed ion chromatography, using a Biotronik IC5000 apparatus equipped with a 100 mm long × 4 mm id BT1AN column (Biotronik, Maintal, Germany). The eluent was a mixture of Na_2CO_3 (1 mmol l^{-1}) and $NaHCO_3$ (2 mmol l^{-1}), at a flow rate of 1 ml min^{-1}.

The formation of cyanate, nitrite and nitrate anions was followed by ion chromatography (IC), using a Metrohm 690 apparatus equipped with a Beckman (Fullerton, CA, USA) 110A pump and a Hamilton (Reno, NV, USA) PRP X100 column (150 mm long × 4.1 mm id). The composition of the eluent employed was: benzoic acid 2×10^{-3} mol l^{-1} and sodium *p*-hydroxybenzoate 4×10^{-3} mol l^{-1}, dissolved in water–methanol (90 + 10 v/v), at pH 8.5. The elution was performed at a constant flow rate (1 ml min^{-1}). For comparison purposes the nitrite analysis was also performed spectrophotometrically, using the Griess method.[2] The absorbance of the reddish azo-compound formed was measured at 525 nm, with a detection limit for NO_2^- of about 0.5 μg l^{-1}.

The determination of ammonium ion was performed using the Nessler spectrophotometric method,[2] measuring the absorbance of the corresponding reaction product at 400 nm against a blank. The calibration graph, prepared using NH_4Cl was linear in the NH_4^+ concentration range of 0.3–10 mg l^{-1}.

Results and Discussion

Substrate Decomposition (Primary Degradation)

Irradiation of air-equilibrated aqueous solutions containing the investigated pollutants and the suspended semiconductor leads to the disappearance of these compounds. Starting from solutions containing 2×10^{-4} mol l^{-1} of substrate and 200 mg l^{-1} of dispersed TiO_2, at pH 5.5, the time required for complete decomposition of the investigated compounds was less than 1 h. These results are in agreement with previous findings concerning the destruction of other aromatic pollutants (having widely different chemical structures) present in water.[3,5,6]

The sequence of events giving rise to the destruction process has been already examined in detail and is reported elsewhere.[7–10] Basically, the TiO_2 (anatase crystalline form) semiconductor has a bandgap energy (E_{bg}) of about 3.2 eV, with a corresponding light absorption threshold at 390 nm. This implies that, under simulated AM1 sunlight irradiation, only a small fraction (about 3%) of the incident light can be absorbed by the semiconductor particles promoting the electrons to the conduction band (CB) and leaving the corresponding valence band holes:

$$TiO_2 + h\nu\ (E \geqslant E_{bg}) \rightarrow e^-_{(CB)} + h^+ \qquad (1)$$

A part of the charge carrier is lost through recombination, whereas a fraction of the carriers can rapidly migrate to the surface of the semiconductor particle, where they can be trapped as Ti^{III} (electrons) or as $[Ti^{IV}–O^{\cdot -}–Ti^{IV}]–OH$ radicals (holes), giving rise to the following set of reactions, $O_{2(ads)}$ indicating oxygen adsorbed on the TiO_2 particles:

$$O_{2(ads)} + e^-_{(CB)} \rightarrow O_2^{\cdot -}{}_{(ads)} \qquad (2)$$

$$Ti^{IV}\text{-}OH^- + h^+ \rightarrow Ti^{IV}/\cdot OH \qquad (3)$$

$$Ti^{IV}\text{-}OH_2 + h^+ \rightarrow Ti^{IV}/\cdot OH + H^+ \qquad (4)$$

The ·OH radicals are highly oxidizing species, capable of attacking the organic substrates. In aqueous acidic media (pH

3) the $O_2^{\cdot -}$ radical protonates forming the hydroperoxide radical $HO_2^{\cdot}$, which in turn gives rise to the formation of H_2O_2.[11,12] Absorption of UV light (λ; 250–300 nm) by H_2O_2 or the interaction of this molecule with $e^-_{(CB)}$ can also originate ·OH radicals. It was already clearly demonstrated that both molecular oxygen and water are essential components in photocatalytic reactions.[13]

Primary degradation kinetics

The primary degradation of all the investigated compounds obeys pseudo-first-order kinetics, described by the following equation:

$$-dc_{subs}/dt = k_{obs}\, c_{subs} \quad (5)$$

where c_{subs} is the concentration of each derivative and k_{obs} is the observed first-order rate constant. According to eqn. (5), linear plots of $-\ln c/c_0$ *versus* time were obtained (see Fig. 2) from which slopes k_{obs} can be evaluated. Table 1 reports the k_{obs} values (together with the corresponding correlation coefficient, r) and the measured half-lifes ($t_{\frac{1}{2}}$) of the examined compounds. It can be noted that the degradation kinetics vary depending on the substituent present on the aniline molecule. Alkyl groups and halogen atoms speed up the primary process, whereas the presence of nitrogen-containing substituents reduces the reaction rate. All the corresponding k_{obs} values are, however, grouped in a quite narrow range, with the sole exception of 4-hydroxyaniline. For this compound, in fact, primary degradation is significantly faster.

Taking into account that the active species attacking the substrate are mainly radicals and that the reaction takes place at the semiconductor/water interface or very near to it, the observed differences in reaction rates depend on the solute partitioning (between the bulk solution and the semiconductor surface), and on the presence of chemical groups or bonds more or less reactive towards the radicals. The increase of substrate hydrophobicity in alkyl- and haloanilines can favour their adsorption onto the particles, thus facilitating the reactions with adsorbed radical species. The formation of halide anions, which is more easy going from fluorine to bromine, could justify the rate sequence observed within the haloaniline group.

The slower degradation rate of nitro- and cyanoaniline could be related to a lower reactivity of the corresponding aromatic rings towards the oxidizing radicals, due to the electrophilic nature of such substituents. However, the very fast degradation of 4-hydroxyaniline is not surprising as it has been already proven that hydroxylation of the aromatic ring favours further attack of the ·OH species.

Experiments performed at increasing pollutant concentrations showed a decrease in k_{obs}. This effect, also reported in other photocatalytic studies, can be explained by assuming competition between reaction intermediates and substrate for the active sites of the semiconductor oxide.[14]

Influence of pH on primary degradation

The influence of pH on the photocatalytic degradation of aniline has been examined in detail. In particular, as expected, it was noted that a relevant decrease of the reaction rate occured at lower pH values (see Fig. 3). At pH 1.5, the half-life of aniline is about ten times longer than at pH 5.5, clearly indicating that the formation of the corresponding cation together with the presence of positively charged TiO_2 particles (the isoelectric point is in the range 5–6 for this oxide) tends to repel the substrate from the catalyst surface. Moreover, the concentration of hydroxy radicals is lower in acid media and, thus, the primary degradation becomes strongly inhibited. Conversely, the pH increase favours the process because the yield of oxidizing radicals increases significantly in basic solutions.

Photochemical contribution to the primary degradation

The degradation of the investigated compounds in the absence of TiO_2 was also investigated, at fixed irradiation times, in order to evaluate the influence of the possible photochemical reactions. Depending on the structure of the examined compound and on the nature of the incident light, the photolytic contribution may be relevant, whereas the influence of photolysis is strongly reduced if the 340 nm cutoff filter is used. Table 2 reports the percentage of substrate still present in the solution after 30 min irradiation when the semiconductor is absent.

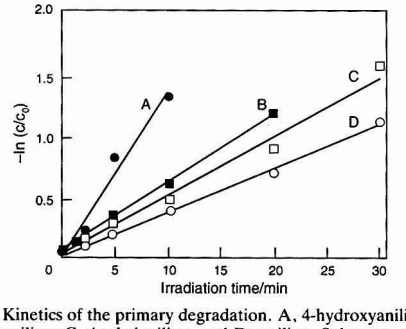

Fig. 2 Kinetics of the primary degradation. A, 4-hydroxyaniline; B, 4-fluoroaniline; C, 4-ethylaniline, and D, aniline. Substrate concentration, 2×10^{-4} mol l^{-1}; TiO_2, 200 mg l^{-1}; cutoff filter, 315 nm; pH 5.5.

Table 1 Kinetic parameters of primary degradation. Initial substrate concentration, 2×10^{-4} mol l^{-1}; TiO_2, 200 mg l^{-1}; initial pH 5.5; cutoff filter, 315 nm

Compound	$t_{\frac{1}{2}}$/min	$k_{obs} \times 10^2$/min^{-1}	r [eqn. (5)]
Aniline	8.30	8.35	0.998
4-Methylaniline	7.28	9.50	0.997
4-Ethylaniline	7.13	9.70	0.999
4-Fluoroaniline	5.53	12.50	0.990
4-Chloroaniline	6.53	11.50	0.9995
4-Bromoaniline	7.60	9.11	0.9995
4-Cyanoaniline	8.43	8.21	0.999
4-Nitroaniline	9.83	7.04	0.9995
4-Hydroxyaniline	2.27	31.00	0.990

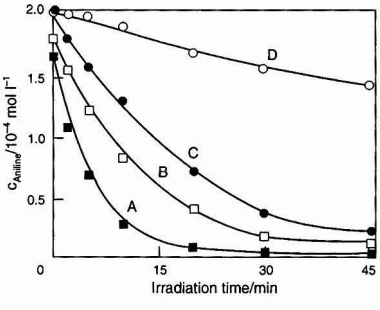

Fig. 3 Variation of aniline degradation rate with the initial pH. A, pH 9.8; B, pH 5.5; C, pH 3.2; and D, pH 1.5. Other experimental conditions as in Fig. 2.

Experiments performed on aniline under the above mentioned conditions showed that the degradation becomes much slower and, in order to obtain reaction rates comparable with those measured using the 315 nm filter, the amount of TiO_2 must be increased. Fig. 4 shows the effect of the semiconductor concentration on primary degradation kinetics of aniline, at pH 5.5, using the 340 nm cutoff filter. It can be seen that the substrate half-life (about 5 min) is comparable to the previously reported value (about 8 min) after roughly doubling the semiconductor concentration. However, a practical limit exists for the use of concentrated TiO_2 suspensions in the reaction vessels owing to the relevant light scattering effects. Thus, in most practical systems the reported concentration of such a component is not higher than approximately 2 g l^{-1}.

Formation of the Reaction End-products

Although the transformation of each substrate occurs through the formation of (several) intermediate compounds, the formation of the end-products from the initial molecule is usually described by an over-all equation that remains valid after long-term irradiation. Working in the presence of an excess of oxygen and assuming complete mineralization, the following equation may be proposed for aniline:

$$C_6H_5\text{–}NH_2 + 9\,O_2 \xrightarrow[TiO_2]{h\nu} 6\,CO_2 + 3\,H_2O + H^+ + NO_3^- \quad (6)$$

Similar equations are valid for the other derivatives and, moreover, halide ions are obtained when haloanilines are degraded. However, the complete oxidation of nitrogen-containing groups present in aromatic molecules to NO_3^- is not always found. Other inorganic end-products are usually detected together with this anion, indicating a more complex transformation scheme for these substituent groups in which reduction reactions involving nitrogen are probably operating.[15] Recent research work performed on a series of nitroaromatic compounds clearly confirmed the presence of such reduction steps.[16]

Mineralization of organic carbon to CO_2

The complete oxidation of the organic carbon to CO_2 in less than 1 h was demonstrated for all the investigated compounds, thus indicating the feasibility of the proposed degradation method. However, the formation of CO_2 is a slow process if compared with primary degradation, and this implies that the reaction proceeds through the formation of other intermediate organic species. In fact, after about 10 min irradiation, the amount of CO_2 formed does not exceed approximately one sixth of the stoichiometric value, whereas under the same irradiation conditions, more than one half of the initial substrate has been decomposed. The presence of some organic intermediates arising from the hydroxylation of the aromatic ring has been confirmed *via* HPLC analysis.

Fig. 5 shows the CO_2 formation profile for aniline and two alkyl derivatives. It can be seen that the presence of the alkyl groups slightly reduces the CO_2 formation rate because, in addition to the aromatic ring, the alkyl chain must also be attacked by the active radicals. The formation of the stoichiometric amount of CO_2 (plateau region) is reached after about 45–50 min for aniline and at longer times for the alkyl derivatives. Conversely, the CO_2 formation rate is practically the same for derivatives having no alkyl substituents.

Formation of halide ions

It appears to be characteristic that hydroxyl radicals add to the halo-organic substrates displacing the corresponding halogen

Table 2 Effect of photolytic processes after 30 min irradiation in Solarbox. Initial substrate concentration, 2×10^{-4} mol l^{-1}

	Percentage of residual aromatic amine	
Compound	$\lambda \geqslant 315$ nm	$\lambda \geqslant 340$ nm
Aniline	88.0	97.5
4-Methylaniline	88.5	97.0
4-Ethylaniline	80.0	94.5
4-Fluoroaniline	56.0	81.0
4-Chloroaniline	46.0	77.5
4-Bromoaniline	78.5	87.5
4-Cyanoaniline	96.0	99.0
4-Nitroaniline	96.0	99.5
4-Hydroxyaniline	85.0	96.0

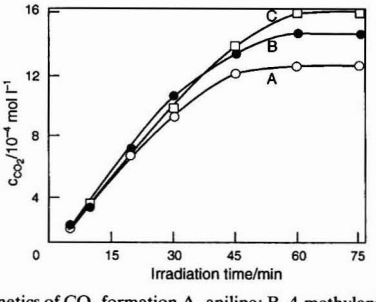

Fig. 5 Kinetics of CO_2 formation A, aniline; B, 4-methylaniline; and C, 4-ethylaniline. Other experimental conditions as in Fig. 2.

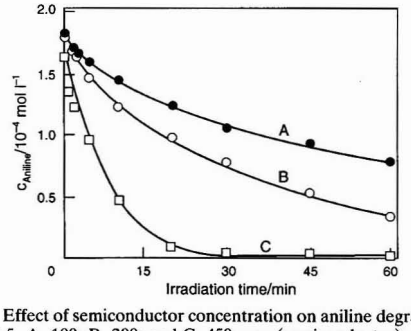

Fig. 4 Effect of semiconductor concentration on aniline degradation at pH 5.5. A, 100; B, 200; and C, 450 ppm (semiconductor).

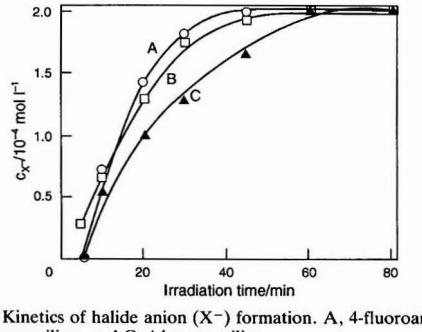

Fig. 6 Kinetics of halide anion (X^-) formation. A, 4-fluoroaniline; B, 4-chloroaniline; and C, 4-bromoaniline.

radical, which is in turn transformed into the corresponding halide *via* the reduction of ·X by the conduction band electrons:

$$\cdot X + e^-_{CB} \rightarrow X^- \quad (7)$$

Fig. 6 shows that the stoichiometric formation of fluoride is faster than the formation of chloride, which is, in turn, faster than bromide. These findings are in agreement with the tendency of each halogen atom to form the corresponding anion. The kinetics of halide formation are comparable to those of CO_2 formation, both processes being faster than nitrogen mineralization.

Formation of nitrogen-containing inorganic products

Most of the experiments were performed on aniline and it was found that the presence of a large excess of oxygen in the reaction cell is a fundamental parameter. In fact, very low amounts of nitrate were obtained working in closed cells (even after several hours irradiation), whereas oxidation became faster if the cells were opened at regular time intervals (typically every hour). It must be underlined that ammonium ion has also been detected in these experiments, thus indicating that oxidation–reduction processes of nitrogen take place simultaneously in the system (see Fig. 7). As the measured final pH in the irradiated cell is about 3.4 (starting from an initial pH of 5.5), there is practically no risk of ammonia loss during cell opening.

Similar profiles were obtained for the other derivatives. For example, after approximately 500 min irradiation, the measured concentration of NO_3^- in the reaction solution was in the range $7–8 \times 10^{-5}$ mol l^{-1} for aniline, 4-ethylaniline and 4-chloroaniline. After the same irradiation periods, the ammonium ion determined was in the range $6–7 \times 10^{-5}$ mol l^{-1}, thus implying that about 25–30% of the total nitrogen must be present in other forms.

These results are in agreement with those reported in studies concerning the photocatalytic transformation of other nitrogen-containing compounds and some authors suggested the possible formation of hydroxylamine as reaction product.[16,17] Moreover, the formation of gaseous compounds (for example N_2) from the oxidation of the above hypothesized intermediate cannot be excluded, but the detection of such products is difficult under the reported experimental conditions.

It must be noted that there is no evidence of nitrite formation (at least within the sensitivity limits of the applied analytical methods) during the degradation of the investigated compounds, with the sole exception of nitroaniline (see Fig. 8). This result is in agreement with recent studies concerning nitroaromatic compounds.[14,16]

Another peculiar behaviour was exhibited by 4-cyanoaniline which, in addition to ammonium ion and nitrate, also

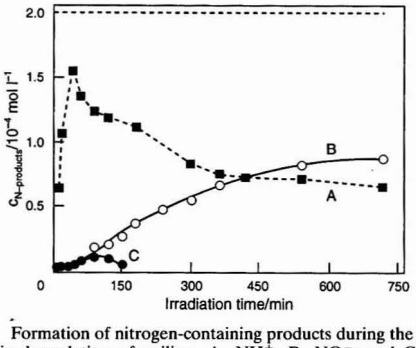

Fig. 7 Formation of nitrogen-containing products during the photocatalytic degradation of aniline. A, NH_4^+; B, NO_3^-; and C, NO_3^- (closed cell). The dashed line at the top of the figure represents the stoichiometric amount of nitrogen.

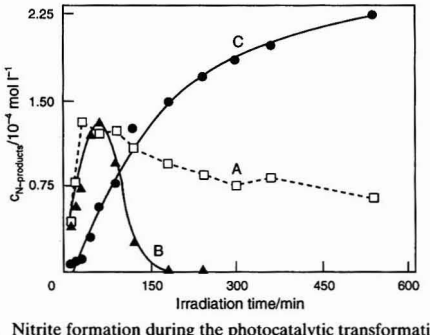

Fig. 8 Nitrite formation during the photocatalytic transformation of 4-nitroaniline. A, NH_4^+; B, NO_2^-; and C, NO_3^-.

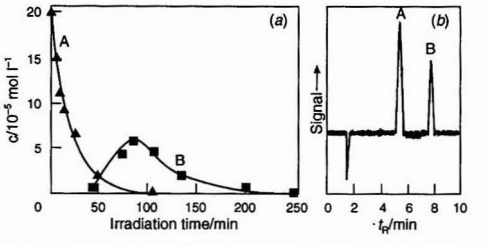

Fig. 9 (*a*) Degradation of A, 4-cyanoaniline and B, intermediate formation of cyanate ion. (*b*) Ion chromatography peaks: A, cyanate; and B, nitrate.

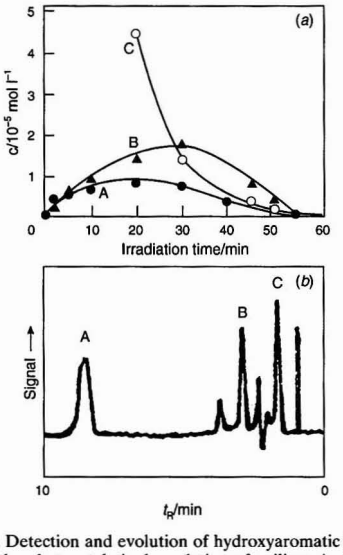

Fig. 10 (*a*) Detection and evolution of hydroxyaromatic intermediates during the photocatalytic degradation of aniline: A, 4-hydroxyaniline; B, 1,3,4-trihydroxybenzene; and C, aniline. (*b*) HPLC peaks: A, aniline; B, 4-hydroxyaniline. and C, 1,3,4-trihydroxybenzene.

showed the presence of cyanate as an intermediate. This compound, which was not previously found in other reported experiments, confirms that the transformation cycle of nitrogen is strongly dependent on the nature of the nitrogen atoms or groups present in the pollutant molecule. The concentration profile of this intermediate [illustrated in Fig. 9(*a*)] shows a maximum after about 100 min, when 4 cyanoaniline is no longer present in the system. After about 200 min cyanate is, in turn, completely degraded. The Fig. 9(*b*) shows the observed IC chromatographic peaks corresponding to nitrate and cyanate ions present in solution after 50 min irradiation.

Presence of Hydroxyaromatic Intermediates

The HPLC pattern of aqueous aniline after photo-oxidation [see Fig. 10(*b*)] shows a group of peaks at retention times shorter than that of the starting substrate, which completely disappear after about 55 min of irradiation. The possible chemical identity of some of these compounds was investigated by comparing their retention times with those of different pure standards and, in particular, peaks B and C were assigned to 4-hydroxyaniline and 1,2,4-trihydroxybenzene, respectively. The presence of polyhydroxyaromatic compounds, already observed during the degradation of other previously investigated aromatic molecules,[13,14,18,19] confirms the nature of the process. It is also known that, after the formation of trihydroxybenzenes, the reaction proceeds *via* the ring opening and the detection of the corresponding products becomes more difficult.

The concentration profiles of the intermediates formed during the aniline transformation are shown in Fig. 10(*a*). Blank experiments performed on solutions containing the corresponding pure standards (each at the concentration of the corresponding maximum) showed the same kinetic profile, thus supporting the previously proposed assignment.

In some instances, for irradiation times in the range 10–20 min, the appearance of a transient yellowish colour was observed. As aromatic amines and phenolic products are simultaneously present at that time (as found during the analysis of the intermediates), coupling reactions between them can occur. However, these hypothesized intermediates are further degraded as the solution again becomes completely colourless after about 30 min of irradiation.

Conclusion

The experiments performed indicated that photocatalysis over suspended TiO_2 particles is an accessible, suitable and cheap degradation method for the destruction of residual aromatic amines present in laboratory wastes. Under the reported conditions, all of the examined aniline derivatives were degraded in less than 1 h, irrespective of the nature of the substituent present.

The final products, arising from the more or less complete mineralization of the initial pollutant, are not dangerous and the detected intermediate compounds do not accumulate in the reaction vessel, but are themselves rapidly degraded by the radical species formed during the irradiation. The presence of abundant oxygen in the reaction cell is important, especially if a more complete oxidation of nitrogen is desired.

The use of direct solar light or simulated solar light containing low percentages of the UV component (as in the experiments performed with the 340 nm cutoff filter) is also possible, taking into account that the degradation kinetics becomes slower in these situations.

Optimization studies performed on larger volume photoreactors are actually under investigation in order to scale up the proposed treatment method.

Financial support from MURST (Rome), CNR, and EEC Contract STEP-CT90-0106-C (DSCN) is gratefully acknowledged.

References

1 *Photometric Determination of Traces of Metals. Part I*, ed. Sandell, E. B., and Onishi, H., Wiley, New York, 1978.
2 *Standard Methods for the Examination of Water and Wastewater*, ed. Clesceri, L. S., Greenberg, A. E., and Rhodes Trussel, R., APHA-AWWA-WPCF, Washington D.C., 17th edn., 1989, ch. 3, pp. 135–137; ch. 4, pp. 79–80; ch. 4, pp. 117–120.
3 Ollis, D. F., Pelizzetti, E., and Serpone, N., in *Photocatalysis. Fundamentals and Applications*, ed. Serpone, N., and Pelizzetti, E., Wiley, New York, 1989, pp. 603–637.
4 Pelizzetti, E., Minero, C., Maurino, V., Sclafani, A., Hidaka, H., and Serpone, N., *Environ. Sci. Technol.*, 1989, **23**, 1380.
5 Mills, A., Davies, R. H., and Worsley, D., *Chem. Soc. Rev.*, 1993, 417.
6 Pelizzetti, E., Minero, C., and Pramauro, E., in *Chemical Reactor Technology for Environmentally Safe reactors and Products*, ed. De Lasa, H. J., Kluwer, Dordrecht, 1993, pp. 577–607.
7 Howe, R. F., and Gratzel, M., *J. Phys. Chem.*, 1987, **91**, 3906.
8 Lawless, D., Serpone, N., and Meisel, D., *J. Phys. Chem.*, 1991, **95**, 5166.
9 Okamoto, K., Yamamoto, Y., Tanaka, H., Tanaka, M., and Itaya, A., *Bull. Chem. Soc., Jpn.*, 1985, **58**, 2015.
10 Al-Ekabi, H., and Serpone, N., *J. Phys. Chem.*, 1988, **92**, 5726.
11 Cundall, R. B., Rudham, R., and Salim, M. S., *J. Chem. Soc., Faraday Trans. 1*, 1976, **72**, 1642.
12 Hermann, J., and Pichat, P., *J. Chem. Soc. Faraday Trans. 1*, 1980, **76**, 1138.
13 Barbeni, M., Pramauro, E., Pelizzetti, E., Borgarello, E., Gratzel, M., and Serpone, N., *Nouv. J. Chim.*, 1984, **8**, 546.
14 Augugliaro, V., Palmisano, L., Schiavello, M., Sclafani, A., Marchese, L., Martra, G., and Miano, F., *J. Appl. Catal.*, 1991, **69**, 323.
15 Low, G. K. C., McEvoy, S. R., and Matthews, R. W., *Environ. Sci. Technol.*, 1991, **25**, 460.
16 Minero, C., Pelizzetti, E., Piccinini, P., and Vincenti, M., *Chemosphere*, 1994, **28**, 1229.
17 Mozzanega, H., Herrmann, J. M., and Pichat, P., *J. Phys. Chem.*, 1979, **83**, 2251.
18 Barbeni, M., Morello, M., Pramauro, E., Pelizzetti, E., Vincenti, M., Borgarello, E., and Serpone, N., *Chemosphere*, 1987, **16**, 1165.
19 Pramauro, E., Vincenti, M., Augugliaro, V., and Palmisano, L., *Environ. Sci. Technol.*, 1993, **27**, 1790.

Paper 4/06440B
Received October 21, 1994
Accepted October 28, 1994

Seasonal and Areal Variations of Polycyclic Aromatic Hydrocarbon Concentrations in Street Dust Determined by Supercritical Fluid Extraction and Gas Chromatography–Mass Spectrometry*

Yu Yang and Wolfram Baumann†

Institute of Inorganic Chemistry and Analytical Chemistry, University of Mainz, 55099 Mainz, Germany

Twenty-four street dust samples were collected from highways, urban streets, a gasoline station, pedestrian tunnels, a civil house and a car park building in some German cities. Polycyclic aromatic hydrocarbons (PAHs) were extracted from these samples with supercritical CO_2 and determined by gas chromatography–mass spectrometry. The PAH concentrations showed distinct variations with the sampling area and the sampling season. In winter, the street dusts were contaminated by PAHs about 2–12 times more than in summer. Fluoranthene, pyrene and phenanthrene always exhibited the highest concentrations, independent of the total PAH concentration, and thus may be used as indicators of PAH pollution of street dusts.

Keywords: Supercritical fluid extraction; supercritical carbon dioxide; polycyclic aromatic hydrocarbon; street dust

Introduction

Polycyclic aromatic hydrocarbons (PAHs) in the environment have received much attention because of both their continuous emission from combustion and their biological activities,[1] such as toxicity, mutagenicity and carcinogenicity. Most of the previous investigations on PAHs in the environment have been concentrated on airborne particles, and little work has been carried out on street dusts.[2–6]

As a first step in an analytical procedure for PAHs, extraction of the investigated environmental samples is necessary. Liquid–liquid (Soxhlet or sonication) extraction and subsequent separation by column chromatography or by adsorption onto special sorbents are widely employed for this purpose. However, such extractions often require large volumes of solvent, which may be toxic and/or expensive, and they often need several hours to even several days to yield acceptable although often incomplete recoveries of some target analytes.

The recovery of many compounds from complex samples should increase with decreasing viscosity. This was the main impetus to developing procedures that incorporate supercritical fluid extraction (SFE) steps[7] and subsequently, applications of this technique also to the determination of PAHs in environmental particulates have been reported.[8–12] For laboratory work, generally the application of CO_2 is preferred over other available fluids as it is non-toxic and its critical point data are easily accessible: at 40 °C and 200 bar the density of CO_2 is of the order of that of non-polar organic liquids, as is the polarity. However, the viscosity is much lower. Therefore, CO_2 under these conditions has the solvent power of at least hexane but shows much better mass transfer characteristics as an extraction medium. Hence it should be the ideal solvent for PAHs in street dust.

In addition to the aforementioned advantages of CO_2 as a non-polar solvent, it is a non-toxic and non-ecotoxic gas that does not necessarily create an additional load for the environment as it can be produced from the CO_2 content of the atmosphere or from natural CO_2 sources. These advantages of CO_2 as a low-viscosity, low polarity solvent and its physiological and ecological advantages make it an ideal candidate solvent for use in clean analytical methods.

Extraction and determination in this investigation were performed by off-line SFE followed by gas chromatography–mass spectrometry (GC–MS), which for the purpose of this work is a more flexible and simpler technique than on-line coupling to, *e.g.*, GC,[10] liquid chromatography[13] or even supercritical fluid chromatography.[14]

Experimental

Sampling and Samples

Street dust samples were collected between April 1990 and December 1991 using a battery-powered vacuum cleaner from a farm road, a civil house, highways, urban streets, a gasoline station, a car park building, an industrial area and pedestrian tunnels in Mainz, Berlin, Frankfurt/Main, Hannover, Wiesbaden and Mannheim. The dusts were sampled directly from the street side, unless stated otherwise. All samples were sieved through a 100 μm metal filter. Some samples were further classified into three classes: < 50, 50–100 and 100–500 μm. In the Mainz district some samples were collected from the same sampling site in different seasons of the year. Table 1. shows the sampling date and site for each sample. Samples were stored for different times (average 6 months) at −4 °C in small glass bottles closed by a PTFE foil capsule until analysis.

In order to prepare well defined but similar model samples, real samples were extracted for 3–5 h with pure supercritical CO_2 at 40 °C and 200 bar, and then a second time for another 3–5 h using supercritical CO_2 at 40 °C and 200 bar saturated with methanol (10% v/v). When used as blanks in the standard extraction procedures, such samples turned out to be real blanks (no PAHs were found in this matrix). A 1 g amount of this matrix was then spiked with 100–300 ng of each target PAH, mixed well and the solvent was allowed to evaporate at low temperature (4–10 °C). These model samples (blank matrix spiked with PAHs) were stable for several weeks in a refrigerator. Some were analysed again after ageing for 3 months and no significant change in the recovery was found.

* Submitted as a paper on Clean Analytical Methods.

† To whom correspondence should be addressed.

Compounds

The following PAHs were found in a first screening experiment on a real dust sample, using GC–MS in the scan mode, and were therefore followed in this study: acenaphthylene (Any), acenaphthene (Ane), fluorene (Flr), phenanthrene (Ph), anthracene (A), 2-methylphenanthrene (2-MePh), 2-methylanthracene (2-MeA), 1-methylphenanthrene (1-MePh), 2-phenylnaphthalene (2-PhyN), 3,6-dimethylphenanthrene (3,6-DiPh), 2,7-dimethylphenanthrene (2,7-DiPh), fluoranthene (F), pyrene (P), benzo[*ghi*]fluoranthene (BghiF), benz[*a*]anthracene (BaA), chrysene (Ch), anthracene-9,10-dione (9,10-Adio) 7*H*-benz[*de*]anthracen-7-one (7H-BA-7-o) and Benzo[*b*]naphtho[1,2-*d*]thiophene (BbNoThio).

Standard PAHs were supplied by Promochem, Amchro Chromatography, Johnson Matthey, Aldrich and Merck.

Table 1 Sampling date (year/month/day) and sampling site for each sample

Sample No.	Sampling date	Sampling site
S1	90/04/04	East Berlin, Heinrich-Mann-Strasse
S2	90/04/05	West Berlin, in front of Zoo railway station
S3	90/04/05	Hannover, in front of the main railway station
S4	90/05/03	Mainz, on the bridge over the main railway station, above S8
S5	90/05/14	Mannheim, at the centre of the pedestrian subway to the main railway station
S6	90/05/21	Mainz, Binger Strasse, in the DEA gas station
S7	90/05/24	Stadecken-Elsheim (a small town 16 km from Mainz), Spielbergstrasse
S8	90/07/04	Mainz, on a rail in a half-sided open pedestrian subway, under the bridge over the main railway station
S9	90/07/13	Mainz–Mombach, industrial area, Rheinallee, under the railway bridge to Wiesbaden
S10	90/07/17	Mainz, Binger Strasse, on the crossway with the tramway
S11	90/08/26	Mainz–Lerchenberg, Koblenzer Strasse, under the A60 highway bridge
S12	90/08/26	Mainz–Lerchenberg, Koblenzer-strasse, on the A60 highway, above S11
S13	90/09/06	Frankfurt airport, on the floor of parking lot 122–123
S14	90/10/10	Same as S9
S15	91/01/10	Same as S11
S16	91/01/10	Same as S12
S17	91/01/15	Same as S9
S18	91/03/25	Same as S8
S19	91/04/15	Wiesbaden, in the pedestrian tunnel in front of the main railway station, 2–10 m from the entrance (station side)
S20	91/05/09	Same as S9
S21	91/05/15	Mainz–Bretzenheim, 300 m from Koblenzer Strasse, on a small farm road
S22	91/05/15	Same as S12
S23	91/05/15	Same as S11
S24	91/12/27	Mainz–Hartenberg, Jakob-Steffan-Strasse 39, dust from a flat on the second floor

Procedures

SFE

The supercritical fluid extractions were performed using a laboratory-made SFE system. Fig. 1 shows the scheme of this experimental set-up, with all necessary instrumental details.

The main parts are a membrane compressor controlled for any settable pressure between 60 and 200 bar (Nova Swiss Model 555.0020), a laboratory-made temperature-controlled water-bath, an extraction cell (Bischoff-type column, 12.5 cm × 2 cm i.d.) and a series of miniature columns (18 mm × 1.5 mm i.d., slurry packed with RP-18, 3 μm particles) which serve both as flow resistors and as sample collectors.

The samples (1 or 3 g) were packed inside a piece of soft paper (*e.g.*, Kleenex) and then positioned roughly in the centre of the extraction cell. The remaining cell volume was filled with glass balls. A 20 l volume of CO_2 was used for all extractions.

As an additional advantage, the series of miniature columns provided a pre-selection with sample precipitation in the different columns of the series, according to the solubility of the sample components at the pressure of the column considered. Details of this method were described previously.[15] For further GC–MS analysis, analytes from the single miniature columns were rinsed using about 1 ml of toluene by an HPLC pump (Bischoff Model 2200). This eluent could then be analysed by GC–MS.

GC–MS

A Hewlett-Packard HP 5890A gas chromatograph and a Hewlett-Packard HP 5970 mass spectrometer with electron impact ionization (70 eV) and helium as carrier gas were used. Separation was carried out with on-column injection onto a 50 m × 0.25 mm i.d. capillary column (Macherey–Nagel, SE-54-CB-0.25). Qualitative analyses were performed in the SCAN mode, from 35 to 350 u. Quantitative analyses were performed by MS in the selected ion monitoring (SIM) mode. For this purpose characteristic ions were observed that were monitored in nine groups of four to eight ions, with a dwell time of 50 ms for each ion. Table 2 shows the analytical SIM conditions. A certified PAH standard solution in toluene that contained 100–200 ng ml^{-1} of each PAH was used. Two internal standards (ε-HCH and Mirex) were added at 144 and 168 ng ml^{-1} to each standard and to each sample solution.

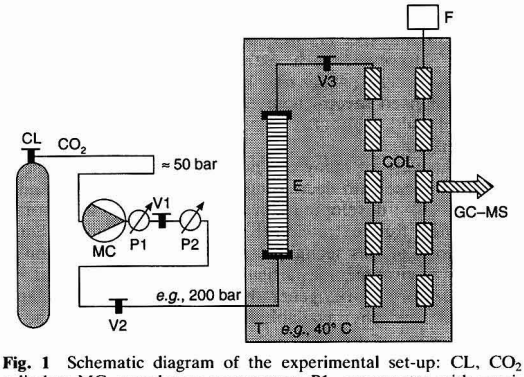

Fig. 1 Schematic diagram of the experimental set-up: CL, CO_2 cylinder; MC, membrane compressor; P1, manometer with maximum/minimum pressure-control switches; V1, pressure-regulating valve; P2, fine manometer; V2 and V3, needle valves; T, water-bath thermostat; E, extraction cell; COL, series of miniature columns; F, flow meter; and GC–MS, off-line transfer to GC–MS analysis.

Selectivity of Extraction Process

Under the extraction conditions (40 °C, 200 bar) used, CO_2 is a powerful eluent for non-polar PAHs. As the solubility of PAHs is very good under these conditions precipitation occurred only on the last three miniature columns of a series of nine or ten columns whereas more polar but still CO_2-soluble compounds precipitated on the first miniature columns. This behaviour is consistent with that found previously with non-polar or medium-polarity pesticides.[15] Hence, only three columns had to be eluted with toluene and the eluate was almost free from interfering compounds, owing to the selectivity of the extraction power of CO_2 and of the fractionated precipitation onto the miniature columns.

Chromatographic Conditions

The selected ion chromatogram was used to optimize the extraction steps and the chromatographic conditions, such as the temperature programme shown in Table 3.

Fig. 2 shows an example of the selected ion chromatogram of a real dust sample. This chromatogram shows the high selectivity of the final procedure with respect to the non-polar PAHs and some other non-polar compounds. Almost all peaks not marked were identified as polychlorinated biphenyls, which will not be discussed in this paper.

Table 2 Selected ions, divided into nine groups, the retention times (t_R) and the recoveries of which are given as average values with standard deviations, from each of three complete SFE–GC–MS experiments on model dust samples

Compound*	Ion mass	Group	t_R/min	Recovery (%)
Any	150/152	1	15.4	91 ± 11
Ane	152/154		16.2	85 ± 9
Flr	163/166	2	18.9	96 ± 11
Ph	176/178	3	26.5	102 ± 11
A	176/178		27.1	98 ± 11
ε-HCH	183/219	4	28.6	
2-MePh	189/192	5	32.3	92 ± 10
2-MeA	189/192		32.8	84 ± 10
1-MePh	189/192		33.7	92 ± 10
2-PhyN	202/204	6	35.8	86 ± 9
9,10-Adio	180/208		36.1	99 ± 11
3,6-DiPh	191/206		38.0	96 ± 11
2,7-DiPh	191/206		38.8	94 ± 11
F	200/202	7	41.4	93 ± 12
P	200/202		44.7	90 ± 12
BghiF	224/226	8	60.6	62 ± 8
BbNoThio	232/234		61.2	60 ± 7
BaA	226/228		62.9	64 ± 8
Ch	226/228		63.5	61 ± 8
7H-BA-7-o	202/230	9	65.0	71 ± 19
Mirex	272/274		68.3	

* For full names, see text.

Table 3 GC temperature programme

	Temperature/°C	
Time/min	Initial	Final
0–4	90	90
4–4.71	90	140
4.71–5.51	140	180
5.51–20.89	180	200
20.89–41.72	200	225
41.73–54.22	225	250
54.23–57.3	250	270
57.3–70	270	270

Recovery

The recoveries of PAHs were determined using the model samples described above, which were extracted with 30 l of CO_2 under the above mentioned conditions. Table 2 gives the recoveries of all 19 PAHs with standard deviations, calculated from three independent complete extraction and determination procedures.

For smaller and more volatile PAHs the recoveries are nearly 100%, in contrast to the more polar or the larger PAHs, with recoveries as low as 60–70%.

As with all analytical work on real matrices, the question arises of how the measured recoveries can be applied to the determination of PAHs in real samples. As mentioned above, the twofold extraction with methanol as modifier did not produce any further target analytes, and the same was true with hexane as the eluent. Hence applying the recoveries to the evaluation of data from real samples probably does not introduce additional errors. This speculation is further supported by the fact that the very non-polar PAHs do not show a good interaction with the much more polar sites of dust, and so also will not sit in pores, *etc.* Further evidence for complete extraction comes from the fact that aged model samples also yielded around 100% recovery. This is also consistent with independent observations that only polar compounds or compounds with polar groups (pesticides) exhibit the problem of undissolvable residues. However, the PAH concentrations found in real dust samples in this study should provide good indications of the minimum PAH concentrations.

Results

Table 4 shows the results for the determination of each PAH in 24 samples. In all samples investigated, PAHs were found and the total concentration (sum of all 19 PAHs) varied from a few to a few hundred μg g^{-1}, depending on sampling area and season.

It is worth-while noting that the size distribution is approximately the same for all dust samples except for S8 and S18. These samples were collected from the frame of a rail in a pedestrian subway, which obviously retains smaller particles better than larger ones, which probably are blown off, as the subway is exposed to wind. Table 5 shows the particle mass distribution for four selected samples, sieved into three fractions.

Of special interest is that the concentrations of fluoranthene, pyrene and phenanthrene, although varying from

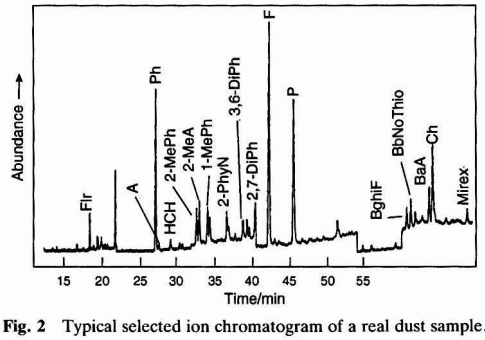

Fig. 2 Typical selected ion chromatogram of a real dust sample.

sample to sample, are the highest in almost all samples. Hence they may be used as indicators of PAH pollution.

Discussion

Areal Variations of PAH Concentrations

As there is a seasonal variation that is discussed in the next section, the discussion here is concentrated on the samples taken in spring. Table 4 reveals that there are samples with total PAH concentrations of less than 5 μg g^{-1} (S4, S5, S7, S21, S22 and S23), an intermediate group containing 6–16 μg g^{-1} (S1, S2, S3 and S19) and another group containing 18–115 μg g^{-1} (S6, S18 and S20).

As expected, the lowest values were found in a small town (S7), in the centre of a 150 m pedestrian tunnel (S5) and on a farm road (S21). However, one would not expect that samples S4, S22 and S23 would also show relatively small PAH loads as there was heavy traffic at these locations. This finding indicates that the PAHs possibly accumulate on dust particles and thus show lower than expected concentrations at locations where the mean standing time of dust particles is low owing to exposure to wind, which is the situation with S4, S22 and S23. However, the extremely highly loaded site S18 is a location where dust may stay and even accumulate for a long time. Of course, the gas station sample S6 shows a high PAH concentration, probably owing to direct pollution from spilled fuels.

Seasonal Variations of PAH Concentrations

The PAH concentration was observed at four sampling sites in Mainz at different times of the year. Fig. 3 shows the observed

Table 5 Relative mass distributions (%) of four dust samples, classified into three size fractions

	Size fraction diameter/μm		
Sample	<50	50–100	100–500
S11	7.6	26.0	66.4
S14	7.9	36.5	55.6
S18	33.8	58.5	7.7
S19	10.4	28.8	60.8

Table 4 Concentrations (ng g^{-1}, determined from one aliquot of each sample) of 19 individual PAHs and the total PAH concentration (rounded to two significant figures) in street dust from sampling sites S1–S24

PAH*	S1	S2	S3	S4	S5	S6	S7	S8	S9	S10	S11	S12
Any	15	16	24	17	8	55	29	36	6	14	7	11
Ane	38	72	47	57	73	210	—†	220	48	40	21	20
Flr	350	180	77	40	64	870	20	400	84	40	31	54
Ph	1300	2400	940	320	480	3600	160	4700	1500	340	540	360
A	220	120	110	73	71	540	22	410	51	48	43	49
2-MePh	400	740	400	260	110	4700	58	1100	510	210	240	230
2-MeA	120	32	53	24	20	460	13	56	26	29	14	24
1-MePh	25	440	240	270	35	2300	34	750	280	110	130	110
2-PhyN	110	550	390	270	180	3200	75	1600	1200	220	210	200
3,6-DiPh	38	290	210	91	98	2200	28	510	170	150	90	76
2,7-DiPh	53	170	140	180	72	1500	18	280	130	150	58	76
F	1200	2400	1600	760	260	2900	280	10000	4700	610	690	650
P	1100	1800	1400	670	160	3300	200	7000	2700	690	610	490
BghiF	250	220	290	39	3	200	43	1100	400	140	95	81
BaA	540	530	400	140	9	640	91	1000	840	170	130	150
Ch	1500	1400	1200	210	19	1600	210	4600	2800	550	370	400
9,10-Adio	87	520	290	230	20	2700	100	3200	1600	150	220	110
7H-BA-7-o	—	130	180	53	48	310	—	1100	530	120	64	12
BpNoThio	91	130	130	36	1	70	—	340	180	77	110	30
Total	7400	12000	8100	3700	1700	31000	1400	38000	18000	3900	3700	3200

	S13	S14	S15	S16	S17	S18	S19	S20	S21	S22	S23	S24
Any	110	9	13	17	27	41	10	10	12	13	21	17
Ane	880	40	26	54	1400	710	53	45	110	25	29	47
Flr	630	94	60	99	2600	1700	220	90	110	52	73	67
Ph	1800	1900	670	820	40000	13000	1900	1500	860	740	550	1400
A	320	160	37	130	2900	1900	310	170	180	54	73	67
2-MePh	1300	560	290	130	11000	7300	1300	600	120	360	250	360
2-MeA	560	35	14	24	8900	620	650	25	32	17	9	4
1-MePh	890	400	160	180	970	3400	510	290	65	210	140	540
2-PhyN	340	1300	300	300	14000	8500	1200	960	110	330	360	390
3,6-DiPh	270	160	120	120	1400	1600	380	150	26	72	110	160
2,7-DiPh	370	130	182	53	820	880	82	110	11	76	150	43
F	3000	6000	1110	1700	46000	16000	3300	5200	480	840	790	1600
P	2600	3500	870	1200	44000	14000	2600	3200	390	810	580	1300
BghiF	260	400	130	130	1500	2400	400	340	31	150	130	260
BaA	480	790	140	360	6400	7600	530	910	210	170	130	160
Ch	460	2800	460	630	10000	15000	670	2200	250	580	400	450
9,10-Adio	800	1800	230	86	23000	17000	1900	1800	88	260	160	670
7H-BA-7-o	2400	530	110	10	610	1800	—	450	—	110	24	—
BbNoThio	110	170	38	42	800	1300	330	160	22	65	27	28
Total	18000	21000	4900	6100	216000	115000	16000	18000	3100	4900	4000	7600

* For full names, see text.

† Dashes indicate below detection limit.

seasonal variations of PAH concentrations. Obviously, the concentrations reveal a trend: concentrations appear to be distinctly higher in winter than in summer, which could be explained by increased coal and oil combustion.

Although there are no reports on the seasonal variations of PAH levels in street dust, the results here may be discussed with reference to some results on airborne particles. In Japan,[5] it was reported that PAHs in airborne particles were related to meteorological factors. Often, the concentrations of PAHs during night-time were higher than those during daytime, both in summer and in winter, and markedly higher concentrations were observed in winter when a surface inversion layer appeared. As another reason for a winter maximum of some PAHs in airborne dust, the use of studded tyres[6] has been reported.

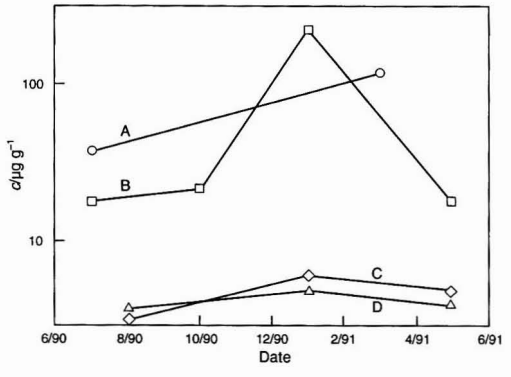

Fig. 3 Seasonal variation of the PAH concentration of street dust from four different sampling sites. A, Mainz railway station; B, Mainz–Mombach; C, on highway A60; and D, under highway A60.

The trend observed in this study is inconclusive as there are only very few data that show the discussed trend, and which also might be due to unknown singular and local effects.

Abundance Distributions of PAHs

It has already been mentioned that the concentrations of fluoranthene, pyrene and phenanthrene are much higher than those of all other PAHs in all the investigated dust samples. Fig. 4 shows the distributions of 15 PAHs in the four samples: S13 (Frankfurt airport parking), S17 (Mainz–Mombach industrial area), S22 (on the A60 highway) and S7 (from a small town).

Basically, all PAH distributions in street dust samples have the same pattern with one interesting peculiarity: the relative amount of chrysene compared with the other dominant PAHs is distinctly smaller in the airport parking (S13) and in the Mainz–Mombach industrial area winter samples (S17) than in the other two samples. This holds true also for the samples S5, S19 and S24. In S5, S13, S17, S19 and S24 the chrysene : fluoranthene ratio is 0.07, 0.15, 0.22, 0.20 and 0.28, respectively, whereas it is between about 0.5 and 0.8 for the other samples investigated. However, the summer and autumn samples from the Mainz–Mombach sampling site (S9, S14 and S20) do not show such a low chrysene : fluoranthene ratio as does the winter sample S17 from this site. With reference to Table 1, one might speculate that the relative chrysene ratio is small at relatively dark and closed sampling sites, and is smaller in winter than in summer, independent of the absolute concentrations.

The PAH distribution in street dust may be compared with distributions of PAHs in other relevant samples. The PAHs emitted from brown coal-fired residential stoves were analysed by Grimmer *et al.*[16] and their abundance distribution was very similar to that found in street dust in this work. Other similar PAH abundance distributions have been found in urban dust,[17] sediments,[18] tobacco smoke condensates[19] and in airborne particulate matter.[20]

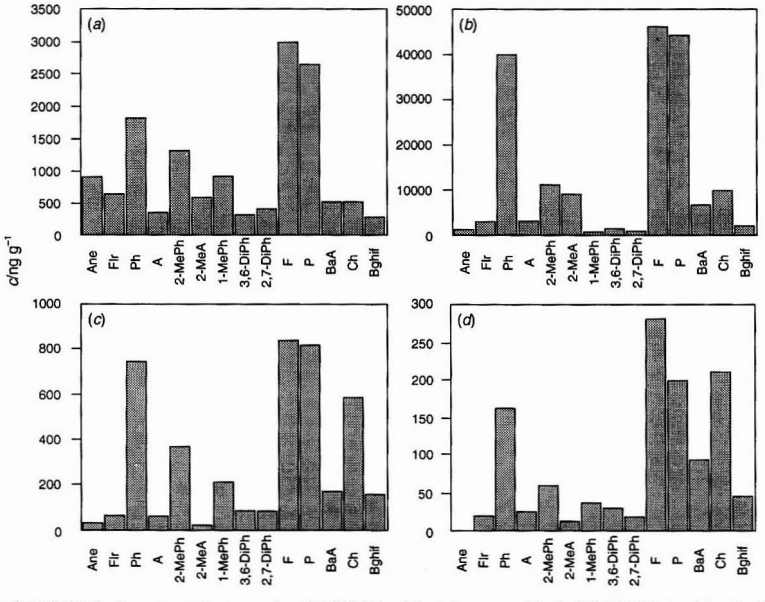

Fig. 4 Abundance of 15 PAHs in four street dust samples. (*a*) S13 (Frankfurt airport parking); (*b*) S17 (Mainz–Mombach industrial area); (*c*) S22 (on the highway A60); and (*d*) S7 (a village).

A completely different type of abundance distribution was found in the gasoline station sample (S6), where the maximum distribution occurs for 2-MePh. This distribution is shown in Fig. 5, together with the respective distribution from diesel particulates.[17] In contrast to the PAH distribution of the other samples, the gasoline station and diesel samples show very high relative concentrations of 2-MePh. Hence it might be concluded that the pollution in the gasoline station is a restricted local pollution caused by the emission from diesel cars.

Conclusion

An attempt has been made to replace non-polar solvents such as hexane by the non-toxic CO_2 under supercritical conditions. It turned out that the properties of inexpensive CO_2 are sufficient for this application. The high recoveries obtained indicate that CO_2 at 40 °C and 200 bar is a good substitute for non-polar organic solvents in this application. Hence extraction of PAHs using supercritical CO_2 is considered to be a good simple, inexpensive step towards a 'cleaner' analytical laboratory.

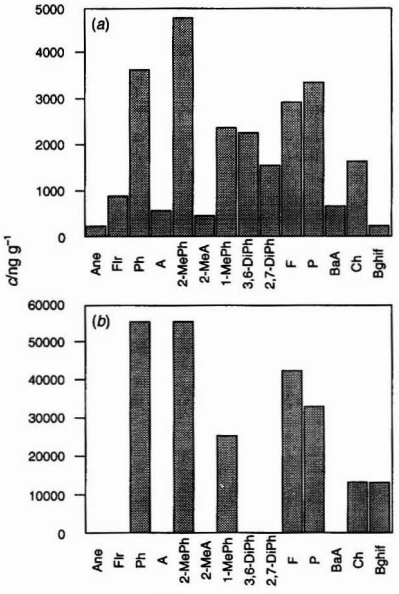

Fig. 5 PAH distribution in (*a*) a sample from a gasoline station (S6); and (*b*) in diesel particulates (from ref. 17).

The authors are indebted to R. Nagel and T. Ternes for making available their GC–MS system. A grant to Y. Y. from the Gottlieb Daimler and Karl Benz Foundation and financial support from the Centre of Environmental Investigations of the University of Mainz are gratefully acknowledged.

References

1 Karcher, W., Fordham, R. J., Dubois, J. J., Glaude, P. G. J. M., and Ligthart, J. A. M., *Spectral Atlas of Polycyclic Aromatic Compounds, Including Data on Occurrence and Biological Activity*, Reidel, Dordrecht, 1985.
2 Takada, H., Onda, T., and Ogura, N., *Environ. Sci. Technol.*, 1990, **24**, 1179.
3 Takada, H., Onda, T., Harada, M., and Ogura, N., *Sci. Total Environ.*, 1991, **107**, 45.
4 Nuekomm, S., Vu Duc, T., and Barblan, C., *Soz.- Praeventivmed.*, 1975, **20**, 65.
5 Kobayashi, S., and Nishikawa, M., *Nagasaki-ken Eisei Kogai Kenkyushoho*, 1983, **25**, 11.
6 Tamakawa, K., Matsumoto, K., Mishima, Y., Seki, T., and Tsunoda, A., *Sendai-shi Eisei Shikenshoho*, 1986, **16**, 305.
7 Hawthorne, S. B., *Anal. Chem.*, 1990, **62**, 633A.
8 Hawthorne, S. B., and Miller, D. J., *Anal. Chem.*, 1987, **59**, 1705.
9 Hawthorne, S. B., and Miller, D. J., *J. Chromatogr.*, 1987, **403**, 63.
10 Hawthorne, S. B., and Miller, D. J., *J. Chromatogr. Sci.*, 1986, **24**, 258.
11 Wright, B. W., Wright, C. W., Gale, R. W., and Smith, R. D., *Anal. Chem.*, 1987, **59**, 38.
12 Lohleit, M., Hillmann, R., and Bächmann, K., *Fresenius' Z. Anal. Chem.*, 1991, **339**, 470.
13 Unger, K. K., and Roumeliotis, P., *J. Chromatogr.*, 1983, **282**, 519.
14 Sugiyama, K., Saito, M., Hondo, T., and Senda, M., *Z. Chromatogr.*, 1985, **332**, 107.
15 Schäfer, K., and Baumann, W., *Fresenius' Z. Anal. Chem.*, 1989, **332**, 884.
16 Grimmer, G., Jacob, J., Naujack, K.-W., and Dettbarn, G., *Anal. Chem.*, 1983, **55**, 892.
17 Niles, R., and Tan, Y. L., *Anal. Chim. Acta*, 1989, **221**, 53.
18 Giger, W., and Blumer, M., *Anal. Chem.*, 1974, **46**, 1663.
19 Lee, M. L., Novotny, M., and Bartle, K. D., *Anal. Chem.*, 1976, **48**, 405.
20 Greaves, R. C., Barkley, R. M., and Sievers, R. E., *Anal. Chem.*, 1985, **57**, 2807.

Paper 4/03300K
Received June 3, 1994
Accepted July 18, 1994

Costs, Laboratory Safety, Productivity and Faster Research Octane Number and Motor Octane Number Determinations in Industrial Chemistry Laboratories*

J. M. Andrade, S. Muniategui, P. López and D. Prada

Departamento de Química Analítica, Universidade da Coruña, A Zapateira s/n, E-15071 A Coruña, Spain

Various aspects of industrial laboratory performance including costs, staff productivity, test urgency, and professional health and hygiene-related topics were investigated in this paper. Because environmental considerations should include the working environment, where one may spend a substantial amount of time, this work was aimed at the development of testing methodologies, taking account of these considerations and meeting the new demands currently imposed by the working environment. In the practical example presented, chemometric and Fourier transform middle infrared (FT–MIR) techniques were jointly used in order to predict the two main features of automotive gasolines (research octane number (RON) and motor octane number (MON). Reduced delay times, and increased repeatability and throughput were additional objectives of this work. In this way, management of smaller amounts of samples and reagents were accomplished.

Keywords: Motor octane number; research octane number; working environment; Fourier transform; infrared

Introduction

The vast amount of scientific work devoted to the 'natural environment' is a clear reflection of the great concern of today's society with nature, its preservation, and avoidance of harmful effects and deterioration. Work in these areas is often carried out by analytical chemists, whose scope has substantially expanded since the inception of chemometrics. Their major goal is not only to make accurate measurements, but also to develop all the steps involved in the analytical process.[1,2] In fact, such steps have benefitted from dramatic advances as regards not only the determination of a wide variety of toxic elements and substances with very low detection limits, but also the development of new, more powerful analytical methods. Currently, the involvement of analytical chemists goes well beyond their traditional former tasks and includes a deep concern with protecting the natural environment. This has aroused the widespread feeling, as pointed out by the Environmental Protection Agency,[3] that new testing methods should use as little sample and reagents as possible, and that the latter should be environmentally 'safe'. This is no doubt a praiseworthy working policy.

Our aim in this work was to take a further step forward and switch from an overall approach to a more specific one. Any substance can be a poison, depending on the dose.[4] It is easy to see that chemical-industry workers are exposed to health hazards that may result in acute or chronic professional diseases.[5] Obviously in such instances, the influence of the working environment should not be overlooked. One can even put forward purely economic arguments in favour of this. Thus, laboratories that are to comply with quality assurance systems (QAS) and/or good laboratory practices (GLP) should be aware that every aspect of the working environment (safety, laboratory design, health and hygiene precautions, *etc.*) directly influence the quality of results achieved.[6]

In this work, we studied a real industrial situation with a view to: decreasing analytical costs; improving professional health and hygiene; diminishing the amount of analytical waste to be disposed of; and developing new, more rapid and precise methods of doing so, than the existing alternatives; the practical example presented involved replacing two essential tests for quality control of automotive gasolines, *i.e.*, the determination of the knock characteristics of motor fuels by the Research Method (research octane number, RON)[7] and those of motor and aviation fuels by the Motor Method (motor octane number, MON).[8] These two standardized methods involved using very expensive equipment, [purchase cost about US$155000 per motor *versus* about US$26000 per Fourier transform middle infrared (FTIR) spectrometer] that was also expensive to run and maintain under optimal conditions, *i.e.*, frequent servicing, large amounts of samples (≈1 l), intensive attention by the analyst (about 30 min per sample) and wide repeatability (about 0.3 octane number (O.N.) for MON and 0.2 for RON) and reproducibility (0.7 O.N. for RON and 0.9 O.N. for MON) ranges. Their reproducibility s_r values strongly depend on the RON or MON values. For the common fluid-catalytic cracking (FCC) values used in this work, reproducibility s_r values were 0.3 for RON and 0.4 for MON. Additionally, the two standard motors used emitted vapours and gases which, however efficiently removed by fume-drawing systems, should be minimized or avoided. Each motor produced a high noise and required about 500 ml of a mixture of isooctane (2,2,4-trimethylpentane) of special purity, *n*-heptane and toluene. Both the noise and the gas exhaust can be anti-hygienic, or even noxious, in the long term.

In addition, the motors worked in a highly sophisticated way and called for skilled operators, therefore, both economic, throughput, and professional health and hygiene considerations made it desirable to develop an alternative that would be specially indicated in routine control applications at refinery-production plants. In fact, the final gasoline analyses preceding shipping must unavoidably be carried out by using the traditional methods for this purpose (this is imposed by widespread trade practices).

The specific objectives of this work, in connection with the system addressed, were (*a*) to suppress noise; (*b*) to reduce the amount of sample required for analysis; (*c*) to eliminate noxious vapours and gases; (*d*) to minimize analytical reagent consumption; (*e*) to improve the precision relative to

* Submitted as a paper on Clean Analytical Methods.

traditional methods; and (*f*) to simplify the operational procedures involved so they can be implemented by unskilled workers.

Experimental

Samples

An overall of 140 samples collected from the daily output of the FCC units of a Spanish refinery were used. The samples contained none of the additives typically used for improved RON or MON (*i.e.*, we determined the 'clean octane number').

The sampling was carried out in compliance with ASTM D4057-standard,[9] and all samples were refrigerated prior to analysis. They were subjected to the classical RON and MON determinations by using standardized motors[7,8] and skilled personnel. For the development of the new method, an aliquot of 40–50 ml from each of the previous samples was placed in a 50 ml chromatographic vial (Supelco ref. 3-3108) and the vial was closed with a silicone-rubber stopper (Supelco ref. 3-3204) and sealed with tear-away seals (Supelco ref. 3-3251). The vials were then stored in a refrigerator at 0 °C in order to avoid potential degradation. Work has been performed to extend the studies to finished gasolines [with methyl *tert*-butyl ether (MTBE) and ethyl *tert*-butyl ether (ETBE) as additives].

None of the samples were subjected to any pre-treatment for application of the two analytical methods. Of the initial 90 samples, 44 were used as the calibration set and the remaining 46 as the testing set. The latter were picked from production batches unrelated to the calibration samples. In this way, the performance of the method in routine work could be assessed. Additionally, 50 samples were taken to follow the new method performance comparing it with the ASTM standard values. All 140 samples were collected in several sampling seasons during one year.

Instrument Set-up

The ASTM standard methods were implemented on two standardized ASTM-CFR motors[7,8] under controlled running conditions. Their performance was checked *via* inter-laboratory experiments.

The proposed alternative method was implemented on a Perkin-Elmer 1610 FTIR spectrometer operating in the middle-infrared (MIR) region and furnished with an NaCl traditional cell of constant thickness (Teflon spacer of 0.01 cm, no optimization was made to select this parameter) that was stored in a desiccator loaded with silica gel at 25 °C prior to use. The spectrometer performance was checked by determining the wavelengths of appearance of the absorption bands for polystyrene (as a 0.038 mm thick film), which were well documented.[6,10] All the bands studied fell within the acceptable error ranges. This test was run periodically (see Table 1). The cell was filled using disposable syringes (2 ml) Becton Dickinson (Huelva, Spain). Spectra were scanned with a 4 cm^{-1} resolution.

Table 1 Polystyrene bands used to monitor FTMIR spectrometer accuracy performance

Theorical peak/cm^{-1}	Maximum acceptable interval	Experimental value/cm^{-1}
2851.5	±5.0	2848.0
1601.8	±2.5	1601.3
1028.3	±2.5	1028.9
907.0	±2.5	907.0

Software

The spectrometer was controlled *via* a 386 DX PC compatible computer interfaced to and equipped with a mathematical co-processor. The Infrared Data Manager from Perkin-Elmer was used as control software. The statistical package employed was developed at the Centre for Process Analytical Chemistry (CPAC, Seattle, WA).[11]

Analytical Procedure

While similar problems had already been addressed by other authors in a similar way[12–15] the proposed procedure had a number of distinct features, namely: (*a*) Excepting the Ichikawa study,[16] to our knowledge the MIR region had not yet been widely used in combination with chemometrics to address this type of problem. (*b*) The example presented involved monitoring real, daily output, which was not stated as being the case in previous, similar studies. (*c*) Currently, each laboratory must perform this type of study in accordance with the type of sample it usually handles. Alternatively, second-order standardization techniques could be used.[17,18] In any case, this is still at research level and application to industrial processes is still remote. (*d*) We focused on improving the off-line process analytical chemistry component[19] rather than the on-line component in accordance with the peculiarities of the company concerned. It should be noted that the new method is also aimed at improving environmental laboratory conditions. (*e*) The laboratory already had the above-mentioned FTMIR equipment, the utility of which was to be augmented (by increasing its throughput and reducing the atomization time), as was the laboratory throughput as a result. In this way, the need to purchase new, medium-to-high cost equipment for the NIR region (used by most authors for the intended purpose) was avoided.

The working methodology used was similar to that typically employed in this type of study,[12–15] so only a brief outline is provided below.

Sample spectra were recorded on the FTMIR spectrometer from 4000 to 600 cm^{-1} at 4 cm^{-1} intervals. Each spectrum was the result of the average of six scans. For chemical reasons, only the region from 1600 to 600 cm^{-1} was used for statistical purposes. Spectra were digitized, and input into the statistical software together with the experimental, classical, RON and MON values. Background spectra were obtained with the

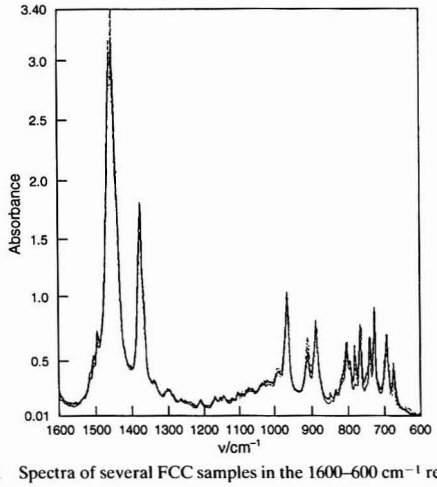

Fig. 1 Spectra of several FCC samples in the 1600–600 cm^{-1} region.

same empty cell, cleaned and dried, and were subtracted from each sample spectrum.

The partial least squares (PLS) regression technique was used in its two variants (one-block and two-block) for statistical modelling. Both provided identical results. Data were auto-scaled prior to all analyses. The optimal number of latent variables for each model was determined by cross-validation. The optimal model chosen in each case was that resulting in the minimum standard error of prediction (SEP) where $SEP = 1/n\,[\Sigma(Y_{exp} - Y_{calc})^2]^{\frac{1}{2}}$ (n = number of samples in the monitoring set).[20]

Fig. 1 shows the general profile for the samples. Each variable of interest (RON and MON) was studied separately (by using the PLS-1 block) and simultaneously (by using the

Table 2 Performance of the statistical model. Routine samples. Classical method *versus* the IR-PLS method.

	RON				MON			
Sample	RON	IR-PLS	95% confidence interval	Δ	MON	IR-PLS	95% confidence interval	Δ
1	91.3	92.0	0.31	0.7	80.1	80.1	0.23	0.0
2	91.5	92.3	0.30	0.8	80.4	80.3	0.22	0.1
3	92.0	92.2	0.24	0.2	80.0	80.3	0.20	0.3
4	91.8	91.8	0.28	0.0	80.2	80.0	0.23	0.2
5	91.5	91.7	0.32	0.2	80.3	79.9	0.25	0.4
6	92.3	92.4	0.28	0.1	81.1	80.4	0.20	0.7
7	91.5	91.8	0.22	0.3	80.0	80.2	0.22	0.2
8	91.3	91.3	0.50	0.0	80.3	80.0	0.40	0.3
9	90.8	91.1	0.57	0.3	80.0	79.9	0.43	0.1
10	94.3	94.0	0.26	0.3	82.0	81.5	0.24	0.5
11	93.5	93.2	0.42	0.2	81.6	80.8	0.29	0.8
12	92.5	92.9	0.33	0.4	80.3	80.6	0.29	0.3
13	92.5	93.1	0.42	0.6	80.3	80.6	0.24	0.3
14	93.3	92.9	0.33	0.4	80.5	80.5	0.30	0.0
15	93.3	92.7	0.32	0.6	80.5	80.5	0.26	0.0
16	94.2	94.2	0.28	0.0	82.2	81.7	0.27	0.5
17	94.1	94.1	0.30	0.0	82.0	81.7	0.27	0.3
18	93.2	92.9	0.28	0.3	80.6	80.7	0.24	0.1
19	93.0	92.9	0.30	0.1	81.4	80.6	0.27	0.8
20	93.9	94.3	0.32	0.4	82.0	81.8	0.29	0.2
21	91.9	92.8	0.38†	0.9	80.0	80.4	0.32	0.4
22	92.6	92.4	0.37	0.2	80.9	80.4	0.23	0.5
23	92.4	92.4	0.33	0.0	80.9	80.3	0.22	0.6
24	92.7	92.5	0.34	0.2	80.6	80.4	0.23	0.2
25	96.0	96.2	0.38	0.2	85.1	84.1	0.28‡	1.0
26	93.4	92.5	0.38†	0.9	81.0	80.4	0.23	0.6
27	92.2	92.3	0.27	0.1	80.9	80.3	0.20	0.6
28	92.5	92.3	0.33	0.2	80.7	80.2	0.27	0.5
29	92.0	92.3	0.35	0.3	80.4	80.3	0.23	0.1
30	92.5	92.3	0.30	0.2	80.0	80.2	0.23	0.2
31	93.0	92.4	0.33	0.6	80.6	80.4	0.21	0.2
32	92.2	93.8	0.41*	1.6	82.8	81.6	0.26*	1.3
33	94.5	93.7	0.44*	0.8	82.5	81.5	0.26*	1.0
34	96.2	97.2	0.57*	1.0	84.0	85.1	0.52*	1.1
35	97.5	97.2	0.71	0.3	85.4	85.3	0.65	0.1
36	93.0	92.3	0.28	0.7	81.0	80.3	0.20	0.7
37	92.9	92.3	0.32	0.6	80.8	80.3	0.22	0.5
38	92.5	92.3	0.29	0.2	80.5	80.2	0.22	0.3
39	97.0	97.0	0.58	0.0	84.7	84.9	0.52	0.2
40	97.1	97.4	0.59	0.3	85.1	85.2	0.52	0.1
41	93.0	92.3	0.43	0.7	80.6	80.3	0.26	0.3
42	97.7	97.4	0.49	0.3	85.6	85.0	0.38	0.6
43	92.9	92.3	0.44	0.6	80.7	80.2	0.27	0.5
44	96.9	96.5	0.58*	0.4	84.9	84.0	0.40*	0.9
45	96.8	96.9	0.45	0.1	84.9	84.5	0.33	0.4
46	92.5	92.4	0.35	0.1	80.6	80.2	0.27	0.4
47	92.3	92.4	0.53	0.1	80.3	80.1	0.35	0.2
48	93.1	92.2	0.41	0.9	81.1	80.1	0.29‡	1.0
49	92.0	92.2	0.37	0.2	80.3	80.1	0.27	0.2
50	92.1	92.6	0.47	0.5	80.0	80.3	0.30	0.3

RON: $SEP^2 = 0.2037$ ($n = 47$); SEP = 0.45 (all samples except those denoted with *).
$SEP^2 = 0.1543$ ($n = 45$); SEP = 0.39 (all samples expect those denoted with *, † or ‡).
MON: $SPE^2 = 0.2015$ ($n = 47$); SEP = 0.45 (all samples except those denoted with *).
$SEP^2 = 0.1594$ ($n = 44$); SEP = 0.40 (all samples except these denoted with *, † or ‡.

* Samples from blending tanks.
† Samples with errors in the ASTM values.
‡ Model faults.

PLS-2 block). The results reported were those obtained in the latter study, as nothing significant was gained by predicting each variable separately. The models discussed below allow the RON and MON to be determined simultaneously, which is very important as the classical method entails using two motors, under different working conditions, in order to measure both quantitities. These results agree with those of the bibliography (*e.g.*, references 12–15).

Results and Discussion

The actual region of interest for statistical analysis was from 1600 to 600 cm^{-1} (Fig. 1). This spectral region was digitized to obtain 250 points per spectrum.

One of the greatest difficulties encountered in the experimental work was assigning the bands in this range, traditionally known as the 'fingerprint region', because most of the organic components of gasolines exhibit a host of peaks that are difficult to interpret. This could be one of the advantages of NIR work, where band interpretation would be simpler due to the existence of fewer bands. However, this problem was irrelevant to this particular work as the chemometric study required no detailed interpretation. The spectra obtained are currently being analysed in detail, as is their relationship to the mathematical models derived.

After raw data were obtained, they were auto-scaled and each spectrum was assigned its RON and MON values as determined by traditional methods. By careful analysis of leverages and students *t*-test values, and with the aid of the cross-validation technique, potential outliers to be eliminated were identified with a view to establishing the final models at a later stage.

After the models were established, they were validated by correlating the results provided by a large number of samples analysed daily by using both the classical methodology and that based on our statistical models. Table 2 summarizes the results obtained. Samples denoted with * correspond to samples from blending tanks (*i.e.*, FCC plus platforming napthas and MTBE as additives). As we did not model these types of samples, we did not obtain good results. Samples 21 and 26 were unreliable as regard to their agreement with ASTM RON values. MON values with † have been considered as model faults because no special circumstances were addressed.

It should be emphasized that the SEP values obtained were consistent with previously reported values[12–14] for the NIR region, which indicates that the proposed method was valid and comparable in terms of performance to the more sophisticated methods using fibre optics and NIR. For MON, we have an SEP of 0.4 (using NIR, values of 0.34 have been obtained[14]); RONs ASTM reproducibility s_r is 0.4. For RON, we have an SEP of ≈0.39 (using NIR, 0.29[14]), and MONs ASTM reproducibility s_r is 0.3.

Using the method proposed, reproducibility s_r values were not dependent on the RON and MON values.

'Long term standard deviation' can be calculated by re-analysing one sample several times during a given period. Using the ASTM methods, one might expect that long term standard deviation may almost be the same as the reproducibility s_r. However, using the proposed IR–PLS method, long term standard deviation values have shown to be about 0.03 ON for both RON and MON ($n = 15$).

Regarding repeatability, using the IR–PLS method, values of 0.01 have been encountered ($n = 6$) for either MON or RON; ASTM methods show values of about 0.15 for MON and 0.10 about for RON (and for the current values used here).

It can be seen that the IR–PLS method has good reproducibility and repeatability compared with the ASTM methods.

Several tests can be used to verify that the IR–PLS method gave the same values as the ASTM method. One such test is to regress IR–PLS values on ASTM values for several samples. It can be statistically tested, if the slope is unity and ordinate is zero. Table 3 shows a good agreement between both methods, as Table 2 suggests.

Table 4 summarizes the advantages of the proposed methodology over the classical methodology in terms of working environment considerations alone. As regards cleaning the NaCl cell used by the MIR equipment in applying the

Table 3 Regression of IR–PLS values on ASTM values to assess performance of the IR–PLS method

Number of latent variables (L.V.) in the model: 2
Variance percentage described by the model

	Independent variables		Dependent variables	
L.V.	This L.V.	Total	This L.V.	Total
1	76.27	76.27	88.95	88.95
2	5.52	81.80	6.42	95.37

Actual (x) *versus* predicted regression (y):

RON—

Regression line: $y = 4.23 + 0.955\,x$
Standard error of calibration (SEC) = 0.48
$r = 0.9770$ ($r^2 = 0.955$; alienation coefficient = 21.21%)

Independent hypothesis tests:
Slope: $|t_{exp}| = (1 - b)/S_b = 1.02$ $t_{(95\%,\ n\ -\ 2\ =\ 39)} = 1.71$
Intercept: $|t_{exp}| = (0 - a)/S_a = 1.02$

Simultaneous hypothesis test:
$F_{cal} = 0.54$ $F_{tab,(95\%,\ 1\ tail,\ 2,\ 23)} = 3.42$
Conclusion: both methods give statistically identical results

MON—

Regression line: $y = 3.92 + 0.952\,x$
Standard error of calibration (SEC) = 0.48
$r = 0.9760$ ($r^2 = 0.952$; alienation coefficient = 21.91%)

Independent hypothesis tests:
Slope: $|t_{exp}| = (1 - b)/S_b = 1.14$
Intercept: $|t_{exp}| = (0 - a)/S_a = 1.14$ $t_{95\%,\ n\ -\ 2\ =\ 39)} = 1.71$

Simultaneous hypothesis test:
$F_{cal} = 0.61$ $F_{tab,\ (95\%,\ 1\ tail,\ 2,\ 23)} = 3.42$
Both methods give statistically identical results

Table 4 Chemometric method compared to ASTM method

Item	ASTM methods	Chemometric methods
Sample	1 l	20 ml
Reagents	approximately 500 ml blends of isooctane, *n*-heptane, toluene	none
Environmental noise	quite high	none
Vapours (fumes)	from reagents, from motor performance, from samples	only from gasoline samples (small amounts)
Delay time to get one characteristic (considering one sample)	35 min	5 min
Residues	fumes, isooctane, *n*-heptane, toluene, gasoline samples (about 200 ml useless blends)	only 10 ml of gasoline per sample. They can be used to clean heavy products from glassware (*e.g.*, fuel, vacuum residues, *etc.*)

classical working method, we initially chose a solvent capable of efficiently flushing any gasoline residue. We selected carbon disulfide for spectroscopy (Merck, ref. 2210:1000) because it removed gasoline residues and could be removed readily from the cell, simply by passing a stream of dry air over it. Even though the amount of solvent residue after each analysis was 2–3 ml per sample, we could not be satisfied because carbon disulfide is a well-known carcinogen.[4] However, we found that washing was not needed as we had about 40 ml of sample, so 10–15 ml could be set aside for flushing the cell before an aliquot was taken. In fact, passing 2–3 ml of each fresh sample through the constant-thickness cell was found not to alter the results obtained for the sample aliquot subsequently assayed. In this way, the need for any solvent clean-up was avoided and the sole residue handled was that of each gasoline sample. Gasoline residues can readily be collected and used to clean other types of products used in refinery laboratories which cannot be flushed by other solvents (*e.g.*, crude oils, fuels, vacuum residues, *etc.*) or be introduced in the general cycle for recovery of residues implemented by each company. As regards this latter alternative, we must emphasize that our method introduced no new products or residues in the cycle.

It should be emphasized that considering all the samples used in this study, we have monitored the real throughput of the FCC unit for about one year and this is still on going. To our knowledge, this had never been done before. By not monitoring the real performance of the model under the changing conditions of real production in a refinery, unexpected problems may arise. We found how easily a model can be derived from a small number of samples that performed well with one another.

The most serious problems in model performance arose from dissimilarities between the samples used to develop it and those actually produced by the refinery. This was usually the result of the typical differences between refinery-feed crudes. Thus, application of the proposed method to daily output was found to call for increased universality, even at the expense of decreased 'predictive goodness' (*i.e.*, increased SEPs). As a rule, this can be accomplished by increasing both the number and the variety of samples included in the calibration group. This was frequently used in our work. Recalibration and new prediction sets were obtained increasing the number of samples included in several data sets, although FCC gasolines did not show great variability.

Acceptance of the new methodology by the laboratory staff was mixed. Among other things, this will be to the benefit of their own health, although we know by experience that industrial workers are reluctant to use extraneous-protection systems.[21]

The authors wish to express their gratitude to Dr. D. J. Veltkamp, of the Center for Process Analytical Chemistry (Seattle, WA) for kind access to his statistical package, and the Spanish government for partial funding of this work.

References

1 Massart, D. L., Vadeginste, B. G. M., Deming, S. N., Michotte, Y., and Kaufman, L., in *Chemometrics: a Textbook*, Elsevier, London, 1988, p. 6.
2 Taylor, J. K., in *Quality Assurance of Chemical Measurements*, Lewis Publishers, Michigan, 1987, pp. 49, 231.
3 Kingston, H. G., *Anal. Chem.*, 1989, **61**, 1381A.
4 Cassaret, L. J., Doull, J., in *Toxicology*, 3rd edn., MacMillan, New York, 1980, p. 3.
5 San Martin, S., in *Salud Pública y Medicina Preventive*, Masson, Barcelona, 1989, p. 68.
6 Garfield, F. M., in *Quality Assurance Principles for Analytical Laboratories*, AOAC, 1991, p. 113.
7 American Society for Testing and Materials, *Annual Book of ASTM Standards Vol. 05.04*, ASTM, Philadelphia, 1993, p. 6.
8 American Society for Testing and Materials, *Annual Book of ASTM Standards Vol. 05.04*, ASTM, Philadelphia, 1993, p. 20.
9 American Society for Testing and Materials, *Annual Book of ASTM Standards Vol. 05.03*, ASTM, Philadelphia, 1993, p. 722.
10 *Infrared Data Manager. User's Manual*, Perkin-Elmer, USA 1990.
11 Veltkamp, J. V., and Kowalski, B. R., *PLS-2 Block Modelling*, Center for Process Analytical Chemistry, University of Washington, Seattle, 1988, personal communication.
12 Kelly, J. J., Barlow, C. H., Jinguji, T. M., and Callis, J. B., *Anal. Chem.*, 1989, **61**, 313.
13 Kelly, J. J., and Callis, J. B., *Anal. Chem.*, 1990, **62**, 1444.
14 Parisi, A. F., Nogueiras, L., and Prieto, H., *Anal. Chim. Acta.*, 1990, **238**, 95.
15 Descales, B., and Lambert, D., *Pètrole et Techniques*, 1989, **349**, 2.
16 Ichikawa, M., Nonaka, K., Takada, I., and Ishimori, S., *Appl. Spectrosc.*, 1992, **46**, 966.
17 Wang, Y., Veltkamp, D. J., and Kowalski, B. R., *Anal. Chem.*, 1991, **63**, 2750.
18 Wang, Y., and Kowalski, B. R., *Anal. Chem.*, 1993, **65**, 1174.
19 Callis, J. B., Illman, L. D., and Kowalski, B. R., *Anal. Chem.*, 1987, **59**, 624A.
20 Shaw, R. C., and Kratochvil, B., *Anal. Chem.*, 1990, **62**, 167.
21 Bird, F. E., and Germain, G. L., in *Practical Loss Control Leadership*, Institute Publishing, Longaville, USA, 1986, p. 98.

Paper 4/01912A
Received March 30, 1994
Accepted September 19, 1994

Spectrophotometric Determination of Copper(II), Nickel(II), and Cobalt(II) as Complexes with Sodium Diethyldithiocarbamate in the Anionic Micellar Media of Dodecylsulfate Salts*

M. P. San Andres, M. L. Marina and S. Vera†

Departamento de Química Analítica, Facultad de Ciencias, Universidad de Alcalá de Henares, 28871 Alcalá de Henares (Madrid), Spain

Copper(II), Ni^{II} and Co^{II} were determined spectrophotometrically as their complexes with diethyldithiocarbamate (DDTC) in the presence of aqueous anionic micellar media of sodium and ammonium dodecylsulfate. The presence of micellar systems allows one to eliminate the previous solvent extraction step that is necessary for the determination of metal–DDTC complexes in the absence of micelles. This reduces the cost and toxicity of the method. The influence of anionic micelles on the analytical characteristics (sensitivity and detection limits) was studied. The proposed method was applied to the determination of Cu^{II} in industrial waste water and in nickel covered metallic samples, and the results were compared with those obtained by flame atomic absorption spectrometry.

Keywords: Micelles; spectrophotometry; metal ions; diethyldithiocarbamate

Introduction

One of the main uses of surfactants in analytical chemistry is in the determination of metal ions as their complexes by spectrophotometry and fluorimetry.[1–7] In such metal complex solutions, the addition of a surfactant may cause a decrease in the pH at which the complex is formed, red-shifts in the absorption bands, and/or increases in the molar absorptivity or fluorescence intensity.

Surfactants contain different hydrophobic and hydrophilic regions, and, depending on their chemical structure and the nature of the medium, can give rise to different organized structures, namely normal and reversed micelles, microemulsions, monolayers, bilayers, and vesicles.

Normal micelles are formed when, in aqueous solution the surfactant reaches a certain concentration [the critical micellization concentration (c.m.c.)] and aggregates spontaneously. These systems and other organized structures have been shown to exhibit some interesting properties.[8–12] For example, they can solubilize, concentrate, and compartmentalize ions and molecules, modify acid–base and redox equilibra, and influence reaction rates, chemical pathways, and stereochemistry. In addition, micellar systems are convenient to use because they are optically transparent, stable, and relatively non-toxic.

These advantages illustrate the relevance of surfactant systems in the development of new spectrophotometric and fluorimetric methods for the determination of micro amounts of metal ions, anions, biological compounds, drugs, and pesticides.

Very sensitive methods for metal-ion determination have been developed by using chelating organic reagents (*e.g.*, triphenylmethane, xanthene, and phenoxazone) and cationic or non-ionic surfactants.[13–16] Comparison of the spectral properties of the complexes in the absence and presence of cationic surfactants typically reveals a one- to 10-fold increase in the molar absorptivity (sensitivity), and bathochromic shifts in the wavelength of maximum absorbance in the range 20–100 nm.[17–21]

Although the majority of research in this area concerns cationic surfactants, anionic micelles have also been shown to provide similar analytical benefits.[22–24] Routine use of anionic micelles in the determination of metal ions may be limited due to the occurrence of direct surfactant–metal ion interactions, which can inhibit metal–dye complex formation.

On the other hand, the ability of micelles to solubilize complexes in aqueous solutions can eliminate the need for non-aqueous extraction steps in a given analysis.[4,6,25]

Diethyldithiocarbamate (DDTC) has been used as a chelating agent in the determination of metal ions by ultraviolet–visible spectrophotometry. However, DDTC metal complexes are water insoluble and therefore a solvent-extraction step is necessary. Generally, carbon tetrachloride has been employed as organic solvent, although chloroform has also been used.[26] These solvents can be classified as toxic and as environmental pollutants,[27] and have been listed as carcinogens by the Environmental Protection Agency (EPA).[28]

This paper describes the spectrophotometric determinations of Cu^{II}, Co^{II}, and Ni^{II} as their DDTC complexes in micellar aqueous solutions of sodium and ammonium dodecylsulfate. This method does not require a solvent-extraction step, hence the use of carbon tetrachloride or chloroform is avoided. In place of these organic solvents, less toxic agents[27] in the form of dodecylsulfate salts were used.

Experimental

Reagents

All reagents used were of analytical-reagent grade (Merck). Stock solutions of Ni^{II}, Co^{II}, and Cu^{II} were prepared from nitrate salts. The sodium diethyldithiocarbamate solutions were freshly prepared in distilled water just before use to avoid acid decomposition. The surfactant ammonium dodecylsulfate (ADS) was synthesized from sodium dodecylsulfate (SDS) using an ion-exchange method with the cationic resin Dowex 50 (20–50 mesh).

Apparatus

A Hewlett-Packard Model HP8452A diode-array spectrophotometer equipped with 1 cm silica cells was used to record the

* Submitted as a paper on Clean Analytical Methods.
† To whom correspondence should be addressed.

absorption spectra used to measure absorbance data at selected wavlengths for calibration and to determine the c.m.c. of ADS.

Flame atomic absorption spectrometry (FAAS) was conducted using a Perkin-Elmer instrument (Model 2380).

A Metrohm pH meter and combined electrode were used to measure the pH of solutions. Some c.m.c.s were determined using a Crison Model 522 conductimeter.

Ultraviolet–visible (UV/VIS) Spectrophotometric and conductimetric measurements were carried out at 25 ± 1 °C in a Braun thermostatic bath (Model Thermomix BU).

Synthesis of Ammonium Dodecylsulfate

The ion-exchange resin was placed in a column. Prior to its use, several ion-exchange cycles were conducted (H^+/Na^+) to generate the H^+ form of the resin. A 1 mol l^{-1} NH_4Cl solution was passed through the column to generate the ammonium form of the resin, and then a 0.25 mol l^{-1} SDS solution was passed slowly through the resin where an ion exchange between the sodium of the SDS and ammonium of the resin occurred. The effluent was collected in a flask. The actual concentration of ADS was determined by titration as follows: a few drops of a formaldehyde solution (20%) were added to 5 ml of ADS; the H^+ generated in the subsequent reaction was titrated with standardized NaOH; the addition of formaldehyde and the titration were repeated until the reaction appeared to be complete; an additional 2 ml of standardized NaOH were added, and the solution was left in the dark for 15 min; and the excess of NaOH was titrated with HCl which had previously been titrated with sodium carbonate. The concentration of ADS was found to be 0.24 mol l^{-1}. The ADS solution was stored in a refrigerator. A second portion of the remaining effluent was precipitated in a freezer and filtered at low temperature to eliminate the solvent. The solid ADS was then dried and kept in a receptacle. The c.m.c. of ADS was determined by both UV spectrophotometric and conductimetric methods.

Procedure

Determination of surfactant c.m.c.

The c.m.c. value for ADS was determined by spectrophotometry as follows. The absorbance of a Calcon (Merck)–ADS mixture at 219.1 nm was measured at different concentrations of ADS. A change in slope occurred at a point near to the c.m.c. In the absence of Calcon, the absorbance of ADS at 219.1 nm also presents a change in the slope near to the c.m.c. In both cases, the c.m.c. was taken as the intersection of the two straight lines.

The c.m.c. of ADS was determined using conductivity measurements and compared with the value obtained by spectrophotometry, for both the titrated solution and the solid ADS. The cmc of SDS was also determined by this method. The surfactant concentrations ranged from 10^{-3} to 2.5×10^{-2} mol l^{-1} for SDS and from 1.1×10^{-4} to 2.2×10^{-2} mol l^{-1} for ADS. The occurrence of a sharp inflection point in the plots of specific conductivity *versus* surfactant concentration indicated the c.m.c.

Determination of surfactant c.m.c. in the presence of DDTC

The c.m.c. values in the presence of different concentrations (5×10^{-5}–5×10^{-4} mol l^{-1}) of DDTC were obtained from conductivity measurements. The surfactant concentration was determined over the same concentration range as in the absence of DDTC, and the c.m.c. was obtained from the sharp inflection point occurring in the plots of specific conductivity *versus* surfactant concentration.

Spectrophotometric determination of metal ion in micellar solutions

Appropriate volumes of stock solutions of metal ion, DDTC, and the selected surfactant were added to a series of 25 ml calibrated flasks, and made up to volume with distilled water. The following concentration ranges of metal ion were used: Ni^{II}, 2×10^{-6}–3×10^{-5} mol l^{-1}; Co^{II}, 5×10^{-6}–5×10^{-5} mol l^{-1}; and Cu^{II}, 1×10^{-5}–8×10^{-5} mol l^{-1}. The concentration of DDTC used was 2×10^{-4} mol l^{-1} for the nickel and cobalt complexes, and 4×10^{-4} mol l^{-1} for the copper complex. The surfactant concentrations, pH values, and analytical wavelengths used are listed in Table 1.

Spectrophotometric determination of metal ion after extraction with CCl_4

Appropriate volumes of stock aqueous solutions of metal ion and DDTC were placed in an extractive funnel and 10 ml of CCl_4 were added. The organic layer was transferred into a 25 ml calibrated flask. In order to obtain complete extraction, the process was repeated twice, the first time with 10 ml of CCl_4 and the second time with 5 ml. For a total volume of the organic layer of 25 ml, absorbances were measured at the appropriate wavelength for each metal ion (Table 1).

Sensitivity and detection limits

The sensitivity of the spectrophotometric method was determined from the slope of the analytical calibration curve and is expressed as the molar absorptivity. The detection limit was

Table 1 Experimental conditions for metal ion determination with DDTC in anionic micellar medium and in carbon tetrachloride

	Surfactant				
Surfactant	SDS (0.020 mol l^{-1})	SDS (0.100 mol l^{-1})	ADS (0.020 mol l^{-1})	ADS (0.100 mol l^{-1})	CCl_4
Co^{II}—					
Wavelength/nm	322	322	322	322	322
pH	9.7	9.0	6.5	6.3	8.0
Ni^{II}—					
Wavelength/nm	318	326	324	324	328
pH	8.3	7.5	7.1	6.6	6.7
Cu^{II}—					
Wavelength/nm	446	440	448	434	436
pH	8.1	8.2	6.8	6.8	7.6

defined as the sample solution concentration giving a signal equal to the blank signal, y_B, plus three times the standard deviation of the blank, s_B; hence the probability of either of two types of error (type 1 type 2) occurring was only 5%. A value of $y_B + 10s_B$ was used to define the determination limit.[29]

A least-squares method was used to calculate the linear relationship between the analytical signal (absorbance) and the concentration. The regression curve thus calculated was used to estimate sensitivity, the detection limit, and the determination limit in accordance with the literature.[29]

Determination of Cu^{II} in real samples

The absorbance of a waste water sample obtained from an industrial effluent was measured following sample preparation as follows. Appropriate amounts of ADS and DDTC were added to a 25 ml calibrated flask to obtain final concentrations of 0.1 mol l^{-1} in ADS and 4 × 10^{-4} mol l^{-1} in DDTC. Then, 0.05 ml of the sample were added and the absorbance was measured. This absorbance reading was used to calculate the concentration of Cu^{II} in the diluted sample and hence in the real sample.

For the determination of Cu^{II} by FAAS, a 0.1 ml aliquot of the sample was diluted with distilled water.

For metallic samples covered with Ni, the solid, metallic matrix was dissolved with nitric acid and subsequently diluted with distilled water to 250 ml. This solution was again diluted to measure the metal ions, the dilution depending on the sample size (samples 1 and 2, 0.02–25 ml; and samples 3 and 4, 0.05–25 ml for the UV/VIS spectrophotometric method as well as for FAAS).

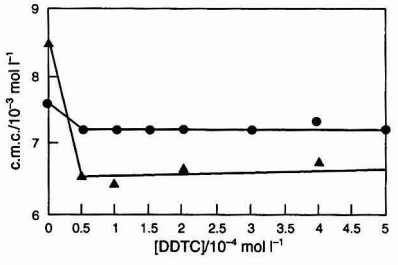

Fig. 1 Variation of critical micellization concentration (c.m.c.) of dodecylsulfate salts (▲, sodium and ●, ammonium) with DDTC concentration.

Results and Discussion

Surfactant c.m.c.

The c.m.c. of SDS was determined from conductivity measurements. In the case of ADS, the c.m.c. was determined by conductivity and spectrophotometry as described in Experimental.

For SDS, a c.m.c. of 8.5 × 10^{-3} mol l^{-1} was obtained in pure aqueous solution. For ADS, a c.m.c. of 7.6 × 10^{-3} mol l^{-1} was obtained regardless of the method employed. These values are in good agreement with literature values.[30]

Surfactant c.m.c. versus DDTC Concentration

The c.m.c.s of SDS and ADS were also determined conductimetrically in solutions containing the complexing ligand

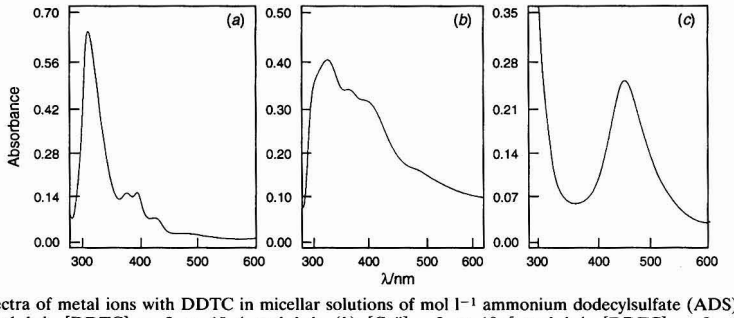

Fig. 2 Absorption spectra of metal ions with DDTC in micellar solutions of mol l^{-1} ammonium dodecylsulfate (ADS). Concentrations: (*a*) [Ni^{II}] = 2 × 10^{-5} mol l^{-1}, [DDTC] = 2 × 10^{-4} mol l^{-1}; (*b*) [Co^{II}] - 2 × 10^{-5} mol l^{-1}, [DDTC] = 2 × 10^{-4} mol l^{-1}; and (*c*) [Cu^{II}] = 2 × 10^{-5} mol l^{-1}, [DDTC = 4 × 10^{-4} mol l^{-1}.

Table 2 Detection limits (DLs), determination limits (DTLs), and molar absorptivities (ε) for the metal ion determinations with DDTC in anionic micellar medium and in carbon tetrachloride

Surfactant	SDS (0.020 mol l^{-1})	SDS (0.100 mol l^{-1})	ADS (0.020 mol l^{-1})	ADS (0.100 mol l^{-1})	CCl_4
Co^{II}—					
DL/μg l^{-1}	220.3 ± 30.2	73.8 ± 1.0	73.9 ± 4.3	49.3 ± 1.8	47.5 + 2.4
DTL/μg l^{-1}	724.1 ± 69.8	226.5 ± 32.3	246.3 ± 14.4	164.3 ± 6.1	159.3 ± 8.1
ε/10^{-3} m^2 mol^{-1}	22.4	22.1	22.5	22.2	23.3
Ni^{II}—					
DL/μg l^{-1}	101.0 ± 16.7	24.1 ± 7.1	25.1 ± 0.6	9.2 ± 1.1	24.3 ± 1.5
DTL/μg l^{-1}	336.7 ± 35.6	86.9 ± 28.7	83.6 ± 2.0	30.5 ± 3.5	81.0 ± 5.2
ε/10^{-3} m^2 mol^{-1}	27.4	30.3	26.3	32.3	32.1
Cu^{II}—					
DL/μg l^{-1}	130.9 ± 13.3	98.7 ± 28.5	77.6 ± 5.6	54.4 ± 1.7	117.3 ± 3.5
DTL/μg l^{-1}	436.2 ± 44.0	329.6 ± 96.2	258.4 ± 18.5	181.4 ± 5.7	423.9 ± 17.2
ε/10^{-3} m^2 mol^{-1}	12.7	13.7	12.0	12.5	14.9

DDTC. Fig. 1 shows the variations of the c.m.c.s of SDS and ADS as functions of the DDTC concentration in solution. Fig. 1 also indicates the c.m.c.s in pure aqueous solution. It is observed that for both surfactants, the presence of DTC causes a decrease in the c.m.c. value. However, the c.m.c. of SDS and of ADS remains constant in all DDTC-containing solutions regardless of the DDTC concentration. A c.m.c. value of 6.6×10^{-3} mol l^{-1} was obtained for SDS and of 7.2×10^{-3} mol l^{-1} for ADS. These results indicate that the presence of DDTC improves micelle formation for both anionic surfactants. However, for SDS, the improvement in micellization is greater than that for ADS. This is the opposite of the results obtained for pure aqueous solution in which micelle formation is favoured more for ADS than for SDS.

The reduced values of c.m.c. obtained for SDS and ADS in the presence of DDTC were also obtained for cationic surfactants,[25] and when certain alcohols and salts were added to the micellar solutions.[31,32]

Spectrophotometric Characteristics of Ni^{II}, Co^{II} and Cu^{II} Complexes with DDTC

To establish the experimental conditions for the determination of metal ions as DDTC complexes, absorption spectra were recorded for complexes of Cu^{II}, Ni^{II}, and Co^{II} with DDTC. Fig. 2 shows the results obtained in the presence of 0.2 mol l^{-1} ADS. Similar spectra were obtained for the three metal ion complexes in the presence of SDS. Fig. 2 shows that, due to the narrow absorption bands obtained for Ni^{II} (*a*) and Cu^{II} (*c*), the latter can be determined in the presence of Ni^{II} with no interference. However, the broad absorption band obtained for the Co^{II} complex makes it impossible to determine this element in the presence of Ni^{II} and/or Cu^{II}. Similarly, neither Ni^{II} nor Cu^{II} can be determined in the presence of Co^{II}. Table 1 lists the analytical wavelength and pH values of the different metal ligand–surfactant systems and metal ligand complexes after solvent extraction of CCl_4.

Comparison of the analytical wavelengths with the wavelengths after solvent extraction (see Table 1) reveals that the presence of anionic micellar systems produces a displacement of the maximum wavelength (λ_{max}) for Ni^{II}–DDTC in 0.02 mol l^{-1} SDS, Cu^{II}–DDTC in 0.2 mol l^{-1} SDS and 0.2 mol l^{-1} ADS. In contrast, the anionic micelles do not cause any displacement in λ_{max} for Co^{II}–DDTC. The interaction that occurs between metal–DDTC complexes and anionic micelles therefore depends on the nature of the metal ion.

It is of interest to note that for the same metal–DDTC complexes, the presence of cationic micelles (hexadecyltrimethylammonium bromide, chloride, and hydroxide) does not have an effect on λ_{max}.[25]

It was observed that the pH for the three metal–DDTC complexes in ADS micellar media was always lower than that in SDS micellar media. This behaviour is in accordance with the acidic character of NH_4^+ as a micellar counter ion.

Table 3 Detection limits (μg l^{-1}) obtained for the anionic surfactants in this work and those obtained for the cationic surfactants (CTAB, CTAC, and CTAOH) in previous work[25]

	Detection limit/μg l^{-1}		
Surfactant*	Co^{II}	Ni^{II}	Cu^{II}
SDS (0.020 mol l^{-1})	220.3 ± 30.2	101.0 ± 16.7	130.9 ± 13.3
SDS (0.100 mol l^{-1})	73.8 ± 1.0	24.1 ± 7.1	98.7 ± 28.5
ADS (0.020 mol l^{-1})	73.9 ± 4.3	25.1 ± 0.6	77.6 ± 5.6
ADS (0.100 mol l^{-1})	49.3 ± 1.8	9.2 ± 1.1	54.4 ± 1.7
CTAB (0.020 mol l^{-1})	37.7 ± 8.2	81.7 ± 7.9	71.9 ± 6.5
CTAB (0.100 mol l^{-1})	136.3 ± 5.9	22.5 ± 5.1	277.6 ± 82.1
CTAC (0.022 mol l^{-1})	53.5 ± 0.4	18.5 ± 0.6	63.1 ± 1.1
CTAC (0.110 mol l^{-1})	46.2 ± 1.4	15.9 ± 0.3	40.6 ± 2.1
CTAOH (0.015 mol l^{-1})	—†	—†	86.5 ± 2.5
CTAOH (0.060 mol l^{-1})	—†	—†	55.7 ± 2.1
CCl_4	47.5 ± 2.4	24.3 ± 1.5	117.3 ± 3.5

* CTAB = Hexadecyltrimethylammonium bromide (CTA bromide); CTAC = CTA chloride; and CTAOH = CTA hydroxide.

† No complex formation.

Spectrophotometric Determination of Ni^{II}, Cu^{II}, and Co^{II} as DDTC Complexes in the Presence of Anionic Micelles of SDS and ADS

The detection and determination limits and the sensitivity of the method (defined as in Experimental) were determined for each metal ion in each micellar system and in CCl_4. Six values were obtained for each parameter, the averages of which are listed in Table 2. The standard deviations of the detection and determination limits ($n = 6$) are also given in Table 2.

From the results given in Table 2, it is possible to deduce that the sensitivity of the spectrophotometric method in the presence of SDS and ADS micelles (expressed as molar absorptivity for each of metal ion) is very similar regardless of the nature of the micelle counterion (Na^+, NH_4^+), and the surfactant concentration. According to the molar absorptivities, the sensitivity of the method is highest for Ni^{II}: $Ni^{II} > Co^{II} > Cu^{II}$. The sensitivity of the method in the presence of anionic micelles is similar to that of the metal ion determination with DDTC after extraction with carbon tetrachloride (Table 2).

The detection limits shown in Table 2 indicate that the determination of Ni^{II}, Co^{II}, and Cu^{II} as their DDTC complexes in anionic micellar medium is possible down to μg l^{-1} levels. The detection limit for Ni^{II} is always lower than that for Co^{II} or Cu^{II}. The lowest detection limit was obtained for Ni^{II} in 0.1 mol l^{-1} ADS (9.2 μg l^{-1}) and the highest for Co^{II} in 0.02 mol l^{-1} SDS (220.3 μg l^{-1}).

But, to what extent does the nature of the surfactant counterion and the concentration influence the detection limit? It does not appear that the micellar counter ion is a

Table 4 Results obtained for the determination of copper in four metalic samples by FAAS and by spectrophotometry in a micellar medium of ADS (0.1 mol l^{-1})

	Cu^{II}/mg		Ni^{II}/mg		
Sample	FAAS	ADS spectrophotometric method	FAAS	Sample mass/g*	Cu^{II} (%)
1	804.2 ± 9.4	782.3 ± 1.6	10.3 ± 0.2	$1.5253 \pm 4.0 \times 10^{-3}$	51.3
2	831.4 ± 7.8	836.6 ± 0.9	11.9 ± 0.2	$1.5253 \pm 4.0 \times 10^{-3}$	54.8
3	419.4 ± 2.9	417.2 ± 0.6	6.6 ± 0.1	$0.7054 \pm 1.9 \times 10^{-3}$	59.1
4	400.4 ± 5.8	409.3 ± 2.9	6.1 ± 0.1	$0.7054 \pm 1.9 \times 10^{-3}$	58.0

* The mean mass of eight samples for samples 1 and 2, and the mean mass of 11 samples for samples 3 and 4.

determining factor, although in the presence of ADS (NH_4^+ counter ion), the detection limits are generally lower than those in SDS (Na^+ counterion). Further, the detection limits were observed to decrease, regardless of the surfactant counter ion, as the surfactant concentration increased.

Table 3 lists the detection limits obtained for Co^{II}, Ni^{II}, and Cu^{II} in the anionic micellar media studied in this work and those obtained for the same metal ions in cationic micellar solutions of hexadecyltrimethylammonium bromide, chloride, and hydroxide (CTAB, CTAC, CTAOH) in previous work.[25] Clearly, the best results were obtained for cationic micelles of CTAC 0.11 mol l^{-1} and anionic micelles of ADS 0.10 mol l^{-1}.

It is interesting to report that detection limits obtained with high concentrations of ADS micelles are the same (determination of Co^{II}–DDTC) or even better (determination of Ni^{II}– and Cu^{II}–DDTC complexes) than those obtained following solvent extraction with CCl_4. Furthermore, the ADS method avoids the previous extraction step and eliminates the use of dangerous organic solvents.

Determination of Cu^{II} in Waste Water

The proposed spectrophotometric method was applied to the determination of Cu^{II} in industrial waste water. As the lowest detection limit for this metal was obtained in 0.1 mol l^{-1} ADS, this surfactant was used in the determination. The result of the determination of Cu^{II} in the diluted sample (see Experimental) using the proposed method was compared with the result obtained by FAAS: (four measurements; mean ± standard deviation) proposed method, 924.3 ± 0.5 μg ml^{-1} Cu^{II}; and FAAS method, 945.3 ± 10.9 μg ml^{-1} Cu^{II}. Agreement between the two methods was good.

The determination of Cu^{II} in one industrial waste water sample (in quadruplicate) required 90 ml of a 0.25 mol l^{-1} ADS solution, whereas the same determination using solvent extraction with CCl_4 required about 225 ml of the organic solvent.

Determination of Cu^{II} in Metallic Samples

The proposed method was also applied to the determination of Cu^{II} in Cu^{II} alloys covered with nickel to prevent oxidation and to allow their use as electronic connectors. Copper(II) was determined in four such samples using the proposed method, and Cu^{II} and Ni^{II} were also determined by FAAS. Table 4 shows that the results obtained for Cu^{II} by the two methods agree well, and that Cu^{II} can be determined without interference from Ni^{II}.

The determination of Cu^{II} in the four metallic samples (in quadruplicate) required 200 ml of a 0.25 mol l^{-1} ADS solution, whereas 525 ml of CCl_4 was necesssary for the solvent extraction determination.

Conclusions

These results for anionic micellar systems and those obtained previously with cationic micellar systems[25] show that Cu^{II}, Co^{II}, and Ni^{II} can be determined as their DTC complexes in aqueous solution. No extraction step is required and hence the use of organic solvents, which are generally toxic pollutants, is avoided.

The authors are grateful to the University of Alcalá de Henares (Spain) (ref. 91 B/14 and 92/27) for providing financial support for this study.

References

1 Hinze, W. L., in *Solution Chemistry of Surfactants*, ed. Mittal, K. L., Plenum Press, New York, 1979, p. 79.
2 Cline-Love, L. J., Habarta, J. G., and Dorsey, J. G., *Anal. Chem.*, 1984, **56**, 1132A.
3 Hinze, W. L., Singh, H. N., Baba, Y., and Harvey, N. G., *Trends Anal. Chem.*, 1984, **3**, 193.
4 Pelizzetti, E., and Pramauro, E., *Anal. Chim. Acta*, 1985, **161**, 1.
5 Diaz-García, M. E., and Sanz-Medel, A., *Talanta*, 1986, **33**, 255.
6 McIntire, G. L., *CRC Crit. Rev. Anal. Chem.*, 1990, **21**, 257.
7 Fernández, F., Marina, M. L., and Rodríguez, A. R., in *Vibrational Spectra and Structure*, ed. Durig, J. R., Elsevier, Amsterdam, 1991, p. 113.
8 Fendler, J. H., and Fendler, E. J., *Catalysis in Micellar and Macromolecular Systems*, Academic Press, New York, 1975.
9 *Micellization, Solubilization and Microemulsions*, ed. Mittal, K. L., Plenum Press, New York, 1977.
10 *Solution Behaviour of Surfactants; Theoretical and Applied Aspects*, eds. Mittal, K. L., and Fendler, E. J., Plenum Press, New York, 1982.
11 *Surfactants in Solution*, eds. Mittal, K. L., and Lindman, B., Plenum Press, New York, 1984.
12 *Surfactants in Solution*, ed. Mittal, K. L., Plenum Press, New York, 1990.
13 Svoboda, V., and Chromy, V., *Talanta*, 1965, **12**, 431.
14 Sauvin, B., *Crit. Rev. Anal. Chem.*, 1979, **8**, 55.
15 Marczenko, Z., *Crit. Rev. Anal. Chem.*, 1981, **11**, 195.
16 Cermakova, L., in *Surfactants in Solution*, eds. Mittal, K. L., and Lindman, B., Plenum Press, New York, 1984, vol. 2, p. 1217.
17 Sanz-Medel, A., Camara, C., and Perez, J. A., *Anal. Chem.*, 1980, **52**, 1035.
18 Marczenko, Z., and Kalowska, H., *Anal. Chim. Acta*, 1981, **123**, 279.
19 Callahan, H., and Kook, K. D., *Anal. Chem.*, 1982, **54**, 174.
20 Jarosz, M., and Marczenko, Z., *Anal. Chim. Acta*, 1984, **159**, 309.
21 Mori, I., Fujita, K., Usami, A., Kawabe, H., Koshiyama, Y., and Tanaka, T., *Bull. Chem. Soc. Jpn.*, 1986, **59**, 1623.
22 Zhang, C. P., Qi, D. Y., and Zhou, T. Z., *Talanta*, 1982, **28**, 1119.
23 Callahan, H., and Kook, K. D., *Anal. Chem.*, 1984, **56**, 1632.
24 León, M. E., Santos, M. J., and Polo, L. M., *Anal. Chim. Acta*, 1985, **178**, 331.
25 San Andrés, M. P., Marina, M. L., and Vera, S., *Talanta*, 1994, **41**, 179.
26 *CRC Handbook of Organic Analytical Reagents*, CRC Press, Boca Raton, FL, 1982, p. 389.
27 Merck and Co. Inc., Rahway, New York, *The Merck Index*, 10th edn., 1983.
28 *Second Annual Report on Carcinogens*, Environmental Protection Agency, NTP 81-43, Dec. 1981, pp. 73–75 and 78–80.
29 Miller, J. C., and Miller, J. N., in *Statistics for Analytical Chemistry*, Ellis Horwood, Chichester, 2nd edn., 1988, chap. 5.
30 Mukerjee, P., and Mysels, K. J., in *Critical Micelle Concentrations of Aqueous Surfactant Systems*. United States Department of Commerce, National Bureau of Standards, Washington, DC, 1971.
31 Zana, R., Yiv, S., Strazielle, C., and Lianos, P., *J. Colloid Interface Sci.*, 1981, **80**, 208.
32 Abu-Handiyah, M., *J. Phys. Chem.*, 1986, **90**, 1345.

Paper 4/00253I
Received January 17, 1994
Accepted April 18, 1994

Quality Concepts and Practices Applied to Sampling—An Exploratory Study

Michael Thompson

Department of Chemistry, Birkbeck College, Gordon House, 29 Gordon Square, London, UK WC1H 0PP

Michael H. Ramsey

Department of Geology, Imperial College, London, UK SW7 2BP

There is now a self-consistent and almost complete body of concepts and practices relating to the quality of analytical data. The need for quality in sampling is also well recognized but there has been no comparable development of an over-all approach or, in some aspects, even of a basic methodology. This paper discusses the prospects for a complete approach to quality in sampling. It shows that virtually all of the concepts and practices used in analysis can be adapted, with only a slight change of detail, for application to sampling. Topics considered include the sampling analogues of trueness, bias, accuracy error, precision, uncertainty, traceability, fitness for purpose, reference materials, collaborative trials, proficiency tests and internal quality control.

Keywords: *Sampling quality; sampling trueness; sampling precision; reference sampling targets; fitness-for-purpose*

Introduction

The quality of data produced by chemical analysis has long been regarded as an important topic. Over the years, methods of ensuring and assessing data quality have evolved piecemeal in several sectors of the analytical community. Because of this, until recently no comprehensive theory of data quality was available to provide a logical basis for these practices. Over the last two decades, however, there has been an accelerating and concerted effort by specialists worldwide to codify the various concepts, techniques and procedures into a self-consistent whole. This process is now almost complete, and the resulting body of knowledge can be justifiably regarded as the basic theory of analytical chemistry. Analytical chemists generally are becoming aware of the importance of this work.

The importance of effective sampling is also well recognized. A large amount of information on best sampling practice is available in many fields of application.[1–7] However, except in a few sectors of analytical chemistry, there is no organized body of concepts and practices relating to the establishment and maintenance of fitness for purpose in sampling. Documentation in relation to the assessment of quality in sampling is sparse and incomplete, despite a general interest in the subject. This is a serious shortcoming, because it is literally true that the quality of a result can be no better than that of the sample analysed. Moreover, it is often suspected (and occasionally demonstrated) that the quality of sampling is poorer than that of the subsequent analysis, so that efforts directed to analytical excellence may be to an extent wasted.

Clearly, there is a case for establishing a complete conceptual framework and methodology for quality in sampling. In this paper we attempt to approach that goal by investigating the applicability to sampling of the concepts and practices established for quality in analytical measurement. Topics covered are trueness, bias, accuracy, error, precision, fitness for purpose, uncertainty, traceability, reference sampling targets, collaborative sampling trials, proficiency testing of sampling and internal quality control. Critical features of each topic are first discussed in relation to analysis, and then appraised for applicability to sampling.

Sampling Protocols, Replication and Independence

There is no intention in this paper of providing instructions for sampling or discussing empirical methods of achieving fitness for purpose in sampling. Sampling targets are diverse, and a considerable amount of expertise on sampling *per se* is already documented. Nevertheless, it is necessary for the present purposes to dwell on some general principles and the terminology of sampling before proceeding with a consideration of quality. It is also important that the concepts of randomness and independence are emphasized, because statistical inference is based on such assumptions.

An essential starting point in the following is that the sampler follows a prescribed *sampling protocol* and does not vary the procedure from one occasion to another. If we are trying to study or characterize a procedure, it can only be a fixed procedure. However, sufficient flexibility must be built into the protocol to allow for the contingencies that may arise during sampling. The total amount of material from which the sample is to be abstracted is here called the *sampling target*, which may be, for instance, a *lot* or *consignment* of a raw material or manufactured product, material flowing through a pipe or along a conveyor during a certain period or a certain *area* or *site* in environmental or geological studies.

Sampling is normally executed by the extraction of a number of *increments*, which are segments from the sampling target selected on a basis defined in the protocol. The increments are then combined to form the *aggregate sample*, which may then be treated in some way (such as comminution and splitting) to produce the *laboratory sample*, the material that is to be analysed. The laboratory sample may be further divided and comminuted before analysis. The portion of the laboratory sample that is subjected to the analytical procedure is the *test portion*.

A number of different styles of sampling are recognized. *Random sampling* is the most effective. If we imagine that the target is made up of a large number of equally sized discrete increments, a random sample results if each increment has an equal chance of being selected. Random sampling will, if excecuted correctly on a well defined target, on average produce a representative (unbiased) sample. *Systematic sampling* is excecuted by taking increments on a regular basis in space or time. For instance, a material moving steadily on a conveyer belt or in a pipe line may be sampled systematically by removing equal increments at fixed time intervals. *Stratified sampling* is executed when the target is segregated in some way, either in reality (as when a bulk

material is distributed in a number of railway wagons) or schematically (as when a field is subdivided into a number of contiguous areas). Sampling is then executed separately in each stratum, either randomly or systematically. A *convenience sample* is taken with no regard to representativeness. Strictly, no statistical inference can be based on a convenience sample.

At several points in the ensuing discussion, the collection of replicate samples from a single target is postulated. Statistical inference requires that such replicates should be random and independent. Therefore, special consideration has to be given to how this can be achieved (or at least approximated to) in practice, because existing sampling protocols usually omit any reference to such requirements. No specific instructions can be given here, because of the wide diversity of sampling targets. However, some general principles can be established, and examples given to illustrate their application to particular circumstances. A simple approach for static samples is to suppose that the sampling protocol (*i.e.*, the method of selecting the increments) must start at a particular physical position in the target. Increments are then collected at successive positions in the target located relative to the previous position according to the protocol. Duplicate aggregate samples could be collected by starting the protocol twice, at two different points selected at random. For flowing targets the principle would be the same: increments, however, would be selected on a temporal rather than a spatial basis. These requirements are best illustrated by examples.

Example 1

Suppose that a protocol for sampling the topsoil in a rectangular field required the sampler to walk the field in a 'W' (Fig. 1), and to collect increments at the vertices of the W and at four points roughly evenly spaced along each leg. To procure independent duplicate samples, the sampling procedure could first be initiated at a corner of the field selected at random in a direction selected at random. For a second sample the procedure is started at one of the remaining three corners selected at random.

If the increments were being collected in a stratified scheme (Fig. 2), the duplicates could be collected at random within each stratum. If the increments were to be collected systematically, say on the intersections of a rectangular grid, the duplicated grids could be rotated and offset in a random fashion (Fig. 3).

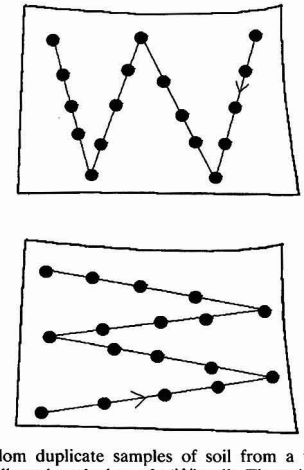

Fig. 1 Random duplicate samples of soil from a field, with the increments collected on the legs of a 'W' walk. The point of origin and the orientation of each walk is selected at random.

Example 2

Suppose that a protocol for sampling a large pile of raw material required the use of coning and quartering. The pile is initially mixed by transferring it to another position by shovelling. A cone is formed by adding material symmetrically over the apex of the new heap. The top of the completed cone is flattened and quartered by a metal cross positioned centrally but with a random orientation. Opposite quarters are taken as the sample and the other two quarters are rejected. This procedure can be repeated a number of times to reduce further the size of the sample. For a second sample the procedure would be to rebuild the cone of the rejected material in a fresh position. The cross could be inserted in a different orientation and the other pair of diagonally opposite segments taken for the sample at each repetition.

Fundamental Concepts

Trueness and Bias

Trueness in an analytical measurement is defined as the closeness of agreement between the average value obtained from a large series of test results and an accepted reference value.[8] Bias, a related concept, is the difference between the expectation of the test results and an accepted reference value.[8] Although a true value is, in most instances, unknowable, it is perfectly clear that a true value must exist. For

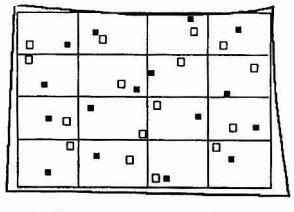

Fig. 2 Random duplicate samples of soil from a field, with the duplicate increments collected from random positions within each stratum.

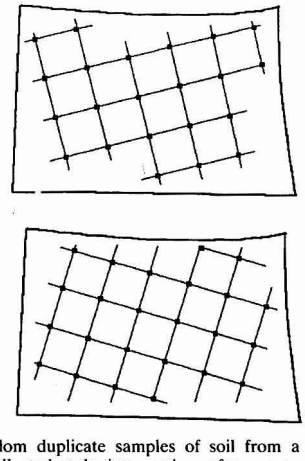

Fig. 3 Random duplicate samples of soil from a field with the increments collected at the intersections of a square grid. The origin and orientation of each grid are selected at random.

example, the copper concentration in a certain amount of material is the combined mass of all of the copper atoms in the material divided by the total mass of the material. This is an example of what could be called a 'conceptual analyte': a method used to determine its concentration could be called a 'conceptual method'. We have a clear physical picture of the analyte, and can envisage analytical methods that will estimate the required mass. Such measurements would be traceable to pure copper.

Despite the unknowable nature of the true value, it is the goal of chemical measurement. The certified value assigned to an analyte in a reference material is, as far as we can achieve, the best estimate of the true value and it is used as such. Analytical chemists believe in the reality of true values.

There is a class of analytes, however, that are not chemically well defined in the way that copper is. 'Fat', for example, comprises a mixture of triglycerides, other fatty esters, fatty acids, sterols, hydrocarbons, *etc.*, in variable proportions. In practical terms it is usual to define as fat everything that is measured by a standard method of analysis, for instance solvent extraction of the test material followed by weighing the extract. Strictly, the consensus of a large number of laboratories making the measurement according to a recognized protocol (the set of specifications and procedures that define the analytical method) is the true value for such 'empirical methods'. Measurements are traceable only to the analytical method in such an instance.

The concepts of trueness, true value and bias can be applied directly to sampling. There is necessarily a true value for a sampling target: it is the mass of analyte in the target divided by the mass of the target. A sample will have a different true value from that of the target, except in the rare case where the target is homogeneous. If the mean true value of a large number of samples (of equal mass) differed from the true value of the target, then we could say that the sampling method was biased. In practice, probably most sampling protocols are empirical rather than conceptual, and in such instances the consensus of a large number of samples is necessarily the true value.

For example, suppose that the sampling target is the soil in a field. A conceptual sampling protocol might refer to the collection of increments from the A-horizon of the soil. This sampling target has a clearly defined true value (assuming that the horizon is sufficiently well developed), which will be realized to a greater or lesser extent [the sampler(s) might misinterpret the description of the boundaries of the A-horizon and thus on average provide a biased sample] by the consensus of a large number of samples. In contrast, an empirical sampling protocol might specify the collection of increments from the topmost 10 cm of soil. The consensus of a large number of such samples is necessarily the true value.

Of course, sampling differs from analysis in that measurements are obtained only through the mediation of the subsequent analysis. In the above discussion we considered the true value of targets and samples, without regard for the additional error introduced by analysis. There is no conceptual problem in such a procedure, and subsequent discussion will show that there is no practical problem either.

One of the few published discussions of sampling bias is that of Gy,[9] who considered process materials. Gy maintains that sampling bias is an invalid concept, apparently on the grounds that all sampling protocols should be regarded as empirical. At the moment it seems appropriate to reserve judgement on this point.

Accuracy and Error

Accuracy is the closeness of agreement between the result of a measurement and the true value of the measurand.[10] Error is the result of a measurement minus a true value of the measurand.[10] (In both of these definitions the result may be the mean of several separate measurements if the measurement protocol so demands. Accuracy and error differ essentially from trueness and bias in that the former concepts refer to a single measurement and thus include both random and systematic elements, whereas the latter refer to the mean or expectation of a large series of results which in principle removes the random element.) Again, we find that both of these concepts are directly transferable to sampling practice. Sampling error would be the difference between the true value of a sample and the true value of a target, and would include systematic and random elements. Accuracy is the term denoting the degree of lack of error in a sample.

Precision

Precision in analysis is the closeness of agreement between independent test results obtained under prescribed conditions.[11] Usually it is quantified in terms of standard deviation or some derivative of it. In sampling one can imagine a number of samples having been collected from a single target by the use of a particular protocol. Each sample has a true value of the concentration of an analyte. The sampling precision is quantified by the standard deviation of these true values. The value of the sampling precision could be estimated practically from the results of a randomized replicated experiment, despite the presence of concomitant analytical variation, by an analysis of variance (ANOVA) procedure. Sampling precision could be measured under a variety of conditions of replication; these conditions are discussed in the section on collaborative trials.

Fitness for Purpose

Fitness for purpose (FFP) is defined here as the property of data produced by a measurement process that enables a user of the data to make technically correct decisions for a stated purpose. FFP is recognized as the fundamental operational criterion in data quality. Broadly the concept refers to the ability of test measurements to support interpretations based on them without a significant probability of compromising the correctness of the decision. Fitness of purpose is clearly equally applicable to analysis and sampling.

The FFP concept has not yet given rise in general to quantitative guidelines or criteria that could be related to uncertainty or quality assurance practices, although in certain sectors empirical rules have evolved. For instance, in clinical biochemistry, 'Tonks' law'[12] suggests that the allowable limits of error for an analyte should be one quarter of the normal range expressed as percentage of the mean of the normal range.

In at least one application field, namely applied geochemistry, FFP has been addressed quantitatively,[13–17] although not by that name. Broad principles have been laid down that allow the estimation of 'ideal' values of sampling precision and analytical precision for specific tasks, such as identifying suspect data and anomalous sites for further investigation. Similar principles could be applied to other application areas.

As an example, we consider the precision requirements for the identification of an anomalous site. An anomalous site in the context of mineral exploration might indicate the presence of a mineral vein or, in environmental surveys, an area of pollution. Success in identifying such sites depends on the use of economically viable methods for sampling and analysis, as large numbers of samples are collected and analysed. An anomaly can be defined only in relation to the variation among normal or 'background' sites. A frequently used definition[18] is

that an anomaly is a measured value that falls above $\mu_{bgd} + 3\sigma_{bgd}$ (for positive anomalies), where μ_{bgd} and σ_{bgd} are the parameters of the background variation. The minimum size of anomaly that can be detected therefore depends on the value of σ_{bgd}.

We find that, if the sources of variation are independent,

$$\sigma^2_{bgd} = \sigma^2_{site} + (\sigma^2_{sam} + \sigma^2_{an}/n)/m$$
$$= \sigma^2_{site} + \sigma^2_{tech}$$

where σ^2_{site} is the variance of the true values of the sites, σ^2_{sam} is the sampling variance, σ^2_{an} is the variance of the analytical method, σ^2_{tech} is the total variance introduced by the measurement technology, n is the number of replicate analyses per sample and m is the number of replicate samples per site.

As σ_{site} is fixed for a given population, the value of σ_{bgd} can be reduced only by the reduction of σ_{tech}. This could be achieved either by amendments to the sampling and/or analytical protocols, or by manipulating the values of m and n. However, there is no practical advantage in reducing the value of σ_{tech} below about $0.3\sigma_{site}$, at which point $\sigma_{bgd} \approx 1.04\sigma_{site}$, because beyond that limit the improvement to σ_{bgd} would be insignificant. Moreover, improvements in precision almost invariably imply increased costs. Hence $\sigma_{tech}/\sigma_{site} \approx 0.3$ is an 'ideal' value for cost effectiveness. (This is equivalent to $\sigma_{tech} \approx 0.3\sigma_{bgd}$.) A similar argument shows that an ideal value for $\sigma_{an}/n\sigma_{sam}$ is approximately 0.3.

In this way, the ideal values of both σ_{an} and σ_{sam} can be related to the minimum magnitude of the anomaly that it is required to detect. Estimates of values of precisions for given protocols can be obtained, together with the mean and standard deviation of the background sites, $\hat{\mu}_{bgd}$ and $\hat{\sigma}_{bgd}$, by nested ANOVA. Data are obtained in a hierarchically designed experiment (Fig. 4) in which duplicate samples are taken at each of a number of background sites, and duplicate analyses are made of each sample under randomized repeatability conditions.[17] Such an experiment is referred to as an 'orientation study'.[18]

Recently, the use of robust ANOVA has been advocated for the analysis of data from orientation studies and the identification of anomalies or pollution.[13–17] This method has the advantage of automatically downweighting the effects of occasional discrepant replicates or anomalous sites, and is the best method of identifying such for further investigation.

In the above instance, the FFP principle has been applied in an equivalent manner to analysis and sampling. There seems to be no reason why the idea could not be quantified in other types of situation.

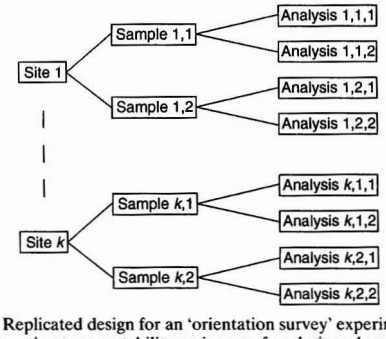

Fig. 4 Replicated design for an 'orientation survey' experiment with k sites to estimate repeatability variances of analysis and sampling for comparison with inter-site variance, to establish the fitness-for-purpose of the sampling and analytical protocols.

Uncertainty

Uncertainty is defined as a parameter, associated with the result of a measurement, that characterizes the dispersion of the values that could reasonably be attributed to the measurand.[8,19] This new concept in metrology has yet to be applied rigorously to chemical measurements, although its introduction will not long be delayed. Uncertainty can be expressed as a standard deviation (the standard uncertainty) or as a half-range (the expanded uncertainty) obtained by multiplying the standard uncertainty by a 'coverage factor' normally between 2 and 3. The standard uncertainty of an analytical measurement is estimated by combining the uncertainties of all of the separate operations and features that constitute the analytical protocol. Short-cut methods for obtaining uncertainties are under discussion and likely to be established.[20]

It seems to be a natural, indeed necessary, extension of the uncertainty concept to include the uncertainty of sampling. Really we need to know the uncertainty range that includes the true value of the bulk material that comprises the sampling target, rather than that of the laboratory sample. Therefore, after the uncertainty of the analysis has been estimated, the uncertainty of the sampling should be combined with it by addition in quadrature, *i.e.*, $u_{total} = \sqrt{u^2_{anal} + u^2_{samp}}$ The immediate question, then, is how to estimate the uncertainty of sampling u_{samp}.

A general or average value of sampling uncertainty could be obtained from the reproducibility standard deviation of sampling obtained in the equivalent of a collaborative trial (to be discussed below). Such a value, however, would suffer from the defect that a sampler employing better than average practice would have a smaller than average sampling uncertainty. It would be unfair to attribute to him/her an average uncertainty. Similarly, a worse than average sampler should not have an undue advantage.

In analysis, the uncertainties in individual laboratories can be addressed through internal quality control (IQC) procedures, although this approach has yet to be formalized. However, internal quality control in analysis is fully effective only if the laboratory uses an external reference point, usually through certified or other reference materials with externally traceable assigned values. Laboratories without this external reference have been found to be worse performers in proficiency tests.[21] A full implementation of the IQC idea in sampling would therefore require the use of reference sampling targets (to be discussed next), and might not be generally possible. However, if we simply assume that the sampling is unbiased (as it would probably be if an empirical sampling protocol were used), we could establish an uncertainty of a particular sampler under 'intermediate' precision conditions,[22] *i.e.*, samples collected on (say) different days. This value could be used for the contribution of sampling to the total uncertainty. The same value would then be used to define a control limit for precision in sampling IQC.

Reference Materials and Reference Sampling Targets

Reference Materials in Analysis

A reference material (RM) is defined as a material or substance one or more of whose property values are sufficiently homogeneous and well established to be used for the calibration of apparatus, the assessment of a measurement procedure or for assigning values to materials.[10] A certified reference material (CRM) is defined as a reference material, accompanied by a certificate, one or more of whose property values are certified by a procedure which establishes traceability to an accurate realization of the unit in which the property values are expressed and for which each certified value is

accompanied by an uncertainty at a stated level of confidence.[10] Tests for trueness in analysis often require the use of reference materials of some kind. Other recognized uses of reference materials include calibration, proficiency testing, internal quality control and method validation (including the collaborative trial), all to be discussed subsequently.

An essential characteristic of a reference material is stability: reference materials cannot be made unless the analyte and the matrix are, for practical purposes, invariant with time. This restriction implies that reference materials must be maintained under appropriate conditions. Most analytical reference materials are divided for distribution into effectively identical portions, and suitable for further subdivision into test portions in each laboratory. The bulk material before subdivision must therefore be effectively homogeneous. Finally, and especially in the case of the CRM, a value of analyte concentration with its associated uncertainty must be assigned to the material. Each of these essential features may require extensive testing.

Testing a reference material for stability in principle requires the analysis of the candidate material before and after an extended period of storage under appropriate conditions and normal handling (*e.g.*, dispatch by post). However, any instability in the material would be confounded with instability in the analytical method if such a naive approach were taken. Consequently, it is better practice to keep a control portion of the material for the same period under conditions that guarantee stability, *e.g.*, under reduced temperature, relative humidity or oxygen partial pressure. The two portions are then analysed in replicate in a random order under repeatability conditions. Any significant difference between the mean results for the two portions shows a lack of stability.

A test for sufficient homogeneity is conducted, after the candidate material has been divided into portions for distribution, by selecting at random a number (usually 10–20) of the portions and analysing them in duplicate under repeatability conditions, the test portions being in a random order in the analytical run. Sufficient homogeneity is manifest if there is no significant difference between the portions or if the between-portion variance is lower than some empirically determined limit.[23]

Essentially two different approaches can be detailed for the evaluation of the assigned value. In one extreme the material is analysed in one laboratory under ideal conditions, using best possible practice and usually some kind of 'definitive' method of analysis. The other extreme is the certification trial, which involves a number of experienced laboratories employing a variety of analytical methods based on a range of physicochemical principles. If significant differences between the participants emerge after a first trial, a second round is conducted after exhaustive investigation of the causes of the discrepancies and remedial action as appropriate. The consensus of the revised results is taken to be the assigned value.[24]

Reference Sampling Targets

Reference sampling targets (RST) are at least conceivable as fulfilling in part duties in sampling analogous to those of the RM in analysis. There seems to be a role for the RST for validating sampling protocols and for quality control, although not for calibration: there is no analogue of calibration in sampling. For example, if a sampling protocol under trial were applied to a putative reference sampling target, a bias in the protocol or in its execution would be manifest as a difference between the assigned value of the RST and the mean value resulting from an unbiased analysis of the samples procured. Occasional use of the RST close to times when sampling was required 'in the real world' might suffice for internal quality control. The realization of such a scenario would depend on whether the notions of stability, homogeneity and true value could be applied to RSTs, in addition to the economic feasibility of establishing and maintaining an RST.

A true value could be assigned to an RST in principle by the same methods that are used for CRMs. One possibility is that 'expert samplers' could take samples from the candidate RST using recognized or validated sampling protocols. After analysis of the samples by a bias-free method, the consensus is the assigned value of the RST. In some instances the RST could be prepared by mixing 'pure' constituents in known quantities, or by spiking. In the environmental field there could be ethical objections to applying such a procedure to toxic analytes or concomitants: it would probably not be acceptable practice deliberately to contaminate a previously clean field, for example.

The stability of an RST would be difficult to test. In principle, a number of samples could be removed from the target according to a fixed protocol and stored under conditions of enhanced stability (*e.g.*, in a deep-freeze). After a suitable period further samples are taken by the same protocol. All of the samples are then analysed under repeatability conditions in a random order. A two-sample test of significance such as the *t*-test would show whether the samplings were different, but not necessarily that the material was stable. There would be no way of determining whether the difference was due to instability of the target or differences in the two implementations of the sampling protocol.

The use of an RST over an extended period has different resource implications in different fields of application. Considering the likely bulk involved, secure warehousing with a degree of management would probably be the minimum requirement for many bulk commodities. Many such materials (*e.g.*, foodstuffs) would require permanent temperature and humidity control, and possibly chemical treatment to inhibit attack by insects or microbiota. There would need to be a considerable space available beyond that needed simply to store the RST, to allow the material to be moved about during sampling where necessary. A heap of ore would need to be coned repeatedly to prevent segregation causing a bias in the results. The RST would need to be of considerable bulk so that biased sampling does not cause a noticeable drift in the content of the analyte. Foodstuff RSTs would require additional security to prevent the accidental use of the material for consumption.

Environmental RSTs have to be sampled *in situ* if any semblance to reality is aimed at. This implies that, because of their flow, targets such as natural waters or the atmosphere are unlikely to be sufficiently stable to qualify as reference materials. Sediments too, although they are quasi-stable much of the time, can be changed radically in a very short period by heavy rainfall and flood conditions. Even for soils, the need for stability demands that the area designated as an RST must be in quasi-equilibrium with environmental features such as hydromorphic or clastic dispersion, and must obviously be free from the danger of flooding. This implies that processes contributing to pollution must have ceased for a considerable period before use as an RST is contemplated, to allow equilibration to take place. For example, for an RST representing pollution from mining or smelting, sites where operations ceased in the 18th or 19th century would therefore be most suitable. Small-scale changes, if they were still occurring, could be allowed for. RST sites would have to be secure and managed, to prevent unauthorized and potentially deleterious uses such as dumping or shooting. Even grazing would have to be carefully considered as a mechanism for depleting the soil of trace elements taken up by herbage. Once established, however, such a soil RST would have an extended useful lifetime. For example, the soil target in a 1 ha field

consists of about 10^6–10^7 kg. Thousands of 1 kg samples could be removed before any deterioration would be apparent.

Sufficient homogeneity as a concept in sampling is not an exact analogue of that in analysis. RSTs are usually heterogeneous—if the target is homogeneous there is no random element to the sampling problem by definition. In fact, the natural heterogeneity of RSTs would have to be carefully safeguarded. It would be legitimate for samplers to re-mix an RST (for instance, by re-coning) to overcome the effects of segregation. However, comminution of an RST by a sampler could not be allowed, because the nature of the material would be permanently changed thereby. The organizer responsible for the preparation of the RST would have to carry out comminution to the required degree before samplers could have access to the material.

The question of sufficient homogeneity arises only when we postulate the division of a bulk RST for distribution, into portions that would be used as equivalent RSTs at a number of locations. This is an exact analogue of the distribution of a CRM. Hence we postulate an experiment depicted in Fig. 5. The bulk RST after preparation could be divided into portions for distribution. Between 10 and 20 of these portions would be selected at random and samples taken in duplicate from each under sampling repeatability conditions. The samples would then be analysed once each under analytical repeatability conditions in a random order. One-way ANOVA would establish whether the portions were significantly different.

The Size of RSTs

Ideally, an RST should be the same size as a normal lot or consignment. This situation would give free scope for all of the normal contingencies of sampling. However, it would probably prove to be prohibitively expensive, in respect of the cost of maintenance and the capital value tied up in it. To maintain its value as a standard, therefore, an RST smaller than a typical lot or consignment should preserve the same range of potential for sampling error. For example, the range of particle size should remain the same. This would probably be one of the main determinants of a minimum size for an RST. A finely divided RST could be much smaller than a coarse material.

Heterogeneity on a broad scale (not just locally) is a feature of certain materials such as ores, and this feature would be impossible to preserve in a smaller representative RST. However, such bulk materials are usually sampled while passing along a conveyor, by the systematic removal of increments by scoops taken at fixed intervals. The aggregate sample is then mixed (and comminuted to a degree if appropriate), and a smaller sample is taken for analysis. It seems much more feasible to restrict the RST concept to such aggregate samples, which are on a more manageable scale. If necessary, the effectiveness of the primary sampling process could be assessed as a separate exercise, for example by duplication.

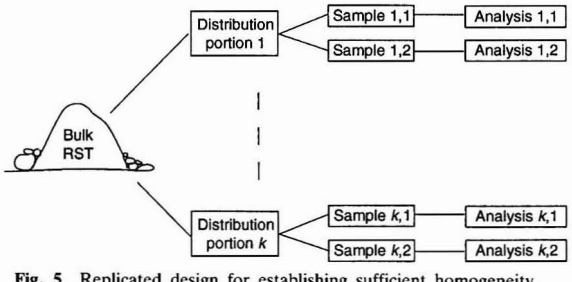

Fig. 5 Replicated design for establishing sufficient homogeneity, with k distributed portions of a candidate reference sampling target. (Sampling and analysis under repeatability conditions.)

Traceability in an RST

Traceability in analysis is defined as a property of the result of a measurement or the value of a standard whereby it can be related to stated references, usually national or international standards, through an unbroken chain of comparisons all having stated uncertainties.[10] For most purposes in analysis traceability to a certified reference material is sufficient. The traceability concept is normally restricted to a testing process and its applicability to sampling is not obvious. Only the analytical process in assigning a value to an RST would need to be traceable.

Reference Sampling Targets—Conclusions

The setting-up of an RST (the analogue in sampling of an RM or CRM) from a product or commodity would necessarily be a large undertaking. Capital cost and maintenance costs would be significant, although probably not excessive in proportion to the normal operational costs of the industries involved. However, the motivation for instituting an RST would arise only from a clear perception that sampling errors themselves, and any incorrect decisions resulting from them, were in themselves an expensive problem. Setting up an RST for contaminated soil might prove easier. Contaminated land unsuitable for development is relatively cheap and could be secured and managed easily.

The Collaborative Trial and its Analogue in Sampling

The Collaborative Trial

A collaborative trial is an interlaboratory exercise designed to characterize the performance of a method that is a candidate standard method. The method has to be clearly specified in a protocol and subjected to extensive preliminary validation in a single laboratory. A collaborative trial may cost of the order of £20 000 to conduct.

Several bodies have issued standards or guidelines for the conduct and interpretation of collaborative trials,[25–28] and individual authors have commented in detail.[29–34] The most general set of guidelines is the Harmonized Protocol produced by ISO, IUPAC and AOAC International.[35] The collaborative trial is regarded as the strongest form of method validation.

The collaborative trial is conducted by the organizing agency distributing samples to a minimum of eight laboratories. The samples come from a number (>5) of sufficiently homogeneous materials that represent the scope of the validation to be attempted. The participants analyse the materials in duplicate, strictly according to the protocol, and report the results to the organizer. The organizer interprets the data by one-way ANOVA for each separate material forming the estimates $s_r = s_0$, $s_L = s_1$, $s_R = (s_r^2 + s_L^2)^{\frac{1}{2}}$ and $\bar{x}$, where s_0 is the within-group standard deviation, s_1 is the between-group standard deviation, s_r is the repeatability standard deviation and s_R is the reproducibility standard deviation. If the trial materials are certified reference materials, the bias at each level is obtained. The materials normally cover a range of concentrations, so that relationships between the precision and concentration can be established. The standard deviation s_r represents repeatability conditions of precision, *i.e.*, where independent test results are obtained with the same method on identical test material in the same laboratory by the same operator using the same equipment

within short intervals of time.[22] Reproducibility conditions of precision, represented by s_R, is obtained where independent results of measurement of the same measurand are obtained with the same measurement procedure in different laboratories with different observers using different equipment.[22] Intermediate precision conditions, such as within-laboratory between-run precision, can also be estimated by a more complex experimental design.

The precisions σ_r and σ_R are conventionally regarded as properties of the analytical method. However, Horwitz *et al.*[36] have shown that two approximate relationships (where the concentration c is expressed as a mass fraction), namely

$$0.01c^{0.8495} < \sigma_R < 0.04c^{0.8495}$$

and

$$\sigma_r \approx 0.6\sigma_R$$

hold irrespective of the analyte, matrix, method or concentration range. Hence the precisions are likely to represent more general features of analytical practice.

The treatment of outliers in the collaborative trial is a contentious issue. Most authorities now recommend before the ANOVA the exclusion of outliers identified by tests of significance. Alternatively, robust ANOVA can be used on the raw data.[37] Either way, the statistics represent the performance of the majority, or the 'good' laboratories. There has also been wide discussion about the degree to which the statistics are representative. Some commentators say that, as a trial is executed before laboratories have become practised in the new (or modified) method, that better performance will be expected in due course. Others contend that collaborative trials are unlikely to explore the full range of variations in procedure that are allowed by the protocol and that test the ruggedness of a method, and that consequently the statistics are unduly rigorous. Likewise, the set of laboratories that participates in a trial is unlikely to be a random sample from the population of potential participants, but probably selected on the basis of known reliability.

A further query concerns the validity of a value for s_r, obtained under conditions of supposed blind duplication. Participants in practice know which test portions are duplicates, and often analyse them contiguously in a run rather than in a random order. A design that partially alleviates this problem is the split-level design where, as an alternative to duplication, two similar but distinct materials are each analysed once.

The Collaborative Trial Analogue in Sampling

At first sight, the collaborative trial in sampling (CTS) seems to be straightforward. A simple scenario has the participants visiting the sampling targets in succession, taking independent duplicate samples according to a fixed protocol and analysing the samples in duplicate (Fig. 6). The data are then treated by nested ANOVA, which for each target provides estimates of the grand mean, the analytical repeatability variance s_0^2, the sampling repeatability variance s_1^2 and the between-sampler variance s_2^2. The reproducibility sampling variance is given by $s_1^2 + s_2^2$. However, in order to separate the sampling and analytical variations between laboratories, it is essential that samples from all of the samplers be analysed together under repeatability conditions, *i.e.*, within a single laboratory and run. There is no equivalent to this necessity in collaborative trials, but is not a serious impediment to the idea of a CTS.

To preserve statistical independence of the samplers, the sampling targets should not show signs of the previous samplers' activities. If necessary, the targets should be restored to their original appearance after each sampler has gone. If an estimate of sampling bias is required, the targets must be RSTs.

Seemingly, the notions of repeatablity and reproducibility conditions can be extended to sampling with no difficulty. Repeatability conditions would apply to variations between samples collected by the same sampler from a single target using a single protocol and equipment within a short period of time. Reproducibility conditions apply to variation between samples collected from a single target by different samplers, using the same protocol and equipment. Intermediate conditions, however, seem to have a less clear meaning in sampling, because it is not immediately apparent that a sampling 'run' is well defined.

A sampling collaborative trial could therefore be conducted fairly easily. The only logistic problem would be that the samplers would have to travel to the targets. No long-term storage or management is implied for the targets, however, and they would not have to be stable for more than the time required for the samplers to visit, which should amount to only a few days. Targets could be restored to their normal use after the trial unless they were RSTs. Collaborative trials in sampling should not be prohibitively expensive, therefore.

The outcome of CTS is not easy to predict. Presumably we would find that reproducibility variance was significantly greater than repeatability variance, as is usually found in analysis, but the general magnitude of the ratio requires experimental estimation: it is not clear that the ratio of about 1.5 found in analysis is applicable. There is a small amount of experimental evidence that sampling repeatability variance increases with increasing analyte concentration in environmental studies.[38] No general impression of the manner of the variation is apparent, however, except that sampling variance 'explodes' in polluted areas. No conjecture about an empirical relationship of the Horwitz type could be entertained until a large number of trials had been conducted. The data obtained in CTSs should be scrutinized by a statistical expert in the early days, because the patten of variation between and within samplers is difficult to predict. The automatic applicability of particular statistical methods cannot be assumed in these circumstances. However, it seems likely that some kind of outlier treatment will be required.

The Sampling Proficiency Test

Analytical Proficiency Testing

Proficiency testing is the use of results generated in inter-laboratory test comparisons for the purpose of continuing assessment of the technical competence of participating testing laboratories.[39] Proficiency tests (PT) can take a number of forms, but the following type is widespread in

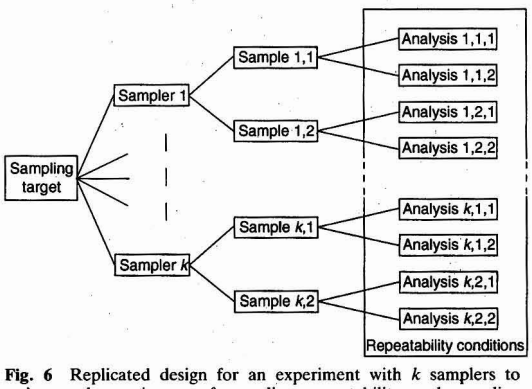

Fig. 6 Replicated design for an experiment with k samplers to estimate the variances of sampling repeatability and sampling reproducibility in a 'collaborative trial' of a sampling protocol.

analytical chemistry.[23] Test materials are prepared by the organizing agency and (ideally) tested for stability and sufficient homogeneity. Samples of the validated test materials are then distributed to the participating laboratories for unsupervised analysis as unknowns. There is usually no prescription of the method to be used, but it is accepted in PT that participants should operate under conditions that normally prevail in routine analysis and report a result exactly in the form that would be given to a normal client. Reporting must be completed by a fixed date, after which the organizer makes a statistical analysis of the results and reports the outcome back to the participants. The whole procedure is repeated regularly at intervals of between 2 weeks and 4 months.

A number of procedures have been devised for converting the raw data into 'scores'. The only score recommended in the International Harmonised Protocol[23] is the z-score, given by

$$z = (x - \hat{X})/\sigma$$

where x is the participant's raw result, $\hat{X}$ is the assigned value (the best available estimate of the true value) and σ, the target value for standard deviation, defines the required standard of performance in terms of interlaboratory error. A z-score that falls outside the range of ± 3 is usually regarded as representing an unsatisfactory performance that requires remedial action.

The ethos of the PT is that it constitutes a method for laboratories to detect unsuspected deficiencies in their analytical and quality practices. It is not a substitute for internal quality control, but rather an incentive for laboratories to install effective IQC systems. PT allows a participant to make three main comparisons: (*i*) between the result obtained and the true value; (*ii*) between the result obtained and the results of the other participants; and (*iii*) between current performance and past performance. Despite the primary purpose of the PT as a service to the participants, both end-users of analytical data and accreditation agencies are beginning to make use of PT performance scores.

A critical feature of the operation of a PT is the utilization of an appropriate value for the assigned value. Several options are available, *viz.*, (*i*) the consensus of several expert laboratories that undertake the analysis under ideal conditions using definitive methods; (*ii*) 'spiking', the addition of known amounts of analyte to a typical test material containing none; and (*iii*) the consensus of the participants. Of these methods (*i*) and (*ii*) are preferable in that they address the true value whereas (*iii*) merely encourages consistency among laboratories and might even institutionalize the use of biased methods. However, (*iii*) is usually regarded as safe when the analytical method is well understood and relatively easy to conduct. Moreover, when an empirical method is used, the consensus of a sufficiently large number of participants is very close to the true value by definition.

Another critical measure is the target value for standard deviation. Ideally this should be determined by fitness for purpose, *i.e.*, by relating the required quality of the data to its intended use. There are problems with expressing fitness for purpose quantitatively at present in most fields of analysis, but PT organizers usually have sufficient experience to set a target value for standard deviation that represents fitness for purpose in their field. An alternative possibility is to use a value that represents contemporary practice, *i.e.*, a robustified standard deviation from the results of all participants in a round of a mature PT scheme. This practice is less satisfactory, because it may perpetuate a standard of performance that is inconsistent with fitness for purpose. The use of the actual standard deviation achieved in each round is not satisfactory, because a comparison of z-scores round by round is then not possible.

While proficiency tests have had a marked beneficial effect on data quality in the fields where they have been introduced, some limitations must be recognized. The scope of a PT scheme, in terms of the range of analytes covered, and the frequency of the rounds are limited by costs. As the distributions are, in most instances, relatively infrequent, the scheme can demonstrate the potential for a laboratory to produce data of an appropriate quality but not the actuality: that is the task of internal quality control. In addition, the range of different materials and analytes tested may be necessarily only a token of the total range of a typical laboratory. Therefore, a single test may have to be regarded as representative of a class of analytes of materials. Sometimes this approach is justified, but often it is not.[40]

The Potential for Proficiency Testing in Sampling

A strict analogue of proficiency testing in sampling would involve each participant sampler travelling to the sampling target and independently taking a sample by his/her method of choice. The sample would be removed to a laboratory for analysis, and the result reported to the scheme organizers.

Several requirements are immediately apparent. The target would need to be sufficiently large to be effectively unchanged by sampling. This precaution would ensure that there was no drift in the true bulk composition of, or other relevant change in, the target during sampling by successive samplers, some of whom might take biased samples. The participants should visit the target separately and not leave perceptible traces of their activities, to preserve the independence of successive samplings. The premises on which the target was located would have to be such that it did not enforce a particular *modus operandi* on successive samplers, again to preserve independence. The target would have to be maintainable in a stable condition and used for no other purpose during the access period. However, no long-term storage or stability would be required, and after the sampling PT the sampling target could be restored to its original use. Unlike analytical PT, there would be no requirement that the target should be homogeneous.

A complication of sampling PT is that the success of sampling is assessed by analysis, but errors can arise independently in both sampling and analysis. The simplest and possibly most satisfactory approach would be to regard the whole process, sampling plus analysis, as the subject of the PT. Then only one result per target would be reported by the participant. This approach has the advantage of simplicity and addresses the matter of direct concern—the total quality of the whole train of activities that represent the composition of the sampling target by the analytical result. It shows an apparent defect by leaving unanswered the interesting question as to whether the greater part of the total error arises in sampling or analysis. However, that is an exact analogue of analytical proficiency testing: the outcome provides the participant with no diagnostic information concering the source of errors, which could arise independently, for example, during the preliminary chemical treatment of the test portion or during instrumental measurement. Alternatively, the PT scheme organizer could arrange to have all of the samples analysed under repeatability conditions (*i.e.*, in a single laboratory and run) by a method of high precision and trueness, so that the outcome reflected variations only in the sampling quality.

The sampling analogue of a z-score could be derived if suitable values of $\hat{X}$ and σ could be established. At the present stage of development it seems unlikely that a credible 'consensus of experts' could be used as the assigned value, and establishing a value by spiking would be impracticable in many areas of activity. Consequently, it would usually be necessary to rely on the consensus of participants, presuming a

consensus to exist. This would have the disadvantage of addressing only consistency rather than trueness, and this might represent a serious defect if, for example, all of the participants tended to collect a sample that was biased in the same direction. If the sampling method is regarded as empirical, however, the consensus is the ideal assigned value. Establishing a value of σ based on fitness for purpose should be no more difficult for sampling-plus-analysis than for pure analysis. In fact, we might anticipate the same value of σ being used initially, because at present sampling variations are not usually included in FFP considerations.

The interpretation of *z*-scores for sampling-plus-analysis could follow the same pattern that is established in analysis, although it could reasonably be assumed that initial attempts at sampling PT would result in a high proportion of extreme values and possibly no consensus.

In conclusion, sampling proficiency tests seem to be inherently feasible and an almost exact analogy of analytical PT. The introduction of a sampling PT in a particular sector of the analytical community would almost certainly be followed by an improvement in sampling quality. Only experience could determine whether the associated problems could be overcome in a cost-efficient manner.

Internal Quality Control

Analytical Internal Quality Control

Internal quality control (IQC) occupies a key role in analytical measurement because it is the ultimate test that a run of analyses is fit for its destined purpose. Even with all of the other methods of quality assurance in place, there is still a possibility of the occurrence of a mistake in procedure or other contingency that adversely affects the accuracy of the results obtained during a run. A well designed IQC scheme can detect such a lapse. This allows the analyst to reject the results, suspend operation of the analytical systems for remedial action, and only then conduct the re-analysis of the run. The 'run' is taken to be a set of analyses conducted under repeatability conditions.

Procedures for IQC have been devised in many sectors of analytical chemistry,[41–46] and they are currently being codified by cooperation between ISO, IUPAC and AOAC International into a set of Harmonized Guidelines.[47] Two basic procedures comprise IQC. First, control materials that are as similar as possible to the test materials are added to the analytical run. Second, the replication of the analysis of some or all of the test materials is undertaken in the run.

The control materials must be either CRMs or traceable with sufficiently small uncertainty to materials of certified or otherwise tested quality. Lack of attention to this point is a weakness in many IQC implementations at this time.[21] Control materials are used in two conceptually different ways. The primary concept is that of statistical control. It is assumed that, in an analytical system used regularly without mistake, run-to-run variations in bias are described by a normal curve with parameters that can be estimated from experience with the system. Therefore, if a control material is analysed regularly in the system, a value outside the range $\mu \pm 3\sigma$ should occur with a probability of about 0.003. Such an occurrence is taken to be so unlikely as to show that the system is no longer 'in control', but is behaving differently on account of an uncontrolled and deleterious change of some kind. The implication is that the errors in the system are no longer predictable, so that no valid uncertainty can be ascribed to the results obtained on the test materials during that run. As a secondary role for the control material, the grand mean of the results obtained in the in-control runs can be compared to the assigned value in a test for overall bias. An additional minor function is to provide diagnostic information for a logical approach to remedying the faults that give rise to an out-of-control condition.

In *ad hoc* analysis (where single unpredictable materials or objects are analysed), the concept of statistical control is void—we have no advance information on the likely magnitudes of the errors in the analytical system. In such an instance, we regard the bias encountered in control materials as representative of that present in the test materials, and simply use fitness for purpose criteria for comparison purposes.

Replication is used to control the magnitude of random errors within a run, *i.e.*, to control the repeatability precision. The best form of replication in most circumstances is the duplication of all, or a proportion, of the test materials in a run. If we consider the absolute difference $|d|$ between duplicated results, only in about 3 instances in 1000 will we find that $|d| > 3\sqrt{2}\sigma_r$, where σ_r is the standard deviation of repeatability of the laboratory. An unduly high proportion of such results in a run is indicative that a within-run out-of-control condition has occurred.

IQC in Sampling

An exact analogue in sampling of the control material in analysis would be a specially designated RST, the control sampling target. The sampler must therefore have access to a control sampling target (CST) that would have to be preserved at a convenient place near where the test sampling targets are normally examined. The CST would be sampled each time that a test sampling was carried out, by exactly the same sampling protocol. The CST sample would be analysed in the same run as the normal test samples, and the result plotted on a control chart (or treated by an equivalent mathematical procedure). The control chart limits would be set by estimates of the sampling plus analytical precision combined. An out-of-control condition would be unambiguous if the analytical IQC were in control. If there was an assigned value associated with the CST, then any over-all bias of the sampling could be estimated as the difference between the mean value obtained by the reproduced sampling of the CST and the assigned value, and a significance test could be carried out. Of course, the CST would need to be stable and secured over long periods of time.

A simpler and far less costly procedure would be the repeat sampling of all or a proportion of the test sampling targets. Indeed, this procedure has been recommended (although not as yet widely adopted) in routine environmental and mineral exploration exercises,[14–16] and is used in an informal way in several sectors of the analytical community. To assess the outcome of such a procedure, the absolute differences between the analytical results on duplicated samples could be compared with a value of $3\sqrt{2(\sigma_r^2 + \sigma_s^2)}$, where σ_s is the repeatability sampling precision in the laboratory. This value would act as an upper bound equivalent to $p \approx 0.003$. When the collection of repeat samples is combined with repeated analysis, the application of nested ANOVA leads to a separate estimation of the sampling variance on a run-wise basis. This in itself is likely to be a salutary experience, but it must be remembered that the repeatability sampling variance is likely to be smaller than the more realistic reproducibility sampling variance. Sampling bias cannot be addressed by such an approach, but if the sampling protocol is regarded as unbiased there is no problem.

Hence it seems that all of the features of analytical IQC could, in principle, be adapted to sampling IQC. The extra cost of conducting sampling IQC is likely to be in a similar proportion of total sampling costs as is found in analysis.

Conclusions

It has been shown that nearly all of the concepts and practices associated with ensuring a satisfactory quality for analytical data can in principle be applied to sampling. Implementing these practices in full would undoubtedly be a significant addition to the over-all cost of sampling, and it may be that a degree of simplification or attenuation of the methods discussed here would be called for. However, in the areas such as setting up reference sampling targets and conducting sampling proficiency tests, sampling quality control and sampling protocol collaborative trials, only experimentation will suffice to establish satisfactory and cost-effective procedures. Likewise, experimentation alone will allow us to assess the magnitude of the sampling quality problem in a particular field of application. It cannot be doubted that such measures are necessary, however. Sampling quality is a little-known area—the analyst's 'skeleton in the cupboard'—and it is of vital concern that analytical excellence is not going to waste on defective samples.

References

1 Ferguson, C. C., *Ground Eng.*, 1992, **25**, 34.
2 *Principles of Environmental Sampling*, ed. Keith, L. H., American Chemical Society, Washington, DC, 1988.
3 Kratochvil, B., Wallace, D., and Taylor, J. K., *Anal. Chem.*, 1984, **56**, 113R.
4 Smith, R., and James, G. V., *The Sampling of Bulk Materials*, Royal Society of Chemistry, London, 1981.
5 Visman, J., Duncan, A. J., and Lerner, M., *Mater. Res. Stand.*, **11**(8), 32.
6 *Instructions on Codex Sampling Procedures*, Codex Alimentarius Commission (WHO), Rome, 1987.
7 *General Principles of Sampling and Accuracy of Results (Methods for the Examination of Waters and Associated Materials)*, HM Stationery Office, London, 1980.
8 *Statistics Vocabulary and Symbols—Part 1: Probability and General Statistical Terms*, ISO 3534-1: 1993 (E/F), International Standards Organization, Geneva, 1993.
9 Gy, P. M., *Sampling of Heterogeneous and Dynamic Materials: Theories of Heterogeneity, Sampling and Homogenising*, Elsevier, Amsterdam, 1992, pp. 569ff.
10 ISO, *International Vocabulary for Basic and General Terms in Metrology*, International Standards Organization, Geneva, 2nd edn., 1993.
11 *Terms and Definitions Used in Connection with Reference Materials*, ISO Guide 30: 1992, International Standards Organization, Geneva, 1992.
12 Tonks, D., *Clin. Chem.*, 1963, **9**, 217.
13 *Handbook of Exploration Geochemistry. Vol. 2: Statistics and Data Analysis in Geochemical Prospecting*, ed. Howarth, R. J. Elsevier, Amsterdam, 1983, pp. 92–107.
14 Ramsey, M. H., Thompson, M., and Hale, M., *J. Geochem. Explor.*, 1992, **44**, 23.
15 Ramsey, M. H., *Appl. Geochem.*, 1993, **2**, 149.
16 Ramsey, M. H., in *Sampling of Environmental Materials for Trace Analysis*, ed. Markert, B., VCH, Weinheim, 1994, pp. 93–108.
17 Thompson, M., and Maguire, M., *Analyst*, 1993, **118**, 1107.
18 Rose, A. W., Hawkes, H. E., and Webb, J. S., *Geochemistry in Mineral Exploration*, Elsevier, Amsterdam, 1979, pp. 34–35.
19 ISO, *Guide to the Expression of Uncertainty in Measurement*, International Standards Organisation, Geneva, 1993.
20 Analytical Methods Committee, personal communication.
21 Thompson, M., and Lowthian, P. J., *Analyst*, 1993, **118**, 1495.
22 *Precision of Test Methods*, ISO 5725-1986, International Standards Organization, Geneva, 1986, under revision.
23 Thompson, M., and Wood, R., *Pure Appl. Chem.*, 1993, **65**, 2123 (also published in *JAOAC Int.*, 1993, **76**, 926).
24 *Reference Materials. Part 4: Guide to General and Statistical Principles for the Certification of Reference Materials*, ISO Guide 35: 1989, International Standards Organization, Geneva, 1989.
25 Youden, W. J., *Statistical Techniques for Collaborative Tests*, Association of Official Analytical Chemists, Washington DC, 1969.
26 *Standard Practice for Conducting an Interlaboratory Study to Determine the Precision of a Test Method*, ASTM E691-87, American Society for Testing and Materials, Philadelphia, 1988.
27 *Institute of Petroleum Standard Methods for the Analysis and Testing of Petroleum and Related Products*, Wiley, Chichester, 1992, IP 367/84.
28 *Guidelines for the Development of Standard Methods by Collaborative Study*, Laboratory of the Government Chemist, London, 4th edn., 1988.
29 Zaalberg, J., *J. Assoc. Off. Anal. Chem.*, 1989, **72**, 34.
30 Kelly, P. C., *J. Assoc. Off. Anal. Chem.*, 1990, **73**, 58.
31 Malanoski, A. J., *J. Assoc. Off. Anal. Chem.*, 1990, **73**, 231.
32 Malanoski, A. J., *J. Assoc. Off. Anal. Chem.*, 1990, **73**, 235.
33 Malanoski, A. J., *J. Assoc. Off. Anal. Chem.*, 1990, **73**, 411.
34 Mandel, J., *Chemom. Intell. Lab. Syst.*, 1991, **11**, 109.
35 Horwitz, W., *Pure Appl. Chem.*, 1988, **60**, 855–864 (revision in preparation).
36 Horwitz, W., Kamps, L. R., and Boyer, K. W., *J. Assoc. Off. Anal. Chem.*, 1980, **63**, 1334.
37 Analytical Methods Committee, *Analyst*, 1989, **114**, 1699.
38 Ramsey, M. H., and Thompson, M., unpublished data.
39 *Development and Operation of Laboratory Proficiency Testing*, ISO Guide 43:1980, International Standards Organization, Geneva, 1980.
40 Thompson, M., unpublished data.
41 Thompson, M., in *Handbook of Exploration Geochemistry. Vol. 2: Stastistics and Data Analysis in Geochemical Prospecting*, ed. Howarth, R. J., Elsevier, Amsterdam, 1983, pp. 39–58.
42 Analytical Methods Committee, *Analyst*, 1989, **114**, 1497.
43 Analytical Methods Committee, *Analyst*, 1995, **120**, 29.
44 Westgard, J. O., Barry, P. L., and Hunt, M. R., *Clin. Chem.*, 1981, **27**, 493.
45 Nix, A. B. J., Rowlands, R. J., Kemp, K. W., Wilson, D. W., and Griffiths, K., *Stat. Med.*, 1987, **6**, 425.
46 Cheeseman, R. V., Wilson, A. L., and Gardner, M. J., *Manual on Analytical Quality Control for the Water Industry*, Water Research Centre, Medmenham, 1989.
47 Thompson, M., and Wood, R., *Pure Appl. Chem.*, in the press.

Paper 4/04337E
Received July 15, 1994
Accepted November 9, 1994

A Horwitz-like Function Describes Precision in a Proficiency Test

Michael Thompson and Philip J. Lowthian

Department of Chemistry, Birkbeck College, University of London, Gordon House, 29 Gordon Square, London, UK WC1H 0PP

Horwitz found that a simple functional relationship described the variation of reproducibility precision in collaborative trials as a fractional power of the concentration of the analyte. This relationship holds reasonably well, irrespective of the analyte, the matrix, or the nature of the test material. A similar relationship has been found in the results of a proficiency test.

Keywords: Horwitz function; reproducibility precision; proficiency test; collaborative trial

Introduction

A collaborative trial is an interlaboratory exercise designed to establish the performance characteristics, especially the precisions, of a specific well defined analytical method.[1,2] Horwitz and co-workers have established that there is an empirical relationship between reproducibility (between laboratory) precision and the concentration of the analyte in statistics derived from collaborative trials.[3–5] The exact equation proposed by Horwitz is

$$RSD_R(\%) = 2^{(1 - 0.5\log_{10}c)} \quad (1)$$

where $RSD_R(\%)$ is the relative standard deviation of reproducibility as a percentage, and c is the concentration of the analyte expressed as a fraction. Remarkably, this relationship seems to hold regardless of the analyte, the matrix or the analytical method and seems to be invariant with time. Most values of RSD_R estimated from collaborative trials fall within a range of 0.5–2.0 of the predicted value (the 'Horwitz band'), over about nine orders of magnitude of analyte concentration.

Proficiency tests are also interlaboratory exercises, but unlike collaborative trials they are designed to assess the competence of the participating laboratories.[6] In analytical proficiency tests, effectively identical portions of a material are distributed to the participating laboratories for blind unsupervised analysis.[7] There is usually no restriction on the choice of the analytical method to be used. It is not obvious from this context whether interlaboratory standard deviations in proficiency tests are likely to be greater or smaller than those from collaborative trials at the same concentration of analyte, or whether they would follow a relationship with concentration similar to the Horwitz function. These questions are considered here.

The Horwitz equation is equivalent to

$$\sigma_R = 0.02c^{0.8495} \quad (2)$$

or to

$$\log_{10}\sigma_R = 0.8495 \log_{10}c - 1.6990 \quad (3)$$

where σ_R is the reproducibility standard deviation. Eqn. 3, the logarithmic form, is valuable for experimental studies as it is linear in form and the transformed data are close to homoscedastic–simple linear regression can, therefore, be used to estimate the empirical parameters of the relationship.

Experimental

Data were obtained from the four rounds preceding August 1994 of the Food Analysis Performance Assessment Scheme (FAPAS) (organised by the FAPAS Secretariat, CSL Food Science Laboratory, Ministry of Agriculture, Fisheries and Food, Norwich Research Park, Colney, Norwich, UK NR4 7UQ). Some 40–50 analytes grouped into eleven 'series' were determined in each round. Between 50–150 laboratories participated in each separate test, depending on the nature of the analyte. A typical data set is shown in Fig. 1. Preliminary rounds of the scheme were excluded from the study on the grounds that the results would be atypical of the mature scheme.

Some of the data sets were rejected before the statistical analysis. These were clearly bi- or multi-modal (indicating that two or more discrepant analytical methods had been used by the participants) or where there was independent evidence of analytical problems among the participants. These rejected data sets would, therefore, have an inflated value of precision associated with them. In all, 141 data sets were subjected to the final statistical analysis.

Statistical Methods

The mean and standard deviations of each data set were estimated by a robust method, by using the Huber 'H15' method and the Analytical Methods Committee (AMC) algorithm.[8] This method has the effect of greatly reducing the influence of outlying results on the statistics, thus, eliminating any inflation of the result by the small proportion of laboratories with unsatisfactory performance. This approach is compatible with the Harmonized Protocol method of dealing with outliers used by Horwitz in his studies of collaborative trials.[2]

Results and Discussion

The standard deviations plotted against the analyte concentrations are shown in Fig. 2, on $\log_{10}$–$\log_{10}$ scales. Visually, most

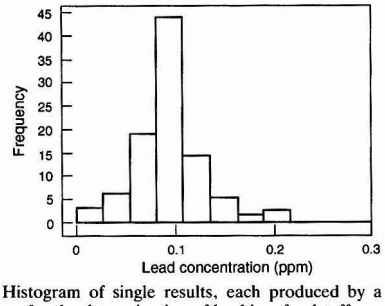

Fig. 1 Histogram of single results, each produced by a separate laboratory, for the determination of lead in a foodstuff.

of the points conform to a linear relationship extending over nearly ten orders of magnitude, with some scatter around the line and some local deviations. A simple regression indicated an underlying relationship of

$$\sigma_I = 0.023\ c^{0.8255}$$

where σ_I is the interlaboratory standard deviation. This result is close to the Horwitz function.

Over most of the range, the standard deviations slightly higher than predicted by the Horwitz function (Fig. 3). This is to be expected, as there is no restriction on analytical method

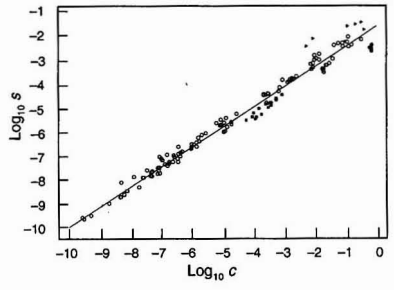

Fig. 2 Interlaboratory standard deviation plotted against analyte concentration, with a simple regression line. Squares show HPLC determinations, triangles show GLC determinations, closed circles show moisture determinations, open circles show other analytes.

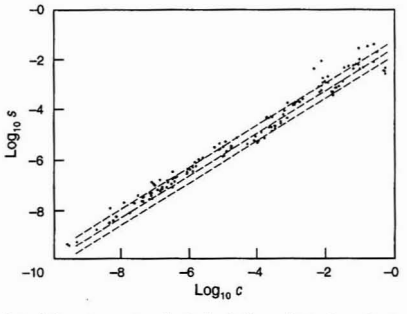

Fig. 3 Interlaboratory standard deviation plotted against analyte concentration, with the 'Horwitz band'. The lines show precisions of 0.5, 1.0, and 2.0 times the Horwitz function.

in FAPAS, whereas the Horwitz function is based on collaborative trials where a single well defined method is used. Where the various analytical methods used in a proficiency test are completely consistent (unbiased), no inflation of the interlaboratory precision would be expected. Where the methods are inconsistent, a bi-modal distribution would result, and such data sets were avoided in this study. Where methods are nearly consistent, some slight inflation of the precisions above the Horwitz function would be expected, and this seems to be the outcome of the present study.

There is no doubt that a Horwitz-like function with a fractional exponent describes the underlying trend of interlaboratory precisions in the FAPAS proficiency test well, although there are some interesting and probably statistically significant deviations among individual results. There are also a few systematic deviations from the general trend among natural groups of data. Thus, moisture determinations and HPLC determinations are consistently more precise than the general trend, whereas GC determinations are less precise (Fig. 2).

These conclusions may have some implications in setting targets for interlaboratory precision based on fitness-for-purpose criteria. The general approach to the examination of precision may be useful for organizers of proficiency tests.

Financial support for this work was provided by the Ministry of Agriculture, Fisheries and Food, UK.

References

1 ISO 5725:1986, *Precision of Test Methods–Determination of Repeatability and Reproducibility for a Standard Test Method by Interlaboratory Test*, International Organization for Standardization, Geneva, 1986.
2 Horwitz, W., *Pure Appl. Chem.*, 1988, **60**, 855.
3 Horwitz, W., Kamps, L. R., and Boyer, K. W., *J. Assoc. Off. Anal. Chem.*, 1980, **63**, 1344.
4 Horwitz, W., *Anal. Chem.*, 1982, **54**, 67A.
5 Boyer, K. W., Horwitz, W., and Albert, R., *Anal. Chem.*, 1985, **57**, 454.
6 ISO Guide 43:1980, *Development and Operation of Laboratory Proficiency Testing*, International Organization for Standardization, Geneva, 1980.
7 Thompson, M., and Wood, R., *Pure Appl. Chem.*, 1993, **65**, 2123.
8 Analytical Methods Committee, *Analyst*, 1989, **114**, 1693.

Paper 4/06565D
Received October 26, 1994
Accepted November 16, 1994

Orthogonal Array Design as a Chemometric Method for the Optimization of Analytical Procedures

Part 3.* Five-level Design and its Application in a Polarographic Reaction System for Selenium Determination

Wei Guang Lan, Ming Keong Wong† and Kok Kay Chee

Department of Chemistry, National University of Singapore, Kent Ridge, Singapore 0511, Republic of Singapore

Yoke Min Sin

Department of Zoology, National University of Singapore, Kent Ridge, Singapore 0511, Republic of Singapore

The theory and methodology of a five-level orthogonal array design for the optimization of analytical procedures were developed. In the theoretical section, the construction and characteristics of the $OA_{25}(5^6)$ matrix are described in detail while orthogonality is proved by means of a fourth-order polynomial model. Next, the assignment of experiments in the $OA_{25}(5^6)$ matrix is illustrated, followed by the data analysis strategy, in which significant/non-significant influence for each factor is quantitatively evaluated by the analysis of variance (ANOVA) technique including the percentage contribution, and the differences among five levels for each factor that has a significant influence are determined by Duncan's multiple *F*-test. Finally, the response surface methodology for the $OA_{25}(5^6)$ matrix is developed by using the equations obtained from the proof on orthogonality. In the application section, the reaction system for selenium determination by differential-pulse polarography, as a practical example, is employed to demonstrate the application of the $OA_{25}(5^6)$ matrix in the area of analytical chemistry.

Keywords: Five-level orthogonal array design; chemometric optimization; response surface methodology; selenium determination; differential-pulse polarography

Introduction

As the response of many analytical procedures is influenced by a variety of factors such as the medium used for the experiments and the instrumental settings employed in an analysis, optimization is a topic of interest to many chemists. Traditionally, the optimization of analytical procedures is carried out by using a one-dimensional search, the so-called one-factor-at-a-time method.[1] However, this method is often unreliable and prone to obtaining a false optimum.[2–3] As an illustration, let us consider an analytical method in which several factors need to be optimized. In the instance of the one-fact-at-a-time method, all factors except one are kept constant. This factor is then varied, and the level setting at which it yields the optimum response is ascertained. This procedure is then repeated as required for all other factors. However, regardless of which factor is being studied, the optimum level value obtained for such experiments is true only if the other conditions are kept identical. Such requirements might be impossible to achieve. At the other extreme is a full-dimensional search performed with a full factorial design. By changing all factors simultaneously, the experimental domain can be scanned efficiently and the real optimum reached. This method was first devised in the 1920s by Fisher[4] as an agricultural research tool but it was not introduced into the area of chemistry until 1947 by Smallwood.[5] Since then, full factorial design has found widespread application in optimizing analytical procedures and numerous literature is available (for example, refs. 6–9). However, one of the main difficulties in using full factorial design is that the number of experimental trials required increases geometrically with increasing factors. Hence, the total number of experimental trials expand so rapidly that it is not feasible to implement these trials.

Fortunately, in recent years, a large number of other chemometric strategies for the optimization of analytical procedures have become available, such as sequential simplex optimization,[10–14] retention mapping,[15,16] iterative regression optimization,[12,17] central composite design,[18,19] mixture design,[18,20] multi-criteria decision making,[21,22] simulated annealing,[23,24] Plackett–Burman design,[25,26] genetic algorithm,[27,28] classic fractional factorial design,[19,29] *etc.* Recently, the use of orthogonal array design as a new chemometric method for the optimization of analytical procedures has been developed by our research group. The source and background of orthogonal array design were described in detail in the first paper on this topic,[30] in which the theory and methodology for two-level orthogonal array design were also developed.[30] Indeed, as shown in Part 1 of this series,[30] for any initial experiments containing many factors to be screened, it is suitable to use a two-level orthogonal array design because a large amount of quantitative information can be extracted using only a few experimental trials. However, it has been pointed out that for continuous factors two-level orthogonal array design also suffers from two major drawbacks.[31] The first drawback is that the response is highly dependent on the high and low levels chosen. For example, if the high and low levels are set too close, the effect might not be noticeable but might be significant if the high and low levels are set further apart. The second drawback is that the non-linear trends for the response surface cannot be estimated.[30] However, in many cases the response surface cannot be adequately described by a linear

* For Part 2, see ref. 31.

† To whom correspondence should be addressed.

model; such an example has also been shown in our previous paper.[30] Therefore, it is desirable that orthogonal array design with more than two level settings is proposed and employed to optimize analytical procedures.

For the reasons mentioned above, after introducing a two-level orthogonal array design,[30] we now proposed a four-level orthogonal array design as a chemometric method for the optimization of analytical procedures.[31] As a continuation of the paper,[31] the present study further introduces the five-level orthogonal array design into the area of analytical chemistry for the optimization of analytical procedures. In the first part of the paper, the theory and methodology for five-level orthogonal array design and data analysis strategy are described in detail. To follow, the reaction system for selenium determination by differential-pulse polarography, which was reported in our previous paper,[32] is presented as a practical example to demonstrate the application of the proposed five-level orthogonal array design in the area of analytical chemistry.

Theoretical

Matrix

For any orthogonal array design, a matrix, which consists of columns and rows, with various numbers at the intersections of each column and row, must be initially constructed. In theory, five-level orthogonal array design can be expressed as the $OA_{4S+1}(5^S)$ matrix, where $4S + 1 = 5^M$ ($M = 1, 2, 3, \cdots,$). It is clear that all of the five-level orthogonal array matrices except the $OA_{25}(5^6)$ matrix are too large to be carried out in practical experiments in analytical chemistry. Therefore, in the present study, attention is focused on the $OA_{25}(5^6)$ matrix, which is displayed in Table 1, and the method of construction of the matrix is given in Appendix A. This is a five-level orthogonal array matrix that is made up of 6 columns and 25 rows. Each column represents a factor, which is an independent parameter, and each row represents an experimental trial. The numbers at the intersections indicate the level settings that apply to the factors for the experimental trials. From this matrix, it can be seen that, each of six columns is varied over five level settings, each level setting repeating five times. Therefore, a total of $5 \times 5 = 25$ experimental trials are necessary for each column. Additionally, in any two columns, the horizontal combinations of any two level numbers appear the same number of times. That is, each combination of the twenty-five ordered pairs (1, 1), (1, 2), $\cdots$, (1, 5); (2, 1), (2, 2), $\cdots$, (2, 5); $\cdots\cdots$; and (5, 1), (5, 2), $\cdots$, (5, 5) appears exactly once. Thus, when the five level numbers of a column are at level 1, for any other columns, the corresponding level numbers are at level 1, 2, 3, 4, and 5, respectively. Similar cases can be seen when the five level numbers of this column are at other four level settings. The above features of the $OA_{25}(5^6)$ matrix provide the orthogonality among all six columns. This can be proved by the following statistical method.

Table 1 $OA_{25}(5^6)$ matrix and the analytical results

Trial no.	Column no. 1	2	3	4	5	6	Experimental $\bar{y} \pm s$ ($n = 3$)	Polynomial Y^*	$\hat{y}^\dagger$	$(\bar{y} - \hat{y})$
1	1	1	1	1	1	1	0.00 ± 0.00	−12.48	−0.16	0.16
2	1	2	2	2	2	2	0.00 ± 0.00	−12.44	−0.12	0.12
3	1	3	3	3	3	3	0.00 ± 0.00	−11.98	0.34	−0.34
4	1	4	4	4	4	4	0.00 ± 0.00	−12.54	−0.22	0.22
5	1	5	5	5	5	5	0.00 ± 0.00	−12.20	0.12	−0.12
6	2	1	2	3	4	5	24.24 ± 0.92	11.69	24.01	0.23
7	2	2	3	4	5	1	12.65 ± 0.63	0.60	12.92	−0.27
8	2	3	4	5	1	2	2.19 ± 0.17	−10.42	1.90	0.29
9	2	4	5	1	2	3	8.71 ± 0.54	−3.41	8.91	−0.20
10	2	5	1	2	3	4	11.27 ± 0.73	−1.05	11.27	0.00
11	3	1	3	5	2	4	11.56 ± 0.90	−0.55	11.77	−0.21
12	3	2	4	1	3	5	21.23 ± 1.04	8.52	20.84	0.39
13	3	3	5	2	4	1	12.06 ± 0.49	−0.01	12.31	−0.25
14	3	4	1	3	5	2	13.27 ± 0.83	0.97	13.29	−0.02
15	3	5	2	4	1	3	1.78 ± 0.12	−10.67	1.65	0.13
16	4	1	4	2	5	3	21.05 ± 1.28	8.40	20.72	0.33
17	4	2	5	3	1	4	9.34 ± 0.76	−2.68	9.64	−0.30
18	4	3	1	4	2	5	11.92 ± 0.64	−0.40	11.92	0.00
19	4	4	2	5	3	1	1.28 ± 0.13	−11.25	1.07	0.21
20	4	5	3	1	4	2	12.35 ± 0.89	0.24	12.56	−0.21
21	5	1	5	4	3	2	12.78 ± 0.63	0.72	13.04	−0.26
22	5	2	1	5	4	3	7.69 ± 0.38	−4.62	7.70	−0.01
23	5	3	2	1	5	4	17.63 ± 0.92	5.09	17.41	0.22
24	5	4	3	2	1	5	6.12 ± 0.48	−5.89	6.43	−0.31
25	5	5	4	3	2	1	1.05 ± 0.10	−11.54	0.78	0.27
r_1	0.00	13.93	8.83	11.98	3.89	5.41	$u \pm s = 8.81 \pm 7.43$			
r_2	11.81	10.18	8.99	10.10	6.65	8.12	$\bar{Y} \pm s = -3.52 \pm 7.41$			
r_3	11.98	8.76	8.54	9.58	9.31	7.85	$\hat{y} \pm s = 8.80 \pm 7.41$			
r_4	11.19	5.88	9.10	7.83	11.27	9.96	$(\bar{y} - \hat{y}) \pm s = 0.00 \pm 0.23$			
r_5	9.05	5.29	8.58	4.54	12.92	12.70				

* Polynomial values excluding β_0 item.
† Polynomial values including β_0 item.

First, the following assumptions are made:

(i) Suppose all the six columns in the $OA_{25}(5^6)$ matrix are assigned an independent parameter, namely factor $A, B, \cdots,$ and F, respectively. Suppose that there are no interactions between factors, then a polynomial model representing a response surface can be expressed as:

$$y = \beta_0 + \sum_{x=A}^{F} \beta_x \phi_x + \sum_{x=A}^{F} \beta_{xx} \phi_x^2 + \sum_{x=A}^{F} \beta_{xxx} \phi_x^3 + \sum_{x=A}^{F} \beta_{xxxx} \phi_x^4 + \varepsilon \quad (1)$$

where

$$\phi_x = \frac{Z_x - \bar{Z}_x}{H_x} \quad (2)$$

in eqn. (2), suppose that

$$H_x = Z_{x2} - Z_{x1} = Z_{x3} - Z_{x2} = Z_{x4} - Z_{x3} = Z_{x5} - Z_{x4} \quad (3)$$

then

$$\bar{Z}_x = \frac{Z_{x1} + Z_{x2} + Z_{x3} + Z_{x4} + Z_{x5}}{5} = Z_{x3} \quad (4)$$

Therefore

$$\phi_{x1} = -2; \quad \phi_{x2} = -1; \quad \phi_{x3} = 0; \quad \phi_{x4} = 1; \quad \phi_{x5} = 2 \quad (5)$$

and

$$\sum_{k=1}^{5} \phi_{xk} = 0; \quad \sum_{k=1}^{5} \phi_{xk}^2 = 10; \quad \sum_{k=1}^{5} \phi_{xk}^3 = 0; \quad \sum_{k=1}^{5} \phi_{xk}^4 = 34 \quad (6)$$

(ii) Suppose that

$$E_x = \beta_x \phi_x + \beta_{xx} \phi_x^2 + \beta_{xxx} \phi_x^3 + \beta_{xxxx} \phi_x^4 \quad (7)$$

Then, the response y_i for each experimental trial can be described as follows:

$$y_i = \beta_0 + E_{Ak} + E_{Bk} + E_{Ck} + E_{Dk} + E_{Ek} + E_{Fk} + \varepsilon \quad (8)$$

where k represents the level setting numbers that vary with intersections in the $OA_{25}(5^6)$ matrix and ε is the statistical error that is an independent random variable from a $N(0, \sigma^2)$

distribution. Therefore,

$$\frac{1}{25}\sum_{i=1}^{25}\varepsilon_i \simeq 0 \qquad \frac{1}{5}\sum_{l=1}^{5}\varepsilon_i \simeq 0 \tag{9}$$

Now, a proof can be given as follows. Let us randomly select a factor at a level, *e.g.*, factor C at level 1; according to the $OA_{25}(5^6)$ matrix given in Table 1 and eqn. (8), it can be concluded that

$$\begin{aligned} R_{C1} &= y_1 + y_{10} + y_{14} + y_{18} + y_{22} \\ &= 5\beta_0 + \sum_{k=1}^{5} E_{Ak} + \sum_{k=1}^{5} E_{Bk} + 5E_{c1} \\ &\quad + \sum_{k=1}^{5} E_{Dk} + \sum_{k=1}^{5} E_{Ek} + \sum_{k=1}^{5} E_{Fk} \\ &\quad + \varepsilon_1 + \varepsilon_{10} + \varepsilon_{14} + \varepsilon_{18} + \varepsilon_{22} \end{aligned} \tag{10}$$

When combined with eqn. (7), eqn. (10) can be rewritten as

$$\begin{aligned} R_{C1} = 5\beta_0 &+ \beta_A \sum_{k=1}^{5} \phi_{Ak} + \beta_{AA} \sum_{k=1}^{5} \phi_{Ak}^2 + \beta_{AAA} \sum_{k=1}^{5} \phi_{Ak}^3 \\ &+ \beta_{AAAA} \sum_{k=1}^{5} \phi_{Ak}^4 + \beta_B \sum_{k=1}^{5} \phi_{Bk} + \beta_{BB} \sum_{k=1}^{5} \phi_{Bk}^2 \\ &+ \beta_{BBB} \sum_{k=1}^{5} \phi_{Bk}^3 + \beta_{BBBB} \sum_{k=1}^{5} \phi_{Bk}^4 \\ &+ 5(\beta_C\phi_{C1} + \beta_{CC}\phi_{C1}^2 + \beta_{CCC}\phi_{C1}^3 + \beta_{CCCC}\phi_{C1}^4) \\ &+ \beta_D \sum_{k=1}^{5} \phi_{Dk} + \beta_{DD} \sum_{k=1}^{5} \phi_{Dk}^2 + \beta_{DDD} \sum_{k=1}^{5} \phi_{Dk}^3 \\ &+ \beta_{DDDD} \sum_{k=1}^{5} \phi_{Dk}^4 + \beta_E \sum_{k=1}^{5} \phi_{Ek} + \beta_{EE} \sum_{k=1}^{5} \phi_{Ek}^2 \\ &+ \beta_{EEE} \sum_{k=1}^{5} \phi_{Ek}^3 + \beta_{EEEE} \sum_{k=1}^{5} \phi_{Ek}^4 + \beta_F \sum_{k=1}^{5} \phi_{Fk} \\ &+ \beta_{FF} \sum_{k=1}^{5} \phi_{Fk}^2 + \beta_{FFF} \sum_{k=1}^{5} \phi_{Fk}^3 + \beta_{FFFF} \sum_{k=1}^{5} \phi_{Fk}^4 \\ &+ \varepsilon_1 + \varepsilon_{10} + \varepsilon_{14} + \varepsilon_{18} + \varepsilon_{22} \end{aligned} \tag{11}$$

Substituting eqns. (6) and (9) into eqn. (11) will lead to

$$\begin{aligned} R_{C1} = 5\beta_0 &+ 10\beta_{AA} + 34\beta_{AAAA} + 10\beta_{BB} + 34\beta_{BBBB} \\ &+ 10\beta_{DD} + 34\beta_{DDDD} + 10\beta_{EE} + 34\beta_{EEEE} \\ &+ 10\beta_{FF} + 34\beta_{FFFF} \\ &+ 5(\beta_C\phi_{C1} + \beta_{CC}\phi_{C1}^2 + \beta_{CCC}\phi_{C1}^3 + \beta_{CCCC}\phi_{C1}^4) \end{aligned} \tag{12}$$

Suppose that

$$\begin{aligned} 5T_C = 5\beta_0 &+ 10\beta_{AA} + 34\beta_{AAAA} + 10\beta_{BB} \\ &+ 34\beta_{BBBB} + 10\beta_{DD} + 34\beta_{DDDD} + 10\beta_{EE} \\ &+ 34\beta_{EEEE} + 10\beta_{FF} + 34\beta_{FFFF} \end{aligned} \tag{13}$$

Then eqn. (12) can be rewritten as

$$r_{C1} = T_C + \beta_C\phi_{C1} + \beta_{CC}\phi_{C1}^2 + \beta_{CCC}\phi_{C1}^3 + \beta_{CCCC}\phi_{C1}^4 \tag{14}$$

Correspondingly

$$r_{C2} = T_C + \beta_C\phi_{C2} + \beta_{CC}\phi_{C2}^2 + \beta_{CCC}\phi_{C2}^3 + \beta_{CCCC}\phi_{C2}^4 \tag{15}$$

$$r_{C3} = T_C + \beta_C\phi_{C3} + \beta_{CC}\phi_{C3}^2 + \beta_{CCC}\phi_{C3}^3 + \beta_{CCCC}\phi_{C3}^4 \tag{16}$$

$$r_{C4} = T_C + \beta_C\phi_{C4} + \beta_{CC}\phi_{C4}^2 + \beta_{CCC}\phi_{C4}^3 + \beta_{CCCC}\phi_{C4}^4 \tag{17}$$

$$r_{C5} = T_C + \beta_C\phi_{C5} + \beta_{CC}\phi_{C5}^2 + \beta_{CCC}\phi_{C5}^3 + \beta_{CCCC}\phi_{C5}^4 \tag{18}$$

Then, by means of eqns. (5) and (14)–(18), the following equations can be obtained:

$$\beta_C = \tfrac{1}{12}\{8(r_{C4} - r_{C2}) - (r_{C5} - r_{C1})\} \tag{19}$$

$$\beta_{CC} = \tfrac{1}{24}\{16(r_{C4} + r_{C2}) - (r_{C1} + 30r_{C3} + r_{C5})\} \tag{20}$$

$$\beta_{CCC} = \tfrac{1}{12}\{(r_{C5} - r_{C1}) - 2(r_{C4} - r_{C2})\} \tag{21}$$

$$\beta_{CCCC} = \tfrac{1}{24}\{(r_{C1} + 6r_{C3} + r_{C5}) - 4(r_{C4} + r_{C2})\} \tag{22}$$

By using the similar method, the following equations for each factor can be inferred

$$\beta_X = \tfrac{1}{12}\{8(r_{X4} - r_{X2}) - (r_{X5} - r_{X1})\} \tag{23}$$

$$\beta_{XX} = \tfrac{1}{24}\{16(r_{X4} + r_{X2}) - (r_{X1} + 30r_{X3} + r_{X5})\} \tag{24}$$

$$\beta_{XXX} = \tfrac{1}{12}\{(r_{X5} - r_{X1}) - 2(r_{X4} - r_{X2})\} \tag{25}$$

$$\beta_{XXXX} = \tfrac{1}{24}\{(r_{X1} + 6r_{X3} + r_{X5}) - 4(r_{X4} + r_{X2})\} \tag{26}$$

From eqns. (5), (7) and (23)–(26), it is clear that the effect for the factor X at each level is only dependent on the averages of the responses for this factor at different levels and is independent of the effects of any other factors. Therefore, the orthogonality has been proven. As a result, the $OA_{25}(5^6)$ matrix which has only 25 trials can effectively represent the possible 5^6 (15 625) combinations, it is clear that the latter number is too large to be carried out in practical experiments.

Assignment of Experiments

The $OA_{25}(5^6)$ matrix can be viewed as a $25/5^6 = 1/625$ fraction of a full 5^6 factorial design. In this matrix, the 25 experimental trials provide a total of 24 degrees of freedom for the entire experiment, owing to each column having five level settings, *i.e.*, four degrees of freedom, six columns can be allocated. As shown in our previous papers,[30,31] it is desirable that at least one column should be used to assign a dummy factor, in which no variable (actual factor) is assigned so that the error

Table 2 ANOVA equations including percentage contribution for the $OA_{25}(5^6)$ matrix: *SS*, sum of square; df, degrees of freedom; *MS*, mean square; *SS′*, purified sum of square; and *PC*, per cent contribution

Source of Variance	*SS*	*df*	*MS*	*F*-value	*SS′*	*PC*
X	$5J\sum_{k=1}^{5}(r_{xk} - u)^2$	4	$\frac{SS_X}{4}$	$\frac{MS_X}{MS_{error}}$	$SS_X - 4MS_{error}$	$\frac{SS'_X}{SS_{total}} \times 100\%$
Error	$\sum_{i=1}^{25}\sum_{j=1}^{J}(y_{ij} - \bar{y}_i)^2$	$25(J-1)$	$\frac{SS_{error}}{I(J-1)}$		$SS_{total} - \Sigma SS'_x$	
Total	$\sum_{i=1}^{25}(y_{ij} - u)^2$	$25J-1$				

variance can be measured. Otherwise, the error variance must be obtained from the repetitions in each experimental trial.

In our statistical model mentioned above, each factor is an independent parameter, and no interactions are expected to require consideration. However, when the interactions cannot be neglected, even if a two-variable interaction with five level settings is expected to be considered, it will require $4 \times 4 = 16$ degrees of freedom, whereas each column in the $OA_{25}(5^6)$ matrix just provides four degrees of freedom. Therefore, four of the six columns must be occupied. This is to say that a two-variable interaction equals four independent parameters. Consequently, for the $OA_{25}(5^6)$ matrix, only two columns can be used to assign the main variables while the other four columns must be employed to assign a two-variable interaction. In view of this, when a two-variable interaction requires consideration, the use of the five-level orthogonal array design is not suitable. In general, when two-variable interactions are expected to be considered, it would be advisable that an orthogonal array design with two level settings instead of five level settings is used to determine the two-variable interactions before embarking on five-level orthogonal array design. The former method had been described in detail in our previous paper.[30]

Data Analysis Strategy

After conducting the experimental trials arranged by using the $OA_{25}(5^6)$ matrix and obtaining data of responses, for each factor, the five level means (r_1, r_2, r_3, r_4 and r_5) must be first calculated. Then, the analysis of variance (ANOVA) technique, including the percentage contribution, is employed to estimate the factor effects. The algorithm used is the same as that shown in our previous paper,[30] except that the equations used must be modified according to the change of the degrees of freedom. The modified equations are shown in Table 2.

It should be noted that, if replicated experiments are carried out, most publishers ask authors to report the mean values of the experimental results and the standard deviation, s, (Mean $\pm\ \sigma_{n-1}$) with a statement of the replicated number (n) instead of all the individual results of replicate experiments. Therefore, it is difficult for the readers to verify the SS_{total} by using the equations given in Table 2. However, in this event, by means of the following equation (which had been inferred in our previous work[30]):

$$\sum_{\delta=1}^{\tau} (\alpha_\delta - \bar{\alpha})^2 = (\tau - 1)\sigma^2_{\delta-1} \tag{27}$$

the equation for calculating SS_{error} in Table 2 can be rewritten as:

$$SS_{\text{error}} = (n-1) \sum_{i=1}^{25} (\sigma_{n-1})_i^2 \tag{28}$$

Then, the total variance can be calculated by using the following equation:

$$SS_{\text{total}} = SS_{\text{error}} + \Sigma SS_X \tag{29}$$

It is worth noting that the ANOVA technique including percentage contribution (shown in Table 2) provides a significant test for the different factor effects by comparing the statistics F_x to F_α. The latter is a critical value at the given degrees of freedom and significant level. However, ANOVA including the percentage contribution does not specify which of the level means is different. Thus, we recommend employing the Duncan's multiple F-test[33] to compare the differences among five level means for each factor having a significant influence. In this instance, the application of Duncan's multiple F-test is briefly described as follows:

(i) After carrying out ANOVA, for each factor that has a significant influence, the five level means are placed in order from small to large.

(ii) According to the degrees of freedom for error [$25(J-1)$, refer to Table 2] and the spans between the level means (SP), the Duncan's coefficient (ρ) is extracted from Duncan's multiple F-test coefficient tables[33] at the different significant levels.

(iii) The shortest significant ranges (SSR) are calculated according to the following equation:

$$\text{SSR} = \rho \times \sqrt{\frac{MS_{\text{error}}}{5J}} \tag{30}$$

where $5J$ represents the number of observations in each level.

(iv) The difference between two level means is compared with the corresponding SSR value, which is calculated by eqn. (30). If the former exceeds the latter, the difference is significant at the corresponding significant level. Otherwise it is not significant.

Furthermore, if one expects to estimate the effect of the factors with significant influences in the model, eqn. (1) can be simplified as

$$y = \beta_0 + \sum_{X_s} \beta_{X_s}\phi_{X_s} + \sum_{X_s} \beta_{X_s X_s}\phi^2_{X_s} + \sum_{X_s} \beta_{X_s X_s X_s}\phi^3_{X_s} + \sum_{X_s} \beta_{X_s X_s X_s X_s}\phi^4_{X_s} + \varepsilon \tag{31}$$

where the calculation of the β values is quite simple according to the equations given in eqns. (23) to (26).

Experimental

Apparatus and Reagents

Differential-pulse polarography was performed using an EG & G Princeton Applied Research Polarographic Analyzer (Princeton, NJ, USA, PAR Model 174A), equipped with a PAR Model 303 static mercury drop electrode (SMDE) and a Graphtec WX 2400 X–Y recorder (Tokyo, Japan). The reference electrode was Ag–AgCl (saturated KCl). Details of the instrumental parameters chosen and reagents used for the selenium determination have been described in our previous work.[32]

Analytical Procedures

A 5 cm^3 volume of standard selenium solution (10 μg dm^{-3}) was pipetted into a 25 cm^3 volumetric flask; A cm^3 of perchloric acid and B cm^3 of sodium sulfite solution were added and mixed well and the solution was allowed to stand for C min at room temperature. Next, D cm^3 of the buffer solution (pH 10.2), E cm^3 of potassium iodate solution and F cm^3 of gelatin solution were added and mixed thoroughly. For different experimental trials, the variables (A–F) were varied with the level setting (shown in Table 3). Then the solution was diluted with de-ionized water to the mark. Before recording a cathodic sweeping differential-pulse polarogram from -0.50 to -0.85 V, oxygen was purged from the solution by bubbling with pure nitrogen for 4 min. The peak potential of the catalytic wave was at -0.79 V *versus* Ag–AgCl (saturated KCl). Finally, the peak currents of the different experimental trials [i_p/μA] were calculated as response (y) for the $OA_{25}(5^6)$ matrix.

Results and Discussion

According to our previous work,[32] six factors needed to be considered in the present study: the volume of perchloric acid (A); the volume of sodium sulfite (B); the waiting time before

adding buffer solution (C); the volume of the buffer solution (D); the volume of the potassium iodate (E); and the volume of gelatin solution (F). The position and five different level values of six factors in the $OA_{25}(5^6)$ matrix are given in Table 3. Since no dummies were available, triplicate runs were carried out for each experimental trial to measure the error variance.

After conducting all the experiments, the mean of the response values ($\bar{y}$) and their standard deviation (σ_{n-1}) obtained were recorded and are given in Table 1. From Table 1 it can be seen that no peak current appears in experimental trials 1–5, where no perchloric acid is added (factor A at level 1). This further confirms the conclusion given in our previous work,[32] in which the reasons resulting in the above phenomenon have been described in detail.

By using eqns. (27)–(29) and the equations shown in Table 2, the ANOVA table including percentage contribution is constructed and given in Table 4. From Table 4 it is clear that all the other factors (A, B, D, E, and F) are statistically significant at $p < 0.001$, whereas no statistical difference is observed for the factor C ($p > 0.1$). The latter demonstrates that after selenite, perchloric acid and sodium sulfite were mixed well, the peak current was not affected by 'the waiting time before adding buffer solution'. This means that it is actually not necessary to stand for about 20 min, which was recommended in previous literature (ref. 32 and references cited therein). Moreover, from percentage contribution, it can be seen that the most significant effect contributing to the response is A (38.45%) and then, in order, E (19.53%), B (18.41%), D (11.80%), F (11.02%), and C (0.05%). The percentage contribution owing to error (unknown and uncontrolled factors) is low (0.74%). This means that no important variables and/or interaction are omitted in this work. Hence, it is reasonable to neglect all the interactions between factors in the present study.

For the factor that has a significant influence, the Duncan's multiple F-test[33] was implemented and the results obtained are shown in Table 5. From Table 5 it can be seen that, firstly, the best level mean for factor A is at level 3, but no significant difference is observed between level 2 and level 3 ($p > 0.05$); and, secondly the best level means for factors B, D, E, and F are at levels 1, 1, 5, and 5 respectively. In addition, for each of these factors, the level mean at the best level is significantly different from that at other levels ($p < 0.01$).

The above conclusions indicate that the best conditions for the polarographic reaction system for selenium determination are 0.25–0.50 cm^3 of perchloric acid (70%), 1.0 cm^3 of sodium sulfite solution (1.3 mol dm^{-3}), 7.0 cm^3 of NH_3–NH_4Cl buffer solution (pH 10.2), 4.5 cm^3 of potassium iodate solution (0.20 mol dm^{-3}), and no gelatin solution (0.08% m/v) is necessary. In practice, to avoid squandering perchloric acid, 0.25 cm^3 of perchloric acid is recommended. As a matter of convenience, no waiting time before adding the buffer solution is also recommended.

Furthermore, using eqns. (23)–(26), the different β values for each variable considered can be calculated. Then according to eqn. (31), the following polynomial model can be obtained

$$\begin{aligned} y = \beta_0 &- 1.17\phi_A - 0.02\phi_A^2 + 0.86\phi_A^3 - 0.46\phi_A^4 \\ &- 2.15\phi_B - 1.04\phi_B^2 + 0.31\phi_B^4 \\ &- 0.89\phi_D - 0.71\phi_D^2 - 0.24\phi_D^3 + 0.09\phi_D^4 \\ &+ 2.33\phi_E - 0.39\phi_E^2 - 0.02\phi_E^3 + 0.04\phi_E^4 \\ &+ 0.62\phi_F + 1.49\phi_F^2 + 0.30\phi_F^3 - 0.30\phi_F^4 + \varepsilon \end{aligned} \quad (32)$$

For each experimental trial, by substituing the ϕ_k values [given in eqn. (5), it should be noted that the level settings (k) for different factors are varied with the level numbers of the intersections as shown in Table 1] into eqn. (32), the polynomial value excluding β_0 item (Y) can be computed and the figures obtained are given in Table 1. Combined with eqn. (9), it is clear that the mean between u and $\bar{Y}$ can be considered as the β_0 item. Therefore, the expected value, y (polynomial value including β_0 item) and the random error item ($\varepsilon = \bar{y} - \hat{y}$) for each experimental trial can be calculated and the figures obtained are also given in Table 1. The results show that the expected value for each experimental trial (y_i) is in good agreement with the corresponding experimental value ($\bar{y}$). The mean of the random error item [$(\bar{y} - \hat{y}), i = 25$] equals

Table 3 Assignment of factors and their level values for the polarographical reaction system of selenium determination in the $OA_{25}(5^6)$ matrix

	Column no.					
	1	2	3	4	5	6
	Factor*					
Level†	A/cm^3	B/cm^3	C/min	D/cm^3	E/cm^3	F/cm^3
1	0.00	1.00	20	7.00	0.50	2.00
2	0.25	2.00	15	6.00	1.50	1.50
3	0.50	3.00	10	5.00	2.50	1.00
4	0.75	4.00	5	4.00	3.50	0.50
5	1.00	5.00	0	3.00	4.50	0.00

* A, 70% perchloric acid; B, 1.3 mol dm^{-3} of sodium sulfite; C, waiting time before adding buffer solution; D, NH_3–NH_4Cl buffer solution (pH 10.2); E, 0.2 mol dm^{-3} potassium iodate; F, 0.08% (m/v) of gelatin.

† Level value for each factor is (i) satisfied with the definition given in eqn. (3); and (ii) randomly arranged from low to high or *vice versa*.

Table 4 ANOVA table including percentage contribution (PC) for experimental responses in the $OA_{25}(5^6)$ matrix

Source	SS	df	MS	F	SS'	PC(%)
$HClO_4$ (A)	1535.80	4	383.95	959.88*	1534.20	38.45
Na_2SO_3 (B)	736.04	4	184.01	460.02*	734.44	18.41
Time (C)	3.64	4	0.91	2.28†	2.04	0.05
Buffer (D)	472.49	4	118.12	295.30*	470.89	11.80
KIO_3 (E)	780.98	4	195.24	488.10*	779.38	19.53
Gelatin (F)	441.18	4	110.30	275.75*	439.58	11.02
Error	19.99	50	0.40		29.59	0.74
Total	3990.12	74			3990.12	100.00

* Critical value 5.45 ($p < 0.001$).
† Critical value 2.58 ($p < 0.05$).

Table 5 Worksheet of the Duncan's multiple F-test for each factor at different levels*

	SP (SSR at $p = 0.01$)				
	2 (0.61)	3 (0.62)	4 (0.65)	5 (0.67)	
A	r_1 (0.00)	r_5(9.05)	r_4(11.19)	r_2(11.81)	r_3(11.98)†
B	r_5(5.29)	r_4(5.88)	r_3(8.76)	r_2(10.81)	r_1(13.93)
D	r_5(4.54)	r_4(7.83)	r_3(9.58)	r_2(10.10)	r_1(11.98)
E	r_1(3.89)	r_2(6.65)	r_3(9.31)	r_4(11.27)	r_5(12.92)
F	r_1(5.41)	r_2(8.12)	r_3(7.85)	r_4(9.96)	r_5(12.70)

* Any two level means not underscored by the same line are significantly different ($p < 0.01$). Any two level means underscored by the same line are not significantly different ($p > 0.01$).
† $p > 0.05$ [$SSR_{(2,50;0.05)}$ is 0.45].

zero (see Table 1), which is in accord with the assumption given in eqn. (9). This means that the fourth-order polynomial model given in eqn. (32) can adequately and accurately represent the response surface for the present study.

Further, in order to precisely express the relationship between output response (y) and input factor value (Z), eqn. (2) with the known Z_x and H_x values should be substituted into eqn. (32), then the following equation can be obtained

$$\begin{aligned} y = {} & 25.00 + 95.80Z_A - 29.39Z_B - 19.01Z_D + 1.40Z_E \\ & -1.16Z_F - 259.52Z_A^2 + 15.70Z_B^2 + 9.19Z_D^2 \\ & + 1.26Z_E^2 - 15.64Z_F^2 + 290.56Z_A^3 - 3.72Z_B^3 \\ & -1.56Z_D^3 - 0.42Z_E^3 + 16.80Z_F^3 - 117.76Z_A^4 \\ & + 0.31Z_B^4 + 0.09Z_D^4 + 0.04Z_E^4 - 4.80Z_F^4 + \varepsilon \end{aligned} \quad (33)$$

Finally, to confirm the validity of the optimization procedure, additional experiments using the best conditions described above (A_2, B_1, C_5, D_1, E_5, and F_5) were performed. The result demonstrated that when compared with that results obtained from 25 experimental trials in the $OA_{25}(5^6)$ matrix, the largest response value (27.62 ± 0.98, $n = 3$) could be achieved. However, the theoretical value predicted by using eqn. (33) is 27.91, which is in good agreement with the former experimental value.

Conclusions

This report discusses an application of the five-level orthogonal array design for the optimization of analytical procedures. When compared with two-level orthogonal array design, more exact relationships between output responses and input variables can be extracted by using five-level orthogonal array design. However, care should be taken as the practical application of five-level orthogonal array design is strongly limited by the presupposition of absence of interactions between factors. In fact, for the $OA_{25}(5^6)$ matrix, if more than two-variable interactions cannot be neglected in addition to two variables requiring consideration, it is impossible to obtain a 'Resolution IV' or 'Resolution V' design. In this instance, it is advisable to use orthogonal array design with two level settings instead of five level settings so as to avoid confounding between main variables and/or two-variable interactions.

In our previous paper,[31] we recommended the use of the polynomial model established with derivative algorithm for estimating the optimum input variable value for each variable considered. Indeed by using this method, the optimum value can be precisely obtained. However, in many instances it may not always be necessary to choose the best experimental condition according to the optimum value acquired because the departure from the optimum value obtained may not always cause the significant variation. For this reason, in this work, we employed Duncan's multiple F-test instead of the polynomial model established with derivative algorithm to decide the best experimental condition for each variable considered. One of the most obvious advantages is that the computational burden of the former method is much smaller than that of the latter.

W. G. Lan thanks the National University of Singapore for the award of a research studentship to read for a PhD degree. This work was supported by a grant from the National University of Singapore (RP 920634).

Appendix A. Construction of the $OA_{25}(5^6)$ Matrix

Suppose that the level settings of the columns 1, 2, 3, 4, 5, and 6 in the $OA_{25}(5^6)$ matrix can be expressed as f_1, f_2, f_3, f_4, f_5 and f_6, respectively, then:

(*i*) Two basic columns (f_1 and f_2) can be constructed by writing five level settings (1, 2, 3, 4, and 5), each level setting is repeated five times. More precisely, for f_1, level 1 is repeated five times, and then level 2, 3, 4, and 5, respectively; for f_2, the five level settings from 1 to 5 are first written in order, and then they are repeated four times.

(*ii*) The columns except for the two basic columns can be constructed by the generating equations described as follows $f_3 = f_2 + (f_1 - 1)$; $f_4 = f_2 + 2(f_1 - 1)$; $f_5 = f_2 + 3(f_1 - 1)$; and $f_6 = f_2 + 4(f_1 - 1)$. All calculations are done in modulo 5 arithmetic (that is, an integer larger than five is replaced with its remainder after division by five).

Hence, the $OA_{25}(5^6)$ matrix shown in Table 1 is constructed.

Appendix B. Definitions of Symbols

β_0	Constant term of the polynomial model, where the input variable is ϕ_X.
β_X	Coefficient of the first-order effect for the factor X, where the input variable is ϕ_X.
β_{XX}	Coefficient of the second-order effect for the factor X, where the input variable is ϕ_X.
β_{XXX}	Coefficient of the third-order effect for the factor X, where the input variable is ϕ_X.
β_{XXXX}	Coefficient of the fourth-order effect for the factor X, where the input variable is ϕ_X.
ρ	Duncan's coefficient.
E_X	Effect of the factor X, when X is at level k, E_X is expressed as E_{Xk}.
H_X	Difference between the level value at level k and that at level $k + 1$. Where $k = 1, 2, 3, 4$.
i	Number of the experimental trials, $i = 1, 2, \ldots, 25$.
j	Number of the observed responses, $j = 1, 2, \ldots, J$.
k	Number of the level settings, unless otherwise specified, $k = 1, 2, \ldots 5$.
l	Number of the replications for the different experimental trials at the same level setting, $l = 1, 2, \ldots 5$.
SP	Span between the level means.
SSR	Shortest significant ranges.
$\hat{y}$	Polynomial value including the β_0 term.
Y	Polynomial value excluding the β_0 term.
$\bar{Y}$	Average of the polynomial value excluding the β_0 term.
Z_X	Any value between Z_{X1} and Z_{X5} for factor X, when X is at level k, Z_X is expressed as X_{Xk}.
$\bar{Z}_X$	Average of the sum of the Z_{X1}, Z_{X2}, ..., and Z_{X5} for factor X.

For other symbols used in the text, the reader is referred to Appendix D of ref. 30 (Part 1 of this series).

References

1 Van Ryswyk, H., and Van Hecke, G. R., *J. Chem. Educ.*, 1991, **68**, 878.
2 Wold, S., Sjostrom, M., Carlson, R., Lundstedt, T., Hellberg, S., Skagerberg, B., Wikstrom, C., and Ohman, J., *Anal. Chim Acta*, 1986, **191**, 17.
3 Grossman, O., *Anal. Chim. Acta*, 1986, **186**, 185.
4 Fisher, R. A., *The Design of Experiments*, Oliver and Boyd, Edinburgh, 4th edn., 1947.
5 Smallwood, H. M., *Ind. Eng. Chem., Anal. Ed.*, 1947, **19**, 950.
6 McMinn, D. G., Eatherton, R. L., and Hill, H. H., *Anal. Chem.*, 1984, **56**, 1293.
7 Dachs, J., and Bayona, J. M., *J. Chromatogr.*, 1993, **636**, 277.
8 Olsson, N. U, and Kaufmann, P., *J. Chromatogr.*, 1990, **600**, 257.

9 Bicking, M. K. L., *J. Chromatogr. Sci.*, 1992, **30**, 358.
10 Walters, F. H., Parker, L. R., Morgan, S. L., and Deming, S. N., *Sequential Simplex Optimization*, CRC Press, Boca Raton, FL, 1991.
11 Burton, K. W. C., and Nickless, G., *Chemom. Intell. Lab. Syst.*, 1987, **1**, 135.
12 Berridge, J. C., *Chemom. Intell. Lab. Syst.*, 1989, **5**, 195.
13 Morgan, E., Burton, K. W., and Nickless, G., *Chemom. Intell. Lab. Syst.*, 1990, **7**, 209.
14 Morgan, E., Burton, K. W., and Nickless, G., *Chemom. Intell. Lab. Syst.*, 1990, **8**, 97.
15 Glajch, J. L., and Kirkland, J. J., *J. Chromatogr.*, 1989, **485**, 51.
16 Glajch, J. L., Kirkland, J. J., Squire, K. M., and Minor, J. M., *J. Chromatogr.*, 1980, **199**, 57.
17 Strasters, J. K., Kim, S. T., and Khaledi, M. G., *J. Chromatogr.*, 1991, **566**, 221.
18 Deming, S. N., Palasota, J. A., and Palasota, J. M., *J. Chemom.*, 1991, **5**, 181.
19 Morgan, E., Burton, K. W., and Church, P. A., *Chemom. Intell. Lab. Syst.*, 1989, **5**, 104.
20 Palasota, J. M., and Deming, S. N., *Anal. Chim. Acta*, 1992, **270**, 13.
21 Hendriks, M. M. W. B., De Boer, J. H., Smilde, A. K., and Doornbos, D. A., *Chemom. Intell. Lab. Syst.*, 1992, **16**, 175.
22 Keller, H. R., Massart, D. L., and Brans, J. P., *Chemom. Intell. Lab. Syst.*, 1991, **11**, 175.
23 Kalivas, J. H., *Chemom. Intell. Lab. Syst.*, 1992, **15**, 1.
24 Shew, S. L., and Olson, C. L., *Anal. Chem.*, 1992, **64**, 1546.
25 Jones, K., *J. Chromatogr.*, 1987, **392**, 1.
26 Vindevogal, J., and Sandra, P., *Anal. Chem.*, 1991, **63**, 1530.
27 Lucasius, C. B., and Kateman, G., *Chemom. Intell. Lab. Syst.*, 1992, **19**, 1.
28 Hibbert, D. B., *Chemom. Intell. Lab. Syst.*, 1993, **19**, 277.
29 Renard, L., Moulin, G., and Sanders, P., *J. AOAC Int.*, 1992, **75**, 1045.
30 Lan, W. G., Wong, M. K., Chen, N., and Sin, Y. M., *Analyst*, 1994, **119**, 1659, and references cited therein.
31 Lan, W. G., Wong, M. K., Chen, N., and Sin, Y. M., *Analyst*, 1994, **119**, 1669, and references cited therein.
32 Lan, W. G., Wong, M. K., and Sin, Y. M., *Talanta*, 1994, **41**, 53, and references cited therein.
33 Duncan, D. B., *Biometrics*, 1955, **11**, 1.

Paper 4/01791I
Received March 25, 1994
Accepted July 1, 1994

Orthogonal Array Design as a Chemometric Method for the Optimization of Analytical Procedures

Part 4.* Mixed-level Design and its Application to the High-performance Liquid Chromatographic Determination of Polycyclic Aromatic Hydrocarbons

Wei Guang Lan, Kok Kay Chee, Ming Keong Wong† and Hian Kee Lee

Department of Chemistry, National University of Singapore, Kent Ridge, Singapore 0511, Republic of Singapore

Yoke Min Sin

Department of Zoology, National University of Singapore, Kent Ridge, Singapore 0511, Republic of Singapore

The theory and methodology of a mixed-level orthogonal array design for the optimization of analytical procedures is described. Firstly, the method of construction of a mixed-level orthogonal array design is discussed in detail, followed by the assignment of experiments and the data analysis strategy in the design. The optimization of the parameters involved in the high-performance liquid chromatographic determination of polycyclic aromatic hydrocarbons is then employed to demonstrate the practical application of the proposed mixed-level orthogonal array design in the area of analytical chemistry.

Keywords: *Mixed-level orthogonal array design; optimization; chemometric method; high-performance liquid chromatography; polycyclic aromatic hydrocarbon*

Introduction

In the previous parts to this series,[1–3] the theory and methodology for orthogonal array design as a chemometric method for the optimization of analytical procedures have been described in detail. We believe that the two-level design discussed in Part 1 of this series[1] is particularly useful because a large number of main-variables and two-variable interactions can be considered simultaneously and a large amount of quantitative information can be extracted with only a few experimental trials. For this reason, we recommend that an initial experimental investigation should begin with a two-level design whenever possible. Once the significant factors are identified, multiple-level design, as discussed in Parts 2 and 3 of this series[2–3] can then be used for estimating non-linear responses. However, in these papers,[1–6] we have considered an orthogonal array design in which all the factors have the same number of level settings. In a practical instance, not all of the variables are expected to be considered at the same number of levels. For example, when other factors have two-level setting numbers, there are some situations in which a factor (or a few factors) will be assigned to an experiment and more than two levels will be required. More specifically, for a qualitative variable, often more than two levels must be considered simultaneously. For a quantitative variable, a non-linear response would be expected. However, for other variables, two-level settings are necessary in order to avoid using a relatively large orthogonal array matrix. Therefore, it would be helpful to introduce mixed-level orthogonal array design into the area of analytical chemistry.

Polycyclic aromatic hydrocarbons (PAHs) are important environmental pollutants because of their ubiquitous presence and their carcinogenic, mutagenic and toxic potential.[7–9] While hundreds of PAHs exist in the environment, 16, in particular, have been selected by the United States Environmental Protection Agency (USEPA) as Consent Decree priority pollutants for regulatory purposes.[10]

Chromatography has been the basis of many analytical methods used for determining PAHs.[11–18] However, owing to the very slight differences in their properties, for example, polarity and polarizability, it is often encountered that various PAHs cannot be easily separated from each other.[19] For this reason, it is desirable to optimize chromatographic conditions in order to improve the separation efficiency of PAHs. Some research has been focused on this topic.[19–21]

In this report the theory and methodology of mixed-level orthogonal array design for the optimization of analytical procedures has been developed. Subsequently, optimization of the parameters for high-performance liquid chromatographic determination of polycyclic aromatic hydrocarbons is described as a practical example to demonstrate the application of the proposed mixed-level orthogonal array design.

Theoretical

Construction Method of Mixed-level Orthogonal Array Design

As an example, let us randomly choose two columns in the $OA_8(2^7)$ matrix (see Table 1 in ref. 1), *e.g.*, column 1 and 2. It is clear that there are four combinations of levels 1 and 2: (1, 1), (1, 2), (2, 1), and (2, 2), which correspond to the levels 1, 2, 3, and 4, respectively, for the four-level column in the mixed-level orthogonal array matrix. However, one column in the two-level design provides only one degree of freedom whereas one four-level column must have three degrees of

* For Part 3, see ref. 3.

† To whom correspondence should be addressed.

freedom. Therefore, in order to construct a four-level column, a total of three two-level columns in the original two-level orthogonal array matrix must be merged. For example, when two columns in the original two-level design are used for constructing a new four-level column, another two-level column must be deleted in order to provide an additional degree of freedom to meet the requirements of the four-level column; otherwise, the orthogonality of the newly formed mixed-level orthogonal array matrix would be destroyed. As for which two-level column needs to be deleted, one can check the balance between the newly formed four-level column and any other two-level column. For the above example, in the $OA_8(2^7)$ matrix, except for column 3, there is a balance between the newly formed four-level column and one of the any two-level columns, in which (1, 1), (1, 2), (2, 1), (2, 2), (3, 1), (3, 2), (4, 1), and (4, 2) appear once, respectively. However, non-balance can be observed between the newly formed four-level column and column 3, in which (1, 1), (2, 2), (3, 2), and (4, 1) appear twice, respectively, whereas (1, 2), (2, 1), (3, 1) and (4, 2) do not appear. Obviously, column 3 in the $OA_8(2^7)$ matrix must be deleted. This is to say that, in the $OA_8(2^7)$ matrix, if column 1 is combined with column 2 for constructing a new four-level column, then column 3 must be deleted. Subsequently, once the numbers of columns in the original two-level design are renamed, the $OA_8(4^1 \times 2^4)$ matrix-a type of mixed-level orthogonal array design will be obtained (as shown in Table 1).

Note that column 3 is the interaction column of columns 1 and 2 (refer to Table 3 in ref. 1). More interestingly, one can find if columns A and B are randomly chosen to construct a new four-level column and in this case if column C needs to be deleted, then it will be certain that column C is the interaction column of columns A and B. In practice, the above conclusion can be considered as a rule for constructing a new four-level column from the original two-level design. It should be pointed out that for the $OA_8(2^7)$ matrix, no second four-level column can be constructed because the column needing to be deleted has been used to construct the first four-level column (refer to Table 3 in ref. 1). As a result, for the $OA_8(2^7)$ matrix, just one mixed-level orthogonal array matrix, the $OA_8(4^1 \times 2^4)$ matrix can be constructed. However, up to four mixed-level orthogonal array matrices can be derived from the $OA_{16}(2^{15})$ matrix according to Tables 2 and 4 in ref. 1, and the rule stated above. If column 1 and column 2 are combined, and column 3 is deleted in the $OA_{16}(2^{15})$ matrix, then the $OA_{16}(4^1 \times 2^{12})$ matrix will be constructed (as shown in Table 2). In the combination of column 1 and column 2, column 4 and column 8, and the deletion of columns 3 and 12 in the $OA_{16}(2^{15})$ matrix, the $OA_{16}(4^2 \times 2^9)$ matrix is constructed (as shown in Table 3). If column 1 and column 2, column 4 and column 8, and column 5 and column 10 are combined, and columns 3, 12 and 15 are deleted, in the $OA_{16}(2^{15})$ matrix, then the $OA_{16}(4^3 \times 2^6)$ matrix is constructed (as shown in Table 4). The combination of column 1 and column 2, column

Table 1 $OA_8(4^1 \times 2^4)$ matrix

	Column no.				
	1	2	3	4	5
1	1	1	1	1	1
2	1	2	2	2	2
3	2	1	1	2	2
4	2	2	2	1	1
5	3	1	2	1	2
6	3	2	1	2	1
7	4	1	2	2	1
8	4	2	1	1	2

Table 2 $OA_{16}(4^1 \times 2^{12})$ matrix with experimental results

	Column no.													Response	
	1	2	3	4	5	6	7	8	9	10	11	12	13	ndp	*IC*
1	1	1	1	1	1	1	1	1	1	1	1	1	1	16	1.55
2	1	1	1	1	1	2	2	2	2	2	2	2	2	15	1.67
3	1	2	2	2	2	1	1	1	1	2	2	2	2	6	0.77
4	1	2	2	2	2	2	2	2	2	1	1	1	1	6	0.77
5	2	1	1	2	2	1	1	2	2	1	1	2	2	15	3.50
6	2	1	1	2	2	2	2	1	1	2	2	1	1	15	3.62
7	2	2	2	1	1	1	1	2	2	2	2	1	1	16	3.88
8	2	2	2	1	1	2	2	1	1	1	1	2	2	16	3.75
9	3	1	2	1	2	1	2	1	2	1	2	1	2	12	2.15
10	3	1	2	1	2	2	1	2	1	2	1	2	1	13	2.70
11	3	2	1	2	1	1	2	1	2	2	1	2	1	6	0.53
12	3	2	1	2	1	2	1	2	1	1	2	1	2	6	0.53
13	4	1	2	2	1	1	2	2	1	1	2	2	1	12	2.75
14	4	1	2	2	1	2	1	1	2	2	1	1	2	14	3.26
15	4	2	1	1	2	1	2	2	1	2	1	1	2	10	2.00
16	4	2	1	1	2	2	1	1	2	1	2	2	1	12	2.58
ndp—															
r_1	10.8	14.0	11.9	13.8	12.6	11.6	12.2	12.1	11.8	11.9	12.0	11.9	12.0		
r_2	15.5	9.8	11.9	10.0	11.1	12.1	11.5	11.6	12.0	11.9	11.8	11.9	11.8		
r_3	9.2														
r_4	12.0														
IC—															
r_1	1.19	2.65	2.00	2.53	2.24	2.14	2.35	2.28	2.21	2.20	2.26	2.22	2.30		
r_2	3.69	1.85	2.50	1.97	2.26	2.36	2.16	2.23	2.29	2.31	2.24	2.28	2.20		
r_3	1.48														
r_4	2.65														

4 and column 8, column 5 and column 10, and column 7 and column 9, and deletion of columns 3, 12, 15, 14 in the $OA_{16}(2^{15})$ matrix, gives the $OA_{16}(4^4 \times 2^3)$ matrix shown in Table 5. Finally, the combination of column 1 and column 2, column 4 and column 8, column 5 and column 10, column 7 and column 9, column 6 and column 11, and deletion of columns 3, 12, 15, 14, 13 in the $OA_{16}(2^{15})$ matrix, give the $OA_{16}(4^5)$ matrix, which has previously been given in Table 1 of Part 2 of this series.[2]

Assignment of Experiments

In principle, the assignment of experiments in a mixed-level orthogonal array design is the same as that in the two-level orthogonal array design except that a variable (or variables) with four level settings must be assigned to the four-level column (or columns). Another exception, is the assignment of the interaction between the four-level variable and any other two-level variable. It is well known that one four-level column contains three degrees of freedom whereas one two-level column has one degree of freedom, and thus the interaction between a four-level column (A) and a two-level column (B) has $3 \times 1 = 3$ degrees of freedom. Consequently, for the interaction between a four-level column and a two-level column, three two-level columns have to be occupied. Furthermore, the three two-level columns occupied should be those interaction columns between column B and three original two-level columns which have been used for constructing column A. For example, if the interaction between column 1 (four-level column) and column 2 [which is in reality column 4 in the orignal $OA_{16}(2^{15})$ matrix] in the $OA_{16}(4^1 \times 2^{12})$ matrix is considered, then one must firstly refer to the original $OA_{16}(2^{15})$ matrix, because the four-level column is derived from columns 1, 2, and 3 in the original $OA_{16}(2^{15})$ matrix. According to the triangular table associated with the original $OA_{16}(2^{15})$ matrix (refer to Table 4 in ref. 1), it is clear that the interaction columns between columns 1, 2, 3 and 4 are 5, 6, and 7, respectively. Therefore, the interaction between column 1 (four-level column) and column 2 [which is in reality column 4 in the original $OA_{16}(2^{15})$ matrix] in the $OA_{16}(4^1 \times 2^{12})$ matrix should be columns 3, 4 and 5 [which are in reality column 5, 6, and 7, respectively in the original $OA_{16}(2^{15})$ matrix]. As a matter of convenience, the assignment table of the main variables and two-variable interactions in the $OA_{16}(4^1 \times 2^{12})$ matrix is constructed according to the corresponding triangular table associated with the $OA_{16}(2^{15})$ matrix (Table 4 in ref. 1) and shown in Table 6.

Table 3 $OA_{16}(4^2 \times 2^9)$ matrix

	Column no.										
	1	2	3	4	5	6	7	8	9	10	11
1	1	1	1	1	1	1	1	1	1	1	1
2	1	2	1	1	1	2	2	2	2	2	2
3	1	3	2	2	2	1	1	1	2	2	2
4	1	4	2	2	2	2	2	2	1	1	1
5	2	1	1	2	2	1	2	2	1	2	2
6	2	2	1	2	2	2	1	1	2	1	1
7	2	3	2	1	1	1	2	2	2	1	1
8	2	4	2	1	1	2	1	1	1	2	2
9	3	1	2	1	2	2	1	2	2	1	2
10	3	2	2	1	2	1	2	1	1	2	1
11	3	3	1	2	1	2	1	2	1	2	1
12	3	4	1	2	1	1	2	1	2	1	2
13	4	1	2	2	1	2	2	1	2	2	1
14	4	2	2	2	1	1	1	2	1	1	2
15	4	3	1	1	2	2	2	1	1	1	2
16	4	4	1	1	2	1	1	2	2	2	1

Table 4 $OA_{16}(4^3 \times 2^6)$ matrix

	Column no.								
	1	2	3	4	5	6	7	8	9
1	1	1	1	1	1	1	1	1	1
2	1	2	2	1	1	2	2	2	2
3	1	3	3	2	2	1	1	2	2
4	1	4	4	2	2	2	2	1	1
5	2	1	2	2	2	1	2	1	2
6	2	2	1	2	2	2	1	2	1
7	2	3	4	1	1	1	2	2	1
8	2	4	3	1	1	2	1	1	2
9	3	1	3	1	2	2	2	2	1
10	3	2	4	1	2	1	1	1	2
11	3	3	1	2	1	2	2	1	2
12	3	4	2	2	1	1	1	2	1
13	4	1	4	2	1	2	1	2	2
14	4	2	3	2	1	1	2	1	1
15	4	3	2	1	2	2	1	1	1
16	4	4	1	1	2	1	2	2	2

Table 5 $OA_{16}(4^4 \times 2^3)$ matrix

	Column no.						
	1	2	3	4	5	6	7
1	1	1	1	1	1	1	1
2	1	2	2	2	1	2	2
3	1	3	3	3	2	1	2
4	1	4	4	4	2	2	1
5	2	1	2	3	2	2	1
6	2	2	1	4	2	1	1
7	2	3	4	1	1	2	2
8	2	4	3	2	1	1	1
9	3	1	3	4	1	2	2
10	3	2	4	3	1	1	1
11	3	3	1	2	2	2	1
12	3	4	2	1	2	1	2
13	4	1	4	2	2	1	2
14	4	2	3	1	2	2	1
15	4	3	2	4	1	1	1
16	4	4	1	3	1	2	2

Data Analysis Strategy

After the mixed level orthogonal array design has been conducted, the analysis of variance (ANOVA) technique including percentage contribution is used for estimating the factor effects. For four-level columns, the algorithm used is the same as that shown in the previous paper[2] describing four-level orthogonal array design; and for two-level columns, the algorithm used is the same as that shown in the earlier paper[1] which discussed a two-level orthogonal array design.

Furthermore, if all the factors having significant influences are quantitative variables, the polynomial model representing response surface can be expressed as follows:

$$y = \beta_0 + \sum_{X_{s4}} \beta_{X_{s4}} \phi_{X_{s4}} + \sum_{X_{s4}} \beta_{X_{s4} X_{s4}} \phi^2_{X_{s4}} + \sum_{X_{s4}} \beta_{X_{s4} X_{s4} X_{s4}} \phi^3_{X_{s4}} + \sum_{X_{s2}} \beta_{X_{s2}} \phi_{X_{s2}} + \varepsilon \quad (1)$$

where the definitions of symbols is the same as that given in Part 1 and 2 of this series except that X_{s4} stands for four-level

factors and X_{s2} stands for two-level ones. Note that the estimate of first-, second-, and third-order coefficients for four-level column(s) ($\beta_{X_{s4}}$,$\beta_{X_{s4}X_{s4}}$,$\beta_{X_{s4}X_{s4}X_{s4}}$) is the same as that described in Part 2 of this series whereas the estimate of first-order coefficient for two-level columns ($\beta_{X_{s2}}$) is the same as that described in Part 1 of this series. Nevertheless, care should be given to when one or more qualitative variables assigned in a mixed-level orthogonal array matrix (have) a significant influence. In this case, it is not appropriate to establish a polynomial model representing the response surface. The reason for which has been explained in detail in Part 1 of this series.

Experimental

Instrumentation and Reagents

High-performance liquid chromatography (HPLC) was performed using the Waters (Milford, MA, USA) Powerline system, comprising the Waters 600E systems controller, Waters 486 Turnable Absorbance Detector and Waters 700 Satellite WISP autosampler. The Maxima 825/Baseline 815 Powerline HPLC software was used to control the HPLC system. For ultraviolet (UV) detection, the wavelength was set at 254 nm.

The following columns were used: 1, Nova-Pak C_{18} column (Waters) (150 mm × 3.9 mm i.d.; 4 μm particle size); 2, Spherex C_{18} column (Phenomenex, Torrance, CA, USA) (250 mm × 4.6 mm i.d.; 5 μm particle size); 3, μ-Bondapak C_{18} column (Waters) (300 mm × 4.6 mm i.d.; 10 μm particle size); 4, LiChrosorb RP-18 column (HiChrom, Berkshire, UK) (250 mm × 4.6 mm I.D.; 5 μm particle size).

PAH standards (naphthalene, acenaphthene, acenaphthylene, fluorene, phenanthrene, anthracene, fluoranthene, pyrene, benz[*a*]anthracene, chrysene, benzo[*b*]fluoranthene, benzo[*k*]fluoranthene, benzo[*a*]pyrene, dibenzo[*a*,*h*]-anthracene, benzo[ghi]perylene and indeno[1,2,3-cd]pyrene) were obtained from Ultra-Scientific (North Kingston, RI, USA) and were of analytical-reagent grade.

Standards were prepared in methanol at a concentration level of 12.5 mg dm^{-3} for each component. The acetonitrile, methanol and methylene chloride (Fisher Scientific, Pittsburgh, PA, USA) used were of HPLC-grade. Analytical-reagent grade water was obtained from a Millipore Milli-Q (Milford, MA, USA) system.

Optimization Strategy

On the basis of the previous publications related to the liquid chromatographic determination of PAHs, the following six variables are chosen in the present study for optimization to obtain the best separation efficiency: four packed standard columns (factor *A*); the percentage of acetonitrile (factor *B*); the percentage of methanol (factor *C*); initial time (factor *D*); program time (factor *E*); and flow rate (factor *F*). Because one four-level variable and five two-level variables are to be optimized, the $OA_{16}(4^1 \times 2^{12})$ matrix is employed to assign the variables considered, and for the two-variable interactions which may occur. From the chemical viewpoint, the following interactions: $A \times B$, $A \times C$, $A \times D$, $A \times E$, and $B \times C$ should be considered. Therefore, with reference to Table 6, positions of the main-variables chosen and those interactions considered in the $OA_{16}(4^1 \times 2^{12})$ matrix are assigned and shown in Table 7. In addition, level setting values of the main-variables used in mixed-level orthogonal array design are displayed in Table 7.

Two response functions, the number of distinguishable peaks (ndp) and the individual contributions (*IC*), which had been used and described in detail in our previous paper,[5] were chosen to judge the quality of the chromatograms. A distinguishable peak means that the top of the peak is not obscured by other peaks. The simplicity is the most obvious advantage when using ndp as the response function. However, care should be given that ndp is a discrete response. This means that if ndp is employed as response function, no polynomial model representing response surface can be established. Individual contributions can be defined as follows: if a mixture of n components is chromatographed and the resulting chromatogram is composed of k_1 singlets, k_1 doublets and k_p p-multiplets with $\Sigma\ (pk_p) = n$, the contribution of the p-multiplets to the quantity of information is given by

$$I_p = (pk_p/n)\log_2(n/p) \qquad (2)$$

Table 6 Assignment table of the factors in the $OA_{16}(4^1 \times 2^{12})$ matrix

	Column no.												
n	1	2	3	4	5	6	7	8	9	10	11	12	13
3	*A*	*B*	$(A \times B)_1$	$(A \times B)_2$	$(A \times B)_3$	*C*	$(A \times C)_1$	$(A \times C)_2$	$(A \times C)_3$	$B \times C$			
4	*A*	*B*	$(A \times B)_1$ $C \times D$	$(A \times B)_2$	$(A \times B)_3$	*C*	$(A \times C)_1$ $B \times D$	$(A \times C)_2$	$(A \times C)_3$	$B \times C$ $(A \times D)_1$	*D*	$(A \times D)_2$	$(A \times D)_3$
5	*A* $D \times E$	*B*	$(A \times B)_1$ $C \times D$	$(A \times B)_2$ $C \times E$	$(A \times B)_3$	*C*	$(A \times C)_1$ $B \times D$	$(A \times C)_2$ $B \times E$	$(A \times C)_3$	$B \times C$ $(A \times D)_1$ $(A \times E)_3$	*D* $(A \times E)_2$	*E* $(A \times D)_2$	$(A \times D)_3$ $(A \times E)_1$

Table 7 Assignment of factors and level settings for liquid chromatographic determination of PAHs in the $OA_{16}(4^1 \times 2^{12})$ matrix

		Column no.												
Level		1	2	3	4	5	6	7	8	9	10	11	12	13
		A	*B*	$(A \times B)_1$	$(A \times B)_2$ $C \times E$	$(A \times B)_3$	*C*	$(A \times C)_1$	$(A \times C)_2$	$(A \times C)_3$	$B \times C$ $(A \times D)_1$ $(A \times E)_3$	*D* $(A \times E)_2$	*E* $(A \times D)_2$	*F* $(A \times D)_3$ $(A \times E)_1$
1	Column 1	50					5					0	25	0.8
2	Column 2	80					0					6	10	1.2
3	Column 3													
4	Column 4													

where pk_p/n is the appearance frequency and $\log_2(n/p)$ is the quantity of specific information brought by the identification of a component in a p-multiplet. The total information from the chromatogram is the sum of the IC of each peak group:

$$IC = \Sigma(pk_p/n)\log_2(n/p) \quad (3)$$

The value of IC varies between zero [when all the components co-elute ($p = n$, $k_p = 1$)], and $\log_2(n)$ [when all the components are separated from each other ($p = 1$, $k_p = n$)].

Results and Discussion

After implementing 16 experimental trials, that were pre-designed according to the $OA_{16}(4^1 \times 2^{12})$ matrix, and obtaining the corresponding chromatograms, for each experimental trial, IC was calculated according to eqn. (3), and the ndp computed. The results obtained are listed in Table 2. The average of the response for each factor at different levels was also calculated and is given in Table 2. As stated above, the ndp is a discrete response. However, in order to eliminate rounding error for ANOVA, this response is assumed to be a continuous function when r_1 and r_2 are calculated.

Based on the methods presented in Parts 1 and 2 of this series, the results of sums of squares for different variables and the so-called interaction columns are first calculated. These are given in Table 8 (ndp) and Table 9 (IC). It is obvious that when either ndp or IC is chosen as a response, the interactions assigned to columns 7, 8, 9, 10 are negligible. This means that the above 4 columns can be treated as dummies and used for estimating the variance in error. Consequently, the ANOVA tables including percentage contributions are constructed and given in Table 8 (for the ndp) and Table 9 (for the IC). In Tables 8 and 9 it can be seen that the use of the two different responses produced similar conclusions: chromatographic column (factor A), acetonitrile (factor B), and the interaction $A \times B$ is statistically significant ($p < 0.01$) whereas no statistical differences are observed for any other variables and interactions considered ($p > 0.05$). The minor differences are, for the IC: factor A is significant at $p < 0.001$ while factors B and $A \times B$ are significant at $p < 0.01$; in contrast, for the ndp, factor B is significant at $p < 0.001$ while factors A and $A \times B$ are significant at $p < 0.01$. The latter seems to indicate that the effect of factor B is much larger than that of factor A. However, it should be pointed out that the significance values (F ratio) merely reflect the relative magnitudes of the incremental effects of both factors A and B. Factor A has three increments adding up to the effect owing to total factor A whereas factor B has only one increment. However, since the total span of levels 1–4 for factor A is available, the total effect for factor A is also available. From the total effects for factor A and B, it is clear that the effect of factor A is larger than that of factor B (for the ndp, $r_{A4} - r_{A1} = 6.25$; $r_{B4} - r_{B1} = 4.25$). Therefore, care should be given when interpreting the significance (F ratio) in mixed-level orthogonal array design, that is, the magnitude of the significance (F ratios) does not necessarily indicate the magnitude of the over-all effect.

Furthermore, from the percentage contribution (shown in Table 8 for the ndp and in Table 9 for the IC), it can be seen that, for both the ndp and the IC, the most important factor contributing to the output response is factor A (36.1% for ndp and 74.2% for IC), then, in order follow B (33.0% for ndp and 11.9% for IC) and C (27.4% for ndp and 10.4% for IC). Note that for the ndp the ranking of the significance (F ratios) is rectified by observing the percentage contribution. Obviously, the percentage contribution indicates that factor A makes the greatest contribution towards the variation observed in the experiments. This is in good agreement with the conclusion obtained from the total effect discussed above. The percentage contribution owing to error (unknown and uncontrolled factors) is quite low (3.4% for the ndp and 2.8% for the IC). This means that no important variables and/or interactions are neglected in our experimental design.

In comparing r_1, r_2, r_3, and r_4 for factor A and r_1 and r_2 for factor B, it is clear that for both the ndp and the IC the optimum levels are A_2 and B_2. However, because the interaction $A \times B$ is statistically significant ($p < 0.01$), the choice of the optimum experimental conditions of factors A and B must depend on their interaction, which can be evaluated by using a four-by-two table. The method of construction of the four-by-two table is the same as that of the two-by-two table, which has been described in detail elsewhere.[1] The four-by-two table constructed is shown in Table 10, from which it is clear that for the IC, the combination of A_2 and B_2 would result in the maximum response; for the ndp, although the combination of A_2 and B_2 would result in the maximum response, the combination of A_1 and B_1 would nevertheless give a comparable result.

In summary, the results obtained from ANOVA indicate that, by using a Spherex C_{18} column from Phenomenex (250 mm × 4.6 mm, i.d.; 5 μm particle size) and 80% acetonitrile in chromatographic analysis the best separation efficiency is obtained. Furthermore, the separation efficiency is not affected when methanol is used under the following conditions: 0–5%; initial time, 0–6 min, time programme, 10–25

Table 8 ANOVA table including percentage contribution for the number of distinguishable peak in the $OA_{16}(4^1 \times 2^{12})$ matrix. SS, sum of squares; df, degrees of freedom; MS, mean square; SS', purified sum of squares; and PC, percentage contribution

Source	SS	df	MS	F	SS'	PC(%)
Column (A	85.2	3	28.4	29.9**	82.4	36.1
Acetonitrile (B)	72.3	1	72.3	76.1***	75.2	33.0
Methanol (C)	1.0	1	1.0			
Initial time (D)	0.0	1	0.0			
Program time (E)	0.0	1	0.0			
Flow rate (F)	0.2	1	0.2			
$A \times B$	65.4	3	21.8	22.9**	62.5	27.4
Error	3.8	4	0.9		7.8	3.4
Total	228.0	15			228.0	100.0

Table 9 ANOVA table including percentage contribution for the number of individual contributions in the $OA_{16}(4^1 \times 2^{15})$ matrix. SS, sum of squares; df, degrees of freedom; MS, mean square; SS', purified sum of squares; and PC, percentage contribution

Source	SS	df	MS	F	SS'	PC(%)
Column (A)	15.77	3	5.26	131.50***	15.65	74.2
Acetonitrile (B)	2.55	1	2.55	63.75**	2.51	11.9
Methanol (C)	0.20	1	0.20	5.00	0.16	0.8
Initial time (D)	0.05	1	0.05			
Program time (E)	0.01	1	0.01			
Flow rate (F)	0.03	1	0.03			
$A \times B$	2.31	3	0.77	19.25**	2.19	10.4
Error	0.18	4	0.04		0.58	2.8
Total	21.10	15			21.10	100.0

Table 10 The four-by-two table for the analysis of the $A \times B$ interaction

	ndp				IC			
	A_1	A_2	A_3	A_4	A_1	A_2	A_3	A_4
B_1	15.5	15.0	12.5	13.0	1.61	3.56	2.43	3.01
B_2	6.0	16.0	6.0	11.0	0.77	3.81	0.53	2.29

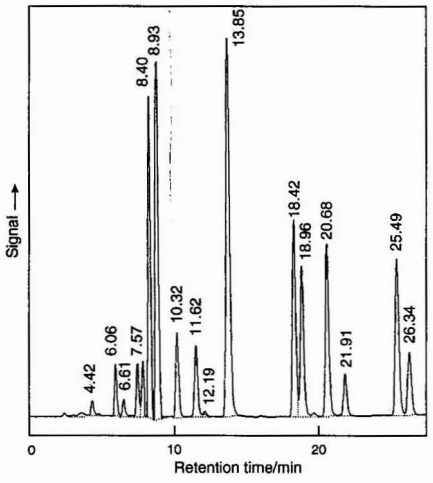

Fig. 1 Chromatogram of a standard mixture of 16 PAHs for experimental trial no. 7. Chromatographic conditions: Spherex C_{18} column; 80% acetonitrile; 5% methanol; initial time (6 min); gradient time (25 min); and flow rate (0.8 ml min^{-1}). Retention times (t_R): naphthalene (t_R 6.06 min), acenaphthylene (t_R 6.61 min), acenaphthene (t_R 7.57 min), fluorene (t_R 8.10 min), phenanthrene (t_R 8.40 min), anthracene (t_R 8.93 min), fluoranthene (t_R 10.32 min), pyrene (t_R 11.62 min), benzo[*a*]anthracene (t_R 12.19 min), chrysene (t_R 13.85 min), benzo[*b*]fluoranthene (t_R 18.42 min), benzo[*k*]fluoranthene (t_R 18.96 min), benzo[*a*]pyrene (t_R 20.96 min), dibenzo[*a,h*]anthracene (t_R 21.91 min), benzo[ghi]perylene (t_R 25.49 min) and indeno[1,2,3-cd] pyrene (t_R 26.34 min).

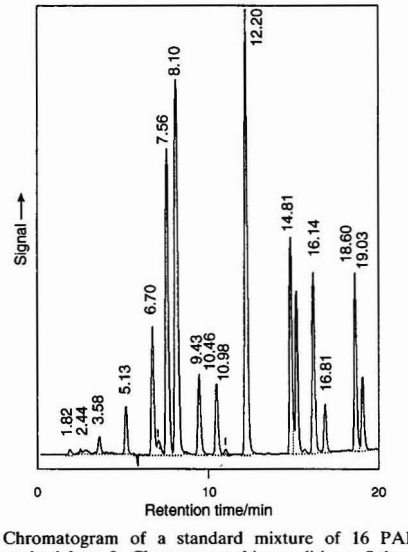

Fig. 2 Chromatogram of a standard mixture of 16 PAHs for experimental trial no 8. Chromatographic conditions: Spherex C_{18} column; 80% acetonitrile; 0% methanol; initial time (0 min); gradient time (10 min); and flow rate (1.2 ml min^{-1}). Retention times: naphthalene (t_R 3.58 min), acenaphthylene (t_R 5.13 min), acenaphthene (t_R 6.70 min), fluorene (t_R 7.03 min), phenanthrene (t_R 7.56 min), anthracene (t_R 8.10 min), fluoranthrene (t_R 9.43 min), pyrene (t_R 10.46 min), benzo[*a*]anthracene (t_R 10.98 min), chrysene (t_R 12.20 min), benzo[*b*]fluoranthene (t_R 14.81 min), benzo[*k*]fluoranthene (t_R 15.10 min), benzo[*a*]pyrene (t_R 16.14 min), dibenzo[*a,h*]anthracene (t_R 16.81 min), benzo[ghi]perylene (t_R 18.60 min) and indeno[1,2,3-cd] pyrene (t_R 19.03 min).

min; and flow rate 0.8–1.2 ml min^{-1}. It is obvious that the above conclusions obtained from ANOVA are the same as those obtained using the direct observation method, which indicates that the optimum separation efficiency was obtained in experimental trial numbers 7 and 8 (refer to Table 2). The chromatograms for experimental trial numbers 7 and 8 are shown in Figs. 1 and 2, respectively. From Figs. 1 and 2, it can be seen that, although the separation efficiency of PAHs is not affected by the variation in methanol composition, initial time, time programme, and flow rate, the retention time is significantly affected. Therefore, if retention time is considered, those factors that do not affect separation efficiency should be taken into account.

Lastly, it is worth mentioning that in the present study the chromatographic column, a discrete variable, is chosen as a factor. Moreover, the results obtained demonstrated that this factor is significantly influential. Therefore, as stated in the theoretical section, the establishment of a polynomial model representing the response surface is inappropriate.

Conclusions

This report is concerned with the optimization of analytical procedures where at least one of the variables exists at more than two-level settings. For this reason, we have described the theory and methodology of the mixed-level orthogonal array design, which can be considered as a supplement to orthogonal array design, in which all the factors have the same level settings. With the introduction of a mixed-level orthogonal array matrix, the feasibility and suitability for orthogonal array design as a chemometric method for the optimization of analytical procedures can be expanded.

In the present study, only the combination of two-level and four-level columns was considered. Although other mixed-level orthogonal array matrices can be constructed, the designs are relatively large even for a modest number of factors, and most of the small fractions have complex alias relationships that would require assumptions that are too restrictive to be useful. Those mixed-level orthogonal array matrices are therefore not recommended for the optimization of analytical procedures.

The authors thank H. B. Wan for technical assistance in the liquid chromatographic analysis. W. G. L. and K. K. C. thank the National University of Singapore for the award of research scholarships. This work was financially supported by the Asean-Canda Cooperative Programme on Marine Science, Phase II.

References

1 Lan W. G., Wong, M. K., Chen, N., and Sin, Y. M., *Analyst*, 1994, **119**, 1659, and references cited therein.
2 Lan, W. G., Wong, M. K., Chen, N., and Sin, Y. M., *Analyst*, 1994, **119**, 1669, and references cited therein.
3 Lan, W. G., Chee, K. K., Wong, M. K., and Sin, Y. M., *Analyst*, 1995, **120**, 273.
4 Lan, W. G., Wong, M. K., Chen, N., and Sin, Y. M., *Talanta*, 1994, **41**, 1917.
5 Wan, H. B., Lan, W. G., Wong, M. K., and Mok, C. Y., *Anal. Chim. Acta*, 1994, **289**, 371.
6 Wan, H. B., Lan, W. G., Wong, M. K., and Mok, C. Y., *J. Chromatogr.*, 1994, **677**, 255.
7 Dong, M. W., Duggan, J. X., and Stefanou, S., *LC-GC*, 1993, **11**, 802.
8 Lee, M. L., Novotny, M. V., and Bartle, K. D., *Analytical Chemistry of Polycyclic Compounds*, Academic Press, New York, 1981, p. 462.
9 Sander, L. C., and Wise, S. A., *LC-GC*, 1990, **8**, 378.
10 Grosser, Z. A., Ryan, J. F., and Dong, M. W., *J. Chromatogr.*, 1993, **642**, 75.

11 Giger, W., and Schaffner, C., *Anal. Chem.*, 1978, **50**, 243.
12 Organ, K., Katz, E., and Slavin, W., *Anal. Chem.*, 1979, **51**, 1315.
13 Das, B. S., and Thomas, G. H., *Anal. Chem.*, 1978, **50**, 967.
14 Dong, M. W., and Greenberg, A., *J. Liq. Chromatogr.*, 1988, **11**, 1887.
15 Scorell, R. K., and Reding, R., *J. Chromatogr.*, 1979, **185**, 655.
16 Murray, A. P., and Gibbs, C. F., *Int. J. Environ. Anal. Chem.*, 1983, **16**, 167.
17 Eiceman, G. A., and Lindley, K., *Int. J. Environ. Anal. Chem.*, 1988, **32**, 29.
18 Brindle, I. D., and Li, X. F., *J. Chromatogr.*, 1990, **498**, 11.
19 Wenclawiak, B. W., and Hees, T., *J. Chromatogr.*, 1994, **660**, 61.
20 Trevelin, W. R., Vidal, L. H., Landgraf, M. D., Silva, I. C. E., and Rezende, M. O. O., *Anal. Chim. Acta*, 1992, **268**, 67.
21 Marriott, P. J., Carpenter, P. D., Brady, P. H., McCormick, M. J., Griffiths, A. J., Hatvani, T. S. G., and Rasdell, S. G., *J. Liq. Chromatogr.*, 1993, **16**, 3229.

Paper 4/03450C
Received June 7, 1994
Accepted July 21, 1994

Chemometric Evaluation of the Solvent Properties of Liquid Organic Salts

Salwa K. Poole and Colin F. Poole*
Department of Chemistry, Wayne State University, Detroit, MI 48202, USA

Abraham's solvation parameter model was used to characterize the solvent properties of 38 liquid organic salts at a reference temperature of 121.4 °C. These salts are strong hydrogen-bond bases with a significant capacity for dipole–dipole and dipole-induced dipole interactions. The primary characteristics that dominate their solvent properties are the extent of charge localization on the anion and the extent of association between solvent molecules resulting from intermolecular hydrogen bonding. Their solvent properties cannot be duplicated by common non-ionic solvents used as stationary phases in gas chromatography.

Keywords: Liquid organic salts; solvent properties; solvation parameter model; stationary phases in gas chromatography

Introduction

The liquid organic salts are a new class of polar, selective solvents suitable for a wide range of chemical and technological applications.[1–5] In particular, alkylammonium and alkylphosphonium salts with weak nucleophilic anions form thermally stable liquids with a low vapour pressure at temperatures exceeding their melting-point by 150 °C or more in favourable cases.[6–15] In addition, a number of these salts have low melting-points including several that are liquid at room temperature.[16–21] The useful liquid ranges for a large number of organic salts as well as information on their physical properties can be obtained from reviews.[1–3] Unlike molten inorganic salts, which have been studied more extensively, the liquid organic salts have lower melting-points, in general, a significant capacity to dissolve a wide range of organic compounds, and lower chemical reactivity,[1,22] making them useful solvents for applications in analytical and organic chemistry. The high-temperature stable liquid organic salts are unique in having a simple, well defined, chemical structure and can be substituted in applications where polymeric solvents are generally used out of necessity (*e.g.*, as stationary phases in gas–liquid chromatography).

The lack of a suitable model to characterize the solvent behaviour of the liquid organic salts in terms of their capacity for fundamental interactions and as a means to compare their solvent properties with those of non-ionic solvents has obscured the novel features of these solvents and inhibited their technical development. Qualitative descriptions of their solvent properties have been made in terms of specific or molar retention volumes,[7,9–13] corrected McReynolds phase constants[7,9–13] and solute activity coefficients.[2,14,23] In a few instances Kamlet–Taft solvatochromic parameters or Reichardt's $E_{T(30)}$ parameter have been determined.[18,20] The latter methods are only suitable for comparing the solvent properties of the salts and non-ionic solvents that are liquids at about room temperature. Gas–liquid chromatography is an ideal technique for studying the solvent behaviour of liquids as it provides precise values for solvent thermodynamic constants, such as the gas–liquid partition coefficient, at any desired temperature the solvent has a low vapour pressure, and is economical in time and volume of solvent required for the determination. A model is required, however, to apportion the contribution of the various intermolecular interactions responsible for retention to the singular observed value of the retention parameter. In earlier work we have used the McReynolds phase constants system for this purpose but now accept the inadequacies of this model for solvent characterization for reasons detailed elsewhere.[24–29] Abraham and co-workers,[30–34] Carr and co-workers[35–37] and Poole and co-workers[29,38–43] have described a new approach to solvent characterization based on a cavity model, free of the problems extant in McReynolds' model.

The cavity model of solvation assumes that the transfer of a solute from the ideal gas state to the solvent at infinite dilution requires: (1) the creation of a cavity in the solvent of suitable size to accommodate the solute; (2) reorganization of the solvent molecules around the cavity (the Gibbs energy change for this process is probably very small compared with the other changes); and (3) interaction of the solute molecule with the surrounding solvent molecules. The total Gibbs energy change associated with this process can be represented by the sum of the individual Gibbs energy contributions to the solvation process. As demonstrated by Abraham and co-workers these changes can be described by eqn. (1)

$$\log K_L = c + rR_2 + s\pi_2^H + a\alpha_2^H + b\beta_2^H + l \log L^{16} \quad (1)$$

where K_L is the solute gas–liquid partition coefficient, c is a constant, R_2 the solute excess molar refraction, π_2^H the effective solute dipolarity/polarizability parameter, α_2^H the effective hydrogen-bond acidity, β_2^H the effective hydrogen-bond basicity and L^{16} the gas–liquid partition coefficient on hexadecane at 25 °C. This model is similar to the solvatochromic theory of solutions except that the explanatory variables R_2, π_2^H, α_2^H, β_2^H and $\log L^{16}$ are solvation parameters derived from equilibrium measurements and further refined (and augmented) by multiple linear regression analysis on solvents of assumed characteristic properties. The solvent parameters r, s, a, b and l are unambiguously defined: the r constant refers to the ability of the solvent to interact with solute π- and n-electron pairs; the s constant to the ability of the solvent to take part in dipole–dipole and dipole-induced dipole interactions; the a constant is a measure of the hydrogen-bond basicity of the solvent; the b constant is a measure of the hydrogen-bond acidity of the solvent; and the l constant incorporates contributions from solvent cavity formation and dispersion interactions, and more specifically in gas–liquid chromatography indicates how well the solvent will separate members in a homologous series. Experimentally, the solvent specific constants are determined from a number of measurements of $\log K_L$ for solutes with known explanatory variables using multiple linear regression analysis.

* To whom correspondence should be addressed.

The model proposed by Carr and co-workers is similar to eqn. (1) but differs in the values taken for the explanatory variables and in the use of an empirical correction term for the influence of the polarizability of the solute on the estimate of dipole-type interactions in place of the R_2 parameter used by Abraham and co-workers. These changes result in small numerical differences in the solvent characteristic constants but the general trends predicted by both models are the same.[29] The general model proposed by Poole and co-workers is different in approach to the above models and results in a single general term for the polar interactions which must be deconvoluted by chemometric procedures to identify the individual intermolecular contributions to the solvation process. The final approach for deconvolution has not been established yet so this model is less useful for the present study, although it should be noted that a single term that relates to the total polar interactions of a functional group is very useful for predicting retention in gas–liquid chromatography. Also, there is good general agreement between the term characterizing the sum of the polar interactions predicted by Poole's model and the equivalent terms in Abraham's model.[29,39,41,42] Hence an interpretation of solvent properties by each model would be redundant for our current purposes and only the model identified by eqn. (1) will be used here. In addition, the largest number of solvents have been characterized using eqn. (1) so that broad comparisons between solvent types is facilitated.[29,30]

Experimental

The gas–liquid partition coefficients, corrected for interfacial adsorption, at 121.4 °C were taken from the literature[10–14,20,23] and augmented by previously unpublished values.[44–47] The general experimental protocol and an evaluation of the typical uncertainty in the gas–liquid partition coefficients is described in detail elsewhere.[48] Briefly, all measurements were made on packed columns with a stationary phase loading of 8–20% (m/m) on Chromosorb W-AW (60–80 mesh). A minimum of four phase loadings for each salt covering the above range were used to determine the gas–liquid partition coefficient by linear extrapolation based on eqn. (2)

$$V_N^*/V_L = K_L + (\text{adsorption})\ (1/V_L) \qquad (2)$$

where V_N^* is the net retention volume per gram of packing, V_L the volume of liquid organic salt per gram of column packing and (adsorption) is a composite term representing the sum of all possible interfacial adsorption retention mechanisms. The experimental conditions are selected so that a linear extrapolation can be used as explained elsewhere.[48] The typical uncertainty in K_L is 2–5% relative standard deviation when the uncertainty in the phase loading is ±0.15% (determined by Soxhlet extraction), carrier gas flow rate ±0.20 ml min^{-1}, column pressure drop ±1 mmHg, column temperature ±0.2 °C and retention time ±0.02 min. The reference temperature of 121.4 °C was selected to be close to the standard temperature at which most studies of stationary phase properties of non-ionic solvents have been made.

The explanatory variables used in eqn. (1) were taken from the compilations of Abraham and co-workers[30,34,41] and are assembled in Table 1 for the reader's convenience. Multiple linear regression analysis was performed on an Epson Apex 200 computer (Epson America, Torrance, CA, USA) using the program SPSS/PC+ V3.1 (SPSS, Chicago, IL, USA) and multivariate analysis using the program Pirouette V1.1 (Infometrix, Seattle, WA, USA).

Results and Discussion

Gas–liquid chromatography is an excellent technique for determining solubility properties of individual compounds but the translation of the data into a more general picture of fundamental solvent behaviour rests on the availability of appropriate interpretive models. Abraham's solvation parameter model is very attractive for this purpose because it leads to a simple interpretation of solvent behaviour in terms of the relative contributions of orientation, induction and hydrogen-bond acid/base character. The cavity and dispersion contributions are correlated with the size of the solute and cannot be independently evaluated as yet. They are represented by the l log L^{16} term and at least part of the equation constant.

The data in Table 2 summarize the characteristic solvent constants for 38 liquid organic salts at 121.4 °C. The experimental data used in their determination have been gathered over about a 10 year period, and hence the number of solutes and their identity are not the same for all salts. This reflects the changes in approach used to characterize solvents in this group as earlier approaches have had to be abandoned in favour of more realistic methods. All results represent retention data from a minimum of four columns of different solvent loading and are corrected for interfacial adsorption. The quality of the fit to eqn. (1) is given by the individual standard deviation of the over-all fit (SD) and the multiple correlation coefficient (R) in Table 2 (n is the number of solutes employed in the regression equation). The fits are acceptable and similar in quality to those observed in similar studies of non-ionic solvents. The data in Table 2 and the results for ten tetraalkylammonium alkanesulfonate and perfluoroalkanesulfonate salts[40] comprise a complete summary of all currently available information.

Based on the data in Table 2 all the liquid organic salts are strong hydrogen-bond bases (a constant) with a significant capacity for dipole–dipole and dipole-induced dipole interac-

Table 1 Explanatory variables used in eqn. (1)

Solute	R_2	π_2^H	α_2^H	β_2^H	Log L^{16}
Dodecane	0.000	0.00	0.00	0.00	5.696
Tridecane	0.000	0.00	0.00	0.00	6.200
Tetradecane	0.000	0.00	0.00	0.00	6.705
Pentadecane	0.000	0.00	0.00	0.00	7.209
Pentan-2-one	0.143	0.68	0.00	0.51	2.755
Hexan-2-one	0.136	0.68	0.00	0.51	3.262
Heptan-2-one	0.123	0.68	0.00	0.51	3.760
Octan-2-one	0.108	0.68	0.00	0.51	4.257
Nonan-2-one	0.119	0.68	0.00	0.51	4.735
Methyl heptanoate	0.079	0.60	0.00	0.45	4.356
Methyl octanoate	0.065	0.60	0.00	0.45	4.838
Methyl nonanoate	0.056	0.60	0.00	0.45	5.321
Methyl decanoate	0.053	0.60	0.00	0.45	5.803
Methyl undecanoate	0.050	0.60	0.00	0.45	6.285
Butan-1-ol	0.224	0.42	0.37	0.48	2.601
Pentan-1-ol	0.219	0.42	0.37	0.48	3.106
Hexan-1-ol	0.210	0.42	0.37	0.48	3.610
2-Methylpentan-2-ol	0.169	0.30	0.31	0.60	3.081
Oct-2-yne	0.225	0.30	0.00	0.10	3.850
1-Nitropropane	0.242	0.95	0.00	0.31	2.894
1,4-Dioxane	0.329	0.75	0.00	0.64	2.892
Benzene	0.610	0.52	0.00	0.14	2.786
Toluene	0.601	0.52	0.00	0.14	3.325
Ethylbenzene	0.613	0.51	0.00	0.15	3.778
Nitrobenzene	0.871	1.11	0.00	0.28	4.557
Chlorobenzene	0.718	0.65	0.00	0.07	3.657
Bromobenzene	0.882	0.73	0.00	0.09	4.041
Iodobenzene	1.188	0.82	0.00	0.12	4.502
1,2-Dichlorobenzene	0.872	0.78	0.00	0.04	4.518
Benzaldehyde	0.820	1.00	0.00	0.39	4.008
Acetophenone	0.818	1.01	0.00	0.48	4.501
Pyridine	0.631	0.84	0.00	0.52	3.022

tions (*s* constant). In general they are not significant hydrogen-bond acids (*b* constant statistically insignificant). The typical range of values for the solvent constants of non-ionic solvents are 0–1.90 for *s* and 0–2.40 for *a* (very few non-ionic solvents have *a* values >1.70).[29,32,33] Plotting the *s* constant against the *a* constant (Fig. 1) for all the solvents in Table 2 indicates a tight grouping of properties. Most salts have *s* constants between 1.5 and 2.1 and *a* constants between 3.0 and 4.0. The exceptions are tetrabutylammonium pentacyanopropionide, picrate, trifluoromethanesulfonate and perfluorobenzenesulfonate (low *a* and *s* constants) and tetrabutylammonium chloride, bromide and nitrite and tetrabutylphosphonium chloride and bromide (large *a* and intermediate to large *s* constants). The hydrogen-bond basicity of the anion depends primarily on the extent of charge localization and size. Anions that can delocalize charge such as picrate, pentacyanopropionide and perfluorobenzenesulfonate are weaker hydrogen-bond bases and are less dipolar than other salts because of the reduction in charge localized on the terminal acidic portion of the anion. The chloride and bromide salts have relatively small atomic radii and no additional mechanism for charge delocalization so they are the most basic of the salts studied.

It is interesting that the solvent constants for the tetrabutylammonium and tetrabutylphosphonium salts with a common anion are identical within the statistical uncertainty of their determinations. Hence the choice of the cation is unimportant in terms of the solvent properties of these sets of analogous salts. A more important consideration for selection is their physical characteristics. The tetrabutylphosphonium salts are generally more stable to higher temperatures and, depending on their melting-point, will usually provide wider useful liquid ranges.[12] On the other hand, the tetrabutylphosphonium salts are very hygroscopic and difficult to manipulate in air.

Table 2 Characteristic solvent constants for the liquid organic salts at 121.4 °C

Counter ion	*c*	*r*	*s*	*a*	*l*	SD	*R*	*n*
(*i*) *Tetrabutylammonium salts*—								
Chloride (LOS-1)	−1.305	0.198	2.036	5.677	0.548	0.081	0.9954	18
Bromide (LOS-2)	−0.894	0.231	1.849	4.425	0.467	0.069	0.9956	18
Nitrate (LOS-3)	−0.829	0.145	1.864	3.535	0.453	0.055	0.9967	18
Nitrite (LOS-4)	−0.821	0.179	1.854	4.476	0.443	0.062	0.9961	18
Picrate (LOS-5)	−0.542	0.100	1.557	1.424	0.445	0.061	0.9935	36
Sulfamate (LOS-6)	−1.040	0.157	1.944	3.956	0.451	0.065	0.9957	17
Tetrabutylborate (LOS-7)	−0.499		1.440	3.230	0.476	0.061	0.9944	15
1,1,2,3,3-Pentacyanopropionide (LOS-8)	−0.406		1.541	1.517	0.438	0.052	0.9956	18
Methanesulfonate (LOS-9)	−0.612	0.334	1.454	3.762	0.435	0.071	0.9970	27
Trifluoromethanesulfonate (LOS-10)	−0.552		1.579	2.135	0.416	0.055	0.9980	27
Ethanesulfonate (LOS-11)	−0.804	0.139	1.805	4.021	0.442	0.079	0.9923	18
Benzenesulfonate (LOS-12)	−0.924	0.121	1.756	3.507	0.464	0.050	0.9955	27
Perfluorobenzenesulfonate (LOS-13)	−0.723	−0.088	1.647	2.238	0.459	0.030	0.9985	21
4-Toluenesulfonate (LOS-14)	−0.686	0.156	1.582	3.295	0.459	0.033	0.9980	36
2-(Cyclohexylamino)ethanesulfonate (LOS-15)	−0.827	0.073	1.572	3.667	0.505	0.060	0.9957	18
3-(Cyclohexylamino)propanesulfonate (LOS-16)	−0.934		1.577	3.710	0.541	0.066	0.9946	18
4-Morpholineethanesulfonate (LOS-17)	−0.631	0.095	1.595	3.408	0.437	0.097	0.9900	34
4-Morpholinepropanesulfonate (LOS-18)	−0.937		1.748	3.538	0.550	0.069	0.9939	18
2-Hydroxy-4-morpholinepropanesulfonate (LOS-19)	−0.906		1.764	3.204	0.494	0.053	0.9963	18
3-[tris(Hydroxymethyl)methyl]amino-1-propanesulfonate (LOS-20)	−1.040	0.396	2.204	3.690	0.265	0.054	0.9974	15
3-[tris(Hydroxymethyl)methyl]amino-2-hydroxy-1-propanesulfonate (LOS-21)	−0.860	0.266	1.959	3.058	0.317	0.048	0.9957	27
2-[bis(2-Hydroxyethyl)amino]ethanesulfonate (LOS-22)	−0.805	0.253	1.760	3.368	0.382	0.046	0.9965	33
2-[(2-acetamido)amino]ethanesulfonate (LOS-23)	−0.666	0.283	1.809	3.417	0.329	0.100	0.9900	34
(*ii*) *Tetraalkylammonium 4-toluenesulfonates*—								
Tetraethylammonium (LOS-24)	−0.762	0.330	2.045	3.429	0.304	0.050	0.9976	22
Tetrapropylammonium (LOS-25)	−0.902	0.165	1.987	3.569	0.404	0.042	0.9981	22
Tetrapentylammonium (LOS-26)	−0.795	0.013	1.636	3.430	0.529	0.064	0.9944	22
(*iii*) *Tetrabutylphosphonium salts*—								
Chloride (LOS-27)	−1.009	0.244	1.854	5.418	0.468	0.078	0.9929	27
Bromide (LOS-28)	−0.848	0.249	1.810	4.255	0.449	0.072	0.9926	27
Iodide (LOS-29)	−0.708	0.210	1.798	3.150	0.429	0.051	0.9956	27
Nitrate (LOS-30)	−0.758	0.183	1.829	3.538	0.421	0.051	0.9956	27
2-(Cyclohexylamino)ethanesulfonate (LOS-31)	−0.816	0.107	1.582	3.633	0.493	0.059	0.9947	26
4-Morpholinepropanesulfonate (LOS-32)	−0.774	0.126	1.682	3.659	0.494	0.054	0.9954	27
3-{[tris(Hydroxymethyl)methyl]amino}-2-hydroxy-1-propanesulfonate (LOS-33)	−0.849	0.205	1.957	3.091	0.330	0.044	0.9960	26
(*iv*) *Miscellaneous*—								
Octyltriphenylphosphonium bromide (LOS-34)	−1.029	0.413	1.926	3.964	0.389	0.046	0.9970	25
Ethylpyridinium 4-toluenesulfonate (LOS-35)	−0.987	0.366	2.119	3.630	0.281	0.044	0.9967	26
1-Ethyl-3-hydroxypyridinium 4-toluenesulfonate* (LOS-36)	−1.030	0.449	1.958	2.890	0.305	0.073	0.9917	26
1-Ethyl-3-hydroxypyridinium bromide† (LOS-37)	−1.083	0.497	2.108	3.214	0.242	0.039	0.9976	22
Tributylammonium 4-toluenesulfonate (LOS-38)	−0.717	0.110	1.546	2.917	0.466	0.069	0.9920	30

* $b = 0.368$.

† $b = 0.320$.

None of the liquid organic salts are significant hydrogen-bond acids. 1-Ethyl-3-hydroxypyridinium bromide and 1-ethyl-3-hydroxypyridinium 4-toluenesulfonate are weak hydrogen-bond acids with b values of 0.320 and 0.368, respectively. This is undoubtedly due to the presence of a phenolic-type hydroxy group attached to the cation. The lack of solvents with significant hydrogen-bond acidity at 121.4 °C has been demonstrated previously for non-ionic solvents.[3,32,36,41,49] Only the phenolic solvent bis(3-allyl-4-hydroxyphenyl)sulfone, b = 1.457, and 4-dodecyl-α,α-bis-(trifluoromethyl)benzyl alcohol, b = 2.686 (at 80 °C), are known to be significant hydrogen-bond acids; docosanol, b = 0.34, sorbitol, b = 0.34, and diglycerol, b = 0.52, are weak hydrogen-bond acids. Several sulfonate anions with hydroxy, amine and amide substituents, such as 3-{[tris(hydroxymethyl)methyl]amino}-2-hydroxy-1-propanesulfonate, 2-[bis(2-hydroxyethyl)amino]ethanesulfonate and 2-[(2-acetamido)amino]ethansulfonate were synthesized by us with a view to creating solvents with significant hydrogen-bond acidity. For these salts the preference to form hydrogen-bonded solvent complexes occurs to the exclusion of significant interactions with solute hydrogen-bond bases. For anions of similar structure the introduction of hydrogen-bonding groups, such as hydroxy groups, results in a small decrease in the solvent s and a constants but more significant reductions in the l constant. Hence hydrogen-bond association between solvent molecules is primarily responsible for an increase in the cohesive energy of the solvent as exemplified by a less favourable endoergic cavity term (smaller value for l).

The contribution of rR_2 to solvent behaviour is small compared with the other terms in eqn. (1) and does not contribute significantly to the solvent properties of the salts in Table 2. We need not discuss this term further. According to Abraham and co-workers[32–34] the l constant in combination with the c term [eqn. (1)] reflects a combination of an endoergic cavity term and an exoergic solute–solvent general dispersion interaction term. Its interpretation is difficult as we lack the means at present to separate the two contributions to the l constant. Abraham *et al.*[33] have shown that there is a general correlation between the l constant and the partial molar Gibbs energy of solution for a methylene group (ΔGCH_2). A plot of (ΔGCH_2) against l for the liquid organic salts in Table 2 (Fig. 2) shows a modest correlation for a linear fit (r^2 = 0.86) confirming the general trend. In addition to experimental error it is possible that inclusion of a portion of the c term is needed to improve the fit.[39,43] At least in a qualitative sense the l constant can be interpreted as an indication of the capacity of a solvent to dissolve higher members of an homologous series and in gas chromatography is an indication of the peak spacing between homologues. The l constant for non-ionic solvents at 121.4 °C ranges from 0.24 to 0.58, representing the solvents poly(dicyanoallylsiloxane), OV-275, and the hydrocarbon squalane, respectivey.[29] The tetrabutylammonium and tetrabutylphosphonium salts with non-associating anions have surprisingly large l constants, 0.44–0.55, compared with non-ionic polar solvents and are unique among polar solvents in their capacity to separate members of a homologous series in gas–liquid chromatography. For anions believed to be associated as hydrogen-bond complexes the l constants are significantly smaller, 0.26–0.37, and equivalent to the values observed for the most polar of the non-ionic solvents. The tetraalkylammonium 4-toluenesulfonate salts show a general increase in the value of the l constant as a function of the cation volume (r^2 = 0.96) accompanied by a decrease in the s constant (r^2 = 0.96), Fig. 3. The a constant is essentially unchanged. Given the small changes in the constants, the approximate method used to calculate the cation volume,[50] and the small number of data points these correlations seem reasonable. It is noteworthy that the l constant for tetrapentylammonium 4-toluenesulfonate is similar to that of the poly(dimethylsiloxane) solvent SE-30. The c terms are very different for these two solvents, however; −0.775 for the liquid organic salt and −0.194 for SE-30.[29] Although the spacing between members of a homologous series is similar for both solvents the absolute retention of the individual members is less by a factor of about 2.4 on the tetrapentyla monium 4-toluenesulfonate salt, indicating the importance of the c term as well as the l term in judging the solubility of non-polar solutes in different solvents.

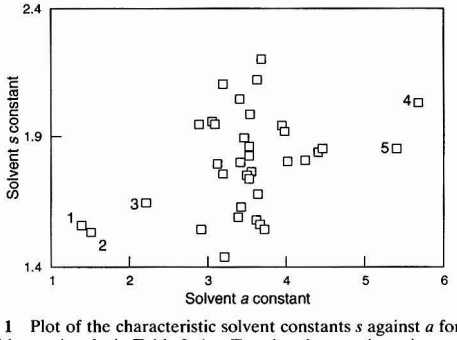

Fig. 1 Plot of the characteristic solvent constants s against a for the liquid organic salts in Table 2. 1 = Tetrabutylammonium picrate, 2 = tetrabutylammonium pentacyanopropionide, 3 = tetrabutylammonium perfluorobenzenesulfonate, 4 = tetrabutylammonium chloride and 5 = tetrabutylphosphonium chloride.

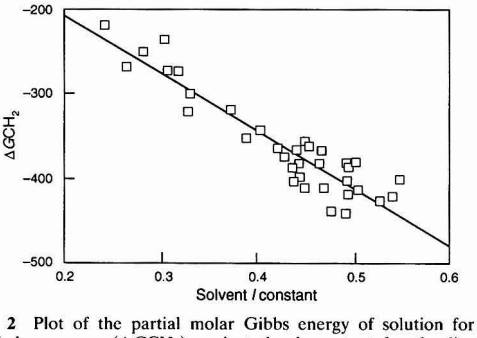

Fig. 2 Plot of the partial molar Gibbs energy of solution for a methylene group (ΔGCH_2) against the l constant for the liquid organic salts in Table 2.

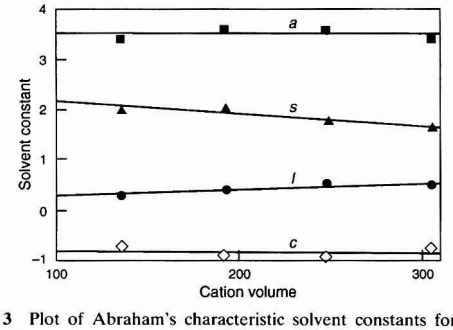

Fig. 3 Plot of Abraham's characteristic solvent constants for the tetraalkylammonium 4-toluenesulfonate salts against the characteristic volume of the cation (calculated without regard for the charge).

Cluster analysis is an alternative to principal component analysis for classification of samples by multivariate analysis. For cluster analysis a distance matrix is formed from the original data matrix. The Euclidean distance between any sample (or groups of samples) to another is used as a measure of how similar the two samples are. The outputs for clustering algorithms are dendrograms. The dendrogram provides a convenient and visual approach to solvent selection. The solvents that are most similar are next to each other and are connected. Connections at the extreme left-hand side of the dendrogram have a similarity of 1, representing duplicates, and those at the extreme right-hand side a similarity of zero, and have no features in common. In an obvious manner solvents with significantly different properties as well as those with near duplicate properties are easily identified. The nearest neighbour single-link dendrogram (Fig. 4) for all 38 liquid organic salts reveals a high level of similarity among most of the solvents. All but eight of the liquid organic salts (LOS-1, LOS-5, LOS-8, LOS-12, LOS-25, LOS-33, LOS-34 and LOS-35) show greater than 70% similarity in their solvent properties. For this group of liquid organic salts there are few grouped descendants or large clusters indicating subtle differences in the solvent properties of individual salts. The greatest similarity is observed for the tetrabutylammonium and tetrabutylphosphonium salts with a common anion. The salts with the least similarity to the major cluster are the tetrabutylammonium and tetrabutylphosphonium chlorides and tetrabutylammonium pentacyanopropionide and picrate. The reasons why these salts show different behaviour to the others were discussed earlier.

A second function of these studies was to demonstrate that the liquid organic salts have unique solvent characteristics that are not duplicated by familiar non-ionic solvents. To this end we have added data for 21 non-ionic solvents determined under identical conditions to those used for the liquid organic salts,[29,33] and after excluding the two liquid organic salts with significant values for b (all the non-ionic solvents have $b = 0$), the combined results were subjected to classification by principal component analysis. These results are summarized in Table 3. The first two principal components account for 95.6% of the total variance of the data. Principal component 1 is heavily weighted towards solvent hydrogen-bond basicity (a constant) while component 2 is weighted more towards dipole–dipole and dipole-induced dipole interactions (s constant) with a smaller contribution from the cavity/dispersion term (l constant). The score plot of principal component 1 against component 2 (Fig. 5) shows three clusters with three solvents behaving independently (tetrabutylammonium chloride and perfluorobenzensulfonate and tetrabutylphosphonium chloride). The membership of groups 1 and 2 is given in Table 3. Group 1 contains phases with weak polar interactions. Group 2 contains the polar non-ionic solvents and the liquid organic salts tetrabutylammonium pentacyanopropionide and picrate. Group 3 contains all the remaining liquid organic salts. This group is well separated from group 1 and 2 and is an indication of the unique characteristic solvent properties of the liquid organic salts. Only for tetrabutylammonium picrate and pentacyanopropionide are common non-ionic solvents available that could duplicate (at least in large part) the solvent properties of the liquid oganic salts.

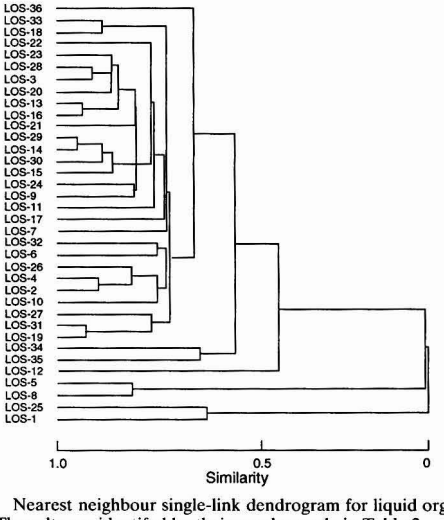

Fig. 4 Nearest neighbour single-link dendrogram for liquid organic salts. The salts are identifed by their number code in Table 2.

Table 3 Summary of results from principal component analysis of 55 solvents

Principal component	Per cent. variance	Cumulative variance
1	76.7	76.7
2	18.9	95.6
3	4.0	99.6

Loadings for principal components—

	PC 1	PC 2	PC 3
r	−0.0137	0.0797	−0.1234
s	0.0594	0.9402	0.0217
a	0.9964	−0.0365	0.0148
l	−0.0540	0.3281	−0.1118
c	−0.0241	0.0271	0.9857

Group membership—*

Group 1	Group 2
Squalane, SE-30	DEHPA, U50HB, OV-275
OV-3, OV-105	OV-330, THPED, TCEP
OV-11, OV-17	OV-225, CW20M, EGAD
OV-22, OV-25	QPIC, QPCP, DEGS
PPE-5, QF-1	
OV-7	

* Full list of chemical names for abbreviations is given in ref. 29.

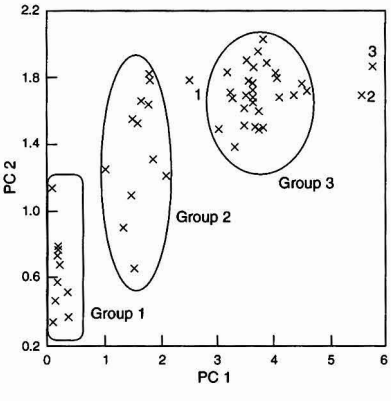

Fig. 5 Score plot for 55 solvents obtained by principal component analysis. The group membership is identified in Table 3 and the text. 1 = Tetrabutylammonium perfluorobenzenesulfonate, 2 = tetrabutylphosphonium chloride and 3 = tetrabutylammonium chloride.

Conclusions

The above results demonstrate the unique solvent properties of the liquid organic salts. The data are generated through studies employing gas–liquid chromatography and hence the possibility of using these materials for separations is well established. The general model used to characterize their properties in terms of identifiable specific intermolecular interactions establishes their unique character and hopefully will serve to promote their wider use in analytical chemistry in applications where the identified solvent characteristics are considered desirable. It is hoped that Table 2 will be useful as a selection aid in these studies as it brings together a significant amount of previously unpublished data as well as providing a consistent method of data evaluation to replace the qualitative approaches used in the past.

References

1 Poole, C. F., Furton, K. G., and Kersten, B. R., *J. Chromatogr. Sci.*, 1986, **24**, 400.
2 Poole, C. F., Furton, K. G., Pomaville, R. M., Poole, S. K., and Kersten, B. R., in *Molten Salt Techniques*, eds. Gale, R. J., and Lovering, D. G., Plenum, New York, 1991, vol. 4, pp. 41–81.
3 Gordon, J. E., in *Techniques and Methods of Organic and Organometallic Chemistry*, ed. Denny, R. E., Marcel Dekker, New York, 1969, vol. 1, pp. 51–88.
4 Tissot, P., in *Molten Salt Techniques*, eds. Lovering, D. G., and Gale, R. J., Plenum, New York, 1983, vol. 1, pp. 137–150.
5 Pagni, R. M., in *Advances in Molten Salt Chemistry*, eds. Mamantov, G., Mamantov, C. B., and Brunstein, J., Elsevier, Amsterdam, 1987, vol. 6, pp. 211–346.
6 Poole, C. F., Butler, H. T., Coddens, M. E., Dhanesar, S. C., and Pacholec, F., *J. Chromatogr.*, 1984, **289**, 299.
7 Furton, K. G., and Poole, C. F., *J. Chromatogr.*, 1985, **349**, 235.
8 Dhanesar, S. C., Coddens, M. E., and Poole, C. F., *J. Chromatogr.*, 1985, **349**, 249.
9 Coddens, M. E., Furton, K. G., and Poole, C. F., *J. Chromatogr.*, 1986, **356**, 59.
10 Furton, K. G., and Poole, C. F., *Anal. Chem.*, 1987, **59**, 1170.
11 Furton, K. G., Poole, C. F., and Kersten, B. R., *Anal. Chim. Acta*, 1987, **192**, 255.
12 Pomaville, R. M., Poole, S. K., Davis, L. J., and Poole, C. F., *J. Chromatogr.*, 1988, **438**, 1.
13 Pomaville, R. M., and Poole, C. F., *Anal. Chem.*, 1988, **60**, 1103.
14 Pomaville, R. M., and Poole, C. F., *J. Chromatogr.*, 1989, **468**, 261.
15 Furton, K. G., and Morales, R., *Anal. Chim. Acta*, 1991, **246**, 171.
16 Hussey, C. L., *Adv. Molten Salt Chem.*, 1983, **5**, 185.
17 Poole, C. F., Kersten, B. R., Ho, S. S. J., Coddens, M. E., and Furton, K. G., *J. Chromatogr.*, 1986, **352**, 407.
18 Shetty, P. H., Youngberg, P. J., Kersten, B. R., and Poole, C. F., *J. Chromatogr.*, 1987, **411**, 61.
19 Arancibia, E. L., Castells, R. C., and Nardillo, A. M., *J. Chromatogr.*, 1987, **398**, 21.
20 Poole, S. K., Shetty, P. H., and Poole, C. F., *Anal. Chim. Acta*, 1989, **218**, 241.
21 Shetty, P. H., Poole, S. K., and Poole, C. F., *Anal. Chim. Acta*, 1990, **236**, 51.
22 Poole, S. K., and Poole, C. F., *J. Chromatogr.*, 1988, **435**, 17.
23 Furton, K. G., and Poole, C. F., *J. Chromatogr.*, 1987, **399**, 47.
24 Kersten, B. R., Poole, C. F., and Furton, K. G., *J. Chromatogr.*, 1987, **411**, 43.
25 Poole, C. F., Poole, S. K., Pomaville, R. M., and Kersten, B. R., *J. High Resolut. Chromatogr.*, 1987, **10**, 670.
26 Poole, C. F., and Poole, S. K., *Chem. Rev.*, 1989, **89**, 377.
27 Poole, S. K., Kersten, B. R., and Poole, C. F., *J. Chromatogr.*, 1989, **471**, 91.
28 Morales, R., Blanco, C., and Furton, K. G., *Talanta*, 1993, **40**, 1541.
29 Poole, C. F., Kollie, T. O., and Poole, S. K., *Chromatographia*, 1992, **34**, 281.
30 Abraham, M. H., *Chem. Soc. Rev.*, 1993, **22**, 73.
31 Grate, J. W., and Abraham, M. H., *Sens. Actuators B*, 1991, **3**, 85.
32 Abraham, M. H., Whitting, G. S., Doherty, R. M., and Shuely, W. J., *J. Chromatogr.*, 1990, **518**, 329.
33 Abraham, M. H., Whiting, G. S., Doherty, R. M., and Shuely, W. J., *J. Chromatogr.*, 1991, **587**, 229.
34 Abraham, M. H., *J. Chromatogr.*, 1963, **644**, 95.
35 Zhang, Y., Dalas, A. J., and Carr, P. W., *J. Chromatogr.*, 1993, **638**, 43.
36 Li, J., Zhang, Y., and Carr, P. W., *Anal. Chem.*, 1993, **65**, 1969.
37 Li, J., Zhang, Y., and Carr, P. W., *Anal. Chem.*, 1992, **64**, 210.
38 Kollie, T. O., and Poole, C. F., *J. Chromatogr.*, 1991, **556**, 457.
39 Kollie, T. O., Poole, C. F., Abraham, M. H., and Whiting, G. S., *Anal. Chim. Acta*, 1992, **259**, 1.
40 Kollie, T. O., and Poole, C. F., *Chromatographia*, 1992, **33**, 551.
41 Abraham, M. H., Haftvan-Andonian, J., Hamerton, I., Poole, C. F., and Kollie, T. O., *J. Chromatogr.*, 1993, **646**, 351.
42 Poole, C. F., and Kollie, T. O., *Anal. Chim. Acta*, 1993, **282**, 1.
43 Poole, S. K., Kollie, T. O., and Poole, C. F., *J. Chromatogr.*, 1994, **664**, 229.
44 Furton, K. G., Ph.D. Thesis, Wayne State University, 1986.
45 Kersten, B. R., Ph.D. Thesis, Wayne State University, 1988.
46 Pomaville, R. M., Ph.D. Thesis, Wayne State University, 1989.
47 Kollie, T. O., Ph.D. Thesis, Wayne State University, 1992.
48 Poole, S. K., and Poole, C. F., *J. Chromatogr.*, 1990, **500**, 329.
49 Li, J., Zhang, Y., Ouyang, H., and Carr, P. W., *J. Am. Chem. Soc.*, 1992, **114**, 9813.
50 Abraham, M. H., and McGowan, J. C., *Chromatographia*, 1987, **23**, 243.

Paper 4/02395A
Received May 15, 1994
Accepted September 6, 1994

Development of a Novel Methodology in the Determination of Magnesium from Chlorophyll *a* by Atomic Absorption Spectrometry Using Chemometric Experimental Design

Pedro W. Araujo, Keyhandokht Kavianpour and Richard G. Brereton*
School of Chemistry, University of Bristol, Bristol, UK BS8 1TS

The amount of Mg from chlorophyll *a* was determined by atomic absorption spectrometry (AAS) with a new procedure involving acetone–water mixtures which was compared with an acid digestion procedure using a composite central design. The amount of chlorophyll *a* was determined using electronic absorption spectrometry and calibrated to AAS. The results demonstrated that there are no significant differences between the two procedures and that the sample matrix does not affect the determination of the analyte. The results from the two-factor design were compared with results using the standard additions method, and were found to be slightly better in this example.

Keywords: Magnesium determination; chlorophyll a*; atomic absorption spectrometry; electronic absorption spectrometry; experimental design*

Introduction

Chlorophylls are tetrapyrroles with a central Mg atom, coordinated to four nitrogen atoms and one or two external ligands. The structure of chlorophyll *a* is given in Fig. 1. Because chlorophylls have vacant coordination sites, pure chlorophyll in the absence of external ligands cannot be obtained; the crystal structure of chlorophyll *a* has yet to be determined. Hence, there are substantial difficulties in the determination of chlorophyll *a*, as weighing is not easy owing to problems with hydrocarbon impurities that associate with the hydrophobic phytyl tail and coordination of external ligands, such as water. An alternative approach is to determine the amount of Mg and to use this for measuring the amount of chlorophyll *a*. Conventionally the Mg is extracted with aqueous mineral acids and determined by an analytical method such as gravimetry, spectrophotometry, spectrofluorimetry or atomic absorption spectrometry (AAS).[1] The methods described in this paper were validated using pure chlorophyll as a standard, but could be applied to mixtures of chlorophylls such as those that occur in whole extracts.

Owing to the sensitivity and low detection limits, AAS was used by Porra *et al.*[2] to confirm the molar absorptivity proposed by Smith and Benitez[3] for chlorophyll *a* and chlorophyll *b*, respectively, in diethyl ether. The method they used was based on the exhaustive extraction of Mg from ethereal solutions with perchloric acid, but the recoveries of metal chlorophyll were not reported. The influence of the solvent in the determination of Mg from chlorophyll *a* samples has been studied by comparing samples dissolved in acetone with 4-cyclohexylbutyric acid Mg salt standard solutions prepared in acetone,[4] but the results obtained were imprecise, probably because of the strong influence of the solvent; for this reason, the mineralization of the sample prior to AAS analysis is conventionally used. Tsunoda *et al.*,[5] without using acid digestion, determined total Mg from chlorophylls by AAS. Their extraction procedure involved the use of different organic solvents and partition chromatography before the AAS determination. The Mg recovery revealed that some analyte was lost, possibly as a result of the sample manipulation.

The existing extraction procedures have the disadvantages that they can result in the loss of analyte and that they are complex and time consuming. In this work, we propose a novel approach to the determination of Mg from chlorophyll *a* by AAS. For this purpose, we studied two sample treatment procedures and compared them using a central composite experimental design. The validity of the results was confirmed through the use of standard additions graphs.

Experimental

Apparatus

A Pye Unicam (Cambridge, UK) Model SP9 atomic absorption spectrometer with an air–acetylene flame and a Pye Unicam Mg hollow-cathode lamp resonating at 285.2 nm with a 0.5 nm spectral width and 4 mA lamp current was used for AAS measurements.

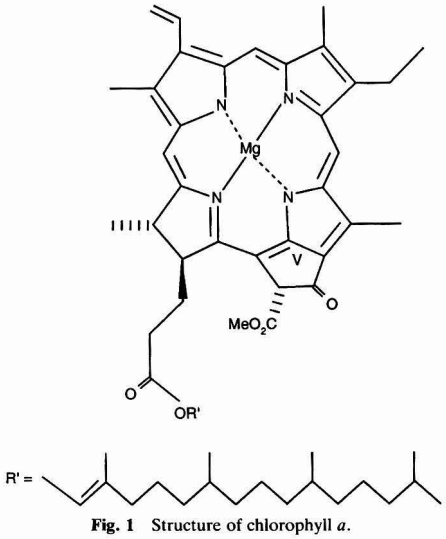

Fig. 1 Structure of chlorophyll *a*.

* To whom correspondence should be addressed.

Electronic absorption spectra were recorded using a Pharmacia (Uppsala, Sweden) LKB BioChrom Ultrospec III UV/VIS spectrophotometer (Model 80-2097-62) equipped with deuterium and tungsten halogen lamps. The spectra were obtained from the Wavescan software package with a resolution of 1 nm.

High-performance liquid chromatography (HPLC) was carried out with a Waters (Milford, MA, USA) Model 600E multi-solvent delivery system and a reversed-phase C_{18} column (300 × 3.9 mm id) and using a Waters Model 990 diode-array detector. Acetone, methanol and water were used for the mobile phase at a flow rate of 1 ml min^{-1}. Chromatograms were recorded between 350 and 800 nm and digitized every 2 s and 2 nm.

Reagents

Stock standard of $Mg(NO_3)_2$ containing 1 mg ml^{-1} of Mg and HNO_3 were obtained from BDH (Poole, Dorset, UK). For chromatography and electronic and atomic spectrometry, HPLC-grade acetone and methanol (Aldrich, Milwaukee, WI, USA) were used. Ultrapure water was obtained from a Milli-Q water-purification system (Millipore-waters, Milford, MA, USA). All test solutions were prepared immediately prior to use.

Preparation of Pure Chlorophyll a

Chlorophyll was extracted from spinach using methods based on those used by Svec,[6] Iriyama *et al.*[7] and Rahmani *et al.*[8] The crude extract was chromatographed to obtain pure chlorophyll *a*. The separation procedure was based on open-column chromatography as described by Brereton *et al.*[9] The purity of the chlorophyll *a* (column purified five times) was qualitatively checked by HPLC with diode-array detection. The chlorophyll *a* was dissolved in diethyl ether and placed in brown glass ampoules (1 ml each). The ether was then removed using a stream of nitrogen and the ampoules were sealed with a flame and stored at 5 °C for further analysis.

The amount of chlorophyll in each ampoule used below was determined by electronic spectrometry using the equation proposed by Lichtenthaler[10] for chlorophyll *a* in acetone at 644 and 661 nm. The contents of the ampoule were dissolved in a known amount of solvent (4 ml) and electronic absorption spectrometry was performed on a 0.1 ml fraction. The estimated amount of chlorophyll *a* for three ampoules gave only a small spread, and the average reading was taken as the amount of chlorophyll per ampoule.

Sample Treatments

Procedure A

One ampoule containing pure, dry chlorophyll *a* was opened, dissolved in 4 ml of acetone and transferred into a beaker. The ampoule was washed using a further 4 ml of acetone in small portions to ensure complete removal of chlorophyll *a* from the ampoule. The acetone was evaporated completely by gently heating the beaker. A 3 ml volume of nitric acid was added to the dry sample and it was heated gently until expulsion of dinitrogen oxide vapour and dissolution of the sample were complete. Finally, the sample solution was diluted with de-ionized water in a 100 ml calibrated flask, in preparation for AAS.

Procedure B

Procedure B is a modification of procedure A. After an 8 ml acetone solution of the contents of the ampoule had been prepared, the sample solution was diluted with de-ionized water in a 100 ml calibrated flask. There was no requirement to perform an extra acid-digestion step.

Central Composite Experimental Design

A central composite experimental design[11,12] was used to investigate whether the sample treatment procedures proposed above influence the determination of magnesium by AAS. The experiments were arranged according to Fig. 2 and the coded and true levels involved in this design are given in Table 1. The amount of chlorophyll per treatment was calculated using the concentrations obtained from the Lichtenhaler equation as described above.

The response selected in this study was the absorbance as measured by AAS and the calculations were carried out using the SAS statistical package.[13]

Standard Additions Graphs

In order to check the analyte concentration, standard addition graphs were prepared varying the concentration of Mg between 0 and 0.8 μg ml^{-1} and adding a constant sample volume (15 ml); in all instances the final volume was 50 ml.

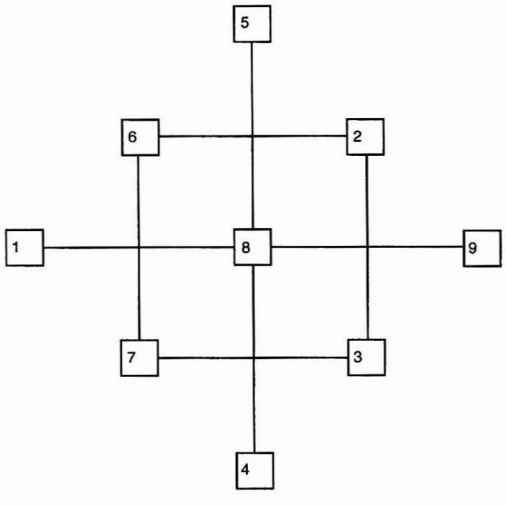

Fig. 2 Distribution of the experimental points in the space of two variables for a central composite experimental design.

Table 1 Design employed in this study

	Code levels		True levels*	
Point	Procedure A	Procedure B	Procedure A	Procedure B
1	−1.0	0.0	0.0	0.2
2	0.5	0.5	0.3	0.3
3	0.5	−0.5	0.3	0.1
4	0.0	−1.0	0.2	0.0
5	0.0	1.0	0.2	0.4
6	−0.5	0.5	0.1	0.3
7	−0.5	−0.5	0.1	0.1
8	0.0	0.0	0.2	0.2
9	1.0	0.0	0.4	0.2

* All the true levels are given in μg ml^{-1} of Mg.

The graphs obtained for the two procedures were compared with an Mg single calibration graph obtained between 0 and 1 μg ml^{-1}

Results and Discussion

The chromatogram of the extracted and purified chlorophyll *a* was recorded. The dry sample for this analysis was dissolved in acetone. The result was compared with a chromatogram obtained for Sigma (St. Louis, MO, USA) standard chlorophyll *a* in acetone. The comparison between these chromatograms suggests that the chlorophyll *a* placed in the ampoules is substantially free from impurities.

The amount of chlorophyll *a* per ampoule determined by electronic spectrometry in acetone using the Lichtenthaler equation was 2.70 ± 0.04 mg, corresponding to the average of three samples. With this value, it was possible to calculate the amount of Mg per ampoule as 73.47 μg. The molecular and atomic masses of the chlorophyll *a* and Mg used in the calculation were 893.48 and 24.312 g mol^{-1}, respectively.

The samples were prepared by procedures A and B and mixed to give the concentrations given in Table 2. In all instances the final volume of solvent was 25 ml.

The results obtained when the central composite design was applied (Table 2) show that the experimental response ($\hat{y}$) as a function of the two treatments applied can be approximated by the following equation:

$$\hat{y} = -0.020 + 0.881\,[A] + 0.876\,[B] \quad (1)$$

where [A] and [B] represent the Mg concentration in μg ml^{-1}

Table 2 AAS results

	True levels*		
Point	Procedure A	Procedure B	Response†
1	0.0	0.2	0.133, 0.135, 0.137
2	0.3	0.3	0.560, 0.561, 0.558
3	0.3	0.1	0.302, 0.299, 0.306
4	0.2	0.0	0.157, 0.159, 0.155
5	0.2	0.4	0.479, 0.480, 0.483
6	0.1	0.3	0.341, 0.343, 0.341
7	0.1	0.1	0.196, 0.195, 0.195
8	0.2	0.2	0.305, 0.305, 0.307
9	0.4	0.2	0.500, 0.504, 0.500

* All the true levels are given in μg ml^{-1}.
† All the responses are given in absorbance.

Table 3 ANOVA table for results in Table 2

Source	Degrees of freedom	Sum of squares	Mean square	*F*-Value	Significance (probability > *F*)
Model	2	0.55581	0.27791	311.876	0.0001
Error	24	0.02139	0.00089		
C_{total}	26	0.57720			

Table 4 Standard addition results (two ampoules). The two ampoules were mixed and divided into equal fractions for procedures A and B. Standard deviations for $n = 3$ given

Procedure	Mg concentration/ μg ml^{-1}	Amount of Mg per ampoule/μg	Amount of chlorophyll per ampoule/mg
A	0.209 ± 0.006	69.54 ± 2.07	2.556 ± 0.076
B	0.221 ± 0.006	73.72 ± 1.92	2.709 ± 0.070

obtained from procedures A and B, respectively. An analysis of variance (Table 3) reveals that a large proportion of the variance can be explained by eqn. (1). This result explains 96.29% of the variance.

The response surface generated by eqn. (1) suggests that both procedures give the same result in the range of acetone, acid and Mg concentrations studied. This observation was confirmed through a statistical comparison (*t*-test), which showed that the coefficients for concentrations estimated by procedures A and B in eqn. (1) are not significantly different at the 95% probability level.

An alternative method for the determination of Mg in each ampoule is to use the standard additions method. Independent experiments were performed, treating one ampoule by procedure A and another by procedure B. Unlike the above, the results of the two treatments were not mixed, and the following equations were obtained:

Sample treatment A:

$$\hat{y} = 0.182 + 0.871\,[Mg] \quad (2)$$

Sample treatment B:

$$\hat{y} = 0.199 + 0.898\,[Mg] \quad (3)$$

The gradients in eqns. (2) and (3), with standard errors of 0.010 and 0.009 absorbance ml μg^{-1}, respectively, did not reveal significant differences when the *t*-test was applied at the 95% probability level. This result is consistent with eqn. (1), which also showed no significant differences between the two treatments.

Using the ratio of the intercept and the slope of the regression line in eqns. (2) and (3), it is possible to calculate the amounts of Mg and chlorophyll *a* in each ampoule for both treatments and to compare these results (Table 4) with the estimate of 0.220 μg ml^{-1} of Mg obtained using the Lichtenthaler equation for electronic absorption. This last estimate was calculated assuming that 2.70 mg of chlorophyll *a* were dissolved in 100 ml (independently of the treatment) in order to prepare the standard addition samples, in which the intercept corresponds to the concentration in Mg as described under Experimental section.

The metal recoveries for procedures A and B were 99 and 98%, respectively. These high values show that both treatments are suitable for Mg determination.

The gradients from eqns. (2) and (3) are close to those from eqn. (1), as are the estimates of the total amount of chlorophyll per ampoule, and verify the results of the designed experiments. It is interesting that better agreement was obtained using the designed experiments than by independently comparing the estimates using the standard additions method.

Conclusion

Although both procedures provide similar estimates of chlorophyll *a* concentrations, the proposed method is a better alternative than acid digestion, because it is simpler and faster, so is suitable for routine analysis, and does not require pure acids, which means that it is safe and inexpensive.

We also find that using a two-treatment, two-factor, central composite design is a better way of comparing treatments than using the standard additions method. The approach in this paper requires only nine unique AAS experiments (although we took replicates), compared with 20 using the standard additions method. Quantification using the two-factor experiments is possible by calibrating to electronic absorption spectrometry and removes the need to perform standard additions, so reducing the amount of work required.

The Consejo Nacional de Investigaciones Cientificas y Tecnologicas de Venezuela (CONICIT) is thanked for financial

support (P.W.A.), and Dr. D. J. Roberts and E. Marcano are thanked for their valuable assistance and collaboration in the AAS measurements and a literature search, respectively.

References

1 Strain, H. H., Cope, B. T., and Svec, W. A., *Methods Enzymol.*, 1987, **23**, 452.
2 Porra, R. J., Thompson, W. A., and Kriedemann, P. E., *Biochim. Biophys. Acta*, 1989, **975**, 384.
3 Smith, J., and Benitez, A., in *Modern Methods of Plant Analysis*, ed. Paech, K., and Tracey, M. V., Berlin, 1955, vol. **4**, p. 42.
4 de Figuereido, J., *MSc Thesis*, University of Bristol, 1991.
5 Tsunoda, K., Inoue, N., Tachibana, M., and Aoyama, M., *J. Food Hyg. Soc. Jpn.*, 1993, **34**, 25.
6 Svec, W. A., *The Porphyrins*, ed. Dolphin, D., Academic Press, New York, 1978, pp. 341–399.
7 Iriyama, K., Ogura, N., and Takamiya, A., *J. Biochem.*, 1974, **76**, 901.
8 Rahmani, A., Eckardt, C. B., Brereton, R. G., and Maxwell, J. R., *Photochem. Photobiol.*, 1993, **57**, 1048.
9 Brereton, R. G., Rahmani, A., Liang, Y., and Kvalheim, O. M., *Photochem. Photobiol.*, 1994, **59**, 99.
10 Lichtenthaler, H. K., *Methods Enzymol.*, Academic Press, New York, 1987, **148**, 350.
11 Brereton, R. G., *Chemometrics, Applications of Mathematics and Statistics to Laboratory Systems*, Ellis Horwood, Chichester, 1993, pp. 27–84.
12 Deming, S. N., and Morgan, S. L., *Experimental Design: a Chemometric Approach*, Elsevier, Amsterdam, 1987, pp. 227–278.
13 *SAS/STAT User's Guide, Version 6*, SAS Institute, Cary, NC, 4th edn., 1989, vol. 2.

Paper 4/03973D
Received June 30, 1994
Accepted September 9, 1994

H-Point Standard Additions Method for Analyte Determination in Ternary Mixtures

J. Verdú Andrés, F. Bosch Reig and P. Campíns Falcó*

Departament de Química Analítica, Facultat de Química, Universitat de València, c/Dr. Moliner, 50, E46100-Burjassot (València), Spain

The use of the H-point standard additions method for resolving ternary mixtures is proposed. The method calculates the analyte concentration from spectral data at two wavelengths where the two species selected as interferents present the same absorbance relationship. These wavelength pairs are easily found, and can be selected to give the most precise results. If a matrix effect is present, use of the standard additions method is necessary in order to obtain good results. If there is no matrix effect, only sample absorbances and molar absorption coefficients are necessary. Ternary mixtures of phenol, *o*-cresol, 4-chlorophenol and 3,4-dichlorophenol, which are species with highly overlapped spectra throughout the wavelength range, were selected to test the method. The results obtained are comparable to those obtained using multilinear regression.

Keywords: *Ternary mixture; H-point standard additions method; analyte determination; bias error; spectrophotometry*

Introduction

The simultaneous determination of two or more compounds in the same sample without previous chemical separation has been developed from several mathematical procedures. For binary mixtures, some of these procedures are based on the use of absorbance data, such as multivariate calibration,[1] multiwavelength linear regression analysis,[2] apparent content curves[3] and other linear algorithms for extension of pattern recognition methods of a more qualitative nature, such as regression on latent variables (principal component regression, PCR, and partial least squares, PLS).[4] Other methods use derivative spectrophotometry, such as zero-crossing measurements[5] and first derivative of the ratios of spectra.[6] Some of these methods have also been developed for resolving ternary mixtures. The accuracy of various graphical (zero-crossing and derivative quotient spectra with standardized divisor) and numerical methods (MULTIC and PLS) has been studied[7,8] for amitriptyline–imipramine–perphenazine and acetylsalicylic acid–caffeine–thiamine binary and ternary mixtures. Numerical methods were found to be particularly suitable for multicomponent analysis, especially for mixtures containing more than two analytes with highly overlapped spectra.

In this work, the previously described basis of the H-point standard additions method (HPSAM) for binary mixtures[9–12] is developed for ternary mixtures. The results are compared with those obtained using multilinear regression (MLR) in some phenol–*o*-cresol–4-chlorophenol–3,4-dichlorophenol ternary mixtures; the spectra of these compounds overlapped severely throughout the wavelength range.

* To whom correspondence should be addressed.

Theoretical Background

Let us suppose that a ternary mixture S consists of compounds X, Y and Z. Their spectra are shown in Fig. 1. The absorbance of the sample at each wavelength will be the sum of the individual absorbances of the species X, Y and Z at this wavelength:

$$A_{S,j} = \varepsilon_{X,j} \times C^0_X + \varepsilon_{Y,j} \times C^0_Y + \varepsilon_{Z,j} \times C^0_Z = A^0_{X,j} + A^0_{Y,j} + A^0_{Z,j};\ \lambda_j \in (\lambda_l, \lambda_k) \quad (1)$$

where $\varepsilon_{X,j}$, $\varepsilon_{Y,j}$ and $\varepsilon_{Z,j}$ are the molar absorption coefficients for the species X, Y and Z at λ_j; C^0_X, C^0_Y and C^0_Z are the concentrations of the species X, Y and Z in the sample, and $A^0_{X,j}$, $A^0_{Y,j}$ and $A^0_{Z,j}$ are the individual absorbances of the species X, Y and Z in the sample.

When a binary mixture is considered, the HPSAM develops a procedure to quantify an analyte X in the presence of a direct interferent Y, by the construction of two standard additions plots, with slopes $M_{X,X(l)}$ and $M_{X,X(k)}$, at two previously selected wavelengths, $\lambda_{X(l)}$ and $\lambda_{X(k)}$, which intersect at the H-point, with coordinates $(-C_{H(X)}, A_H)$. The H-point is a function of the analyte concentration (C^0_X) according to the expression:[9–12]

$$-C_{H(X)} = \frac{[A^0_{X,X(k)} - A^0_{X,X(l)}] + [A^0_{Y,X(k)} - A^0_{Y,X(l)}]}{M_{X,X(l)} - M_{X,X(k)}} = -C^0_X + \frac{A^0_{Y,X(k)} - A^0_{Y,X(l)}}{M_{X,X(l)} - M_{X,X(k)}} \quad (2)$$

If $\lambda_{X(l)}$ and $\lambda_{X(k)}$ are selected in such a way that the interferent absorbance values are equal $[A^0_{Y,X(l)} = A^0_{Y,X(k)}]$, the abscissa of the H-point will be the analyte concentration, $-C_{H(X)}$:

$$-C_{H(X)} = \frac{A^0_{X,X(k)} - A^0_{X,X(l)}}{M_{X,X(l)} - M_{X,X(k)}} = -C^0_X \quad (3)$$

according to the basis of the HPSAM.

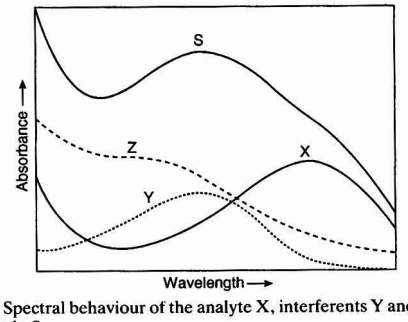

Fig. 1 Spectral behaviour of the analyte X, interferents Y and Z, and the sample S.

For ternary mixtures, if we wish to determine one compound, for example the species X, in the presence of the other two species Y and Z, by using the HPSAM, we have to find two wavelengths $\lambda_{X(l)}$ and $\lambda_{X(k)}$ where the following condition is fulfilled:

$$\frac{A_{Y,X(l)}}{A_{Y,X(k)}} = \frac{A_{Z,X(l)}}{A_{Z,X(k)}} = r_{Y,Z} \quad (4)$$

Fig. 2(*a*) shows the spectral behaviour of the sample at the two selected wavelengths, if only $\lambda_{X(l)}$ and $\lambda_{X(k)}$ are considered. Fig. 2(*b*) gives the same plot after transformation of the data taking into account the factor $r_{Y,Z}$, which depends only on the molar absorption coefficients of compounds Y and Z. The factor $r_{Y,Z}$ allows the transformation of the analytical signals for Y and Z at $\lambda_{X(l)}$ and $\lambda_{X(k)}$ into a null slope line. In this way, the fundamentals of the previously described HPSAM for binary mixtures[9–12] are now of use.

The equations for the HPSAM lines at the two previously selected wavelengths $\lambda_{X(l)}$ and $\lambda_{X(k)}$ will be (Fig. 3):

For $\lambda_{X(l)}$:

$$A[\lambda_{X(l)}] = A^0_{X,X(l)} + A^0_{Y,X(l)} + A^0_{Z,X(l)} + M_{X,X(l)} \times C^i_X; \quad i = 0, 1, \ldots, n \quad (5)$$

For $\lambda_{X(k)}$:

$$A[\lambda_{X(k)}] = A^0_{X,X(k)} + A^0_{Y,X(k)} + A^0_{Z,X(k)} + M_{X,X(k)} \times C^i_X; \quad i = 0, 1, \ldots, n \quad (6)$$

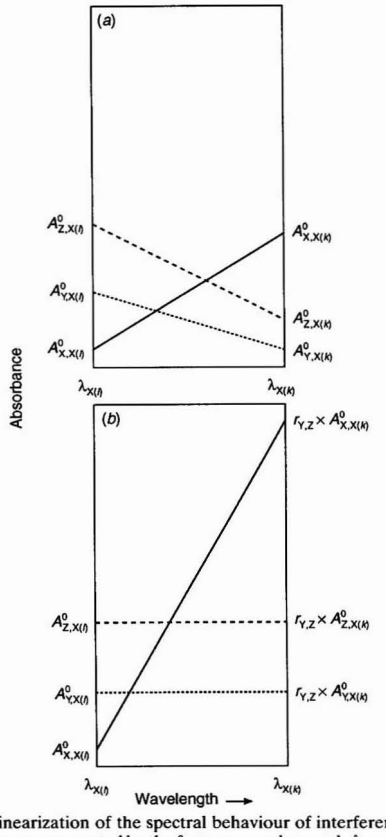

Fig. 2 Linearization of the spectral behaviour of interferents Y and Z when they are corrected by the factor $r_{Y,Z}$, where only $\lambda_{X(l)}$ and $\lambda_{X(k)}$ are taken into account.

where $A[\lambda_{X(l)}]$ and $A[\lambda_{X(k)}]$ are the measured absorbances at the two previously selected wavelengths; $M_{X,X(l)}$ and $M_{X,X(k)}$ are the slopes of the lines obtained at $\lambda_{X(l)}$ and $\lambda_{X(k)}$; C^i_X is the concentration of analyte X in the solution i; and n is the number of additions of pure analyte. When $i = 0$, this corresponds to the situation where the solution is the sample.

If we multiply eqn. (6) by the value for $r_{Y,Z}$ obtained in expression (4) we obtain (Fig. 3):

$$r_{Y,Z} \times A[\lambda_{X(k)}] = r_{Y,Z} \times A^0_{X,X(k)} + r_{Y,Z} \times A^0_{Y,X(k)} + r_{Y,Z} \times A^0_{Z,X(k)} + r_{Y,Z} \times M_{X,X(k)} \times C^i_X = r_{Y,Z} \times A^0_{X,X(k)} + A^0_{Y,X(l)} + A^0_{Z,X(l)} + r_{Y,Z} \times M_{X,X(k)} \times C^i_X \quad (7)$$

Eqns. (5) and (7) permit the calculation of the unbiased analyte concentration from the abscissa of their intersection point, which is the H-point $[-C_{H(X)}, A_{H(Y,Z)}]$.

$$A^0_{X,X(l)} + A^0_{Y,X(l)} + A^0_{Z,X(l)} + M_{X,X(l)} \times [-C_{H(X)}] = r_{Y,Z} \times A^0_{X,X(k)} + A^0_{Y,X(l)} + A^0_{Z,X(l)} + r_{Y,Z} \times M_{X,X(k)} \times [-C_{H(X)}]$$

$$-C_{H(X)} = \frac{A^0_{X,X(l)} - r_{Y,Z} \times A^0_{X,X(k)}}{r_{Y,Z} \times M_{X,X(k)} - M_{X,X(l)}} \quad (8)$$

where $C_{H(X)} = C^0_X$ is the unbiased analyte concentration in the sample, because eqn. (6) depends only on the variables related to the analyte. The incorrigible error due to the presence of two interferents has been transformed into a constant systematic error, as the basis of the HPSAM predicts. In effect, the value of $A_{H(Y,Z)}$ obtained will be:

$$A_{H(Y,Z)} = A^0_{Y,X(l)} + A^0_{Z,X(l)} = r_{Y,Z} \times [A^0_{Y,X(k)} + A^0_{Z,X(k)}] \quad (9)$$

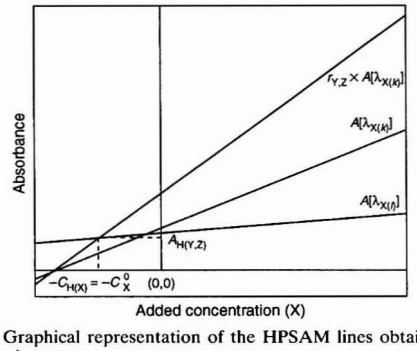

Fig. 3 Graphical representation of the HPSAM lines obtained for ternary mixtures.

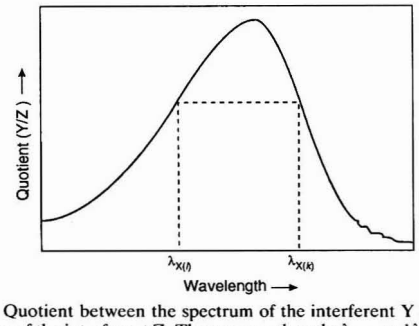

Fig. 4 Quotient between the spectrum of the interferent Y and the spectrum of the interferent Z. The two wavelengths $\lambda_{X(l)}$ and $\lambda_{X(k)}$ are such that eqn. (10) is fulfilled.

Table 1 Composition of the four samples assayed

Sample	X/10^{-5} mol l^{-1}	Y/10^{-5} mol l^{-1}	Z/10^{-5} mol l^{-1}
A	*o*-Cresol 4.467	4-Chlorophenol 3.730	3,4-Dichlorophenol 2.983
B	3,4-Dichlorophenol 2.983	Phenol 5.104	*o*-Cresol 4.467
C	Phenol 5.104	*o*-Cresol 4.467	4-Chlorophenol 3.730
D	4-Chlorophenol 3.730	Phenol 5.104	3,4-Dichlorophenol 2.983

The wavelengths at which eqn. (4) is fulfilled are easily found, as it is derived from this equation, re-written in the following form:

$$\frac{A_{Y,X(l)}}{A_{Z,X(l)}} = \frac{r_{Y,Z} \times A_{Y,X(k)}}{r_{Y,Z} \times A_{Z,X(k)}} = \frac{A_{Y,X(k)}}{A_{Z,X(k)}} \quad (10)$$

because in this case $r_{Y,Z}$ will be the same for the compounds Y and Z.

Only one spectrum of the species Y and another of the species Z are needed. The quotient between both spectra is then applied and the wavelength pairs that show the same value for this quotient are sought. Although this relationship depends on the concentrations of Y and Z, it will be equal at the two selected wavelengths, independently of the concentrations chosen. Fig. 4 shows the quotient between a spectrum of the species Y and a spectrum of the species Z, and two

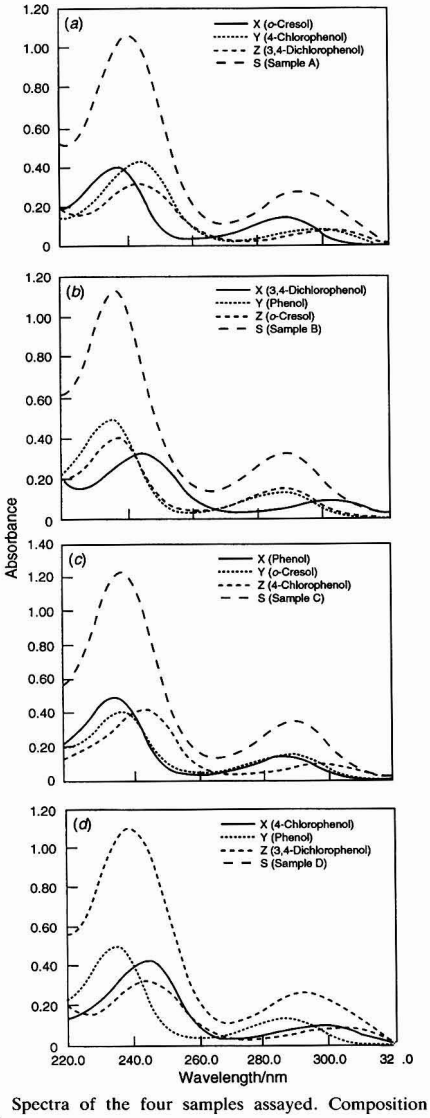

Fig. 5 Spectra of the four samples assayed. Composition as in Table 1.

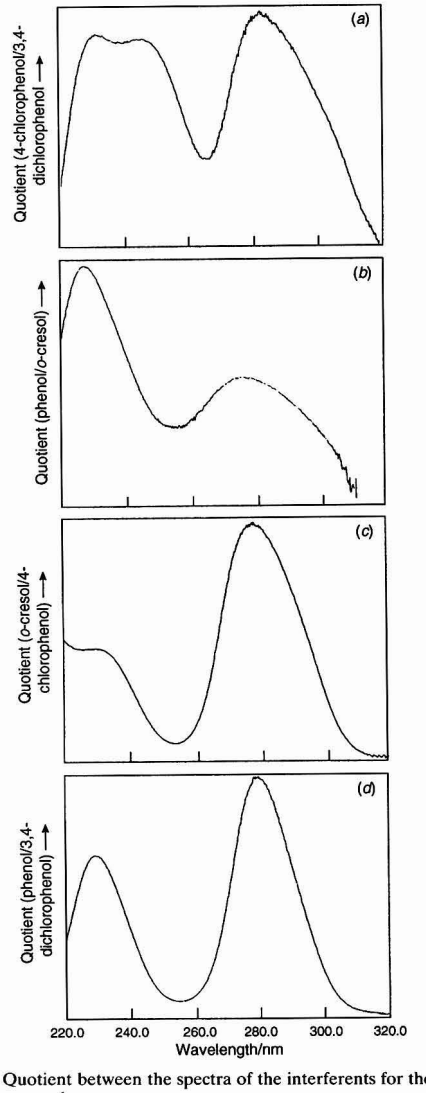

Fig. 6 Quotient between the spectra of the interferents for the four samples assayed.

wavelengths $\lambda_{X(l)}$ and $\lambda_{X(k)}$ where eqn. (10) is fulfilled. These wavelength pairs depend only on the nature of the species Y and Z, and not on the nature of X. Hence, these wavelength pairs allow the determination of any analyte X in the presence of the interferents Y and Z simultaneously. From all the possible wavelengths pairs, it will be demonstrated that for every analyte there are some pairs that provide the best sensitivity.

The quotient of eqn. (8) should be optimized to give the greatest value, and hence to obtain the most precise results. As the wavelength pairs which obey eqn. (4) are known, the optimization is easily performed for each analyte.

If matrix effects are known not to be present, the method can be simplified experimentally by using sample absorbances. The $M_{X,X(l)}$ and $M_{X,X(k)}$ values used can be obtained from the calibration lines for the species X: the molar absorption coefficients. In this instance eqn. (8) transforms to:

$$-C_{H(X)} = \frac{A_{S,X(l)} - r_{Y,Z} \times A_{S,X(k)}}{r_{Y,Z} \times \varepsilon_{X,X(k)} - \varepsilon_{X,X(l)}} \quad (11)$$

which permits the calculation of the concentration of the analyte X without the need for standard additions. The optimization of the value of the denominator in eqn. (8) or (11) can be performed for each analyte in order to obtain the most precise results.

Experimental

Apparatus

A detection system consisting of a Perkin-Elmer Lambda 16 UV/VIS double-beam spectrophotometer, equipped with 1 cm pathlength quartz cells, was used. The slit-length was 1 nm and a scan speed of 60 nm min^{-1} was selected. The spectra were recorded at 0.2 nm intervals. The spectophotometer was interfaced to an Ataio S-2000 AT computer and an Epson LQ-4000 printer.

Reagents

Sodium hydroxide (Panreac; Barcelona, Spain) (0.5 mol l^{-1}) was used. Stock solutions (1000 ppm) of the different phenols were prepared by weighing the appropriate amount of the substance and dissolving it in 250 ml of distilled water. Phenol (Merck, Darmstadt, Germany), *o*-cresol (Merck, Schuchardt, Germany), 4-chlorophenol (Aldrich, Steinheim, Germany) and 3,4-dichlorophenol (Aldrich, Gillingham, Dorset, UK) were used). Stock solutions were stored in borosilicate glass vessels in a refrigerator. Working solutions were prepared daily by appropriate dilution of the stock solutions.

Table 3 Results obtained for analyte X concentration (10^{-5} mol l^{-1}) in the four samples assayed, using the proposed HPSAM and multivariate calibration (501 points)

	HPSAM		Multivariate calibration	
Sample A: (*o*-cresol as analyte)				
Replicate 1	4.56 ± 0.01		4.69 ± 0.01	
Replicate 2	4.64 ± 0.01		4.42 ± 0.01	
Replicate 3	4.55 ± 0.07		4.24 ± 0.01	
Mean of three values	4.58 ± 0.05		4.45 ± 0.23	
s_r* (%) E_r† (%)	1.01	2.57	5.11	−0.38
Sample B: (3,4-dichlorophenol as analyte)				
Replicate 1	2.96 ± 0.04		3.03 ± 0.01	
Replicate 2	3.10 ± 0.01		3.08 ± 0.01	
Replicate 3	3.19 ± 0.01		3.11 ± 0.01	
Mean of three values	3.09 ± 0.11		3.07 ± 0.04	
s_r* (%) E_r† (%)	3.77	3.45	1.35	3.05
Sample C: (phenol as analyte)				
Replicate 1	5.50 ± 0.18		5.52 ± 0.02	
Replicate 2	4.71 ± 0.39		4.99 ± 0.02	
Replicate 3	4.52 ± 0.49		5.11 ± 0.02	
Mean of three values	4.91 ± 0.52		5.11 ± 0.37	
s_r* (%) E_r† (%)	10.62	−3.84	7.17	0.06
Sample D: (4-chlorophenol as analyte)				
Replicate 1	4.34 ± 0.18		4.31 ± 0.02	
Replicate 2	3.62 ± 0.17		3.57 ± 0.01	
Replicate 3	4.04 ± 0.51		3.80 ± 0.03	
Mean of three values	4.00 ± 0.36		3.89 ± 0.38	
s_r* (%) E_r† (%)	9.07	7.16	9.75	4.29

* s_r = Relative standard deviation.
† E_r = Relative error.

Table 2 Selected wavelength pairs for analyte determination in the four samples, together with values for $r_{Y,Z}$ and $r_{Y,X} \times M_{X,X(k)} - M_{X,X(l)}$ at those wavelengths

	Selected wavelength pairs/nm				
	$r_{Y,Z}$				
Sample	$r_{Y,Z} \times M_{X,X(k)} - M_{X,X(l)}$				
A (*o*-cresol as analyte)	246.4, 276.4 12.1210 −20 387	245.0, 276.4 12.3984 −20 001	244.6, 276.4 12.4340 −19 787	248.8, 276.2 11.1835 −19 697	244.4, 276.4 12.4547 −19 684
B (3,4-dichlorophenol as analyte)	243.6, 283.2 2.1189 8087	243.0, 279.8 2.6334 8029	2440, 285.0 1.9157 8016	243.8, 284.4 1.9916 8015	243.0, 280.6 2.5352 8013
C (phenol as analyte)	232.8, 295.6 3.2031 3695	234.4, 296.0 3.5074 3565	235.2, 296.2 3.6347 3461	233.0, 266.4 7.7956 3095	229.8, 266.6 6.5184 3066
D (4-chlorophenol as analyte)	220.0, 241.4 0.6420 −3350	220.2, 241.2 0.6351 −3191	220.8, 240.4 0.6126 −2750	245.4, 300.0 3.8146 2101	243.0, 298.0 4.0208 1618

Procedures

The absorption spectra of phenol, *o*-cresol, 4-chlorophenol and 3,4-dichlorophenol, solutions (prepared in 0.1 mol l^{-1} NaOH immediately before the measurements) were recorded in order to obtain the spectral data for multivariate calibration. The wavelength interval selected was 220–320 nm. The baseline correction was made with 0.1 mol l^{-1} NaOH immediately before each replicate measurement. In order to apply the proposed HPSAM, ternary mixtures were prepared. Their compositions are shown in Table 1, where the species considered as the analyte is denoted by X. The analyte concentrations added to each sample varied from 0 to 1.063×10^{-4} mol l^{-1} for phenol, from 0 to 9.307×10^{-5} mol l^{-1} for *o*-cresol, from 0 to 7.771×10^{-5} mol l^{-1} for 4-chlorophenol and from 0 to 6.215×10^{-5} mol l^{-1} for 3,4-dichlorophenol.

Results and Discussion

Fig. 5 shows the spectra of the synthetic ternary mixtures prepared according to the data in Table 1. As can be observed, the spectra of the analyte and interferents overlaps severely throughout the wavelength range for the four samples. In addition, in two of the samples, C and D, the analyte spectrum also completely overlaps that of one of the interferents (sample C: phenol maxima at 234.6 and 287.0 nm and *o*-cresol maxima at 236.6 and 288.4 nm; sample D: 4-chlorophenol maxima at 243.8 and 298.4 nm and 3,4-dichlorophenol maxima at 243.8 and 303.0 nm). Hence, extreme situations have been selected in order to study the possibilities of using the proposed method to determine an analyte in ternary mixtures.

In order to resolve the mixtures, the quotients between the spectra of Y and Z must be obtained, according to eqn. (8). Fig. 6 shows these quotients. It must be noted that if the spectral behaviour of the two interferents is similar, as in mixtures A and B [Fig. 5(*a*) and (*b*)], then the quotients are obtained with some noise [Fig. 6(*a*) and (*b*)]. However, for the mixtures C and D, where the spectral behaviour of the interferents is different [Fig. 5(*c*) and (*d*)], the quotients obtained are smoother. From these results we can obtain the wavelength pairs that show the same value in order to calculate the analyte concentration. This method can be employed to determine any analyte in the presence of a selected pair of interferents. As an example, Table 2 shows the five best wavelength pairs [those that give the greatest value for the denominator in eqn. (8)] for the four samples assayed, the $r_{Y,Z}$ values estimated according to eqn. (4) and $r_{Y,Z} \times M_{X,X(k)} - M_{X,X(l)}$ at those wavelengths. Five pairs of values are selected in order to minimize the error introduced by the noise. As can be seen in Table 3, which shows the results obtained for three replicates of each sample, the standard deviation of the results obtained for samples A and B is smaller than that obtained for samples C and D, because the precision of the method depends principally on the denomin-

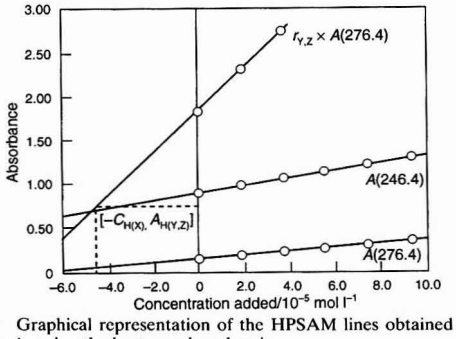

Fig. 7 Graphical representation of the HPSAM lines obtained for sample A, using the best wavelength pair.

Table 4 Results obtained for the concentrations of the interferents Y and Z (10^{-5} mol l^{-1}) in the four samples assayed, using the proposed HPSAM (employing sample absorbance values and molar absorption coefficients for each compound as *M* values) and multivariate calibration (501 points)

	HPSAM		Multivariate calibration	
Sample A: (4-chlorophenol as analyte)				
Replicate 1	4.16 ± 0.28		3.87 ± 0.01	
Replicate 2	3.56 ± 0.23		4.63 ± 0.03	
Replicate 3	4.00 ± 0.12		4.29 ± 0.02	
Mean of three values	3.91 ± 0.31		4.17 ± 0.26	
s_r* (%) E_r† (%)	8.07	4.80	6.25	11.87
Sample A: (3,4-dichlorophenol as analyte)				
Replicate 1	2.52 ± 0.08		2.75 ± 0.01	
Replicate 2	3.18 ± 0.12		2.43 ± 0.03	
Replicate 3	3.09 ± 0.10		2.59 ± 0.02	
Mean of three values	2.93 ± 0.36		2.59 ± 0.16	
s_r* (%) E_r† (%)	12.27	−1.75	6.16	−13.14
Sample B: (phenol as analyte)				
Replicate 1	5.13 ± 0.05		5.20 ± 0.02	
Replicate 2	4.85 ± 0.03		4.76 ± 0.01	
Replicate 3	4.64 ± 0.05		4.63 ± 0.02	
Mean of three values	4.87 ± 0.24		4.86 ± 0.30	
s_r* (%) E_r† (%)	5.03	−4.53	6.08	−4.73
Sample B: (*o*-cresol as analyte)				
Replicate 1	4.70 ± 0.05		4.49 ± 0.01	
Replicate 2	4.68 ± 0.13		4.78 ± 0.01	
Replicate 3	4.78 ± 0.09		4.84 ± 0.03	
Mean of three values	4.72 ± 0.05		4.70 ± 0.19	
s_r* (%) E_r† (%)	1.11	5.65	3.97	4.75
Sample C: (*o*-cresol as analyte)				
Replicate 1	4.18 ± 0.06		4.22 ± 0.02	
Replicate 2	4.44 ± 0.10		4.58 ± 0.02	
Replicate 3	4.71 ± 0.09		4.65 ± 0.02	
Mean of three values	4.44 ± 0.27		4.48 ± 0.24	
s_r* (%) E_r† (%)	6.00	−0.60	5.25	0.38
Sample C: (4-chlorophenol as analyte)				
Replicate 1	3.66 ± 0.01		3.63 ± 0.01	
Replicate 2	3.82 ± 0.04		3.84 ± 0.01	
Replicate 3	3.85 ± 0.02		3.88 ± 0.01	
Mean of three values	3.78 ± 0.10		3.78 ± 0.14	
s_r* (%) E_r† (%)	2.72	1.21	3.63	1.46
Sample D: (phenol as analyte)				
Replicate 1	4.84 ± 0.01		5.10 ± 0.01	
Replicate 2	5.02 ± 0.02		5.10 ± 0.01	
Replicate 3	5.05 ± 0.01		4.95 ± 0.01	
Mean of three values	4.97 ± 0.11		5.05 ± 0.09	
s_r* (%) E_r† (%)	2.25	−2.63	1.74	−1.11
Sample D: (3,4-dichlorophenol as analyte)				
Replicate 1	2.12 ± 0.23		2.35 ± 0.01	
Replicate 2	2.87 ± 0.11		3.20 ± 0.01	
Replicate 3	3.73 ± 0.12		3.34 ± 0.03	
Mean of three values	2.91 ± 0.80		2.96 ± 0.54	
s_r* (%) E_r† (%)	27.65	−2.43	18.21	−0.67

* s_r = Relative standard deviation.
† E_R = Relative error.

ator of eqn. (8). As can be deduced from Fig. 5, this value depends on the similarity of the spectra of the analyte and the interferents. The greater the similarity between the analyte and the interferents, the lower the value of the slope.

Table 3 compares the results obtained using the proposed method with those obtained by using multivariate calibration over the entire wavelength range measured (501 points), following the matricial algorithm described in ref. 13. It can be observed that, with only five points (ten measured wavelengths), the proposed method yields results of comparable accuracy to those provided by multivariate calibration. This is because, for each sample, the wavelength pairs were selected in order to obtain the best results, and this selection is made before starting the measuring process. This is an important point to take into account in the experimental design. In addition, this step can lead to an increase in the sensitivity of the method, as shown in Fig. 7, because correction with the factor $r_{Y,Z}$ can lead to lines with higher slope than the maximum shown by the analyte. However, the standard deviation of the method for each replicate is more similar to the standard deviation observed among replicates than those obtained by MLR, as can be seen in Table 3.

Table 4 shows the results obtained for species Y and Z employing sample absorbance values and the molar absorption coefficients for each compound (because the matrix effect is absent) as M values [eqn. (11)]. As can be observed, the values obtained are comparable to those obtained using MLR. Even in the less favourable cases, when the spectrum of the species considered as the analyte overlaps completely that of the interferent (sample A), previous optimization of the selected wavelengths allows better accuracy to be obtained than that provided by MLR. As regards the standard deviation, the discussion above is also valid in this case.

Conclusions

Based on the results obtained, it has been shown that the proposed HPSAM for resolving ternary mixtures calculates the analyte concentration free from bias error from the abscissa of the H-point. The principal advantages of the method are: (1) Absorbance data, and not first derivative data, are used; hence the signal-to-noise ratio is not diminished. In addition, the method takes into account the matrix effect. (2) The wavelength pairs for measuring the analyte are easily obtained from the spectral behaviour of the interferents. (3) Only five points (ten measured wavelengths) are necessary to obtain good results. (4) The method works well even if the interferents overlap the analyte band(s) completely.

The authors are grateful to the DGICYT (Project No. PB 91-0651) for financial support. Jorge Verdú Andrés acknowledges a grant from the Conselleria d'Educació i Ciència of the Generalitat Valenciana for carrying out Ph.D. studies.

References

1 Martens, H., Dr. Techn. Thesis, University of Trondheim, Norway, 1985.
2 Blanco, M., Gene, J., Iturriaga, H., Maspoch, S., and Riba, J., *Talanta*, 1987, **34**, 987.
3 Llobat Estellés, M., Marín Saez, R., and San Martín Ciges, M. D., *Fresenius' J. Anal. Chem.*, 1992, **342**, 538.
4 Chemometrics: a Textbook, eds. Massart, D. L., Vandeginste, B. G. M., Deming, S. N., Michote, Y., and Kaufman, L., Elsevier, Amsterdam, 1988.
5 O'Haver, T. C., *Anal. Chem.*, 1979, **51**, 91A.
6 Salinas, F., Berzas Navarro, J. J., and Espinosa Mansilla, A., *Talanta*, 1990, **37**, 347.
7 García Fraga, J. M., Jiménez Abizanda, A. I., Jiménez Moreno, F., and Arias León, J. J., *Anal. Chim. Acta*, 1991, **252**, 107.
8 Bautista, R. D., Jiménez, F., Jiménez, A. I., and Arias, J. J., *Talanta*, 1993, **40**, 1687.
9 Bosch Reig, F., and Campíns Falcó, P., *Analyst*, 1988, **113**, 1011.
10 Bosch Reig, F., and Campíns Falcó, P., *Analyst*, 1990, **115**, 111.
11 Campíns Falcó, P., Bosch Reig, F., and Molina Benet, A., *Fresenius' J. Anal. Chem.*, 1990, **338**, 16.
12 Campíns Falcó, P., Bosch Reig, F., and Verdú Andrés, J., *Talanta*, 1992, **39**, 1.
13 Draper, N. R., and Smith, H., *Applied Regression Analysis*, Wiley, New York, 1981.

Paper 4/04173I
Received July 8, 1994
Accepted September 13, 1994

Simultaneous Determination of Several Amino Acids With Multivariate Calibration Methods by Using a Continuous-flow System

J. Saurina and S. Hernández-Cassou*

Departament de Química Analítica, Universitat de Barcelona, Diagonal 647, 08028 Barcelona, Spain

An initial approach to the simultaneous determination of several amino acids by using multivariate calibration methods is proposed. The method is based on the development of the reaction between amino acids and 1,2-naphthoquinone-4-sulfonate. Spectra of the corresponding derivatives obtained from a continuous-flow system were used to provide multivariate data for the multivariate procedure. Two multivariate calibration methods were applied, principal component regression (PCR) and partial least-squares regression (PLS). In order to compare the resolution capabilities of these multivariate methods, a series of synthetic solutions containing different concentrations of lysine, proline, phenylalanine and tryptophan were prepared. The selection of solutions for calibration and problem sets was performed on the basis of the distribution of the amino acid derivatives spectra on the first and second principal components. The effects of the number of working wavelengths, the number of principal components and the mathematical treatment of data (smoothed and derivative spectra) on the predictions were also investigated. The method was applied to the analysis of feed samples, where the determination of some particular amino acids such as lysine are of special interest. The results were in good agreement with those obtained with the standard amino acid autoanalyser procedure.

Keywords: *Continuous-flow analysis; principal component regression; partial least-squares regression; amino acid determination; 1,2-naphthoquinone-4-sulfonate*

Introduction

The coupling of detection systems to data acquisition units has permitted the collection of large amounts of data. Continuous-flow methodologies have facilitated the generation of data in an easier way. Several multivariate calibration methods have recently been developed for the treatment of this information and they have become important tools for analytical chemistry. In contrast to univariate counterparts, these methods use more than one variable (*e.g.*, absorbance at different wavelengths). The application of multivariate calibration techniques to flow systems data has been reported in several papers.[1–9]

Typical procedures for amino acid determination have usually been based on chromatography. Chromatographic techniques provide accurate results but may be unsuitable for the analysis of large sets of samples because the separation step is time consuming. However, the simultaneous determination of several analytes is also possible using multivariate calibration and these techniques present advantages over chromatography as they are faster, sample treatment is usually reduced and the removal of interferences is not strictly required in many instances.

* To whom correspondence should be addressed.

A continuous-flow spectrophotometric method based on the reaction with 1,2-naphthoquinone-4-sulfonate (NQS) has been developed previously for amino acid determination.[10] NQS is a general spectrophotometric reagent for both primary and secondary amino groups. The reaction has to be developed on-line because NQS decomposes in alkaline medium. In this work, this reaction was applied to the resolution of some synthetic mixtures of four amino acids (Phe, Lys, Trp and Pro). The continuous-flow method was used for the generation on-line of the corresponding NQS derivatives, the spectra of which provide the multivariate data to be used in the multivariate calibration procedure. This study is a preliminary step for further application to the determination of particular amino acids such as Lys in feed samples.

The analyses were performed by using two multivariate calibration methods, principal component regression (PCR) and partial least-squares regression (PLS). PCR and PLS model the concentration values as a function of response (inverse calibration). The main advantage of inverse calibration is that only the species of interest need to be known, although unknown species have to be included in the samples because they have to be modelled implicitly. A common requirement for all these calibration techniques is that problem and calibration samples must have the same nature. PCR and PLS are based on the concentration of the total information of a response matrix in the fewest number of new variables, called principal components, which are able to describe the significant information contained in multivariate data such as spectra, kinetics and others. In PCR the first initial component describes the largest variance in the response matrix. The second principal component describes the next largest variance of the residual information and it is orthogonal to the first. In this way, the following principal components are calculated. The difference between PCR and PLS lies in how the calculations of principal components are performed. Whereas PCR uses only the information of the response matrix, PLS utilizes both the response matrix and the concentration matrix for calibration. The orthogonality of the principal components is lost in the PLS model. PCR and PLS allow the treatment of the full spectrum without the need for wavelength selection because the use of principal components overcomes the collinearity problems due to redundant information. More detailed descriptions are given elsewhere.[11–13]

In this work, as PLS provided the most accurate predictions, it was applied to the determination of amino acids in extracts of commercial feed samples.

Experimental

Reagents

All chemicals were of analytical-reagent grade.

Sodium 1,2-naphthoquinone-4-sulfonate (NQS) (Aldrich,

Milwaukee, WI, USA) was used to prepare a 1×10^{-3} mol l^{-1} stock standard solution in 0.1 mol l^{-1} HCl. This solution is stable for at least 2 weeks.

A stock standard buffer solution of 0.1 mol l^{-1} sodium carbonate (Scharlau)–0.75 mol l^{-1} sodium hydroxide (Merck, Elmsford, NY, USA) was used for the development of the reaction at pH 10, whereas 0.1 mol l^{-1} sodium carbonate–0.12 mol l^{-1} sodium hydroxide was used to obtain a pH of 12.

All amino acids used in the preparation of the mixture solutions were supplied by Merck.

Commercial feed samples were obtained from Cooperativa Agropecuaria de Guissona (Lleida, Spain).

Apparatus and Flow Manifold

The continuous-flow manifold used (Fig. 1) is described as follows. Solutions were pumped through standard Tygon tubing by using a peristaltic pump (Scharlau HP4). The sample solution S merged with an alkaline reagent stream emerging from the mixing chamber. This alkaline solution was generated on-line from the NQS stock standard solution R and the stock standard buffer solution B. The analytical reaction was developed in a PTFE reaction coil (10 m × 0.35 mm i.d.) which was placed in a thermostated bath (SBS TFB-3) kept at 70 °C. Spectra were recorded in the range 290–590 nm using a Beckman DU7 spectrophotometer with a Hellma flow cell (path length 10 mm and volume 18 μl). The measurement process started by recording the background spectrum, which was obtained by pumping water instead of sample solution through channel S. Next, samples were pumped and their spectra were recorded when the absorbance values had attained the steady state.

Data Acquisition and Treatment

Data acquisition was performed with a microcomputer using Dumod software[14] and the absorbance values of NQS–amino acid derivatives were stored at wavelengths from 290 to 590 in steps of 1 nm. The data treatment was done with MATLAB for Windows (Version 4.0).[15] The multivariate calibration software was implemented for MATLAB use.[16]

Results and Discussion

The continuous-flow system (Fig. 1) was utilized for the generation of the NQS derivative spectra to be used as multivariate data. Multivariate calibration methods are suitable for the analysis of large numbers of samples (such as those generated in the elaboration of feed samples). However, they are not advisable for the determination of large numbers of analytes because the complexity of the calibration becomes too great. Moreover, the preparation and analysis of the standards belonging to the calibration set are the most expensive step in the multivariate calibration procedure.

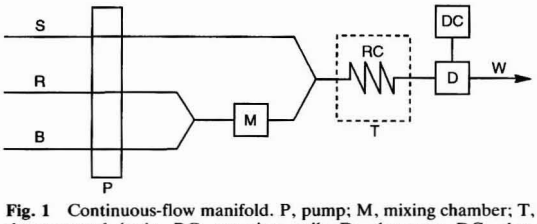

Fig. 1 Continuous-flow manifold. P, pump; M, mixing chamber; T, thermostated bath; RC, reaction coil; D, detector; DC, data acquisition unit; S, sample; R, reagent: 10^{-3} mol l^{-1} NQS in 0.1 mol l^{-1} HCl; B, buffer: 0.1 mol l^{-1} sodium carbonate–0.75 mol l^{-1} sodium hydroxide; W, waste. Flow rates: channel S = 0.4 ml min^{-1}, channel R = 0.4 ml min^{-1} and channel B = 0.3 ml min^{-1}.

A previous study[10] showed that several amino acids (*e.g.*, Lys, Pro, Trp and Cys) have NQS derivatives with spectra sufficiently differentiated from the others. In contrast, other amino acids showed similar spectra of their NQS derivatives (*e.g.*, Phe, Ile, Leu, His, Thr and Gly). On this basis, Lys, Trp, Pro and Phe were selected. Lys was chosen because its determination is of special interest in the feed sample field, and Phe was taken as a model for amino acids with similar derivative spectra.

Multivariate calibration methods require a suitable experimental design of the standards belonging to the calibration set in order to provide good predictions. A synthetic set of 35 solutions of mixtures of Phe, Lys, Trp and Pro were prepared (Table 1). Fig. 2 shows the spectra of NQS–amino acid derivatives for 1×10^{-3} mol l^{-1} solutions of Phe, Lys, Pro and Trp at pH 10. These spectra were obtained using the continuous-flow system described previously. It can be seen that the degree of overlap is high and there is no selective wavelength that allows their determination by classical univariate calibration. However, there are some spectral differences that can be used to resolve this mixture by multivariate calibration methods.

From the series, 25 solutions were chosen for the calibration set and the other 10 were used as problem solutions. This selection was performed on the basis of their distributions on the first and second principal components shown in Fig. 3. Problem solutions were chosen according to their situation on the graph, inside the range of calibration solutions. Fig. 3 also

Table 1 Composition of amino acid solutions for the synthetic series. Concentrations in mol $l^{-1} \times 10^{-4}$

Solution	Type*	Phe	Lys	Trp	Pro
1	P	1.5	0.5	0.5	0.5
2	C	1.5	1.0	0.5	0.5
3	P	1.5	0.5	1.0	0.5
4	C	1.5	0.5	0.5	1.0
5	P	0.5	1.5	0.5	0.5
6	C	1.0	1.5	0.5	0.5
7	C	0.5	1.5	1.0	0.5
8	P	0.5	1.5	0.5	1.0
9	C	0.5	0.5	1.5	0.5
10	P	1.0	0.5	1.5	0.5
11	C	0.5	1.0	1.5	0.5
12	P	0.5	0.5	1.5	1.0
13	C	0.5	0.5	0.5	1.5
14	C	1.0	0.5	0.5	1.5
15	P	0.5	1.0	0.5	1.5
16	C	0.5	0.5	1.0	1.5
17	C	1.0	1.0	0.5	0.5
18	C	1.0	0.5	1.0	0.5
19	C	1.0	0.5	0.5	1.0
20	C	0.5	1.0	1.0	0.5
21	P	0.5	1.0	0.5	1.0
22	C	0.5	0.5	1.0	1.0
23	C	1.5	1.0	1.0	0.5
24	P	1.5	1.0	0.5	1.0
25	C	1.5	0.5	1.0	1.0
26	C	1.0	1.5	1.0	0.5
27	C	1.0	1.5	0.5	1.0
28	C	0.5	1.5	1.0	1.0
29	C	1.0	1.0	1.5	0.5
30	C	1.0	0.5	1.5	1.0
31	C	0.5	1.0	1.5	1.0
32	C	1.0	1.0	0.5	1.5
33	C	1.0	0.5	1.0	1.5
34	C	0.5	1.0	1.0	1.5
35	P	1.0	1.0	1.0	1.0

* P = problem solution; C = calibration solution.

shows that, in general, mixtures with high concentrations of proline lie at the bottom right of the plot, whereas mixtures with large amounts of tryptophan are at the top right. The differences between lysine and phenylalanine derivatives are small, so samples with high concentrations of lysine and phenylalanine were at the left of the graph.

The selection of the number of principal components or factors to be used in the calibration with PCR and PLS algorithms is very important in order to achieve the best predictions. As a first approach, this number can be estimated by the indicator function (IND),[17] or by binary cross-validation, by plotting the standard error of the residuals in the prediction (SEP function) *versus* the number of principal components.[18] In binary cross-validation, the whole data matrix is divided into two halves, one half matrix being utilized for the calibration and the other for predictions (leaving out the half matrix for prediction). These treatments were performed by taking the absorbance in steps of 5 nm for each spectrum of the calibration set in the range 290–590 nm (Fig. 4). From Fig. 4, the number of variables deduced to be considered is five. Hence, as principal components involve causes of variation for the explanation and fitting of the model, four of the five were due to the presence of the four amino acids and the fifth factor was attributed to the baseline drift during the recording of spectra. The main drawback of SEP and IND functions is that they only use the information of the calibration set. In contrast, external cross-validation make predictions on independent samples that are not used in the calibration. In consequence, the influence of the number of factors on the predictions was studied for both the PCR and PLS methods to be taken as a model of external cross-validation. The effect of the number of working wavelengths was also considered. Figs. 5 and 6 show the results obtained for PCR and PLS, respectively, in which the percentage error was calculated as follows:

$$\text{Error (\%)} = [\Sigma(c_{\text{true}} - c_{\text{calc}})^2]^{1/2}/(\Sigma c_{\text{true}}^2)^{1/2} \quad (1)$$

where c_{true} and c_{calc} are the known and found concentrations for each analyte, respectively. This calculation was performed for each individual amino acid and for the whole set of four amino acids for both calibration and prediction sets.

Figs. 5 and 6 were constructed from 72 points (percentage error) calculated by performing predictions with nine different numbers of factors (from 4 to 12 factors) and eight different numbers of working wavelengths, which resulted from measuring the full spectra at regular steps of 3, 4, 5, 6, 8, 10, 12 and 15 nm. These figures show that in all instances minimum errors were obtained by using a number of principal components higher than that found with SEP and IND functions. The number of working wavelengths utilized in the calibration affected the evolution of the percentage error. Thus, predictions with a small number of wavelengths, such as 21, achieved the minimum error using seven principal components whereas with many wavelengths such as 101 the error was minimum with 11 principal components. By comparing Figs. 5 and 6, PLS provides higher accuracy than PCR, so PLS was chosen for further calculations.

Spectra of NQS–amino acid derivatives were subjected to a smoothing or a derivative procedure in order to test the influence of these mathematical treatments on the predictions. The analysis of spectra belonging to the calibration set by means of SEP and IND functions showed that, as with original data, when smoothed spectra were used the number of components was five. In contrast, four principal components were found when derivative spectral data were utilized. As mentioned previously, a fifth factor was attributed to the background drift. This drift was studied by recording the background spectrum for several hours. The results showed that the shapes of these spectra were horizontal lines

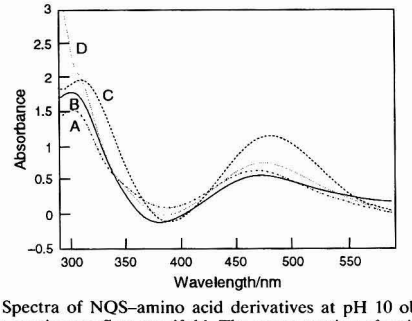

Fig. 2 Spectra of NQS–amino acid derivatives at pH 10 obtained using the continuous-flow manifold. The concentration of amino acid is 10^{-3} mol l^{-1} in all cases. Reagent solution, 10^{-3} mol l^{-1} NQS–0.1 mol l^{-1} HCl; buffer solution, 0.1 mol l^{-1} sodium carbonate–0.075 mol l^{-1} sodium hydroxide; temperature, 70 °C; total flow rate, 1.1 ml min^{-1}; reaction coil; 1000 cm × 0.35 mm i.d. A, Phe; B, Lys; C, Pro; and D, Trp.

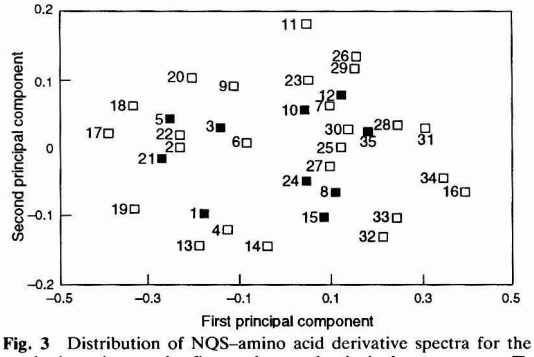

Fig. 3 Distribution of NQS–amino acid derivative spectra for the synthetic series on the first and second principal components. □, Calibration; ■, problem.

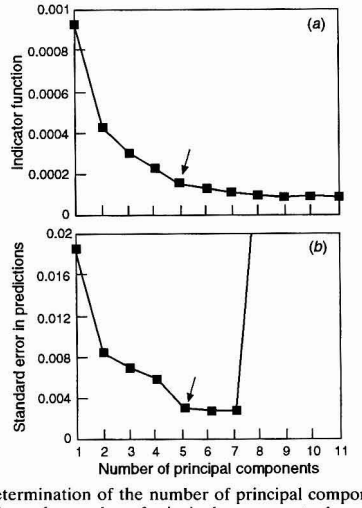

Fig. 4 Determination of the number of principal components. The arrows indicate the number of principal components chosen. (*a*) IND function; (*b*) SEP function.

with low absorbance values that increased slightly with time. Hence, when spectra were derivatized, the constant contribution from background drift was removed and the number of principal components decreased to four. In further studies the background was registered after recording the spectrum of NQS–amino acid derivatives of each solution to suppress the contribution of the drift.

The variation of the percentage error of predictions with the number of principal components for spectra treated mathematically was studied using the PLS method. Fig. 7 shows the results obtained for the three kinds of data taking the spectra in steps of 10 nm (31 working wavelengths). Nine and ten factors were needed to obtain the most accurate predictions of the problems for smoothed and derivative spectral data, respectively, so in this instance an overfitting with respect to the number of factors found by SEP and IND functions is also suitable. Table 2 contains the prediction, as percentage error, for each particular amino acid and for the total set. Table 2 indicates that the lowest errors correspond to Pro and Trp because their NQS derivatives have specific spectral characteristics that can be distinguished from the others. The over-all error is greater for derivative spectra attributable to Lys, as it presents a certain spectral selectivity about 590 nm that is lost in the mathematically derived spectrum.

In order to investigate the possible interferences in the determination of Phe, another series of 35 synthetic solutions containing His, Ile and Leu apart from Phe were prepared. As mentioned previously, all of these amino acids have similar spectra to their NQS derivatives. Three different concentrations of each amino acid were chosen (2×10^{-4}, 1×10^{-4} and 5×10^{-5} mol l^{-1}). The design of the composition of this series was made by analogy with that listed in Table 1. The error in the prediction of the concentration of Phe using PLS with nine factors was 8.5%, which is slightly higher than that for the series with differentiated spectra (5.8% in the prediction of Phe). These results illustrate some possibilities of multivariate calibration methods in the discrimination of substances with similar spectral characteristics.

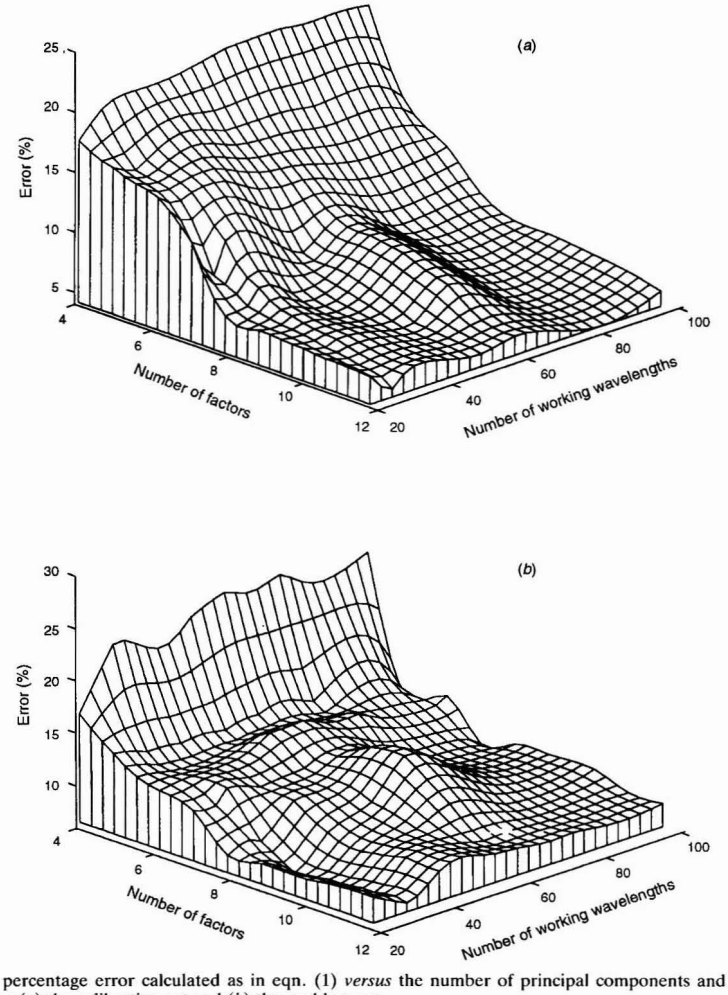

Fig. 5 Variation of the percentage error calculated as in eqn. (1) *versus* the number of principal components and the number of working wavelengths using PCR for (*a*) the calibration set and (*b*) the problem set.

Application to Feed Samples

Several essential amino acids are added to animal feed samples in certain steps of the elaboration process. In particular, free lysine is often supplied to the diet of herbivores because this amino acid is hardly present in vegetable products. Although the main aim of this work was focused on the control of the amount of free lysine added in the elaboration of these feed samples, the concentrations of other amino acids such as Phe, Trp and Pro were also determined.

The PLS method was applied to the determination of Phe, Lys, Pro and Trp in commercial feed samples. These samples were subjected to a solid–liquid extraction in order to recover the free amino acids. Amounts of 3 g of feed sample were extracted with 50 ml of a 1% aqueous solution of phenol for 30 min in a conical flask with magnetic stirring. The extracts obtained were filtered through a nylon membrane of 0.45 μm

Table 2 Percentage error for the synthetic series using the PLS method for different types of spectral data calaculated as in eqn. (1). Spectra were taken in the range 290–590 nm in steps of 10 nm

			Error (%)				
Spectra	NPC*	Step	Phe	Lys	Trp	Pro	Global
Original	9	Calibration	5.9	8.6	6.0	2.3	6.1
		Prediction	5.9	6.7	5.2	2.4	5.3
Smoothed	9	Calibration	3.3	6.6	3.1	1.6	4.1
		Prediction	7.7	8.0	3.8	1.6	6.0
Derivative	10	Calibration	4.7	8.3	2.5	1.7	4.4
		Prediction	7.5	10.9	5.0	2.1	7.3

* Number of principal components considered.

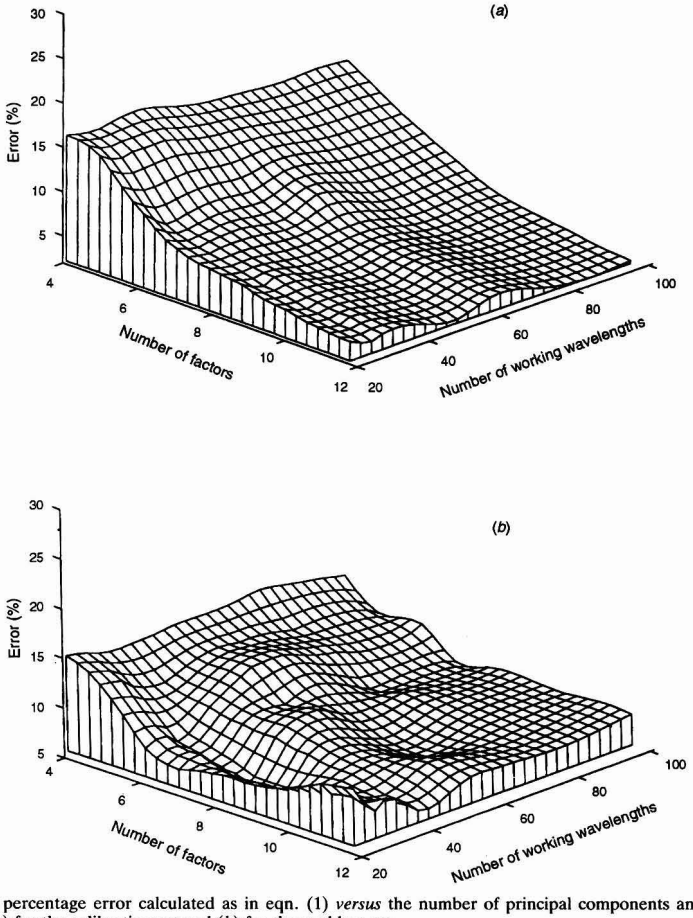

Fig. 6 Variation of the percentage error calculated as in eqn. (1) *versus* the number of principal components and the number of working wavelengths using PLS (*a*) for the calibration set and (*b*) for the problem set.

pore size. Solutions to be pumped through the continuous-flow system were prepared from 5 ml of the filtered extract solutions, which were diluted to 25 ml. Twenty extract solutions were finally obtained from ten feed samples, as two independent extractions were carried out on each sample.

Feed samples were analysed by an independent method in order to determine the concentration of each amino acid. For this purpose, a standard amino acid analysis procedure based on the ninhydrin reaction was used.[19] Solutions injected into the amino acid analyser were prepared with 250 μl of the extract solution plus 25 μl of norleucine (internal standard), and were filtered through an Ultrafree-MC low-binding cellulose membrane from Millipore.

PLS involves the use of problem and calibration samples of the same nature, so 12 of the 20 extract solutions were taken for the calibration set and the eight remaining solutions were chosen as problems. As previously in the synthetic series, the selection of these calibration and problem sets was based on their distribution on the first and second principal components (Fig. 8).

The spectra of feed samples were also recorded from 290 to 590 nm. However, in this instance, the experimental absorbances in the region of 290–320 nm were very high, owing to the interference of the feed sample matrix. In this zone the spectra of amino acid derivatives were masked by the matrix absorption and, in consequence, the determination of the optimum spectral range for the calibration was studied. Fig. 9 shows the variation of the error on both calibration and prediction steps *versus* the spectral range and the number of principal components. This figure was obtained from 45 points (percentage error), as the number of factors was varied from five to nine and nine different spectral ranges were used (spectra were always taken in steps of 5 nm started at the nine initial wavelengths of 330, 350, 370, 390, 410, 430, 450, 470 and 490 nm, and always finished at 590 nm). The best predictions were found for intermediate spectral ranges while both the narrow and the wide ranges led to worse results. This behaviour could occur because in narrow spectral ranges (such as 490–590 nm) some important information was lost and in the wide ranges (such as 330–590 nm) the interference from the sample matrix was also included. In consequence, the optimum zone chosen for further calculations was an intermediate range from 390 to 590 nm.

Predictions from original, smoothed and derivative spectra of feed samples were compared in order to determine whether these mathematical treatments of data could improve the results. Fig. 10 shows the variation of the percentage error with the number of factors for the three kinds of spectra (in the range 430–590 nm) using PLS. This figure confirms that, in this instance, the original spectra can be used directly without mathematical treatment as they provide the best results. In contrast, predictions with derivative spectra were significantly worse, mainly owing to the bad determination of Lys.

SEP and IND functions were also applied to determine the number of factors to be used in the calibrations and five factors were found. However, Fig. 10 indicates that the best predictions are obtained using more than these five factors. As in the synthetic series, Fig. 10 was used as a model of external cross-validation and, in consequence, seven factors were chosen for the calibration with original spectra. Table 3 shows the comparison between results obtained by the proposed continuous-flow method using PLS and those obtained by the standard method. There is good agreement in spite of the complexity of the feed sample matrix.

In order to test the robustness of the calibration, two feed samples containing 0.155 and 0.077 g of Lys in 100 g of feed sample were chosen. These samples were analysed on four different days by the NQS method. Fresh solutions of NQS and buffer were prepared daily, in addition to extract solutions. The calibration model was constructed on the first day of this study and was used to make predictions. The calibration was performed with the PLS method using seven principal components and working in the spectral range 390–590 nm in steps of 5 nm. The percentage error in the determination of Lys during the study was 6.9%. In consequence, the method could be used for routine analysis of these samples without the need for daily calibration.

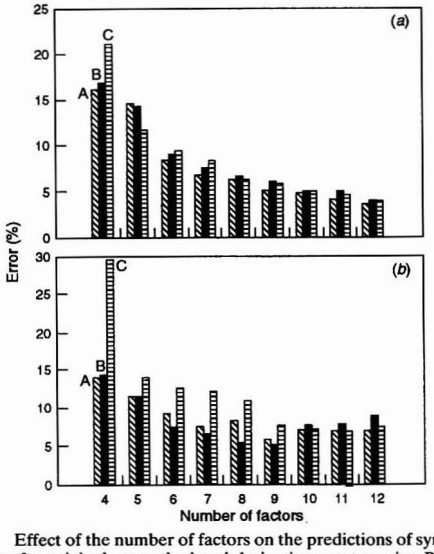

Fig. 7 Effect of the number of factors on the predictions of synthetic samples for original, smoothed and derivative spectra using PLS for (*a*) the calibration set and (*b*) the problem set. A, Original spectra; B, smoothed spectra; and C, derivation spectra.

Conclusions

Continuous-flow analysis methodology with spectrophotometric detection coupled to multivariate calibration techniques seems to be a useful tool in the resolution of some particular amino acid mixtures, even in presence of complex matrix samples. The system was focused on the determination of some amino acids such as Lys which is of special interest in the feed analysis field. Two different multivariate calibration methods were used, PCR and PLS, and PLS was shown to

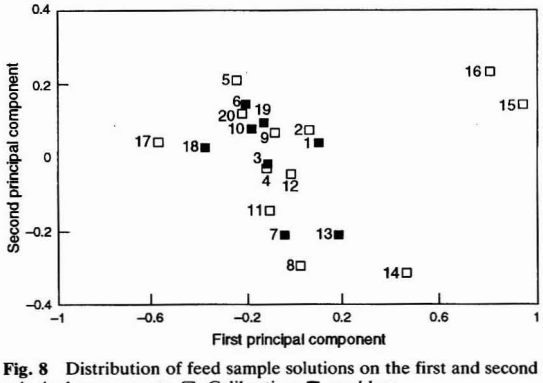

Fig. 8 Distribution of feed sample solutions on the first and second principal components. □, Calibration; ■, problem.

Table 3 Comparison between amino acid concentrations determined with the standard amino acid autoanalyser and by the proposed continuous-flow method (NQS method) using PLS. Calibration performed with seven factors for the spectral range 390–590 nm in steps of 5 nm. Amino acid concentrations of the extract solution used in the continuous-flow system expressed in mol $l^{-1} \times 10^{-5}$

		Phe		Lys		Trp		Pro	
Feed sample	Type*	Standard method	NQS method	Standard method	NQS method	Standard method	NQS method	Standard method	NQS method
1	P	0.42	0.42	3.14	4.98	0.55	0.75	2.26	2.69
2	C	0.40	0.40	2.93	2.95	0.52	0.66	2.10	2.32
3	P	0.66	0.75	5.54	3.99	0.63	0.59	3.58	3.30
4	C	0.67	0.82	5.62	5.67	0.64	0.48	3.63	3.51
5	C	0.40	0.30	2.88	2.87	0.66	0.60	2.48	2.29
6	P	0.46	0.35	3.25	4.56	0.74	0.64	2.79	2.61
7	P	0.72	0.82	11.0	9.80	0.57	0.63	3.73	3.75
8	C	0.82	0.82	12.6	12.6	0.65	0.70	4.26	4.31
9	C	0.57	0.52	2.94	2.99	0.65	0.64	3.22	3.24
10	P	0.56	0.46	2.89	1.67	0.64	0.70	3.16	2.27
11	C	1.08	0.93	3.90	3.92	0.64	0.74	4.90	5.01
12	C	0.92	0.87	3.30	3.21	0.54	0.58	4.15	4.09
13	P	0.61	0.69	1.01	1.75	1.35	1.33	11.4	11.1
14	C	0.69	0.72	1.14	1.14	1.52	1.51	12.9	12.9
15	C	0.43	0.53	0.94	0.92	1.25	1.23	4.19	4.18
16	C	0.43	0.37	0.95	0.97	1.25	1.24	4.23	4.20
17	C	0.52	0.51	5.23	5.26	0.54	0.47	1.53	1.44
18	P	0.56	0.42	5.62	6.39	0.58	0.50	1.64	2.52
19	P	0.44	0.44	3.36	3.22	0.65	0.65	2.34	2.59
20	C	0.42	0.45	3.16	3.16	0.61	0.61	2.19	2.24

* C = used in the calibration; P = used in the prediction.

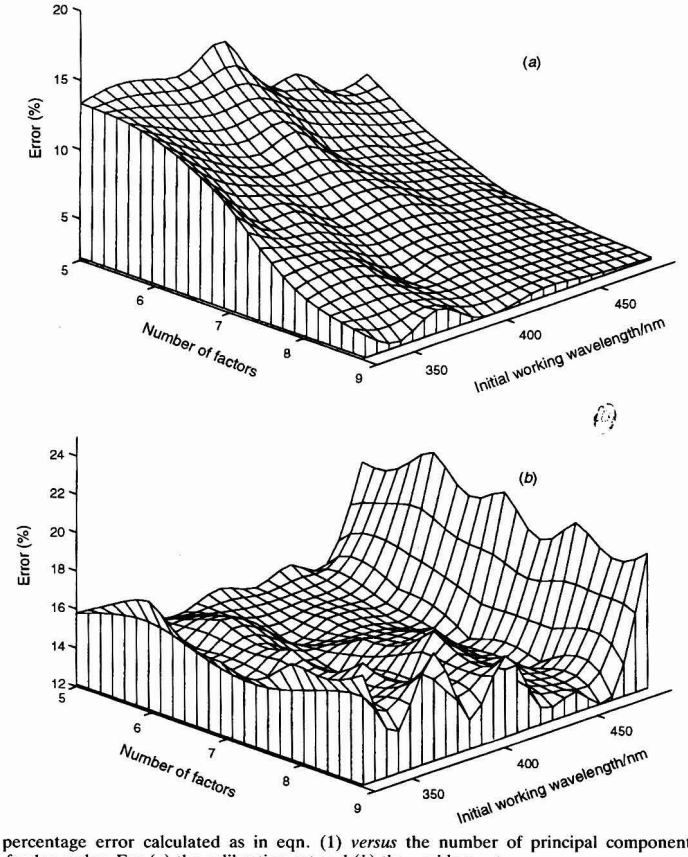

Fig. 9 Variation of the percentage error calculated as in eqn. (1) *versus* the number of principal components and the initial working wavelengths using PLS for feed samples. For (*a*) the calibration set and (*b*) the problem set.

provide the most accurate predictions of the amino acid composition. Original data can be used directly as generated by the spectrophotometer because the mathematical treatments tested (smoothed and derivative spectra) do not improve the determination significantly. If derivative spectra are used the predictions become worse as some spectral selectivity in the spectrum of the NQS–lysine derivative is lost. Because the determination of the number of factors to be used in the calibration by SEP and IND functions does not give the best results, external cross-validation on samples that will not be included in the calibration set can be utilized. The proposed method can be applied for the rapid, routine simultaneous determination of several particular amino acids by simply recording the spectra.

The authors thank Dr. R. Tauler and Dr. A. Izquierdo-Ridorsa for their interest in and help with this work, and the Cooperativa Agropecuaria de Guissona for providing the feed samples. J. S. also thanks the Ministerio de Educación y Ciencia for an FPI grant. This work was partially financed by DGICYT project PB90-0821.

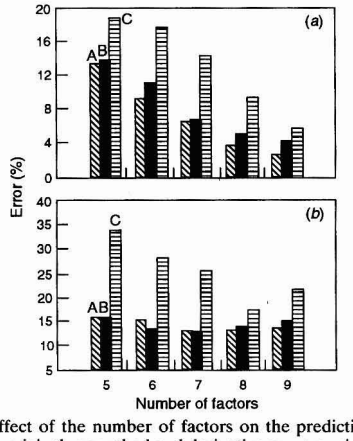

Fig. 10 Effect of the number of factors on the predictions of feed samples for original, smoothed and derivative spectra using PLS. For (*a*) the calibration set and (*b*) the problem set. A, Original spectra; B, smoothed spectra; C, derivative spectra.

References

1 MacLaurin, P., Worsfold, P. J., Norman, P., and Crane, M., *Analyst*, 1993, **118**, 617.
2 Poppi, R. J., and Pasquini, C., *Chemom. Intell. Lab. Syst.*, 1993, **19**, 243.
3 Saurina, J., and Hernández-Cassou, S., *Anal. Chim. Acta*, 1993, **281**, 593.
4 Blanco, M., Coello, J., Iturriaga, H., Maspoch, S., Redón, M., and Riba, J., *Anal. Chim. Acta*, 1992, **259**, 219.
5 Whitman, D. A., Seasholtz, M. B., Růžička, J., Christian, G. D., and Kowalski, B. R., *Anal. Chem.*, 1991, **63**, 775.
6 Gerritsen, M. J. P., Kateman, G., van Opstal, M. A. J., Bennekom, W. P., and Vandegiste, B. G. M., *Anal. Chim. Acta*, 1990, **241**, 23.
7 Erickson, B. C., Růžička, J., and Kowalski, B. R., *Anal. Chim. Acta*, 1989, **218**, 303.
8 Lukkari, I., and Lindberg, W., *Anal. Chim. Acta*, 1988, **211**, 1.
9 Blanco, M., Gené, J., Iturriaga, H., and Maspoch, S., *Analyst*, 1987, **112**, 619.
10 Saurina, J., and Hernández-Cassou, S., *Anal. Chim. Acta*, 1993, **283**, 414.
11 Martens, H., and Naes, T., *Multivariate Calibration*, John Wiley, New York, 1989.
12 Haaland, D., and Thomas, E., *Anal. Chem.*, 1988, **60**, 1193.
13 Beebe, K., and Kowalski, B. R., *Anal. Chem.*, 1987, **59**, 1007A.
14 Beltrán, J. L., Centeno, G., Izquierdo, A., and Prat, M. D., *Talanta*, 1992, **39**, 981.
15 *Matlab*, Math Works, Natick, MA, 1993.
16 Wise, B. M., *PLS_Toolbox*, Richland, WA, 1992.
17 Malinowski, E. R., *J. Chemom.*, 1988, **3**, 39.
18 Wold, S., *Technometrics*, 1978, **20**, 397.
19 Spackman, D. H., Stein, W. H., and Moore, S., *Anal. Chem.*, 1958, **30**, 1190.

Paper 4/03077J
Received May 23, 1994
Accepted August 8, 1994

Application of the Partial Least-squares Calibration Method to the Simultaneous Kinetic Determination of Propoxur, Carbaryl, Ethiofencarb and Formetanate

J. M. García, A. I. Jiménez and J. J. Arias*

Department of Analytical Chemistry, Food Chemistry and Toxicology, University of La Laguna, E-38204 La Laguna, Tenerife, Spain

Karim D. Khalaf, Angel Morales-Rubio and Miguel de la Guardia*

Department of Analytical Chemistry, University of Valencia, 50 Dr. Moliner St., E-46100 Burjassot, Valencia, Spain

A method based on the application of partial least-squares analysis to bilinear data was used for the simultaneous determination of propoxur, carbaryl, ethiofencarb and formetanate by a kinetic–spectrophotometric method. The procedure is based on the different rate constants of the reactions between *p*-aminophenol, in the presence of potassium metaperiodate, and the phenolic and naphtholic compounds obtained from the alkaline hydrolysis of the pesticides using a stopped-flow injection procedure. Mixtures containing 2–10 μg ml^{-1} of propoxur, 2–8 μg ml^{-1} of carbaryl, 2–10 μg ml^{-1} of ethiofencarb and 2–10 μg ml^{-1} of formetanate were successfully resolved with errors of less than 5%.

Keywords: *Multicomponent determination; partial least-squares analysis; carbamate pesticide; kinetic–spectrophotometric method*

Introduction

One of the greatest challenges traditionally faced in analytical chemistry, *viz.*, the simultaneous determination of several components in mixtures, has recently experienced dramatic advances thanks to major breakthroughs in instrumental development. Thus, measurements at a single wavelength have been superseded by entire spectra recorded over a wavelength range which provides first-order data that are subsequently converted into vectors (one-way arrays) for a single sample and matrices (two-way arrays) for several samples. By coupling measuring instruments one can also obtain second-order or bilinear data for each sample and hence construct three-way matrices (three-way arrays) for a set of samples.[1] While chromatography in its various combinations with detection systems is one of the major instrumental choices, second-order data can still be obtained without it; in fact, emission–excitation spectrofluorimetry,[2] photometric titrations[3] and spectrophotometric measurements at different times[4] or pH values[5] all provide bilinear data at a lower cost by using more straightforward equipment for the resolution of a wide variety of mixtures of analytical interest.

In addition, the use of mathematical algorithms formerly employed in other branches of science has boosted advances in analytical instrumentation by facilitating processing of the large amounts of information typically produced. First-order multivariate calibration methods such as the classical least-squares (CLS), principal component regression (PCR) and partial least-squares (PLS) methods[6] have so far been the most frequently used choices for treating first-order data; however, bilinear data call for more complicated alternatives, *viz.*, multi-way methods[7] such as: PARAFAC,[8] GRAM,[9] U-PLS[10] and DTDM.[11]

On the other hand, the ability of diode-array spectrophotometers to record entire spectra in a fraction of a second and their ease of handling *via* an interfaced computer have fostered the development of applications that use bilinear methods to process the data provided by kinetic–spectrophotometric methods for resolving mixtures of rare earths,[12] metals[13] and pharmaceuticals,[14] among others. The three-dimensional matrices initially constructed are reduced to two dimensions by converting the vectors obtained for each sample at different times into large vectors and subsequently processing the resulting two-dimensional matrices using a PCR or PLS method.

In this work, we have applied PLS regression to the bilinear data obtained from changes in the absorption spectra of the products of the alkaline hydrolysis of propoxur, carbaryl, ethiofencarb and formetanate by reaction with *p*-aminophenol in the presence of potassium metaperiodate in a stopped-flow system. As shown below, application of PLS regression to kinetic–spectrophotometric data allows the simultaneous determination of the four pesticides.

Experimental

Apparatus and Software

The manifold used has been described in previous work[20] and consisted of a Gilson Minipuls P2 peristaltic pump and a Hewlett-Packard (Avondale, PA, USA) HP8452A diode-array spectrophotometer furnished with a flow cell of 50 μl internal volume and 1 cm pathlength and interfaced to a Hewlett-Packard Vectra ES computer; each channel was employed to transport different carrier solutions and the connection between channels was carried out by using Y-shaped merging zones. Flexible poly(vinyl chloride) tubes of 1.52 mm bore were used to transport solutions in each channel. Reaction coils were made of Teflon with 0.8 mm bore. The temperature was kept constant with the aid of an MS Lauda thermostat.

Absorption spectra were recorded and processed with the aid of the spectrophotometer software. The data were transferred to a PC/AT 386 personal computer (DTK, Taiwan) furnished with an Intel 80387 mathematical co-processor for its treatment with UNSCRAMBLER program.[15]

* To whom correspondence should be addressed.

Reagents

Stock standard solutions containing 15 μg ml^{-1} of carbaryl (Union Carbide), 100 μg ml^{-1} of ethiofencarb (Bayer), or 100 μg ml^{-1} formetanate (Riedel-de Haën) were prepared by direct weighing of the required amount from the commercial products and dissolved in distilled, de-mineralized water.

A stock standard solution of propoxur (Bayer) was prepared by dissolving 25 mg of the pesticide in 1 ml of methanol and diluting to 250 ml with distilled water. A 50 ml volume of this solution was diluted to 100 ml to give a working standard solution of 50 μg ml^{-1} propoxur.

A 100 μg ml^{-1} *p*-aminophenol (PAP) solution was prepared by weighing the required amount from the commercial product (Fluka) and dissolved in boiled and cooled distilled water.

A 0.004 mol l^{-1} KIO_4 solution and a 0.05 mol l^{-1} NaOH solution were prepared from analytical-grade reagents (Probus).

Procedure

Complex mixtures of propoxur, carbaryl, ethiofencarb and formetanate were treated with 0.05 mol l^{-1} NaOH at 90 °C for 60 min and were subsequently continuously injected into the manifold. The phenolate and naphtholate compounds obtained by hydrolysis were mixed with the quinoneimine compound obtained from the continuous oxidation of 100 μg ml^{-1} of PAP solution with 0.004 mol l^{-1} KIO_4 solution. After mixing, the flow was stopped and the absorbance spectra were recorded between 556 and 648 nm, every 2 nm, at 5 s intervals for 60 s. The three-way data obtained were transferred to the DTK computer, transformed into two-way data and treated with the UNSCRAMBLER program.

Results and Discussion

The carbamate pesticides propoxur, carbaryl, ethiofencarb and formetanate are hydrolysed to phenolate and naphtholate derivatives in an alkaline medium at 25 °C. The first three are quantitatively hydrolysed within 15 min by 0.05 mol l^{-1} NaOH at 25 °C, whereas the last is incompletely hydrolysed under the same conditions. The hydrolysis products from these pesticides react with quinoneimide, obtained by oxidation of PAP in the presence of KIO_4, to yield coloured products.[16–19]

In previous work,[20] the above-mentioned reactions were used for the simultaneous determination of the four pesticides with errors less than 6% for propoxur, carbaryl and ethiofencarb and a much larger error for formetanate; the last pesticide was incompletely hydrolysed under the working conditions used, *viz.*, 15 min at 25 °C, so its hydrolytic derivative exhibited a very low absorbance relative to those of the other three pesticides. In order to improve the sensitivity, the hydrolysis conditions were made more drastic: heating at 90 °C for 1 h. Fig. 1 shows the spectra for the products obtained by reaction of the hydrolysed pesticides with PAP under these conditions; comparison of the spectra for the products obtained under the two types of hydrolysis conditions reveals that those for carbaryl and ethiofencarb were similar, that for propoxur increased slightly and that for formetanate increased by a factor of approximately ten in terms of absorbance. On the other hand, the extensive spectral overlap (the absorption maxima for formetanate, carbaryl, propoxur and ethiofencarb are at 576, 592, 600 and 638 nm, respectively) precluded resolution of the mixture by using spectra recorded at a fixed time.

As can be seen from Fig. 2, the reaction of the hydrolysed carbamates with PAP in the presence of KIO_4 takes place at a different rate depending on the particular pesticide; this, in addition to small differences between the derivatized products could, in principle, be used to address the simultaneous determination of the four pesticides.

When the simultaneous determination of these carbamate pesticides was carried out at 25 °C, the concentration ranges used to construct the calibration matrix were 2–10, 1–4, 2–10 and 4–20 μg ml^{-1} of propoxur, carbaryl, ethiofencarb and formetanate, respectively;[20] the high absorbance exhibited by carbaryl at the initially tested concentrations compelled us to lower them in order to bring its signal closer to the low levels exhibited by formetanate. However, the product obtained by hydrolysis of formetanate at 90 °C for 60 min provided a high enough signal, thereby avoiding the need to use a high concentration of this pesticide. Therefore, to carry out the simultaneous determination of the four pesticides under the new conditions a calibration matrix was constructed by using pesticide concentrations in the ranges 2–10 μg ml^{-1} for propoxur, ethiofencarb and formetanate and 2–8 μg ml^{-1} for carbaryl. The experimental design used involved four factors at two levels (Table 1) and recording the absorbance spectra for the quaternary mixtures from 450 to 750 nm every 2 nm (151 wavelengths) for 60 s at 5 s intervals (13 times).

The results thus obtained were grouped by placing the spectrum recorded every 5 s next to the previous one, in such a way that the resulting vector contained the 13 spectra in a sequential order (151 wavelengths × 13 times). In order to avoid the redundancy of information caused by two adjacent wavelengths, only the wavelengths, λ, between 450 and 750 nm every 4 nm were taken (76 wavelengths × 13 times). First, to select the range of λ providing more information, a previous

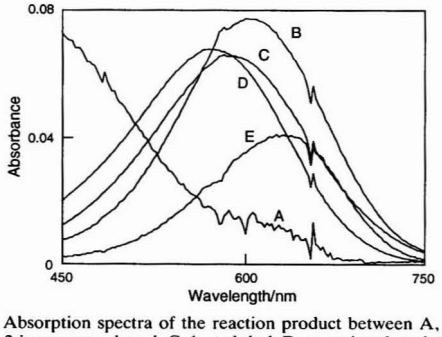

Fig. 1 Absorption spectra of the reaction product between A, PAP and B, 2-isopropoxyphenol, C, 1-naphthol, D, *m*-aminophenol and E, phenol sulfone obtained from NaOH hydrolysis (60 min at 90 °C) of 8 μg ml^{-1} propoxur, 4 μg ml^{-1} carbaryl, 4 μg ml^{-1} formetanate and 8 μg ml^{-1} ethiofencarb, respectively.

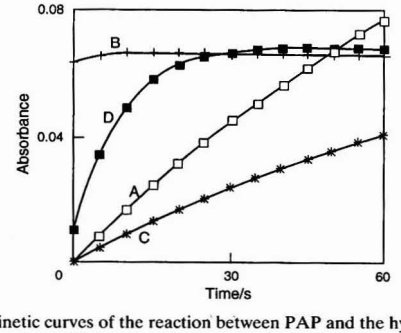

Fig. 2 Kinetic curves of the reaction between PAP and the hydrolysis products of the carbamate pesticides: A, 8 μg ml^{-1} propoxur, B, 4 μg ml^{-1} carbaryl, C, 8 μg ml^{-1} ethiofencarb and D, 4 μg ml^{-1} formetanate.

calibration was carried out, where data were centred about the mean and leverage correction method was used for validation.[6] When the model was established, the selection of the optimum wavelength interval was realized using several approaches. (a) In the first, the calibration residual variance was plotted against the leverage for the individual variables. The variables with too high residual variance and too low leverages must be eliminated because they have a poor fitting between the absorbances measured and the added concentrations for the calibration objects. A plot of the residual variance *versus* the leverage showed that most of the variables out of the range 556–648 nm had high residual variance and low leverage; when the fifth factor was included, the plot showed that the residual variance of variables decreased, but the leverage remained low. Hence the fifth factor corrects the high residual variance obtained with those variables when four factors were used. (b) Likewise, the outliers, variables with a high relative error (absolute value of residual/square root of the mean values of the squares of the residual), identified by the computer program, revealed that most of these variables were those out of the interval 556–648 nm. (c) Also, the normal probability distribution plot of regression coefficients describing the relationships between absorbances and concentrations for the fifth factor showed a risk of systematic errors for most of the pesticides or a lack of linearity for the variables associated with 0 s. For these reasons, the spectra obtained at this time were all discarded.

The calibration was repeated by using the spectra recorded at times between 5 and 60 s and 5 s intervals from 556 to 648 nm every 4 nm (23 wavelengths × 12 times). The model was then centred about the mean values and the cross-validation method was applied to eight randomly chosen segments with two objects each.[6] Fig. 4 shows the percentage residual variances obtained in the cross-validation process for both the absorbance and the concentration matrix; as can be seen, 99.5% of the absorbance variance was accounted for using two factors only. On the other hand, the residual variances for the concentrations of the validation objects, which are indicative of how good the model is and how good predictions can be, were satisfactorily accounted for (98.8, 99.7, 99.1 and 99.7% for propoxur, carbaryl, ethiofencarb and formetanate, respectively) by five factors. Using a further factor increased all the previous values to above 99.8% but, as shown in Fig. 5 (a plot of scores of absorbance data matrix *versus* scores of concentration data matrix for the sixth factor), the objects dispersed about the regression line, which can be ascribed to the presence of noise and hence overfitting of the model.

Table 1 Composition of calibration matrix

Sample No.	Amount added/μg ml^{-1}			
	Propoxur	Carbaryl	Ethiofencarb	Formetanate
1	10.00	8.00	10.00	10.00
2	10.00	8.00	10.00	2.00
3	10.00	8.00	2.00	10.00
4	10.00	2.00	10.00	10.00
5	2.00	8.00	10.00	10.00
6	10.00	8.00	2.00	2.00
7	10.00	2.00	2.00	10.00
8	2.00	2.00	10.00	10.00
9	2.00	8.00	10.00	2.00
10	10.00	2.00	10.00	2.00
11	2.00	8.00	2.00	10.00
12	10.00	2.00	2.00	2.00
13	2.00	8.00	2.00	2.00
14	2.00	2.00	10.00	2.00
15	2.00	2.00	2.00	10.00
16	2.00	2.00	2.00	2.00

Fig. 6 shows a plot of score 2 *versus* score 1. As can be seen, score 1 is related to the formetanate + carbaryl and propoxur + ethiofencarb over-all concentrations; the first two pesticides absorb maximally at shorter wavelengths and higher reaction rates than the last two. Lines A–C group objects in the calibration matrix with formetanate + carbaryl overall concentrations of (A) 4, (B) 10–12 and (C) 18 μg ml^{-1}; the

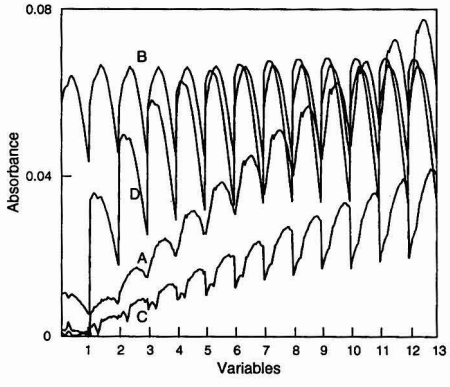

Fig. 3 Graph of data for A, 8 μg ml^{-1} propoxur, B, 4 μg ml^{-1} carbaryl, C, 8 μg ml^{-1} ethiofencarb and D, 4 μg ml^{-1} formetanate measured 13 times in the wavelength range 556–648 nm.

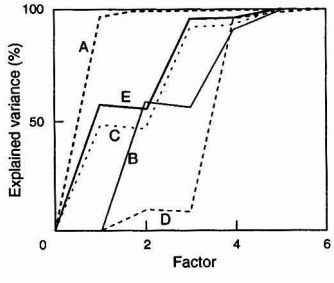

Fig. 4 Graph of explained variance (when cross-validation is used) of the validation objects as a function of number of factors: A, absorbance data; B, propoxur; C, carbaryl; D, ethiofencarb; and E, formetanate.

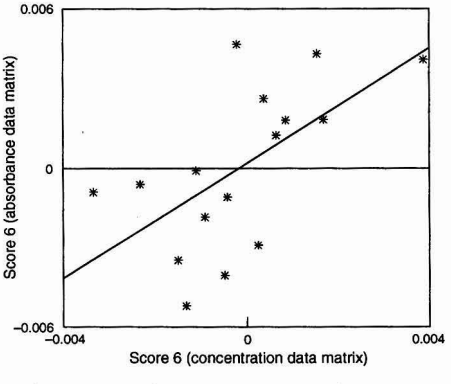

Fig. 5 Plot of scores of absorbance data matrix *versus* scores of concentration data matrix for the sixth factor.

increase in the first score is consistent with an increase in the formetanate + carbaryl concentration. Within each group, objects are distributed according to their propoxur + ethiofencarb over-all concentration; the greater value of score 1 for objects with the same propoxur + ethiofencarb concentration corresponded to that with the higher propoxur concentration. Because of slanting of the hypothetically parallel lines formed by the above-mentioned groups, some of the pesticides related to the first factor should also presumably be related to the second score. In fact, the calibration objects distributed horizontally (score 2) according to their propoxur + ethiofencarb over-all concentration, which increased with increase in the second score; for objects with the same propoxur + ethiofencarb concentration, the propoxur concentration was

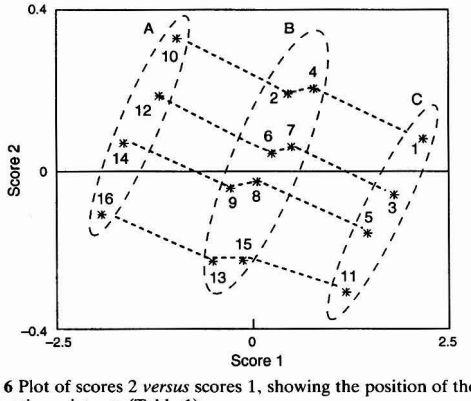

Fig. 6 Plot of scores 2 *versus* scores 1, showing the position of the 16 calibration mixtures (Table 1).

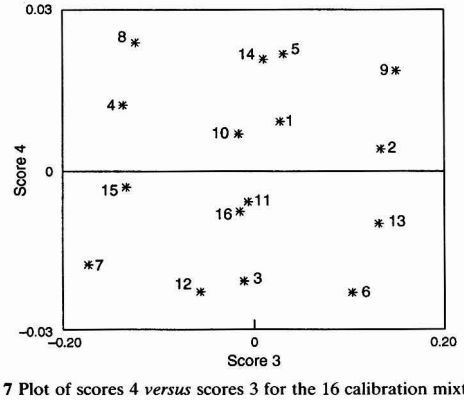

Fig. 7 Plot of scores 4 *versus* scores 3 for the 16 calibration mixtures (Table 1).

the dominant factor, as was the case with score 1. This can be ascribed to the propoxur derivative exhibiting a higher absorbance and a higher reaction rate.

As can be seen in Fig. 7, a plot of score 3 *versus* score 4, objects are distributed vertically according to their carbaryl-to-formetanate ratio; the third score increased with increase in this ratio. On the other hand, the fourth score was found to be related to the ethiofencarb concentration and, to a lesser extent, that of propoxur; hence, objects with high ethiofencarb concentrations gave rise to positive scores, whereas those with low concentrations resulted in negative scores. For a given ethiofencarb concentration, objects are distributed according to their propoxur concentration.

From the foregoing, it follows that the first factor is related to the carbaryl and formetanate concentrations and, to a lesser extent, those of propoxur and ethiofencarb; the second factor is related to the concentration of propoxur and, to a lesser extent, that of ethiofencarb; the third factor is related to the concentrations of carbaryl and formetanate; and the fourth factor is related to the concentration of ethiofencarb and, to a lesser extent, that of propoxur. These relationships between the analytes and factors, derived from the score plots, are consistent with the increase in the percentage residual variance accounted for by each factor (Fig. 4); hence the greatest variance increments for each analyte in each factor were matched by the greatest influence of the pesticide concerned on the corresponding score.

The fifth factor was found to be related to none of the pesticides based on the score plots. On the other hand, a plot of amount added *versus* amount found for the calibration objects when four factors were used showed that the concentration of pesticides were quantified in excess. If five factors were used, the plot obtained indicated that the estimated concentration of the objects of calibration decreased. Because of an excess of PAP was added in order to ensure a complete hydrolysis reaction, it is possible to consider that the fifth factor corrects the excess of PAP and reduces the pesticide concentration.

The variation of the root-mean-square error of prediction in the cross-validation process (RMSEP) provides an estimate of the error of prediction to be expected; when five factors were used the RMSEP found for each pesticide were 0.10, 0.24, 0.15 and 0.12 μg ml^{-1} for propoxur, carbaryl, ethiofencarb and formetanate, respectively.

In order to test the performance of the proposed method, it was applied to the resolution of synthetic mixtures containing various concentrations of the four pesticides. Table 2 gives the errors obtained by using five factors for various mixtures of the four pesticides following treatment with 0.05 mol l^{-1} NaOH at 90 °C for 60 min. As can be seen, the amounts added and found were consistent and the relative standard deviations low, with an error of less than 5% in every instance. The relative root-mean-square errors of prediction (RRMSEP)[6] previously obtained by hydrolysis at 25 °C[20] were 2.86, 1.4, 4.45 and 17.3% for propoxur, carbaryl, ethiofencarb and formetanate, respectively; the proposed model (Table 2) decreased RRMSEP for formetanate and ethiofencarb by

Table 2 Simultaneous determination of propoxur (PRO), carbaryl (CAR), ethiofencarb (ETH) and formetanate (FOR) in synthetic mixtures

Amount added/μg ml^{-1}				Amount found ± standard deviation/μg ml^{-1}				Relative error (%)			
PRO	CAR	ETH	FOR	PRO	CAR	ETI	FOR	PRO	CAR	ETH	FOR
3.00	6.00	6.00	3.00	2.98 ± 0.19	5.93 ± 0.16	5.91 ± 0.25	3.12 ± 0.17	−0.67	−1.17	−1.50	4.00
7.00	7.00	4.00	4.00	6.90 ± 0.31	7.22 ± 0.26	3.96 ± 0.22	3.88 ± 0.15	−1.43	3.14	−1.00	−3.00
6.00	3.00	4.00	3.00	6.02 ± 0.27	2.88 ± 0.22	4.01 ± 0.23	2.90 ± 0.17	0.33	−4.00	0.25	−3.33
5.00	4.00	5.00	9.00	4.76 ± 0.24	4.19 ± 0.17	4.76 ± 0.30	9.06 ± 0.21	−4.80	4.75	−4.80	0.67
6.00	5.00	6.00	6.00	5.96 ± 0.23	5.24 ± 0.18	5.99 ± 0.28	6.01 ± 0.18	−0.67	4.80	−0.17	0.17

factors of 9 and 2, respectively, and increased that for carbaryl slightly; the latter may have been the result of the broader concentration range used for carbaryl and the higher variance to be accounted for by the model as a result. The fact that carbaryl gave rise to the largest error can be tentatively ascribed to its being the only pesticide of the four whose hydrolysis products had fully reacted with PAP by the time measurements were started (Fig. 2), so the variation resulting from this substance during the measurement process was zero.

The absence of systematic errors was checked by subjecting the added and found amounts to the test in the joint confidence region for the slope and intercept developed by Mandel and Lining.[21]

Conclusions

The longer analytical time required by the proposed method relative to a previously reported alternative[20] is more than offset by the increased sensitivity obtained for formetanate, which allows its determination at lower concentrations (2–10 μg ml^{-1}) with smaller errors (1.84% *versus* 17.36%). Also, the high molar absorptivities of carbaryl derivatives in the earlier method entailed using fairly low concentrations (1–4 μg ml^{-1}) in order to obtain comparably small signals relative to those of formetanate. In addition, the increase in the formetanate signal achieved by altering the hydrolysis conditions expands the working concentration range for carbaryl (2–8 μg ml^{-1}). These beneficial effects are reflected in errors of less than 5% in the determination of the four pesticides studied.

The proposed method testifies to the great potential of using bilinear methods such as PLS for processing kinetic–spectrophotometric data. By plotting various parameters associated with the models, one can readily select those variables which characterize the system best. In addition, application of these algorithms requires no prior knowledge of the rate constants, reaction mechanisms or molar absorptivities involved. A variety of mixtures of analytes can thus be readily resolved, even if their absorption maxima lie no further away than a few nanometres from one another, provided that their rates of reaction with a common reagent are sufficiently different.

K. D. Khalaf acknowledges the financial support of the Institute of International Cooperation of the Ministerio de Asuntos Exteriores (Spain) and the University of Baghdad (Iraq) to carry out the PhD studies at the University of Valencia (Spain).

References

1 Smilde, A. K., Wang, Y., and Kowalski, B. R., *J. Chemom.*, 1994, **8**, 21.
2 Russell, M. D., and Gouterman, M., *Spectrochim. Acta, Part A*, 1988, **44**, 857.
3 Tauler, R., and Casassas, E., *Analusis*, 1992, **20**, 255.
4 Havel, J., Jiménez, F., Bautista, R. D., and Arias, J. J., *Analyst*, 1993, **118**, 1355.
5 García, J. M., Martín, E., Jiménez, A. I., Jiménez, F., and Arias, J. J., *Proceedings of the Chemometrics III Congress, Brno, Czech Republic, 1993.*
6 Martens, H., and Naes, T., *Multivariate Calibration*, Wiley, Chichester, 1991.
7 Geladi, P., *Chemom. Intell. Lab. Syst.*, 1989, **7**, 11.
8 Harshman, R. A., *UCLA Working Papers in Phonetics*, 1970, **16**, 1.
9 Sánchez, E., and Kowalski, B. R., *Anal. Chem.*, 1986, **58**, 496.
10 Wold, S., Geladi, P., Esbensen, K., and Ohman, J., *J. Chemom.*, 1987, **1**, 41.
11 Sánchez, E., and Kowalski, B. R., *J. Chemom.*, 1990, **4**, 29.
12 García, J. M., Jiménez, A. I., Jiménez, F., Arias, J. J., and Havel, J., *Proceedings of the Chemometrics III Congress, Brno, Czech Republic, 1993.*
13 Blanco, M., Coello, J., Iturriaga, H., Maspoch, S., Riba, J., and Rovira, E., *Talanta*, 1993, **40**, 261.
14 Hernández, O. M., Jiménez, A. I., Jiménez, F., and Arias, J. J., *Proceedings of the VI Jornadas de Análisis Instrumental, Barcelona, 20–22 October, 1993*, paper P-II-52.
15 *Unscrambler-ex v.5.0*, Computer-Aided Modelling, Trondheim, 1993.
16 Khalaf, K. D., Sancenón, J., and de la Guardia, M., *Anal. Chim. Acta*, 1992, **266**, 119.
17 Khalaf, K. D., Morales-Rubio, A., and de la Guardia, M., *Anal. Chim. Acta*, 1993, **280**, 231.
18 Khalaf, K. D., Sancenón, J., and de la Guardia, M., *Fresenius' Z. Anal. Chem.*, 1993, **347**, 52.
19 Khalaf, K. D., Sancenón, J., and de la Guardia, M., *Talanta*, 1993, **40**, 1173.
20 Khalaf, K. D., Morales-Rubio, A., de la Guardia, M., García, J. M., Jiménez, F., and Arias, J. J.,*Proceedings of the 6th International Conference on Flow Analysis, Toledo, June 8–11, 1994*, paper PII-43.
21 Mandel, J., and Lining, F. J., *Anal. Chem.*, 1957, **29**, 743.

Paper 4/04091K
Received July 5, 1994
Accepted October 5, 1994

Application of Near-infrared Reflectance Analysis to the Integrated Control of Antibiotic Tablet Production

Elena Dreassi, Giuseppe Ceramelli, Luisa Savini and Piero Corti

Dipartimento Farmaco Chimico Tecnologico, Università degli Studi di Siena, via Banchi di Sotto 55, 53100 Siena, Italy

Piero Luigi Perruccio

Stabilimento Chimico Farmaceutico Militare, via R. Giuliani 201, 50144 Florence, Italy

Silvano Lonardi

Glaxo SpA, via Fleming 2, 37100 Verona, Italy

The possibility of applying near-infrared reflectance analysis to the integrated control of the production cycle of cefuroxime axetil tablets was investigated. The results were good for the identification of cefuroxime axetil primary material, granules, cores and tablets. The determination of the compound and of its water content also gave satisfactory results.

Keywords: *Near-infrared reflectance analysis; antibiotic cefuroxime axetil; industrial control*

Introduction

The possibility of determining the physical and chemical parameters of complex mixtures in the solid state, without prior modification of the sample, is certainly the most interesting feature of near-infrared reflectance analysis (NIRA).[1] Its simplicity and speed of analysis are also positive aspects, especially when applied to the analytical control of production cycles.[2–9] On the basis of these features, we focused on the possibility of using NIRA for the integrated control of production cycles in the pharmaceutical industry.[10–19].

In this work, we applied this technique to the qualitative and quantitative analysis of tablets containing cefuroxime axetil (**I**), (*RS*)-1-acetoxyethyl(6*R*,7*R*)-3-carbamoyloxymethyl-7-[(2)-2-methoxyimino-2-(fur-2-yl)acetamido]ceph-3-em-4-carboxylate, having the composition reported in Table 1.

Different analytical aspects were studied. A calibration map for the qualitative analysis of various primary materials was constructed. The materials were drugs and excipients that could conceivably be used in the same area of production. Maps were developed for the global control of the drug during the various steps of the production cycle: primary material (cefuroxime axetil), granules ready for compression, cores and finished tablets.

Table 1 Composition of tablets containing cefuroxime axetil

Component	Composition of core (%)
Cefuroxime axetil	66.8
Microcrystalline cellulose	21.1
Sodium carboxymethylcellulose	8.9
Sodium lauryl sulfate	1.0
Hydrogenated vegetable oil	1.9
Silica precipitate	0.3

By far the most interesting aspect was the success obtained in the quality control of granules (G_1 and G_2, produced by different granulation parameters), which it was possible to distinguish.

Using the qualitative maps developed and the appropriate quantitative calibrations for assay and water content determination, it was possible to check the quality of the product at each step of the production cycle.

Experimental

NIRA

All the samples used were supplied by Glaxo (Verona, Italy). For NIRA the samples were placed in 0.5 cm deep polyethylene cells, covered with microscope slides and analysed in triplicate with an InfraAlyzer 500 apparatus (Bran & Luebbe), interfaced to an IBM PS/2 Model 50 computer. The cores and the tablets were milled with a Cyclotec 1093 sample mill (Tecator) before the analysis. All the samples were read in triplicate, refilling the cells with powder for each reading.

Qualitative analysis was performed by discriminant analysis (DA) on the raw absorbance data or on their principal component analysis (PCA) and clustering (Statgraphic Plus v.6.0, Statistical Graphic). Quantitative analysis was performed using multiple linear regression (MLR) (Idas-pc v.1.41, Bran & Luebbe) and partial least squares (PLS) (Unscrambler v.3.40, Camo) methods on the raw absorbance data and their derivatives.

Preparation of Laboratory Sample of Cefuroxime Axetil

Laboratory raw material samples, to widen the range of concentrations in the calibration phase, were prepared separately for assay and water content determinations. For assay, cefuroxime axetil was degraded by exposure to sunlight in petri dishes for different periods of time; for water content determination, samples of primary material were kept in an environment with 100% relative humidity for different periods of time.

For granules, cores and tablets, laboratory samples were prepared starting from a single pool of powders for each of the three species studied. The assay of the active ingredient was increased or decreased by adding primary material or a mixture of excipients. The same process was followed to vary the water content, keeping several samples in an environment with 100% humidity for different periods of time.

HPLC Identification and Determination of Cefuroxime Axetil

An HPLC method was used with the following equipment and conditions: Series 410 LC pump connected to an SEC-4 solvent environmental controller (Perkin-Elmer), LC 85B spectrophotometric detector (Perkin-Elmer), Model 3390A integrator (Hewlett-Packard); Hypersil SAS (5 μm) column (20 × 0.46 mm i.d.); column temperature, 25 °C; mobile phase, 0.2 mol l^{-1} ammonium dihydrogenphosphate–methanol (37.5 + 62.5); flow rate, 1 ml min^{-1}; and detection wavelength, 278 nm. The concentrations of cefuroxime axetil in the primary material, granules, cores and tablets were determined by comparing the areas of the chromatographic peaks with those of a standard.

The samples for HPLC analysis were prepared using the above mobile phase.

Determination of Water Content

The cores and the tablets were milled before water content determination by the Karl Fischer method. Exact masses of powder (500 mg) were added to 30 ml of neutralized Hydranal solvent (Riedel-de Haën) and titrated with Hydranal titrant. The end-point was determined electrometrically using an Amel Model 233-234 apparatus with a double-point Amel 880/TPG/12 electrode. The titrant was standardized with sodium tartrate dihydrate. Each sample was analysed in duplicate.

Sieve Analysis

An Octagon 200 test sieve shaker (Endecotts) was used. The time of analysis was 40 min with an intermittent vibration cycle of 1 min with a 40 s pause. The sieves used were Endecott 710, 500, 300, 250, 180, 125 and 90 μm. Granules and milled granules were subjected to the sieve test. The near-infrared spectrum of each sample was recorded before and after sieve analysis. After sieve analysis, each fraction collected was read in triplicate on the InfraAlyzer 500 apparatus.

Results and Discussion

Qualitative Analysis

Three calibration maps were constructed with the available samples: a general calibration containing all the chemical species in the production cycle; a specific calibration for cefuroxime axetil including primary material, granules and milled cores and tablets; and a specific calibration for the two granules.

Different chemometric approaches were used: discriminant analysis (DA) of spectral data, discriminant analysis of PCA scores and cluster analysis (CA). The results obtained by the first approach for the three calibrations on the basis of wavelengths giving sufficiently high Mahalanobis distances are given in Table 2. For the general calibration, DA was applied to the second derivative of the spectral data so as to give smaller spectral differences in the cefuroxime axetil group, that included samples with very different particle sizes (primary material, granules, milled cores and tablets), and to limit dispersion as much as possible.

Some randomly chosen samples were taken as unknowns and used to evaluate the predictive capacity of each of the calibrations. No wrong assignments occurred for the general calibration. The parameter considered was the normalized distance from the parent group. This was always more than 3 with respect to the other groups. For the specific calibration for cefuroxime axetil, all samples were identified correctly. With the third map, it was possible to distinguish the granules of different origin. This is very interesting because the two types of granules turned out to have different parameters for compression. None of the test samples was wrongly assigned (the normalized distance from the parent group was less than 2 and the distance from other groups was greater than 7). These calibrations make it possible to follow the cefuroxime axetil samples during the production cycle, irrespective of origin and stage of production, and to distinguish them from all other products present in the same area of production.

The results of DA of scores (the first six components were used), developed in the same way as for spectral data, for a

Table 2 Results of discriminant analysis of spectral data of the three calibrations

General calibration—

Component	Distance of cefuroxime axetil from other groups
Ceftazidime	171.3
Avicel	47.1
Sodium lauryl sulfate	153.1
Vegetable oil	352.2
Croscaramellose	76.4
Cefalexin	128.3
Cefuroxime	358.6
Silica	48.2

Specific calibration for cefuroxime axetil—

Distance from the group	Primary material	Granules	Cores and tablets
Primary material	—		
Granules	50.8	—	
Cores and tablets	52.6	11.3	—

Specific calibration for granules G_1 and G_2—

Distance from the group	Granules G_1	Granules G_2
Granules G_1	—	
Granules G_2	15.7	—

Table 3 Results of discriminant analysis of PCA scores in the three calibrations

General calibration—

Component	Distance of cefuroxime axetil from other groups
Ceftazidime	187.2
Avicel	62.3
Sodium lauryl sulfate	170.9
Vegetable oil	434.7
Croscaramellose	71.2
Cefalexin	184.4
Cefuroxime	392.3
Silica	160.1

Specific calibration for cefuroxime axetil—

Distance from the group	Primary material	Granules	Cores and tablets
Primary material	—		
Granules	60.3	—	
Cores and tablets	68.5	17.8	—

Specific calibration for granules G_1 and G_2—

Distance from the group	Granules G_1	Granules G_2
Granules G_1	—	
Granules G_2	20.7	—

general calibration, one specific for cefuroxime axetil and another exclusively for granules, are given in Table 3. In the calibration phase, all samples were correctly assigned in all three calibrations and verification with samples taken as unknowns confirmed the validity of the calibrations, as none of the samples was wrongly assigned.

Cluster analysis was used to distinguish samples of cefuroxime axetil in the specific calibration for primary material, granules and milled cores and tablets and in the specific calibration for the two types of granules. The variables used were the scores of the first six principal components. The results of the general map including all forms of cefuroxime axetil are given in Fig. 1. In this instance the optimum cluster number was four; in fact, with five groups (in the hope of distinguishing milled cores and tablets) there was overlap between core and tablet samples. The centroid method of clustering was used to distinguish the granules of different origin, imposing the formation of two clusters (Fig. 2). As shown by the figures, the centroid method gave good results in line with those obtained by discriminant analysis on spectral data and scores.

We were interested in investigating the analytical possibilities as far as the granules were concerned. The significant differences in their densities and compressibilities affected the NIRA readings. In fact, the different particle size distribution of the two granule types (Fig. 3) could have been the fundamental element in distinguishing G_1 and G_2. However, the spectra of the different size ranges (Fig. 4) gave the impression of significant differences, even when size ranges were matched. This is most evident in Fig. 5, where incomplete or partial overlapping of the two spectra is evident, even when there is no difference in particle size. Hence it seems logical to attribute the differences to the physical parameters mentioned above (density and compressibility).

It was interesting to observe that the granules G_1 and G_2 maintained their differences even after milling. Even though they have the same distributions of particle sizes after milling,

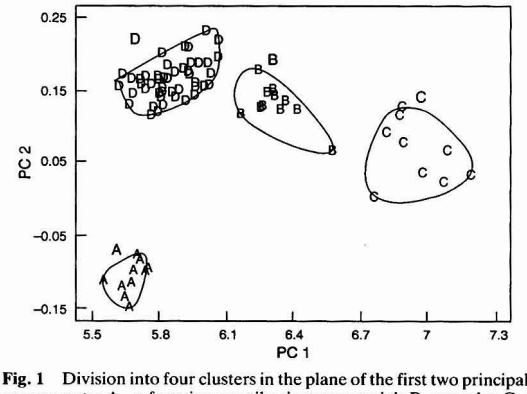

Fig. 1 Division into four clusters in the plane of the first two principal components: A, cefuroxime axetil primary material; B, granules G_1; C, granules G_2; D, milled cores and tablets.

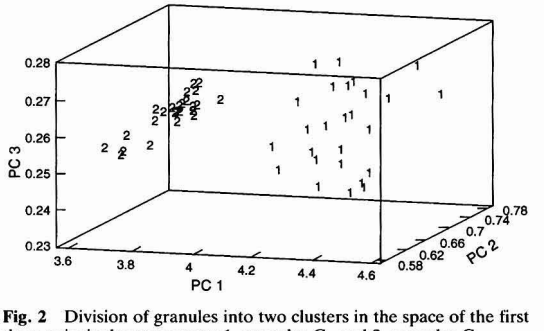

Fig. 2 Division of granules into two clusters in the space of the first three principal components: 1, granules G_1 and 2, granules G_2.

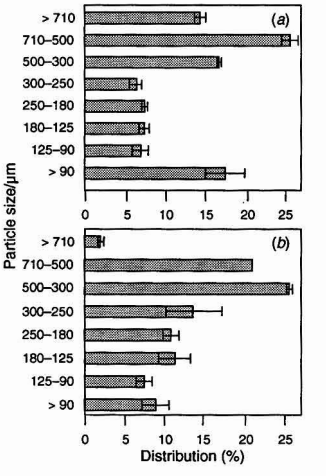

Fig. 3 Distribution of grain size of granules: (*a*) G_1 and (*b*) G_2.

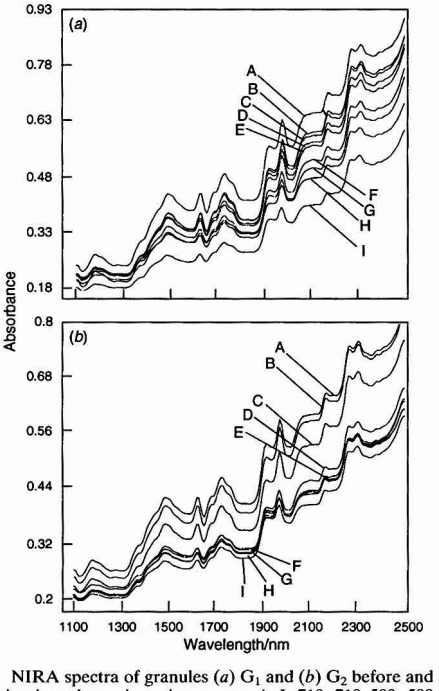

Fig. 4 NIRA spectra of granules (*a*) G_1 and (*b*) G_2 before and after separation into the various size ranges: A–I, 710, 710–500, 500–300, 300–250, 250–180, 180–125, 125–90, before separation and <90 μm, respectively.

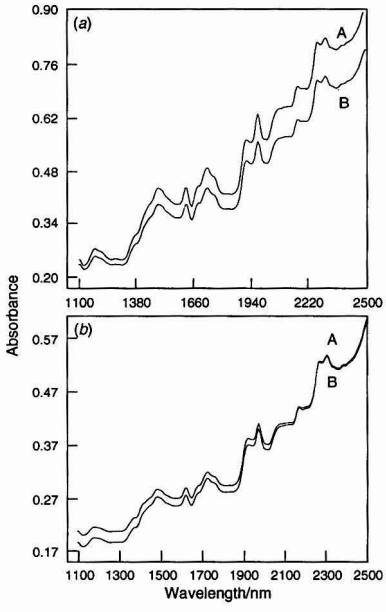

Fig. 5 NIRA spectra of granules A, G_1 and B, G_2 in the following size ranges: (*a*) 710–500 μm and (*b*) <90 μm.

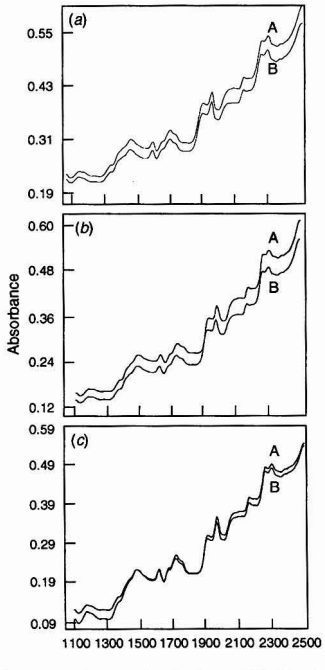

Fig. 6 NIRA spectra of granules A, G_1 and B, G_2 after milling: (*a*) before, (*b*) after sieving 250–180 μm and (*c*) after sieving <90 μm.

the spectra of milled granules as such and of the various size ranges were not the same (Fig. 6). Microscope observation revealed that the granules broke in different ways and this was confirmed by the NIRA spectra.

Quantitative Analysis

As with qualitative analysis, we again tested and compared different methods of processing spectral data, namely multiple linear regression (MLR) and partial least squares (PLS). The same production samples as in the previous analysis were used, plus laboratory samples prepared to give a sufficiently wide calibration interval, as described in previous papers.[10,11]

Calibrations with MLR and PLS were developed for assay and water content determination of the primary material in order to compare their respective performances. The results are shown in Table 4. The two methods are equivalent in the calibration phase, but for prediction of the amount of active ingredient the PLS calibration gave a better standard error. The main differences occur in the calibration phase, which is more laborious for MLR and hence more subject to error. As far as water content is concerned, the percentage error was sometimes high (>10%), but only for samples having a water content of less than 1% (acceptability limit = 2%). This demonstrates that water may not be detected by reflectance at levels of less than 1%. In terms of production control, such errors would never lead to the erroneous acceptance or rejection of samples having the required specifications.

Table 4 Results of assay and water content determination of cefuroxime axetil primary material by multiple linear regression and partial least squares

	Calibration for the cefuroxime axetil assay			
Chemometric approach	r*	*SEE**	Range of calibration	*SEP**
MLR	0.986	1.021	79.4–101.2	1.614
PLS	0.985	1.075	79.4–101.2	1.240
	Calibration for water content determination			
	r*	*SEE**	Range of calibration	*SEP**
MLR	0.992	0.091	0.49–4.19	0.098
PLS	0.990	0.095	0.49–4.19	0.110

* r = Correlation coefficient; *SEE* = standard error of estimate; *SEP* = standard error of prediction.

Table 5 Results of assay and water content determination of granules, cores and tablets by multiple linear regression and partial least squares

	Calibration for the cefuroxime axetil assay			
Chemometric approach	r*	*SEE**	Range of calibration	*SEP**
MLR	0.960	0.407	62.6–70.1	0.524
PLS	0.974	0.305	62.6–70.12	0.481
	Calibration for water content determination			
	r*	*SEE**	Range of calibration	*SEP**
MLR	0.983	0.160	0.91–4.12	0.259
PLS	0.989	0.124	0.91–4.12	0.203

* r = Correlation coefficient; *SEE* = standard error of estimate; *SEP* = standard error of prediction.

For the assay of granules, the same two methods were used and the results are given in Table 5. Polyvalent calibrations were constructed with samples of granules and with milled cores and tablets. For the determination of water content, the idea of constructing a single calibration for granules, cores and tablets was justified. The results are shown in Table 5. In all instances the calibrations were verified with a test set of samples and the results in terms of standard error were good. The histograms in Figs. 7 and 8 show the distributions of the percentage errors obtained for the various calibrations with the test samples.

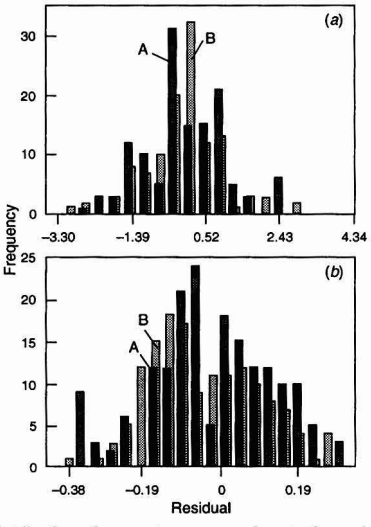

Fig. 7 Distribution of percentage errors of a set of samples taken as unknowns for calibrations for (*a*) the assay and (*b*) water content determination of primary material, by A, PLS and B, MLR.

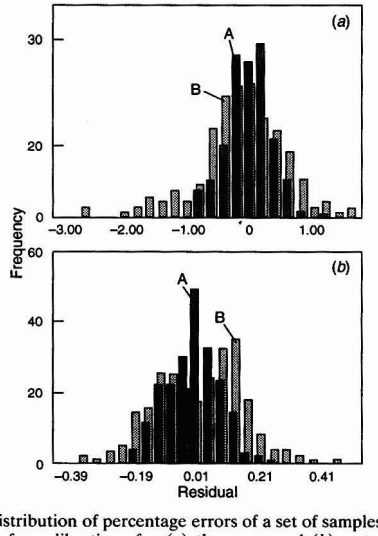

Fig. 8 Distribution of percentage errors of a set of samples taken as unknowns for calibrations for (*a*) the assay and (*b*) water content determination of granules, cores and tablets, by A, PLS and B, MLR.

Conclusions

The proposed method for the analyses investigated (identification, assay of active ingredient and determination of water content) for a solid pharmaceutical form and its production cycle intermediates was fully satisfactory, giving results comparable to those of the reference methods (HPLC and Karl Fischer).

As far as identification is concerned, the results obtained were excellent, in terms of both statistical parameters of control and the results obtained in the verification phase. In addition to a good discriminating capacity with respect to extraneous substances, various production intermediates and granules of different origin could be distinguished. The possibility of analysing the sample in the solid state also provides information on the physical characteristics of the sample, as shown in the testing of the two granules. This is an advantage over the simple determination of identity by HPLC.

The results obtained for the determination of the active ingredient and water content were also good, both in the calibration phase and in the phase of verification with unknown samples. All the calibrations obtained, whether with MLR or PLS, gave good standard errors in the prediction phase.

Overall, the results obtained by NIRA were completely satisfactory. The analytical determinations are performed in one step and much more quickly than with traditional methods of analysis. The results again confirm the appropriateness of NIRA for the analysis of solid pharmaceuticals.

References

1 Corti, P., Dreassi, E., and Lonardi, S., *Farmaco*, 1993, **48**, 1.
2 Mark, H. L., and Tunnell, D., *Anal. Chem.*, 1985, **57**, 1449.
3 Ciurczak, E. W., and Maldacker, T. A., *Spectroscopy*, 1986, **1**, 36.
4 Ciurczak, E. W., *Appl. Spectrosc. Rev.*, 1987, **23**, 147.
5 Whitfield, R. G., Gerger, M. E., and Sharp, R. L., *Appl. Spectrosc.*, 1987, **41**, 1204.
6 Lodder, R. A., Selby, M., and Hieftje, G. M., *Appl. Spectrosc.*, 1987, **59**, 1921.
7 Lodder, R. A., and Hieftje, G. M., *Appl. Spectrosc.*, 1988, **42**, 556.
8 Drennen, J. K., and Lodder, R. A., *J. Pharm. Biomed. Anal.*, 1990, **79**, 622.
9 Plugge, W., and Van der Vlies, C., *J. Pharm. Biomed. Anal.*, 1992, **10**, 837.
10 Lonardi, S., Viviani, R., Mosconi, L., Bernuzzi, M., Corti, P., Dreassi, E., Murratzu, C., and Corbini, G., *J. Pharm. Biomed. Anal.*, 1989, **7**, 303.
11 Corti, P., Dreassi, E., Murratzu, C., Corbini, G., Ballerini, L., and Gravina, S., *Pharm. Acta Helv.*, 1989, **64**, 140.
12 Corti, P., Dreassi, E., Corbini, G., Ballerini, L., and Gravina, S., *Pharm. Acta Helv.*, 1990, **65**, 189.
13 Corti, P., Dreassi, E., Corbini, G., Lonardi, S., and Gravina, S., *Analusis*, 1990, **18**, 112.
14 Corti, P., Dreassi, E., Corbini, G., Montecchi, L., and Paggi, J., *Analusis*, 1990, **18**, 117.
15 Corti, P., Dreassi, E., Corbini, G., Lonardi, S., Viviani, R., Mosconi, L., and Bernuzzi, M., *Pharm. Acta Helv.*, 1990, **65**, 28.
16 Corti, P., Dreassi, E., Franchi, G. G., Corbini, G., Moggi, A., and Gravina, S., *Int. J. Crude Drug Res.*, 1990, **28**, 185.
17 Corti, P., Dreassi, E., Ceramelli, G., Lonardi, S., Viviani, R., and Gravina, S., *Analusis*, 1991, **19**, 198.
18 Corti, P., Dreassi, E., Savini, L., Petriconi, S., Genga, R., Montecchi, L., and Lonardi, S., *Proc. Control Qual.*, 1992, **2**, 131.
19 Corti, P., Savini, L., Dreassi, E., Ceramelli, G., Montecchi, L., and Lonardi, S., *Pharm. Acta Helv.*, 1992, **67**, 57.

Paper 4/03947E
Received June 29, 1994
Accepted September 5, 1994

Signal and Noise Analysis of Non-modulated Polarimeters Using Mueller Calculus Simulations

Uma Kale and Edward Voigtman*

Chemistry Department, Lederle GRC Tower, University of Massachusetts, Box 34510, Amherst, MA 01003-4510, USA

Two non-modulated polarimeters have been modelled using the Mueller optical calculus. The effects of polarizer extinction ratio, orientation of the polarizer, source shot noise, 1/*f* noise and polarization ratio, on the signal-to-noise ratio of the measurement of optical activity, are evaluated. It is shown that the performance of a conventional polarimeter consisting of a crossed polarizer pair is strongly influenced by the arrangement of the optics and the type of dominant noise. The quality of the optics used is also important, if the measurement is source 1/*f* noise limited. The other polarimeter modelled, consists of a polarizer in combination with a polarizing prism, which resolves the light into orthogonally polarized components. Numerical simulation of this design shows that its performance is not degraded by the use of inferior optics, provided that the optics are positioned appropriately. The optimum arrangement is influenced by the dominant noise type, and in some instances, the polarization ratio and the quality of the optical components. However, the optimum arrangement may prove difficult to achieve experimentally. This design is also shown to be superior to the other scheme because of its ability to discriminate against source noise effectively.

Keywords: Optical polarimetry; signal-to-noise ratio optimization; noise analysis; Mueller calculus; numerical simulation

Introduction

The development and evaluation of spectrometric instrumental analysis techniques requires a clear understanding of the underlying principles of optics, electronics, and signal processing methods, as well as knowledge of the various sources of error in the experiment, such as errors produced by imperfect optical and electronic components, and their effect on the measurement of the property of interest. However, a theoretical analysis of these techniques, and the numerous experimental configurations possible for each technique, is often impeded by the inherent complexity of the transfer functions of such systems. In such situations numerical analysis proves to be extremely useful.

The numerical analysis approach is particularly well suited to the study of optical polarimetry techniques, as polarized or partially polarized light and various optical elements may be modelled using the Jones or Mueller formalism.[1] Analytical matrix methods have been successfully applied to the analysis of ideal systems,[2] but real polarimeters with non-ideal light sources and optical components are difficult to model and analyse, except by numerical simulation.

The numerical simulation approach has been applied previously to the quantitative analysis of a polarimeter design which employs polarization modulation and a lock-in amplifier to demodulate the signal.[3] Frequency domain noise calculations were performed to analyse the effects of polarizer extinction ratio, modulation frequency, preamplifier noise and analyte concentration on the signal-to-noise (S/N) ratio.[3] This design, reported by Yeung *et al.*,[4] is known to be superior, in terms of sensitivity of the measurement, to other simpler non-modulated schemes described in the literature. It is of interest similarly to model and analyse the non-modulated designs in order to gain an understanding of how various factors interact and influence the performance of these schemes.

This paper describes the numerical simulation and analysis of two non-modulated polarimeters. The first scheme, probably the simplest and the most commonly described one, is depicted in Fig. 1. It consists of a light source and two polarizers with their transmission axes crossed at 90°. The optical activity of a sample placed between the two polarizers is measured by monitoring the intensity of the light transmitted with the polarizers in the crossed orientation.

An alternative non-modulated design, shown in Fig. 2, consists of a polarizer oriented with its fast axis at 45°, followed by the sample and a polarizing prism which resolves the light into two orthogonally polarized components.[5] In the absence of an optically active sample between the polarizer and the prism, the linearly polarized light beam oriented at 45° exiting the sample cell is resolved into components having equal intensity. However, a small rotation of the plane of polarization induced by an optically active sample causes the intensities of the two components to be unequal, the difference being a possible signal measured.

Simulations were performed to evaluate the performance of both these designs under various experimental conditions. The influence of source intensity, stability and polarization state, quality of the optics and their orientation and the magnitude of optical rotation on the precision of the measurement was evaluated.

The numerical simulations were performed using a commercially available program (Extend; Imagine That, San Jose, CA, USA), in combination with optical calculi and signal

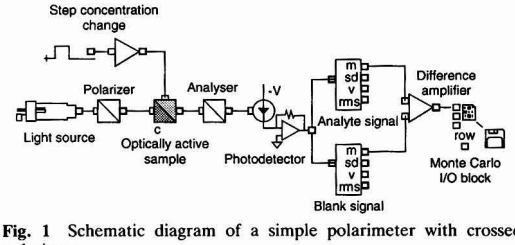

Fig. 1 Schematic diagram of a simple polarimeter with crossed polarizers.

* To whom correspondence should be addressed.

processing software, called Voigt fx, which has been described elsewhere.[6–12] The simulation program allows users to create a block diagram of a process by sequentially connecting appropriate blocks. Vectors or real numbers, as appropriate, are passed and received by each of the blocks during the simulation. Each block processes its input as described in the code which is built into the blocks, and passes the data to the next block in the sequence. Although the code is invisible to the user, all blocks have a dialogue box into which various input parameters are specified. Using this software, models of experimental schemes are constructed and analysed with great ease and speed. The use of this program for modelling spectrometric techniques is described in greater detail in refs. 6–12.

Experimental

Simulation Parameters

All simulations were performed on a Macintosh IIfx computer (Apple Computer, Cupertino, CA, USA) with 8 M RAM. The models shown in Figs. 1 and 2, with minor modifications, were used for all calculations. A general explanation of the two schemes was given in the previous section, and a detailed description of the simulation parameters used by each block follows.

The light source generated either horizontally polarized light, with a polarization ratio of 500 : 1, or unpolarized light. Light intensities of 10 μW, 1 mW and 10 mW were used. Noise was digitally generated and imposed on the light source and the relative standard deviation specified was either 0.1 or 0.001%. The probability distribution function of the noise was Gaussian, and the noise power spectral density was inversely dependent on frequency. The Gaussian distributed 1/*f* noise was band-limited from 1 mHz to 10 Hz. Thus, the lower frequency components, between 1 mHz and 10 Hz, made the greatest contribution to the noise and above 10 Hz, the noise power spectral density was independent of frequency. For shot noise calculations, the wavelength of light was assumed to be 500 nm.

The models used imperfect linear polarizers, *i.e.*, the extinction ratios (ε) of the polarizers were non-zero. The extinction ratio, which is the ratio of the light intensity transmitted by a pair of polarizers with their transmission axes crossed at 90° to the intensity of the light transmitted with the axes parallel, was varied between zero and 10^{-2}. Commercially available high-quality polarizers have extinction ratios of the order of 10^{-6}, with $\varepsilon = 0$ representing ideal polarizers. Yeung *et al.*[4] have reported achieving ε values as low as 10^{-10}, by selecting strain-free localized regions within the polarizers. For the second scheme, which uses a polarizing prism, the ε was specified separately for each polarization state of the light. The extinction ratio for each beam was selected to match that of the polarizer.

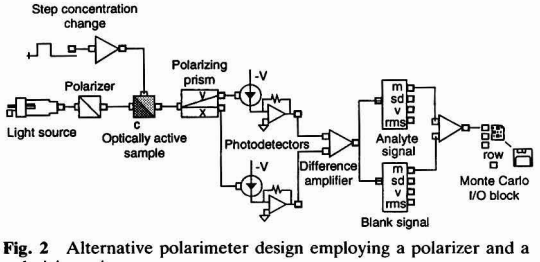

Fig. 2 Alternative polarimeter design employing a polarizer and a polarizing prism.

The optically active sample had an activity of $-10°$ l mol^{-1} cm^{-1}, and although sample circular dichroism effects are easily included in the models, they were ignored here. The temporal concentration profile was modelled as a step function, allowing the sample concentration to be maintained at zero for 1 s and then instantaneously changed to 1 mmol l^{-1} during the next second. This allows for accurate noise calculation, by inclusion of noise from the blank measurement. Although the blank was optically inactive, the light intensity transmitted by a pair of non-ideal crossed polarizers may be equivalently considered to be a signal from an optically active blank. Pathlength was assumed to be 1 cm, so that the true sample optical rotation was -10×10^{-3} degrees.

Ideal photodetectors, with a responsivity of 0.1 A W^{-1}, and a transimpedance preamplifier gain of 10 kΩ, were used to measure the light intensity transmitted by the analyser or the prism. The block following the preamplifier in the sequence merely calculated the mean light intensity measured over a specified period. In this manner, signals obtained from the blank and the sample were calculated, the difference was computed and the result was recorded by the Monte Carlo I/O block, at the end of the simulation.

Each simulation was performed in 250 steps over a simulation period of 2 s, *viz.*, 1 s each per sample and blank measurement. The simulation was repeated 1000 times, and S/N ratios were calculated by dividing the mean of the 1000 simulations by their standard deviation. The Mueller calculus was used for all simulations, in preference to the Jones calculus, as it has the advantage of greater speed and the ability to handle unpolarized light.

Shot Noise Calculations

Although theoretical noise calculations involving non-white noise present challenging problems, the simulations described here are able to handle these calculations with almost trivial ease. On the other hand, shot noise effects cannot be directly incorporated into the models, because of the dependence of shot noise on the light intensity, whereas analytically, shot noise is often handled fairly easily. These calculations therefore require a slightly different approach than the multiple simulation procedure described earlier. As shot noise is known normally to follow Poisson statistics, the only information required is the intensity of the light, expressed as number of photons per second, the S/N ratio of the measured intensity then being given by the square-root of the intensity. Thus, digital generation of noise is not required, as with the 1/*f* noise, and hence a single calculation can be performed to obtain the S/N ratios and multiple runs of 250 step simulations are not required.

The scheme for calculation of shot noise limited S/N ratios is shown in Fig. 3. The measured voltages were expressed as number of photons per second, using the appropriate conversion factor for light at 500 nm. For a photodetector with a responsivity of 0.1 A W^{-1} and a transimpedance preamplifier gain of 10 kΩ, the conversion factor is 2.52×10^{15} (photons s^{-1})/V, if the light is assumed to be at 500 nm. Thus, a 1 V signal corresponds to a photon arrival rate of 2.52×10^{15}

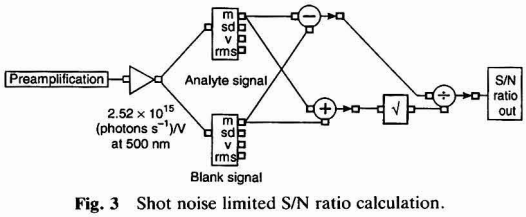

Fig. 3 Shot noise limited S/N ratio calculation.

photons s^{-1} at the detector. The net signal was divided by the square root of the total number of photons observed during the blank and sample measurements, to give the absolute S/N ratio. An integration time of 1 s was assumed. Actual S/N ratios would depend on the integration time.

Effect of Polarizer Offset Angle on S/N Ratio

Earlier reports in the literature indicate that for a non-modulated polarimeter, the S/N ratio in the shot noise limit is determined not by the quality of the optics, but by their orientation.[2] Thus, use of polarizers with large extinction ratios are expected to yield near-optimum S/N ratios, if they are offset appropriately, at an angle $\arctan(\varepsilon^{1/4})$, which was shown to be the optimum offset angle.[2] It is desirable to know whether this result may be extended to other non-modulated designs, and to find the optimum experimental parameters for measurements limited by noise other than shot noise, as in practical situations, shot noise is unlikely to be the limiting noise source. Real polarimeters often have a significant amount of low frequency noise, especially if laser light sources are used. In such a situation, it is intuitive that the polarizers should be perfectly crossed in order to minimize the noise. However, it should be recognized that the signal magnitude is not independent of the offset angle, so that an optimum orientation should also exist for $1/f$ noise limited measurements.

Calculations were performed to evaluate numerically the optimum offset angle of the polarizers for each scheme in the shot noise and source $1/f$ noise limit. The effect of the polarization state of the light (*i.e.*, x polarized or unpolarized) on the dependence of S/N ratio on the offset angle was also evaluated. The S/N ratios were calculated using the equations in Table 1. It is assumed that the measurement time of 1 s for the blank and sample signals ensures that there is no correlation between the noises on the two intensities measured. It should also be noted that although the shot noise calculations yield absolute S/N ratios, the $1/f$ noise limited S/N ratios are scaled by a factor dependent on the magnitude of the source noise. As the root mean square (rms) noise is directly proportional to the source intensity for $1/f$ noise, any attenuation of the source intensity also results in a proportional decrease in the noise. Thus, the S/N ratio of the light intensity measured at the detector is constant, and independent of the measured intensity. Therefore, the scale factor is expected to be independent of the offset angle and ε and is determined only by the magnitude of the source noise. Absolute S/N ratios may be calculated by running multiple simulations, but scaled S/N ratios are computed more rapidly. As the scaled S/N ratios are calculated indirectly, a noisy light source is not required. For all these calculations an ideal light source, with no noise on its output intensity, was used. Calculation of absolute S/N ratios would require multiple simulation runs using a light source with $1/f$ noise on the light intensity. The offset angle of the polarizer following the light source was varied from 0 to 20°, in 0.020° increments, and for each offset angle, the equations in Table 1 were used to calculate the S/N ratio.

As the offset angle of the polarizer cannot be controlled externally *via* a modulation input, an unpolarized light source and a Faraday rotator following the polarizer were use to adjust the orientation of the light beam appropriately. The model for Scheme 1 is shown in Fig. 4 and a similar model was constructed for Scheme 2. The block that performed the S/N ratio calculation was an hierarchical block, *i.e.*, it was comprised of other blocks, depending on the calculation to be performed. For example, the internal structure of the block was as shown in Fig. 3, for calculation of shot noise limited S/N ratios for Scheme 1. For the other calculations, the structure of this block was modified according to the equations in Table 1. The simulations were also performed using x polarized light, and for these calculations the polarizer and Faraday rotator were replaced by a general Mueller matrix block. The Mueller matrices for polarizers with different extinction ratios were calculated and entered in this block, the offset angle of which can be controlled externally.

Results and Discussion

Effect of Source Noise on Precision

Tables 2 and 3 show the S/N ratios obtained for Schemes 1 and 2, respectively, for the measurement of an optical rotation of -10×10^{-3} degrees using polarizers of varying quality and an x polarized light source with $1/f$ noise on the intensity. It can be seen that the performance of the two schemes is comparable, if ideal optics are used. In practical situations, however, Scheme 2 is predicted to provide superior performance, if the limiting noise source is the light source. The improvement in S/N ratios can be attributed to the design of the second instrument, which allows for cancellation of any correlated noise on the two light beams, by calculating a difference of the two intensities measured. It is interesting that although this design resembles a double-beam type instrument, it is neither

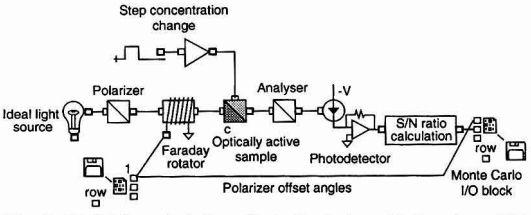

Fig. 4 Model for calculating effect of polarizer offset angle on S/N ratio.

Table 1 Equations used for calculation of S/N ratios

Source noise type	Scheme 1*	Scheme 2†
Shot noise	$\frac{I_s - I_b}{(I_s + I_b)^{1/2}}$	$\frac{I_{ys} - I_{xs} - I_{yb} + I_{xb}}{(I_{ys} + I_{xs} + I_{yb} + I_{xb})^{1/2}}$
$1/f$ noise‡	$\frac{I_s - I_b}{(I_s^2 + I_b^2)^{1/2}}$	$\frac{I_{ys} - I_{xs} - I_{yb} + I_{xb}}{[(I_{ys} - I_{xs})^2 + (I_{yb} - I_{xb})^2]^{1/2}}$

* I_s and I_b are sample and blank signals, respectively.

† I_{xs} and I_{xb} are the x polarized components of the sample and blank signals, and I_{ys} and I_{yb} are the y polarized components.

‡ These equations give scaled S/N ratios and the scale factors have been omitted here.

Table 2 Source $1/f$ noise limited S/N for Scheme 1, using crossed polarizers

		10 μW	1 mW	10 mW
$\varepsilon = 0$				
	0.1% $1/f$	1.5×10^3	1.4×10^3	1.4×10^3
	0.001% $1/f$	1.5×10^5	1.4×10^5	1.5×10^5
$\varepsilon = 10^{-6}$				
	0.1% $1/f$	1.3×10^2	1.3×10^2	1.3×10^2
	0.001% $1/f$	1.3×10^4	1.3×10^4	1.2×10^4
$\varepsilon = 10^{-2}$				
	0.1% $1/f$	0.339	0.042	0.046
	0.001% $1/f$	1.3	1.3	1.4

a true double beam in space type instrument, as it requires sequential measurement of blank and sample signals, nor is it a double beam in time type instrument; nevertheless, it allows for excellent cancellation of source noise. Evidently, effective noise cancellation requires that the light beam be oriented as close to 45° as possible, prior to entering the sample cell. Thus, it is likely that in this instance the quality of the polarizers is not as critical as their orientation, the most favourable orientation being the one that allows for total cancellation of the noise from the blank measurement. On the other hand, Scheme 1 is extremely sensitive to source noise, and the best approach to maximize S/N ratios is to lower the extinction ratio of the polarizers.

The theoretical S/N ratios, in the shot noise limit, are given in Tables 4 and 5. A 10 mW shot noise limited light source is probably not a realistic assumption, as such a source is not readily available, but the calculations merely serve to ensure that the S/N ratios scale as expected. For Scheme 1, results similar to the 1/*f* noise limited case are obtained, *i.e.*, the S/N ratio decreases rapidly as ε increases. On the other hand, Scheme 2 is not especially sensitive to changes in ε, because for polarizers oriented at 45°, the change in light intensity transmitted is insignficiant, for varying ε values. Combining the shot noise and 1/*f* noise results, it can be seen that for Scheme 1, extremely good polarizers (better than $\varepsilon = 10^{-6}$) are required, as is a high intensity, quiet light source. This is in agreement with the results of a semi-quantitative noise analysis previously reported by Yeung.[13,14] For the second scheme, commercially available high-quality polarizers ($\varepsilon = 10^{-6}$) are adequate, and not much improvement is to be expected by lowering ε. Use of a high intensity low noise source is preferred by both schemes, but this is not unexpected as a high intensity shot noise limited source is, indeed, an ideal source for these measurements.

Effect of Polarizer Offset Angle on S/N Ratio Using Unpolarized Light

All simulations involving calculation of dependence of S/N ratio on polarizer offset angle were run using six different ε values, ranging from 0 to 10^{-2}. However, in Figs. 5–9 only the results for three of the six cases have been plotted. Some of the results not plotted are described in the text.

For unpolarized light, the shot noise and 1/*f* noise limited S/N ratios were calculated for various orientations of the polarizers, as described in Table 1. Figs. 5 and 6 show the dependence of shot noise limited S/N ratios on the offset angle for Schemes 1 and 2, respectively. It can be seen that for the first design, appropriately offsetting inferior quality polarizers does indeed allow S/N ratios close to the optimum (within 10%) to be achieved, if shot noise is the dominant noise

Table 3 Source 1/*f* noise limited S/N ratios for Scheme 2

	10 μW	1 mW	10 mW
$\varepsilon = 0$			
0.1% 1/*f*	1.5×10^3	1.4×10^3	1.4×10^3
0.001% 1/*f*	1.4×10^5	1.4×10^5	1.5×10^5
$\varepsilon = 10^{-6}$			
0.1% 1/*f*	5.4×10^2	5.8×10^2	6.0×10^2
0.001% 1/*f*	5.7×10^4	5.6×10^4	5.9×10^4
$\varepsilon = 10^{-2}$			
0.1% 1/*f*	5.4	5.3	5.1
0.001% 1/*f*	5.4×10^{-2}	5.4×10^{-2}	5.4×10^{-2}

Table 4 Source shot noise limited S/N ratios for Scheme 1, using crossed polarizers

	10 μW	1 mW	10 mW
$\varepsilon = 0$	875	8752	27 676
$\varepsilon = 10^{-6}$	150	1504	4 756
$\varepsilon = 10^{-2}$	1.5	15	48

Table 5 Source shot noise limited S/N ratios for Scheme 2

	10 μW	1 mW	10 mW
$\varepsilon = 0$	876	8756	27 690
$\varepsilon = 10^{-6}$	876	8756	27 689
$\varepsilon = 10^{-2}$	858	8582	27 140

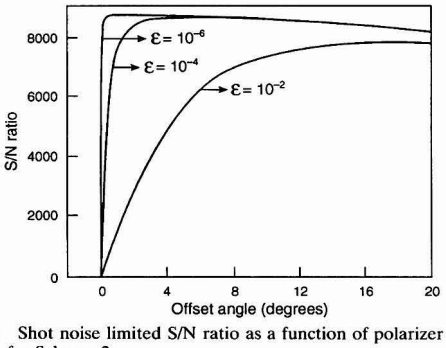

Fig. 5 Shot noise limited S/N ratio as a function of polarizer offset angle, for Scheme 2.

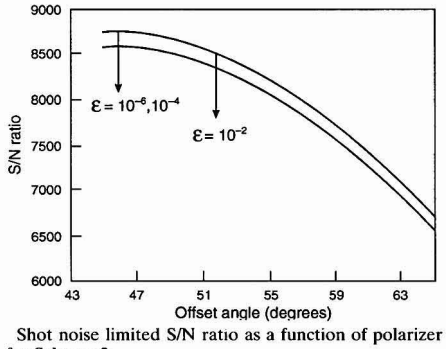

Fig. 6 Shot noise limited S/N ratio as a function of polarizer offset angle, for Scheme 2.

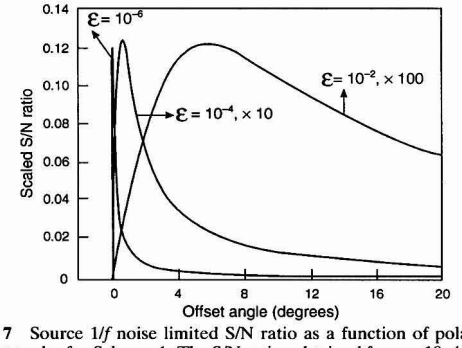

Fig. 7 Source 1/*f* noise limited S/N ratio as a function of polarizer offset angle, for Scheme 1. The S/N ratios obtained for $\varepsilon = 10^{-4}$ and $\varepsilon = 10^{-2}$ have been multiplied by factors of 10 and 100, respectively, so that they may be plotted to the same axis. The factor by which all S/N ratios are scaled is independent of ε.

source. The optimum offset angle was in exact agreement with the value of arctan($\varepsilon^{1/4}$) predicted by Kankare and Stephens.[2] It should be noted that the offset angle of arctan($\varepsilon^{1/4}$) has been derived to be the optimum only in the limit of zero optical activity. Thus, for ideal polarizers the optimum orientation is not 0° but is determined by the optical activity measured, whereas, for non-ideal polarizers, the influence of the magnitude of optical activity is not as important, and the optimum angles matched the predicted values. The optimum angle was found to vary from about 0.54° for $\varepsilon = 0$ to 17.56° for $\varepsilon = 10^{-2}$. For $\varepsilon = 0$, the calculated optimum angle for a sample optical rotation of -10×10^{-6} degrees was 0.02°, which is indeed much closer to the predicted value. Below the optimum angle, the S/N ratio decreased rapidly, but for angles greater than the optimum, the S/N ratio was largely independent of offset angle. It is important to recognize that for this scheme, the common practice of crossing the transmission axes of the polarizers does not yield the highest S/N ratios. The crossed orientation is the optimum only for ideal polarizers and an ideal, *i.e.*, shot noise limited, light source in the limit of zero optical activity, as noted by Kankare and Stephens in their paper.[2]

In the shot noise limit, the second scheme was found to be largely insensitive to variation in the offset angle, the optimum orientation being 45°, regardless of polarizer quality. For angles as large as 65°, *i.e.*, 20° greater than the optimum, the S/N ratio was found to have degraded to about 75% of the maximum value. This is because if 1 mW unpolarized light is used, regardless of the ε value and the offset angle, the intensity of the light beam emerging from the polarizer is 0.5 mW. After separation into the two components of perpendicular polarization, all the photons are detected by the photodetectors. It follows from the equations in Table 1, that although the magnitude of the signal may change by a small amount, that of the noise remains constant, leading to only a small decrease in the S/N ratio.

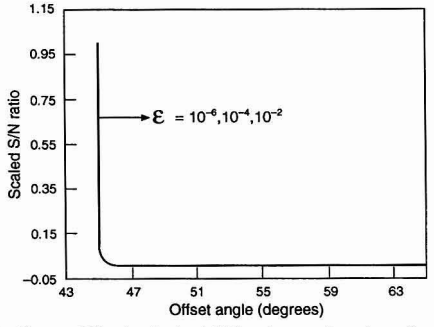

Fig. 8 Source 1/*f* noise limited S/N ratio as a function of polarizer offset angle, for Scheme 2. The factor by which all S/N ratios are scaled is independent of ε.

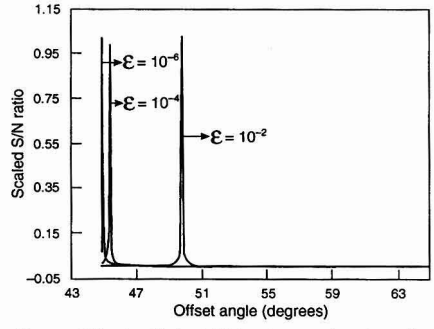

Fig. 9 Source 1/*f* noise limited S/N ratio as a function of polarizer offset angle, for Scheme 2, using *x* polarized light. The factor by which all S/N ratios are scaled is independent of ε.

The scaled 1/*f* noise limited S/N ratios for Schemes 1 and 2 are plotted as a function of the offset angle in Figs. 7 and 8, respectively. For Scheme 1, it can be seen that in agreement with the results in Table 2, the precision of the measurement is severely compromised by use of poor quality optics. Nevertheless, an optimum offset angle does exist for these measurements, and in practical situations this angle is in the range of a few hundredths of a degree. Again, the crossed orientation is not the optimum arrangement for this scheme, regardless of the fact that the rms noise is directly proportional to the transmitted intensity.

For Scheme 2, the 1/*f* noise limited S/N ratios are independent of polarizer quality, over a very wide range of ε values. For unpolarized light, this is to be expected, as regardless of ε, the light beam entering the sample cell has an intensity of 0.5 mW, and a polarization ratio determined by the offset angle, and not greatly affected by the extinction ratio, even for ε as large as 10^{-2}. The degree of polarization of the light transmitted by a polarizer with $\varepsilon = 10^{-2}$ is only 1% lower than the degree of polarization obtained by use of ideal polarizers. Thus, use of polarizers with high ε values is not found to have a detrimental effect, but if ε is greater than 10^{-2} it is expected that the S/N ratio will degrade, as the degree of polarization decreases. The optimum angle, in all instances, is 45°, and for an offset angle only 0.02° greater, the S/N ratio is lower by 70%. The S/N ratio is a strong function of the polarizer offset, and as the tolerance on the optimum angle is not large, as with the shot noise case, precise control of the offset angle is critical.

It is apparent that if polarized light is used, the optimum angle will not be independent of ε, as both the ε and the offset angle dictate the orientation of the plane of polarization of the light. All the simulations described in this section were also run using polarized light in order to evaluate the influence of the source polarization ratio on the precision of the measurement and the optimum experimental arrangement. The results appear in the next section.

Effect of Polarizer Offset Angle on S/N Ratio Using Polarized Light

For Scheme 1, the dependence of the shot noise limited S/N ratio on the offset angle, obtained using 500 : 1*x* polarized light, was seen to be similar to the results obtained using unpolarized light. The absolute S/N ratios were greater by a factor of $\sqrt{2}$ but the shape of the curves remained unchanged. The $\sqrt{2}$ improvement in S/N is obtained as a result of the intensity of *x* polarized light transmitted by a pair of crossed polarizers being twice the intensity of unpolarized light transmitted by the polarizer pair. It should be recognized that the increase in the shot noise limited S/N ratio is not directly influenced by the polarization ratio of source, but by the source intensity. The optimum angles for the various polarizers were smaller than the optimum angles obtained using unpolarized light. The decrease was about 0.5° for $\varepsilon = 10^{-6}$, and 4.5° for $\varepsilon = 10^{-2}$. However, this is not a very significant decrease as the S/N curves are fairly flat above the optimum offset angle.

The shot noise results for Scheme 2 were similar to those shown in Fig. 6. Although the curves were not identical with those in Fig. 6, the differences were small, and they lead to similar conclusions. The S/N ratios were not greater by a factor of $\sqrt{2}$ as the intensity of the light emerging from the

polarizer was unchanged, *i.e.*, 0.5 mW of light is transmitted by an ideal polarizer oriented at 45°, regardless of polarization ratio. However, in contrast to the use of unpolarized light, as the intensity of x polarized light transmitted by the polarizer decreases for angles greater than 45°, the shot noise limited S/N ratios worsened as compared with the S/N ratios obtained with unpolarized light. For example, with unpolarized light the S/N ratio at an offset angle of 65° is about 6700 for $\varepsilon = 10^{-6}$, but the S/N ratio obtained with polarized light was about 4000. For all values of ε, the optimum offset angle was 45°.

In the $1/f$ noise limit, Scheme 1 again did not appear to be influenced by the polarization properties of the source. All curves were similar to the corresponding curves obtained with unpolarized light, but the optimum offset angles were slightly smaller. The decrease was 0.02° for an ε of 10^{-6}, and approximately 1.36° for an ε of 10^{-2}. However, this is of little practical importance as the S/N ratios would be too small, as seen from Table 2, to permit a useful measurement to be made, if ε is large.

The $1/f$ noise results for Scheme 2, shown in Fig. 9, indicate that close to maximum S/N ratios can indeed be obtained for inferior quality polarizers if they are offset such that the light emerging from the polarizer has x and y polarization components of equal intensity. Thus, the optimum orientation of the polarizer is not 45°, but may vary between a few tens of a millidegree and a few degrees. It can also be seen that a polarizer with $\varepsilon = 10^{-2}$ gives a slightly larger S/N ratio at the optimum angle than does a polarizer with $\varepsilon = 10^{-4}$. This is due to a small difference in the azimuth of the polarized light transmitted by the polarizer. Finer adjustment of the offset angle does allow equal S/N ratios to be obtained. In general, independent of ε, the optimum S/N ratio is very sensitive to small changes in the position of the polarizer, as was the case with the unpolarized light.

All the simulations described in the previous two sections were run with a lower analyte concentration, *i.e.*, the optical rotation measured was lowered to -10×10^{-6} degrees in order to assess the effect of the magnitude of the rotation on the optimum experimental conditions. In all cases involving use of non-ideal polarizers, the magnitude of the rotation had no effect on the optimum arrangement of the optics. However, for Scheme 2, it was found that when the analyte concentration was decreased, the optimum orientation, for the $1/f$ noise limited polarized light case, changed by a few tenths of a millidegree as compared with the optimum offset for a -10×10^{-3} degree rotation. Although this is not a large difference, it does require much greater precision in the positioning of the optics, owing to the sensitivity of the S/N ratio to the offset angle.

Conclusions

It has been shown that the numerical implementation of the optical calculi allows for accurate, quantitative analysis of spectrometric experimental schemes, the theoretical description of which is impeded by the difficulty posed by a rigorous noise analysis. Two simple polarimeters were modelled and analysed to compare and predict their performance under various conditions.

It was found that the first scheme, which employs a crossed pair of polarizers, requires use of very high quality optics if source low frequency noise is the dominant noise source in the experiment. Furthermore, the optimum orientation of the optics is not the crossed position but, depending on the quality of the optics, may vary between a few millidegrees and a few degrees. In the shot noise limit, however, expensive polarizers are not required and inferior quality optics can provide close to the optimum S/N ratio, if positioned correctly. The optimum orientation is with the fast axis of the polarizer at an angle arctan ($\varepsilon^{1/4}$), as given by Kankare and Stephens.[2]

Analysis of Scheme 2, which uses a polarizer and a polarizing prism, showed that this design was superior to the first design because of its partial immunity to source noise, and because it does not require the use of expensive optics, regardless of the dominant noise type. Furthermore, the precision of a measurement limited by source $1/f$ noise was so sensitive to the orientation of the optical components, although not their quality, that even though the optimum conditions may be known or calculated, they may be difficult to achieve experimentally. Thus, despite the ability of this design to allow cancellation of source noise, it is still most likely to be limited by source noise. For shot noise limited measurements, the S/N ratio is largely uninfluenced by the offset angle, relaxing the requirement of precise orientation of the optics. The polarization properties of the light source cannot be ignored as they have a strong influence on the optimum experimental conditions for the $1/f$ noise limited case.

Thus, it can be seen that the precision of the measurement of the optical activity, and the optimum experimental conditions for this measurement, are influenced by many factors such as the design of the instrument, polarization of the light, the quality of the optics, and the dominant type of noise. A fair comparison of the two designs requires consideration of other factors such as analyte circular dichroism, preamplifier noise, effect of ε on calibration function, and so on. The models are easily modified to include these, and many other, effects. All calculations described here were performed using monochromatic light, but the polychromatic version of the optical calculus software will provide the opportunity to perform calculations far more elaborate than those described here.

The authors gratefully acknowledge support of this work by the National Science Foundation through grant No. CHE-9108707. Part of this work was presented at Pittcon '94, Chicago, IL.

References

1 Kliger, D. S., Lewis, J. W., and Randall, C. E., *Polarized Light in Optics and Spectroscopy*, Academic Press, Boston, MA, 1990.
2 Kankare, J. J., and Stephens, R., *Talanta*, 1984, **31**, 689.
3 Voigtman, E., *Anal. Chem.*, 1992, **64**, 2590.
4 Yeung, E. S., Steenhoek, L. E., Woodruff, S. D., and Kuo, J. C., *Anal. Chem.*, 1980, **52**, 1399.
5 Dawson, J. B., King, P. R., Duffield, R. J., and Ellis, D. J., *J. Anal. At. Spectrom.*, 1989, **4**, 245.
6 Voigtman, E., *Anal. Chim. Acta*, 1991, **246**, 9.
7 Voigtman, E., *Appl. Spectrosc.*, 1991, **45**, 890.
8 Kale, U., and Voigtman, E., *Appl. Spectrosc.*, 1992, **46**, 1636.
9 Voigtman, E., *Spectrochim. Acta, Part B*, 1992, **47**, E1549.
10 Voigtman, E., *Anal. Instrum.*, 1993, **21**, 43.
11 Voigtman, E., *Anal. Chim. Acta*, 1993, **283**, 559.
12 Voigtman, E., *Anal. Chem.*, 1993, **65**, 1029A.
13 Yeung, E. S., in *Chemical Analysis*, ed. Yeung, E. S., Wiley-Interscience, New York, 1986, vol. 89, pp. 204–227.
14 Yeung, E. S., *Talanta*, 1985, **32**, 1097.

Paper 4/02871F
Received May 16, 1994
Accepted July 19, 1994

Determination of Levamisole in Animal Tissues Using Liquid Chromatography–Thermospray Mass Spectrometry

A. Cannavan, W. J. Blanchflower and D. G. Kennedy*

Veterinary Sciences Division, Department of Agriculture for Northern Ireland, Stoney Road, Stormont, Belfast, UK BT4 3SD

A method is described for the determination of the anthelmintic levamisole in liver, kidney and muscle using liquid chromatography–thermospray mass spectrometry. Samples are extracted by homogenizing with ethyl acetate, applied to Bakerbond CN solid-phase extraction columns, washed with chloroform–hexane and eluted with methanol. The extracts are evaporated to dryness under nitrogen and the residues are dissolved in mobile phase and injected into the LC–MS system. The positive M + 1 ion at *m/z* 205 is monitored. The detection limit for the assay is 5 ng g^{-1}. Mean recoveries were about 93% for liver, 85% for kidney and 79% for muscle. The assay has been used for statutory testing purposes and for measuring levamisole concentrations in liver, kidney and muscle from sheep dosed with a commercial drench containing levamisole.

Keywords: Levamisole determination; anthelmintic; animal tissue; liquid chromatograph–thermospray mass spectrometry

Introduction

Levamisole [L-(−)-2,3,5,6-tetrahydro-6-phenylimidazo(2,1-*b*)thiazole], the laevorotatory isomer of tetramisole, is an anthelmintic drug widely used for the control of gastrointestinal parasites in cattle, sheep and pigs. It is normally administered as the hydrochloride salt orally or by injection. The maximum residue limit (MRL) permitted in animal products for human consumption, set by the European Union, is 10 ng g^{-1}.[1]

Various methods have been published for the determination of levamisole in milk, biological fluids and meat. Techniques reported include high-performance liquid chromatography (HPLC),[2,3] gas chromatography (GC) with nitrogen–phosphorus detection[4] or mass spectrometric (MS) detection,[5] supercritical fluid chromatography–mass spectrometry,[6] mass-analysed ion kinetic energy spectrometry[7] and on-line high-performance liquid chromatography–gas chromatography–tandem ion-trap mass spectrometry.[8] Of these methods, HPLC, GC and GC–MS have been used recently for determination or confirmation of the drug in meat. Mass spectrometry is the preferred technique for confirmatory residue analyses because of its specificity and it has been shown[9,10] that LC–MS can provide quantitative data for drug residue analyses using relatively simple extraction and clean-up steps. This paper describes the determination of levamisole in animal tissues using LC–MS. The sensitivity compares favourably with those of previously published methods and the method is also simpler and more rapid. The method has been used to measure levamisole levels in liver, kidney and muscle samples submitted for national plan testing and from sheep dosed with a commercial drench containing levamisole.

* To whom correspondence should be addressed.

Experimental

Materials

All solvents were of HPLC grade and other chemicals were of analytical-reagent grade. Levamisole hydrochloride was obtained from Sigma Chemical (Poole, Dorset, UK). A stock standard solution (1 mg ml^{-1}) was prepared in acetonitrile–water (1 + 1 v/v) and was stable for at least 3 months when stored at 4 °C. A dilute standard (1 μg ml^{-1}) was prepared monthly in the LC–MS mobile phase (described below) and stored at 4 °C.

The mobile phase was acetonitrile–tetrahydrofuran–triethylamine–water (350 + 50 + 2 + 598, v/v) containing ammonium acetate (0.1 mol l^{-1}).

Animals

Twelve adult sheep, of approximately 80 kg body mass, were each treated orally with the recommended therapeutic dose (7.5 milligrams of levamisole hydrochloride per kilogram of body mass) of Levacide Worm Drench [Norbrook Laboratories (GB), Bewdley, UK]. The sheep were housed in concrete-floored, indoor pens and fed hay *ad libitum*. Three animals were killed by an overdose of intravenous pentobarbitone sodium at each of four times after dosing (24, 48, 72 and 96 h). Samples of liver, kidney and quadriceps muscle were removed and frozen at −70 °C until analysis.

Equipment

The HPLC system consisted of a Hewlett-Packard (Stockport, UK) Series 1050 LC pump and autosampler and a LiChrospher 60 RP-select B (5 μm) 125 × 4 mm i.d. cartridge and guard column with holders (Merck, Poole, Dorset, UK).

The mass spectrometer was a Hewlett-Packard 5989A MS Engine with a thermospray LC–MS interface and MS Chemstation. The instrument was tuned daily using the data system software autotune program and the HP standard poly(propylene glycol) tuning solution. Positive-ion data were acquired using filament-initiated chemical ionization. The vaporizer probe stem temperature was maintained at 15 °C below the take-off temperature. The mass spectrometer ion source and quadrupole were set to 250 and 100 °C, respectively. The electron multiplier voltage was set to +200 V with respect to the autotune voltage (typically 1800–2000 V). Initially spectra were obtained by scanning from *m/z* 10 to 500 with a scan threshold abundance of 1000. For maximum sensitivity in sample analyses the instrument was operated in

the selected-ion monitoring (SIM) mode with a dwell time of 500 ms and with low mass resolution enabled. Peak-area data were obtained for the ion at *m/z* 205.

Bakerbond spe Cyano (CN) 3 ml disposable extraction columns (J. T. Baker, Phillipsburg, NJ, USA) were conditioned immediately before use with ethyl acetate–hexane (1 + 1 v/v) (5 ml). The solvent level was maintained about 2 mm above the column packing to prevent the material from drying out. The columns were used in conjunction with a Vac-Elut ten-place vacuum manifold fitted with stainless-steel Luer stop-cocks (Varian, Harbour City, CA, USA).

Tissue extraction

Frozen tissue samples were pulverized in a domestic food blender to form a fine powder and stored at −20 °C until analysis. Aliquots (3 g) were weighed into 110 × 30 mm i.d. centrifuge tubes. Fortified samples were prepared at this stage by adding an appropriate amount of dilute standard solution. The spiked samples were allowed to stand for 10 min before extraction. Anhydrous sodium sulfate (2 g), ethyl acetate (9 ml) and potassium hydroxide solution (50% m/v) (0.5 ml) were added and the tissues were homogenized immediately for 1 min using a Silverson homogenizer. The tubes were centrifuged (2000 rev min^{-1}, 10 min) and aliquots (6 ml) of supernatants transferred into clean 110 × 30 mm i.d. tubes. Hexane (6 ml) was added and mixed with the ethyl acetate extracts and the mixtures applied to Bakerbond CN columns. The columns were washed with chloroform–hexane (1 + 1 v/v) (5 ml) and dried by allowing air to pass through under vacuum for 10 min. Levamisole was eluted using two 2 ml portions of methanol. The eluate was collected and evaporated to dryness at 70 °C under nitrogen. The residues were dissolved in the LC mobile phase (200 μl) by sonicating for 5 min.

LC–MS Analysis

The system was allowed to equilibrate by pumping mobile phase through the column at a flow rate of 1 ml min^{-1} for 10 min prior to analysis. Aliquots (50 μl) of dilute standard solution were injected until reproducible peak areas were obtained (normally about three injections). Aliquots (50 μl) of sample extracts were then injected followed by a standard after every three samples. Peak areas for the ion at *m/z* 205 were recorded.

Results and Discussion

The structure of levamisole and its positive-ion thermospray mass spectrum are shown in Fig. 1. The most prominent ion is the molecular ion (M + 1) at *m/z* 205. This is typical of positive-ion LC–MS, with few fragment ions being produced.

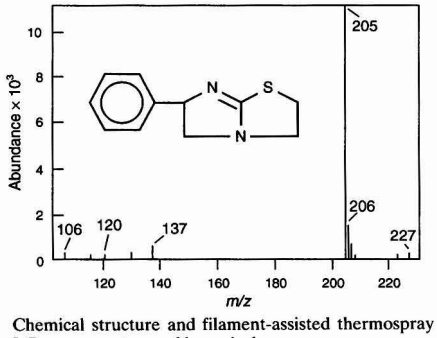

Fig. 1 Chemical structure and filament-assisted thermospray positive-ion LC–mass spectrum of levamisole.

Fig. 2 shows single-ion chromatograms at *m/z* 205 for a levamisole standard, a negative liver extract and an extract of liver containing 34.8 ng g^{-1} of levamisole. At the retention time of the levamisole peak (3.5 min), the chromatograms are clean and free from interferences. Chromatograms for kidney and muscle were similar to those shown for liver.

The linearity of the assay was determined by injecting 50 μl aliquots of a series of standard solutions ranging from 50 to 5000 ng ml^{-1} (equivalent to 5–500 ng g^{-1} in tissue) into the LC–MS system. The linearity over this range was excellent, the linear regression coefficient, *r*, being 0.9999.

The detection limit of the assay, based on a signal-to-noise ratio of 3:1, was estimated to be less than 3 ng g^{-1}. This was checked by analysing four replicates of liver spiked at 5 ng g^{-1} with levamisole. A mean result of 4.1 ng g^{-1} (82% recovery) with a relative standard deviation of 11.3% was obtained. The limit of determination was therefore set at 5 ng g^{-1}.

Reproducibility and recovery values for the assay were determined by analysing five replicates of liver fortified at 25 and 50 ng g^{-1} on each of three days (Table 1). The over-all values for recovery and relative standard deviation were 91 and 7.8%, respectively, for liver fortified with levamisole at

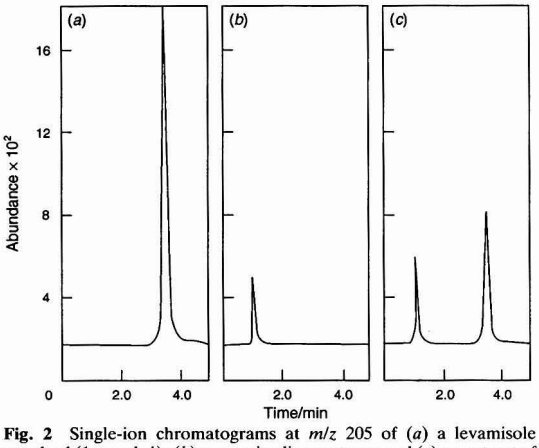

Fig. 2 Single-ion chromatograms at *m/z* 205 of (*a*) a levamisole standard (1 μg ml^{-1}); (*b*) a negative liver extract; and (*c*) an extract of liver containing 34.8 ng g^{-1} of levamisole.

Table 1 Inter- and intra-assay reproducibility and recovery for levamisole in liver

	Day 1	Day 2	Day 3	Over-all
Spiked at 50 ng g^{-1}—				
Mean/ng g^{-1}	44.3	45.7	46.5	45.5
s*/ng g^{-1}	2.54	2.74	5.15	3.53
s_r† (%)	5.7	6.0	11.1	7.8
Mean recovery (%)	88.5	91.4	92.9	91.0
n‡	5	5	5	15
Spiked at 25 ng g^{-1}—				
Mean/ng g^{-1}	22.9	23.4	24.2	23.5
s/ng g^{-1}	3.64	1.99	2.01	2.52
s_r (%)	15.9	8.5	8.3	10.7
Mean recovery (%)	91.6	93.7	96.7	94.0
n	5	5	5	15

* s = Standard deviation.
† s_r = Relative standard deviation.
‡ n = Number of replicates.

50 ng g^{-1} and 94 and 10.7%, respectively, for liver fortified at 25 ng g^{-1}. Recoveries from muscle and kidney were assessed by spiking five replicates of each tissue with levamisole at 50 ng g^{-1} (Table 2). For muscle the mean recovery was 85% with a relative standard deviation of 2.2% and for kidney the mean recovery was 79% with a relative standard deviation of 6.2%.

The reproducibility of the assay was further assessed by analysing an incurred liver sample singly on eight occasions over a period of about 2 months. The tissue was stored at −20 °C between assays. The mean result obtained was 34.2 ng g^{-1} with a relative standard deviation of 1.0%.

Table 2 Recovery and precision of the method for muscle and kidney. Tissues were spiked with levamisole at 50 ng g^{-1}

	Muscle	Kidney
Mean/ng g^{-1}	42.5	39.3
s/ng g^{-1}	0.92	2.46
s_r (%)	2.2	6.2
Mean recovery (%)	84.9	78.7
n	5	5

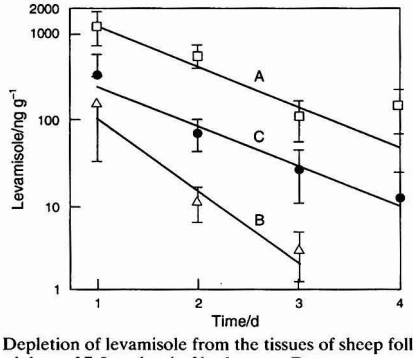

Fig. 3 Depletion of levamisole from the tissues of sheep following a single oral dose of 7.5 mg kg^{-1} of body mass. Data are means ± SEM (n = 3). A, liver; B, muscle; and C, kidney.

The depletion of levamisole from the tissues of dosed sheep is shown in Fig. 3. The half-lives of levamisole in liver, kidney and muscle, with the corresponding correlation coefficients in parentheses, were 0.64 (r = 0.990), 0.65 (r = 0.989) and 0.35 d (r = 0.997), respectively. By extrapolation, liver levamisole concentrations should be below the MRL (10 ng g^{-1}) within 6 d of dosing. Hence, if the withdrawal period for sheep of 14 d is observed, levamisole at concentrations above the MRL should not be detectable.

Conclusions

The method described is rapid, simple, sensitive and specific, providing mass-related data that are desirable in confirmatory residue analyses. The simple extraction and single-step solid-phase clean-up enable a batch of 15 samples to be analysed within one working day. The assay is currently used to fulfil the requirements of the UK National Surveillance Scheme, required under EC Directive 86/469/EEC.[11]

References

1 *European Union Council Regulation 675/92*, 18 March 1992.
2 Osterdahl, B. G., Johnsson, H., and Nordlander, I., *J. Chromatogr.*, 1985, **337**, 151.
3 Wyhowski de Bukanska, B., Degroodt, J. M., and Beernaert, H., *Z. Lebensm.-Unters. Forsch.*, 1991, **193**, 545.
4 Westenborghs, R., Michielsen, L., and Heykatis, J., *J. Chromatogr.*, 1981, **224**, 25.
5 Stout, S. J., DaCunha, A. R., Tondreau, R. E., and Boyd, J. E., *J. Assoc. Off. Anal. Chem.*, 1988, **71**, 1150.
6 Perkins, J. R., Games, D. E., Startin, J. R., and Gilbert, J., *J. Chromatogr.*, 1991, **540**, 257.
7 Maffei Facino, J., and Carini, M., *Biol. Mass. Spectrom.*, 1992, **21**, 195.
8 Chappell, C. G., Creaser, C. S., Stygall, J. W., and Shepherd, M. J., *Biol. Mass Spectrom.*, 1992, **21**, 688.
9 Blanchflower, W. J., *Spectrosc. Int.*, 1990, **4**, 37.
10 Blanchflower, W. J., Cannavan, A., and Kennedy, D. G., *Analyst*, 1994, **119**, 1325.
11 Council Directive of 16 September 1986 on the Determination of Residues in Animals and in Fresh Meat, *Off. J. Eur. Commun.*, No. L 275/36, 1986.

Paper 4/06077/F
Received October 5, 1994
Accepted October 24, 1994

Simultaneous Measurement of Lithium and Boron Isotopes as Lithium Tetraborate Ion by Thermal Ionization Mass Spectrometry

Sarata K. Sahoo and Akimasa Masuda

Department of Chemistry, University of Electro-Communications, 1-5-1 Chofugaoka, Tokyo-182, Japan

A method for the measurement of $Li_2BO_2^+$ ions by thermal ionization mass spectrometry employing a Daly ion-counting system was examined. By solving simultaneous quadratic equations of intensity ratios ranging between *m/z* 55 and 57, and between *m/z* 56 and 57, precise and accurate measurement of lithium and boron isotope ratios can be carried out simultaneously. The intensity ratio between *m/z* 54 and 57 can be used to check the internal consistency of the lithium and boron isotope ratios obtained. The isotopic fractionation rate with the species $Li_2BO_2^+$ was low. Prior to measurement, a two-column ion-exchange process was used to separate lithium from the sample matrix and then to convert LiCl into LiOH, which subsequently reacts with H_3BO_3 to form lithium tetraborate. Lithium and boron isotope ratios were successfully measured simultaneously with precisions (relative standard deviations) of 0.05% for lithium and 0.01% for boron.

Keywords: Lithium; boron; isotopic composition; Daly ion-counting system; thermal ionization mass spectrometry

Introduction

The determination of lithium and boron isotope ratios in natural materials is of interest in geochemical exploration as a guide to hydrothermal alteration. It also has useful applications in the exploration of ore deposits and geothermal reservoirs.[1] Lithium and boron have not only experienced natural variations in their isotopic abundances but have also been subject to extensive mass separation for technological applications. Variations in the isotopic abundance can be traced to a variety of causes including natural mass fractionation, isotopic effects during chemical treatment, isotopic fractionation in the instrument, or due to segregated nuclear reactions. In the last example, the products and depleted parents are prevented from re-entering the general pool of elements for remixing. In addition, lithium and boron are important because of the nuclear spallation effect on both elements and the high lithium content of iron meteorites.

The isotopic composition of lithium has been studied by many workers.[2–11] Reported values show a spread of several per cent. in the isotopic abundance ratio in lithium reagents and natural lithium-bearing minerals. The most precise assays to date involve standardization of reference materials and the atomic mass of lithium. Flesch *et al.*,[3] for example, reported the absolute $^6Li/^7Li$ ratio as 0.0832 ± 0.0002 from a high-purity Li_2CO_3 sample, manufactured by The Lithium Corporation of America, whereas Michiels and de Bievre[4] reported this ratio as 0.08137 ± 0.00034 from a natural lithium sample. Both groups measured the ratio from commercial natural lithium samples using conventional mass spectrometers. Isakov *et al.*[6] reported a range of 6.77–9.28% in mica samples analysed by mass spectrometry. It should be noted that the $^6Li/^7Li$ abundance ratiod can be subject to relatively large natural variations owing to the large mass ratio between 6 and 7. A few researchers have recommended the iodide[2–5] or chloride[7] salts of lithium as filament loading forms. Some have specially designed mass spectrometers suitable only for lithium isotope analysis.[7]

Theoretical and experimental data have shown that the ratio of molecular to atomic species volatilized is a major factor in the fractionation rate, particularly for triple filament sources in which the evaporation and ionization processes are spatially separated.[8] The large relative mass difference between the two lithium isotopes, because of the low atomic mass, makes the control of isotope fractionation particularly difficult in the precise isotopic analysis of lithium. Several thermal ionization mass spectrometric methods have been developed using both single and multiple filament techniques. In order to obtain reproducible results, the volatilization rate of each atomic and molecular species must be constant or controllable during the analysis and reproducible from one loading to the next. However, it is difficult to determine the volatilization rates in thermal ionization mass spectrometry because neutral species are not detectable. One approach for circumventing this difficulty is to use a molecular species that greatly reduces the fraction of lithium vaporized as atomic Li^+ ions or neutral atomic or low molecular mass species and the extent of isotopic fractionation during the measurement.

In a triple filament procedure, LiI has been used[2–5] as the loading material and its high molecular mass reduced the fractionation factor. Similarly, another triple filament procedure for the isotopic analysis of lithium is based on the measurement of the Li_2F^+ ion with a precision of 0.2%.[8] Lithium fluoride is one of the most stable compounds of lithium. More recently, lithium isotope ratios have been measured, with lithium loaded as the tetraborate ($Li_2BO_2^+$), by using both single[9] and double filament procedures.[10] The measurement of $Li_2BO_2^+$ reduces isotopic fractionation for the single filament procedure and a precision (relative standard deviation) of 0.13% was achieved. Chan[9] observed a peak at mass 55, but an accurate measurement of masses 54 and 55 was not possible. In the double filament procedure, with lithium loaded as $Li_2B_4O_7$, the measurement of the Li^+ ion was achieved with a precision better than 0.1%. When adjusting the conditions of filament assembly and geometry, it is possible to obtain Li^+ ions stronger than $Li_2BO_2^+$ ions. However, such a problem is beyond the scope of this paper.

Refined thermal ionization mass spectrometry and ultra-clean chemical separation techniques have been the primary focus of our efforts to analyse lithium isotopes. Previous work using similar techniques facilitated the measurement at mass 55 but could not measure mass 54 using a multicollector system.[11] In this paper, we describe clean separation techniques prior to improved mass spectrometric analysis. A Daly ion-counting system was used, which allows measurement of the four possible nuclear isotopic species of $Li_2BO_2^+$ at masses 54, 55, 56 and 57, in addition to small efficient loadings on the

filament and stable ionization efficiencies at reduced temperatures.

Experimental

Instrument and Apparatus

A VG (VG Isotech, Cheshire, UK) Sector 54-30 thermal ionization mass spectrometer equipped with a Daly ion-counting system was used. The detection system was linear and accurate to 0.04% under the conditions used here. Ion count rates were corrected by using background correction. The counting time used for an isotopic species was 5 s for masses 54, 55, 56 and 57. Each redundant piece of data consists of the average of seven ratio measurement sets while the final ratio is the mean of 15 data sets.

Reagents and Materials

A cation-exchange column was prepared by packing a 2 cm i.d. Pyrex column with AG 50W-X8 (200–400 mesh) resin (Bio-Rad Laboratories, Richmond, CA, USA) to a height of 8 cm. The resin was pre-cleaned by soaking in 6 mol dm^{-3} HCl and washed with distilled water prior to packing into a column. The resin in the column was converted into the H^+ form by passing 10 cm^3 of 1 mol dm^{-3} HCl through it, followed by washing with distilled water until the washings were free from chloride.

An anion-exchange column was prepared by packing a similar column to a height of 6 cm with AG 1-X8 (200–400 mesh) resin (Bio-Rad Laboratories). The resin was pre-cleaned by soaking in 6 mol dm^{-3} HNO_3 and washing with distilled water prior to packing into a column. The exchanger was converted into the OH^- form by repeated washing with 1 mol dm^{-3} NaOH (Suprapur grade; Merck, Darmstadt, Germany). As this column was used for the conversion of LiCl into LiOH, extra care was taken to prevent contamination.

Ultrapure HCl and HNO_3, purchased from Wako Pure Chemical Industries (Osaka, Japan), were further purified by carrying out up to three sub-boiling distillations. Aqueous solutions were prepared from distilled water from a Milli-Q water purification system (with a resistivity of 18 MΩ cm).

A lithium isotopic standard [National Institute of Standards and Technology (NIST) L-SVEC lithium carbonate] and a boron isotopic standard [NIST Standard Reference Material (SRM) 951 boric acid] were used for the synthesis of $Li_2B_4O_7$.

Table 1 Possible nuclide combination species of the $Li_2BO_2^+$ molecular ion

Mass number	Species
54	$(^6Li)_2\ ^{10}B\ (^{16}O)_2$
55	$^6Li\ ^7Li\ ^{10}B\ (^{16}O)_2$ $(^6Li)_2\ ^{10}B\ (^{16}O)\ (^{17}O)$ $(^6Li)_2\ ^{11}B\ (^{16}O)_2$
56	$(^7Li)_2\ ^{10}B\ (^{16}O)_2$ $^6Li\ ^7Li\ ^{11}B\ (^{16}O)_2$ $(^6Li)_2\ ^{11}B\ ^{16}O\ ^{17}O$ $(^6Li)_2\ ^{10}B\ (^{17}O)_2$ $^6Li\ ^7Li\ ^{10}B\ ^{16}O\ ^{17}O$ $(^6Li)_2\ ^{10}B\ ^{16}O\ ^{18}O$
57	$(^7Li)_2\ ^{11}B\ (^{16}O)_2$ $^6Li\ ^7Li\ ^{10}B\ ^{16}O\ ^{18}O$ $(^6Li)_2\ ^{11}B\ ^{16}O\ ^{18}O$ $(^7Li)_2\ ^{10}B\ ^{16}O\ ^{17}O$ $(^6Li)_2\ ^{11}B\ (^{17}O)_2$ $(^6Li)_2\ ^{10}B\ ^{17}O\ ^{18}O$ $^6Li\ ^7Li\ ^{11}B\ ^{16}O\ ^{17}O$ $^6Li\ ^7Li\ ^{10}B\ (^{17}O)_2$

In all the experiments lithium was separated from a mixture by cation-exchange chromatography. For the standards, a cation-exchange column was not necessary. In order to check the effect of the cation-exchange column on lithium isotope composition, both cation- and anion-exchange columns were employed. A solution containing lithium was passed through the cation-exchange column to separate any other cations present in the solution. Lithium was eluted from the column using 0.5 mol dm^{-3} HCl. The column was then washed with Milli-Q water to ensure that lithium was not retained on the column. The eluate was preconcentrated to a small volume in a Teflon beaker by evaporation almost to dryness at a low temperature. The main aim was to convert the LiCl solution into LiOH for the synthesis of $Li_2B_4O_7$. Therefore, this step helped to reduce the amount of chloride loaded onto the anion-exchange column. Subsequently, the LiCl solution was passed through the anion-exchange column, which had been preconditioned with 1 mol dm^{-3} NaOH, thus converting LiCl into LiOH. Lithium carbonate can be used for the synthesis of $Li_2B_4O_7$. However, LiOH was found to be the best choice for the synthesis of $Li_2B_4O_7$ in this work.

Instrumental Procedure

Prior to sample loading, zone-refined rhenium ribbon (ESPI Marz Grade, 99.996%) filaments were de-gassed at 4.0 A in an evacuated chamber ($<1.0 \times 10^{-6}$ Torr; 1 Torr ≡ 133.322 Pa) for 1 h.

In the single filament procedure, 0.5 μg of lithium (as LiOH) and 1 μl of 1 mg g^{-1} H_3BO_3 were found to be the optimum values. The mass ratio of LiOH to H_3BO_3 taken is nearly stoichiometric in relation to $Li_2B_4O_7$. A 1 μl volume of 1 mg g^{-1} H_3BO_3 was taken and deposited onto the rhenium filament using a micropipette. The droplets were dried at a current of 0.8 A. After evaporation of H_3BO_3 to dryness, 0.5 μg of lithium (as LiOH) was loaded onto the same filament. The LiOH sample solution was dried with a current of 0.8 A passing through the filament. The filament was further heated for 10 s at 1.8 A, and held for 5 min at 0.8 A before introduction into the mass spectrometer.

Mass spectrometric analysis was started when the ion-gauge pressure in the instrument reached 1.0×10^{-8}–2.0×10^{-8} Torr. Liquid nitrogen was added to the cold finger over the source. An accelerating voltage of 8 kV was used. In this procedure, $Li_2BO_2^+$ ions were thermally ionized from $Li_2B_4O_7$ on the same filament and monitored at masses 54, 55, 56 and 57. After ensuring that the instrumental calibration between magnetic field strength and atomic mass scale was stable, the sample was slowly heated and de-gassed under vacuum using a filament current of 0.7 A for 3 h. The filament current was then increased very slowly until a $Li_2BO_2^+$ signal started to appear. Once the $Li_2BO_2^+$ ion signals appeared, the system was allowed to stabilize until the signal ceased to increase with time. Generally, the signal from a 0.5 μg load of lithium increases from approximately 120 000–150 000 counts s^{-1} to 250 000–300 000 counts s^{-1} by the end of a run (after 2 h). The baseline was determined at the beginning of a set of measurements. Typical baseline count rates varied from 0 to 8 counts s^{-1} at mass 55.5. The target intensity was focused at $<2.0 \times 10^{-13}$ A for measurement. The selection of ion beams was made by varying the magnetic field, and the ion beams were focused on masses 54, 55, 56 and 57. Data acquisition was started after stable emission and at a desired signal strength ($\approx 2.0 \times 10^{-12}$ A) using an ion-counting pulse system. After the completion of each set comprising a pre-set number (7) of measurements, the instrument measures the baseline after beam focusing and peak centring. The computer automatically adjusts the filament current to maintain a smooth increase in the ion current. The integration time was

5 s, whereas the magnetic settlement time was 2 s. Typically, 100–150 ratios were obtained during a sample run with the ion current increasing from 2.9×10^{-12} to 4.3×10^{-12} A. Results were discarded if they consisted of less than 70 reproducible ratios.

Results and Discussion

Determination of $^6Li/^7Li$ Ratio

The relative ion intensity measurement is made for the molecular ion of $Li_2BO_2^+$ produced from $Li_2B_4O_7$. Considering the isotopic abundances of the constituent elements, *e.g.*, lithium, boron and oxygen, 36 isotopically distinct Li_2BO_2 molecules having mass numbers ranging from 54 to 61 are obtained. The possible species with nuclide combinations corresponding to $Li_2BO_2^+$ ions of masses 54–57 are given in Table 1. Theoretical ion intensity ratios and abundances of Li_2BO_2 molecules are summarized in Tables 2 and 3.

Even if the contributions of the isotopes ^{17}O and ^{18}O are ignored, this does not have a significant effect on the results of the calculations. In order to maintain mathematical exactness, however, the contributions of these trace oxygen isotopes to the 'isobaric' molecular ions are quantitatively taken into account in the present calculations. Specifically, the ion with mass number 54 contains exclusively two ^{16}O atoms. It is self-evident that $Li_2BO_2^+$ ions involving two ^{16}O atoms are the 'dominant' species for ions with mass numbers 55, 56 and 57. Isobaric contributions of molecular ions involving ^{17}O and/or ^{18}O to the bulk intensities (I' s) are calculated as 0.002, 0.010 and 0.050%, corresponding to mass numbers 55, 56 and 57, respectively. Hence the following equations for the measured ion intensity ratios for $I_{54/57}$, $I_{55/57}$ and $I_{56/57}$ should hold:

$$\frac{I_{54}}{I_{57}} \times 1.00050 = \frac{(^6Li)_2\,{}^{10}B\,(^{16}O)_2}{(^7Li)_2\,{}^{11}B\,(^{16}O)_2} = \frac{(^6Li)_2}{(^7Li)_2} \times \frac{^{10}B}{^{11}B} = X^2Y \quad (1)$$

$$\frac{I_{55}}{I_{57}} \times 1.00047 = \frac{2 \times {}^6Li\,{}^7Li\,{}^{10}B\,(^{16}O)_2}{(^7Li)_2\,{}^{11}B\,(^{16}O)_2} + \frac{(^6Li)_2\,{}^{11}B\,(^{16}O)_2}{(^7Li)_2\,{}^{11}B\,(^{16}O)_2} = 2XY + X^2 = X(X + 2Y) \quad (2)$$

$$\frac{I_{56}}{I_{57}} \times 1.00040 = \frac{2 \times {}^6Li\,{}^7Li\,{}^{11}B\,(^{16}O)_2}{(^7Li)_2\,{}^{11}B\,(^{16}O)_2} + \frac{(^7Li)_2\,{}^{10}B\,(^{16}O)_2}{(^7Li)_2\,{}^{11}B\,(^{16}O)_2} = 2X + Y \quad (3)$$

where $X = {}^6Li/{}^7Li$ and $Y = {}^{10}B/{}^{11}B$.

Chan[9] has calculated X ($^6Li/^7Li$) by substituting the known value of Y ($^{10}B/^{11}B$) using eqn. (3).

As with measurements obtained by other methods, the solution obtained here can reflect the effect of fractionation. The potentially unique advantage of the proposed method is that it can provide an approach for investigating the relationship between the simultaneous effects of '*in situ*' fractionation of boron and lithium isotopes. Therefore, we have solved simultaneous quadratic equations to determine the isotopic composition of lithium and boron in the Li_2BO_2 molecular ion. Taking into consideration eqns. (2) and (3) as a set of simultaneous equations, we obtain

$$X^2 + 2XY = \alpha \quad (4)$$

and

$$2X + Y = \beta \quad (5)$$

where α and β are the product of the measured intensity ratios and the isobaric correction factors.

Mathematically, the simultaneous quadratic equations give two values. Needless to say, one of them has no physical meaning.
Therefore,

$$X = \frac{2\beta - (4\beta^2 - 4 \times 3 \times \alpha)^{1/2}}{2 \times 3} \quad (6)$$

Once X has been calculated, Y can be calculated using eqn. (3). From these values, eqn. (1) can be checked and compared with the measured value. This provides a verification of the extent of isotope fractionation.

In order to test the precision and accuracy of the thermal ionization mass spectrometric method used in this work, measurements of $Li_2BO_2^+$ ions at masses 54, 55, 56 and 57 were carried out individually using ten filaments. Each filament was loaded with 0.5 μg of NIST L-SVEC lithium carbonate and the results are presented in Table 4. Applying eqns. (2) and (3), the averages of the intensity ratios shown in Table 4 yield $X = 0.082289$ and $Y = 0.24779$.

Different methods for loading the lithium samples onto the filament were attempted. For example, LiCl and $LiNO_3$ samples were mixed with H_3BO_3, but the results were not satisfactory. However, a mixture of LiOH and H_3BO_3 produced the most stable isotope ratio measurements for lithium. In general, LiOH reacts chemically with H_3BO_3 to

Table 2 Abundance ratios of $Li_2BO_2^+$

Theoretical ratio	Abundance ratio
54/57	0.00163
55/57	0.04684
56/57	0.41044
58/57	0.00241
59/57	0.00401
60/57	0.000003
61/57	0.000004

Table 3 Mathematically calculated mass spectrum distribution abundances of the Li_2BO_2 molecule

Mass number	Abundance (%)
54	0.11141
55	3.19650
56	28.00990
57	68.24387
58	0.16427
59	0.27356
60	0.00022
61	0.00027

Table 4 Measured isotope ratios of NIST L-SVEC Li_2CO_3 as the $Li_2BO_2^+$ ion

No.	54/57	55/57	56/57
1	0.00167	0.04748	0.41203
2	0.00167	0.04753	0.41219
3	0.00167	0.04752	0.41221
4	0.00167	0.04751	0.41212
5	0.00168	0.04754	0.41225
6	0.00168	0.04756	0.41233
7	0.00167	0.04753	0.41220
8	0.00168	0.04755	0.41224
9	0.00167	0.04751	0.41217
10	0.00168	0.04757	0.41229
Average	0.001674	0.04753	0.41220
s^*	0.000005	0.000026	0.000085
$s_r^\dagger$ (%)	0.31	0.021	0.050

* s = Standard deviation.
† s_r = Relative standard deviation.

form $Li_2B_4O_7$. Therefore, H_3BO_3 followed by LiOH was loaded directly onto the filament to form $Li_2B_4O_7$, the most stable loading form, which produces a strong $Li_2BO_2^+$ signal. This permits lithium isotope ratio measurements to be made with high precision.

According to our experiments, the recommended B/Li atomic ratio for stable and precise lithium isotope ratio measurements ranges from 2 to 2.5, corresponding to, or higher than, the stoichiometric B/Li ratio.

The ionization filament temperature is a crucial parameter which governs the rate of fractionation. This has been demonstrated by most researchers in this field. At optimum sample vaporization temperatures, lithium evaporates primarily as molecular species containing boron. In our studies, it was observed that the fractionation was higher at temperatures above 850 °C.

In order to check the blank before sample loading, a de-gassed filament was loaded with H_3BO_3 only, and without any lithium sample. It did not produce any detectable $Li_2BO_2^+$ ion signals under the conditions used for lithium isotope ratio measurements. This verified that there was no background from the filament material under these conditions.

The analysis was, therefore, carried out with a low signal intensity at low temperature to reduce fractionation, and the isotope ratio measured as a function of time showed negligible variations. For precise measurement of lithium isotope ratios, the amount of sample and control of the filament temperature are important factors to be considered.

As mentioned above, we observed ratios of 0.082289 ± 0.000043 and 0.24779 ± 0.00032 for $^6Li/^7Li$ (X) and $^{10}B/^{11}B$ (Y), respectively. The isotopic ratio obtained ($^{10}B/^{11}B$ = 0.24779) agrees well with the certified value ($^{10}B/^{11}B = 0.2473 \pm 0.0002$).[12] It would be significant to calculate X^2Y from the values obtained for X and Y from eqns. (2) and (3), because, as mathematically derived above [eqn. (1)], X^2Y corresponds to I_{54}/I_{57} multiplied by the correction factor. Evaluation based on $X = 0.082289$ and $Y = 0.24779$ gives $X^2Y = 0.001678$, while the observed mean value for the corrected I_{54}/I_{57} ratio is 0.001675, which is in good agreement with the calculated value for X^2Y within the experimental uncertainty. The uncertainty of ± 0.02% for α results in uncertainties of ± 0.076, ± 0.18 and ± 0.048% for X, Y and X^2Y, respectively. In turn, the uncertainty of ± 0.02% for β results in uncertainties of ± 0.01, ± 0.13 and ± 0.17% for X, Y and X^2Y, respectively. This suggests that the degree of isotopic fractionation during the measurements was negligible. Further, it endorses the high linearity of the Daly ion-counting system for intensity ratio magnitudes of 10^5–10^6 and the high dependability and internal consistency of the X and Y values obtained.

The same method was applied to high-purity Sumitomo Li_2CO_3 samples. Results of these analyses are given in Table 5. Taking the correction factor into consideration, we found $X = 0.082415$ and $Y = 0.24775$. The results are similar and the isotope ratio of boron is identical. The Sumitomo sample was similar to the standard lithium sample, and the same H_3BO_3 was used in both instances. The results obtained in this work were compared with those obtained by other workers, and are summarized in Tables 6 and 7. The proposed method is reproducible and has an analytical precision (relative standard deviation) of 0.05% for lithium and 0.01% for boron.

Table 5 Analytical reproducibility for the Sumitomo Li_2CO_3 sample

	54/57	55/57	56/57	$^6Li/^7Li$	$^{10}B/^{11}B$
	0.00168	0.04761	0.41242	0.08243	0.24754
	0.00168	0.04762	0.41244	0.08245	0.24752
	0.00167	0.04759	0.41238	0.08239	0.24758
Average	0.00167	0.047606	0.41241	0.08242	0.24755
s*	0.000005	0.000015	0.00003	0.000031	0.000031
s_r† (%)	0.34	0.032	0.007	0.037	0.012

* s = Standard deviation.
† s_r = Relative standard deviation.

Conclusions

This study demonstrates that precise measurement of the isotope ratios of lithium and boron can be carried out by using a thermal ionization mass spectrometer equipped with a Daly ion-counting detection system. The sample loading procedure, purity of chemical form and control of the filament temperature are the salient features in achieving precise measurement of ratios. In order to apply this technique to the measurement of samples, it is essential to achieve quantitative recovery and clean separation of lithium from other inorganic ions during the separation process. In order to apply the technique to the precise measurement of boron isotope ratios, the boron in the sample should preferably be in the form of

Table 6 Comparison of lithium isotopic composition of NIST L-SVEC standard

Researcher	Measured ion	Loaded as (chemical) form	$^6Li/^7Li$ ratio (X)	Reference
Flesch *et al.*	Li^+	LiI	0.0832 ± 0.00033	3
Chan	$Li_2BO_2^+$	$Li_2B_4O_7$	0.08282 ± 0.0001	9
Lamberty *et al.*	Li^+	LiI	0.08214 ± 0.00009	5
Green *et al.*	Li^+	LiF	0.08201 ± 0.00013	8
Xiao and Beary	Li^+	$Li_2B_4O_7$	0.082212 ± 0.000019	10
Sahoo and Masuda	$Li_2BO_2^+$	$Li_2B_4O_7$	0.082289 ± 0.000043	This work

Table 7 Comparison of boron isotopic composition of NIST SRM 951 boric acid

Researcher	Measured ion	Loaded as (chemical) form	$^{10}B/^{11}B$ (Y)	Reference
Spivack and Edmond	$Cs_2BO_2^+$	$Cs_2B_4O_7$	0.24718 ± 0.00024	13
Xiao *et al.*	$Cs_2BO_2^+$	$Cs_2B_4O_7$	0.24689 ± 0.00011	14
Nakamura *et al.*	$Cs_2BO_2^+$	$Cs_2B_4O_7$	0.24684 ± 0.00035	15
Zeininger and Heumann	BO_2^-	$H_3BO_3 + La(NO_3)_3$	0.2489 ± 0.0002	16
Sahoo and Masuda	$Li_2BO_2^+$	$Li_2B_4O_7$	0.24779 ± 0.00032	This work

either borate or H_3BO_3. The $Li_2BO_2^+$ ion beam technique described here for the isotopic analysis of lithium and boron can be applied to samples of either element of whatever origin. One advantage of the technique is that no isotope standard is required.

The authors thank Dr. H. Tominaga, NMK, for helpful suggestions concerning the theoretical aspects of the work. Financial support by the NMK and experimental discussions with Drs. Qi-Lu and M. B. Shabani are gratefully acknowledged. Dr. E. Opare-Addo is also thanked for critical review of the manuscript.

References

1 Divis, A. F., and Clark, J. R., *Geochemical Exploration 1978: Proceedings of the Seventh International Geochemical Exploration Symposium, Golden, Colorado*, The Association of Exploration Geochemists, Rexdale, Ontario, 1978, p. 273.
2 Svec, H. J., and Anderson, A. R., Jr., *Geochim. Cosmochim. Acta*, 1965, **29**, 633.
3 Flesch, G. D., Anderson, A. R., Jr., and Svec, H. J., *Int. J. Mass Spectrom. Ion Phys.*, 1973, **12**, 265.
4 Michiels, E., and de Bievre, P., *Int. J. Mass Spectrom. Ion Phys.*, 1983, **49**, 265.
5 Lamberty, A., Michiels, E., and de Bievre, P., *Int. J. Mass Spectrom. Ion Processes*, 1987, **79**, 311.
6 Isakov, Y. A., Plyusin, G. S., and Brandt, S. D., *Geochem. Int.*, 1969, **6**, 598.
7 Brown, H. L., Biltz, C., and Anbar, M., *Int. J. Mass Spectrom. Ion Phys.*, 1977, **25**, 167.
8 Green, L. W., Leppinen, J. J., and Elliot, N. L., *Anal. Chem.*, 1988, **60**, 34.
9 Chan, L. H., *Anal. Chem.*, 1987, **59**, 2662.
10 Xiao, Y. K., and Beary, E. S., *Int. J. Mass Spectrom. Ion Processes*, 1989, **94**, 101.
11 Datta, B. P., Khodade, P. S., Parab, A. R., Goyal, A. H., Chitambar, S. A., and Jain, H. C., *Int. J. Mass Spectrom. Ion Processes*, 1992, **116**, 87.
12 Lamberty, A., and de Bievre, P., *Int. J. Mass Spectrom. Ion Processes*, 1991, **108**, 189.
13 Spivack, A. J., and Edmond, J. M., *Anal. Chem.*, 1986, **58**, 31.
14 Xiao, Y. K., Beary, E. S., and Fassett, J. D., *Int. J. Mass Spectrom. Ion Processes*, 1988, **85**, 203.
15 Nakamura, E., Ishikawa, T., Birck, J. L., and Allegre, C. J., *Chem. Geol.*, 1992, **94**, 193.
16 Zeininger, H., and Heumann, K. G., *Int. J. Mass Spectrom. Ion Phys.*, 1983, **48**, 377.

Paper 4/04089I
Received July 5, 1994
Accepted September 22, 1994

Investigations Into the use of Inductively Coupled Plasma Mass Spectrometry for the Determination of Gold in Plant Materials

Carl A. Williams, Fadi R. Abou-Shakra and Neil I. Ward

ICP-MS Facility, Chemistry Department, University of Surrey, Guildford, Surrey, UK GU2 5XH

The measurement of gold in plant materials using inductively coupled plasma mass spectrometry is assessed in terms of instrument conditions and methodology problems encountered with the type of digestion method used. Factors including the nebulizer flow rate, forward power and selection of internal standard were optimized for maximum sensitivity and signal stability. Furthermore, different digestion procedures were compared for their recovery and reproducibility. Indigenous plants collected from the vicinity of a mine were analysed for their gold content. Levels of gold in the plant materials ranging from 5 to 7450 ng g^{-1} (dry mass) were noted with an instrumental detection limit of 0.04 ng ml^{-1}. The data obtained provide an indication of the concentration and dispersal of gold within the surficial environment of the mine and surrounding area.

Keywords: *Inductively coupled plasma mass spectrometry; gold; plant material; digestion*

Introduction

The use of plants in prospecting for gold is a well established technique of geochemical research.[1] Reported levels from non-mineralized areas show typical values around 0.005 μg g^{-1} ashed mass (ash m).[2] However, levels as high as 125 μg g^{-1} (ash m) have been reported for plants collected from mineralized regions.[3] The main analytical techniques used for analysis have been instrumental neutron activation analysis (INAA), electrothermal vaporization atomic absorption spectrometry (ETAAS) and inductively coupled plasma mass spectrometry (ICP-MS). Table 1 shows a listing of the work carried out on gold determination in plant materials using the aforementioned techniques.

Table 1 Reported gold levels from background and mineralized locations using various analytical techniques

	Au content/ng g^{-1}		
Material	Ash*	Dry†	Analytical technique
Plant[1]	—	1–8	INAA
Douglas Fir[4]	290	—	INAA
Twigs[5]	10–20	—	INAA
Bark (Spruce)[5]	5–15	—	INAA
Bark (Pine)[6]	10–20	—	INAA
Leaves[6]	8–18	—	INAA
Leaves[7]	20	—	INAA
Plant[8]	—	50	AAS
Plant[9]	180–1038	—	ETV-AAS
Plant[10]	—	100	ETV-AAS
Twigs[11]	570	—	ICP-MS
Tree bark[12]	340	—	ICP-MS
Humus[13]	—	16 200	ICP-MS

* Ashed mass basis.
† Dry mass basis.

The major advantage of INAA is that the technique is non-destructive and subsequently no sample dissolution is required. Typical detection limits[14] of INAA are in the range 2–5 ng g^{-1}. A more sensitive technique for the analysis of gold is ETAAS with typical detection limits[15] of 0.4 ng ml^{-1}. However, for measurements on plant materials, the major disadvantage of ETAAS is the need for sample dissolution prior to analysis. Furthermore, non-spectroscopic matrix interferences have been observed when large amounts of iron, copper and/or calcium are present in the sample.

Since its development in the early 1980s, ICP-MS has emerged as a front runner for trace elemental and isotopic analysis. The technique is fast and sensitive, with reported detection limits for gold[11] of the order of 0.5 ng ml^{-1}. However, for the analysis of gold in plant materials, the disadvantage of sample dissolution also applies.

The most popular chemical treatment for the dissolution of gold utilizes *aqua regia* or $HBr–Br_2$, followed by extraction into isobutyl methyl ketone (IBMK). The latter step is necessary to separate the large levels of silica normally encountered in plant materials. However, the use of organic materials significantly impairs the performance of the ICP-MS, causing instabilities in the plasma and blockage of the orifices of the sampler and skimmer cones through carbon build up. Therefore other dissolution steps based on the use of hydrofluoric acid (HF) have been investigated. Hydrofluoric acid is well known for its ability to dissolve silicate-containing materials where the silica is lost from the matrix as volatile SiF_4.

In this study, two different digestion procedures are described and compared. In addition, the analytical problems encountered during the analysis of gold by ICP-MS are discussed and recommendations made.

Experimental

Chemicals

Aqua regia acid solutions were prepared by mixing 1 part Aristar 69% HNO_3 and 3 parts AnalaR 72% HCl and diluting to the necessary final concentration with doubly distilled, de-ionized water (resistivity of 18 MΩ cm). Dissolution was then carried out using AnalaR 48% HF. Elemental standards were prepared by diluting various volumes of 1000 μg ml^{-1} standard solutions with doubly distilled, de-ionized water. The tellurium solution was prepared from 1000 μg ml^{-1} telluric acid solution and $SnCl_2$ solution was prepared from a stock of AnalaR stannous chloride. All the chemicals were from Merck (Poole, Dorset, UK).

Instrumentation

ICP-MS determinations were carried out on a Finnigan-MAT SOLA ICP-MS (Finnigan-MAT, Hemel Hempstead, England). A summary of the instrumental and operational parameters is shown in Table 2.

Method

The study falls into two parts. Firstly, synthetic gold solutions were used to optimize the performance of the instrument. Secondly, different digestion procedures were investigated and applied to plant materials collected from various sampling sites around an operating gold mine, prior to analysis by ICP-MS.

ICP-MS Analysis of Gold in Synthetic Solutions

Optimization of the gold signal

A 100 ng ml^{-1} gold solution in 5% *aqua regia* was prepared and introduced into the ICP-MS. The effect of varying the forward power and nebulizer flow rate on the gold signal was evaluated to determine the optimum conditions. The forward power was varied between 1.1–1.5 kW, and for each of these settings the nebulizer flow rate was varied between 0.72–1.12 l min^{-1}. The ion peak intensity for Au was corrected for the background at mass 198.

Internal standardization

In the analysis of biological samples by ICP-MS, it is common practice to employ an internal standard. A review of the literature shows that indium has been extensively utilized as an internal standard for the analysis of a variety of elements including gold in different materials. Therefore, the suitability of indium as an internal standard for gold analysis was investigated. A 5% *aqua regia* solution containing 100 ng ml^{-1} of gold and indium was employed to observe the behaviour of the Au : In signal ratios over a time period of 10 h. The same approach was then adopted for iridium, platinum and bismuth.

Memory effects in ICP-MS

An evaluation of possible gold memory effects caused by reverse adsorption of the sample solution onto the ICP-MS uptake tubing was undertaken. Initially a 100 ng ml^{-1} gold solution was introduced for 10 min. This solution was then washed through with either doubly distilled, de-ionized water, or 1% HNO_3, until the signal returned to background. In both these cases *aqua regia* was then passed through the tubing and the gold signal monitored. The experiment was carried out for varying strengths of *aqua regia*, namely, 1, 5 and 8%.

Table 2 Finnigan-MAT SOLA ICP-MS instrument and operating conditions

Instrument	Finnigan-MAT SOLA
RF forward power	Varied
RF reflected power	<5 W
Spray chamber	Scott double pass
Nebulizer	Spetec V-groove
Solution uptake	Gilson minipuls (2 ml min^{-1})
Operating conditions	
Argon flow rates/l min^{-1}	
Nebulizer	Varied
Intermediate	0.4
Coolant	15

Detection limits

A solution of 100 ng ml^{-1} of gold in 5% *aqua regia* was prepared together with a blank of the same acid solution. Using ICP-MS, six separate analyses for each solution were recorded, with each of these analyses representing three individual readings.

ICP-MS Analysis of Gold in Plant Materials

Digestion procedures

The aim of this experiment was to investigate potential digestion procedures for the analysis of gold in plant materials. Essentially such procedures consist of an ashing and a dissolution stage. Two methods of dissolution were tested for their recovery and reproducibility.

Bulk plant material was prepared by mixing a cross-section of several bryophyte species, crushing them and homogenizing the mixture using a commercial food processor. Aliquots (10 g) of this bulk material were removed and dry ashed at 200 °C for 2 h in a muffle furnace (Gallenkamp, Loughborough, UK). The temperature in the muffle furnace was then raised to 450 °C and held at this level for 24 h. The ashed aliquots (approximately 1 g) were then homogenized, weighed and subjected to one of the two wet-digestion procedures.

Procedure 1. To the ashed material, 15 ml of *aqua regia* and 5 ml of 48% HF were added and the resulting solution was heated at 200 °C to incipient dryness. *Aqua regia* (10 ml) was added and the solution was heated for 1 h at 80 °C. The samples were centrifuged (at 4500 rpm for 5 min), the supernatant was decanted and evaporated to incipient dryness, and the remaining sample discarded. Concentrated (12 mol l^{-1}) HCl (5 ml) was then added, the contents warmed and 45 ml of water added. Subsequently, 5 ml of Te solution (prepared by dissolving 1 ml of 1000 μg ml^{-1} Te standard solution in 10 ml of 1.2 mol l^{-1} HCl) and 5 ml of $SnCl_2$ solution (prepared by weighing 20 g of $SnCl_2 \cdot 2H_2O$, adding 17 ml of 12 mol l^{-1} HCl and diluting to 100 ml with water) were added, in order to precipitate the Au onto Te. The contents were heated to near boiling. A further 2 ml of $SnCl_2$ solution was added to ensure complete reduction and the solution heated for 20 min. The sample was filtered through a 0.45 μm type HAWP filter paper (Millipore, Watford, UK), washing with 1 mol l^{-1} HCl. The filter paper and precipitate were placed in a glass beaker and 5 ml of *aqua regia* added. The contents were evaporated to about 0.75 ml and diluted to 10 ml with a solution which was 0.2% in HNO_3 and 0.02% in HCl (see Fig. 1).

Procedure 2. To the ashed material, 15 ml of *aqua regia* and 5 ml of 48% HF were added, and the contents evaporated to incipient dryness. *Aqua regia* (5%, 10 ml) was then added, the samples centrifuged (at 4500 rpm for 5 min) and the supernatant decanted and the remaining sample discarded. From each sample 1 ml of the solution was pipetted and diluted to 10 ml with 5% *aqua regia* (see Fig. 1).

Recovery and reproducibility tests were carried out on the two procedures by spiking a piece of filter paper (<0.01 g) with 10 μl of 10 μg ml^{-1} gold solution and adding this to the dry material prior to ashing. Ten aliquots were prepared for each procedure and analysed.

Analysis of bryophyte material collected from a gold mining area

As an application of the methodologies developed in this study, plant materials were collected from four sample locations around an operating gold mine, namely, the mine open pit, treatment plant, tailings pond and background area.

Investigations into the gold content of the samples removed from these sites should give an indication of the extent of the environmental impact of the mining operations on the gold content of the surficial environment of the immediate vicinity.

Bryophyte species collected from the vicinity of the gold mine were separated manually from their associated substrate. The samples were then washed with copious amounts of de-ionized water to remove any further soil particles adhering to them. However, the plant material was not vigorously agitated while washing in order to avoid possible cellular damage and thence cellular leakage. After washing, the samples were dried in a drying oven (Gallenkamp) at 60 °C for 3 d. Then 8–10 g aliquots were weighed and digested as described in the previous section using procedure 2. Note that in order to reduce the percentage of total dissolved solids, 0.25 g of ash were dissolved instead of 1 g as previously described, though the same acid volumes were used.

Results and Discussion

ICP-MS Analysis of Gold in Synthetic Solutions

Optimization of the gold signal

A maximum signal is obtained for gold by varying the nebulizer flow rate at particular power settings. Based on the results shown in Fig. 2, it can be observed that there are different local maxima depending on the nebulizer flow rate and the power setting of the ICP. The position of these maxima shift towards higher nebulizer flow rates as the power increases. Furthermore, the magnitude of the signal at these points appears to increase as the forward power increases.

As has been suggested in the literature,[16] it can be assumed that there is a zone within the central channel of the plasma in which there is a maximum density of gold ions. An increase in the nebulizer flow rate shifts this zone closer to the sampling cone and further away from the load coil. A maximum signal for the gold ions is obtained when the tip of the sampling cone is positioned in the centre of this zone. A further increase in the nebulizer flow rate results in the sampling of ions from outside the zone thus registering as a drop in signal.

In agreement with the above mentioned reference, the results from this study fit the theory that an increase in plasma power pulls the zone of maximum ion density towards the load coil. As a result it is necessary to increase the nebulizer flow rate in order to obtain an optimal signal. The fact that the magnitude of the signal for the observed optimum increases with increasing power can be explained by the increase in plasma temperature at higher power settings.

Based on the observed trend, one can conclude that optimum settings of the instrument would be achieved by selecting the highest power/nebulizer flow rate combination. Although such a combination is a rich ground for the formation of doubly charged species, the relatively high second-ionization energy of gold makes such an occurrence unlikely. However, since the maximum nebulizer flow rate that could be used under the current settings of our system was 1.12 l min^{-1} the optimum conditions used for the rest of the study were a forward power of 1.2 kW and a nebulizer flow rate of 1.02 l min^{-1}.

Internal standardization

Changes in the $^{197}Au:^{115}In$ signal ratios during the course of the analysis are plotted in Fig. 3. It can be observed, that the $^{197}Au:^{115}In$ signal ratio varies considerably with time. A careful consideration of the distribution of the data points in Fig. 3 indicates the presence of a certain trend which is not clearly defined. The $^{197}Au:^{115}In$ ratios appear to drop steadily over a period of 60–120 min before jumping back to a higher level. The reason for such behaviour is not clear and further investigations are required to identify it. However, for the

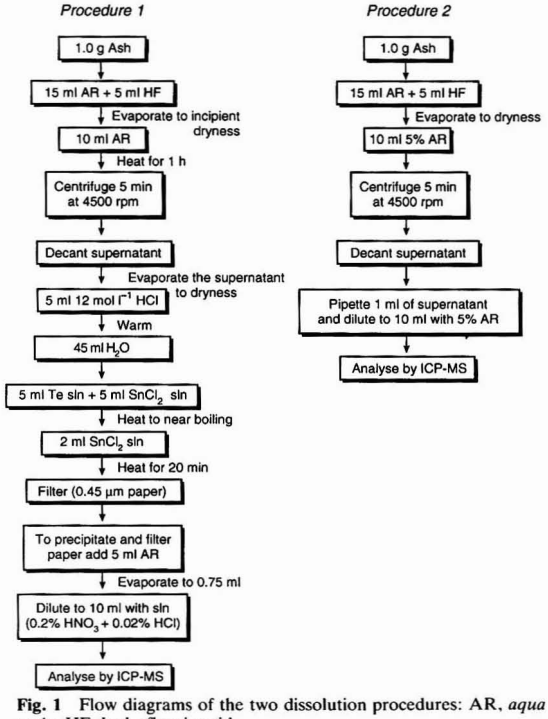

Fig. 1 Flow diagrams of the two dissolution procedures: AR, *aqua regia*; HF, hydrofluoric acid.

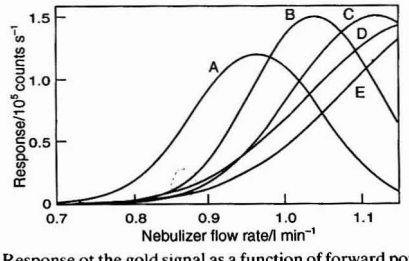

Fig. 2 Response of the gold signal as a function of forward power and nebulizer flow rate. A, 1.1; B, 1.2; C, 1.3; D, 1.4; and E, 1.5 kW.

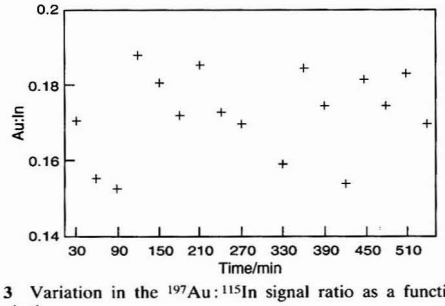

Fig. 3 Variation in the $^{197}Au:^{115}In$ signal ratio as a function of analysis time.

purposes of this study, it is clear that the use of indium as an internal standard for the analysis of gold can lead to erroneous results and that there is a need to investigate alternative internal standards.

Owing to their proximity to gold in mass and ionization energy, iridium, platinum and bismuth (as the isotopes ^{193}Ir, ^{194}Pt, ^{195}Pt, ^{198}Pt and ^{209}Bi) were tested as potential internal standards. The variation in signal ratios (with a comparison of the $^{197}Au:^{115}In$ signal ratio) as a function of analysis time can be seen in Fig. 4.

The variation of the $^{197}Au:^{115}In$ signal again displays an erratic response. However, the $^{197}Au:^{193}Ir$, $^{197}Au:^{194}Pt$, $^{197}Au:^{195}Pt$, $^{197}Au:^{198}Pt$ and $^{197}Au:^{209}Bi$ ratios display very good stability over the analysis period. In deciding which of these isotopes to employ for internal standardization, several factors must be taken into consideration. Firstly, the internal standard must have a similar mass to charge ratio (m/z) as the isotope under investigation. For the above isotopes iridium and platinum closely match this prerequisite. Secondly, the internal standard must also have a similar ionization potential to the isotope under investigation. The ionization potentials for iridium, platinum, and bismuth are 880, 870 and 703.2 kJ mol^{-1}, respectively. These values are in close proximity to the ionization potential for gold (890 kJ mol^{-1}). Thirdly, the internal standard must be mono-isotopic, or have a high-abundance isotope (^{193}Ir has an abundance of 62.7%, platinum has six isotopes, namely, 190, 192, 194, 195, 196 and 198 with abundancies of 0.01, 0.79, 32.9, 33.8, 25.3 and 7.2%, respectively, whilst bismuth is mono-isotopic at 209). Finally, the internal standard must not be present to a high concentration in the matrix under investigation. Of the three elements under scrutiny, Ir is the least naturally abundant element in plant materials.

From the above discussion it can be seen that ^{193}Ir is the best choice of internal standard for gold analysis.

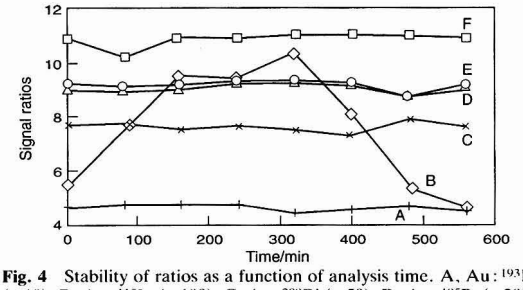

Fig. 4 Stability of ratios as a function of analysis time. A, Au: ^{193}Ir (×10); B, Au: ^{115}In (×100); C, Au: ^{209}Bi (×50); D, Au: ^{195}Pt (×20); E, Au: ^{194}Pt (×20); F, Au: ^{198}Pt (×5).

Memory effects in ICP-MS

Following the introduction of a 100 ng ml^{-1} gold solution (signal reading about 300 000 counts), Fig. 5 shows that a period of 20 min washing with de-ionized water is necessary for the gold signal to return to background levels (about 300 counts). However, on addition of the *aqua regia* wash solutions, the gold signal increases dramatically (11 813 counts for 1% *aqua regia*; 15 693 counts for 5% *aqua regia*; and 22 613 counts for 8% *aqua regia*). The *aqua regia* wash solutions were run through until the gold signal was observed to reach background levels, which occurred after 16, 11 and 6 min, for the 1, 5 and 8% *aqua regia* solutions, respectively.

The second experiment was performed by employing 1% HNO_3 instead of doubly distilled, de-ionized water. As can be observed in Fig. 5, the wash with this solution took about 16 min to return the gold signal to background levels. Again, on addition of the *aqua regia* wash solutions, there was a significant increase in the gold signal, with an increase from background levels to 10 153 counts for 1%, 15 583 counts for 5% and 19 913 counts for 8% *aqua regia*.

From these observations it can be concluded that a residual gold signal is still present in the system, even after a thorough wash with 1% HNO_3 solution. However, on addition of the *aqua regia* wash solutions it appears that the signal returns to background levels with no residual gold adhered to the tubing. The most efficient of these *aqua regia* wash solutions is 8% *aqua regia*, which returns the signal to background levels in the shortest time period, thus improving sample throughput.

Following the introduction of 100 ng ml^{-1} iridium (signal reading about 700 000 counts), the uptake tubing was washed with doubly distilled, de-ionized water. A period of 20 min, was required for the signal to drop to background levels (signal reading about 500 counts). In a similar manner to that observed for gold, the addition of *aqua regia* stripped an appreciable amount of iridium from the tubing. Fig. 5 shows clearly that the use of 8% *aqua regia* clears the uptake from both gold and iridium within the shortest time period.

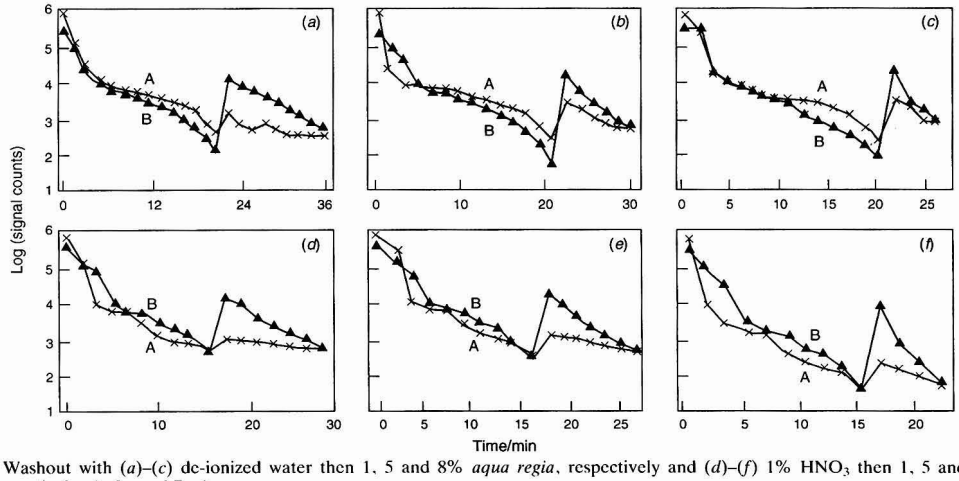

Fig. 5 Washout with (*a*)–(*c*) de-ionized water then 1, 5 and 8% *aqua regia*, respectively and (*d*)–(*f*) 1% HNO_3 then 1, 5 and 8% *aqua regia*, respectively. A, Ir; and B, Au.

Detection limits

The detection limit for gold, calculated as three times the standard deviation of the signal produced from 18 readings of a 5% *aqua regia* solution, was found to be 0.04 ng ml^{-1}. This detection limit is very favourable when compared with detection limits cited in the literature for ICP-MS (0.5 ng ml^{-1}).[11] Although this improved detection limit is partly due to the high sensitivity of the instrument in use, it must be noted that detection limits are dependent on other factors such as the instrument set-up, quality of the blanks, the age (sensitivity) of the channel electron multiplier and the status of the sampling cones. One should therefore be very cautious when comparing detection limits from different ICP-MS instruments.

ICP-MS Analysis of Gold in Plant Materials

Digestion procedures

Procedures 1 and 2 were assessed in terms of their reproducibility (Fig. 6) and recovery (Table 3).

The lower recovery and poor reproducibility of procedure 1 indicate that gold present in the material has been lost during the pre-analysis stage. This may be owing to the fact that this procedure has many stages where gold may be lost from the sample, notably taking the sample to incipient dryness repeatedly, with subsequent transfer between containers. However, in contrast, procedure 2 displays excellent recovery and reproducibility and is far less complex than the first procedure. Therefore, this procedure was adopted for all further analysis of gold in plant materials.

Gold in bryophyte material from a gold mining area

Table 4 shows the range and mean values of gold concentrations obtained from the analysis of bryophyte material collected from the vicinity of the mine and surrounding areas.

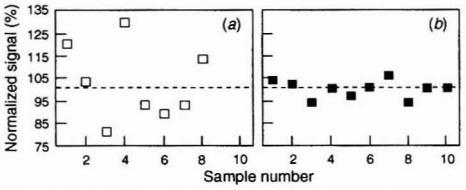

Fig. 6 Reproducibility of the digestion procedures. (*a*) Procedure 1; (*b*) procedure 2.

Table 3 Recovery of a 100 ng ml^{-1} gold spike by the two digestion procedures

Procedure	Recovery (%)*
1	65.8 ± 16.9
2	102 ± 3.6

* Mean ± standard deviation (n = 10).

Table 4 Gold concentrations in plant material from the vicinity of the gold mine

Location	Bryophyte material/ng g^{-1}*
Mine open pit	9–2088 (223)
Treatment plant	2560–7450 (4310)
Tailings pond	57–2072 (571)
Background	81–131 (106)

* All concentrations expressed on a dry mass basis.

From Table 4 it can be observed that the bryophytes removed from the treatment plant area display the highest level of gold accumulation. This observation can be accounted for by the fact that at this sampling site the gold is leached from the rock, and thus there is a greater loss of gold to the immediate environment. These values are elevated in comparison with the gold concentrations for material removed from 'background' locations.

The gold concentrations observed for samples removed from around the mine open pit display a very large range (9–2088 ng g^{-1} with a mean of 223 ng g^{-1}). This spread in gold level is also apparent in samples removed from the tailings pond area. The spread in gold concentration may be due to the fact that these sampling locations represent the largest areas available for removal of plant materials, with the open mine pit covering a surface area of about 24 ha. A large range of concentration was therefore to be expected.

Investigations into the observed high background levels led to the discovery that the sampling site was the location of an old gold mine which had been closed for many years. It can be assumed therefore that this area still has gold available for accumulation by the local flora.

Reading *et al.* reported that in a mineralized zone in the Canadian arctic, gold levels were as high as 2300 ng g^{-1} (dry m) in species of *Betula glandulosa* and *Ledum decumbens*.[10] Concentrations of 1380 ng g^{-1} in the ash of *Dictronia squarrosa* from around an operating gold mine were also reported.[9] These data are in good agreement with the results of this work, in so much as anomalously high levels of gold were also found. Furthermore, a study carried out on the gold concentration of alder leaves reported levels ranging from 5–48 ng g^{-1} (ash m) in early June to 8–24 ng g^{-1} (ash m) in September of the same year.[5] In a similar study, the same author[6] reported levels of gold from a mineralized area of 50 ng g^{-1} in the ash of alder twigs and 10 ng g^{-1} for the same samples from background locations. These values suggest that the concentrations of gold in plant material (leaves and twigs) are lower than those observed in this study (bryophytes).

Conclusions

The research discussed in this paper indicates that a high recovery, fast and reproducible digestion procedure has been developed for the analysis of gold in plant materials by ICP-MS. However, before such a pre-analysis protocol could be employed, certain instrument parameters had to be investigated. Optimization of the instrument signal response to the ^{197}Au ion was addressed through varying the forward power and nebulizer flow rate. An increase in the forward power produced an increase in signal, though for optimum response this necessitated a shift to a higher nebulizer flow rate. Under the conditions adopted in this study, a forward power of 1.2 kW and a nebulizer flow rate of 1.02 l min^{-1} were found to be optimal.

The use of indium as an internal standard led to an erratic response over an analysis period of 10 h. In contrast, by using iridium, a stable signal over the same analysis period was achieved. Iridium was therefore adopted as the appropriate internal standard.

This research has clearly demonstrated that there is a definite problem of reverse adsorption of both gold and iridium onto the sample uptake tubing. However, preparation of samples and standards in 5% *aqua regia* and the employment of an 8% *aqua regia* wash solution between samples appears to eliminate this problem.

These methodologies were adopted for the analysis of gold in plant materials from various sample sites around an operating gold mine, with a detection limit of 0.04 ng ml^{-1}. It

can be observed from the results in this paper that a large order of magnitude variation in gold concentration is reported for the same mass to volume ratio of sample. This reflects the wide linear dynamic range of the ICP-MS.

Finally it must be noted that the data presented in this study are reported on a dry mass basis in contrast to most of the data available in the literature where the ash mass is used. On ashing, the inorganic ions are effectively preconcentrated in the material by a factor of 8–10. Thus, our data, reported on dry mass prior to ashing, and therefore without the benefit of this preconcentration, illustrate the excellent sensitivity of ICP-MS for ultra-trace elemental analysis.

Useful technical discussions with Dr. M. P. Rayman are gratefully acknowledged.

References

1 Erdman, J. A., and Olson, J. C., *J. Geochem. Explor.*, 1985, **24**, 281.
2 Brooks, R. R., *Geobotany and Biogeochemistry in Mineral Exploration*, Harper and Row, New York, 1972, p. 215.
3 Shacklette, H. T., Erdman, J. A., and Harms, T. F., *Toxicity of Heavy Metals in the Environment, Part 1*, ed. Oetime, F. W., Marcel Dekker, New York, 1978, p. 25.
4 Warren, H. V., and Barakso, J., *Western Miner*, 1982, 27.
5 Dunn, C. E., *J. Geochem. Explor.*, 1986, **63**, 418.
6 Dunn, C. E., *J. Geochem. Explor.*, 1986, **25**, 21.
7 Cohen, D. R., Hoffman, E. L., and Nichol, I., *J. Geochem. Explor.*, 1987, **29**, 49.
8 Michailova, T. P., and Rezepina, V. A., *Analyst*, 1970, **95**, 769.
9 Ward, N. I., and Brooks, R. R., *New Zealand J. Botany*, 1978, **16**, 175.
10 Reading, K. A. L., Brooks, R. R., and Naidu, S. D., *J. Geochem. Explor.*, 1987, **27**, 143.
11 Hall, G. E. M., Pelchat, J. C., and Dunn, C. E., *J. Geochem. Explor.*, 1990, **37**, 1.
12 Hall, G. E. M., and Bonham-Carter, E. F., *J. Geochem. Explor.*, 1988, **30**, 255.
13 Perry, B. J., and Van Loon, J. C., in *Applications of Plasma Source Mass Spectrometry*, Blackie, Glasgow, eds. Holland, G., and Eaton, A. N., 1991, p. 38.
14 Hoffman, E. L., and Brooker, E. J., *Assoc. Explor. Geochemist, Rexdale, Ont., Spec.*, 1982, **10**, 69.
15 Brooks, R. R., and Naidu, S. D., *Anal. Chim. Acta*, 1985, **170**, 325.
16 Vanhaecke, F., Vandecasteele, C., Vanhoe, H., and Dams, R., *Mikrochim. Acta*, 1992, **108**, 41.

Paper 4/03075C
Received May 23, 1994
Accepted October 10, 1994

Quantitative Analysis of Impurities in ε-Caprolactam by Raman Spectroscopy

Christos G. Kontoyannis, Nicolaos Ch. Bouropoulos and Petros G. Koutsoukos

Institute of Chemical Engineering and High Temperature Chemical Processes and Department of Pharmacy, University of Patras, P.O. Box 1414, GR 26500 Patras, Greece

Laser Raman spectroscopy was used for the quantitative analysis of the most common impurities contained in ε-caprolactam: adipic acid, sodium sulfate and ammonium sulfate. Calibration graphs were constructed from spectra obtained from pellets with known quantities of ε-caprolactam and each of the impurities. Linear relationships between the caprolactam content and the ratio of the relative intensities at characteristic wavelengths were found for the impurities examined. The calibration lines were defined as: adipic acid–ε-caprolactam $I_{915}/I_{746} = \chi^{-1}_{cap}\ 0.62 - 0.58$; ammonium sulfate–ε-caprolactam $I_{975}/I_{746} = \chi^{-1}_{cap}\ 2.78 - 2.23$; and sodium sulfate–ε-caprolactam $I_{994}/I_{746} = \chi^{-1}_{cap}\ 4.26 - 4.45$. I is the relative Raman intensity at the wavenumber noted by the subscript and χ_{cap} is the molar fraction of caprolactam. The detection limits are better than 1 mol% for the impurities examined.

Keywords: Raman spectroscopy; ε-caprolactam; sodium sulfate; ammonium sulfate; adipic acid

Introduction

ε-Caprolactam is one of the basic raw materials used in manufacturing high-quality synthetic fibres and various plastics. The world production of caprolactam for 1992 was 3.6×10^6 t.[1] The quality of products made of caprolactam is strictly dependent on its purity grade. Therefore, continuous monitoring of the impurities during the different stages of its synthesis is imperative.

One of the major by-products formed and subsequently occluded as an impurity is either sodium sulfate or ammonium sulfate,[2,3] depending on the method used. The crude product may contain up to 50 mol% of these salts while after purification (with simultaneous recovery of the sulfates) the content of the impurities is 1–10 mol%. Quantitative determination of other impurities, such as the adipic acid[4] which plays an important role in the acidity of the final product and consequently on its quality, is also important. The content of adipic acid in the crude product may exceed 10 mol% but in the final product this impurity is quite low (<0.1 mol%).

Considerable research has been carried out in the determination of the organic impurities using gas chromatographic analysis.[5–9] For inorganic ions, separate analyses are performed using classical chemical analytical methods. For the complete analysis of the impurities contained in the system of interest a combination of gas and ion chromatography should be employed for the analysis of adipic acid and the inorganic (Na^+, NH_4^+ and SO_4^{2-}) ions, respectively. The procedure, besides requiring different instrumentation, necessitates the preparation of different eluents and use of different columns, conditioning, *etc*, which make it difficult to apply for rapid analyses. A fast, reliable qualitative and quantitative method, suitable for routine analysis, is needed in order to determine the level of impurities in ε-caprolactam at the production line.

In the present work, laser Raman spectroscopy (LRS) was used for the quantitative analysis of ε-caprolactam containing Na_2SO_4, $(NH_4)_2SO_4$ and adipic acid impurities. The ratio of the relative intensities of the easily defined LRS peaks of ε-caprolactam and each of the impurities was applied to the determination of the impurities. A calibration graph was obtained by mixing known quantities of the ε-caprolactam with each of the impurities. Infrared (IR) spectroscopy was also used in order to compare the two spectroscopic techniques.

Methods and Materials

Sample Preparation and Chemicals

ε-Caprolactam, sodium sulfate and ammonium sulfate were purchased from Merck (Darmstadt, Germany) while adipic acid was acquired from Serva (Heidelberg, Germany). All chemicals were used without further treatment except ε-caprolactam, which was dried at 60 °C in a laboratory oven for at least 24 h prior to use.

In order to construct a calibration graph, mixtures of ε-caprolactam and each of the impurities were prepared, by careful weighing and subsequent grinding in an agate mortar. The solid mixture was placed in a cylindrical die and a pellet was formed by applying a pressure of 8 t m^{-2} for 1 min. The homogeneity of the pellets was verified by obtaining several spectra, from different points on the surface, for each pellet.

LRS System Configuration and IR Spectroscopy System

Raman spectra were excited with the 488 nm line of a 4 W Spectra Physics argon laser. The plasma lines were removed from the laser beam by using a small monochromator as filter. A cylindrical lens, with 5 in focal length, was used to focus the laser line on the sample giving a probed area of approximately 1 mm^2. The scattered light was collected at an angle of 90° and analysed with a SPEX 1403, 0.85 m double monochromator equipped with an RCA photomultiplier cooled to −20 °C and EG & G/Ortec photon counter and electronic amplifier. The power of the incident laser beam on the sample surface was about 100 mW. The typical spectral width and time constant were 1 cm^{-1} and 1 s, respectively. The system was also interfaced with a computer and the spectra were recorded on *x–t* recorder paper and simultaneously digitized and stored in diskettes.

The IR spectra were obtained using an FTIR Perkin-Elmer 16 PC spectrometer.

Results and Discussion

LRS versus FTIR

Evaluation of the quantitative capabilities of the two spectroscopic techniques is possible only by comparison of the spectra

obtained from the pure compounds. In Figs. 1 and 2 the IR and Raman spectra, respectively, of ε-caprolactam, sodium sulfate, ammonium sulfate and adipic acid are presented. In the IR spectra ε-caprolactam exhibits a rather well defined band at around 1650 cm^{-1} which is due to the valence and deformation vibrations.[10] This band coincides with a band at 1690 cm^{-1} in the adipic acid spectral. Sodium sulfate and ammonium sulfate exhibit a band at around 1120 cm^{-1}, which unfortunately overlaps with several caprolactam peaks. On the other hand, in the Raman spectra ε-caprolactam exhibits a well defined peak,[10] at 746 cm^{-1}, while the ammonium sulfate and sodium sulfate bands at 975 cm^{-1} and 994 cm^{-1}, respectively, are due to the S–O bond. The most characteristic band of pure adipic acid is at 915 cm^{-1}. Thus, LRS is a better quantitative method than IR spectroscopy.

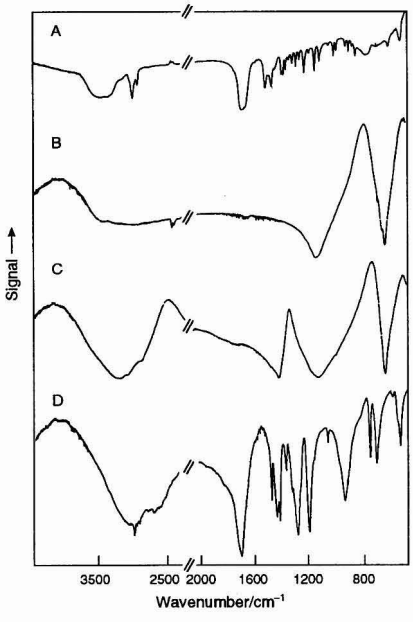

Fig. 1 FTIR spectra: A, caprolactam; B, sodium sulfate; C, ammonium sulfate; and D, adipic acid.

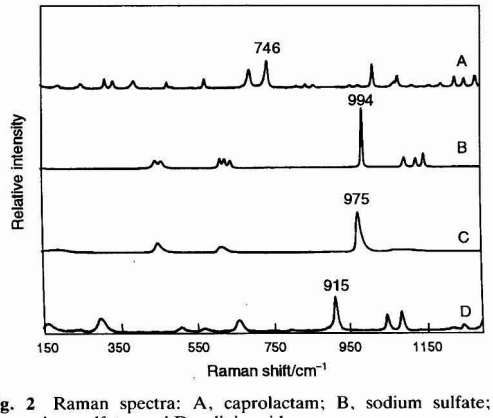

Fig. 2 Raman spectra: A, caprolactam; B, sodium sulfate; C, ammonium sulfate; and D, adipic acid.

Theory for the Construction of the Calibration Graphs

The objective was to find a simple, reliable method to calculate the impurity content of the caprolactam samples. The peak height was used rather than the integrated intensities of the bands. The differences in the measured intensities of the various spectra made it apparent that only relative factors within each spectrum, *e.g.*, ratio of the intensities, could be used.

The intensity of a Raman line depends on a number of factors, including incident laser power, frequency of the scattered radiation, absorptivity of the materials involved in the scattering, and the response of the detection system. Thus, the measured Raman intensity, $I(\nu)$, can be represented[11] as

$$I(\nu) = I_0 K(\nu) c \qquad (1)$$

where I_0 is the intensity of the excitation laser line, ν is the Raman shift, $K(\nu)$ is a factor which includes the frequency dependent terms, *viz.*, the over-all spectrophotometer response, the self-absorption of the medium and the molecular scattering properties and c is the concentration of the Raman active species.

If χ_{cap} and χ_{imp} are the molar fractions of the ε-caprolactam and of the impurity examined, respectively, then for the ε-caprolactam–impurity pellets $\chi_{cap} + \chi_{imp} = 1$. Thus, the ratio of the relative intensity of the impurity peak to the relative intensity of the ε-caprolactam peak at 746 cm^{-1} can be represented as

$$\frac{I_{imp}}{I_{746}} = \frac{K_{imp}}{K_{746}} \frac{1}{\chi_{cap}} - \frac{K_{imp}}{K_{746}} \qquad (2)$$

where I_{746} and I_{imp} represent the intensities of the 746 cm^{-1} and the impurity peaks, respectively. The subscript of the K represents the Raman shift of the peak.

ε-Caprolactam and Sodium Sulfate

The plot of the ratio of I_{994}/I_{746} *versus* $\chi^{-1}{}_{cap}$ is shown in Fig. 3(*a*). The value of both intensities was obtained by subtracting the 'background' intensity. Typical spectra of sodium sulfate in pellets with ε-caprolactam are shown Fig. 4.

A linear regression on all data yields the following equation

$$\frac{I_{994}}{I_{746}} = \frac{1}{\chi_{cap}} 4.26 - 4.45 \qquad (3)$$

The correlation coefficient, r, was 0.999 while the standard errors for the slope and the intercept were $\pm 3.7 \times 10^{-2}$ and ± 0.18, respectively.

ε-Caprolactam and Ammonium Sulfate

The plot of the ratio of I_{975}/I_{746} *versus* $\chi^{-1}{}_{cap}$ is shown in Fig. 3(*b*). The value of both intensities was obtained by subtracting the 'background' intensity. Typical spectra of ammonium sulfate in pellets with ε-caprolactam are shown in Fig. 5.

A linear regression on all data yields the following equation

$$\frac{I_{975}}{I_{746}} = \frac{1}{\chi_{cap}} 2.78 - 2.23 \qquad (4)$$

The r value was 0.998 while the standard errors for the slope and the intercept were $\pm 6.3 \times 10^{-2}$ and ± 0.23, respectively.

ε-Caprolactam and Adipic Acid

The plot of the ratio of I_{915}/I_{746} *versus* the $\chi^{-1}{}_{cap}$ is shown in Fig. 3(*c*). The value of both intensities was obtained by subtracting the 'background' intensity. Typical spectra of adipic acid in pellets with ε-caprolactam are shown in Fig. 6.

A linear regression on all data yields the following equation

$$\frac{I_{915}}{I_{746}} = \frac{1}{\chi_{cap}} 0.62 - 0.58 \quad (5)$$

The value of r was 0.998 while the standard errors for the slope and the intercept were $\pm 1.0 \times 10^{-2}$ and $\pm 3.7 \times 10^{-2}$, respectively.

Calibration Graphs

According to eqn. 2 the absolute values for the intercepts obtained from the calibration lines were expected to be equal to the absolute values of their respective slopes. The standard errors of the intercepts and the slopes for the eqns. 3–5 account for the deviation from the theoretically derived equation.

Five Raman spectra were recorded for each composition of caprolactam with each impurity and thus the intensity ratios of Fig. 3 are the mean values of the experimental data. The relative standard deviation for each of the mean values was of the order of three.

From the standard errors for each calibration line and by using the error propagation theory the standard error for χ_{cap} was calculated to be of the order of 0.01. This value (1 mol%) also represents the quantitative limitation for the described spectroscopic determination. As may be seen from the calibration lines in the insets in Fig. 3, the accuracy mentioned is valid over the entire range of interest (1–90%) for the impurities in caprolactam.

In the range of our spectra measurements the over-all spectrometer response can be considered to be constant, and thus, the K ratios depend only on the scattering parameter associated with each band. Consequently, the value assigned to the K ratios may be applied to any Raman spectrometric system.

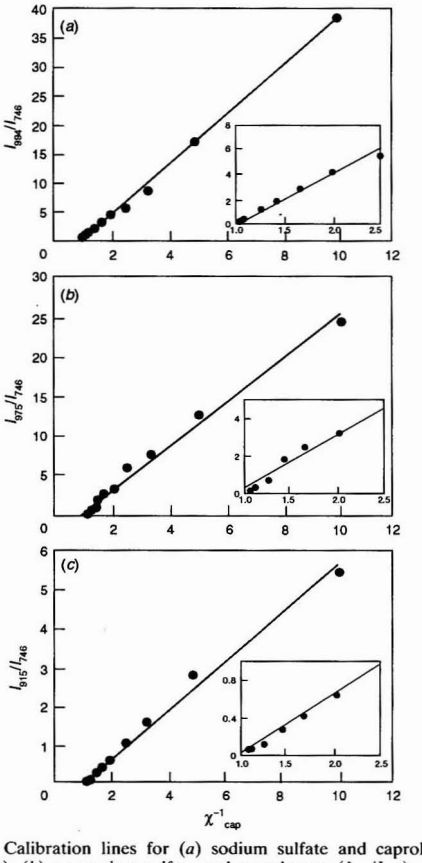

Fig. 3 Calibration lines for (*a*) sodium sulfate and caprolactam (I_{994}/I_{746}), (*b*) ammonium sulfate and caprolactam (I_{975}/I_{746}) and (*c*) adipic acid and caprolactam (I_{915}/I_{746}).

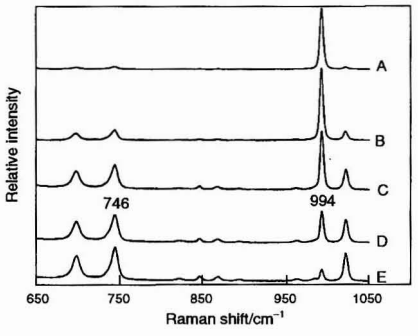

Fig. 4 Raman spectra from mixtures of sodium sulfate and caprolactam. The molar fraction ratio of Na_2SO_4 in the pellets was: A, 0.90; B, 0.70; C, 0.50; D, 0.30; and E, 0.10.

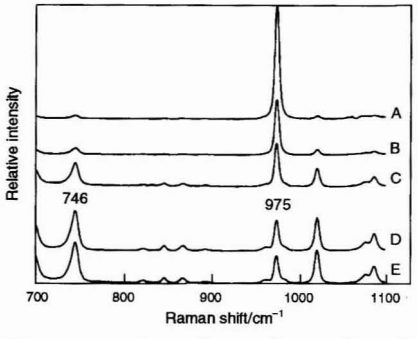

Fig. 5 Raman spectra from mixtures of ammonium sulfate and caprolactam. The molar fraction ratio of $(NH_4)_2SO_4$ in the pellets was: A, 0.90; B, 0.70; C, 0.40; D, 0.20; and E, 0.10.

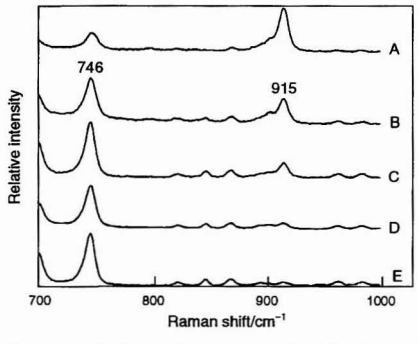

Fig. 6 Raman spectra from mixtures of adipic acid and caprolactam. The molar fraction ratio of adipic acid in the pellets was: A, 0.80; B, 0.50; C, 0.30; D, 0.20; and E, 0.10.

Note that the analytical method presented here does not depend on the simultaneous existence of the sulfate salts and the adipic acid since there is neither interaction (chemical) between these species nor overlap of the corresponding bands in the Raman spectra. As a result the relative intensities used in the analysis according to eqns. 2–4 are not affected. Moreover, as may be seen from eqn. 1 the intensity of the Raman bands depends upon the concentration of the investigated species alone.[11]

The above described procedure may be adapted for any other impurity provided that the impurity exhibits a well-defined peak in the Raman spectrum.

Conclusions

Linear calibration lines were obtained for the quantitative determination of ε-caprolactam containing impurities such as adipic acid, sodium and ammonium sulfate, using LRS. The calibration lines were constructed from plots of the ratio of the intensity of the peak due to the impurity divided by that due to the caprolactam as a function of the inverse concentration of ε-caprolactam in the standards. LRS clearly demonstrated its potential as a quantitative analytical technique which may be used efficiently for monitoring the different stages of ε-caprolactam production. The method is adaptable for any impurity.

The authors are indebted to Professor G. N. Papatheodorou for helpful suggestions and for providing the experimental facilities. This work has been supported by the E.C. Commission (JOULE program, contract no. JOU2-CT92-0077).

References

1 Jansens, P. J., Ph.D. Thesis, Technical University of Delft, The Netherlands, 1994.
2 Barduhn, A., and Handley, M., *J. Chem. Eng. Data*, 1982, **27**, 306.
3 *Ullmann's Enzyklopädie der technischen Chemie*, Verlag chemie, Weinheim, 1975, pp. 96–114.
4 Austin, G. T., in *Shreve's Chemical Process Industries*, 5th edn, McGraw-Hill, New York, 1984, p. 767.
5 Czerwinski, W., Wiejcka, M., Malikowska, H., and Dyjas, S., *J. Chromatogr.*, 1981, **208**, 27.
6 Unger, P., and Friedman, M., *J. Chromatogr.*, 1980, **187**, 429.
7 Krajvik, V., Bozek, P., Kondelikova, J., and Kralicel, J., *J. Chromatogr.*, 1982, **240**, 539.
8 Jodra, L., Romero, A., Garcia-Ochoa, F., and Aracil, J., *J. Appl. Polym. Sci.*, 1981, **26**, 3271.
9 Jodra, L., Romero, A., Garcia-Ochoa, F., and Aracil, J., *Ind. Eng. Chem. Prod. Res. Dev.*, 1981, **20**, 562.
10 Kabo, G. J., Kozyro, A., Krouk, V., Sevruk, V., Yursha, I., Simirksy, V., and Gogolinsky, V., *J. Chem. Thermodyn.*, 1992, **24**, 1.
11 Strommen, D., and Nakamoto, K., in *Laboratory Raman Spectroscopy*, Wiley, New York, 1984, pp. 71–75.

Paper 4/02829E
Received May 12, 1994
Accepted July 12, 1994

Qualitative and Semiquantitative Analysis of Annatto and its Content in Food Additives by Photoacoustic Spectrometry

Ulrich Haas

Institut für Physik, Universität Hohenheim, Garbenstrasse 30, D-70599 Stuttgart, Germany

Carlos A. Vinha*

Departamento de Física, Universidade Federal de Mato Grosso do Sul (UFMS), 79070-900 Campo Grande, MS, Brazil

Photoacoustic spectrometry in the ultraviolet, visible and near-infrared regions was employed to study the absorption behaviour of the colourant annatto and to determine its content in commercial seasoning products *via* the intensity of an absorption peak compared with the absorption of standard samples with a known content of annatto. Owing to strong absorption and as a consequence saturation of the signal of the pigment in the ultraviolet and visible regions, a peak of weak absorption in the near-infrared region was used, guaranteeing a linear relationship between peak intensity and annatto content for the usually applied low to medium levels of dye contents in commercial products.

Keywords: Semiquantitative food analysis; ultraviolet–visible–near-infrared photoacoustic spectrometry; natural pigment; annatto; 'Colorífico de Urucum'

Introduction

In the last two decades, photoacoustic spectrometry (PAS)[1–4] has proved to be an important technique for the observation of fingerprint spectra and has been used to to determine the contents and composition of various substances,[5–14] and also for the investigation of foods and agricultural products.[10,15–18] In addition to the unique possibility of using PAS for depth profiling by variation of the modulation frequency of the incident light,[1–4,19–22] this technique also has the advantage of being applicable to the investigation of materials in intact form without prior sample preparation.[18–24]

In this work, PAS was applied to study the natural colour annatto as the pure substance and in diverse mixtures in the ultraviolet (UV), visible (VIS) and near-infrared (NIR) spectral regions. Annatto can be extracted from the shells of seeds of *Bixa orellana* L. and is commercially available as a powder, suspended matter or reddish–brown solution.[25,26] The main pigment of annatto extracts is bixin, a yellow to orange–red substance belonging to the group of carotenoids. The pigments of the shells of seeds of *Bixa orellana* L. consist of about 90% of bixin, and the mass content of bixin relative to the total mass of a seed is about 2.5–7%. In the international colour index bixin is CI 75120 and is called L-Orange 4, and is known in the European Union as E160b.[26–28] It is employed to colour foods, *e.g.*, butter, margarine, cheese, oils, mayonnaise, sausage and macaroni, and to dye cosmetics and textiles.[26,29–33] Using diverse adsorbing substances, the natural colour annatto is also utilized to produce food additives with a content of 1–30% of bixin.[26] A mixture of corn meal with powdered seeds of *Bixa orellana* L. or powdered annatto extracts is a well known red–orange powder and one of the most important dyes, especially used in Brazil as a colourant and also as a food seasoning substance with the trade name 'Colorífico de Urucum'.[32,33]

The objective of this study was to show the possibility of determining by PAS the content of annatto (abbreviated to CA) and of bixin in three commercial products of 'Colorífico de Urucum' produced in Brazil. Therefore, standards of 'Colorífico de Urucum' with known contents of powdered seeds of *Bixa orellana* L. (in this paper also named annatto) and of corn meal were prepared. The CA of the commercial products could be derived *via* the intensity of an absorption peak in the NIR region by interpolation from a graph of the same absorption peak of the standards *versus* the known contents of annatto and corn meal.

Experimental

Apparatus

The PA spectra were recorded using an EG&G PAR Model 6001 photoacoustic spectrometer equipped with a 1 kW high-pressure xenon arc lamp, which allows the recording of spectra from 200 to 2600 nm. Light modulation over the frequency range 10 Hz–2 kHz was accomplished by electronic modulation of the lamp current. The sample cell was made of stainless steel, with a rectangular (4 × 8 × 22 mm) sample cup. The PA signal was detected by a sensitive microphone (Brüel & Kjær Type 4166) and 'source-compensated' by a real-time signal, derived from a pyroelectric detector which was exposed, *via* a fused-silica beam-splitter, to a fraction of the incident modulated light beam.

For milling of the samples, a three-dimensional oscillating mixer mill (Retsch Model MM2) with grinding vessels made of agate was used and for sieving a vibrating sieving machine (Retsch Model Vibro) was employed, using ISO standard stainless-steel test sieves with wire gauges of 180, 125, 90, 45 and 20 μm. Samples of materials were weighed using an electronic analytical balance (Kern Type 410-11; resolution 0.1 mg at 41 g capacity). Liquid extracts of the seeds of *Bixa orellana* L. were prepared using a temperature-controlled magnetic stirrer (IKA Kombimak RCT).

Materials

The ingredients of the three commercial products of 'Urucum' as given by the manufacturers were as follows: first product (S1), seeds of annatto, corn meal, soybean oil; second product

* On leave at the Institut für Physik, Universität Hohenheim, Garbenstrasse 30, D-70599 Stuttgart, Germany.

(S2), annatto, corn meal, soybean oil; and third product (S3), not specified. Examination of these products by optical microscopy revealed great variations in the particle size of the corn meal and inhomogeneity of pigment distribution.

The standards were produced using commercial source materials of corn meal, soybean oil and seeds of *Bixa orellana* L.

Extracts of pigments were obtained by applying soybean oil or acetone as solvent.

Procedure

The commercial products were in powdered form. They were used as received or in definite ranges of grain sizes by milling the material and subsequently passing it through standard test sieves.

Annatto was produced by milling the intact seeds of *Bixa orellana* L. and subsequent sieving. The standards were prepared by weighing and carefully mixing known amounts of powdered annatto, corn meal and a small amount of soybean oil. Homogeneity of the mixtures was monitored with an optical microscope. Three independent series of concentrations of the standards were prepared and investigated.

To determine the CA of the commercial products, measurements only of comparable fractions of grain sizes, *e.g.*, 125 μm $< d \leqslant$ 180 μm, of the standards and of the commercial products were made. All investigations were executed with a fixed modulation frequency $f = 13$ Hz of the incident light and the spectra were normalized to graphite ('carbon black') as 100% absorber. To average several scans and to test the reproducibility, up to ten measurements with new fillings of each samples were executed.

Results and Discussion

To determine the annatto content of the commercial products, we first studied the absorption behaviour of the various components of 'Colorífico de Urucum' as pure substances in the UV, VIS and NIR regions.

The PA spectra from 200 to 1200 nm of bixin in soybean oil, prepared as an extract of bixin in soybean oil as solvent, and of pure soybean oil are shown in Fig. 1A and B, respectively. The absorption peaks centred at 442, 467 and 498 nm can be assigned to bixin in solution, whereas the peak at about 260 nm is mainly due to the absorption of soybean oil. A contribution to this UV peak, seen as a shoulder at the long-wavelength side, arises from bixin, as revealed by the PA spectrum of intact seeds of *Bixa orellana* L. (Fig. 2, A). In the UV region both intact and milled seeds show an absorption peak at about 286 nm. However, for intact seeds the typical absorption peaks of bixin in the VIS region are broadened and therefore not well separated. Signal saturation due to strong absorption of this pigment, embedded in high concentrations in the shell of the seeds, could be the reason, as revealed in Fig. 3 by comparing the PA amplitudes and also the absorption behaviour in the wavelength range 350–550 nm of annatto (Fig. 3, A) and the commercial product (Fig. 3, B). The latter shows a more characteristic absorption curve of bixin with an increased PA amplitude due to the lower content of annatto. To remove saturation effects, investigations of annatto and of the commercial products were also performed by diluting the samples with MgO and by increasing the modulation frequency of the incident light. For all dilutions and modulation frequencies applied, no decrease in saturation effects with utilizable signal-to-noise ratio of the PA signal could be obtained in the UV/VIS region.

Further, in the VIS region the absorption peaks of the solid samples are shifted to longer wavelengths, a well known fact for the absorption of a substance in the solid phase compared with its solution in a convenient solvent, as demonstrated by comparing Fig. 1A with Figs. 2A and 3A. A further small absorption of intact seeds at 663 nm (Fig. 2, A) can be attributed to an absorption of the supporting texture of the shell of seeds. This could be confirmed from the PA spectrum of seeds washed with acetone to remove the pigments quantitatively. In Fig. 2 the spectra of corn meal (Fig. 2, C) and of one of the commercial products (Fig. 2, B) in the UV to NIR regions are also shown. Both samples were investigated as received, whereas the spectra in Fig. 3 were acquired using

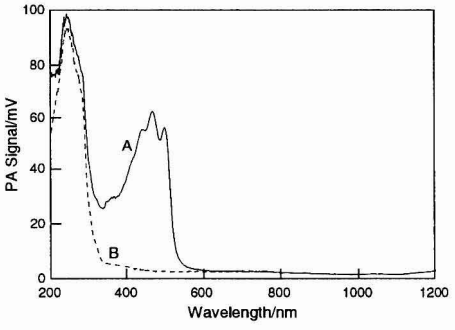

Fig. 1 Photoacoustic spectrum of A, bixin in soybean oil, prepared as an extract from seeds of *Bixa orellana* L. with soybean oil as solvent; and B, of pure soybean oil in the spectral range 200–1200 nm.

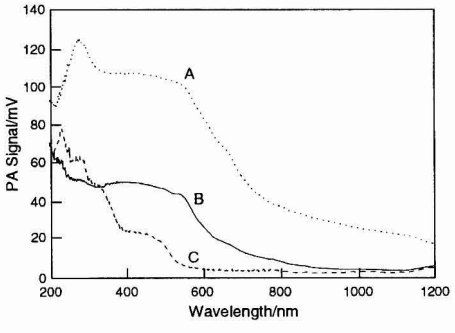

Fig. 2 Photoacoustic absorption behaviour from the UV to NIR regions of A, intact seeds of *Bixa orellana* L.; B, one of the commercial products (S1) of 'Colorífico de Urucum'; and C, Corn meal. All samples were used as received.

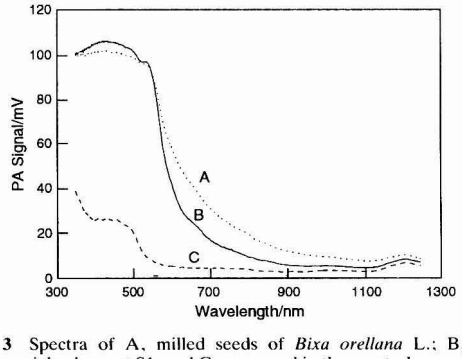

Fig. 3 Spectra of A, milled seeds of *Bixa orellana* L.; B, the commercial colourant S1; and C, corn meal in the spectral range from 350 to 1250 nm for particle size range 125 μm $< d \leqslant$ 180 μm.

powdered samples of grain sizes 125 μm < d ≤ 180 μm. Figs. 2 and 3 reveal the absorption behaviour of the commercial product compared with the pigments of the seeds and of pure corn meal, respectively, with all characteristic features of both components.

It is well known that the particle size of powdered samples has a strong influence on the signal amplitude of PA spectra. In order to decrease this influence to a minimum, the same fraction of particle sizes (125 μm < d ≤ 180 μm) of the standards and of the commercial colourants was always used. This fraction of particle sizes was selected from three different fractions on the basis of classification of the homogeneity by an optical microscope and of the reproducibility of the PA response to the different particle size fractions of the various samples.

The standards were prepared as described above with mass-to-mass ratios of annatto and corn meal of 100:0 (pure annatto), 90:10, 80:20, 70:30, 60:40, 50:50, 45:55, 40:60, 35:65, 30:70, 25:75, 20:80, 15:85, 10:90, 5:95 and 0:100 (pure corn meal). Fig. 4 shows PA spectra in the NIR region from 800 to 1300 nm of the following mixtures of annatto to corn meal: 80:20 (B), 60:40 (C), 40:60 (D) and 20:80 (E), and for pure corn meal (F). Beginning with pure annatto (Fig. 4, A), a decreasing PA signal amplitude with increasing content of corn meal of the standards is observed. Commercial 'Colorífico de Urucum' products were investigated for the same range of particle sizes (125 μm < d ≤ 180 μm) as for the standards. The results are demonstrated in Fig. 5 for the three commercial products S1 (B), S2 (C) and S3 (D), together with pure annatto (A) and pure corn meal (E).

For all quantitative calculations, we used an absorption peak of corn meal in the NIR region at 865 nm, which is increasingly superimposed by the absorption of annatto with increasing content in the standards. The non-specific absorption of annatto at this wavelength indicates its choice to decrease saturation effects and hence non-linearities. An advantage for these investigations is the relatively low content of annatto in the commercial 'Colorífico de Urucum' products, since over this range the standards produced show no saturation effects. Therefore, a relatively simple method could be applied without the need to consider the entire range of concentrations of the pigment or by using, *e.g.*, linearizing procedures.[15]

The effective amplitude ['PA-Intensity (compensated)'] of the PA signal at 865 nm was calculated to compensate for background effects by subtracting the minimum amplitude of each spectrum. In Fig. 6 the experimentally determined values of 'PA-Intensity (compensated)' are plotted *versus* the content of annatto (CA in % m/m) for the standards and for pure corn meal and annatto. Good linearity occurs for CA values up to about 50%, as shown by the straight line (Fig. 6) obtained by a least-squares fit, whereas for higher concentrations an asymptotic behaviour is observed owing to increasing PA saturation effects.[15,34] For CA values below 25% the data points for the standards conform very well with the straight line, whereas up to 50% increasing scatter of the plotted points is observed. Taking into account that for lower values of CA the pigmented grains of corn meal remain as single particles with a minor tendency to agglomerate, there is almost a constant compactness of the material in the sample cup for the multiple investigations with new fillings. Therefore, the experimental results reveal a low standard deviation. However, with increasing CA a greater tendency for particle agglomeration is observed, hence it becomes increasingly difficult to adjust a comparable compactness of the samples for repeated measurements, and the scatter of the experimental data increases. This can also be seen for values of CA above 50% (Fig. 6) when the signal saturation increases.

To extend the range of calibration to higher contents of annatto, saturation effects must be decreased with an increased modulation frequency or by diluting the samples in an inert matrix; dilution can have the added benefit of decreasing packing effects observed for the standards at higher contents of annatto. By increasing the modulation

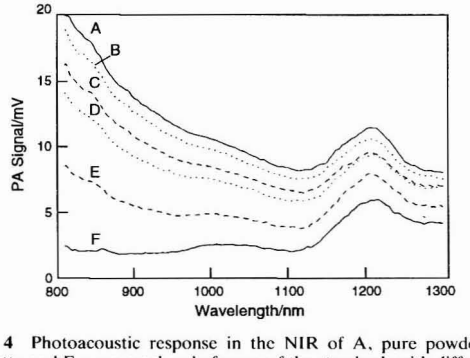

Fig. 4 Photoacoustic response in the NIR of A, pure powdered annatto and F, corn meal and of some of the standards with different mixture ratios of the colourant annatto to corn meal (% m/m): B, 80:20; C, 60:40; D, 40:60; E, 20:80. Range of particle size for all samples, 125 μm < d ≤ 180 μm.

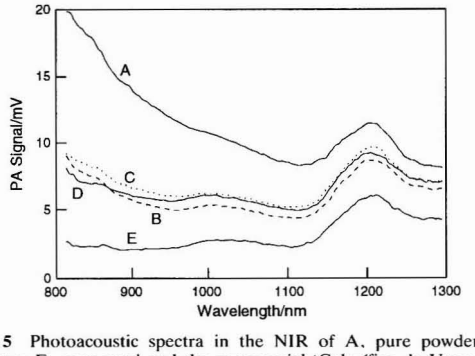

Fig. 5 Photoacoustic spectra in the NIR of A, pure powdered annatto; E, corn meal and the commercial 'Colorífico de Urucum' products: B, S1; C, S2; and D, S3. Range of particle size for all samples: 125 μm < d ≤ 180 μm.

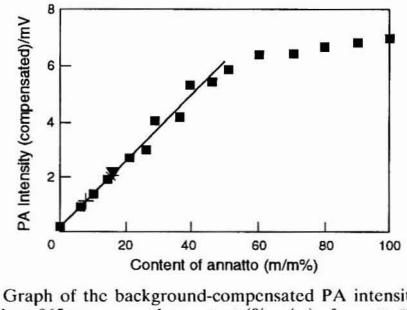

Fig. 6 Graph of the background-compensated PA intensity of the standards at 865 nm *versus* the content (% m/m) of annatto (■). The commercial colourants S1 (*), S2 (▼), S3 (+) are also marked, by plotting their spectroscopically determined compensated PA intensities. The point of intersection with the fitted straight line allows the determination of the CA of S1, S2 and S3.

frequency, the beginning of a decrease in saturation and an improvement in spectral resolution are observed in the NIR region at frequencies of over 500 Hz for pure annatto and also for the standards with contents of annatto above 50%. However, no gain can be obtained owing to the low signal-to-noise ratio of the PA amplitudes with increased modulation frequencies. Dilution of the samples with MgO, *e.g.*, with 1% of annatto, decreases the saturation effects and improves the spectral resolution in the NIR region. Therefore, dilution would be essential to determine bixin, *e.g.*, in materials with high contents of the pigment, produced as a direct extract of *Bixa orellana* L., as saturation effects now cannot be avoided. However, as mentioned above, the contents of the pigments in the commercial 'Colorífico de Urucum' products are typically in a range where saturation effects of the standards are not observed. Therefore, in this instance there is no need to extend the range of calibration for the objective of our study.

The unknown contents of annatto of the commercial 'Colorífico de Urucum' products can be determined graphically from the plot for standard samples (Fig. 6) or with the data for the regression line using the compensated PA signals at 865 nm of S1, S2 and S3. The results for CA in the products investigated in this work are CA(S1) = 16 ± 1%, CA(S2) = 17 ± 1% and CA(S3) = 7 ± 1%.

To evaluate the content of bixin in the commercial products, it is necessary to know its net content in the seeds. By weighing intact seeds of *Bixa orellana* L. and powdered bixin from an acetone extract of seeds, the content of bixin was determined to be about 4.6 ± 0.1%, a reasonable result compared with the values mentioned in the Introduction. The product of this value and the experimentally determined CA of commercial samples results in the content of bixin in the commercial colourants.

Conclusions

The concentration of annatto in three commercial 'Colorífico de Urucum' products could be determined by employing a comparison method with standards, prepared as powdered samples of a definite fraction of grain sizes with a known content of annatto and corn meal. A calibration graph for the standards was obtained by plotting the normalized amplitude of an absorption band in the NIR region, determined by using PAS, *versus* the content of annatto in the standards. The only handling of the commercial colourants required is homogenization by milling and subsequent selection of the same fraction of particle sizes as for the standards.

The authors are grateful to Dr. P. R. N. Carvalho (ITAL, Campinas, SP, Brazil) for providing information about the industrial method for the production of annatto colourants. The support for C. A. V. by a post-doctoral scholarship from the Conselho Nacional de Desenvolvimento Científico e Tecnológico (CNPq), Brazil, is gratefully acknowledged.

References

1 Rosencwaig, A., *Photoacoustics and Photoacoustic Spectroscopy*, Wiley, New York, 1980.
2 McClelland, J. F., *Anal. Chem.*, 1983, **55**, 89A.
3 West, G. A., Barrett, J. J., Siebert, D. R., and Reddy, K. V., *Rev. Sci. Instrum.*, 1983, **54**, 797.
4 Vargas, H., and Miranda, L. C. M., *Phys. Rep.*, 1988, **161**, 45.
5 Adams, M. J., Beadle, B. C., and Kirkbright, G. F., *Anal. Chem.*, 1978, **50**, 1371.
6 Castleden, S. L., Kirkbright, G. F., and Menon, K. R., *Analyst*, 1980, **105**, 1076.
7 Jin, Q., Kirkbright, G. F., and Spillane, D. E. M., *Appl. Spectrosc.*, 1982, **36**, 120.
8 Lewis, L. N., *J. Organomet. Chem.*, 1982, **234**, 355.
9 Ashworth, C. M., Kirkbright, G. F., and Spillane, D. E. M., *Analyst*, 1983, **108**, 1481.
10 Haas, U., *Verhandl. DPG*, 1984, **1**, 618, MO117.
11 Haas, U., and Seiler, H., *Z. Naturforsch., Teil A*, 1984, **39**, 1242.
12 Moore, T. A., *Photochem. Photobiol. Rev.*, 1983, **7**, 188.
13 Braslawsky, S. E., *Photochem. Photobiol.*, 1986, **43**, 667.
14 Buschmann, C., and Prehn, H., *Phys. Methods Plant Sci.*, 1990, **11**, 148.
15 Belton, P. S., and Tanner, S. F., *Analyst*, 1983, **108**, 591.
16 Cesar, C. L., Vargas, H., Lima, C. A. S., Mendes Filho, J., and Miranda, L. C. M., *J. Agric. Food Chem.*, 1984, **32**, 1355.
17 Haas, U., and Jäger, M., *J. Food Sci.*, 1986, **51**, 1087.
18 Vinha, C. A., Hennies, C. E., da Silva, E. C., Vargas, H. R., Reis, F. de A. M., and Cortez, J. G., *Rev. Bras. Fis. Apl. Instrum.*, 1989, **4**, 267.
19 Campbell, S. D., Yee, S. S., and Afromowitz, M. A., *IEEE Trans. Biomed. Eng.*, 1979, **26**, 220.
20 Haas, U., *Can. J. Phys.*, 1986, **64**, 1063.
21 Haas, U., Franz, J., and Nimmerfall, F., in *Photoacoustic and Photothermal Phenomena*, ed. Hess, P., and Pelzl, J., p. 552.
22 Nery, J. W., Pessoa O., Jr., Vargas, H., Reis, F. de A. M., Gabrielli, A. C., Miranda, L. C. M., and Vinha, C. A., *Analyst*, 1987, **112**, 1487.
23 Gould, J. M., *Plant Physiol.*, 1982, **10**, 1521.
24 Giese, K., Nicolaus, A., Sennhenn, B., and Kölmel, K., *Can. J. Phys.*, 1986, **64**, 1139.
25 Dendy, D. A. V., *East Afr. Agric. For. J.*, 1966, **32**, 126.
26 Bertram, B., *Farbstoffe in Lebensmitteln und Arzneimitteln*, Wissenschaftliche Verlagsgesellschaft, Stuttgart, 1989.
27 Ingram, J. S., and Francis, B. J., *Trop. Sci.*, 1969, **9**, 97.
28 *Colour Index*, Society of Dyers and Colourists, Bradford, 3rd edn., 1971, vols. I–V.
29 *CRC Handbook of Food Additives*, ed. Furia, T. E., CRC Press, Boca Raton, FL, 1980, vol. II.
30 Marmion, D. M., *Handbook of US Colorants, Foods, Drugs, Cosmetics and Medical Devices*, Wiley, New York, 3rd edn., 1991.
31 Engelhardt, J., Roed, B. L., and Didriksen, C., *NATCOL Q. Inf. Bull.*, 1988, **2**, 4.
32 Ghiraldini, J. E., in *Resumos do Seminário Corantes Naturais para Alimentos–ITAL*, Campinas, Brazil, 1989, p. 21.
33 Guimaraes, I. S., de S., in *Resumos do Seminário Corantes Naturais para Alimentos–IAL*, Campinas, Brazil, 1988, p. 42.
34 Paula, M. H., de, and Aegerter, M. A., *Anal. Lett.*, 1986, **19**, 251.

Paper 4/04530K
Received July 25, 1994
Accepted August 26, 1994

Extraction of Surfactants From Aqueous Media by Supercritical Fluid Extraction*

M. Kane, J. R. Dean† and S. M. Hitchen

Department of Chemical and Life Sciences, University of Northumbria at Newcastle, Ellison Building, Newcastle upon Tyne, UK NE1 8ST

C. J. Dowle

ICI plc, Wilton Research Centre, P.O. Box 90, Wilton, Middlesbrough, Cleveland, UK TS6 8JE

R. L. Tranter

Glaxo Manufacturing Services, Harmire Road, Barnard Castle, Co. Durham, UK DL12 8DT

Two methods for the supercritical fluid extraction (SFE) of analytes from aqueous media were evaluated: direct extraction and solid-phase extraction (SPE) discs. SPE discs were used to isolate an alcohol phenol ethoxylate (APE) non-ionic surfactant from an aqueous matrix prior to extraction using supercritical CO_2. This method was compared with the direct SFE of surfactant from the aqueous matrix. The second method allowed the continuous extraction of analyte from water using a modified extraction cell. The extraction cell was designed to maximize the exposure of the analyte to supercritical CO_2 interactions and thereby allow the continuous extraction of the analyte from an aqueous sample. The results suggest that there is a difference in the effects of diffusion and equilibrium on the extraction process for the two methods of extraction studied.

Keywords: Supercritical fluid extraction; solid-phase extraction; direct aqueous extraction; non-ionic surfactant; extraction model

Introduction

In recent years the use of supercritical fluid extraction (SFE) has become widely accepted as an alternative to more traditional methods of extraction.[1–3] Higher diffusion rates and selective solvent strengths are often quoted as the main advantages of SFE over traditional methods such as liquid–liquid and liquid–solid extraction.[4–6]

However, the published literature on analytical SFE often considers the extraction of analytes from solid matrices with little or no water content. In these, the supercritical fluid is thought to interact with the analyte on the matrix by first dissolving the analyte. Once the analyte is dissolved, diffusion forces control the rate at which it is transported into the bulk supercritical fluid. Aqueous phase extraction differs from this in that water has a very limited solubility in supercritical CO_2[7] and under standard SFE conditions mixing is by diffusion through the sample.

Research on the solubility of pure surfactants[8,9] in supercritical CO_2 has demonstrated that non-polar non-ionic surfactants tend to exhibit significant solubility, whereas those of both anionic and cationic nature show very little or no solubility. The chemical nature of surfactants, in particular their amphilic properties, and also their tendency to exist in micellar form above a concentration known as the critical micellization concentration (c.m.c.) make the extraction of surfactants using supercritical CO_2 of particular interest.

SFE has the potential to reduce significantly the complexity of the multi-step analyses currently used for the sample preparation of aqueous-based surfactant samples.[10] It has been suggested that on a larger scale SFE may prove to be a low energy, and hence a low cost, alternative to distillation and evaporation techniques currently used to isolate analytes.[11] These benefits would be valuable in the measurement of surfactants in waste waters and groundwaters.

In this paper we consider two methods currently used in SFE for the extraction of analytes from aqueous media, and compare the results for the extraction of a non-ionic surfactant by the two methods. The first method studied was the use of solid-phase extraction (SPE) discs in conjunction with SFE.[12–14] The use of SPE discs allows the removal of the aqueous part of the sample and effects preconcentration of analyte on the disc. The analyte is removed from the disc by conventional SFE. This method is particularly useful when trace levels of analyte are present in the aqueous phase. The second method, using a headspace extraction cell, allows the direct and continuous extraction of analytes from a bulk water sample.[15,16] Unlike flow-through cells, this type of cell contains the aqueous sample in the cell and avoids unwanted carryover of liquid from the extraction chamber into the collection device.

Mechanism of Extraction From Water

A non-ionic surfactant introduced into water causes a disruption of ordered hydrogen bonded regions owing to the presence of its hydrophobic chains. However, the hydrophilic oxyethylene chains provide sufficient hydrogen bonding with water molecules to compensate for the loss in energy due to the disruption process. The removal of the hydrophobic portions of the molecule from the aqueous phase in a two-phase system is entropically favoured. Hence, the surfactant will probably accumulate at the supercritical CO_2–water interface in such an orientation that its hydrophobic part is oriented towards the supercritical CO_2 phase, whereas the hydrophilic oxyethylene chain remains in the water (Fig. 1). An over-all effect of this is a disruption of the order of the water molecules at the surface resulting in a lowering of surface tension. There is a sharp cut-off point in the lowering of interfacial surface tension as the c.m.c. is reached. If we relate this to the experimentally observed behaviour of a non-ionic surfactant extracted from water using SFE, we can

* Presented by M. Kane on receipt of the Ronald Belcher Memorial Lectureship, R & D Topics Meeting, University of Hertfordshire, July, 18–19, 1994.

† To whom correspondence should be addressed.

suggest a mechanism of extraction based on two distinct stages within the extraction, *i.e.*, an equilibration stage followed by a kinetically controlled diffusion stage.

Initially, surfactant molecules present at the water–air interface, in water above its c.m.c., are aligned with the hydrophobic part towards the air and the remainder of the molecule is randomly oriented in and between micelles. When extraction begins the air phase is rapidly replaced with supercritical CO_2. Equilibrium conditions are achieved for the pressure and temperature conditions used in the experiment and the surfactant is distributed between the water and supercritical phase. Surfactant at the interface partitions into the supercritical phase and is replaced by surfactant from the bulk water. This equilibrium process continues until the concentration of surfactant reaches its c.m.c. At this point, it is suggested that the movement of surfactant across the supercritical CO_2 boundary is exothermically feasible and that the remaining surfactant is contained within the bulk water phase and is unable to be extracted owing to break up of the micelles.

Experimental

Instrumentation

For SFE, a Jasco Model 880-81 SFE/SFC back-pressure regulator (BPR) was coupled to a modular Jasco pump (880-PU) and oven (860-CO) system (Mettler–Toledo, Halstead, Essex, UK) as shown in Fig. 2. A Rheodyne (Cotati, CA, USA) 7010 switching valve was used to switch the extraction chamber in-line with the fluid path. The master pump was cooled by a refrigerated head which allows for the pumping of liquid CO_2 (Air Products, Sunderland, Tyne and Wear, UK). Supercritical conditions were attained in the oven where the flowing liquid was heated above its critical temperature *via* a pulse damper and 2 m of standard 1/16 in stainless-steel tubing. Modifier was added at an exact concentration by the second pump. This arrangement is similar to a standard gradient high-performance liquid chromatography (HPLC) system. The extraction was monitored *via* a high-pressure UV/VIS spectrophotometric detector (Jasco UV979). The system pressure was maintained by the BPR based on a high-speed needle valve, periodically opening and closing the flow path.

Collection of the analytes was at the BPR exhaust where a suitable receptacle allows trapping of the analyte and also the escape of gaseous CO_2. A modified collection vial (Fig. 3) allowed efficient separation of CO_2 and analyte. Volatile components were trapped on a Bond Elut cartridge (Phase Separations, Deeside, Clwyd, UK) and back-flushed into the vial at the end of the extraction.

Extracted analytes were quantified by UV spectrophotometry using a Shimadzu (Tokyo, Japan) UV-160 double-beam instrument with 10 mm silica cells. Alcohol phenol ethoxylate non-ionic surfactant (APE) has a wavelength of maximum absorbance at 276 nm. The extracts were quantified using a six-point calibration plot. The plot was linear over the concentration range 0–400 μg ml^{-1} with a correlation coefficient of 0.9996.

Extraction Cell Configuration for Aqueous Samples

The cell arrangement used for the extraction of analytes from the aqueous phase is shown in Fig. 4. The cell is made of 12.0 mm thick stainless steel, and has a total internal volume of 50.0 ml. The cell top screws on to the base with a 24.0 mm section of threading. A Teflon coating is used on the threading to ensure a pressure-tight seal. The seal is also maintained by a

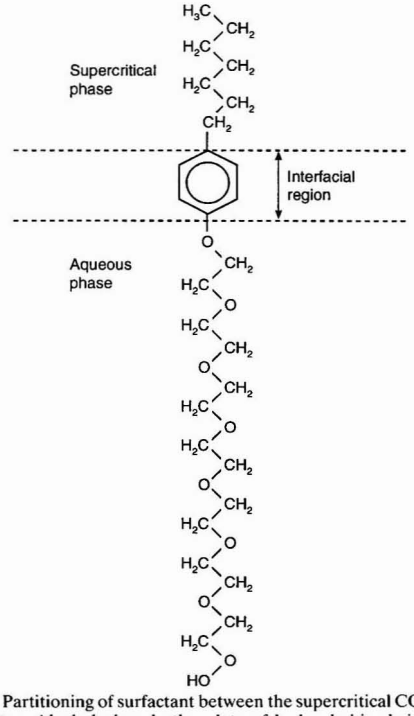

Fig. 1 Partitioning of surfactant between the supercritical CO_2 phase and water. Alcohol phenyl ethoxylate of hydrophobic chain length $n = 8$ and oxyethylene chain length $n = 8$–10.

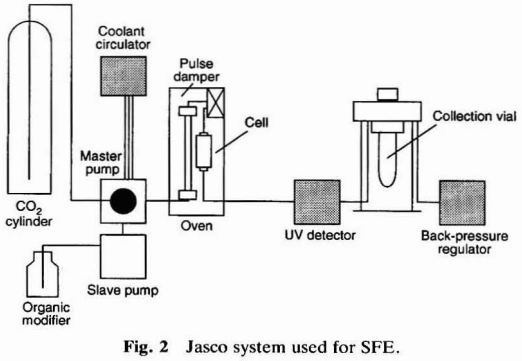

Fig. 2 Jasco system used for SFE.

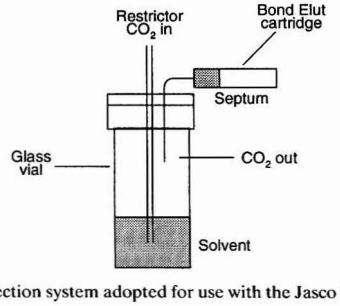

Fig. 3 Collection system adopted for use with the Jasco SFE system.

PEEK O-ring placed between the cell top and base. The 1/16 in inlet tubing is extended to the base of the chamber where it is coiled to allow a swirling motion of the flowing CO_2. The headspace configuration of the extraction cell allows the supercritical fluid to flow through the sample prior to exiting. The outlet is covered by a frit which allows only dissolved analytes to flow from the extraction chamber into the collection vessel.

A second extraction cell configuration designed to improve the mixing of the CO_2 and the area of contact between the fluid and the bulk water was also used. The modified cell configuration is shown in Fig. 5. The inlet tubing was replaced with a standard solvent filter normally used for helium sparging in HPLC. The porous 10 μm frit outlet enabled the fluid to escape through a larger surface area into the aqueous sample as a continuous stream of supercritical fluid.

Preconcentration Onto SPE Discs

Empore C_{18} bonded silica SPE discs (Jones Chromatography, Hengoed, Clwyd, UK) were used for the preconcentration of the non-ionic surfactant (APE 8–10). The aqueous sample was passed through SPE discs at flow rates of about 10 ml min^{-1}. A standard filtration apparatus was used in preconcentrating aqueous samples. Methanol (5 ml) and distilled water (10 ml) were used to activate the extraction disc immediately prior to filtering the sample through the preconcentration apparatus. A 45 ml aqueous sample took approximately 20 min to pass through the disc. The disc was partially dried by pulling air for 5 min through the filter and then drying it in an oven at 45 °C for 30 min. The discs were then ready for extraction by SFE.

Standard Sample Preparation

A 1 ml aliquot of a 1% m/v stock solution containing 10 mg of the alcohol phenyl ethoxylate (APE 8-10) (ICI, Wilton, Cleveland, UK) was diluted to 45 ml with distilled water giving an initial concentration of 222 μg ml^{-1} of APE. Samples were prepared by this method to ensure that the initial concentration of sample was consistent. The 45 ml of sample solution were then treated according to the following extraction method. For extraction using SPE discs the solution was filtered through the discs and then extracted by SFE. With continuous extraction from water the 45 ml sample was placed in the extraction cell and then extracted by SFE.

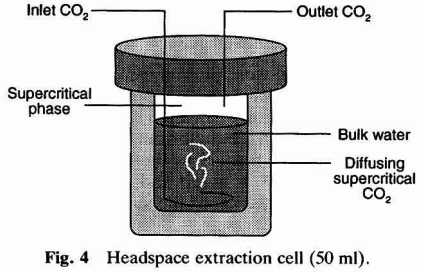

Fig. 4 Headspace extraction cell (50 ml).

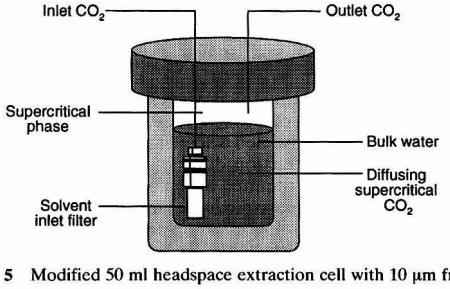

Fig. 5 Modified 50 ml headspace extraction cell with 10 μm frit.

SFE Conditions

The pressure was kept constant at 220 kg cm^{-2} and the oven temperature was set at 45 °C, resulting in a supercritical fluid density of 0.84 g ml^{-1}. The fluid was pumped at 1 ml min^{-1}. The BPR outlet, held at a temperature of 40 °C, was placed in the collection vial containing 5 ml of HiPerSolv grade methanol (Merck, Poole, Dorset, UK). SPE discs were extracted with both unmodified supercritical CO_2 and supercritical CO_2 modified with 10 vol.-% methanol. Modified CO_2 was not used when extracting from water.

Results and Discussion

Effect of Modifier on Extraction

Initial extractions from SPE discs demonstrated that the solvent strength of pure CO_2 was insufficient to extract more than 2.0 mg of the 10 mg of APE preconcentrated on the disc. Table 1 shows the results of a 30 min extraction from three separate SPE discs using first CO_2 only followed by 10 vol.-% methanol-modified CO_2. It is apparent that most of the 10 mg of APE is extracted only with the presence of modifier.

Re-use of SPE Discs

An experiment to investigate the possible re-use of SPE media was undertaken. Three discs were preconcentrated, extracted and then cleaned four times to assess the feasibility of

Table 1 Extraction of non-ionic surfactant from SPE discs. Effect of CO_2 and methanol-modified CO_2 on extraction efficiency

Sample	Recovery of APE using CO_2 only/mg	Recovery of APE using 10 vol.-% methanol-modified CO_2/mg	Total extracted (%)
Disc 1	1.6	7.1	87
Disc 2	1.9	6.9	89
Disc 3	2.2	7.3	95
			Average = 90 ± 4.3% (n = 3)

Table 2 Effect on extraction recovery from SPE discs of repeated supercritical CO_2 extraction of 10 mg of APE

Disc number	Extraction number	Extraction (%)	Mean amount extracted (%) (n = 3)
1	1	78	
2	1	92	
3	1	90	
			87 ± 7.6
1	2	100	
2	2	103	
3	2	91	
			98 ± 6.2
1	3	88	
2	3	76	
3	3	70	
			78 ± 9.2
1	4	70	
2	4	45	
3	4	65	
			60 ± 13.2

repeated use. The discs were cleaned by filtering extracted discs with 10 ml of methanol and allowing to dry for 1 h in an oven at 45 °C. Subsequent extraction of the cleaned discs showed no residual APE on the discs. The results (n = 3) demonstrate how the percentage recovery of APE decreased from 87 ± 7.56 to 60 ± 13.2% with re-use. This suggests that the effectiveness of the extraction discs deteriorates with repeated use and is consistent with the experimental observations of foaming (owing to analyte breakthrough) occurring in the filtration apparatus with re-used discs. It was also observed that re-used discs become deformed.

Effect of Static Equilibration Time on the Extraction of APE From SPE Discs

It has been reported that the inclusion of a static extraction step, where the fluid is allowed to equilibrate and permeate the sample matrix, can enhance sample extraction.[17] The repeatability of static extraction was compared with that of a dynamic extraction. A period of static extraction (5 min) followed by a 25 min dynamic extraction was performed. The supercritical CO_2 was methanol-modified (10 vol.-% methanol) with all other conditions the same as described previously. The repeatability of extraction was 100 ± 3.4% (n = 6) which was better than the previous reproducibility study with dynamic extraction alone, shown in Table 2, of 92 ± 8.8% (n = 6). Therefore, it is clear that a period of static extraction prior to dynamic extraction allows excellent recovery of the APE. Also, the results demonstrate that non-ionic surfactants can be effectively preconcentrated from aqueous samples using a combined SPE–SFE method and methanol-modified CO_2.

Table 3 Continuous extraction of APE from aqueous sample using modified cell

Extract number	Time of extraction/min	Amount extracted (%)
1	5	10
2	10	12
3	15	12
4	20	15
5	25	15
6	30	29
7	60	34
8	90	40
9	120	41

Table 4 Continuous extraction of APE from aqueous sample using modified extraction cell with 10 μm solvent filter

Extract number	Time of extraction/min	Amount extracted (%)
1	5	15
2	10	20
3	15	22
4	20	25
5	25	27
6	30	32
7	60	40
8	90	47
9	120	60

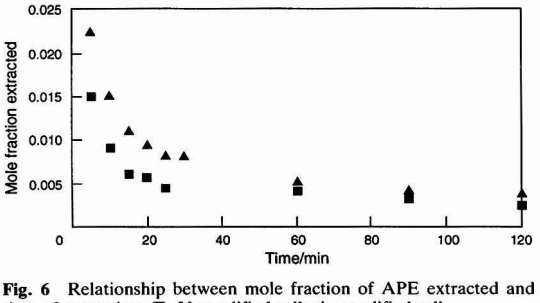

Fig. 6 Relationship between mole fraction of APE extracted and time of extraction. ■, Unmodified cell; ▲, modified cell.

Continuous Extraction of APE From Water

The practical problems of containing a liquid sample were overcome by using a headspace extraction cell of the type shown in Fig. 4. The extraction cell was modified to include a solvent filter on the inlet tube of the cell (Fig. 5). The two sample inlet configurations were compared in order to evaluate their effectiveness in continuously extracting 10 mg of the APE sample.

Initial experiments indicated that there were practical difficulties in implementing a continuous system for the direct extraction from water. The headspace extraction cell design meant that water carryover into the collection device was not a problem, although trace amounts of water observed in the collector were probably associated with the small, but finite solubility of water in CO_2.[7] However, the main problem was that even at relatively long extraction times (2 h), the amount of APE recovered was below 100% (Table 3). As discussed earlier, these poor extraction recoveries from water may be attributable to the hydrogen bonding that exists between the water and non-ionic surfactant.

It is also thought that the surface area of the extracting fluid in contact with the sample may affect the diffusion controlled part of the extraction. A larger surface area was created by the addition of a solvent filter to the inlet tube of the extraction cell (Fig. 5). The results in Table 4 show clearly that there is an improvement in extraction efficiency with the addition of the solvent filter.

The total amount of APE extracted is related to the amount of CO_2 used in the extraction and it can be expressed as the mole fraction, x,

$$x = \text{moles of APE}/(\text{moles of APE} + \text{moles of } CO_2 \text{ used})$$

Data for the extraction were plotted using this function (Fig. 6). The plot is characteristic of extraction/time profiles predicted for the extraction of an analyte from a matrix.[18] The first part of the extraction is equilibrium-controlled and results in rapid extraction with respect to the CO_2 used. The latter part of the graph is not as steep and is a result of kinetic diffusion-controlled extraction of the surfactant.

Conclusions

Two different approaches to the extraction of surfactants from a water sample have been investigated. Both methods are simple in design and require little sample preparation. Continuous extraction directly from the water matrix was improved by the addition of a 10 μm frit to the inlet tube of the extraction cell. However, the process seems to be kinetically limited as the amount of surfactant extracted with respect to the amount of CO_2 consumed is small at long extraction times. The advantage of extraction directly from water is that no sample preparation is required as the aqueous sample can be placed directly into the extraction chamber. The method has potential for use as a sample clean-up procedure for non-ionic, anionic and cationic surfactants. The possibility for selective extraction from an aqueous sample has been identified as a

major benefit of these methods owing to the potential insolubility of both anionic and cationic surfactants[8] in supercritical CO_2.

SPE discs have proved to be efficient in the trapping of surfactant molecules. The use of SFE with SPE discs has been shown to be quantitative and reproducible provided that the supercritical CO_2 is modified with methanol.

The speed of sample analysis is a major advantage of these methods. The sample throughput for one sample with the direct method is approximately 1–2 h including the time of extraction. The time is slightly longer with SPE discs, but shorter extraction times with better extraction efficiencies are possible. In comparison, current methods[19] of determining non-ionic surfactants in environmental samples involve eight separate stages prior to chromatographic analysis which can take up to 24 h per analysis.

References

1 Synder, J. L., Grob, R. L., McNally, M. E., and Oostdyk, T. S., *Anal. Chem.*, 1992, **64**, 1940.
2 King, J. W., *J. Chromatogr. Sci.*, 1989, **27**, 355.
3 Hawthorne, S. B., *Anal. Chem.*, 1990, **62**, 633A.
4 Alexandrou, N., Lawrence, M. J., and Pawliszyn, J., *Anal. Chem.*, 1992, **64**, 311.
5 Larson, K. A., and King, M. L., *Biotechnol. Prog.*, 1986, **2**, 73.
6 *Analytical Supercritical Fluid Chromatography and Extraction*, eds. Lee, M. L., and Markides, K. E., Chromatography Conferences, Provo, UT, 1990.
7 *Chemical Engineering at Supercritical Fluid Conditions*, eds. Paulitis, J. M., Gray, R. D., and Davidson, K. P., Ann Arbor Science Publishers, Ann Arbor, MI, 1983, p. 101.
8 Consani, K. A., and Smith, R. D., *J. Supercrit. Fluids*, 1990, **3**, 51.
9 Sandra, P., and David, F., *J. High Resolut. Chromatogr.*, 1990, **13**, 415.
10 *Nonionic Surfactants Chemical Analysis*, ed. Cross, J., Marcel Dekker, New York, 1987.
11 Knez, Z., Possel, F., Goblob, J., and Bauman, D., *Vestn. Slov. Kem. Drus.*, 1989, **36**, 155.
12 Tang, P. H., Ho, J. S., and Eichelbergwer, J. W., *J. Assoc. Off. Anal. Chem.*, 1993, **76**, 72.
13 Barnabas, I. J., Dean, J. R., Hitchen, S. M., and Owen, S. P., *Anal. Chim. Acta*, 1994, **291**, 261.
14 Barnabas, I. J., Dean, J. R., Hitchen, S. M., and Owen, S. P., *J. Chromatogr.*, 1994, **665**, 307.
15 Hedrick, J., and Taylor, L. T., *Anal. Chem.*, 1989, **61**, 1986.
16 Hedrick, J., and Taylor, L. T., *J. High Resolut. Chromatogr.*, 1990, **13**, 312.
17 *Applications of Supercritical Fluids in Industrial Analysis*, ed. Dean, J. R., Blackie Academic and Professional, Glasgow, 1993, p. 54.
18 *Supercritical Fluid Extraction and its use in Chromatographic Sample Preparation*, ed. Westwood, S. A., Blackie Academic and Professional, Glasgow, 1992.
19 Mattijs, E., and Hennes, E. C., *Tenside Surfactants Deterg.*, 1991, **28**, 22.

Paper 4/04535A
Received July 25, 1994
Accepted September 14, 1994

Speciation of Selenium and Arsenic Compounds in Natural Waters by Capillary Zone Electrophoresis After On-column Preconcentration With Field-amplified Injection

Ke Li and Sam F. Y. Li*

Department of Chemistry, National University of Singapore, 10 Kent Ridge Crescent, Singapore 0511, Republic of Singapore

A method for the separation and determination of selenium and arsenic compounds by capillary zone electrophoresis (CZE) was developed. On-column enrichment of selenium and arsenic was performed by stacking large volumes of samples injected onto the column with the field-amplified injection technique. Over a 100-fold preconcentration for selenium and arsenic compounds could be achieved within 3.7 min. This method was applied to the determination of selenium and arsenic species in real water samples. The detection limits were below 25 ppb. The relative standard deviations for the determination of selenium and arsenic species in water samples were in the range 4.0 to 15.6%.

Keywords: Capillary zone electrophoresis; on-column preconcentration; field-amplified injection; selenium; arsenic

Introduction

Selenium has been recognized to be an essential nutrient at low concentrations and a toxic species at higher concentrations for both humans and animals. The dietary deficiency of selenium has been known to be associated with diseases in man such as Keshan disease.[1] Studies have suggested that selenium plays a preventive role in the etiology of cancer.[2] High selenium concentrations can cause symptoms such as inflammation of feet, softening or loss of hooves and horns in animals, or loss of hair and nails and irritation of the skin and eyes in humans.[3] Therefore, there is the need for an appropriate method to be established for the accurate determination of selenium in its different chemical forms or oxidation states in various environmental and biological samples.

Compounds of arsenic are known to be highly toxic, although there is an indication that arsenic may be an essential element.[4] The toxicity of arsenic is dependent on its chemical form, the oxidation state and its solubility in biological media. The toxicity of arsenic compounds decreases in the order: arsine, inorganic As^{III}, organic As^{III}, inorganic As^{V}, organic As^{V}, arsonium compounds and elemental arsenic.[4,5] Naturally existing compounds of organic arsenic are non-toxic or of low toxicity.[4]

Various methods have been used for the determination and speciation of selenium and arsenic species. The determination of selenium(IV) by gas chromatography (GC) is an established method, which is based on the formation of the volatile compound piazselenol through the reaction between selenious acid and different substituted *o*-phenylenediamine (PDA). This reaction takes 2–4 h to go to completion.[6] Very few papers have been published on the separation and determination of arsenic using GC owing to the difficulty of converting arsenic into a volatile form.[7,8] Laintz *et al.*[9,10] reported on the separation of arsenic compounds using supercritical fluid chromatography (SFC) by complexing As^{III} with bis(trifluoroethyl)dithiocarbamate, but As^{V} cannot be determined directly. High-performance liquid chromatography (HPLC) has previously been used successfully for the separation and determination of selenium and arsenic include atomic absorption spectrometry (AAS) and inductively coupled plasma atomic emission spectrometry (ICP-AES) after hydride generation,[14–20] and cathodic stripping voltammetry.[21,22] However, these methods are difficult to use for the purpose of chemical speciation and are subject to interferences.

Recently, there has been an increasing interest in the separation and determination of ionic species using capillary zone electrophoresis (CZE) owing to its very high efficiency and simplicity. Wildman *et al.*[23] reported on the speciation of arsenite and arsenate by CZE with indirect ultraviolet (UV) detection, but only relatively high concentrations of arsenite and arsenate can be determined. There has not been any report on the separation and determination of selenium compounds using CZE methods. it is expected that CZE would be superior to GC or SFC owing to the elimination of the derivatization steps, and to HPLC because of its higher efficiency. Compared with AAS, ICP-AES and electroanalytical methods, CZE has relatively fewer interferences owing to the highly efficient separations achieved.

However, it should be noted that CZE has a relatively lower concentration sensitivity than HPLC or GC because in CZE much smaller volumes (at nanolitre levels) of samples are used, although the absolute detection limits achieved using CZE are as low as picograms. Off-line preconcentration methods such as solvent extraction[17,24–28] and cartridge extraction[17,29,30] have been used to enrich selenium and arsenic compounds. These methods are often time-consuming and laborious. In most instances it is impossible to extract Se^{IV} and Se^{VI} or As^{III} and As^{V} simultaneously. Recently, several elegant techniques such as isotachophoresis and field-amplified injection, have been employed to carry out on-column preconcentration to enhance the detection sensitivity in CZE.[31–38] Chien and Burgi[33,34] described a method to stack large volumes of analytes while pumping out the water plug in the sample matrix with an electroosmotic flow. These methods are preferred over off-line preconcentration methods because of their simplicity, rapidity, and high enrichment factors achievable.

This paper presents the separation of several selenium and arsenic species using CZE. The speciation and determination of selenium and arsenic in water samples were performed after on-column preconcentration by stacking large volumes of samples injected onto the column.

* To whom correspondence should be addressed.

Experimental

Chemicals and Reagents

Sodium selenite and sodium selenate decahydrate were purchased from Merck (Darmstadt, Germany). Sodium arsenite and disodium hydrogen arsenate were obtained from Aldrich (Milwaukee, WI, USA). Dimethylarsinic acid sodium salt was obtained from Fluka (Buchs, Switzerland). Stock solutions of about 10 mg ml^{-1} for the above standards were prepared by dissolving accurately weighed amounts of the individual standards in de-ionized water **[CAUTION:** the above compounds are toxic and should be handled with great care].

Standards at ppm and ppb levels were prepared fresh daily by stepwise dilution of the stock solutions. Sodium tetraborate and sodium dihydrogen phosphate (Merck) were used to prepare electrolyte buffer, which was passed through 0.45 μm membrane filters and degassed by ultrasonication before use. All other chemicals and reagents were of analytical-reagent grade or better. De-ionized water (18 MΩ) generated from a Millipore-Q system was used throughout the experiments.

Instrumentation

A model 270A capillary electrophoresis system (Applied Biosystems, Foster City, CA, USA), that was equipped with a reversible-polarity power supply, was used to perform the preconcentration and determination of selenium and arsenic compounds. A piece of fused silica capillary tube (Polymicro Technologies, AZ, USA) with dimensions 500 mm length and 50 μm i.d. was used to separate selenium and arsenic compounds. The detection window was at 300 mm from the injection end of the column. Ultraviolet detection was carried out at 195 nm. The electropherograms were recorded and processed with Model C-R6A Chromatopac integrator (Shimadzu, Kyoto, Japan).

Vacuum injections were used for the introduction of samples throughout the experiments. For the introduction of large volumes of samples, one of the following procedures was adopted. The first method was to inject the analyte for several successive cycles of 30 s using the 'sampling' cycle. With this method, a 1 s injection corresponded to 2.5 mm length or 4.9 nl of sample or standard solution in the capillary column. Another method was to inject the sample using the 'washing' cycle, which allowed faster introduction of samples, every 6 s, and introduced 65.4 mm or 128 nl of sample into the capillary column.

The mineral water samples were purchased from a supermarket, and were used directly for the determinations. The tap water was passed through 0.45 μm filters before analysis. The method of standard additions was used for quantitation.

Procedures of Analyte Stacking and Water Plug Removal

A large volume of standard or sample was injected onto the column using a vacuum programme in either the 'sampling' of the 'washing' cycle. A negative polarity was applied to stack the anions whilst removing the water plug with the electroosmotic flow. The gradually increasing currents were carefully monitored. The current was cut-off when it reached 95% of that of the electrophoretic buffer, which had been measured by filling the column with the buffer before injection of the sample or standard. The polarity of the power supply was then changed to positive to start the normal CZE separation and the determination of selenium and arsenic species.

Results and Discussion

CZE Separation of Selenium and Arsenic Compounds

The pH of the electrophoretic buffer affected the separation of selenium and arsenic significantly. The pH effects were attributed to its influence on the bulk electroosmotic flow and the electrophoretic flows of selenium and arsenic species, as well as on the chemical form (protonation and decomposition) of the selenium and arsenic compounds, which resulted in changes in migration times and sensitivities for both selenium and arsenic. Fig. 1 illustrates the effect of pH on the migration times of selenium and arsenic compounds. A general trend of increasing migration times of selenium and arsenic species with an increase in pH was observed.

In a normal CZE separation configuration of positive polarity, selenium and arsenic anions would be expected to reach the detection window by the electroosmotic flow overcoming the electrophoretic flows of the individual anions. As the pH is decreased, the weak acid anions could be partially protonated, and slower electrophoretic flows for the anions would be expected. Therefore, faster observed mobilities ($\mu_{ob} = \mu_{oe} - \mu_{op}$) were obtained. With an increase in pH, the separation of selenium and arsenic compounds was improved, particularly for selenate, which overlapped with the negative water peak at pH < 7.5. The separation beween selenate and arsenite could also be further improved at pH > 8.3. At pH > 9.2, selenite had the fastest electrophoretic flow. Consequently, it had the slowest observed mobility ($\mu_{eo} - \mu_{ep}$), and migrated out behind arsenate.

Fig. 2 shows the separation by CZE of five selenium and arsenic species at different pH values. Although the separation of selenate and arsenite was improved at higher pH, the separation time increased and the peak efficiencies decreased significantly under such conditions. Therefore the separation of selenium and arsenic compounds was mainly performed at low pH because high peak efficiency is more important for better stacking efficiencies.

On-column Stacking of Selenium and Arsenic Without Sample Matrix Removal

When analytes are dissolved in a matrix which has a lower conductivity than the supporting electrolyte buffer in the capillary column, the analytes will experience a locally increased electric field strength and will migrate with higher velocities. Furthermore, the analytes will slow down at the boundary between the sample and support electrolyte and stack into a much narrower zone than the original sample zone once they cross the boundary between the sample plug and the

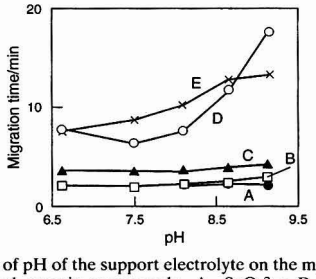

Fig. 1. Effect of pH of the support electrolyte on the mgiration time of selenium and arsenic compounds. A, SeO_4^{2-}; B, AsO_2^-; C, $Me_2AsO_2^-$; D, SeO_3^{2-}; and E, AsO_4^{2-}. Separation column, 500 mm × 0.05 μm i.d. fused capillary tube (effective length 330 nm); support electrolyte, different ratios of 0.075 mol l^{-1} NaH_2PO_4 and 0.025 mol l^{-1} $Na_2B_4O_7$; applied voltage, 20 kV.

electrophoresis buffer. Hence, the analytes are preconcentrated on-column. Obviously, this stacking effect, *i.e.*, the field-amplified injection process, is proportional to the ratio of the conductivity of the background electrolyte to that of the sample matrix. Fig. 3 shows the electropherograms of different injection volumes of selenium and arsenic compounds, without matrix water-plug removal from the capillary column. Fig. 3(*a*) was obtained for a 2.5 mm injection (*i.e.*, a volume of sample solution which occupied a 2.5 mm length of the column); Fig. 3(*b*) for a 25 mm injection of the sample used in Fig. 3(*a*) after 10 times dilution; Fig. 3(*c*) for a 50 mm injection of the sample as used in Fig. 3(*b*). It can be seen that, without water matrix removal from the column, the volume of the sample which could be injected onto the column without affecting the resolution was very limited. Although the sample was prepared in de-ionized water to be suitable for field-amplified injection, the efficiency was decreased significantly with increasing injection volume. When the injection volume was further increased to a volume corresponding to 100 mm of column, the peaks for selenium and arsenic could not be resolved [Fig. 3(*d*)]. This could be explained by the laminar broadening mechanism[31] owing to the mismatch in the electroosmotic flows between the sample plug and the support buffer. As a result, broadened peaks were obtained, which made stacking with a large enrichment factor impossible. The shortened migration times obtained for large-volume injections could be explained by the combined effects of the changed electroosmotic flow, the electrophoretic flows of the anions, and the shorter distance of migration of the anions to the detection window.

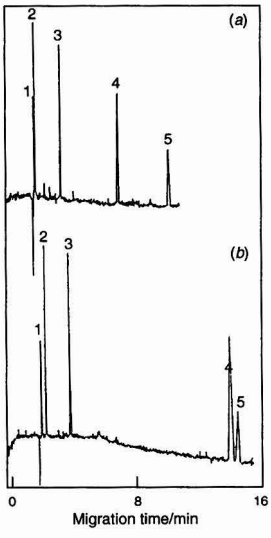

Fig. 2. CZE separation of selenium and arsenic compounds. (*a*) pH 7.65, (*b*) pH 8.65. Peak identification: 1, SeO_4^{2-}; 2, AsO_2^-; 3, $Me_2AsO_2^-$; 4, SeO_3^{2-}; 5, AsO_4^{3-}. Other conditions as in Fig. 1.

On-column Stacking of Selenium and Arsenic With Sample Matrix Removal

To eliminate the laminar broadening effect, a reversed voltage (negative) was applied to remove the water plug from the sample at the injection end whilst stacking was in progress. In a CZE configuration of negative polarity, selenium and arsenic anions could be stacked at the back of the sample plug. Concurrently, the cations were stacked at the front of the boundary and could be pumped into the buffer vial first. When the water plug was almost completely removed from the column (when the current reached about 95% of that of the background buffer as described in Experimental), the CZE system was changed back to the normal separation configuration. Fig. 4 shows the electropherograms obtained for diluted samples of selenium and arsenic compounds in de-ionized

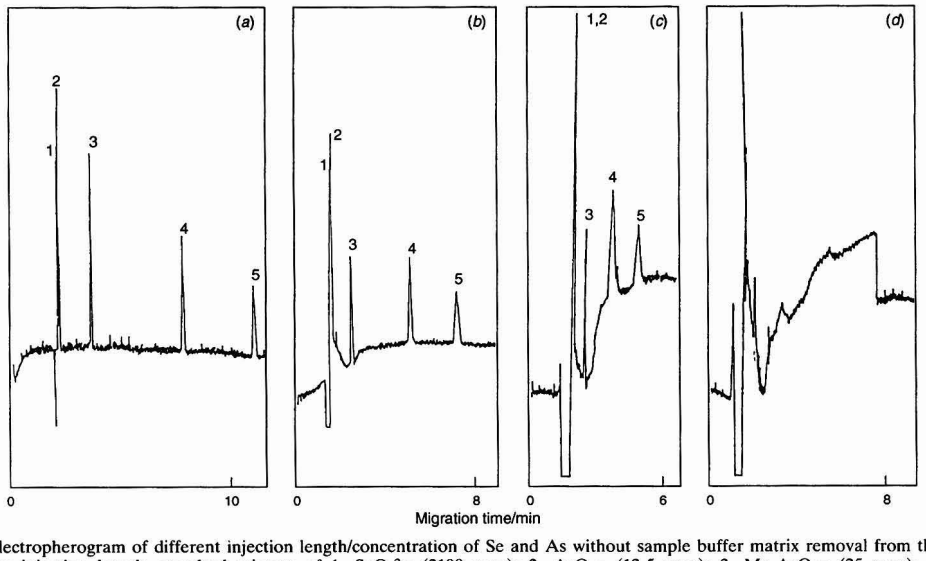

Fig. 3. Electropherogram of different injection length/concentration of Se and As without sample buffer matrix removal from the column. (*a*) 2.5 mm injection length, standard mixture of 1, SeO_4^{2-} (2190 ppm); 2, AsO_2^- (12.5 ppm); 3, $Me_2AsO_2^-$ (25 ppm); 4, SeO_3^{2-} (13.8 ppm); and 5, AsO_4^{3-} (19.3 ppm). (*b*) 25 mm injection length, standard mixture as used in (*a*) was diluted 10 times. (*c*) 50 cm injection length, standard mixture as used in (*b*). (*d*) 100 mm injection length, standard mixture as used in (*a*) was diluted 20 times. Support electrolyte, pH = 7.8, adjusted with 0.075 mol l^{-1} NaH_2PO_4–0.025 mol l^{-1} $Na_2B_4O_7$. Other conditions as in Fig. 1.

water after on-column stacking and water-plug removal. Fig. 4(*a*), (*b*) and (*c*) present the electropherograms obtained for injection lengths of a quarter, a half and a whole column, respectively. A good linear relationship between the injection length and peak area was observed, and a significant improvement in the stacking efficiencies was obtained.

As can be seen in Fig. 4, selenate was found to co-migrate with the water plug (negative peak) because it appeared very close to the water peak. It was also noted that slightly broadened peaks and decreased migration times for selenium and arsenic were obtained when very large sample volumes were injected onto the column. This could be because the analyte anions were stacked in a zone slightly wider than the sample plug normally obtained when a very small volume (generally several nanolitres) of sample was injected onto the column directly. Arsenite was also partially masked by the water peak. However, dimethylarsenite, selenite and arsenate were successfully stacked on-column.

The effects of the voltages for stacking and matrix removal on the detection sensitivity were investigated and the results are summarized in Table 1. With an increasing stacking voltage, slight decreases in the peak area were observed for AsO_2^- and $Me_2AsO_2^-$, whilst for AsO_4^{3-} and SeO_3^{2-}, no clear trend was noted. Although a high stacking voltage could stack the analytes and pump out the sample matrix within a short time, monitoring the current became difficult because of

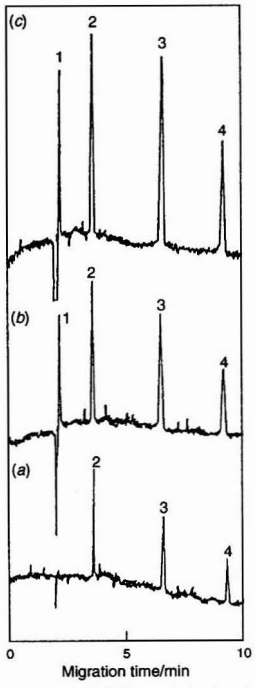

Fig. 4. Electropherograms of different injection lengths of selenium and arsenic after stacking, with sample buffer removal from the column. (*a*) Injection length of 1/4 of the column. (*b*) Injection length of 1/2 of the column. (*c*) Injection length of whole column length (500 mm). Sample: standard mixture of selenium and arsenic in de-ionized water. Peak identification: 1, SeO_4^{2-} (21.9 ppm) + AsO_2^- (249 ppb); 2, $Me_2AsO_2^-$ (250 ppb); 3, SeO_3^{2-} (185 ppb); and 4, AsO_4^{2-} (193 ppb). Electrolyte buffer pH 7.65. Stacking voltage 10 kV. Other conditions as in Fig. 1.

Table 1 Effect of stacking voltage on detection sensitivity (peak area) for selenium and arsenic compounds*

Stacking voltage/ kV	i_0†/ μA	i_s‡/ μA	t§/ min	Peak area¶/arbitrary units AsO_2^-	$Me_2AsO_2^-$	AsO_4^{3-}	SeO_3^{2-}
5	10	9	8.2	4205	8097	9046	11551
10	20	19	3.7	3712	7710	8510	11502
20	45	43	1.7	3037	7295	9102	10259

* CZE separation performed at 20 kV. Concentrations of selenium and arsenic as in Fig. 4.

† Current for the electrophoresis buffer measured at the stacking voltage.

‡ Current at which stacking was terminated.

§ Time needed for stacking and sample matrix removal.

¶ Mean value of 3–4 measurements.

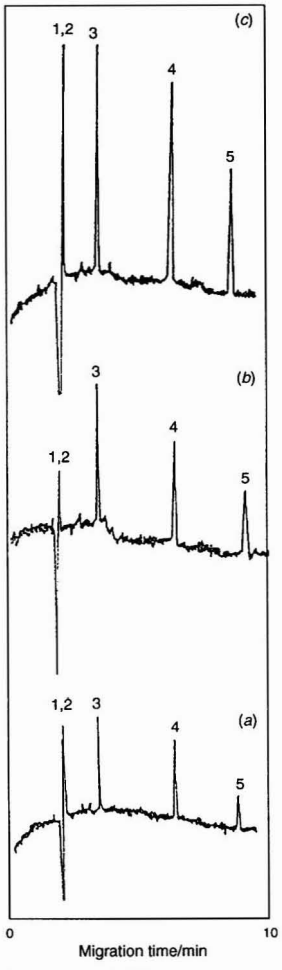

Fig. 5. Electropherograms of different concentrations of selenium and arsenic compounds after stacking. (*a*) 1, SeO_4^{2-} (5.3 ppm); 2, AsO_2^- (63 ppb); 3, $Me_2AsO_2^-$ (43 ppb); 4, SeO_3^{2-} (47 ppb); and 5, AsO_4^{3-} (48 ppb). (*b*) Injection concentration for each compound was twice that used in (*a*), peak identification as in (*a*). (*c*) Injection concentration for each compound was 4 times that used in (*a*). Injection length was 480 mm. Other conditions as in Fig. 1.

the rapid increase in current at the final stage of the stacking. Since SeO_4^{2-} and AsO_2^- had slow electrophoretic flows, they reached the detection window first owing to the large ($\mu_{eo} - \mu_{ep}$). Consequently, they could be completely (for selenate) or partially (for arsenite) pumped into the buffer container when a high stacking voltage was used. In this study, a stacking voltage of 10 kV was used to perform on-column preconcentration using the field-amplified injection technique.

Fig. 5 illustrates the results obtained for the on-column stacking of different concentrations of selenium and arsenic compounds. An excellent linear relationship between the concentrations of selenium and arsenic species and the peak areas was obtained.

Table 2 Analytical results for several water samples

	AsO_2^-	$Me_2AsO_2^-$	SeO_3^{2-}	AsO_4^{3-}
Tap water—				
Added (ppb)	0	0	0	0
Measured (ppb)	0	0	0	0
Added (ppb)	63	125	69	96.5
Measured (ppb)	—*	143	73.8	97.1
s_r (%)		4.0 ($n = 3$)	12.0 ($n = 3$)	7.8 ($n = 3$)
Added (ppb)	125	250	138	193
Measured (ppb)	—*	277	135	177
s_r (%)		15.6 ($n = 3$)	4.2 ($n = 3$)	6.0 ($n = 3$)
Mineral spring water 'Amust'†—				
Added (ppb)	0	0	0	0
Measured (ppb)	0	0	0	0
Added (ppb)	63	125	69	96.5
Measured (ppb)	—*	141	80	96.1
s_r (%)		8.5 ($n = 3$)	9.8 ($n = 3$)	4.0 ($n = 3$)
Added (ppb)	125	250	138	193
Measured (ppb)	—*	237	121	192
s_r (%)		7.0 ($n = 4$)	10.8 ($n = 4$)	10.1 ($n = 4$)

* Peak overlapped with matrix peak.
† Commercially available mineral water.

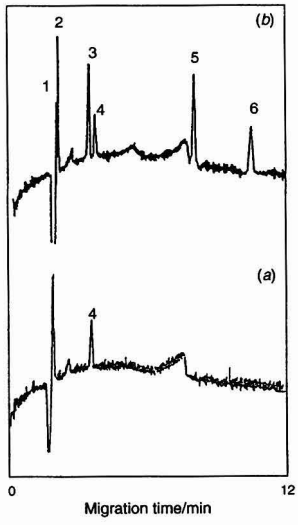

Fig. 6. Electropherograms of tap water after stacking. (*a*) Tap water and (*b*) tap water spiked with selenium and arsenic compounds. Peak identification: 1, water + SeO_4^{2-} (10.9 ppm); 2, AsO_2^- (63 ppb); 3, $Me_2AsO_2^-$ (125 ppb); 4, unknown; 5, SeO_3^{2-} (69 ppb); and 6, AsO_4^{3-} (96.5 ppb). Injection length was 480 mm. Other conditions as in Fig. 4.

Applications

In commonly encountered water samples, such as fresh water, rain water and groundwater, the concentrations of selenium and arsenic are often below 1 ppm.[4,25] These low concentrations would be beyond the detection capacity of direct CZE analysis for these compounds. However, such samples, generally, have relatively weak matrices and low conductivities. The CZE method described here is ideally suited to the determination of selenium and arsenic after on-column preconcentration by stacking large volumes of sample with field-amplified injection techniques.

Fig. 6 shows the electropherograms of selenium and arsenic species in tap water after on-column preconcentration with

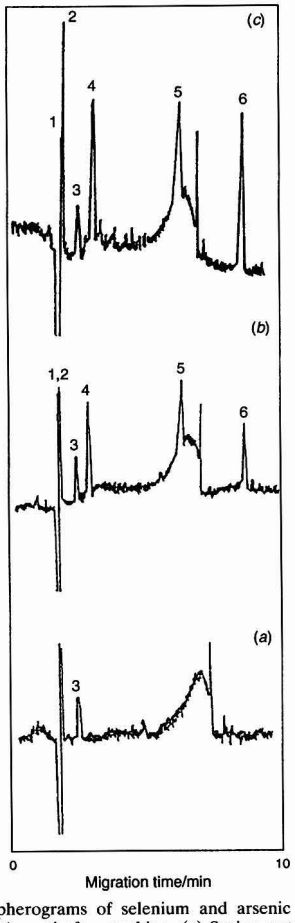

Fig. 7 Electropherograms of selenium and arsenic compounds in mineral water 'Amust' after stacking. (*a*) Spring water 'Amust'. (*b*) 'Amust' spiked with selenium and arsenic compounds. Peak identification: 1, SeO_4^{2-} (5.5 ppm); 2, AsO_2^- (63 ppb); 3, unknown; 4, $Me_2AsO_2^-$ (125 ppb); 5, SeO_3^{2-} (69 ppb); and 6, AsO_4^{3-} (96 ppb). (*c*) 'Amust' spiked with selenium and arsenic compounds. Peak identification as in (*b*), the concentration of each compound was twice that in (*b*). The CZE conditions are as in Fig. 6.

Table 3 Detection limits* of selenium and arsenic compounds obtained using the CZE method

	SeO_4^{2-}	AsO_2^-	$Me_2AsO_2^-$	SeO_3^{2-}	AsO_4^{3-}
Direct CZE (ppm)	202	0.8	2.1	1.9	3.7
CZE with stacking (ppb)	—†	—†	13	12	25
Enrichment factor	—†	—†	161	158	148

* Signal to noise ratio = 3.
† Peak overlapped with matrix peak.

field-amplified injection. It could be seen that the electropherograms were free of interferences from the simple matrix. In addition, some cations could be separated from the analytes during the stacking process. Fig. 7 shows the electropherograms of selenium and arsenic in a mineral spring-water sample. This sample had a relatively strong matrix (total ion concentrations of 80 ppm anions and cations according to the label). Although unknown peaks were detected after preconcentration, the three selenium and arsenic species were clearly identified and quantitatively preconcentrated. The results obtained for the determination of the selenium and arsenic compounds in the water samples are presented in Table 2.

Table 3 shows the detection limits for the determination of selenium and arsenic species using CZE with and without on-column stacking. It can be seen that over a 100-fold enrichment for selenium and arsenic species was readily achieved within several minutes (stacking times are listed in Table 1).

Conclusion

The CZE method for the separation of selenium and arsenic compounds reported in this work has the advantages of high efficiency and speed. It eliminates the complexing or derivatization steps often required in conventional separation techniques, such as HPLC, GC and SFC, and the efficiencies achieved are better than those of the other methods. Enrichment of selenium and arsenic compounds by stacking a large volume of sample using field-amplified injection should be a very promising preconcentration technique for the determination of these compounds in water samples owing to its simplicity and high efficiency. Compared with off-line preconcentration methods, such as solvent extraction and cartridge extraction, field-amplified injection is less labour intensive, is less time-consuming, and the sample volumes needed are much smaller than those for conventional extraction methods.

References

1 Levanda, O. A., *J. Am. Diet. Assoc.*, 1991, **91**, 1572.
2 Greeder, G. A., and Milner, J. A., *Science*, 1980, **209**, 825.
3 Shamberger, R. J., *Trace Elem. Med.*, 1986, **3**, 105.
4 Morita, M., and Edmond, J. S., *Pure Appl. Chem.*, 1992, **64**, 575.
5 McKenzie, H. A., and Smythe, L. E., *Quantitation Trace Analysis of Biological Materials*, Elsevier, Amsterdam, 1988.
6 Johansson, K., and Olin, A., *J. Chromatogr.*, 1992, **589**, 105.
7 Daughtrey, E. H., Fitchett, A. W., and Mushak, P., *Anal. Chim. Acta*, 1975, **79**, 199.
8 Yu, J. J., and Wai, C. M., *Anal. Chem.*, 1991, **63**, 842.
9 Laintz, K. E., Yu, J. J., and Wai, C. M., *Anal. Chem.*, 1992, **64**, 311.
10 Laintz, K. E., Shieh, J. M., and Wai, C. M., *J. Chromatogr. Sci.*, 1992, **30**, 120.
11 Nakagawa, A., Aoyama, E., Hasegawa, N., Kobayashi, N., and Tanaka, H., *Anal. Chem.*, 1989, **61**, 233.
12 Handelman, G. J., Kosted, P., Short, S., and Dratz, E. A., *Anal. Chem.*, 1989, **61**, 2244.
13 Maitani, T., Uchiyama, S., and Saito, Y., *J. Chromatogr.*, 1987, **391**, 161.
14 Colon, L. A., and Barry, E. F., *HRC CC J. High Resolut. Chromatogr. Chromatogr. Commun.*, 1991, **14**, 608.
15 Nham, T. T., and Brodie, K. G., *J. Anal. At. Spectrom.*, 1989, **4**, 697.
16 Ericzon, C., Petterson, J., Andersson, M., and Olin, A., *Environ. Sci. Technol.*, 1989, **23**, 1524.
17 Mentasti, E., Nicolotti, A., Porta, V., and Sarzanini, C., *Analyst*, 1989, **114**, 1113.
18 Cutter, G. A., *Anal. Chem.*, 1985, **57**, 2951.
19 Sheppard, B. S., and Caruso, J. A., *Analyst*, 1992, **117**, 971.
20 Lm-Lenung, S. Y., Cheng, V. K. W., and Lam, Y. W., *Analyst*, 1991, **116**, 957.
21 van den Berg, C. M. G., and Khan, S. H., *Anal. Chim. Acta*, 1990, **231**, 221.
22 Zelic, M., and Branica, M., *Electroanalysis*, 1990, **2**, 455.
23 Wildman, B. J., Jackson, P. E., Jones, W. R., and Alden, P. G., *J. Chromatogr.*, 1991, **546**, 459.
24 Subramanian, K., and Meranger, J. C., *Anal. Chim. Acta*, 1981, **124**, 131.
25 Putteman, F., and Massart, D. L., *Anal. Chim. Acta*, 1982, **141**, 225.
26 Jitoh, F., Imura, H., and Suzuki, N., *Anal. Chim. Acta*, 1990, **228**, 85.
27 Hocquellet, P., and Candillier, M. P., *Analyst*, 1991, **116**, 505.
28 Ritsema, R., *Microchim. Acta*, 1992, **109**, 61.
29 Johansson, K., Ornemark, U., and Olin, A., *Anal. Chim. Acta*, 1993, **274**, 129.
30 Aoyama, E., Akamatsu, K., Nakagawa, T., and Tanaka, H., *Anal. Sci.*, 1991, **7**, 617.
31 Kaniansky, D., and Marak, J., *J. Chromatogr.*, 1990, **498**, 191.
32 Jandik, P., and Jones, R., *J. Chromatogr.*, 1991, **546**, 431.
33 Chien, R. L., and Burgi, D. S., *Anal. Chem.*, 1992, **64**, 1046.
34 Chien, R. L., and Brugi, D. S., *Anal. Chem.*, 1992, **64**, 489A.
35 Stegehuis, D. S., Tjaden, U. R., and Van der Greef, J., *J. Chromatogr.*, 1992, **591**, 341.
36 Nielen, M. W. F., *TRAC, Trends Anal. Chem.*, 1993, **12**, 345.
37 Reinhoud, N. J., Tjaden, U. R., and Van der Greef, J., *J. Chromatogr.*, 1993, **641**, 155.
38 Burgi, D. S., *Anal. Chem.*, 1993, **65**, 3726.

Paper 4/05467A
Received September 7, 1994
Accepted September 15, 1994

Time-resolved Luminescence Detection of Europium(III) Chelates in Capillary Electrophoresis

Martti Latva, Timo Ala-Kleme, Heidi Bjennes, Jouko Kankare and Keijo Haapakka*

Department of Chemistry, University of Turku, FIN-20500 Turku, Finland

An instrumentally simple on-column time-resolved luminescence capillary electrophoresis (CE) detector for determining and characterizing migrated europium(III) chelates on the basis of their long-lived $^5D_0 \rightarrow {}^7F$-multiplet transitions has been constructed. In addition to the background fluorescence arising from the cell walls, this time-resolved luminescence method of measurement also allows an efficient discrimination of the analyte emission against the short-lived background fluorescence caused by possible fluorescent impurities in the electrophoresis buffer; this should provide a feasible means of constructing a CE detector for the trace analysis of europium(III) chelates and also of samples of biological interest labelled with europium(III) chelates. If supplied additionally with a device for determining the excited-state lifetimes of separated europium(III) chelates, this time-resolved luminescence detector should make possible the peak identification of migrated europium(III) chelates.

Keywords: *Capillary electrophoresis; time-resolved luminescence detection; luminescent europium(III) chelates*

Introduction

Capillary electrophoresis (CE) has established itself as an important and widely utilized tool for routine analytical separations. Presently, an important research area of CE is the development of new instrumentally simple on-column detectors which allow the detection of separated analytes at low concentration levels. So far, a wide range of detection methods based on well-known principles have been demonstrated to be useful for CE, including spectrophotometry,[1–10] fluorescence,[11–15] refractive index,[16] conductimetry,[17–22] amperometry[23–28] and mass spectrometry.[29–32] Of these detectors, the spectrophotometric detector is the most widely used and can be evaluated as follows: (*i*) it is relatively universal, (*ii*) it is instrumentally simple but (*iii*) it does not provide a low detection limit owing to the short optical pathlength available across the capillary column; to some extent, the optical pathlength can be increased by using Z-shaped[7,9] and multireflection[8,10] flow cells. However, this makes the spectrophotometric detector considerably more complicated. The conductimetric detector is also universal and instrumentally simple but provides only a relatively poor detection limit. The amperometric detector can be used for selective and sensitive detection of a variety of electroactive species; the major drawbacks of this detector are (*i*) the periodical cleaning of the working electrode required for optimum detector performance and (*ii*) the difficulty of isolating electrically the working electrode from the high-potential field across the electrophoresis capillary. The mass spectrometry detector is an ideal detector for the structural elucidation of small amounts of analytes eluting from the capillary tubing but it is not the detector for conventional analytical applications.

The second most widely used detector in CE is based on on-column fluorescence. Unlike the spectrophotometric detector, the fluorescence detector can provide (*i*) a low detection limit because its signal-to-noise ratio does not depend on the detection-cell pathlength and (*ii*) a good selectivity because only a limited number of compounds are capable of generating a sufficiently intense fluorescence at analytically useful wavelengths; this selectivity can, however, be considerably changed by using pre- or post-column derivatization of non-fluorescent analytes with a strongly fluorescent label. The chemiluminescence detector, where instead of optical excitation the analyte molecule is excited by means of an energetic chemical reaction,[33] is sensitive and selective, but its construction is complicated because of additional reagent supply pumps, reagent capillaries and the reaction capillary.

In the conventional detection mode of fluorescence in CE, the analyte response is measured against the background which actually consists of the fluorescence arising (*i*) from the cell walls and (*ii*) from fluorescent impurities in the electrophoresis buffer. The use of a confocal optical system, which limits the observation volume to a depth of several micrometres in the capillary tubing, eliminates the interference effects from cell wall fluorescence but not from impurity fluorescence. However, in order to attain a reasonably good signal-to-noise ratio to conduct trace analysis by CE, an efficient discrimination of the analyte response against this impurity fluorescence is also required; the present paper proposes a time-resolved luminescence detection method of measurement[34] as an alternative for this background discrimination.

The lowest excited state $^5D_0$ of europium(III) is efficiently shielded from interactions that lead to a rapid loss of electronic energy, and hence the europium(III) cation exhibits an exceptionally long-lived luminescence; the lifetime of the excited $^5D_0$-state of the hydrated europium(III) cation is reported to be 0.11 ms.[35] This excited state lifetime can be made longer by utilizing an appropriate multidentate chelation of europium(III) which removes coordinated radiationless water molecules from the europium(III) solvation shell, *e.g.*, the chelation of the hydrated europium(III) cation by the heptadentate ligand diethylenetriaminepentaacetic acid (DTPA) increases the $^5D_0$-state lifetime to about 0.50 ms.[36] Provided that additionally (*i*) the ligand portion of the europium(III) chelate has a strong absorption band in the ultraviolet (UV) range, (*ii*) this ligand portion has an efficient intersystem crossing, (*iii*) the lowest triplet stage energy of this ligand portion is nearly equal to or above the excited singlet state of europium(III) and (*iv*) the intramolecular

* To whom correspondence should be addressed.

energy transfer from this lowest triplet state to the excited singlet state of coordinated europium(III) is fast, a europium(III)-based luminescence may be induced, which is considerably more intense than that initiated by the hydrated europium(III) cation. In connection with pulsed nitrogen-laser excitation and with time-resolved luminescence detection to discriminate the long-lived europium(III) luminescence against the short-lived background fluorescence, it has been pointed out that the europium(III)-based luminescence provides a versatile means for the analytical determination where the ultimate detection limit is a prerequisite, *e.g.*, the use of europium(III) chelates as highly luminescent labels makes possible time-resolved fluoroimmunoassays from biological fluids such as urine, serum and plasma.[37,38]

The research group of Wallac Oy (Turku, Finland) has conducted important work as regards the synthesis and development of novel multidentate chelating agents capable of forming thermodynamically and kinetically stable europium(III) chelates that can be used as luminescent labels in time-resolved fluoroimmunoassay.[39–44] Utilizing the long-lived luminescence from the europium(III) chelates with the heptadentate ligands 2,6-bis[*N*,*N*-bis(carboxymethyl)aminomethyl]-4-benzoylphenol and 4-(phenylethynyl)-2,6-bis[*N*-*N*-bis(carboxymethyl)aminomethyl]pyridine as model chelates with exceptionally long luminescence decays, this paper describes an instrumentally simple and highly sensitive on-column time-resolved luminescence CE detector that provides the means for an efficient discrimination of the analyte luminescence not only against the background fluorescence arising from the cell walls but also against the background fluorescence resulting from fluorescent impurities in the electrophoresis buffer.

Experimental

Instrumentation

Fig. 1 shows a schematic diagram of the principal components of the CE apparatus, where the detector is located close to the cathodic end of the capillary tubing. The high voltage (HV) power supply was laboratory-made; it provided a constant 25 kV output voltage and made possible electrokinetic injections from 1 to 10 s. The 3 cm long pieces of 0.3 mm diameter platinum wire were used to fabricate the electrodes, which were located at a distance of about 5 mm from the ends of the capillary tubing. Under conditions where 120 cm long, deactivated fused silica capillary tubing (i.d. 75 μm, o.d. 330 μm) and a 0.005 mol dm^{-3} borate buffer adjusted to pH 9.2 were used, the electrophoretic current was found to be 18 μA. The capillary tubing was a product from SGE and no chemical derivatization of the capillary inner surface was carried out. The on-column luminescence microcell was fabricated by burning a 5 mm piece of polyimide coating from the capillary tubing at a distance of 100 cm from the anodic injection end; the resulting cell volume was estimated to be 20 pl.

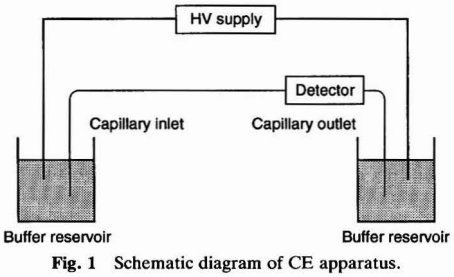

Fig. 1 Schematic diagram of CE apparatus.

A block diagram of the on-column luminescence detector is given in Fig. 2. The microcell luminescence was initiated by using a 0.5 ns, 337 nm excitation pulse from a laboratory-made compact sealed-off nitrogen laser;[45] the laser operation was controlled by a 3 ms TTL-pulse at 100 Hz obtained from a function generator supplied by GW Instruments (Model GFG-8016D). The time-resolved luminescence response was achieved using a laboratory-made conventional gated integrator which allowed freely adjustable delay and gate times of 0.1–2.0 and 0.5–10.0 ms, respectively, from the rising edge of the aforementioned TTL-pulse; a 0.1 ms delay time and a 1.0 ms gate time were found to be optimum in the present work (see Fig. 6). The head-on type photomultiplier was a product of Hamamatsu (Model R580).

Fig. 3 shows the luminescence microcell compartment in more detail. The 60 × 60 × 60 mm body of the cell compartment was made of aluminium and was supplied with an opening for the lightproof attachment of a 20 × 20 × 60 mm aluminium capillary holder (C) which was provided with two 4 mm diameter holes to attain a 90° optical pathway. The capillary was installed in this holder along a 0.4 mm diameter passage and was tightly clamped to this holder by two special screws located adjacent to the 20 pl capillary microcell in order to secure a proper focusing of the excitation laser beam onto the microcell and thus to attain an efficient detection of the emitted luminescence during CE. Additionally, a 580 nm long-pass cut-off filter (thickness 2 mm, diameter 20 mm; transmittance at 610 nm (70%) (D) and a microscope objective (×20) (E) were placed in the aluminium body as shown in Fig. 3. A focusing lens (B) inside a 40 mm diameter aluminium tube was used to focus the 337 nm excitation pulse from the nitrogen laser (A) onto the 20 pl capillary microcell. In order to minimize the interfering effect of light leaks on the emitted luminescence, the inside of the optical pathway was painted black.

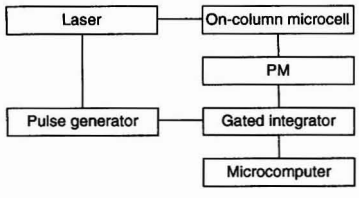

Fig. 2 Block diagram of time-resolved luminescence on-column detector.

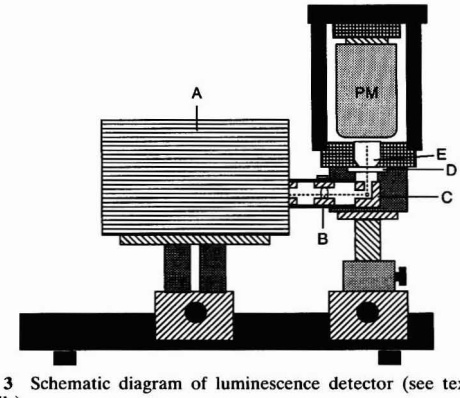

Fig. 3 Schematic diagram of luminescence detector (see text for details).

Reagents and Procedures

The reagents were purchased from the following manufacturers: sodium tetraborate decahydrate (*pro analysi*), hydrochloric acid (*pro analysi*), nitric acid (*pro analysi*) and sodium hydroxide (Suprapur) from Merck, and europium(III) nitrate (99.9%) and gadolinium(III) nitrate (99.9%) from Aldrich. All these reagents were used without further purification. 2,6-Bis-[*N*,*N*-bis(carboxymethyl)aminomethyl]-4-benzoylphenol was prepared as described in a previous paper;[46] 4-(phenylethynyl)-2,6-bis[*N*,*N*-bis(carboxymethyl)aminomethyl]pyridine was synthesized as described elsewhere.[39] Glycerin was a *pro analysi* product of Merck and was filtered through activated carbon (Aldrich, Darco G-60). Quartz-distilled water was used for the preparation of all solutions.

The capillary tubing was occasionally washed with a 0.1 mol dm^{-3} mixture of hydrochloric and nitric acids followed by careful rinsing with quartz-distilled water, with 0.1 mol dm^{-3} sodium hydroxide and, finally, with the electrophoresis buffer. In general, the electrophoretic measurements were carried out as follows: an appropriate sample solution was prepared in the electrophoresis buffer in a separate vessel, the anodic injection end of the capillary column together with the platinum electrode was immersed in this buffer vessel and a 2 s, 18 μA electrokinetic injection was conducted; the anodic end of the capillary tubing was transferred into the electrophoresis buffer reservoir and the 18 μA CE was carried out.

The luminescence measurements were made by using an LS-5 spectrometer (Perkin-Elmer); the phosphorescence experiments were performed by using appropriate gadolinium chelates in glycerol–water (5 + 4) at 77 K. A Hewlett-Packard 500 MHz digitizing oscilloscope (HP 54503A) was used to record the luminescence pulses displayed in Fig. 6.

All the luminescence intensity values are reported in arbitrary units.

Results and Discussion

Sensitized Long-lived Europium(III) Luminescence

As shown in Fig. 4(*a*), 2,6-bis[*N*,*N*-bis(carboxymethyl)-aminomethyl]-4-benzoylphenol, denoted by H_5L (according to our measurements, the acid dissociation constants of this chelating agent are $pK_{a_1} = 2.3$, $pK_{a_2} = 2.8$, $pK_{a_3} = 5.7$, $pK_{a_4} = 10.8$ and $pK_{a_5} = 12.5$, where pK_{a_3} depicts the dissociation of the phenolic hydroxyl group), is a heptadentate chelating agent, which is capable of forming a thermodynamically and kinetically stable chelate with europium(III), in which the cation is located deep inside the chelating cage formed by the phenolic hydroxyl group and two 2,2′-(methylenenitrilo)-bis(acetic acid) moieties with their one nitrogen and two oxygen donor atoms. As the dashed line in Fig. 5 shows, this europium(III) chelate has a strong excitation maximum at 324 nm and its highly intense luminescence consists of two distinct peak emissions at 590 and 613 nm; these peak emissions can be assigned to the well-known $^5D_0 \rightarrow {}^7F$-multiplet transitions of europium(III).[47] On the basis of luminescence measurements, the following mechanism can be proposed for the formation of these light-emitting europium(III) transitions: (*i*) the ligand portion of the chelate is raised to one of its higher excited singlet states at 3.8 eV by absorbing the 324 nm photon, (*ii*) this excited ligand portion immediately loses some of its excitation energy by vibrational relaxation and by internal conversion and is relaxed to its lowest excited singlet state S_1 at 2.8 eV, (*iii*) as with most aromatic carbonyl compounds, the energy difference between the lowest singlet and triplet states is small [*i.e.*, according to the phosphorescence experiments with the analogous gadolinium(III) chelate, the lowest triplet state T_1 was found to be at 2.7 eV], which makes an efficient intersystem crossing $S_1 \rightarrow T_1$ possible, (*iv*) the coordinated europium(III) cation has its excited state $^5D_2$ at 2.6 eV, which is only approximately 0.1 eV below the triplet state T_1 of the ligand portion of the chelate, thus making the intramolecular energy transfer $T_1 \rightarrow {}^5D_2$ highly probable and, finally, (v) it is proposed that this higher excited singlet state of europium(III) is immediately relaxed to the lowest excited state $^5D_0$ of europium(III), which, in turn, is deactivated to the vibrational ^7F-multiplet ground state, thus inducing the well-known peak emissions of europium(III) shown in Fig. 5; subsequently, this luminescence process has been called a sensitized luminescence of the europium(III) chelate.[48] In aqueous solution containing equimolar amounts of europium(III) and 2,6-bis[*N*,*N*-bis(carboxymethyl)aminomethyl]-4-benzoylphenol at pH 9.2, the lifetime τ_{EuL} of the radiative first-order $^5D_0 \rightarrow {}^7F$-multiplet transition was found to be 0.905 ms.

4-(Phenylethynyl)-2,6-bis[*N*,*N*(carboxymethyl)aminomethyl]pyridine [see Fig. 4(*b*)], denoted by H_4Y, is also a heptadentate chelating agent that is capable of forming a thermodynamicaly and kinetically stable europium(III) chelate, which produces an intense radiative $^5D_0 \rightarrow {}^7F$-multiplet transition of chelated europium(III) with the excitation maximum occurring at 290 nm as shown by the dotted line in Fig. 5.

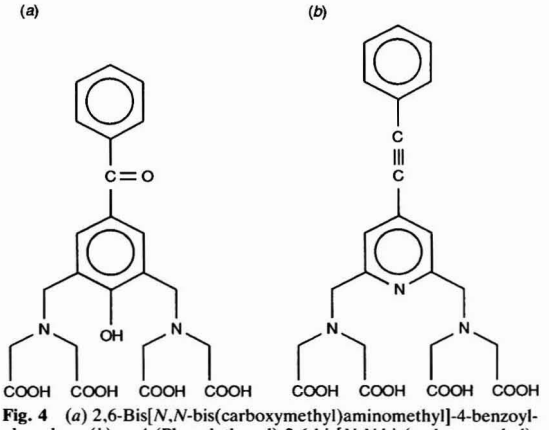

Fig. 4 (*a*) 2,6-Bis[*N*,*N*-bis(carboxymethyl)aminomethyl]-4-benzoylphenol. (*b*) 4-(Phenylethynyl)-2,6-bis[*N*,*N*-bis(carboxymethyl)-aminomethyl]pyridine.

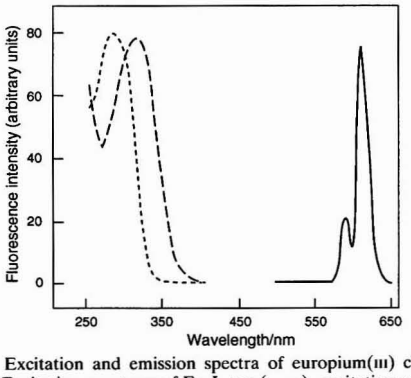

Fig. 5 Excitation and emission spectra of europium(III) chelates. (– – –), Excitation spectrum of $Eu_xL_y^{n-}$; (·····), excitation spectrum of EuY^-; (——), emission spectrum of these europium(III) chelates. Conditions: excitation wavelength, 320 or 290 nm; emission wavelength, 615 nm; 1.0×10^{-6} mol dm^{-3} europium(III); 1.0×10^{-6} mol dm^{-3} chelating agent; pH 9.2.

This europium(III)-based luminescence also shows a well-defined first-order decay with a lifetime τ_{EuY} of 0.394 ms; the lowest singlet and triplet states of this chelating agent are located at 2.8 and 2.6 eV, respectively, and on this basis, it is probable that the mechanism of this europium(III) luminescence is analogous to that of the chelate of europium(III) with 2,6-bis[*N*,*N*-bis(carboxymethyl)aminomethyl]-4-benzoylphenol presented above.

In general, the experimental lifetime (τ_{obs}) of the lowest excited state $^5D_0$ of europium(III) in an aqueous solution can be defined as follows:

$$\tau_{obs} = \tau_{H_2O} + \tau_{non\text{-}rad} + \tau_{nat} \quad (1)$$

where τ_{H_2O} is the lifetime for a radiationless energy transfer to the H_2O oscillators in the first coordination sphere of europium(III), $\tau_{non\text{-}rad}$ is the lifetime for a non-radiative de-excitation which does not involve H_2O oscillators and τ_{nat} is the natural lifetime for photon emission; the values of these lifetimes are reported to be 0.11, 4.0 and 5.3 ms, respectively.[36] These lifetime values show that the number of coordinated water molecules in the europium(III) coordination sphere plays a dominant role in the relaxation of the $^5D_0$-excited state of europium(III). The coordinated water molecule can actually be regarded as an independent radiationless oscillator, and its replacement, *e.g.*, by a D_2O molecule, causes the vibronic de-excitation pathway to become less probable which, in turn, may prolong the lifetime of this excited state of europium(III).

Horrocks and Sudnick[36] have pointed out that in H_2O–D_2O mixtures, the number of radiationless H_2O oscillators left in the europium(III) coordination sphere (q_{H_2O}) can be calculated from the equation

$$q_{H_2O} = A_{Eu^{III}}(\tau_{obs}^{-1} - \tau_{D_2O}^{-1}) \quad (2)$$

where the europium(III)-specific constant $A_{Eu^{III}}$ is reported to be 1.05, τ_{obs} and τ_{D_2O} are the lifetimes of the $^5D_0 \rightarrow {}^7F$-multiplet transitions of europium(III) in an appropriate aqueous solution and in a pure solution of deuterium oxide [*i.e.*, in a solution where instead of radiationless H_2O oscillators, all nine coordination sites of europium(III) are filled with D_2O molecules]; in general, it is accepted that τ_{D_2O} is approximately 1.8 ms. For the chelate of europium(III) with 4-(phenylethynyl)-2,6-bis[*N*,*N*-bis(carboxymethyl)aminomethyl]pyridine, in which τ_{EuY} was found to be 0.394 ms, the Horrocks and Sudnick equation predicts that the solvation shell of europium(III) contains two H_2O oscillators and, consequently, this europium(III) chelate seems to have a conventional 1:1 structure in which 4-(phenylethynyl)-2,6-bis[*N*,*N*-bis(carboxymethyl)aminomethyl]pyridine is coordinated to europium(III) by all seven of its coordination sites; this chelate will subsequently be denoted by EuY^-.

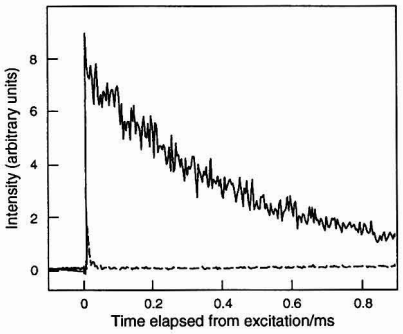

Fig. 6 Luminescence pulses from the on-column flow cell. (– – –), Background fluorescence; (——), luminescence of $Eu_xL_y^{n-}$ at the moment of the 102 s zone (see Fig. 7). Conditions: 5.0×10^{-3} mol dm^{-3} borate buffer at pH 9.2; 1.0×10^{-5} mol dm^{-3} $Eu_xL_y^{n-}$.

Correspondingly, the lifetime of the $^5D_0 \rightarrow {}^7F$-multiplet transition in the chelate of europium(III) with 2,6-bis[*N*,*N*-bis(carboxymethyl)aminomethyl]-4-benzoylphenol was found to be 0.905 ms, which can be regarded as exceptionally long and on the basis of the Horrocks and Sudnick equation, this chelate contains only half a coordinated H_2O oscillator in the europium(III) solvation shell. Taking into account that this chelating agent is only a heptadentate chelating agent, this result may well be an indication of the formation of a structurally more complicated europium(III) chelate than the aforementioned EuY^- chelate; this chelate will subsequently be denoted by $Eu_xL_y^{n-}$. Further work to elucidate the exact structure of this luminescent europium(III) chelate is currently in progress in our laboratory.

Basis and Feasibility of the Time-resolved On-column Luminescence Detector

A prerequisite in trace analysis is the efficient discrimination of the analyte response against the background response. In the luminescence CE detector, the background response (I_{BF}) can be divided into two components as follows:

$$I_{BF} = I_{CC} + I_{EB} \quad (3)$$

where I_{CC} and I_{EB} are used to depict the fluorescence responses resulting (*i*) from the cell compartment (*e.g.*, from the black-painted cell walls, from the capillary tubing, *etc.*) and (*ii*) from the fluorescent impurities in the electrophoresis buffer, respectively. A proper confocal optical system, which limits the observation volume to a depth of several micrometres in the capillary tubing, discriminates efficiently against the I_{CC} component but not against the I_{EB} component. On the other hand, a time-resolved luminescence detection may also discriminate against the I_{EB} component, provided that the analyte response is longer-lived than that of the fluorescent impurity in the electrophoresis buffer; excluding a few exceptional cases, it can be postulated that the fluorescence decay occurs on the nanosecond timescale in an aqueous solution.

As measured from the 20 pl flow cell containing the electrophoresis buffer (*i.e.*, 5.0×10^{-3} mol dm^{-3} borate buffer adjusted to pH 9.2), the dashed line in Fig. 6 shows the background fluorescence pulse after a 0.5 ns excitation pulse from the nitrogen laser; this fluorescence pulse actually consists of the I_{CC} and I_{EB} components and shows an observed lifetime of approximately $\tau_{BF} = 0.0006$ ms. Taking into account the aforementioned exceptionally long lifetimes of $\tau_{EuY} = 0.394$ ms and $\tau_{EuL} = 0.905$ ms (the solid line in Fig. 6 shows the luminescence decay curve of the $Eu_xL_y^{n-}$ chelate) obtained for the sensitized emission of the EuY^- and $Eu_xL_y^{n-}$ chelates, it is possible to conclude that these strongly luminescent europium(III) chelates can be detected in the present CE detector by a time-resolved luminescence method of measurement, which is capable of discriminating efficiently against both components of the 0.006 ms I_{BF} background fluorescence.

Fig. 7 shows a time-resolved luminescence electrophoregram, where the detection window is 0.1–1.0 ms (see Fig. 6), obtained for a 2 s, 25 kV electrokinetic injection of a mixture containing 1.0×10^{-5} mol dm^{-3} $Eu_xL_y^{n-}$ chelate and 5.0×10^{-4} mol dm^{-3} EuY^- chelate; this sample mixture was diluted from separately prepared 2.0×10^{-2} mol dm^{-3} stock solutions of $Eu_xL_y^{n-}$ and EuY^- chelates at pH 9.2. The electrophoregram shows two completely resolved zones at migration times of 61 and 102 s, and the decay times τ_{61} and

τ_{102} of the sensitized europium(III) luminescence pulses (as an example, the solid line in Fig. 6 shows the luminescence pulse measured at the moment of the 102 s zone) at the moments of zone intensity maxima were found to be 0.390 and 0.910 ms, respectively; on the basis of these decay times, the 61 and 102 s zones can be attributed to the EuY^- and $Eu_xL_y^{n-}$ chelates, respectively. As compared with that of the EuY^- chelate, the unexpectedly long migration time of the $Eu_xL_y^{n-}$ chelate may well be evidence for a polynuclear chelate in which a stronger negative charge is responsible for this comparatively slow electrophoretic migration. The EuY^- chelate produces about a 100-fold weaker time-resolved response than the $Eu_xL_y^{n-}$ chelate, which is mainly due to its inefficient excitation by the 337 nm nitrogen laser used in this work (*i.e.*, the excitation maxima of the EuY^- and $Eu_xL_y^{n-}$ chelates are 290 and 324 nm, respectively). Finally, Fig. 8 shows the electrophoretic peak intensity as a function of the concentration of the $Eu_xL_y^{n-}$ chelate in the injected sample solution; on this basis, the detection limit for the electrophoretically migrated $Eu_xL_y^{n-}$ chelate is approximately 1×10^{-7} mol dm^{-3}, and this time-resolved detection mode responds linearly to chelated europium(III) over about three orders of magnitude up to about 1×10^{-4} mol dm^{-3}. In conclusion, these results can be regarded as reasonable, particularly when it is taken into account that the present time-resolved luminescence CE detector has not been constructed from any sophisticated commercial devices and does not contain any system to compensate for the variations in the intensity of the excitation pulses of the nitrogen laser.

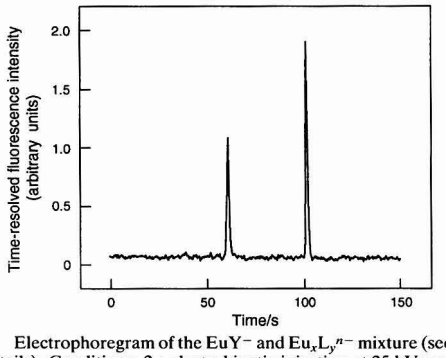

Fig. 7 Electrophoregram of the EuY^- and $Eu_xL_y^{n-}$ mixture (see text for details). Conditions: 2 s electrokinetic injection at 25 kV; applied voltage, 25 kV; effective length of capillary tubing, 50 cm; 5.0×10^{-3} mol dm^{-3} borate buffer adjusted to pH 9.2; 5.0×10^{-4} mol dm^{-3} $Eu_xL_y^{n-}$; solutions de-aerated with nitrogen; time-resolved luminescence detection: delay time, 0.1 ms; gate time, 1.0 ms.

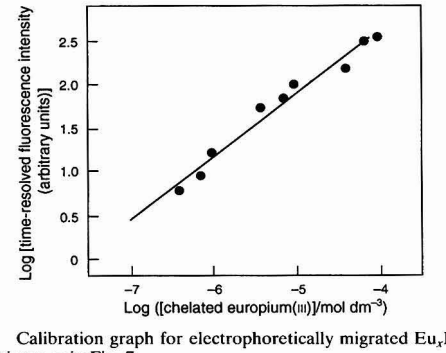

Fig. 8 Calibration graph for electrophoretically migrated $Eu_xL_y^{n-}$. Conditions: as in Fig. 7.

It is obvious that as in conventional time-resolved lanthanide(III) spectrofluorimetry,[37] the furnishing of these kinetically stable europium(III) chelates with appropriate linking groups provides a means of using these chelates as luminescent labels in conventional pre- and post-column derivatization of a variety of samples of biological interest, *e.g.*, amino acids, peptides and proteins, which makes possible the CE determination of these europium(III)-labelled analytes using a time-resolved luminescence detector. Under optimized experimental conditions, this time-resolved detection technique may provide a significant selectivity improvement because only the migrated compounds attached covalently to the europium(III) chelate by the appropriate linking group are capable of producing a detectable luminescence response. Finally, the furnishing of the time-resolved on-column luminescence detector with a device for determining the excited-state lifetimes of migrated europium(III) chelates creates the basis for peak identification and for the evaluation of the structures of these chelates.

The research group of Wallac Oy, Turku, Finland is thanked for the gift of 2,6-bis[*N*,*N*-bis(carboxymethyl)aminomethyl]-4-benzoylphenol and 4-(phenylethynyl)-2,6-bis[*N*,*N*-bis(carboxymethyl)aminomethyl]pyridine.

References

1 Walbroehl, Y., and Jorgenson, J., *J. Chromatogr.*, 1984, **315**, 135.
2 Prusik, Z., Kasicka, V., Stanek, S., Kuncova, G., Hayer, M., and Vrkoc, J., *J. Chromatogr.*, 1987, **390**, 87.
3 Wang, T., Hartwick, R., and Chaplin, P., *J. Chromatogr.*, 1989, **462**, 147.
4 Kobayashi, S., Ueda, T., and Kikumoto, M., *J. Chromatogr.*, 1989, **480**, 179.
5 Sepaniak, M., Swaile, D., and Powell, A., *J. Chromatogr.*, 1989, **480**, 185.
6 Rohlicek, V., and Deyl, Z., *J. Chromatogr.*, 1989, **494**, 87.
7 Chevret, J., van Soest, R., and Ursen, M., *J. Chromatogr.*, 1991, **543**, 439.
8 Taylor, J., and Yeung, E., *J. Chromatogr.*, 1991, **550**, 831.
9 Xi, X., and Yeung, E., *Appl. Spectrosc.*, 1991, **45**, 1199.
10 Wang, T., Aiken, J., Huie, C., and Hartwick, R., *Anal. Chem.*, 1991, **63**, 1372.
11 Jorgenson, J., and Lukacs, K., *Anal. Chem.*, 1981, **53**, 1298.
12 Green, J., and Jorgenson, J., *J. Chromatogr.*, 1986, **352**, 337.
13 Rose, D., and Jorgenson, J., *J. Chromatogr.*, 1988, **447**, 117.
14 Tsuda, T., Weinberger, R., Sapp, E., and Moring, S., *Anal. Chem.*, 1991, **63**, 417.
15 Hernandez, L., Escalona, J., Joshi, N., and Guzman, N., *J. Chromatogr.*, 1991, **559**, 183.
16 Chen, C., Demana, T., Huang, S., and Morris, M., *Anal. Chem.*, 1989, **61**, 1590.
17 Huang, X., Pang, T., Gordon, M., and Zare, R., *Anal. Chem.*, 1987, **59**, 2747.
18 Huang, X., Gordon, M., and Zare, R., *J. Chromatogr.*, 1988, **425**, 385.
19 Beckers, J., Verheggen, T., and Evaraerts, F., *J. Chromatogr.*, 1988, **452**, 591.
20 Huang, X., Luckey, J., Gordon, M., and Zare, R., *Anal. Chem.*, 1989, **61**, 766.
21 Huang, X., Gordon, M., and Zare, R., *J. Chromatogr.*, 1989, **480**, 285.
22 Huang, X., Zare, R., Sloss, S., and Ewing, A., *Anal. Chem.*, 1991, **63**, 189.
23 Wallingford, R., and Ewing, A., *Anal. Chem.*, 1987, **59**, 678.
24 Wallingford, R., and Ewing, A., *Anal. Chem.*, 1987, **59**, 1762.
25 Wallingford, R., and Ewing, A., *Anal. Chem.*, 1988, **60**, 258.
26 Wallingford, R., and Ewing, A., *Anal. Chem.*, 1988, **60**, 1972.
27 Wallingford, R., and Ewing, A., *J. Chromatogr.*, 1988, **441**, 299.

28 Wallingford, R., and Ewing, A., *Anal. Chem.*, 1989, **61**, 98.
29 Olivares, J., Nguyen, N., Yonker, C. , and Smith, R., *Anal. Chem.*, 1987, **59**, 1230.
30 Smith, R., Barinaga, C., and Udseth, H., *Anal. Chem.*, 1988, **60**, 1948.
31 Moseley, M., Deterding, L., Tomer, K., and Jorgenson, J., *J. Chromatogr.*, 1989, **480**, 197.
32 Thibault, P., Pleasance, S., and Laycook, M., *J. Chromatogr.*, 1991, **542**, 483.
33 Wu, N., and Huie, C., *J. Chromatogr.*, 1993, **634**, 309.
34 Soini, E., and Lövgren, T., *CRC Crit. Rev. Anal. Chem.*, 1987, **18**, 105, and references cited therein.
35 Stein, G., and Wurzberg, E., *J. Chem. Phys.*, 1975, **62**, 208.
36 Horrocks, W., Jr., and Sudnick, D., *Acc. Chem. Res.*, 1981, **14**, 384.
37 Hemmilä, I., *Applications of Fluorescence in Immunoassays*, Wiley, New York, 1991.
38 Diamandis, E., and Christopoulos, T., *Anal. Chem.*, 1990, **62**, 1149A.
39 Takalo, H., Pasanen, P., and Kankare, J., *Acta Chem. Scand., Ser. B*, 1988, **42**, 373.
40 Takalo, H., Kankare, J., and Hänninen, E., *Acta Chem. Scand., Ser. B*, 1988, **42**, 448.
41 Takalo, H., Hänninen, E., and Kankare, J., *Helv. Chim. Acta*, 1993, **76**, 877.
42 Mukkala, V.-M., Sund, C., Kwiatkowski, M., Pasanen, P., Högberg, M., Kankare, J., and Takalo, H., *Helv. Chim. Acta*, 1992, **75**, 1621.
43 Mukkala, V.-M., and Kankare, J., *Helv. Chim. Acta*, 1992, **75**, 1578.
44 Mukkala, V.-M., Helenius, M., Hemmilä, I., Kankare, J., and Takalo, H., *Helv. Chim. Acta*, 1993, **76**, 1361.
45 Harju, R., Laiho, R., Kojola, H., and Soini, E., *Wallac Report*, 1981.
46 Kankare, J., Fälden, K., Kulmala S., and Haapakka, K., *Anal. Chim. Acta*, 1992, **256**, 17.
47 Reisfeld, R., *J. Res. Natl. Bur. Stand., Sect. A*, 1972, **76**, 613.
48 Nugent, L., Bhaumik, M., George, S., and Lee, S., *J. Chem. Phys.*, 1964, **41**, 1305.

Paper 4/03939D
Received June 29, 1994
Accepted September 11, 1994

Determination of Baclofen in Human Plasma and Urine by High-performance liquid chromatography with Fluorescence Detection

Sedat Tosunoğlu and Lale Ersoy

Faculty of Pharmacy, Department of Analytical Chemistry, University of Istanbul, 34452 Beyazit, Istanbul, Turkey

An isocratic reversed-phase column liquid chromatographic assay for baclofen was developed. Prior to analysis, derivatization of urine or deproteinized plasma with 4-chloro-7-nitrobenzofurazan (NBD-Cl) reagent was employed. After solid-phase extraction on a small silica gel column, the mixture was chromatographed on a 10 μm Bondapak C_{18} column using methanol–water (45 + 55 v/v) as the mobile phase. The NBD-baclofen derivative was detected spectrofluorimetrically by monitoring the emission at 524 nm with excitation at 463 nm. The method was tested for suitability in routine analysis. After a single oral dose of 20 mg of baclofen, the plasma concentration and the cumulative urinary excretion of the drug were determined. The average recoveries were 99.5 and 98.5% for plasma and urine, respectively.

Keywords: Baclofen determination; 4-chloro-7-nitrobenzofuran; high-performance liquid chromatography; biological fluid

Introduction

Baclofen is a *p*-chlorophenyl analogue of γ-aminobutyric acid (GABA) and is widely used as a muscle relaxant in the treatment of spastic disorders. To obtain the maximum effect and to carry out pharmacokinetic studies, sensitive and specific analytical procedures are necessary. For this purpose, several methods to determine baclofen in biological fluids have been reported. Degen and Riess[1] and Kochak and Honc[2] developed gas–liquid chromatographic methods with electron-capture detection involving extraction and derivatization steps. Another GC method was developed by Sioufi *et al.*[3] utilizing a capillary column. Several high-performance liquid chromatographic (HPLC) methods have been published for the assay of baclofen in biological fluids. The drug was determined by utilizing either UV absorbance[4–6] or fluorescent derivatives[7,8] after various extraction procedures. Thin-layer chromatographic[9] and mass fragmentographic[10] methods have also been used for the determination of baclofen in biological fluids.

In this paper, a selective and sensitive HPLC method for the determination of baclofen in plasma and urine which is based on a derivatization reaction with 4-chloro-7-nitrobenzofurazan (NBD-Cl) is reported. After the derivatization procedure, small silica gel columns were used to separate the fluorescent NBD-baclofen derivative from the endogenous amino acid derivatives. The method was tested for suitability in routine analysis after the therapeutic doses of baclofen.

Experimental

Materials and Reagents

Baclofen was supplied by Ciba-Geigy (Basle, Switzerland). Solvents and other chemicals were of analytical-reagent grade (Merck, Darmstadt, Germany) and were used as received. Water was doubly distilled. For solid-phase extraction, small columns (25 mm × 6 mm i.d.) were prepared by using silica gel of 0.063–0.200 mm particle size (Merck).

A stock standard solution of baclofen was prepared in water (0.5 μg ml^{-1}) and stored at 4 °C. Plasma or urine samples containing known amounts of baclofen were prepared by adding the appropriate volume of this baclofen solution to the drug-free plasma or urine.

Apparatus

HPLC determinations were performed with a Model 6000 A solvent-delivery system, a U6K universal injector and a Model 470 fluorescence detector (Waters, Milford, MA, USA) using an excitation wavelength of 463 nm, an emission wavelength of 524 nm and a time constant of 0.5 s. The detector was connected to a strip-chart recorder (Linear 355). The HPLC column used was 10 μm Bondapak C_{18}, 300 mm × 3.9 mm i.d. (Waters). The mobile phase was methanol–water (45 + 55 v/v). The mobile phase was filtered through a 0.45 μm filter (Millipore, Bedford, MA, USA) and a flow rate of 0.4 ml min^{-1} at ambient temperature was employed.

The concentration of baclofen in the samples was determined from the peak areas.

Procedure

The preparation of blood samples for analysis and the derivatization reaction with NBD-Cl were similar to those described previously.[11] Blood samples placed in citrated tubes were centrifuged immediately to obtain the plasma, which was stored −20 °C until assayed.

A 0.5 ml plasma sample was deproteinized by adding 2 ml of methanol. After centrifugation, 1 ml of the supernatant liquid or 0.1 ml of urine sample was reacted with NBD-Cl by adding 0.5 ml of sodium tetraborate buffer solution (pH 9) and 0.25 ml of methanolic reagent solution (0.2%). The mixture was heated at 60 °C for 45 min and acidified with 0.1 mol l^{-1} HCl, then extracted with 5 ml of ethyl acetate. In contrast to the densitometric study,[11] the ethyl acetate extract should be purified prior to HPLC by solid-phase extraction using a small silica gel column. For this reason, 3 ml of the extract were evaporated to about 0.5 ml and dried with anhydrous Na_2SO_4, then passed through the column wetted with ethyl acetate.

The extract was eluted with the same solvent to obtain a final volume of 2 ml. The solvent was evaporated to dryness under nitrogen in a block heater at 50 °C. The residue was generally dissolved in 1 ml of mobile phase and 10 μl were injected into the HPLC system with a Hamilton injector.

Recovery and Linearity Studies

The recovery of baclofen from plasma or urine was determined by comparing the results obtained with those for an aqueous baclofen standard solution at the same concentration and under the same conditions. The recoveries were determined as the means of triplicate measurements.

The linearity between baclofen concentration and peak area was determined with samples containing 25, 50, 100, 150, 200 and 250 ng of baclofen per 0.5 ml of plasma or 0.1 ml of urine.

Reproducibility

The relative standard deviation was determined at three different concentrations of baclofen in plasma and urine by using the proposed method.

Experiment with a Healthy Volunteer

After oral administration of 20 mg of baclofen (2 h after breakfast) to a 45-year-old healthy woman, venous blood samples of 1–2 ml were drawn at pre-determined intervals for a total period of 24 h. Urine samples were also collected at intervals for up to 30 h. The blood specimens collected in citrated tubes and the urine samples were stored at −20 °C until analysis.

Results and Discussion

Typical chromatograms obtained from drug-free and spiked plasma samples are shown in Fig. 1. The drug-free plasma showed no interferences at the retention time of the NBD-baclofen derivative. The chromatograms of urine samples are the same as those obtained for plasma samples. The excitation and emission maxima of the fluorescent NBD-baclofen derivative are 463 and 524 nm, respectively. The retention time of the derivative is 4.0 min and the run time is 20 min.

To obtain an isolated NBD-baclofen peak, a solid-phase extraction procedure seemed to be necessary. For this purpose, the ethyl acetate extract of reaction mixture was passed through a small silica gel column. To retain the interfering substances successfully, the extract should contain no water, *i.e.*, it must be completely dried with anhydrous Na_2SO_4, otherwise interfering substances cannot be retained by inactive silica gel. A small amount of anhydrous Na_2SO_4 can be placed at the top of the silica gel column.

The mean recoveries of baclofen were in the range 97.4–101.5% for plasma and 96–101% for urine at three different concentrations and the relative standard deviations were below 7% (Table 1).

For the concentration range 25–250 ng of baclofen per 0.5 ml of plasma (r = 0.9997) or 0.1 ml of urine (r = 0.9995), a linear calibration graph was obtained. The limit of detection was 10 ng for 0.5 ml of plasma or 0.1 ml of urine, at a signal-to-noise ratio of 3. These values correspond to 40 pg in an injection volume of 10 μl.

Although the working range of present method was higher than those of GC–mass fragmentographic[10] or HPLC[6,7] methods, its limit of quantification is suitable for pharmacokinetic investigations. The recoveries are similar to[7,9,10] or even higher than[4] those of previous methods.

To test the applicability of proposed HPLC method for pharmacokinetic studies, an experiment was performed with a healthy volunteer. After a single oral dose of 20 mg of baclofen, the plasma concentration–time curve shown in Fig. 2 was obtained. A maximum concentration of 270 ng ml^{-1} in plasma was reached at 2.5 h. The cumulative urinary excretion

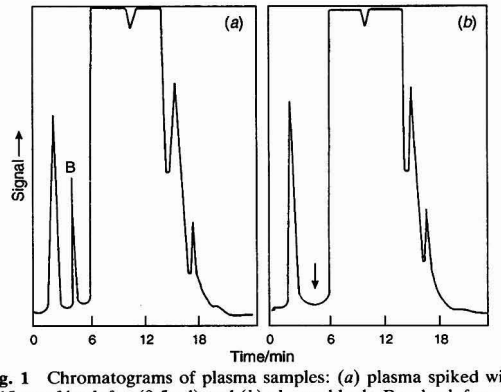

Fig. 1 Chromatograms of plasma samples: (*a*) plasma spiked with 0.15 μg of baclofen (0.5 ml) and (*b*) plasma blank. B = baclofen.

Table 1 Relative standard deviations (s_r) and recoveries in the assay of baclofen added to plasma and urine (n = 3)

Sample	Amount added/ng	Amount found: Mean	Amount found: s_r (%)	Mean recovery (%)
Plasma (0.5 ml)	50	48.7	6.3	97.4
	100	98.3	6.2	98.3
	200	203.0	4.0	101.5
Urine (0.1 ml)	50	48.0	5.5	96.0
	100	101.0	3.0	101.0
	200	197.7	3.3	98.9

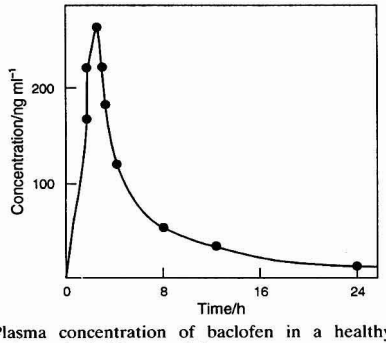

Fig. 2 Plasma concentration of baclofen in a healthy woman volunteer after a single 20 mg oral dose.

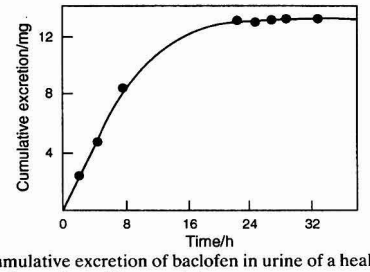

Fig. 3 Cumulative excretion of baclofen in urine of a healthy woman volunteer after a single 20 mg oral dose.

of the drug is shown in Fig. 3; 65% of the baclofen taken was excreted unchanged within 30 h after oral administration.

The proposed method showed high sensitivity and reproducibility. The derivatization and purification procedures are relatively simple and derivatized baclofen can be extracted with high recovery. Hence this method provides a sensitive and selective analytical procedure for use in bioavailability and pharmacokinetic studies.

References

1 Degen, P. H., and Riess, W., *J. Chromatogr.*, 1976, **117**, 399.
2 Kochak, G., and Honc, F., *J. Chromatogr.*, 1984, **310**, 319.
3 Sioufi, A., Kaiser, G., Leroux, F., and Dubois, J. P., *J. Chromatogr.*, 1988, **450**, 221.
4 Harrison, P. M., Tonkin, A. M., and McLean, A. J., *J. Chromatogr.*, 1985, **339**, 424.
5 Wuis, E. W., van Beijsterveldt, L. E. C., Dirks, R. J. M., Vree, T. B., and van der Kleyn, E., *J. Chromatogr.*, 1987, **420**, 212.
6 Sallerin-Caute, B., Monsarrat, B., Lazorthes, Y., Cros, J., and Bastide, R., *J. Liq. Chromatogr.*, 1988, **11**, 1753.
7 Wuis, E. W., Dirks, R. J. M., Vree, T. B., and van der Kleyn, E., *J. Chromatogr.*, 1985, **337**, 341.
8 Spahn, H., Krauss, D., and Mutschler, E., *Pharm. Res.*, 1988, **5**, 107.
9 Krauss, D., Spahn, H., and Mutschler, E., *Arzneim.-Forsch.*, 1988, **38**, 1533.
10 Swahn, J. G., Beving, H., and Sedvall, G., *J. Chromatogr.*, 1979, **162**, 433.
11 Ersoy, L., *Analyst*, 1990, **115**, 1559.

Paper 4/04172K
Received July 8, 1994
Accepted September 5, 1994

Real-time Analysis of Multicomponent Chromatograms: Application to High-performance Liquid Chromatography

Atsushi Yamamoto, Akinobu Matsunaga, Mikiya Ohto and Eiichi Mizukami

Toyama Institute of Health, 17-1, Nakataikoyama, Kosugi-machi, Toyama 939-03, Japan

Kazuichi Hayakawa and Motoichi Miyazaki

Faculty of Pharmaceutical Sciences, Kanazawa University, 13-1, Takara-machi, Kanazawa 920, Japan

In liquid chromatography with photodiode array detection, a number of approaches have been developed in chemometrics to determine an analyte of interest in the presence of one or more unknown compounds. So far, these techniques have required time-consuming data analysis programs, and are not suitable for routine analysis. A 'derivative spectrum chromatogram' is proposed as a new approach for resolving overlapped peaks in real time. This procedure is based on the following assumptions: (*i*) an absorption spectrum of an analyte with rounded humps changes to steep peaks by high-order derivatization; and (*ii*) the principle of superposition is valid for the derivative spectra of a sample mixture. The performance of this procedure is assessed with real data for the separation of pesticides by liquid chromatography.

Keywords: *Chemometrics; overlapped peaks; derivative spectrometry; high-performance liquid chromatography; photodiode array detector*

Introduction

A photodiode array (PDA) UV/VIS detection permits the continuous measurement of spectral changes in column effluents during chromatographic analysis without stopping the delivery. A large amount of data obtained by PDA, however, have merely been utilized for peak purity checks by the ratiogram technique owing to the limitations in ability of the data processor. Recently, these data have come to be used very often for the analysis of multicomponent chromatograms. In particular, procedures based on factor analysis[1] have been rapidly developed in chemometrics to resolve overlapped peaks along with the development of PDA.[2–5] These procedures have enabled one to estimate both the elution profile and the absorption spectrum of a component in a cluster of closely eluting peaks with high accuracy.[6–8] However, these PDA data were analysed off-line by time-consuming data analysis programs, so it is desirable to develop a procedure for real-time analysis.

The lack of selectivity of photometric detectors is attributable to the breadth and continuity of the absorbance spectra of analytes. However, this continuity allows analysis *via* derivative spectra. The aspect in which the derivative spectrum differs from the parent spectrum is the presence of the 'zero-crossing point', and derivative spectrophotometry at this wavelength has been used to determine drug contents in pharmaceutical dosage forms[9] and nutrient contents in foodstuffs[10,11] without separation. The shapes of derivative spectra vary from rounded humps to steep bands as their orders become higher, which may permit more selective identification and determination of overlapping chromatographic peaks. In this work, we have established a novel approach to the analysis of multicomponent chromatograms processed in real time by plotting the maximum or minimum amplitude of a high-order derivative spectrum of the analyte against analysis time. We have named this approach a 'derivative spectrum chromatogram' and as an example applied it to the HPLC separation of pesticides.

Experimental

Chromatography

The liquid chromatographic system consisted of a Shimadzu (Kyoto, Japan) LC-9A pump, a Rheodyne (Cotati, CA, USA) Model 7125 injector and a Shimadzu CTO-10AC column oven. Chromatographic separation was performed on a 25 cm × 4.6 mm i.d. reversed-phase column (LiChrospher 100 RP-18; Cica-Merck, Tokyo, Japan) maintained at 40 °C. Acetonitrile–water was used as the mobile phase at a flow rate of 1 ml min^{-1}. The PDA detector was a Shimadzu SPD-M6A, set up to collect spectra at 2 s sampling intervals and covering the wavelength range 210–360 nm. Data were stored on an NEC (Tokyo, Japan) PC-9801 RA personal computer.

Reagents

Acetonitrile was of HPLC grade (Wako, Osaka, Japan) and water was distilled and de-ionized. All pesticides were of analytical–pesticide grade purchased from Wako or GL Sciences (Tokyo, Japan), and were dissolved in acetonitrile at a concentration of 100 ppm to prepare stock standard solutions.

Data Analysis

For calculating the derivative values from the digital data of the absorbance spectra stored on floppy disks, the Savitzky–Golay polynomial algorithm[12] was used. All the programs were written by the authors in N_{88}-BASIC version 5.0 (Microsoft, Redmond, WA, USA).

Results and Discussion

Preparation of Derivative Spectrum

In order to obtain high-order derivative values from PDA data, the least-squares method can be used. When a polynomial of degree m was determined by mean square fitting through a set of n consecutive data, an arbitrary order derivative value at an arbitrary wavelength could be calculated

from this polynomial. For data points at uniform intervals on the abscissa, Savitzky and Golay[12] developed a very simple procedure for derivative convolution.

The SPD-M6A PDA detector used in this experiment measures the spectra of analytes at intervals of about 1 nm. Fig. 1 shows the zeroth-(smoothing) to fourth-order derivative spectra of the fungicide chlorothalonil, which were prepared from PDA data at the peak maximum by using the Savitzky–Golay procedure. The following relationship exists between the number of data, n, and the degree of polynomial, m: when n is much larger than m, the most minute details of the spectrum disappear, whereas the calculated spectrum becomes noisy by affecting the fluctuating data as n becomes small. When m is fixed (the sixth-degree polynomial convolution was employed in Fig. 1), n should decrease as the order of the derivative increases. It was found that the most suitable conditions were to use the fourth-order derivative spectrum at $n = 11$, whereas $n = 25$ was suitable for smoothing. All points of the maxima and minima in each spectrum in Fig. 1 corresponded to the zero-crossing points of the next higher order derivative spectra. Fifth-order derivative spectra or higher were impractical as they showed poor signal-to-noise ratios (S/N).

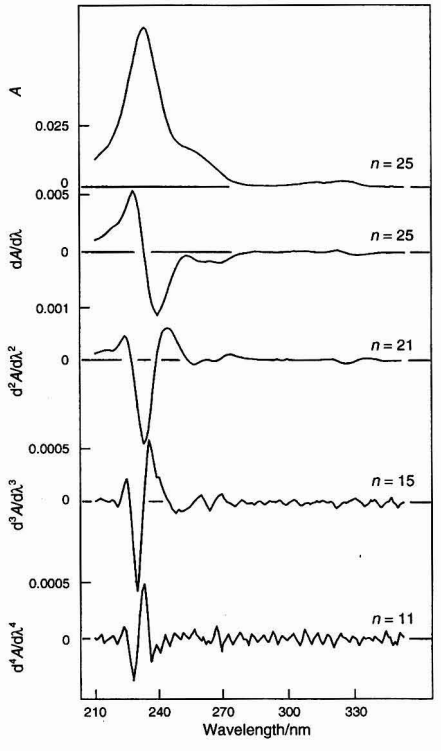

Fig. 1 Derivative spectra of chlorothalonil obtained by the multilinear least-squares fitting method.

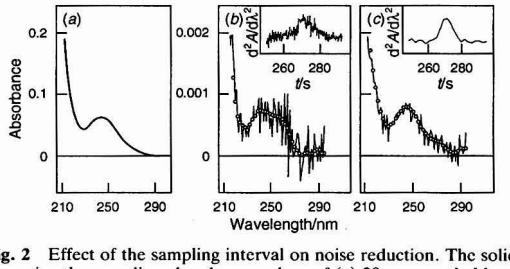

Fig. 2 Effect of the sampling interval on noise reduction. The solid lines give the sampling absorbance values of (*a*) 30 ppm methyldymron at a 0.24 s; (*b*) 0.3 ppm at a 0.24 s and (*c*) 0.3 ppm at a 2 s sampling interval. Circles give the results of 25-point smoothing. The chromatograms in the insets were drawn by connecting the second-derivative values ($m = 6$, $n = 25$) at 226.6 nm.

Sensitivity

Fig. 2(*a*) shows the raw spectrum obtained from a 20 μl injection of 30 ppm of the herbicide methyldymron with 0.24 s PDA detector sampling intervals. In this interval, a single spectrum was stored over 25.6 ms and nine successive scans were averaged. A high concentration of the analyte brought about a noise-free, smoothed UV absorbance spectrum. Fig. 2(*b*) shows the spectrum under the same conditions except that the concentration of methyldymron was 100 times lower. The circles in Fig. 2(*b*), calculated by polynomial smoothing ($m = 6$, $n = 25$), could not reproduce the spectrum accurately, and the second-derivative spectrum chromatogram obtained from these data was very noisy (S/N = 2.5). When the sampling interval was 2 s (78 successive scans), the reproduci-

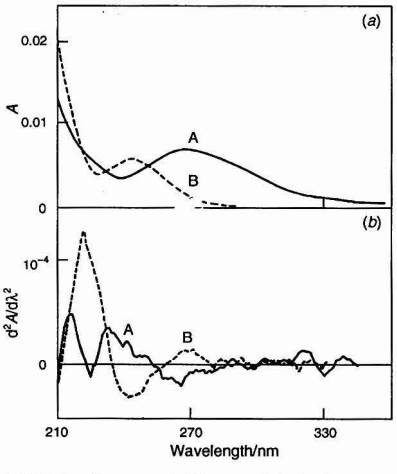

Fig. 3 (*a*) UV absorbance and (*b*) second-derivative spectra of, A, MEP and, B, methyldymron.

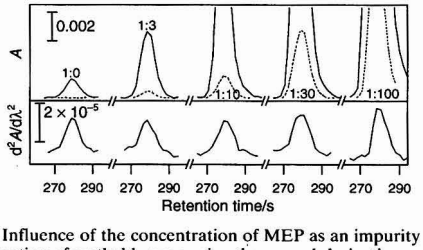

Fig. 4 Influence of the concentration of MEP as an impurity on the determination of methyldymron using the second-derivative spectrum chromatogram. The solid lines give the univariate chromatograms at 245.5 nm and the broken lines those at 329.5 nm. The numbers on each chromatogram are the ratios of methyldymron to MEP.

bility of the spectrum was satisfactory and the S/N of the derivative spectrum chromatogram was improved to almost 6 [Fig. 2(*c*)]. It can be assumed increased as square root of the ratio of successive scans. The baseline noise level of the SPD-M6A detector at 226.6 nm with 3 nm resolution was about 10^{-4} absorbance at a 2 s sampling interval, hence the S/N in the univariate chromatogram at this wavelength was about 7 [Fig. 2(*c*)]. Consequently, for methyldymron the detection limit calculated from the S/N of the proposed technique is not inferior to the inherent performance of the PDA detector.

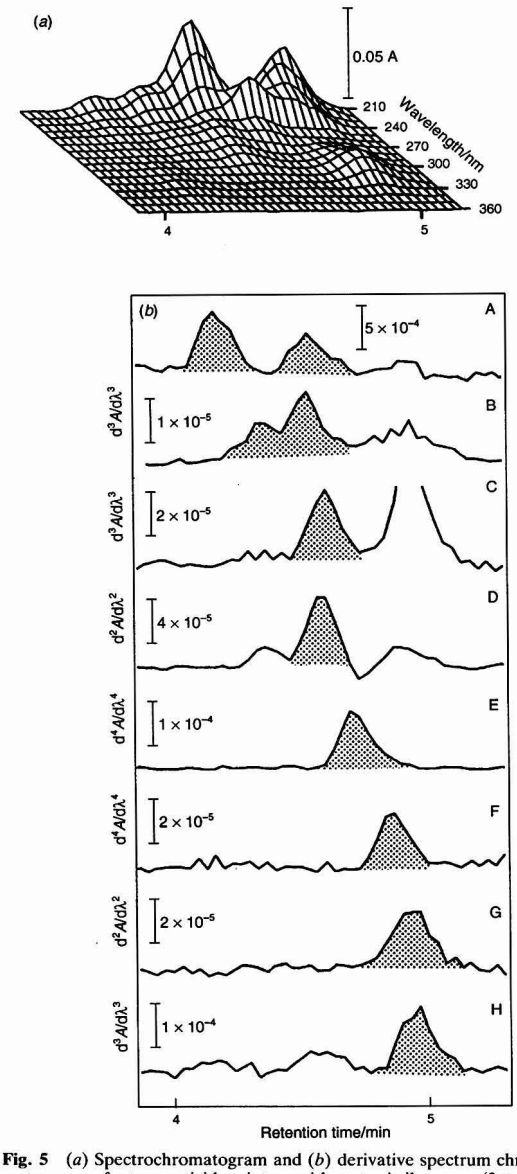

Fig. 5 (*a*) Spectrochromatogram and (*b*) derivative spectrum chromatograms of a ten pesticide mixture with acetonitrile–water (3 + 1) as eluent on a LiChrospher 100 RP-18 analytical column. The values in parentheses were calculated for the shaded regions. From top to bottom: A, pyridaphenthion (0.92 ppm) and fenitrothion (1.08 ppm) at 350.1 nm; B, flutolanil (0.80 ppm) and mepronil (1.10 ppm) at 294.4 nm; C, iprodion (1.04 ppm) at 214.1 nm; D, methyldymron (1.18 ppm) at 225.6 nm; E, chlorothalonil (1.02 ppm) at 232.9 nm; F, napropamide (1.01 ppm) at 236.1 nm; G, isoprothiolane (1.11 ppm) at 331.6 nm; and H, chloroneb (1.07 ppm) at 212 nm.

Two-component System

A reversed-phase column permitted the adjustment of the elution order between methyldymron and fenitrothion (MEP) as desired, by varying the ratio between acetonitrile and water in the mobile phase. Using a mobile phase of acetonitrile–water (73 + 27) on a LiChrospher column, the two peaks overlapped completely. Fig. 3(*a*) shows the UV absorbance spectra obtained from the LC-PDA data by 20 μl injections of both pesticides at 5 ppm each over the wavelength range 210–360 nm ($m = 6$, $n = 25$). MEP exhibits a broad spectrum above 300 nm and prevents the direct determination of methyldymron using the univariate chromatogram for the mixture. When the second-derivative spectra are obtained from the PDA data ($m = 6$, $n = 21$), the zero-crossing point of MEP is produced at 222.5 nm, where methyldymron shows a large amplitude [Fig. 3(*b*)]. The top traces in Fig. 4 show the univariate chromatograms obtained from sample solutions containing 1 ppm of methyldymron and various concentrations of MEP ranging from 0 to 100 ppm under above chromatographic conditions at 245.5 and 329.5 nm, where methyldymron shows maximum and no absorption, respectively. The presence of MEP led to a lack of clarity of the elution profiles of methyldymron. The bottom traces in Fig. 4 are the second-derivative spectrum chromatograms of methyldymron at 222.5 nm. It is clear that the proposed technique could remove the influence of an impurity whose concentration is two orders of magnitude higher than that of the analyte in a binary mixture.

Multicomponent System

A mixture of ten pesticides at 1 ppm each which possess various UV absorbance spectra was used as a sample solution. Using acetonitrile–water (3 + 1) as the mobile phase, these pesticides were eluted with overlapping peaks in a time span of 4–5 min. The top part of Fig. 5 shows the multivariate chromatogram of the pesticide mixture, and the bottom part shows the derivative spectrum chromatograms obtained from these PDA data. When an analyte, such as pyridaphenthion or MEP, has absorption bands at longer wavelengths than others, we recommend the use of the univariate chromatogram at this wavelength for quantification. If an analyte has large absorption bands, the higher order derivative values can be used, with more selective and accurate chromatograms being obtained, *e.g.*, chlorothalonil or napropamide. The time spent on calculations was short, and most of the necessary time per derivative spectrum chromatogram was required for reading off the data from the floppy disk. If the PDA data can be processed on-line, the proposed technique will make real-time analysis possible.

Conclusion

The derivative spectrum chromatogram technique can be successfully applied to the analysis of overlapped peaks in LC-PDA. In a two-component system, completely overlapped peaks can reliably be resolved by this technique. The most striking features of this technique are its simplicity and rapidity, coming from the simple algorithm, which render it suitable for routine analysis.

We gratefully acknowledge the technical assistance of M. Nishimura and Y. Mito of Shimadzu.

References

1 Brown, S. D., *Anal. Chem.*, 1990, **62**, 84R.
2 Lorber, A., *Anal. Chim. Acta*, 1984, **164**, 293.
3 Lindberg, W., Oehman, J., and Wold, S., *Anal. Chem.*, 1986, **58**, 299.
4 Sanchez, E., and Kowalski, B. R., *Anal. Chem.*, 1986, **58**, 496.
5 Li, S., Hamilton, J. C., and Gemperline, P. J., *Anal. Chem.*, 1992, **64**, 599.
6 Sakuma, I., Takai, N., Dohi, T., Fukui, Y., and Ohkubo, A., *J. Chromatogr.*, 1990, **506**, 223.
7 Keller, H. R., Massart, D. L., and DeBeer, J. O., *Anal. Chem.*, 1993, **65**, 471.
8 Liang, Y-Z., Brereton, R. G., Kvalheim, O. M., and Rahmani, A., *Analyst*, 1993, **118**, 779.
9 Abdel-Hay, M. H., El-Din, M. S., and Abuirjeie, M. A., *Analyst*, 1992, **117**, 157.
10 Gallignani, M., Garrigues, S., and Guardia, M., *Analyst*, 1993, **118**, 1167.
11 Botsoglou, N. A., Fletouris, D. J., Papageorgiou, G. E., and Mantis, A. J., *J. Agric. Food Chem.*, 1993, **41**, 1635.
12 Savitzky, A., and Golay, M. J. E., *Anal. Chem.*, 1964, **36**, 1627.

Paper 4/02275K
Received May 18, 1994
Accepted August 12, 1994

Enantiomeric Separation and Spectrofluorometric Detection of the Racemic Drugs, (±)-1-(2,6-Dimethylphenoxy)-2-propamine (Mexiletine) and (3*RS*)-4-Amino-3-hydroxybutanoic Acid (GABOB), Derivatized With 4-Fluoro-7-nitro-2,1,3-benzoxadiazole on a Phenylcarbamylated Cyclodextrin Bonded Stationary Phase

Takeshi Fukushima, Masaru Kato, Tomofumi Santa and Kazuhiro Imai*

Faculty of Pharmaceutical Sciences, University of Tokyo, 7-3-1 Hongo, Bunkyo-ku, Tokyo 113, Japan

(±)-Mexiletine [(±)-1-(2,6-dimethylphenoxy)-2-propamine] and (3*RS*)-4-amino-3-hydroxybutanoic acid (GABOB) were derivatized with a fluorogenic reagent, 4-fluoro-7-nitro-2,1,3-benzoxadiazole (NBD-F). They were then separated on a phenylcarbamylated β-cyclodextrin [cyclomaltoheptaose] bonded stationary phase (Ultron ES-phCD) with a mobile phase of water–acetonitrile–methanol (50 + 10 + 40, v/v/v) for mexiletine and 50 mmol dm^{-3} citric acid–acetonitrile (90 + 10, v/v) for GABOB and detected by spectrofluorimetry at 530 nm with excitation at 470 nm. The derivatives of the enantiomers were well separated from each other. The separation factors (α) for the NBD-(±)-mexiletine and -(*RS*)-GABOB derivatives were 1.08 and 1.07, respectively. The data suggest that the enantiomers of drugs having an amino group at the chiral centre but lacking the carboxy group and drugs having an amino moiety at the β-position from a chiral centre but bearing a carboxy moiety following derivatization with NBD-F are effectively separated on the modified cyclodextrin stationary phase. Using either Pirkle-type stationary phases (K. Imai, *et. al.*, *Biomed. Chromatogr.*, 1993, 7, 177) or the modified cyclodextrin bonded stationary phase (proposed here) and the derivatization with NBD-F, many chiral drugs having an amino functional group could be separated enantioselectively and sensitively detected.

Keywords: 4-Fluoro-7-nitro-2,1,3-benzoxadiazole; mexiletine; (3R) (or 3S)-4-amino-3-hydroxybutanoic acid; enantiomer separation; modified beta-cyclodextrin bonded stationary phase; high-performance liquid chromatography

Introduction

The enantioselective determination of the racemic drugs in body fluids is very important in studying their pharmacological and toxicological properties.

We have found that amino acids or amino acid-type drugs derivatized with 4-fluoro-7-nitro-2,1,3-benzoxadiazole (NBD-F)[1–5] were separated into their enantiomers on the Pirkle-type stationary phases and sensitively detected at the sub-pmol range.[6,7] Thus racemic drugs having both an amino functional group at the chiral centre and a carboxy group can be enantioselectively separated from each other on Pirkle-type stationary phases following derivatization with NBD-F. On the other hand, racemic drugs having an amino group at the chiral centre but lacking the carboxylic acid moiety or drugs having an amino moiety at the β-position from the chiral centre but bearing a carboxy group moiety were not separated enantiomerically.

In order to broaden the usefulness of the derivatization method the enantiomeric separation of such racemic drugs on a β-cyclodextrin (cyclomaltoheptaose, β-CD) bonded stationary phase is investigated, because the steric surroundings of the derivatives in the cavity of cyclodextrin might be effective in separating the enantiomers. Thus, in this paper, we investigate the chiral separation on a modified β-CD bonded stationary phase of (±)-mexiletine [(±)-1-(2,6-dimethylphenoxy)-2-propamine] (Fig. 1), an anti-arrhythmic drug[8] as a representative for the chiral drugs having an amino group at the chiral centre but lacking the carboxy group and (3*RS*)-4-amino-3-hydroxybutanoic acid [(*RS*)-GABOB], a GABA agonist,[9] as a representative of the drugs having an amino moiety at the β-position of the chiral centre but bearing a carboxy group moiety, derivatized with NBD-F.

Experimental

Materials

A phenylcarbamylated β-CD type chiral column (Ultron ES-phCD, 150 × 60 mm i.d., 5 μm) (Fig. 2) was donated by Sinwa Kakou (Kyoto, Japan). The acetonitrile, methanol and water of the mobile phase were of high-performance liquid chromatography (HPLC) grade (Wako Pure Chemicals, Osaka, Japan). (*R*)-(−)-, (*S*)-(+)- and (*RS*)-(±)-mexiletine hydrochlorides were donated by Boeringer Ingelheim (Ingelheim, Germany). (3*R*)-(−)- and (3*S*)-(+)-GABOB were from Ono Yakuhin Kogyo (Osaka, Japan).

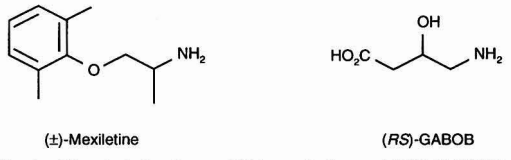

(±)-Mexiletine (*RS*)-GABOB

Fig. 1 Chemical structures of (±)-mexiletine and (*RS*)-GABOB.

* To whom correspondence should be addressed.

Derivatization With NBD-F

A 10 μl portion of 100 μmol l^{-1} (−)-, (+)- or (±)-mexiletine hydrochloride or 3*R*- or 3*S*-GABOB in 0.2 mol l^{-1} borate buffer (pH 8.0) containing 4 mmol l^{-1} Na_2EDTA and 30 μl of 50 mmol l^{-1} NBD-F in acetonitrile were mixed and heated at 60 °C for 5 min. Then, 960 μl of 1% acetic acid in methanol were added to the solution to stop the reaction. A 10 μl aliquot of the solution was analysed by HPLC.

High-performance Liquid Chromatography

An HPLC intelligent pump L-6200 (Hitachi, Tokyo, Japan), a spectrofluorimetric detector F-1050 (Hitachi) and an integrator D-2000 (Hitachi) were used. The mobile phase consisted of H_2O–CH_3CN–MeOH (50 + 10 + 40, v/v/v) for (±)-mexiletine and 50 mmol l^{-1} citric acid in H_2O–CH_3CN (90 + 10, v/v) for (*RS*)-GABOB. The flow rate was 0.8 ml min^{-1}. Spectrofluorimetric detection was carried out at 530 nm with excitation at 470 nm.

Results and Discussion

Previously,[6,7] the chiral separation of NBD-amino acids was performed on a Pirkle-type chiral stationary phase (Sumichiral OA series) with ammonium acetate in methanol as the mobile phase. In this case, in order to achieve enantiomeric separation, the interaction of the carboxy group in the analytes is essential in the π–π interaction between the NBD or 4-alkylamino-7-nitro-benzofurazan moiety and the stationary phase such as (*S*)-1-naphthylglycyl-3,5-dinitrophenylamide silica gel or *N*-[(*R*)-1-naphthylethylaminocarbonyl]-(*S*)-*tert*-leucylaminopropyl silica gel. Hence, chiral drugs lacking the carboxy group such as (±)-mexiletine are difficult to separate into their enantiomers. Moreover, the derivatization site should be at the amino group at the chiral centre of the enantiomer separation, judging from the defect of the enantioselective separation of NBD-(*RS*)-GABOB. In this work, Ultron ES-phCD (Fig. 2) was used as a chiral stationary phase in which the primary and secondary hydroxy groups of the β-CD were modified quantitatively (20 mol per β-CD) by phenylcarbamylation, in the hope that the hydrophobic and π–π interaction with the NBD-derivatives would be favourable to enantioseparation.

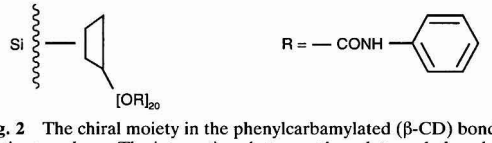

Fig. 2 The chiral moiety in the phenylcarbamylated (β-CD) bonded stationary phase. The interactions between the solute and phenylcarbamylated β-CD and solute may be ascribed to the π–π and hydrophobic interactions in addition to the inclusion into the cavity of β-CD.

The chromatogram obtained for NBD-(±)-mexiletine with water–acetonitrile–methanol (50 + 10 + 40, v/v/v) as the mobile phase is shown in Fig. 3. NBD-(−)- and -(+)-mexiletine were well separated, with a separation factor (α) of 1.08. They were not eluted in more than 80 min with a mobile phase of water–methanol and not enantioselectively separated with a mobile phase of water–acetonitrile (retention time, about 9.0 min). According to Reeuwijk *et al.*,[10] acetonitrile could penetrate to the hydrophobic cavity of β-CD and displace the compound included in the cavity. Therefore, the use of acetonitrile is not convenient for the chiral separation through the inclusion process into the cavity. On the other hand, methanol has a weak ability to penetrate into the β-CD cavity owing to its high polarity. In this work, the use of acetonitrile in the mobile phase was necessary since the mexiletine enantiomer was not displaced from the β-CD cavity by methanol alone. Thus, the above mobile phase was appropriate for enantiomeric separation of (±)-mexiletine.

Although enantiomeric separation of the (±)-mexiletine derivatized with 1-naphthoyl chloride on a Pirkle-type chiral stationary phase with propan-2-ol–hexane (5.5 + 94.5) as a mobile phase has been reported,[11,12] the low excitation (230 nm) and emission (340 nm) wavelengths necessitated the use of an extensive cleanup procedure for mexiletine in the plasma. In contrast, the NBD-derivatives, having the long excitation (470 nm) and emission (530 nm) wavelengths could avoid the tedious cleanup procedure of mexiletine from biological samples.

NBD-(*RS*)-GABOB derivatives were not separated enantiomerically with the mobile phase suitable for the mexiletine derivatives. GABOB, appears to interact mainly with β-CD through hydrogen bonding of the carboxylic acid moiety with the amide moiety of the derivatized β-CD. Methanol in the mobile phase may interfere with this hydrogen bond. Thus, the separation of NBD-(*RS*)-GABOB was achieved in the absence of methanol with water and acetonitrile as the mobile phase (α = 1.07, Fig. 4).

Accordingly, many racemic drugs having a primary or secondary amino functional group at the chiral centre, which lack a carboxy group, or drugs having an amino group at the β-position from the chiral centre, which possess a carboxy group, may be enantioselectively separated and sensitively detected using either a Pirkle-type stationary phase or a β-CD phase following derivatization with NBD-F.

The enantiomer separation of the other type of chiral drugs bearing an amino group at a remote position from a chiral centre should be the next stage of investigation.

The proposed chiral separation and sensitive detection methods would be useful in the tracing of the metabolic fate of racemic drugs in animals.

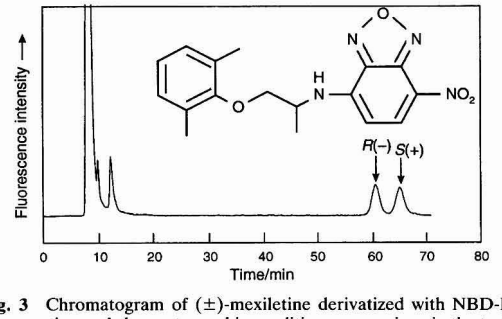

Fig. 3 Chromatogram of (±)-mexiletine derivatized with NBD-F. The reaction and chromatographic conditions are as given in the text.

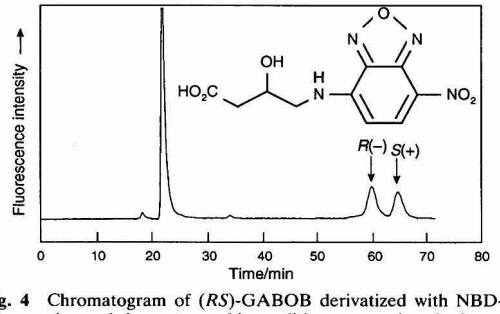

Fig. 4 Chromatogram of (*RS*)-GABOB derivatized with NBD-F. The reaction and chromatographic conditions are as given in the text.

The authors thank Boeringer Ingelheim Co. Ltd. and Ono Yakuhin Kogyou Co. Ltd. for supplying mexiletine and GABOB, respectively. The authors also thank Sinwa Kako Co. Ltd. for the gift of a phenylcarbamylated β-cyclodextrin bonded stationary phase.

References

1 Watanabe, Y., and Imai, K., *Anal. Chim. Acta*, 1981, **130**, 377.
2 Watanabe, Y., and Imai, K., *Anal. Biochem.*, 1981, **116**, 471.
3 Watanabe, Y., and Imai, K., *J. Chromatogr.*, 1982, **239**, 723.
4 Watanabe, Y., and Imai, K., *J. Chromatogr.*, 1984, **309**, 279.
5 Watanabe, N., Toyo'oka, T., and Imai, K., *Biomed. Chromatogr.*, 1987, **2**, 99.
6 Imai, K., Fukushima, T., and Uzu, S., *Biomed. Chromatogr.*, 1993, **7**, 177.
7 Imai, K., and Fukushima, T., *Biomed. Chromatogr.*, 1993, **7**, 275.
8 Turgeon, J., Uprichard, A. C. G., Belanger, P. M., Harron, D. W. G., and Grech-Belanger, O., *J. Pharm. Pharmacol.*, 1991, **43**, 630.
9 Katayama, Y., *Okayama Igakkai Zasshi*, 1976, **88**, 209.
10 Reeuwijk, H. J. E. M., Irth, H., Tjaden, U. R., Merkus, F. W. H. M., and Van der Greef, J., *J. Chromatogr.*, 1993, **614**, 95.
11 McErlane, K. M., and Igwemenzie, L., *J. Chromatogr. Biomed. Appl.*, 1987, **415**, 335.
12 Igwemenzie, L., Kerr, C. R., and McErlane, K. M., *Xenobiotica*, 1989, **19**, 677.

Paper 4/03334E
Received June 6, 1994
Accepted July 17, 1994

Development of Optically Active Fluorescent Edman-type Reagents

Toshimasa Toyo'oka

Department of Analytical Chemistry, School of Pharmaceutical Sciences, University of Shizuoka, 52-1 Yada, Shizuoka 422, Japan

Yi-Ming Liu

Division of Environmental Chemistry, National Institute of Health Sciences, 1-18-1 Kamiyoga, Setagaya-ku, Tokyo 158, Japan

The optically active fluorescent Edman-type reagents 4-(3-isothiocyanatopyrrolidin-1-yl)-7-nitro-2,1,3-benzoxadiazole [(*R*)-(−)- and (*S*)-(+)-NBD-PyNCS] and 4-(3-isothiocyanatopyrrolidin-1-yl)-7-(*N*,*N*-dimethylaminosulfonyl)-2,1,3-benzoxadiazole [(*R*)-(−)- and (*S*)-(+)-DBD-PyNCS] were synthesized and characterized by their physico-chemical properties. High optical purities of all four enantiomers were identified by high-performance liquid chromatography (HPLC) with a chiral stationary phase (CSP) column. Good stability in both solid and liquid forms is one of the excellent properties of these novel Edman-type reagents. The applicability of these reagents to the resolution of mirror-image enantiomers of amines, including amino acids and some drugs (β-adrenergic blocking agents), by reversed-phase HPLC was demonstrated. The proposed reagents read quantitatively with primary and secondary amino functional groups under mild conditions (55 °C for 10 min) in the presence of triethylamine (TEA) to produce the corresponding fluorescent thiourea derivatives. The maximum excitation/emission wavelengths of the resulting diastereomers in acetonitrile–water (1 + 1) are around 490/530 nm for NBD-PyNCS derivatives and around 460/550 nm for DBD-PyNCS derivatives. The fluorescence wavelengths are independent of the amino compounds. The diastereomers that were derived from the amines were efficiently resolved on an achiral ODS column with water–acetonitrile containing 0.05% trifluoroacetic acid (TFA). The R_s values were in the range 0.83–4.12 for the diastereomers obtained with NBD-PyNCS and 1.35–6.06 for those with DBD-PyNCS. The diastereomer corresponding to the *R* configuration of the amines elute faster than those of the *S* configuration with the (*R*)-(−)-enantiomer of the Edman-type reagents used as the derivatization reagent. As expected, the opposite elution order is obtained with the use of the (*S*)-(+)-enantiomers.

Keywords: Chiral derivatization reagents; pre-column derivatization; resolution of racemates of primary and secondary amines; fluorescence detection; high-performance liquid chromatography

Introduction

More than half of the organic compounds marketed as drugs possess asymmetric centres; nevertheless, most are used therapeutically as racemates. The chiral drugs and their metabolites would be expected to interact stereoselectively with biological compounds, since asymmetry and optical activity are widely distributed in biological systems, as illustrated by enzymes and receptors, *etc.* In fact, enantiomers of some racemic drugs have been found to differ in pharmacological activity, side-effects, stability and pharmacokinetics.[1,2] If the toxicites (one of the side-effects) are drastically different for the individual enantiomers of the drugs, as in the case of thalidomide, the drug must be supplied as a single enantiomer. Therefore, enantiomeric separation of racemic drugs is of critical importance for the pharmaceutical industry.

Many kinds of polypeptides such as insulin and opioid peptides are produced by biotechnology, organic synthesis or a combination of both. The possibility exists that the product will be contaminated with small amounts of D-amino acids. Contamination with D-isomers in bioactive materials decreases the activation values in some instances. If toxicity increases with increasing amounts of D-amino acids, then there is a need to monitor the quality of the peptides produced. Therefore, the determination of trace amounts of optical isomers is an important subject in terms of the safety and efficacy of pharmaceuticals. Some naturally occurring bioactive peptides do not have adequate stability and biological activity for marketing as pharmaceuticals. However, some benefits can be derived if some of the amino acids in the peptide sequence are converted into the D-isomers. Conformational changes based on the introduction of D-amino acid(s) can increase biological activity and stability and may even decrease side-effects. Therefore, it is highly desirable to determine with chiral peptide sequences the configuration of each amino acid in the peptide.

Various fluorescent tagging reagents have been developed for the derivatization of the amino functional group.[3,4] Amino acids and drugs incorporating primary and secondary amino functional groups have been determined by high-performance liquid chromatography (HPLC) after derivatization. As various kinds of fluorophores with high quantum efficiency (ϕ) can be used as the derivatization reagents, highly sensitive detection is possible.[5,6] HPLC separation combined with sensitive detection, such as fluorescence, is also suitable for the determination of trace amounts of individual enantiomers. Several optically active reagents have been used for the resolution and determination of enantiomers of amines by conversion into diastereomers that can be separated with conventional achiral columns such as silica gel (SIL) and octadecylsilica gel (ODS).[7–11]

In previous papers,[12,13] we described the syntheses of chiral fluorescent derivatization reagents [(*S*)-(−)- and (*R*)-(+)-enantiomers of 4-(2-chloroformylpyrrolidin-1-yl)-7-(*N*,*N*-dimethyaminosulfonyl)-2,1,3-benzoxadiazole (DBD-Pro-COCl) and 4-(2-chloroformylpyrrolidin-1-yl)-7-nitro-2,1,3-benzoxadiazole (NBD-Pro-COCl)] and evaluated their application to the resolution of chiral molecules. The enantiomers of alcohols were completely separated by normal-phase HPLC after derivatization. However, inadequate separation of chiral amines was obtained with these reagents.[14] In this work, the development of optically active fluorescent derivati-

zation reagents for the resolution of racemic amines was undertaken. This paper deals with the synthesis of novel Edman-type fluorescence chiral tagging reagents [(*S*)-(+)- and (*R*)-(−)-enantiomers of 4-(3-isothiocyanatopyrrolidin-1-yl)-7-nitro-2,1,3-benzoxadiazole (NBD-PyNCS) and 4-(3-isothiocyanatopyrrolidin-1-yl)-7-(*N*,*N*-dimethylaminosulfonyl)-2,1,3-benzoxadiazole (DBD-PyNCS)], which have the isothiocyanate (NCS) functional group as the reactive site, and the application of these compounds to the resolution of various chiral amines, including amino acids and drugs. The fluorescence characteristics and reversed-phase HPLC resolution of the resulting diastereomers were also investigated.

Experimental

Materials and Reagents

4-(3-Aminopyrrolidin-1-yl)-7-nitro-2,1,3-benzoxadiazoles [(*R*)-(−)- and (*S*)-(+)-NBD-APys] and 4-(3-aminopyrrolidin-1-yl)-7-(*N*,*N*-dimethylaminosulfonyl)-2,1,3-benzoxadiazoles [(*R*)-(−)- and (*S*)-(+)-DBD-APys] were synthesized as described previously.[15] Enantiomers of 1-(1-naphthyl)ethylamine (NEA) and 1-phenylethylamine (PEA) were purchased from Wako (Osaka, Japan). Enantiomers of 1-cyclohexylethylamine (CEA) were supplied by Fluka (Buchs, Switzerland). Enantiomers of phenylalanine, valine, proline, 1-(*o*-allylphenoxy)-3-(isopropylamino)propan-2-ol hydrochloride (alprenolol) and 1-(isopropylamino)-3-(1-naphthyloxy)propan-2-ol hydrochloride (propanolol) were purchased from Sigma (St. Louis, MO, USA). Trifluoroacetic acid (TFA), acetonitrile, methanol and water were of HPLC grade (Wako). All other chemicals were of analytical-reagent grade and were used as received.

Apparatus

Proton nuclear magnetic resonance (^{1}H NMR) spectra were recorded on a Varian (Palo Alto, CA, USA) Jemini-300 spectrometer at 300 MHz using tetramethylsilane (0.00 ppm) as the internal standard. For describing NMR characteristics, the following abbreviations are used: s = singlet, d = doublet and m = multiplet. Mass spectrometry (MS) was performed with a JEOL (Tokyo, Japan) DX-300 mass spectrometer with electron impact (EI) ionization at 70 eV. Infrared (IR) spectra were measured using potassium bromide (KBr) discs with a Shimadzu (Kyoto, Japan) Model IR-460 spectrometer. For measurement of excitation and emission spectra, a Hitachi Model 650-60 spectrofluorimeter with a 1 cm quartz cell was employed without spectral correction. Optical rotations were measured on a DIP-370 digital polarimeter (JASCO, Tokyo, Japan) with 50 × 3.5 mm diameter cylindrical cell. Melting-points (m.p.) were measured with a Yanagimoto (Tokyo, Japan) micro melting-point apparatus.

HPLC

The high-performance liquid chromatograph consisted of two LC-10AD pumps (Shimadzu) and an SCL-10A system controller (Shimadzu). Sample solutions were injected with a SIL-10A autoinjector (Shimadzu). The analytical column was Inertsil ODS-80A (150 × 4.6 mm i.d., 5 μm) for reversed-phase chromatography (GL Sciences, Tokyo, Japan). A CSP column of Ultron ES-PhCD (150 × 6.0 mm i.d., 5 μm) (Shinwa Chemicals, Kyoto, Japan) was used for the determination of the optical purity of the proposed reagents. The columns were maintained at 40 °C with a CTO-10AC column oven (Shimadzu). A Shimadzu RF-10A fluorescence monitor equipped with a 12 μl flow cell was employed for detection. The excitation and emission wavelengths were fixed at 490 and 530 nm, respectively, for the derivatives with NBD-PyNCS and 460 and 550 nm, respectively, for the derivatives with DBD-PyNCS. The peak areas obtained from the fluorescence monitor were computed with a C-R7A Chromatopac integrator (Shimadzu). All mobile phases were de-gassed with an on-line de-gasser (DGU-3A, Shimadzu). The flow rate of the eluent was 1.0 ml min^{-1}.

Preparation of Reagents

To (*S*)-(+)-4-(3-aminopyrrolidin-1-yl)-7-nitro-2,1,3-benzoxadiazole [(*S*)-(+)-NBD-APy] (0.1 g, 0.4 mmol) dissolved in 100 ml of acetone was added 0.1 ml of thiophosgene ($CSCl_2$) in 10 ml of benzene. After refluxing for 60 min, the solvent in the reaction mixture was evaporated under reduced pressure. The remaining residue was suspended in 100 ml of water and extracted with 25 ml of benzene. The extraction procedure was repeated three times. The combined benzene extracts were washed with 20 ml of water, dried over anhydrous sodium sulfate and evaporated *in vacuo*. The raw product obtained was recrystallized from hexane–benzene (1 + 2).

(*S*)-(+)-4-(3-Isothiocyanatopyrrolidin-1-yl)-7-nitro-2,1,3-benzoxadiazole [(*S*)-(+)-NBD-PyNCS]: red crystals; m.p. 165–170 °C (decomp.); yield 75 mg (65%); NMR (ppm) in $CDCl_3$, 8.46 (1H, d, J_{ab} = 8.8 Hz, a), 6.08 (1H, d, J_{ab} = 8.8 Hz, b), 4.69 (1H, m, c), 3.6–4.7 (4H, m, d + e), 2.52 (2H, m, f); EI-MS, *m*/*z* 291 (M^+); IR (KBr), 2160, 2100, 1610, 1550, 1495, 1320, and 1290 cm^{-1}; $[\alpha]_D^{30}$ +478°, *c* = 0.4 in CH_3CN. Analysis: calculated for $C_{11}H_9N_5O_3S$, C 45.36, H 3.11, N 24.04; found, C 45.21, H 3.13, N 23.43%.

(*R*)-(−)-4-(3-Isothiocyanatopyrrolidin-1-yl)-7-nitro-2,1,3-benzoxadiazole [(*R*)-(−)-NBD-PyNCS] was obtained from the reaction of (*R*)-(−)-4-(3-aminopyrrolidin-1-yl)-7-nitro-2,1,3-benzoxadiazole [(*R*)-(−)-NBD-APy] with $CSCl_2$ in the same manner described above.

(*R*)-(−)-NBD-PyNCS; yield 75 mg (65%); $[\alpha]_D^{30}$ −472°, *c* = 0.4 in CH_3CN. Analysis: calculated for $C_{11}H_9N_5O_3S$, C 45.36, H 3.11, N 24.04; found, C 45.14, H 3.12, N 23.30%. Other data were the same as those for (*S*)-(+)-NBD-PyNCS.

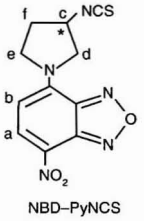

NBD–PyNCS

Similarly, (*S*)-(+)- and (*R*)-(−)-DBD-PyNCS were obtained from the reaction of the corresponding enantiomers of DBD-APy with $CSCl_2$.

(*S*)-(+)-4-(3-Isothiocyanatopyrrolidin-1-yl)-7-(*N*,*N*-dimethylaminosulfonyl)-2,1,3-benzoxadiazole [(*S*)-(+)-DBD-PyNCS): yellow crystals; m.p. 160–170 °C (decomp.); yield 62 mg (55%); NMR (ppm) in $CDCl_3$, 7.88 (1H, d, J_{ab} = 8.8 Hz, a), 6.01 (1H, d, J_{ab} = 8.8 Hz, b), 4.61 (1H, m, c), 3.9–4.3 (4H, m, d + e), 2.87 (6H, s, g), 2.46 (2H, m, f); EI-MS, *m*/*z* 353 (M^+); IR (KBr), 2170, 2110, 1600, 1560, 1420, 1335, and 1140 cm^{-1}; $[\alpha]_D^{30}$ + 256°, *c* = 0.4 in CH_3CN. Analysis: calculated for $C_{13}H_{15}N_5O_3S_2$, C 44.18, H 4.28, N 19.82; found, C 43.69, H 4.24, N 19.68%.

(*R*)-(−)-DBD-PyNCS: yield 60 mg (53%); $[\alpha]_D^{30}$ −257°, *c* = 0.4 in CH_3CN. Analysis: calculated for $C_{13}H_{15}N_5O_3S_2$, C 44.18, H 4.28, N 19.82; found, C 43.79, H 4.20, N 19.60%. Other data were the same as those for (*S*)-(+)-DBD-PyNCS.

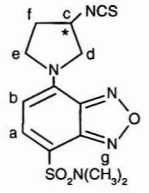

DBD–PyNCS

Derivatization and HPLC Separation

A 10 μl volume of the reagent [5 mmol l^{-1} (*R*)-(−)- or (*S*)-(+)-enantiomer] in acetonitrile and 10 μl of chiral amines (1 mmol l^{-1} of each enantiomer) in acetonitrile–water (1 + 1) containing 2% triethylamine (TEA) were mixed in a 1.5 ml mini-vial (GL Science). The vials were tightly capped and heated at 55 °C with a dry heat block for 10 min. Then 480 μl of 1 mol l^{-1} acetic acid (AcOH) in acetonitrile–water (1 + 1) was added to the reaction mixture to stop the derivatization reaction. The acidic solution was diluted tenfold with acetonitrile and then a 5 μl portion of the diluted solution was analysed by HPLC. The reagent blanks without amines were also treated in the same manner.

For the fluorescencent spectra measurements, 50 μl of the acid solution before dilution were injected on to the column and the peak corresponding to amine derivative was collected at the outlet of the detector (approximately a 2 ml portion). Fluorescence maximum wavelengths of the chiral reagents themselves were also measured at 2 μmol l^{-1} concentration without chromatographic separation.

Results and Discussion

Synthesis and Purity of the Reagent

The optical isomers [(*S*)-(+)- and (*R*)-(−)-enantiomers] of NBD-PyNCS and DBD-PyNCS were synthesized by reacting $CSCl_2$ with the corresponding enantiomers of NBD-APy and DBD-APy that have been reported previously as chiral fluorescent tagging reagents for the carboxyl functional group.[12,13] Fig. 1 shows the synthetic pathway for the reagents and the subsequent reaction with chiral amines. The structure was confirmed by the physico-chemical properties described under Experimental.

For the determination of trace amounts of the opposite enantiomer in the presence of a large excess of the optical isomer, high optical purity of the tagging reagent is essential. Therefore, the optical purity was measured for the proposed reagents by HPLC utilizing an ES-PhCD column, packed with β-cyclodextrin phenylcarbamate derivatives as the chiral stationary phase.[16] As shown in Figs. 2 and 3, each pair of the reagent enantiomers were completely separated with aqueous eluents. The enantiomeric impurities were calculated from the comparison for the peak areas of (*R*)-(−)- and (*S*)-(+)-isomers after injection of large amounts of the reagents. As shown in Table 1, the optical purities were found to be

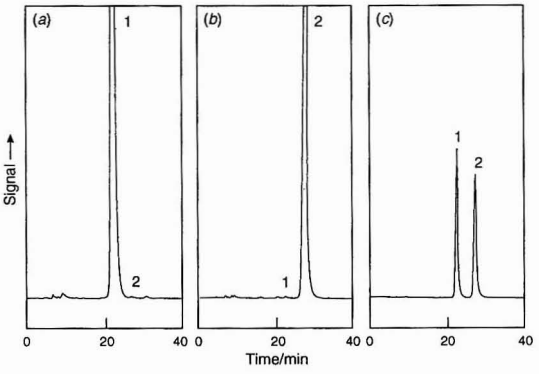

Fig. 2 Separation of a pair of enantiomers of NBD-PyNCS by a CSP column: (*a*), injection of (*R*)-(−)-NBD-PyNCS; (*b*), injection of (*S*)-(+)-NBD-PyNCS; and (*c*), injection of both enantiomers of NBD-PyNCS. Peaks: 1, (*R*)-(−)-NBD-PyNCS; and 2, (*S*)-(+)-NBD-PyNCS. Eluent, water–acetonitrile–methanol (4 + 3 + 3). Other HPLC conditions are given under Experimental.

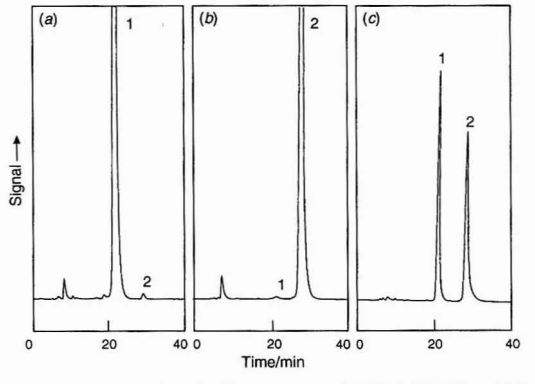

Fig. 3 Separation of a pair of enantiomers of DBD–PyNCS by a CSP column: (*a*), injection of (*R*)-(−)-DBD-PyNCS; (*b*), injection of (*S*)-(+)-DBD-PyNCS; and (*c*), injection of both enantiomers of DBD-PyNCS. Peaks: 1, (*R*)-(−)-DBD-PyNCS; and 2, (*S*)-(+)-DBD-PyNCS. Eluent, water–acetonitrile (2 + 8). Other HPLC conditions are given under Experimental.

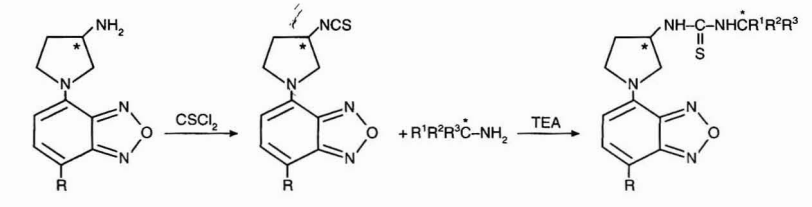

NBD–APy: R=NO_2 NBD–PyNCS: R=NO_2

DBD–APy: R=$SO_2N(CH_3)_2$ DBD–PyNCS: R=$SO_2N(CH_3)_2$

Fig. 1 Syntheses of the chiral derivatization reagents and subsequent reaction with chiral amines.

>99.5% for all four reagent enantiomers. The proposed reagents exhibit excellent stability, not only as the solid, but also in solution. No significant degradation was observed in acetonitrile solution after storage for 2 weeks at room temperature and 1 month at 5 °C in a refrigerator. This is obviously an important advantage not found with phenyl isothiocyanate (PITC)[17] and 1-(9-fluorenyl)ethyl chloroformate (FLEC),[18] which are volatile liquids. Another interesting characteristic of the reagents is the large values of optical rotation (more than 470° for the enantiomers of NBD-PyNCS and 270° for the enantiomers of DBD-PyNCS). The direction of the optical rotation is the same as that of the corresponding starting material, NBD-APy or DBD-APy.

Derivatization

The reagents react with chiral amines in a manner similar to other Edman-type reagents to produce corresponding thiourea derivatives (Fig. 1). Edman-type reagents such as PITC and fluorescein isothiocyanate (FITC) require a base catalyst for the derivatization of amines.[19–22] As triethylamine (TEA) is usually used as the catalyst, 1% TEA was also used in this work. The derivatization reaction with the amines is essentially completed after 10 min at 55 °C in water–acetonitrile (1 + 1) containing 1% TEA. The excitation and emission maxima of the resulting diastereomers are essentially the same as those of the derivatizing reagent and independent of the amine portion of the molecule. The reagents fluoresce at similar excitation and emission wavelengths to their derivatives (Table 2). Also, the maximum wavelengths and fluorescence intensities of the reagents are dependent on the solvent.

Table 1 Resolution and optical purity of the reagent enantiomers

	NBD-PyNCS		DBD-PyNCS	
Parameter*	(*R*)-(−)-Isomer	(*S*)-(+)-Isomer	(*R*)-(−)-Isomer	(*S*)-(+)-Isomer
t_R (min)	22.53	27.26	20.84	28.19
k'	16.74	20.46	15.41	21.20
α	1.22		1.38	
R_s	4.11		5.63	
Concentration of opposite enantiomer (%)	0.05	0.23	0.43	0.36

* t_R = Retention time; k' = capacity factor; α = separation factor; R_s = resolution.

The excitation and emission at long wavelengths is a distinct advantage for analysis of biological samples, because interference by intrinsic fluorescent compounds, which are excited and fluoresce at shorter wavelengths, is negligible.

HPLC Separation of Resulting Diastereomers

The utility of the chiral derivatization reagents for the analyses of chiral amines was investigated by HPLC. Protonated solvents in the mobile phase interfere with the interaction of the diastereomers with the stationary phase owing to hydrogen bond formation between the diastereomer and water. Therefore, normal-phase chromatography with nonpolar solvents was generally adopted for the separation of the diastereomers derived from chiral molecules. Although efficient resolution is usually obtained by the normal-phase chromatography, this technique may not be suitable for biological specimens because of sample handling difficulties and the use of harmful organic solvents such as benzene and chloroform. Therefore, separation by reversed-phase chromatography with aqueous solvent system was investigated in this work.

The capacity factor (k'), separation factor (α) and resolution value (R_s) for each pair of diastereomers are listed in Table 3. Seven amines, including amino acids and drugs, are well resolved on the Inertsil ODS-80A column with water–acetonitrile containing 0.05% TFA as the eluent. When (*R*)-(−)-isomers of the reagents are used as the derivatization reagents, amines of *R* configuration elute faster than those of *S* configuration. As expected, the opposite elution order was observed with use of (*S*)-(+)-isomers of the reagents. The elution order does not depend on the optical rotation of the enantiomers of amines. No exceptions were observed among the pairs of enantiomers tested. Among the amines and amino acids, the best resolution was observed with the β-blocker with NBD-PyNCS and DBD-PyNCS. The R_s values of β-blockers obtained with DBD-PyNCS were larger than those with NBD-PyNCS, whereas the values for PEA, NEA and CEA were essentially the same with both reagents. For amino acids, the resolution was dependent on both the analytes and the chiral reagents (Table 3). Fig. 4 shows some separation examples for the diastereomers formed from (*R*)-(−)-isomers of the reagents by reversed-phase chromatography. The largest peak observed in each chromatogram was the reagent itself; other small peaks are due to impurities in the analytes.

Conclusions

The proposed chiral fluorescent Edman-type reagents NBD-PyNCS and DBD-PyNCS provide excellent HPLC resolution

Table 2 Fluorescence characteristics of the chiral reagents and the derivatives with propranolol. Fluorphore concentration = 2×10^{-6} mol l^{-1}

		NBD-PyNCS		DBD-PyNCS	
Solvent	Parameter*	Reagent	Derivative	Reagent	Derivative
CH_3CN	λ_{ex}/nm	482	—†	451	—
	λ_{em}/nm	530	—	535	—
	I_{fluo} (arbitrary units)	850	—	410	—
CH_3CN–H_2O (1 + 1)	λ_{ex}/nm	491	491	460	460
	λ_{em}/nm	531	532	550	552
	I_{fluo} (arbitrary units)	390	(240‡)	125	(105‡)
H_2O	λ_{ex}/nm	502	—	457	—
	λ_{em}/nm	531	—	560	—
	I_{fluo} (arbitrary units)	55	—	10	—

* I_{fluo} = fluorescence intensity.
† Dashes indicate not measured.
‡ Concentration of the fluorophore undetermined.

of enantiomers of amino compounds by formation of diastereomers. The derivatization reaction with amines proceeds selectively and rapidly without detectable racemization. The resulting diastereomers are very stable and highly fluorescent with excellent spectral properties. The separation of the diastereomers derived from amines including amino acids and drugs is easily achieved by reversed-phase chromatography with an aqueous solution as the eluent. As the elution order of enantiomers can be changed with the use of a different enantiomer of the chiral reagent, the determination of trace amounts of one enantiomer in the presence of a much greater amount of the other enantiomer is easily accomplished. Good stability of the reagents is another important aspect.

Although DBD-Pro-COCl[12] and NBD-Pro-COCl[13] can also be used for the enantioseparation of chiral amines,[14] the proposed Edman-type reagents not only offer better selectivity with respect to the amino functional group, but also the resulting diastereomers are easily separated by reversed-phase chromatography. When the chloroformyl-based reagents are employed for tagging β-blockers, for example, care with the derivatization conditions must be taken in order to avoid incomplete double tagging towards amino and hydroxy groups, which can react with the reagents. Another excellent aspect of the isothiocyanate-based reagents is that the reaction proceeds in both organic solvents and aqueous solutions. The fluorescence at long wavelengths is another advantage for detection with biological samples, because the likelihood of interference by intrinsic compounds without amino functional groups is less likely. As the excitation wavelengths of the derivatives with NBD-PyNCS are close to the argon-ion laser light emission at 488 nm, the determination of primary and secondary amines at the attomole level should be possible with laser-induced fluorescence detection.[23] In addition, DBD-PyNCS derivatives are suitable for chemiluminescence detection, which provides high sensitivity, as demonstrated in previous work.[24] Consequently, the proposed methods may

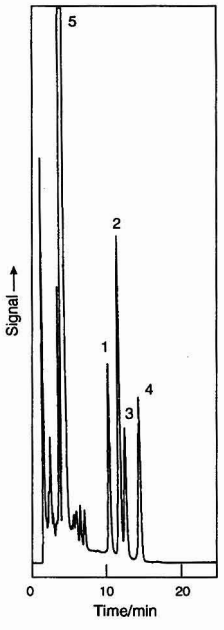

Fig. 4 Chromatograms of diastereomers derived from chiral drugs with (*R*)-(−)-NBD-PyNCS. Peaks: 1, (*R*)-(+)-propranolol; 2, (*S*)-(−)-propranolol; 3, (*R*)-(+)-alprenolol; 4, (*S*)-(−)-alprenolol; and 5, (*R*)-(−)-NBD-PyNCS. Each peak except the reagent corresponds to 25 pmol. An isocratic elution of water–acetontirile (60 + 40) containing 0.05% TFA for 20 min was used. Other HPLC conditions are given under Experimental.

Table 3 Resolution of diastereomers derived from chiral amino compounds by reversed-phase chromatography

		NBD-PyNCS				DBD-PyNCS			
		(*S*)-(+)-Isomer		(*R*)-(−)-Isomer		(*S*)-(+)-Isomer		(*R*)-(−)-Isomer	
Amino compound*	Isomer	k'	R_s	k'	R_s	k'	R_s	k'	R_s
PEA	(*R*)-(+)-	15.47		13.23		22.51		19.20	
	------		3.17†		3.20†		3.91†		3.97†
	(*S*)-(−)-	13.51		15.58		18.94		22.63	
CEA	(*R*)-(−)-	15.20		14.54		20.48		19.23	
	------		0.84†		0.83†		1.35†		1.37†
	(*S*)-(+)-	14.52		15.16		19.31		20.42	
NEA	(*R*)-(+)-	15.22		14.38		11.86		10.84	
	------		2.15‡		2.19‡		1.73‡		1.76‡
	(*S*)-(−)-	14.37		15.24		10.92		11.85	
Alprenolol	(*R*)-(+)-	10.31		8.13		13.04		9.81	
	------		4.10§		4.12§		6.03§		6.06§
	(*S*)-(−)-	8.20		10.23		9.82		12.91	
Propranolol	(*R*)-(+)-	8.70		6.96		14.58		11.56	
	------		3.75§		3.80§		5.52§		5.57§
	(*S*)-(−)-	6.99		8.62		11.60		14.56	
Valine	(*R*)-(+)-	6.81		6.13		10.87		10.40	
	------		1.62¶		1.60¶		1.83†		1.87†
	(*S*)-(−)-	6.11		6.85		10.40		10.96	
Phenylalanine	(*R*)-(+)-	14.90		12.48		13.89		13.09	
	------		3.57¶		3.50¶		2.28†		2.29†
	(*S*)-(−)-	12.52		14.83		13.04		13.95	

* PEA = 1-phenylethylamine; CEA = 1-cyclohexylethylamine; NEA = 1-(1-naphthyl)ethylamine.

†,‡,§,¶ CH_3CN–H_2O mixtures containing 0.05% v/v trifluoracetic acid were used as the mobile phases. CH_3CN contents (isocratic): † 40% v/v; ‡ 50% v/v; § 60% v/v and ¶ 35% v/v.

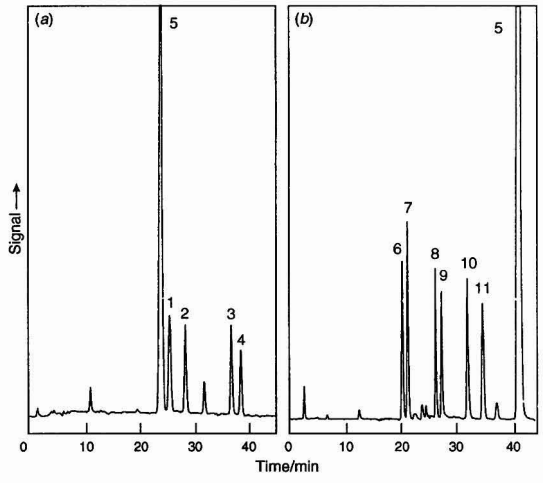

Fig. 5 Chromatograms of diastereomers derived from (*a*), chiral amines or (*b*), amino acids with (*R*)-(−)-DBD-PyNCS. Peaks: 1, (*R*)-(+)-PEA; 2, (*S*)-(−)-PEA; 3, (*R*)-(+)-NEA; 4, (*S*)-(−)-NEA; 5, (*R*)-(−)-DBD-PyNCS; 6, (*R*)-(+)-proline, 7, (*S*)-(−)-proline; 8, (*R*)-(+)-valine; 9, (*S*)-(−)-valine; 10, (*R*)-(+)-phenylalanine; and 11, (*S*)-(−)-phenylalanine. Each peak except the reagent is corresponding to 20 pmol. Eluent: A, water containing 0.05% TFA; and B, acetonitrile containing 0.05% TFA. Elution for amines: an isocratic elution of A–B (6 + 4) for 20 min, a linear gradient elution from A–B (6 + 4) to A–B (5 + 5) for 10 min, and then isocratic elution with A–B (5 + 5) for 15 min. Elution for amino acids: an isocratic elution with A–B (75 + 25) for 5 min, a linear gradient from A–B (75 + 25) to A–B (65 + 35) for 15 min, and then isocratic elution with A–B (6 + 4) from 20 min to 50 min. Other HPLC conditions are given under Experimental.

serve for the enantiomeric determination of various kinds of chiral amines such as drugs and amino acids in complex biological specimens.

Chiral sequence analysis of peptides and proteins might be another important application. If the chiral sequencing of amino acids is performed, not only the identification of the optical isomer but also the determination of the optical purity in each amino acid in peptides might be possible. Further studies on trace chiral drug and amino acid determination and peptide sequence analyses are in progress.

The authors thank Dr. C. R. Warner, Food and Drug Administration, Washington, DC, for reviewing the manuscript.

References

1 Stinson, S. C., *Chem. Eng. News*, 1992, Sept. 28, 46.
2 *Chirotechnology*, ed. Sheldon, R. A., Marcel Dekker, New York, 1993, ch. 2, p. 39.
3 Imai, K., and Toyo'oka, T., in *Selective Sample Handling and Detection in High-performance Liquid Chromatography*, ed. Frei, R. W., and Zech, K., *Journal of Chromatography Library*, vol. 39A, Elsevier, Amsterdam, 1988, p. 209.
4 Lingeman, H., Underberg, W. J. M., Takadate, A., and Hulshoff, A., *J. Liq. Chromatogr.*, 1985, **8**, 789.
5 *Chiral Separation by HPLC*, ed. Krstulovic, A. M., Ellis Horwood, Chichester, 1989.
6 *Chromatographic Chiral Separation*, ed. Zief, M., and Crane, L. J., Marcel Dekker, New York, 1988.
7 Srinvas, N. R., and Igwemezie, L. N., *Biomed. Chromatogr.*, 1992, **6**, 163.
8 Goto, J., Hasegawa, M., Nakamura, S., Shimada, K., and Nambara, T., *J. Chromatogr.*, 1978, **152**, 413.
9 Goto, J., Goto, N., Hikichi, A., and Nambara, T., *J. Liq. Chromatogr.*, 1979, **2**, 1179.
10 Aswad, D. W., *Anal. Biochem.*, 1984, **137**, 405.
11 Nimura, N., and Kinoshita, T., *J. Chromatogr.*, 1986, **352**, 169.
12 Toyo'oka, T., Ishibashi, M., Terao, T., and Imai, K., *Analyst*, 1993, **118**, 759.
13 Toyo'oka, T., Liu, Y.-M., Hanioka, N., Jinno, H., Ando, M., and Imai, K., *J. Chromatogr.*, 1994, **675**, 79.
14 Toyo'oka, T., Liu, Y.-M., Jinno, H., Hanioka, N., Ando, M., and Imai, K., *Biomed. Chromatogr.*, 1994, **8**, 85.
15 Toyo'oka, T., Ishibashi, M., and Terao, T., *Analyst*, 1992, **117**, 727.
16 Toyo'oka, T., Ishibashi, M., and Terao, T., *Anal. Chim. Acta*, 1993, **278**, 71.
17 Heinrikson, R. L., and Meredith, S. C., *Anal. Biochem.*, 1984, **136**, 65.
18 Einarsson, S., Josefsson, B., Moller, P., and Sanchez, D., *Anal. Chem.*, 1987, **59**, 1191.
19 Jin, S.-W., Chen, G.-X., Palacz, Z., and Wittmann-Liebold, B., *FEBS Lett.*, 1986, **198**, 158.
20 Imai, K., Uzu, S., Nakashima, K., and Akiyama, S., *Biomed. Chromatogr.*, 1993, **7**, 56.
21 Imakyure, O., Kai, M., Mitsui, T., Nohta, H., and Ohkura, Y., *Anal. Sci.*, 1993, **9**, 647.
22 Muramoto, K., Kamiya, H., and Kawauchi, H., *Anal. Biochem.*, 1984, **141**, 446.
23 Toyo'oka, T., Ishibashi, M., and Terao, T., *J. Chromatogr.*, 1992, **625**, 357.
24 Toyo'oka, T., Ishibashi, M., and Terao, T., *J. Chromatogr.*, 1992, **627**, 75.

Paper 4/03452J
Received June 7, 1994
Accepted July 12, 1994

Liquid–Liquid Extraction and Separation of Lanthanum(III) from Titanium(IV), Zirconium(IV), Hafnium(IV), Thorium(IV) and Uranium(VI)

N. G. Bhilare and V. M. Shinde*

Analytical Laboratory, The Institute of Science, 15 Madam Cama Road, Bombay-400 032, India

A method for the solvent extraction of lanthanum from salicylate media by using triphenylphosphine oxide is presented. Lanthanum is extracted quantitatively from 2.0×10^{-2}–5.0×10^{-2} mol dm^{-3} sodium salicylate solution at pH 4.0–5.0 using 1.5% triphenylphosphine oxide dissolved in toluene. The extracted metal ion is stripped using water and estimated spectrophotometrically following complexation with Thoron-I. A possible mechanism of extraction is discussed. The method permits the separation of lanthanum from titanium, zirconium, hafnium, thorium and uranium.

Keywords: Lanthanum(III) separation; solvent extraction; triphenylphosphine oxide

Introduction

Lanthanum is an important constituent of aluminium and copper alloys, used as a hardening agent. It is also used in glass polishing agents and semiconductors, and has a promising future in nuclear technology. The preconcentration and purification of lanthanum can be achieved by solvent extraction. The existing solvent extraction methods are listed in Table 1.

In this communication we propose a method for the extractive separation of lanthanum from salicylate media using triphenylphosphine oxide (TPPO). The method is free from limitations such as a long equilibration period, the use of salting out agents, multiple extraction and co-extraction.

Experimental

Apparatus and Reagents

Absorbance and pH were measured on Spectronic 20D (Milton Roy and Co, New York) and Control Dynamic digital pH meter with a combined glass electrode.

A stock solution of lanthanum was prepared by dissolving 0.587 g of lanthanum oxide (BDH, now Merck, Poole, Dorset, UK) in 5 cm^3 of concentrated hydrochloric acid (11.3

Table 1 Critical review of the methods for the solvent extraction of lanthanum(III)

Extractant	Aqueous medium	Special features	Reference number
Tributyl phosphate (TBP) Trioctylphosphine oxide (TOPO) Tributylphosphine oxide (TBPO)	Thiocyanate	Extractable species defined $La(SCN)_3$–5TBP, $La(SCN)_3$–4TOPO, $La(SCN)_3$–4TBPO	1
Tributyl phosphate	Nitrate	Requires salting out agent and multiple extraction (three times)	2
Tributyl phosphate	Thiocyanate	Equilibration time 5 min, extracted species $La(SCN)_3$–5TBP	3
Trioctylphosphine oxide Tributylphosphine oxide	Nitrate	Requires salting out agents	4
Trioctylphosphine oxide	Chloride	Extraction of hydroxide complex, $La(OH)_3$–3TOPO. Equilibration time 15 min	5
Diisopentylmethyl phosphonate	Nitrate	Requires salting out agent	6
Di(2-ethylhexyl)phosphoric acid	Chloride	Batch extraction and purification of lanthanum	7
Di(2-ethylhexyl)phosphoric acid	pH	Study of fluoride, oxalate and sulfate complexes	8
Amine substituted phosphine oxide	Nitrate	Study of effect of amino group substituents	9
Dialkyl dithiophosphoric acid	Nitrate or chloride	Separation from thorium(IV)	10
Bis(2-ethylhexyl)phosphorodithioate	pH	Co-extraction of thorium(IV)	11
(2-Ethylhexyl-3-pentadecylphenyl) phosphoric acid	Chloride	Comparative study with di(2-ethylhexyl)phosphoric acid	12
Tris(1-methylheptyl)phosphine oxide	Thiocyanate	Four-fold decrease in distribution coefficient with 10 °C rise in temperature	13
Trialkylmethylammonium nitrate + tributyl phosphate	Nitrate	Separation from actinium(III)	14
Primary amine + bis(2-ethylhexyl) hydrogenphosphate	Sulfate	Synergistic effect study. Equilibration time 15 min	15
Bis(2,4,4-trimethylpentyl)phosphinic acid	pH	Extraction coefficient and separation factor determined	16
Dioctylphosphoric acid	Nitrate or chloride	Separation from barium	17
Di-*n*-butyl carbamoyl phosphonate	Chloride	—	18
N-Phenylbenzohydroxamic acid	Perchlorate	Separation from cerium. Equilibration time 15 min	19

* To whom correspondence should be addressed.

mol dm^{-3}) and diluting to 100 cm^3 with distilled water. The solution was standardized by a previous method[20] and further diluted, as required, for the working solutions.

TPPO (1.5% m/v) (Fluka Buchs, Switzerland) dissolved in toluene was used for the extraction studies. A 0.1% aqueous solution of Thoron-I was used for the spectrophotometric determination of lanthanum.[21] All other reagents were of analytical-reagent grade.

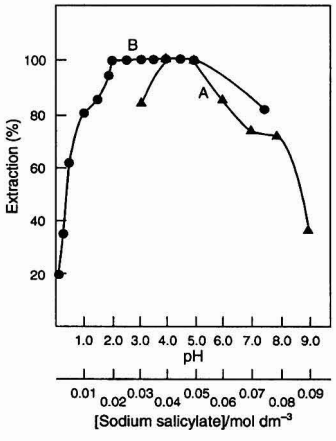

Fig. 1 Extraction of lanthanum(III) as a function of A, pH at a fixed sodium salicylate concentration (5×10^{-2} mol dm^{-3}) and TPPO concentration (1.5%) and B, salicylate concentration at a fixed pH (4.5) and TPPO concentration (1.5%).

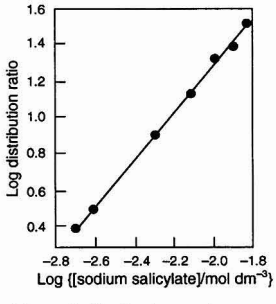

Fig. 2 Graph of log of distribution ratio *versus* log of sodium salicylate concentration at a fixed pH (4.5) and TPPO concentration (1.5%).

Extraction Procedure

A 25 cm^3 aliquot of a solution containing 80 μg of lanthanum and 5.0×10^{-2} mol dm^{-3} of sodium salicylate was adjusted to pH 4.5 using dilute hydrochloric acid (0.1 mol dm^{-3}) and sodium hydroxide solution, and was equilibrated for 30 s in a 100 cm^3 separatory funnel with 5 cm^3 of 1.5% TPPO dissolved in toluene. After phase separation, lanthanum was stripped from the TPPO using 10 cm^3 of water and estimated spectrophotometrically: 2 cm^3 of Thoron-I solution was added, the pH of the solution was adjusted to 5.0–6.0 using dilute hydrochloric acid and sodium hydroxide solution and the absorbance was measured at 545 nm.[21]

Results and Discussion

Extraction Conditions

The variation in TPPO concentrations (0.1–2.0%), pH (3.0–9.0) and sodium salicylate concentrations (1.0×10^{-3}–7.5×10^{-2} mol dm^{-3}) indicated that quantitative extraction of lanthanum from 2.0×10^{-2}–5.0×10^{-2} mol dm^{-3} sodium salicylate at pH 4.0–5.0 (Fig. 1) using 1.5% TPPO is feasible. A 30 s equilibration time was adequate. Various solvents, such as toluene, xylene, benzene, chloroform, and carbon tetrachloride were tried and the results showed that TPPO dissolved in toluene and xylene gave 99.6 and 99.2% extraction, respectively. With the other three diluents, the extraction was 93.75, 92.15 and 95.08%, respectively.

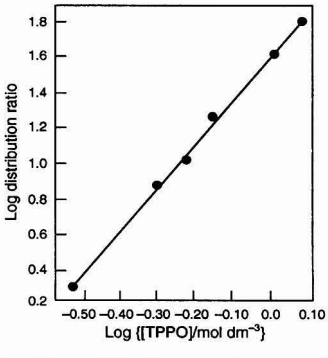

Fig. 3 Graph of log of distribution ratio *versus* log of TPPO concentration at a fixed pH (4.5) and salicylate concentration (5.0×10^{-2} mol dm^{-3}).

Table 2 Separation of lanthanum(III) from binary mixtures and a multicomponent system

Composition of mixture/μg	Recovery of lanthanum (triplicate analysis) (%)	Relative error (%)	Recovery of added ion (triplicate analysis) (%)	Relative error (%)	Estimation procedure for added ions
La*, 80.0; Ti, 100.0	99.6	0.4	99.9	0.1	H_2O_2[25]
La, 80.0; Zr, 100.0	99.4	0.6	99.2	0.8	Alizarin Red S[25]
La, 80.0; Hf, 100.0	99.5	0.5	99.6	0.4	Xylenol Orange[25]
La, 80.0; Th, 100.0	99.6	0.4	99.3	0.7	Thoron-I[25]
La, 80.0; U, 100.0	99.2	0.8	99.7	0.3	PAR[26]
La, 80.0; Ti, 100; Zr, 100; Hf, 100; Th, 100; U, 100	99.0	1.0	—	—	—

* Lanthanum was determined using Thoron-I as described under Extraction Procedure.

Nature of the Extracted Species

An attempt was made to ascertain the composition of the extracted species. In aqueous solution the salicylate ion generally functions as a divalent bidentate ligand[22] that can function either as a singly-charged or a doubly-charged anion in solvent extraction systems.[23,24] A graph of log of distribution ratio *versus* log of salicylate concentration at fixed pH (4.5) and TPPO concentration (1.5%) gave a slope of 1.2 with respect to salicylate (Fig. 2).
As

$$\frac{\mathrm{d}\log D}{\mathrm{d}\log[\mathrm{HSal_{aq}}]} = n(\mathrm{org}) - n(\mathrm{aq})$$

where n (org) and n (aq) are the number of ligands associated with each metal ion in the organic and aqueous phase, respectively, D is the distribution ratio and $[\mathrm{HSal_{aq}}]$ is the concentration of salicylate. The observed slope indicates that the number of salicylate ions per lanthanum in the organic phase is one greater than the number of salicylate ions per lanthanum in the aqueous phase. The number of ligands associated with the metal ion in the aqueous phase is dependent on the pH and salicylate concentration. The predominant species in the aqueous phase is La^{3+} and $LaSal^{+}$, as only uncharged species are extracted into the organic phase by a neutral extractant; the extracted species in the organic phase is therefore LaSal–HSal–x TPPO where x is the number of TPPO molecules associated with each metal ion. A plot of log of distribution ratio *versus* log of TPPO concentration at a fixed pH (4.5) and salicylate concentration (5.0×10^{-2} mol dm^{-3}) gave a slope of 2.3 (Fig. 3) indicating that two moles of TPPO are associated with each mole of lanthanum. Hence, a probable extraction mechanism is

$$La^{3+}(aq) + Sal^{2-}(aq) \rightleftharpoons LaSal^{+}(aq)$$
$$LaSal^{+}(aq) + HSal^{-}(aq) \rightleftharpoons LaSal\text{–}Hsal(aq)$$
$$LaSal\text{–}HSal(aq) + 2TPPO(org) \rightleftharpoons LaSal\text{–}HSal\text{–}2TPPO(org)$$

TPPO, being more basic than water displaces the latter and renders the lanthanum salicylate more hydrophobic.

Effect of Foreign Ions

Varying amounts of foreign ions were added to a fixed amount of lanthanum (80 μg) to study interferences in the recommended procedure. The tolerance limit was set as the amount of foreign ion required to cause a ±2% error in lanthanum recovery. There was no interference from 5000 μg each of Ba^{II}, Mg^{II} and sulfate; 3000 μg each of Au^{III}, U^{VI}, Hg^{II}, Ca^{II}, ascorbic acid and nitrate, 2000 μg each of Ag^{II}, Mo^{VI}, Al^{III}, Mn^{II}, Cd^{II}, thiocyanate and tartrate; 1000 μg each of Cr^{VI}, Co^{II}, Zr^{IV}, Fe^{III}, V^{V}, Zn^{II}, Th^{IV}, Bi^{III} and Cu^{II}; 500 μg each of Ti^{IV}, W^{VI} and thiourea; 100 μg each of Ni^{II}, Pb^{II}, Sn^{II}. However, oxalate, ethylenediaminetetraacetic acid (EDTA) and phosphate interfered severely.

Separation of La^{III} from Ti^{IV}, Zr^{IV}, Hf^{IV}, Th^{IV} and U^{VI}

Zirconium, hafnium, thorium and uranium showed 100.0, 100.0, 65.0 and 87.0% extraction, respectively, using the optimum extraction conditions for lanthanum. The co-extracted metal ions were separated from lanthanum by selective stripping of the latter with water and its subsequent determination using Thoron-I. None of the co-extracted metal ions are stripped with water. Zirconium, hafnium and thorium can be removed from the organic phase by stripping with 0.1 mol dm^{-3} hydrochloric acid and uranium with 0.05 mol dm^{-3} ammonium hydroxide, and are spectrophotometrically determined, in the aqueous phase, using previous methods.[25,26] Titanium, however, remains completely in the aqueous phase and is estimated by using a standard procedure.[25] The separation and recovery of lanthanum and added ions was found to be ≥99.0%. Lanthanum was also separated from a multicomponent system. The results are reported in Table 2. Six determinations with 80.0 μg of lanthanum gave a mean absorbance value of 0.3 ± 0.01 with a standard deviation (s) of 5.76×10^{-2} and a relative standard deviation (s_r) 1.92%. The total procedure required only 15 min. The proposed method is precise, accurate and permits a rapid separation and determination of lanthanum.

The authors thank the Council of Scientific and Industrial Research (CSIR), New Delhi, India for financing this project.

References

1 Khopkar, P. K., and Narayanankutty, P., *J. Inorg. Nucl. Chem.*, 1972, **34**, 2617.
2 Edge, R. A., *Anal. Chim. Acta*, 1962, **27**, 396.
3 El-Yamani, I. S., and Shabana, E. I., *J. Radioanal. Chem.*, 1984, **84**, 307.
4 Goffart, J., and Duyckaerts, G., *Anal. Chim. Acta*, 1969, **46**, 91.
5 Cecconie, T., and Freiser, H., *Anal. Chem.*, 1990, **62**, 622.
6 Mikhlin, E. B., and Korpusov, G. V., *Zh. Neorg. Khim.*, 1965, **10**, 2787.
7 Nair, S. G. K., and Smutz, M., *J. Inorg. Nucl. Chem.*, 1967, **29**, 1787.
8 Aziz, A., and Lyle, S. J., *J. Inorg. Nucl. Chem.*, 1970, **32**, 1925.
9 Rusina, M. N., Polikarpov, Y. M., Yaroshenka, G. F., and Timakoka, L. M., *J. Gen. Chem. USSR (Engl. Transl.)*, 1973, **43**, 238.
10 Curtui, M., and Haiduc, I., *J. Radioanal. Chem.*, 1992, **164**, 91.
11 Curtui, M., and Haiduc, I., *Rev. Chim. (Bucharest)*, 1988, **39**, 1099.
12 Sreelatha, S., Rao, T. Prasada, Narayanan, C. S., and Damodaran, A. D., *Talanta*, 1994, **41**, 433.
13 Korpusov, G. V., Danilov, N. A., Volodin, I. A., Kotova, L. V., and Filippov, E. A., *Radiokhimiya*, 1980, **22**, 111.
14 Mikhailichenko, A. I., Goryacheva, E. G., Aksenava, N. M., and Denisov, A. F., *Radiokhimiya*, 1982, **24**, 207.
15 Watanabe, H., *Bull. Chem. Soc. Jpn.*, 1970, **43**, 100.
16 Komatsu, Y., and Freiser, H., *Anal. Chim. Acta*, 1989, **227**, 397.
17 Peppard, D. F., Mason, G. W., and Moline, S. W., *J. Inorg. Nucl. Chem.*, 1957, **5**, 141.
18 Perricon, D. C., Tsolis, A. K., and Belkas, E. P., *Talanta*, 1970, **17**, 551.
19 Riedel, A., *J. Radioanal. Chem.*, 1970, **6**, 75.
20 Welcher, F., *The Analytical Uses of EDTA*, Van Nostrand, New York, 1958, p. 50.
21 Sangal, S. P., and Dey, A. K., *Chimie Analytique*, 1964, **46**, 223.
22 Perrin, D. D., *Nature*, 1958, **182**, 741.
23 Aggett, J., and Crossley, P., *J. Inorg. Nucl. Chem.*, 1967, **29**, 1113,
24 Aggett, J., Evans, D., and Hancock, R., *J. Inorg. Nucl. Chem.*, 1968, **30**, 2529.
25 Marczenko, Z., *Spectrophotometric Determination of Elements*, Ellis Horwood, Chichester, 1976, pp. 539, 556, 611 and 613.
26 Dalvi, M. B., and Khopkar, S. M., *Talanta*, 1978, **25**, 599.

Paper 4/05041J
Received August 16, 1994
Accepted September 13, 1994

Determination of Free Selenomethionine in Nutritional Supplements by High-performance Liquid Chromatography Coupled with Thermochemical Hydride Generation Atomic Absorption Spectrometry

G. Matni and R. Azani

Macdonald Campus, Department of Food Science and Agricultural Chemistry, McGill University, 21 111 Lakeshore Road, Ste-Anne-de-Bellevue, Québec, H9X 3V9, Canada

M. R. Van Calsteren

Agriculture Canada, Food Research and Development Centre, 3600 Casavant Blvd. West, Saint-Hyacinthe, Québec, J2S 8E3, Canada

M. C. Bissonnette

Environment Canada, Environmental Technology Centre, 3439 River Road, Ottawa, Ontario, K1A 0H3, Canada

J. S. Blais*

Macdonald Campus, Department of Food Science and Agricultural Chemistry, McGill University, 21 111 Lakeshore Road, Ste-Anne-de-Bellevue, Québec, H9X 3V9, Canada and Agriculture Canada, Food Research and Development Centre, 3600 Casavant Blvd. West, Saint-Hyacinthe, Québec, J2S 8E3, Canada

Selective isolation and HPLC–AAS protocols were developed to determine free selenomethionine (SeMet) in complex matrices such as nutritional supplements and mixtures of free amino acids. The selenoamino acid in alkaline solution was first derivatized with 1-fluoro-2,4-dinitrobenzene (FDNB, Sanger's reagent). After removal of excess of reagent by partitioning with diethyl ether, the *N*-dinitrophenyl (DNP)-derivatized SeMet was protonated by acidification and extracted with diethyl ether. DNP-SeMet was determined selectively by HPLC–thermochemical hydride generation (THG) AAS. A selective chromatographic mechanism based on π-electron interactions was optimized using a silica stationary phase derivatized with *p*-nitrophenyl moieties. Primary analytical validation parameters including stability, linearity and limit of detection were obtained using a purified DNP-SeMet standard which was characterized by $^{1}H/^{13}C/^{77}Se$ NMR and fast atom bombardment MS techniques. The calibration graphs for sequential dilutions of this standard were linear (averge r = 0.997) and the limit of detection from the resultant calibration graphs was estimated to be 17 ng as Se or 81 ng as DNP-SeMet. The standard was found to decompose slowly (0.08% h^{-1}) via photolytic cleavage of a Se–C bond. MS and HPLC–THG-AAS studies demonstrated that the cleavage intermediates ($CH_3Se^{\cdot}$) combined to form dimethyl diselenide. Ascorbic acid present in large amounts in nutritional supplements was revealed to be the major interferent during the DNP derivatization step. This interference was removed using a cation-exchange treatment of the crude extract prior to derivatization. The recovery of the SeMet from stock solutions and nutritional supplements was virtually quantitative (99 ± 4.5%). In the presence of a 500-fold excess of other amino acids, this recovery decreased (95 ± 2.6%), but remained in an acceptable range to allow the accurate determination of SeMet in a protein hydrolysate.

***Keywords:** Selenomethionine determination; 1-fluoro-2,4-dinitrobenzene derivatization; Sanger's reagent; nutritional supplements; high-performance liquid chromatography–thermochemical hydride generation atomic absorption spectrometry*

Introduction

Interest in the role of selenium (Se) in human nutrition has increased rapidly since studies have demonstrated the complex biochemistry of this trace element. Dietary Se supplementation has become a popular health fad, with claims being made in the popular press for the prevention of angina, arthritis, cancer, cerebrovascular disease, ageing, infections, infertility, *etc.*[1,2] The effectiveness of this supplementation in the prevention of chronic selenium deficiency symptoms such as those in Keshan disease has been demonstrated unambiguously.[3] Peptidic selenomethionine (SeMet) has been shown to be the major Se species present in soybean,[4] wheat[5] and yeast.[6] Free selenomethionine and selenized yeast are present in the formulation of several nutritional supplements available commercially for human consumption. In the lactating rat, selenium ingested as free SeMet or selenized yeast has been shown to be more bioavailable than selenite.[7] Moreover, because SeMet may not be differentiated from methionine by enzymes,[8] selenium from free SeMet or selenized yeast/wheat tends to distribute less specifically than selenite (rat)[6] or selenate (human).[9] The latter inorganic forms have been shown to be incorporated more rapidly in the seleno-enzyme glutathione peroxidase.

The potential benefits of a dietary supplementation in selenium are limited by its relatively narrow 'therapeutic window' above which toxicity symptoms may develop.[10,11] Thus, the consumption of intentionally (supplements) or biogeochemically selenium-enriched diets may lead to a

* To whom correspondence should be addressed, at Agriculture Canada.

chronic condition referred to as selenosis.[1,12,13] SeMet is embryotoxic to fish, amphibians and most notably to avian species. Recent studies conducted with Mallard ducklings for 14 weeks revealed a dose-dependent accumulation of Se (fed as SeMet) in the liver with evidence of hepatoxicity, which compromised growth and, at high doses, survival.[14]

Studying the relatively singular biological activity of SeMet or running routine quality control of selenium-enriched nutritional supplements require access to a rapid, quantitative and selective method for the determination of this selenoamino acid. Ion-exchange chromatographic and radiometry techniques for protein hydrolysates have been used successfully to characterize ^{75}Se-radiolabelled selenoamino acids.[6,8] Several selenoamino acids were first identified using other classical characterization techniques such as preparative thin-layer chromatography (TLC)[4,15,16] or GC–MS of trimethylsilylated SeMet.[4] SeMet has been determined indirectly *via* reaction with cyanogen bromide, forming CH_3SeCN, which was then determined by HPLC[17] or derivatized to a piazselenol followed by GC.[18] Although the latter GC approach provides limits of detection that allow the routine determination of peptidic SeMet at trace levels, it would also respond to *Se*-methylated amino acids such as *Se*-methylselenocysteine, which may be present in plants and microorganisms.[15] For direct HPLC analysis, the main problem remains the fact that SeMet exists in a vast excess over other amino acids. Using non-specific detection, the determination of peptidic SeMet by cation-exchange HPLC is difficult because it elutes with a retention time similar to those of leucine and isoleucine.[17,19]

The method described here is based on the application of a selenium-selective HPLC detector which allows the determination of SeMet in the presence of a large excess of other components present in nutritional supplements. For this purpose, we used a gas-phase thermochemical hydride generator (THG) which was configured as an interface between HPLC and atomic absorption spectrometry (AAS).[20,21] We report the analytical performance of an integrated analytical procedure involving (a) a solvent extraction protocol based on the derivatization of SeMet with the Sanger's reagent [forming a 2,4-dinitrophenyl (DNP) derivative]; (b) a selective π-electron HPLC separation of derivatized SeMet; and (c) on-line THG-AAS detection. The preparation, purification and characterization of a DNP-SeMet standard are described along with stability and calibration parameters.

Experimental

Reagents

Diethyl ether, methanol, acetonitrile (distilled in glass, anhydrous) and 2,4-dinitrophenol (ACS reagent grade) were purchased from BDH (Montreal, Canada). Triethylamine (TEA), 1-fluoro-2,4-dinitrobenzene (FDNB, Sanger's reagent), DL-selenomethionine and dimethyl diselenide were purchased from Sigma (St. Louis, MO, USA).

Instrumentation

The instrument consisted of a binary HPLC system (Gilson Model 305) coupled to an atomic absorption spectrometer (Model 200A; Buck Scientific, Norwalk, CT, USA) *via* a thermochemical hydride generator.[20,21] Narrow-bore tubing (2 mm i.d.) was used post-injector (50 μl sample loop). The THG interface was configured and operated as described previously for selenonium species.[21] Chromatograms were recorded and integrated by chromatographic software (JCL 6000; Jones Chromatography, Littleton, CO, USA).

HPLC Conditions

Chromatography was performed on a silica-based Nucleosil column (*p*-nitrophenyl, 5 μm, 200 × 4.0 mm i.d.; Macherey–Nagel, Dueren, Germany) using methanol as the mobile phase at a flow rate of 0.65 ml min^{-1}. Triethylamine was added to the mobile phase in various proportions (0–1000 μg ml^{-1}) during chromatographic optimization. For each mobile phase composition, peak areas and retention times from three replicate injections (50 μl) of DNP-SeMet standard were recorded.

Synthesis and Purification of DNP-SeMet Standard

A 3 g amount of DL-SeMet was dissolved in 100 ml of 0.2 mol l^{-1} phosphate buffer (pH 10.0). Five equivalents of FDNB were added under a gentle flow of nitrogen and the reaction was carried out in darkness for 6 h under an inert atmosphere with continuous magnetic stirring. The pH of the reaction mixture was readjusted to 10.0 with 1 mol l^{-1} NaOH and the mixture was extracted with diethyl ether (50 ml) several times to remove excess of FDNB. The removal of excess of FDNB was monitored by TLC on silica gel (Polygram, SIL G/UV$_{254}$, Macherey–Nagel) using ethyl acetate–hexane (3 + 1) containing 1% of acetic acid as the mobile phase. The pH of the aqueous phase was then adjusted to 2.0 with 6 mol l^{-1} HCl and the mixture was re-extracted with diethyl ether (50 ml) several times. Residual water present in the ether extracts was frozen on the surface of the reaction flask after immersion in liquid air for 15–20 s. The etheral phase was transferred into a dry flask and the solvent was removed using a rotary evaporator.

The yellow–reddish oily product was dissolved in 2 ml of ethyl acetate–hexane (1 + 1), applied on a preparative chromatography column (silica gel, 230–400 mesh, 60 Å) and eluted with the same solvent. Fractions of 1 ml were collected and analysed by TLC on a pre-coated silica plate (PK5 silica gel, Whatman, Maidstone, UK) using the same mobile phase. The TLC bands were detected at 365 and 254 nm. The relative retention indices for DNP-SeMet, 2,4-dinitrophenol (basic hydrolysis product of FDNB) and FDNB were 0.15, 0.56 and 0.93, respectively. Aliquots from the same fractions were also analysed for Se content by THG-AAS in the flow injection mode (HPLC column removed). Selenium-containing fractions eluting as one band in TLC were combined and the solvent was evaporated. The product crystallized on freezing at −20 °C.

Characterization of DNP-SeMet

DNP-SeMet was analysed by NMR spectrometry on a Bruker AM-300 wide-bore spectrometer using a 5 mm ^{1}H/^{19}F probe for ^{1}H and a 10 mm broadband probe for ^{13}C and ^{77}Se. The 300.13 MHz ^{1}H, 75.47 MHz ^{13}C and 57.24 MHz ^{77}Se NMR analyses of DNP-SeMet were performed in $CDCl_3$–CD_3OD (1 + 2) at 298 K. Connectivities between protons were established by the two-dimensional correlated spectroscopy (COSY) technique.[22] Proton chemical shifts were obtained by spectral simulations performed with the Bruker PANIC program. Normal-mode ^{13}C NMR spectra were acquired with composite-pulse decoupling as implemented in the spectrometer software. Carbons were assigned using the following pulse sequences: distorsionless enhancement by polarization transfer (DEPT),[23] heteronuclear ^{13}C–^{1}H correlation 2D experiments (HETCORR)[24] and ^{1}H-detected heteronuclear multiple bond correlation (HMBC).[25] Characterization of DNP-SeMet was also carried out by mass spectrometry (VG Model 7070) using fast atom bombardment (FAB) in the negative-ion mode. The sample was introduced in a glycerol matrix and bombarded with xenon (8 kV, 1 a) at a pressure of 2 × 10^{-6} Torr (1 Torr = 133.3 Pa).

Linearity, Reproducibility and Limits of Detection

Calibration graphs were obtained by HPLC–THG-AAS analysis of sequential dilutions of a fresh standard of DNP-SeMet. The same experiment was conducted in the flow injection mode. Correlation coefficients were obtained by linear regression of peak area *versus* concentration of the analyte. The limit of detection (LOD) was calculated from the resultant calibration graphs as three standard deviations above the averaged background noise. The reproducibility of the interface was determined by calculating the relative standard deviation of triplicate injections under the optimum conditions of sequential dilutions of the standard.

Photodegradation Experiments

Aliquots of 2 ml of the pure standard of DNP-SeMet were distributed in glass tubes and stored at room temperature under air or a nitrogen atmosphere (in deoxygenated methanol) and in darkness or under continuous fluorescent lighting. The four treatments were analysed periodically by HPLC–THG-AAS. Dimethyl diselenide was identified as a degradation product of DNP-SeMet by HPLC–THG-AAS and confirmed by MS. The mass spectrum was obtained by electron impact ionization (70 eV) using the direct unheated probe technique at a pressure of 5×10^{-5} Torr.

Determination of SeMet in Aqueous Solutions

In 50 ml glass tubes, 0.5, 1.0, 1.5, 2.0 and 3.0 ml of a fresh aqueous solution containing 100 μg ml^{-1} of DL-SeMet were added to 9 ml of 0.2 mol l^{-1} phosphate buffer (pH 10.0). Under a gentle flow of nitrogen, 1.5 ml of FDNB was added to each tube. The tubes were tightly closed wtih PTFE stoppers and the reaction was carried out for 2 h, in darkness, with continuous reciprocal shaking. The pH of the buffered solutions was routinely measured (double-strip pH paper) and, if necessary, readjusted to pH 10 in order to correct for acidification by reaction by-products (HF and 2,4-dinitrophenol). After 2 h, the reaction medium was extracted with 3×10 ml of diethyl ether at alkaline pH (10.0), then acidified to pH 2.0 with 6 mol l^{-1} HCl and extracted with 3×10 ml of diethyl ether. The etheral extracts were combined, dried by freezing and evaporated to dryness; the residue was dissolved in 10 ml of methanol and analysed by HPLC–THG-AAS. Blank solutions were submitted to the same treatments. The etheral extract from the basic reaction mixture was also analysed for total Se in the flow injection THG-AAS mode.

Determination of SeMet in the Presence of an Excess of Amino Acids

A 1 ml volume of DL-SeMet at 100 μg ml^{-1} in water was spiked in 9 ml of phosphate buffer (pH 10.0). A 500-fold excess of amino acids (isoleucine, leucine, aspartic acid, lysine histidine, serine, methionine, phenylalanine, tryptophan, proline, glycine, valine, alanine, threonine and arginine) was spiked in the SeMet solution. A 2 ml volume of FDNB was added under nitrogen and the reaction and isolation procedures were carried out as described previously. Blanks containing the sample concentration of amino acids (except SeMet) were conducted simultaneously.

Determination of SeMet in Nutritional Supplement

Tablets of a dietary supplements (BioSelen + Zinc, Pharma Nord, Denmark) labelled as containing (per tablet) vitamin A (1.0 mg), vitamin B_6 (2.2 mg), vitamin C (90 mg), vitamin E (15 mg), zinc gluconate (15 mg) and L-SeMet (100 μg) were used as test samples. The tablets were weighed, then homogenized with a mortar and pestle. Amounts of powder equivalent to 50, 100, 150 and 200 μg of SeMet were weighed and distributed in glass tubes (in triplicate). Water (30 ml) was added and the mixture was shaken thoroughly and centrifuged at 12096 *g* for 20 min. The supernatant was transferred and extracted with 10 ml of diethyl ether in order to remove organo-soluble materials. The pH of the aqueous phase was around 4.9. The sample was applied on a cation-exchange column (5 cm × 1.0 cm i.d., Dowex 50W-X8, Bio-Rad, Hercules, CA, USA). The column was washed with distilled water (5×5 ml) and the sample was immediately eluted with 30 ml of 2 mol l^{-1} ammonia solution. The eluate was buffered at pH 10.0 (with phosphate buffer) and ammonia was displaced from the solution using a nitrogen bubbler at 40 °C for 1 h. FDNB (1.5 ml) was then added and the reaction and isolation procedure was carried out as described above. The recovery of SeMet was calculated from calibration graphs obtained from control samples (buffer spiked with the same amounts of SeMet of 50, 100, 150 and 200 μg in triplicate). Samples of nutritional supplement were also analysed without the cation-exchange chromatography step. Blanks containing no supplement were also analysed.

Results and Discussion

Sanger's reagent (1-fluoro-2,4-dinitrobenzene, FDNB) has been widely used for decades to prepare 2,4-dinitrophenyl (DNP) derivatives of amino acids for *N*-terminal amino acid analysis, modification of proteins and identification of peptide fragments.[26] In the context of determining SeMet in complex matrices, we found that the use of DNP derivatization offered several elements of selectivity that allowed the development of simple isolation and chromatographic protocols. The water-soluble and amphoteric characteristics of free SeMet allowed the preliminary removal of organic or neutral/anionic contaminants via extraction with diethyl ether or preparative cation-exchange chromatography, respectively. A flow chart describing the derivatization and isolation protocol is presented in Fig. 1. After derivatization under basic conditions, DNP-SeMet remained insoluble in diethyl ether, allowing the selective extraction of unreacted FDNB. Under acidic conditions, the protonated DNP-SeMet was extracted with diethyl ether, allowing rapid concentration of the extract *via* solvent evaporation. As several DNP-amino acids derivatives remain water soluble at low pH (arginine, histidine, tyrosine, lysine, *etc.*),[26] this treatment was considered as a potential sample purification step for the purpose of determining SeMet in protein hydrolysates.

Given that the DNP group is a particularly effective π-electron acceptor, an analytical chromatographic mechanism based on π-electron interactions was selected. A silica support derivatized with *p*-nitrophenyl groups was used for this purpose. The analyte emerging from the HPLC column was channelled to a thermochemical hydride generation atomic absorption spectrometer system providing a high selectivity for selenium. This system was previously optimized for the determination of organoselenonium compounds,[21,27] and was used under the same operating conditions.

Effect of pH on DNP Derivatization Efficiency

The nucleophilic aromatic substitution mechanism of the reaction between FDNB and the amino group of SeMet implies a pH-dependent reaction rate. The effect of pH on derivatization efficiency is shown in Fig. 2. Maximum recoveries of the DNP-SeMet derivative were obtained at pH values ranging from 9 to 10. At lower pH, the nucleophilic electron pair of the amino group become increasingly protonated, causing a sharp decrease in derivatization efficiency. In

separate experiments, the conversion of FDNB to 2,4-dinitrophenol was monitored by TLC. This undesirable reaction involving nucleophilic attacks from hydroxyl groups became progressively important at higher pH values (≥11). From these data, and taking into account that hydrofluoric acid is formed as a side-product during the reaction, the standard derivatization pH was set to 10.0. At this pH, a small proportion of 2,4-dinitrophenol was also formed during the reaction.

Purification and Characterization of DNP-SeMet

Purification of the DNP-SeMet standard was achieved by chromatography on a silica gel column that was eluted with 1 + 1 ethyl acetate–hexane. The 1 ml fractions 24–32 gave one spot in TLC (detection by UV quenching) and revealed a high content of Se by flow injection THG-AAS. Structural confirmation of the DNP-SeMet standard was obtained by FAB-MS and $^{1}H/^{13}C/^{77}Se$ NMR analyses, which are presented in Fig. 3 and Tables 1 and 2, respectively. A mass spectrometric characterization of the standard was more difficult to obtain. A molecular ion was not observed using the conventional gas-phase (heated probe) sample introduction or positive-ion FAB-MS modes. On the other hand, the negative-ion FAB mass spectrum of the analyte induced the molecular ion [DNP-SeMet − H (*m/z* 362)] and its glycerol adduct (*m/z* 454). Other masses (91, 107, 183, 275) were typical artifacts inherent to the glycerol matrix. The NMR spectra did not show resonance peaks other than those of the analyte and internal standard, confirming the high purity observed by TLC. The NMR chemical shift (Ξ) of ^{77}Se was 19.073058 MHz (absolute frequency).

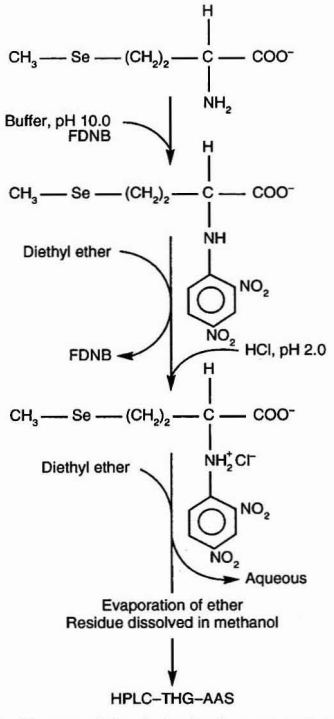

Fig. 1 Flow diagram of the derivatization and isolation protocol.

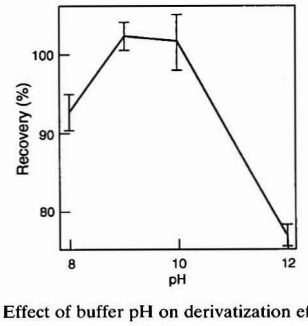

Fig. 2 Effect of buffer pH on derivatization efficiency.

Chromatographic Conditions

The principal limitation of the THG-AAS system is the requirement for an organic-rich mobile phase to support the combustion process.[20,21] Using pure methanol as a mobile

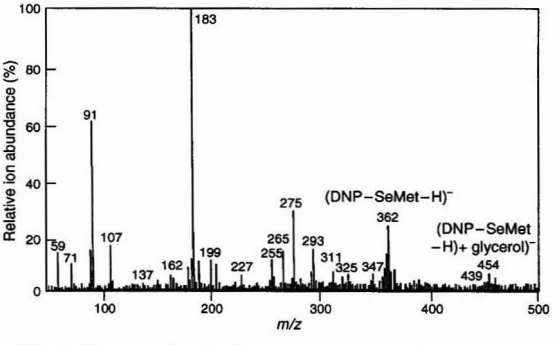

Fig. 3 Fast atom bombardment mass spectrum of DNP-SeMet.

Table 1 300.13 MHz ^{1}H NMR data for DNP-SeMet in $CDCl_3$–CD_3OD (1 + 2) at 298K

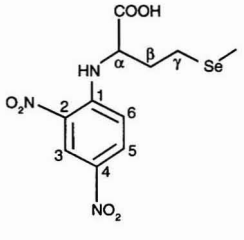

N-(2,4-dinitrophenyl)selenomethionine

Proton	δ (ppm)*	Multiplicity†	*J* (Hz)	Interpretation
a	9.078	d	2.7	H-3
b	8.253	dd	9.7, 2.7	H-5
c	7.083	d	9.7	H-6
d	4.343	t	5.9, 5.5	H-α
e	2.702	m	−12.3, 9.6, 5.9	H-γ_1
f	2.611	m	−12.3, 9.6, 5.6	H-γ_2
g	2.302	m	−14.2, 9.6, 5.9, 5.6	H-β_1
h	2.272	m	−14.2, 9.6, 5.9, 5.5	H-β_2
i	1.980	s	—	CH_3

* Chemical shifts downfield from internal TMS.
† s = Singlet; d = doublet; t = triplet; m = multiplet.

phase (providing optimum THG performance), conventional HPLC stationary phases such as octadecyl- and cyanopropyl-derivatized silica or styrene–divinylbenzene copolymeric supports did not retain DNP-SeMet. On the other hand, underivatized SeMet was completely retained via adsorption of the amino group on residual silanol moieties in a cyanopropyl column.[20,21] A small proportion of triethylammonium (100 μg ml^{-1} triethylamine + 1% v/v acetic acid) added to the methanolic mobile phase competed effectively with these silanophilic interactions and eluted SeMet as a sharp peak with a retention time of 6.1 min. This method was used to assess the purity of the commercial SeMet used to prepare the DNP-SeMet standard.

π-Electron interactions have been shown to be an important chromatographic mechanism during the separation of unsaturated analytes on aromatic copolymeric supports.[28] With an electron-rich cyano group, acetonitrile effectively competes with these interactions and has been used as such to elute unsaturated analytes from aromatic copolymers.[28] *p*-Nitrophenyl-derivatized silica stationary phases have also been used to separate aromatic hydrocarbons.[29] Using pure methanol as the mobile phase, DNP-SeMet was completely retained *via* the formation of π-complexes between the DNP group and the *p*-nitrophenyl-derivatized stationary phase. At concentrations up to 1% v/v, acetonitrile, used as a weak π-electron donor, did not elute the analyte. On the other hand, the lone electron pair present in the basic form of triethylamine (TEA) effectively competed with the π-interactions. Thus, methanol spiked with small volumes of TEA (100–500 μg ml^{-1}) eluted the analyte as a sharp peak. Evidence for a π-interaction chromatographic mechanism was obtained by acidifying the mobile phase with 0.1% HCl. Under acidic conditions, the lone electron pair normally available in the basic form of TEA coordinated a proton, and as such could not compete with π-interactions. The net result was complete retention of the analyte. A schematic description of the chromatographic retention mechanism is presented in Fig. 4.

It was also noted that the analyte was more retained when analysed in crude extracts. This effect was attributed to the presence of 2,4-dinitrophenol (from hydrolysis of FDNB) which, as a weak organic acid, was co-isolated with DNP-SeMet. The effect of co-injecting a high concentration (1 mg ml^{-1}) of 2,4-dinitrophenol on the retention time of DNP-SeMet injected as a pure standard or from a crude extract is presented in Table 3. Although this retention effect may be explained by the protonation of basic TEA by 2,4-dinitrophenol (which would shift the equilibrium towards the formation of π-complexes during chromatography), the possibility of the formation of a π-complex between 2,4-dinitrophenol and DNP-SeMet during the chromatography cannot be excluded and remains to be investigated. Subsequent HPLC–THG-AAS analyses were performed using 500 μg ml^{-1} TEA in methanol. As 2,4-dinitrophenol appeared to increase the retention time of the analyte, peak confirmation and calibration were achieved by the method of standard additions.

Table 2 75.47 MHz ^{13}C NMR data for DNP-SeMet in $CDCl_3$–CD_3OD (1 + 2) at 298 K

Carbon	δ (ppm)*	Multiplicity†	One-bond coupling to	Long-range coupling to	Interpretation
A	176.93	Q	—	d, g, h	COOH
B	147.73	Q	—	a, b, d	C1
C	136.05	Q	—	a, b, c	C4
D	130.92	Q	—	a, c‡	C2
E	130.59	T	b		C5
F	124.78	T	a	b	C3
G	115.23	T	c	—	C6
H	58.18	T	d	e, f, g, h	Cα
I	33.34	S	g, h	d, e, f	Cβ
J	20.87	S	e, f	d, g, h	Cγ
K	4.20	P	i	e, f	CH_3

* Chemical shifts downfield from internal TMS.
† P = primary; S = secondary; T = tertiary; Q = quaternary.
‡ Carbons not resolved.

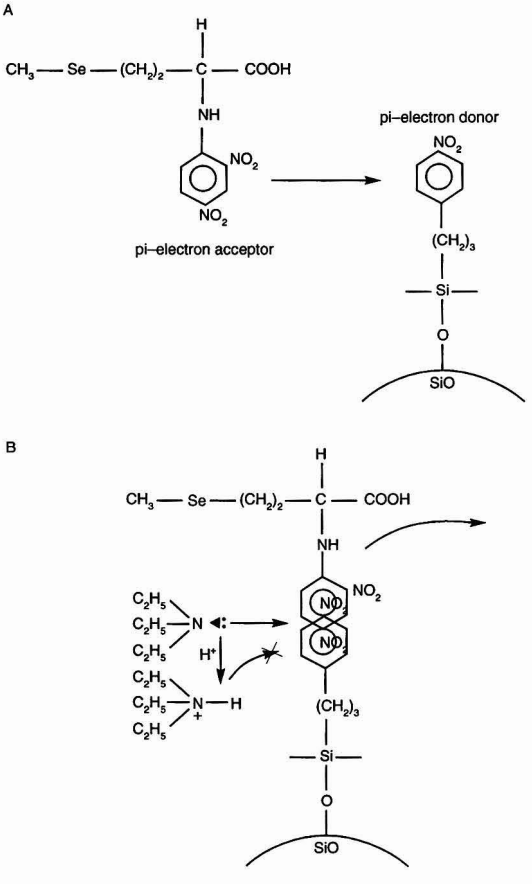

Fig. 4 Model of the chromatographic mechanism where A shows the DNP moiety carried by the analyte acting as a π-electron acceptor prone to undergo π-complexation with the *p*-nitrophenyl group bonded on the HPLC stationary phase; and B shows basic triethylamine (TEA) acting as a stronger electron donor competing with the stationary phase. This competing effect was reversed on acidification of the mobile phase where TEA was converted into triethylammonium.

Table 3 Retention times of DNP-SeMet in the presence and absence of 2,4-dinitrophenol (DNPol)

	Retention time/min	
Sample	−DNPol	+DNPol
Purified DNP-SeMet	1.99	3.22
DNP-SeMet crude extract	4.06	4.89

Photodegradation of DNP-SeMet

Given the photochemical sensitivity of DNP-amino acids[26] and the marked tendency of organic Se species to oxidize,[17,18] a stability study was undertaken in order to define the handling conditions and conservation time of the standard. Oxygenated and deoxygenated methanolic solutions of DNP-SeMet (100 μg ml^{-1}) were stored at room temperature under ambient fluorescent lighting or in darkness, and analysed periodically. Chromatograms observed after 10 d are presented in Fig. 5. Slow degradation of DNP-SeMet was observed in all samples exposed to light. Both oxic and anoxic standards degraded at a constant rate (r = −0.97 and −0.90, respectively), which averaged at 0.08 ± 0.01 μg ml^{-1} h^{-1}. Samples conserved in darkness remained stable at room temperature for at least 552 h. A dimethyl diselenide (DMDSe) standard co-chromatographed with the degradation product present in air/light-exposed samples. A mass spectrum of this volatile degradation product obtained in the chemical (H_2O) ionization mode is presented in Fig. 6. Mass assignments (Fig. 6) confirmed DMDSe as the major degradation product. Under anoxic conditions, DMDSe further degraded to a species eluting with a slightly longer retention time. This apparently oxygen-labile product was not positively confirmed. DMDSe was not found in underivatized SeMet solutions exposed to light, leaving little doubt about the active role of the DNP group in the photodegradation mechanism. The most probable mechanism involves the homolytic cleavage of the weak selenium–γ-carbon bond by photosensitized aromatic nitro groups, followed by the recombination of two $CH_3Se^{\bullet}$ radicals to DMDSe. This photodegradation route was confirmed by the presence of DMDSe in test solutions of underivatized SeMet spiked with 2,4-dinitrophenol and exposed to light.

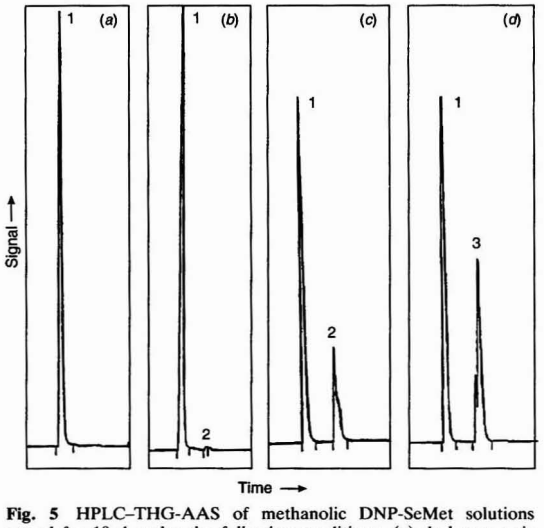

Fig. 5 HPLC–THG-AAS of methanolic DNP-SeMet solutions stored for 10 d under the following conditions: (*a*) darkness, oxic atmosphere; (*b*) darkness, anoxic atmosphere; (*c*) fluorescent lighting, oxic atmosphere; and (*d*) fluorescent lighting, anoxic atmosphere. Peak 1 (2.0 min), DNP-SeMet; peak 2 (3.2 min), dimethyl diselenide; and peak 3 (3.3 min) unconfirmed.

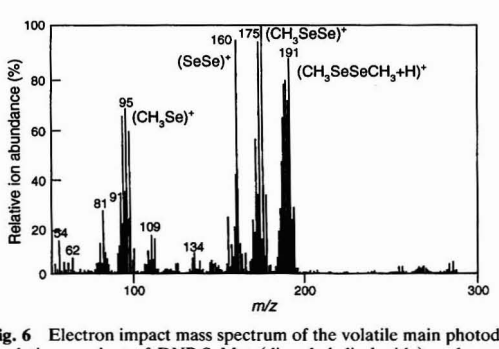

Fig. 6 Electron impact mass spectrum of the volatile main photodegradation product of DNP-SeMet (dimethyl diselenide) under oxic conditions.

Linearity, Limit of Detection and Reproducibility

Calibration graphs obtained in the flow injection THG-AAS and HPLC–THG-AAS modes were linear (r = 0.996 and 0.997, respectively) from the limit of detection (81 ng of DNP-SeMet) to 5 μg in 50 μl injections. The short-term reproducibility of the interface expressed in terms of relative standard deviation (s_r) at different concentrations of the analyte is presented in Table 4. The average efficiency of the derivatization and isolation method over a sample concentration ranging from 50 to 300 μg ml^{-1} was 99 ± 4.5%, which was reflected in a linear standard (SeMet) addition calibration (r = 0.996). The recovery of SeMet decreased to 95 ± 2.6% when derivatized in the presence of a large excess of amino acids.

The recovery of SeMet from the nutritional supplement was low (12 ± 8%) when derivatization was performed on a crude aqueous extract. Ascorbic acid (vitamin C), a major component of several food supplements containing SeMet, was identified as the major interferent. In separate experiments we found that the interference was concentration dependent, as demonstrated by a decrease in the recoveries of SeMet (in water) from a quantitative to 91.5, 81 and 13% with increasing vitamin C to SeMet molar ratios (1:10, 1:1 and 10:1, respectively). Ascorbic acid is known to reduce *o*-dinitrobenzene[30] and, given the high proportion of vitamin C relative to SeMet in the nutritional supplements, we attributed this interference to a possible reduction of the 2,4-dinitrophenyl groups of the derivatized analyte. As FDNB was added in a large excess (relative to ascorbic acid), the possibility of quantitative reduction of the reagent by ascorbic acid was excluded. In additional experiments, the derivatized product (DNP-SeMet) was spiked in buffer (pH 10.0) containing a 334-fold molar excess of ascorbic acid. The solutions were shaken for 2 h in the presence or absence of FDNB and the analyte was isolated as described earlier (Fig. 1). In both instances, the proportion of analyte recovered (69 ± 5% and 69 ± 3%) contrasted sharply with the poor recovery (13%) observed when SeMet was derivatized in the presence of a tenfold excess of ascorbic acid. These results suggest that, in addition to affecting the recovery of the derivatized analyte (presumably via reduction of the DNP moieties), ascorbic acid interferes with the nucleophilic aromatic substitution reaction between FNDB and SeMet. A possible affinity between the

Table 4 Reproducibility of the HPLC–THG-AAS system for various concentrations of DNP-SeMet

Concentration/μg ml^{-1}	cv (%)*
100	0.85
60	3.3
36	0.9
21.6	3.0
12.9	5.1
6.48	3.25

* (Standard deviation/mean) × 100. Triplicate injections.

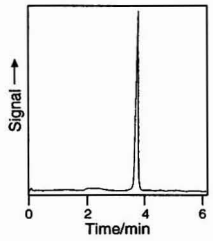

Fig. 7 HPLC–THG-AAS of DNP-derivatized SeMet isolated from nutritional supplement tablets.

ene-diol group of ascorbic acid[30,31] and the amino group of SeMet is under investigation. Removal of ascorbic acid by a preparative cation-exchange step resulted in quantitative derivatization and isolation of SeMet from the nutritional supplement (100 ± 7%, based on the supplier's specifications). Ascorbic acid was not retained on the cation-exchange column, and as such was rapidly eluted with water. SeMet was then eluted with ammonia solution. Displacement of excess of ammonia before derivatization was essential to avoid an undesirable reaction with FDNB (forming 2,4-dinitroaniline). A chromatogram of DNP-SeMet obtained from the supplement tablets is presented in Fig. 7.

Conclusion

The integration of a series of selective derivatization, isolation and chromatographic steps allowed the determination of free SeMet in complex matrices containing vitamin C, free amino acids, transition metals and lipophilic components. The limit of detection provided by the THG-AAS detector (81 ng as DNP-SeMet in a 50 µl injection) allows the analysis of samples that were originally enriched in selenium, such as nutritional supplements. A high proportion of SeMet present in biological materials is incorporated in proteins. Given that the final organic extract may be concentrated about 100-fold prior to HPLC–THG-AAS analysis, we expect that this method will be useful for determining trace levels of SeMet present in protein hydrolysates.

The authors gratefully acknowledge financial support by the Natural Science and Engineering Research Council of Canada (J. S. B.) and the Fonds pour la Formation de Chercheurs et l'Aide à la Recherche (J. S. B.).

References

1 Fan, A. M., and Kizer, K. W., *West. J. Med.*, 1990, **153**, 160.
2 Salbe, A. D., and Levander, O. A., *J. Nutr.*, 1990, **120**, 207.
3 Yang, G., Zhou, R., Yin, S., Gu, L., Yan, B., Liu, Y., Liu, Y., and Li, X., *J. Trace Elem. Electrolytes Health Dis.*, 1989, **3**, 77.
4 Yamasuto, K., Tetsuya, S., and Yoshiba, M., *J. Agric. Food Chem.*, 1988, **36**, 463.
5 Olson, O. E., Novacek, E. J., Whitehead, E. I., and Palmer, I. S., *Phytochemistry*, 1970, **9**, 1181.
6 Beilstein, M. A., and Whanger, P. D., *J. Nutr.*, 1986, **116**, 1701.
7 Smith, A. M., and Picciano, M. F., *J. Nutr.*, 1987, **117**, 725.
8 Butler, J. A., Beilstein, M. A., and Whanger, P. D., *J. Nutr.*, 1989, **119**, 1001.
9 Butler, J. A., Thomson, C. D., Whanger, P. D., and Robinson, M. F., *Am. J. Clin. Nutr.*, 1991, **53**, 748.
10 Choy, W. N., Henika, P. R., Willhite, C. C., and Tarantal, A. F., *Environ. Mol. Mutagen.*, 1993, **21**, 73.
11 Willhite, C. C., Hawkes, W. C., Omayes, S. T., Choy, W. N., Cox, D. N., and Cukierski, M. J., *Food Chem. Toxicol.*, 1992, **30**, 903.
12 Yang, G., Wang, J., Zhou, R., and Sun, S., *Am. J. Clin. Nutr.*, 1983, **37**, 872.
13 Olson, O. E., *J. Am. Coll. Toxicol.*, 1986, **5**, 45.
14 Hoffman, D. J., Heinz, G. H., LeCaptain, L. J., Bunck, C. M., and Green, D. E., *J. Toxicol. Environ. Health*, 1991, **32**, 449.
15 Bottino, N. R., Banks, C. H., Irgolic, K. J., Micks, P., Wheeler, A. E., and Zingaro, R. A., *Phytochemistry*, 1984, **23**, 2445.
16 Hasunuma, R., Ogawa, T., Ishii, J., and Kawanishi, Y., *J. Chromatogr.*, 1991, **537**, 1991.
17 Wolf, W. R., LaCroix, D. E., and Slagt, M. E., *Analyst. Lett.*, 1992, **25**, 2165.
18 Zheng, O., Jiang, W., and Qi, X. L., *Anal. Biochem.*, 1989, **178**, 77.
19 Tschursin, E., and Wolf, W. R., *Fresenius' J. Anal. Chem.*, 1993, **345**, 243.
20 Blais, J. S., Momplaisir, G. M., and Marshall, W. D., *Anal. Chem.*, 1990, **62**, 1161.
21 Blais, J. S., Huyghues-Despointes, A., and Marshall, W. D., *J. Anal. At. Spectrom.*, 1991, **6**, 225.
22 Bax, A., and Freeman, J., *J. Magn. Reson.*, 1981, **48**, 542.
23 Doddrell, D. M., Pegg, D. T., and Bendall, M. R., *J. Magn. Reson.*, 1982, **48**, 323.
24 Bax, A., and Morris, G., *J. Magn. Reson.*, 1981, **42**, 501.
25 Bax, A., and Summers, M. F., *J. Am. Chem. Soc.*, 1986, **108**, 2093.
26 Mills, G. L., in *Chromatographic and Electrophoretic Techniques*, ed. Smith, I., Interscience, New York, 1960, p. 157.
27 Huygues-Despointes, A., Momplaisir, G. M., Blais, J. S., and Marshall, W. D., *Chromatographia*, 1991, **31**, 481.
28 Thévenon-Emeric, G., Tchapla, T., and Martin, M., *J. Chromatogr.*, 1991, **550**, 267.
29 Blumer, G. P., Gundermann, K. D., and Zander, M., *Chem. Ber.*, 1976, **109**, 1991.
30 Fearon, W. R., and Kawerau, E., *Biochemistry*, 1943, **37**, 326.
31 Kimoto, E., Tanaka, H., Ohmoto, T., and Choami, M., *Anal. Biochem.*, 1993, **214**, 38.

Paper 4/03485F
Received June 9, 1994
Accepted September 2, 1994

Salicylic Acid Functionalized Polystyrene Sorbent Amberlite XAD-2. Synthesis and Applications as a Preconcentrator in the Determination of Zinc(II) and Lead(II) by Using Atomic Absorption Spectrometry

Reena Saxena and Ajai K. Singh*

Department of Chemistry, Indian Institute of Technology, New Delhi-110 016, India

Devendra P. S. Rathore

Chemical Laboratory, Atomic Mineral Division, Department of Atomic Energy, West Block VII, R. K. Puram, New Delhi-110 066, India

Amberlite XAD-2 has been functionalized by coupling it through an –N=N– group with salicylic acid. The resulting chelating resin has been characterized by using elemental analyses, thermogravimetric analysis (TGA) and infrared (IR) spectra. It has been used for preconcentrating Pb^{II} and Zn^{II}, prior to their determination by flame atomic absorption spectrometry. The optimum pH values for quantitative sorption of Zn^{II} and Pb^{II} are 5.0 and 4–6, respectively. The two metals can be desorbed (recovery 98–100%) with 1 mol dm^{-3} HCl and a mixture of 2–4 mol dm^{-3} HCl/3–4 mol dm^{-3} HNO_3, respectively. The sorption capacity of the resin is 1146 and 461 μg g^{-1} of resin, respectively, for Zn and Pb. From F^-, Cl^-, NO_3^-, SO_4^{2-} and PO_4^{3-} ions, only PO_4^{3-} interferes with Pb. The preconcentration factor was found to be 140 for Pb (at 7 ppb concentration level) and 180 for Zn (at 5.5 ppb concentration level). Simultaneous determination of the two metals is possible. Cations commonly present in water do not affect the sorption of both metal ions by the resin. The method was applied to determine Zn and Pb contents of well-water samples ($s_r < 7.0\%$).

Keywords: Amberlite XAD-2; salicylic acid; chelating resin; zinc; lead; preconcentration; atomic absorption spectrometry

Introduction

The iminodiacetate containing resin, Chelax-100, is the most commonly employed chelating resin for the preconcentration of trace heavy metals.[1–2] However, its selectivity for metal ions is not good and, therefore, elaborate and careful washing procedures are required.[3–4] Several other metal ion-sorbing matrices of better selectivity have been developed by sorbing appropriate chelating ligands on organic polymers or silica[5–11] but they suffer from ligand-leaching problems. The chemical coupling of a ligand with an organic-polymer resin results in a rugged sorption matrix, but its sorption capacity is comparatively lower,[12–16] particularly when the size of the ligand molecule is large. Salicylic acid is a ligand which can selectively complex with metal ions like Zn^{II}, Pb^{II}, Fe^{III}, *etc.*, at controlled pH. Its molecular size is also suitable for achieving a reasonable level of sorption capacity. However, salicylic acid-loaded resins have not been much explored for preconcentration of metal ions, except the report in 1974, in which Vernon and Eccles[17] synthesized four such resins and made preliminary investigations on their metal-sorption behaviour after their characterization by elemental analyses. It was, therefore, thought worthwhile to synthesize salicylic acid-loaded Amberlite XAD-2, and study its metal-sorption behaviour and its applications as a metal preconcentrator. In the present paper results of such studies carried out for Zn^{II} and Pb^{II} are described.

Experimental

Apparatus and Reagents

Atomic absorption spectrometric measurements were made with a Hitachi (Tokyo, Japan) atomic absorption spectrometer Model Z-8100 using an air–acetylene flame (air and acetylene flow rates of 15 dm^3 min^{-1} and 1.5 dm^3 min^{-1}, respectively). The pH measurements were made on an Elico (Hyderabad, India) pH meter, Model LI-120-digital. Infrared (IR) spectra (4000–200 cm^{-1}) were recorded on a Nicolet (Madison, USA) DX-5 FT IR spectrometer. Stanton Redcroft (London, UK) simultaneous thermal analyzer Model STA-780 was used for recording thermogravimetric analysis (TGA). The resin was packed in columns (diameter 1 cm, Pharmacia; Bromma, Sweden) for metal-sorption studies. The flow of liquid through these columns was controlled with a peristaltic pump (Watson-Marlow Model 101/U/R; Falmouth, UK).

Stock solutions (1000 ppm) of zinc(II) and lead(II) were prepared by dissolving appropriate amounts of analytical-reagent grade zinc(II) sulfate, and lead(II) acetate, respectively, in doubly-distilled water, acidified with a small amount of the corresponding acid and standardized[18] before use. The pH adjustments were made with 0.01 to 1.0 mol dm^{-3} HCl and NaOH. Amberlite XAD-2 resin (surface area 330 m^2 g^{-1}, pore diameter 90 Å and bead size 20–60 mesh) was obtained from Aldrich (Milwaukee, USA). Salicylic acid (BDH; Bombay, India) was used as received. All other reagents used were of analytical-reagent grade. The glassware was soaked in 5% HNO_3 for one week before use and cleaned with doubly distilled water.

Synthesis of Amberlite XAD-2 Loaded With Salicylic Acid

A 5 g sample of Amberlite XAD-2 was mixed with 10 cm^3 of concentrated HNO_3 and 25 cm^3 of concentrated H_2SO_4 (18 mol dm^{-3}) and stirred at 60 °C for 30 min. Thereafter, the reaction mixture was poured into an ice–water mixture. The

* To whom correspondence should be addressed.

nitrated resin was filtered, washed with water until free from acid and mixed with 40 g of $SnCl_2$, 45 cm^3 of concentrated HCl (11.5 mol dm^{-3}) and 50 cm^3 of ethanol. This mixture was refluxed for 10 h. The solid precipitate was filtered and washed with water and 2 mol dm^{-3} NaOH which released amino-resin (R-NH_2) from $(R\text{-}NH_3)_2SnCl_6$. The amino resin was first washed with 2 mol dm^{-3} HCl and finally with an excess of water. It was slurried in an ice–water mixture (350 cm^3) and treated with 1 mol dm^{-3} HCl and 1 mol dm^{-3} $NaNO_2$ (added in small aliquots of 1 cm^3) until the reaction mixture began to give a dark blue colour with starch–iodide paper. The diazotized resin was filtered, washed with cold water and reacted with salicylic acid (2.5 g in 350 cm^3 of glacial acetic acid and 150 cm^3 of acetone) at 0–3 °C for 24 h. The resulting brown-coloured beads were filtered and washed with water. Elemental analyses found: C, 63.34; H, 4.52; N, 10.10%. Calculated values for $C_{15}H_{14}N_2O_4$: C, 62.94; H, 4.89 and N, 9.81%.

Recommended Procedure for Preconcentration and Determination of Pb^{II} and Zn^{II}

Amberlite XAD-2 (1 g), loaded with salicylic acid, was packed in a glass column C10/10 (Pharmacia). This was treated with 4 mol dm^{-3} HCl (20 cm^3) and washed with water until free from acid. A solution containing 10 μg of Zn^{II}/Pb^{II} in a volume of up to 1.4/1.8 dm^3 was passed through the column, after adjusting its pH to 5.0 and at a flow rate of 2 cm^3 min^{-1} (controlled with a peristaltic pump). The column was washed with either 7.5 cm^3 of HCl (1 mol dm^{-3} for Zn and 2–4 mol dm^{-3} for Pb) or 3–4 mol dm^{-3} HNO_3 for Pb. The volume of eluate was made up to 10 cm^3. Its Zn and Pb contents were determined at 213.9 and 212 nm, respectively, by using flame atomic absorption spectrometry (AAS) standardized prior to determination.

Results and Discussion

The TGA of the resin showed slow mass loss up to 550 °C. However, the 5% mass loss up to 130 °C may have been due to the sorbed water (one molecule per unit of the polymer). The results of elemental analyses of the resin in conjunction with electronic effects and steric reasons suggested that on average one salicylic acid molecule per unit of polymer was present, as shown in Fig. 1. The IR spectrum of salicylic acid-loaded Amberlite XAD-2 in comparison with the IR spectrum of pure Amberlite XAD-2 depicted four additional bands at 1635, 1535, 1460 and 1395 cm^{-1}. These appear to originate from the ligand molecule and are characteristic of carboxylate, –N=N–, O–H (bending) and phenolic group vibrations, respectively.

Optimum Conditions for Sorption

The column C10/10 (Pharmacia) was packed with 1 g of Amberlite XAD-2 loaded with salicylic acid, treated with 20 cm^3 of 4 mol dm^{-3} HCl and washed several times with water to remove the acid. The sorption and desorption of Pb(II), Cd^{II}, Zn^{II} and Ni^{II} on this column were studied. The maximum sorption of Ni^{II} and Cd^{II} was 55% at pH 5 and 4.5–8.0, respectively, using flow rates of 2–3 and 2–5 cm^3 min^{-1}, respectively. The desorption of both these metals was quantitative with 4 mol dm^{-3} HCl or 4–6 mol dm^{-3} HNO_3. The sorption of Pb^{II} and Zn^{II} was quantitative and optimum conditions for their sorption and desorption are recorded in Table 1. Flow rates slower than 2 cm^3 min^{-1} were not studied to avoid long analyses times. An acid concentration of >4 mol dm^{-3} was not used for desorption because the necessity for its partial neutralization in the eluate would reduce the preconcentration factor. The capacity of sorption was found to be almost the same (variation $\leqslant \pm 4$ μg g^{-1} of resin) for different batches of salicylic acid-loaded Amberlite XAD-2 prepared separately. The capacity of resin was also found to be practically unaffected (lower by $\leqslant \pm 5$ μg g^{-1} of resin) by its 40 repeated uses for preconcentration. Therefore, resin may be used for multiple preparations.

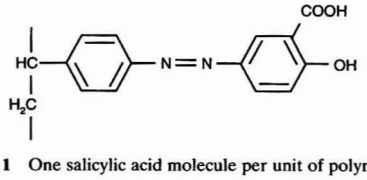

Fig. 1 One salicylic acid molecule per unit of polymer.

Effect of Electrolytes and Cations

The effect of NaF, NaCl, $NaNO_3$, Na_2SO_4 and Na_3PO_4 on the sorption of Zn^{II} and Pb^{II} by salicylic acid-loaded Amberlite XAD-2 was studied. The tolerance limits are given in Table 2.

In the sorption of 10 μg of Zn, 5 μg of each of Cu^{II}, Co^{II}, Fe^{II} and Cr^{III} did not interfere. An amount of 40 μg of each of these metals did not affect the sorption of 10 μg of Pb. 5 μg of Hg^{II} was tolerable in the sorption of 10 μg Pb and 5 μg Zn. Simultaneous sorption of Zn and Pb was found to be quantitative from mixtures containing up to 200 μg of each. The tolerance limits of electrolytes (except Na_3PO_4) and cations were found to increase 10- and 40-fold, respectively, when the column was packed with 5 g of resin. Further increase in the tolerance limits was not observed with this amount of resin.

Limit of Preconcentration and Preconcentration Factor

Lead(II) can be collected quantitatively from solutions of concentrations of the order of 7 ppb (recovery 96%), resulting in a preconcentration factor of the order 140. For Zn^{II}, the preconcentration factor was found to be 180 for the concentration level 5.5 ppb (recovery 98%).

Table 1 Optimum experimental conditions for sorption and desorption of lead(II) and zinc(II)

	Metal ion	
Experimental parameter	Zn^{II}	Pb^{II}
pH	5.0	4–6
Flow rate/cm^3 min^{-1}	2	2–5
Acid for desorption	1 mol dm^{-3} HCl	2–4 mol dm^{-3} HCl or 3–4 mol dm^{-3} HNO_3
Capacity of sorption/μg g^{-1} of resin	1146	461
Average recovery (%)	98	100
Standard deviation* (ppm)	0.062	0.036
Relative standard deviation (S_r) (%)	6.07	3.2

* In the six determinations of 0.102 ppm of Zn and 0.112 ppm of Pb: blank values: 0.5 ± 0.2 and 0.4 ± 0.2 ppb, respectively, for Pb and Zn.

Table 2 Tolerance limits of electrolytes

	Tolerance limit/mol dm^{-3}				
Metal ion (10 μg)	NaF	NaCl	$NaNO_3$	Na_2SO_4	Na_3PO_4
Pb^{II}	0.01	0.05	0.01	0.1	Interfered
Zn^{II}	0.5	0.1	0.1	0.01	0.3

IR Spectra of Metal Ion-sorbed Amberlite XAD-2 Loaded With Salicylic Acid

IR spectra of the chelating resin saturated with Zn^{II} or Pb^{II} were compared to those of metal-ion free resin. The carboxylate and phenolic bands underwent a red shift of the order 12–15 cm^{-1} when the resin was saturated with Zn or Pb, whereas the –N=N– band remained unchanged. This suggested that the chelation with salicylic acid functionality is responsible for sorption of metal ions by this resin.

Determination of Lead and Zinc in Water Samples

Water samples (1 dm^3) were collected from wells situated in Janak Puri, New Delhi, India and Patel Nagar, Gurgaon, India and subjected to the recommended procedure for preconcentrating and determining Zn and Pb (given in experimental). The results are reported in Table 3. These results in conjunction with those of synthetic water samples (Table 3) demonstrate the applicability of the present method to water analysis.

In comparison to Chelax-100[3,19–26] (the more commonly used resin) the main advantages of using salicylic acid-loaded Amberlite XAD-2 for preconcentrating Zn^{II} and Pb^{II} were the high preconcentration factor, lower matrix effects and good precision. The preconcentration factors achievable for the two metals with the present resin were also much higher than those reported for many other matrices, like bis(2-hydroxyethyl)dithiocarbamate-loaded Amberlite XAD-4,[11] oxine-immobilized silica,[7] C-18-bonded silica-gel loaded with oxine and Alizarin Red-S-loaded Amberlite XAD-2.[16] In comparison to dithizone and dithiocarbamate-based solvent extraction methods recommended for preconcentrating Pb and Zn in water samples[23] Amberlite XAD-2 loaded with salicylic acid gives much better preconcentration factors with lower matrix effects.

Table 3 Determination of Zn and Pb/μg cm^{-3}, in well-water samples

Origin of sample	Method	Metal			
		Zinc	s_r (%)	Lead	s_r (%)
New Delhi	Direct	0.48	5.0	0	—
	SA	0.60	5.1	0	—
	Lit.[21]	0.60	5.1	0	—
Gurgaon	Direct	2.56	2.1	0.03	6.1
	SA	2.68	2.2	0.04	6.2
	Lit.[21]	2.80	6.1	0.04	7.0
Synthetic	Direct	6.4†	10.1	9.2†	9.7
Water samples*	SA	8.0†	10.8	11.0†	8.0

SA = Standard additions method

* Containing 10 and 7 ng cm^{-3} of Pb and Zn, respectively.

† ng cm^{-3}.

The authors wish to thank CSIR (India) for financial support towards this work.

References

1 Kantipuly, C., Katragadda, S., Chow, A., and Gesser, H. D., *Talanta*, 1990, **37**, 491.
2 Akelah, A., and Moet, A., in *Functionalized Polymers and Their Applications*, Chapman and Hall, London, 1st edn., 1990, p. 139.
3 Kingston, H. M., Barnes, I. L., Brady, T. J., Rains, T. C., and Champ, M. A., *Anal. Chem.*, 1978, **50**, 2064.
4 Sturgeon, R. E., Berman, S. S., Desaluniers, A., and Russell, D. S., *Talanta*, 1980, **27**, 85.
5 Singh, A. K., and Dhingra, S. K., *Analyst*, 1992, **117**, 889.
6 Singh, A. K., and Rita, P., *Microchem. J.*, 1991, **43**, 112.
7 Sturgeon, R. E., Berman, S. S., Willie, S. N., and Desaulniers, J. A. H., *Anal. Chem.*, 1981, **53**, 2337.
8 McLaren, J. W., Mykytiuk, A. P., Willie, S. N., and Berman, S. S., *Anal. Chem.*, 1985, **57**, 2907.
9 Howard, A. G., and Abbab-Zavar, M. H., *Talanta*, 1979, **26**, 895.
10 Volkan, M., Ataman, O. Y., and Howard, A. G., *Analyst*, 1987, **112**, 1409.
11 King, J. N., and Fritz, J. S., *Anal. Chem.*, 1985, **57**, 1016.
12 Chwastowska, J., and Kosiarska, E., *Talanta*, 1988, **35**, 439.
13 Yebra-Biurrun, M. C., Garcia-Dopazo, M. C., Bermejo-Barrera, A., and Bermejo-Barrera, M. P., *Talanta*, 1992, **39**, 671.
14 Persuad, G., and Cantwell, F. F., *Anal. Chem.*, 1992, **64**, 89.
15 Bastia, T. K., Lenka, S., and Nayak, P. L., *J. Appl. Polym. Sci.*, 1992, **46**, 739.
16 Saxena, R., Singh, A. K., and Sambi, S. S., *Anal. Chim. Acta*, 1994, **295**, 199.
17 Vernon, F., and Eccles, H., *Anal. Chim. Acta*, 1974, **72**, 331.
18 Vogel, A. I., in *A Text Book of Quantitative Inorganic Analysis*, Longman, London, 3rd edn., 1973, pp. 610, 680.
19 Paulson, A. J., *Anal. Chem.*, 1986, **58**, 183.
20 Greenberg, R. R., and Kingston, H. M., *Anal. Chem.*, 1983, **55**, 1160.
21 Sturgeon, R. E., Berman, S. S., and Willie, S. N., *Talanta*, 1982, **29**, 167.
22 Brooks, R. R., Presley, B. J., and Kaplan, I. R., *Talanta*, 1967, **14**, 809.
23 Allen, H. E., and Minear, R. A., in *Examination of Water for Pollution Control*, ed. Suess, M. J., Pergamon, New York, 1982, p. 43.

Paper 4/05042H
Received August 16, 1994
Accepted September 27, 1994

Atomic Absorption Spectrometric Determination of Platinum and Rhodium in Cobalt Oxide Catalyst

Barbara Różańska

Department of Analytical Chemistry, Warsaw University of Technology, Noakowskiego 3, 00-664 Warsaw, Poland

A procedure is proposed for the flame atomic absorption spectrometric determination of Rh and Pt in Co_3O_4 catalyst. The samples are reduced in a stream of hydrogen and dissolved in *aqua regia*. The accuracy of Rh determination was confirmed by the fusion method. The method of Pt extraction with triphenylphosphine in isobutyl methyl ketone was optimized from the point of view of precision and accuracy.

Keywords: *Rhodium and platinum determination; cobalt oxide catalyst; triphenylphosphine; solvent extraction; flame atomic absorption spectrometry*

Introduction

In the manufacture of nitric acid, rhodium–platinum gauzes are used to catalyse the oxidation of ammonia. Recently oxide catalysts, usually based on iron or cobalt oxides, have been investigated as a substitute or together with noble metal gauzes, *e.g.*, Pt–Rh and Au–Pd trap gauzes. During the process of ammonia oxidation, the noble metals from Pt–Rh gauzes are lost by volatilization of their oxides.[1] Depending on the position of the oxide catalyst level, and other factors, different amounts of the platinum and rhodium oxides are trapped on the oxide catalyst bed. For process control, it is important to know the amount of trapped noble metals.

The determination of trace and small amounts of platinum and rhodium in cobalt oxide catalyst[2] by flame AAS encounters some difficulties. The main component of the matrix, Co_3O_4,[3] is resistant to chemical dissolution. To bring it into solution, fusion with $K_2S_2O_7$, alkali fusion or prolonged heating with concentrated H_2SO_4, can be applied. However, these procedures (not always suitable for both noble metals) lead to high salt or sulfuric acid contents in solution.

Co_3O_4, when heated to about 1100 K, decomposes to give CoO (soluble in acids) with evolution of molecular and atomic oxygen.[4] However, under these conditions some amount of platinum oxide can be lost by volatilization.

The reduction of Co_3O_4 in a stream of hydrogen allows its conversion into the metallic form, which is readily soluble in acids. It can be assumed that noble metal oxides can also be reduced.

The low content of platinum in some samples of catalysts and its poor sensitivity to flame AAS make the separation and preconcentration of platinum necessary. Extraction is an efficient method for the separation of platinum[5–8] before flame and furnace AAS determination; however, precise and efficient extraction is not always possible when working with a complex and concentrated matrix.[9,10]

The purpose of this work was to check the proposed method of sample decomposition and to develop a method for the extractive separation of platinum before its determination by flame AAS.

Experimental

Apparatus

A Thermo Jarrel Ash S-H 1150 atomic absorption spectrometer with flame and furnace CTF 188 and hollow-cathode lamps produced by Cathodeon were used for the determination of platinum and rhodium in isobutyl methyl ketone and aqueous solutions. The instrumental parameters and flame conditions were as follows: for Pt (265.9 nm), lamp current 4.5 mA, bandwidth 0.15 nm, lean oxidizing flame [air 16 standard cubic feet per hour (SCFH), acetylene 3 SCFH, burner height (h) 10 mm in aqueous solutions and air 17 SCFH, acetylene 2 SCFH and h = 14 mm in organic solutions]; and for Rh (343.5 nm), lamp current 4 mA, bandwidth 0.3 nm, lean oxidizing flame (air 14 SCFH, acetylene 3 SCFH, h = 7 mm in aqueous solutions and the same as for platinum in organic solutions).

A laboratory-made quartz tube furnace with a 10% Rh–Pt/Pt thermocouple was used for heating samples in a stream of hydrogen.

Reagents

All chemicals were of analytical-reagent grade.

Stock solution of Pt, 1 mg ml^{-1}. Prepared by dissolving 100 mg of Pt 4N wire in *aqua regia*, expelling nitric acid by repeated evaporations with small volumes of hydrochloric acid and finally dissolving in 20 ml of HCl (1 + 1) and diluting to 100 ml with water.

Stock solution of Rh, 1025 μg ml^{-1} *in* 5% HCl. Aldrich.

Acetone. POCH.

Triphenylphosphine (TPP). Merck.

Isobutyl methyl ketone (IBMK). Loba, pure.

Lanthanum buffer (5% *La*). Prepared by dissolving 13.4 g of $LaCl_3 \cdot 7H_2O$ in water with addition of 25 ml of concentrated HCl and 1.5 ml of concentrated H_2SO_4 and diluting to 100 ml with water.

Lanthanum buffer (10% *La*). Prepared by dissolving of 13.4 g of $LaCl_3 \cdot 7H_2O$ in 50 ml of 1 mol l^{-1} HCl.

Tin(II) chloride, 1 mol l^{-1} *in* 3 mol l^{-1} *HCl*. Prepared by dissolving $SnCl_2 \cdot 2H_2O$ in concentrated HCl and subsequent dilution with water.

Cobalt(II) chloride solution, 2.5 mol l^{-1} *in* 1 mol l^{-1} *HCl*. Prepared using $CoCl_2 \cdot 6H_2O$ (POCH).

Procedure

Decomposition of catalyst

A weighed portion of the catalyst (about 2 g of ground sample) was placed in a quartz boat in the quartz tube of the furnace and heated for 3 h at 650 °C in a stream of hydrogen at a flow rate of 5 l h^{-1}. After cooling in a stream of nitrogen, the sample was transferred into a quartz beaker, moistened with 8 ml of water and dissolved in 8 ml of *aqua regia* in the covered

beaker. After evaporation almost to dryness on a steam-bath, 12 ml of *aqua regia* were added, digested for 30 min and evaporated to humidity. Then 4 ml of concentrated HCl were added and the mixture was evaporated to humidity. (Evaporation with HCl should be repeated if an extraction procedure is to be applied.) Finally, the residue was dissolved in 20 ml of 2 mol l^{-1} HCl, transferred into a 25 ml calibrated flask and diluted to the mark with 2 mol l^{-1} HCl.

Extraction and determination of platinum

A 10 ml volume of the solution was pipetted into a separating funnel, 0.2 ml of $SnCl_2$ solution was added and the mixture was stirred, allowed to stand for 5 min and then shaken with 5 ml of 0.025 mol l^{-1} TPP in IBMK for 10 min. After separation of the layers, the aqueous layer was removed, the organic phase was transferred into the flask and the absorbance was measured in the air–acetylene flame.

For the calibration graph aqueous standard solutions containing 1–15 μg ml^{-1} of Pt^{IV} in 2 mol l^{-1} HCl were prepared and extracted in the same way as that used for the sample solutions.

Extraction procedures

(1) A 2 ml volume of 0.01 mol l^{-1} TPP in acetone was added to 5 ml of Pt^{IV} solution (20 μg ml^{-1}) in 6 mol l^{-1} HCl, heated for 15 min on a steam-bath and, after cooling, extracted with 5 ml of IBMK for 5 min.

(2) A 2 ml volume of 0.01 mol l^{-1} TPP in acetone and 0.5 ml of $SnCl_2$ solution were added to 5 ml of Pt^{IV} solution (20 μg ml^{-1}) in HCl of various concentrations, heated for 15 min on a steam-bath and, after cooling, extracted with 5 ml of IBMK for 5 min.

(3) A 0.5 ml volume of $SnCl_2$ solution was added to 5 ml of Pt^{IV} solution (20 μg ml^{-1}) in HCl of various concentrations, heated for 15 min on a steam-bath and, after cooling, extracted with 5 ml of 0.1 mol l^{-1} TPP in IBMK for 5 min.

(4) A 1 ml volume of $SnCl_2$ solution was added to 5 ml of Pt^{IV} solution in HCl of various concentrations, stirred and after 5 min extracted with 5 ml of 0.1 mol l^{-1} TPP solution in IBMK for 5 min.

Determination of Rh after fusion with potassium pyrosulfate

A 0.4 g amount of sample was fused with 4 g of $K_2S_2O_7$ and dissolved in and diluted to the mark with 2 mol l^{-1} HCl in a 25 ml calibrated flask. Rhodium was determined by flame AAS, using the standard additions method and Smith–Hieftje background correction. Lanthanum buffer (10% La) was added (1% of La in final solutions).

Aqua regia *leaching*

Freshly prepared *aqua regia* (10 ml) was added to the ground sample (1 g) in a quartz beaker, the beaker was covered and the contents were stirred for 1 h. After filtration followed by washing with the minimum volume of water, the solution was evaporated to humidity on a steam-bath, then dissolved in and transferred into a 10 ml calibrated flask with 2 mol l^{-1} HCl. Rhodium was determined by flame AAS, using the standard additions method, using 5% lanthanum buffer (1% of La in final solutions) and Smith–Hieftje background correction, and by the extraction method. Platinum was determined by the extraction method.

Results and Discussion

Dissolution of the Catalyst

Reduction of Co_3O_4 catalyst was investigated with the use of a thermobalance. The change in mass of a dried 1.0300 g sample heated in hydrogen at 650 °C for 1–6 h (mass of the sample = 0.7693, 0.7653, 0.7642, 0.7641, 0.7641 and 0.7641 after 1 h intervals), indicated that heating for 3 h was sufficient for reduction of the catalyst.[11] The samples of (dry) analysed catalyst were weighed before and after heating in the furnace. The ratio of the masses, *e.g.*, 0.7384 (1.7500/2.3700), 0.7379 (1.9915/2.6989) and 0.7388 (2.8989/3.9233), was almost equal to the value of the molecular mass ratio $3Co/Co_3O_4 = 0.7342$, so it can be concluded that reduction of almost pure Co_3O_4 oxide to metallic Co had occurred.

Dissolution of platinum in *aqua regia* is usually carried out without any problems but rhodium can be dissolved only when in dispersion. The accuracy of Rh determination using the proposed procedure for dissolution of the catalyst should be checked. The results of Rh determination after oxide reduction and dissolution in *aqua regia* were compared with the results after fusion with pyrosulfate, and good agreement was found (Table 1).

After pressure digestion in concentrated H_2SO_4, the recovery of rhodium was only about 75%.

The leaching with *aqua regia* of the ground raw samples was also tested. In comparison with the results after sample dissolution, 15% of rhodium and 66% of platinum were leached. Leaching with hot *aqua regia* solution and a prolonged leaching time did not increase amounts of Rh and Pt leached.

Determination of Pt and Rh in Cobalt Chloride Solutions

Replacement of fusion of samples by hydrogen reduction followed by dissolution in acids allows larger samples to be dissolved, but for low platinum concentrations the spectral background is a significant part of the absorbance in the presence of high cobalt concentrations. The detection limit in 1–1.2 mol l^{-1} Co solutions was increased to about 0.4 μg ml^{-1} (the detection limit was calculated according to the IUPAC recommendation[12] as c_L for $x_L = x_b + 3s_b$ for $n = 10$). The influence of the cobalt ion concentration on the platinum signals in solutions with and without buffer addition is shown in Fig. 1(*a*). The total signal and the spectral background of Pt measurement increase with increase of cobalt concentration, depending on conditions of measurement [Fig. 1(*b*)], but the background-corrected curve (difference between the two curves) always decreases with increase in Co concentration.

Table 1 Results of Rh determination after different decomposition procedures

	Catalyst I*		Catalyst II*	
	H_2 reduction, acid dissolution	Pyrosulfate fusion	H_2 reduction, acid dissolution	Pyrosulfate fusion
Mean value (%) ($n = 4$)	2.54×10^{-2}	2.53×10^{-2}	2.07×10^{-2}	2.05×10^{-2}
s_r (%)	0.9	1.9	1.0	2.1

* The catalysts from a plant installation were provided by Dr. J. Petryk, Department of Inorganic Technology, Warsaw University of Technology.

For Rh measurements the spectral background increases slightly with increasing Co concentration, but the total and background-corrected signals decrease.

The shapes of the background-corrected curves are similar to analyte *versus* interferent concentration plots when the analyte forms a compound with the interferent.

Both effects, the increase in background and decrease in Rh absorbance, are, as in Pt measurements, more intense in a sharp oxidizing flame and at higher burner heights. The most important factor influencing the extent of interferences was the efficiency of nebulization, which is known but difficult to elucidate without special equipment.

The spectral background in Pt and Rh measurements could be corrected by Smith–Hieftje correction, but remained dependent on the Co concentration, hence demanding the use of the matrix matching method. Buffer addition is necessary. Lanthanum buffer eliminates the mutual interference of Pt and Rh even in the presence of high Co concentrations.

Because of the relatively low Pt contents in some samples of Co_3O_4 catalyst, the poor Pt sensitivity in flame AAS and the influence of the matrix, separation and preconcentration of Pt were required.

The determination of rhodium except at very low concentrations can be carried out in matrix solution, with La buffer, by the matrix matching method.

Determination of Platinum in Organic Solvent After Solvent Extraction

The sensitivity of the flame AAS determination of Pt in organic extracts depends on the solvent used[13] and extracted and co-extracted species. The best characteristic concentration of Pt in an air–propane flame was found with chloroform as solvent and 8-mercaptoquinoline as a reagent.[14]

In this work, IBMK was chosen as the organic solvent because of its well known combustion properties. Extraction of chelate complexes [ammonium tetramethylenedithiocarbonate (ammonium pyrrolidinedithiocarbamate) (APDC)] was not considered because of the concentrated cobalt chloride matrix, although for the group extraction of some metals the extraction system HCl–quaternary ammonium salts–APDC–IBMK was found to be effective for concentrated cobalt salt solutions.[15] Extraction with triisooctylamine (TIOA) in IBMK was also tested but was found to be less useful because a long time was required for phase separation.

It was found that the cobalt concentration in the aqueous phase up to 0.5 mol l^{-1} does not affect the Pt absorbance in IBMK when Pt was extracted (as in often-used Pt extraction methods) as iodide and tin chloride complexes. However, the sensitivity of the flame AAS determination of Pt in the presence of extracted iodine and tin was poor. As follows from preliminary experiments concerning the extraction of Pt with TPP in IBMK instead of dichloroethane, as applied in the original method,[16,17] the sensitivity of Pt determination is better.

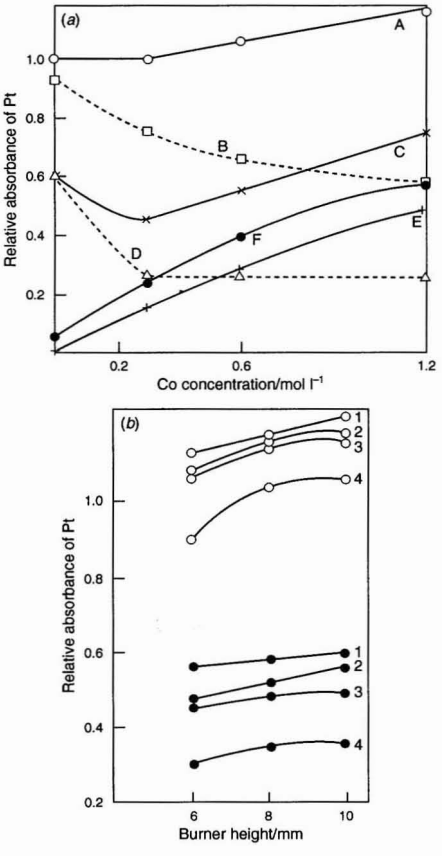

Fig. 1 (*a*) Influence of Co on the determination of Pt (20 μg ml^{-1}) with flame AAS. The relative absorbance was calculated relative to the absorbance of Pt in La buffer solution. A, total and, B, background-corrected signals in buffer solution (1% La, 2 mol l^{-1} HCl); C, total and, D, background-corrected signals in acid solution (2 mol l^{-1} HCl); E, spectral background of Co solutions in 2 mol l^{-1} HCl; F, spectral background of Co solutions in buffer solution. (*b*) Influence of flame conditions on total and background signal of Pt (20 μg ml^{-1}) measurements. The relative absorbance was calculated relative to the absorbance of Pt in La buffer solution. ○, Total signals in buffer solution (1% La, 2 mol l^{-1} HCl, 1.2 mol ml^{-1} Co); ●, spectral background of 1.2 mol l^{-1} Co solution in 1% La, 2 mol l^{-1} HCl. 1, Air 12, acetylene 2; 2–4, acetylene 3, air 16, 14, 12, respectively (fuel and oxidant flow in SCFH, aspiration rate 5 ml min^{-1}, air pressure 3.5 kg cm^{-2}, fuel pressure 1.1 kg cm^{-2}).

Table 2 Comparison of extraction procedures

	Procedure				
Parameter	1 (6 mol l^{-1} HCl)	2 (2 mol l^{-1} HCl)	3 (2 mol l^{-1} HCl)	4 (2 mol l^{-1} HCl)	Proposed procedure
Characteristic concentration in organic solution/μg ml^{-1}*	0.6	0.4	0.4	0.4	0.3
Precision of extraction, s_r (%) (n = 4)†	0.5	4.5 0.9‡	1.5	1.3	0.3

* The characteristic concentration in the aqueous phase was 1 μg ml^{-1}.

† For four replicate extractions. Solutions were measured three times and the average was used in calculations.

‡ In 0.5 mol l^{-1} Co solution.

The following variants of the TPP extraction method were tested and are discussed from the point of view of sensitivity, precision and matrix influence:

(1) 6 mol l^{-1} HCl/TPP–acetone solution/heating/IBMK extraction;

(2) 1–6 mol l^{-1} HCl/$SnCl_2$/TPP–acetone solution/heating/IBMK extraction;

(3) 1–6 mol l^{-} HCl/$SnCl_2$/heating/0.1 mol l^{-1} TPP in IBMK extraction;

(4) 1–6 mol l^{-1} HCl/$SnCl_2$/0.1 mol l^{-1} TPP in IBMK extraction.

The sensitivity (characteristic concentration based on the concentration in the organic phase) was similar in the extraction procedures with addition of $SnCl_2$, but the precision of the extractions was different (Table 2).

Platinum is virtually unextractable with 0.01 mol l^{-1} TPP in IBMK from solutions (20 μg ml^{-1}) in 1–6 mol l^{-1} HCl, but good efficiency and precision were obtained by extraction according to procedure 1, even though $SnCl_2$ was not added. This can be explained by different extraction mechanisms independent of the kinetics of exchanging the ligand in the central ion, as suggested by Mojski.[16] Absorbance of Pt in the organic phase does not depend on the Co concentration in the aqueous phase up to 0.5 mol l^{-1} of Co, even though a small amount of Co was extracted.

The precision in procedures 3 and 4 was similar for HCl concentrations of 1–1.5 mol l^{-1}. Increasing amounts of precipitate (probably $SnCl_3^-$ $TPPH^+$) were observed in the organic phase when the HCl concentration in the aqueous phase increased. In extractions from 2 mol l^{-1} HCl the precipitate was not observed immediately in the organic phase, but nebulization of the saturated solution resulted in less precise measurements.

The poor precision in procedure 2, where the reagent added in acetone solution was not completely dissolved in 2 mol l^{-1} HCl, which can hinder the attainment of equilibrium of complexation and where transfer of solutions with the precipitate into a separating funnel can be a source of random errors, can be understood. However, the reason for the improved precision in the presence of 0.5 mol l^{-1} Co ions is difficult to explain (the average values of the signals are not statistically different).

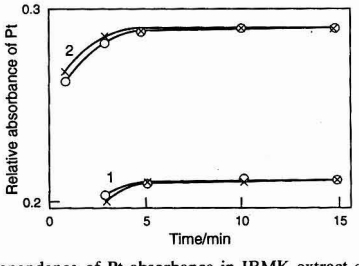

Fig. 2 Dependence of Pt absorbance in IBMK extract on shaking time. 0.025 mol l^{-1} TPP, $V_w/V_o = 2$; 1, ×, 15 μg ml^{-1} Pt in 2 mol l^{-1} HCl; ○, 15 μg ml^{-1} Pt, 2 mol l^{-1} HCl, 1.2 mol l^{-1} Co; 2, ×, 20 μg ml^{-1} Pt, 1 mol l^{-1} HCl; ○, 20 μg ml^{-1} Pt, 1 mol l^{-1} HCl, 1.2 mol l^{-1} Co.

Table 3 Results of Pt determination after extractive separation of Co_3O_4 catalyst

	Catalyst I*	Catalyst II	Catalyst II†
Mean value (%) ($n = 4$)	1.63×10^{-2}	1.12×10^{-2}	1.10×10^{-2}
s_r (%)	0.4	0.7	1.5

* A weighed portion (about 10 g) of ground sample of catalyst was reduced and, after cooling, weighed. The ratio of the masses was checked. Next, weighed portions of about 1.5 g of reduced sample were analysed.

† Extraction according to procedure 3. Heating after addition of $SnCl_2$, cooling and extraction with 0.025 mol l^{-1} TPP.

Optimization of the extraction procedure

TPP and $SnCl_2$ concentration. The signal did not change when the concentration of TPP in IBMK and $SnCl_2$ in the aqueous phase decreased to 0.02 mol l^{-1}, but the precision improved. Concentrations of 0.025 mol l^{-1} TPP in IBMK and 0.02 mol l^{-1} $SnCl_2$ in the aqueous phase were chosen.

Extraction time. Because of the complex dependence of the extraction of Pt on TPP, $SnCl_2$ concentration, acidity and time of shaking,[18] the dependence of Pt absorbance in organic phase on the shaking time was checked for extraction with 0.025 mol l^{-1} TPP in IBMK from Pt solution in 1–2 mol l^{-1} HCl containing 0–1.2 mol l^{-1} cobalt chloride (Fig. 2). In each instance the plateau was reached after shaking for 5 min, but after 10 min of extraction the results were more precise.

Ratio of phase volumes. The absorbance of a fixed amount of Pt in the organic phase slightly increased with variation of the V_w/V_o ratio in range 1–5, but not more than would be expected from the solubility of IBMK in 2 mol l^{-1} HCl (a wider range of phase volume ratios was not examined.

Interferences. Rhodium does not influence the Pt signal up to $c_{Rh}/c_{Pt} = 5$.

No interference was observed up to 1 mol l^{-1} Co concentration in the aqueous phase. Two calibration graphs ($a + bx$) obtained for 0, 5, 10 and 15 μg ml^{-1} of Pt in the aqueous phase (2 mol l^{-1} HCl), $V_w/V_o = 2$, without Co and in 1 mol l^{-1} Co solution, were compared using regression analysis:[19]

Graph 1: $a = 2.594 \times 10^{-4}$, $s_a = 2.427 \times 10^{-3}$, $t_{crit} = 4.478$ ($P = 0.95$), $t_{calc} = 0.107$, so a is not different from zero; $b = 2.0655 \times 10^{-2}$, $s_b = 2.5955 \times 10^{-4}$.

Graph 2: $a = -8.623 \times 10^{-4}$, $s_a = 4.888 \times 10^{-3}$, $t_{crit} = 4.478$ ($P = 0.95$), $t_{calc} = 0.176$, so a is not different from zero; $b = 2.1368 \times 10^{-2}$, $s_b = 5.2256 \times 10^{-4}$ (s_a = standard deviation of intercept of regression line, s_b = standard deviation of slope of regression line).

Comparison of graphs: $F_{calc} = 4.0537$, $F_{crit} = 18.2497$, so the scatter of the results is the same; $variance_{sum} = 2.128 \times 10^{-5}$, $t_{calc} = 1.2236$, $t_{crit} = 2.7908$, so $b_1 = b_2$. $b_{average} = 2.1012 \times 10^{-2}$, variance of $b_{av} = 9.357 \times 10^{-8}$, $variance_{sum} = 2.339 \times 10^{-5}$, $t_{calc} = 1.2377$, $t_{crit} = 2.5779$, so the straight lines are identical.

Percentage extraction. The aqueous phases after extraction under optimum conditions of 5, 10 and 15 μg ml^{-1} Pt, $V_w/V_o = 2$, were analysed by electrothermal AAS, and average value 99.4 + 0.05% extraction of Pt was obtained.

Extraction of Rh

Rhodium can also be extracted with the TPP–$SnCl_2$–IBMK system, but equilibrium of extraction is not reached without heating, similarly to other Rh extraction systems.[20,21] The extraction of Rh was only 75% following the procedure proposed for Pt extraction. The calibration graph obtained with extraction from matching standards was a straight line, and the precision of extraction was fairly good, but the results for the determination of Rh in solutions of samples were not accurate. Accurate results (in comparison with direct measurement in sample solution) were obtained only using procedure 3; after addition of $SnCl_2$ to the aqueous phase (up to a concentration of 0.02 mol l^{-1}) the samples were heated for 15 min, and extracted with 0.025 mol l^{-1} TPP in IBMK. The extraction of Rh obtained was then 95%.

Results of determination of Pt in the catalyst

Examples of the results are presented in Table 3. The precisions obtained for catalyst I (treatment) and catalyst II (reduction and treatment) correspond to the level of precision of extraction procedures. The results of determination obtained according to procedure 3 (heating after addition of $SnCl_2$, and extraction with 0.025 mol l^{-1} TPP in IBMK) were in good agreement with those in proposed procedure.

The accuracy was tested only for the treatment stage: 100 μg of Pt^{IV} were added to the dissolved sample, and 100% recovery was obtained. From a previous study concerning the volatilization of platinum,[22] it was known that 95% of microgram amounts (10–250 μg) of Pt^{IV} placed in the form of H_2PtCl_6 on a quartz or alumina surface was reduced in a stream of hydrogen or argon (1 h, 600 °C), without any losses of Pt. Volatilization of microgram amounts of Pt placed as H_2PtCl_6 on a quartz or alumina surface and heated at 650 °C was hardly noticeable even in a stream of air. A spike with platinum oxides is not available but from the vapour pressure data[23] no volatilization of PtO_2 and PtO in a stream of hydrogen at 650 °C can be expected. Concerning the formation of sparingly soluble species, rhodium can form it more easily, so the positive results of rhodium determination with regard to accuracy can be considered as a test for both metals.

Conclusion

The proposed method of decomposition of Co_3O_4 catalyst by reduction in hydrogen and *aqua regia* dissolution allows the accurate and precise determination of Rh and Pt by flame AAS. The optimized variant of the TPP–IBMK extractive separation of platinum is precise and efficient.

This work was supported by the State Committee for Scientific Research (project No. 200778 9101) sponsored in 1991–94.

References

1 Rubel, M., Pszonicka, M., Ebel, M. F., Jablonski, A., and Palczewska, W., *J. Less-Common Met.*, 1986, **125**, 7.
2 Petryk, J., and Krawczyk, K., *Przem. Chem.*, 1988, **67**, 272.
3 Petryk, J., and Krawczyk, K., *Pol. Pat.*, 149619, 1988.
4 *Comprehensive Chemical Kinetics, Vol. 22, Reaction in the Solid State*, ed. Bamford, C. H., and Tipper, C. F. H., Elsevier, Amsterdam, 1980.
5 Judelewicz, I. G., Starcewa, E. A., and Gordejew, G. A., *Zavod. Lab.*, 1982, **48**, 23.
6 Eller, R., Alt, F., and Tölg, G., *Fresenius' Z. Anal. Chem.*, 1989, **334**, 723.
7 Brooks, R. R., and Lee, B. S., *Anal. Chim. Acta*, 1988, **204**, 333.
8 Vest, P., Schuster, M., and König, K.-H., *Fresenius' Z. Anal. Chem.*, 1989, **335**, 759.
9 Wood, S. A., and Vassopoulous, *Anal. Chim. Acta*, 1990, **229**, 227.
10 Shkil, A. N., and Rukhadze, E. G., *Zh. Anal. Khim.*, 1988, **44**, 1204.
11 Petryk, J., unpublished work.
12 IUPAC, *Pure Appl. Chem.*, 1976, **45**, 99.
13 Pitts, A. E., and Beamish, F. E., *Anal. Chim. Acta*, 1970, **52**, 405.
14 Pilipenko, A. T., Prishchep, N. N., and Demchenko, V. Ya., *Zh. Anal. Khim.*, 1989, **44**, 1378.
15 Vassileva, E., and Arpadjan, S., *Analyst*, 1990, **115**, 399.
16 Mojski, M., *Talanta*, 1980, **27**, 7.
17 Seeverens, P. I. H., Klaasen, E. I. M., and Maessen, F. J. M. J., *Spectrochim. Acta*, 1983, **38**, 727.
18 Koch, K. R., and Yates, J. E., *Anal. Chim. Acta*, 1983, **147**, 235.
19 Brownlee, K. A., *Statistical Theory and Methodology in Science and Engineering*, Wiley, New York, 1965.
20 Diamantatos, A., *Anal. Chim. Acta*, 1981, **131**, 53.
21 Watanabe, H., Aihara, M., and Kiboka, M., *Bunseki Kagaku*, 1990, **39**, T61.
22 Różańska, B., *Zesz. Nauk. Politech. Śląsk. Chem.*, 1988, **119**, 99.
23 Kazenas, E. K., and Chizhikow, D. M. M., *Davlenie i Sostav Para nad Okislami Khimicheskih Elementov*, Nauka, Moscow, 1976, p. 270.

Paper 4/00585F
Received January 31, 1994
Accepted July 8, 1994

Determination of Trace Metals in Tea Using Both Microwave Digestion at Atmospheric Pressure and Inductively Coupled Plasma Atomic Emission Spectrometry

Kathryn Lamble and Steve J. Hill*

Department of Environmental Sciences, University of Plymouth, Drake Circus, Plymouth, Devon, UK PL4 8AA

A microwave digestion method for tea leaves has been developed using an open focused microwave digester. The optimized procedure involves initial reaction with nitric acid followed by perchloric acid to give a clear, colourless solution. Digestions are complete in 35 min, thus offering a substantial time saving on the conventional hot-plate procedure which may take in excess of 2 h. The optimized method has been employed to digest a standard reference material, a number of tea samples of different origins, four commercial blends and a herbal tea. Tea liquors were also prepared. The subsequent determination of Al, Ba, Ca, Cu, Mg, Mn and Zn was achieved using inductively coupled plasma atomic emission spectrometry. The results obtained for the standard tea were in excellent agreement with the certified values. A large variation in the trace element composition of the tea samples was observed and these results are discussed with reference to both existing literature values and country of origin.

Keywords: Focused microwave digestion; tea; trace metal analysis; inductively coupled plasma atomic emission spectrometry

Introduction

Sample dissolution is an integral part of sample treatment due to the intrinsic requirement of most quantitative analytical techniques for the sample to be in liquid form. However, the two most common digestion methods, dry digestion (calcination) and wet digestion are generally very time consuming and may be the source of possible contamination of the sample. A great deal of interest has been generated over the last two decades regarding the use of microwaves as a source of energy to break down a wide range of sample matrices which have proved to be time consuming or troublesome to digest by conventional techniques. Such samples include biological, botanical and geological materials.[1–3] An authoritative account of microwave digestion has been presented elsewhere.[4]

In the UK, on average, 1 litre of tea is consumed per person per day.[5] The accurate determination of the trace element content of tea is thus very important in assessing any potential implications for health. Aluminium is an important element to consider as it is associated with a number of health conditions and is accumulated in high concentrations by the tea bush (*Camellia sinensis*). Up to 23 000 ppm of Al[6] has been reported in tea leaves which is a far higher concentration than that for other plants which do not normally exceed 200 ppm.[7] However, other elements may have nutritional qualities, for example it has been suggested that tea is a valuable source of calcium and potassium.[5] In addition, trace metals have also been associated with the flavouring characteristics of tea.

A number of papers have been published on the aluminium content of tea leaves (*Camellia sinensis*),[6–8] although the results obtained are often in poor agreement. Coriat and Gillard[6] report dry mass concentrations (by gravimetric analysis) of aluminium in tea leaves from China, India and Russia of 8700 ppm to 23 000 ppm which is consistent with the levels of up to 20 000 ppm quoted by Talibudeen and Sivasubramanian.[7] However conflicting results have since been generated by Koch *et al.*[8] who found much lower levels of aluminium in a range of teas from India and Africa of between 400 and 1000 ppm. This was achieved using a nitric–perchloric acid hot-plate digestion.

Little work has been published on the use of microwave digestion techniques for tea leaves. Kojima *et al.*[3] used a closed vessel pressurized microwave digestion technique for biological and botanical samples, including tea leaves. However, aluminium was not included in this analysis and the certified reference material was the only tea sample digested. In addition, this procedure employed hydrofluoric acid, the use of which may be restricted in some laboratories.

Discrepancies also exist in the literature over the aluminium levels found in tea liquors. Coriat and Gillard[6] report levels of 40–100 mg l^{-1} for tea samples infused for up to 30 min, whereas Fairweather-Tait *et al.*[9] record much lower levels of between 2.7 and 4.9 mg l^{-1} for 1 g of tea infused in 100 ml of water. However, incomplete experimental detail is provided in the literature in both cases. Koch *et al.*[8] carried out similar analyses with results more in agreement with those of Fairweather-Tait *et al.*[9] They quote aluminium levels of 0.9 to 3.2 mg l^{-1} for 0.5 g of tea infused in 45 ml of water for 5 min. Takeo[10] undertook trace element determinations of Sen-cha and Kamairi-cha tea (Japanese) which were prepared by infusing 3 g of tea, in 200 ml of boiling water, twice. They report lower aluminium levels of 0.8–1.41 mg l^{-1}.

This paper reports on a study of the trace element content of tea leaves and tea liquors prepared from teas from a range of origins. Various digestion methods were investigated employing an open-focused microwave system and avoiding reagents which may be of restricted use in some laboratories, due to the associated safety risks involved.

* To whom correspondence should be addressed.

Experimental

Instrumentation

Digestions were carried out in a single-mode reflux microwave system (Microdigest 301, Prolabo, Paris) with a maximum power setting of 200 W. This system employs a focused microwave beam thus offering an efficient mechanism for transferring energy to the sample.

Analysis of all samples was performed using inductively coupled plasma atomic emission spectrometry (ICP-AES) (Liberty 200, Varian Instruments, Warrington, UK). The instrumental operating parameters used are shown in Table 1.

Reagents

Nitric acid (AnalaR), hydrogen peroxide (AnalaR) and 70% perchloric acid (ARISTAR) were obtained from Merck, Poole, Dorset, UK. De-ionized water (18 MΩ cm^{-1}) purified through a Millipore purification system (Millipore-waters, Bedford, MA 01730, USA) was used for all dilutions. All glass and plasticware was thoroughly cleaned in Decon 90 (Merck), acid washed in 5% v/v nitric acid (AnalaR, Merck) and then rinsed in de-ionized water prior to use.

Multi-element working standards were prepared containing Al, Ba, Ca, Cu, K, Mg, Mn and Zn by diluting high-purity 1000 mg l^{-1} stock solutions (SpectrosoL, Merck) with de-ionized water, nitric and perchloric acids in order to obtain the same acid concentration as in the samples (10% nitric acid, 2% perchloric acid). For the tea liquor analysis, standards were prepared without acid in calibrated plastic flasks.

The certified reference material employed was NIES No. 7 'Tea Leaves', obtained from the National Institute for Environmental Studies (Japanese Environment Agency).

Sample Preparation

Nitric Acid and Hydrogen Peroxide Digestion

Initial digestions were undertaken with concentrated nitric acid and also with nitric acid and hydrogen peroxide. Both methods were ineffectual, resulting in solutions which were yellow in colour and contained a substantial amount of undissolved material. Filtration was required before analysis. A nitric–perchloric acid mixture was therefore investigated due to its powerful oxidizing properties in hot concentrated solution.

Table 1 Optimized ICP-AES instrumental operating conditions

Instrument	Varian, Liberty 200
R.f. frequency	40.68 MHz
Operating power	1 kW
Plasma gas flow rate	15 l min^{-1}
Auxiliary gas flow rate	1.5 l min^{-1}
Torch type	Standard one piece quartz torch with 1.4 mm i.d. injector tube
Nebulizer type	V Groove
Nebulizer pressure	150 kPa
Sample flow rate	3 ml min^{-1}
Pump rate	20 rpm
Integration time	3 s
Peak search window width	0.08 nm
Viewing height	Optimized on SBR except for Ca, K and Mg which are optimized on intensity
Background correction	Dynamic
PMT voltage	650 V [except for Ca (550 V)]
Grating order	Default
Filter position	Default
Snout purge	Low

Perchloric Acid Digestion

A 0.25 g amount of tea leaves was initially heated with 5 ml of nitric acid in order to totally digest all of the easily oxidized organic matter. This is necessary before the addition of perchloric acid in order to minimize the risk of explosion. A 1 ml aliquot of 70% perchloric acid was subsequently added and heating was continued until a clear, colourless solution was obtained. De-ionized water was added, where necessary, to avoid charring the sample. When cool, the digest was transferred quantitatively into a 50 ml calibrated flask and made up to volume with de-ionized water. All samples were stored in plastic bottles before analysis by ICP-AES.

Optimization studies were carried out on the power setting and heating time for the two stages of the digestion procedure. Samples (n = 3) were heated for 15 mins with nitric acid followed by 20 mins with perchloric acid and the power setting increased systematically from 30 to 90 W. Fig. 1 shows the recoveries obtained for Al, Cu, K, Mg, Mn and Zn. Generally, recoveries increased with increasing power setting up to a maximum at 70 W power. At higher settings the reaction became very vigorous and the sample tended to boil up into the reflux column. It was therefore necessary to add anti-bumping granules to the sample flask. The lower recoveries experienced at ≥80 W (*i.e.*, above a 40% power setting) can therefore be explained by loss of sample rather than incomplete digestion.

The power setting was then set at 70 W (35%) for various combinations of heating times for the two stages of the digestion procedure. Fig. 2 shows the effect of heating times on the elemental recoveries using this two-stage procedure (n

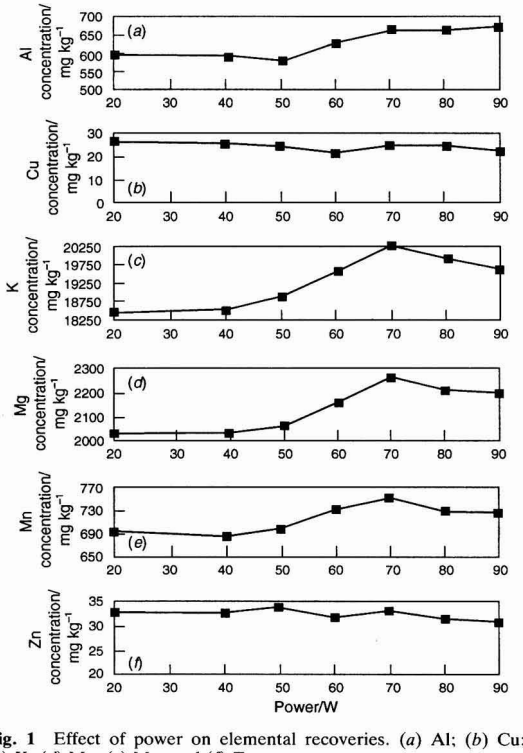

Fig. 1 Effect of power on elemental recoveries. (*a*) Al; (*b*) Cu; (*c*) K; (*d*) Mg; (*e*) Mn; and (*f*) Zn.

= 3). As can be seen, optimum recoveries are generally obtained after 15 min heating with nitric acid and 20 min with perchloric acid. The lower recoveries for the samples heated for longer periods of time can again be explained by losses due to extensive heating rather than to incomplete digestion. Table 2 summarizes the details of the optimized digestion procedure which is used throughout the rest of this work.

Hot-plate Digestion

For comparison, hot-plate digestion of the sample was also carried out. A 0.25 g amount of tea sample was initially heated on a hot-plate with 5 ml of nitric acid for approximately 30 min. Heat was supplied to maintain gentle boiling of the solution. The reaction was carried out in a 100 ml beaker covered with a watch-glass to prevent loss of the sample. A further 5 ml of nitric acid was then added and heating continued for a further 30 min. A 1 ml portion of 70% perchloric acid was subsequently added and heating continued for a further 60 min. This procedure was not vigorously optimized although it was found that the sample was not digested completely after only 30 min heating with perchloric acid.

It was necessary to keep adding small aliquots of de-ionized water to the flask to prevent evaporation to dryness and thus reducing the risk of explosion. After cooling, the digest was transferred quantitatively into a 50 ml calibrated flask, rinsing with de-ionized water. Washings from the watch-glass were also added before making the total volume up to 50 ml. Again a clear, colourless solution was obtained and filtration was unnecessary.

Tea Liquor Preparation

Experiments were carried out to examine the effect of the degree of agitation and the brewing time on the 'strength' of the tea liquor. It was found that constant stirring throughout a 5 min brewing process produced an increase in the concentration of certain elements by up to 250% when compared to samples prepared without agitation. Further experiments showed that samples brewed for 15 min (continuous stirring) contained between 0 and 56% higher concentrations of certain elements than samples brewed for only 5 min. It was therefore important to ensure that when preparing the tea liquors that the degree of agitation and the brewing time were identical for each sample.

The following procedure was adopted for preparing the tea liquors. A 0.5 g sample of tea was infused in 50 ml of boiling de-ionized water for 5 min. The mixture was not agitated until 10 s before the end of the brewing time. The flask was then gently swirled before filtering and storing the liquor in plastic bottles. Samples were analysed immediately by ICP-AES, to minimize the potential loss of trace elements by absorption onto the container walls.

Results

Microwave Digestion of Certified Reference Material

The certified reference material was digested using the optimized microwave digestion procedure (see Table 2). A clear, colourless solution was obtained. The results of the subsequent analysis by ICP-AES are shown in Table 3. It can be seen that the results are in excellent agreement with the certified values. For comparison, hot-plate digestions were also undertaken. The recoveries are compared with the

Table 2 Summary of conditions for the optimized microwave digestion procedure

Step	Procedure
1	Heat 0.25 g of tea leaves with 5 ml of nitric acid, power = 70 W (35%), time = 10 min
2	Add 2 ml of de-ionized water resume heating, power = 70 W, time = 5 min
3	Add 1 ml of 70% perchloric acid resume heating, power = 70 W, time = 5 min
4	Add 5 ml of de-ionized water resume heating, power = 70 W, time = 15 min
5	Cool digest, make up to 50 ml with de-ionized water

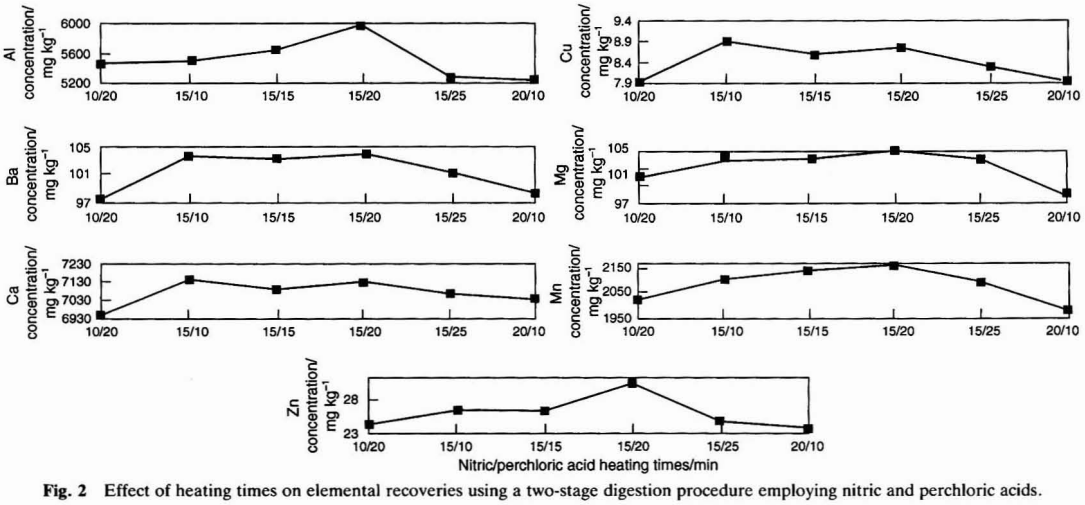

Fig. 2 Effect of heating times on elemental recoveries using a two-stage digestion procedure employing nitric and perchloric acids.

certified values in Table 3 and again are in very good agreement although the zinc recoveries are slightly high.

Trace Element Analysis of Tea Samples From Different Origins

The optimized microwave digestion method was finally employed to digest a range of samples originating from China, Japan, Africa, India and Sri Lanka. In addition a number of commercial blends and a herbal tea were analysed. Prior to digestion, coarse samples were ground in a pestle and mortar to aid digestion. Tea liquor samples were also prepared and both digests and liquors were then analysed by ICP-AES for Al, Ba, Ca, Cu, Mg, Mn and Zn. The results are shown in Tables 4 and 5, respectively.

Table 3 Comparison of certified and experimental results for certified reference material NIES No. 7 'Tea Leaves'. Values in parentheses are relative standard deviations (%) and $n = 5$ for all digestions

Element	Certified values/mg kg^{-1}	Microwave digestion/mg kg^{-1}	Hotplate digestion/mg kg^{-1}
Al	775 ± 20	766 ± 23* (1.49)	754 ± 22 (1.45)
Ca	3200 ± 120	3213 ± 129 (2.00)	3139 ± 63 (1.01)
Mg	1530 ± 60	1498 ± 70 (2.32)	1496 ± 74 (2.46)
Mn	700 ± 25	697 ± 3 (0.22)	689 ± 28 (2.04)
K	18600 ± 700	18800 ± 1051 (2.80)	18776 ± 1109 (2.95)
Zn	33 ± 3	35 ± 4.5 (6.43)	37.3 ± 2.4 (3.24)
Cu	7.0 ± 0.3	7.0 ± 0.4 (2.72)	7.08 ± 3.1 (22)
Ba	5.7†	5.4 ± 0.04 (0.65)	5.66 ± 0.2 (1.74)

* Uncertainties for the experimental results are calculated as twice the standard deviation.
† Reference value.

Discussion

Tea Leaf Digestion

The analysis highlighted the variability of trace metal levels in tea leaves from different origins. For the teas analysed it was found that generally aluminium levels fell between 500 and 1000 ppm, although two samples contained higher levels, *i.e.*, Yunnan 1517 ppm and Bancha 3566 ppm. These results are thus in agreement with those of Koch *et al.*[8] who quote levels of aluminium in tea leaves of between 400 and 1000 ppm, and much lower than earlier workers who cite aluminium levels of 8700–23 000 ppm.[6,7]

Camomile, the herbal tea, contained the lowest aluminium (542 ppm) and manganese (101 ppm) levels. Ba, Cu and Zn levels were also generally low but the calcium and magnesium levels far higher than in the other teas analysed.

Excluding the herbal tea, a number of trends can be seen. The African tea (Kenya) contained the lowest aluminium levels (631 ppm) (and the lowest calcium levels). The Indian teas (Assam and Darjeeling) contain the next highest aluminium levels; followed by Ceylon tea and then the Chinese teas. The Japanese tea (Bancha) contains by far the highest aluminium levels (and calcium and manganese levels) but in contrast has the lowest copper levels. The commercial blends of tea contain aluminium levels in the middle of the range, as may be expected.

Tea Liquor Analysis

The majority of the tea liquors contained aluminium levels in the range 1.0–3.1 mg l^{-1}. The exceptions were the Japanese tea, Bancha (8.4 mg l^{-1}) and Camomile tea (0.03 mg l^{-1}). Results are thus in good agreement with those of Fairweather-Tait *et al.*[9] and Koch *et al.*[8] but are much lower than those of

Table 4 Trace element content of a variety of tea samples. Values in parentheses are the relative standard deviations (%). In all cases $n = 3$. All values are given in mg kg^{-1}

Sample	Origin	Al	Ca	Mg	Mn	Ba	Zn	Cu
Assam	India	687 (1.1)	4249 (0.7)	2171 (1.5)	734 (2.0)	33.3 (5.0)	31.3 (4.3)	28.4 (3.4)
Darjeeling	Himalayas (India)	619 (2.2)	4486 (7.5)	2433 (1.2)	551 (2.1)	35.1 (2.9)	32.8 (1.7)	21.0 (5.7)
Yunnan Pu-erh	China	1517 (1.8)	5089 (1.1)	2823 (0.6)	799 (1.9)	26.4 (2.0)	47.8 (0.2)	22.0 (1.4)
Gunpowder (green tea)	China	939 (1.4)	3782 (4.2)	2247 (1.2)	881 (3.3)	32.6 (5.7)	27.9 (3.0)	13.2 (4.2)
Earl Grey (blend)	China	917 (1.2)	3915 (2.0)	2330 (0.04)	873 (1.9)	22.9 (1.1)	33.9 (2.8)	24.9 (0.3)
China (blend)	China	861 (0.0)	3769 (1.6)	2623 (2.7)	731 (0.4)	24.0 (5.7)	44.2 (2.6)	25.0 (2.8)
Ceylon	Sri Lanka	856 (2.7)	4906 (0.5)	2203 (0.02)	310 (0.9)	14.7 (5.5)	39.5 (0.5)	24.6 (1.3)
Kenya	Africa	631 (0.8)	3263 (0.9)	2124 (0.3)	842 (2.1)	15.3 (1.6)	26.7 (4.5)	11.6 (3.8)
Bancha	Japan	3566 (2.2)	6261 (0.9)	1847 (0.9)	2678 (2.6)	33.3 (4.0)	31.8 (12.1)	10.1 (9.7)
E. Breakfast (blend)	Unknown	959 (3.5)	4741 (0.8)	2467 (0.8)	453 (1.6)	18.7 (3.0)	41.5 (8.7)	29.6 (1.5)
'Commercial Blend'	Unknown	781 (2.2)	3875 (0.1)	2137 (1.0)	1244 (0.2)	17.5 (1.9)	23.2 (1.5)	12.0 (1.3)
Camomile	Unknown	542 (4.9)	14302 (4.9)	5369 (4.7)	101 (4.8)	15.9 (1.8)	31.6 (1.8)	12.0 (1.7)

Table 5 Trace element content of tea liquors. Values in parentheses are the percentage of the element leached into solution during the brewing process and $n = 5$ for all samples. All values are given mg l^{-1}

Sample	Al	Ca	Mg	Mn	Ba	Zn	Cu
Assam	3.08 (44.8)	3.12 (7.4)	9.86 (45.4)	2.61 (35.6)	0.0082 (2.47)	0.141 (45.1)	0.068 (24.0)
Darjeeling	1.86 (30.1)	2.61 (5.8)	6.79 (27.9)	1.24 (22.5)	0.0067 (1.90)	0.132 (40.3)	0.058 (27.5)
Gunpowder	1.40 (14.9)	2.75 (6.8)	5.93 (26.4)	1.69 (19.2)	0.0056 (1.7)	0.101 (36.1)	0.050 (37.7)
Yunnan	0.99 (6.5)	2.64 (5.2)	5.12 (17.2)	1.31 (16.4)	0.0078 (2.96)	0.108 (22.5)	0.019 (8.82)
Earl Grey	2.27 (24.8)	2.59 (6.9)	6.56 (28.2)	2.02 (23.1)	0.0061 (2.7)	0.136 (40.1)	0.053 (15.5)
China	1.47 (17.0)	2.50 (6.6)	5.87 (22.4)	1.30 (17.9)	0.0049 (2.0)	0.141 (31.6)	0.046 (18.2)
Ceylon	2.88 (33.7)	3.19 (6.5)	7.28 (33.0)	0.81 (26.2)	0.0040 (2.7)	0.159 (40.3)	0.073 (29.6)
Kenya	1.79 (28.4)	2.74 (8.4)	8.53 (40.2)	3.09 (36.6)	0.0031 (2.0)	0.145 (54.5)	0.035 (30.0)
Bancha	8.35 (23.4)	4.11 (6.6)	4.93 (26.7)	4.72 (17.6)	0.0319 (9.6)	0.110 (34.6)	0.017 (17.3)
E. Breakfast	3.12 (32.5)	2.85 (6.0)	7.45 (30.2)	1.09 (24.1)	0.0067 (3.6)	0.154 (37.0)	0.076 (25.6)
'C Blend'	3.04 (38.9)	3.14 (6.8)	9.60 (44.9)	3.88 (31.2)	0.0069 (4.0)	0.141 (60.7)	0.055 (46.1)
Camomile	0.03 (0.6)	45.62 (31.9)	32.82 (61.1)	0.25 (25.1)	0.0214 (13.4)	0.090 (28.5)	0.043 (36.1)

Coriat and Gillard.[6] Such comparisons must, however, be treated with care because the preparation of the samples varies greatly. For example, Coriat and Gillard[6] do not state the amount of tea and water infused, they use local tap water and liquors are brewed for the much longer time of 30 min. Also infusions are carried out in a teapot which could be a significant source of contamination.

Copper levels were determined in the tea liquors at between 0.02 and 0.08 mg l^{-1} and the insoluble copper complex reported by Takeo[10] was not observed. With regard to calcium levels Camomile tea contained by far the highest levels of 45.6 mg l^{-1}. For the other teas levels fell between 2.50 and 4.11 mg l^{-1} and thus are higher than the results of Takeo[10] (1.55 to 1.74 mg l^{-1}), but much lower than the levels of 13–110 mg kg^{-1} reported by Gurses and Artik[11] in Turkish black tea liquors.

For Camomile tea, magnesium levels were determined at 45.6 mg l^{-1} and so are again far higher than the 4.9–9.9 mg l^{-1} determined in the other tea liquors. Barium levels were also high but, in contrast, the manganese and zinc levels were the lowest of all the tea liquors analysed.

It is interesting to note that the percentage of each element leached out of the tea leaves into the liquor during the brewing process. These values are displayed in parentheses in Table 5. It can be seen that although the percentage of each element leached into the liquor varies with the type of tea, certain elements do seem to be more readily leached than others. Predictably barium and calcium appear to be the least soluble elements (although high levels are leached for Camomile tea) and zinc the most soluble. The percentage of calcium leached into solution was determined to be 31.9% for Camomile tea and between 5.2 and 8.4% for the other samples, thus it is lower than the 10–12% reported by Jackson and Lee.[12] In contrast, the percentage of aluminium leached into the liquor in this study is generally higher than the 15% recorded by Koch *et al.*[8] Camomile tea is again the exception with less than 1% being leached out of the leaves into the liquor during the brewing process.

Conclusions

To conclude, the microwave digestion procedure developed in this study offers an effective method for the digestion of tea leaves. This is reflected by the excellent recoveries obtained for the elements Al, Ba, Ca, Cu, K, Mg, Mn and Zn for the certified reference tea NIES No. 7 'Tea Leaves'. Digestions are complete within 35 min, a factor of at least 3.5 times faster than for the conventional hot-plate digestion. In addition, the reagents are delivered automatically through a set of pumps into the sample flask, thus requiring minimal operator attention. The use of a fully automated microwave system which has the ability to run a number of samples in succession would therefore result in substantial time saving on the conventional techniques. The analysis of a number of different tea samples from a range of origins highlighted the variability in their trace metal content. Further work is planned to examine the possibility of correlating the trace element content of the tea with it's origin. This will involve the digestion of a wider range of samples and the use of chemometric techniques to substantiate any trends in the data.

The tea liquor analyses highlighted the need to prepare samples by the same method if comparisons are to be made with past work. This should include details of the mass and physical nature of the tea used, volume of water used, infusion time and the degree of agitation applied to the sample. Our study showed that the latter point, which has often been overlooked in previous work, together with the brewing time, has a vital effect on determining the strength of the tea liquor.

The authors would like to thank Prolabo Ltd, Paris, France for supporting this work.

References

1 Kingston, H. M., and Jassie, L. B., *Anal. Chem.*, 1986, **58**, 2534.
2 Schramel, P., and Hasse, S., *Fresenius' Z. Anal. Chem.*, 1983, **346**, 794.
3 Kojima, I., Uchida, T., and Iida, C., *Anal. Sci.*, 1988, **4**, 211.
4 Kingston, H. M., and Jassie, L. B., *Introduction To Microwave Sample Preparation Theory and Practice*. American Chemical Society, Washington DC, 1988.
5 Nas, S., Gokalp, H. Y., and Sahin, Y., *Lebensmittel-Untersuchung Forschung*, 1993, **196**, 32.
6 Talibudeen, O., and Sivasubramanian, S., *J. Sci. Food Agric.*, 1971, **22**, 325.
7 Coriat, A. M., and Gillard, R. D., *Nature (London)*, 1986, **321**, 570.
8 Koch, K. R., Pougnet, M. A. B., and De Villiers, S. D., *Analyst*, 1989, **114**, 911.
9 Fairweather-Tait, S. J., Moore, G. R., and Jemil Fatemi, S. E., *Nature*, 1987, **330**, 213.
10 Takeo, T., *Jpn. Agric. Res. Quarterly*, 1985, **19**, No. 1, 32.
11 Gurses, O. L., and Artik, N., *Food J. (Turkish)*, 1983, **8**, 55.
12 Jackson, L. S., and Lee, K., *J. Food Prot.*, 1988, **151**, 711.

Paper 4/03000A
Received May 20, 1994
Accepted September 14, 1994

Comparison of a Combined Helium–Argon Plasma With Pure Helium Plasmas for Gas Chromatography With Atomic Emission Detection

Antonio L. Pires Valente* and Peter C. Uden

Department of Chemistry, Lederle Graduate Research Tower A, University of Massachusetts, Box 34510, Amherst, MA 01003-4510, USA

The use of a concentric flow sheath gas of argon or helium for a helium microwave-induced plasma (MIP) shows useful characteristics for gas chromatographic detection, by virtue of minimizing direct contact of reactive products formed in the plasma with the cell wall. Such MIPs show fewer emission bands than the capillary-type MIP, argon sheathing being more effective at much lower flow rates than helium. This plasma has a notable cost advantage, while losing little in elemental sensitivity for the plasma. Comparisons of chlorine detection are made for Ar–He and He–He plasmas.

Keywords: *Microwave-induced plasma; concentric flow; sheath gas; atomic emission; gas chromatography; chlorine detection*

Introduction

The most frequently used mode of microwave-induced plasma (MIP) for atomic spectral emission detection in gas chromatography (GC-AED) is the helium plasma sustained in quartz capillary discharge tubes.[1–3] Alumina and boron nitride capillary discharge tubes have also been used for measurements that require the absence of interfering silicon emissions[4,5] or when silica tubes generate spurious elemental signals resulting, for example, from oxygen produced from plasma–tube surface reactions.[6] The use of an argon MIP is less favoured as it is less energetic and permits effective detection of fewer elements than the helium MIP; hence, halogens respond very poorly in argon plasmas.[7] Reports on the use of the helium MIP have shown numerous background emissions due to the presence of helium and other elements in the plasma environment[4] and these can interfere with the detection of some elements. The production of a 'cleaner' spectral background is important in GC-MIP-AED and this paper discusses the use of argon as a sheathing gas for helium to accomplish this result.

Experimental

The argon-sheathed helium plasma is generated in a torch in which the sheathing gas is fed through several 0.2 mm i.d. capillary tubes that surround the 1 mm i.d. tube through which the helium support gas is supplied. In order to make direct comparisons with previous data, the torch was tested using the same plasma spectrometer and signal processing system as described previously.[4,5] This consisted of a Beenakker TM_{010} cylindrical resonance cavity, equipped with a 2.45 GHz microwave generator (Applied Chromatography Systems, Luton, Bedfordshire, UK). Frequency and impedance matching between generator and cavity was provided by a coaxial stub stretcher (Model SL-10N tuner, Microlab/FXR, Livingstone, NJ, USA) attached to the plasma cavity by a UG-58 connector. The torch assembly, shown in Fig. 1, holds a 3 mm i.d. quartz tube into which flow the support and sheath gas streams. This 3 mm i.d. discharge tube arrangement is larger than the conventional capillary system. The line that feeds the (inner) helium support gas is independent of that feeding the outer sheath gas. The latter may be helium or argon, allowing operation in two alternative modes: He–Ar or He–He.

For comparison purposes, background spectrograms, scanned from 225 to 600 nm, were obtained with the torch operating in each mode. These were further compared with parallel scans obtained in the same MIP system for a conventional helium plasma sustained in a quartz capillary tube. Comparisons were also made with scans obtained in earlier studies on this system,[4,5] which included background spectrograms of He-MIPs in quartz, boron nitride and alumina capillary discharge tubes. Table 1 summarizes these data. Both He–He and He–Ar plasmas were also tested for responses to halogenated compounds. Table 2 summarizes the results obtained for the calibration graphs for chloroform, monitoring the 480.9 nm chlorine emission line.

Results and Discussion

In Table 1 are summarized data showing similarities and differences in relative intensities of emission lines for the He–He and He–Ar plasmas (columns 6 and 7) and by comparison, information from a number of other MIP studies (columns 3, 4, 5, 8 and 9). The various sources were selected to indicate the differences among the spectrograms obtained for different instruments and under differing operating conditions. Hence, data in columns 3, 4 and 5 were all obtained for the same quartz capillary cell system but at different times; differences in intensities are noted for Si (243.0 nm), He (447.1 nm, *etc.*) and Ar/CN (419.0 nm). These variations may

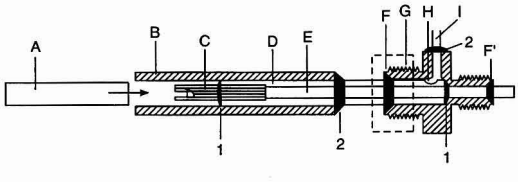

Fig. 1 Gas-sheathed torch. A = Quartz discharge cell, B = 1/4 in o.d. copper tube, C = package of fused silica capillaries, D = 1/8 in o.d. copper tube, E = 1/16 in o.d. stainless-steel tube, F, F' = ferrules (1/8 and 1/16 in), G = reducing connector, H = hole drilled in tube D, I = intake for sheath gas, 1 = cement and 2 = solder.

* Present address: Instituto de Quimica, Universidade Estadual de Campinas, Campinas, SP 13081-970, Brazil.

be attributed to differences in flow rate and purity of the support gas and power applied to the cavity, but may also be due to less tangible factors such as the quality of the quartz or undefined interactions of the support gas with other elements in the plasma.

In Table 1, emissions in rows 1–8 are attributed to silicon.[4,5] Asterisks for emission in columns 3–5 indicate that the silicon signals are generally very intense in helium plasmas sustained in quartz capillary cells. Intensities for these emissions in the He–He and He–Ar plasmas (columns 6 and 7) are much reduced or below measurement levels at the range displayed, confirming that these MIPs are almost free of silicon emission. This is attributable to protection against plasma attack on the quartz cell wall afforded by the sheath gas, a characteristic also

Table 1 Comparison of relative intensities* of some emission lines observed with He–He and He–Ar plasmas, and lines observed with capillary quartz discharge cells.

	1	2	3	4	5	6	7	8	9
			Band intensity as height (%) relative to chart full scale†						
		Attribution	Quartz capillary						
Column	Band/nm	(ref. 4)				He–He	He–Ar	Al_2O_3	BN
1	243.0	Si	OS‡	78	60	5	—§	—	—
2	250.6	Si	OS	OS	96	7	—	—	—
3	251.6	Si	OS	OS	OS	22	—	—	—
4	252.4	Si	OS	OS	OS	7	—	—	—
5	252.8	Si	OS	OS	OS	8	—	—	—
6	263.0	Si	20	28	11	0.4	—	—	—
7	288.1	Si	OS	OS	OS	3	2	—	—
8	443.0	Si	30	13	28	—	—	—	—
9	388.9	He	OS	OS	OS	—	—	OS	OS
10	447.1	He	OS	38	47	3	—	OS	OS
11	318.8	He	75	—	13	—	—	90	54
12	492.2	He	48	6	9	0.4	0.8	57	45
13	471.3	He	25	—	5	0.4	0.8	30	27
14	402.6	He	25	—	27	—	—	30	30
15	396.5	He	18	—	4	—	—	27	—
16	419.0	Ar/CN	30	7	3	6	80	66	90

* Data for columns 3, 8 and 9 from ref. 5; for columns 2 and 4 from ref. 4; for columns 5, 6 and 7 from this work.

† Data for columns 3, 8 and 9 corrected to 3×10^{-6} A mV^{-1} electronic gain; other column measurements were made with 3×10^{-6} A mV^{-1} electronic gain.

‡ OS, Off Scale.

§ Not measurable.

Table 2 Results of calibration graphs* obtained for the He–He and He–Ar plasmas using chloroform as analyte and signal monitoring at the chlorine 480.9 nm emission line. Linear regression equation: h (peak height) = $A \times$ mass + B

Data obtained for the He–He plasma—

		Regression analysis		*t*-test (95%)	
Mass of Cl/ng	Peak height (h)/mm	Parameter†	Standard deviation	Lower value	Upper value
111.0	100.0	$A = 0.9018$	0.0089‡	0.8770‡	0.9266‡
55.5	48.0				
27.8	24.0				
13.9	11.7	$B = -0.7790$	0.00893§	−2.0757§	0.5176§
7.0	5.9				
3.5	3.0	$r^2 = 0.9996$			

Data obtained for the He–Ar plasma—

		Regression analysis		*t*-test (95%)	
Mass of Cl/ng	Peak height (h)/mm	Parameter†	Standard deviation	Lower value	Upper value
111.0	91.0	$A = 0.8244$	0.00524‡	0.8077‡	0.8411‡
55.5	44.5				
27.8	22.1				
13.9	10.5	$B = -0.7622$	0.30040§	−1.7182§	0.1938§
7.0	5.5				
—	—	$r^2 = 0.9998$			

* Experimental conditions. For both plasmas: emission line = 480.9 nm (Cl); sample = $CHCl_3$ in toluene; injected volumes = 0.3 μl; split ratio = 1:200; temperatures: column = 120 °C, injector = 240 °C, transfer line = 240 °C; column flow rate = 2 ml min^{-1}. For the He–He MIP: forward power = 54 W reflected power = 0 W; inner He flow = 30 ml min^{-1}; outer He flow = 1 l min^{-1}. For the He–Ar MIP: forward power = 52 W, reflected power = 0 W; inner He flow = 35 ml min^{-1}, outer Ar flow = 115 ml min^{-1}.

† A = Slope (mm ng^{-1}); B = intercept (mm).

‡ of A.

§ of B.

noted for the tangential flow torch[8] and the concentric dual flow torch[9] which also utilize concentric flow of gases. Comparison of the silicon emissions between the He–He (column 6) and He–Ar (column 7) plasmas shows them to be still present at low levels in the former but less intense or absent in the latter, indicating the superiority of argon sheathing for cell protection. Supporting evidence that the listed emissions are due to silicon arises from the observation that they are not present in helium plasmas sustained in the alumina and boron nitride cells (as noted in entries in rows 1–8 of columns 8 and 9 in Table 1).

Comparison of the characteristics of the helium emissions noted in rows 9–15 of Table 1 is also useful. The data in columns 6 and 7 show that the helium emission lines are either absent or are of very low intensity for both He–He and He–Ar modes, while they are generally of higher intensities in the plasmas sustained in the quartz, alumina and boron nitride capillary cells. In the He–He plasma the reduced helium emissions must be attributed to a reduction of cell wall interactions by the action of the sheathing gas. For ths He–Ar plasma, the effect could also be partly attributed to the presence of a less energetic plasma owing to total or partial quenching of the helium plasma energy by the argon used for sheathing.

In order to address the latter possibility, the detection at 480.9 nm of chlorine, introduced as chloroform, was examined. The results shown in Table 2 indicate that, under the experimental conditions employed, the calibration graph obtained for chlorine response in the He–Ar plasma is not substantially different from that observed for the He–He plasma. The value for the slope of the response calibration graph for the latter situation (0.9018 ± 0.0089 mm ng^{-1}) is approximately 10% greater than for the former (0.8185 ± 0.0081 mm ng^{-1}), but this difference is insufficient to conclude that there is any substantive lowering of sensitivity due to a less energetic He–Ar plasma. Within the 95% confidence interval of the *t*-test, the response factors obtained for both situations are almost overlapped. For both He–He and He–Ar plasmas these chromatograms, corresponding to injected chlorine masses of 3.5 ng, showed peak heights approximately four times the baseline noise. Absolute extrapolated detection limits were not obtained as post-run digital noise filtration on the collected data was not available.

Although it cannot be unequivocally stated that the He–Ar MIP is as energetic as the He–He MIP under the experimental conditions employed, it is possible to conclude that the former does not behave as a pure argon plasma in that its response to chlorine as chloroform in the GC introduction mode closely resembles that of the He–He plasma. The conditions used to collect these data also indicate a more effective sheathing capacity for argon as it was effective at a flow rate of 115 ml min^{-1} whereas the same effect with helium sheathing required a flow of 1 l min^{-1}.

In conclusion, it appears that torches that operate with a sheath gas are of potential use in GC-MIP spectroscopic detectors, by virtue of their ability to minimize direct contact of reactive products formed in the plasma with the cell wall. As a consequence, such MIPs show fewer emission bands than the capillary-type MIP and hence may find broader use for various element-selective detection applications. Argon is effective as a sheath gas as it is more effective at much lower flow rates than helium, affording a notable cost advantage, while losing little in elemental sensitivity for the plasma. The greater cell wall protection imparted by argon sheathing may result in an increased lifetime for discharge tubes, and the testing of longer term operational characteristics of the He–Ar MIP will be reported in a subsequent paper.

One of the authors, A. L. P. V., thanks the 'Fundaçao de Amparo a Pesquisa do estado de Sao Paulo, FAPESP', São Paulo, Brazil, for the sponsorship of postdoctoral study at the University of Massachusetts. This project was supported in part by project No. 551/89-FAEP (Fundo de Amparo ao Ensino e Pesquisa) of the State University of Campinas-UNICAMP, Campinas, Brazil.

References

1 Uden, P. C., in *Element Specific Chromatographic Detection by Atomic Emission Spectroscopy,* ed. Uden, P. C., American Chemical Society, Washington, DC, 1992, *ACS Symposium Series No. 479*, pp. 1–24.
2 Bradley, C., and Carnahan, J. W., *Anal. Chem.*, 1988, **60**, 858.
3 Quimby, B. D., and Sullivan, J. J., *Anal. Chem.*, 1990, **62**, 1027.
4 Estes, S. A., Uden, P. C., and Barnes, R. M., *Anal. Chem.*, 1981, **53**, 1829.
5 Slatkavitz, K. J., Hoey, L. D., Uden, P. C., and Barnes, R. M., *Anal. Chem.*, 1985, **57**, 1846.
6 Slatkavitz, K. J., Uden, P. C., and Barnes, R. M., *J. Chromatogr.*, 1986, **355**, 117.
7 Beenakker, C. I. M., Boumans, P. W. J. M., and Rommers, P. J., *Philips Tech. Rev.*, 1980, **39**, 65.
8 Bollo-Kamara, A., and Codding, E. G., *Spectrochim. Acta, Part B,* 1981, **36**, 973.
9 Dowling, T. M., Seeley, J. A., Feuerbacher, H., and Uden, P. C., in *Element Specific Chromatographic Detection by Atomic Emission Spectroscopy*, ed. Uden, P. C., American Chemical Society, Washington, DC, 1992, *ACS Symposium Series No. 479*, pp. 90–104.

Paper 4/04683H
Received July 29, 1994
Accepted September 21, 1994

New Spectrofluorimetric Reagent, 2,3-Diamino-1,4-dibromonaphthalene, for the Determination of Selenium in Biological Materials

Karin Johansson, Örjan Andersson and Åke Olin

Department of Analytical Chemistry, University of Uppsala, P.O. Box 531, S-751 21 Uppsala, Sweden

2,3-Diamino-1,4-dibromonaphthalene (Br_2-DAN) has been investigated as a new reagent for the spectrofluorimetric determination of selenium. It has advantages in comparison with the commonly used 2,3-diaminonaphthalene (DAN) as ligand. The values of the acidity constants of Br_2-DAN make the adjustment to the optimum pH for the piazselenol reaction easy, and the reaction can be performed in a strongly acidic medium. The stability of the reagent is good and there is no need to work in subdued daylight. In cyclohexane, the fluorescence of the selenium complex, 4,7-dibromo-5,6-benzopiazselenol, is measured at 577 nm and with excitation at 383 or 518 nm. The background is low and equivalent to less than 0.1 ng of selenium for excitation at the longer wavelength. An analytical procedure is presented for the determination of total selenium in small biological samples where the whole analysis is performed in a single test tube. The reduction of Se^{VI} to Se^{IV} is performed by hydrobromic acid at 85 °C over 15 min. This is followed by derivatization into piazselenol at 70 °C for 10 min. Iron(III) and copper(II) do not interfere.

Keywords: Selenium; 2,3-diamino-1,4-dibromonaphthalene; fluorescence; hydrogen bromide reduction; biological samples

Introduction

Selenium(IV) reacts in aqueous solution with aromatic *o*-diamines to form piazselenols, which can be extracted into an organic solvent and quantified. Substituted *o*-diaminobenzenes are used in determinations made by gas chromatography[1–3] whereas 2,3-diaminonaphthalene (DAN), introduced by Parker and Harvey,[4] is the most extensively used reagent when molecular fluorescence spectrometry is utilized. Both techniques are important and frequently used for the determination of selenium in various matrices.[1–13]

Piazselenol is formed in a reaction between undissociated selenous acid and the monoprotonated diamine,[14–16] and consequently it is important that the prevailing reaction conditions are selected so that these species predominate. With DAN as derivatization ligand the useful pH range is limited to 1–2.[5,8,15,17–19] Since biological samples require decomposition with strong acids and subsequent reduction of Se^{VI} to Se^{IV}, normally by the use of 4–6 mol l^{-1} hydrochloric acid,[20] extensive pH adjustment is necessary before spectrofluorimetry is performed. This is usually accomplished by the addition of a base or concentrated buffer solution. In order to achieve reproducible results, the pH of the reaction medium must be controlled quite carefully. Hence, a pH indicator has to be added or a pH meter used to monitor the pH adjustment. In addition to being lengthy, this manipulation of the sample is prone to introduce errors at low analyte concentrations by contamination. Further, it is reported that the solution of DAN is unstable, needs repeated cleaning prior to use and has to be stored cold in the dark under a layer of cyclohexane.[7,8,15,18,19,21] Since the piazselenol (5,6-benzopiazselenol) is sensitive to light, the derivatization and extraction of the piazselenol are often performed in the dark. The spectrofluorimetric method using DAN is thus somewhat time-consuming and laborious, but frequently used. The last steps in the analysis have been automated.[21,22]

A ligand with a considerably larger first acidity constant than that of $DANH_2^{2+}$[15,16] would shift the optimal concentration of strong acid for the derivatization reaction to the mol l^{-1} range. Such a ligand would be more compatible with the conditions resulting from the pre-treatment of the sample. Substituted *o*-diaminobenzenes have been studied as ligands when selenium is derivatized to piazselenol for determination by gas chromatography. Then the efforts were directed towards finding substituents in the aromatic ring, such as halogens or nitro groups, that yield a high sensitivity in the electron capture detector.[1–3] These substituents also shift the usable pH range of the piazselenol reaction towards a lower pH owing to changes in the acidity constants.[16,23] Corresponding alterations in the acidity constants can be expected for derivatives of DAN. Such derivatives have been little used in gas chromatography, but Zheng *et al.*[24] reported on the use of 2,3-diamino-1,4-dibromonaphthalene (Br_2-DAN). The applicability of this ligand to the spectrofluorimetric determination of selenium has not yet been examined.

This paper reports on Br_2-DAN as a reagent in the spectrofluorimetric determination of selenium. This ligand offers several advantages over DAN. The pH adjustment is obviated and the piazselenol reaction is faster with Br_2-DAN. The background fluorescence signal is low. The stability of the ligand is good and no precautions against daylight are necessary. An analytical procedure for the determination of selenium in biological materials is also presented and evaluated. It is based on the new reagent and the steps prior to the spectrofluorimetric measurement are carried out in a single test tube.

Experimental

Apparatus

All the spectrofluorimetric recordings were made on an Aminco SPF-500 Corrected Spectra Fluorimeter, equipped with a standard four-position cell compartment. A Hamamatsu R928P photomultiplier tube with extended red-sensitivity (near S-20 response) was used for monitoring the fluorescence. Fused silica cells, 1 cm, were used for all measurements. When possible, the excitation beam was filtered by a

2 mm WG 360 cut-off filter (Schott Glaswerke, Mainz, Germany), blocking second-order reflections of short wavelengths. Gas chromatography–mass spectrometry (GC–MS) measurements were made on a Hewlett-Packard (HP) 5890 Series II gas chromatograph connected to a HP 5971A Mass Selective Detector (Hewlett-Packard, Avondale, PA, USA). A HP-5 column (25 m × 200 μm id) with 0.33 μm film thickness was used. The chromatographic conditions were: carrier gas, helium at 60 kPa; split vent, 50 ml min^{-1}; purge vent, 1 ml min^{-1}; injector temperature, 250 °C; detector temperature, 280 °C; column temperature programme, 100 °C held for 2 min, increased at 20 °C min^{-1} to 275 °C, and held for 15 min. Manual injections (1 μl sample + 1 μl toluene) were made in the splitless mode, with a change to the split mode after 1 min. The mass sensitive detector was operated in the scan mode, continuously scanning over the range 100–400 *m/z*. The detector was activated 5 min after the injection in order to avoid the toluene peak.

All the sample treatments were performed in 8 ml Pyrex glass tubes equipped with poly(tetrafluoroethylene) (PTFE) faced screw caps in a laboratory-built aluminium block (150 × 150 mm) with a capacity of 25 samples and placed on a 2000 W hot-plate. The temperature was regulated by an Eurotherm 904 temperature regulator (Eurotherm International, Strängnäs, Sweden).

Reagents

All chemicals were of analytical-reagent grade from Merck (Darmstadt, Germany) unless otherwise stated. Milli-Q-filtrated (MQ) water (Millipore waters, Milford, MA, USA) was used throughout. All the glassware was cleaned in 7 mol l^{-1} nitric acid and rinsed with MQ water. The standard solution of selenium(IV) was prepared and analysed as described before.[23] A solution of DAN was prepared by dissolving 0.1 g of the chemical (Fluka, Buchs, Switzerland) in 100 ml of 0.1 mol l^{-1} hydrochloric acid. It was purified by extraction as described by Alfthan.[10] 2,3-Diamino-1,4-dibromonaphthalene was synthesized, with some modifications, by the method described by Zheng *et al.*[24] About 0.5 g of DAN was weighed into a 50 ml round-bottomed flask and dissolved in 10 ml of glacial acetic acid. A mixture of 0.3 ml of bromine and 3 ml of glacial acetic acid was added dropwise under vigorous stirring at room temperature. After 10 min, the precipitate was filtered off and washed with 10 ml of glacial acetic acid followed by 50 ml of 2% sodium carbonate solution and finally dried at 80 °C for 3 h. The crude pink product was purified by flush chromatography using a Silica-60 column and a mixture of 83% toluene, 15% acetonitrile and 2% triethylamine. Mass spectrometry (MS) and thin layer chromatography (TLC) were used to identify the fraction containing the pure product. The solvent was evaporated, yielding a solid residue of light orange–red needles. A working solution of Br_2-DAN was prepared by dissolving 16.2 mg of the chemical in 25 ml of methanol. The solution was stored at room temperature in the dark. It was stable for at least one week.

Kinetic Experiments

A 1 ml amount of a 10 μg l^{-1} Se^{IV} solution in 2 mol l^{-1} hydrobromic acid was added to a set of 8 ml Pyrex test-tubes with PTFE faced screw caps. The tubes were closed and placed in a thermostated aluminium block. When the desired temperature had been reached, 25 μl of a 2.05×10^{-3} mol l^{-1} Br_2-DAN solution were added. At predetermined times, a tube was withdrawn from the heating block and the reaction stopped by changing the pH to 5 by addition of a strong Na_3PO_4 solution. The tube was then stored in an ice bath. The extraction of the piazselenol was performed at room temperature with 3 ml of cyclohexane.

Analytical Procedure

Digestion of Sample

Weigh about 0.1 g of dry homogeneous sample into an 8 ml Pyrex test tube. Add 0.3 g of magnesium nitrate hexahydrate, 1 ml of 14 mol l^{-1} nitric acid and 50 μl of 12 mol l^{-1} hydrochloric acid. Place the tube in the aluminium block and apply the following temperature programme [temperature (°C), ramp time (min), dwell time (min)]: 50, 20, 60; 85, 20, 100; 105, 20, 100; 125, 20, 100; 175, 120, 30; 225, 40, 30; 500, 180, 120. An end step may also be included, allowing the temperature to decrease to 85 or 110 °C, the temperatures used for the reduction to selenium(IV) by hydrobromic acid or hydrochloric acid, respectively. In the following text (*i*) and (*ii*) represent hydrobromic and hydrochloric acid medium, respectively.

Reduction of Se^{VI}

(*i*) Add 1 ml of a solution containing 2 mol l^{-1} hydrobromic acid and 2.5 mol l^{-1} perchloric acid and maintain the capped tube in the block at 85 °C for 15 min. Then add 50 μl of 0.5 mol l^{-1} hydroxylammonium sulfate to reduce any bromine formed to bromide. (*ii*) Add 1.2 ml of 6 mol l^{-1} hydrochloric acid and place the capped tube in the aluminium block at 110 °C for 45 min.

Derivatization and Extraction of the piazselenol

Cool the tube. (*i*) Add 25 μl of 2.05×10^{-3} mol l^{-1} Br_2-DAN. (*ii*) Add 2.8 ml of MQ-water and 75 μl of 2.05×10^{-3} mol l^{-1} Br_2-DAN. Close the tube, shake well and place it in a heating block at (*i*) 70 °C for 10 min or (*ii*) 50 °C for 30 min. Cool to room temperature and extract with 3 ml of cyclohexane. Rapid phase separation is obtained by spinning the test-tubes.

Spectrofluorimetric determination

Measure the fluorescence of the piazselenol extract at an excitation wavelength of 518 nm and emission wavelength of 577 nm.

Results and Discussion

Spectra

DAN has been used for over 30 years as a reagent for the spectrofluorimetric determination of selenium and the spectral characteristics of the DAN-Se complex have been investigated.[4–6,17] The use of Br_2-DAN for the same purpose does not seem to have been attempted yet. The reason for this could be that it is known that the fluorescence quantum yield is diminished when heavy atom substituents are introduced in aromatic systems. However, at the same time the probability of singlet → triplet intersystem crossing is enhanced resulting in a higher yield of phosphorescence instead.[25]

Spectra of the two ligands and corresponding selenium complexes were recorded in cyclohexane. The excitation and emission spectra of 5,6-benzopiazselenol (DAN-Se) are shown in Fig. 1. The excitation and emission maxima are at 378.5 and 521 nm, respectively. The corresponding maxima for 4,7-dibromo-5,6-benzopiazselenol (Br_2-DAN-Se) are at 383 and 577 nm as shown in Fig. 2. Additional excitation bands are found for Br_2-DAN-Se at 518 and 559 nm, Fig. 2(*a*).

The shift of the emission band of Br_2-DAN-Se towards longer wavelengths initiated a study of the lifetimes of the excited state of DAN-Se and Br_2-DAN-Se using a pulsed laser for excitation.[26] In both cases the lifetimes were approximately 20 ns in aerated solutions and 50 ns in deaerated solutions. Therefore, it was concluded that the emissions are of the same origin. Note that one heavy atom, *i.e.* selenium, is already present in the ring systems and the effect of this atom is perhaps dominating.

The emission intensity is lower with Br_2-DAN-Se as ligand, approximately 65, 35 and 45% of that of DAN-Se for excitation at 383, 518 and 559 nm, respectively. The decreases are probably caused by lower absorbances and diminishing sensitivity of the photomultiplier tube with increasing wavelength. As seen in Figs. 1 and 2, the background is substantially smaller with Br_2-DAN as the ligand. The differences are reflected in the corresponding average selenium equivalents which are 0.6 ng ($n = 6$) for DAN, and 0.15 ($n = 6$) and 0.08 ng ($n = 14$) for Br_2-DAN at the excitation wavelengths 383 and 518 nm. The value obtained for DAN is somewhat lower than the figure reported by Alfthan.[10] The differences between the DAN and Br_2-DAN blanks are probably caused by the higher ligand concentration needed for derivatization with DAN.

From the spectral data, excitation at 518 and measurement at 577 nm was selected for the quantitation of selenium. The more favourable excitation at 559 nm was excluded because it was feared that the proximity of the excitation and emission bands would cause problems with stray light in our instrument.

Acidity Constants

The acidity constants of Br_2-DANH_2^{2+} were determined by spectrophotometric measurements at room temperature. The value of $pK_{a,2}$ was found to be 0.65 ± 0.05, but the value of $pK_{a,1}$ could not be properly established. The spectrum of Br_2-DANH$^+$ did not start to change until the medium was 4 mol l^{-1} in strong acid and it then changed continuously in the region 4 to 8 mol l^{-1} acid, which indicates that the value of $K_{a,1}$ must be large.

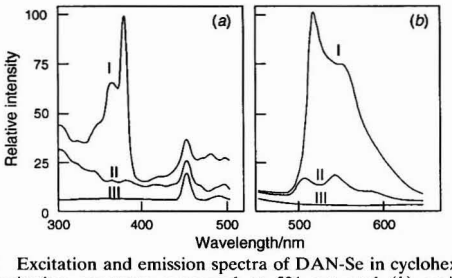

Fig. 1 Excitation and emission spectra of DAN-Se in cyclohexane. (*a*) Excitation spectrum measured at 521 nm and (*b*) emission spectrum excited at 378.5 nm. I, DAN + 5 ng Se; II, DAN (blank); III, solvent.

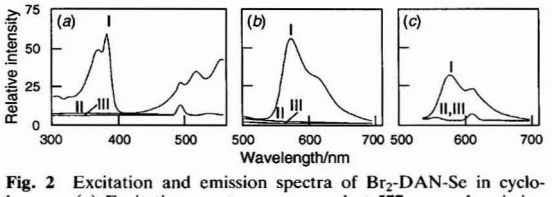

Fig. 2 Excitation and emission spectra of Br_2-DAN-Se in cyclohexane. (*a*) Excitation spectrum measured at 577 nm and emission spectra excited at (*b*) 383 nm, (*c*) 518 nm. I, Br_2-DAN + 5 ng Se; II, Br_2-DAN (blank); III, solvent.

According to Cukor and Lott,[15] $pK_{a,1}$ is 0.51 and $pK_{a,2}$ is 2.11 for DANH_2^{2+} whereas Nève *et al.* reported the values as 0.95 and 3.99.[16] For selenous acid $pK_{a,1}$ is 2.6.[27] These constants indicate that the useful pH range is 1–2 for the piazselenol reaction with DAN.[5,8,15,18,19] The substituents introduced on DAN have increased the values of the acidity constants, which implies that the pH adjustment before the derivatization of Se^{IV} to the piazselenol is less critical and the reaction can be carried out in 1–2 mol l^{-1} acid.

Piazselenol Formation

The formation of piazselenol occurs in a bimolecular reaction between undissociated selenous acid and the monoprotonated ligand and can be represented by

$$H_2SeO_3 + Br_2\text{-DANH}^+ \rightleftharpoons Br_2\text{DAN-Se} + 2\,H_2O + H_3O^+$$

For fast piazselenol formation, the pH of the derivatization step in the analytical procedure must be situated in the range where H_2SeO_3 and Br_2-DANH$^+$ simultaneously constitute large fractions of the total concentrations of Se^{IV} and Br_2-DAN, respectively. The effect of pH on the concentration of Br_2-DAN-Se must also be considered in the choice of the optimal pH for piazselenol formation, since the reaction proceeds to an equilibrium. Computer simulations based on the data for several substituted diaminobenzenes given by Nève *et al.*[16] indicated that the rate of the piazselenol formation is quite sensitive to pH, whereas the equilibrium concentration of the piazselenol stays almost constant over a rather broad range in pH. The reaction is only moderately fast, hence the optimal pH for the derivatization of Se^{IV} is determined by the kinetics rather than by the equilibrium position of the piazselenol reaction.

The kinetic experiments were carried out in a medium of constant acidity with the ligand present at constant concentration and in great excess over Se^{VI}. Concentrations given refer to the value at room temperature (20 °C) for practical reasons. From the previous discussion, the rate law for the main forward reaction is expected to follow

$$r = \frac{\mathrm{d}[Br_2\text{-DAN-Se}]}{\mathrm{d}t} = k_2[H_2SeO_3][Br_2 - \text{DANH}^+] \quad (1)$$

in analogy with the results of earlier kinetic studies of piazselenol formation. Under the conditions used here, eqn. (1) can be simplified to

$$r = k_2'[Se^{IV}]_{tot}[Br_2DAN]_{tot} \quad (2)$$

owing to the constant acidity, and further to

$$r = k_1'[Se^{VI}]_{tot} \quad (3)$$

owing to the excess of the ligand. The latter constants will be referred to as the conditional (apparent) second- and first-order constants, respectively. The reverse reaction is assumed to be of the first order with respect to [Br_2-DAN-Se].

The rate of formation of Br_2-DAN-Se was studied as a function of ligand concentration in 2 mol l^{-1} hydrobromic acid at 70 °C. The results are presented in Fig. 3 which shows that the reaction rate increases with ligand concentration and the reaction proceeds to a state of equilibrium. The rate equation for a first-order, reversible reaction is expected to be obeyed and hence the fluorescence intensity is expected to follow

$$S_t = S_\infty(1 - e^{-kt}) \quad (4)$$

where S_t is the measured fluorescence intensity at time t and S_∞ is the corresponding quantity at equilibrium. The rate constant, k, is the sum of the conditional constants of the forward and backward reaction. The values of S_∞ were obtained by fitting the function $S_t = A - Be^{-kt}$ to the (S_t, t)

data and they are plotted against ligand concentration in Fig. 4.

The conditional equilibrium constant, β', of the piazselenol reaction can be written

$$\beta' = \frac{[\text{Br}_2\text{-DAN-Se}]}{[\text{Se}^{\text{IV}}]_{\text{tot}}[\text{Br}_2\text{-DAN}]_{\text{tot}}} \quad (5)$$

The total selenium concentration, c_0, is

$$c_0 = [\text{Se}^{\text{IV}}]_{\text{tot}} + [\text{Br}_2 - \text{DAN} - \text{Se}] \quad (6)$$

Eqn. (5) and (6) give

$$S_\infty = \frac{\beta' S_0[\text{Br}_2\text{-DAN}]_{\text{tot}}}{1 + \beta'[\text{Br}_2\text{-DAN}]_{\text{tot}}} \quad (7)$$

where, as before, S_∞ is the fluorescence intensity at equilibrium and S_0 is the intensity expected for complete conversion of Se^{IV} into the piazselenol. By fitting eqn. (7) to the experimental (S_∞, $[Br_2\text{-DAN}]_{tot}$) data, β' was estimated to be 1.7×10^5 l mol^{-1}. The value of β' was confirmed by a measurement of the amount of Se^{IV} present at equilibrium for $[Br_2\text{-DAN}]_{tot} = 50 \times 10^{-6}$ mol l^{-1}. The value of β' so determined was 1.8×10^5 l mol^{-1}.

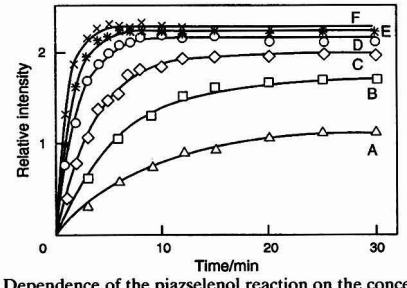

Fig. 3 Dependence of the piazselenol reaction on the concentration of Br_2-DAN (ligand) in 2 mol l^{-1} hydrobromic acid at 70 °C. Ligand concentrations: A 6; B, 13; C, 26; D, 51; E, 78; and F, 108 μmol l^{-1}.

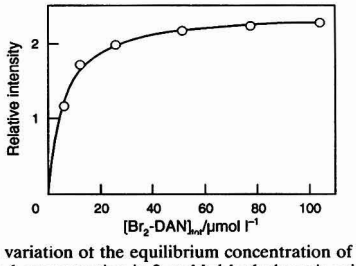

Fig. 4 The variation ot the equilibrium concentration of Br_2-DAN-Se with ligand concentration in 2 mol l^{-1} hydrobromic acid at 70 °C.

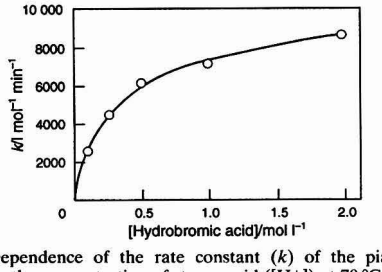

Fig. 5 Dependence of the rate constant (k) of the piazselenol reaction on the concentration of strong acid ([H$^+$]) at 70 °C.

The equilibrium constant for the piazselenol reaction

$$\beta = \frac{[\text{H}_3\text{O}^+][\text{Br}_2\text{-DAN-Se}]}{[\text{H}_2\text{SeO}_3][\text{Br}_2\text{-DANH}^+]} \quad (8)$$

can be calculated from β' and the values of the acidity constants of H_2SeO_3 and Br_2-DANH$^+$. The value of β so obtained was 3.4×10^5. For comparison, the β-values for piazselenols derived from 1,2-diaminobenzenes have been calculated from the compilation by Nève *et al.*[16] The values range from 1.4 to 8.6×10^5, *i.e.*, the β-values of the ligands are of the same order of magnitude. The equilibrium constants must be of this magnitude in order to make the ligand a useful derivatization reagent. The small values for DAN reported by Cukor and Lott[15] should probably be multiplied by 1000 to put them on the mol l^{-1} scale.

The variation of the conditional rate constant with acidity at constant ligand concentration (50×10^{-6} mol l^{-1}) is shown in Fig. 5. The variation should be mainly a result of the variation of [Br_2-DANH$^+$]. However, with increasing acid concentration the backward reaction will become more pronounced. An expression for the rate constant, k, can be derived from the rate law including the forward and backward reactions and the assumption that $K_{a,1}$ is large.

$$k = k_f[\text{Br}_2\text{-DAN}]_{\text{tot}}\frac{[\text{H}^+]}{K_{a,2} + [\text{H}^+]} + k_b[\text{H}^+] \quad (10)$$

k_f and k_b are the rate constants of the forward and the backward reactions, respectively. Eqn. (10) was fitted to the data in Fig. 5 and the value of p$K_{a,2}$ obtained was 0.62, which is close to the result obtained from the spectrophotometric determinations at 20 °C.

The temperature dependence of the reaction rate was determined in 2 mol l^{-1} hydrobromic acid between 20 and 80 °C, Fig. 6. The results can be represented by

$$\ln k_2' = 23.2 - \frac{4820}{T} \quad (11)$$

with k_2' in l mol^{-1} min^{-1}. The equilibrium concentration of the piazselenol decreases with temperature, indicating a moderate temperature dependence of the equilibrium constant.

The data presented allow, at least semiquantitatively, predictions to be made about the piazselenol formation by computer simulations. Fig. 7 shows the variation with pH of the relative rate of formation and the degree of formation of Br_2-DAN-Se with pH at a ligand concentration of 50×10^{-6}

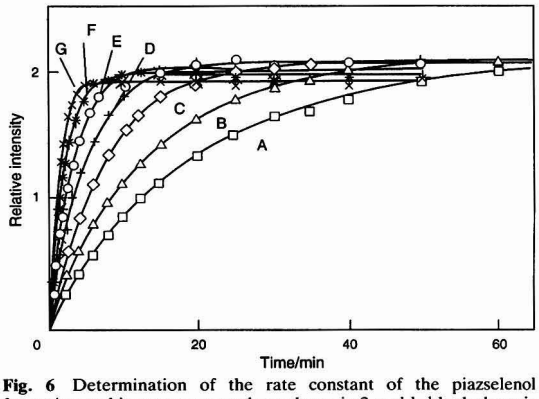

Fig. 6 Determination of the rate constant of the piazselenol formation and its temperature dependence in 2 mol l^{-1} hydrobromic acid and 50×10^{-6} mol l^{-1} of Br_2-DAN. A, 20; B, 30; C, 40; D, 50; E, 60; F, 70; and G, 80 °C.

mol l^{-1} and 70 °C. It can be concluded that the derivatization can be carried out in 1–2 mol l^{-1} of strong acid and that the equilibrium of the reaction is only slightly affected by the concentration of acid within this range. Fig. 7 also shows the kinetic pH profile of DAN, which necessitates a careful pH adjustment prior to the derivatization. From measurements at 50 °C, the second-order rate constant for Br_2-DAN in 2 mol l^{-1} hydrobromic acid was found to be about 10 times larger than for DAN measured at pH 1.5. This is in accordance with the findings of Nève *et al.*[16] who investigated the reaction rate of five differently substituted *o*-diaminobenzenes. They found that diamines having a substituent that lowered the basicity of the amino group had faster reaction kinetics. Consequently, derivatization with DAN is usually carried out with about 10-fold larger concentrations of the ligand than with Br_2-DAN. This contributes to the larger blank signal observed for DAN, since much of the ligand is extracted into the organic phase.

Deviations from the expected results were found when the derivatization was performed in a hydrochloric acid medium. At temperatures above 50 °C, the fluorescence signal first increased to a maximum and then gradually decreased with time. Since the results in hydrobromic acid indicated good thermal stability of the ligand and piazselenol, it was suspected that an exchange of bromide with chloride had occurred. This was confirmed by GC–MS measurements as follows: solutions containing 50×10^{-6} mol l^{-1} Br_2-DAN in 1 mol l^{-1} HCl were heated at 90 °C. At predetermined times they were then cooled to room temperature and extracted with 1 ml of toluene. The toluene extracts were injected into the GC–MS instrument. Each chromatogram showed the presence of several components in the injected sample.

Most of the components could be identified from their molecular masses and the characteristic isotope patterns occurring in mass spectra of compounds containing Br and Cl. From the chromatograms in Fig. 8 and the assignments made to the peaks, it is clear that exchange of halogens occurs with a transformation of Br_2-DAN to Cl_2-DAN. The corresponding exchange in the piazselenol could not be followed since the solubility of Br_2-DAN-Se in the reaction medium is not high enough to yield a sufficiently large concentration in the toluene extract for the GC–MS measurements. The exchange reaction has analytical implications. A moderate temperature and a reaction time of about 30 min must be used when the reaction medium is hydrochloric acid.

Reduction of Se^{VI} to Se^{IV} with Hydrobromic Acid

Several authors have investigated the reduction of Se^{VI} to Se^{IV} with reagents other than hydrochloric acid but this reagent is by far the most often used. A few articles have reported on the application of hydrobromic acid as a reducing agent.[11,28,29] Shibata *et al.*[28] reported that an almost quantitative reduction of Se^{VI} to Se^{IV} was obtained within 5 min with 4, 3 or 1.8 mol l^{-1} hydrobromic acid at 70, 87 and 100 °C, respectively. The reduction of Se^{VI} with 2 mol l^{-1} hydrobromic acid was studied at 85 °C. The results presented in Table 1 show that the reduction is complete after 15 min. Hydrobromic acid is, therefore, suitable both with regard to the stabilities of the ligand and the complex, and the efficiency of the reduction.

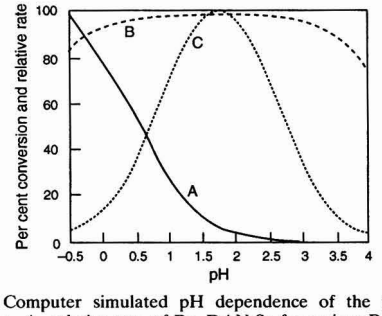

Fig. 7 Computer simulated pH dependence of the piazselenol formation. A, relative rate of Br_2-DAN-Se formation; B, degree of formation of Br_2-DAN-Se; and C, the relative rate of DAN-Se formation.

Interferences

Metals are known to interfere in methods using DAN, but the interference can often be masked by the addition of EDTA.[5,7,21] This method cannot be expected to work in a strongly acidic medium. Interference studies were performed for Fe^{III}, which is ubiquitously present in biological materials, and Cu^{II} which forms strong complexes with nitrogen donors. Using cyclohexane for extraction of the piazselenol from 2 mol l^{-1} hydrobromic acid, no interference was observed for additions of Fe (≤150 μg) or Cu (≤50 μg) and a sample volume of 2 ml. With 1 mol l^{-1} hydrochloric acid as medium, as little as 0.1 μg of Cu interfered by increasing the fluorescence signal by about 5%. Surprisingly, the interference did not increase significantly with the amount of Cu up to 100 μg. Iron also interferes, but the increase in fluorescence signal did not exceed 5% for a 150 μg addition.

Determination of Selenium in Reference Materials

For the determination of selenium in biological samples the organic material has to be digested. Usually, this is performed by treatment with strong, oxidizing acids. Most commonly

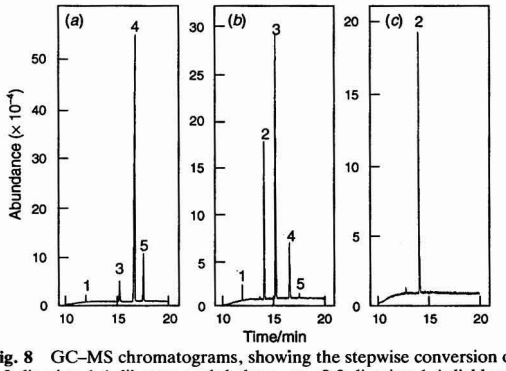

Fig. 8 GC–MS chromatograms, showing the stepwise conversion of 2,3-diamino-1,4-dibromonaphthalene to 2,3-diamino-1,4-dichloronaphthalene in 1 mol l^{-1} HCl at 90 °C. The samples were analysed after a reaction time of (*a*) 5 min, (*b*) 2 h and (*c*) 18 h, respectively. The peaks are: 1, unknown; 2, 2,3-diamino-1,4-dichloronaphthalene; 3, 2,3-diamino-1-bromo-4-chloronaphthalene; 4, 2,3-diamino-1,4-dibromonaphthalene; and 5, unknown.

Table 1 Reduction of Se^{VI} to Se^{IV} with 2 mol l^{-1} hydrobromic acid at 85 °C

Reduction time/min	Recovery of Se^{VI} (%)
2.5	67
5	89
7.5	96
10	99
15	100
20	100

employed is a mixture of nitric, perchloric and sulfuric acid. Hansson *et al.*[30] have described a combined wet/dry ashing procedure, in which the digestion of the organic material is performed with a mixture of magnesium nitrate, nitric and hydrochloric acid. This digestion method was used as it avoids the risks and the regulations connected with use of hot perchloric acid and permits the entire procedure to be performed in a single 8 ml test-tube.[31] Samples of mass 0.1 g were generally used. The residue after the digestion consists mainly of magnesium oxide, about 50 mg, which has to be accounted for when the proper conditions are established for the reduction of Se^{VI} to Se^{IV} and the subsequent derivatization of Se^{IV}. The reductions by hydrochloric acid were performed in 4 mol l^{-1} of acid. The dilution of the acid to about 1 mol l^{-1} is necessary before the addition of Br_2-DAN in order to avoid the bromide–chloride exchange in the ligand. With bromide as reducing agent the digestion residue was dissolved in a solution containing 2 mol l^{-1} of hydrobromic acid and 2.5 mol l^{-1} of perchloric acid. Perchloric acid was included only in order to reduce the consumption of hydrobromic acid. The medium contained 2 mol l^{-1} hydrobromic acid after dissolution of the decomposed sample. This concentration ensured rapid reduction of Se^{VI} and fast derivatization. When the mixture of acids was added to the digest the solution became straw coloured. Trace amounts of nitrite left from the digestion probably oxidize bromide to bromine. The formation of a small amount of bromine does not interfere in the reduction step. Rather, the presence of some bromine is beneficial, since the Br_2/Br^- redox couple stabilizes the tetravalent oxidation state of selenium. Bromine must, however, be removed before the derivatization step. This was accomplished by addition of hydroxylammonium sulfate.

The following reference materials were analysed; SRM 1567 wheat flour (1100 ± 200 ng g^{-1}), RM 8412 corn stalk (16 ± 8 ng g^{-1}), RM 8413 corn kernel (4 ± 2 ng g^{-1}), SRM 1577a bovine liver (710 ± 70 ng g^{-1}) and IAEA MA-B-3/TM fish tissue (1460 ng g^{-1}, 1350–1700 ng g^{-1}, 95% confidence interval). The results are presented in Tables 2 and 3 for the respective reaction media. The measured concentrations fall within the specified concentration limits of the reference materials. The result obtained for SRM 1567 is close to the lower end of the certified concentration range. Low results for this reference material were also found in a previous study[31] where selenium was determined by hydride generation–atomic absorption spectrometry. It was concluded that the low results probably arose from incomplete digestion. Any influence of the amount of sample on the analytical result was studied on the fish tissue, Table 4, and no significant dependence was found on the sample mass. For the other materials, 1 g samples were also digested and the results are presented in Table 5. The value for bovine liver has increased significantly and reflects difficulties with the small-scale version of the present digestion method on this type of material. For no apparent reason, obvious outliers were obtained now and then for small samples of bovine liver, but not for the other materials.

The results of the present investigation indicate that 2,3-diamino-1,4-dibromonaphthalene could advantageously be used for the spectrofluorimetric determination of selenium. The advantages of the new reagent include less strict conditions for piazselenol formation, a lower blank and less interference from metal ions. Hydrobromic acid appears to be the best reaction medium for biological samples for which the volumes can to be kept small.

Table 2 Selenium concentrations (dry mass) found in some reference materials. Sample mas 0.1 g and reduction with 2 mol l^{-1} hydrobromic acid

Reference material	Mean/ ng g^{-1}	s*/ ng g^{-1}	n	Specified concentration/ ng g^{-1}
SRM 1567, wheat flour	925	21	9	1100 ± 200
SRM 1577a, bovine liver	667	28	7	710 ± 70
IAEA MA-B-3/TM, fish tissue	1400	35	9	1350 – 1700†
RM 8412, corn stalk	11.7	0.6	4	16 ± 8
RM 8413, corn kernel	4.9	0.5	8	4 ± 2

* s = standard deviation.
† 95% confidence interval.

Table 3 Selenium concentrations (dry mass) found in some reference materials. Sample mass 0.1 g and reduction with hydrochloric acid

Reference material	Mean/ ng g^{-1}	s/ ng g^{-1}	n	Specified concentration/ ng g^{-1}
SRM 1567, wheat flour	914	27	13	1100 ± 200
SRM 1577a, bovine liver	677	30	11	710 ± 70
IAEA MA-B-3/TM, fish tissue	1409	18	8	1350–1700*
RM 8412, corn stalk	14.0	0.6	10	16 ± 8
RM 8413, corn kernel	5.7	0.6	9	4 ± 2

* 95% confidence interval.

Table 4 Influence of the amount of sample used on the analytical result for IAEA-MA-B-3/TM, fish tissue (1350–1700 ng g^{-1}, 95% confidence interval)

Sample weight/mg	Selenium/ng g^{-1}
50	1383, 1402
100	1401, 1396
150	1402, 1403
200	1423, 1418

Table 5 Selenium concentrations (dry mass) found in some reference materials. Sample mass 1 g and reduction with hydrochloric acid

Reference material	Mean/ ng g^{-1}	s/ ng g^{-1}	n	Specified concentration/ ng g^{-1}
SRM 1567, wheat flour	920	20	4	1100 ± 200
SRM 1577a, bovine liver	720	7	4	710 ± 70
RM 8412, corn stalk	11.3	1.1	3	16 ± 8
RM 8413, corn kernel	5.6	0.6	3	4 ± 2

References

1 Shimoishi, Y., and Tôei, K., *Anal. Chim. Acta*, 1978, **100**, 65.
2 Dilli, S., and Sutikno, I., *J. Chromatogr.*, 1984, **298**, 21.
3 Al-Attar, A. F., and Nickless, G., *J. Chromatogr.*, 1988, **440**, 333.
4 Parker, C. A., and Harvey, L. G., *Analyst*, 1962, **87**, 558.
5 Lott, P. F., Cukor, P., Moriber, G., and Solga, J., *Anal. Chem.*, 1963, **35**, 1159.
6 Allaway, W. H., and Cary, E. E., *Anal. Chem.*, 1964, **36**, 1359.
7 Watkinson, J. H., *Anal. Chem.*, 1966, **38**, 92.
8 Grant, A. B., *N. Z. J. Sci.*, 1981, **24**, 65.
9 Koh, T.-S., and Benson, T. H., *J. Assoc. Off. Anal. Chem.*, 1983, **66**, 918.
10 Alfthan, G., *Anal. Chim. Acta*, 1984, **165**, 187.
11 Nakaguchi, Y., Hiraki, K., Tamari, Y., Fukunaga, Y., Nishikawa, Y., and Shigematsu, T., *Anal. Sci.*, 1985, **1**, 247.
12 Tamari, Y., Ohmori, S., and Hiraki, K., *Clin. Chem. (Winston-Salem, N.C.)*, 1986, **32**, 1464.
13 Wang, D., Alfthan, G., and Aro, A., *Environ. Sci. Technol.*, 1994, **28**, 383.
14 Barza, L., *Mikrochim. Acta*, 1964, 136.

15 Cukor, P., and Lott, P. F., *J. Phys. Chem.*, 1965, **69**, 3232.
16 Nève, J., Hanocq, M., and Molle, L., *Mikrochim. Acta*, 1980, 41.
17 Cukor, P., Walzcyck, J., and Lott, P. F., *Anal. Chim. Acta*, 1964, **30**, 473.
18 Analytical Methods Committee, *Analyst*, 1979, **104**, 778.
19 Bayfield, R. F., and Romalis, L. F., *Anal. Biochem.*, 1985, **144**, 569.
20 Pettersson, J., and Olin, Å., *Talanta*, 1991, **38**, 413.
21 Brown, M. W., and Watkinson, J. H., *Anal. Chim. Acta*, 1977, **89**, 29.
22 Watkinson, J. H., *Anal. Chim. Acta*, 1979, **105**, 319.
23 Johansson, K., and Olin, Å., *J. Chromatogr.*, 1992, **598**, 105.
24 Zheng, O., Xu, P.-Y., Xiong, G.-L., and Liu, Y., *Talanta*, 1986, **33**, 443.
25 Schulman, S. G., *Molecular Luminescence Spectroscopy; Methods and Applications, Part 1*, Chemical Analysis, vol. 77, Wiley, New York, 1985, ch. 1.
26 Andersson, Ö., Johansson, K., and Olin, Å., unpublished work.
27 Baes, C. F. Jr., and Mesmer, R. E., *The Hydrolysis of Cations*, Wiley, New York, 1976, ch. 17.
28 Shibata, Y., Morita, M., and Fuwa, K., *Analyst*, 1985, **110**, 1269.
29 D'Ulivo, A., *J. Anal. At. Spectrom.*, 1989, **4**, 67.
30 Hansson, L., Pettersson, J., and Olin, Å., *Talanta*, 1987, **34**, 829.
31 Hansson, L., Johansson, K., Olin, Å., and Simán, G., *Acta Agric. Scand, Sect. B*, 1994, in the press.

Paper 4/05958A
Received September 29, 1994
Accepted October 10, 1994

Pyoverdin-doped Sol–Gel Glass for the Spectrofluorimetric Determination of Iron(III)

J. M. Barrero, C. Cámara and M. C. Pérez-Conde*

Departamento de Química Analítica, Facultad de Ciencias Químicas, Universidad Complutense de Madrid, 28040 Madrid, Spain

C. San José and L. Fernández

Departamento de Nutrición y Bromatología III, Facultad de Veterinaria, Universidad Complutense de Madrid, 28040 Madrid, Spain

Pyoverdin, a natural fluorescent pigment biosynthesized by *Pseudomonas fluorescence*, was entrapped in sol–gel glass and used as a reactive solid phase for the determination of trace amounts of Fe^{III}. No leaching or bleaching of the trapped reagent was observed. The fluorescent siderophore was more stable in sol–gel glass than on controlled-pore glass. Iron(III) was determined by continuous flow and flow injection (FI) methods. Both methods provided a fast response. The detection limits were 3 ng ml^{-1} (relative standard deviation, 3.0% for 150 ng ml^{-1} of Fe^{III}) and 20 ng ml^{-1} (relative standard deviation, 4.5% for 500 ng ml^{-1} of Fe^{III}) for the continuous and FI (sample injection 1 ml) systems, respectively. The selective sensor was successfully used to determine iron in tap waters (continuous system) and human serum (FI system).

Keywords: *Sol–gel glass; pyoverdin; siderophore; iron(III) determination; fluorescence; serum; water*

Introduction

Reactive solid phases prepared by the sol–gel process at room temperature (sol–gel glasses doped with the different reagents) are an attractive support for the immobilization of biomolecules in silica matrices. This simple process allows the entrapment of a wide range of organic and inorganic compounds including enzymes and other molecules.

The sol–gel entrapment conditions (temperature, container, ageing, *etc.*) must be carefully controlled in order to obtain a satisfactory active phase.[1–4] As the reagent occupies cavities in the sol–gel glass, it reacts readily when the test solution passes through the channels connecting the cavities. Hence, cavity size is a critical parameter that must be carefully selected to allow the entry of the analyte and avoid reagent leaching.

Zusman *et al.*[5] were among the first to entrap organic reagents in sol–gel glasses and to report the qualitative determination of metals. We have evaluated three supports, including the sol–gel glass used for the determination of Fe^{III}.[6]

Wolfbeis *et al.*[7] have prepared a sensitive sol–gel containing an entrapped dye for pH determination. MacCraith *et al.*[8] have recently described an evanescent wave sensor to determine oxygen based on the sol–gel entrapment of an organic reagent. Lev *et al.*[9] have determined Fe^{II} spectrophotometrically using 1,10-phenanthroline entrapped in a silica matrix by the sol–gel method.

Sol–gel solid supports are particularly suitable for the entrapment of enzymes and several attempts have been described in the literature. Trypsin was successfully entrapped by Johnson and Whateley[10] in silica xerogel, and subsequently showed activity that was not removed by washing. Braun *et al.*[11] immobilized alkaline phosphatase in a silica matrix using the sol–gel procedure and reported better stability and selectivity than in aqueous solutions. Glucose oxidase has been entrapped by the sol–gel method and used in a glucose sensor by Tatsu *et al.*[12]

An optical sensor for Fe^{III} based on pyoverdin immobilized on controlled-pore glass (CPG) has been described in a previous paper.[13]

This paper reports the preparation and properties of the highly fluorescent pigment pyoverdin when entrapped in sol–gel glass and its application to the determination of Fe^{III}.

Two sampling systems were used: continuous sample introduction and flow injection (FI), the latter being useful when only small amounts of sample are available.

Experimental

Apparatus and Materials

Fluorescence intensity was measured on a Perkin-Elmer LS-50 spectrofluorimeter, which was equipped with a xenon-lamp source and an IBM Model 55 SX computer and used in combination with a Hellma quartz flow cell. All measurements were made with 5 nm bandwidths for the emission and excitation monochromators. The temperature was controlled by means of a thermostated bath. All spectra were uncorrected.

UV/VIS absorbance was recorded on a Hewlett-Packard 8452-A diode-array spectrophotometer and pH was measured on a Crison 2001 pH-meter. Solutions were pumped from a Gilson Minipuls 2 pump. An Omnifit injection valve (six-way) was used for FI measurements.

A Perkin-Elmer 2380 atomic absorption spectrometer was used for the reference technique.

A Zeiss fluorescence microscope equipped with a camera was used to take pictures of the solid phase.

Ultrafree-CL low binding cellulose units from Millipore were used for desalination or clarification of serum samples.

Reagents

Pyoverdin, a natural fluorescent pigment, was biosynthesized and purified from *Pseudomonas fluoresecens* strain AR-11 by a previously described method.[14] The sol–gel glass was prepared from tetramethylorthosilicate (Aldrich) and methanol (Carlo Erba). A 1000 mg l^{-1} stock Fe^{III} solution was prepared by dissolving $Fe(NO_3)_3 \cdot 9H_2O$ in 1% HNO_3 and titrating it with potassium permanganate solution. The buffer

* To whom correspondence should be addressed.

solutions used included 2-(*N*-morpholino)ethanesulfonic acid (MES), tris(hydroxymethyl)methylamine hydrochloride (TRIS), hexamethylenetetramine (HMTA), imidazole, phthalic acid and acetic acid. Freshly prepared ultrapure water obtained from a Milli-Q water purification system and analytical-reagent grade reagents were used in all experiments.

Cromatrol T, obtained from Cromatest, is a freeze-dried human serum without preservative and with certified values for 23 components; it was used as a control for validating the proposed method.

Procedure

Glass preparation

Pyoverdin was entrapped in sol–gel glasses by the standard sol–gel procedures described by Zusman *et al.*,[5] which were as follows: 1 ml of tetramethoxysilane, 1.2 ml of methanol, 0.48 ml of distilled water, 0.08 ml of aqueous 1×10^{-3} mol l^{-1} pyoverdin and any catalyst used were mixed and allowed to gel under ambient conditions for 3 d. The container was then covered with perforated aluminium paper and dried to constant mass. When a sol–gel glass of constant mass was obtained (about 2 weeks), it was dried overnight under vacuum to remove any remaining solvents. All sol–gel glasses were prepared with and without pyoverdin. The final amount of pyoverdin in the sol–gel glasses was 0.124 mmol g^{-1}.

The glass disc obtained was ground and passed through sieves of different mesh sizes (1 and 0.16 mm). The powder was washed with different solvents and finally with distilled water. The cleaning solutions were analysed by absorption spectrometry at the peak wavelength of aqueous pyoverdin (385 nm)[14,15] and by fluorescence spectrometry at emission and excitation wavelengths of 465 and 390 nm, respectively, and no leaching was observed.

The flow cell was filled with 200 mg of sol–gel glass powder and was kept at 4 °C.

Iron determination

Continuous system. Buffer (0.05 mol l^{-1} MES, pH 6.5), Fe^{III} at any of several different concentrations and regenerator (1 mol l^{-1} HCl) were pumped alternately through the cell. The fluorescence intensity at 405 nm (excitation at 330 nm) was recorded *versus* time. The formation of the pyoverdin–Fe^{III} complex was evidenced by the decrease in fluorescence intensity when the Fe^{III} solution flowed through the cell. Fluorescence intensity decreased with increasing Fe concentration. The Fe^{III} was pumped through the cell for 2 min. When the pyoverdin–Fe^{III} complex had formed, 1 mol l^{-1} HCl was pumped for 1 min to cleave the complex and then the buffer solution was circulated to restore the fluorescence intensity to the initial level, ready for another Fe concentration measurement.

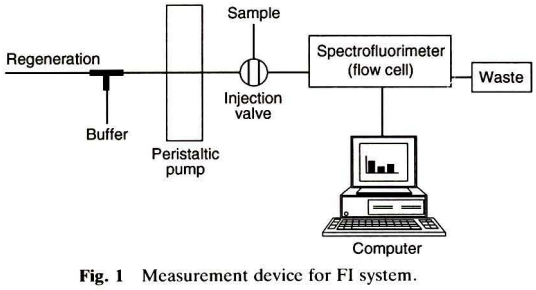

Fig. 1 Measurement device for FI system.

The calibration graph was obtained by plotting the slope of the decrease in fluorescence intensity (2 min after addition of Fe solution) *versus* Fe concentration. The same procedure was followed for water analyses.

FI system. An injection valve was inserted in the system (Fig. 1) in order to control the exact volume of sample (from several microlitres to 1 ml). The decrease in the fluorescence intensity after passage of the injected sample was evaluated instead of the slope as in the continuous system. This was because the system generated only a baseline signal when no Fe was pumped and a (lower) constant signal when the Fe^{III} in the loop reached and reacted with the reagent phase. A typical FI peak was not observed because of the irreversibility of the reaction. Once the Fe^{III} had passed through the cell, the reactive solid phase was regenerated with 1 mol l^{-1} HCl to re-establish the initial signal. Different Fe concentrations were injected after injection of the buffer solution (0.05 mol l^{-1} MES, pH 6.5).

In order to obtain the calibration graph, the difference in fluorescence intensity recorded when the buffer passed through the cell and that obtained when Fe^{III} was injected and retained in the solid phase was plotted against Fe concentration.

Serum preparation

Freeze-dried reference serum sample was kept at 4 °C and reconstituted according to the instructions. Distilled water (5 ml) was added to the freeze-dried powder and shaken. This solution was either used immediately, refrigerated or frozen for later use.

The Fe^{III} was complexed to proteins from which it had to be separated by standard methods without protein precipitation.[15] Serum (0.3 ml) plus 1.5 ml of 0.8 mol l^{-1} acetate buffer (pH 4.5) were centrifuged in a Millipore Ultrafree-CL unit containing a filter that retained molecules above 5000 Da. The Fe^{III} passed through and was analysed by the standard additions method.

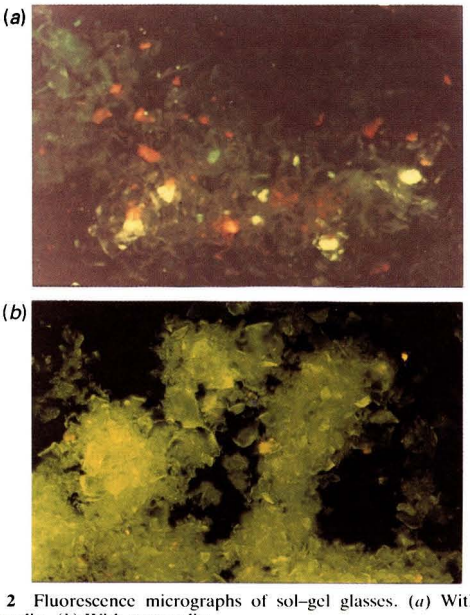

Fig. 2 Fluorescence micrographs of sol–gel glasses. (*a*) Without pyoverdin. (*b*) With pyoverdin.

Results and Discussion

Once the sol–gel glass powder doped with pyoverdin had been obtained, it was placed in the flow cell and test solutions at different pH (acidic, basic and neutral) were pumped through. No leaching was observed in any instance.

When solutions containing different concentrations of Fe^{III} were passed through the flow cell, the fluorescence intensity decreased with increasing Fe concentration. Hence, the pyoverdin immobilized in the sol–gel glass acts as an active phase and has potential as a sensor for Fe^{III}.

Fluorescence microscopy photographs of the pigment immobilized in sol–gel glass revealed the cavities in which the fluorescent pigment is located as well as the non-fluorescent undoped sol–gel glass (Fig. 2).

The flow cell was filled with 200 mg of doped sol–gel glass and placed in the spectrofluorimeter. The fluorescence spectrum of pyoverdin (excitation and emission maxima were 330 and 405 nm, respectively) was similar to that of pyoverdin in solution (excitation and emission maxima 390 and 465 nm, respectively) but very different to that of pyoverdin on CPG (excitation and emission maxima 500 and 552 nm, respectively), which shows that entrapment causes few changes in the luminophore environment and/or electronic structure.[13]

Continuous System

The following tests were performed to identify the best operating conditions. The pH was varied from 3 to 9; the fluorescence intensity of the entrapped pyoverdin in the sol–gel glass was constant within the pH range 5.0–7.5, whereas at pH values higher than 7.5 and lower than 5.0 it significantly decreased and increased, respectively. At pH values lower than 5.0, the pyoverdin Fe^{III} complex was not formed. The optimum pH was found to be between 6.2 and 7.2 (Fig. 3); within this pH range the decrease in fluorescence intensity was maximum. Different buffers at the same concentration were used to obtain the optimum pH; maximum sensitivity was obtained in the absence of buffer, with MES giving the next best sensitivity (Fig. 4). Hence, MES was chosen to obtain the required pH and the effect of its concentration was evaluated. As can be seen in Fig. 5, increasing the buffer concentration significantly decreased the sensitivity of the determination of Fe^{III}; therefore, 0.05 mol l^{-1} MES was chosen for further experiments. As a constant response was obtained at a buffer flow rate of 1.5–2.5 ml min^{-1}, 1.8 ml min^{-1} was used (Fig. 6).

The electrolytes $NaClO_4$ and NaCl were tested at concentrations from 0.05 to 1 mol l^{-1} to ascertain the effect of ionic strength. Concentrations lower than 0.5 mol l^{-1} did not affect the sensor response.

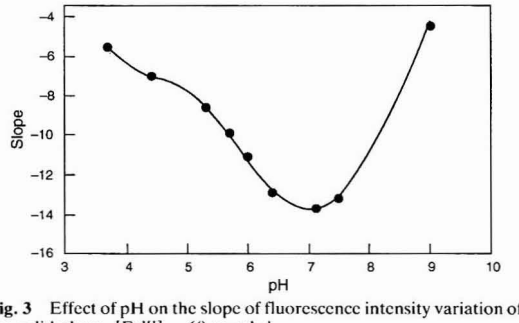

Fig. 3 Effect of pH on the slope of fluorescence intensity variation of the solid phase. [Fe^{III}] = 60 ng ml^{-1}.

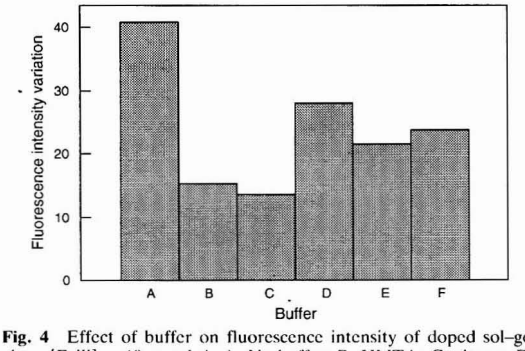

Fig. 4 Effect of buffer on fluorescence intensity of doped sol–gel glass. [Fe^{III}] = 60 ng ml^{-1}. A, No buffer; B, HMTA; C, citrate; D, MES; E, TRIS; and F, imidazole.

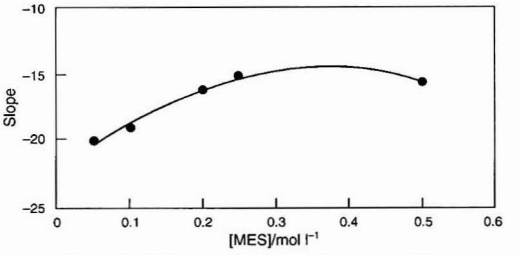

Fig. 5 Effect of MES concentration on the slope of fluorescence intensity variation. [Fe^{III}] = 150 ng ml^{-1}.

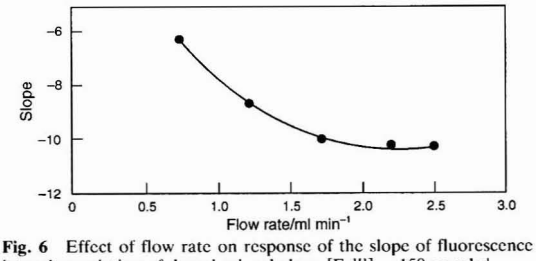

Fig. 6 Effect of flow rate on response of the slope of fluorescence intensity variation of doped sol–gel glass. [Fe^{III}] = 150 ng ml^{-1}.

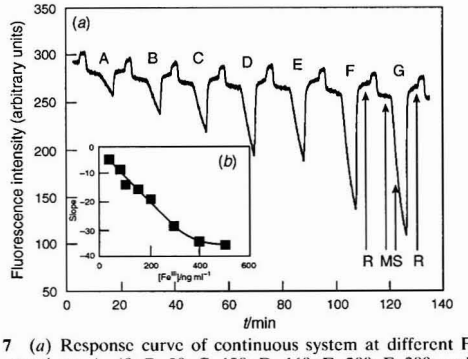

Fig. 7 (*a*) Response curve of continuous system at different Fe^{III} concentrations: A, 40; B, 80; C, 120; D, 160; E, 200; F, 300; and G, 400 ng ml^{-1}. R, Regeneration; M, MES (pH 6.5); S, sample. (*b*) Linear range, slope *versus* Fe^{III} concentration.

The proposed solid phase showed an immediate response to Fe^{III} and, furthermore, as a consequence of the high thermodynamic formation constant of the complex, very strong regeneration conditions (1 mol l^{-1} HCl) were required.

Regeneration was very fast and it was sufficient to pump the 1 mol l^{-1} HCl regenerator for 1 min. The whole analysis procedure and the calibration graph are shown in Fig. 7. When solutions of Fe^{III} were pumped through the cell a significant decrease in fluorescence intensity was achieved [proportional to Fe^{III}; Fig. 7(*a*), S]. The reactive phase was then regenerated [Fig. 7(*a*), R] and the baseline was re-established by pumping the buffer solution [Fig. 7(*a*), M]. As the baseline was not completely recovered, the slope achieved for each Fe solution was used. The calibration graph, obtained by plotting the slope of the response *versus* Fe concentration, was linear from 3 to 300 ng ml^{-1} and the correlation coefficient was 0.997 [Fig. 7(*b*)].

The detection limit, calculated as three times the standard deviation of the blank, was 3 ng ml^{-1}. The precision, expressed as the relative standard deviation, was 3% for ten determinations of 150 ng ml^{-1} of Fe^{III}.

Table 1 Study of interferences. All experiments were carried out at an Fe^{III} concentration of 150 ng ml^{-1} at pH 6.5

Ion	Ion : Fe^{III} ratio*	Relative sensitivity (%)†
Na^{I}	500	104
K^{I}	500	102
Ca^{II}	200	105
Mg^{II}	500	106
Cu^{II}	100	97
Ni^{II}	100	103
Zn^{II}	500	98
Pb^{II}	100	100
Al^{III}	50	99
Mn^{II}	10	100
Cr^{III}	100	101
Fe^{II}	100	103
F^-	100	97
Cl^-	1000	100
CO_3^{2-}	50	95
SO_4^{2-}	1000	96

* Maximum ratio tested.

† Expressed as the ratio of the signal of Fe^{III} in the presence of interferent to that of Fe^{III} alone.

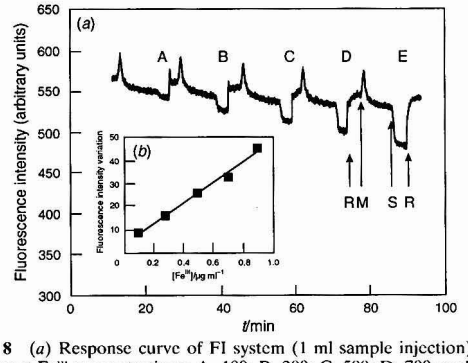

Fig. 8 (*a*) Response curve of FI system (1 ml sample injection) at different Fe^{III} concentrations: A, 100; B, 300; C, 500; D, 700; and E, 900 ng ml^{-1}. R, Regeneration; M, MES (pH 6.5); S, sample. (*b*) Linear range, fluorescence intensity variation *versus* Fe^{III} concentration.

The effect of the most common substances (cations and anions) present in water was evaluated. The results, given in Table 1, show that the method is very selective and that the main interferences are caused by fluoride and carbonate. The selectivity provided by the proposed solid phase is slightly better than that obtained with CPG.[13]

FI System

The proposed solid phase must be combined with a sample injection system when it is necessary to determine Fe^{III} in samples available in only small volumes, such as human serum. The measurement device used is illustrated in Fig. 1.

The optimum operating parameters for FI measurements were the same as for the continuous system, except that the flow rate was slightly more critical, with 1.2 ml min^{-1} being the optimum. As expected, sample volume affected the response: fluorescence intensity decreased with increasing sample volume. Although the injection volume was varied depending on the amount of sample available, 1 ml was considered to be a good compromise between sample amount and sensitivity. A sample volume of 250–1000 μl was used.

The working conditions and the calibration graph are shown in Fig. 8. Classical FI peaks were not obtained because of the irreversibility of the system. In this instance, the calibration graph was obtained by plotting the decrease in fluorescence intensity *versus* Fe^{III} concentration and was linear from 20 to 900 ng ml^{-1} [Fig. 8(*b*)] with a correlation coefficient of 0.997. The detection limit was 20 ng ml^{-1} and the precision 4.5% for ten determinations of 500 ng ml^{-1} of Fe^{III} when 1 ml of sample was injected. The detection limit and precision were 70 ng ml^{-1} and 6%, respectively, when the injection volume was 250 μl. The interferences were the same as for the continuous system.

Applications

Continuous system

The optimized method was applied to the determination of Fe^{III} in Madrid tap water. Samples were diluted with the MES buffer to obtain the optimum pH for measurement. The slope of the decrease in fluorescence intensity was measured and the Fe^{III} concentration was obtained from the calibration graph.

The method was validated by using flame atomic absorption spectrometry (FAAS) as an alternative technique (Table 2). There were no significant differences between the results obtained by the two methods at the 95% confidence level.

FI system

Serum was analysed by the FI procedure described above. As a significant matrix effect was observed, the standard additions method was required. The results were validated by use of the standard ferrozine method and in all instances were

Table 2 Spectrofluorimetric determination of Fe^{III} using pyoverdin immobilized in sol–gel glass

Continuous system—		
Sample	Sol–gel glass*	FAAS*
Tap water 1	0.69 ± 0.03	0.71 ± 0.02
Tap water 2	1.10 ± 0.02	1.15 ± 0.03
FI system—		
Sample	Sol–gel glass*	Ferrozine
Serum 1	2.46 ± 0.05	2.23 ± 0.24
Serum 2	1.63 ± 0.07	1.54 ± 0.26

* Average of three measurements ± *s* (mg l^{-1}).

within the range of the certified values (Table 2). The precision of the proposed method is higher than that of the reference method.

Conclusions

The pyoverdin-doped sol-gel glass was stable for up to 12 months, significantly longer than for CPG, where the reagent was located on the surface. This stability was due to the protection afforded to the pigment by the sol–gel cavities.

The proposed solid phase allows the selective determination of Fe^{III}, and the effect of Fe^{II} is almost negligible. The method does not require the reduction of Fe^{III} to Fe^{II} as do most classical clinical methods. A further feature of the method is that it could be used in an optical sensor by coupling an optical fibre at the active phase.

The authors thank the CICYT for financial support under project AMB92-0092-C03-02 and M. Gormann for revising the manuscript.

References

1 Hench, L. L., and West, J. K., *Chem. Rev.*, 1990, **90**, 1, 33.
2 Livage, J., and Sanchez, C., *J. Non-Cryst. Solids*, 1992, **145**, 11.
3 Tillotson, T. M., and Hrubesh, L. W., *J. Non-Cryst. Solids*, 1992, **145**, 44.
4 Levy, D., and Avnir, D., *J. Phys. Chem.*, 1988, **92**, 4734.
5 Zusman, R., Rottman, C., Ottolenghi, M., and Avnir, D., *J. Non-Cryst. Solids*, 1990, **122**, 107.
6 Pulido, P., Barrero, J. M., Pérez-Conde, M. C., and Cámara, C., *Quím. Anal.*, 1993, **12**, 48.
7 Wolfbeis, O. S., Rodriguez, N. V., and Werner, T., *Mikrochim. Acta*, 1992, **108**, 133.
8 MacCraith, B. D., McDonagh, C. M., O'Keeffe, G., Keyes, E. T., Vos, J. G., O'Kelly, B., and McGilp, J. F., *Analyst*, 1993, **118**, 385.
9 Lev, O., Kuyavskaya, B. I., Gigozin, I., Ottolenghi, M., and Avnir, D., *Fresenius' J. Anal. Chem.*, 1992, **343**, 370.
10 Johnson, P., and Whateley, T. L., *J. Colloid Interface Sci.*, 1971, **37**, 557.
11 Braun, S., Rappoport, S., Zusman, R., Avnir, D., and Ottolenghi, M., *Mater. Lett.*, 1990, **10**, 1.
12 Tatsu, Y., Yamashita, K., Yamaguchi, M., Yamamura, S., Yamamoto, H., and Yoshikawa, S., *Chem. Lett.*, 1992, 1615.
13 Barrero, J. M., Moreno-Bondi, M. C., Pérez-Conde, M. C., and Cámara, C., *Talanta*, 1993, **40**, 1619.
14 Meyer, J. M., and Abdallah, M. A., *J. Gen. Microbiol.*, 1978, **107**, 319.
15 Pesce, A. J., and Kaplan, L. A., *Química Analítica: Métodos*, Panamericana, Buenos Aires, 1990.

Paper 4/03074E
Received May 23, 1994
Accepted July 29, 1994

Solvent Extraction of Acenaphthene from Dodecane into Aqueous β-Cyclodextrin Medium and Application to Synchronous Spectrofluorimetric Determination in Kerosene

Masaki Tachibana and Motohisa Furusawa

Faculty of Engineering, Yamanashi University, 4-3-11 Takeda, Kofu, Yamanashi 400, Japan

Acenaphthene can be selectively extracted from a dodecane phase into a water–dimethyl sulfoxide (20% v/v) medium containing β-cyclodextrin (10 mg cm^{-3}), potassium iodide (300 mg cm^{-3}) and sodium thiosulfate pentahydrate (15 mg cm^{-3}) with a shaking time of 3 min. The distribution ratio for the solvent extraction was 0.292 with a relative standard deviation of 8.3% at 20 ± 1 °C. The amount of acenaphthene extracted from 1 cm^3 of dodecane by three 8 cm^3 successive batch extractions was 97.3% in calculations and 95.1% in practice. The extraction behaviours of several typical two- and three-ring aromatic compounds were investigated under the same conditions. Selective extraction based on complexation with β-cyclodextrin was applied to the synchronous spectrofluorimetric determination of acenaphthene in commercially available kerosene.

Keywords: Solvent extraction; acenaphthene; synchronous fluorescence spectrometry; aqueous β-cyclodextrin medium; kerosene analysis

Introduction

Cyclodextrins (CDxs) are well known for their ability to form inclusion complexes with a variety of molecules on the basis of spatial fitting. Owing to their selective complexing ability, there has been considerable interest in their analytical utilization. We have recently reported[1] the usefulness of β-CDx for the selective detection of acenaphthene, a typical three-ring aromatic hydrocarbon, which is of great environmental and industrial concern because of its existence in fossil fuels. It was demonstrated that only the peaks of acenaphthene interacting with β-CDx can be measured with an appreciable intensity in an iodide-quenching state by synchronous spectrofluorimetry. Consequently, acenaphthene in mixtures of analogous three-ring compounds was selectively detected by using an aqueous dimethyl sulfoxide (DMSO) medium containing β-CDx and potassium iodide. This advantageous interaction between acenaphthene and β-CDx could be expected to be of further utility.

In this work, solvent extraction of acenaphthene was investigated with emphasis on application to synchronous spectrofluorimetric determination. The distribution of acenaphthene between dodecane and a water–DMSO (20% v/v) medium containing β-CDx, potassium iodide and sodium thiosulfate was studied, and then multiple batch extractions were performed for separative extraction into the aqueous β-CDx phase. A few studies on the use of CDxs for solvent extraction have been described.[2,3] Blyshak and co-workers[4,5] investigated CDx-modified solvent extraction for polycyclic aromatic hydrocarbons. They submitted that the extraction technique may be particularly useful for simplifying complex mixtures of organic materials such as oil samples or air sample adsorbates. However, no application to such real samples was reported.

Kerosene is a complicated mixture of petroleum hydrocarbons, chiefly of the alkane series having 10–16 carbon atoms per molecule, and generally used as a representative fuel in lamps and stoves. Various methods for hydrocarbon type analysis[6–8] and determination of total aromatics[9–11] in petroleum-distilled kerosene fractions have been developed in order to assess the quality. Despite the developments in such class characterization, the identification and determination of an individual three-ring compound contained as a trace constituent have always been a formidable analytical task.[12–15] The selective extraction studied in this work was actually applicable to the direct determination of acenaphthene in commercial kerosene fuels by synchronous spectrofluorimetry. Such information on the acenaphthene content in kerosene would be very useful not only for qualitative evaluation, but also as an indication for more detailed analysis with more sophisticated techniques. The proposed method provides a simple and cost-effective procedure without tedious sample pre-treatments or chromatographic separations.

Experimental

Reagents

Commercially available acenaphthene, other three-ring aromatic compounds and DMSO were purified as detailed previously.[1] Naphthalene derivatives (purchased from Tokyo Kasei Kogyo or Wako) were used as received, except naphthalene and 2-methyl- and 2,3-dimethylnaphthalene, which were purified by zone melting. β-Cyclodextrin and dodecane (Tokyo Kasei Kogyo) and potassium iodide and sodium thiosulfate pentahydrate (Kanto Chemical) were of guaranteed-reagent grade and used as received. Kerosene fuels were obtained directly from different petrol stations.

Apparatus

Synchronous spectrofluorimetric measurements were made using a Hitachi Model 650-40 spectrofluorimeter equipped with a Hitachi Model 056 recorder. A 150 W xenon arc lamp was used as the excitation source and 1.00 cm pathlength quartz cells as the measurement vessel. Both excitation and emission spectral bandpasses were always set at 2 nm. Batch extractions were carried out using 50 cm^3 separating funnels and a Irie TS shaker equipped with a holder for attachment of the three funnels.

Procedure for Determination of Acenaphthene in Kerosene

Transfer 1 cm³ of a kerosene sample into a 50 cm³ separating funnel. Add 8 cm³ of a water–DMSO (20% v/v) medium containing β-CDx (10 mg cm^{-3}), potassium iodide (300 mg cm^{-3}) and sodium thiosulfate pentahydrate (15 mg cm^{-3}) to the funnel. Shake the mixture for 3 min at room temperature and then allow the two immiscible liquid phases to separate. After completion of the separation, draw the bottom layer into a 25 cm³ calibrated flask. Successively perform the two additional extractions with a fresh 8 cm³ portion of the aqueous β-CDx medium in the same manner as above. Dilute the triplicate bottom layers collected in the flask to volume with the aqueous β-CDx medium. Measure the synchronous fluorescence spectrum of the resultant solution with a wavelength interval of 7 nm. Evaluate the relative intensity at a peak wavelength of 328 nm by the baseline method. Use a 0.400 μg cm^{-3} DMSO solution of acenaphthene as the standard for the evaluation of relative values. Determine the concentration of acenaphthene in kerosene from the calibration graph prepared similarly *via* triple batch extractions.

Results and Discussion

Synchronous Fluorescence Spectra in Aqueous β-CDx Medium

As detailed previously,[1] acenaphthene in an aqueous DMSO medium can be selectively detected by synchronous spectrofluorimetry in the presence of both β-CDx and potassium iodide. Fig. 1 shows the synchronous fluorescence spectrum ($\Delta\lambda$ = 7 nm) of acenaphthene in a water–DMSO (20% v/v) medium containing β-CDx (10 mg cm^{-3}), potassium iodide (300 mg cm^{-3}) and sodium thiosulfate pentahydrate (15 mg cm^{-3}). The additional presence of the thiosulfate helps to prevent interference with the absorption from coloured molecular iodine, which will be readily formed by oxidation of iodide ion. The fluorescence of acenaphthene in this aqueous β-CDx medium was stable for at least a few weeks when the solution was stored in a stoppered flask. It can be seen from Fig. 1 that acenaphthene exhibits characteristic double peaks at 322 and 328 nm under these measurement conditions. A UV absorption spectrum of the aqueous β-CDx medium is shown in Fig. 2. It is confirmed that there are no inner-filter effects in the wavelength range to be measured.

Distribution Between Aqueous β-CDx Medium and Dodecane

A mixture of the aqueous β-CDx medium as described above and a dodecane solution of acenaphthene was shaken in a separating funnel. After separation of the two immiscible phases, acenaphthene extracted into the aqueous β-CDx layer was characterized by measuring the relative synchronous fluorescence intensity at 322 nm with $\Delta\lambda$ = 7 nm by the baseline method. In addition, the batch extraction from the dodecane layer was successively repeated with equal amounts of the medium. The intensities of the aqueous β-CDx layers thus obtained were also measured in the same manner. By using 5 cm³ of the aqueous β-CDx medium, three types of the successive batch extractions were performed for dodecane volumes of 5, 2 and 1 cm³. The temperature of the two solvents used was kept constant at 19–21 °C throughout the experiments. The results of these experiments are shown in Fig. 3, which demonstrates that this medium should be useful for the quantitative extraction of acenaphthene from dodecane.

The proportion of DMSO in the aqueous β-CDx medium had a significant influence on the extraction. Acenaphthene was hardly extracted into a DMSO-free aqueous β-CDx solution, whereas with 40% v/v DMSO mixture its extraction efficiency increased appreciably compared with the result with the above 20% v/v solution. A water–DMSO mixture of 20% v/v was nevertheless used in our studies, because the inclusion effect of β-CDx and the separation efficiency of acenaphthene

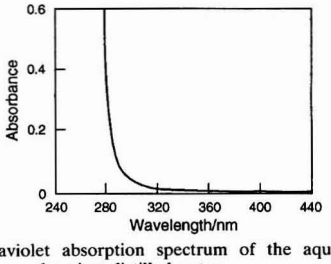

Fig. 2 Ultraviolet absorption spectrum of the aqueous β-CDx medium, measured against distilled water.

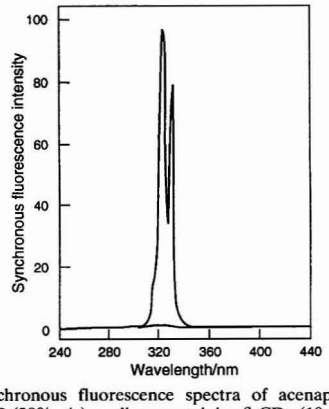

Fig. 1 Synchronous fluorescence spectra of acenaphthene in a water–DMSO (20% v/v) medium containing β-CDx (10 mg cm^{-3}), KI (300 mg cm^{-3}), and $Na_2S_2O_3 \cdot 5H_2O$ (15 mg cm^{-3}), and only the medium, measured with a wavelength interval ($\Delta\lambda$) of 7 nm. The wavelength corresponds to that of the emission monochromator, and the spectra are not corrected.

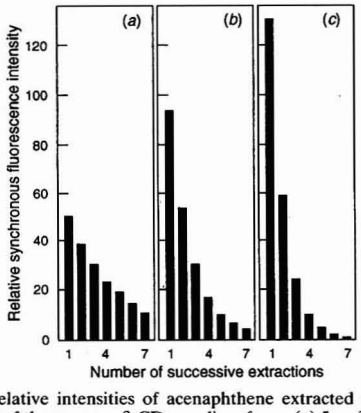

Fig. 3 Relative intensities of acenaphthene extracted successively into 5 cm³ of the aqueous β-CDx medium from: (*a*) 5 cm³, (*b*) 2 cm³, and (*c*) 1 cm³ of dodecane, respectively. Acenaphthene, 10.2 μg; temperature, 19–21 °C; shaking time, 5 min; and measurement conditions: at 322 nm peak with $\Delta\lambda$ = 7 nm by the baseline method. The intensity of a DMSO solution of acenaphthene (1.00 μg cm^{-3}) was used as the standard for the evaluation of relative values.

from foreign compounds was considered rather than the extraction efficiency.

Distribution Ratio for Extraction

Assuming that the inclusion complex of acenaphthene with β-CDx is essentially insoluble in non-polar hydrocarbons, the distribution ratio, D, for the extraction of acenaphthene from dodecane into the aqueous β-CDx medium is given by

$$D = ([AN]_a + [AN\text{–}CDx]_a)/[AN]_d \quad (1)$$

where [AN] and [AN–CDx] are the concentrations of acenaphthene and acenaphthene–β-CDx (1:1) complex, respectively, and the two subscripts (a and d) represent the aqueous β-CDx and dodecane phases, respectively. In this work, as β-CDx should be present in a large enough amount to shift the inclusion equilibrium to its complex formation (*i.e.*, $[AN]_a \ll [AN\text{–}CDx]_a$), eqn. (1) can be simplified to

$$D = [AN\text{–}CDx]_a/[AN]_d \quad (2)$$

In these equations, terms for the proportion of the acenaphthene that exists as 1:2, 2:1 and more complicated complexes are neglected because it forms exclusively the 1:1 complex with β-CDx.[16–18] When the extraction of a certain amount (AN_0 nmol) of acenaphthene is performed with different volumes of the aqueous β-CDx and the dodecane phases (V_a and V_d cm^3, respectively), the concentration (mmol m^{-3}) of acenaphthene remaining in the dodecane phase can be expressed as

$$[AN]_d = (AN_0 - [AN\text{–}CDx]_a V_a)/V_d \quad (3)$$

Substitution of eqn. (3) into eqn. (2) and rearrangement yields

$$D = \frac{[AN\text{–}CDx]_a V_d}{AN_0 - [AN\text{–}CDx]_a V_a} \quad (4)$$

The value of D can consequently be obtained by measuring only the concentration (mmol m^{-3}) of the fluorescent 1:1 complex present in the aqueous β-CDx layer after a single extraction. Table 1 gives the values calculated by substituting experimental data in eqn. (4). The mean of the 16 results was 0.292 with a relative standard deviation (s_r) of 8.3%.

Percentage Extracted in Calculations

For analytical purposes, the percentage extracted may be more accessible than the distribution ratio. If n separate extractions are performed with equal volumes of the aqueous β-CDx medium, then the percentage of acenaphthene extracted into the aqueous β-CDx layer by the nth extraction, E_n, is given by

$$E_n = \frac{AN_{n-1} - AN_n}{AN_0} \times 100 \quad (5)$$

where AN_0, AN_{n-1} and AN_n are the initial amount of acenaphthene and the amounts remaining in the dodecane layer after $n-1$ and n extractions, respectively. According to the basic theory for multiple batch extractions, AN_n is related to the distribution ratio and the volumes of the two layers by

$$AN_n = AN_0\left(\frac{V_d}{DV_a + V_d}\right)^n \quad (6)$$

and hence AN_{n-1} can be also derived as

$$AN_{n-1} = AN_0\left(\frac{V_d}{DV_a + V_d}\right)^{n-1} \quad (7)$$

By using eqns. (6) and (7), therefore, $AN_{n-1} - AN_n$ can be calculated and rearrangement gives

$$AN_{n-1} - AN_n = \frac{AN_0 D V_a V_d{}^{n-1}}{(DV_a + V_d)^n} \quad (8)$$

Substitution of eqn. (8) into eqn. (5) gives finally

$$E_n = \frac{100\, DV_a V_d{}^{n-1}}{(DV_a + V_d)^n} \quad (9)$$

Table 2 gives the results of calculations for the percentage extracted, based on eqn. (9) in which $D = 0.292$ and $V_d = 1$ cm^3 were used. Four different volumes of aqueous β-CDx medium (V_a = 24, 12, 8 and 6 cm^3) were used as examples. It can be seen from Table 2 that three successive 8 cm^3 extractions are necessary to separate acenaphthene in a total volume of 24 cm^3 of the medium almost quantitatively.

Effect of Shaking Time

A mixture of the aqueous β-CDx medium (8 cm^3) and dodecane (1 cm^3) containing acenaphthene (10.2 μg) was shaken once for various time periods from 0.5 to 5 min at 20 ± 1 °C. Fig. 4 shows the relative synchronous fluorescence intensities (at 322 nm with $\Delta\lambda$ = 7 nm) of the aqueous β-CDx layers after separation. As can be seen the intensities are almost unchanged with shaking for more than 1.5 min. It is therefore recommended that in rapid batch extractions the mixture of the two immiscible solvents be shaken for 3 min.

Table 1 Distribution ratio for solvent extraction of acenaphthene from dodecane into the aqueous β-CDx medium. Initial amount of acenaphthene (AN_0) = 66.1 nmol and temperature = 19–21 °C

Volumes of the two layers/cm^3		Concentration of acenaphthene–β-CDx complex found in the aqueous medium,	
Dodecane, V_d	Aqueous medium, V_a	$[AN\text{–}CDx]_a$/mmol m^{-3}	Distribution ratio, D*
1.00	2.00	12.2, 12.4	0.293, 0.300
2.00	2.00	6.68, 7.72	0.253, 0.305
5.00	2.00	2.99, 3.92	0.249, 0.336
1.00	5.00	7.86, 8.01	0.293, 0.307
2.00	5.00	5.69, 5.78	0.302, 0.311
5.00	5.00	3.02, 3.10	0.296, 0.306
1.00	10.0	4.84, 4.93	0.273, 0.293
2.00	10.0	3.67, 3.99	0.250, 0.305
			Mean: 0.292
			s_r: 8.3%

* These values were calculated from eqn. (4).

Table 2 Percentage extracted, calculated for the multiple batch extractions of acenaphthene from 1 cm^3 of dodecane into four different volumes (V_a) of the aqueous β-CDx medium

Multiple batch extraction	Extraction* (%)			
	24 cm^3	12 cm^3	8 cm^3	6 cm^3
1st	87.5	77.8	70.0	63.7
2nd	10.9/98.4	17.3/95.1	21.0/91.0	23.1/86.8
3rd	1.4/99.8	3.8/98.9	6.3/97.3	8.4/95.2
4th	0.2/100.0	0.9/99.8	1.9/99.2	3.1/98.3
5th	0.0	0.2/100.0	0.6/99.8	1.1/99.4
6th	0.0	0.0	0.2/100.0	0.4/99.8
7th	0.0	0.0	0.1/100.1	0.1/99.9

* For these calculations, $E_n = 29.2V_a/(0.292V_a + 1)^n$ was used.

Application to Synchronous Spectrofluorimetric Determination of Acenaphthene

Recovery in three successive extractions

The accurate recovery of acenaphthene and the temperature effect on the recovery were checked in practice according to the triple extraction scheme described above. The results obtained at temperatures of 15, 20 and 25 °C are summarized in Table 3. It can be seen that the recovery decreases with increase in temperature. This decrease was predictable to some extent from the dependence of the inclusion formation constants of CDxs on temperature.[19,20] The variation of the recovery is negligible, however, at temperatures between 15 and 20 °C, and not very serious even at 20–25 °C if the temperature is kept constant during extractions. Table 3 also indicates that 95.1% of acenaphthene can be recovered at 20 °C, and that it is approximately 2% lower than the 97.3% calculated from the percentage extracted. The slight difference between the experimental and calculated values may be due to the loss of acenaphthene resulting from triple extraction processes. Such an incomplete recovery of acenaphthene, in either event, can be readily corrected for by using a calibration graph prepared in a similar manner as for samples.

Effect of two- and three-ring aromatic compounds

The extraction behaviour and spectral effect of analogous two- and three-ring compounds were investigated by measuring the spectra of their aqueous β-CDx solutions prepared under the same conditions as for acenaphthene. Table 4 gives the resulting spectral data, including fluorescence signal range, peak wavelength and relative peak intensity, for the 16 different compounds and acenaphthene for comparison. The amounts of the analogues used were mostly 100–190 times higher than that of acenaphthene, but those of carbazole and anthracene were 11 and 15 times higher, respectively, because of their poor solubility in dodecane. It can be seen from Table 4 that the most intense peak and the next one correspond to carbazole and fluorene, respectively. As their peaks at 343 and 309 nm are approximately 15 nm distant from the double peaks of acenaphthene, the spectral interference is of little interest. On the other hand, a few naphthalene derivatives such as 1-methyl-, 1,2-dimethyl- and 1,5-dimethylnaphthalene fluoresce recognizably with doublets similar to that of acenaphthene. However, although large amounts of these naphthalenes have a considerable effect, their influence was negligible in amounts smaller than 20 μg.

The aqueous β-CDx solutions used for these spectral measurements, except for carbazole, hardly showed UV absorption in the wavelength range above 320 nm. Therefore, the absorption effect of the foreign compounds on the determination of acenaphthene was insignificant in this work.

Direct determination of acenaphthene in kerosene

Commercially available kerosene is a complex mixture of chemicals containing hundreds of various aliphatic and aromatic compounds. Two different synchronous fluorescence spectra ($\Delta\lambda$ = 7 nm) of a typical kerosene sample are shown in Fig. 5. One spectrum was obtained from neat

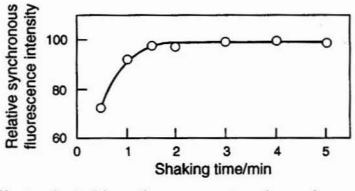

Fig. 4 Effect of shaking time on extraction of acenaphthene. Acenaphthene, 10.2 μg; dodecane; 1 cm³; aqueous β-CDx medium, 8 cm³; temperature, 19–21 °C; and measurement conditions: at 322 nm peak with $\Delta\lambda$ = 7 nm by the baseline method, using the acenaphthene DMSO solution as the standard.

Table 3 Recovery of acenaphthene extracted by three 8 cm³ portions of the aqueous β-CDx medium from 1 cm³ of dodecane

Temperature/ °C	Added to dodecane/μg	Found in the aqueous β-CDx medium/μg	Recovery (%)
20	2.03	1.87, 1.98	92.1, 97.5
	2.03	1.95, 1.95	96.1, 96.1
	10.2	9.58, 9.76	93.9, 95.7
	10.2	9.95, 9.75	97.5, 95.6
	50.8	47.4, 48.7	93.3, 95.9
	50.8	47.1, 48.0	92.7, 94.5
			Mean: 95.1
			s_r: 1.9%
15	2.03	2.00, 1.95	98.5, 96.1
	10.2	9.72, 9.73	95.3, 95.4
	50.8	46.9, 49.4	92.3, 97.2
			Mean: 95.8
25	2.03	1.89, 1.87	93.1, 92.1
	10.2	8.76, 9.20	85.9, 90.2
	50.8	45.3, 45.5	89.2, 89.6
			Mean: 90.0

Table 4 Synchronous spectrofluorimetric data for the aqueous β-CDx solutions (25 cm³) prepared finally after three successive extractions (8 cm³) of different two- and three-ring aromatic compounds from dodecane (1 cm³)

Compound	Amount added to dodecane/mg	Synchronous fluorescence signal* Spectral range/nm	Peak wavelength†/nm
Acenaphthene	0.010	305–340	322 (108.2), 328 (92.5)
Dibenzofuran	1.14	290–320	304 (33.7)
Fluorene	1.10	295–325	309 (138.0)
Dibenzothiophene	1.16	320–340	332 (10.0)
Carbazole	0.11	325–360	343 (180.2)
Phenanthrene	1.07	345–360	348 (8.8), 356 (6.6)
Anthracene	0.15	375–390	383 (5.9)
Naphthalene	1.07	Not detected	
1-Methylnaphthalene	1.27	300–335	321 (37.9), 325 (34.2)
2-Methylnaphthalene	1.10	315–330	321 (1.3), 327 (2.1)
1-Ethylnaphthalene	1.22	310–330	323 (2.2)
2-Ethylnaphthalene	1.65	Not detected	
1,2-Dimethylnaphthalene	1.86	315–340	323 (63.7), 330 (99.4)
1,3-Dimethylnaphthalene	1.61	315–335	323 (1.5), 329 (1.8)
1,5-Dimethylnaphthalene	1.08	305–335	321 (20.2), 328 (18.6)
2,3-Dimethylnaphthalene	1.01	300–320	311 (1.3)
2,7-Dimethylnaphthalene	1.05	Not detected	

* All spectra were measured with $\Delta\lambda$ = 7 nm, uncorrected.

† Relative peak intensities obtained by the baseline method are given in parentheses; the intensity (at 322 nm) of an acenaphthene standard solution (0.40 μg cm⁻³ in DMSO) was taken as 100.0 for the evaluation of relative values.

kerosene and another from a 1000-fold dilute solution in dodecane. Fig. 5 demonstrates that it is impossible to detect and/or determine the small amount of acenaphthene in the kerosene even with this highly selective spectrofluorimetric method.

The proposed separative extraction and the following synchronous technique were applied to the determination of acenaphthene in such kerosene fuels without any pre-treatment. Because the commercial fuels usually contain a few hundred μg cm^{-3} of 1-methylnaphthalene, a less sensitive peak wavelength of 328 nm was preferred for the synchronous fluorimetric measurements of acenaphthene. Interference from the 1-methylnaphthalene in kerosene was consequently negligible up to 200 μg cm^{-3}. The calibration graph for acenaphthene was prepared by treating 1 cm^3 of its dodecane solutions (0–10 μg cm^{-3}) according to the determination procedure. The graph thus obtained was linear over this concentration range. The determination limit of acenaphthene was approximately 0.5 μg under the conditions adopted.

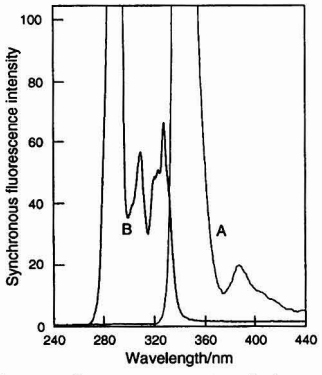

Fig. 5 Synchronous fluorescence spectra of: A, a neat kerosene sample; and B the dilute solution (approximately 0.1% in dodecane) measured with $\Delta\lambda$ = 7 nm. The wavelength corresponds to that of the emission monochromator, and the spectra are not corrected.

Table 5 Determination of acenaphthene in four different kerosene samples

Sample	Added/ μg cm^{-3}	Relative synchronous fluorescence intensity (arbitrary units)	Found/ μg cm^{-3}
A	0.00	68.5	6.97
B	0.00	66.1	6.72
C	0.00	41.0	4.17
D	0.00	49.3*	5.01
	0.53	55.6†	5.65
	1.06	59.3†	6.03
	2.11	67.4†	6.85
	4.23	88.4†	8.99

*,† Means of four and two measurements, respectively.

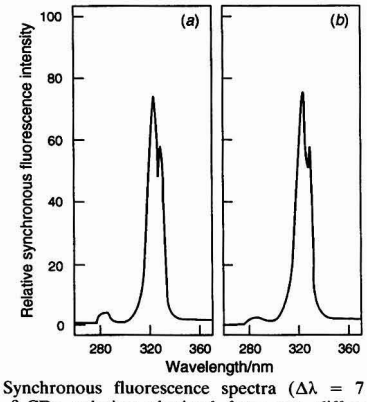

Fig. 6 Synchronous fluorescence spectra ($\Delta\lambda$ = 7 nm) of the aqueous β-CDx solution obtained from two different kerosene samples according to the determination procedure. (*a*) and (*b*): commercially available kerosene, samples A and B given in Table 5, respectively. The wavelength corresponds to that of the emission monochromator, and the spectra are not corrected.

Table 5 gives the results for four different kerosene samples purchased from various manufacturers and also for kerosene spiked with acenaphthene at concentrations in the range 0.53–4.23 μg cm^{-3}. The results for the spiked samples suggest the presence of interfering constituents that affect the extraction efficiency of acenaphthene from kerosene. The unexpected effect of such constituents is not serious, however, because the relative errors in determining acenaphthene in the spiked kerosene were within 4%. Fig. 6 shows the synchronous fluorescence spectra obtained from the two unspiked samples. The peak wavelengths of the two spectra agree well with those of the spectrum of pure acenaphthene shown in Fig. 1, although the characteristic doublet structure of the peaks is indistinct. All aqueous β-CDx solutions used for these spectrofluorimetric measurements had little UV absorption in the wavelength range above 320 nm. From these experiments, therefore, it is concluded that the proposed extraction method is applicable to the direct determination of acenaphthene in kerosene fuels.

References

1 Tachibana, M., and Furusawa, M., *Analyst*, 1994, **119**, 1081.
2 Nakai, Y., Yamamoto, K., Terada, K., and Horibe, H., *Chem. Pharm., Bull.*, 1982, **30**, 1796.
3 Matsunaga, K., Imanaka, M., Ishida, T., and Oda, T., *Anal. Chem.*, 1984, **56**, 1980.
4 Blyshak, L. A., Rossi, T. M., Patonay, G., and Warner, I. M., *Anal. Chem.*, 1988, **60**, 2127.
5 Blyshak, L. A., Patonay, G., and Warner, I. M., *ACS Symp. Ser.*, 1989, **383**, 167.
6 Al-Thamir, W. K., *J. Chromatogr. Sci.*, 1988, **26**, 345.
7 Hayes, P. C., Jr., and Anderson, S. D., *J. Chromatogr.*, 1988, **437**, 365.
8 Kosal, N., Bhairi, A., and Ali, M. A., *Fuel*, 1990, **69**, 1012.
9 Tameesh, A. H. H., Hanna, M. H., and Komers, R., *J. Chromatogr.*, 1985, **328**, 207.
10 Mohammed, A.-H. A.-K., and Hankish, K., *Analyst*, 1985, **110**, 1477.
11 Ramaswamy, V., Kothiyal, V., Singh, I. D., and Krishna, R., *J. Chem. Technol. Biotechnol.*, 1988, **41**, 255.
12 Shiomi, K., *Anal. Sci.*, 1985, **1**, 327.
13 Dixit, L., Ram, S., Gupta, R. B., Chandola, H. C., and Kumar, P., *Analyst*, 1986, **111**, 101.
14 Davies, I. L., Bartle, K. D., Andrews, G. E., and Williams, P. T., *J. Chromatogr. Sci.*, 1988, **26**, 125.
15 Bagheri, H., and Creaser, C. S., *Analyst*, 1988, **113**, 1175.
16 Hamai, S., *J. Am. Chem. Soc.*, 1989, **111**, 3954.
17 Mohseni, R. M., and Hurtubise, R. J., *J. Chromatogr.*, 1990, **499**, 395.
18 Muñoz de la Peña, A., Durán-Merás, I., Salinas, F., Warner, I. M., and Nodou, T. T., *Anal. Chim. Acta*, 1991, **255**, 351.
19 Blyshak, L. A., Dodson, K. Y., Patonay, G., Warner, I. M., and May, W. E., *Anal. Chem.*, 1989, **61**, 955.
20 Blyshak, L. A., Warner, I. M., and Patonay, G., *Anal. Chim. Acta*, 1990, **232**, 239.

Paper 4/03449J
Received June 7, 1994
Accepted August 9, 1994

Determination of Three Aspirin Metabolites in Human Urine by Derivative Synchronous Spectrofluorimetry

Patricia Damiani, María Élida Ribone, Gabriela Ibáñez and Alejandro C. Olivieri*

Departamento de Química Analítica, Facultad de Ciencias Bioquímicas y Farmacéuticas, Universidad Nacional de Rosario, Suipacha 531, Rosario (2000), Argentina

The direct and simultaneous determination of three aspirin metabolites present in human urine (salicylic acid, salicyluric acid and gentisic acid) is described. The method involves the measurement of synchronous fluorescence spectra ($\Delta\lambda$ = 100 nm) of untreated urine samples at a single pH (borate buffer giving pH 9.0). The combination of first- and second-derivative spectra and the zero-crossing technique allows calibration plots for the three metabolites to be obtained that are linear in the range 0.02–0.2 ppm. The solution of a system of three simultaneous linear equations is discussed. Better results are obtained by transferring the second-derivative spectra in the range λ_{exc} = 325–375 nm to a microcomputer and performing a least-squares fit of the sample to a combination of spectra of three standard solutions. This choice of wavelengths makes it unnecessary to eliminate normal fluorescent urine components.

Keywords: Aspirin metabolites; salicylic acid; salicyluric acid; gentisic acid; derivative synchronous spectrofluorimetry

Introduction

The determination of the metabolites of aspirin in human biological fluids such as blood serum and plasma, synovial fluid and urine has attracted attention.[1–14] Of the several techniques that are available for their determination, namely chromatography,[1–3] spectrophotometry[4–6] and spectrofluorimetry,[7–15] the last has been preferred owing to its simplicity, sensitivity and specificity. The three main metabolites of aspirin present in human urine are salicylic acid (SA), salicyluric acid (SU) and gentisic acid (GE). The simultaneous determination of the first two has been carried out by zero-crossing first-derivative synchronous fluorescence spectrometry ($\Delta\lambda$ = 90 nm) of urine samples that were previously extracted in acidic media and re-extracted with NaOH.[12] The latter procedure was necessary in order to remove normal urine components that are fluorescent at wavelengths near those corresponding to the emission of SA, SU and GE. However, the direct determination of SA and SU in unextracted, alkalinized urine is also possible by a careful selection of wavelengths in both first- and second-derivative synchronous fluorescence spectrometry (with $\Delta\lambda$ = 90 nm).[14,15] The determination of all three metabolites has been described, requiring extraction/re-extraction treatment of the urine sample followed by measurement of first-derivative synchronous fluorescence spectra at two different pH values on separate samples.[12] The pH values are selected in such a way that at one of them SU does not fluoresce, whereas at the other one the emission of GE is negligible.

In this paper, we propose a method by which all three metabolites can be determined directly and simultaneously in an untreated urine sample and at a single pH. It involves the adjustment of the pH by means of a borate buffer (pH 9.0) where SA, SU and GE are all fluorescent, the selection of the optimum $\Delta\lambda$ for the best spectral differentiation of these species and the combination of first- and second-derivative synchronous fluorescence spectrometry. Two different techniques are discussed: (1) solution of a set of three simultaneous linear equations by applying the zero-crossing technique in order to decrease the number of calibration plots to be constructed and (2) least-squares fitting of the sample second-derivative synchronous fluorescence spectra to those of three standard solutions of the studied metabolites. As all measurements are restricted to the region λ_{exc} = 325–375 nm, where the fluorescence of normal urine components has considerably decayed, the method can be applied directly to untreated urine samples.

Experimental

Apparatus

All fluorescence measurements were carried out on a JASCO FP 770 spectrofluorimeter equipped with a 150 W xenon lamp. Synchronous fluorescence spectra were recorded by scanning both monochromators with a constant difference of 100 nm between excitation and emission. The usual experimental parameters were scan speed 200 mm min^{-1}, response time 0.025 min and bandwidth 5 nm. First- and second-derivative spectra were then obtained.

Reagents

Stock standard solutions of salicylic acid (Merck) (10.0 mg l^{-1}), salicyluric acid (Aldrich) (10.0 mg l^{-1}) and gentisic acid (Aldrich) (10 mg l^{-1}) in distilled water were prepared. Dilutions of these stock standard solutions (1 + 9) were prepared daily.

Procedure for Ternary Mixtures

From each stock standard solution a dilution from 1 ml to 10 ml was prepared. In order to prepare working standard solutions containing mixtures of the three standard metabolites, appropriate volumes were taken from these latter dilutions and placed in 50 ml calibrated flasks. Borate buffer of pH 9.0 (5 ml) was then added and the mixture was diluted to volume with distilled water. In this way the range of concentrations of each standard was between 0.01 and 0.10 ppm.

* To whom correspondence should be addressed.

Results and Discussion

Fig. 1(*a*) and (*b*) show the first- and second-derivative synchronous fluorescence spectra (using $\Delta\lambda$ = 100 nm) of aqueous solutions containing 0.100 ppm of each of the three metabolites and a representative salicylate-free human urine (after a 1 + 499 dilution) at the pH given by borate buffer (pH 9.0). As can be seen, normal urine components show a fluorescent band which considerably decays beyond λ_{exc} = 325 nm. Hence, if all fluorescence measurements are restricted to a range $\lambda_{exc} > 325$ nm, the extraction/re-extraction procedure (or other alternatives) in order to remove these components is not necessary, and urine samples can be studied directly after dilution and pH adjustment. Further, Fig. 1(*a*) and (*b*) show that the fluorescence spectra of SU and GE are very similar. As the appearance of these spectra depends on $\Delta\lambda$, their simultaneous determination (together with SA) requires a careful selection of this parameter. After recording several spectra using $\Delta\lambda$ values in the range 70–130 nm, it was found that $\Delta\lambda$ = 100 nm provides the best differentiation between the spectra of SU and GE.

In principle, the simultaneous determination of the contents of the three metabolites SA, SU and GE requires the solution of the following set of simultaneous equations:

$$\begin{aligned}[SA]m^{1,2}{}_{\lambda1}(SA) + [SU]m^{1,2}{}_{\lambda1}(SU) + [GE]m^{1,2}{}_{\lambda1}(GE) &= I^{1,2}{}_{\lambda1}\\ [SA]m^{1,2}{}_{\lambda2}(SA) + [SU]m^{1,2}{}_{\lambda2}(SU) + [GE]m^{1,2}{}_{\lambda2}(GE) &= I^{1,2}{}_{\lambda2}\\ [SA]m^{1,2}{}_{\lambda3}(SA) + [SU]m^{1,2}{}_{\lambda3}(SU) + [GE]m^{1,2}{}_{\lambda3}(GE) &= I^{1,2}{}_{\lambda3}\end{aligned} \quad (1)$$

where [X] (X = SA, SU, GE) denotes the concentration of SA, SU and GE and $m^{1,2}{}_{\lambda1,2,3}(X)$ are the slopes of the corresponding calibration graphs of the first- or second-derivative intensity measured at $\lambda_{exc} = \lambda_1$, λ_2 and λ_3 and $I^{1,2}{}_{\lambda1,2,3}$, are the corresponding intensities measured for the unknown. This would require obtaining nine calibration graphs. However, if the wavelengths are selected according to the zero-crossing technique [see Fig. 1(*a*) and (*b*)], eqns. (1) would be considerably simplified. Consideration of the spectra shown in Fig. 1(*a*) and (*b*) in the range $\lambda_{exc} > 325$ nm shows two appropriate zero-crossing points in the second-derivative spectra [Fig. 1(*b*)]: λ_{exc} = 345 nm, where the intensity corresponding to GE is zero, and λ_{exc} = 350 nm, where that from SA has considerably decayed. A further point of interest is λ_{exc} = 325 nm in the first-derivative mode [Fig. 1(*a*)], where the intensity from SU is zero. Hence eqns. (1) reduce to

$$\begin{aligned}[SA]m^{1}{}_{325}(SA) + [GE]m^{1}{}_{325}(GE) &= I^{1}{}_{325}\\ [SA]m^{2}{}_{345}(SA) + [SU]m^{2}{}_{345}(SU) &= I^{2}{}_{345}\\ [SU]m^{2}{}_{350}(SU) + [GE]m^{2}{}_{350}(GE) &= I^{2}{}_{350}\end{aligned} \quad (2)$$

which requires only six calibration graphs (in fact, as the first- and second-derivative intensities are directly determined by the spectrofluorimeter, only three sets of standard solutions are required). These plots were found to be linear in the range 0.02–0.2 ppm for all three metabolites. The limit of determination (0.02 ppm) is significantly lower than that obtained by using chromatographic methods.[1,3] The corresponding results are summarized in Table 1. An alternative procedure involves the use of standard solutions of SA, SU and GE (0.100 ppm in each instance), in which case eqns. (2) become

$$\begin{aligned}xI^{1}{}_{325}(\text{std. SA}) + zI^{1}{}_{325}(\text{std. GE}) &= I^{1}{}_{325}\\ xI^{2}{}_{345}(\text{std. SA}) + yI^{2}{}_{345}(\text{std. SU}) &= I^{2}{}_{345}\\ yI^{2}{}_{350}(\text{std. SU}) + zI^{2}{}_{350}(\text{std. GE}) &= I^{2}{}_{350}\end{aligned} \quad (3)$$

where $I^{1,2}{}_{\lambda}$(std. X) are the first- or second-derivatives intensities of each standard at the indicated excitation wavelengths, and x, y and z are the ratios [X]/[std. X]. Results for representative ternary mixtures of SA, SU and GE are given in Table 2, where both the precision [relative standard deviation (s_r), %] and accuracy (percentage recovery) of the method can be appreciated. Note that all fluorescence data correspond to the spectral range $\lambda_{exc} > 325$ nm, and therefore that the natural fluorescent components of human urine do not cause interference.

An alternative procedure that we also found to be useful is to transfer the spectral data from the spectrofluorimeter to a microcomputer, and to perform a least-squares fitting of the experimental sample spectrum to a weighted sum of the spectra of the standards. We selected the second derivative of the synchronous fluorescence spectra, as it displays more spectral features that would allow a better differentiation among the three components of the sample. Also, only the spectral range λ_{exc} = 325–375 nm was considered for the fitting procedure, in order to avoid interference from urine components. Least-squares fitting over the latter range was therefore performed with the equation

$$I^{2}{}_{\lambda}(\text{sample}) = xI^{2}{}_{\lambda}(\text{std. SA}) + yI^{2}{}_{\lambda}(\text{std. SU}) + zI^{2}{}_{\lambda}(\text{std. GE}) \quad (4)$$

where x, y and z have been defined before. The fitting was

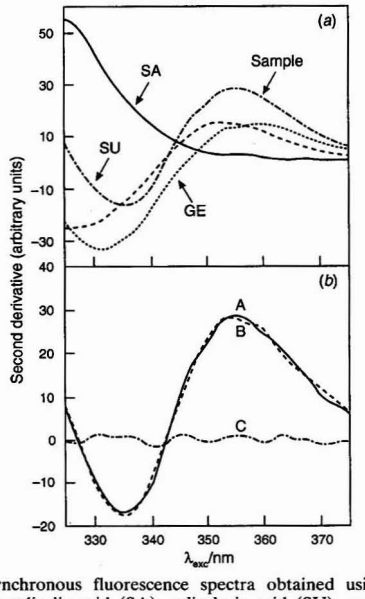

Fig. 1 Synchronous fluorescence spectra obtained using $\Delta\lambda$ = 100 nm for salicylic acid (SA), salicyluric acid (SU), gentisic acid (GE) and human urine, as indicated. In all instances the pH was adjusted to 9.0. Concentration of the three standard metabolites, 0.100 ppm: (*a*), first-derivative mode, (*b*), and second-derivative mode.

Table 1 Results for the calibration graphs after measuring first- and second-derivative synchronous fluorescence spectral intensities at different wavelengths

Compound	Parameter measured	Slope*	Intercept*	Correlation coefficient
SA	$I^{2}{}_{345}$	0.012(3)	$2(2) \times 10^{-4}$	0.978
	$I^{2}{}_{345}$	0.7(1)	$3(5) \times 10^{-3}$	0.990
SU	$I^{2}{}_{345}$	0.021(3)	$1(2) \times 10^{-4}$	0.995
	$I^{2}{}_{350}$	0.060(7)	$-7(4) \times 10^{-4}$	0.997
GE	$I^{1}{}_{325}$	0.028(7)	$-3(4) \times 10^{-4}$	0.969
	$I^{2}{}_{350}$	0.063(7)	$-2(4) \times 10^{-4}$	0.996

* Values in parentheses are standard deviations (n = 3).

Table 2 Recoveries from ternary mixtures of SA, SU and GE using both methods described in the text

SA/SU/GE taken (ppm)	SA/SU/GE found (ppm)* Eqns. (2)	Eqns. (3)†
0.100/0.100/0.100	0.110(2)/0.082(1)/0.121(1)	0.095(1)/0.091(3)/0.092(3)
	110% 82% 121%	95% 91% 92%
0.100/0.100/0.050	0.105(2)/0.096(1)/0.050(2)	0.094(1)/0.086(4)/0.045(3)
	105% 96% 100%	94% 86% 90%
0.050/0.100/0.050	0.057(1)/0.084(1)/0.049(2)	0.044(1)/0.078(3)/0.044(3)
	114% 84% 98%	88% 78% 88%
0.050/0.050/0.100	0.047(1)/0.054(2)/0.092(1)	0.049(1)/0.040(3)/0.110(2)
	94% 108% 92%	98% 80% 110%
0.020/0.020/0.050	0.020(1)/0.024(2)/0.049(1)	0.022(1)/0.022(1)/0.052(2)
	100% 120% 99%	108% 109% 104%

* Values in parentheses are s_r corresponding to the average of three determinations. Percentage values are recoveries.
† The s_r values given were calculated from the standard deviation for the fitting procedure as given by a sigma plot.

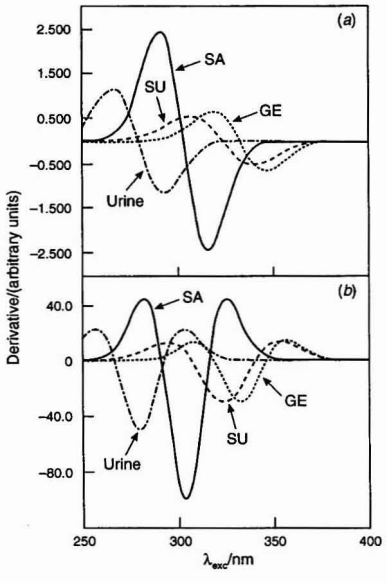

Fig. 2 (*a*), Second-derivative synchronous fluorescence spectra of salicylic acid (SA, 0.100 ppm), salicyluric acid (SU, 0.100 ppm), gentisic acid (GE, 0.100 ppm), and an aqueous solution containing 0.100 ppm of each of the three metabolites. (*b*) Superposition of the sample spectrum (A) and the computer-calculated least-squares plot (B) according to eqns. (3) ($x = 0.95$, $y = 0.91$, $z = 0.92$), together with the fitting residuals (C).

done by transferring the data in ASCII format to a microcomputer and processing them with SigmaPlot 5.0. The corresponding results for the ternary mixtures referred to above are given in Table 2. As can be seen, both the relative standard deviations and recoveries are also satisfactory with this method. Fig. 2 shows the second-derivative spectrum of a selected ternary mixture, together with the computer least-squares fitting solution (and residuals). As can be seen, the agreement between the calculated and experimental values is good.

We are currently applying the methods described to a pharmacological study of the distribution of the metabolites of aspirin. Although they are in principle applicable to cases of aspirin overdose in patients, the latter are better handled through the rapid determination of blood levels of salicylate, as reported previously.[14] Other drugs that may be used in combination with aspirin, such as paracetamol, do not interfere. Fluorescence methods have not been reported for the determination of anti-inflammatory drugs used in the treatment of arthritis rheumatoidea.[16] We are currently pursuing this topic, to investigate both the possibility of interferences and the development of methods of determination based on the emission of fluorescence. Finally, it should be noted that acetylsalicylic acid itself is fluorescent and can also be determined, as reported,[17] but it is not present as such in human urine.

In conclusion, a method has been described for the direct and simultaneous determination of the aspirin metabolites salicylic acid, salicyluric acid and gentisic acid in human urine. This confirms the utility of fluorescence measurements combined with synchronous scanning techniques and derivative spectra.

References

1 Bekerski, I., Boxembaum, H. G., Whitson, M. H., Publisi, C. V., Pocelinko, R., and Kaplan, S. A., *Anal. Lett.*, 1977, **10**, 539.
2 Amick, E. N., and Mason, W. D., *Anal. Lett.*, 1979, **12**, 629.
3 Moore, C. M., and Tebbett, I. R., *Forensic Sci. Int.*, 1987, **34**, 155.
4 Trinder, P., *Biochem. J.*, 1954, **57**, 301.
5 Truitt, E. B., Morgan, A. M., and Little, J. M., *J. Am. Pharm. Assoc. Sci. Ed.*, 1955, **44**, 142.
6 Bermejo, A. M., Lopez-Rivadulla, M., Fernandez, P., and Cruz, A., *Anal. Lett.*, 1991, **24**, 1147.
7 Schachter, D., and Manio, J. G., *J. Clin. Invest.*, 1958, **37**, 800.
8 Pitet, G., Cros, J., and Caujolle, R., *C.R. Acad. Sci., Ser. D*, 1969, **268**, 868.
9 Gupta, R. N., and Zamkanei, M., *Clin. Chem.*, 1990, **36**, 1690.
10 Jacobs, J. C., and Pesce, M., *Arthritis Rheum.*, 1978, **21**, 129.
11 Bailey, M. P., Rochs, B. F., and Riley, C., *Anal. Chim. Acta*, 1987, **201**, 335.
12 Salinas, F., Muñoz de la Peña, A., Durán-Merás, I., and Durán, M. S., *Analyst*, 1990, **115**, 1007.
13 Muñoz de la Peña, A., Salinas, F., and Durán-Merás, I., *Anal. Chem.*, 1988, **60**, 2493.
14 Damiani, P., Ibáñez, G., and Olivieri, A. C., *Anal. Lett.*, 1993, **26**, 247.
15 Damiani, P., Ibáñez, G., and Olivieri, A. C., *J. Pharm. Biomed. Anal.*, in the press.
16 Ichinose, N., Schwedt, G., Schnepel, F. M., and Adachi, K., *Fluorometric Analysis in Biomedical Chemistry. Trends and Techniques Including HPLC Applications*, Wiley, New York, 1991.
17 Konstantianos, D. G., Ioannou, P. C., and Efstathiou, C. E., *Analyst*, 1991, **116**, 373.

Paper 4/02585G
Received May 3, 1994
Accepted July 1, 1994

Upgrading a Rapid-scanning Spectrometer With Microcomputerized Data Acquisition and Treatment to Measure Spectrokinetic Parameters of Photochromic Compounds

Jean-Jacques Meyer

LAB.El, Université de Haute Alsace, IUT, 61 rue Albert Camus, 68093 Mulhouse Cedex, France

Patrick Levoir and Roger Dubest*

Institut de Topologie et de Dynamique des Systèmes, CNRS URA 34, Université Paris 7, 1 rue Guy de la Brosse, 75005 Paris, France

An interface circuit between a rapid scanning spectrometer and a 486 compatible personal computer is described. A specific unit was also designed in order to study multi-phase kinetic processes with high accuracy. Major spectrokinetic parameters, specifying the properties of photochromic compounds, can thus be readily obtained. The improvement of the apparatus highlighted that up to four different kinetic constants are involved in the thermal bleaching process of a new series of compounds. Owing to the modular design of the menu-driven software, written in C language, the system is very flexible and easy to use.

Keywords: Microcomputer-controlled rapid scanning spectrometer; spectrokinetic parameters; photochromic compounds; analysis of multi-exponential decay

Introduction

Photochromism describes the colour change of a substance when exposed to light.[1] Under UV irradiation, the C–O bond breaking in spiro compounds leads to a coloured species, photomerocyanine, according to the scheme in Fig. 1.

After numerous studies on the spiropyrans and particularly the nitroindoline derivatives, our recent work has been devoted to the synthesis and characterization of new structures in the oxazine series.[2,3]

In order to specify photochromic properties, a knowledge of the following four major parameters is necessary: (*i*) the thermal ring closure kinetic constant, k_Δ; (*ii*) the maximum absorption wavelength λ_{max} of the coloured species; (*iii*) the colourability A_0; and (*iv*) the photodegradation parameter t_R or n_R, expressed either as the fatigue resistance time t_R or as the number n_R of degradation flash shots before the colourability becomes $A_0/2$. This latter measurement is performed with a new specific apparatus recently developed.[4] The first three parameters were obtained in a single experiment using a fast scanning spectrometer.[2,5]

Despite considerable technological advances in the field of opto-electronics and related instrumentation[6] during the last ten years, including a new method[7] using high-speed framing with slow-scan readout on two-dimensional CCD arrays, allowing time-resolved spectroscopy in the 1 μs range, with a multi-channel advantage when compared with a single photomultiplier tube detector, our spectrophotometer[5] (Model 501, Warner and Swasey, Flushing, NY, USA) with a 1 ms scanning time at a rate of 800 scans per second remains today, like similar commercial designs,[8] a powerful investigative tool suitable for the study of transient species in the 10^{-3}–10^{+2} s time range, which is the field of thermal bleaching in photochromic reactions. Therefore, it was of interest to upgrade inexpensively our spectrometer on a personal computer.

In order to acquire a series of spectra, to control efficiently the course of the experiment and to process the acquired data, we designed an interface circuit between the spectrometer and a 486 compatible personal computer. A specific kinetic measurement unit was also developed in order to acquire and treat multi-exponential kinetics. A user-friendly program, written in C language, fully controls the experiment and performs many specific spectral and kinetic data treatments.

Results from spectrokinetic experiments on spiro[1,3,3-trimethylindolinenaphthoxazine] and other compounds in a new series are presented in order to illustrate the performance of the system.

Experimental

The complete system designed to measure the spectral and kinetic parameters is depicted in Fig. 2. To preserve the spectrometer's resolution (approximately 1 nm) and accuracy (approximately 1%) and to ensure reliable analogue-to-digital conversion, we selected a high-speed (1 μs conversion time) 12 bit analogue-to-digital converter (ADC). Our 486 PC is equipped with an advanced transient recorder plug-in board (BAK) (Model BE490, Bakker Electronics, Atlanta, GA, USA) fitted with a segmentable buffer memory (1 Mo). The intensity spectra collected by the Warner and Swasey fast-scanning spectrometer (FSS), after conditioning by the analogue signal conditioning circuit (ASC), are numbered by the fast ADC and stored in the PC memory.

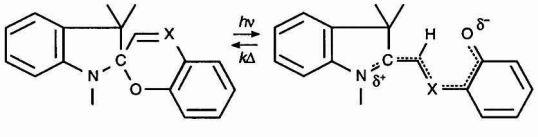

Spirocompound Photomerocyanine

X = CH: Spiropyrans
X = N: Spiro-oxazines

Fig. 1. Photochromic reaction scheme.

* To whom correspondence should be addressed.

Only first-order kinetics can be treated because only 20–30 measurement points, taken from the spectra sequence, are available at best. To obtain accurate multi-exponential parameters, a kinetic measurement mode is provided. For this purpose, as one part of the optical beam is reflected by a small mirror (SM) to the monochromator (M) (Model 7155, Oriel, Stratford, CT, USA) and the photomultiplier tube (PMT), the other enters the Cassegrainian collector system of the spectrometer. The signal is conditioned by the kinetic unit (KU), converted by the 12 bit ADC of the interface card (PCLAB) (Model PCL-812PG in the PCLabCard series, by Advantech) and collected in the PC memory.

Logic Control Unit

Functional description

For spectroscopic measurements, two main operating modes, namely manual and auto, can be selected by the mode switch located on the front panel of the logic control unit (LCU). The manual mode is especially used for initial tests and calibration purposes. In the auto mode, the experiment is under program control.

Two kinds of synchronization capabilities, continuous and triggered, are provided (Fig. 3). Under continuous synchronization, each Scan Time Marker signal, which is the spectrometer's mirror position synchronization signal occurring at the start of each scan (RT = 1.25 ms), gives rise to a corresponding Outscan output generated even in the absence of a flash event. This synchronization is used to acquire the initial spectrum I_0 (before flash). In the auto mode, the synchro selection is provided by the A. Synchro signal. In the manual mode, this task is performed by setting the synchro switch located on the front panel of the LCU. Triggered synchronization gives rise to the Outscan signal only after the flash has fired. This triggering is selected for the acquisition of spectral data in the course of a photolysis experiment. In both modes, on request from the operator, the program can acquire or disregard pre-selected numbers of spectra. The Outscan pulses are software counted, the Select Conv flag is set and the ADC is triggered only at the occurrence of pre-selected spectra numbers.

Manual and computer-controlled operations are 'ORed', the manual settings overriding the automatic settings. After completion of an experiment, the operator by actuating the RAZ switch, or the program by re-setting the A. RAZ line, re-initializes the LCU.

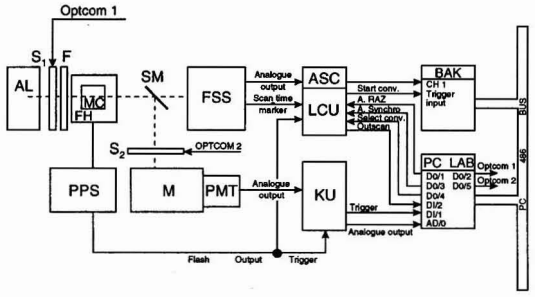

Fig. 2 Block diagram of the complete system: AL, analysis lamp; S_1 and S_2, optical shutters; F, filter; FH, flash housing; MC, measurement cell; PPS, photolysis power supply; FSS, fast-scanning spectrometer; SM, small mirror; M, monochromator; PMT, photomultiplier tube; LCU, logic control unit; ASC, analogue signal conditioning circuit; KU, kinetic unit; BAK and PC LAB, interface boards; PC, personal computer; and dashed line, optical path.

Circuit description

The schematic diagram of the LCU is given in Fig. 4. The Flash Output Trigger and Scan Time Marker signals are fed to LM311 comparators IC1 and IC2, whose outputs trigger IC3 and IC5-1 monostables. If triggered synchronization is selected, the flash output trigger signal clocks IC4-1, sets the Q_2 output of IC4-2 D flip-flop and, thus, opens the IC9-A Nand gate; Scan-2 then triggers 100 μs monostable IC5-2 whose output $\bar{Q}_2$ is buffered by open-collector buffer IC7-B. Outscan clocks a software counter which detects the number of 0 to 1 transitions in the signal. This count is compared with the numbers in the sequence of the spectra to be acquired: a coincidence then sets the Select Conv flag, which in turn opens Nand gate IC9-C and outputs the Start Conv signal which finally triggers the ADC. After the last selected spectrum has been digitized, D flip-flops IC4-1 and IC4-2 are cleared by the A. RAZ signal. The mode and synchro select functions are wired by IC-7, -8 and -9 gates and inverters. All input and output signals fed to or issued from the LCU are buffered by 74LS05 open-collector circuits.

In order to adjust the Analogue output signal of the Warner and Swasey FSS to the input span of the ADC, we used the A1 OPA627 operational amplifier, wired in a variable-gain, non-inverting configuration. This gain is set by means of a ten-turn potentiometer located on the front panel of the logic control unit.

The shape of the spectra obviously changes with the studied compounds. A Fourier analysis of the frequency content of the periodic analogue output signal of the Warner and Swasey spectrometer did not show any noticeable amplitudes above

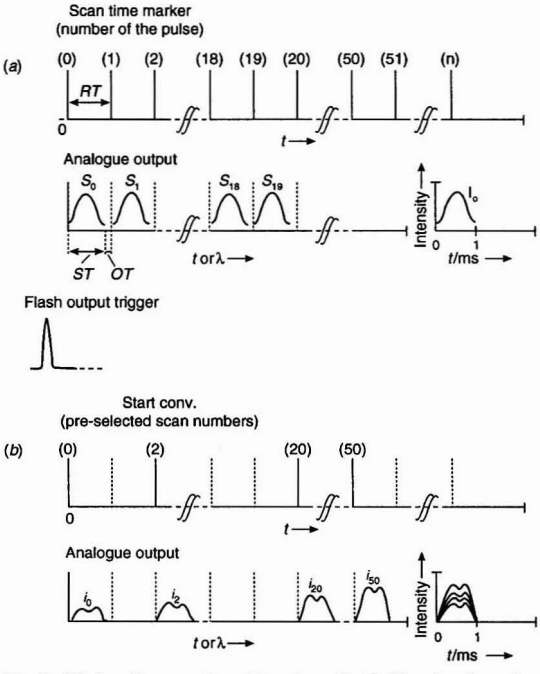

Fig. 3 Timing diagram. Repetition time, RT (1.25 ms) = Scanning time, ST (1 ms) + Off time, OT (0.25 ms). The output signal is linear in time and wavelength. (*a*), Continuous synchronization, $I_0 = \frac{1}{20}\sum_{n=0}^{n=19} S_n$. (*b*), Triggered synchronization.

30–40 kHz. Taking into account that the study of solutions giving rise to broad bands is not the only kind of experiment that can be carried out, but that it is possible that higher frequencies may appear in the spectrum, an accurate estimate of the signal bandwidth is difficult. The noise amplitude, highly dependent on the experimental conditions, can also vary from a few to 10–20% of the full-scale signal. Nevertheless, despite the difficult accurate definition of its characteristics, an anti-aliasing filter in front of the ADC is useful. The higher we make the sampling rate compared with the signal bandwidth, the simpler this filter will be. Hence, by programming, we may select a high oversampling ratio (the highest sampling frequency of the ADC is 1 MHz). We designed three Sallen and Key third-order Butterworth filters, built around AD845 operational amplifiers, with −3 dB cut-off frequencies of 50, 75 and 100 kHz. Provision was also made by means of the filter switch to select first-order RC filtering provided by the Warner and Swasey spectrophotometer.

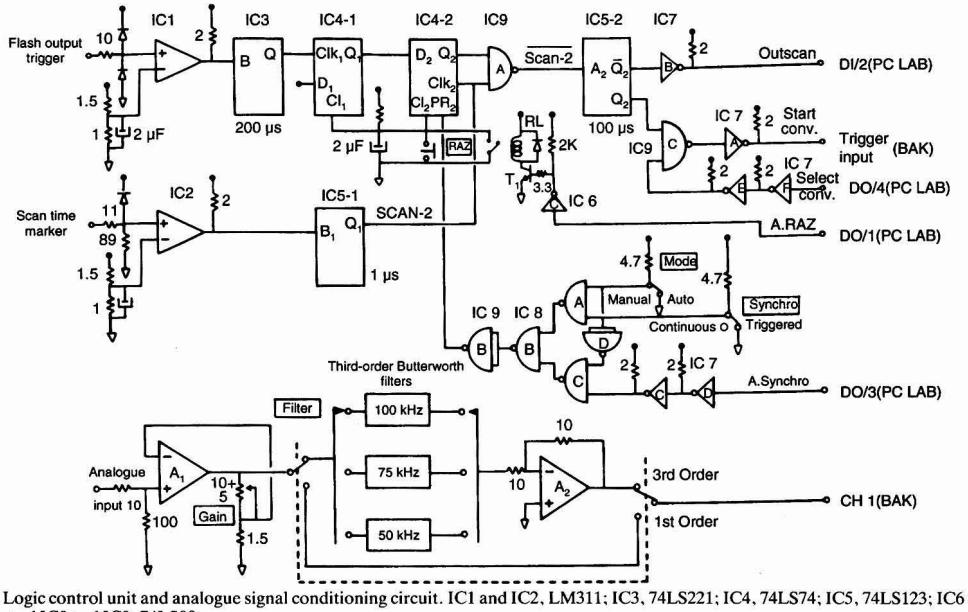

Fig. 4 Logic control unit and analogue signal conditioning circuit. IC1 and IC2, LM311; IC3, 74LS221; IC4, 74LS74; IC5, 74LS123; IC6 and IC7, 74LS05; and IC8 and IC9, 74LS00.

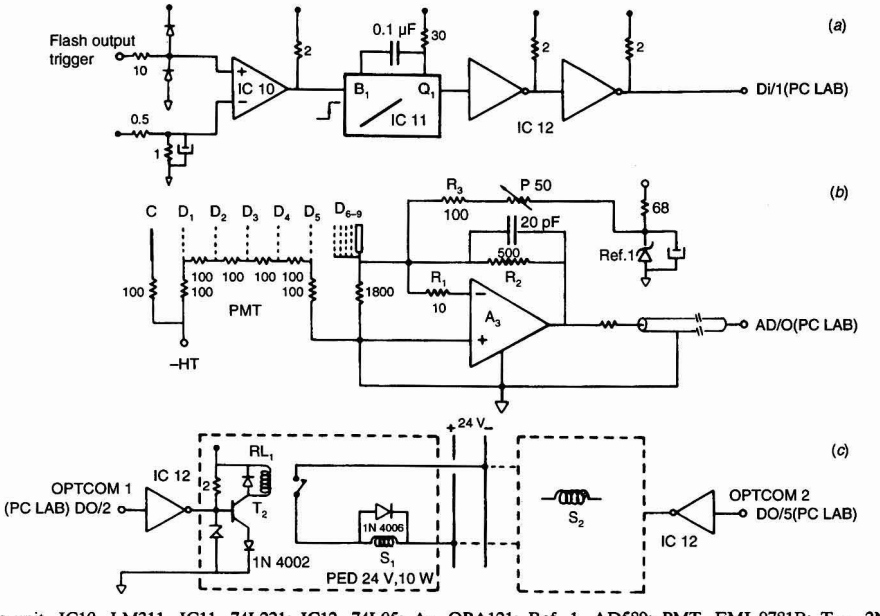

Fig. 5 Kinetic unit. IC10, LM311, IC11, 74L221; IC12, 74L05; A_3, OPA121; Ref. 1, AD589; PMT, EMI 9781B; $T_{2,3}$, 2N2219A; and $RL_{1,2}$, DSE 5V.

On the peaks of a reference mercury lamp, we measured, under our standard experimental conditions, a maximum wavelength shift of 2 nm, due to the non-linear frequency phase shift of the Butterworth filters, with a wavelength repeatability of about 0.3 nm. As the grating used in the system (258 lines mm^{-1}) is blazed at a small angle (2°20′) it follows simply from the grating equation that the dispersion is linear to better than 1% over the whole useful range of the grating. The wavelength calibration performed on the filtered signal gives the function of wavelength related to the time in one scan (t between 0 and 1 ms): $\lambda\,(nm) = 0.285\,t\,(\mu s) + 417.6$. It should be noticed that the major limitation in λ_{max} determination is due to broad bands of the absorbance spectra for the compounds studied.

Kinetic Unit (KU)

When the flash fires, the Flash Output Trigger signal, delivered by the photolysis power supply (PPS), is fed to IC10 comparator, shaped by IC11 monostable and buffered by IC12 open-collector gates [Fig. 5(*a*)]. When the trigger signal is fed to the PCLAB board, the program checks for a 0 to 1 level transition in the DI/1 line and thereafter triggers the board's ADC.

The kinetic signal is issued from the photomultiplier tube (PMT) wired in a five-stage configuration. The A3 transimpedance amplifier, loaded with resistor R2, converts the anodic PMT current into a low-impedance output voltage which is fed to the ADC input (AD/0) [Fig. 5(*b*)]. In order to make use of the whole input voltage span of the ADC (−5 to +5 V), the no-input light condition is set to the −5 V level by the compensation network made of resistor R3, potentiometer P and voltage reference REF1. Resistor R1 protects the A3 input circuits against a possible PMT current surge. To reduce the circuit's stray electromagnetic fields (EMF) sensitivity, this amplifier is wired closely near the PMT socket and enclosed in a well shielded metallic box.

S1 and S2 are optical shutters triggered by OPTCOM1 and OPTCOM2 signals on program request [Fig. 5(*c*)]. Shutter S2 prevents the PMT from being exposed to input light when no kinetic measurement is in progress. Shutter S2 contributes also to reduce current drifts due to mean anodic current levels in excess of a few microamperes.

Software

A user-friendly and menu-driven software, written in C language, fully controls the experiment by means of the PCLAB board (flash trigger, count of scan time marker signals, *etc.*), collects the data by means of the BAK or the PCLAB boards and performs the spectroscopic and kinetic data treatments (Fig. 6).

The Warner and Swasey spectrophotometer is a single-beam instrument. In order to calculate the absorbance, an initial spectrum I_0 must be acquired before the flash perturbation. It should be noticed that I_0 is computed from the average of 20 consecutive spectra in order to improve its signal-to-noise ratio (S/N).

The acquisition module permits the following operations to be realized: the direct visualization of the initial spectrum; the acquisition of the I_0 spectrum before the flash is fired; and the collection of the spectral data in the desired sequence.

In the direct visualization mode, the signal is displayed in real time on the PC screen in order to adjust the position and the amplitude of the signal to be acquired under continuous synchronization. With the help of user-friendly graphics software, the experimenter enters the desired sequence of the intensity spectra to be acquired by the arrow keys. Once the flash has triggered, the chosen spectra are acquired *via* the LCU and stored in the segmented memory of the BAK board. At the end of the acquisition process, all the selected spectra are transferred into the PC memory and displayed on the PC screen, hence, the user can store the spectral data in files on the PC hard disk.

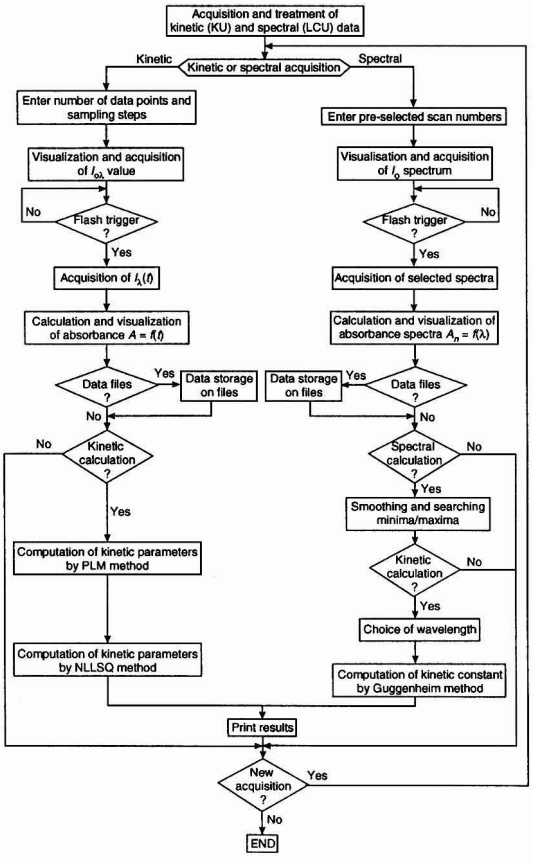

Fig. 6 Flow chart of the software.

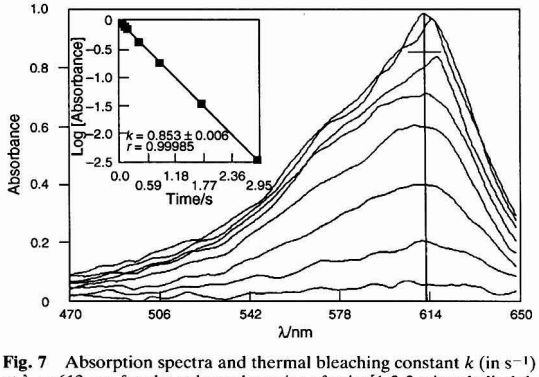

Fig. 7 Absorption spectra and thermal bleaching constant k (in s^{-1}) at λ = 613 nm for the coloured species of spiro[1,3,3-trimethylindolinenaphthoxazine] in DMSO.

The acquired signal can be smoothed by a binomial algorithm[9] and/or piecewise zoomed to select the useful spectral range, then the absorbance spectra $A_n = \log(I_0/i_n) = f(\lambda)$ are calculated and displayed as shown in Fig. 7. These spectra can be saved in ASCII or JCAMP format files for more elaborate treatments such as band decomposition (Spectra Calc software by Galactic Industries, Salem, NH, USA). By means of a horizontally and vertically movable cursor, the wavelength and absorbance values of maxima and minima can be determined graphically for each spectrum.

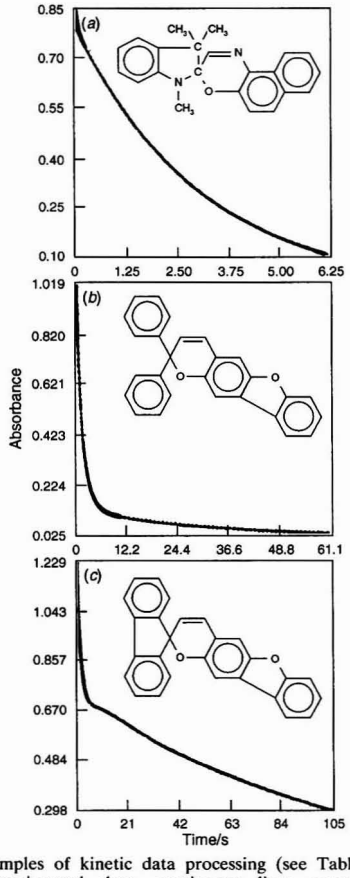

Fig. 8 Examples of kinetic data processing (see Table 1 for k_i values). Experimental data, continuous line; computed data (obtained from NLLSQ procedure: see text), crosses. (*a*), Spiro[1,3,3-trimethylindolinenaphthoxazine] in toluene at $\lambda = 600$ nm. Two sampling steps (0.5 ms for the first 500 points and 12 ms for the following 500 points) were pre-set. (*b*), 7,7-Diphenyl-7*H*-benzofurano[2,3-*g*]chromene in toluene at $\lambda = 450$ nm. Two sampling steps (15 ms for the first 700 points and 195 ms for the following 260 points) were preset. (c), Spiro[7*H*-benzofurano[2,3-*g*]chromene-7,9′-fluorene] in toluene at $\lambda = 490$ nm. Two sampling steps (10 ms for the first 500 points and 200 ms for the following 500 points) were present.

At a wavelength fixed by the arrow keys, a rough estimate of time parameters of mono-exponential kinetics can be gained using a classical linear least-squares method.[10]

However, higher accuracy for thermal ring closure kinetic constants k_Δ of the photomerocyanines can be obtained using the kinetic unit. To pre-set kinetic data acquisition, the operator enters the desired number of data points and the sampling step (from 100 μs to 1 s). At the chosen wavelength λ, once the $I_{o\lambda}$ (initial transmittance) data have been acquired, the flash is fired and the software monitors the sampling of the kinetic process.

In a multi-phase kinetic process, it is possible to enter two different sampling steps t_1 and t_2 ($t_2 = nt_1$, n being an integer).

The kinetic signals can be adequately described by a sum of exponentially decaying functions:

$$A(t) = \sum_i A_i e^{-k_i t}$$

and the computation of the spectrokinetic parameters is carried out by either the well known Marquardt non-linear least-squares method[11,12] (NLLSQ) or the newly developed Padé–Laplace method (PLM).[13,14]

Structurally, the PLM is an analytical technique providing a direct estimation of the components without any *a priori* assumption as to their number. Moreover, this method is free from the effects of overfitting which can occur in statistical methods. An efficient approach to analyse such complex signals reliably is to associate PLM with NLLSQ.[15] In this way, PLM provides a first estimate of the parameters, which are then used in NLLSQ as initial values. The PLM results are thereby enriched by the confidence parameters of the statistical procedure.

Results and Discussion

First, we present (Fig. 7) the absorption spectra and the thermal bleaching constant k_Δ calculated by a linear least-squares method at $\lambda_{max} = 613$ nm for the coloured species of spiro[1,3,3-trimethylindolinenaphthoxazine] in DMSO, obtained in a single experiment. Our measurement on the A_0 reproducibility under our standard experimental conditions led to a mean of 1 and a relative standard deviation of about 10%. For k_Δ, despite of the obvious satisfactory accuracy observed in its determination, the use of our kinetic unit (with 1000 data points and a sampling step of 3 ms) will show that we have a bi-phase kinetic process: $A(t) = A_1 e^{-k_1 t} + A_2 e^{-k_2 t}$ with $k_1 =$

Table 1 Kinetic parameters (k_i values) for Fig. 8(*a*), (*b*) and (*c*)

Kinetic parameter	k_i/s^{-1} (*a*)	(*b*)	(*c*)
A_1	$6.84 \times 10^{-2} \pm 3 \times 10^{-4}$	$9.22 \times 10^{-1} \pm 1.4 \times 10^{-4}$	$6.85 \times 10^{-1} \pm 3 \times 10^{-5}$
k_1	$2.03 \times 10^{-1} \pm 1.4 \times 10^{-1}$	$5.82 \times 10^{-1} \pm 1.26 \times 10^{-4}$	$5.16 \times 10^{-1} \pm 3.5 \times 10^{-5}$
A_2	$7.98 \times 10^{-1} \pm 1.3 \times 10^{-4}$	$1.15 \times 10^{-1} \pm 4.50 \times 10^{-5}$	$-3.34 \times 10^{-1} \pm 2.1 \times 10^{-5}$
k_2	$3.17 \times 10^{-1} \pm 1.3 \times 10^{-4}$	$3.30 \times 10^{-2} \pm 4.44 \times 10^{-5}$	$2.12 \times 10^{-1} \pm 2.9 \times 10^{-5}$
A_3			$1.35 \times 10^{-1} \pm 1.7 \times 10^{-5}$
k_3			$1.02 \times 10^{-1} \pm 4.2 \times 10^{-5}$
A_4			$7.36 \times 10^{-1} \pm 1.2 \times 10^{-5}$
k_4			$8.70 \times 10^{-3} \pm 5.8 \times 10^{-7}$

2.48 s^{-1}, $A_1 = -0.14$, $k_2 = 0.89\ s^{-1}$, $A_2 = 0.88$ (for an initial absorbance $A_0 = 0.74$).

Hence, for our studies, the best way will be to obtain in a first experiment (using the Warner and Swasey spectrophotometer) the absorption spectra (λ_{max}, A_0) and an estimate of the major k_Δ value. The use of the kinetic unit is necessary to take advantage of the performance of our apparatus. In this instance, although data smoothing routine is available, we can use raw data in the fitting routines; indeed, the noise on the data is less than 0.01 peak to peak in absorbance.

To illustrate these remarks, we now present some examples of kinetic measurements (Fig. 8, Table 1), including two new compounds recently synthesized.[16,17] These examples show that, in the case of multi-exponential signals, our system allows the computation with excellent accuracy of the spectrokinetic parameters even when the amplitude of one exponentially decaying function is small [a few per cent of the total amplitude: 8% and 11% in Fig. 8(*a*) and (*b*), respectively].

Moreover, we could highlight four species involved in the thermal bleaching process of the coloured form for a new compound in the heteroannelated spiro[fluorenechromenes] series [Fig. 8(*c*)]. Owing to the interest in such a series for application in the field of variable optical transmission materials, further chemical developments based on these results will be published later.

Owing particularly to the modular design of the software, we can easily obtain with our apparatus the major spectrokinetic parameters of photochromic compounds. The results are very useful for comparisons within the same series or between different series of compounds. Moreover, these measurements, particularly the kinetic measurements, could help to achieve a better understanding of the species involved in the photochromic reaction.

The authors thank R. Guglielmetti (Université Aix–Marseille II) and J. Aubard (Université Paris VII) for helpful discussions during this work.

References

1 Bertelson, R. C., in *Photochromism*, ed. Brown, G. H., Wiley, New York, 1971, ch. 3.
2 Pottier, E., Dubest, R., Guglielmetti, R., Tardieu, P., Kellmann, A., Tfibel, F., Levoir, P., and Aubard, J., *Helv. Chim. Acta*, 1990, **73**, 303.
3 Tardieu, P., Dubest, R., Aubard, J., Kellmann, A., Tfibel, F., Samat, A., and Guglielmetti, R., *Helv. Chim. Acta*, 1992, **75**, 1185.
4 Dubest, R., Levoir, P., Meyer, J. J., Aubard, J., Baillet, G., Giusti, G., and Guglielmetti, R., *Rev. Sci. Instrum.*, 1993, **64**, 1803.
5 Dolin, S. A., Kruegle, H. A., and Penzias, G. J., *Appl. Opt.*, 1967, **6**, 267.
6 Yip, W. T., and Tse, R. S., *Rev. Sci. Instrum.*, 1992, **63**, 3777.
7 Aikens, R. S., Epperson, P. M., and Denton, M. B., *Proc. SPIE*, 1984, **501**, 49.
8 *Olis RSM Spectrophotometer*, On-Line Instrument Systems, Bogart, GA.
9 Marchand, P., and Marmet, L., *Rev. Sci. Instrum.*, 1983, **54**, 1034.
10 Guggenheim, E. A., *Philos. Mag.*, 1926, **2**, 538.
11 Marquardt, D. W., *J. Soc. Ind. Appl. Math.*, 1963, **11**, 431.
12 Press, W. H., Flannery, B. P., Teukolsky, S. A., and Vetterling, W. T., *Numerical Recipes in C*, Cambridge University Press, Cambridge, 1989, pp. 540–565.
13 Aubard, J., Levoir, P., Denis, A., and Claverie, P., *Comput. Chem.*, 1987, **11**, 163.
14 Yeramian, E., and Claverie, P., *Nature (London)*, 1987, **366**, 169.
15 Tellier, C., Guillou-Charpin, M., Le Botlan, D., and Pelissolo, F., *Magn. Reson. Chem.*, 1991, **29**, 167.
16 Pozzo, J. L., Lokshin, V. A., Harié, G., Samat, A., and Guglielmetti, R., to Essilor, *Fr. Pat.*, 94 04028, 1994.
17 Pozzo, J. L., Samat, A., and Guglielmetti, R., to Essilor, *Fr. Pat.*, 94 04029, 1994.

Paper 4/02250E
Received April 15, 1994
Accepted August 1, 1994

Optical Fibre Fluorosensor for Cadmium With Diethylaminoethyl-Sephadex as a Substrate

Jianzhong Lu

Department of Chemistry, Nanjing University, P.O. Box 210008, Nanjing, China

Zhujun Zhang*

Department of Chemistry, Shaanxi Normal University, P.O. Box 710062, Xi'an, China

An optical fibre fluorosensor for cadmium ion was prepared by immobilizing 8-hydroxy-7-iodoquinoline-5-sulfonic acid on diethylaminoethyl (DEAE) Sephadex. Owing to the lowest excited singlet changing from n–π^* to π–π^*, complexation between cadmium ion and the immobilized reagent resulted in a weakly fluorescent ligand becoming a strongly fluorescent complex. Based on the fluorescence intensity change of the immobilized phase at 505 nm, cadmium ion in solution was determined. The characteristics of the fluorosensor were studied by using both the kinetic and equilibrium methods. As DEAE-Sephadex is a colourless and transparent gel containing diethylaminoethylglucan with a low transfer resistance in water, the fluorosensor reached 90% of the steady-state response in 10 s. The relationship between the response and the logarithm of cadmium ion concentration was linear in the range of 2.0×10^{-7}–7.0×10^{-5} mol dm^{-3}. The detection limit for Cd^{II} was 8.0×10^{-8} mol dm^{-3}. Using KI solution, the sensing layer saturated by cadmium ion can be regenerated, but the immobilized 8-hydroxy-7-iodo-quinoline-5-sulfonic acid was not destroyed. The results of this study demonstrate that DEAE-Sephadex is a good substrate for an optical fibre fluorosensor for cadmium ion. With appropriate separation it can be applied to the determination of cadmium ion in flour samples.

Keywords: Cadmium ion determination; optical fibre fluorosensor; diethylaminoethyl-Sephadex

Introduction

Owing to the inherent advantages of optical fibres, a variety of chemical sensors have been developed[1–8] and many sensors have been successfully applied in process control, environmental and medical analysis, *etc.* In addition to the sensitivity and selectivity considered, the key to devising a good sensor is to shorten the response time and obtain good reversibility. The response time is controlled by mass transfer processes in the substrate and the reversibility is dominated by the binding constant of the indicating reaction. Saari and Seitz[9] reported an optical fibre copper sensor, which was based on the fluorescence quenching between calcein immobilized on cellulose and copper ion. About 90% of the steady-state response could be reached in 5 min, and the sensor was irreversible. Zhang *et al.*[10] prepared an optical fibre sensor responding to Al^{III}, Mg^{II}, Zn^{II} and Cd^{II}. Amberlite CG-400 anion-exchange resin was used as the substrate, the response time was 1.5–2.5 min and the linear response range to metal ions was narrow.

* To whom correspondence should be addressed.

In this paper, an optical fibre fluorosensor for cadmium ion using diethylaminoethyl (DEAE)-Sephadex as the substrate and immobilized 8-hydroxy-7-iodoquinoline-5-sulfonic acid (ferron) as the indicator is described. The characteristics of the fluorosensor were studied by using both the kinetic and equilibrium methods.

Experimental

Instrumentation

A schematic diagram of the fluorosensor used in the kinetic method is shown in Fig. 1. The excitation light is passed through one arm of the bifurcated optical fibre to a thin layer of immobilized ferron and the fluorescence intensity is monitored through the other arm of the optical fibre by a Perkin Elmer LS-50 luminescence spectrometer with a xenon discharge excitation source (equivalent to 20 kW for an 8 μs duration, pulse width at peak half-height <10 μs). The configuration of the sensing layer used in the equilibrium method is similar to that reported previously.[10] The pH was measured with a Model pHs-3C pH meter. The solution was transmitted with a three-channel peristaltic pump.

Reagents

8-Hydroxy-7-iodoquinoline-5-sulfonic acid (ferron) was of analytical-reagent grade and was purchased from the Chemicals Reagents Factory (Beijing, China). All other chemicals were of analytical-reagent grade and were obtained from the Chemical Reagents Factory (Xi'an, China) and A-50-120 DEAE-Sephadex was purchased from Sigma (St. Louis, MO, USA). A 0.0100 mol dm^{-3} cadmium stock standard solution

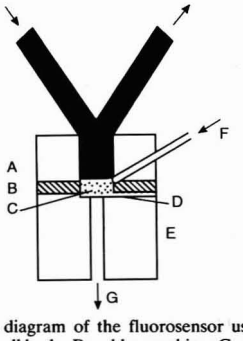

Fig. 1 Schematic diagram of the fluorosensor used in the kinetic method: A, upper cell body: B, rubber packing; C, substrate; D, filter disc; E, lower cell body; F, solvent entrance; and G, exit.

was prepared by dissolving 0.1125 g of pure cadmium metal in a minimum amount of dilute nitric acid (1 + 5) and diluting to 100 cm^3 with water. A 0.01 mol dm^{-3} ferron solution was prepared by dissolving 0.3511 g in a minimum volume of sodium hydrate solution (0.1 mol dm^{-3}) and diluting to 100 cm^3 with water. All solutions were prepared with de-ionized water.

Immobilization Procedure

A 0.10 g amount of DEAE-Sephadex was stirred with 20 cm^3 of the ferron solution for 40 min, then filtered and washed five times with de-ionized water. The substrate was kept wet for storage.

Measurement Procedure

In the kinetic method, 1 mg of substrate immobilized with ferron was packed into a small cell formed by a filter disc and rubber packing (Fig. 1); the diameter of the cell was 4 mm and the indicator layer was 1 mm thick. An optical fibre was fixed in the light channel of the cell and the common end of the optical fibre was contacted exactly with the substrate. The lower cell body was fixed on the lower end of the cell. The standard and sample cadmium solutions were passed from the solvent entrance. The excitation and emission wavelengths were 410 and 505 nm, respectively, and the slit widths for both the excitation and emission light were 15 nm. The fluorescence intensity was recorded as a function of time and the concentration of cadmium ion was determined by using the fluorescence intensity at 60 s.

In the equilibrium method, a thin layer of the substrate with immobilized ferron was spread onto a piece of Cellophane tape by placing the tape over a vial containing the substrate. The vial was shaken until a uniform layer formed. The tape was held in place on the optical fibre by an O-ring. The end of the optical fibre was immersed directly into the cadmium solution and the concentration of cadmium ion was determined by using the fluorescence intensity obtained when the fluorosensor was inserted in the cadmium solution for 10 s to reach 90% of the steady-state response.

Results and Discussion

Spectral Characteristics

Fig. 2 shows the excitation and emission spectra of ferron before and after reaction with cadmium ion on DEAE-Sephadex. It can be seen that the immobilized ferron alone has a very weak fluorescence and complexation between cadmium ion and the immobilized ferron resulted in a strongly fluorescent complex, which was due to the lowest excited singlet changing from n–π^* to π–π^*. The maximum excitation and emission wavelengths were 410 and 505 nm, respectively. Compared with that in solution, immobilization on DEAE-Sephadex causes 20 nm blue shifts of the maximum emission wavelength of the complex.

Effect of pH

The optimum pH range for the formation of the complex is 5.5–7.5 with 0.1 mol dm^{-3} KH_2PO_4–0.1 mol dm^{-3} NaOH buffer solution. When the pH is below 5.0 or above 8.0, the fluorescence intensity decreases rapidly.

Response to Cadmium Ion

When using the kinetic method to carry out the determinations, the adsorption of cadmium ion is a dynamic process. Fig. 3 shows the adsorption curves of the sensing

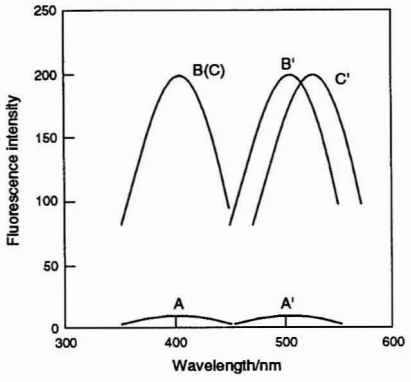

Fig. 2 Excitation and emission spectra: A and A′, ferron before reaction with cadmium ion on DEAE-Sephadex; and B and B′, ferron after reaction with cadmium ion on DEAE-Sephadex; C and C′, the complex in solution.

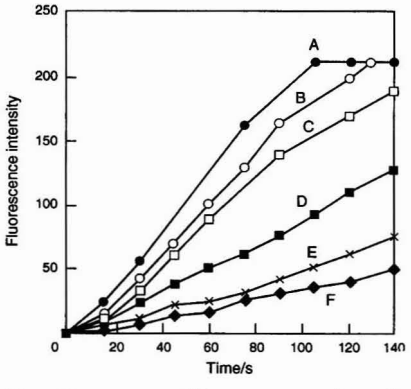

Fig. 3 Absorption curves at different concentrations of cadmium ion: A, 7.0 × 10^{-5}; B, 1.75 × 10^{-5}; C, 9.9 × 10^{-6}; D, 1.75 × 10^{-6}; E, 3.5 × 10^{-7}; and F, 3.5 × 10^{-8} mol dm^{-3}.

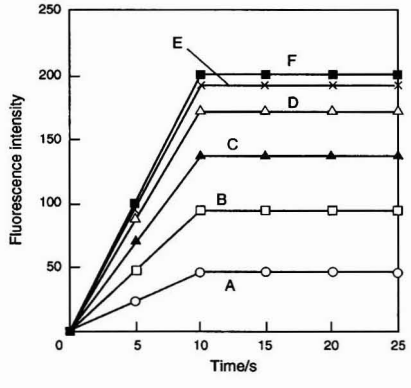

Fig. 4 Response curves at different concentrations of cadmium ion on DEAE-Sephadex using the equilibrium method: A, 1.75 × 10^{-6}; B, 3.5 × 10^{-6}; C, 5.25 × 10^{-6}; D, 7.0 × 10^{-6}; E, 8.75 × 10^{-6}; and F, 10.5 × 10^{-6} mol dm^{-3}.

layer at different concentrations of cadmium ion with DEAE-Sephadex as the substrate at a 2.0 cm min^{-1} flow rate. It can be seen that the slopes of the adsorption curves are smaller at lower concentrations of cadmium ion. However, all the curves reach the same constant value of fluorescence intensity, representing the state where all of the binding sites were saturated. The concentrations of cadmium ion can be determined by using the fluorescence intensity at 60 s. The relationship between the response and the logarithm of the concentration of cadmium ion is linear in the range 2.0×10^{-7}–7.0×10^{-5} mol dm^{-3} with a correlation coefficient of 0.993; the regression equation is $F = 341.96 + 49.97 \log C_{cd}$.

As discussed previously,[10] if the stoichiometry of the reaction is 1:1 and if the amount of metal combining with the immobilized reagent phase is small relative to the amount in solution, an equilibrium between the solution and immobilized reagent phase will be established when the fluorosensor is inserted in the cadmium solution in the equilibrium method, and the following equation applies:

$$C_M/F = C_M/kC + 1/kCK \quad (1)$$

where F is the fluorescence intensity, k is a proportionality constant relating fluorescence intensity to the amount of complex, C_M is the concentration of metal ion, C is the amount of immobilized ligand and K is the conditional equilibrium constant for complex formation. As predicted by eqn. (1), the plot of C_M/F *versus* C_M is linear, confirming a 1:1 stoichiometry and that the amount of bound metal is small relative to the amount in solution. The conditional binding constant determined from the slope and the intercept of the plot is 1.0×10^6. Under the same conditions, the conditional binding constant in the solution is 3.0×10^6, which was measured by spectrophotometry with the continuous variation method.

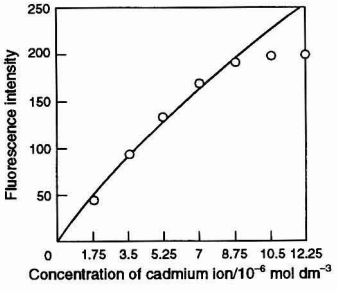

Fig. 5 Graph of fluorescence intensity *versus* cadmium concentration using the equilibrium method. The solid line shows the theoretical curve and the marked points show the experimental curve.

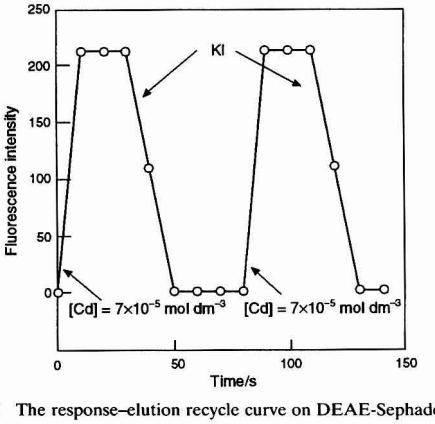

Fig. 6 The response–elution recycle curve on DEAE-Sephadex.

Fig. 4 shows the response curves of the sensing layer at different concentrations of cadmium ion on DEAE-Sephadex, which was obtained by using the equilibrium method. The 90% steady-state response can be reached in 10 s at any cadmium concentration. Fig. 5 shows the fluorescence intensity as a function of concentration of cadmium ion determined by the equilibrium method. It includes a theoretical curve calculated from eqn. (1) assuming a conditional binding constant of 1.0×10^6. The agreement between theory and experiment is good, although at high cadmium ion concentrations the experimental intensities are less than predicted. Using KI solution, the sensing layer saturated by cadmium can be regenerated quickly and completely, but the immobilized ferron was not destroyed. From the response–elution recycle curve in Fig. 6, it can be seen that the response of the sensing layer is fast as well as reversible, with good reproducibility.

Effect of Foreign Ions

The effect of foreign ions was studied using the above procedure. A foreign ion was considered not to interfere if it caused a relative error of less than 5% in the determination of 1.0×10^{-6} mol dm^{-3}. Equal amounts of La^{III}, WO_4^{2-}, Co^{II}, Ni^{II} and Cu^{II} did not interfere. K^I and Na^I up to 1.0×10^{-3} mol dm^{-3} and Mg^{II} and Ca^{II} at up to ten times the concentration of cadmium did not interfere. Equal amounts of Al^{III}, Zn^{II} and Fe^{III} interfered. Most interfering ions can be eliminated by pre-separation with an anion-exchange resin.

Sample Analysis

The sensor was applied to the analysis of two flour samples. The relative standard deviation was less than 5.0%. The amounts of cadmium ion measured per gram of flour were 8.0×10^{-9} and 8.5×10^{-9} mol, respectively, which corresponds to the concentrations measured by the spectrophotometric method.

The authors thank the National Natural Science Fund of China for its support of this research.

References

1 Seitz, W. R., *CRC Crit. Rev. Anal. Chem.*, 1988, **19**, 135.
2 Narayanaswamy, R., and Sevilla, F., *Analyst*, 1986, **111**, 1085.
3 Zhang, Z.-J., and Seitz, W. R., *Anal. Chim. Acta*, 1984, **160**, 47.
4 Zhang, Z.-J., Mullin, J. L., and Seitz, W. R., *Anal. Chim. Acta*, 1986, **184**, 251.
5 Narayanaswamy, R., *Biosensors Bioelelectron.*, 1991, **6**, 467.
6 De Oliveira, W. A., and Narayanaswamy, R., *Talanta*, 1992, **39**, 1499.
7 Arnold, M. A., *Anal. Chem.*, 1992, **64**, 1051A.
8 Watanabe, K., and Nakagawa, E., Yamada, H., Hisamoto, H., and Suzuki, K., *Anal. Chem.*, 1993, **65**, 2704.
9 Saari, L. A., and Seitz, W. R., *Anal. Chem.*, 1984, **56**, 810.
10 Zhang, Z.-J., and Seitz, W. R., *Anal. Chim. Acta*, 1985, **171**, 251.
11 Lin, Q.-Z., Si, Z.-Y., and Xu, J.-G., *Huaxue Shiji*, 1988, **10**, 106.

Paper 4/02336F
Received April 20, 1994
Accepted August 19, 1994

Optical Oxygen Sensing Materials Based on the Room-temperature Phosphorescence Intensity Quenching of Immobilized Erythrosin B

Marta Elena Diaz-Garcia, Rosario Pereiro-García and Nieves Velasco-García

Department of Physical and Analytical Chemistry, Faculty of Chemistry, C/Julian Claveria, 8, University of Oviedo, 33006 Oviedo, Spain

The organic dye, Erythrosin B, exhibits strong room-temperature phosphorescence (RTP) when adsorbed on non-ionic resins or when encapsulated in silicone rubber films. In this paper, oxygen transducers based on the RTP intensity quenching of the immobilized dye (on Amberlite XAD-2 or embedded in silicone) have been optically and analytically characterized using continuous and gas-phase flow injection systems. The sensing phases proved to have good photochemical stability. Detection limits of 0.0005% of oxygen in dry argon were found and s_r values of around 0.3% (at 0.02% oxygen level) were achieved. Typical response times were less than 2 s for full signal change and no hysteresis in the response was observed.

Keywords: Room-temperature phosphorescence; oxygen sensing; Erythrosin B; flow injection; quenching

Introduction

Monitoring concentrations of molecular oxygen is of great importance in medical care, *e.g.*, in critical care, assisting in anaesthesiology, in pulmonary examinations, *etc.*[1,2] The development of new techniques and methods to measure molecular oxygen has attracted continuous effort over the last decade. The inherent advantages of optical sensors for oxygen, based on the quenching of the luminescence of appropriate indicators (such as lack of oxygen consumption and inertness against sample flow rates or stirring[3]) have encouraged research in that area. The possibility of being coupled to long fibre optics provides a means for remote-sensing of oxygen.

Polycyclic aromatic hydrocarbons[4,5] and transition metal complexes (especially those with platinum metals[6–9]) are the most commonly used fluorescent indicators for oxygen sensing. The application of the quenching of room-temperature phosphorescence (RTP) by oxygen was first described more than fifty years ago: the detection of traces of oxygen produced in photosynthetic processes and the measurement of the diffusion coefficient of oxygen in acrylics was performed using organic dyes such as, trypaflavine, acridine, safranine or hematoporphyrin adsorbed on silica gel or aluminium oxide.[3,10] Unfortunately, most dyes are photolabile, and traces of water interfere strongly.[3,10,11] Recently, the use of RTP metal chelates like Pd^{II}- [or Pt^{II}-] coprophorphyrins in solution, or immobilized on polymer films,[12,13] the platinum dimer tetrakis(pyrophosphito) diplatinate(II) embedded in silicone,[14] and 8-hydroxy-7-iodo-5-quinolinesulfonic acid (ferron) chelates of some transition metals retained on anion-exchange resin beads[15] have been proposed for oxygen sensing. In principle, RTP quenching based oxygen sensors offer several advantages over fluorescent ones. Most of these advantages arise from the longer excited-state lifetimes of phosphorescent reagents, which give rise to high-quenching effectiveness by oxygen, and to low-noise analytical signals.[16,17] Moreover, the RTP backgrounds from conventional solid supports, where the luminophor is usually immobilized (*e.g.*, organic resins or common polymer films), are negligible. These properties makes the search and characterization of new RTP oxygen sensing phases a field of great research interest.

In this paper, an RTP phase, based on immobilized Erythrosin B, is proposed for the optical sensing of oxygen. Non-ionic resin beads of Amberlite XAD-2 and silicone membranes have been studied as dye solid supports. Optimization and optical characterization of the sensing phases is described, the effect of water as a quencher of the RTP emission and the sensor's analytical performance for gaseous mixtures is evaluated using continuous flow and flow injection (FI) systems. In this last case, gas samples are transiently introduced into the flow system with a gas exponential dilution manifold.[18]

Experimental

Materials

The selected reagent, Erythrosin B, was provided by Carlo Erba (Milan, Italy) and was used without further purification. The non-ionic polymeric adsorbent Amberlite XAD-2 (20–60 mesh) (Sigma, St. Louis, MO, USA) was used as the dye solid support. The Amberlite impurities were removed by washing the resin first with ethanol, in order to displace air from the pores of the resin and to remove residual monomers and solvents, and then with de-ionized water. The washed resins were dried at 120 °C for 3 h. Lower mesh particle sizes (200–400 mesh) were prepared in the laboratory by applying crushing and sieving procedures to the commercial resin.

Silicone rubber (Silicex, Silicona Hispania SA) used was a clear rubber without a filler, such as silica. Air, argon, oxygen, carbon dioxide, nitrogen and helium, all with purity higher than 99.995%, were purchased from Sociedad Española del Oxígeno. All other chemicals were of analytical-reagent grade.

Preparation of the Oxygen-sensing Beads and the Sensing Films

Impregnated resins (active phases) with different concentrations of adsorbed reagent were prepared by immersing 0.1 g of the dry support in 4 ml of Erythrosin B solution for 10 h, with intermittent stirring. Erythrosin B solutions of different concentrations were prepared by dissolving the appropriate amount of reagent in 100 ml of liquid solution containing 90 ml of ethanol and 10 ml of 0.1 mol l^{-1} acetic acid–sodium acetate buffer solution, at pH 6. To evaluate the exact amount of reagent fixed per gram of support, the dye not adsorbed in the immobilization process was quantified by measuring the fluorescence of the remaining solution. The phosphorescent

sensing beads were washed with de-ionized water, dried at 40 °C, and kept dry until use.

The oxygen sensing films were prepared by either one of the following methods: (*i*) dispensing the sensing beads [Erythrosin B immobilized on small size Amberlite XAD-2 resin particles (200–400 mesh)] in silicone rubber (following a similar procedure to that described previously[15]), (*ii*) mixing the dye (50 μl of 10^{-3} mol l^{-1} solutions of Erythrosin B in ethanol) thoroughly with 0.068 g of silicone rubber, before casting the silicone to make the film.

Instrumentation

All RTP data were collected with a Perkin-Elmer LS 5 luminescence spectrometer, which employs a xenon-pulsed (10 μs half-width, 50 Hz) excitation source and is equipped with a Perkin-Elmer 3600 data station. The delay time was normally set at 0.04 ms and the gate time was 2 ms for RTP measurements. The triplet lifetimes were obtained by using the 'Obey-Decay' application program. To apply this program it is necesssary to set six delay time values. The delay times selected for our studies were: 0.04, 0.06, 0.08, 0.10 0.12 and 0.15 ms.

For some experiments, 20–60 mesh active beads were directly packed on a conventional Hellma (Mullheim, Germany) flow-cell (Model 176.52) as previously described.[15] In the case of experiments with sensing films, the membrane was positioned on a laboratory-made front-surface flow-through cell with an inner volume of about 150 μl. The flow cell, fabricated from Perspex, has a rectangular quartz window to which the sensing membrane is adhered. The design and dimensions of this flow cell, which fitted in the spectrometer sample compartment, are given elsewhere.[15]

The phosphorescence intensities were monitored at 625 nm and/or at 700 nm, with excitation (in all cases) at 550 nm, and all the measurements were made at room temperature (20 ± 2 °C) and 101.325 KPa (1 atm).

Gas Flow Optosensing Manifolds and Procedures of Operation

Fig. 1 illustrates the two optosensing systems for continuous and transient (*i.e.*, discrete) introduction of gas mixtures. For the continuous mode [Fig. 1(*a*)], a steady environment with various concentrations of oxygen was maintained in the flow cell by varying the relative flow rates of compressed oxygen (or pure air, 21.0% O_2) and argon. Two mass flow controllers were used to measure the relative flow rates of oxygen and argon. The total gas flow rate was kept constant at 200 ml min^{-1}. Back diffusion processes in the mixing tee limit the use of this system to air–argon ratios higher than 2% of oxygen.

A transient sample introduction manifold, which can be considered as a gas-phase FI system, was used to lead to the sensor levels of oxygen lower than 2%. In this case, the gas sample is introduced into the gas flow system using an exponential dilution chamber.[18] This device consists of a 140 ml glass vessel, as shown in Fig. 1(*b*), containing a magnetic stirrer to allow gas homogeneity. Samples (air or pure oxygen) are introduced into the vessel (filled with argon) with a Hamilton gas-tight syringe (Teknokroma, Barcelona, Spain), through a septum. The exponential dilution chamber is provided with a three-way stopcock which allows the carrier gas (argon at a flow rate of 200 ml min^{-1}) to pass directly to the sensor or to go through the vessel dragging the sample to the sensing phase. In this second step, an initial concentration, c_o, in the vessel is diluted continuously according to[18]

$$c(t) = c_o \exp(-Ft/V)$$

where $c(t)$ is the concentration at time t; F is the flow rate of the argon carrier gas; t is the time spent after the stopcock was turned, and V is the volume of the vessel. Therefore, this sample introduction system gives rise to the formation of sample plugs which reach the detector with an exponential decay concentration profile.

Results and Discussion

Optical Characteristics of Erythrosin B in Solution and Immobilized on Amberlite XAD-2

Erythrosin B is a tetraiodo-substituted xanthene dye. Solutions of Erythrosin B in ethanol or in aqueous buffers 0.1 mol l^{-1} acetic acid–sodium acetate at pHs ranging from 4.5 to 6.5 proved to be fluorescent but no RTP emissions were observed either in the presence of oxygen or in deoxygenated

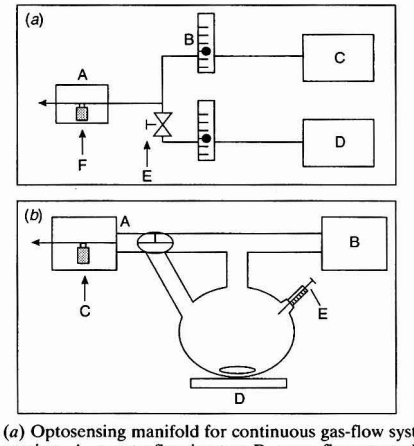

Fig. 1 (*a*) Optosensing manifold for continuous gas-flow system for oxygen sensing. A, spectrofluorimeter; B, mass flow controller; C, argon cylinder; D, air cylinder; E, needle valve; and F, sensor. (*b*) Manifold for gas-flow injection oxygen sensing. A, spectrofluorimeter; B, argon cylinder; C, sensor; D, magnetic stirrer; and E, septum for gasesous sample injection.

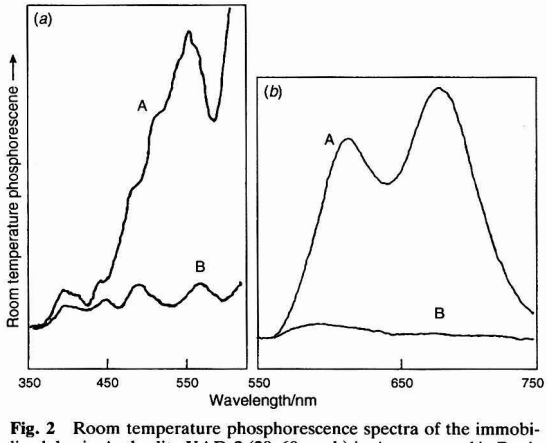

Fig. 2 Room temperature phosphorescence spectra of the immobilized dye in Amberlite XAD-2 (20–60 mesh) in A, argon and in B, air environments. Sensing beads with 6.2×10^{-7} mol Erythrosin B per gram of XAD-2. (*a*) excitation spectrum and (*b*) phosphorescence spectrum.

media (in this latter case, solutions were chemically deoxygenated with 1×10^{-2} mol l^{-1} sodium sulfite).[19] The excitation and the RTP spectra of Erythrosin B immobilized on XAD-2 are recorded in Fig. 2. A delay time of 0.04 ms was used for these experiments to ensure that any fluorescence from the dye and the support had ceased. As can be seen, the excitation spectra obtained in the absence of oxygen (argon environments) has an intense maximum at about 550 nm, while two maxima, at 625 nm and 700 nm, respectively, were observed for the RTP emission spectra. The RTP emission intensity is severely quenched in the presence of air. As can be seen, air environments decrease completely the intensity of both RTP emission bands. The more intense maximum at 700 nm, which has also larger single–triplet splitting, was chosen for most subsequent experiments.

Selection of the Concentration of Erythrosin B Immobilized on the Resin Beads

Sensing beads 20–60 mesh with different concentrations of adsorbed dye, prepared following the procedure described in the Experimental Section, were packed in a conventional flow cell.[15] The RTP emission intensity in the absence of oxygen (I_{Ar}) and the ratios I_{Ar}/A_{air} (I_{air} corresponds to the RTP intensity in air) were measured. Results are shown in Fig. 3. As can be seen, the concentration which provided higher I_{Ar} intensities was 3.6×10^{-7} mol of Erythrosin B per gram of XAD-2. This concentration of reagent adsorbed on the sensing beads was obtained using a 1×10^{-5} mol l^{-1} solution of Erythrosin B in the preparation of the sensing phase. However, insignificant differences in the I_{Ar}/I_{air} ratios were observed for the five types of sensing beads assayed. The resin with higher RTP emission intensities was selected for further work.

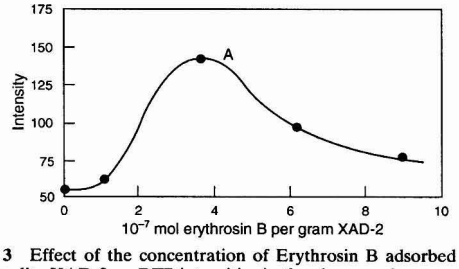

Fig. 3 Effect of the concentration of Erythrosin B adsorbed onto Amberlite XAD-2 on RTP intensities in the absence of oxygen. A = 3.6×10^{-7} mol erythrosin B per gram XAD-2.

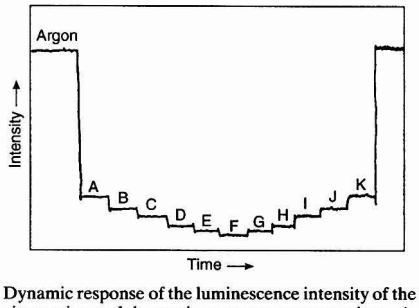

Fig. 4 Dynamic response of the luminescence intensity of the sensing beads to increasing and decreasing oxygen concentrations. A, 1.4; B, 1.7; C, 3.0; D, 4.2; E, 5.7; F, 7.6; G, 5.7; H, 4.2; I, 3.0; J, 1.7; and K, 1.4% O_2.

Performance of the Selected Sensing Beads

It was found that the sensing beads, when packed directly into the flow cell, respond reversibly to the presence of oxygen in gaseous mixtures and that the response time for full signal change was less than 2 s. Also, as shown in Fig. 4, no hysteresis effects were observed. Moreover, the proposed sensing beads proved to be photochemically stable in the presence of both oxygen and argon. No substantial decrease in the RTP intensity of this active phase was observed after more than 30 h of continuous illumination.

The influence of the temperature on the Stern–Volmer responses for oxygen was tested. As expected, the higher the temperature, the poorer the sensitivity. For example, an increase from 20 to 50 °C worsened the oxygen detection limit by 45%. A temperature of 20 °C was maintained for the subsequent experiments.

The effect of some foreign gases on the photochemical characteristics of the proposed sensor was evaluated. The selectivity study was focused on the major air components, nitrogen and carbon dioxide (the latter very important in pulmonary examinations). Light helium was also investigated in order to preclude a possible role of argon as the external heavy atom of the RTP emission of the immobilized dye. Results confirmed that none of these gases produce any effect in the determination of oxygen. In fact, it was observed that even if nitrogen, carbon dioxide or helium were used as carrier gases instead of argon, no influence in the I_o/I ratios for oxygen was observed (the study was performed with 5% oxygen levels).

Analytical performance characteristics of the proposed sensing beads were evaluated. As was stated under Experimental, standard calibration graphs for oxygen concentrations lower than 2% were prepared using an exponential dilution manifold, which gives rise to FI-like signals [see Fig. 5(*a*)]. Calibration graphs, for Stern–Volmer intensity quenching plots are shown in Fig. 5(*b*). The lack of linearity of the plot could be attributed to inhomogeneities of the

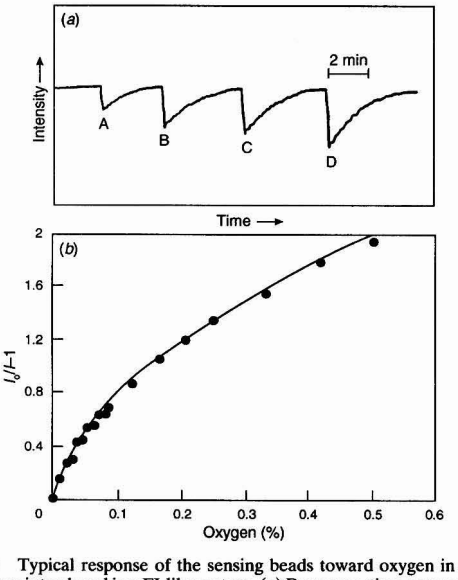

Fig. 5 Typical response of the sensing beads toward oxygen in gas mixtures introduced in a FI-like system. (*a*) Response–time curves. A, 0.008; B, 0.02; C, 0.025; and D, 0.034% O_2. (*b*) Stern–Volmer calibration plot.

environment where the luminophor is immobilized.[7] For the chosen sensing phase, mathematical data treatment showed a linear correlation of $I_o/I - 1$ *versus* the square root of the concentration of oxygen, being the linear regressions higher than 0.9995. The detection limit, estimated as the concentration of oxygen which produced an analytical signal equal to 3 times the relative standard deviation (s_r) of the RTP intensity in argon was 0.0005% (5 ppm) oxygen in argon, and the precision at 0.02% oxygen level for five determinations was ±0.2%.

Triplet lifetimes obtained using the Obey-Decay program are shown in Table 1. As expected, the triplet lifetime decreases both in the presence of oxygen and of moisture.

Effect of Moisture on the RTP Background Intensity and on the Response to Oxygen of the Sensing Beads

It is well known that the RTP emission of many compounds adsorbed in filter paper, cellulose, silica, *etc.*, decreases drastically in the presence of moisture. In these cases, traces of water disrupt the hydrogen bonds between the RTP luminophor and the support.[16,17] In order to evaluate the effect of moisture in our system, a humidifier with pure de-ionized water was placed immediately before the detector. For experiments with sensing beads, results showed that 100% humidity in the gas flow stream decreased the RTP emission intensities observed in the absence of oxygen (Ar environments) by 38%. However, it was found that in the presence of moisture, the sensing beads also respond to oxygen and, interestingly, the slopes of the calibration graphs, I_o/I *versus* the square root of the concentration of oxygen, were a little higher for humidified than for dry gases, *e.g.*, linear plots:

$$I_o/I - 1 = -0.17 + 2.57\ (\%\ O_2)^{\frac{1}{2}}$$ for dry mixtures, and
$$I_o/I - 1 = -0.14 + 2.88\ (\%\ O_2)^{\frac{1}{2}}$$ for humidified gases

were obtained; the linear regressions were 0.9996 and 0.9998, respectively.

The differences in the slopes could be explained by considering that the water contained in the moisturized gases decreased the degree of fixation of the adsorbed dye to the non-ionic resin. This effect makes the RTP emission of the luminophor more sensitive to quenching by oxygen.

Furthermore, it was observed that the sensing beads also respond to oxygen in liquid media (see Fig. 6), as it was demonstrated using a liquid flow system similar to that described previously.[15] For these experiments an aqueous buffer, 0.1 mol l^{-1} acetic acid–sodium acetate at pH 6, was continuously pumped through the system.

Table 1 Triplet lifetimes of immobilized erythrosin B in different environments

Environment	Lifetime/ms	Correlation
Dry argon	0.404 ± 0.002	0.999
Wet argon	0.357 ± 0.003	0.999
Dry argon + 1.26% O_2	0.185 ± 0.010	0.995
Wet argon + 1.26% O_2	0.167 ± 0.010	0.995

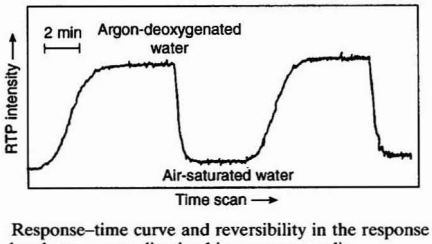

Fig. 6 Response–time curve and reversibility in the response of the sensing beads to oxygen dissolved in aqueous media.

Experiments with Sensing Membranes

The response to oxygen of silicone-sensing membranes prepared under different procedures was evaluated. Fig. 7 shows typical response curves obtained for the gas FI system, using two sensing phases of different thicknesses. The rounded shape of the profiles is indicative of the higher impediments for the oxygen to reach the RTP indicator when sensing membranes are used instead of sensing beads [Fig. 5(*a*)]. Also, as can be seen in Fig. 7, the thicker the membranes the lower the oxygen diffusion processes.

Oxygen detection limits for these membranes were evaluated using the gas FI system and results are collected in Table 2. Table 2 also shows detection limits obtained when using membranes with sensing beads embedded. It can be observed in the latter case that better detection limits are obtained for higher bead density in the silicone membrane.

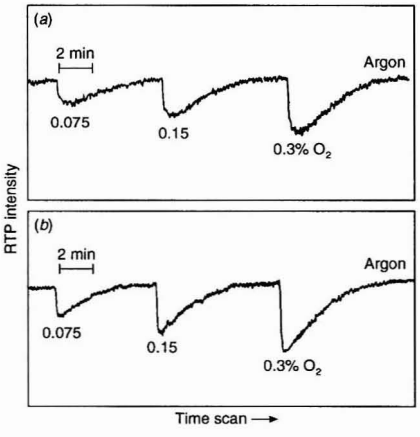

Fig. 7 Response-time signals for the gas FI system using a silicone sensing film of: (*a*) 0.40 mm thickness and (*b*) 0.20 mm thickness.

Table 2 Detection limits and precisions attained for different sensing phases using the gas–FI system

Phase	Detection limits (%)	Precision (%)
Sensing beads (20–60 mesh beads with 3.6×10^{-7} mol adsorbed reagent per gram of XAD-2)	0.0005	±0.3 (at 0.02% O_2)
Sensing films		
(*a*) prepared from a solution of the reagent:		
film 0.20 mm thick	0.0046	±0.4 (at 0.15% O_2)
film 0.40 mm thick	0.0060	±0.4 (at 0.15% O_2)
(*b*) prepared from sensing beads of 200–400 mesh (films of 0.25 mm thickness):		
0.063 g beads per gram of silicone	0.0150	±0.3 (at 0.15% O_2)
0.144 g beads per gram of silicone	0.0085	±0.3 (at 0.15% O_2)

Conclusions

The oxygen sensing phases proposed in the present study offer excellent analytical sensitivities. In fact, the sensing beads prepared by adsorbing Erythrosin B on Amberlite XAD 2 particles give a detection limit for oxygen which is 200 times lower than other RTP sensing phases described for oxygen, which used similar instrumentation.[15] In those studies, negatively charged room-temperature phosphorescent metal chelates were strongly bonded *via* ion-exchange processes to strong anion-exchange resins.[15] A higher degree of immobilization of the indicators bonded by ion-exchange, which make the RTP sensor less susceptible to the presence of quenchers such as oxygen,[1,3] are among the reasons which could account for the lower Stern–Volmer quenching efectiveness observed for the sensing phases with those metal chelates.

These good sensitivities, which could allow the use of minute sensor sizes, along with the long excitation and emission maxima wavelengths (cheap light sources and detectors are available in these regions) open the way for the coupling of the assayed sensing phase to simple instrumentation and to fibre optics for remote oxygen sensing.

Insight into the transduction mechanism of this RTP probe, using triplet lifetime measurements, has also been outlined in studies performed in our laboratory.[20]

The financial support from Fondo de Investigaciones de la Seguridad Social (FISss) Project Ref. 93/0469 is gratefully acknowledged and Dr. A. Sanz-Medel is thanked for helpful discussions.

References

1 Leiner, M. J. P., *Anal. Chim. Acta*, 1991, **255**, 209.
2 Wolfbeis, O. S., and Leiner, M. J. P., *J. Soc. Photo-Opt. Instrum. Eng.*, 1988, **906**, 42.
3 O. S. Wolfbeis, in *Molecular Luminescence Spectroscopy. Methods and Applications: Part 2*, ed. S. G. Schulman, John Wiley, New York, 1988, ch. 3.
4 Peterson, J. I., Fitzgerald, R. V., and Buckhold, D. K., *Anal. Chem.*, 1984, **56**, 62.
5 Optiz, N., Graf, H. J., and Luebbers, D. W., *Sens. Actuators*, 1988, **13**, 159.
6 Wolfbeis, O. S., Weis, L. J., Leiner, M. J. P., and Ziegler, W. E., *Anal. Chem.*, 1988, **60**, 2028.
7 Lippitsch, M. E., Pusterhofer, J., Leiner, M. J. P., and Wolfbeis, O. S., *Anal. Chim. Acta*, 1988, **205**, 1.
8 Sacksteder, L., Demas, J. N., and DeGraff, B. A., *Anal. Chem.*, 1993, **65**, 3480.
9 Li, X. M., Ruan, F. Ch., and Wong, K. Y., *Analyst*, 1993, **118**, 289.
10 Kautsky, H., *Trans. Faraday Soc.*, 1939, **35**, 216.
11 Lee, E. D., Werner, T. C., and Seitz, W. R., *Anal. Chem.*, 1987, **59**, 279.
12 Papkovsky, D. B., *Sens. Actuators, B*, 1993, **11**, 293.
13 Gewehr, P. M., and Delpy, D. T., *Med. Biol. Eng. Comput.*, 1993, **1**, 11.
14 Li, X. M., and Wong, K. Y., *Anal. Chim. Acta*, 1992, **262**, 27.
15 Liu, Y. M., Pereiro-García, R., Valencia-González, M. J., Diaz-García, M. E., and Sanz-Medel, A., *Anal. Chem.*, in the press.
16 Hurtubise, R. J., *Phosphorimetry. Theory, Instrumentation and Applications*, VCH Publishers, New York, 1990, ch. 6.
17 Vo-Dinh, T., *Room Temperature Phosphorimetry for Chemical Analysis*, ed. Elving, P. J., Winefordner, J. D., and Kolthoff, I. M., Wiley, New York, 1984, ch. 4.
18 Lovelock, J. E., *Anal. Chem.*, 1961, **33**, 162.
19 Diaz Garcia, M. E., and Sanz-Medel, A., *Anal. Chem.*, 1986, **58**, 1936.
20 Velasco-García, N., Pereiro García, R., and Diaz-García, M. E., *Spectrochim. Acta Part A*, submitted.

Paper 4/01821D
Received March 28, 1994
Accepted June 28, 1994

Chemiluminescence Determination of Tetracyclines Based on Their Reaction With Hydrogen Peroxide Catalysed by the Copper Ion

X. R. Zhang, W. R. G. Baeyens, A. Van den Borre and G. Van der Weken

University of Ghent, Faculty of Pharmaceutical Sciences, Department of Pharmaceutical Analysis, Laboratory of Drug Quality Control, Harelbekestraat 72, B-9000 Ghent, Belgium

A. C. Calokerinos

University of Athens, Chemistry Department, Laboratory of Analytical Chemistry, Panepistimiopolis 157 71, Athens, Greece

S. G. Schulman

University of Florida, College of Pharmacy (Box J-485), Medicinal Chemistry, J. Hillis Miller Health Center, Gainesville 32610, Florida, USA

A flow injection-based method for the determination of tetracycline, chlortetracycline and oxytetracycline has been proposed. It is based on the reaction of the tetracyclines with hydrogen peroxide, catalysed by the copper ion in ammonia medium. Persulfate was used as a co-oxidizing agent. The procedure allows the determination of 0.025–2.5 nmol of chlortetracycline and 0.25–25 nmol of tetracycline and oxytetracycline (50 μl per injection) by the flow-injection method compared with 0.005–50 μmol l^{-1} of chlortetracycline and 0.05–500 μmol l^{-1} of tetracycline and oxytetracycline by the classical batch method. The method is sensitive, selective and easy to operate and can be used for the determination of tetracyclines in pharmaceutical preparations. A discussion on the possible reaction mechanism is presented.

Keywords: Chemiluminescence; tetracycline; flow injection; pharmaceutical analysis

Introduction

Tetracyclines are broad-spectrum antibiotics, which possess a hydronaphthacene skeleton with a wide variety of functional groups. They are commonly used in veterinary medicine, animal nutrition and feed additives.

Tetracyclines are determined mainly by microbiological,[1] chromatographic,[2–4] spectrophotometric,[5–8] spectrofluorimetric[9,10] and electrochemical[11] procedures. The disadvantages of microbiological assays are long incubation periods, lack of precision and low specificity, although the assays are relatively sensitive. Direct spectrophotometric methods are simple, but not very sensitive and often suffer from interferences from other materials. The remaining methods are more sensitive, but need elaborate instrumentation.

Chemiluminescent methods have already been used successfully for the determination of tetracyclines. Most systems involve the reaction of bromine or bromine-containing compounds. The first direct chemiluminescent method, described in the literature, was based on the reaction of 1,3-dibromo-5,5- dimethylhydantoin.[12] The use of bromine as an oxidizing agent has also been cited.[13] Halvatzis *et al.*[14] proposed a more sensitive method using *N*-bromosuccinimide, allowing a 5.0 ng l^{-1} detection limit for tetracycline (**1**), which is quite sensitive. Chlortetracycline (**2**) and oxytetracycline (**3**) detection limits, however, (200 and 500 ng ml^{-1}, respectively) still need to be improved. (The structures of **1**, **2** and **3** are given below.) Hexacyanoferrate and lucigenin are also used for tetracycline determinations.[15]

In this paper, a flow-injection (FI) method is described for the determination of **1**, **2** and **3** based on oxidation with hydrogen peroxide, catalysed by the copper(II) ion in ammonia medium using persulfate as a co-oxidizing agent. Compounds **1**, **2** and **3** showed chemiluminescence following the above procedure; **2** could be determined more sensitively than **1** and **3**. The investigation also showed different degradation speeds for the various tetracyclines. Compound **1** reacted more slowly than **2** and **3**, owing to the substituted chloro- and

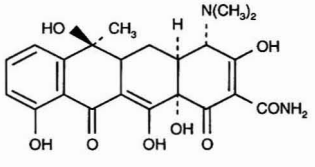

1

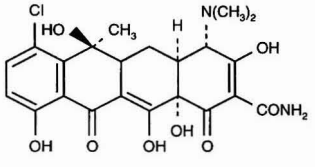

2

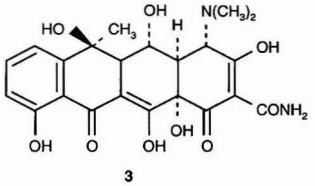

3

hydrogen-groups in the latter molecules which lead to accelerated reactions.

Experimental

Reagents

All the chemicals were of analytical-reagent or reagent grade and the solutions were prepared with distilled, de-ionized water.

Tetracycline hydrochloride (Pfizer Corporation, Brussels, Belgium), oxytetracycline hydrochloride (Pfizer Corporation, Brussels, Belgium), chlortetracycline hydrochloride (Janssen Chimica, Geel, Belgium), copper(II) sulfate pentahydrate ($CuSO_4 \cdot 5H_2O$, Merck, Darmstadt, Germany), ammonium carbonate (Janssen Chimica, Brussels, Belgium), potassium persulfate ($K_2S_2O_8$, UCB, Brussels, Belgium), hydrogen peroxide (30% H_2O_2, Merck, Darmstadt, Germany), tetrasodiumdiphosphate decahydrate $Na_4P_2O_7 \cdot 10H_2O$ (Merck, Darmstadt, Germany) were used.

Solutions

A 5 mmol l^{-1} Cu^{2+} solution [from copper(II)sulfate] was prepared in 50 mmol l^{-1} ammonium carbonate medium at pH 9 to obtain the $Cu(NH_3)_4^{2+}$ complex. $K_2S_2O_8$ (0.1 mol l^{-1}) and $Na_4P_2O_7$ (0.1 mol l^{-1}) were prepared by dissolving the chemicals in water. Hydrogen peroxide (0.01 mol l^{-1}) solution was freshly prepared by cautious dilution of the 30% (m/m) H_2O_2 solution with water.

Stock solutions of **1**, **2** and **3** were made by dissolving each tetracycline in water.

The injection sample was prepared by the subsequent addition of 2.0 ml of 0.01 mol l^{-1} H_2O_2, 10 ml of 0.1 mol l^{-1} $K_2S_2O_8$ and of 0.5 ml of 0.1 mol l^{-1} $Na_4P_2O_7$ to different concentrations of the tetracycline under investigation, followed by dilution with water to 20 ml.

Procedure

Flow injection was applied to the determination of the tetracyclines. Therefore, the sample was injected (injection volume: 50 μl) into a carrier stream, containing only de-ionized water, and mixed with the reagent stream [$Cu(NH_3)_4^{2+}$] in a T-piece (Fig. 1). The reaction takes place after mixing and the light is measured in the chemiluminescence detection cell. The signal is displayed on the computer screen *via* a photomultiplier tube.

The FI instrumentation used in the present work consisted of two high-performance liquid chromatography (HPLC) pumps (Waters Chromatography Division, Milford, PN, USA), a chemiluminescence detector (Luminometer 1250, Bio-orbit Oy, Turku, Finland), and an IBM-compatible computer (PC-systems, Lokeren, Belgium) with a 1250 Luminometer Program (Bio-orbit Oy, Turku, Finland).

An off-line batch method was used to determine the speed of the chemiluminescent reaction. Therefore, 0.5 ml of the analyte solution is pipetted into the chemiluminescence cell, which is positioned in the cell holder of the luminometer. The cell is rotated into the measuring position, 0.25 ml of oxidizing solution and 0.50 ml of the Cu^{2+}-solution are injected consecutively and the signal is measured.

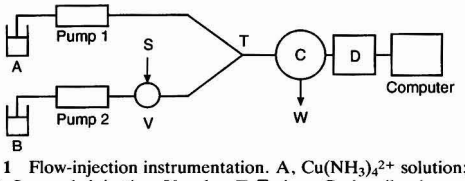

Fig. 1 Flow-injection instrumentation. A, $Cu(NH_3)_4^{2+}$ solution; B, H_2O; S, sample injection; V, valve; T, T-piece; C, chemiluminescence cell; W, waste; and D, detector.

Results and Discussion

Optimization

The optimum conditions for the tetracycline determination were examined by injecting analyte samples of 50 μl into the carrier stream, the flow rates of both streams (pumps 1 and 2) were 1 ml min^{-1}. Preliminary work indicated that the use of $Cu(NH_3)_4^{2+}$ gave highest chemiluminescence signals, when compared with other metal ions such as Co^{II}, Cr^{III} and Fe^{III}, which all are strong catalysts for several chemiluminescent reactions involving hydrogen peroxide. The relative signals from Co^{II} and Fe^{III} were 8 and 9 while Mn^{II} and Cr^{III} did not have any effect. Therefore this reagent system was chosen for the present investigation. Initially, the effect of the Cu^{2+}-solution was examined; optimum intensity was obtained at a concentration of 5 mmol l^{-1}. For the ammonium carbonate solution, the optimum intensity was at 50 mmol l^{-1} at a pH of 9 (Fig. 2).

The optimum H_2O_2 concentration in the sample solutions was 1 mmol l^{-1}. Persulfate was added as a co-oxidizer. The chemiluminescence signal increased with increasing concentrations of the latter, a 50 mmol l^{-1} solution being finally chosen because of solubility limitations.

Next, the effect of the flow rate was studied. After mixing the **1**, **2** and **3** solutions with the H_2O_2 and $K_2S_2O_8$ reagents and standing for some time (35, 5 and 0 min, for **1**, **2** and **3**, respectively) causing the conversion of the tetracycline into an intermediate compound, the solutions were injected *via* the valve into the system and the chemiluminescence signals were detected by the FI instrument (Fig. 1). Equal flow rates for each channel were used, ranging from 0.75 to 1.50 ml min^{-1}. The signal increased with increasing flow rates. The reason for this is that the chemiluminescence reaction of H_2O_2 with the degraded intermediate, catalysed by the copper ion, is rapid. The time needed to reach a maximum signal after mixing, is 1.8 for **1**, 2.4 for **2** and 4.2 s for **3**. Fig. 3 shows the relation between flow speed and the intensity of **1** under the optimized reagent conditions. The reaction involves two steps, the first being the oxidation of **1** to the intermediate by H_2O_2 and $K_2S_2O_8$, which occurs very slowly (about 35 min is needed). The second step involves the chemiluminescent reaction of the copper ion catalysing the reaction of the **1**-intermediate with H_2O_2 and $K_2S_2O_8$ and proceeds quickly; only a few seconds are required.

Measurement of Chemiluminescence Signals

After mixing solutions **1**, **2** or **3** with the H_2O_2- and $K_2S_2O_8$-reagents, the mixture needs to be allowed to stand to

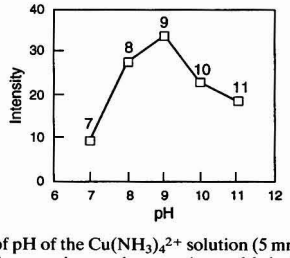

Fig. 2 Effect of pH of the $Cu(NH_3)_4^{2+}$ solution (5 mmol l^{-1} of Cu^{2+}, 50 mmol l^{-1} of ammonium carbonate, 1 mmol l^{-1} of H_2O_2 and 0.2 mmol l^{-1} of $K_2S_2O_8$) on the chemiluminescence of **1** (50 μl per injection).

attain stable chemiluminescence signals; for **1** this standing time is 35 min, for **2** 5 min, whilst **3** reaches its maximum emission immediately after mixing, followed by a decrease. The amplitude of the increase in signal is different for the three compounds: for **2** an increase of about 24% is noticed, the **3** signal remains unchanged whilst the signal for **1** is about five-fold higher at its maximum. Measurements were carried out immediately after mixing the tetracycline solution with the oxidizing solution.

Calibration Graphs

The calibration graphs obtained using the proposed FI and batch methods under the optimized conditions were established. Table 1 shows linear ranges, regression equations and limits of detection for the three tetracyclines. The correlation coefficients from the FI method are more than satisfactory in comparison to average chemiluminescence calibrating methods.

Interference Studies

Effect of metal ions

In this experiment, the effect of some metal ions on the chemiluminescence was studied using a 5 μmol l^{-1} solution of **1**. Several metal ions were added to a concentration of 50 μmol l^{-1}. The effect of ethylenediaminetetraacetic acid (EDTA) was examined as well as it may be possible to exploit its complexing properties towards metal ions. Table 2 shows the effect of some metal ions on the chemiluminescence signal obtained from **1**. Only Mn^{2+} provides significant interference with the emission; this interference, however, can be masked by the addition of EDTA at the optimum reagent conditions of pH 9.

Effect of some pharmaceutical additives

The influence of some frequently used pharmaceutical adjuvants upon the chemiluminescence was studied using a 10 μg ml^{-1} solution of **1**; the pharmaceutical components were added to the sample in a theoretical concentration corresponding to 100 μg ml^{-1} in the solution to be analysed, taking into account the solubility limitations of cellulose and of magnesium stearate. As can be seen from Table 3, negligible interference was observed.

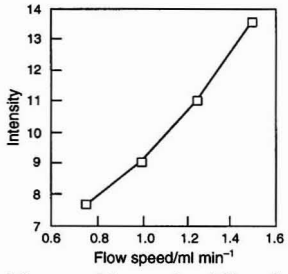

Fig. 3 Effect of flow speed (pumps 1 and 2) on the chemiluminescence of **1** under optimum reagent conditions.

Applications

The proposed method was applied to the determination of tetracyclines in a pharmaceutical dosage form. The results are shown in Table 4. As can be seen, there are no significant differences between the labelled values and those obtained by the suggested method. In order to evaluate the validity of the proposed method for the determination of tetracyclines in pharmaceuticals, recovery studies were carried out on samples to which known amounts of tetracycline standards were added. Recovery values of greater than 95% were found.

Possible Chemiluminescence Mechanism of Tetracyclines on Peroxide Treatment

In order to obtain more information on the chemiliminescence of the tetracyclines under investigation, measurements of chemiluminescence were performed in parallel with spectrophotometry. A solution of **1** (20 μmol l^{-1}) was prepared following the proposed method, and at various times after preparation, the ultraviolet (UV) spectrum was compared with the chemiluminescence results, so as to obtain information about structural changes. To accelerate the reaction rate,

Table 2 Effect of some metal ions and of EDTA on the chemiluminescence of **1**

Metal ion added	Relative signal (%)
none	100
Al^{3+}	97
Ca^{2+}	103
Mg^{2+}	104
Mn^{2+}	58
Zn^{2+}	98
(EDTA	102)

Table 3 Effect of some pharmaceutical additives on the chemiluminescence of **1**

Added compound	Relative signal (%)
None	100
Cellulose	100
Galactose	104
Magnesium stearate	104
Poly(ethylene glycol)	96
Saccharose	100

Table 1 Calibration graphs, regression equations and detection limits for tetracycline, chlortetracycline and oxytetracycline

	Tetracycline	Chlortetracycline	Oxytetracycline
Linear range—			
FI method (50 μl sample)	0.25–25 nmol	25–2500 pmol	0.25–25 nmol
Batch method	0.05–50 μmol l^{-1}	0.005–50 μmol l^{-1}	0.05–50 μmol l^{-1}
Regression—			
FI method	$I = 0.0878\,C + 0.1526$ $r = 0.9987$	$I = 0.5791\,C + 0.7155$ $r = 0.9999$	$I = 0.0341\,C - 0.1236$ $r = 0.9976$
Batch method	$I = 0.4236\,C + 0.0749$ $r = 0.9998$	$I = 10.195\,C - 0.1164$ $r = 0.9991$	$I = 1.234\,C - 1.969$ $r = 0.9996$
Detection limit—			
FI method (50 μl sample)	0.1 nmol	10 pmol	0.1 nmol
Batch method	0.01 nmol	1.0 pmol	0.01 nmol

Table 4 Determination of tetracyclines in pharmaceutical preparations by the chemiluminescent reaction with the hydrogen peroxide–Cu^{II} system

Sample	Amount/mg				
	Label	Found ± s*	Added/mg	Recovered/mg	Recovery (%)
Hostacycline (containing **1**)	500	521.7 ± 24.3	500	999.9	100.0
			1000	1585.3	105.7
Terramycine (containing **3**)	100	104.0 ± 4.9	100	205.9	103.0
			200	315.1	105.0

* s = Standard deviation; n = 0.

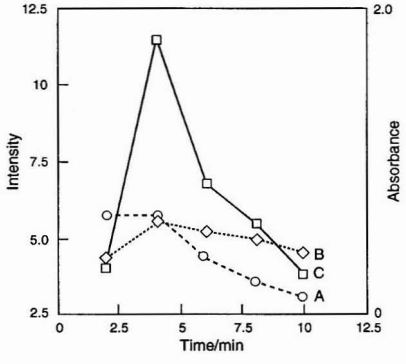

Fig. 4 Chemiluminescence intensity and UV absorbance of **1** *versus* incubation time at 60 °C. A, UV absorbance at 267.6 nm; B, UV absorbance at 238.5 nm; C, chemiluminescence.

a temperature of 60 °C was chosen for the studies recommended in ref. 14. The results are given in Fig. 4.

On comparing UV and chemiluminescence results, a two-step reaction mechanism may be suggested. First, **1** is converted into its iso- or anhydro-derivatives which are fluorescent compounds[15,16] and responsible for the chemiluminescence reaction;[14] next, by reaction with strong oxidizing agents such as H_2O_2 and $K_2S_2O_8$, the tetracycline skeleton is broken and chemiluminescence takes place. Since Cu^{2+} is a catalyst, the reaction is accelerated by its addition.

Immediately after mixing **1** with H_2O_2 and $K_2S_2O_8$, the first conversion step of **1** to its iso- or anhydro-derivative apparently does not take place, as a result of which chemiluminescence is low. With time, conversion occurs and chemiluminescence starts to increase, providing a chemiluminescence maximum when all of the **1** has been converted into the degraded intermediates. The UV absorption at 238.5 nm, which will vary with the degradation of the structure of **1** into the intermediate, starts to increase during the mixing of **1** with H_2O_2 and $K_2S_2O_8$. The absorbance at 267.6, which was assumed to respond to changes in the tetracycline-skeleton only, remains unchanged. This assumption is based on the fact that the **1**, **2** and **3** tetracyclines with similar skeletons show a similar maximum in the UV spectrum at around 267 nm; no similar UV absorption at about 238 nm is observed for **2** and **3** since these molecules bear different functional groups. When all the **1** has been converted into the intermediate, the reaction of **1** with H_2O_2 and $K_2S_2O_8$ will still slowly take place. The skeleton of **1** starts to break owing to oxidation by the latter reagents even in the absence of a catalyst. On increase of the broken structure and decrease of the degraded structure, the chemiluminescence starts to decrease. At this point, owing to a serious structural conversion, both absorption wavelengths change.

For **2** and **3**, the chemiluminescence mechanism is expected to be similar. With both molecules, the cited steps appear quite rapidly, especially for **3**, almost immediately after mixing. It is assumed that substitution with Cl-groups (**2**) or with OH-groups (**3**) produces a chemiluminescence accelerating effect. Further research needs to be performed in order to elucidate the exact reaction mechanism.

Conclusion

The proposed method for the determination of tetracyclines is sensitive, selective and precise, offering satisfactory linear ranges. The procedure allows the determination of the three tetracyclines in pharmaceutical products. Owing to the application of an FI procedure, the method is simple and the speed of determination is high. The system should be easily combined with an HPLC set-up and this is to be the subject of further investigations.

S. Croubels from the Laboratory of Food Analysis (Faculty of Pharmaceutical Sciences) of the University of Ghent is gratefully acknowledged for helpful discussions and for providing specific chemicals.

References

1 *Antibiotic Residues in Milk, Dairy Products and Animal Tissues: Methods, Reports and Protocols*, National Centre for Antibiotic and Insulin Analysis, Food and Drug Administration, Department of Health, Education and Welfare, Washington, DC, 1968.
2 Oka, H., Uno, K., Harada, K. I., Yasaka, K., and Suzuki, M., *J. Chromatogr.*, 1984, **298**, 435.
3 Hasan, T., and Cooperman, B. S., *J. Chromatogr.*, 1985, **321**, 462.
4 Ragazzi, E., and Veronese, G., *J. Chromatogr.*, 1977, **134**, 223.
5 Salinas, F., Berzas Nevado, J. J., and Espinosa, A., *Analyst*, 1989, **114**, 1141.
6 Mahrous, M. S., and Abdel-Khalek, M. M., *Talanta*, 1984, **31**, 289.
7 Sultan, S. M., Al Zamil I. Z., and Alarfaj, N. A., *Talanta*, 1988, **35**, 375.
8 Saha, U., *J. Assoc. Off. Anal. Chem.*, 1987, **70**, 686.
9 Salinas, F., Munoz de la Pena, A., and Duran Meras, I., *Anal. Lett.*, 1990, **23**, 863.
10 Poiger, H., and Schlatter, Ch., *Analyst*, 1976, **101**, 808.
11 Ghandour, M. A., and Ali, A. M. M., *Anal. Lett.*, 1991, **24**, 2171.
12 Owa, T., Masjujima, T., Yoshida, H., and Imai, H., *Bunseki Kagaku*, 1984, **33**, 570.
13 Alwarthan, A. A., and Townshend, A., *Anal. Chim. Acta*, 1988, **205**, 261.
14 Halvatzis, S. A., Timotheou-Potamia, M. M., and Calokerinos, A. C., *Analyst*, 1993, **118**, 633.
15 *Analytical Profiles of Drug Substances*, ed. Florey, K., Academic Press, Orlando, 1984, vol. 13.
16 Waller, C. W., Hutchings, B. L., Wolf, C. F., Goldman, A. A., Broschard, R. W., and Williams, J. H., *J. Am. Chem. Soc.*, 1952, **74**, 4981.

Paper 4/03486D
Received June 9, 1994
Accepted September 28, 1994

Sensitized Determination of Sulfite Using Flow Injection With Chemiluminescent Detection

David A. Paulls and Alan Townshend*
School of Chemistry, University of Hull, Hull, UK HU6 7RX

The acidic oxidation of sulfite by Ce^{IV} is weakly chemiluminescent. A comparative study of the chemiluminescent determination of sulfite with the use of 3-cyclohexylaminopropanesulfonic acid (CAPS) and of cyclooctylamine as sensitizers of the reaction was made using a flow injection procedure. Despite a slight decrease in sensitivity, it was found that cyclooctylamine was superior to CAPS as a sensitizer and a detection limit of 5.4×10^{-7} mol l^{-1} sulfite was achieved compared with 1×10^{-5} mol l^{-1} using CAPS.

Keywords: *Chemiluminescence; sulfite; flow injection; 3-cyclohexylaminopropanesulfonic acid; cyclooctylamine*

Introduction

Because of their cheapness, efficiency and versatility, sulfur dioxide and sulfite are extensively used in industry. Sulfite is used as an antioxidant in the pharmaceutical and food industries, an inhibitor of yeasts and bacteria in the wine industry, a reducing agent in bleaching, an oxygen scavenger in water for steam generation, in the production of paper pulp and in the treatment of sulfide ores. Sulfur dioxide is also a major air pollutant, believed to be responsible for acidifying soil and water due to acid rain. Human exposure to sulfite is on the increase and concern has arisen that at high levels sulfite exposure can have toxic effects.

There are many methods available for the determination of SO_2 in the atmosphere, but all suffer from either lack of sensitivity at ambient levels, lack of specificity, use of mercury or its salts, instrumental and procedural complications or long response times. In 1975, Stauff and Jaeschke[1] published a method for measuring SO_2 using chemiluminescence. They found that the oxidation of sulfite with potassium permanganate, cerium(IV) sulfate or hydrogen peroxide was accompanied by chemiluminescence.

Yamada *et al.*[2] greatly simplified the existing instrumentation by constructing a system that combined flow injection with chemiluminescence detection. The addition of riboflavin phosphate as a sensitizer of the reaction also enabled conventional detection equipment to be used as opposed to the photon-counting device that had been used by Stauff and Jaeschke.

Dilute solutions of sulfite are unstable and are readily oxidized by air. However, various compounds can be added to the solutions that will stabilize the sulfite, *e.g.*, potassium tetrachloromercurate(II) and carbonyl compounds. In an attempt to stabilize sulfite solutions, Wheatley and co-workers[3,4] added cyclohexanone, chosen as a typical carbonyl compound, to the sulfite–permanganate system. They found that at the concentrations recommended for sulfite stabilization the emission intensity was diminished but, at lower concentrations, the intensity was more than doubled. Further, they found that other carbonyl compounds (*p*-benzoquinone, acetone and acetaldehyde) diminished the intensity at all concentrations. Several other cyclohexyl derivatives were investigated as possible sensitizers. 3-Cyclohexylaminopropanesulfonic acid (CAPS), cyclohexanecarboxylic acid, cyclohexylamine, cyclohexanol, 2-methylcyclohexanone and cyclohexane-1,4-diol all gave enhancements to various extents, whereas 1,2-diaminocyclohexanetetraacetic acid did not. This study was expanded by Koukli *et al.*,[5] who successfully used CAPS, 2-cyclohexylaminoethanesulfonic acid (CHES) and 3-cyclohexylamino-2-hydroxypropane-1-sulfonic acid (CAPSO) to sensitize the oxidation of sulfite by cerium(IV). In both studies, CAPS was found to be the most effective sensitizer.

CAPS is non-fluorescent and therefore cannot be excited, like riboflavin phosphate, by energy transfer but, although the sensitizing action of these types of compounds is unclear, this phenomenon has been exploited not only for the determination of SO_2 and sulfite, but also for the determination of corticosteroids, steroids and sodium cyclamate.[6–8]

During a study of the sensitizing nature of CAPS, it was found that cyclooctylamine acted as a far superior sensitizer of the chemiluminescent oxidation of sulfite. In this paper, a comparison between the two sensitizers is presented. An explanation of the sensitizing nature of CAPS and other cycloalkyl-containing compounds will be presented at a later date.

Experimental

Instrumentation

The flow manifold used (Fig. 1) consisted of a peristaltic pump (Gilson Minipuls 3), which continuously pumped the oxidant and sensitizer solutions at equal flow rates (1.4 ml min^{-1}) through PTFE flow lines (0.5 mm i.d.). The pump tubing was grey/grey PharMed tubing (1.3 mm i.d.). The two solutions were mixed at a PTFE T-piece just before the flow coil, which was glass (0.8 mm i.d.) coiled to a diameter of 18 mm. The mixing piece, flow coil and photomultiplier tube (Thorn-EMI 9844 B) were within a light-tight aluminium housing. Samples of 25 μl of sodium sulfite were injected into the sensitizer stream using a low-pressure rotary injection valve (Rheodyne Model 5020). The signal was recorded on a chart recorder (Chessell BD 40 04).

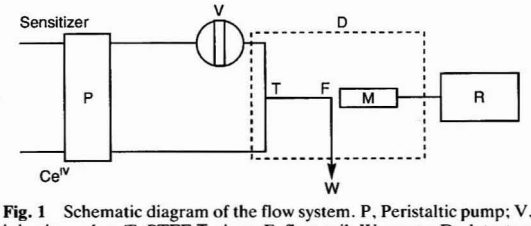

Fig. 1 Schematic diagram of the flow system. P, Peristaltic pump; V, injection valve; T, PTFE T-piece; F, flow coil; W, waste; D, detector; M, photomultiplier tube; and R, recorder.

* To whom correspondence should be addressed.

Reagents

Cerium(IV) sulfate solution (0.1 mol l^{-1}, AnalaR) was purchased from BDH (now Merck) and diluted to the required volume with 0.1 mol l^{-1} H_2SO_4 (analytical-reagent grade; Rhône-Poulenc). Sulfite solutions were prepared daily by dissolving the required amount of anhydrous sodium sulfite (AnalaR; BDH) in distilled water. CAPS and cyclooctylamine were purchased from Aldrich.

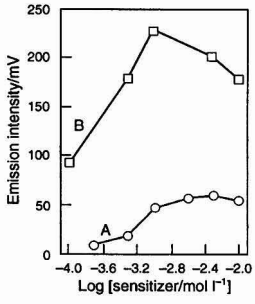

Fig. 2 Effect of sensitizer concentration on the emission intensity. A, CAPS sensitized. Conditions: 1×10^{-3} mol l^{-1} sulfite, 3×10^{-4} mol l^{-1} Ce^{IV} in 0.1 mol l^{-1} H_2SO_4, total flow rate 2.8 ml min^{-1}. B, Cyclooctylamine sensitized. Conditions: 1×10^{-3} mol l^{-1} sulfite, 4×10^{-4} mol l^{-1} Ce^{IV} in 0.1 mol l^{-1} H_2SO_4, total flow rate 2.8 ml min^{-1}.

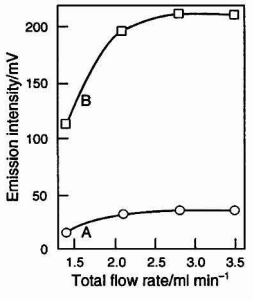

Fig. 3 Effect of flow rate on the emission intensity. A, CAPS sensitized. Conditions: 1×10^{-3} mol l^{-1} sulfite, 3×10^{-4} mol l^{-1} Ce^{IV} in 0.1 mol l^{-1} H_2SO_4, 5×10^{-3} mol l^{-1} CAPS. B, Cyclooctylamine sensitized. Conditions: 1×10^{-3} mol l^{-1} sulfite, 4×10^{-4} mol l^{-1} Ce^{IV} in 0.1 mol l^{-1} H_2SO_4, and 1×10^{-3} mol l^{-1} cyclooctylamine.

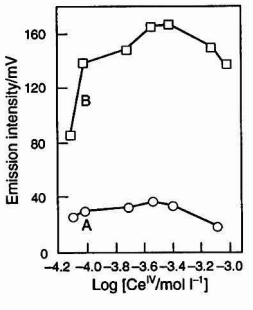

Fig. 4 Effect of cerium(IV) concentration on the emission intensity. A, CAPS sensitized. Conditions: 1×10^{-3} mol l^{-1} sulfite, 1×10^{-3} mol l^{-1} CAPS, total flow rate 2.8 ml min^{-1}. B, Cyclooctylamine sensitized. Conditions: 1×10^{-3} mol l^{-1} sulfite, 1×10^{-3} mol l^{-1} cyclooctylamine, total flow rate 2.8 ml min^{-1}.

Results and Discussion

Early investigations into the sensitizing nature of CAPS revealed that the cycloalkyl group was responsible for the sensitization and that the emission intensity increased with increasing ring size of the cycloalkyl group. The greatest emission was observed when cyclooctylamine was used as a sensitizer. It was decided to conduct a comparative study between CAPS and cyclooctylamine in order to determine whether it would be advantageous to use cyclooctylamine instead of CAPS in the chemiluminescent determination of sulfite.

The effect of CAPS and cyclooctylamine concentration on the emission intensity of the oxidation of sulfite is shown in Fig. 2. With cyclooctylamine the emission intensity increased to a maximum with increasing cyclooctylamine concentration up to 1×10^{-3} mol l^{-1} and then decreased, whereas with CAPS, the peak height reached a maximum at a concentration of approximately 5×10^{-3} mol l^{-1} and then became constant. The oxidation of sulfite by Ce^{IV} is a relatively fast reaction (<1 s)[9] and, in accordance with such a reaction, it was found that as the flow rate increased the emission intensity reached a constant level (Fig. 3). In both instances a total flow rate of 2.8 ml min^{-1} (1.4 ml min^{-1} for each channel) was chosen as an optimum. This gave the greatest emission intensity with the least consumption of reagents. As with many chemiluminescent reactions, the concentration of oxidant has a significant effect on emission intensity. The effects of Ce^{IV} concentration on the sensitized reactions are shown in Fig. 4. The optimum concentrations of Ce^{IV} were almost identical, 3×10^{-4} and 4×10^{-4} mol l^{-1} for the CAPS- and cyclooctylamine-sensitized reactions, respectively. Above these concentrations the emission intensity decreased, in part owing to the cerium absorbing the emitted light.

Using the optimum conditions for each sensitized reaction (summarized in Table 1), calibration graphs were obtained for sulfite. The analytical characteristics of the graphs are summarized in Table 2. Although there is a slight decrease in sensitivity for cyclooctylamine, as shown by the slopes of the log–log plots, a substantial decrease in detection limit is obtained. This occurs because CAPS is relatively less effective than cycloctylamine at lower sulfite concentrations. Thus the cyclooctylamine system approximates closely to a first-order reaction in sulfite producing the luminescence, but the

Table 1 Optimum conditions for the determination of sulfite using CAPS and cyclooctylamine as sensitizers

	Sensitizer	
Parameter	CAPS	Cyclooctylamine
Flow rate/ml min^{-1}	2.8	2.8
$[Ce^{IV}]$/mol l^{-1}	3×10^{-4}	4×10^{-4}
[Sensitizer]/mol l^{-1}	5×10^{-3}	1×10^{-3}

Table 2 Analytical characteristics of sulfite in the presence of CAPS and cyclooctylamine

Parameter	With CAPS	With cyclooctylamine
Limit of detection*/mol l^{-1}	1.0×10^{-5}	5.4×10^{-7}
Linear range/mol l^{-1}	1×10^{-5}–1×10^{-3}	5.4×10^{-7}–1×10^{-4}
Intercept/log mV	5.33	5.46
Slope	1.28	1.04
r ($n = 6$)	0.998	0.998

* Signal-to-noise ratio = 3.

suppressed emission at lower sulfite concentration in the presence of CAPS causes a greater calibration slope and thus a greater apparent reaction order. There is also a decrease in the relative standard deviation (s_r). The standard deviations for six determinations of 1×10^{-4} mol l^{-1} sulfite were 0.01 mV (s_r, 4.4%) and 0.06 mV (s_r, 2.8%) for the CAPS- and cyclooctylamine-sensitized reactions, respectively.

In conclusion, it is clear that cyclooctylamine has several advantages over CAPS as a sensitizer for the chemiluminescent determination of sulfite. Less sensitizer is required to give a greater emission intensity. The limit of detection has decreased from 1×10^{-5} mol l^{-1} sulfite for CAPS to 7.4×10^{-7} mol l^{-1} and a better relative standard deviation has been achieved (2.8% for 1×10^{-4} mol l^{-1} sulfite, $n = 6$).

The authors thank the School of Chemistry, University of Hull, for funding this study.

References

1 Stauff, J., and Jaeschke, W., *Atmos. Environ.*, 1975, **9**, 1038.
2 Yamada, M., Nakada, T., and Suzuki, S., *Anal. Chim. Acta*, 1983, **147**, 401.
3 Wheatley, A. R., *PhD Thesis*, University of Hull, 1983.
4 Al-Tamrah, S. A., Townshend, A., and Wheatley, A. R., *Analyst*, 1987, **112**, 883.
5 Koukli, I. I., Sarantonis, E. G., and Calokerinos, A. C., *Anal. Lett.*, 1990, **23**, 1167.
6 Syropoulos, A. B., Sarantonis, E. G., and Calokerinos, A. C., *Anal. Chim. Acta*, 1990, **239**, 195.
7 Koukli, I. I. and Calokerinos, A. C., *Analyst*, 1990, **115**, 1553.
8 Psarellis, I. M., Sarantonis, E. G., and Calokerinos, A. C., *Anal. Chim. Acta*, 1993, **272**, 265.
9 Stauff, J., and Jaeschke, W., *Z. Naturforsch, Teil B*, 1978, **33**, 293.

Paper 4/05342G
Received September 1, 1994
Accepted October 10, 1994

Flow-injection Chemiluminometric Determination of Citrate Based on a Photochemical Reaction

Tomás Pérez-Ruiz, Carmen Martínez-Lozano, Virginia Tomás and Otilia Val

Department of Analytical Chemistry, Faculty of Chemistry, University of Murcia, 30071 Murcia, Spain

A flow injection configuration for the chemiluminometric determination of citrate is proposed. The procedure is based on the photochemical decomposition of the iron(III)–citrate complex. Iron(II) formed in the photochemical reaction was measured by its catalysis of the chemiluminescent luminol reaction in the absence of added oxidant. Linear calibration graphs were obtained between 2.0×10^{-7} and 1.0×10^{-4} mol l^{-1} citrate, with a throughput of 30 samples h^{-1} and relative standard deviations between 0.45 and 1.5%. The applicability of the method to the determination of citrate in pharmaceutical preparations and soft drinks was demonstrated by investigating the effect of potential interferences and by the analysis of commercial preparations.

Keywords: Citrate; flow injection; photochemical reaction; chemiluminescence detection; pharmaceuticals and soft drinks

Introduction

L-Citric acid is found in plants, animals and bacteria. It takes part directly in the production of energy through the tricarboxylic acid cycle and plays an important role in the study of nephrolithiasis[1] and prostate function.[2] In the food industry, citrate is used as an antibacterial substance and as an additive in fruit drinks.

Citrate is also widely used in the pharmaceutical industry. It is used therapeutically as an anticoagulant to preserve blood for transfusion purposes, as an antacid and to dissolve renal calculi. It is also used in preparing effervescent granules and tablets and for improving the taste of pharmaceutical formulations.

The analytical methods employed for the assay of citrate can be classified into four main groups: gravimetric and volumetric methods,[3] spectrophotometry,[3] enzymic analysis[4] and chromatographic determinations.[5,6] Traditionally, the formation of chromophores using pyridine, acetic anhydride and citrate or by oxidation of citrate to pentabromoacetone and subsequent reaction with alkaline pyridine has been applied to the determination of citrate in different matrices. Enzyme-catalysed reactions have been applied to citrate with proven specificity and are considered a suitable reference method;[7,8] however, limitations of sample throughput and tediousness make the enzyme assay unattractive for high frequency determinations. High-performance liquid chromatography is increasingly applied although sample clean-up still remains a problem in many instances.[9,10]

Automated systems that permit continuous determinations, *e.g.*, in continuous-flow analysis or flow injection (FI), have rarely been applied to the determination of citrate and only two methods have been described. The first is based on the formation of a hydroxamate from the reaction between citrate and hydroxylamine with the aid of a water-soluble carbodiimide. The hydroxamate is converted into the coloured iron(III) complex which is monitored.[11] The other procedure makes use of two enzymes, citrate lyase and malate dehydrogenase, and of the reduced nicotinamide adenine dinucleotide (NADH) by monitoring spectrophotometrically the NADH consumed.[12]

Interest in using chemiluminescence (CL) to determine trace and ultratrace concentrations of inorganic and organic species has increased in the last few years.[13–16] The most notable characteristics of CL methods are the higher sensitivity and larger dynamic concentration range compared with other analytical methods. CL analysis is also useful because the instrumentation can be very simple. Furthermore, the introduction of FI has made CL methods even more attractive, because it is possible to mix samples and reagents rapidly with a high degree of reproducibility.[17,18] Recently, it has been established that the irradiation of photoreactive analytes leads to the formation of species that can be detected by CL. However, until now, such photochemical–CL detectors have rarely been used in simple hydrodynamic systems such as FI.[19,20]

The purpose of the present investigation was to develop a simple, sensitive and rapid assay for citrate using an FI system coupled to photochemically induced CL. The method uses the photochemical decomposition of the iron(III)–citrate complex, and the iron(II) generated is determined by the production of CL in a luminol system in the absence of added oxidant. Levels as low as 2×10^{-7} mol l^{-1} citrate can easily be determined by measuring the intensity of the light produced.

Experimental

Apparatus

The measurement of the emitted light was made with a laboratory-built apparatus. A shield and separately housed SLM-Aminco Model JD 490 photomultiplier tube (PMT) was used as a light detection system; the PMT output was amplified and quantified by an SLM-Aminco Series 2 spectrofluorimeter connected to a personal computer fitted with the SLM-Aminco Data Manager software. A Gilson Minipuls-4, an Omnifit rotary valve and a Eurolight tungsten halogen lamp (500 W, 250 V) were also used. Except for the pump tubing (Tygon), poly(tetrafluoroethylene) (PTFE) tubing (0.5 mm i.d.) was used throughout the manifold. The CL cell was a Hellma 170.QS flow cell placed in a thermostated cell holder immediately in front of the PMT, with a mirror behind; the volume of the cell was 80 μl, exposing a large surface area to the adjacent PMT. Extreme precautions were necessary to ensure that the sample compartment and PMT were light-tight, in view of the high instrument gain settings used.

The photoreactor was a 250 cm PTFE tube (0.5 mm i.d.) coiled around a glass tube of 0.5 cm diameter placed inside a

Pyrex cylinder with a double-walled well through which cooling water continuously flowed. This assembly was housed in a metal box to protect it from light other than that of the lamp. The inside of the box was covered with aluminium foil to permit maximum reflectance of the light from the lamp.

A timer synchronized to the injection system allowed the flow to be stopped at any delay time for any length of stop time.

Manifold

A schematic diagram of the instrumental set-up is shown in Fig. 1 with optimum conditions as stated. The sample was injected into the iron(III) stream with the aid of a rotary valve with a 235 μl loop. When the sample zone was located in the photochemical reactor the flow was stopped and the irradiation was carried out with the halogen lamp placed at a distance of 10 cm from the reactor. After irradiation, the pump was triggered by the timer and the iron(II) generated in the photochemical decomposition of the iron(III)–citrate complex merged with the buffered luminol stream at the Y-piece in front of the flow cell. The distance between the Y-piece and the flow cell was 10 cm (minimum distance achieved). The light emitted by the iron(II)–luminol system was detected with the PMT with no wavelength discrimination and amplified by the spectrofluorimeter. The tubing of the luminol and buffer streams and that leading from the photoreactor to the flow cell was covered with black insulating tape in order to prevent a 'fibre optic' effect introducing stray light into the detector.

Reagents

All chemicals were of analytical-reagent grade and were used without further purification. Doubly distilled water was used throughout.

Citrate stock solution (0.01 mol l^{-1}) was prepared from trisodium citrate (Merck) and was determined by the pentabroacetone method.[3]

Iron(III) stock solutions were prepared from iron(III) sulfate in 0.01 mol l^{-1} sulfuric acid. These solutions also contained 0.01% poly(vinyl alcohol) in order to prevent precipitation of iron(III) in the manifold.

Borate buffers were prepared from 0.25 mol l^{-1} sodium tetraborate and sufficient 5 mol l^{-1} sodium hydroxide or hydrochloric acid to give the desired pH.

Results and Discussion

Basis of the Method

The irradiation of solutions containing iron(III) and citrate in aqueous acidic media yields iron(II). The photochemical determination of citrate using CL detection can be illustrated by the following reactions:

$$Fe^{III}\text{–citrate} \xrightarrow{h\nu} Fe^{2+} + CO_2$$

$$\text{Luminol} + O_2 + 2HO^- \xrightarrow{Fe^{2+}} \text{3-aminophthalate} + N_2 + 2H_2O + h\nu$$

Both reactions have to be developed under different conditions, *viz.*, an acidic medium for the photochemical reaction and a basic medium for the CL reaction; hence a flow system provides a very suitable approach to develop such a scheme.

CL reaction

It is very important to know the speed of the CL reaction and the effect of mixing the reagents on the CL intensity for the design of the flow system. In general, the way in which the reagent solutions are mixed (*i.e.*, mixing order and mixing time interval) plays a key role in the CL reaction; no, or weakened, light emission may often be observed according to the mixing procedure used and the speed at which the CL reaction proceeds is the dominant factor that governs the sensitivity in flow CL analysis because transient light emission is monitored.

It was found that the emission intensity was dependent on the way in which the reagent [buffer, iron(II) and luminol] solutions were mixed. The greatest CL signal was obtained when the buffer and luminol streams were mixed within the flow system prior to merging with the iron(II) stream. On the other hand, light emission occurred with very high speed and reached maximum intensity within 1 s. This suggests that the sample and reagent stream should be mixed as close as possible to the flow cell.

Photochemical reaction

The photochemical reduction of the iron(III)–citrate complex to produce iron(II) ions must be carried out in an acidic medium in order to obtain reproducible results. A sulfuric acid concentration of 0.1–0.01 mol l^{-1} is sufficient to avoid the deleterious action of oxygen.

Manifold design

The manifold shown in Fig. 1 was designed taking into account the characteristics of both the CL and photochemical reactions. The solution emerging from the photoreactor contains small amounts of iron(II) in the presence of a large amount of iron(III); when this solution merges with the alkaline buffered luminol solution, the precipitation of iron(III) hydroxide occurs with concomitant instability of the CL signal and blocking of the tubes. Iron(III) hydroxide is colloidal in nature and can be stabilized by the addition of surfactants. In addition to overcoming the solubility problem, their presence also alters the pathway of the chemical and photophysical processes and can be an effective means of enhancing the photochemical and CL reactions.[21] Hence, the effects of aqueous micellar systems of each charge type (*i.e.*, cationic, anionic, zwitterionic or non-ionic) were studied in order to eliminate the solubility problem and improve sensitivity and precision.

The surfactants employed were hexadecyltrimethylammonium bromide and chloride, sodium dodecyl sulfate, Triton X-100, poly(vinyl alcohol) (PVA), 3-(*N*-dodecyl-*N*,*N*-

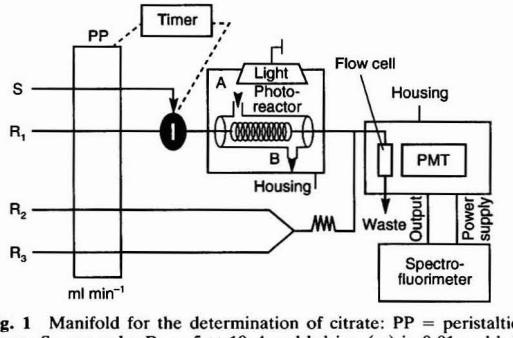

Fig. 1 Manifold for the determination of citrate: PP = peristaltic pump; S = sample; $R_1 = 5 \times 10^{-4}$ mol l^{-1} iron(III) in 0.01 mol l^{-1} sulfuric acid and 0.01% m/v PVA; $R_2 = 1$ mol l^{-1} borate buffer of pH 11; $R_3 = 5 \times 10^{-4}$ mol l^{-1} luminol; A and B = water inlet and outlet, respectively. Broken lines represent synchronous control line.

dimethylammonium) propane-1-sulfonate and Span-20. PVA was chosen because it gave the best results as regards sensitivity and reproducibility.

Optimization of Manifold Parameters

The variables studied were flow rate, volume injected and time of irradiation. The reagent concentrations used in these experiments were as follows: iron(III) line, 4×10^{-4} mol l^{-1} Fe^{3+}, 0.01 mol l^{-1} H_2SO_4 and 0.02%; luminol line, 6×10^{-4} mol l^{-1}; buffer line, 1 mol l^{-1} borate buffer of pH 10.5; sample solution, 2×10^{-5} mol l^{-1}. The mixing ratio between the luminol and buffer lines was always 1:1. The irradiation time used was 24 s.

Determination of the total flow rate is important because the time taken to transfer the irradiated sample to the photon counter is critical for obtaining a high CL intensity. Stopped-flow experiments revealed that the time taken to reach maximum intensity is about 0.05 s, which corresponds to the time required to travel from the mixing point to the inlet of the flow cell when the total flow rate is 20 ml min^{-1}. However, at total flow rates higher than 14 ml min^{-1} the signal became noisy and irreproducible. A flow rate of 12 ml min^{-1} was chosen as a compromise between sensitivity and reproducibility.

The sample volume was varied between 35 and 285 μl. The peak heights increased with increasing volumes injected up to 235 μl, above which they remained virtually constant. A sample volume of 235 μl was chosen for further experiments.

The photoreactor length selected was 250 cm, of which 200 cm was irradiated with the lamp located 10 cm from the reactor.

Particular attention was paid to the influence of the irradiation time on the CL signal. Different irradiation times were achieved by halting the flow when the sample was located in the photoreactor and then irradiating it for different times. The development of the photochemical reaction increased with the length of the irradiation time. An irradiation of 60 s was chosen as a compromise between sensitivity and sampling rate.

Optimization of Reagent Concentration

The effects of pH and various concentrations of luminol and iron(III) solutions were tested in the optimized flow system.

The pH of the solution in the flow cell has a great influence on peak height (Fig. 2), the maximum CL intensity being obtained at pH 10.4. Of several buffers tested, borate buffer exhibited the best properties although its buffering capacity is low at that pH. The sulfuric acid concentration of the iron(III) solution should be at the lowest end of the recommended range (0.01 mol l^{-1}) so that the pH after mixing with the luminol stream remains as close as possible to the optimum value. Taking all these points into consideration, a 1 mol l^{-1} borate buffer of pH 11 was chosen in order to obtain a pH of about 10.4 in the flow cell.

The CL signal increased steeply with increasing concentration of luminol solution up to 4×10^{-4} mol l^{-1}, above which it remained virtually constant. The working luminol solution chosen was 5×10^{-4} mol l^{-1}.

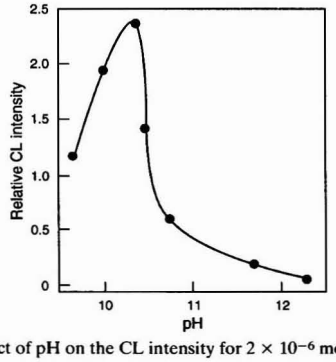

Fig. 2 Effect of pH on the CL intensity for 2×10^{-6} mol l^{-1} citrate.

Table 1 Determination of citrate in synthetic samples

Sample	Taken/ ng ml^{-1}	Found*/ ng ml^{-1}	Error (%)
1	37.8	36.9	−2.4
2	56.7	57.3	+1.1
3	94.5	95.2	+1.8
4	945	953	+0.7
5	1890	1880	+0.9
6	9450	9375	−0.5

* Average of four determinations.

Table 2 Tolerance to different ions in the determination of citrate*

Species added	Maximum tolerable mole ratio
NO_3^-, SO_4^{2-}, Cl^-, acetate, formate, barbituric acid, cyclamate, urea, K^+, Na^+, Mg^{2+}, Ca^{2+}, Ba^{2+}, Cd^{2+}, Zn^{2+}	500†
PO_4^{3-}, hippuric acid, malonate, manitol, glycerol, vitamin B_6, caffeine	100
Succinate	20
Cr^{3+}, Ni^{2+}, nicotinamide, calcium panthothenate	10
Picrate, lactate, thiamine, cyanocobalamin, acetylsalicylic acid	1
Tartrate, paracetamol, Co^{2+}, Mn^{2+}	0.1
Cu^{2+}, uric acid, riboflavin	0.01

* Citrate concentration, 4×10^{-6} mol l^{-1}.
† Maximum ratio tested.

Table 3 Determination of citrate in pharmaceutical preparations

Preparation*	Supplier	Found: Proposed method†	Found: Reference method‡
Citrocil drops (320 mg ml^{-1})	Cepa	325 ± 0.9	323
Citrocil tablets (400 mg per tablet)	Cepa	397 ± 1.2	398
Bicarbonate (0.43 g g^{-1})	SmithKline-Beecham	0.44 ± 0.02	0.42
Natreen (mg per tablet)	Bayer	3.19 ± 0.12	3.29
Dulzol (mg ml^{-1})	Santiveri	1.68 ± 0.21	1.75
Alka-Seltzer (1.05 g per tablet)	Bayer	1.04 ± 0.15	0.97

* Composition of samples: Citrocil drops: dihydrostreptomycin sulfate, 40 mg; sodium citrate, 320 mg; saccharin sodium, 3 mg; excipient and water (1 ml). Citrocil tablets: dihydrostreptomycin sulfate, 50 mg; sodium citrate, 400 mg; excipient. Bicarbonate: sodium hydrogencarbonate, 0.46 g; citric acid, 0.43 g; anhydrous sodium carbonate, 0.1 g. Natreen: sodium cyclamate; saccharin sodium; sodium hydrogencarbonate; sodium citrate. Dulzol: sodium cyclamate, saccharin sodium; citric acid, phosphoric acid, water. Alka-Seltzer: acetylsalicylic acid, 0.32 g; monocalcium phosphate, 0.20 g; sodium hydrogencarbonate, 1.90 g; citric acid, 1.05 g.
† Mean ± standard deviation for four samples.
‡ Boehringer method (ref. 8). Mean of two samples.

The CL signal also increased steeply with increasing concentrations of iron(III) solution from 1×10^{-5} to 4.5×10^{-4} mol l^{-1}, above which it remained virtually constant. A 5×10^{-4} mol l^{-1} iron(III) solution was used for further experiments.

The influence of the amount of PVA added to the iron(III) solution was studied over the range 0–0.2% m/v. Reproducible CL intensities were only obtained when the PVA concentration was higher than 0.005% m/v. The concentration adopted in the procedure was 0.02% m/v.

Dissolved oxygen is involved in the luminol CL reaction with iron(II) in the absence of oxidants[22–24] and so all reagent solutions were run without de-aeration.

Calibration Graph and Reproducibility

A series of standard solutions were injected into the manifold under the optimized conditions in order to test the linearity of the calibration graph. The calibration graph was linear from 2.0×10^{-7} to 1.0×10^{-4} mol l^{-1}. The throughput was about 30 samples h^{-1}. A statistical study performed on ten samples with triplicate injections of 5.5×10^{-6} and 5.5×10^{-7} mol l^{-1} citrate yielded relative standard deviations of 0.45 and 1.5%, respectively.

The method was tested on several synthetic samples of citrate. Some of the results obtained are given in Table 1 and, as can be seen, the errors of these determinations were always less than 3%.

Interferences

An extensive interference study with a view to determining citrate in pharmaceutical formulations and soft drinks was performed. Samples containing a fixed concentration of citrate and various concentrations of the foreign substance were injected into the flow system. A substance was considered not to interfere if the variation in the peak height of citrate was less than ±3%.

The results are shown in Table 2. There are at least three types of interference. The first acts on the CL reaction, the second on the photochemical reaction and the third by reducing Fe^{3+} to Fe^{2+}.

The interferences of Cu^{2+}, Mn^{2+}, Cr^{3+} and Ni^{2+} may be due to their catalytic effect on the oxidation of Fe^{2+} to Fe^{3+}, while Co^{2+} interferes because it acts as a catalyst in the CL reaction.[22–24]

Oxalate, tartrate and lactate form photochemically active complexes and interfere by producing Fe^{2+} in a competing reaction.[25,26]

Table 4 Determination of citrate in soft drinks

		Found/mg ml^{-1}	
Sample*	Added/ mg ml^{-1}	Proposed method†	Reference method‡
Carbonated soft drink	—	3.22 ± 0.3	3.30
	1.00	4.21 ± 0.4	4.32
	2.00	5.19 ± 0.3	5.28
	3.00	6.28 ± 0.2	6.35
Gatorade	—	2.87 ± 0.4	3.00
	1.00	4.02 ± 0.3	3.86
	2.00	4.93 ± 0.2	5.12
	3.00	5.87 ± 0.3	5.85

* Composition of samples: Carbonated soft drink: water, saccharin, citric acid, sodium hydrogencarbonate. Gatorade: citric acid; ascorbic acid; saccarose; glucose; water.

† Mean ± standard deviation for four samples.

‡ Boehringer method (ref. 8).

The interference of ascorbic acid can be minimized by incorporating a mini-column containing ascorbate oxidase. The sample is passed through the column prior to injection into the flow system.

Analysis of Real Samples

The proposed FI method has great potential for the sensitive and rapid determination of citrate in real samples. This was confirmed by the results obtained for the determination of citrate in pharmaceutical formulations and soft drinks.

Several pharmaceutical dosage forms containing citrate in tablets or syrups were diluted with distilled water prior to injection into the manifold. The results obtained by the proposed method and by the Boehringer citrate lyase, malate dehydrogenase and lactate dehydrogenase method[8] are given in Table 3.

Table 4 summarizes the results obtained in the determination of citrate in soft drinks using the proposed method and the Boehringer method.[8]

Conclusion

The results presented in this work demonstrate that the coupling of CL and photochemical reactions in an FI system has great analytical potential.

The proposed method, based on the photoinduced Fe^{2+}–luminol–O_2 CL system, provides a simple and sensitive approach to the determination of citrate at nanogram levels. The dynamic range of the method is very wide (2.2×10^{-7}–1.0×10^{-4} mol l^{-1} citrate) with a throughput of 30 samples h^{-1}. In addition, the method can be used successfully for the determination of citrate in pharmaceutical formulations and soft drinks and it appears to be a viable alternative to other continuous methods.

This investigation was supported by a grant from the Spanish DGYCT (PB93-1139).

References

1 Nicar, M. J., Skurla, C., Sakhae, K., and Pak, C., *Urology*, 1983, **21**, 8.
2 Wetterauer, U., and Heite, H., *Aktuel. Dermatol.*, 1976, **2**, 239.
3 Williams, W. J., *Handbook of Anion Determination*, Butterworth, London, 1979, pp. 62–67.
4 Moellering, H., and Gruber, W., *Anal. Biochem.*, 1966, **17**, 369.
5 Molnar-Perl, I., and Pinter-Szakacs, M., *J. Chromatogr.*, 1986, **365**, 171.
6 Ashoor, S. H., and Knox, M. J., *J. Chromatogr.*, 1984, **299**, 288.
7 Henniger, G., and Mascaro, L., *J. Assoc. Off. Anal. Chem.*, 1985, **68**, 1024.
8 *UV-method for the Determination of Citric Acid in Foodstuffs*, Boehringer Mannheim, Mannheim, Cat. No. 139076.
9 Marsili, R. T., Ostapenko, H., Simmons, R. E., and Green, D. E., *J. Food Sci.*, 1981, **46**, 52.
10 Caccano, F., Carfagnini, G., Di Corcia, A., and Samperi, R., *J. Chromatogr.*, 1986, **362**, 177.
11 Plantá, M., Lázaro, F., Puchades, R., and Maquieira, A., *Analyst*, 1993, **118**, 1193.
12 Dunemann, L., *Anal. Chim. Acta*, 1989, **221**, 19.
13 Seitz, W. R., *C.R.C. Crit. Rev. Anal. Chem.*, 1981, **13**, 1.
14 Townshend, A., *Analyst*, 1990, **115**, 495.
15 Birks, J. W., *Chemiluminescence and Photochemical Reaction Detection in Chromatography*, VCH, New York, 1989, pp. 149–230.
16 Nakashima, K., and Imai, K., in *Molecular Luminescence Spectroscopy*, ed. Schulman, S. G., Wiley, New York, 1993, pt. 3, pp. 1–23.
17 Růžička, J., and Hansen, E. H., *Flow Injection Analysis*, Wiley, New York, 2nd edn., 1988.

18 Valcárcel, M., and Luque de Castro, M. D., *Flow Injection Analysis. Principles and Applications*, Ellis Horwood, Chichester, 1987.
19 Suzuki, S., Nakuzawa, H., and Fujita, M., *Anal. Chim. Acta*, 1989, **202**, 247.
20 Pérez-Ruiz, T., Martínez-Lozano, C., Sanz, A., and Val, O., *Anal. Chim. Acta*, 1993, **284**, 173.
21 Riehl, T. E., Malchorn, C. L., and Hinze, W. L., *Analyst*, 1986, **111**, 931.
22 Seitz, W. R., and Hercules, D. M., *Anal. Chem.*, 1972, **44**, 2143.
23 Sarantonis, E. G., and Townshend, A., *Anal. Chim. Acta*, 1986, **184**, 311.
24 Kolpf, L. L., and Nieman, T. A., *Anal. Chem.*, 1983, **55**, 1080.
25 Fitzgeral, J. M., *Analytical Photochemistry and Photochemical Analysis*, Marcel Dekker, New York, 1971, pp. 128–129.
26 Riggs, W. M., and Bricker, C. E., *Anal. Chem.*, 1966, **38**, 897.

Paper 4/04587D
Received July 26, 1994
Accepted September 26, 1994

Investigation Into the Detection of Chlorine Species by Rhodamine 6G Chemiluminescence With Electrochemical Modification

Gordon P. Irons and Gillian M. Greenway*
School of Chemistry, University of Hull, Hull, UK HU6 7RX

A flow system for the determination of free chlorine by a chemiluminescence reaction with Rhodamine 6G in aqueous solution is described. The system was optimized such that a detection limit (signal-to-noise ratio = 3) of 90 μg l^{-1} was obtained for free chlorine. The system was found to detect bound available chlorine in water by electrochemiluminescence under the same conditions, but in the presence of a charged electrode. In principle, this system could be used to monitor both free chlorine and total available chlorine by switching the electrode voltage. The mechanism of the chemiluminescence is discussed with reference to the analytical advantages of linear calibrations.

Keywords: Xanthene dye; electrochemiluminescence; chemiluminescence; free chlorine; bound available chlorine; singlet oxygen

Introduction

The chlorine content of water is of significance to suppliers, as well as to both domestic and industrial consumers. Adequate chlorination ensures that drinking water is disinfected before it enters the water distribution system. Disinfection is maintained by the presence of trace amounts of other chlorine-containing species such as chloramines, which remain in the water after the chlorine has dissipated. There are a variety of methods for determining the chlorine content of water samples, only some of which can distinguish between the weakly disinfecting combined chlorine species (chloramines) and the strongly disinfecting free chlorine species.

There are two main volumetric methods that are used to calibrate other instrumental methods. Iodimetric titrations give the total residual chlorine content, while Fe^{2+} titrations with DPD (*N,N*-diethyl-1,4-phenylenediamine) can give separate results for the free and combined chlorine concentrations when performed under the appropriate conditions.[1]

More recently, flow injection methods based on spectrophotometric,[2–5] electrochemical[6–9] and chemiluminescence[10–13] techniques have been developed, giving highly reproducible results and high sample throughputs. Among these, chemiluminescence methods have the lowest reported detection limits, although they suffer from interferences from other chlorine-containing species and oxidizing agents. Rhodamine 6G (R6G) (Fig. 1) chemiluminescence[14] has been reported as having a good combination of specificity and sensitivity. It was, therefore, chosen for further investigation as a possible detection technique that could be combined with electrochemical modification to quantify a number of chlorine-containing species in water.

* To whom correspondence should be addressed.

Experimental

Materials

Rhodamine 6G was obtained as the hydrochloride salt (>99%) from Fluka (Gillingham, Dorset, UK) and concentrated sodium hypochlorite solution from A & J Beveridge (Edinburgh, UK). Tween 60 and Tween 40 (non-ionic surfactants) were from Koch-Light Laboratories (Colnbrook, Buckinghamshire, UK); all other reagents were of AnalaR grade and were supplied by Merck (Poole, Dorset, UK). The water used had a resistivity of 12 MΩ cm and was produced by reverse osmosis followed by ion exchange.

Instrumentation

Continuous chemiluminescence monitoring was performed using a Thorn EMI (Ruislip, Middlesex, UK) 9789 QB photomultiplier, powered by a Thorn EMI high voltage power supply (Model 3000 R), placed as close as possible to the window of the laminar-flow cell, which was based on a laminar-flow cell used by Lancaster and Worsfold.[15] The cell volume was formed by a poly(tetrafluoroethylene) (PTFE) spacer with an elliptical orifice sandwiched between a PTFE back plate and the cell window. This assembly was held together by a stainless-steel plate and four screws. Set in the surface of the back PTFE plate facing the photomultiplier were two platinum disc electrodes, and within this plate situated downstream of the main cell volume there was a small chamber housing the reference and counter electrodes. When a controlled potential was required on an electrode, it was connected to a two-channel three-electrode potentiostat that was constructed in-house from chopper-stabilized operational amplifiers. At all other times the electrodes were electrically insulated from the remainder of the system.

The peristaltic pump was an Ismatec (Wallington, Surrey, UK) Mini S 820 fitted with poly(vinyl chloride) (PVC) pump tubing; the flow system was constructed from 0.5 mm i.d. PTFE tubing (Anachem, Luton, Bedfordshire, UK), and the injection valve was a Rheodyne (Supelco, Poole, Dorset, UK) Model 5020. All spectra were recorded using a Perkin-Elmer

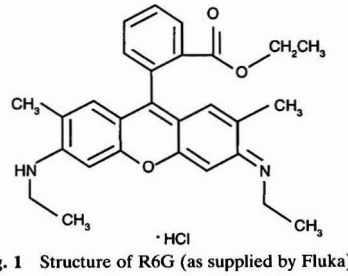

Fig. 1 Structure of R6G (as supplied by Fluka).

(Beaconsfield, Buckinghamshire, UK) Model 3000 fluorescence spectrometer. Batch studies were carried out using a Berthold (St. Albans, Hertfordshire, UK) Biolumat LB 9500 T.

Results and Discussion of Chemiluminescence Study

Flow Injection Measurements

As in most chlorine analysis the analyte solution is available in large volumes, the initial experiments were based on reversed flow injection, as described by Nakagama *et al.*[14] (injecting a slug of reagent into a stream of sample). These experiments were disappointing, as even when the temperature was raised to accelerate the reaction, only a poor detection limit (350 $\mu g\ l^{-1}$) and a very small non-linear calibration range (less than one order of magnitude) were obtained. A precipitate was also formed which eventually blocked the small channels in the flow cell; therefore, an alternative method using a different flow system was designed and optimized (Fig. 2).

Samples were injected into a carrier stream of buffer, and merged with a stream of R6G solution at a T-piece within a light-tight housing, before being fed into the flow cell. Tween 60 was added to the R6G solution, both to enhance the chemiluminescence and to keep the precipitate in solution. A simplex method based on that suggested by Betteridge *et al.*[16] was chosen to optimize the flow system. The factors optimized were as follows: length of the tubing between the T-piece and the flow cell (to enable the simplex to optimize the match between reaction rate and flow cell position), injection volume, R6G concentration and the concentration of the surfactant (Tween 60). The flow rate was fixed at 2 ml min^{-1} and a pH of 8.7 was selected as providing a compromise between sensitivity and reproducibility.

The conditions that provided the optimum signal output were as follows: R6G (2×10^{-3} mol l^{-1}) in water containing 10% v/v Tween 60, a 140 µl injection volume with 8 cm of tubing between the T-piece and the cell. A background chemiluminescence reaction was found to mask the chlorine chemiluminescence resulting in a limit of detection (3 × baseline noise) of 1.9 mg l^{-1} of free chlorine. The only material in the carrier stream that could cause this background was the phosphate buffer; therefore, a further calibration was performed with a water carrier stream and buffered samples. This was found to eliminate the background; however, the reagent solution was difficult to prepare. The problems were caused by the viscosity and insolubility of cold Tween 60 and were considerably reduced by substituting 5% v/v Tween 40. This modified reagent was used to obtain a calibration (Fig. 3) for hypochlorous acid (free chlorine at pH 6.7 in phosphate buffer) which gave a detection limit of 90 $\mu g\ l^{-1}$ of free chlorine (3 × standard deviation of baseline noise).

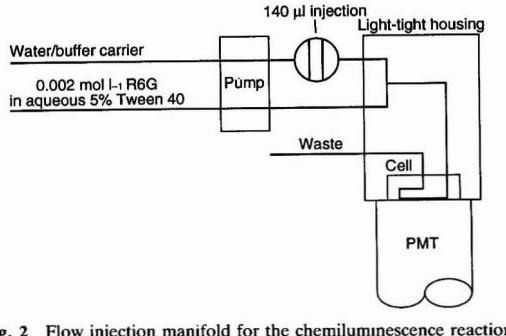

Fig. 2 Flow injection manifold for the chemiluminescence reaction of R6G and free chlorine. PMT = Photomultiplier tube.

In order to observe the effect of chlorine species on the calibration, a second curve was produced for hypochlorite, which is also classed as free chlorine when present in water. This was quadratic to 150 mg l^{-1} and gave a detection limit of 3.7 mg l^{-1}.

The hypochlorous acid calibration was reproducible and was usable from 0 to 1.5 mg l^{-1} where it followed a quadratic curve. It was also usable for samples containing more than 2 mg l^{-1} of free chlorine, as above this level it was linear. If a sample fell in the range 1.5–2 mg l^{-1} a rough estimate could be obtained for its concentration, which could be refined by diluting the sample so that it fell within the quadratic part of the calibration. Clearly, if the conditions of the analysis could be altered to obtain a linear calibration then a far more convenient and more easily automated method would result. The conditions above were selected to optimize the signal-to-noise ratio and to avoid negative blanks. In order to be able to develop an alternative method with a linear calibration it was first necessary to have a better understanding of the reaction, and then to revise the experimental conditions appropriately.

Review of R6G/Xanthene Dye Chemiluminescence

A range of dyes were studied by Yamada *et al.*[17] and were shown to emit light when mixed with free chlorine. Nakagama *et al.* have published two different methods that use this group of reactions (reverse flow injection with R6G[14] and a sensor using immobilized Uranine[13]). They also speculated that the chemiluminescence results from a bleaching reaction involving chlorination of the π system of the dyes; however, this speculative mechanism is not consistent with the results of Yamada *et al.*[17] There are two relevant results in the work of Yamada *et al.*:[17]

(1) Two of the dyes emitted light when treated with hypochlorite but their spectra remained unaltered; therefore, this chemiluminescence cannot be due to a reaction that bleaches, or otherwise alters, the dye.

(2) All the dyes tested were reported to be totally bleached by chlorine in acid. For most of the dyes tested, higher chemiluminescence intensities were recorded from experiments in alkaline or neutral solutions, even though the mechanism suggested by Nakagama *et al.* implies that the chemiluminescence should be associated with dye bleaching.

These two observations clearly allow the 'chemiluminescence from bleaching' theory to be discounted for alkaline solutions, and cast doubt on its relevance to near-neutral solutions.

The fact that a variety of fluorescent dyes can be involved, and that the spectra of the dyes are not necessarily altered by the chemiluminescence reaction in alkali, suggested that the

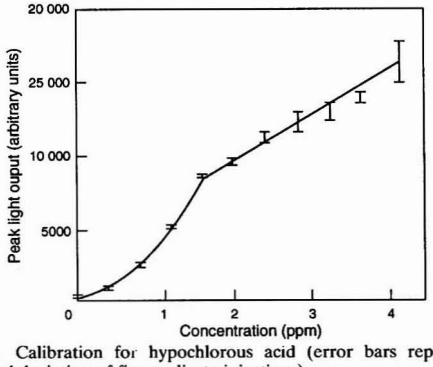

Fig. 3 Calibration for hypochlorous acid (error bars represent standard deviation of five replicate injections).

reaction is sensitized and that chemiluminescence does not directly result from chlorine attacking the dye molecule. As this could be consistent with the dyes sensitizing a reaction between the chlorine and a ubiquitous contaminant, a literature survey was performed to identify chemiluminescence reactions involving chlorine and other species. This search highlighted the generation of singlet oxygen by chlorine–hydrogen peroxide mixtures,[18] and a variety of other sources including alkaline hydrogen peroxide,[19,20] and peroxyacid decomposition.[21] It also confirmed that a number of materials can sensitize singlet oxygen chemiluminescence.[18,22,23]

Identification of One Product

The following experiments were performed to investigate a precipitate that was found to form when a solution of R6G came into contact with a solution of hypochlorite. This red material was produced by mixing equal volumes of R6G solution (0.2 g in 100 ml of water) and sodium hypochlorite solution containing about 1% free chlorine (general-purpose reagent from A & J Beveridge). The precipitate was filtered off and recrystallized from hot ethanol, and air-dried. The resulting material was studied by proton nuclear magnetic resonance spectrometry and mass spectrometry and was shown to be the free carboxylic acid formed by hydrolysis of R6G (Fig. 4).

It appears that the alkali present in the hypochlorite solution is sufficient to hydrolyse the ester link in the dye molecules. There is no indication that this material is involved in the production of an excited state; however, the fact that it is formed does imply that attack by hypochlorite on the π system of the dye molecule is slow compared with hydrolysis.

Spectral Study

In order to obtain an insight into the nature of the emitting species involved in the chemiluminescence reaction, the fluorescence and chemiluminescence spectra of R6G were recorded under as near identical conditions as possible. The fluorescence spectrometer was fitted with a flow cell consisting of a normal fluorescence cell with a short piece of glass tubing fused on to its open end. A rubber seal (suba seal) was fitted to this and the flow lines were inserted. A 1×10^{-4} mol l^{-1} solution of R6G in water at 50 °C was merged with a stream of aqueous sodium hypochlorite solution (1 + 49) at a T-piece and fed into the flow cell. The spectrum of the resulting chemiluminescence was then recorded by scanning the emission from 250 to 800 nm, with a slit-width of 2.5 nm and a shutter over the excitation source.

The fluorescence spectra were then recorded using the same flow system with the sodium hypochlorite solution replaced with water. The excitation spectrum was recorded with both excitation and emission slits of 2.5 nm and scanned from 250 to 500 nm. The emission monochromator was set to 560 nm to keep the signal on scale. Finally, the emission spectrum was recorded with the excitation set to 250 nm.

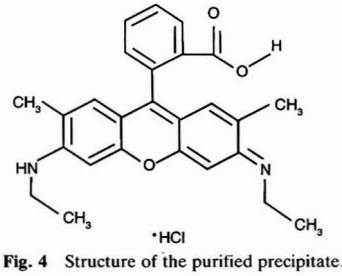

Fig. 4 Structure of the purified precipitate.

The chemiluminescence spectrum contained two bands, a wide, weak band from 360 to 490 nm with an almost flat top from 420 to 450 nm and a strong band centred on 555 nm extending from 520 to 640 nm. The R6G emission spectrum contained only one band which was centred on 550 nm and extended from 520 to 640 nm, *i.e.*, the main chemiluminescence emission is red-shifted by 5 nm compared with the emission of R6G. The excitation spectrum of R6G contained a number of bands from 250 to 500 nm, with the maxima of the most significant signals being at about 280, 345 and 470 nm.

The first weak chemiluminescence band occurs in the same area of the spectrum as the red end of the R6G excitation spectrum. This suggests that this band is characteristic of the initial excited species. It was noted that this band overlaps those of a number of dual molecule singlet oxygen transitions identified by Khan and Kasha.[24] The extreme width of this band means that it cannot be regarded as diagnostic; its precise interpretation is complicated further because R6G absorbs in part of this region, and may, therefore, alter the shape of this emission band.

The spectral evidence clearly shows that the reaction is sensitized by either R6G or a similar substance. It also suggests that singlet oxygen is a plausible candidate for the initial excited species.

Experimental Demonstration of Sensitizing Effects

The spectroscopic study has shown that most of the light is emitted by either R6G or a species that is closely related to it. It is difficult to prove that singlet oxygen is present in the chemiluminescence reaction mixture; literature methods for detecting the production of singlet oxygen are long and complex.[21,25] As this was an analytical study this line of enquiry was not followed further.

Although steps were not taken to prove the existence of singlet oxygen in the reaction mixture, short experiments were performed to obtain evidence for or against the supposition that singlet oxygen is involved. Hydrogen peroxide and hypochlorite react rapidly to give a high yield of singlet oxygen; therefore, the theory that singlet oxygen is involved would predict that the addition of hydrogen peroxide to a mixture containing R6G and free chlorine would enhance the chemiluminescence. This enhancement of the chemiluminescence by hydrogen peroxide could be analytically useful; therefore, it was investigated using the batch luminometer.

Effect of Hydrogen Peroxide on Chemiluminescence Intensity

The following solutions were prepared using boiled water to minimize the background chemiluminescence, R6G (1×10^{-4} mol l^{-1}), H_2O_2 (4×10^{-4} mol l^{-1}) and NaOCl (4×10^{-3} mol l^{-1}). The mixtures in Table 1 were prepared in the luminometer cell, which was inserted into the instrument and the sample chamber closed. A blank reading was then recorded (peak during a period of 1 min) followed by a signal reading recorded in the minute following a manual injection of 0.5 ml of the NaOCl solution. These results are shown in Fig. 5.

Clearly, the chemiluminescence output is far higher in the presence of hydrogen peroxide than in its absence. It is also clear that up to a point the chemiluminescence signal rises with R6G concentration. If two independent chemiluminescence reactions were occurring, then the effect of increasing the R6G concentration would be the same both in the presence and absence of hydrogen peroxide. If, however, a mechanism

exists that uses R6G, hypochlorite and hydrogen peroxide to produce light, then the chemiluminescence signal should rise faster in the presence of hydrogen peroxide. Doubling the amount of R6G from 0.1 ml of reagent added to 0.2 ml of reagent added increased the signal on average by 100 counts in the absence of hydrogen peroxide, but the same change with hydrogen peroxide gave an average increase of 2033 counts. Clearly, the addition of hydrogen peroxide has made the system more sensitive to this change in R6G concentration. This is consistent with a sensitized mechanism.

The fact that the graphs level off at about 0.25 ml of added R6G solutions could be due to a variety of reasons, two of which are: (*i*) R6G is highly coloured and absorbs light at the chemiluminescence wavelengths; (*ii*) as the R6G concentration is increased, increasing amounts of free chlorine are likely to be lost in dark side reactions.

This experiment has shown that R6G appears to sensitize a reaction that involves hypochlorite and hydrogen peroxide. Although hydrogen peroxide and hypochlorite are known to react to produce singlet oxygen, there is no proof that this is the reaction that generates the light in the absence of added hydrogen peroxide. Similarly, as R6G and free chlorine produce light in the absence of added hydrogen peroxide, it could be that the hydrogen peroxide is enhancing some reaction of the dye; therefore, a second experiment was performed to confirm that R6G can accept energy from singlet oxygen.

From an analytical viewpoint, this experiment has shown that the addition of hydrogen peroxide can enhance the chemiluminescence intensity by a factor of 20 or more. It has also shown that when hydrogen peroxide is present the concentration of dye used should be large so as to minimize the effect of small changes in dye concentration.

Table 1 Effect of the addition of peroxide on chemiluminescence with various levels of R6G

Volumes/ml				
R6G	H_2O	H_2O_2	Light/counts (blank/counts)	Light/counts (blank/counts)
0.0	0.5	0.5	1530 (9)	794 (16)
0.1	0.4	0.5	2508 (9)	638 (14)
0.2	0.3	0.5	3970 (11)	264 (13)
0.3	0.2	0.5	4090 (10)	4018 (15)
0.4	0.1	0.5	4687 (8)	1329 (16)
0.5	0.0	0.5	3461 (7)	3365 (16)
0.0	1.5	0.0	13 (9)	32 (18)
0.1	1.4	0.0	55 (9)	118 (18)
0.2	1.3	0.0	148 (11)	226 (17)
0.3	1.2	0.0	205 (10)	148 (10)
0.4	1.1	0.0	190 (9)	162 (9)
0.5	1.0	0.0	182 (8)	152 (10)

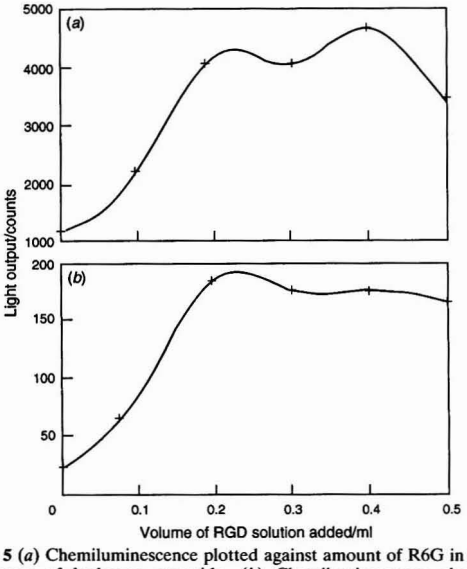

Fig. 5 (*a*) Chemiluminescence plotted against amount of R6G in the presence of hydrogen peroxide. (*b*) Chemiluminescence plotted against amount of R6G in the absence of hydrogen peroxide.

Demonstration of Singlet Oxygen Chemiluminescence Sensitized by R6G

In order to confirm that the increased chemiluminescence found in the previous experiment is due to R6G sensitizing a reaction between peroxide and chlorine rather than peroxide enhancing a reaction between R6G and chlorine, the following experiment was performed. The following solutions were prepared in boiled water: alkaline hydrogen peroxide (0.3 mol l^{-1} NaOH and 0.3 mol l^{-1} H_2O_2), R6G (1×10^{-4} mol l^{-1}) and sodium chloride (1×10^{-4} mol l^{-1}). The peak light output in the first minute after mixing was then measured for the mixtures listed in Table 2 and the results were summarized. Although there is a great deal of scatter (owing to differences in timing between replicates resulting from manual mixing and triggering of the light measuring system), only the mixture containing both alkaline hydrogen peroxide and R6G produced significant amounts of light.

The fact that the solution of sodium chloride did not produce a significant amount of light demonstrates that it is the organic part of the dye, and not the chloride associated with it, that is involved in light production. The blanks of the previous experiments have already shown that R6G and hydrogen peroxide do not produce chemiluminescence in the absence of alkali, which is significant, as in neutral solution hydrogen peroxide disproportionates very slowly and does not produce significant amounts of singlet oxygen, whereas in alkaline solutions it disproportionates to give a (1 + 3) mixture of singlet and triplet oxygen.[19,20]

This experiment has shown that R6G can accept energy from singlet oxygen. This, combined with the results of the previous experiment, suggests that a sensitized singlet oxygen mechanism is possible.

Effect of pH

As the calibration for hypochlorous acid was distinctly different from the calibration for hypochlorite, the effect of pH over a range of values between these two extremes was investigated using the batch luminometer. In each experiment 1 ml of 0.1 mol l^{-1} buffer (borate or phosphate) was placed in the cell of the luminometer. This was then spiked with 0.1 ml

Table 2 Mixtures used to show chemiluminescence in the absence of free chlorine

Mixture	A	B	C	D
R6G (1×10^{-4} mol l^{-1})/ml	—	0.5	—	—
Sodium chloride (1×10^{-4} mol l^{-1})/ml	—	—	0.5	—
Alkaline hydrogen peroxide (0.3 mol l^{-1})/ml	0.5	0.5	0.5	—
Water/ml	1.0	0.5	0.5	1.5
Mean/counts	44.25	222.5	35.75	39.5
Sample standard deviation/counts	13.2	50.4	5.7	7.9

of approximately 1.5×10^{-4} mol l^{-1} free chlorine solution (sodium hypochlorite in water) and the chart recorder started. The luminometer was then closed, and 6 s after the spike had been added the R6G solution (1×10^{-4} mol l^{-1} in water) was injected. This timing was chosen to allow the injection to be performed carefully and consistently, 6 s being the time taken for the chart paper to advance from one ruling to the next. Each experiment was repeated with unspiked buffers to obtain blank values. From the chart recordings the peak light output, the blank light output and time taken to reach the peak were measured where possible and are summarized in Table 3.

It is noted that the chemiluminescence intensity rose with pH, from pH 5.6 to 8.4, above which a plateau was found. The time taken to reach peak chemiluminescence output dropped from 3.3 s at pH 5.6 to 0.8 s at pH 8.2 before becoming unmeasurable using this method. It was also noted that the blank rose exponentially in the pH range 8.2–0.25. Although the chemiluminescence intensity rises with pH, the blank rises faster, causing the signal-to-blank ratio to fall. This is consistent with the results of the hypochlorite and hypochlorous acid calibrations described above.

Mechanism of Singlet Oxygen Production

The above experiments have shown that the chemiluminescence reaction between R6G and free chlorine could involve the production of singlet oxygen followed by the transfer of energy from singlet oxygen to the dye. It is assumed that this may also be true for the other dyes investigated by Yamada *et al.*[17]

There are a number of reactions that are known to generate singlet oxygen, including the reaction of hydrogen peroxide with chlorine, hypochlorite or bromine and the decomposition of hydrogen peroxide or peracids in alkaline solution. All of the above materials that are associated with the production of singlet oxygen have one feature in common: they can be regarded as acids with an oxygen atom inserted between the proton and the conjugate base, *i.e.*, they can call be regarded as peracids.

This could suggest that they all react in the same way; however, there are significant differences both in their structure and behaviour. For example, when singlet oxygen is produced by reactions involving peracids and hydrogen peroxide, or hypochlorite and hydrogen peroxide, isotopic studies indicate that the oxygen produced is derived entirely from the hydrogen peroxide.[26] If a peracid generates singlet oxygen in the absence of hydrogen peroxide, then this cannot occur; therefore, at least two mechanisms are possible.

One explanation for the generation of singlet oxygen in the absence of added hydrogen peroxide can be summarized as follows. Hypochlorous acid may be able to oxidize carboxylate ions to produce peroxyacids, which then decompose to yield singlet oxygen. This theory predicts that the rate of production of singlet oxygen and, therefore, of light will be related to the number of carboxylate ions present in the reaction mixture. As R6G is an ester, the amount of carboxylate formed by hydrolysis will depend on the concentration of hydroxide. The production of peroxyacids from carboxylate would be most efficient at a pH where the parent carboxylic acid is fully dissociated and the chlorine is still in the form of hypochlorous acid; however, the decomposition of peroxyacids is fastest when they are half dissociated. This combination of effects would predict the exponential rise in chemiluminescence intensity at moderate pH values followed by a plateau at high pH, as shown in Table 3.

Both the direct decomposition of hydrogen peroxide to singlet oxygen and the production of singlet oxygen from peracids created from hydrogen peroxide are favoured at very high pH and this is consistent with the exponential rise in blank signals found in Table 3. Therefore, the theory that singlet oxygen is involved can explain the effect of pH on chemiluminescence from both the spiked and unspiked solutions.

Various energy pooling mechanisms have been suggested to explain the fact that a number of materials sensitize singlet oxygen chemiluminescence even though a single molecule of singlet oxygen does not carry sufficient energy to excite them to their first singlet state. Ogryzlo and Pearson[22] studied dibenzanthrone sensitized singlet oxygen chemiluminescence and proposed an energy pooling mechanism that predicted a quadratic relationship between chemiluminescence intensity and concentration at low levels of singlet oxygen, and a linear relationship at high levels. This form of calibration was found in Fig. 3, further supporting the theory that the chlorine produces singlet oxygen, the chemiluminescence of which is sensitized by the dye. This theory suggests that the addition of hydrogen peroxide could simplify the calibration by increasing the efficiency of singlet oxygen production, a possibility that is currently being explored.

Table 3 Effect of pH on chemiluminescence intensity, blank and rate of reaction

Buffer	pH	Peak light output (spiked)/ counts	Peak light output (no spike)/ counts	Time to peak/s
Phosphate	5.6	175	Not measured	3.3
Phosphate	6.1	362	Not measured	2.5
Phosphate	6.7	1212	Not measured	2.1
Phosphate	7.1	2850	Not measured	1.73
Phosphate	7.8	16250	Not measured	1.16
Phosphate	8.3	67000	Not measured	0.8
Borate	8.2	178750	25	Not measured
Borate	8.45	250000	38	Not measured
Borate	8.6	249375	50	Not measured
Borate	8.93	258750	94	Not measured
Borate	9.25	247500	181	Not measured

Electrogenerated Chemiluminescence

Other factors that affect the reaction are also currently being investigated, but for the purpose of identifying which chlorine compounds can be detected by electrochemically modified chemiluminescence, the conditions used for the calibration described earlier were adequate. A series of experiments were performed to screen a variety of inorganic chlorine compounds not normally detected by R6G chemiluminescence, to identify those that could be detected by R6G chemiluminescence when in the presence of an appropriately charged electrode. The injection valve was removed from the flow system, as for these experiments a continuous stream of each analyte solution was required. The analytes tested were as follows: 1×10^{-3} mol l^{-1} sodium chloride, 1×10^{-3} mol l^{-1} ammonium chloride, 1×10^{-3} mol l^{-1} potassium chlorate, 1×10^{-3} mol l^{-1} sodium perchlorate, 1×10^{-3} mol l^{-1} sodium hypochlorite and a mixture of chloramines produced by preparing a solution containing 1×10^{-3} mol l^{-1} ammonium chloride and an equal concentration of sodium hypochlorite. The above analyte solutions were prepared one at a time in 0.1 mol l^{-1} phosphate buffer of pH 6.7, and at least three replicate sets of data collected; a duplicate blank experiment was also performed using only phosphate buffer and the R6G reagent.

The system was programmed to step the working electrode voltage from −3 to +3 V in 0.3 V steps and simultaneously to sample the photomultiplier tube output and the current through the electrode 1600 times for each voltage step. In order to reduce the bulk of the data and the effect of random

noise, the data recorded from the two channels (the photomultiplier tube and the potentiostat) were averaged to obtain two data points for each channel and each step. This produced 42 data points per channel per replicate. The data were loaded into SuperCalc (Computer Associates version 5.5); the data sets for each of the test analytes were averaged and plotted against time (as there were two data points at each voltage), with error bars indicating the standard error of the mean of three replicates (four for the chloramines). As could have been predicted, the solution of hypochlorite gave a very high chemiluminescence response that was not greatly affected by the potential of the electrode. All the other mixtures tested did exhibit voltage-dependent chemiluminescence and these results are shown in Fig. 6; the corresponding electrochemical data with the blank subtracted are shown in Fig. 7.

It was noted that the main peak in the optical data obtained from the chloramines occurred after 37 s at +2.4 V relative to the mercury–mercury sulfate reference electrode used. A smaller peak was found at this point in the blank, and was unaltered on the addition of chloride, chlorate or perchlorate, *i.e.*, the addition of chloramines to the solution significantly increased the chemiluminescence intensity found when the electrode was at +2.4 V. This is significant as at this potential

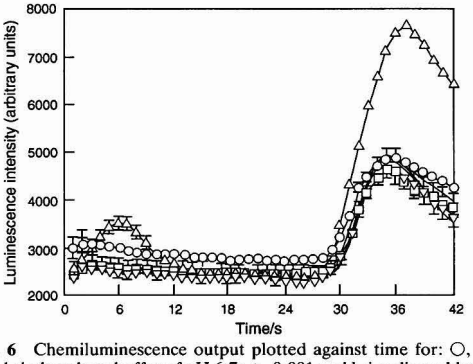

Fig. 6 Chemiluminescence output plotted against time for: ○, 0.1 mol l^{-1} phosphate buffer of pH 6.7; +, 0.001 mol l^{-1} sodium chloride in buffer; □, 0.001 mol l^{-1} ammonium chloride in buffer; ×, 0.001 mol l^{-1} potassium chlorate in buffer; ▽, 0.001 mol l^{-1} sodium perchlorate in buffer; and △, 0.001 mol l^{-1} sodium hypochlorite and 0.001 mol l^{-1} ammonium chloride in buffer.

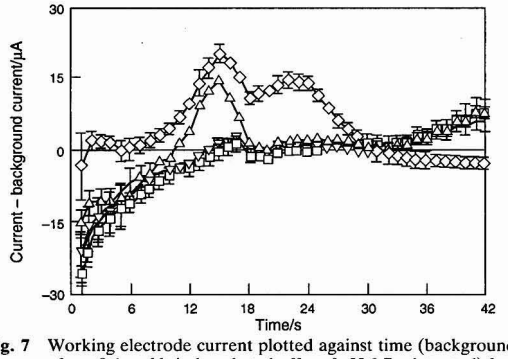

Fig. 7 Working electrode current plotted against time (background response from 0.1 mol l^{-1} phosphate buffer of pH 6.7 subtracted) for: +, 0.001 mol l^{-1} sodium chloride in buffer; □, 0.001 mol l^{-1} ammonium chloride in buffer; ×, 0.001 mol l^{-1} potassium chlorate in buffer; ▽, 0.001 mol l^{-1} sodium perchlorate in buffer; ◇, 0.001 mol l^{-1} sodium hypochlorite in buffer; and △, 0.001 mol l^{-1} sodium hypochlorite and 0.001 mol l^{-1} ammonium chloride in buffer.

the chloramines have no real impact on the current through the electrode, suggesting that either the chemiluminescence reaction is highlighting an otherwise insignificant electrode reaction involving the chloramines, or the chloramines enhance the chemiluminescence resulting from the oxidation of another species at the electrode.

A similar argument involving reduction applies to the chemiluminescence peak found after 7 s (−2.4 V), although at this point potential-dependent chemiluminescence was only noted with chloramines.

The chloramines produced by adding hypochlorite to an ammonium-containing solution were found to give a significant chemiluminescence signal in the presence of a platinum electrode held at either +2.4 or −2.4 V relative to mercury–mercury sulfate. They were also found to give a significant electrochemical signal at −1 V (this electrochemical signal is due to the reduction of the chloramines whereas the luminescence signal at 2.4 V is due to the oxidation of one or more species in the mixture). It is clear from Figs. 6 and 7 that either an electrochemiluminescent method or an electrochemical method could be used to detect chloramines; however, any free chlorine present would be likely to swamp the signals. It is also clear that chloride, chlorate and perchlorate are unlikely to interfere.

Throughout this work, the active electrode used was a 4 mm diameter platinum disc, an electrode type that can only influence a thin layer of the solution passing over it. As a result the electrochemical reactions required for the electrochemiluminescent detection of the chloramines observed above can only have involved a small fraction (20% or less) of the solution, *i.e.*, changing the electrode could have a significant effect on the relative intensities of the free chlorine chemiluminescence and chloramine electrochemiluminescence responses, although it would not alter the relative electrochemical responses. A system could, therefore, be developed using a porous flow-through electrode, that would give a far stronger response to chloramines. Such a system could be calibrated for free chlorine with the electrode at 0 V and total chlorine (free chlorine and chloramines) with the electrode at 2.4 V; separate estimates of free and combined chlorine could then be obtained by subtraction. Further development of this work is required to realize the potential of this technique fully.

Conclusion

The use of electrochemical modification allows the R6G chemiluminescence reaction to be used for the detection of additional chlorine species, at a level defined by the efficiency of electrochemical conversion and the sensitivity of the original method. Work is continuing in a number of areas:

(*i*) The efficiency of the electrochemical step may be increased by using a porous flow-through electrode and changing the flow cell. This would require re-optimizing the conditions used, and would also involve comparing the response with the reagent flowing through the electrode with the response with the samples flowing through the electrode. This would clarify which materials are involved in the electrochemical step, and hence the origin of the electrochemiluminescence observed.

(*ii*) As hydrogen peroxide enhanced the intensity of the chemiluminescence in the batch system the effect of hydrogen peroxide on the calibration is being investigated, both by adding additional hydrogen peroxide and by taking steps to eliminate any traces of hydrogen peroxide from the water used.

A number of the features of the chemiluminescence reaction when it occurs in neutral or alkaline solution can be explained by a theory involving the generation of singlet

oxygen. The chemiluminescence that occurs in acidic solution may be due either to the presence of very small amounts of hypochlorous acid/hypochlorite or to the ring oxidation/chlorination theory proposed by Nakagama *et al.*[14]

References

1 HM Stationary Office, *Chemical Disinfecting Agents in Water and Effluents and Chlorine Demand 1980*, HM Stationery Office, London, 1980.
2 Leggett, D. J., Chen, N. H., and Mahadevappa, D. S., *Analyst*, 1982, **107**, 433.
3 Aoki, T., and Munemori, M., *Anal. Chem.*, 1983, **55**, 209.
4 Zenki, M., Komatsubara, H., and Tôei, K., *Anal. Chim. Acta*, 1988, **208**, 317.
5 Aoki, T., *Environ. Sci. Technol.*, 1989, **23**, 46.
6 Trojanowicz, M., Matuszewski, W., and Hulanicki, A., *Anal. Chim. Acta*, 1982, **136**, 85.
7 Tsaousis, A. N., and Huber, C. O., *Anal. Chim. Acta*, 1985, **178**, 319.
8 Ishibashi, N., Imato, T., Ohura, H., and Yamasaki, S., *Anal. Chim. Acta*, 1988, **214**, 349.
9 Ge, H., Wallace, G. G., and O'Halloran, R. A. J., *Anal. Chim. Acta*, 1990, **237**, 149.
10 Marino, D. F., and Ingle, J. D., *Anal. Chem.*, 1981, **53**, 455.
11 Marino, D. F., and Ingle, J. D., *Anal. Chim. Acta*, 1981, **123**, 247.
12 Gord, J. R., Gordon, G., and Pacey, G. E., *Anal. Chem.*, 1988, **60**, 2.
13 Nakagama, T., Yamada, M., and Hobo, T., *Anal. Chim. Acta*, 1990, **231**, 7.
14 Nakagama, T., Yamada, M., and Hobo, T., *Analyst*, 1989, **114**, 1275.
15 Lancaster, J. S., and Worsfold, P. J., *Anal. Chim. Acta*, 1990, **239**, 189.
16 Betteridge, D., Wade, A., and Howard, A., *Talanta*, 1985, **32**, 709.
17 Yamada, M., Hobo, T., and Suzuki, S., *Anal. Lett.*, 1988, **21**, 1887.
18 Khan, A., and Kasha, M., *J. Am. Chem. Soc.*, 1970, **92**, 3293.
19 Smith, L., and Kulig, M., *J. Am. Chem. Soc.*, 1976, **98**, 1027.
20 Evans, D., and Upton, M., *J. Chem. Soc., Dalton Trans.*, 1985, 2525.
21 McKeown, E., and Waters, W., *J. Chem. Soc. (B)*, 1966, 1040.
22 Ogryzlo, E. A., and Pearson, A. E., *J. Phys. Chem.*, 1968, **72**, 2913.
23 Wilson, T., *J. Am. Chem. Soc.*, 1969, **91**, 2387.
24 Khan, A., and Kasha, M., *J. Am. Chem. Soc.*, 1966, **88**, 1574.
25 Aubry, J., *J. Am. Chem. Soc.*, 1985, **107**, 5844.
26 Cahill, A., and Taube, H., *J. Am. Chem. Soc.*, 1952, **74**, 2312.

Paper 4/04176C
Received July 8, 1994
Accepted September 12, 1994

Determination of Total Base Number of Used Lubricating Oils From Marine Engines by Potentiometric Titration

Maria Purificación Hernández Artiga and Juan Antonio Muñoz Leyva
Analytical Chemistry Department, University of Cádiz, Puerto Real, Cadiz, Spain
Ramón Cózar Sievert
Department of Heat Engines and Marine Propulsion, University of Cadiz, Puerto Real, Cadiz, Spain

A modification of the IP 276-83–ASTM D2896-92 standardized method for the determination of the total base number of petroleum products is described. This method allows this determination in used lubricating oils from marine engines, which was not possible with the standardized procedure. It shows a better precision, shorter voltage stabilizing time and in many instances avoids back titration. It can be suggested as an alternative to ASTM-IP methods.

Keywords: *Total base number determination; lubricating oils; marine engines; potentiometric titration*

Introduction

The degradation of lubricating oils by oxidation can lead to the development of corrosive organic acids. Further, the residual fuels used in marine internal combustion engines frequently contain sulfur, which is oxidized during combustion and H_2SO_4 is formed. Basicity is therefore an important property of lubricating oils, as bases neutralize acidity and therefore offset corrosion. The basicity of an oil is produced by additives (auxiliary materials added to liquid lubricants to enhance their properties), nitrogen compounds and salts of weak acids.

The total base number (TBN) of an oil is defined as the amount of acid, expressed in milligrams of potassium hydroxide, that is needed to neutralize all basic constituents present in 1 g of sample.[1–4] The TBN initial value of an unused lubricating oil, decreases after several hundred hours of working (until a re-equilibrium value is reached). This implies an increase in metal wear in the oil. The change depends on several factors, such as sulfur content of fuel, motor refrigerating temperature and quality and consumption of lubricating oil.

The determination of TBN by a simple, precise and reproducible method is of great technological interest. Most of the methods described for this determination are based on acid–base reactions using a chromogenic indicator[5–7] or potentiometry[1–4] to detect the end-point. A flow injection potentiometric method[8] and a high-frequency microtitration method[9,10] have also been described. A method consisting of measuring the gas pressure at the end of the acid–base reaction has been proposed.[11]

The ASTM D664-58 and IP 177/64 methods[1,2] for measuring TBN involve the potentiometric titration of a solution of the oil in toluene–propan-2-ol with a standardized solution of hydrochloric acid in propan-2-ol, but the graph obtained does not always show a satisfactory end-point, particularly with used oils. The IP 276-83 and ASTM D2896-92 methods[3,4] using chlorobenzene as a solvent for oil and perchloric acid in acetic acid as titration reagent, is more widely accepted, but it often requires a back titration and with used marine oils the detection of the end-point is not always possible.

This paper describes a modification of the IP 276-83–ASTM D2896-92 method in order to be able to determine the TBN of used lubricating oils from marine engines. Different solvents were tested to increase the sensitivity of the TBN determination and shorten the voltage stabilization time. The results were compared with those obtained by the IP 276-83–ASTM D2896-92 method.

Experimental

Apparatus

A Crison 2.000 pH meter with a glass–calomel combined electrode for non-aqueous media was used for normal determinations. A Mettler DL20 pH meter was used for automatic determinations.

Reagents

All chemicals were of analytical-reagent grade. Potassium hydrogenphthalate and 60% perchloric acid were obtained from Merck. Propan-2-ol, xylene and glacial acetic acid were purchased from Panreac.

Sampling

Thirty-one samples of used lubricating oils of several tradenames with different TBN values were taken from different ship engines. They were collected with the engine hot and running to provide a homogeneous and representative sample; they were stored in poly(propylene) bottles.

Procedure

Standardize the perchloric acid as follows. Heat an amount of potassium hydrogenphthalate in an oven at 120 °C for 2 h and allow it to cool. Take 0.1–0.2 g of the potassium hydrogenphthalate and dissolve it in 40 ml of warm glacial acetic acid. Add 80 ml of xylene, cool and titrate with 0.1 mol l^{-1} perchloric acid in acetic acid using the electrode system and procedures given for TBN determination.

Carry out a blank titration on 40 ml of glacial acetic acid plus 80 ml of xylene.

Sample Titration

Shake the used oil thoroughly to ensure homogeneity before sampling. Calculate the amount of sample required from the TBN expected:

Approximate mass of sample (g) = 28/expected TBN

Add 120 ml of xylene–glacial acetic acid (2 + 1) by volume and stir the solution until the sample has dissolved. Position the electrodes immersed in the solution. Continue the stirring throughout the determination. Adjust the meter so that it reads in the upper part of the millivolt scale. Fill the burette with 0.1 mol l^{-1} perchloric acid in glacial acetic acid and record the initial cell potential reading.

For manual titration, add suitable small portions of titrant and, after waiting until a constant potential has been established, record the burette and meter readings.

For automatic titration, adjust the instrument in accordance with the manufacturer's instructions and set the titration speed at 1.0 ml min^{-1} maximum.

For each set of samples make a blank titration on 120 ml of xylene–glacial acetic acid (2 + 1).

Calculate the total base number as follows:

$$\text{TBN (mg g}^{-1}\text{ KOH)} = \frac{(V - V')\,M \times 56.1}{g}$$

where V = volume of perchloric acid (ml) used to titrate the sample to the inflection point on the titration curve, V' = volume (ml) corresponding to V for the blank titration, M = $HClO_4$ concentration (mol l^{-1}) and g = amount of sample (g).

Results and Discussion

Previous Tests

The determination of the TBN of used lubricating oils from marine engines following the IP–ASTM method was tested, but for this type of sample the repeatability was poor, the voltage stabilization was very slow and often the end-point was hardly detected. Several attempts were made to improve this method.

It was taken into account that the solvent used as the medium for the titration of weak bases in petroleum products must dissolve the sample completely, enhance the basicity of the species to be titrated and have a low solvating power for cations.[10]

Different solvents for both titrant and sample were tested and the other reagents were maintained as specified in the IP–ASTM method. Perchloric acid in dioxane as titrant reagent was tested, but no end-point was detected and the potential readings were very unstable. The use of xylene–propan-2-ol (9 + 1) as the sample solvent improved the voltage readings but there was no clear end-point detection (probably the weak bases to be titrated need an acidic solvent to enhance their basic properties).

Subsequently, several mixed solvents were tried, always containing acetic acid: toluene–acetic acid (2 + 1), toluene–propan-2-ol–acetic acid (9 + 1 + 5) and xylene–propan-2-ol–acetic acid (9 + 1 + 5). We thought that a ternary mixture solvent would be suitable owing to the complexity of the samples. In all three instances the voltage values were unstable and no sharp breaks at the end-point were detected. The addition of acetic anhydride to the samples to avoid problems due to the water content was also tested but the results were the same as described above.

Further trials were made, replacing the monochlorobenzene, used in the standardized method, with xylene. The solubility of the oils in this solvent was acceptable, the voltage stabilization was very rapid and the end-point could be detected very clearly owing to the high potential increments at the end-point. Some improvements were also observed when the perchloric acid was titrated with the standardized method but replacing the chlorobenzene–acetic acid used to dissolve phthalate with xylene–acetic acid. The time of analysis was shortened and sharper breaks at the end-point were observed.

Repeatability

The criteria used for judging repeatability results (95% confidence) with the IP–ASTM standard method of test for TBN of petroleum products by potentiometric perchloric acid titration when applied to used oils are 5% when forward titration is employed and 24% when back titration is required. During the development of this method the complete range of TBN was not covered. It was believed that reasonable interpolation and extrapolation from the ranges used would not introduce serious errors. The TBN range studied was 2.9–11 for used oils (TBN of 5.5–13 for fresh oils and 60–99 for additive concentrates were also studied).

The repeatability of the proposed method was evaluated by determining the TBN of 11 aliquots of the same sample following the procedure. A sample with a high TBN was chosen because it is very representative of the oils used in marine trunk engines. The results were mean = 26.63, standard deviation = 0.143, relative standard deviation =

Table 1 Potential increments at the end-point in the titration of different samples and TBN results obtained by both methods

	IP 276-83–ASTM D2896-92		Proposed method	
Sample No.	Potential increment/ mV ml^{-1}	TBN	Potential increment/ mV ml^{-1}	TBN
1	220	2.84	220	2.99
2	240	2.89	270	2.87
3	210	2.49	260	2.73
4	170	19.75	200	19.67
5	160	19.63	180	19.34
6	190	17.70	200	17.87
7*	130	21.43	210	21.42
8*	130	23.76	240	23.85
9	160	23.17	180	22.97
10	150	25.05	180	24.65
11	150	22.92	170	22.94
12	150	21.29	180	23.74
13	200	18.57	210	18.05
14	140	18.13	180	18.08
15	160	25.12	220	25.04
16	150	23.26	190	23.36
17	170	23.58	220	23.63
18	180	32.43	230	32.20
19	130	24.45	160	23.91
20*	140	26.65	190	26.62
21	130	30.11	190	30.17
22	140	30.11	180	30.02
23	150	28.39	220	28.51
94	140	27.41	210	27.90
25*	120	26.63	180	26.66
26	140	27.25	190	26.66
27	130	23.05	160	23.27
28	130	27.90	160	27.43
29	140	23.05	170	23.07
30	140	22.07	200	22.50
31*	130	26.36	150	25.45

* Samples requiring back titration in the IP–ASTM method.

0.043% and error = 0.36%. This percentage error is far better than that obtained by the standardized method (5% for forward titration or 24% for back titration).

Accuracy

The results obtained as described under Experimental were compared with those obtained by the IP–ASTM method for 31 samples of used oils of several tradenames taken from different ship engines. The TBN values obtained by both methods are given in Table 1. The Youden graph obtained showed that the correlation is very good (slope = 1, r = 0.997). The results obtained by the proposed method are considered to be more accurate because they show a better repeatability. The TBN of the unused oil was around 30 (very common in the crankcase of marine trunk engines). Used lubricating oil samples in this TBN range are not mentioned in the description of the IP–ASTM method. The TBN values obtained were lower than that of the unused oil, as expected.

Voltage Increases at the End-point

Comparison of the titration curves obtained by the two methods are shown in Fig. 1 for $HClO_4$ titration and in Fig. 2 for a sample titration.

The sample shown in Fig. 2(*b*) could not be titrated following the direct standardized method and required a back titration; however, it is easily titrated following the proposed direct method. As can be observed, the IP–ASTM method is not adequate for this application but TBN determination is possible when the modified method is used. This is not an exceptional case and it always occurs when the used oil results from many working hours.

The voltage increases at the end-point were compared. It is higher when the proposed method is used, mainly when the initial TBN is high. Also, the $HClO_4$ titration in both methods showed that the voltage increase at the end-point is higher for the proposed method.

Table 1 shows the voltage increase at the end-point for the titration of the 31 samples described above for both methods.

The voltage stabilization time after each addition of titrant is shortened when the proposed method is used. This is another advantage of the proposed method over the standardized method.

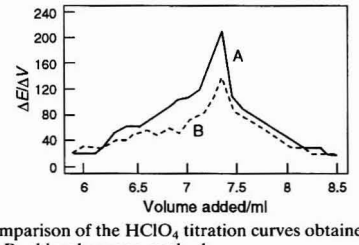

Fig. 1 Comparison of the $HClO_4$ titration curves obtained by A, the xylene and B, chlorobenzene methods.

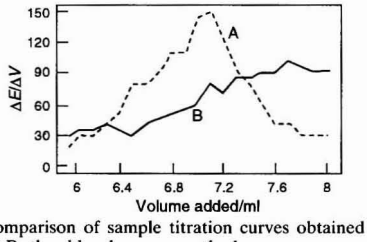

Fig. 2 Comparison of sample titration curves obtained by A, the xylene and B, the chlorobenzene methods.

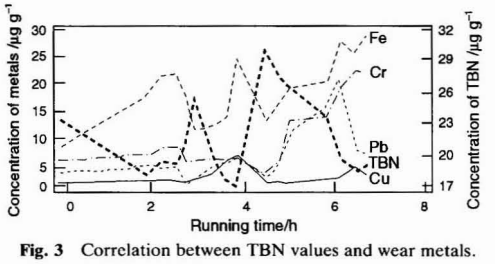

Fig. 3 Correlation between TBN values and wear metals.

Correlation Between TBN Values and Wear Metals

The TBN value of a used oil decreases with increased engine working time. It has also been found that there is a correlation between TBN decrease and wear metal increase with time.

To verify this correlation, several samples were taken from the same engine (with the engine running) at fortnightly intervals. Iron, Cr, Cu and Pb wear metals were measured by atomic absorption spectrometry following a procedure developed previously.[12] The TBN was determined by the procedure proposed in this paper. The results are shown in Fig. 3.

As it can be seen, when the TBN decreases the wear metal concentration increases. Therefore, there is a direct relationship between TBN value and engine wear.

The peaks show the addition of new oil and therefore a TBN increase and wear metal decrease, but in spite of this a tendency for the TBN to decrease and the wear metal concentration to increase can be seen.

On some occasions, apart from the corrosive wear, it is necessary to take into account the abrasive wear, and in this event the correlation between wear and TBN is not so clear. However, in any case a decrease in the TBN values implies higher wear and the possibility of engine failure.

Conclusions

The control of quality-related parameters in marine internal combustion engines is of great importance because the oil is not usually changed. In spite of this, there is no accepted and reliable method for the analysis of used lubricating oil samples from marine engines with many working hours. A very simple modification of the standardized IP–2ASTM method suitable for used oils from marine engines has been proposed. The results of comparisons of the modified and standardized methods allowed us to draw the following conclusions when the modified method is used: the results are more precise; the voltage stabilizing time is shorter; it avoids back titration; and it allows the TBN determination in used lubricating oil samples from marine engines with many working hours, which is not possible with the standardized method. Consequently, the proposed method can be suggested as an alternative to the IP and ASTM methods.

References

1 *1977 Book of ASTM Standards, Part 23*, American Society for Testing and Materials, Philadelphia, 1977, Method D664-58.
2 *Institute of Petroleum Standards 1978, Part I*, Institute of Petroleum, London, 1978, vol. 1, Method 177/64.
3 *1977 Book of ASTM Standards, Part 24*, American Society for Testing and Materials, Philadelphia, 1977, Method D2896-73.

4 *Institute of Petroleum Standards 1978, Part I,* Institute of Petroleum, London, 1978, vol. 2, Method 276/75.
5 Houghton, G. L., Moore, E. J., and Simpson, C. A., (Mobil Oil), *Eur. Pat. Appl.,* EP 170 466, 1986.
6 Andersen, U., and Zielke, E., *Schimierungstecnik*, 1985, **16** (2), 58.
7 Mitshubishi Oil, *Jpn. Kokai Tokkyo Koho,* 5 954 964, 1982.
8 Bauer, W., *The Motor Ship,* November, 1967.
9 Fernandez, T., Rocha, J. M., Rufino, N., García, A., and García Montelongo, F., *Analyst*, 1978, **103**, 1249.
10 Fernandez, T., Rocha, J. M., Rufino, N., García, A., and García Montelongo, F., *Analyst*, 1979, **104**, 739.
11 Clark, G. H., *Marine Diesel Lubrication*, Burmah-Castrol Publications, 1974, p. 192.
12 Hernandez Artiga, M. P., Muñoz Leyva, J. A., and Cózar Sievert, R., *Analyst*, 1992, **117**, 963.

Paper 4/02412E
Received April 25, 1994
Accepted July 13, 1994

Kinetic Model of pH-based Potentiometric Enzymic Sensors.

Part 4.* Enzyme Loading and Lifetime Factors

Robert Koncki and Stanisław Głąb

Department of Chemistry, University of Warsaw, 02-093 Warsaw, Pasteura 1, Poland

Two factors: enzyme loading factor and lifetime factor, are defined on the basis of a kinetic model for pH-based enzymic sensors. The enzyme loading factor is independent of measurement conditions, such as pH and concentration of buffer or concentration of analyte. It allows a quantitative description of enzyme activity in the sensing membrane, and so is helpful in comparisons of various biosensors working under different conditions. The lifetime factor is defined in terms of the dependence of the enzyme loading factor with time. Both factors are universal parameters for pH-based enzymic sensors. The utility of these factors in a description of biosensors is exemplified with pH-membrane electrodes sensitized for urea using different methods of enzyme immobilization.

Keywords: Potentiometric enzymic pH sensors; kinetic model; enzyme loading factor; lifetime factor; urea biosensors

Introduction

Theoretical descriptions of potentiometric enzymic sensors are usually based on diffusional models.[1–4] Special modifications of these models are useful for describing pH-based enzymic sensors.[5–8] One of the most important factors in diffusional models for all types of enzymic sensors is the enzyme loading factor (ELF). It is defined as:

$$\alpha = \frac{V_{max} L^2}{K_M D_S} \quad (1)$$

where V_{max} is the maximal rate of the enzymic reaction, K_M is the Michaelis–Menten constant, D_S is the diffusion coefficient of the substrate and L is the thickness of the enzyme membrane (which is a dimensionless parameter that describes the properties of the enzymic layer). Its numerical value, the ratio of the rate of the enzymic reaction to the rate of mass transport, provides information about diffusional or kinetic control of the various processes occurring inside the sensing layer. The ELF was shown to be the most important factor for potentiometric enzymic probes.[3,4] It gives information about the stability (sensitivity to pH changes and the presence of inhibitors or activators), sensitivity, linear range, detection limit and the upper determination limit of the sensor. The ELF is also an important factor in the description of the non-steady-state and transient analytical response of biosensors. In these cases it provides information about the rate of response of biosensors.[9,10]

A similar parameter is defined in diffusional models of pH-based enzyme sensors. The measurements with pH-based enzymic sensors require pH changes inside the sensing layer, therefore, most models for this type of sensor take into account the influence of pH on the kinetics of enzyme reaction. In this case ELF is replaced by the so called Thiele modulus:[5–7]

$$\Phi = L \sqrt{\frac{V_{max}}{K_M D_S \left(1 + \frac{K_a}{[H]} + \frac{[H]}{K_b}\right)}} \quad (2)$$

where K_a and K_b are the acid and base dissociation constants for the substrate–enzyme complex, respectively. The Thiele modulus is a dimensionless parameter which corresponds to the square root of the ELF, and additionally takes into account the influence of pH on the kinetic parameters of the enzyme reaction (V_{max}, K_M) according to Waley's model.[11] It has been reported that for $\Phi > 10$ the processes in the enzymic layer are diffusion-controlled, and for $\Phi < 10$ they are kinetically controlled.[5] For high enzyme activity in the sensing layer the parameter Φ is not determinable (the maximal determinable value for Φ is 18.8)[6,7]. Sensors with $\Phi < 1$ are useless from an analytical point of view, because of their negligible sensitivity.[5] A rarely used parameter which is similar to the Thiele modulus is the Damkohler number.[8]

In a series of papers[12–16] we have developed a kinetic model for pH-based enzymic sensors. It is based on Morf's kinetic model[17] for potentiometric enzymic electrodes. In the present paper we define the ELF for kinetic models and compare it with the Thiele modulus for diffusional models. On the basis of the ELF we define a new parameter: the lifetime factor (LTF). We present a theoretical description for both parameters and methods for their determination. Theoretical predictions are experimentally verified for several pH-based membrane enzyme electrodes for urea.[18,19]

Experimental

Apparatus and Reagents

A digital pH-meter (Radiometer Model PHM85, Copenhagen, Denmark) was used throughout this work. Glass electrode bodies (Radelkis Model OP-0718P, Budapest, Hungary) were used for the construction of the membrane electrodes. A saturated calomel electrode (Radelkis Model OP-0820P) was used as a reference electrode.

Urease (EC 3.5.1.5; 5 U mg^{-1}) was obtained from Merck (Darmstadt, Germany). Membrane materials and other reagents were: tridodecylamine (Fluka, Buchs, Switzerland), bis(2-ethylhexyl) sebacate (Fluka), potassium tetrakis(4-chlorophenyl)borate (Fluka), cellulose triacetate (Merck, Poole, UK), 1-ethyl-3-(3-dimethylaminopropyl), carbodiimide (Sigma, St Louis, MO, USA), carboxylated PVC (Aldrich, Milwaukee, USA), glutaraldehyde (J. T. Baker, Phillipsburg, NJ, USA) and sodium tetrahydroborate (Merck). Analytical

* For part 3 of this series see ref. 15.

grade reagents were used to prepare buffers and standard urea solutions. Doubly-distilled water was used for all experiments.

Preparation of Urea Electrodes

Four types of urea biosensors were tested. All sensors were obtained by enzymic sensing of pH membrane electrodes with tridodecylamine as hydrogen ionophore. The preparation of the pH electrode has been described elsewhere.[18,19] Enzyme electrodes of different types were prepared in the following way.

Enzyme electrode 1 was prepared by urease adhesion to the surface of a pH membrane electrode.[18]

Enzyme electrode 2 was prepared by the deposition of a cellulose triacetate membrane which includes urease on the surface of a pH membrane electrode.[18]

Enzyme electrode 3 was prepared by covalent binding of urease to the surface of a pH membrane made of carboxylated PVC.[18,19]

Enzyme electrode 4 was prepared by covalent binding of a second layer of urease to the enzymic layer of enzyme electrode 3, using glutaraldehyde and by reduction of the Schiff bases produced.[19]

Conditioning and Storage of Urea Electrodes

All types of urea electrodes were conditioned in a stirred solution of similar composition with respect to ionic strength, pH and buffer concentration to that used during the measurements. After use the urea electrodes were washed in stirred water for 15 min. When not in use they were stored in a refrigerator.

Measurements

The urea electrodes were used in the measurements for about 5–8 h per day. To compare the properties of the different urea electrodes calibrations were made in the standard test solution (phosphate buffer, pH 6.0, c_B = 5.0 mmol dm^{-3}). The electrodes (within the range of urea concentration of 0.1–100 mmol dm^{-3}) were calibrated by stepwise addition of standard urea solutions (0.20 and 2.0 mol dm^{-3} in the buffer containing 0.10 mol dm^{-3} NaCl) to the test solution. These measurements were used for the preparation of the calibration graph. Such calibrations were repeated every day to examine the lifetime of the electrodes.

The properties of all the sensors have been described earlier.[18,19]

Description of Enzyme Loading Factor

In the reported kinetic model,[12,13] the normalized rate constant for an enzyme reaction was defined as

$$k_v = \frac{V_{max}}{k_S} \tag{3}$$

where V_{max} is the maximal rate of the enzymic reaction, and k_S is the transport rate constant for the substrate. This parameter, proportional to the ratio of the rates of the enzymic reaction and mass transport, has the dimensions of concentration. On the basis of this factor the dimensionless parameter ELF can be defined:

$$\mathrm{ELF} = \frac{k_V}{K_M} = \frac{V_{max}}{K_M k_S} \tag{4}$$

where K_M is the Michaelis–Menten constant. This parameter is analogous to ELF in the diffusional models [eqn. (1)].[1–4]

The influence of pH on the enzymic reaction can be taken into account by introducing an equation from the concept of conditional maximal rate constant (V'_{max}) and conditional Michaelis–Menten constant (K'_{max}):[11–13]

$$V'_{max} = \frac{V_{max}}{1 + \frac{K_{a1}}{[H]} + \frac{[H]}{K_{b1}}} \tag{5}$$

$$K'_M = K_M \frac{1 + \frac{K_{a2}}{[H]} + \frac{[H]}{K_{b2}}}{1 + \frac{K_{a1}}{[H]} + \frac{[H]}{K_{b1}}} \tag{6}$$

where K_{a1}, K_{b1}, K_{a2}, K_{b2} are the acid (a) and base (b) dissociation constants for enzyme (1) and substrate–enzyme complex (2), respectively. Introduction of eqns. (5) and (6) into the kinetic model significantly increases the quality of the fit of the theoretical curves to the experimental data.[15] The conditional enzyme loading factor, ELF′, taking into account the influence of pH on the kinetics of the enzymic reaction, can be given as:

$$\mathrm{ELF}' = \frac{\mathrm{ELF}}{1 + \frac{K_{a2}}{[H]} + \frac{[H]}{K_{b2}}} \tag{7}$$

This parameter is similar to the Thiele modulus[5–7] and Damkohler number[8] defined in the diffusional models of pH enzyme sensors.

Determination of ELF (or ELF′) requires determination of k_V and K_M or the direct determination of the ratio of these parameters. In our previous work[12,13] three methods for the determination of kinetic parameters were presented. The first method is based on the general equation describing the whole calibration curve:

$$K_H(H^B - H) + K_W c_W \left(\frac{1}{1 + K_{aW}/H^B} - \frac{1}{1 + K_{aW}/H}\right) + \left(\frac{n_A}{1 + H/K_{aA}} - \frac{n_B}{1 + K_{aB}/H}\right) \cdot \{c_S - \tfrac{1}{2}[\sqrt{(k_V + K_M - c_S)^2 + 4K_M c_S} - (k_V + K_M - c_S)]\} = 0 \tag{8}$$

where c_W is the buffer concentration, c_S is the enzyme substrate concentration, H^B is the hydrogen ion concentration in the bulk solution, H is the hydrogen ion concentration in the sensing layer, n_A and n_B are stoichiometric coefficients in the enzymic reaction for acid (A), and base (B), respectively, K_{aA}, K_{aB}, K_{aW} are dissociation constants for protolytic products (acid and base) and buffer, respectively. The normalized transport rate constants K_H and K_W for hydrogen ions and buffer, take into account differences in the transport rate of various species.[13]

Both parameters, k_V and K_M, can be determined by fitting the theoretical calibration curves [eqn. (8)] to the experimental data. The simplex method[14,16] is useful for this purpose. This procedure minimizes determination errors by using all calibration data.

Parameter k_V can also be easily determined from the upper limit of determination (ULD), using an equation for the zero-order enzymic reaction ([S] ≫ K_M):[13]

$$k_V^{ULD} = \frac{K_H(H^B - H) + K_W c_W \left(\frac{1}{1 + K_{aW}/H^B} - \frac{1}{1 + K_{aW}/H}\right)}{\frac{n_B}{1 + K_{aB}/H} - \frac{n_A}{1 + H/K_{aA}}} \tag{9}$$

The error in determining k_V in this way may be higher than in the first method, as calculations are based on single experimental data only (signal of upper limit of determination). Determination of K_M by this method is impossible.

The value of ELF can also be determined from the first part of the calibration data using an equation for the first-order enzymic reaction ($[S] \ll K_M$):[13]

$$\frac{k_V}{k_V + K_m} = \frac{K_H(H^B - H) + K_W c_W \left(\frac{1}{1 + K_{aW}/H^B} - \frac{1}{1 + K_{aW}/H}\right)}{c_S\left(\frac{n_B}{1 + K_{aB}/H} - \frac{n_A}{1 + H/K_{aA}}\right)} \quad (10)$$

This method does not allow K_M and k_V to be determined separately, but only their ratio. For membranes with very high enzyme activity this method cannot be used. In this case all the substrate can be converted into the product (as occurs for high enzyme activity and low substrate concentration), and the analytical response is a function of the protolytic equilibrium taking place inside the membrane only, and the response is given then by eqn. (11):[13]

$$K_H(H^B - H) + K_W c_W\left(\frac{1}{1 + K_{aW}/H^B} - \frac{1}{1 + K_{aW}/H}\right) + c_S\left(\frac{n_A}{1 + H/K_{aA}} - \frac{n_B}{1 + K_{aB}/H}\right) = 0 \quad (11)$$

which does not include kinetic parameters of the enzymic reaction. A similar situation is described in the diffusional models.[6,7]

Determination of k_V is always possible, using eqn. (8) or (9). Determination of K_M is, however, impossible on the basis of eqn. (9), and, if the membrane enzyme activity is high, eqn. (8) gives erratic values of K_M. Similar reasons (high enzyme activity of membrane) cause high values of the Thiele modulus to be non-determinable.[6,7]

In such a situation the ELF cannot be determined (because of the non-determinability of K_M). The third method presented here, leading directly to a value for ELF, also has limitations if the enzyme activity of membranes is high. For these reasons we suggest the use of the k_V value, instead of ELF, to describe the enzyme activity of the membranes. The k_V value gives the same information as ELF, and its estimation is less problematic.

The k_V value describes the enzymic membrane at a given moment. Changes in k_V with time should give information about the stability of the enzyme sensor. We suggest the introduction of a new parameter, the lifetime factor (LTF), which gives information about the rate of decay of membrane activity. The exact definition of LTF is presented in the next section.

The lifetime of a sensor is dependent on both parameters: LTF and k_V (ELF). A good sensor should have high k_V and LTF values.

Results

In our investigations we used four pH-based enzyme electrodes sensitized for urea using different methods of enzyme immobilization. For each electrode, calibration data were collected during several days and from the data obtained, k_V, K_M and LTF were determined. Calculations were based on eqns. (8) and (9) taking into account Waley's corrections [eqns. (5) and (6)]. The urea decomposition reaction, catalyzed by urease, is given by:

$$(H_2N)_2CO + 2H_2O \xrightarrow{\text{Urease}} H_2CO_3 + 2NH_3 \quad (12)$$

so the stoichiometric coefficients are $n_A = 1$ and $n_B = 2$. Other constants used in calculations were: $K_{aA} = 4.3 \times 10^{-7}$ mol dm^{-3}, $K_{aB} = 5.6 \times 10^{-10}$ mol dm^{-3}, $K_{aW} = 6.2 \times 10^{-8}$ mol dm^{-3}. The acid and base dissociation constants for urease and urease–urea complex ($K_{a1} = 7.0 \times 10^{-9}$ mol dm^{-3}, $K_{b1} = 3.6 \times 10^{-5}$ mol dm^{-3}, $K_{a2} = 3.1 \times 10^{-8}$ mol dm^{-3}, $K_{b2} = 1.4 \times 10^{-6}$ mol dm^{-3}), were taken from refs. 20 and 21. K_H and K_W were assumed to be equal to unity.

Fig. 1 shows experimental data (dots) from calibrations of enzyme electrode 1 prepared by urease adhesion to the surface of the pH membrane electrode. The solid lines in this Figure represent the theoretical calibration curves [fitted on the basis of eqn. (8)] to experimental points using the simplex method.[14,16] The parameters determined: k_V, K_M and ELF, are presented in Table 1. The k_V^{ULD} values presented in Table 1 are the normalized rate constant for the enzymic reaction, k_V, determined from the upper limit of determination [eqn. 9)]. The differences between k_V [eqn. (8)] and k_V^{ULD} [eqn. (9)] are negligible. Also the values of K_M calculated for consecutive days are similar, with the exception of the K_M value obtained for the first day. This very low value of K_M obtained on the first day arises from an error caused by high enzyme activity. The values of both K_M ($\approx 10^{-7}$ mol dm^{-3}) and ELF ($\approx 10^7$) calculated on its basis have no physical reality.

The trends in the results obtained for the three other electrodes were similar to the trends for electrode 1. Fig. 2 presents values of k_V obtained for consecutive days for all the electrodes investigated. In all cases the k_V values obtained from eqns. (8) and (9) were similar. The decay of the membrane activities for all the electrodes investigated is logarithmic:

$$k_V(t) = k_V(0)\exp(-At) \quad (13)$$

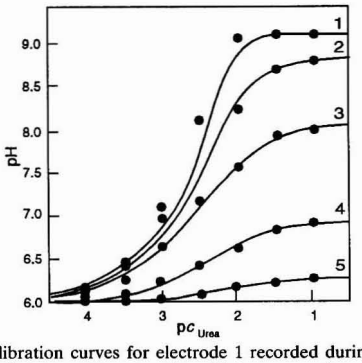

Fig. 1 Calibration curves for electrode 1 recorded during the first five days after sensor preparation. Dots represent experimental points, solid lines are theoretical curves, and numbers are the number of days after sensor preparation.

Table 1 Analytical parameters, obtained from calibration curves, for electrode 1

Day	pH(ULD)	k_V^{ULD} /mol dm^{-3}	k_V /mol dm^{-3}	K_M/O^{-3} mol dm^{-3}	ELF
1	9.11	0.2786	0.2786	3×10^{-4}	10^7
2	8.81	0.0543	0.0655	6.9	9.50
3	8.00	0.0075	0.0086	8.2	1.05
4	6.93	0.0013	0.0013	8.5	0.16
5	6.29	0.0002	0.0002	8.3	0.02

where $k_V(0)$ is the initial value of k_V at the time of membrane preparation. Parameter A gives information about the rate of membrane activity decay and, therefore, we propose that LTF is defined as

$$\mathrm{LTF} = -\left(\frac{\mathrm{d}\ln k_V}{\mathrm{d}t}\right)^{-1} = \frac{1}{A} \qquad (14)$$

Both parameters LTF and $k_V(0)$ can be easily determined from the linear regression $\ln(k_V) = f(t)$. Table 2 lists the values obtained for LTF and $k_V(0)$ for the sensors investigated.

Discussion

It was shown that k_V can be used instead of ELF in the kinetic model. Both parameters give the same information, but determination of ELF is more difficult. Determination of k_V is simple and both methods presented here [based on eqns. (8) and (9)] give coherent results.

ELF [eqn. (4)] is fully analogous to the ELF in the diffusional models, and after introducing Waley's corrections for the influence of pH, ELF′ [eqn. (7)] gives the same information as the Thiele modulus. In spite of this, ELF is a less certain parameter then k_V. Its uncertainty results from errors in the determination of K_M in the case of high enzymic membrane activity. This problem can be bypassed using K_M values obtained from other sources.

Both parameters presented here, k_V and LTF, are useful for comparison of biosensors. In the case of the sensors investigated, both electrodes with physically immobilized urease (electrodes 1 and 2; Table 2) have short lifetimes (low LTF values). The comparison of $k_V(0)$ for these two sensors shows better enzyme loading for the electrode obtained by enzyme adhesion (electrode 1) than enzyme inclusion (electrode 2). The chemical immobilization of urease results in more stable sensors (high values of LTF for electrodes 3 and 4) compared to physical immobilization. Such sensors (electrodes 3 and 4) are better, although the initial enzyme loading is higher for the electrode obtained by enzyme adhesion (electrode 1). Electrode 3 is less stable than electrode 4, although the initial enzyme loading is slightly better for electrode 3. This is the result of more stable enzyme binding in electrode 4, which was discussed in detail elsewhere.[19]

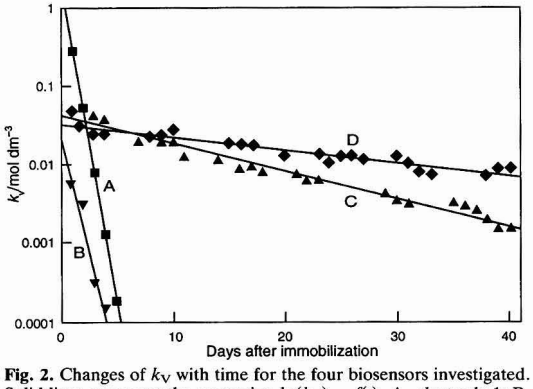

Fig. 2. Changes of k_V with time for the four biosensors investigated. Solid lines represent the regression $\ln(k_V) = f(t)$. A, electrode 1; B, electrode 2; C, electrode 3; and D, electrode 4.

Table 2 $k_V(0)$/mol dm^{-3} and LTF value for the biosensors investigated calculated from the linear regression $\ln[k_V(t)] = \ln[k_V(0)] + \mathrm{LTF}\cdot t$; r = regression coefficient

Electrode	$k_V(0)$/ mol dm^{-3}	LTF/d	r
1	1.986	1.25	0.99
2	0.025	1.75	0.97
3	0.040	28.25	0.99
4	0.032	58.15	0.98

For electrodes with similar values of $k_V(0)$, comparison of LTF values gives information about the ratio of lifetimes. This applies for electrodes 3 and 4. The comparison of LTF values for these sensors shows that the lifetime of electrode 4 is twice as long as the lifetime of electrode 3.

It is worth noting that parameters k_V and ELF are independent of measurement conditions. Changes in pH or concentration of buffer will, of course, modify the protolytic equilibrium in the enzymic membrane and, therefore, will change the analytical signal (ΔpH).[12,13] In spite of this, k_V and ELF do not change, as shown before.[15] This is, of course, not true in the pH range where the enzyme is destroyed.

On the basis of changes of k_V with time it is possible to estimate k_V for any day, and using this value to calculate the magnitude of the analytical signal [eqn. (8)] for this day. Such calculations allowed the lifetime of electrode 3 (more than two months) and electrode 4 (more than four months) to be estimated.

Conclusions

The two parameters presented here: k_V (or ELF) and LTF, are useful for a description of the quality and lifetime of pH enzymic sensors and the comparison of such sensors. The ELF defined in the kinetic model has the same meaning as the ELF defined in the diffusional models, but its determination is much simpler. Moreover, it can be used more widely than the ELF defined in the diffusional models. It can be used to describe sensors with a very thin enzymic membrane or with a monomolecular layer of enzyme covalently bound to the pH detector surface. Diffusional models in these cases lead to erratic results.[5]

The parameter k_V or ELF may be used to describe the enzyme activity of a sensitized membrane, and also the activation or inhibition of an enzyme. It should be useful for a quantitative description of enzyme biosensors used for determination of inhibitors (*e.g.*, determination of toxins, pesticides or insecticides using pH-based enzyme sensors for acetylcholine or butyrylcholine[22–25]) or pH-based immunoenzymic sensors (*e.g.*, determination of herbicides and immunoglobulins).[25–27] The analytical signal in both types of these biosensors is a function of the biocatalytic activity of a sensitized membrane in contrast to typical substrate-sensitive enzyme electrodes.

The concept of k_V (or ELF) and LTF presented here may be adopted for potentiometric enzyme sensors other than pH-based enzyme electrodes. To achieve this, Morf's model[17] should be used to describe such sensors in the same way as was carried out for pH-based enzyme electrodes. The utility of this model for the description of potentiometric enzyme sensors and tissue electrodes has been presented elsewhere.[16]

The concept of LTF can be adopted in the diffusional models of enzyme sensors.

The authors are grateful to Professor A. Hulanicki for valuable discussions. This study was supported by the Committee of Scientific Research (grant KBN 2P30300107).

References

1 Blaedel, W. J., Kissel, T. R., and Boguslaski, R. C., *Anal. Chem.*, 1972, **44**, 2030.
2 Hameka, H. F., and Rechnitz, G. A., *Anal. Chem.* 1981, **53**, 1586.

3 Carr, P. W., and Bowers, L. D., *Immobilized Enzymes in Analytical and Clinical Chemistry. Fundamentals and Applications*, Wiley, New York, 1980.
4 Brady, J. E., and Carr, P. W., *Anal. Chem.*, 1980, **52**, 977.
5 Caras, S. D., Janata, J., Saupe, D., and Schmitt, K., *Anal. Chem.*, 1985, **57**, 1917.
6 Varanasi, S., Stevens, R. L., and Ruckenstein, E., *AIChE J.*, 1987, **33**, 558.
7 Varanasi, S., Ogundiran, S. O., and Ruckenstein, E., *Biosensors*, 1988, **3**, 269.
8 Moynihan, H. J., and Wang, N.-H. L., *Biotechnol. Progr.*, 1987, **3**, 90.
9 Carr, P. W., *Anal. Chem.*, 1977, **49**, 799.
10 Hameka, H. F., and Rechnitz, G. A., *J. Phys. Chem.*, 1983, **87**, 1235.
11 Waley, S. G., *Biochim. Biophys. Acta*, 1953, **10**, 27.
12 Głąb, S., Koncki, R., and Hulanicki, A., *Electroanalysis*, 1991, **3**, 361.
13 Głąb, S., Koncki, R., and Hulanicki, A., *Analyst*, 1991, **116**, 453.
14 Głąb, S., Koncki, R., and Holona, I., *Analyst*, 1992, **117**, 1671.
15 Głąb, S., Koncki, R., and Hulanicki, A., *Analyst*, 1992, **117**, 1675.
16 Koncki R., Głąb, S., and Hulanicki, A., *Anal. Chim. Acta*, 1993, **273**, 477.
17 Morf, W. E., *Mikrochim. Acta*, 1980, **2**, 317.
18 Głąb, S., Koncki, R., Kopczewska, E., Wałcerz, I., and Hulanicki, A., *Talanta*, 1994, **41**, 1201.
19 Koncki, R., Kopczewska, E., and Głąb, S., *Anal. Lett.*, 1994, **27**, 475.
20 Barth, A., and Michel, H.-J., *Biochem. Physiol. Pflanzen*, 1972, **163**, 103.
21 Atkinson, B., and Rousseau, I., *Biotechnol. Bioeng.*, 1977, **19**, 1065.
22 Stein, K., and Schwedt, G., *Anal. Chim. Acta*, 1993, **272**, 73.
23 Kumaran, S., and Tran-Minh, C., *Electroanalysis*, 1992, **4**, 949.
24 Nyamsi Hendji, A. M., Jaffrezic-Renault, N., Martelet, C., Clechet, P., Shul'ga, A. A., Strikha, V. I., Netchiporuk, L. I., Soldatkin, A. P., and Wlodarski, W. B., *Anal. Chim. Acta*, 1993, **281**, 3.
25 Barbaro, A., Colapicchioni, C., Davini, E., Mazzamurro, G., Piotto Piotto, A., and Porcelli, F., *Adv. Mater.*, 1992, **4**, 402.
26 Colapicchioni, C., Barbaro, A., Porcelli, F., and Giannini, I., *Sens. Actuators*, 1991, **B4**, 245.
27 Sakai, H., Kaneki, N., Hara, H. and Ito, K., *Anal. Chim. Acta*, 1990, **230**, 189.

Paper 4/01739K
Received March 23, 1994
Accepted September 9, 1994

Determination of Lead Using a Poly(vinyl chloride)-based Crown Ether Membrane

Suresh K. Srivastava, Vinod K. Gupta and Suresh Jain
Department of Chemistry, University of Roorkee, Roorkee (U.P.), India

A poly(vinyl chloride) (PVC)-based membrane of 15-crown-5 exhibits a good response for lead(II) ions over a wide concentration range. The response time of the sensor is 30 s and the membrane can be used for more than four months without observing any divergence. The selectivity of the sensor is comparable with those reported for other such electrodes. It was possible to determine lead in polluted waters using this electrode assembly.

Keywords: Membrane sensor; lead determination; water analysis; ion-selective electrode; crown ether membrane

Introduction

Crown ethers have played an important role in the development of ion-selective electrodes (ISEs) owing to their specific selectivity and extraction efficiency for metal ions. Taking advantage of their ion discriminating power, the macrocyclic ethers have been shown to be highly suitable materials for the development of metal ion sensors. A good deal of work has already been reported on such compounds and the same is summarized in reviews in *Analytical Chemistry* from time to time. The review by Janata[1] covers all reports appearing on this subject up to 1991–92. Some recent papers on diaza and thia crowns are of particular interest.[2,3]

Efforts made to develop lead(II) ion-selective electrodes based on crown ethers were reviewed by Sheen and Shih.[4] This paper deals with the determination of lead using a 15-crown-5 membrane. This particular compound has only rarely been used as a complexing ligand for alkali metals and so far its utility as an electroactive phase for metal ion activity measurements has not been explored. The performance of this sensor is comparable to, and in some respects superior to, those of others reported in the literature.

Experimental

Reagents

15-Crown-5 was obtained from Fluka (Buchs, Switzerland). All other chemicals were of analytical-reagent grade from Merck (Darmstadt, Germany).

Equipment

A Perkin-Elmer Model 3100 atomic absorption spectrometer with a graphite furnace, and a Model 8440 ICP spectrometer (Labtam, Australia) were used. A Radiometer pH M64 millivoltmeter coupled to a Servoscribe recorder was used for e.m.f. measurements.

Electrode Preparation

The method reported by Craggs *et al.*[5] was adopted for the preparation of membranes. They were prepared by dissolving 250 mg of poly(vinyl chloride) (PVC), 50 mg of dibutyl phthalate and 20 mg of 15-crown-5 in 10 cm^3 of tetrahydrofuran. After shaking the mixture vigorously and removing all air bubbles it was poured into a holder and the solvent was made to evaporate at room temperature. The resulting membrane was cut to size, attached to a Pyrex tube with the help of Araldite and equilibrated with Pb^{2+} solution (1.0 mol dm^{-3}) for 6 d. The equilibration time and the ratio of the membrane ingredients, *i.e.*, electroactive phase, plasticizer, PVC, *etc.*, were optimized first so that the membrane developed reproducible potentials and remained stable for a long time. Table 1 gives the data obtained with membranes having various ratios of different constituents. The membrane chosen for subsequent work (No. 2) exhibited the optimum slope and concentration range in which it can sense lead(II) ions.

Potentials were measured by direct potentiometry at 25 ± 0.1 °C with the help of ceramic junction calomel electrodes. The cell set-up was the same as that reported earlier.[6]

Pure solutions of lead(II) ions, if taken in the functional concentration range, do not need any pH adjustment. Their pH lies between 3 and 6, which is the functional pH range of the sensor (see Fig. 2). If necessary, pH adjustments were made using very dilute solutions of nitric acid and ammonia solution. The pH measurements were made with a pH meter using a glass electrode.

Results and Discussion

The PVC-based membrane of 15-crown-5 generated stable potentials when placed in contact with lead nitrate solution. The e.m.f. response of the membrane in presence of a wide range of concentrations of Pb^{2+} solution is shown in Fig. 1. The electrode exhibits a linear response in the region 5.20 mg dm^{-3} –20.72 × 10^3 mg dm^{-3} and can therefore be used for the determination of lead in this concentration range. The slope of the plot, 30 mV per decade of concentration, indicates the Nernstian nature of this sensor.

The static response time of the membrane sensor, *i.e.*, the time in which stable and constant potentials are recorded, is 30 s over the entire concentration range. Potentials remain constant for more than 10 min, after which a very slow divergence is recorded. The standard deviation of 20 identical measurements is ±2 mV. One membrane can be used for more than four months if properly stored (dipped in water)

and cross-contamination is avoided. Under laboratory conditions the sensor has actually been used for six months, but the membrane was again equilibrated with Pb^{2+} solution (1.0 mol dm^{-3}) for 2 d. The time for subsequent equilibration is much shorter than the initial one.

The working of the membrane electrode in relation to the variation in concentration of reference solutions was also observed. Functioning of the membrane sensor with reference solutions of various concentrations, *viz.*, 0.01, 0.05 and 0.10 mol dm^{-3} (Fig. 1) reveals that 0.10 mol dm^{-3} is most appropriate Pb^{2+} concentration as internal reference, and all subsequent observations were made at this concentration. At lower concentrations a decrease in the working concentration range and a change in slope were observed.

The pH dependence of the membrane electrode was tested over the pH range 1.5–6.0 at a 1.0×10^{-3} mol dm^{-3} Pb^{2+} concentration (Fig. 2). The potentials remained constant from pH 3 to 6 and the sharp fall at pH <3 could be due to the protonation of the crown ether in the membrane phase, which results in a loss of its ability to complex with lead ions. Such observations, *i.e.*, of crowns losing their metal-binding capacity owing to protonation, have also been reported by other workers.[4]

In order to investigate the selectivity of this new membrane, the response of the electrode was examined in the presence of various foreign ions. The potentiometric selectivity coefficient ($k^{Pot}_{Pb,M}$) was evaluated by the fixed interference method using the expression $\ln k^{Pot}_{A,B} = \ln a_A/(a_B)^{Z_A/Z_B}$, where a_A is the activity of primary and a_B that of interfering ions, at a 0.01 mol dm^{-3} concentration of interfering ions. The value of this parameter is generally low for polyvalent ions. As such these ions would normally not interfere. Despite the high selectivity coefficients of monovalent ions, they may not interfere unless present at high concentrations. Fixed interference or separate solution methods are based on the Nikolsky equation:

$$E_{ISE} = E_0 \pm RT/Z_AF \ln[a_A + \sum_{a_B} k^{Pot}_{A,B} (a_B)^{Z_A/Z_B}]$$

which is an empirical relationship and works well in modelling the non-specific response of a membrane electrode when the ions under investigation have the same charge. This equation is not well suited, however, when ions of different charges are involved. The coefficients are either deceptively large or small depending on whether the ion of higher charge is considered as the primary or interfering species. These distorted values are caused by the superscripts on the activity/concentration terms, which are necessary in the Nikolsky equation to account for the different response slopes for ions with different charges. These problems have already been recognized[7–11] and earlier recommendations in this regard are being revised. In spite of existing IUPAC recommendations, the referred to methodology and expression are being used by various workers,[7–11] in a modified manner, to their advantage and there is no consistent approach in this regard.

In view of this, the selectivity coefficients were evaluated with the help of normal expression bearing superscripts, *i.e.*, $\ln k^{Pot}_{A,B} = \ln a_A/(a_B)^{Z_A/Z_B}$, and also by the same expression excluding superscripts, *i.e.*, in $k^{Pot}_{A,B} = \ln a_A/a_B$ (Fig. 3), at a slightly higher level of interference (0.01 mol dm^{-3}). It is observed that in spite of large $k^{Pot}_{Pb,M}$ values for monovalent interfering ions, these do not seem to interfere unless present at high concentrations. To confirm this point, mixed runs were made at different concentrations of a monovalent interfering ion (Na^+) (Fig. 4) and for the sake of comparison a mixed run at different interfering concentrations of bivalent Ca^{2+} was also recorded (Fig. 4). As is evident from the plots, the monovalent ion does not interfere if present at concentrations of $\leq 10^{-4}$ mol dm^{-3}. On the other hand, calcium shows very little interference even at a 10^{-4} mol dm^{-3} concentration (Fig. 4). The behaviour of the monovalent (Na^+) and bivalent (Ca^{2+}) ions is thus more truly depicted in the selectivity

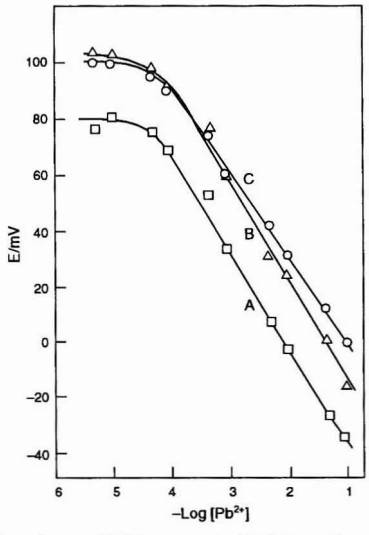

Fig. 1 Plots of potential (*E*) *versus* $-\log [Pb^{2+}]$ at various concentrations of internal reference solution: A, 0.01; B, 0.05 and C, 0.10 mol dm^{-3}.

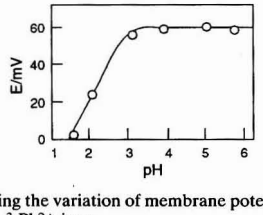

Fig. 2 Plot showing the variation of membrane potential with pH for 1×10^{-3} mol dm^{-3} Pb^{2+} ions.

Table 1 Optimization of membrane ingredients (electroactive phase, plasticizer and PVC)

	Composition				
Membrane no.	Crown ether (%)	PVC (%)	Plasticizer (%)	Detection limit/mg dm^{-3}	Slope/mV per decade
1	1	10.0	2.5	103.60	25
2	1	12.5	2.5	5.20	30
3	1	15.0	2.5	18.65	36
4	1	20.0	2.5	41.44	40
5	2	12.5	2.5	14.50	33
6	1	12.5	2.0	20.72	27
7	1	12.5	3.0	14.50	32

coefficient values, as calculated by the expression without using superscripts (Fig. 3).

Heavy metal ions, such as Ag^+, Hg^{2+}, Cd^{2+}, Cu^{2+} and Fe^{3+}, would not disturb the functioning of this sensor, whereas these ions are reported to be serious interferents with other lead ISEs reported in literature.[12–15] Copper and iron interfere with lead electrodes more severely.[16]

Anions such as acetate and carbonate also do not interfere with the working of this electrode assembly.

The functioning of the electrode system was also observed in a partially non-aqueous medium. It was found that the assembly works well in solutions having a non-aqueous (alcohol) content of up to 35% v/v. Above this level (non-aqueous content) serious divergence is observed. In addition, the electrode was found to work well in presence of cationic or anionic surfactants at low concentrations (approximately 10^{-5} mol dm^{-3}). Even the presence of proteinous matter, at low concentrations, does not cause any disturbance.

This electrode assembly was also successfully applied as an indicator electrode in the potentiometric titration of 20.0 cm^3 of Pb^{2+} solution of concentration 10^{-3} mol dm^{-3} with EDTA solution of concentration 0.01 mol dm^{-3}. Calomel electrodes along with an NH_4NO_3 bridge were also used for titration. Dilution effects were taken into consideration and duly accounted for. Fig. 5 exhibits the change in potential with gradual addition of EDTA. A very good inflection point, showing perfect stoichiometry, is observed in the titration plot.

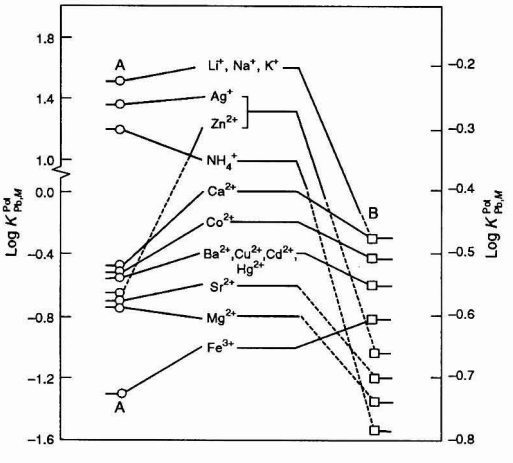

Fig. 3 Selectivity coefficients (log $k^{Pot}_{Pb,M}$) of various interfering ions (M^{Z+}) with (A) and without (B) superscript for lead ion-selective electrode based on 15-crown-5.

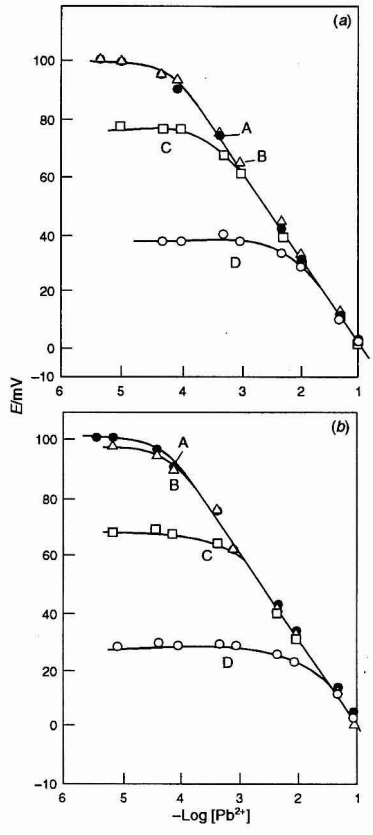

Fig. 4 Potential *versus* log [Pb^{2+}] plots in presence of (*a*) sodium and (*b*) calcium ions at varying levels of interference. A, 0.0; B, 1.0×10^{-4}; C, 1.0×10^{-3}; and D, 1.0×10^{-2} mol dm^{-3}.

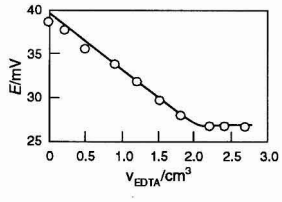

Fig. 5 Titration graph of 20.0 cm^3 of 1.0×10^{-3} mol dm^{-3} $Pb(NO_3)_2$ solution with 0.01 mol dm^{-3} EDTA.

Table 2 Analytical data for river water samples and lead contents as determined with the membrane sensor

Sample no.	Reported values/mg dm^{-3}														Pb^{2+} concentrations determined with membrane sensor/mg dm^{-3}
	Na^+		Ca^{2+}		Zn^{2+}		Hg^{2+}		Cu^{2+}		Cr^{3+}		Pb^{2+}		
	AAS	ICP	AAS	ICP	AAS	ICP	AAS	ICP	AAS	ICP	AAS	ICP	AAS	ICP	
1	2.2	2.4	3.5	3.2	4.2	4.5	6.8	6.8	5.8	5.8	5.8	5.5	10.5	10.4	10.4
2	1.9	2.3	3.4	3.3	4.2	4.3	5.4	5.8	5.2	5.4	6.4	6.3	12.4	12.2	12.4
3	2.0	2.2	3.5	3.3	4.0	4.5	6.2	6.4	6.6.	6.6	6.8	6.4	16.5	16.2	16.4
4	2.2	2.5	3.2	3.3	4.2	4.2	5.0	5.6	6.0	6.0	6.2	6.1	20.7	20.8	20.6

The electrode works well under laboratory conditions in pure solutions and also in synthetic mixtures. To assess its applicability to waste water or actual systems, an attempt was made to determine lead in water samples from a local river, Hindon, which is highly polluted and the monitoring of which has already been conducted by the Ministry of Environment, Government of India. The government analysts have used atomic absorption (AAS) and inductively coupled plasma (ICP) spectrometry for the determination of metal ions and the official data were made available on request. Each sample was run in triplicate (a number of times) using these instruments and the divergence in the results was of the order of 0.3 and 0.2 mg dm^{-3} for AAS and ICP, respectively. Table 2 shows the agreement between the reported values obtained by the two techniques for lead and other matrix metals in Hindon river water. In this work, four samples were collected, from locations identified by the government agency, for which the official values are available. The samples also contained Hg^{2+}, Cu^{2+} and Pb^{2+} in the concentrations given in Table 2. The samples were collected by a routine technique (grab method) and preserved with the help of HNO_3, stored in plastic containers and analysed within 12 h of collection. Each sample was analysed in triplicate and the analysis by ISE was repeated under identical conditions, a number of times (four to six), to assess the reliability of the results. As the samples contained particulate matter, they were centrifuged at 20000 rev min^{-1} for 5 min and the potentials were measured after adjusting their pH with HNO_3 if necessary. No other adjustment was found to be necessary. The amounts of lead evaluated with the help of the sensor under investigation are also given in Table 2. The values obtained with this electrode match those determined by ICP and AAS, thereby reflecting the utility of this membrane sensor.

Conclusion

The membrane sensor incorporating 15-crown-5 as the electroactive phase can be used to determine lead in the concentration range 5.20 mg dm^{-3}–20.72 × 10^3 mg dm^{-3}. The functional pH range is 3–6 and most of the ions that interfere with other lead electrodes do not cause any disturbance with this assembly. Its response time is 30 s and the sensor, if properly stored, can be used for more than four months. It can also be successfully employed for the determination of lead in waste water.

One of the authors (S. J.) is grateful to CSIR, India, for providing a Senior Research Fellowship.

References

1 Janata, J., *Anal. Chem.*, 1992, **64**, 196R.
2 Brzozka, Z., and Pietraszkiewie, Z. M., *Electroanalysis*, 1991, **3**, 855.
3 Sakamoto, H., *Bunseki Kagaku*, 1992, **41**, 468.
4 Sheen, S.-R., and Shih, J.-S., *Analyst*, 1992, **117**, 1691.
5 Craggs, A., Moody, G. J., and Thomas, J. D. R., *Analyst*, 1970, **95**, 910.
6 Srivastava, S. K., Sahgal, V., and Vardhan, H., *Sensors Actuators B*, 1993, **13–14**, 391.
7 Craggs, A., Keil, L., Moody, G. J., and Thomas, J. D. R., *Talanta*, 1975, **22**, 907.
8 Johnson, S., Moody, G. J., and Thomas, J. D. R., *Analyst*, 1989, **114**, 1025.
9 Glazier, S. A., and Arnold, M. A., *Anal. Chem.*, 1991, **63**, 754.
10 Moody, G. J., and Thomas, J. D. R., *Ion-Sel. Electrode Rev.*, 1979, **1**, 3.
11 Jaber, A. M. Y., Moody, G. J., and Thomas, J. D. R., *Analyst*, 1988, **113**, 1409.
12 Hirata, H., and Date, K., *Anal. Chem.*, 1971, **43**, 279.
13 Hirata, H., and Higashiyama, K., *Anal. Chim. Acta*, 1971, **57**, 276.
14 Mascini, M., and Liberti, A., *Anal. Chim. Acta*, 1972, **60**, 405.
15 Midgley, D., *Anal. Chim. Acta*, 1984, **159**, 63.
16 Heijne, G. J. M., van der Linden, W. E., and den Boef, G., *Anal. Chim. Acta*, 1978, **193**, 100.

Paper 4/00748D
Received February 7, 1994
Accepted August 16, 1994

Nitrite-sensitive Liquid Membrane Electrodes Based on Metalloporphyrin Derivatives

De Gao, Jun Gu and Ru-Qin Yu

Department of Chemistry and Chemical Engineering, Hunan University, Changsha, 410082, China

Guo-Dong Zheng

Department of Chemistry, Jilin University, Changchun, 130023, China

Liquid membrane electrodes based on some metalloporphyrin derivatives exhibit an anti-Hofmeister selectivity pattern: NO_2^- > SCN^- > I^- > F^- > Br^- > Cl^- > ClO_4^- > NO_3^-. These derivatives include chloro(5,10,15,20-tetraphenylporphyrinato)indium, chloro[5,10,15,20-tetra(*p*-methoxyphenyl)porphyrinato]indium and chloro(2-nitro-5,10,15,20-tetraphenylporphyrinato)indium. The selectivity pattern is interpreted on the basis of the coordination chemistry of metalloporphyrins. The membrane electrode with optimum composition shows a linear potentiometric response towards nitrite ion in the range 6.3×10^{-5}–0.1 mol l^{-1} with a slope of 51 mV/pNO_2^- and a detection limit of 5.0×10^{-6} mol l^{-1}. The electrode was applied to the determination of nitrite in Chinese cabbage.

Keywords: Nitrite-selective electrode; liquid membrane electrode; metalloporphyrins

Introduction

Since the pioneering work of Simon's group, discovering that vitamin B_{12} derivatives can be used as anion carriers for the preparation of liquid membrane electrodes,[1] similar compounds such as metalloporphyrin derivatives have been tried as candidates for anion-sensing materials.[2–14] One interesting potentiometric response characteristic of such metalloporphyrins as anion carriers is their selectivity pattern, different from the so-called Hofmeister selectivity sequence: ClO_4^- > SCN^- > I^- > NO_3^- > Br^- > NO_2^- > Cl^-.[2] The origin of the anti-Hofmeister selectivity order with metalloporphyrin derivatives as anion carriers comes from the interaction between the central metal and the analyte anions, and therefore the nature of the central metal plays an important role in the realization of the selectivity pattern of electrodes based on the metalloporphyrins. Tetraphenylporphyrins of cobalt, manganese, molybdenum and iron sensing SCN^-,[2,4,12,14] those of tin sensing salicylate[6] and octalethylporphyrinatoindium sensing Cl^-,[9] have been reported. In this paper, the use of substituted tetraphenylporphyrinatoindium derivatives is reported together with their potentiometric response characteristics and preliminary application to the determination of nitrite in vegetable samples.

Experimental

Reagents

The synthesis of 5,10,15,20-tetraphenylporphyrin (TPP) was carried out according to the method of Alder *et al.*[15] 5,10,15,20-Tetra(*p*-methoxyphenyl)porphyrin [(*p*-OCH_3)-TPP] was synthesized according to the method described by Walker.[16] The nitro derivative 2-nitro-5,10,15,20-tetraphenyl porphyrin [(2-NO_2)TPP] was prepared from TPP following the procedure of Hombrecher *et al.*[17] Chloro(5,10,15,20-tetraphenylporphyrinato)indium (InTPPCl), chloro-[5,10,15,20-tetra(*p*-methoxyphenyl)porphyrinato]indium [(*p*-OCH_3)InTPPCl] and chloro(2-nitro-5,10,15,20-tetraphenyl-porphyrinato)indium [(2-NO_2)InTPPCl] were synthesized according to the method of Alder *et al.*[18] The structure of these metalloporphyrins is shown in Fig. 1. The carrier 5,10,15,20-tetraphenylporphyrinatoaluminum (AlTPPCl) was prepared from TPP according to the literature.[19] Methyltrioctylammonium iodide (MTOAI) was also synthesized according to the literature.[20] All ionophores synthesized were purified by chromatography using a neutral Al_2O_3 column and identified by UV/VIS and IR spectrometry and elemental analysis. Poly(vinyl chloride) (PVC) powder of chromatographic grade and tetrahydrofuran (THF) and didecyl sebacate (DDS) of analytical-reagent grade were purchased from Shanghai Chemical. Doubly distilled, de-ionized water was used throughout.

Apparatus

Potentiometric and pH measurements were carried out on a Model 901 Microprocessor Ionalyzer (Orion, Cambridge, MA, USA). Cell assemblies of the following type were used:

$Hg|Hg_2Cl_2|KCl$(satd.)‖sample solution|membrane|0.1 mol l^{-1} KCl|Ag|AgCl

Procedures

The solution was buffered with 0.01 mol l^{-1} H_3PO_4 and the pH was adjusted with NaOH solution. The membrane composition was 1% m/m ionophore, 33% m/m PVC and 66% m/m solvent mediator. The membranes were prepared by using 165 mg of PVC, 330 mg of solvent mediator and 5 mg of ionophore. First, the ionophore was dissolved in the solvent

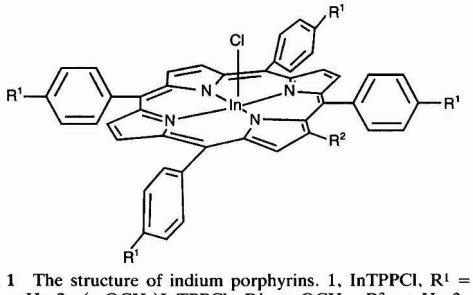

Fig. 1 The structure of indium porphyrins. 1, InTPPCl, R^1 = H, R^2 = H; 2, (*p*-OCH_3)InTPPCl, R^1 = OCH_3, R^2 = H; 3, (2-NO_2)InTRPPCl, R^1 = H, R^2 = NO_2.

mediator, then the PVC and a sufficient amount of THF were added and mixed to obtain a transparent solution. This mixture was transferred onto a 20 cm^2 glass plate and the THF was allowed to evaporate at room temperature, leaving a tough, flexible membrane trapped in a PVC matrix.

The potentiometric selectivity coefficients, $\log k^{pot}_{NO_2^-,X^-}$ were obtained by the separate solution method.[21] The solution was buffered with 0.01 mol l^{-1} H_3PO_4 and adjusted to pH 5.5. with NaOH solution. The single-ion activity was calculated by the following equations[22]

$$\log\gamma_+ = |Z^+/Z^-|\log\gamma_\pm$$
$$\log\gamma_- = |Z^-/Z^+|\log\gamma_\pm$$

Macerated Chinese cabbage kept for 24 h at 25 °C was treated according to the literature method.[23] The sample was analysed by both the electrode method and by spectrophotometry after being diluted 20-fold. The measurements of both the potentiometric selectivity coefficients and the concentration of NO_2^- in Chinese cabbage were carried out in triplicate.

Results and Discussion

Potentiometric Anion Response Characteristics of Electrodes

Table 1 gives the selectivity coefficients of the electrodes based on (*p*-OCH_3)InTPPCl, InTPPCl, (2-NO_2)InTPPCl, AlTPPCl and MTOAI. The selectivity sequence of substituted indium porphyrin derivatives for anions differs from the Hofmeister selectivity pattern of the classical liquid ion-exchange type ionophores under comparable experimental conditions. This behaviour is determined by the properties of both the carriers and the anions. For classical liquid ion-exchange type electrodes, the anion response is based on the ion-exchange properties between analyte anions and the counter ion,[22] and electrostatic interaction plays a dominate role in the transfer of an anion across the organic–water interface. The hydration energy of the analyte anions must be overcome by the electrostatic affinity and the selectivity sequence is determined by the order of hydration energy or hydrophilicity of the analyte anions. For ionophores based on metalloporphyrins, in addition to the electrostatic interaction between the central metal and analyte anions, there is a coordination action between both species and the anion hydration energy is dominated by both electrostatic and coordination forces. As the charges of the carriers and analyte anions are fixed, the Hofmeister selectivity sequence of classical liquid ion-exchange membrane electrodes can be altered by the coordination affinity. Taking the anions ClO_4^- and NO_2^- as examples, the hydration energy of NO_2^- is larger than that of ClO_4^- when a lipophilic quaternary ammonium salt is used as the sensing material, the Hofmeister selectivity sequence is realized and the ClO_4^- ion preferentially enters the membrane phase. For the indium porphyrin membrane electrodes, however, in addition to the electrostatic interaction between the membrane active component and the analyte anions, there is an unoccupied coordination site at the sixth axial position, the ionophore can preferentially coordinate with NO_2^- and the selectivity sequence of the analyte anions deviates from the Hofmeister selectivity behaviour.

It is interesting that the selectivity coefficients of the electrodes based on indium porphyrins for nitrite ion with respect to ClO_4^- and NO_3^- are much less than unity. For comparison, chloro(5,10,15,20-tetraphenylporphyrinato)aluminium was synthesized.

Aluminium and indium atoms have the similar electronic structures and it was expected that the electrodes based on AlTPPCl and InTPPCl would exhibit the similar potentiometric response characteristics. The results in Table 1 show that the selectivity patterns of these electrodes are different, particularly the selectivity coefficients for NO_2^- ion with respect to ClO_4^- ion. For the electrode based on AlTPPCl, the selectivity coefficient $\log k^{pot}_{ClO_4^-,NO_2^-}$ is 1.76, whereas for InTPPCl it is −2.43. The difference in the selectivity patterns of these electrodes is obviously related to the electronic structure of the central metal. For liquid membrane electrodes, the process of the potentiometric response for ionic species includes the entry of these species into the membrane phase and their interaction with the carriers, hence the selectivity pattern of the electrodes depends not only on the hydration energy of the analyte ions, but also on the interaction between the carriers and the analyte ions. For the ions located at the end of the classical Hofmeister selectivity order, the hydration energy is too high to be overcome by the interaction energy between the carriers and the analyte ions, and the selectivity pattern of these ions will follow the classical Hofmeister order. Although aluminium and indium are located in the same Group IIIA in the Periodic Table, their electronic configuration, electronegativity and Pauling radii, *etc.*, are different from each other. The differences in the central metal incorporated in the porphyrin ligand will induce changes in the electronic structure of the metalloporphyrin ring, affecting the coordination of metalloporphyrins with the analyte anions along the fifth or sixth axial positions and resulting in InTPPCl$^-$ and AlTPPCl-based electrodes exhibiting different selectivity patterns. Park *et al.*[9] demonstrated that when chloro(2,3,7,8,12,13,17,18-octaethylporphyrinato)-indium [In(OEP)Cl] was incorporated into the membrane phase, the electrode exhibited the selectivity order $I^- > SCN^- > Br^- \approx Cl^- > ClO_4^-$. The difference in the selectivity patterns between In(OEP)Cl and InTPPCl may be due to the increased basicity of the porphyrin ring in In(OEP)Cl.[24]

As In^{III} and Al^{III} tend to form stable complexes with fluoride ion, it is considered that InTPPCl or AlTPPCl preferentially coordinates F^- with relatively high affinity. Indeed, the potentiometric selectivity coefficients of the InTPPCl$^-$ and AlTPPCl-based electrodes for NO_2^- with respect to F^- ion

Table 1 Potentiometric selectivity coefficients of electrodes based on different carriers. The selectivity coefficients, $\log k^{pot}_{NO_2^-,X^-}$, were determined using the separate solution method in 0.01 mol l^{-1} H_3PO_4–NaOH buffered solution (pH 5.5); results are averages of three determinations

X^-	(*p*-OCH_3)InTPPCl	InTPPCl	(2-NO_2)InTPPCl	AlTPPCl	MTOAI
NO_2^-	0.0	0.0	0.0	0.0	0.0
ClO_4^-	−2.68	−2.43	−2.36	1.76	1.65
SCN^-	−0.74	−1.0	−0.98	1.38	0.55
NO_3^-	−2.98	−2.65	−2.93	−0.62	−0.35
I^-	−1.52	−1.03	−1.02	0.06	0.25
Br^-	−1.65	−1.35	−1.40	−0.54	−0.15
Cl^-	−1.74	−1.85	−2.09	−1.04	−0.85
F^-	−1.57	−1.20	−1.20	−0.30	—

are −1.20 and −0.30, respectively. The results obtained show that the higher affinity of the central metal for fluoride anions will favour the destruction of the water shell around the analyte species.

To a certain extent, the results obtained show that an electrode based on a metalloporphyrin derivative with an electron-donating group such as (*p*-OCH_3)InTPPCl possesses an enhanced selectivity for NO_2^- with respect to other anions, whereas the electrode based on (2-NO_2)InTPPCl, containing an electron-withdrawing group, would have a lower selectivity for NO_2^-. The result can be explained in terms of the coordination chemistry of metalloporphyrins. The coordination action between the metalloporphyrin and the analyte anion can be treated by the concept of generalized acid–base reactions;[25] the acidity of the central metal determines the coordination strength between the porphyrin and the analyte anion and also the selectivity for the primary anion with respect to other anions. For (2-NO_2)InTPPCl, the electron-withdrawing group increases the acidity of the central indium ion and enhances the coordination action between the metalloporphyrin and all the analyte anions, reducing the selectivity for the primary anion NO_2^- with respect to other anions. On the other hand, for (*p*-OCH_3)InTPPCl, the electron-donating effect decreases the acidity of the indium porphyrin and enhances the selectivity for the primary anion.

Effect of pH on Response Characteristics of Electrodes

Fig. 2 shows the effect of pH on the response characteristics of InTPPCl, (2-NO_2)InTPPCl and (*p*-OCH_3)InTPPCl-based electrodes. NO_2^- and OH^- ions seem to coordinate competitively with the indium porphyrin; the coordination ability of NO_2^- towards indium porphyrins is stronger than that of OH^-. When the concentration of NO_2^- is relatively high (0.1–10^{-3} mol l^{-1}), the NO_2^- ion is the primary analyte ion and OH^- interferes only slightly with the NO_2^- response, and the linear response characteristics of the electrode for NO_2^- ion are not affected substantially by OH^-. When the concentration of NO_2^- is relatively low (10^{-3}–10^{-6} mol l^{-1}), with increase in OH^- concentration OH^- becomes the primary analyte anion and the potentiometric response characteristics of the electrode for NO_2^- deviates from linearity, especially at high pH.

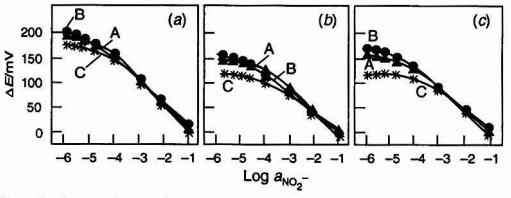

Fig. 2 Potentiometric pH response of electrodes: (*a*) (*p*-OCH_3)InTPPCl; (*b*) InTPPCl; and (*c*) (2-NO_2)InTPPCl. A, pH 5.0; B, pH 5.5; and C, pH 6.5.

Table 2 Comparison of results obtained by different methods for Chinese cabbage

Storage time/h	NO_2^- content/g kg^{-1}* Spectrophotometric method	Electrode method
0	1.3×10^{-3}	1.24×10^{-3}
24†	0.152	0.156

* The relative standard deviation was 2.5% for three determinations.

† The measurement of the sample solution was made after 20-fold dilution.

Determination of Nitrite in Rotten Chinese Cabbage

Nitrite can react directly with secondary amines to form nitrosamines, most of which are carcinogenic. It is important to check whether vegetables such as Chinese cabbage contain relatively high concentrations of NO_2^- after a certain period of storage without refrigeration. There are numerous methods for measuring nitrite in foods. The AOAC method is based on the classical Griess spectrophotometric method.[26] In this method, sulfamic acid is diazotized by free nitrite ion in acid form to form a diazonium salt of sulfamic acid. The latter is then coupled with 1-naphthylamine, forming a pink azo dye with an absorption maximum at 525 nm. Table 2 gives the results of the measurement of nitrite in rotten Chinese cabbage using the spectrophotometric[23] and electrode methods. It can be seen that there is a fair correlation between the values obtained by the two methods.

Conclusions

Liquid membrane electrodes based on indium porphyrins exhibit an anti-Hofmeister selectivity pattern: $NO_2^- > SCN^- > I^- > F^- > Br^- > Cl^- > ClO_4^- > NO_3^-$. When the porphyrin ring is fixed, the selectivity pattern of the electrodes based on metalloporphyrin derivatives is determined by the nature of the central metal. The electrode with optimum membrane composition can be used to determine the nitrite content of vegetables such as Chinese cabbage.

This project was supported by the National Natural Science Foundation of China and partially by the Laboratory of Electroanalytical Chemistry, Changchun Institute of Applied Chemistry, Chinese Academy of Science. The authors thank Professor M. E. Meyerhoff for sending a reprint of ref. 9.

References

1 Schulthess, P., Ammann, D., Simon, W., Caderas, C., Stepanek, R., and Krautler, B., *Helv. Chim. Acta*, 1984, **67**, 1026.
2 Ammann, D., Huser, M., Krauther, B., Rusterholz, B., Schulthess, P., Lindemann, B., Halder, E., and Simon, W., *Helv. Chim. Acta*, 1986, **69**, 849.
3 Chang, Q., and Meyerhoff, M. E., *Anal. Chim. Acta*, 1988, **186**, 81.
4 Chaniotakis, N. A., Chasser, A. M., and Meyerhoff, M. E., *Anal. Chem.*, 1988, **60**, 188.
5 Hodinar, A., and Jyo, A., *Chem. Lett.*, 1988, 993.
6 Chaniotakis, N. A., Park, S. B., and Meyerhoff, M. E., *Anal. Chem.*, 1989, **61**, 566.
7 Hodinar, A., and Jyo, A., *Anal. Chem.*, 1989, **61**, 1171.
8 Daunert, S., Wallace, S., Florido, A., and Bachas, L. G., *Anal. Chem.*, 1991, **63**, 1676.
9 Park, S. B., Matuszewski, W., Meyerhoff, M. E., Liu, Y. H., and Kadish, K. M., *Electroanalysis*, 1991, **3**, 909.
10 Kibbey, C. E., Park, S. B., De Adwyler, G., and Meyerhoff, M. E., *J. Electroanal. Chem.*, 1992, **335**, 135.
11 Wang, E., and Meyerhoff, M. E., *Anal. Chim. Acta*, 1993, **283**, 673.
12 Jyo, A., Minakami, R., Kanda, Y., and Egawa, H., *Sens. Actuators B*, 1993, **13/14**, 200.
13 Blair, T. L., Allen, J. R. Daunert, S., and Bachas, L. G., *Anal. Chem.*, 1993, **65**, 2155.
14 Gao, D., Li, J. Z., Yu, R. Q., and Zheng, G. D., *Anal. Chem.*, 1994, **66**, 2245.
15 Alder, A. D., Longo, F. R., and Finarelli, J. D., *J. Org. Chem.*, 1967, **32**, 476.
16 Walker, F. A., *J. Am. Chem. Soc.*, 1970, **92**, 4235.

17 Hombrecher, H. K., Gherdan, V., and Ohm, S., *Tetrahedron*, 1993, **49**, 8569.
18 Alder, A. D., Longo, F. R., Kampas, F., and Kim, J., *J. Inorg. Nucl. Chem.*, 1970, **32**, 2443.
19 Youoh, K., Naoaki, M., Katsuhisa, T., Yoshiaki, K., and Hiroshi, K., *Bull. Chem. Soc. Jpn.*, 1988, **58**, 103.
20 Hartman, K., Luterotti, S., Osswald, H. F., Oehme, M., Meier, P. C., Ammann, D., and Simon, W., *Mikrochim. Acta, Part II*, 1978, 235.
21 Guilbault, G. G., Durst, R. A., Frant, M. S., Freiser, H., Hansen, E. H., Light, T. S., Pungor, E., Rechnitz, G. A., Rice, N. M., Rohm, T. J., Simon, W., and Thomas, J. D. R., *Pure Appl. Chem.*, 1976, **48**, 127.
22 Morf, W. E., *The Principles of Ion-Selective Electrodes and of Membrane Transport*, Elsevier, Amsterdam, 1981.
23 Nicholas, R. A., and Fox, J. B., *J. Assoc. Off. Anal. Chem.*, 1973, **56**, 922.
24 Kadish, K. M., Cornillon, J. L., Cocolios, P., Tabard, A., and Guilard, R., *Inorg. Chem.*, 1985, **24**, 3645.
25 Pearson, R. G., *J. Am. Chem. Soc.*, 1963, **85**, 33.
26 *Official Methods of Analysis of the Association of Official Analytical Chemists*, AOAC, Washington, DC, 12th edn., 1975, Sects. 24.037–24.038.

Paper 4/03941F
Received June 29, 1994
Accepted August 30, 1994

Incorporation of Dodecylbenzenesulfonic Acid in a Poly(vinyl chloride) Matrix Chloride Ion-selective Membrane Based on Tertiary Ammonium

Satoshi Nomura

Horiba Ltd., 2 Kisshoin Miyanohigashimachi, Minami-ku, Kyoto 601, Japan

A chloride ion-selective electrode based on a tertiary ammonium ion exchanger was studied. By incorporating dodecylbenzenesulfonic acid in a conventional poly(vinyl chloride) matrix membrane, the electrode performance was improved in terms of linearity and selectivity against lipophilic anions. The slope of the emf response for a chloride ion concentration of between 0.1 and 1 mmol l^{-1} increased from 22 to 39 mV. Selectivity coefficients against interfering anions decreased by 20–80%.

Keywords: Ion-selective electrode; chloride ion; tertiary ammonium; dodecylbenzenesulfonic acid

Introduction

Since the pioneering work of Coetzee and Friser,[1,2] anion-selective electrodes based on the ion-association extraction of tertiary ammonium ions has been widely studied. Studies to improve their properties, such as selectivity and durability, have widened their applicability, particularly for clinical use.[3] We have found that a mixture of epoxy resin and poly(vinyl chloride) (PVC) is effective in increasing the selectivity and durability of a chloride anion-selective membrane based on a tertiary ammonium ion exchanger. A resin–PVC mixture was used in Horiba's human blood electrolyte analyser for the measurement of chloride anions in human blood.[4]

In this work, a cation exchanger, dodecylbenzenesulfonic acid (DBS), was incorporated as an additive in the liquid selective membrane based on the tertiary ammonium ion exchanger. By the addition of DBS, the electrode performance was improved. The slope of the emf response at lower chloride concentrations increased with the addition of DBS though the slope decreased at relatively higher chloride ion concentrations. The selectivity against interfering anions was also improved. In this paper, we describe the effect of incorporating DBS into the tertiary ammonium ion exchanger based liquid selective membrane.

Experimental

Reagent

The anion exchanger, tridodecylmethylammonium chloride (TDMA) was supplied by Dojin Kagaku, Kumamoto, Japan. The plasticizer, phthalic acid di-*n*-amyl ester (DAP) and the additive, DBS were supplied by Tokyo Kasei, Tokyo, Japan. The PVC and tetrahydrofuran (THF) were supplied by Shinetu Kagaku, Tokyo, Japan and Nacalai Tesque, Kyoto, Japan, respectively.

For all electrochemical measurements, test solutions were prepared from de-ionized water and analytical-reagent grade. Tris(hydroxymethyl)methylamine (TRIS), boric acid, potassium chloride, sodium hydrogencarbonate, magnesium sulfate, sodium acetate and sodium dihydrogenphosphate were supplied by Nacalai Tesqu, Kyoto, Japan.

Membrane and Electrode Preparation

The chloride ion-selective membrane (membrane 1) is composed of 200 mg of TDMA, 500 mg of DAP, 400 mg of PVC and 100 mg of DBS. A reference membrane without DBS (membrane 2) was prepared with 200 mg of TDMA, 600 mg of DAP and 400 mg of PVC. Both membranes were obtained by dissolving the components in THF and evaporating the THF in a 80 mm diameter petri dish at room temperature.

Circular membrane pieces 10 mm in diameter were stamped out from the master disk and the pieces were then attached to the electrode described in the previous paper.[4] The inner reference solution was TRIS (boric acid) buffer solution consisting of 5 mmol l^{-1} TRIS and 65 mmol l^{-1} boric acid (pH 7.5) containing 3 mmol l^{-1} potassium chloride.

Electrochemical Measurement

Measurements were carried out with the Horiba blood electrolyte analyser SERA-520 (Kyoto, Japan).[4] The electrochemical cell was as follows:

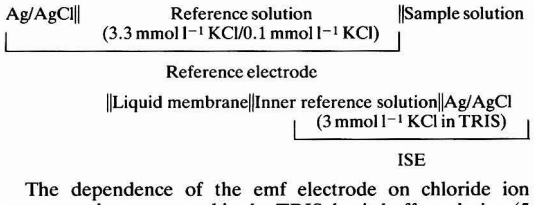

The dependence of the emf electrode on chloride ion concentration was tested in the TRIS–boric buffer solution (5 mmol l^{-1} TRIS–65 mmol l^{-1} boric acid, pH 7.5). Selectivity against interfering anions was evaluated by the mixed solution method[5] which consisted of keeping the chloride ion concentration at 1 mol l^{-1} and varying the interfering anion concentration from 0.01 mmol l^{-1} to 0.1 mmol l^{-1}.

Results and Discussion

In order to confirm the effect induced by DBS, the slopes of the emf responses at different chloride ion concentrations (0.1 to 10 mmol l^{-1}) and selectivity against interfering anions were evaluated for both membranes 1 and 2.

Table 1 shows the slopes obtained by both membranes. Membrane 1 had a greater slope at low chloride ion concentrations (*i.e.*, <1 mmol l^{-1}), but a smaller slope at high concentrations (*i.e.*, 0.5 mmol l^{-1}) compared with the reference membrane 2.

Table 2 shows selectivity coefficients of the four anions, *i.e.*, hydrogen carbonate, sulfate, acetate and dihydrogenphosphate anions. In the case of all four anions tested, membrane 1 improved the selectivity.

The improved selectivity can be explained by the cationic function of DBS: cation exchanger DBS blocked the interfering anions from approaching the ion-exchange site in the membrane.[6] The increased slope of the emf response at low chloride ion concentration is due to the improved selectivity against the anions present in the TRIS–boric buffer. The smaller slope at relatively higher concentrations can also be explained by the cationic function generated by DBS.

The effect of DBS has already been shown by Oka *et al.* in their study on plasticized polystyrene matrix chloride ion-selective membranes soaked in DBS solution.[6] Note that in the present study DBS was retained in conventional PVC matrix and the same effect was still observed. In addition, Schaller *et al.* recently described that the addition of an ionic site was effective in improving electrode performance not only in membranes based on neutral carriers but also in those based on charged carriers.[7] In the context of Schaller's findings, DBS in this work corresponds to the ionic additive which is incorporated in the calcium-selective membrane.[8]

The addition of the cation-exchanger DBS increased the slope of the emf response at low chloride ion concentrations, but decreased the slope at higher concentrations, with respect to the reference membrane. Selectivity against interfering anions was also improved. Further research will allow us to determine the membrane composition for optimum performance at both high and low chloride ion concentrations. However, in order to apply membrane 1 to blood analysis, an increased linear response at lower chloride ion concentrations ($\leq$1 mmol l^{-1}) is of more importance than a greater slope at higher concentrations. This is owing to the fact that in current blood electrolyte measurements, which are carried out by diluting blood samples in buffer solutions such as TRIS–boric acid to reduce the amount of sample required, the chloride ion concentration is less than 1 mmol l^{-1}. Studies on practical applications of the membrane to blood sample measurements are now being undertaken.

Table 1 Slopes of the emf response of membranes 1 and 2 at various chloride ion concentrations

	Slope/mV*	
Concentration range/mmol l^{-1}	Membrane 1	Membrane 2
10–1	52	57
5–0.5	52	54
1–0.1	39	22

* Average of five electrodes.

Table 2 Selectivity coefficient ($K^{pot}_{Cl^-,j}$) against interfering anions

	Selectivity coefficient ($K^{pot}_{Cl^-,j}$)*	
Interfering anion (j)	Membrane 1	Membrane 2
HCO_3^-	0.018	0.042
SO_4^{2-}	0.024	0.032
CH_3COO^-	0.045	0.083
$H_2PO_4^-$	0.083	0.45

* Average of three electrodes.

References

1 Coetzee, C. J., and Freiser, H., *Anal. Chem.*, 1968, **40**, 2071.
2 Coetzee, C. J., and Freiser, H., *Anal. Chem.*, 1969, **49**, 1128.
3 Koryta, J., *Anal. Chim. Acta.*, 1990, **233**, 1.
4 Uematsu, H., Kono, T., Usui, S., and Aomi, T., *Denki Kagaku*, 1987, **55**, 532.
5 Moody, G. J., and Thomas, J. D. R., *Selective Ion Sensitive Electrodes*, 1971, Merrow, Watford, England.
6 Oka, S., Sibazaki, Y., and Tahara, S., *Anal. Chem.*, 1981, **53**, 588.
7 Schaller, U., Bakker, E., Spichiger, U. E., and Pretsch, E., *Anal. Chem.*, 1994, **66**, 391.
8 Morf, W. E., Kahr, G., and Simon, W., *Anal. Lett.*, 1974, **7**, 9.

Paper 4/03618B
Received June 14, 1994
Accepted September 1, 1994

Use of Solid-phase Extraction Cartridges With Differential-pulse Cathodic Stripping Voltammetry at a Hanging Mercury Drop Electrode: Determination of Nedocromil Sodium and Pentamidine Isethionate in Urine

Maria Valnice B. Zanoni, Josino C. Moreira and Arnold G. Fogg*

Department of Chemistry, Loughborough University of Technology, Loughborough, Leicestershire, UK LE11 3TU

Nedocromil sodium (an antiasthma drug) and pentamidine isethionate (an antiprotozoal agent) were determined in urine by cathodic stripping voltammetry after adsorptive accumulation at a hanging mercury drop electrode as examples of the use of solid-phase extraction cartridges with this technique. Prior separation from matrix interferents was necessary and this was carried out using either a C_{18} solid-phase extraction cartridge or liquid–liquid extraction. For nedocromil, a recovery of 100.5 ± 6.5% (± 2 standard deviations) was obtained from urine spiked with 0.42 μg ml^{-1} of the drug using a C_{18} cartridge (five determinations). A 97% recovery of pentamidine isethionate was obtained by solid-phase extraction when the drug was added to urine at a level of 1.48 μg ml^{-1}. At lower levels of pentamidine isethionate, better recovery was obtained using liquid–liquid extraction: recoveries of between 60 and 100% were obtained at levels of 0.04–29.6 μg ml^{-1}. Linear calibration graphs were obtained for the determination of both drugs at concentration levels in the measured solution lower than 1 × 10^{-7} mol l^{-1} (*i.e.*, less than approximately 0.05 μg ml^{-1}): standard additions method was preferred for quantification. Relative standard deviations of 4.5% for the determination of pentamidine isethionate and of 5.2% for the determination of nedocromil (n = 5) were obtained for urine samples containing 2.96 μg ml^{-1} of pentamidine isethionate and 0.42 μg ml^{-1} of nedocromil.

Keywords: *Cathodic stripping voltammetry; solid-phase extraction; nedocromil sodium; pentamidine isethionate*

Introduction

The pharmacokinetic and clinical evaluation of any medical drug requires the use of a very sensitive analytical method capable of determining the compound in biological matrices at ng ml^{-1} or pg ml^{-1} levels. Biological fluids such as blood and urine are the most frequently used sample sources in such studies owing to the ease of collection of the necessary samples for analysis and because these media are important routes for transportation and excretion of drugs in the body. However, these matrices are very complex and their analysis, in general, demands the use of previous separation or even preconcentration steps.

A radioimmunoassay method[1] has been reported for the determination of nedocromil in plasma and urine. For pentamidine isethionate, chromatographic methods employing ultraviolet and fluorescence detection have been described.[2–6]

Cathodic stripping voltammetry following adsorptive preconcentration is a very powerful technique that has been shown to be suitable for the quantification of a large variety of organic compounds at levels that match the range of concentrations necessary for such studies.[7–10] This method has the advantages that it is inexpensive and easy to use, but here too the use of a separation step before the voltammetric measurement is usually necessary in analysing biological fluids.[11–13] Nedocromil sodium (disodium 9-ethyl-6,9-dihydro-4,6-dioxo-10-propyl-4*H*-pyrano[3,2*g*]quinoline-2,8-dicarboxylate), an antiasthma drug, and pentamidine isethionate [4,4′-(pentamethylenedioxy)dibenzamidine bis(2-hydroxyethanesulfonate)], an antiprotozoal agent (structures shown in Fig. 1), were shown to be strongly adsorbed at a hanging mercury drop electrode (HMDE) and to be readily determined at levels as low as 1 × 10^{-10} mol l^{-1} from aqueous solutions.[14,15] Differential-pulse cathodic stripping voltammetry of nedocromil gives three peaks when accumulation is performed at −0.3 V at pH 1.0 in HCl solution.[15] The first peak (A) occurs at about −0.5 V, the second peak (B) at −0.57 V and the third peak (C) at −0.94 V. All three peaks give linear calibration graphs. A differential-pulse cathodic stripping voltammogram

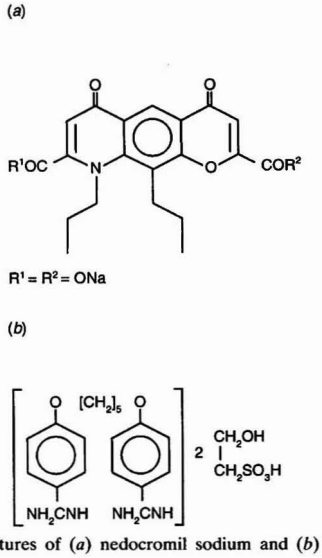

Fig. 1 Structures of (*a*) nedocromil sodium and (*b*) pentamidine isethionate.

* To whom correspondence should be addressed.

of pentamidine isethionate in 0.2 mol l^{-1} sodium hydroxide[14] obtained at an accumulation potential (E_{acc}) of −1.3 V and an accumulation time (t_{acc}) of 180 s showed a well defined peak at −1.60 V, which is used for analytical purposes. However, in both instances, strong interference from urinary components was observed.

The present work illustrates the use of solid-phase extraction cartidges in conjunction with cathodic stripping voltammetry, and describes the determination of nedocromil and pentamidine isethionate in urine at very low levels after separation from matrix interferences using a solid-phase or liquid–liquid extraction.

Experimental

For nedocromil determinations, Metrohm 626/663 (analogue) or 646/647 (microprocessor) voltammetric units were used to carry out cathodic stripping voltammetry. For pentamidine isethionate determinations, a Metrohm E612 voltammetric scanner and an E611 voltammetric detector and 663 stand were used with a Houston Instruments 2000 *x–y* recorder. The Metrohm multimode electrode in the 663 and 647 voltammetric stands was used in the HMDE mode. The 'large' mercury drop size was used with the 663 stand and drop size 5 on the 647 stand; these both correspond to a reproducible drop size of about 0.40 mm^2. The three-electrode system was completed with a glassy carbon auxiliary electrode and an Ag–AgCl reference electrode. All potentials are referred to the Ag–AgCl (3 mol l^{-1} KCl) electrode. A pulse amplitude of 50 mV was used with scan rates of 10 mV s^{-1} and a pulse interval of 1 s.

Nedocromil sodium and pentamidine isethionate samples were kindly supplied by Fisons Pharmaceuticals. The general procedure used for obtaining cathodic stripping voltammograms of these compounds in aqueous standard solutions has been described previously.[14,15]

Solid-phase extractions were carried out as follows. A Waters Associates Sep-Pak C_{18} cartridge was pre-washed with 6 ml of methanol and twice with 3 ml of water followed by 3 ml of 0.1 mol l^{-1} hydrochloric acid (for nedocromil) or 2 ml of phosphate buffer of pH 2.8 composed of primary and secondary phosphate (0.1 mol l^{-1}) adjusted to pH 2.8 with phosphoric acid (for pentamidine isethionate). Aliquots of 1 ml of urine containing the drug were diluted with 10 ml of 0.1 mol l^{-1} hydrochloric acid (nedocromil) or water (pentamidine isethionate) and passed through the cartridge. Water (6 ml) (for nedocromil) or 4 ml of diethyl ether (for pentamidine isethionate) was used to wash the C_{18} phase. Elution of the drugs was effected with 3 ml of 0.1 mol l^{-1} acetate buffer of pH 4.5–methanol (3 + 1) for nedocromil and 2 ml of acetonitrile–0.1 mol l^{-1} phosphate buffer of pH 2.8 (4 + 6) for pentamidine isethionate. For the determination of nedocromil, the eluate containing the drug was transferred into the voltammetric cell and 7 ml of 0.1 mol l^{-1} acetate buffer of pH 4.5 plus 120 μl of concentrated hydrochloric acid were added prior to the accumulation step. The pH after the addition of hydrochloric acid was about 1.0. The addition of hydrochloric acid to the acetate buffer after the extraction was necessary because, although better extraction was obtained at pH 4.5, better adsorption of nedocromil was obtained at about pH 1.0. For pentamidine isethionate, after evaporation of the residual diethyl ether under a stream of nitrogen (5 min), the extract was treated with 200 μl of 1 mol l^{-1} sodium hydroxide (in accord with our previous procedure[14]), diluted with 10 ml of 0.2 mol l^{-1} sodium hydroxide and placed in the voltammetric cell. Diethyl ether has to be evaporated completely, otherwise the signal is suppressed: it is not necessary to evaporate the extract to dryness.

Liquid–liquid extraction was performed using a slight modification of the method of Ericsson and Rais[5] as follows. Aliquots of 1 ml of the urine spiked with the appropriate amount of pentamidine isethionate were shaken with 300 μl of 0.2 mol l^{-1} sodium hydroxide and 5 ml of acetonitrile–chloroform (4 + 6) for 10 min on a sonicator or mechanical shaker. The upper aqueous phase was removed and the organic solvent was evaporated under a stream of nitrogen.

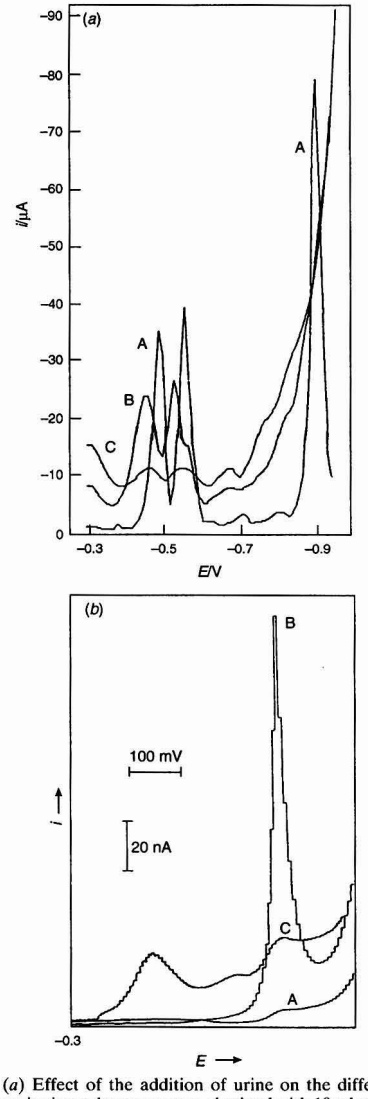

Fig. 2 (*a*) Effect of the addition of urine on the differential-pulse cathodic stripping voltammograms obtained with 10 ml of a 1.0×10^{-7} mol l^{-1} solution of nedocromil in 0.1 mol l^{-1} hydrochloric acid. A, No urine added; B, addition of 100 μl of urine; and C, addition of 300 μl of urine. Accumulation step: 60 s at −0.3 V. (*b*) Differential-pulse cathodic stripping voltammograms obtained with 20 ml of a 1.0×10^{-7} mol l^{-1} solution of pentamidine isethionate in 0.2 mol l^{-1} sodium hydroxide. A, Without accumulation; B, after 3 min accumulation; and C, voltammogram obtained from 1 ml of urine spiked with 0.59 μg ml^{-1} of the drug diluted to 20 ml with 0.2 mol l^{-1} sodium hydroxide. Accumulation step: 3 min at −1.3 V.

The residue was dissolved in 20 ml of 0.2 mol l^{-1} sodium hydroxide and transferred into the voltammetric cell.

Results and Discussion

The effect of the addition of urine on the differential-pulse cathodic stripping voltammograms of 10 ml of a 1.0×10^{-7} mol l^{-1} solution of nedocromil and 20 ml of a 1.0×10^{-7} mol l^{-1} solution of pentamidine isethionate is shown in Fig. 2. It can be seen that normal components of human urine such as proteins, surfactants and urinary pigments have a strong effect on the height of the adsorption peaks of these drugs, and complete suppression of the peaks is observed after addition of higher volumes of urine. Although three peaks are observed for the reduction of nedocromil adsorbed on the mercury electrode at an accumulation potential of −0.3 V, accumulation in urine was performed at −0.4 V because of the presence of a compound that adsorbs if accumulation is performed at −0.3 V and which produces some interference including an increase in the baseline. When accumulation was performed at −0.4 V, this interference was greatly suppressed: the second peak was used for the determination. Pentamidine isethionate is administered by intramuscular injection in a daily dose of about 2–4 mg kg^{-1}; 10–30% of this dose is excreted in the urine within 24 h; 50–70% is excreted in the first 6 h.[16,17] Nedocromil is excreted in urine from 2800 ng ml^{-1} (maximum concentration obtained 1–2 h after the drug is taken) to 18 ng ml^{-1} 12–24 h later.[1] Both drugs are reported to be excreted unchanged. In order to permit determinations at levels comparable to those present in the urine of subjects receiving treatment based on these drugs, a previous clean-up step must be used. Solid-phase separation using a C_{18} cartridge and liquid–liquid extraction were used to isolate these compounds from the urinary interferents.

Solid-phase Extraction

Because of the advantages presented by the use of solid-phase extraction cartridges such as faster analytical protocol, use of

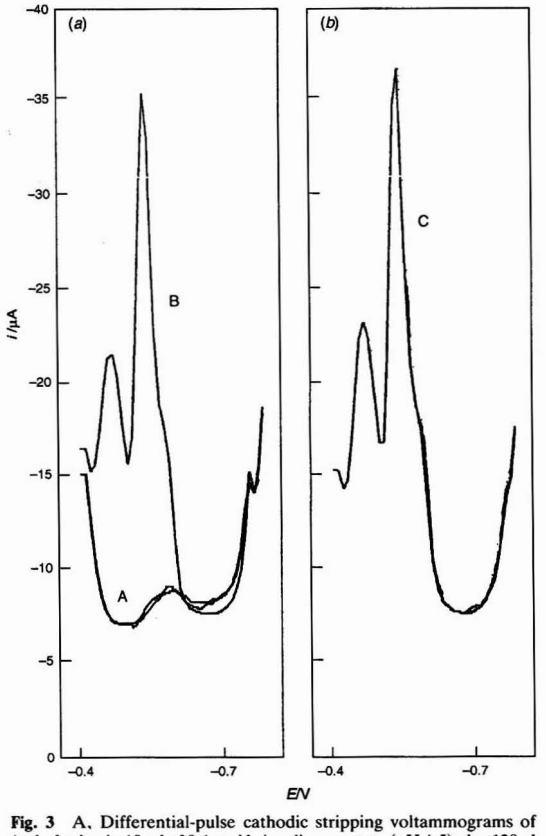

Fig. 3 A, Differential-pulse cathodic stripping voltammograms of 1 ml of urine in 10 ml of 0.1 mol l^{-1} sodium acetate (pH 4.5) plus 120 μl of hydrochloric acid after clean-up using a C_{18} cartridge; B, addition of 0.42 μg of nedocromil to the cell containing the cleaned urine; and C, addition of 0.42 μg of nedocromil to the urine prior to the clean-up. Accumulation step: 60 s at −0.4 V.

Table 1 Results obtained for the determination of pentamidine isethionate in human urine using a C_{18} extraction cartridge. E_{acc} = −1.3 V, t_{acc} = 3 min

Sample	Urine spiked concentration/ μg ml^{-1}	Mean concentration found/ μg ml^{-1}	Extraction recovery (%)
1	2.96	2.93	99
2	1.48	1.42	96
3	0.89	0.80	91
4	0.59	0.37	62

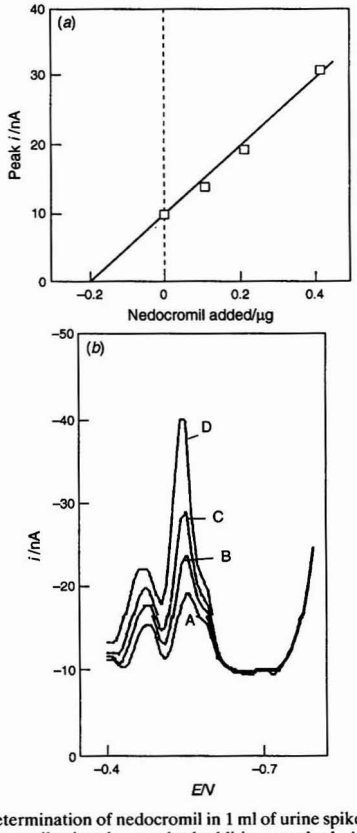

Fig. 4 Determination of nedocromil in 1 ml of urine spiked with 0.21 μg of nedocromil using the standard additions method. A, Urine; B, addition of 0.105 μg; C, addition of 0.21 μg; D, addition of 0.42 μg of nedocromil. Accumulation step: 60 s at −0.4 V.

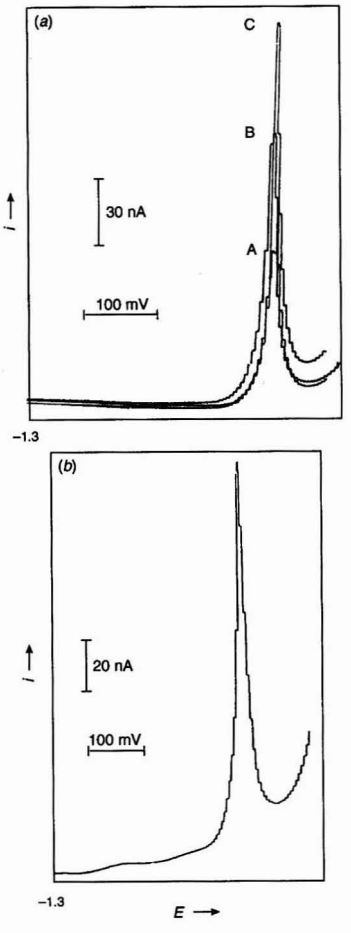

Fig. 5 (*a*) Differential-pulse cathodic stripping voltammograms of pentamidine isethionate recovered from 1 ml of human urine spiked with 1.48 μg ml^{-1} of the drug (A). Successive standard additions of 200 μl of 5.92 μg ml^{-1} of the drug (B and C). Accumulation step: 3 min at − 1.3 V. (*b*) Differential-pulse cathodic stripping voltammogram of urine spiked with 0.59 μg of pentamidine isethionate, after liquid–liquid clean-up. Accumulation step: 3 min at −1.3 V.

Table 2 Results obtained for the determination of pentamidine isethionate in 1 ml of human urine using acetonitrile–chloroform (4 + 6) as extractant. $E_{acc} = -1.3$ V, $t_{acc} = 3$ min

Sample	Urine spiked concentration/ μg ml^{-1}	Mean concentration found/μg ml^{-1}	Extraction recovery (%)
1	29.6	30.1	102
2	5.93	5.89	99
3	2.96	2.80	95
4	1.19	1.12	94
5	0.59	0.52	88
6	0.15	0.10	70
7	0.04	0.03	65

less solvent and reagents, greater safety and accuracy, solid-phase separation was chosen as the initial system to be studied. Excellent results were obtained using C_{18} cartridges. The urine samples were diluted in 0.1 mol l^{-1} hydrochloric acid for nedocromil determination or in phosphate buffer of pH 2.8 for pentamidine isethionate determination as outlined above.

The effect of the clean-up using the C_{18} cartridge on the determination of nedocromil can be seen in Fig. 3. As shown, the use of solid-phase extraction is very effective in preventing interference and no loss of nedocromil occurs in the separation step. In fact, recoveries of 100.5 ± 6.5% for nedocromil at levels as low as 0.2 μg ml^{-1} were obtained. Stripping voltammograms from aqueous standard solutions without the need for clean-up are given elsewhere.[15] The results obtained for pentamidine isethionate (0.59–2.96 μg ml^{-1}) are shown in Table 1. In this instance, the average recovery at a pentamidine isethionate concentration of 1.48–2.96 μg ml^{-1} was calculated to be 95–99%. However, for a pentamidine isethionate concentration of 0.6 μg ml^{-1}, an average recovery of 62% was obtained and better results were obtained using the liquid–liquid extraction method. All the results were obtained by standard additions, as shown in Figs. 4 and 5. The shoulder at the back of the second peak of nedocromil is caused by the urine blank (see Fig. 3).

Berger *et al.*[6] indicated that several makes of cartridge gave low recoveries (*e.g.*, Sep-Pak C_{18}, 61%) at the level of pentamidine isethionate under study (approximately 60 μg ml^{-1}). The modified method described in the present paper, which involves substantial changes in the pre-treatment of the column and composition of the elution solvents, gave recoveries of 91–99% with Sep-Pak C_{18} cartridges at much lower levels than this (see Table 1). The liquid–liquid extraction method described below was used at even lower pentamidine isethionate concentrations, where recoveries with the cartridge were low.

Calibration graphs obtained in urine were linear from 0.2 to 1.2 μg ml^{-1} of nedocromil ($r = 0.998$) with a slope of 590 nA ml μg^{-1} and from 0.9 to 4.7 μg ml^{-1} of pentamidine isethionate (slope = 87 nA ml μg^{-1} and $r = 0.993$).

The reproducibility of the results obtained for urine analyses with five samples containing 0.42 μg ml^{-1} of nedocromil and 2.96 μg ml^{-1} of pentamidine isethionate resulted in relative standard deviations of 5.2 and 4.5%, respectively.

Liquid–Liquid Extraction

In order to improve the recovery of pentamidine isethionate from human urine at levels lower than 0.6 μg ml^{-1}, a liquid–liquid extraction method was studied. A mixture of acetonitrile–chloroform was used as extractant.[5] The results obtained using this method are shown in Table 2 and in Fig. 5(*b*). In the concentration range from 0.6 to 29.6 μg ml^{-1}, recoveries higher than 88% were generally obtained. At very low levels (0.04–0.15 μg ml^{-1}), the results obtained (65–70% recovery suggest the loss of the drug by adsorption onto the glass wall or during the separation of the phases.

The precision of this method was good, given a relative standard deviation of 2.6% ($n = 5$) for urine spiked with 2.96 μg ml^{-1} of pentamidine isethionate.

The authors thank Fisons Pharmaceuticals plc for providing samples of pentamidine isethionate and nedocromil sodium. M. V. B. Z. thanks FAPESP (Brazil) for financial support and the Instituto de Quimica (UNESP), Araraquara, Brazil, for leave of absence. J. C. M. thanks CESTEH (Oswaldo Cruz Foundation) and Departamento de Quimica (UFRRJ), Brazil, for leave of absence.

References

1 Gardner, J. J., Preston, J. R., Gilbert, C. M., Wilkinson, D. J., Lockley, W. J. S., and Brown, K., *J. Pharm. Biomed. Anal.*, 1988, **6**, 285.
2 Dickinson, C. M., Navin, T. R., and Churchill, F. C., *J. Liq. Chromatogr.*, 1986, **9**, 2035.
3 Lin, J. M. H., Shi, R. J., and Li, E. T., *J. Liq. Chromatogr.*, 1986, **9**, 2935.
4 Dusci, L. J., Hackett, L. P., Forbes, A. M., and Ilett, K. F., *Ther. Drug Monit.*, 1987, **9**, 422.
5 Ericsson, O., and Rais, M., *Ther. Drug. Monit.*, 1990, **12**, 36.
6 Berger, B. J., Hall, E. J., and Tidwell, R. R., *J. Chromatogr. Biomed. Appl.*, 1989, **494**, 191.
7 Kalvoda, R., and Kopanica, M., *Pure Appl. Chem.*, 1989, **61**, 97.
8 Wang, J., and Freiha, B., *Anal. Chim. Acta*, 1983, **154**, 87.
9 Wang, J., Freiha, B., and Desmuth, B. K., *Bioelectrochem. Bioenerg.*, 1985, **14**, 457.
10 Telting-Diaz, M., Ordieres, A. J. M., Garcia, A. C., Blanco, P. T., Diamond, D., and Smyth, M. R., *Analyst*, 1990, **115**, 1215.
11 Hernandez, L., Zapardiel, A., Perez Lopez, J. A., and Bermejo, E., *Analyst*, 1987, **112**, 1149.
12 Hernandez, L., Zapardiel, A., Perez Lopez, J. A., and Bermejo, E., *Talanta*, 1988, **35**, 287.
13 Barrio Diez-Caballero, R., Lopez de la Torre, L., Arranz Valentin, J. F., and Arranz Garcia, A., *Talanta*, 1989, **36**, 501.
14 Zanoni, M. V. B., and Fogg, A. G., *Analyst*, 1993, **118**, 1163.
15 Pirzad, R., Moreira, J. C., Davies, A. E., and Fogg, A. G., *Analyst*, 1994, **119**, 2439.
16 *The British Pharmacopoeia 1993*, The Pharmaceutical Press, London, 1993.
17 *Martindale: The Extra Pharmacopoeia*, ed. Reynolds, J. E. F., The Pharmaceutical Press, London, 29th edn., 1989.

Paper 4/04309J
Accepted July 14, 1994

Square-wave Voltammetric Determination of Copper(II) With a Nafion–Dimethylglyoxime Mercury-film Electrode

Jyh-Myng Zen, Nai-Yuen Chi, Fu-Shien Hsu and Mu-Jye Chung

Department of Chemistry, National Chung-Hsing University, Taichung, 402, Taiwan

The use of a dimethylglyoxime-modified Nafion-coated mercury-film electrode in square-wave anodic stripping voltammetry for the determination of copper(II) is described. Compared with a Nafion-coated mercury-film electrode, this modified electrode showed improved resistance to interferences from surface-active compounds and much better selectivity. In addition, detection can be achieved without deoxygenation and the electrode can be easily renewed.

Keywords: Square-wave anodic stripping voltammetry; mercury-film electrode; Nafion; copper determination; dimethylglyoxime

Introduction

Mercury-film electrodes (MFEs) have found wide application in anodic stripping voltammetry (ASV).[1] The electrodes are prepared by electroplating a thin mercury film onto a suitable substrate, but generally glassy carbon is claimed to be the most favourable.[2–8] The advantages of this type of electrode include simple preparation, high sensitivity and excellent resolution of neighbouring signals. However, one of the most common problems when applying MFEs in ASV is the interference effects caused by organic constituents of the sample matrix.[9,10] This problem can be largely solved by coating the working electrode with a permselective membrane, such as Nafion ionomer, cellulose acetate films and cellulose dialysis membranes.[10–17] The function of the membrane is to prevent the organic interferent from reaching the interface at which the deposition/stripping process takes place. A Nafion-coated mercury-film electrode (NCMFE) has been extensively studied in this respect. Unfortunately, considering the interference effects of common ions, the NCMFE generally offers no more advantage than the MFE with regard to the selectivity aspect. However, by incorporating a suitable modifying group capable of binding only a few metals, a number of highly selective determinations should be possible.

Recently, our group has been developing a new kind of NCMFE by incorporating suitable chelating agents into the electrode. For example, an NCMFE containing appropriate amounts of dimethylglyoxime (DMG), designated NC(DMG)MFE, was used for the determination of nickel(II) by an adsorptive stripping process.[18] Further, NCMFE containing appropriate amounts of 2,2′-bipyridyl (Bpy), designated NC(Bpy)MFE, was used in the determination of lead(II) by an anodic stripping process.[19] In this approach, one can take advantage of three effects: the preconcentration effect of the ion-exchange polymer (Nafion), the selective chelating effect of the chelating agent (DMG) and the accumulation effect of the electrode (Hg).

In this paper, the analytical applications of the NC(DMG)MFE are further demonstrated for the determination of copper(II) using an anodic stripping process. Most important, the relative advantages of using square-wave anodic stripping voltammetry (SWASV) in combination with an NC(DMG)MFE as the working electrode for the determination of nickel(II) and copper(II) were assessed. As opposed to differential-pulse stripping voltammetry (DPSV) and linear-sweep stripping voltammetry (LSSV), the advantages include higher sensitivity (especially for reversible reactions),[20,21] effective discrimination against the capacitive current,[22] speed of analysis[22] and insensitivity to dissolved oxygen in the sample.[23,24] This work was intended to extend the applications of SWASV on the NC(DMG)MFEs in order to investigate and establish the advantages of the technique in the trace determination of various species in real sample applications.

Experimental

Apparatus

All voltammetric experiments were performed with a BAS-100B electrochemical analyser. The three-electrode system consists of an NC(DMG)MFE working electrode, a Ag–AgCl, NaCl (3 mol l^{-1}) reference electrode and a platinum wire counter electrode. Spectrophotometric measurements were carried out using a Hitachi U-3000 spectrophotometer.

Reagents and Chemicals

Doubly distilled, de-ionized water was used to prepare all solutions. Nafion perfluorinated ion-exchange powder, 5% m/v solution in a mixture of lower aliphatic alcohols and 10% water, was obtained from Aldrich. Butane-2,3-dione dioxime (dimethylglyoxime), mercury(II) nitrate, ammonium chloride and sodium acetate were of analytical-reagent grade. All buffers and supporting electrolyte solutions were prepared from Merck Suprapur reagents. Copper(II) standard solution (1000 mg l^{-1}) and all other standard metal solutions used in interference studies were also obtained from Merck. Model organic compounds were used as received. Solutions of Triton X-100 (BDH), sodium dodecyl sulfate (SDS) (Wako), humic acid (Fluka), albumin (Sigma) and gelatin (Sigma) were prepared by dissolution in water. D-Camphor (Eastman) was dissolved in 1 ml of 95% v/v ethanol before dilution with water. Starch (Fisher) solution was prepared (without preservative) using a standard procedure. Fulvic acid was extracted from Taichung landfill leachate using XAD-8 (Sigma), generally following the procedures reported earlier.[25]

Procedure

The glassy carbon disc electrode (A = 0.0685 cm^2, BAS) was polished with the BAS polishing kit and rinsed with de-ionized water, then further cleaned ultrasonically in 1 + 1 nitric acid

and de-ionized water successively. Nafion coating solutions (the total volume of the coating solution was always 4 μl, except that there were different ratios between Nafion and ethanol) were spin-coated onto the electrode surface at 2800 rev min^{-1}. A uniform thin film was formed by evaporating the solvent after about 5 min of spinning.

Mercury was deposited on the glassy carbon–(Nafion, DMG) substrate by adding 5×10^{-4} mol l^{-1} mercury(II) nitrate solution to the supporting electrolyte medium at −800 mV *versus* Ag–AgCl for 6 min as described previously.[10] The supporting electrolyte medium contained 0.07 mol l^{-1} acetate buffer (pH 4.0), prepared from sodium acetate and nitric acid. Unless stated otherwise, a medium containing ammonia–ammonium chloride buffer (pH 9.0) was used in the electrochemical experiments. The performance of the electrode was then optimized by improving the coating solutions in three stages as described previously.[18] Electrodes prepared with the optimum coating solution of 1.7 ml of Nafion + 1 ml of the DMG (2% m/v in ethanol) were used throughout.

Underground water was collected from the campus of Chung-Hsing University, located about 5 km from several electroplating facilities. In order to fit into the linear detection range of SWASV, the sample was diluted as described previously.[18] The underground water used for copper(II) measurement was diluted by a factor of ten. Electroplating waste solution was first acidified to pH < 2.0 with an appropriate amount of H_2SO_4 and then filtered with a 0.45 μm sterilized membrane. Following the same dilution procedure as for the underground water, the dilution factor of electroplating waste solution used for copper(II) measurement was ten.

Results and Discussion

Electrochemical Behaviour

The cyclic voltammograms clearly demonstrate that the Cu^{II}–DMG reaction is reversible and the Ni^{II}–DMG reaction is irreversible. After ten successive cycles, the reversible Cu^{II}–DMG peaks remain almost at the same height, whereas the irreversible Ni^{II}–DMG peaks almost disappear. As Ni^{II} has a much better chelating ability than Cu^{II} with DMG, in order to observe both peaks at the same scale of sensitivity, the Cu^{II} concentration is 500 times higher than that of Ni^{II}. It is well known that the sensitivity of SW stripping of adsorbed species is proportional to the degree of reversibilty of the electrochemical reaction.[20,21] Therefore, the species that undergo reversible reactions benefit more by the application of SWs than those that undergo quasi-reversible or totally irreversible reactions. By carrying out the experiments with SWASV, DPSV and LSSV at the same effective scan rate, the above prediction agrees well with the observed behaviour, as shown in Fig. 1. Comparing the sensitivity between SWASV and LSSV, the reversible Cu^{II}–DMG reduction shows an obvious improvement, being at least 15 times more sensitive [Fig. 1(*b*)], whereas for the irreversible Ni^{II}–DMG reduction, SWASV is only about three times more sensitive than LSSV [Fig. 1(*a*)]. In terms of background rejection, LSSV gives the highest sloping baselines, which causes a difficulty in the measurement of low concentrations. SWASV competes with DPSV for background rejection ability, with DPSV having a small advantage in that respect. Overall, even though SWASV has small disadvantage in terms of background discrimination compared with DPSV, it makes up for that with its superior sensitivity in practical applications.

Optimum Conditions for Electrochemical Determinations

In order to arrive at the optimum conditions for the determination of copper(II), there are two aspects that should be considered, the electrode and the detection. Concerning the electrode, the principal factors governing the performance of the Nafion–DMG thin mercury-film CME are the concentration of DMG in the film, the thickness of the Nafion–DMG film and the deposition of mercury. Regarding the detection aspect, the factors involved are the pH of the solution, the preconcentration time, the preconcentration potential and the SW parameters.

The optimum conditions with respect to the electrode aspect for copper(II) determination were found to be similar to those in a previous study on the use of this CME in the determination of nickel(II).[18] CMEs prepared from coating solutions that contain 2 ml of Nafion + 1 ml of DMG (0.01, 0.1, 0.5, 1, 1.5 and 2% m/v in ethanol) were examined under identical conditions. In all instances copper responses could be obtained and the peak current increased as the content of DMG in the coating solution increased, as shown in Fig. 2.

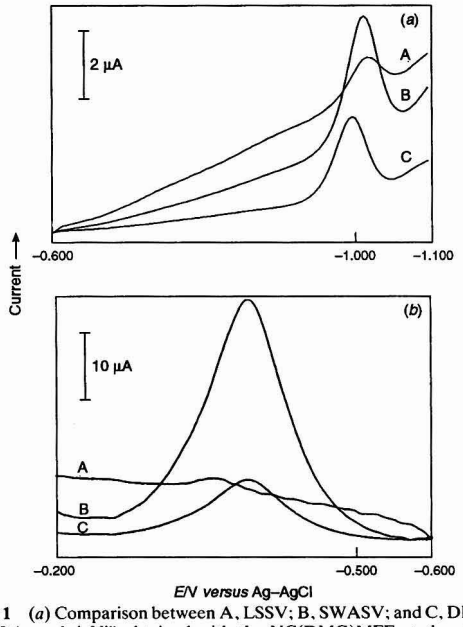

Fig. 1 (*a*) Comparison between A, LSSV; B, SWASV; and C, DPSV for 0.1 mg l^{-1} Ni^{II} obtained with the NC(DMG)MFE at the same effective scan rate of 200 mV s^{-1}. Conditions: B, modulation amplitude, 25 mV; modulation frequency, 100 Hz; C, pulse height, 50 mV, pulse width, 20 ms. (*b*) Same comparison as in (*a*) for 1 mg l^{-1} Cu^{II} except that the SW modulation amplitude was 50 mV.

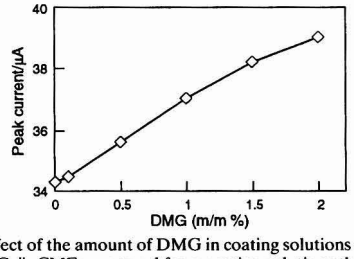

Fig. 2 Effect of the amount of DMG in coating solutions on the peak current of Cu^{II}. CMEs prepared from coating solutions that contain 2 ml of Nafion + 1 ml of DMG (0.01, 0.1, 0.5, 1, 1.5, and 2% m/v in ethanol) were examined under identical conditions: $[Cu^{2+}]$ = 40 μg l^{-1}, preconcentration time (t_p) = 3 min and preconcentration potential (p_p) = −0.8 V *versus* Ag–AgCl.

Apparently, the chelating ability of DMG with copper(II) functions properly in the CME. In summary, electrodes prepared with the optimum coating solution of 1.7 ml of Nafion + 1 ml of DMG (2% m/v in ethanol) at a spin-coating rate of 2800 rev min^{-1} and with a mercury deposition time of 6 min were used in all subsequent work.

For the CME, the optimum conditions for copper(II) accumulation were observed when the sample was slightly basic (pH 8–10), as shown in Fig. 3. The absorbance of the CuA_2 complex in different pH solutions is also shown in Fig. 3 for comparison. As can be seen, the pH region was slightly different from the measured optimum absorption region of pH 6–8 for the CuA_2 complex. This change is due to the fact that the SO_3^- sites of Nafion can attract protons and hold them inside the polymer matrix, an effect which is apparently equivalent to lowering the pH of the solution.

The effect of preconcentration potential on the SW response for copper(II) is shown in Fig. 4. As can be seen, between −0.6 and −0.9 V *versus* Ag–AgCl, the peak current increases as the potential of the electrode becomes more negative. This behaviour is explained by the fact that copper(II) bears a positive charge, and as a result the accumulation of copper(II) is favoured at more negative potentials. However, the peak current drops rapidly as the potential becomes more negative than −0.9 V. A preconcentration potential of −0.8 V was therefore chosen in all subsequent work. As preconcentration of copper(II) takes place at −0.8 V, which is far on the negative side of the copper reduction peak, the preconcentration mechanism of copper is mainly based on electrolysis. Nevertheless, the contribution from the chelating process between DMG and copper(II) cannot be ignored, as indicated by substantial evidence in this study. In summary, the signal was attributed to the following reactions:

$$Cu^{II} + Hg \rightarrow Cu(Hg)$$
$$Cu^{II} + 2HA \rightarrow CuA_2 + 2H^+$$
$$CuA_2 + 2H^+ + 2e^- + Hg \rightarrow Cu(Hg) + 2HA$$

where HA = DMG.

The dependence of the peak current on the preconcentration time for different copper(II) concentrations is shown in Fig. 5. The rate of copper(II) uptake is dependent on concentration. For higher concentrations of copper(II), (40 μg l^{-1}), the peak current increases as the preconcentration time increases and starts to level off around 6 min. For a lower concentation of copper(II) (1 μg l^{-1}), it takes about 15 min for the peak current to level off. This phenomenon is as expected and further confirms the chelation process between DMG and copper(II) in the CME. Apparently, as the electrodes were prepared at a spin-coating rate of 2800 rev min^{-1} with 4 μl of the optimum coating solution, which is composed of 1.7 ml of Nafion + 1 ml of DMG (2% m/v in ethanol), the amount of DMG on the CME was actually fixed. Therefore, in order to chelate with all the DMG sites available, a longer time is needed for a lower concentration of copper(II).

The SW parameters that were investigated were the frequency, the pulse height and the pulse increment. These parameters are interrelated and have a combined effect on the response. The response for copper(II) increases with increasing SW frequency, but at frequencies higher than 160 Hz the sloping background current renders the measurement difficult. An increase in the pulse height causes an increase in the copper(II) peak of up to 50 mV and the peak potential shifts in the positive direction with increasing frequency. The scan increment together with the frequency defines the effective scan rate; hence, an increase in either the frequency or the scan increment results in an increase in the effective scan rate. Overall, the best signal-to-background current characteristic can be obtained with the following instrumental settings: modulation amplitude, 50 mV; modulation frequency, 160 Hz; and effective scan rate 640 mV s^{-1}.

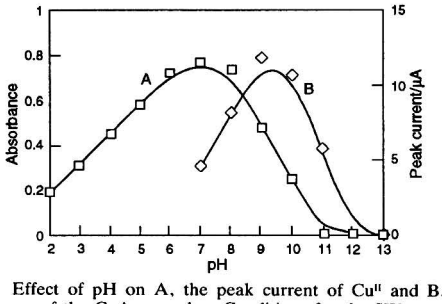

Fig. 3 Effect of pH on A, the peak current of Cu^{II} and B, the absorbance of the CuA_2 complex. Conditions for the SW measurement: $[Cu^{2+}]$ = 1 mg l^{-1}, t_p = 3 min, and p_p = −0.8 V *versus* Ag–AgCl. Conditions for the spectrophotometric measurement: $[Cu^{2+}]$ = 10 mg l^{-1}, [DMG] = 8.5 × 10^{-3} mol l^{-1}.

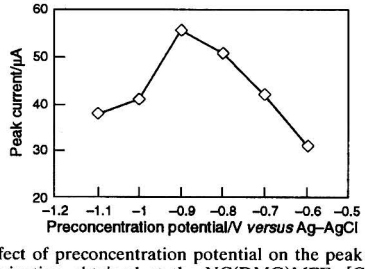

Fig. 4 Effect of preconcentration potential on the peak current of Cu^{II} determination obtained at the NC(DMG)MFE. $[Cu^{2+}]$ = 50 μg l^{-1}, t_p = 5 min.

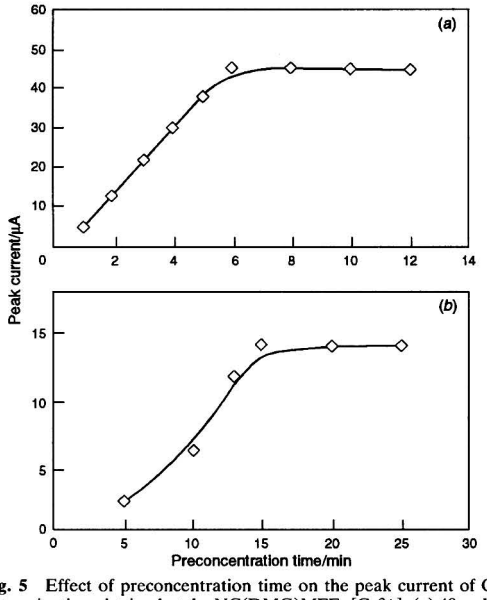

Fig. 5 Effect of preconcentration time on the peak current of Cu^{II} determination obtained at the NC(DMG)MFE. $[Cu^{2+}]$: (*a*) 40 μg l^{-1}; and (*b*) 1 μg l^{-1}, p_p = −0.8 V *versus* Ag–AgCl.

Effect of Oxygen

As the reduction of oxygen is a totally irreversible reaction, the SW waveform is expected not to respond to it,[20,21] thus providing a means of carrying out the analysis without deoxygenating the sample. Fig. 6 shows the results for copper(II) measured both before and after deoxygenation of the sample, with identical sensitivity. As can be seen, the peak currents are almost identical. A similar comparison was also made for nickel(II), but oxygen interfered more with the measurement, probably owing to the Ni^{II}–DMG reduction that occurs near the oxygen reduction wave. The higher background current for the voltammogram obtained without deoxygenation is good support for the above explanation. Therefore, deoxygenation is required for the precise determination of nickel(II), as indicated in our previous study.[18]

Electrode Renewal

The optimum conditions for copper(II) accumulation were observed when the sample was slightly basic (pH 9–11). This behaviour proved in fact to be useful, as it provided a chemical method for removal of the deposit. A 5 s immersion in 1 mol l^{-1} nitric acid was generally sufficient to remove all visual and electrochemical evidence of the preceding copper(II) deposition. However, the first three cycles were generally found to be less efficient for preconcentration than virgin CME surfaces, but after a few cycles the deposition efficiency generally reached a steady value. Nevertheless, this phenomenon was not observed when 1 ml l^{-1} hydrochloric acid was used. For ten successive preconcentration–determination–renewal cycles, the SW voltammetric response could be reproduced with a 4% relative standard deviation for the detection of 40 μg l^{-1} of copper(II).

Analytical Characteristics of CME

Our previous study showed that nickel(II) can be easily determined at the μg l^{-1} level by SWASV on the NC(DMG)MFE.[18] After a 5 min preconcentration period, a blank of 0.1 μg l^{-1} nickel could be detected and a linear response was observed from 1 to 80 μg l^{-1}. The limit of detection can be further decreased by using purer chemicals and a longer deposition time. The same NC(DMG)MFE can also be used in determining copper(II) at the μg l^{-1} level even in the presence of oxygen. Calibration data were obtained for ammonia buffer spiked with copper(II) following a 5 min preconcentration. Fresh sample solutions were used for each individual concentration and preconcentration time and at least six determinations for each data point. For 5 min preconcentration experiments, the relative standard deviation was 1–5%. The calibration graphs thus obtained show a very linear behaviour with slope, intercept and correlation coefficients of 0.8112 μA μg^{-1} l, 0.0269 μA and 0.9997, respectively. The linear range for 5 min preconcentration was investigated by adding copper(II) at concentrations ranging from 0.1 to 100 μg l^{-1}. The copper(II) concentrations calculated from the observed signals and the slope of the regression line were in good agreement with the experimental concentrations, thus indicating essentially constant sensitivity from 1 to 80 μg l^{-1} copper(II). The sensitivity started to decrease when the concentration of copper(II) was higher than 80 μg l^{-1}.

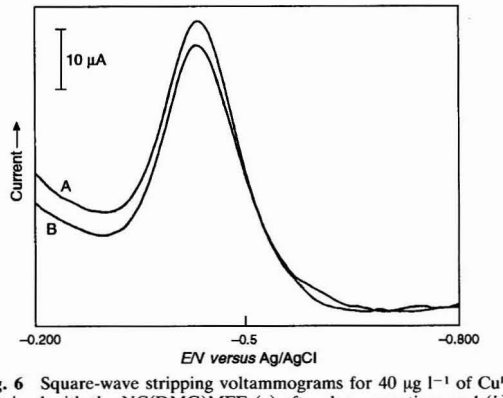

Fig. 6 Square-wave stripping voltammograms for 40 μg l^{-1} of Cu^{II} obtained with the NC(DMG)MFE (*a*) after deoxygenation; and (*b*) before deoxygenation.

The detection limit is defined as the concentration of the analyte resulting in a signal three times the standard deviation of the blank, as recommended by IUPAC. For preconcentration times of 5 and 10 min, the detection limits for copper(II) were 1 and 0.1 μg l^{-1}, respectively. Of course, with shorter preconcentration times, higher concentrations were required for detection. However, an even lower detection limit could be achieved for copper(II) provided that the preconcentration time is longer than 10 min.

Interferences

Any electroactive species that forms a precipitate with DMG might interfere in the determination of copper(II). The metals commonly cited as forming stable DMG complexes are nickel(II), palladium(II), cobalt(II) and bismuth(III). However, the chemical conditions in effect during the preconcentration step might easily be optimized to favour the formation of the copper(II) complex over that of most of the other metals. Therefore, the number of species interacting in this manner is limited. For 0.01 mg l^{-1} copper(II), the results show that over 1000-fold excess concentrations of aluminium(III), boron(III), cobalt(II), calcium(II) and magnesium(II) did not influence the copper response. Zinc(II), mercury(II), antimony(III) and bismuth(III) were found to interfere at a 1000-fold excess, palladium(II) at a 100-fold excess and cadmium(II) and nickel(II) at a 10-fold excess. The most serious interference was from lead(II), for which only a one-fold excess affected the copper signal.

The interference effects caused by surface-active compounds in ASV when using MFEs are recognized.[10] Coating of the MFE with permselective membranes has been introduced as a means of circumventing the organic interferences in ASV.[10–17] The function of the membrane is to prevent the organic interferents from reaching the interface at which the deposition/stripping takes place. For comparison, the effects of the surfactants on both the NCMFE and the conventional MFE were also recorded. The two surfactants chosen were non-ionic (Triton X-100) and anionic (fulvic acid) solutions. For the NCMFE, in comparison with the MFE, the tolerance was improved by a factor of two for both surfactants, as can be seen from Fig. 7. For the NC(DMG)MFE, the tolerance was improved by a factor of 20 up to about 10 mg l^{-1} for both surfactants. The effects of model surfactants (SDS, Triton X-100), proteins (albumin, gelatin) and carbohydrates (starch) and also D-camphor and humic acid on the NC(DMG)MFE in SWSV were further studied. Comparison of the 50 μg l^{-1} Cu^{II} normalized peak current data for model organic compounds (15 mg l^{-1}) with the bare MFE, the NCMFE and the NC(DMG)MFE are summarized in Table 1. As can be seen, for each of the seven model organic compounds, the NC(DMG)MFE shows a clear improvement over the bare MFE. The NCMFE can prevent most of the interferences, with the exception of those of Triton X-100 and humic acid. The NC(DMG)MFE shows an even better

improvement for all the interferents, especially Triton X-100 and humic acid. Hoyer *et al.*[10] pointed out that a membrane coating ultimately cannot eliminate all interferents in a sample from reaching the electrode surface. Even interfering components that are excluded from the electrode surface may still complicate the signal by their accumulation at the outer membrane surface. The role of DMG in the protection against surfactants apparently has something to do with the improvement of the two factors mentioned above.

Practical Applications

The analytical utility of the NC(DMG)MFE was assessed by applying it to the determination of copper(II) in underground water and electroplating waste solution. The results are summarized in Table 2 and indicate good accuracy for all the samples. Real values for the copper(II) content in underground water and electroplating waste solution were calculated from the dilution factors for each sample during preparation.

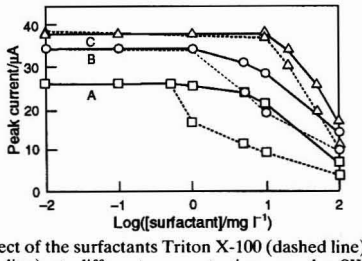

Fig. 7 Effect of the surfactants Triton X-100 (dashed line) and fulvic acid (solid line) at different concentrations on the SW stripping response for 40 μg l^{-1} of Cu^{II} on the A, MFE; B, NCMFE; and C, NC(DMG)MFE; t_p = 5 min, p_p = −0.8 V *versus* Ag–AgCl.

Table 1 Comparison of normalized peak currents for model organic compounds (15 mg l^{-1}) at 50 μg l^{-1} Cu^{II}

	Normalized peak current (100%)		
Compound	MFE	NCMFE	NC(DMG)MFE
Gelatin	40.6	97.8	99.9
Albumin	45.1	91.1	97.7
SDS	82.3	97.1	98.8
Triton X-100	28.0	81.8	97.1
Humic acid	49.3	88.8	95.1
Camphor	85.8	102.6	100.5
Starch	88.7	104.6	100.7

Table 2 Determination of copper(II) in underground water and electroplating waste solution

Parameter	Underground water	Electroplating waste solution
Detected value,* original/μg l^{-1}	4.3 ± 0.2	31.1 ± 2.8
Spike/μg l^{-1}	20.0	20.0
Detected value* after spiking/ μg l^{-1}	24.2 ± 0.5	50.2 ± 4.1
Recovery (%)	99.5	95.5
Real value*/μg l^{-1}	43.1 ± 2.0	311.2 ± 28.2

* n = 6.

Conclusions

It has been demonstrated that SWASV in conjunction with the NC(DMG)MFEs is a potentially interesting development for the determination of copper(II). The CME offers considerably higher resistance to organic interferences than does the NCMFE and the mechanical stability of the mercury film is also better than that of the MFE. The NC(DMG)MFE's characteristics of good sensitivity and selectivity and the capability to be easily regenerated by exposure to acid make the technique very attractive in the trace determination of various species in real sample applications. Future work in this direction is being carried out in order to assess the applicability of the technique in flowing streams.

The authors gratefully acknowledge financial support from the National Science Council of the Republic of China under grant NSC 82-0208-M005-053.

References

1 Wang, J., *Stripping Analysis—Principles, Instruction and Applications*, VCH, Deerfield Beach, FL, 1985.
2 van der Linden, W. E., and Dieker, J. W., *Anal. Chim. Acta*, 1980, **177**, 1.
3 Florence, T. M., *J. Electroanal. Chem.*, 1970, **27**, 273.
4 Copeland, T. R., Christie, J. H., Osteryoung, R. A., and Skogerboe, R. K., *Anal. Chem.*, 1973, **45**, 2171.
5 Lund, W., and Salberg, M., *Anal. Chim. Acta*, 1975, **76**, 131.
6 Valenta, P., Mart, L., and Rützel, H., *J. Electroanal. Chem.*, 1977, **82**, 327.
7 Economou, A., and Fielden, P. R., *Anal. Chim. Acta*, 1993, **273**, 27.
8 Frenzel, W., *Anal. Chim. Acta*, 1993, **273**, 123.
9 Brezonic, P. L., Brauner, P. A., and Stumm, W., *Water Res.*, 1976, **10**, 605.
10 Hoyer, B., Florence, T. M., and Batley, G. E., *Anal. Chem.*, 1987, **59**, 1608.
11 Hoyer, B., and Florence, T. M., *Anal. Chem.*, 1987, **59**, 2839.
12 Wang, J., Bonakdar, M., and Pack, M., *Anal. Chim. Acta*, 1987, **132**, 215.
13 Morrison, G. M. P., and Florence, T. M., *Electroanalysis*, 1989, **1**, 485.
14 Wang, J., and Hutchins-Kumar, L. D., *Anal. Chem.*, 1986, **58**, 402.
15 Stewart, E. E., and Smart, R. B., *Anal. Chem.*, 1984, **56**, 1131.
16 Smart, R. B., and Stewart, E. E., *Environ. Sci. Technol.*, 1985, **19**, 137.
17 M. J. Kelly, M. J., and Heineman, W. R., *J. Electroanal. Chem.*, 1987, **222**, 243.
18 Zen, J.-M., and Lee, M.-L., *Anal. Chem.*, 1993, **65**, 3238.
19 Zen, J.-M., and Huang, S.-Y., *Anal. Chim. Acta*, 1994, **296**, 77.
20 Lovric, M., and Branica, M., *J. Electroanal. Chem.*, 1987, **226**, 239.
21 Lovric, M., and Komorsky-Lovric, S., *J. Electroanal. Chem.*, 1988, **248**, 239.
22 Osteryoung, J. G., and Osteryoung, R. A., *Anal. Chem.*, 1985, **57**, 101A.
23 Woljciechowski, M., Go, W., and Osteryoung, J. G., *Anal. Chem.*, 1985, **57**, 155.
24 Ostapzuk, P., Velenta, P., and Nürnberg, H. W., *J. Electroanal. Chem.*, 1986, **214**, 51.
25 Town, R. M., and Powell, H. K. J., *Anal. Chim. Acta*, 1993, **271**, 195.

Paper 4/02335H
Received April 20, 1994
Accepted August 4, 1994

Application of Crown Ether Coated Piezoelectric Crystal as a Detector for Ion Chromatography

Yih-Song Jane and Jeng-Shong Shih*

Department of Chemistry, National Taiwan Normal University, Taipei, Taiwan 11718, China

A reusable and sensitive piezoelectric quartz crystal detector was developed for the detection of either cations or anions in ion chromatography. The quartz crystal electrode coated with crown ether (sym-dibenzo-16-crown-5-oxydodecanic acid) was prepared and was found to give the best results in terms of stability, sensitivity and reproducibility. Linear frequency (voltage) responses on a 10 MHz AT-cut crystal for ions were found on the range 0.1–5 $\times$ 10^{-5} mol l^{-1}. Variations of the crystal frequencies were converted to voltage using a TC 9400 chip. Polystyrene–poly(divinyl benzene) with cryptand [2,2] as an anchoring group was synthesized and applied as a bifunctional ion chromatographic packing material for the separation of both cations and anions. The crown ether coated piezoelectric crystal detector with detection limits of 2 $\times$ 10^{-5} (1 $\times$ 10^{-10} mol)–5 $\times$ 10^{-5} mol l^{-1} (2.5 $\times$ 10^{-10} mol) for various ions showed a similar detection limit to that of a commercial conductivity detector in ion chromatography. The effects of solvents, reproducibility of responses and competitiveness with respect to a commercial conductivity detector were also investigated.

Keywords: Crown ether; piezoelectric crystal; ion chromatography; cryptand; detector

Introduction

Piezoelectric crystals (PECs), *e.g.*, quartz, can be used as microbalances for thin film technology, *i.e.*, a thin film substance applied to a certain cut of a piezoelectric quartz crystal can be treated as an equivalent mass change of the crystal itself. Any increase in thickness will result in a decrease in the resonance frequency of the fundamental shear oscillation. This implies that the mass sensitivity of the crystal can detect and compute any mass change from its resonance frequency on the crystal quantitatively.[1] This is known as Sauerbrey's equation.[2] This concept has long been exploited extensively in the design of selective sensors for the gas phase. However, there are very few reported studies on the operation of PEC sensors in the liquid phase. Knash and Bastiaans,[3] Thompson *et al.*[4] and Bruckenstein and Shay[5] have recently developed quartz crystals as both high-performance liquid chromatography (HPLC) detectors and biosensors. However, these reports have dealt with organic species detected in solutions: the detection of ions in solutions using a PEC received little attention and has never been systematically investigated. In this paper, a crown ether-coated PEC for the detection of various ions in solutions is presented.

* To whom correspondence should be addressed.

Since Pedersen reported his pioneering work on the preparation of crown ethers[6] and their complexing properties,[7] numerous papers have been written that describe the metal cation bonding properties of various synthesized crown ethers as phase-transfer catalysts, solvent extraction agents, ion-selective electrodes and ion transfer carriers. In the previously reported metal ion–crown ether interaction system, different substitutional group or cavity size of crown ethers played an important role in the determination of the metal ion–crown ether complexation ability, stability and lipophilicity. Owing to the highly complexing ability of crown ethers to metal ions, crown ether-coated piezoelectric quartz crystal can be expected to function as a sensitive detector for various metal ions.

In general, ion chromatography with a conductivity detector is coupled to two columns in series: the separator column that resolves the mixture into individual ions, and the suppressor column that removes the excess of eluent ions. The disadvantage of ion chromatography is the suppresser column, which causes additional peak broadening, and requires regenerating from time to time. The concentration of analyte should be low enough to avoid overloading the suppressor column. This work is cumbersome, although, it is possible to obviate the suppressor column and still use an electrical conductivity detector by eluting with very dilute eluents that have a low conductivity and strong displacing power.[8,9] However, the greater background conductivity cancels out this advantage and, moreover, the detector reads, not only the conductance of the eluted ions, but also the difference between their conductance and that of the equivalent quantity of displacing ions.[10] Instead of using a supressed column, membrane supressors and fibre supressors allow continuous 'regeneration', so that analyses do not need to be interupted for supressor regeneration. These advances have made the use of a suppressor far more convenient; but, they are still two column systems, using different functional resins as the separator column, different eluents and different supressed column to separate anions or cations. Our previous work[11] has successfully coped with these problems. Instead of using a two-column separator and suppressor ion-exchange system, one column (using cryptand [2,2] as a bifunctional packing material) had been used for the separation of both cations and anions, still using an electrical conductivity detector by eluting with neutral water, CH_3CN and methanol.

In the present work, a crown ether (sym-dibenzo-16-crown-5-oxydodecanic acid) coated PEC detector was prepared and applied to the detection of either cations or anions separated using ion chromatography. One column of cryptand 22 (used as a bifunctional packing material) was used to separate both cations and anions by eluting with various non-ionic solvents. All of the separated ions were detected on both the electric conductiviy detector and the crown ether-coated crystal detectors. The sensitivity and detection limits of the crown

ether-coated PEC detectors were investigated and compared with the performance of a commercial conductivity detector.

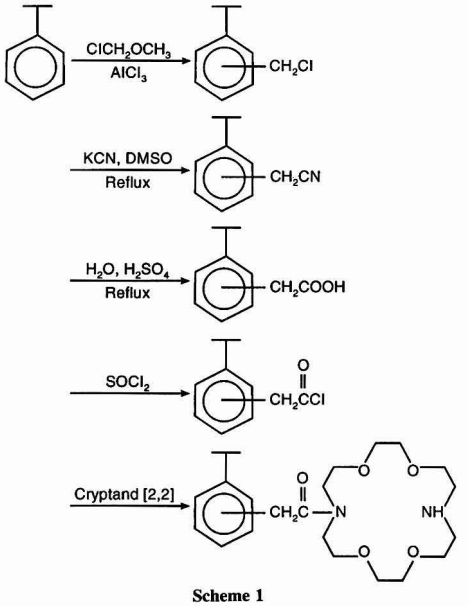

Scheme 1

Experimental

Preparation of Packing Material

The over-all preparation of the polystyrene–poly(divinyl benzene) cryptand [2,2] resin is depicted in Scheme 1. The details of this procedure are presented in ref. 11.

Synthesis of Crown Ether Coating Material

The over-all reaction process is presented in Scheme 2. The details of this process are presented in ref. 11.

Preparation of Crown Ether-coated PEC

Piezoelectric quartz AT-cut crystals of 10 MHz resonance frequency were obtained from TXT Crystal (Taipei, Taiwan). The crystals were plated with a film width of approximately 500 nm of silver by vacuum deposition. The electrodes of crystals were coated with poly(vinyl chloride) (PVC)–sym-dibenzo-16-crown-5-oxydodecanic acid (1 + 1) in tetrahydrofuran (THF) solution *via* the dropped method using a microsyringe. After evaporation of the THF at room temperature for 2 h, the crystal was housed in a flow-through acrylate cell and clamped between two O-rings recessed into the housing (Fig. 1).

Apparatus

Fourier transfer-nuclear magnetic resonance (FT-NMR) (Jeol JMS-EX 400, Palo Alto, CA, USA), infrared (IR) (Jasco IR700, Tokyo, Japan) and mass (Jeol-JMS-D300) spectrometers were applied to identify the synthesized lariat

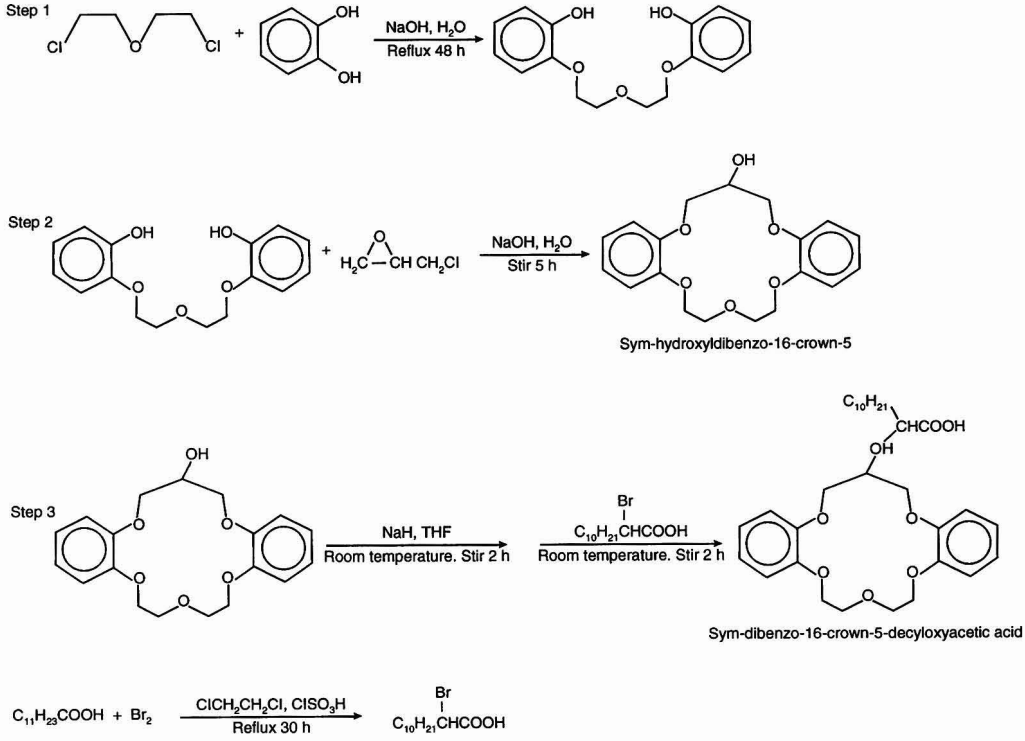

Scheme 2

carboxylate crown ethers. A 30 × 0.4 cm id ion chromatographic column with polystyrene–poly(divinyl benzene) cryptand 22 was prepared at 3000 psi with a packer connected to the pump of an HPLC system (Jasco BIP-BI). All separations of ions were performed using a Dionex Model 4000i one-column ion chromatograph (Sunnyvale, CA, USA) with an electric conductivity detector (TOA) ICA-5220) and piezoelectric quartz crystal (set-up as in Fig. 1). A Jasco IR-810 infrared spectrophotometer was applied for the identification of the synthesized cryptand resins and intermediates. The elemental analysis of the resin was carried out using a Perkin Elmer 240 elemental analyser (Norwalk, CT, USA).

The set-up of the piezoelectric crystal detection system is shown in Fig. 1. After assembling the whole cell, this setup was sealed with wax to prevent leakage. In this system, the oscillating frequency (F) was converted to electric potential (V) signal using an F/V converter TC 9400 (Teledyne) chip with a working range on two modes (0–10 kHz and 0–100 kHz) covering from 0.000 to 6.500 V. In order to appropriate the oscillating frequency into the working range of the TC 9400, another 10 MHz oscillating frequency reference crystal should be used and applied to reduce the frequency of crystal in working-cell by 74LS74 (NEC) chip. The voltage signal was processed with a 12 bit 16 channel ADC connected to a microcomputer for monitoring and recording. The fluid from the ion chromatographic column flows through conductivity detector first and subsequently through the piezoelectric crystal detector.

Reagents

Cryptand 22 was obtained from E. Merck (Darmstadt, Germany). Polystyrene–poly(divinyl benzene) resin XAD-4 (from Sigma, St. Louis, MO, USA) was purified by washing with NaOH (1 mol l^{-1}), followed by HCl (1 mol l^{-1}), H_2O–CH_3OH/CH_2Cl_2 (1 + 10) and finally drying in vacuum at about 0 °C before use. KCl, NaCl, LiCl, CsCl, $CoCl_2$, $NiCl_2$ and $LaCl_3$ were from Merck; KF, KNO_2, KNO_3, KBr, KI and $FeCl_2$ were purchased from Aldrich (Milwaukee, WI, USA). Methanol, CH_3CN, dichloromethane and THF were of LC grade. De-ionized eluent water was prepared by passing distilled water through a Millipore Milli-RO60 ultrapure water purification system. (Milford, MA, USA). All other chemicals were either of analytical-reagent or reagent grade.

Results and Discussion

In our iron chromatography PEC detection system, the crown ether was coated onto the surface of quartz crystal and the eluents used for ion chromatography were water, methanol and a water–methanol mixture. As the solubility of 2-sym-dibenzo-16-crown-5-oxydodecanic acid in water is very low (2.8×10^{-5} mol l^{-1}),[12] this was measured in our previous paper using its ultraviolet (UV) absorption. However, after mixing with PVC to form a thin film, 2-sym-dibenzo-16-crown-5-oxydodecanic acid cannot be detected in water by ultraviolet absorption. This kind of lariat (side arm) crown ether not only forms strong complexes with alkali[13] and alkali-earth[14] metal ions, but also exhibits better extraction ability with transition and lanthanide metal ions.[15] The response of the crown ether-coated quartz crystal electrode in the presence of 0.01 mol l^{-1} KCl (5 μl) aqueous solution has been measured. It was found that the greater the PVC–crown ether coating, the greater the response of the quartz detector. This increase in response is proportional to the amount of coated load until the load exceeds 8 μg. After 8 μg, the frequency response increases less dramatically. Because the surface area of electrode on crystal is constant, the active metal ion capture ability of crown ether has covered all of the electrode surface using an amount of 8 μg. However, there is still a frequency shift response for no crown ether coating on the crystal. Previously, Kanazawa and Gordon[16] or Bruckenstein and Shay[5] derived a theoretical equation describing the oscillating frequency (ΔF) in a quartz crystal in solution

$$\Delta F = -(2.26 \times 10^{-6}) n f^{3/2} (\rho_1 \eta_1)^{1/2} = -K(\rho_1 \eta_1)^{1/2} \quad (1)$$

Where n is the numbers of faces (1 or 2), and depends on the quartz crystal being in contact with the liquid, f is the original oscillating frequency, ρ_1 is the density of the liquid and η_1 is the viscosity of the liquid. Thus, the change in viscosity or density from eluent (H_2O) to KCl solution can probably lead to a shift in frequency.

The frequency changes on the quartz crystal detector should be monitored continuously and recorded on a microcomputer. TC 9400 has been applied as an F/V converter; the TC 9400 generates an output voltage linearly proportional to the frequency. The equation of F/V conversions show the linearity of our experiment

$$V = 0.06512 \times F \text{ (0–100 kHz mode)} \quad (2)$$

$$V = 0.6489 \times F \text{ (0–10 kHz mode)} \quad (3)$$

where V is electric potential (in V) and F is the frequency shift (in kHz).

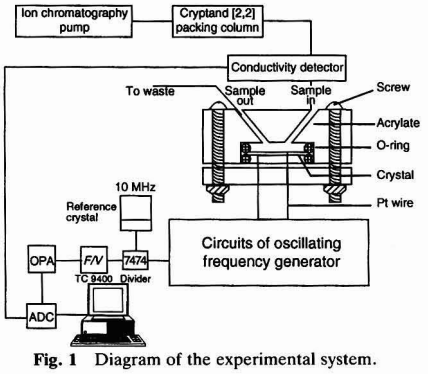

Fig. 1 Diagram of the experimental system.

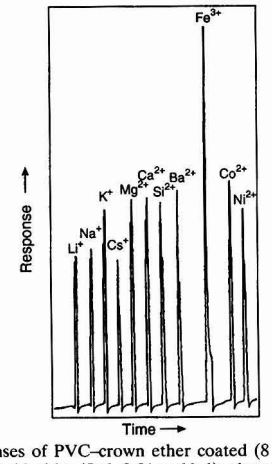

Fig. 2 Responses of PVC–crown ether coated (8 μg) piezoelectric crystal on metal chlorides (5 μl, 0.01 mol l^{-1}); eluent, H_2O; flow rate, 1.0 ml min^{-1}.

The frequency response caused by various metal chlorides (0.01 mol l^{-1}) flowing through our piezoelectric quartz detector (coated with 8 μg PVC-crown ether) has been investigated and is shown in Fig. 2, where the K^+ ion exhibits a great frequency change for alkali metal ions. This result is not surprising, as the complexation of metal ions to crown ether follows the order, $K^+ > Na^+ > Li^+ > Cs^+$. The same selectivity order is followed on the extraction of alkaline metal ions using chloroform.[13] The frequency shift sequence for alkakline earth metal chlorides by using the PVC–$C_{10}H_{21}$DB16C5COOH detector is $Ba^{2+} > Ca^{2+} > Sr^{2+} > Mg^{2+}$. The same selectivity ordered is also shown for the extraction of alkaline earth metal ions in chloroform.[14] It should be noted that at a similar viscosity and density to the other ions solutions, Fe^{3+} provokes the greatest frequency shift response of the piezoelectric crystal detector. Hager[17] suggested that in addition to the viscosity and density of liquids, the relative polarity of solution and charges of the metal ions also influence the oscillating frequency. This could be the reason why trivalent cations cause a greater frequency change than bivalent and monovalent cations of the same concentration.

The voltage and frequency response of the PVC–crown ether coated crystal detector in the flowing cell for KCl, $CoCl_2$ and $LaCl_3$ at various concentrations are shown in Fig. 3. The crown ether-coated piezoelectric crystal detector seems to exhibit linear responses to the concentration of these halides over the concentration range 0.1–30 × 10^{-3} mol l^{-1}. The sensitivity of a piezoelectric detector is defined as the frequency shift (in Hz) per unit concentration (mol l^{-1}) of analytes. The sensitivity of the crown ether-coated piezoelectric crystal detector for these metal chlorides in the order: KCl (2.110 MHz l mol^{-1}) < $CoCl_2$ (3.064 MHz l mol^{-1}) < $LaCl_3$ (3.819 MHz l mol^{-1}). It should be noted that the slope ratio of electric potential (oscillating frequency change or sensitivity) *versus* concentration of variously charged metal ions (2+, 3+) in this figure is 1 : 1.46 : 1.81 which is very similar to the ratio of the square root of the charges on these metal ions ($1 : \sqrt{2} : \sqrt{3}$).

The response of PVC–crown ether-coated piezoelectric quartz crystal to metal ions is also highly reproducible. Detection peaks for a series of 17 repetitive assays of 0.01 mol l^{-1} KCl sample were measured using the PEC detector. This series yielded a relative standard deviation (s_r) of 2.8%. The fast response and rapid return to the baseline made this detector a good competitor for the commercial electric conductivity detector (s_r = 2.1%). The short and long term stability and reproducibility were tested and monitored using a control chart, where s_r values for 5 repetitive assays of 0.01 mol l^{-1} KCl were in the range $\pm 2(s_r)$ after making a survey everyday over 10 d. IUPAC[18] recommends the detection limit, c_L, be defined as the concentration of an analyte equal to a background-corrected signal, $X_L - X_B$, three times the estimated standard deviation of a single determination using 20 measurements of the blank.

$$X_L = X_B + ks_B \quad (4)$$

$$c_L = ks_B/m \quad (5)$$

where X_L is the uncorrected signal; X_B the blank measure; s_B the estimated standard deviation of the blank measure; c_L the detection limit, which is the concentration derived from the smallest measure (x_L) that can be detected with reasonable confidence; k the numerical factor chosen in accordance with the confidence level desired; and, m the analytical sensitivity (slope).

As pointed out by Long and Winefordner,[19] the use of $k = 3$ allows a confidence level of 99.86% for a normal distribution of X_B. Hence, the detection limits for $LaCl_3$, $CoCl_2$ asnd KCl in our PEC detection system are approximately 2 × 10^{-5} (1 × 10^{-10} mol), 3 × 10^{-5} (1.5 × 10^{-10} mol) and 5 × 10^{-5} mol l^{-1} (2.5 × 10^{-10} mol). Although the detection limit for KCl is much higher than a well 'supressed' conductivity detector (2.5 × 10^{-12} mol), the detection of transition metal chlorides and lanthanoid (La^{3+}, Eu^{3+}, *etc.*) salts by PEC detection are easier and more convenient than the conductivity detector method.

The sensitivity of the piezoelectric crystal and the electric conductivity detector for $LaCl_3$ and KCl are compared in Figs. 4 and 5, respectively. The PEC detector seems to display the same order or competitive response as the conductivity detector for these metal chlorides, when the eluent and sample flow through the conductivity detector first and subsequently through the piezoelectric crystal detector. However, the peak widths of the PEC responses are slighly broader than those of the electric conductivity detector. This broadening disadvantage reduces the resolution of the separating procedure. The principle reason for this is that the greater cell volume (250 μl) of the PEC detector causes the eluent and sample to circulate in the cell, thus, it is important to reduce cell volume in order to reduce the broadening effects in the near future.

As shown previously,[11] F^-, Cl^-, Br^-, NO_3^- and I^- can be separated using the protonated cryptand ion chromatography

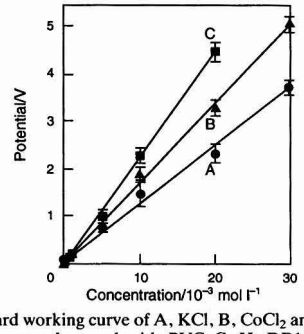

Fig. 3 Standard working curve of A, KCl, B, $CoCl_2$ and C, $LaCl_3$ on a piezoelectric crystal coated with PVC–$C_{10}H_{21}$DB16C5COOH (8 μg); eluent, H_2O; flow rate, 1.0 ml min^{-1}.

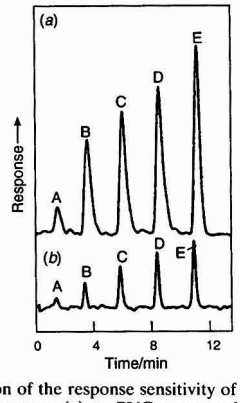

Fig. 4 Comparison of the response sensitivity of various concentrations of $LaCl_3$ between (*a*) a PVC–crown ether coated (8 μg) piezoelectric crystal detector and (*b*) a commercial conductivity detector, where the eluent and sample flow through conductivity detector first and subsequently through the piezoelectric crystal detector. A, 1 × 10^{-4} mol l^{-1}; B, 3 × 10^{-4} mol l^{-1}; C, 5 × 10^{-4} mol l^{-1}; D, 8 × 10^{-4} mol l^{-1}; and E, 1 × 10^{-3} mol l^{-1}; eluent, H_2O; flow rate, 1.0 ml min^{-1}.

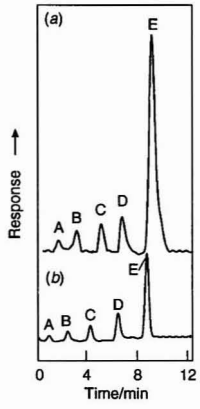

Fig. 5 Comparison of the response sensitivity of various concentrations of KCl between (*a*) a, PVC–crown ether coated (8 μg) piezoelectric crystal detector and (*b*) a commercial conductivity detector, where the eluent and sample flow through the conductivity detector first and subsequently, through the piezoelectric crystal detector, A, 3×10^{-4} mol l^{-1}; B, 5×10^{-4} mol l^{-1}; C, 8×10^{-4} mol l^{-1}; D, 1×10^{-3} mol l^{-1}; and E, 5×10^{-3} mol l^{-1}; eluent, H_2O; flow rate, 1.0 ml min^{-1}.

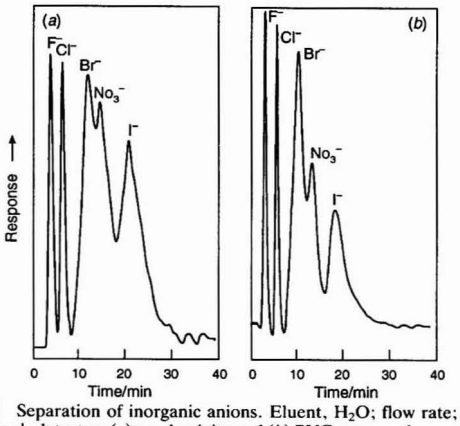

Fig. 6 Separation of inorganic anions. Eluent, H_2O; flow rate; 2.0 ml min^{-1}; detector, (*a*) conductivity and (*b*) PVC–crown ether coated (8 μg) piezoelectric sensor; sample volume, 5 μl; sample, F^-, 20 ppm, Cl^-, 30 ppm, Br^-, 180 ppm, NO_3^-, 250 ppm, and I^-, 800 ppm.

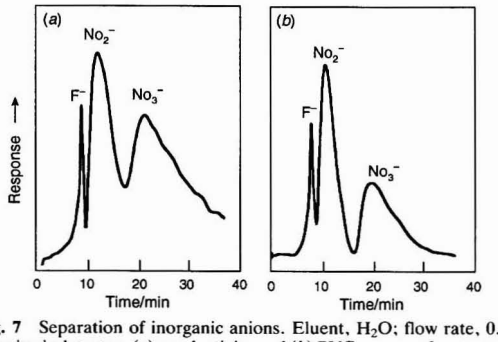

Fig. 7 Separation of inorganic anions. Eluent, H_2O; flow rate, 0.5 ml min^{-1}; detector, (*a*) conductivity and (*b*) PVC–crown ether coated (8 μg) piezoelectric sensor; sample volume, 5 μl; sample, F^-, 20 ppm, NO_2^-, 80 ppm, and NO_3^-, 120 ppm.

column. The order of elution for these ions is $F^- > Cl^- > Br^- > NO_3^- > I^-$ on the cryptand column, the same order as that achieved on the common ion-exchange resin column.[20,21] Fig. 6 shows the responses of F^-, Cl^-, Br^-, NO_3^- and I^- on both the PVC–crown ether piezoelectric crystal detector and the commercial conductivity detector which is separated by a protonated cryptand ion chromatography column. The cryptand ion chromatography column was also successfully applied to separate NO_3^- and NO_2^-, which both gave responses on the two detectors (as shown in Fig. 7). The NO_3^- ion (appoximately 1.86 Å) fits well into the cavity (approximately 1.8–2.2 Å)[22] of cryptand [2,2] but NO_2^- is too small (approximately 1.55 Å) for the cavity of protonated cryptand [2,2]; therefore, NO_3^- forms stronger complexes than NO_2^- with protonated cryptand [2,2], hence the retention time for NO_3^- is longer than that of NO_2^-. Similarly, F^-, SO_4^{2-}, Br^- and SCN^- can also be separated by this column; the responses on these two detectors are significant (Fig. 8).

The cryptand ion chromatography column can also be used as a cation exchanger for the separation of cations after de-protonation on a cryptand ion chromatography column. In aqueous solution, after basification using NaOH (0.05

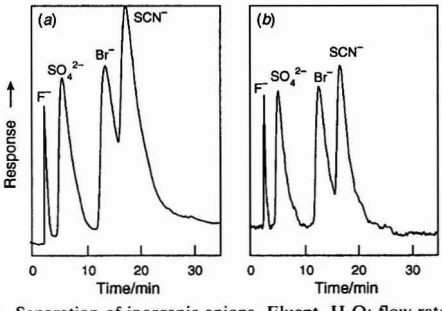

Fig. 8 Separation of inorganic anions. Eluent, H_2O; flow rate, 2.0 ml min^{-1}; detector, (*a*) conductivity and (*b*) PVC-crown ether coated (8 μg) piezoelectric sensor; sample volume, 5 μl; sample, F^-, 20 ppm, SO_4^{-2}, 40 ppm, Br^-, 150 ppm, and SCN^-, 250 ppm.

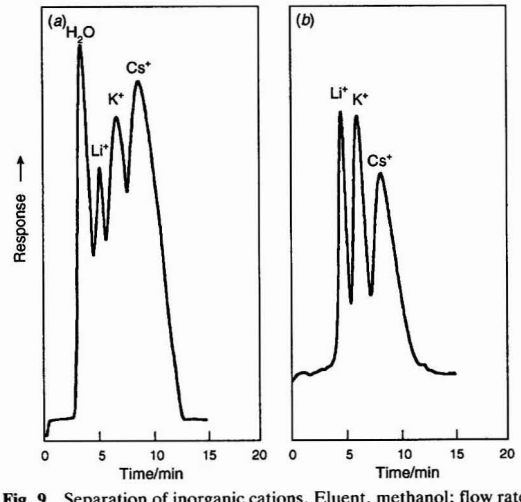

Fig. 9 Separation of inorganic cations. Eluent, methanol; flow rate, 0.5 ml min^{-1}; detector (*a*) conductivity and (*b*) PVC–crown ether coated (8 μg) piezoelectric sensor; sample volume, 5 μL; sample, Li^+, 10 ppm, K^+, 25 ppm, and Cs^+, 200 ppm.

mol l^{-1}), the cryptand column was switched for a cation exchanger column. Fig. 9 shows that alkali metal ions are separated by the cryptand column using methanol as the eluent. It should be noted that there is an extra peak resolved using the PVC–crown ether piezoelectric crystal detector; however, this peak was not detected by the conductivity detector. As the piezoelectric quartz crystal is sensitive to density, viscosity and the relative permittivity of the liquids, in the present system aqueous alkali metal chloride solution was injected into the cryptand ion chromatography column using methanol as the eluent. The density, viscosity and relative permittivity between water and methanol are disimilar, and the retention times of this peak are kept constant by repetitive injections of pure water. It was concluded that this water caused the crown ether piezoelectric crystal detector to detect this extra peak.

It is well known that mixing water with solvents of lower relative permittivity, such as methanol, profoundly affects (lowers) the response of a conductivity detector, but what about the affect on the response of a piezoelectric crystal detector? In the present work, 5 μl of 0.01 mol l^{-1} KCl were injected into the crystal detector with various compositions of eluent (H_2O–methanol). The mixing solvent (H_2O–MeOH) effect on the responses of the crown ether-coated crystal for KCl is shown in Fig. 10. Fig. 10 shows that the more methanol added, the smaller the signal produced by piezoelectric crystal detector. Fig. 10 supports the earlier mentioned fact that the relative permittivity affects the oscillating frequency of the crystal.

There are, of course, several drawbacks inherent in the use of a quartz piezoelectric crystal as an ion chromatography detector. It cannot be used in the gradient elution as it will increase or decrease the oscillating frequency greatly. In the H_2O–MeOH gradient system the change in background signal detected by the conductivity detector method is smaller than that of the PEC method, as $\Delta F = K(\rho\eta)^{1/2}$. Despite of the weakness in applying a PEC in a gradient elution system, relatively small dynamic range (flow rate change will alter the oscillating frequency) is the other shortcoming in PEC method.

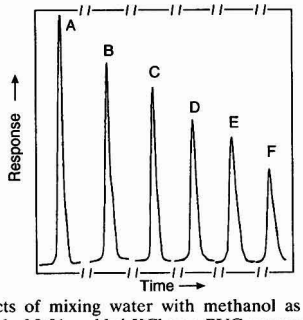

Fig. 10 Effects of mixing water with methanol as eluent on the response of 5 μl of 0.01 mol l^{-1} KCl on a PVC–crown ether coated (8 μg) piezoelectric crystal detector. A, H_2O; B, H_2O–methanol (4 + 1); C, H_2O–methanol (3 + 2); D, H_2O–methanol (2 + 3); E, H_2O–methanol (1 + 4); and F, methanol.

In conclusion, the detection limits for MCl_3, MCl_2 and MCl are approximately 2×10^{-5} (1×10^{-10} mol), 3×10^{-5} (1.5×10^{-10} mol) and 5×10^{-5} mol l^{-1} (2.5×10^{-10} mol). The slope ratio of electric potential (oscillating frequency change) *versus* concentrations of different charged metal ions is very similar to the ratio of the square root of the charges of these metal ions ($1:\sqrt{2}:\sqrt{3}$). The oscillating frequency of piezoelectric quartz crystal depends not only on the viscosity and the density of liquid but also on the relative permittivity of the liquid and the charges on the ions. Moreover, the response of PVC–crown ether coated piezoelectric quartz crystal to metal ions is also highly reproducible. The detection of transition metal chlorides and lanthanoids (La^{3+}, Eu^{3+}, *etc.*) salts using a PEC is more easy and convenient than a conductivity detector method.

The authors thank the National Science Council of Republic of China in Taiwan for financial support.

References

1 Lu, C., *Applications of Piezoelectric Quartz Crystal Microbalances*, ed. Lu, C., and Czanderna, A. W., Elsevier, New York, 1984, ch. 2, p. 27.
2 Sauerbrey, G., *Z. Phys.*, 1964, **178**, 457.
3 Knash, P. L., and Bastiaans, *Anal. Chem.*, 1980, **52**, 1929.
4 Thompson, M., Arthur, C. L., and Dhaliwal, G. K., *Anal. Chem.*, 1986, **58**, 1206.
5 Bruckenstein, S., and Shay, M., *Electrochim. Acta*, 1985, **30**, 1295.
6 Pedersen, C. J., *J. Am. Chem. Soc.*, 1967, **89**, 7017.
7 Pedersen, C. J., *J. Am. Chem. Soc.*, 1970, **92**, 386.
8 Heftmann, E., *Chromatography*, Elsevier, New York, 1983.
9 Gjerde, D. T., Schmuckler, G., and Fritz, J. S., *J. Chromatogr.*, 1980, **187**, 35.
10 Pohl, C. A., and Johnson, E. L., *J. Chromatogr. Sci.*, 1980, **18**, 442.
11 Chen, S. J., and Shih, J. S., *J. Chin. Chem. Soc.* (*Taipei*), 1991, **38**, 216.
12 Jane, Y. S., and Shih, J. S., *J. Chin. Chem. Soc* (*Taipei*), 1994, **41**, 719.
13 Strzelbicki, J., and Bartsch, R. A., *Anal. Chem.*, 1981, **53**, 2247.
14 Strzelbicki, J., and Bartsch, R. A., *Anal. Chem.*, 1981, **53**, 2251.
15 Tang, J., and Wai, C. M., *Anal. Chem.*, 1986, **58**, 3233.
16 Kanazawa, K. K., and Gordon, J. G., *Anal. Chim. Acta*, 1985, **175**, 99.
17 Hager, H. E., *Chem. Eng. Commun.*, 1986, **25**, 43.
18 IUPAC, *Anal. Chem.*, 1976, **48**, 2294.
19 Long, G. L., and Winefordner, J. D., *Anal. Chem.*, 1983, **55**, 712A.
20 Small, H., Stevens, T. S., and Bauman, W. C., *Anal. Chem.*, 1975, **47**, 1801.
21 Smith, F. C., and Chang, R. C., *The Practice of Ion Chromatography*, Wiley, New York, 1983, p. 15.
22 Buschmann, H. J., *Inorg. Chim Acta.*, 1986, **120**, 125.

Paper 4/04578E
Received July 26, 1994
Accepted October 18, 1994

'One-pot' Electrochemical Determination of Copper and Formaldehyde in Electroless Copper Plating Baths

G. Bryan Balazs, Robert S. Glass and Leslie J. Summers

Chemistry and Materials Science Department, Lawrence Livermore National Laboratory, Livermore, CA 94550, USA

A simple electrochemical method has been developed for the determination of copper and formaldehyde concentrations in electroless copper plating baths. This method uses dc amperometry and anodic stripping voltammetry for the determination of formaldehyde and copper concentrations, respectively. The analyses are done sequentially using a single gold electrode in the same sample solution. The advantages of this 'one-pot' technique are simplicity and speed of analysis, important advantages over alternative methods of analysis which are either more time consuming, involve multiple samples, or use more elaborate instrumentation. A commercial plating bath was analysed using the described technique, yielding results which had a precision of within 5% for formaldehyde and copper. While not rigorously precise, this method can be used in process control to indicate when bath replenishment or replacement is necessary. The method can easily be implemented in plating facilities by operators using portable equipment, and an automated, on-line procedure is also possible.

Keywords: *Electroless plating; copper; formaldehyde; electroanalysis; amperometry; stripping voltammetry*

Introduction

Electroless plating baths[1,2] are extensively used in such areas as electronics manufacturing, jewellery making, and other applications where appropriate conductivity, corrosion protection, or other surface properties are desired. The use of electroless deposition largely avoids the problems of dendrite formation and uneven deposits which are often produced using electrolytic deposition, where non-uniform current densities can occur. For this reason electroless deposition is particularly useful for plating through holes in printed wiring boards,[3] and in other areas where the throwing power of electrolytic baths is an issue. Sinee no electrical connection to the substrate is required, plating may even be accomplished on appropriately sensitized non-conductive substrates.

One of the most common electroless plating baths is based on the copper–formaldehyde system.[4,5] The reduction of Cu^{2+} by formaldehyde at the plating surface is given as:

$$Cu^{2+} + 2HCHO + 4OH^- \rightarrow Cu^0 + H_2 + 2H_2O + 2HCOO^- \quad (1)$$

It should be emphasized that this simplified equation is representative of the overall stoichiometry only and the actual oxidative process involves the $H_2C(OH)O^-$ anion.[6,7]

In order for the bath to function effectively, the concentrations of copper ions and formaldehyde must be maintained within a specified range. If the values fall outside the set levels, the coatings produced may be off-colour, too thin or brittle, or uneven or 'spotty' coverage may result. Also, plating times may be inconveniently long if the components become depleted. Quality control mandates that the copper and formaldehyde concentrations be frequently determined to ensure good, consistent plating results.

Currently, copper/formaldehyde baths are analysed by wet chemical or spectroscopic means,[8] a procedure usually done in remote analytical labs and which can require a considerable amount of time and effort (if just from sample turnaround times). Because the concentrations of copper and formaldehyde change continuously during the lifetime of a bath, it would be desirable to have a rapid means of analysis which can be implemented in the plating facility, or on-line using portable equipment. In fact, electrochemical techniques based on stripping voltammetry using mercury[9–11] and platinum[12] electrodes have been developed for just this purpose. The use of a mercury electrode offers the advantage of being able to analyse for many plating bath components in a single analysis.[9–11]

Our results show that the analysis can be simplified even further, especially avoiding the potential complications arising from the use of a mercury electrode. As plating bath compositions must fall within a supplier-specified window which is often somewhat generous, extreme accuracy and precision are not required. As an example, the manufacturer of the electroless copper plating bath analysed in this work (see Experimental section) specifies a range of 2.5 to 3.5 ppt copper and 6 to 9 ppt formaldehyde. The important aspect is that the results be reliable (in a process control sense) and be obtained quickly and easily by shop analysts. To this end, we have developed a convenient, 'one-pot' electrochemical technique for the determination of both copper and formaldehyde concentrations in electroless plating baths. The method described in this article is sufficient to establish if a plating bath has exceeded its useful lifetime or requires replenishment. This method is easily implemented using commercially available instrumentation. In addition, compact, user-friendly systems are under development which will make implementation even easier.

Experimental

All chemicals used were of analytical-reagent grade. Distilled water was further purified by passage through a Corning Mega Pure water purification system (Corning, NY, USA). Copper standards and standard additions were performed by appropriate dilution of a 1000 ppm Cu atomic absorption standard (Aldrich, Milwaukee, WI, USA). Formaldehyde standards and standard additions were performed by dilution of a 37% HCHO reagent solution (J. T. Baker, Phillipsburgh, NJ, USA). All solutions were prepared fresh each day.

The copper plating bath solutions were made fresh each day by mixing commercial solutions (MacDermid, Waterbury, CT, USA) 22A and 22B. This product is a two-component formulation with one solution containing copper(II) ions and

formaldehyde, the other containing sodium hydroxide. The components 22A and 22B and de-ionized water were mixed in the ratio 1:1:8. A plating bath solution mixed as directed initially contains 3.1 ppt of Cu^{2+}, 7.5 ppt of HCHO and 11.5 ppt of NaOH. A complexing agent such as EDTA is also present to prevent precipitation of copper hydroxide.[4,5]

Electrochemical measurements were performed using a Bioanalytical Systems (West Lafayette, IN, USA) Model 100W electrochemical analyser. Before use, conventionally sized disk electrodes (1.6 mm diameter) and microelectrodes (10 μm diameter) were polished using 0.05 μm alumina powder slurries. A platinum wire coil was used as the counter electrode. All potentials given are *versus* an Ag/AgCl reference electrode. The solutions were not deoxygenated before analysis, and all measurements were performed at room temperature. Other electrochemical parameters are given in the figure captions.

Results and Discussion

General Considerations

Although mercury film and hanging mercury drop electrodes have previously been used for both anodic stripping voltammetry of copper[9–11,13] and fundamental studies of the electrochemical reduction[9–11,14,15] and oxidation[16] of formaldehyde, a solid electrode would be easier to use and more acceptable considering the potential contamination aspects. This would be especially true for monitors used directly in plating baths.

Many studies have been done on the electrochemistry of formaldehyde at solid electrodes such as platinum[6,17–20] and gold.[7,21–24] A good review of the oxidation reactions is provided in ref. 23. The reaction mechanisms are dependent on the electrode used and both oxidized products ($HCOO^-$, CO_2) and reduced products [CH_3OH, $(CH_2OH)_2$] are possible.

In an actual electroless copper plating bath, the potentials required for the reduction of formaldehyde at electrodes other than mercury resulted in the plating of copper[24,25] onto the electrode surface. For this reason, an analytical technique based on the oxidation reactions of formaldehyde[6,7,17–23] was the obvious choice. In fact, oxidative processes at platinum electrodes have been used specifically for determining formaldehyde concentrations in electroless copper plating baths[12] and in chromatography.[26]

The use of anodic stripping voltammetry (ASV)[13] has proved valuable for the analysis of copper in plating baths[9–11] and was thus chosen to measure copper concentrations in the present work. Since the copper ion concentration in the copper plating bath studied (see Experimental) is high relative to the concentrations usually determined by ASV, no deoxygenation of the solution was necessary and solid (non-mercury-based) electrodes worked well. After examining several electrode materials (Pt, Ag, Cu, Au, C) with both copper and formaldehyde determinations in mind, it was found that a gold electrode worked best.

While it may be desirable to perform the analysis directly in the plating bath itself, there are certain problems with this approach. The concentrations of copper and formaldehyde in a typical plating bath are large enough so that the range of linear response can be exceeded using conventional electrochemical parameters (deposition time, scan rates, *etc.*). More importantly, the presence of any metal electrode such as gold or platinum, which provides a catalytic surface for reaction (1) to occur, resulted in the plating out of copper on the electrode surface. Therefore, a copper electrode surface was formed after a short immersion time, a result which made an accurate determination of the copper and formaldehyde concentrations difficult. Although the use of carbon-based (graphite or glassy carbon) electrodes did not result in the spontaneous plating out of copper, formaldehyde exhibited no electrochemical oxidation at these electrodes.

In order to circumvent the problems mentioned above, the analysis for both copper and formaldehyde is performed by injecting a small aliquot of the plating bath solution into a 1 mol l^{-1} NaOH solution. Conditions of very high pH were used in order to shift the formaldehyde speciation equilibrium towards the most readily oxidized species, $H_2C(OH)O^-$.[6,7,22] Typical dilutions were on the order of 1:20 to 1:100, the latter dilution factor being used for fresh plating baths. This dilution has the desirable effect of minimizing the spontaneous plating of copper onto the electrode surface, while still maintaining copper and formaldehyde concentrations at levels convenient for the sensitivity of the electroanalytical techniques used. Of course, an added benefit of this procedure is that the electrolyte is well defined from one analysis to the next.

Electrochemical Response of a Gold Electrode in Formaldehyde–NaOH Solutions

The voltammetric response of a conventionally sized (1.6 mm diameter) gold disk electrode in 1 mol l^{-1} NaOH is shown in Fig. 1. Scanning anodically from −1.0 V, the voltammogram exhibits a small wave beginning at −0.15 V, followed by a peak at 0.35 V. On the return scan, a sharp peak occurring at 0 V and a smaller broad peak with a maximum at −0.3 V can be seen. These features have been noted by other researchers,[18,21] and are attributed to the formation (forward scan) and reduction (reverse scan) of gold oxide(s).

The solid trace in Fig. 1 represents the voltammogram obtained in a 1 mol l^{-1} NaOH solution in which 0.73 ppt formaldehyde is also present. An anodic scan starting from −1.0 V exhibits a peak at −0.45 V followed by another anodic process occurring at about 0 V. Overlap of the decreasing portion of the peak at −0.45 V with the broad peak at 0 V results in a step-wise form of the *I–E* curve. These peaks are due to the oxidation of formaldehyde,[6,7,20–22] and increased in magnitude with the addition of more formaldehyde. Further increases in potential (positive of 0.2 V) result in a decrease of the current to almost zero. Because this latter potential is the potential at which the oxidation of the gold electrode itself occurs (see Fig. 1, B), it is reasonable to relate the inhibition of the formaldehyde oxidation to the formation of a gold oxide surface layer. As noted by previous researchers,[6,20,26] the presence of a gold oxide layer on the electrode surface is sufficient to completely block the oxidation of formaldehyde.

On the return scan, the reduction of the gold oxide layer (beginning at 0.1 V) is sufficient to cause the resumption of

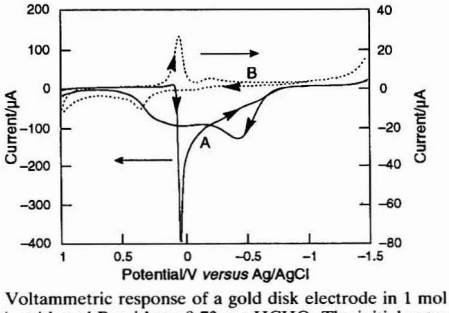

Fig. 1 Voltammetric response of a gold disk electrode in 1 mol l^{-1} NaOH A, with and B, without 0.73 ppt HCHO. The initial potential was −1.0 V and the scan rate was 0.1 V s^{-1}.

formaldehyde oxidation, a phenomena which is indicated by the sudden anodic current spike seen in Fig. 1. It is possible that the adsorption of reaction intermediates on the electrode surface is also responsible for this inhibition effect, as has been proposed with platinum electrodes.[17,18,23] Alternatively, the spike at 0 V may also be due to the oxidation of adsorbed reactants at the electrode surface.[7,23] It is beyond the scope of this work to explain fully the above observations as previous research has discussed the complexity of the formaldehyde oxidation reaction.[6,7,17–23]

Formaldehyde Analysis

Owing to the complications arising from the plating of copper onto the electrode surface and the resulting inhibition of formaldehyde oxidation, it was felt that voltammetric techniques for the determination of formaldehyde at a gold electrode were not adequate. However, an amperometric experiment at a carefully chosen potential proved to give reasonable results. The electrode was potentiostated at 0.1 V and the current due to the oxidation of added formaldehyde was measured as the solution was stirred. The stirring insured solution homogeneity and established plateau currents which are easier to measure.

The choice of electrode potential was not arbitrary. It was chosen to be negative enough to avoid electrode passivation due to gold oxide formation; amperometric experiments at potentials positive of 0.1 V showed less current and more fluctuations. These decreases were no doubt due to the formation of gold oxide at the electrode surface. On the other hand, the optimum potential was positive enough to show a significant rate of oxidation of formaldehyde and to avoid complications arising from copper plating onto the electrode surface. At this potential, any copper metal which plated out onto the electrode surface by electroless deposition is immediately re-oxidized. It has been verified that an addition of Cu^{2+} ions to the solution had no effect on the oxidation of formaldehyde at that potential.

Fig. 2 shows the amperometric response of a conventionally sized (1.6 mm diameter) gold disk electrode potentiostated at 0.1 V in a 1 mol l^{-1} NaOH solution to which formaldehyde has been added in four steps to give total concentrations of 185, 370, 555, and 740 ppm. The noise observed in the plateau regions is probably due to stirring irregularities, while the slight decrease in current with time immediately after each injection may be due to fouling of the electrode surface by

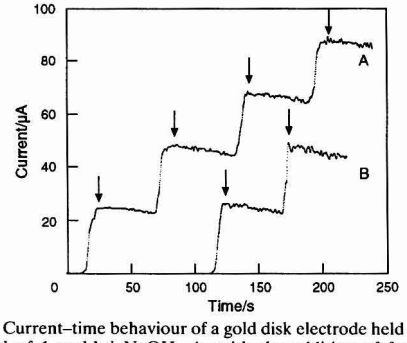

Fig. 2 Current–time behaviour of a gold disk electrode held at 0.1 V in 10 ml of 1 mol l^{-1} NaOH. A, with the addition of four equal amounts of HCHO to yield concentrations after addition of 185, 370, 555 and 740 ppm; B, (offset 100 s for clarity) with the addition of 25 μl of a freshly prepared plating bath (see Experimental), followed by a standard addition of HCHO (50 μl of 3.7% HCHO). The arrows indicate times of current measurement.

reaction intermediates.[6,21,23] Repolishing the electrode after each step restored the response to its former value. However, for the purposes of this analytical technique, sufficient precision was obtained by measuring the current at a consistent time after the injection. This point was chosen by visually inspecting the current steps and choosing the first point after the maximum current for each step was reached, allowing for noise fluctuations.

For each injection (chosen to yield equal concentration increases), the increase in current was approximately 23 μA. Additional experiments showed that this linearity was valid over a concentration range of at least 10 to 2000 ppm. In the absence of formaldehyde, the measured current was negligible compared to the large current obtained for the oxidation of formaldehyde (see Fig 1). This small background current is no doubt due to the oxidation of the gold electrode. The observation that the current for the oxidation of formaldehyde at gold was linear with respect to reactant concentration has been noted by other researchers.[7] Although a stirred solution does not provide the well defined hydrodynamics of a rotating disk electrode, the nearly plateau current shapes observed are sufficient to provide reasonable results.

The analysis of a plating bath was performed in a similar fashion. The current was monitored as an aliquot of a freshly prepared plating bath solution was injected into the stirred 1 mol l^{-1} NaOH solution, followed by the injection of a formaldehyde standard addition. The current response for the two injections is shown in Fig. 2. The standard addition equation [eqn (2)] yields the concentration of the unknown, c_u, given the known values of V (initial solution volume), i_u (current of unknown), c_s (concentration of spike), v (volume of spike) and i_{tot} (total current of unknown and standard addition).[27]

$$c_u = \frac{-vc_s i_u}{i_u V - i_{tot}(V + v)} \quad (2)$$

From this equation, a value of 7.3 ppt for the concentration of formaldehyde in the original plating bath solution can be calculated. This compares well with the 7.5 ppt value given in the product specifications and is within the specified range of 6 to 9 ppt.

Copper Analysis

Although the analysis of metal ions by anodic stripping voltammetry is usually performed in acidic media,[13] the concentration of copper in most plating bath solutions is sufficient to yield a response in 1 mol l^{-1} NaOH. Since the copper and formaldehyde determinations in this method are performed in different potential regions, and the dilution factor is the same, it is possible to perform the analysis for copper in the same solution in which the formaldehyde analysis was performed. This greatly simplifies the procedure.

Fig. 3 shows the currents observed for an anodic stripping experiment in which increasing amounts of copper were added to a 1 mol l^{-1} NaOH solution, deposited on the gold disk electrode at −0.6 V for 10 s, then stripped using an anodic scan. The magnitude of the peak at −0.2 V varies linearly with copper concentration throughout the range given ($\Delta i/\Delta c$ = 0.034 ± 0.006 μA per ppm Cu), but deviated from linearity at higher concentrations or longer deposition times. The deposition times were thus chosen so that linear response conditions would be obtained. Another, much smaller peak is observed at about −0.45 V, but the height of this peak did not correlate linearly with bulk copper ion concentration. A small shoulder at about −0.1 V was seen at the tail end of the larger copper stripping peak. This feature was also seen in a blank and did not depend on deposition time or potential. The shoulder is

likely to be indicative of the oxidation of the gold electrode surface.

To perform the analysis for copper, an anodic stripping experiment was done with the solution used for the formaldehyde analysis above. Again, standard addition can be used to provide quantitative results. Fig. 4 shows the stripping response for copper using the parameters given in the figure caption. From eqn (2), a value of 3.3 ppt copper in the original plating bath can be calculated. This value is in reasonable agreement with the value of 3.1 ppt given in the product specifications, and within the specified range of 2.5 to 3.5 ppt.

The presence of components other than copper in the plating bath solution did not substantially affect the anodic stripping response for copper, as shown in Fig. 3. The two experiments were identical, except that in one case an aliquot of an old plating bath solution was added. It was assumed that the old plating bath solution provides essentially the same matrix as a new one, except for the presence of copper ions and formaldehyde. The only significant difference observed in the two responses was due to dilution effects, and thus the presence of complexing agents, stabilizers, or other proprietary ingredients in the bath does not significantly affect the analytical method.

Recommended Procedures for Determination of Copper and Formaldehyde

The analytical procedure can be summarized as follows: (1) The working electrode may be lightly polished with 0.05 μm alumina slurry before use. (2) The current at a gold electrode potentiostated at 0.1 V in a small volume (10 ml) of 1 mol l^{-1} NaOH is continuously measured. (3) An aliquot (typically 100–250 μl) of the plating bath solution is injected into the stirred solution, followed by a known aliquot of a HCHO standard addition. (4) From the relative magnitude of the two current plateaus, a concentration of HCHO in the original bath is calculated [see eqn (2)]. (5) The electrode potential is then set at −0.6 V for a fixed period (5–30 s), and then scanned to 0.2 V as the current is monitored. Stirring may be required during the deposition step. (6) A known aliquot of a copper standard is added, and step (4) is repeated. (7) From the relative magnitude of the two dominant stripping peaks (at −0.2 V) observed in steps (5) and (6), a concentration of copper in the original bath is calculated, again using the standard addition expression [eqn (2)].

The above procedure was found to give good results with plating bath solutions which were relatively new. The analysis of solutions much lower in copper or formaldehyde concentration (such as those present in old baths or rinse tanks) requires some modifications. Larger amounts of the plating bath aliquot, or longer deposition times for the copper stripping experiment, may be needed. We analysed older plating bath solutions with much less copper and formaldehyde and found that the method described above gave good results.

As noted earlier, copper will plate out onto the electrode surface if the electrode is left unpotentiostated in a plating bath solution. Fortunately, the dilution of the reactants in the above analytical procedure decreased this plating rate considerably. As evidence of this, no significant copper stripping peak was observed for an unpotentiostated electrode immersed in a dilute solution for the time required for an analysis. Although metallic copper plated out on the platinum counter electrode after a period of time, this did not appear to have an effect on the calculated results. However, if prolonged contact with the diluted plating solution were allowed prior to analysis, the amount of copper lost may be sufficient to lead to erroneously low copper values.

In general, the formaldehyde analysis yielded better precision than the copper analysis. Despite repeated attempts, the stripping peaks for copper were only good to about 5% precision. Many concentration ranges and conditions were tried, but no source of error could be identified. Note that a plating bath contains components other than copper and formaldehyde, including complexing agents, stabilizers, and other proprietary ingredients. Owing to the uncertainty of the exact matrix, electroanalysis will not be as 'clean' as in a one- or two-component medium. In addition, anodic stripping voltammetry of copper in basic solutions at bare electrodes is not the accepted quantitative method reported in the literature.[13]

The above results were obtained using a conventionally-sized disk electrode. A substantiai advantage could be realized if the procedure were based on a gold microelectrode since plateau rather than peak currents are observed[28] in quiescent solutions. Enhanced signals have also been noted in ASV using microelectrodes without stirring.[29–31] In addition, the obviation of the requirement for a stirring apparatus would offer true advances in simplifying this entire method. Unfortunately, the current response obtained using a gold microelectrode under the same conditions as detailed above produced a signal which was noisy and did not give a steady-state response. For this reason, it was not possible to use the gold microelectrodes for quantitative analysis of either formaldehyde or copper. Possible reasons for these microelectrode results, such as surface fouling, are being investigated.

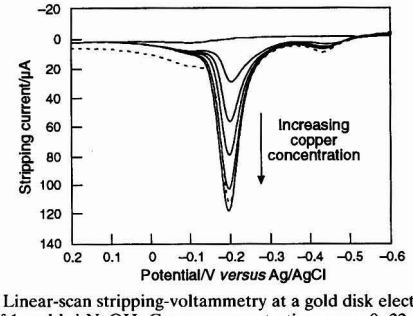

Fig. 3 Linear-scan stripping-voltammetry at a gold disk electrode in 10 ml of 1 mol l^{-1} NaOH. Copper concentrations were 0, 32, 64, 96, 128 and 160 ppm (solid lines). The dashed line is the same solution with a copper concentration of 160 ppm but with the addition of 250 μl of an old plating bath. A 10 s deposition time at −0.6 V with stirring and a 10 s standing time prior to scan initiation were used. The scan rate was 0.1 V s^{-1}.

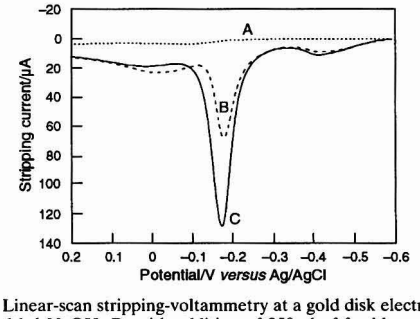

Fig. 4 Linear-scan stripping-voltammetry at a gold disk electrode in A, 1 mol l^{-1} NaOH; B, with addition of 250 μl of freshly prepared plating bath; C, with plating bath addition and standard addition of 250 μl of 3.2 ppt Cu (additional concentration of Cu was 80 ppm). A 10 s deposition time at −0.6 V with stirring and a 10 s standing time prior to the scan initiation were used. The scan rate was 0.1 V s^{-1}.

Conclusions

We have demonstrated the validity of an electrochemical method which can be used for the determination of copper and formaldehyde concentrations in electroless copper plating baths. Only one solution and minimal effort and instrumentation are required. The method could be performed using portable equipment and automated for on-line control.

For the purpose of deciding whether a plating bath needs to be replenished or replaced, extremely accurate or precise numbers are generally not required. The described method for the determination of copper and formaldehyde provides precision and accuracy sufficient for such a decision. The advantages of speed and simplicity far outweigh the small loss of precision or accuracy.

This work is performed under the auspices of the U.S. Department of Energy by the Lawrence Livermore National Laboratory under contract number W-7405-ENG-48.

References

1 *Electroless Plating: Fundamentals and Applications*, eds. Mallory, G. O., and Hajdu, J. B., American Electroplaters and Surface Finishers Society, Orlando, 1990.
2 *Modern Electroplating*, ed. Lowenheim, F. A., Wiley, New York, 1974.
3 Stone, F. E., in *Electroless Plating: Fundamentals and Applications*, eds. Mallory, G. O., and Hajdu, J. B., American Electroplaters and Surface Finishers Society, Orlando, 1990, ch. 13.
4 Bindra, P., and White, J. R., in *Electroless Plating: Fundamentals and Applications*, eds. Mallory, G. O., and Hajdu, J. B., American Electroplaters and Surface Finishers Society, Orlando, 1990, ch. 12.
5 Pearlstein, F., in *Modern Electroplating*, ed. Lowenheim, F. A., Wiley, New York, 1974, ch. 31.
6 Adzic, R. R., Avramov-Ivic, M. L., and Tripkovic, A. V., *Electrochim. Acta*, 1984, **29**, 1353.
7 Beltowska-Brzezinska, M., *Electrochim. Acta*, 1985, **30**, 1193.
8 Parthasaradhy, J. V., *J. Sci. Ind. Res.*, 1988, **47**, 639.
9 Okinaka, Y., *Plat. Surf. Finish*, 1985, **72**, 34.
10 Rothstein, R. L., *Plat. Surf. Finish*, 1984, **71**, 36.
11 Rothstein, R. L., *Met. Finish*, 1984, **82**, 35.
12 Tam, T. M., *J. Electrochem. Soc.*, 1985, **132**, 806.
13 Wang, J., *Stripping Analysis: Principles, Instrumentation and Applications*, VCH, Deerfield Beach, FL, 1985.
14 Montenegro, M. I., Pletcher, D., Liolios, E. A., Mazur, D. J., and Zawodzinski, C., *J. Appl. Electrochem.*, 1990, **20**, 54.
15 Barnes, D., and Zuman, P., *J. Electroanal. Chem.*, 1973, **46**, 323.
16 Vaskelis, A., and Norkus, E., *J. Electroanal. Chem.*, 1991, **318**, 373.
17 Olivi, P., Bulhoes, L. O. S., Beden, B., Hahn, F., Léger, J.-M., and Lamy, C., *J. Electroanal. Chem.*, 1992, **330**, 583.
18 Bagotzky, V. S., and Vasilyev, Y. B., *Electrochim. Acta*, 1964, **9**, 869.
19 Liang, C., and Franklin, T. C., *Electrochim. Acta*, 1964, **9**, 517.
20 Sibille, S., Moiroux, J., and Marot, J.-C., *J. Electroanal. Chem.*, 1978, **88**, 105.
21 Enyo, M., *J. Electroanal. Chem.*, 1985, **186**, 155.
22 Van Den Meerakker, J. E. A. M., *J. Appl. Electrochem.*, 1981, **11**, 387.
23 Parsons, R., and VanderNoot, T., *J. Electroanal. Chem.*, 1988, **257**, 9.
24 MacDonald, D. D., *J. Electrochem. Soc.*, 1974, **121**, 651.
25 Fletcher, S., Barrada, R. G., and Porter, J. D., *J. Electrochem. Soc.*, 1978, **127**, 1960.
26 Rocklin, R. D., in *Formaldehyde: Analytical Chemistry and Toxicology*, ed. Turoski, V., American Chemical Society, Washington, *Advances in Chemistry*, vol. 210, 1985, ch. 2.
27 Willard, H. H., Merritt, L. L., Jr., Dean, J. A., and Settle, F. A., Jr., *Instrumental Methods of Analysis*, Wadsworth, Belmont, CA, 1981, 6th edn., Pp. 719.
28 Fleischmann, M., Pons, S., Rolison, D. R., and Schmidt, P. P., *Ultramicroelectrodes*, Datatech Systems, Morgantown, NC, 1987.
29 Wang, J., Angnes, L., Tobias, H., Roesner, R. A., Hong, K. C., Glass, R. S., Kong, F. M., and Pekala, R. W., *Anal. Chem.*, 1993, **65**, 2300.
30 Wang, J., Brennsteiner, A., Angnes, L., Sylwester, A., LaGasse, R. R., and Bitsch, N., *Anal. Chem.*, 1992, **64**, 151.
31 Wehmeyer, K. R., Wightman, R. M., *Anal. Chem.*, 1985, **57**, 1989.

Paper 4/02146K
Received May 11, 1994
Accepted September 15, 1994

Quantitative Determination of Cadmium, Zinc Thioneins Using Differential-pulse Polarography

Amalia Muñoz* and Adela Rosa Rodríguez

Commission of the European Communities, Joint Research Centre, Institute for Reference Materials and Measurements, Retieseweg, B-2440 Geel, Belgium

The quantitative determination of five commercial Cd–Zn thioneins (MT) and of two organic molecules intrinsic to the structure of metallothioneins, the peptidic fragment Lys-Cys-Thr-Cys-Cys-Ala thionein fragment [56-61] MT I and cysteine, was carried out using differential-pulse polarography (DPP). Metallothioneins of different origins, rabbit liver and horse kidney, presenting different isoforms and with a wide range of total contents of cadmium and zinc were studied. At pH 7.5, polarograms exhibit three peaks, labelled pMT, pCdT and pZnT and previously attributed to the oxidation of the mercury electrode in the presence of thiol groups and to the reduction of cadmium and zinc complexed by the thionein, respectively. Linear relationships between peak intensities and concentrations were observed. The intensity of the peak corresponding to the organic part of the molecule as a function of three times the molar concentration of metal ions initially contained in the MT was a single calibration curve for the five metallothioneins. DPP is proposed as a quantitative determination method.

Keywords: Polarography; metallothionein; protein analysis

Introduction

The electrochemical behaviour at the dropping mercury electrode of Cd, Zn thioneins (MT) from rabbit liver (RL) and horse kidney (HK) was previously studied[1] using differential-pulse polarography (DPP). In a given medium, the MT polarogram exhibits three well defined peaks at potentials different from those corresponding to pure Cd^{2+} and Zn^{2+}, $E_{pCd2+} = -0.58$ V and $E_{pZn2+} = -1.01$ V. For example, at pH 7.5 in Tris-HCl of 2.5×10^{-2} mol dm^{-3}, the values of the potential of the three peaks labelled E_{pMT}, E_{pCdT} and E_{pZnT} are -0.40, -0.83 and -1.10 V, *versus* the Ag/AgCl reference electrode, respectively. The peak labelled E_{pMT} appearing at the least negative potential is attributed to the oxidation of the mercury electrode in the presence of thiol groups of the metallothionein, while E_{pCdT} and E_{pZnT} correspond to the reduction of cadmium and zinc, respectively, complexed by the thionein. The polarogram of the peptide Lys-Cys-Thr-Cys-Cys-Ala thionein fragment [56–61] MT I (FT) exhibits, under the same experimental conditions, one peak labelled E_{pFT} attributed to the oxidation of the mercury electrode in the presence of FT, as a complexing agent.[2]

Consequently, the polarographic responses allow one to distinguish the chemical forms of the compound, the organic part of the molecule and the complexed cadmium or/and zinc with the thionein.

To our knowledge no study has been published on the systematic determination of Cd, Zn Thioneins, considering from an analytical point of view, the characteristics of the DPP technique as a determination method allowing speciation.

The present work studies the polarographic intensity as a function of the concentration of the different compounds. The intensity of peaks can be measured at the potentials corresponding to the electrochemical systems in which the organic part of the molecule is involved and at those corresponding to the CdT and ZnT complexes. With this aim five MT from RL and HK were selected. These MT present different isoforms depending on their amino acid sequence, either the mixture of isoforms I and II or each of them separately. Likewise, the total contents of cadmium and zinc in the MT vary by a factor of two between the different products[3] which reveals relations between the polarographic response and the metal content of each metallothionein. The present study compares the polarographic response $i_p = f(c)$ of MT with those found for two organic molecules intrinsic to the metallothionein structure: cysteine and the peptidic fragment [56–61] of MT I.

Experimental

Apparatus

Analysis was performed with an EG & G Princeton Applied Research Polarographic/Voltammetric Analyser model 384B (Princeton, NJ, USA). An EG & G model 303A Electrode housing was used with a medium size mercury drop as the working electrode, a platinum wire as the counter electrode and a Ag–AgCl reference electrode. A Houston Plotter DMP-40 (Austin, TX, USA) was used. The pH meter was a Tacussel model Minisis 5000 (Villeurbanne, France). A Barnstead Nanopure II water de-ionization system (Dubuque, Iowa, USA) was used in conjunction with a Jencons double distillation still (Bedfordshire, UK).

Procedure

Solutions and samples were degassed for at least 20 min before commencement of the electrochemical experiment. Nitrogen was passed over the solution during the experiments. The polarographic measurements were performed under potentiostatic control in the differential pulse mode. The amplitude of the pulses was 50 mV, the scan rate was 2 mV s^{-1} and the drop time was 1 s. The measurements were carried out at room temperature. The peak intensity is the average of at least three measurements with correction for the background current.

Chemicals

Cd, Zn Thioneins (Sigma, St. Louis, MO, USA) were as follows: MT I + II horse kidney M 4766 lot 79 F 9670 (45.1 ± 1.5 mg Cd g^{-1}, 16.8 ± 0.4 mg Zn g^{-1}); MT I + II horse kidney M 4766 lot 28 F 9545 (36.0 ± 0.7 mg Cd g^{-1}, 8.8 ± 0.2 mg Zn

* Present address: Department of Chemistry, University of Wisconsin, Milwaukee, WI 53211, USA.

g^{-1}); MT I + II rabbit liver M 7641 lot 20 H 9650 (83.2 ± 1.5 mg Cd g^{-1}, 13.3 ± 0.4 mg Zn g^{-1}); MT I rabbit liver M 5267 lot 129 H 9575 (64.3 ± 1.5 mg Cd g^{-1}, 11.1 ± 0.3 mg Zn g^{-1}); MT II rabbit liver M 5392 lot 79 H 9510 (72.1 ± 1.4 mg Cd g^{-1}, 10.0 ± 0.3 mg Zn g^{-1}).

The metal concentrations in the metallothioneins were previously determined[3] by electrothermal atomic absorption spectrometry. L-Cysteine was from Sigma (C 7755 lot 114 F 0672). The Lys-Cys-Thr-Cys-Cys-Ala Peptidic Fragment [56–61] MT I, acetate salt, was synthesized from mouse liver, containing mercaptoethanol as stabilizer (purity 87%) L 4512 lot 39 F 5810 (Sigma). (For calculation of concentrations only the peptide content was taken into account.)

Tris(hydroxymethyl)aminomethane was from Merck (Rathway, NJ, USA). Na_2HPO_4, and NaH_2PO_4 were also from Merck.

Results and Discussion

The peak intensities were measured for five commercial MT, for the FT and for cysteine over a wide range of concentrations in Tris-HCl. In all cases the pH value was 7.5. Several experiments were also performed at pH 2.

The peak intensity (E_{pMT} = −0.30 V) of the electrochemical system, attributed to the thiol groups, is given in Fig. 1 as a function of the molar concentration of MT, which was calculated assuming a molecular weight of 6500 Da. Linear relationships are observed between peak intensities and molar concentrations for a given metallothionein. In all cases, the correlation coefficients ($r > 0.998$) are close to unity. Nevertheless, a single straight line is not obtained as would have been expected if it is assumed that the electrochemical behaviour is the same for each metallothionein independent of their origin and that the electrochemical response is due only to the organic part of these molecules, *i.e.*, to the thiol content.

The variation of I_{pMT} as a function of three times the total concentration of metal ions is shown in Fig. 2. This representation is justified because the amino acid sequence containing three cysteinyl residues is considered as the basic structural unit involved in binding one divalent ion.[4] In this case, the polarographic response is related to the content of thiol groups bound to the metal ions. In fact, the wide range of metal contents in the MT studied should be noted, *e.g.*, MT I + II, HK lot 288 and MT I + II RL lot 20, 44.76 and 96.97 mg (Cd + Zn) g^{-1} (MT), respectively. This fact is difficult to explain assuming that MT synthesized *in vivo* have all their thiol groups saturated, as mentioned in most of the publications. It is possible that several thiol groups can form disulfide bridges which do not participate in the electrochemical mechanism. This has been already indicated in the polarographic study of FT in the presence and in the absence of cadmium and zinc[2] and in a chromatographic study.[5] Fig. 2 shows that plots of $I_{pMT} = f\,3c(Cd + Zn)$ give a single straight line for the five compounds, independent of their origins and metal contents. The equation of the line is $I_p = 1.36c + 0.39$ ($r = 0.982$) with the slope expressed as mA dm^3 mol^{-1}.

The intensities of the peak (CdT), attributed to the reduction of cadmium complexed by the thionein, as a

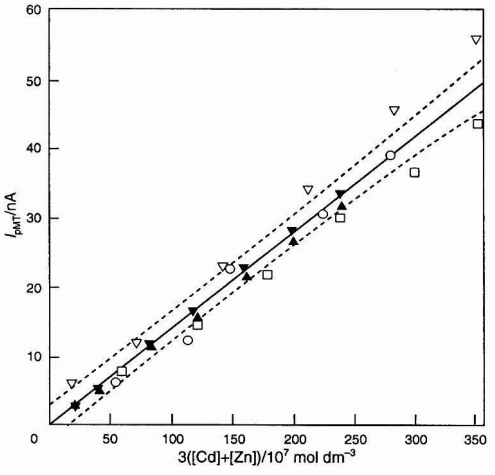

Fig. 2 Intensity of peak MT as a function of three times the total molar concentration of cadmium and zinc. The confidence limits (95%) are shown by the broken lines. Symbols as in Fig. 1.

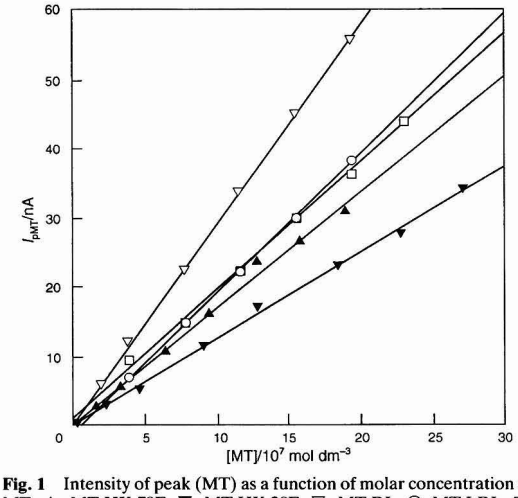

Fig. 1 Intensity of peak (MT) as a function of molar concentration of MT. ▲, MT HK 79F; ▼, MT HK 28F; ▽, MT RL; ○, MT I RL; □, MT II RL.

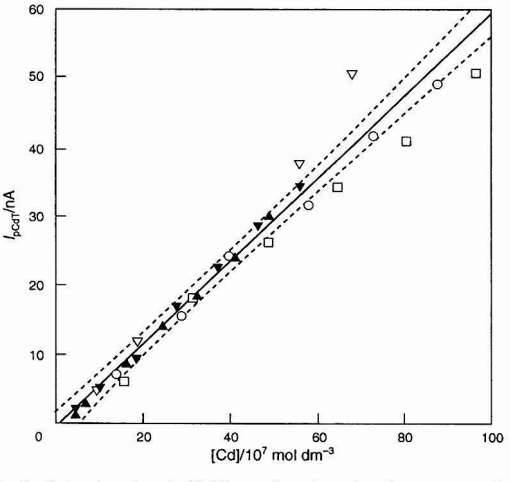

Fig. 3 Intensity of peak (CdT) as a function of molar concentration of cadmium. The confidence limits (95%) are shown by the broken lines. Symbols as in Fig. 1.

function of the molar concentration of cadmium are presented in Fig. 3. A single straight line is obtained indicating that the polarographic response is only dependent on the content of Cd in each MT. The equation of the line is $I_p = 6.00c + 0.69$ ($r = 0.984$). Fig. 4 shows the peak intensity of ZnT complex as a function of the concentration of zinc in the metallothioneins. In this case the peak intensity for zinc–thionein complexes is difficult to measure with precision because its peak potential is

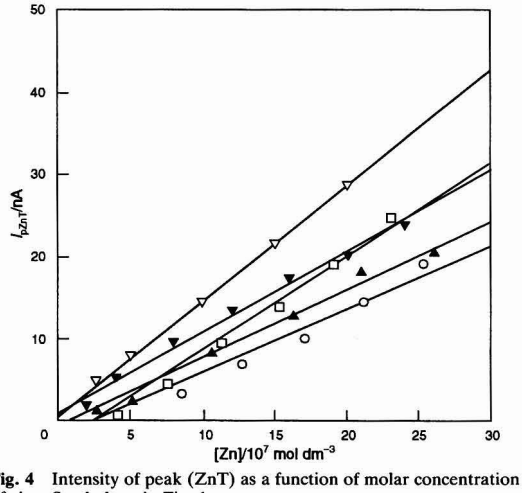

Fig. 4 Intensity of peak (ZnT) as a function of molar concentration of zinc. Symbols as in Fig. 1.

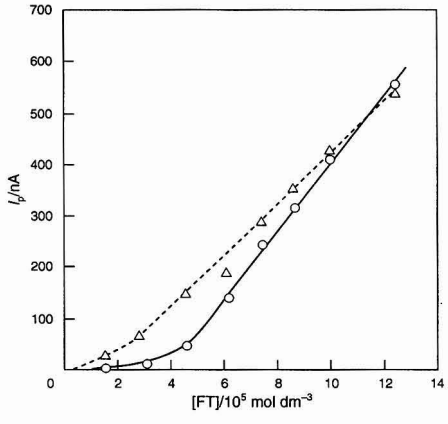

Fig. 5 Peak intensities corresponding to FT as a function of the molar concentration at pH: ○, 7.5; and △, 2.

very close to the potential corresponding to the cathodic limit current due to the reduction of ions contained in the supporting electrolyte. Likewise, the ZnT peak is sometimes not well defined depending on the MT lot used. This leads to the obtention of dispersed straight lines.

Concerning the molecules intrinsic to the metallothionein structure, cysteine and FT, measurements of peak intensity as a function of concentration were performed in 10^{-2} mol dm^{-3} TRIS at pH 7.5 and 2, in the range 1×10^{-5}–2×10^{-4} mol dm^{-3}. In the case of FT, plots of peak intensity *versus* (FT) concentration are given in Fig. 5, showing the dependence on the pH of solution. The response is non-linear at low concentrations of FT. Plots with a similar shape were found[6] for other compounds containing thiol groups.

In Table 1 values of slopes obtained from the plots of the intensity of three peaks as a function of the concentration expressed in different ways (molar concentration of MT, total metal concentration and concentration of Cd or Zn) are given to enable comparison. Note that the slopes corresponding to $I_{MT} = f(c_{3M})$ and $I_{pCdT} = f_{Cd}$ are very close to each other for the five MT and from these plots a single straight line was obtained. These results indicate that the polarographic response corresponding to the organic part of the molecule is dependent, not on the total amount of thiol groups, but on the saturated ones. The percentage of cysteinyl residues bound to the metal ions has been calculated, for each MT, taking into account the total molar concentration of cadmium and zinc experimentally determined and assuming the ratio of complexation to be equal to seven, that means 1 mol of thionein is necessary to complex 7 mol of divalent cation.[7] These values, given in Table 2, are very similar to those calculated from the ratio of the slope values of the straight line $I_{pMT} = f(c_{MT})$ obtained for each thionein. Likewise, slopes of $I_{pMT} = f(c_{MT})$ exhibit linear relationships with the metallic content initially present in MT: c_{Cd},c_{Zn} or $c_{Cd + Zn}$, for the five compounds.

Plots of slopes of curves (see Table 1) corresponding to the peak MT as a function of the concentration expressed in different manners *versus* slopes obtained for the peak CdT are given in Fig. 6, in which the bisectric is also represented. Points are very close to this line indicating a similar electrochemical response for both systems, one of them attributed to the oxidation of the mercury in the presence of thiol groups and the other to the reduction of cadmium(II) complexed by the thionein.

Table 2 Percentage of saturated thiol groups*

Calculation method	MT HK lot 79F	MT HK lot 28F	MT RL I + II	MT I RL I	MT RL II
7[(Cd + Zn)]	64.2	41.4	93.8	73.4	72.4
Slopes ratio	53.1	39.8	93.8	66.7	60.2

* Calculated from seven times the total molar concentration of Cd and Zn and from the ratios of $I_{pMT} = f(c_{MT})$.

Table 1 Slopes (mA dm^3 mol^{-1}) of linear relationships $I_p = f(c)$ for MT, cysteine and FT*

Sample	$I_{pMT} = f(c_{MT})$	$I_{pMT} = f(c_{3M})$	$I_{pCdT} = I(c_{MT})$	$I_{pCdT} = I(c_{Cd})$	$I_{pZnT} = f(c_{MT})$	$I_{pZn} = f(c_{Zn})$
MT HK 79 F 9670	16.4	1.26	16.5	6.32	14.2	8.50
MT HK 28 F 9545	12.3	1.40	13.2	6.50	8.70	9.80
MT RL 20 H 9650	28.8	1.57	34.5	7.18	18.1	13.70
MT RL I 129 F 9545	20.6	1.44	21.5	5.67	10.1	9.20
MT RL II 79 F 9510	18.6	1.20	22.5	5.31	12.5	12.5
Cysteine	0.56					
FT	6.42					

* c_{MT} and c_M indicate the molar concentration of MT and total metal, respectively.

Conclusions

DPP allows, on the one hand, the distinction of the chemical forms of Cd, Zn thioneins by means of the three well defined peaks attributed to three electrochemical systems. On the other hand, this method can be used for the simultaneous and quantitative determination of the organic part of the molecule and of the CdT and ZnT complexes, I_{pMT} being a linear function of the saturated thiol groups and obtaining linearity of calibration curves between I_{pCdT} and I_{pZnT} and the concentration of cadmium and zinc, respectively. However, no relationship was found between the values of the slopes for cysteine, FT and MT and the number of thiol groups in these molecules (1, 3 and 20, respectively). It is probable that in the case of more complex molecules such as FT and MT, the secondary and tertiary structures play important roles in the access of thiol groups to the electrode surface and the polarographic response is modified. Likewise, the possibility that the thiol groups in FT and MT molecules exist, at least partially, as intra- or inter-molecular disulfide bonds is envisaged.

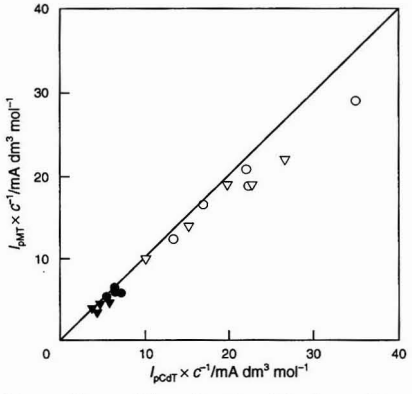

Fig. 6 Slopes of $I_{pMT} = f(c)$ as a function of the slopes of $I_{pCdT} = f(c)$. ▼, $I_p = f[c\,(Cd + Zn)]$; ▽, $I_p = f[c\,(Zn)]$; ○, $I_p = f[c(MT)]$; and $I_p = f[c\,(Cd)]$.

To our knowledge the DPP method was not previously applied to the quantitative determination of Cd, Zn thioneins. Polarography is a simple and accessible method which can be used to obtain quickly information on the characteristics of compounds, to study whether the metal ions are complexed by the thiol groups and to determine and quantify CdT and ZnT complexes.

References

1 Muñoz, A., and Rodríguez, A. R., *Electroanalysis*, in the press.
2 Muñoz, A., and Rodríguez, A. R., *Electroanalysis*, in the press.
3 Muñoz, A., PhD Thesis, Complutense University Madrid, 1992.
4 Furey, W. F., Robbins, A. H., Clancy, L. L., Winge, D. R., Wang, B. C., and Stout, C. D., *Science*, 1986, **231**, 704.
5 Bordin, G., Cordeiro, F., and Rodríguez, A. R., *Can. J. Chem.*, 1994, **74**, 1238.
6 Peter, F., and Rosset, R., *Anal. Chim. Acta*, 1975, **79**, 79.
7 Robbins, A. H., and Stout, C. D., in *Metallothioneins: Synthesis, Structure and Properties of Metallothioneins, Phytochelatins and Metal Thiolate Complexes*, eds. Stillman, M. J., Shaw III, C. F., and Suzuki, K. T., VCH, New York, 1992 Ch. 3.

Paper 4/03623I
Received June 6, 1994
Accepted July 29, 1994

Inclusion Complexes and Stability Studies of an Organophosphorous Insecticide With Cyclodextrins: Spectrophotometric and Kinetic Determination of Stability Constant

Yannis L. Loukas, Ekaterini A. Vyza* and Aspasia P. Valiraki

Department of Pharmacy, Division of Pharmaceutical Chemistry, University of Athens, Panepistimioupoli Zografou 15710, P.O. Box 64064, Athens, Greece

DCPE [α-(diethoxyphosphinoximino)dicyclopropylmethane] is a potent organophosphorous insecticide. It is an oily liquid and therefore the most suitable formulation is an 'emulsifiable concentrate'. In an attempt to develop better formulations, complexes of this insecticide with the cyclodextrins (CDs) αCD, βCD and hydroxypropyl-βCD (HP-βCD) were examined. Stability constants were determined spectrophotometrically, in the case of DCPE–βCD, according to the spectral changes of DCPE due to the complexation and kinetically, in the case of DCPE–HP-βCD, according to the changes in the rate constant of DCPE degradation. HP-βCD has a stabilizing effect on DCPE by decelerating its degradation in aqueous solutions, but αCD and βCD have no effect. Finally, the thermodynamic parameters for the inclusion complex formation between DCPE and HP-βCD in aqueous solutions were calculated by correlating the changes in the stability constant with temperature.

Keywords: Cyclodextrin; organophosphorus insecticide; stability; stability constant

Introduction

DCPE [α-(diethoxyphosphinoximino)dicyclopropylmethane] (Scheme 1), a powerful insecticide that has been synthesized

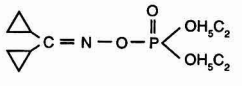

Scheme 1

in our laboratory[1] is a yellow oily liquid that is unstable in aqueous media and poorly soluble in water. This insecticide shows mammalian toxicity orally (LD_{50} 10.86 mg kg^{-1} for male and 7.85 mg kg^{-1} for female rats).[2] DCPE has been formulated as an 'emulsifiable concentrate'.[3] In an attempt to develop better formulations and application methods, better handling, improved storage stability and reduction of its contact toxicity to humans, liquid DCPE was converted into a solid form by the use of cyclodextrins and therefore could be formulated as pellets or granules.

Cyclodextrins (CDs) are a family of water-soluble cyclic oligosaccharides with a preformed hydrophobic cavity, known to form non-covalent inclusion complexes with water-insoluble molecules, and thus have been applied in pharmaceutical development as solubilizing and stabilizing agents.[4] α-Cyclodextrin and βCD have a torus shape, formed by six and seven linked α(1–4) glucose units, respectively. Their cavities have diameters of about 6 Å for αCD and 7 Å for βCD and can accommodate a guest molecule without covalent bonding. Owing to its more favourable complexing ability, the most commonly studied CD is βCD. Recently, chemically modified cyclodextrins have received considerable attention because of their greater complexing abilities and their improved aqueous solubility. The relatively low aqueous solubility of the unmodified CDs appears to be related to their greater tendency to form intramolecular hydrogen bonds between the secondary O-2 and O-3 of adjacent glucopyranose units.

Hydroxypropyl-β-cyclodextrin (HP-βCD)[5] is prepared by hydroxypropylation of some or all of the hydroxyl groups (2-, 3- and 6-OH) of βCD, depending on the conditions (strongly or weakly alkaline) and on the reagents used (propylene oxide, epichlorohydrin, 2-bromoethanol, *etc.*). The degree of substitution (DS) is the main characteristic property for quality control purposes. It gives a measure of the extent to which the reactive hydroxyls in each group of pyranose units of the CD ring have been substituted. The maximum value of this parameter is 3 for all CDs.

Experimental

Materials

DCPE was synthesized and purified in our laboratory. αCD and βCD were obtained from Sigma (St. Louis, MO, USA). HP-βCD was obtained from Janssen (Beerse, Belgium) with a DS of 0.4 and a relative molecular mass (M_r) calculated to be 1300. The DS was calculated from the ^1H NMR spectrum of HP-βCD in deuterium oxide [Fig. 2(*a*)]. Acetonitrile was of HPLC grade and water was de-ionized and doubly distilled using a Millipore Milli-Q Plus system.

Preparation of Complexes

Inclusion complexes of DCPE with αCD and βCD were prepared by the coprecipitation method and that with HP-βCD by the freeze-drying method,[6] as follows.

Preparation of DCPE–αCD 1:2 complex

According to the coprecipitation method, 3 g of αCD (3 mmol) were dissolved in 10 ml of water and the solution was added dropwise to an excess amount of DCPE (3 g or 11.5 mmol, M_r = 262) with stirring. The mixture was stirred for 1 h at ambient temperature and for a further 3 h in an ice-bath. The white precipitate that formed was filtered off and washed with diethyl ether (3 × 5 ml) to remove any uncomplexed DCPE and the decomposition products of DCPE (the corresponding amide **III**, Scheme 2). Finally, the product was

* To whom correspondence should be addressed.

dried in a desiccator under vacuum over P_2O_5, to give a yield of 2.5 g of DCPE–αCD complex.

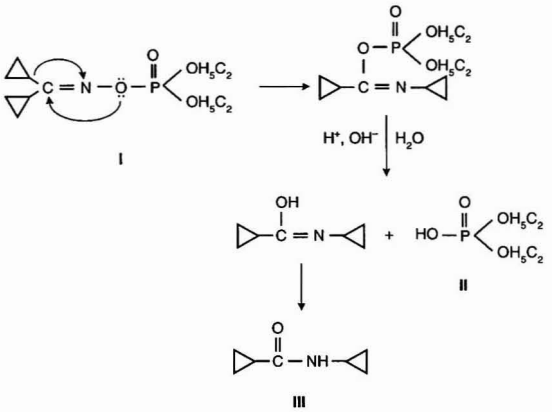

Scheme 2

Preparation of DCPE–βCD 1 : 1 complex

The complex was obtained according to the previously described method and gave a yield of 2.7 g of DCPE–βCD complex.

Preparation of DCPE–HP-βCD 1 : 1 complex

According to the freeze-drying method, 4 g of HP-βCD (3 mmol) were dissolved in 10 ml of water and the solution was added dropwise to an excess amount of DCPE (3 g or 11.5 mmol) with stirring. The mixture was stirred for 1 h at ambient temperature and for a further 2 h in an ice-bath. The solution was then placed in a freezer at −12 °C until it was completely frozen (5–6 h). The frozen solution was then freeze-dried and 3.5 g of DCPE–HP-βCD complex were obtained.

NMR Spectrometry

In aqueous solution, the structures of the complexes were investigated by ^{1}H NMR spectrometry. NMR spectra were recorded on a Bruker AC 200 spectrometer in 99.9% D_2O (Sigma). The chemical shifts were related to the external standard TSP (sodium 2,2,3,3-$^2H_4$-trimethylsilylpropionate) at 0 ppm with calibration having been carried out using the residual solvent signal (hydrogen–deuterium oxide = 4.84 ppm at 293 K). Typical conditions were 16K data points with zero filling, sweep width 1.4 kHz giving a digital resolution of 0.17 Hz per point, pulse width 2 μs (90° pulse 5.5 μs) and acquisition time 2.9 s. Gaussian enhancement was used for the displayed spectra (GB = 0.2, LB = −2).

Differential Scanning Calorimetry (DSC)

Thermograms were obtained using a Perkin-Elmer DSC 7 differential scanning calorimeter, with vented aluminium pans. Typical conditions were temperature range 50–250 °C, scanning rate 10 °C min^{-1} and sample mass 3–10 mg. Baseline optimization was performed before each run.

High-performance Liquid Chromatography (HPLC)

All HPLC assays for DCPE were performed on a Waters (Milford, MA, USA) chromatographic system consisting of a (Model 590) pump and a (Lambda-Max Model 481) multi-wavelength UV detector. The separation of DCPE from its degradation products was performed on a reversed-phase, 10 μm μBondapak C_{18} column (300 × 3.9 mm i.d.) (Waters). The mobile phase was acetonitrile–water (55 + 45), vacuum filtered through a 0.45 μm pore-size nylon membrane filter (Millipore, Watford, UK) prior to use. A flow rate of 1.5 ml min^{-1} was maintained and the effluent was monitored at 215 nm with a detector sensitivity of 0.05 a.u.f.s. The sample volume was 20 μl (Rheodyne 717S injector fitted with a 20 μl loop). Quantification was performed by peak-height integration (Waters, Baseline-810 integration system for personal computer).

Kinetics

All kinetic studies were performed on DCPE in aqueous solutions containing various concentrations of HP-βCD by the HPLC assay described above. The reactions were initiated by placing volumes of 1 ml of an aqueous solution of DCPE in 10 ml calibrated flasks and diluting to volume with aqueous HP-βCD solution to give an initial DCPE concentration of 0.07 mmol l^{-1}. Samples were taken at appropriate intervals and analysed for remaining DCPE. First-order rate constants for the disappearance of DCPE (k_{obs}) were determined from the slopes given by the linear plots of the logarithm of the percentage of the remaining DCPE against time. The degradation pathway of DCPE in aqueous media is shown in Scheme 2. The conversion to amide **III** was due to a Beckmann rearrangement.[7]

Ultraviolet Spectrophotometry

This analysis was carried out using a Perkin-Elmer spectrophotometer. Complex formation between DCPE and βCD in aqueous solutions was investigated according to the spectral shift method. Aliquots of 500 μl of aqueous solution of DCPE were pipetted into 10 ml calibrated flasks ([DCPE]$_t$ = 5 × 10^{-5} mol l^{-1}) containing increasing amounts of aqueous βCD stock standard solutions and diluted to volume with water. The contents were quickly mixed and transferred into a cuvette of 1 cm pathlength. The solutions were analysed at room temperature (25 °C) against a blank reference cell, containing βCD at the same concentration, in order for both cells to have the same refractive index.

In the presence of αCD and HP-βCD, the spectral shift was of insufficient magnitude for quantitative interpretation.

Results and Discussion

Characterization of the Inclusion Complex in the Solid State

DSC indicated true complexation.[8] Thus, in all instances the DSC thermograms of the complexes were different in the number and/or position of peaks compared with DSC curves for both the mechanical mixtures of CDs with DCPE and the pure CDs. Fig. 1 illustrates the DSC curves of solid complexes and pure CDs.

Characterization of the Complex in Solution

Proton NMR spectrometry is commonly used for the investigation of the nature of the complexes in solution.[9] For our soluble complexes, the observed resonances were the time-averaged peaks of pure and complexed compounds (fast exchange regime on the NMR time scale at 293 K). The formation of inclusion complexes of DCPE with CDs in aqueous solutions (D_2O) is evidenced by the modification of NMR spectra of both the guest and host molecules. The

partial 200 MHz ^{1}H NMR spectra of the pure compounds and of the complexes are displayed in Fig. 2. Under the present conditions, only shifts of the signals were observed and no new peaks appeared that could be assigned to the pure complex. This observation implies that the complexation is a dynamic process, the included guest being in fast exchange (relative to the NMR time scale) between the free and bonded states.

Protons located inside the cavity of cyclodextrins (H-3 and H-5) are expected to experience large chemical shift variations on inclusion of the guest, whereas those residing outside the cavity (H-1, H-2 and H-4) should undergo no or minimal changes [Fig. 2(*c*) and (*d*)]. Specifically, the ^{1}H NMR spectrum of the DCPE complexes with β-CD and HP-βCD in D_2O showed upfield shifts of H-3 and H-5 (Tables 1 and 2), whereas the frequencies of H-1, H-2 and H-4 were not altered. In the case of complex with αCD, none of the protons of αCD showed shift (Table 3). Maybe this is a shallow complex, with the DCPE on the rim of the αCD cavity.[10] The induced chemical shifts of the peaks due to methylene and methyl groups of DCPE, which are centred at 4.1 and 1.19 ppm, respectively, undergo downfield shifts (Tables 1–3) in all complexes. It is also evident that for the pure guest the triplets at 1.19 ppm, corresponding to methyl group of DCPE and the same group of its degradation product diethylphosphoric acid **II** (Scheme 2), are overlapped. For all complexes, these two triplets are separated owing to the large downfield shift of the triplet which corresponds to the DCPE [Fig. 2(*b*) and (*e*)–(*g*)]. The triplet corresponding to the diethylphosphoric acid **II** (Scheme 2) did not show any chemical shift. Also, the protons of DCPE's cyclopropyl groups and those of the second degradation product in D_2O, amide **III** (Scheme 2), were not altered. All these observations lead to the conclusion that the DCPE entered the CD cavities from the side of the ethoxy groups.

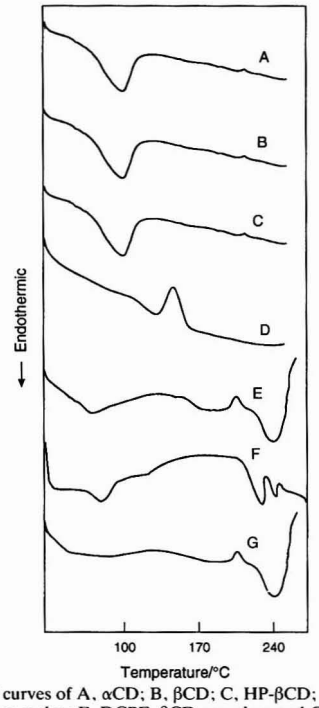

Fig. 1 DSC curves of A, αCD; B, βCD; C, HP-βCD; D, DCPE; E, DCPE–αCD complex; F, DCPE–βCD complex; and G, DCPE–HP-βCD complex.

Stoichiometry of the Inclusion Complexes

The stoichiometries were measured by ^{1}H NMR, HPLC and elemental analysis. Digital integration of selected ^{1}H NMR signals from the host and guest molecules in the soluble complexes provided direct access to the stoichiometry coefficient.[11] In HPLC, a known amount of complex was dissolved in water, the sample was injected and the concentration of the guest (DCPE) in the chromatogram was calculated using a calibration graph. Finally, independent confirmation of the stoichiometry of the complex was obtained from elemental

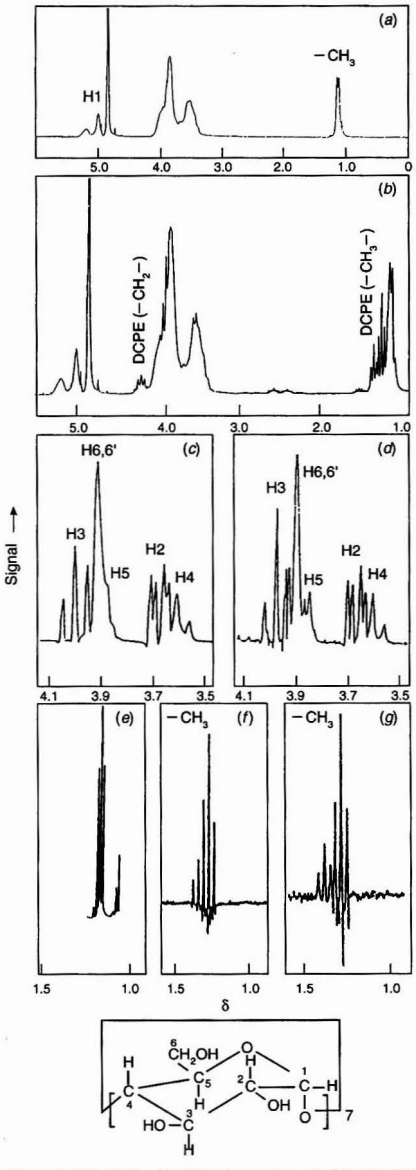

Fig. 2 Partial 200 MHz ^{1}H NMR spectra of (*a*) HP-βCD, (*b*) DCPE–HP-βCD, (*c*) βCD (structure shown above), (*d*) DCPE–βCD, (*e*) DCPE, (*f*) DCPE–αCD, and (*g*) DCPE–βCD.

analysis, which was carried out at the Central Department of Microanalysis (CNRS, Vernaison, France). The results agreed with those calculated by the other two methods. For DCPE complexes with βCD and HP-βCD, the calculated stoichiometry coefficient was found to be 1:1, whereas that with αCD was found to be 1:2 (one molecule of DCPE with two molecules of αCD).

Stability Studies

The complexes were stored as solids and assayed in solutions. The stability of each complex in the solid state was measured by HPLC. Solutions of known concentration of each complex were analysed by HPLC and the DCPE content was calculated from the calibration graph. These experiments were repeated many times for all complexes and for a period of 6 months. The DCPE content of the complexes remained the same.

Determination of Stability Constant for DCPE–βCD complex

The stability constant of the DCPE–βCD complex was studied in aqueous solution by UV spectrophotometry. The zero-order UV absorption spectra of DCPE exhibit a bathochromic shift in the presence of various concentrations of βCD (Fig. 3). This is probably due to the high electron density inside the hydrophobic CD cavity, which creates partial shielding of the excitable electrons of DCPE, when the latter is included inside the cavity of βCD.[12] The change in absorbance (ΔA) at 200.4 nm as a function of βCD concentration ([βCD]) follows the typical binding isotherm:

$$\frac{\Delta A}{b} = \frac{[\text{DCPE}]\, K_{st}\, \Delta\varepsilon_{11}\, [\beta\text{CD}]}{1 + K_{st}\, [\text{DCPE}]} \quad (1)$$

Transformation of the eqn. (1) according to Benesi and Hildebrand[13] gives the more widely utilized approach shown in the equation

$$\frac{b}{\Delta A} = \frac{1}{[\text{DCPE}]\, K_{st}\, \Delta\varepsilon_{11}\, [\beta\text{CD}]} + \frac{1}{[\text{DCPE}]\, \Delta\varepsilon_{11}} \quad (2)$$

where b is the pathlength (b = 1 cm); ε_{11}, ε_S and ε_L are the molar absorptivities for the 1:1 inclusion complex, DCPE and the βCD, respectively; and $\Delta\varepsilon_{11} = \varepsilon_{11} - \varepsilon_S - \varepsilon_L$. The plot of $b\Delta A^{-1}$ *versus* $[\beta\text{CD}]^{-1}$ is a straight line (correlation coefficient = 0.99) (Fig. 4) with $1/[\text{DCPE}]\, K_{st}\, \Delta\varepsilon_{11}$ as the slope and $1/[\text{DCPE}]\, \Delta\varepsilon_{11}$ as the intercept. K_{st} was calculated to be 555 l mol^{-1}.

Determination of Stability Constant for DCPE–HP-βCD complex

The stability constant was determined kinetically. Comparative stability studies of DCPE in the free and complexed form showed that for complexes with αCD and βCD the determined degradation rate remained the same. However, for HP-βCD this reaction undergoes a decelerating effect which shows that the HP-βCD has a pronounced stabilizing effect on DCPE. Specifically, the rate constant for the degradation reaction is

Table 1 Chemical shifts (ppm) of the protons of βCD and DCPE in the free and complexed states

Proton*	δ_0 (free)	δ_c (complex)	$\Delta\delta$ (δ_c-δ_0)
βCD			
H3	3.997	3.981	0.016
H5	3.864	3.843	0.02
DCPE			
$-CH_2-$	4.1	4.25	0.15
$-CH_3$	1.19	1.34	0.15

* Only the protons that show chemical shifts.

Table 2 Chemical shifts (ppm) of the protons of HP-βCD and DCPE in the free and complexed states

Proton*	δ_0 (free)	δ_c (complex)	$\Delta\delta$ (δ_c-δ_0)
HP-βCD			
H3	3.954	3.969	0.015
H5	3.682	3.697	0.015
DCPE			
$-CH_2-$	4.1	4.21	0.11
$-CH_3$	1.19	1.34	0.15

* Only the protons that show chemical shifts.

Table 3 Chemical shifts (ppm) of the protons of αCD and DCPE in the free and complexed states

Proton*	δ_0 (free)	δ_c (complex)	$\Delta\delta$ (δ_c-δ_0)
αCD			
H3	3.998	3.989	0.009
H5	3.843	3.834	0.009
DCPE			
$-CH_2-$	4.1	4.12	0.02
$-CH_3$	1.19	1.34	0.15

* Only the protons that show chemical shifts.

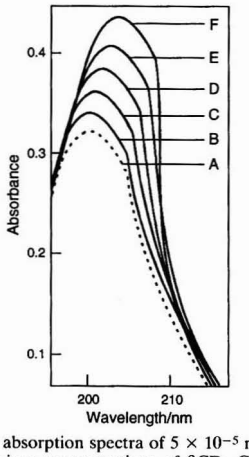

Fig. 3 Ultraviolet absorption spectra of 5 × 10^{-5} mol l^{-1} DCPE in the presence of various concentrations of βCD. Concentrations of βCD: A, 0; 8 × 10^{-4}; C, 11 × 10^{-4}; D 12 × 10^{-4}; E 13 × 10^{-4}; and F 15 × 10^{-4} mol l^{-1}.

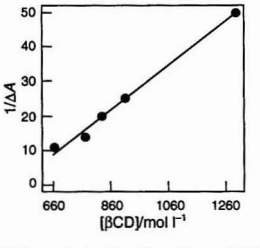

Fig. 4 Benesi–Hildebrand plot for the effect of βCD on the DCPE absorbance at 200.4 nm (y = 0.06x + 33.32).

decreased from 30.3×10^{-3} to 15.7×10^{-3} min^{-1} in the presence of 3.5 mmol l^{-1} of HP-βCD.

Fig. 5 shows the relationship between HP-βCD concentration and the observed pseudo-first-order rate constant for the degradation of the DCPE. It is evident that k_{obs} is not a linear function of the concentration of added HP-βCD, but rather asymptotically approaches a minimum value with increasing HP-βCD concentration.[14] This so-called 'saturation behaviour', is characteristic of the reaction through complex formation, occurring prior to the rate-determining step, and may be accommodated by the reaction mechanism illustrated in Scheme 3, where k_0 is the rate constant for decomposition of free DCPE, k_c is the rate constant for totally complexed DCPE and K_{st} is the apparent stability constant for complex formation.[15]

Usually, a ten-fold excess of CD should be present to ensure the conditions of a first-order reaction. From Scheme 3, the following rate expression can be derived:

$$\frac{-d[DCPE]}{dt} = k_0[DCPE] + k_c[DCPE\text{–}HP\text{-}\beta CD] \quad (3)$$

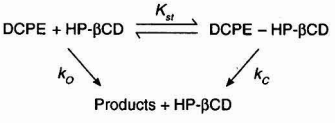

Scheme 3

The observed reaction rate for DCPE degradation in the presence of HP-βCD is a weighted average of the rate of reaction of free DCPE and the rate of reaction of DCPE included in the HP-βCD and, therefore, K_{st} can be determined from the dependence of the observed rate constant on the concentration of added HP-βCD. The actual measurable rate constant is

$$k_{obs} = k_0 + \frac{(k_c - k_0)[HP\text{-}\beta CD]}{1/K_{st} + [HP\text{-}\beta CD]} \quad (4)$$

This equation can be solved graphically according to the Lineweaver–Burke transformation and on rearrangement gives

$$\frac{1}{k_0 - k_{obs}} = \frac{1}{K_{st}(k_0 - k_c)} \frac{1}{[HP\text{-}\beta CD]} + \frac{1}{k_0 - k_c} \quad (5)$$

The plot of $1/k_0 - k_{obs}$ *versus* $1/[HP\text{-}\beta CD]$ gives $1/K_{st}(k_0 - k_c)$ as the slope and $1/k_0 - k_c)$ as the intercept. In Fig. 6, the rate data of Fig. 5 are plotted according to eqn. (5). From the slope and intercept of the plot, the values of K_{st} and k_c were obtained. The data are given in Table 4.

The complexation of DCPE with αCD and βCD did not change the degradation rate of DCPE in aqueous solutions and so the stability constant could not be determined kinetically. The most probable explanation is that with αCD and βCD the active site of DCPE maybe resides outside of the cavity or has a conformation that cannot be protected by the attack of the aqueous medium. Another possible explanation is that HP-βCD may be able to include more of the DCPE molecule or its reactive group within the cavity than can αCD and βCD.

In order to calculate the activation energy for the degradation of DCPE in the absence and presence of HP-βCD, the rate of degradation for DCPE was measured at several temperatures. The activation energy (E_a) was obtained graphically from the temperature dependence of the rate constants for free (k_0) and complexed (k_c) DCPE, according to the Arrhenius equation. The Arrhenius plot in the presence of HP-βCD was parallel to that in its absence (Fig. 7),

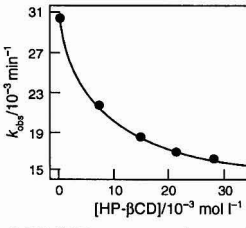

Fig. 5 Effect of HP-βCD concentration on the pseudo-first-order rate constant for the degradation of DCPE.

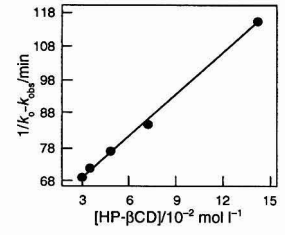

Fig. 6 Graph of the rate data in Fig. 5 according to eqn. (5).

Table 4 Kinetic parameters for the degradation of DCPE and DCPE–HP-βCD complex at various temperatures

Temperature/°C	$k_0 \times 10^{-3}$/min^{-1})	$k_c \times 10^{-3}$/min^{-1})	K_{st}/l mol^{-1}
35	30.3	12.8	1421
40	44.5	21.1	1008
45	77	34.4	739
50	115	55.2	526

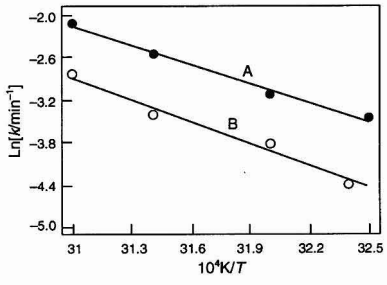

Fig. 7 Arrhenius diagrams for the degradation of A, DCPE alone and B, DCPE–HP-βCD complex.

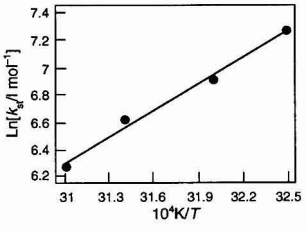

Fig. 8 Van't Hoff plot for the stability constant of DCPE–HP-βCD complex.

suggesting that the mechanism of degradation remained the same.

The activation energy (E_a) for DCPE degradation was calculated and found to be 17.75 kcal mol^{-1}. When DCPE is totally in complexed form, E_a is increased to 19.3 kcal mol^{-1}. The increase in activation energy may be due to steric hindrance preventing the formation of the intermediate compound (Scheme 2), perhaps because the inclusion phenomenon creates a shield to the susceptible moiety of DCPE molecule, so as to protect it from the attack by the aqueous medium.

The enthalpy of complexation of DCPE and HP-βCD was evaluated from the temperature dependence of the stability constant K_{st}. The enthalpy (ΔH_0) of DCPE–HP-βCD complex formation, determined by using the van't Hoff relationship, is exothermic and equal to −12.7 kcal mol^{-1} (Fig. 8).

Negative enthalpies of CD complex formation may be due to enhanced van der Waals interactions between the guest and CD, hydrogen bonding between the guest and the hydroxyl groups of the CD or changes in the degree of aggregation of water associated with the molecules on complex formation.[16] Water molecules inside the CD cavity are in an energetically unfavourable position, owing to polar–non-polar interactions, and therefore cannot form as many hydrogen bonds as in the bulk. These high-enthalpy water molecules are readily displaced by a less polar guest[17] and are combined with the bulk of the solvent to increase the number of solvent–solvent hydrogen bonds.

A negative entropy change (ΔS_0) of −27 cal mol^{-1} K^{-1} was observed for complex formation between DCPE and HP-βCD, showing that the order of the system increases. The ΔS_0 value may indicate a difference between the hydrogen bonds before and after complex formation. Hence, this observed negative entropy, indicates that there is a greater number of hydrogen bonds in the complex than in free molecules.[18]

References

1 Kostakis, E., and Rouman, A., *PhD Thesis*, University of Athens, 1984.
2 Machera, K., and Kostakis, E., *Bull. Environ. Contam. Toxicol.*, 1992, **48**, 108.
3 Loukas, Y., Antoniadou-Vyza, E., E., and Papadaki-Valiraki, A., *J. Chromatogr.*, 1994, **677**, 53.
4 Duchene, D., and Wouessidjewe, D., *Drug Dev. Ind. Pharm.*, 1990, **16**, 2487.
5 Duchene, D., *New Trends in Cyclodextrins and Derivatives*, Editions de Santé, Paris, 1991, pp. 55–97.
6 Duchene, D., and Wouessidjewe, D., *Acta Pharm. Technol.*, 1990, **36**, 1.
7 Donamura, G., and Heldt, W., *Org. React.*, 1960, **11**, 2.
8 Ford, L., and Timmins, P., *Pharmaceutical Thermal Analysis*, Wiley, New York, 1989, pp. 152, 164–165 and 171–172.
9 Duchene, D., *New Trends in Cyclodextrins and Derivatives*, Editions de Santé, Paris, 1991, pp. 179–246.
10 Duchene, D., *Cyclodextrins and Their Industrial Uses*, Editions de Santé, Paris, 1987, pp. 134–136.
11 Duchene, D., *New Trends in Cyclodextrins and Derivatives*, Editions de Santé, Paris, 1991, pp. 221–223.
12 Bettinetti, G. P., Mura, P., Liguori, A., and Bramati, G., *Pharmacology*, 1988, **44**, 195.
13 Benesi, H. A., and Hildebrand, J. H., *J. Am. Chem. Soc.*, 1949, **71**, 2073.
14 Szejtli, J., *Cyclodextrins and Their Inclusion Complexes*, Akadémiai Kiadó, Budapest, 1982, pp. 115–116.
15 Duchene, D., *Cyclodextrins and Their Industrial Uses*, Editions de Santé, Paris, 1987, pp. 144–146.
16 Tabushi, I., Kiyosuke, Y., Sugimoto, T., and Yamamura, K., *J. Am. Chem. Soc.*, 1978, **100**, 916.
17 Saenger, W., *Angew. Chem.*, 1980, **19**, 344.
18 Cramer, F., Saenger, W., and Spatz, H., *J. Am. Chem. Soc.*, 1967, **89**, 14.

Paper 4/03338H
Received June 6, 1994
Accepted October 4, 1994

Spectrophotometric Determination of Alkaline Phosphatase and α-Fetoprotein in Human Serum With 5,10,15,20-Tetrakis (4-phosphonooxyphenyl)porphine

Takanori Kawakami and Shukuro Igarashi

Department of Materials Science, Faculty of Engineering, Ibaraki University, Nakanarusawa, Hitachi, 316, Japan

A highly sensitive kinetic spectrophotometric determination for alkaline phosphatase (ALP) using 5,10,15,20-tetrakis (4-phosphonooxyphenyl)porphine (approximately $\Delta\varepsilon \approx 3.0 \times 10^5$ l mol^{-1} cm^{-1}) was studied. With a measuring time of 30 min, the determination range was 2.0×10^{-12}–8.0×10^{-9} mol l^{-1} and the detection limit (3s) was 1.0×10^{-12} mol l^{-1}. The detection limit became lower on increasing the measuring time. For example, the detection limit was up to 10^{-15} mol l^{-1} for 12 h. This method was applied to the assay of ALP in human serum. Using 0.50 ml of sample without any pre-treatment, a good correlation was obtained with the *p*-nitrophenyl phosphate method, and the relative standard deviation was 4.7%. The method was also applied to the enzyme immunoassay of α-fetoprotein in human serum and provided a good correlation with the 4-methylumbelliferone derivative ($r = 0.999$) with approximately half the relative standard deviations (1.3–2.7%) obtained with a commercial kit. The proposed method requires very small sample volumes, is highly sensitive, highly accurate, and shows good stability of the reagent; it will be applied to various assays using ALP as a label.

Keywords: 5,10,15,20-Tetrakis(4-phosphonooxyphenyl)-porphine; alkaline phosphatase; α-fetoprotein; human serum; kinetic spectrophotometry

Introduction

Recently, in immunoserological assays, enzyme immunoassay (EIA) has displaced the method using a radioactive isotope as a labelling reagent, and the proportion of EIA used in diagnosis has increased year after year. Among these, the methods using alkaline phosphatase (ALP) have been extensively applied not only in clinical diagnosis but also in various studies utilizing their low specification for the substrate and their high sensitivity and precision.[1]

There are three major methods for the determination of ALP: absorption spectrophotometry, spectrofluorimetry and chemi- and bioluminescence methods. In absorption spectrophotometry, chromogenic reagents such as *p*-nitrophenyl phosphate[2] and phenolphthalein phosphate[3] have been used. However, the lowest detection limit was defined on the basis that the molar absorptivities of the reagents are of the order of 10^4 l mol^{-1} cm^{-1} and these reagents are unstable. In fluorescence determinations, umbelliferone derivatives have generally been used,[4] although spectrofluorimetry has the disadvantage of undergoing concentration extinction. Recently, several determination methods making use of chemi- or bioluminescence have been reported.[5] However, their backgrounds for detection are unstable, resulting in a problem with precision. Therefore, a new method for the determination for ALP that is simple, highly sensitive and highly precise is required.

Porphyrin compounds are known as analytical reagents with highly sensitive spectrometric and/or spectrofluorimetric properties. Porphyrin compounds have a Soret band with molar absorptivities of the order of several hundred thousand at 400–500 nm. The peak wavelength is shifted by a change in the electronic conditions in the porphine ring. Also, porphyrin stably complexes over 50 kinds of metal ions; hence many methods of determination using porphyrin have been reported,[6–8] such as the determination of metal ions using complexation in the inner/outer ring and the determination of anionic species using the dissociation reaction of a metal ion from a metal–porphyrin complex.

5,10,15,20-Tetrakis(4-phosphonooxyphenyl)porphine ($TPPP_m$; Fig. 1), which has phosphate ester groups on the outer portion of the porphine ring, was recently synthesized, with the aim of developing an MRI (magnetic resonance imaging) arteriographic reagent for arteriosclerosis that adsorbs selectively on the atheroma.[9] We have found a significant spectral change in this porphyrin on ALP enzymolysis. Based on this phenomenon, a highly sensitive method for the determination of ALP was developed and successfully applied to the determination of ALP in human serum. Moreover, this method was applied to (EIA) and was successfully used in the determination of α-fetoprotein (AFP) in human serum as an indicator of liver disease.

Experimental

Apparatus

A Hitachi Model 200-10 double-beam spectrophotometer (with a 1 cm or microcell) and a Hitachi Model 057 *X*–*Y* recorder were used for the measurement of spectra. A Horiba F-8AT pH meter was used for the measurement of pH. A Yamato-Komatsu CTE42A thermostat circulator with a water-bath was used to control the temperature to within ±0.1 °C.

Reagents

All reagents used were of analytical-reagent grade and were used as received, and all working solutions were prepared just before use. Distilled water was de-ionized and further purified by distillation in glass (SWAC-500, Shimazu). An aqueous buffer solution was prepared as follows: 10.5 g of diethanolamine (Wako) was dissolved in water and diluted to 100 ml, and the pH was adjusted by adding 1.0 mol l^{-1} NaOH (Wako) solution; its temperature was controlled by immersion into a water-bath with a thermostat before use. Other aqueous buffer solutions were also prepared. Alkaline phosphatase (Type I-S from bovine intestinal mucosa, 5.8 U mg^{-1}; Type

XVII from human placenta, 3.8 U mg^{-1}) was obtained from Sigma. Human serum (blood type AB) was obtained from Whittaker Bioproducts. A commercial AFP EIA kit (Tosoh) was used for immunoassay. Control serum (QC-RIA I, II, III) was supplied by Eiken Chemical. $TPPP_m$ was synthesized by phosphorylation of 5,10,15,20-tetrakis(4-hydroxyphenyl)porphine (THPP) and prepared according to the following procedure.

Synthesis of THPP. Synthesis was carried out according to the method of Adler *et al.*[10] as follows. A 20 g amount of *p*-hydroxybenzaldehyde and 10.1 g of pyrrole (equal to the molar amount of the aldehyde) were refluxed in 500 ml of propionic acid at 130 °C. After refluxing for 20 min, the reactant was cooled to room temperature. Purple crystals then appeared and were filtered off with a G4 glass filter. The crystals were washed with propionic acid and water, in turn, and recrystallized from ethanol. The total yield was approximately 40%.

Phosphorylation of THPP. This was carried out by the standard method using pyrophosphoric acid. A 10 g amount of pyrophosphoric acid, 3.0 g of diphosphorus pentaoxide and 0.5 g of THPP were mixed and heated to 120 °C with stirring. Heating of the mixture was continued for 2 h. The product solution was cooled to room temperature and recrystallized from cooled acetone (below 0 °C) several times to remove the free phosphates and the impurities (above 80% yield). The structure of the product was identified by NMR, IR, and UV spectrometry and elemental analysis.

A stock standard solution of $TPPP_m$ was prepared by dissolution in distilled water. A working standard solution was prepared by dilution of the stock solution and its concentration was determined by absorption spectrophotometry.

Procedure

Determination of ALP

Place aliquots of $TPPP_m$ solution in 25 ml calibrated flasks in order to obtain a final concentration 2.0×10^{-6} mol l^{-1}. Add 1.0 ml of 1.0 mol l^{-1} diethanolamine buffer and several drops of 1.0 mol l^{-1} NaOH solution to obtain a final of pH 9.0. Add 1.0 ml of ALP solution, which provides the final concentration between 1.0×10^{-12} and 1.0×10^{-8} mol l^{-1}. Dilute to volume with water. Incubate the resulting solution for 30 min and 1, 2 and 4 h in a water-bath at 37 °C. Measure the variation in the absorbance as ΔA, which is given by $\Delta A = A_0 - A_t$ at 416 nm.

Determination ALP in human serum

Place aliquots of $TPPP_m$ solution in 25 ml calibrated flasks in order to obtain a final concentration of 2.0×10^{-6} mol l^{-1}. Add 1.0 ml of 1.0 mol l^{-1} diethanolamine buffer and several drops of 1.0 mol l^{-1} NaOH solution to obtain a final pH of 9.0. Add 0.5 ml of 1.0×10^{-4} mol l^{-1} $Zn(NO_3)_2$ and 0.5 ml of 1.0×10^{-4} mol l^{-1} $Mg(NO_3)_2$ to avoid interference in serum. Add 0.5 ml of human serum and dilute to volume with water. Incubate the resultant solution for 30 min in a water-bath at 37 °C. Measure the variation in the absorbance as ΔA, which is given by $\Delta A = A_0 - A_{30}$ at 416 nm.

Determination of AFP in human serum

A commercial AFP EIA kit was used and the antigen–antibody reaction was performed according to the recommended procedure in the kit instructions. Place 0.025 ml of control serum containing AFP in the reagent pack, which includes the anti-AFP monochronal antibody immobilized beads and anti-AFP monochronal antibody–ALP bonding solution. Dilute with 0.1 ml of 0.1 g l^{-1} Triton-X100 aqueous solution. Incubate the resultant solution with stirring for 40 min in a water-bath at 37 °C. Wash with pH buffer solution for bonded/free separation. Determine the immobilized ALP activity according to the proposed method; place ALP immobilized beads in 0.220 ml of 2.0×10^{-6} mol l^{-1} $TPPP_m$ aqueous solution, which contains diethanolamine to achieve a pH of 9.0. Incubate for 30 min in a water-bath at 37 °C. Measure the variation in the absorbance as ΔA, which is given by $\Delta A = A_0 - A_{30}$ at 416 nm, with a microcell.

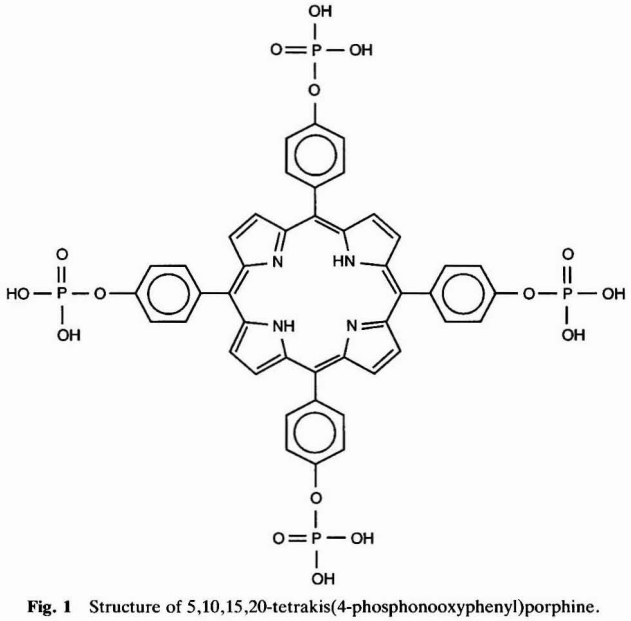

Fig. 1 Structure of 5,10,15,20-tetrakis(4-phosphonooxyphenyl)porphine.

Results and Discussion

Characterization of Reagent

Spectral change

$TPPP_m$ has an absorption maximum wavelength of the Soret band at 416 nm at pH > 8. On adding an aliquot of ALP sample solution in the optimum pH range, as time passed, the absorbance peak of the Soret band underwent a shift from 416 nm to a long wavelength and its molar absorptivity was significantly decreased ($\Delta\varepsilon \approx 3.0 \times 10^5$ l mol^{-1} cm^{-1}; Fig. 2). This phenomenon was explained as follows. The phosphate ester group became a phenol group by enzymolysis at pH > 9. Proton (H^+) was then dissociated from the phenol group, and the phenol group was immediately transformed into a quinone structure. In general, when a chromogenic reagent is formed as a quinone structure, its absorbance is enhanced by means of extension of the π-electronic resonance plane. In this reagent, however, the 18π-electronic resonance structure at the porphine ring was disturbed owing to the $+I$ effect of the outer quinone structure. Hence its absorbance was significantly decreased. It was considered that this spectral change arose from the first hydrolysis of at least one ester group. The reason is as follows. For THPP, which we reported previously,[11] according to the slope analysis, the analogous chromogenic reaction due to the quinone structure was caused by the dissociation of the first proton among the four hydroxy groups.

Stability of reagent

To confirm the pH stability of the reagent itself, pH–absorbance plots were measured (see Fig. 3). Although the major change in absorbance was observed in the pH range 5.5–7.5, this phenomenon means that the absorbance peak shift was caused by the dissociation of protons which were inside the porphine ring (free base form, H_2P, 416 nm; acidic form, H_4P^{2+}, 438 nm). A decrease in absorbance was also observed at pH < 1.0 or pH > 12, however, which was caused by depression of the solubility and subsequent salting-out. Based on the absence of a spectral change in the pH range 8–10, high stability of the phosphate ester groups in $TPPP_m$ was demonstrated in the pH range used for determination. On the other hand, stability with time was demonstrated; when the spectra of the $TPPP_m$ aqueous solution was monitored at pH

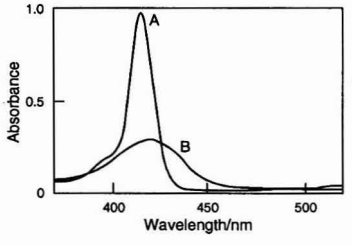

Fig. 2 Spectral change of $TPPP_m$ aqueous solution. $[TPPP_m] = 2.56 \times 10^{-6}$ mol dm^{-3}; $[ALP] = 1.0 \times 10^{-8}$ mol l^{-1}; pH = 9.0. A, $t = 0$; B, $t = 30$ min.

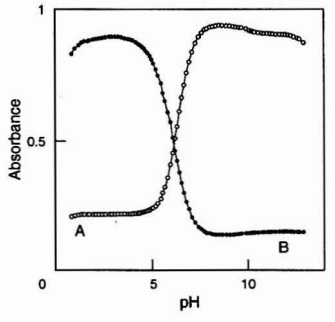

Fig. 3 Absorbance *versus* pH plots for $TPPP_m$. A, 416; and B, 438 nm. $[TPPP_m] = 2.56 \times 10^{-6}$ mol l^{-1}.

Table 1 Determination of ALP in human serum

Method	ALP/mg l^{-1}	s_r (%)*
This work	26.2	4.7
Standard method†	23.4	8.7

* 10 Determinations.
† *p*-Nitrophenyl phosphate method.[2]

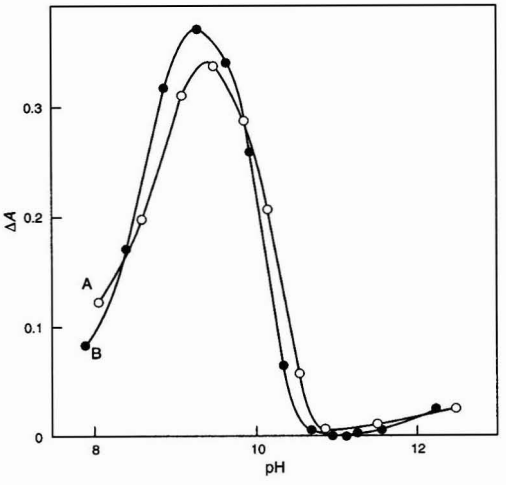

Fig. 4 Influence of pH: $[TPPP_m] = 1.80 \times 10^{-6}$ mol l^{-1}, $[ALP] = 2.05 \times 10^{-9}$ mol l^{-1}, $t = 30$ min. A, 24; B, 37 °C.

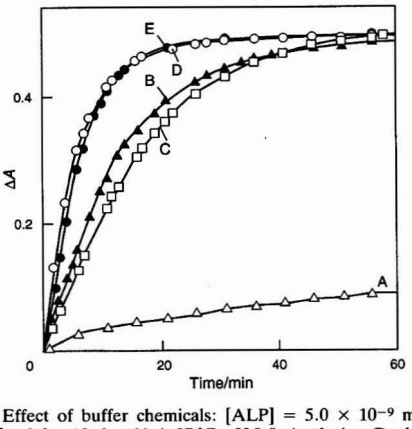

Fig. 5 Effect of buffer chemicals: $[ALP] = 5.0 \times 10^{-9}$ mol l^{-1}, $[TPPP_m] = 2.0 \times 10^{-6}$ mol l^{-1}, 37 °C, pH 9.0. A, glycine; B, glycine + $[Zn(NO_3)_2]$, $Mg(NO_3)_2]$; C, sodium acetate; D, diethanolamine; E, diethanolamine + $[Zn(NO_3)_2]$, $Mg(NO_3)_2]$. [Buffer chemicals] = 4.0×10^{-2} mol l^{-1}; $[Zn(NO_3)_2] = [Mg(NO_3)_2] = 2.0 \times 10^{-6}$ mol l^{-1}.

Table 2 Determination of AFP in human serum

Method	Sample A AFP/ ng ml^{-1}	Sample A s_r (%)*	Sample B AFP/ ng ml^{-1}	Sample B s_r (%)*	Sample C AFP/ ng ml^{-1}	Sample C s_r (%)*
This work	24.3	1.9	115.7	1.3	278.9	2.7
Standard method†	20.8	3.8	120.9	4.2	277.1	4.4

* 10 Determinations.
† 4-Methylumbelliferyl phosphate method.[4]

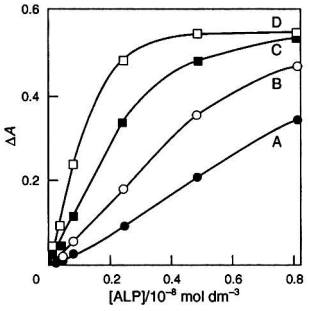

Fig. 6 Calibration graphs for ALP. [$TPPP_m$] = 2.0 × 10^{-6} mol l^{-1}. A, 30; B, 60 min; C, 120; and D, 240 min.

1.0, 7.0, 9.0 and 12.0, no spectral change was observed at room temperature for more than 7 d. This means that $TPPP_m$ is very stable in aqueous solution over a wide pH range for a long time.

Optimization of Conditions

Effect of pH

Fig. 4 shows the effect of pH on the reaction conditions. The enzyme activity was decreased at room temperature (25 °C), but no significant temperature dependence occurred in the optimum pH range. High reactivity was obtained in the pH range 9.0–9.4. All subsequent determinations were carried out at pH 9.0.

Inhibitory effect of buffer solution

As shown in Fig. 5, the enzyme activity was diminished in the presence of a glycine buffer, but high activity was observed with a diethanolamine buffer. Because ALP is a metalloenzyme which has zinc in the activity centre, the coexistence of an excess of a masking ligand such as glycine was assumed to inhibit the enzyme activity. The inhibition of activity was minimized by doping with Zn^{II} and Mg^{II} ions to prevent the masking effect even in glycine buffer. Diethanolamine solution, which hardly inhibited the activity, was used in the buffer in subsequent determinations.

Incubation time and calibration graph

As shown in Fig. 6, a calibration graph was obtained for each run. As the incubation time became longer, the determination range shifted to lower levels. In this study, considering the concentration range of the actual analyte and simplification of the procedure, an incubation time of 30 min was selected for subsequent determinations. The determination range under these conditions was 2.0 × 10^{-12}–8.0 × 10^{-9} mol l^{-1} and the linear range of the calibration graph was 4.0 × 10^{-10}–8.0 × 10^{-9} mol l^{-1}. The relative standard deviation was 3.5% (2.5 × 10^{-10} mol l^{-1}, ten determinations). The detection limit (3s) was 1.0 × 10^{-12} mol l^{-1}. The detection limit can be improved by changing the incubation time. For example, the detection limit reached 1.0 × 10^{-15} mol l^{-1} with a 12 h incubation.

Application to Practical Samples

Determination of ALP in human serum

As an example of application to a practical sample, a calibration graph was constructed using ALP in human serum (Sigma Type XVII from human placenta, 3.8 U mg^{-1}), and ALP in human serum (Whittaker Bioproducts human serum, type AB) was assayed with $TPPP_m$. Comparing the proposed method with the standard method using *p*-nitrophenyl phosphate, the standard method could not detect ALP activity in human serum with the same sample volume (0.5 ml) as that in the proposed method. Hence a 2.0 ml sample volume was used and determinations were carried out under the same conditions as those of the proposed method. The results are given in Table 1. The proposed method provided a smaller relative standard deviation using a smaller sample volume in comparison with the standard method.

Determination of AFP in human serum

As shown in Table 2, the proposed method provided a high correlation coefficient of above 0.999, compared with the 4-methylumbelliferyl phosphate method. This method showed good reproducibility for each control serum sample (low, medium and high AFP concentrations), and all the relative standard deviations were about half those obtained using only the commercial kit.

References

1 Oshihara, W., *Kagaku To Kogyo*, 1993, **7**, 1100.
2 Bessey, O. A., Lowry, O., H., and Brock, M. J., *J. Biol. Chem.*, 1946, **164**, 321.
3 Klein, B., Read, P. A., and Babson, A. L., *Clin. Chem. (Winston-Salem, N.C.)*, 1960, **6**, 269.
4 Guilubault, G. G., Sadar, S. H., Glazer, R., and Haynes, J., *Anal. Lett.*, 1968, **1**, 333.
5 Wood, K. V., in *Bioluminescence and Chemiluminescence; Current Status*, ed. Stanly, P., and Kricka, L., Wiley, Chichester, 1991, p. 543.
6 Chang, K. L., Ueno, K., and Imamura, T., *Handbook of Organic Analytical Reagents*, CRC Press, Boca Raton, FL, 1988, p. 355.
7 Igarashi, S., *Bunseki*, 1989, **3**, 190.
8 Tabata, M., and Tanaka, M., *Trends Anal. Chem.*, 1991, **10**, 121.
9 Kawakami, T., and Igarashi, S., *Nippon Kagaku Kaishi*, 1994, **4**, 396.
10 Adler, A. D., Longo, F. R., Finarelli, F. D., Goldmacher, J., Assour, J., and Korsakoff, K., *J. Org. Chem.*, 1967, **32**, 476.
11 Igarashi, S., Hashimoto, T., Matsumoto, Y., and Yotsuyanagi, T., *Bunseki Kagaku*, 1983, **32**, 591.

Paper 4/04747H
Received August 2, 1994
Accepted August 9, 1994

Mechanism of Nitrite-catalysed Oxidation of Chlorpromazine With Hydrogen Peroxide and/or Dissolved Oxygen Used for the Determination of Nitrite

Bing Liang, Masaaki Iwatsuki* and Tsutomu Fukasawa

Department of Applied Chemistry and Biotechnology, Faculty of Engineering, Yamanashi University, Takeda-4, Kofu 400, Japan

The mechanism of nitrite-catalysed oxidation of chlorpromazine with hydrogen peroxide in an acetic acid medium is inferred from absorption spectra, absorbance change and the properties of gas generated by reacting solutions under different conditions. (*i*) In a nitrite chlorpromazine hydrochloride (CPH)–dissolved O_2 system, nitrite is reduced by CPH to NO, which in turn is oxidized to NO_2 by the dissolved O_2. Much of the NO_2 oxidizes the CPH directly, and is converted into NO. The residual NO_2 disproportionates to HNO_3 and HNO_2. Nitrite and NO_2 oxidize residual CPH cyclically, until they are consumed. (*ii*) When a fresh CPH–H_2O_2 mixture is added to the nitrite-containing solution, peroxonitrous acid (HO_2NO) instantly forms, oxidizes CPH and is reduced to HNO_2, which reacts again with H_2O_2. The HO_2NO is also partially converted into its inactive isomer, HNO_3. The CPH is oxidized cyclically until the nitrite ions are consumed. (*iii*) When CPH and then H_2O_2 are added to the nitrite-containing solution, nitrite is reduced by CPH to NO, and then NO is oxidized by the H_2O_2 to produce mainly HNO_2 and some NO_2. The newly produced HNO_2 reacts with excess H_2O_2 to form HO_2NO, followed by the same cyclic reaction as in (*ii*). In reactions (*ii*) and (*iii*) a maximum absorbance proportional to the nitrite concentration is rapidly attained.

Keywords: Nitrite; catalytic reaction; cyclic reaction; peroxonitrous acid; chlorpromazine; spectrophotometry

Introduction

The authors previously proposed a maximum absorbance method for the rapid determination of nitrite (NO_2^-) down to 3 ng ml^{-1}, using catalytic oxidation of chlorpromazine hydrochloride (CPH) with hydrogen peroxide in an acetic acid medium.[1] The oxidation reaction proceeded sequentially, accelerated by trace nitrite ions as shown by eqn. (1), and gave a maximum in the absorbance *versus* elapsed time curve, that was proportional to nitrite concentration.

$$\underset{\text{Colourless}}{\text{CPH}} \xrightarrow{NO_2^-} \underset{\text{Red}}{\text{CPH}^*} \longrightarrow \underset{\text{Colourless}}{\text{CPH}(O_x)} \qquad (1)$$

Where CPH^* is a metastable free radical.

However, the nitrite-catalysed oxidation of CPH was dependant on the oxidant used (hydrogen peroxide or dissolved O_2) and the order of addition of the reagents (which gave different changes in absorbance and maximum absorbance). The recommended procedure for the determination of nitrite[1] stated that a fresh CPH–H_2O_2 mixture should be added to an acetic acid solution containing nitrite and oxalic acid (added as a masking agent for iron). The present paper discusses the mechanism of the reaction on the basis of absorption spectra and absorbance *versus* time curves, obtained using reacting solutions under different conditions, and reaction vessels of different sizes, and also the properties of the gas generated by the reacting solutions. The results gave a theoretical and practical background to the recommended procedure for the determination of nitrite.

Experimental

Reagents and Apparatus

Details not given here are described in the previous paper.[1] A 0.25 mol l^{-1} CPH stock solution was prepared by dissolving chlorpromazine hydrochloride (Wako, Osaka, Japan) in water. The working solution of nitrite was prepared just before use, by diluting its stock solution of 1.0 mg ml^{-1} which was prepared less than 4 d before use. A mixed acid solution of oxalic and acetic acids was made by dissolving 0.28 g of oxalic acid dihydrate in 20 ml of 3.3 mol l^{-1} acetic acid. All solutions described above were refrigerated in polystyrene or poly(propylene) bottles. A fresh reactant mixture was prepared by mixing 0.10 ml of 0.25 mol l^{-1} CPH and 0.10 ml of 2.5 mol l^{-1} H_2O_2 just before use.

A purpose-built reaction set (Fig. 1) was used for testing gas-generation from the reacting solutions.

Eppendorf (Hamburg, Germany) micropipettes of 100–1000 μl and 10–100 μl volumes were used for reagent addition. A Shimadzu (Kyoto, Japan) UV 140-01 double-beam spectrophotometer with a chart recorder and a 10 mm cell of 4.2 ml was used to obtain measurements for the absorbance–time curves. The temperature of the cell compartment was kept constant by circulating the water from a thermostated

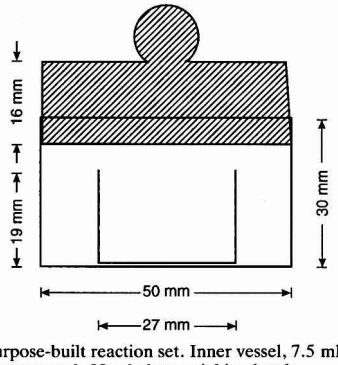

Fig. 1 A purpose-built reaction set. Inner vessel, 7.5 ml polystyrene bottle and outer vessel, 30 ml glass weighing bottle.

* To whom correspondence should be addressed.

water-bath. A Shimadzu UV 160A double-beam UV/VIS spectrophotometer was used for spectral measurements.

Experimental Procedures

Unless otherwise stated, the concentrations of acetic acid, oxalic acid, CPH and H_2O_2 in the reaction solutions were 0.2, 6.6×10^{-3}, 5×10^{-3} and 5×10^{-2} mol l^{-1}, respectively. These concentrations were recommended in the previous paper.[1] A nitrite concentration of 80 ng ml^{-1} was used throughout except when testing for gas generated by the reaction solutions. All working solutions and water were kept in the water-bath before use, at 20 °C unless otherwise stated.

Measurements of absorption spectra and absorbance changes of reacting solutions

A nitrite working solution of 0–0.32 ml was taken into the 10 mm cell and diluted to exactly 3.60 ml (or 3.68 ml for the reaction system without H_2O_2) with water (which was bubbled with oxygen or argon gas to study the effect of dissolved oxygen). After addition of 0.24 ml of the mixed-acid solution, 0.16 ml of the fresh reactant mixture, or 0.08 ml each of CPH and H_2O_2 was added. The cell was covered with a lid and turned upside down three times in order to ensure that the reaction proceeded homogeneously. Absorption spectra of reacting solutions were measured at 360–800 nm for 10 s after various reaction times. The absorbance change at 527 nm against reaction time was recorded on a strip-chart recorder until a maximum absorbance (A_{max}) appeared.

Test of gas generated by reacting solutions

Oxidizing gases, such as nitrogen monoxide (NO) or nitrogen dioxide (NO_2) may be generated from the reacting solutions depending on the experimental conditions. The gas generation and its effects were tested using the reaction set. The mixed-acid solution (0.3 ml), 0.10 ml of 0.25 mol l^{-1} CPH and 4.5 ml of water were taken into the inner vessel which was used as an acceptor for the generated gas. Nitrite working solutions (of different volumes), water and reactant solutions were taken into the outer vessel, in that order, to allow the reaction to proceed as shown in Fig. 2. Here, a higher concentration, *i.e.*, ppm level of nitrite was added to the outer vessel to give appropriate absorbance to the acceptor solution. The reaction set was immediately covered with the lid, and kept in a thermostated water-bath at 20 °C for 30 min, in order to deliver the generated gas into the acceptor solution through the closed atmosphere by diffusion. In order to confirm the oxidative and catalytic properties of the gas absorbed in the acceptor, 0.10 ml of 2.5 mol l^{-1} H_2O_2 was added to the acceptor, and its absorbance change was recorded at 527 nm using the 10 mm cell until an A_{max} was attained.

Use of reaction vessels with different void volumes

In the previous paper,[1] reactions were carried out using a 20 ml glass test tube and 5 ml of the reacting solution. However, the gas released from the reacting solution may have different effects on the reaction depending on the void volume or closed atmosphere in the reaction vessel used. A 20 ml stoppered glass test tube, a 5 ml measuring flask and a 10 mm cell with a lid (which had different void volumes during reaction) were used to test the generation and escape of the gas and the effect of the reaction vessel on the sensitivity of nitrite determination. A reaction solution of 4.0 ml was used for the 10 mm cell and 5.0 ml for the others. Then the absorbance change was recorded in the same manner as above.

Results and Discussion

Absorption Spectra

Fig. 3 and Table 2 show that the order of addition of reagents had no effect on the wavelength of the absorption maximum, but an effect on the peak height. The wavelength of the maximum was 527 nm, which is within the range of 525–530 nm as reported by Mottola *et al.*[2] who used cerium(IV) as an oxidant in a sulfuric acid medium, and near 528 nm, as reported by Gowda *et al.*[3] who used cerium(IV) as an oxidant

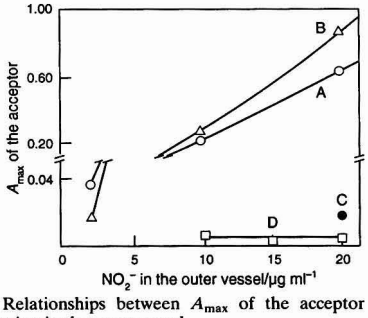

Fig. 2 Relationships between A_{max} of the acceptor and nitrite concentration in the outer vessel.

Table 1 Order of addition of reagents in the outer vessel*

Curve	NO_2^- (2–20 μg ml^{-1})	Mixed acid†	CPH (0.005 mol l^{-1})	H_2O_2 (0.05 mol l^{-1})
A	1	2	NA‡	NA
B	1	2	3	NA
C	1	2	3	4
D	1	2	3	3

* Reagents with the same number were added at the same time as a mixed solution.

† Acids: 0.2 mol l^{-1} acetic acid; 6.6×10^{-3} mol l^{-1} oxalic acid.

‡ NA = not added.

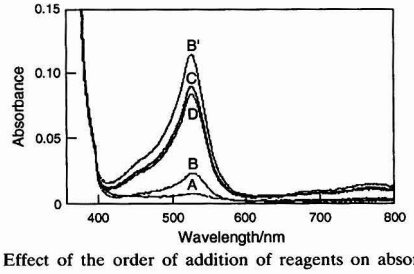

Fig. 3 Effect of the order of addition of reagents on absorbance spectrum.

Table 2 Order of addition of reagents*

Curve	NO_2^- (80 ng ml^{-1})	Mixed acid	CPH (0.005 mol l^{-1})	H_2O_2 (0.05 mol l^{-1})	Reaction time/min
A	NA	1	2	2	110.0
B	1	2	3	NA	2.0
B′	1	2	3	NA	90.0
C	1	2	3	4	2.5
D	1	2	3	3	2.0

* A 10 mm cell of 4 ml was used for reaction and measurements. Scanning time, in the range of 360–800 nm, was 10 s. See footnote in Table 1 for conditions.

in a phosphoric acid medium. This indicates that the oxidation product was the same as that described here and was independent of the oxidants and acids used, or the order of addition of reagents.

Gas Generation From Reacting Solutions

In the experiments represented by Fig. 2, A and B the acidified CPH solutions in the inner vessel gradually became red, even before the addition of H_2O_2 to the inner vessel. This means that both the acidified nitrite solution without CPH (A) and the acidified nitrite solution containing CPH (B) generated an oxidizing gas, which gradually oxidized CPH in the acidic solution, which included naturally dissolved O_2. It is well known that NO is formed from the decomposition of nitrite in acidic medium. Among the many nitrogen compounds which have a valency lower than that of nitrite-nitrogen, only NO is oxidizing and gaseous. Therefore, NO is inferred to be the reduction product of nitrite by CPH in the absence of H_2O_2 (B). The results described above also indicate that NO oxidized CPH in the acidic CPH–dissolved O_2 solution.

After the addition of H_2O_2 to the acceptor solutions (A and B), the A_{max} of the acceptor solutions increased with the nitrite concentration in the outer vessel. This means that the NO produced had a catalytic effect on the CPH–H_2O_2 reaction. Fig. 2, B, however, shows a significantly higher A_{max} than that of A. This means that the reacting solution containing the same amount of nitrite in the outer vessel generated a significantly larger amount of the oxidizing or more catalytic gas, *i.e.*, to escape into the atmosphere and to be transferred into the acceptor solution. The black area, C, shows a result from the addition of H_2O_2 just after CPH to acidified nitrite solution in the outer vessel. This gave a low A_{max}, but it was significantly larger than that of the reagent blank (as described later) (Fig. 2, D). The succeeding addition of H_2O_2 significantly suppressed the generation of oxidizing and catalytic gas. The absorbance of D, which was obtained by adding the CPH–H_2O_2 mixture as described in the previous paper,[1] was as low as the reagent blank. This suggests that there is no release of the oxidizing and catalytic gas from the reacting solution, *i.e.*, nitrite may effectively work in the reacting solution.

Table 3 Effects of the reaction vessel on the colouring rate and A_{max} for different adding procedures of CPH and H_2O_2

	Test tube	Measuring flask	Cell 10 mm
Nominated volume/ml	20.0	5.0	
Practical volume/ml	30.0	6.4	4.2
Reacting solution/ml	5.0	5.0	4.0
Void volume/ml	25.0	1.4	0.2
$Volume_{void}/volume_{sln}$	5.0	0.28	0.05
dA/dt in 1–2 min (without H_2O_2)	0.0022	0.0032	0.0034
A_{max} (without H_2O_2)	Not measured*		
A_{max} (H_2O_2 added just after CPH)†	0.067 ±0.002	0.085 ±0.002	0.089 ±0.001
A_{max} (CPH–H_2O_2 mixture added)‡	0.080 ±0.003	0.082 ±0.003	0.078 ±0.002

Nitrite of 80 ng ml^{-1} was used.
* Required too long time for A_{max} to appear.
† The values of A_{max} are shown as average ± σ (n = 4).

Effect of Void Volume in the Reaction Vessel

Table 3 shows the effect of the void volume or size of reaction vessel on the rate of colour development and A_{max} for the procedures of adding only CPH into the acidified-nitrite solution (nitrite–CPH–dissolved O_2 system), of adding H_2O_2 just after CPH (nitrite–CPH–H_2O_2 system) and of adding the fresh reactant mixture of CPH and H_2O_2 (nitrite–CPH·H_2O_2 mixture system). In the case of the nitrite–CPH–O_2 system or nitrite–CPH–H_2O_2 system, both the measuring flask and cell, which have smaller void volumes or atmosphere for gas to be released from reacting solutions, gave high rates of colour development and high A_{max} in comparison with those in the test tube. This suggests that there was less oxidative gas release when using the flask and cell, whereas there is a considerable release when using the test tube. Each vessel, however, gave almost the same and higher values of A_{max} when the fresh CPH–H_2O_2 mixture was added; this indicates that the reaction did not generate the oxidizing gas and the reaction proceeded effectively. All subsequent experiments were performed using the 10 mm cell which led to the release of less gas.

Effect of Order of Addition of Reagents and of Dissolved Oxygen

In the case of the reagent blank without nitrite, dissolved O_2, and H_2O_2 used, gave a very small absorbance change against elapsed time as shown by Fig. 4, A, B and B′. This means that both dissolved oxygen and H_2O_2 scarcely oxidize CPH in an acetic acid solution without nitrite. Addition of H_2O_2 before CPH to the acidic solution of 80 ng ml^{-1} nitrite gave curve C, bearing a small absorbance change, similar to that of the reagent blanks (B and B′). This indicates that nitrite was oxidized rapidly with H_2O_2 to nitrate, which had no effect on the oxidation of CPH (as described in ref. 1). Curves D, D′ and D″ showed the effect of concentration of dissolved O_2 on the reaction of the nitrite-CPH-dissolved O_2 system. Each of the three curves consisted of an absorbance jump (A_0) at the beginning and a moderate increase of absorbance accompanied by a maximum (A_{maxD}) after 2 h. In the gas bubbling column, Ar, Not and O_2 indicate a lower oxygen concentration, naturally-dissolved oxygen concentration and a higher oxygen concentration, respectively, in the water used for dilution. Therefore, it can be said that A_0 values were independent of the dissolved O_2 concentration, but dependent on nitrite concentration as shown in Fig. 5. Therefore, A_0 is attributable to the direct oxidation of CPH by nitrite. However, the slope of the moderate increase of absorbance

Table 4 Order of addition*

Curve	NO_2^- (80 ng ml^{-1})	Mixed acid	CPH (0.005 mol l^{-1})	H_2O_2 (0.05 mol l^{-1})	Gas bubbling
A	NA	1	2	NA	Not†
B	NA	1	2	2	Not†
B′	NA	1	2	3	Not†
C	1	2	4	3	Not†
D	1	2	3	NA	Ar
D′	1	2	3	NA	Not†
D″	1	2	3	NA	O_2
E	1	2	3	4	Ar
E′	1	2	3	4	Not†
E″	1	2	3	4	O_2
F	1	2	3	3	Ar
F′	1	2	3	3	Not†
F″	1	2	3	3	O_2

* See footnote in Table 1 for the conditions.
† Naturally dissolved oxygen.

and A_{maxD} were dependent on the concentration of dissolved oxygen, as shown by the differences between D, D′ and D″. The moderate increase of absorbance after A_0 suggests that the residual CPH was oxidized by an oxidizing and catalytic gas, *i.e.*, NO_2, which was the oxidation product of NO by dissolved O_2.

Addition of H_2O_2 just after CPH gave curves E–E″ bearing a maximum absorbance (A_{maxE}) which appeared rapidly (within 3 min). The A_{maxE} included the direct oxidation of CPH by nitrite and the subsequent catalytic reaction as described below. As shown by curves F–F″, the addition of the fresh CPH–H_2O_2 mixture gave a slightly lower maximum absorbance (A_{maxF}) appearing earlier than that of curves E–E″. Curves F–F″ resulted from the oxidation of CPH by peroxonitrous acid (HO_2NO), as described later. When using the fresh reactant mixture, dissolved O_2 had little effect on the absorbance, *i.e.*, the reaction, as shown by the slight difference between F, F′ and F″.

Effect of Temperature

Fig. 6 shows that the absorption jump, A_0, defined in Fig. 4, was almost constant (average value = 0.0175) independent of reaction temperature. This result also supports the fact that A_0 is attributable to the direct oxidation of CPH by nitrite as described above. The values of A_{maxE} and A_{maxF} in the two reaction systems including H_2O_2 increased with decreasing temperature. This result may be due to the instability of peroxonitrous acid at higher temperatures,[5] and/or to the competition between the developing- and fading-colour reactions of CPH.

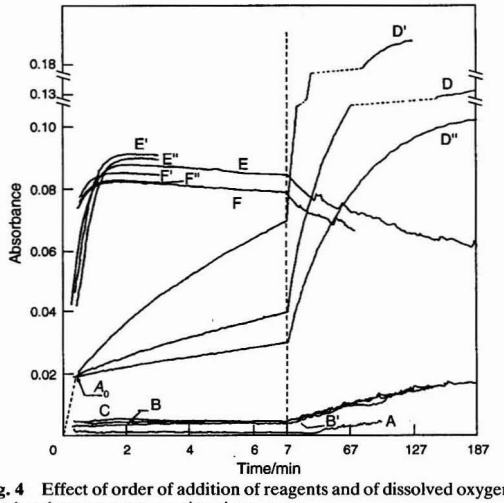

Fig. 4 Effect of order of addition of reagents and of dissolved oxygen on absorbance *versus* reaction time curves

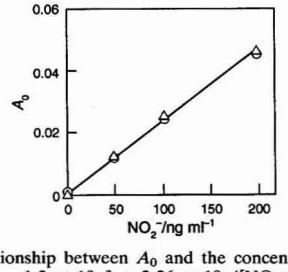

Fig. 5 Relationship between A_0 and the concentration of nitrite. ○, 20 °C, $A_0 = 1.2 \times 10^{-3} + 2.26 \times 10^{-4}[NO_2^-]_{ppb}$, $r = 0.9995$; △, 30 °C, $A_0 = 1.4 \times 10^{-3} + 2.27 \times 10^{-4}[NO_2^-]_{ppb}$, $r = 0.9993$.

Reaction Mechanism for Nitrite–CPH–Dissolved O_2 system

On the basis of the experimental results described above, the reactions of the nitrite–CPH–dissolved O_2 system are inferred to consist of NO_2-participating cyclic reactions as shown in Scheme 1. Nitrite directly oxidizes CPH to give the absorbance jump, A_0, and is converted into NO as shown in eqn. (2). Nitrogen monoxide is known to be easily oxidized to NO_2 by dissolved oxygen as shown in eqn. (3). A large part of NO_2 may directly oxidize CPH and be converted into NO as shown in eqn. (4) and the remainder may disproportionate to nitric acid (HNO_3) and nitrous acid (HNO_2) as shown in eqn. (5). Nitrite and NO_2 will oxidize CPH cyclically until they are consumed, because A_{maxD} for this system was several times larger than A_0.

$$NO_2^- + CPH \rightarrow NO + CPH^* \quad (2)$$

$$NO + (1/2)O_2 \rightarrow NO_2 \quad (3)$$

$$2\,CPH^* + NO \leftarrow 2CPH + NO_2 \quad (4)$$

(Major / Minor)

$$(1/2)HNO_2 + (1/2)HNO_3 \leftarrow (1/2)H_2O + NO_2 \quad (5)$$

Scheme 1 Reactions of nitrite–CPH–dissolved O_2 system

Provided that there was no direct oxidation of CPH by NO_2, as shown in eqn. (4), the oxidation continued only by nitrite produced sequentially in the cyclic process until all the nitrite ions were converted into HNO_3. After the cyclic reaction finished, accumulated [CPH*], *i.e.*, $[CPH^*]_{acc}$, can be expressed as shown in eqn. (6):

$$[CPH^*]_{acc} = [NO_2^-]_0(1 + 1/2 + 1/4 + \cdots + 1/2^n + \cdots) = 2[NO_2^-]_0 \quad (6)$$

where $[NO_2^-]_0$ is the initial concentration of nitrite. As the absorbance of the reacting solution is equal to $\varepsilon[CPH^*]$, where ε is the molar absorption coefficient,

$$A_{maxD} = \varepsilon[CPH^*]_{acc} = 2\varepsilon[NO_2^-]_0$$

and

$$A_0 = \varepsilon[NO_2^-]_0 \quad (7)$$

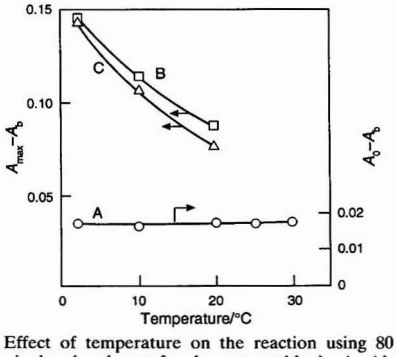

Fig. 6 Effect of temperature on the reaction using 80 ng ml^{-1} NO_2^-. A_b is the absorbance for the reagent blank. A, Absorbance jump (A_0) in the nitrite–CPH–O_2 system. B, A_{maxE} in the nitrite–CPH–H_2O_2 system. C, A_{maxF} in the nitrite–CPH·H_2O_2 mixture system.

Part of CPH* is consumed owing to its further oxidation, *i.e.*, fading reaction as shown by eqn. (1).

$$A_{maxD}/A_0 < 2 \quad (8)$$

However, the experimental values of A_{maxD}/A_0 were 5–9, significantly larger than 2, as shown in Table 5. Therefore, NO_2 should be a participant in the oxidation reaction of CPH as shown in Scheme 1.

Reaction Mechanism for Nitrite–CPH·H_2O_2 Mixture System

In the oxidation process of nitrite with H_2O_2 to nitrate in an acidic medium, peroxonitrous acid (HO_2NO) is formed as an unstable intermediate.[4] In organic chemistry, cooled and acidified H_2O_2 is added to cooled nitrite solution to obtain HO_2NO for oxidation of concomitant organic materials.[5] In the nitrite–CPH·H_2O_2 mixture system, HO_2NO is inferred to be formed when the fresh mixture of CPH–H_2O_2 was added to the acidic solution including nitrite.

Since the nitrite–CPH·H_2O_2 mixture system did not generate an oxidizing gas as described earlier, the reduction product of HO_2NO with CPH is inferred not to be NO and/or NO_2. Glev *et al.*[6] have reported that the reduction product of HO_2NO with bromide was nitrite. The authors have also inferred that the reduction product here was nitrite.

For the nitrite–CPH·H_2O_2 mixture system, cyclic reactions are inferred as shown in Scheme 2. Nitrite is instantly oxidized by H_2O_2 to form HO_2NO, and a fraction (q) of HO_2NO is reduced immediately to HNO_2 by CPH. The newly formed HNO_2 reacts with H_2O_2 to form HO_2NO again, and so cyclic reactions take place. However, residual fraction ($1 - q$) of HO_2NO may be converted into its isomer, *i.e.*, HNO_3 which is inactive for the catalytic reaction.

$$NO_2^- + H_2O_2 \rightarrow HO_2NO \xrightarrow{(1-q)} HNO_3 \quad (9)$$
$$\uparrow \qquad \downarrow (q)$$
$$HNO_2 + 2CPH^* \leftarrow HO_2NO + 2CPH \quad (10)$$
$$(A_{maxF})$$

Scheme 2 Reactions of nitrite–CPH·H_2O_2 mixture system

Table 5 Effect of oxygen concentration on A_{maxD}/A_0

	Bubbling argon	Naturally dissolved O_2	Bubbling oxygen
A_0	0.018	0.0183	0.0185
A_{maxD}	0.102	0.132	0.184
A_{maxD}/A_0	5.7	7.2	9.9

An 80 ng ml^{-1} concentration of nitrite was used.

Accumulated [CPH*] after consumption of all nitrite ions by the cyclic reaction as described above, can be represented in eqn. (11)

$$[CPH^*]_{acc} = 2[NO_2NO](q + q^2 + \cdots + q^n + \cdots)$$
$$= 2[NO_2^-]_0 \sum_{n=1}^{\infty} q^n \quad (11)$$

where n is the cycle number, and the constant, 2, means that one molecule of HO_2NO oxidizes two CPH molecules. Thus, eqn. (12) is obtained.

$$A_{maxF}/A_0 = \varepsilon[CPH^*]_{acc}/A_0$$
$$= 2\varepsilon[NO_2^-]_0 \sum_{n=1}^{\infty} q^n/\varepsilon[NO_2^-]_0$$
$$= 2\sum_{n=1}^{\infty} q^n = 2q/(1-q) \quad (12)$$

Considering that parts of CPH* may be further oxidized to CPH(O_x) and consumed,

$$q < (A_{maxF}/A_0)/(2 + A_{maxF}/A_0). \quad (13)$$

The q values in Table 6 were estimated by using the ratios of the heights of A_{maxF} to A_0 obtained at different temperatures as shown in Fig. 6. The lower the reaction temperature was, the higher the value of q: this is consistent with the instability of HO_2NO at higher temperatures.

Reaction Mechanism for Nitrite–CPH–H_2O_2 System

When H_2O_2 is added, after addition of CPH, to an acidified nitrite solution, it is inferred that NO is produced first from reduction of nitrite by CPH as shown in eqn. (2), and oxidized

Table 6 Experimental and/or calculated values of A_{maxF}/A_0, q and A_{maxE}/A_{maxF} at different reaction temperatures

	Reaction temperature		
	2 °C	10 °C	20 °C
A_0	0.0175	0.016	0.0183
A_{maxE}	0.149	0.116	0.088
A_{maxF}	0.146	0.108	0.082
Ratio of A_{maxF}/A_0	8.4	6.2	4.4
$q = (A_{maxF}/A_0)/(2 + A_{maxF}/A_0)$	0.81	0.76	0.69
Ratio of A_{maxE}/A_{maxF}:			
Experimental	1.01	1.09	1.13
Estimated, route B in Scheme 3	1.12	1.16	1.23
Estimated, route A in Scheme 3	0.62	0.66	0.73

Nitrite of 80 ng ml^{-1} was used.

$$NO_2^- + CPH \rightarrow NO + CPH^* \quad (2)$$

A ↓ Minor

$$H_2O_2 + NO \rightarrow NO_2 + H_2O \quad (14)$$

$$\downarrow$$

$$(1/2)H_2O + NO_2 \rightarrow (1/2)\,HNO_2 + (1/2)HNO_3 \quad (16)$$

B ↓ Major

$$(1/2)H_2O_2 + NO \rightarrow HNO_2 \quad (15)$$

Cyclic reactions (9) and (10) in Scheme 2

Scheme 3 Reactions of nitrite–CPH–H_2O_2 system

to HNO_2 which will act in the manner shown in Scheme 2. Reactions of this system are inferred to follow Scheme 3, which contains two routes, A and B, for NO conversion to HNO_2.

For route A, which produces HNO_2 *via* NO_2,

$$[NO_2^-]_0 = [NO] = [NO_2] = 1/2[HNO_2] = 1/2[HO_2NO]$$

$$A_{maxE} = A_0 + \varepsilon(1/2)2[NO_2^-]_0 \sum_{n=1}^{\infty} q^n$$

$$= A_0 + \varepsilon[NO_2^-]_0\{1/(1-q) - 1\} \quad (17)$$

$$A_{maxE}/A_0 = 1 + \{1/(1-q) - 1\} = 1/(1-q) \quad (18)$$

From eqns. (12) and (18), eqn. (19) is obtained.

$$A_{maxE}/A_{maxF} = 1/2q \quad (19)$$

For route B, which produces HNO_2 directly,

$$[NO_2^-]_0 = [NO] = [HNO_2] = [HO_2NO]$$

Therefore,

$$A_{maxE}/A_{maxF} = (1 + q)/2q$$

Table 6 also shows the calculated values of A_{maxE}/A_{maxF} based on the two routes and their experimental values. As route B gave calculated A_{maxE}/A_{maxF} values nearer to the experimental values, it was inferred to be the major route for the change of NO to nitrite.

Recommended Procedure for Nitrite Determination

The procedure of addition of CPH and then H_2O_2 to an acidified nitrite solution using the 10 mm cell gave an A_{max} a little higher than that achieved by the addition of the fresh reactant mixture. However, use of the cell required especially skillful and careful procedures and was inconvenient. The reaction before addition of H_2O_2 was the nitrite–CPH–dissolved O_2 system. Therefore, the procedure may cause some escape of NO gas from the reacting solution depending on the size of vessel (as shown by the black area, C, in Fig. 2) and is also susceptible to the dissolved O_2 concentration.

The procedure of addition of the fresh mixture of CPH–H_2O_2 gave no gas-generation and gave the same result even when a different reaction vessel was used. The reaction mechanism and the above detailed experiments showed that the recommended procedure in ref. 1 was reasonable and practical.

References

1 Liang, B., Iwatsuki, M., and Fukasawa, T., *Analyst*, 1994, **119**, 2113.
2 Mottola, H. A., and Hanna, A., *Anal. Chim. Acta*, 1978, **100**, 167.
3 Gowda, H. S., and Ahmed, S. A., *Anal. Chim. Acta*, 1978, **99**, 343.
4 Cotton, F. A., and Wilkinson, G., *Advanced Inorganic Chemistry*, Wiley, New York, 4th edn., 1980, p. 430.
5 Ohki, M., Ohsawa, T., Tanaka, M., and Chihara, H., *Encyclopedic Dictionary of Chemistry*, Tokyo Kagaku Dojin, Tokyo, 1989, p. 2154.
6 Glev, K., and Hubold, R., *Z. Anorg. Allg. Chem.*, 1935, **223**, 316.

Paper 4/04964K
Received August 12, 1994
Accepted September 29, 1994

Spectrophotometric Determination of Silver and Gold with 5-(2,4-Dihydroxybenzylidene)rhodanine and Cationic Surfactants

F. M. El-Zawawy, M. F. El-Shahat, A. A. Mohamed and M. T. M. Zaki*

Department of Chemistry, Faculty of Science, Ain Shams University, Abbassia, Cairo, Egypt

The synthesis, characteristics and analytical reactions of 5-(2,4-dihydroxybenzylidene)rhodanine (2,4-DHBR) with silver and gold are described. Maximum enhancement of the absorbance of the chelates is obtained in the presence of the cationic surfactants cetyltrimethylammonium bromide (CTAB) and cetylpyridinium bromide (CPB), respectively. Each metal ion forms two ternary complexes depending on 2,4-DHBR concentration. The stoichiometries of the complexes are 1 : 1 : 1 and 1 : 2 : 3 (Ag–2,4-DHBR–CTAB) and 1 : 2 : 3 and 1 : 3 : 4 (Au–2,4-DHBR–CPB). The complexes with higher reagent/metal ratio were used for the spectrophotometric determination of silver and gold. In the pH ranges 9.2–10.6 and 9.3–10.8, the molar absorptivities are 7.11×10^4 (Ag) and 8.45×10^4 (Au) dm^3 mol^{-1} cm^{-1} at 547 and 558 nm, respectively. The methods adhere to Beer's law for 0.13–1.83 μg cm^{-3} of silver and 0.16–2.24 μg cm^{-3} of gold and the corresponding sensitivities are 0.0015 and 0.0023 μg cm^{-2}. The methods were used successfully to determine trace amounts of silver and gold in silicate rocks and a sulfide ore.

Keywords: Silver determination; gold determination; spectrophotometry; 5-(2,4-dihydroxybenzylidene)rhodanine; surfactants

Introduction

The spectrophotometric determination of silver is usually preceded by reaction with dithizone,[1] 4-(2-quinolylazo)phenol,[2] 2-[4-amino-3-(1,2,4-triazolylazo)]naphthol-4-sulfonate,[3] 4,4′-bis(dimethylamino)thiobenzophenone,[4] ammonium 2-cyano-3-iminodithiobutyrate[5] or ammonium (2′,3′-dihydroxypyridyl-4′-azo)benzene-4-arsonate[6] and that of gold with dithizone,[7] methiomeprazine hydrochloride,[8] dithiodiantipyrylmethane,[9] 2,2,2-trifluoroethyl xanthate,[10] 4-(2-quinolylazo)phenol,[11] 4-(2-pyridylazo)resorcinol[12] or 4-(2-thiazolylazo)resorcinol (TAR).[13] However, most of these methods lack sensitivity, selectivity and/or reproducibility.

Rhodanine derivatives have also found wide application in the determination of silver[14–18] and gold.[19–23] However, many problems are associated with their use, including the solubility of reagents and chelates and the instability of the developed colours.[24,25] Consequently, a protective colloid is added to stabilize the pseudo-solution, or a water-miscible organic solvent is used throughout.

Surfactants and micellar systems are currently used in the spectrophotometric determination of metals to solubilize reactants and products and to improve the sensitivity and selectivity of these methods.[26,27] However, little attention has been directed to the determination of silver[28,29] and gold[30] in micellar media.

In this work, 5-(2,4-dihydroxybenzylidene)rhodanine (2,4-DHBR) was synthesized and tested as a possible chromogenic reagent for the determination of silver(I) and gold(III). The protolytic equilibria of the reagent were determined. The effects of some surfactants and protective colloids on the spectral characteristics of silver– and gold–2,4-DHBR chelates were investigated. Maximum sensitization of the colour reactions was obtained in the presence of cetyltrimethylammonium bromide (CTAB) and cetylpyridinium bromide (CPB), respectively. The experimental variables affecting colour formation and the possible interference of co-existing ions were thoroughly studied. The optimum conditions established were incorporated in the recommended procedures, which were applied to determine silver and gold in silicate rocks and a sulfide ore.

Experimental

Apparatus

Absorbance measurements were obtained with a Perkin-Elmer Lambda 3B UV–VIS spectrophotometer using 1 cm matched quartz cells. An Orion Model 920A Ion-Analyzer equipped with a combination glass–calomel electrode was used for pH determinations.

Reagents

All chemicals were of analytical-reagent grade. Surfactants and protective colloids were used as received. Doubly distilled water was used throughout.

2,4-DHBR was synthesized according to the general method of Julian and Strugis,[31] by adding 10 g of fused sodium acetate to 100 cm^3 of glacial acetic acid containing 0.1 mol each of rhodanine and 2,4-dihydroxybenzaldehyde. The mixture was refluxed for 2 h with occasional shaking. 2,4-DHBR was separated by cooling. The whole mass was poured into 1 dm^3 of cold water. The solid was separated and crystallized several times from acetic acid. The yield was 82%. The purity of the reagent was checked by thin-layer chromatography with benzene–light petroleum (b.p. 40–60 °C) (1 + 4 v/v) as eluent. A single orange–yellow band was obtained for the pure product. Results of elemental analysis confirmed the purity of 2,4-DHBR (calculated, C 47.43, H 2.77, N 5.53; found, C 47.3, H 2.7, N 5.5%). The solid reagent was kept for as long as 18 months without any change in structure, as evidenced from IR, UV and NMR spectroscopic measurements. An ethanolic solution of 2,4-DHBR (5×10^{-3} mol dm^{-3}) was prepared by dissolving 0.3163 g in warm

* To whom correspondence should be addressed. Present address: Department of Chemistry, Faculty of Science, United Arab Emirates University, PO Box 17551, Al-Ain, United Arab Emirates.

ethanol and diluting to 250 cm^3 with the same solvent. This solution was stable for more than 3 months.

Silver(I) stock standard solution (0.01 mol dm^{-3}) was prepared by dissolving 0.8494 g of silver nitrate (dried at 110 °C) in water containing 1 cm^3 of nitric acid and diluting to 500 cm^3 in a calibrated flask.

Gold(III) stock standard solution (1 mg cm^{-3}) was prepared by dissolving 0.5 g of gold in aqua regia by warming, evaporating the solution to dryness and dissolving the residue in hydrochloric acid, evaporating the solution to half its volume, cooling and diluting with water to 500 cm^3 in a calibrated flask.

Cetyltrimethylammonium bromide (CTAB) and cetylpyridinium bromide (CPB) were prepared as 0.01 mol dm^{-3} solutions.

Borax buffer of pH 10 was prepared by adjusting the pH of 0.05 mol dm^{-3} sodium tetraborate solution with dilute sodium hydroxide solution.

Recommended Procedures

Transfer an aliquot of the sample solution containing not more than 45 μg of silver(I) or 56 μg of gold(III) into a 25 cm^3 calibrated flask. Add 0.5 cm^3 of 2,4-DHBR solution and 5 cm^3 of CTAB or CPB, respectively. Dilute to volume with borax buffer. Leave at room temperature for 5 min and measure the absorbance at 547 or 558 nm, respectively, against a blank. Determine the silver or gold concentration using calibration graphs prepared in the same manner.

Results and Discussion

Several rhodanine derivatives were synthesized and tested as reagents for silver(I) and gold(III): 5-(4-chlorobenzylidene)-rhodanine, 3-(5-chlorobenzylidene)rhodanine, 5-(3-chloro-2-hydroxybenzylidene)rhodanine, 5-(3,4-diethoxybenzylidene)rhodanine, 5-(4-hydroxy-3-methoxybenzylidene)rhodanine and 5-(2,4-dihydroxybenzylidene)rhodanine (2,4-DHBR). The study revealed that the first five reagents have no advantage over 5-(4-dimethylaminobenzylidene)rhodanine in the determination of silver(I) and gold(III). However, the colour reactions of 2,4-DHBR are more sensitive in basic media. Therefore, 2,4-DHBR was selected for further studies.

Characteristics of 2,4-DHBR

Assuming the reagent to be H_3L, five species are involved in the acid dissociation behaviour. The equilibria between these species can be written as

$$H_4L^+ \overset{K_1}{\rightleftharpoons} H_3L \overset{K_2}{\rightleftharpoons} H_2L^- \overset{K_3}{\rightleftharpoons} HL^{2-} \overset{K_4}{\rightleftharpoons} L^{3-}$$

where H_4L^+ is

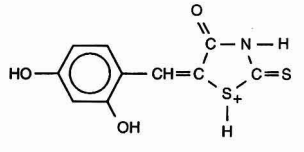

The respective ionization constants were determined in ethanol–water (1 + 1), maintaining the ionic strength at 0.2 with potassium nitrate, by spectrophotometric[32] and potentiometric[33] methods (Table 1). K_1, K_2, K_3 and K_4 are assigned to the deprotonation of SH, NH, *p*-OH and *o*-OH, respectively.

Fig. 1 shows the influence of pH on the absorption spectra of the reagent. The spectra reveal the presence of an absorption band, in acidic medium, with a wavelength maximum at 413 nm, which shows a bathochromic shift to 460 and 512 nm in slightly and strongly basic media, respectively.

Choice of Surfactant

The effect of some surfactants (cationic, anionic and non-ionic) and protective colloids on the spectral characteristics of the binary silver– and gold–2,4-DHBR chelates was studied. Surfactants were used at concentrations above their critical micellization concentration (c.m.c.). The results are given in Table 2. Maximum enhancement of the absorbance of the chelates is obtained in the presence of cationic surfactants. CTAB and CPB are the optimum sensitizers for the colour reactions of silver and gold, respectively.

Absorption Spectra

The absorption spectra of the binary and sensitized silver– and gold–2,4-DHBR chelates, along with their reagent blank in the presence of surfactants, are shown in Fig. 2. All the spectral curves were recorded at pH 10. The binary chelates have absorption maxima at 557 and 560 nm, respectively (curves C and E). Addition of CTAB to the silver complex cause a marked enhancement of the absorbance with a hypsochromic shift of 10 nm (curve D). Moreover, in the presence of CPB, the absorbance of the gold complex is more than doubled (curve F).

Table 1 Determination of the ionization constants of 2,4-DHBR

Method	pK_1	pK_2	pK_3	pK_4
Potentiometric	2.32	6.77	9.05	10.85
Spectrophotometric	—	6.87	9.08	10.81

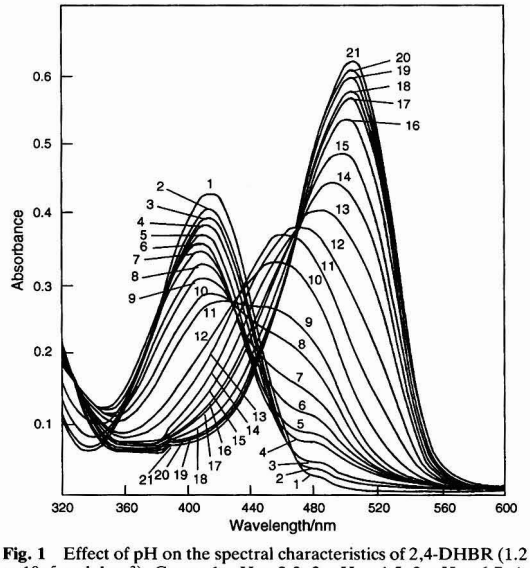

Fig. 1 Effect of pH on the spectral characteristics of 2,4-DHBR (1.2 × 10^{-5} mol dm^{-3}). Curve: 1, pH = 2.3; 2, pH = 4.5; 3, pH = 6.7; 4, pH = 7.0; 5, pH = 7.35; 6, pH = 7.75; 7, pH = 8.1; 8, pH = 8.25; 9, pH = 8.45; 10, pH = 8.81; 11, pH = 9.25; 12, pH = 9.45; 13, pH = 10.0; 14, pH = 10.55; 15, pH = 10.8; 16, pH = 11.1; 17, pH = 11.29; 18, pH = 11.55; 19, pH = 12.1; 20, pH = 12.5; and 21, pH = 12.7.

Optimum Experimental Conditions

The influence of pH on the absorbance of the sensitized silver– and gold–2,4-DHBR complexes was studied over the pH range 2–11. The pH was adjusted to the desired value using dilute nitric acid or sodium hydroxide solution. Maximum and constant absorbances of the complexes were obtained in the pH ranges 9.2–10.6 and 9.3–10.8, respectively. In the optimum pH ranges, no differences in absorbance were noticed when borax buffer was used. Consequently, pH 10 adjusted with borax buffer was adopted in the procedures.

The effect of reagent concentration was investigated, at the optimum pH, by measuring the absorbance of a solution containing 0.85 or 1.72 ppm of silver or gold, 2×10^{-3} mol dm^{-3} of surfactant and various amounts of 2,4-DHBR ranging between 2×10^{-5} and 4×10^{-4} mol dm^{-3}, at 547 or 558 nm, respectively. Full colour development was obtained in the presence of $\geqslant 6 \times 10^{-5}$ and $\geqslant 8 \times 10^{-5}$ mol dm^{-3} of reagent, respectively. In the procedures, 0.5 cm^3 of reagent (1×10^{-4} mol dm^{-3}) was utilized.

The function of surfactants in the colour reactions was studied. The binary silver chelate was solubilized in the presence of $\geqslant 2.4 \times 10^{-4}$ mol dm^{-3} of CTAB and the corresponding CPB concentration for the gold complex was $\geqslant 3.2 \times 10^{-4}$ mol dm^{-3}. Moreover, the absorbance of the sensitized complexes was maximum for CTAB and CPB concentrations of $\geqslant 4 \times 10^{-4}$ and $\geqslant 6.2 \times 10^{-4}$ mol dm^{-3}, respectively.

It is apparent that sensitization of the colour reactions occurs at surfactant concentrations well below their c.m.c.s. The c.m.c.s of CTAB and CPB have been reported as 9.5×10^{-4} and 1.02×10^{-3} mol dm^{-3}, respectively.[34] Consequently, the surfactants interact with the binary chelates to form true ternary complexes.[35]

The ternary complex colours are instantaneously established. Moreover, the absorbance of the silver complex is stable for more than 3 days, whereas the corresponding gold complex is stable for 2 h, after which the stability slightly decreases with time.

Stoichiometry of the Complexes

The molar ratio and continuous variation methods were used to determine the metal-to-reagent ratio in the complexes at pH 10. The study revealed that each metal ion forms two complexes, depending on 2,4-DHBR concentration (Figs. 3 and 4). The complexes of ratios 1 : 1 and 1 : 2 (Ag : 2,4-DHBR) have absorption maxima at 560 and 547 nm, respectively, whereas the corresponding 1 : 2 and 1 : 3 (Au : reagent) complexes absorb at 585 and 558 nm.

The metal complex-to-surfactant ratios in the ternary complexes were determined in an analogous study by the

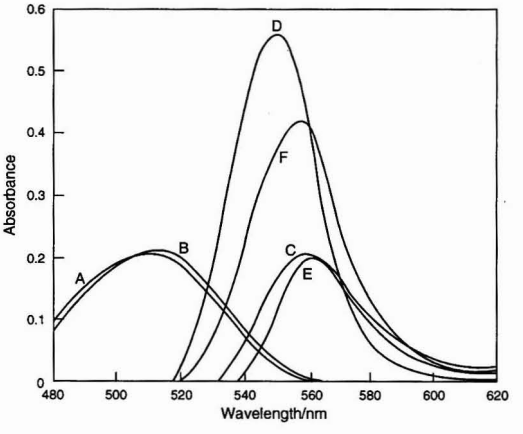

Fig. 2 Absorption spectra of silver and gold binary and ternary complexes and their reagent blank. [Ag] = 1.4×10^{-5} mol dm^{-3} (7.8×10^{-6} mol dm^{-3} for the ternary complex), [Au] = 4.7×10^{-6} mol dm^{-3}, [2,4-DHBR] = 1×10^{-4} mol dm^{-3} (7.2×10^{-6} mol dm^{-3} for curves A and B) and [CTAB] = [CPB] = 2×10^{-3} mol dm^{-3} at pH 10. Curve A, 2,4-DHBR *versus* buffer; B, 2,4-DHBR + surfactant *versus* blank; C, silver chelate in aqueous medium; D, sensitized silver complex; E, gold chelate in aqueous medium; and F, sensitized gold complex.

Table 2 Influence of some surfactants and protective colloids on the spectral characteristics of silver– and gold–2,4-DHBR chelates. Conditions: [Ag$^+$] = 7.87×10^{-6} mol dm^{-3}; [Au^{3+}] = 8.12×10^{-6} mol dm^{-3}; [2,4-DHBR] = 1×10^{-4} mol dm^{-3}; [surfactant] = 2×10^{-3} mol dm^{-3} (0.4% for non–ionic surfactants); protective colloid, 0.2% m/v; pH = 10; 1 cm cells

Surfactant or protective colloid*	Type	Ag–2,4-DHBR chelate			Au–2,4-DHBR chelate		
		$\lambda_{max.}$/nm	Absorbance	$\varepsilon \times 10^{-4}$/dm^3 mol^{-1} cm^{-1}	$\lambda_{max.}$/nm	Absorbance	$\varepsilon \times 10^{-4}$/dm^3 mol^{-1} cm^{-1}
None	—	557	0.117	1.49	560	0.343	4.22
CTAB	Cationic	547	0.559	7.11	553	0.650	8.00
CPB	Cationic	550	0.497	6.32	558	0.686	8.45
CPC	Cationic	560	0.518	6.57	558	0.627	7.72
Zephiramine	Cationic	550	0.461	5.86	558	0.459	5.65
Triton X-100	Non-ionic	545	0.140	1.78	555	0.263	3.24
Emulsifier S	Non-ionic	558	0.114	1.45	545	0.252	3.10
Tween 20	Non-ionic	563	0.093	1.18	555	0.347	4.27
Tween 40	Non-ionic	550	0.124	1.58	550	0.213	2.62
Tween 60	Non-ionic	560	0.103	1.31	555	0.213	2.62
Tween 80	Non-ionic	560	0.109	1.39	552	0.235	2.89
SLS	Anionic	542	0.060	0.71	545	0.196	2.41
SAS	Anionic	567	0.052	0.66	550	0.179	2.20
PVP	Protective colloidal	558	0.067	0.85	555	0.414	5.10
PVA	Protective colloidal	555	0.078	0.99	555	0.206	2.54
Gelatine	Protective colloidal	565	0.098	1.25	545	0.330	4.06

* CTAB, cetyltrimethylammonium bromide; CPB, cetylpyridinium bromide; CPC, cetylpyridinium chloride; zephiramine, benzyldimethyltetradecylammonium chloride; Triton X-100, polyoxyethylene-*p*-*tert*-octylphenol; Tween 40, polyoxyethylene sorbitan monopalmitate; Tween 60, polyoxyethylene sorbitan monostearate; Tween 80, polyoxyethylene sorbitan monooleate; SLS, sodium lauryl sulfate; SAS, sodium alkylbenzene sulfonate; PVP, polyvinylpyrrolidone; PVA, poly(vinyl alcohol).

molar ratio method, by increasing the CTAB or CPB concentration whilst maintaining a constant concentration of 1:1(2) or 1:2(3) silver- or gold-2,4-DHBR complex. The study confirmed the formation of 1:1:1 and 1:2:3 (Ag–2,4-DHBR–CTAB) and 1:2:3 and 1:3:4 (Au–2,4-DHBR–CPB) complexes.

Calibration and Precision

The proposed methods adhere to Beer's law over the concentration ranges 0.13–1.83 and 0.16–2.24 ppm of silver and gold at 547 and 558 nm, respectively. The corresponding molar absorptivities, as determined by a least-squares fit for 15 results each, are 7.11×10^4 and 8.45×10^4 dm^3 mol^{-1} cm^{-1}, respectively. Sandell's sensitivities are 0.0015 μg cm^{-2} and 0.0023 μg cm^{-2}, respectively.

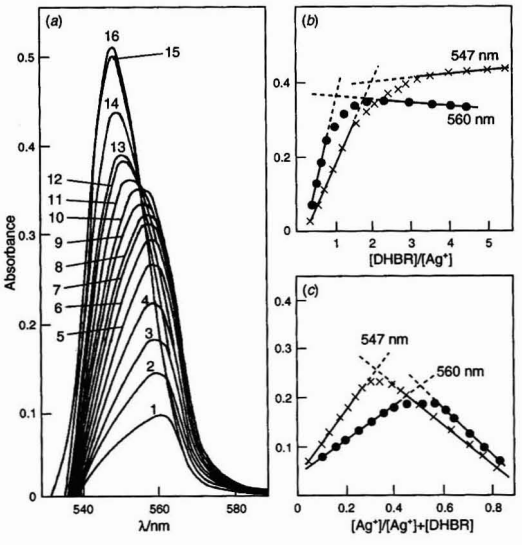

Fig. 3 Influence of 2,4-DHBR concentration on the formation of silver ternary complexes. (*a*) Spectral curves of the complexes; (*b*) molar ratio graphs; (*c*) Job's continuous variation graph.

Effect of Co-existing Ions

The influence of foreign ions on the determination of silver and gold was examined using the recommended procedures. The tolerance limit was taken as the ratio of foreign ion to that being determined that causes a ±2% error in the absorbance value.

Several metal ions interfered with the determination of silver. Consequently, some masking agents were utilized to improve the selectivity of the developed method. The results obtained are given in Table 3. However, halides and cyanide interfered.

Common masking agents slightly improved the tolerance limits for foreign ions in the determination of gold (Table 3). Thus, the Mg–EDTA complex (log β = 8.6)[36] was prepared and tested as a masking agent for interfering metal ions. The study was conducted by adjusting the pH of Mg–EDTA solution to 5.3 to facilitate the replacement reaction. The masking solution was added to an aliquot containing gold(III) plus the foreign ion. After 2 min, the reagent and surfactant

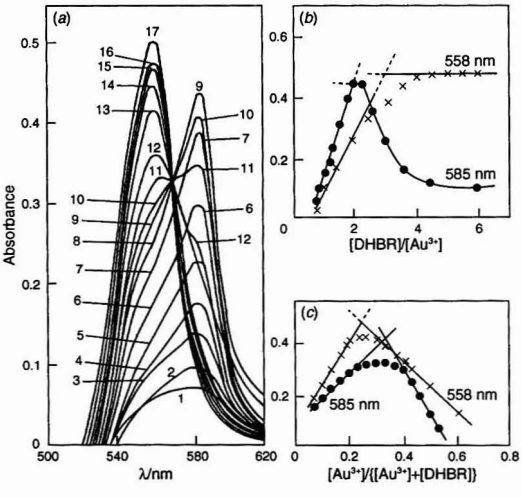

Fig. 4 Influence of 2,4-DHBR concentration on the formation of gold ternary complexes. (*a*) Spectral curve of the complexes; (*b*) molar ratio graph; (*c*) Job's continuous variation graph.

Table 3 Effect of foreign ions on the determination of silver(I) and gold(III) as the ternary complexes. $[Ag^+] = 4.8 \times 10^{-6}$ mol dm^{-3}; $[Au^{3+}] = 4.4 \times 10^{-6}$ mol dm^{-3}

Ternary silver complex method		Ternary gold complex method	
Foreign ion*	Tolerance limit ([ion]/[Ag])	Foreign ion	Tolerance limit ([ion]/Au])
H_2O_2, tartrate, citrate, F^-	8000	Tartrate, citrate, malonate, Cl^-	10000
Ba^{2+}, Ca^{2+}, Co^{2+} (b), Mg^{2+}, Mn^{2+}, Ni^{2+}, Zn^{2+} (b)	5000	Ba^{2+}, Ca^{2+}, Mg^{2+}, F^-, Br^-, I^-	5000
Cd^{2+} (b), Cu^{2+} (b), Mo^{6+}, W^{6+}	1000	$NH_2OH{\cdot}HCl$, $NH_2NH_2{\cdot}H_2SO_4$	3000
Sn^{2+} (a), Ti^{4+} (a), $NH_2OH{\cdot}HCl$	750	EDTA, oxalate, PO_4^{3-}	1000
Al^{3+} (b), Be^{2+} (b), Fe^{3+} (b), Pb^{2+} (b)	500	Al^{3+}, Zn^{2+}, SCN^-	500
Pd^{2+} (c), Pt^{4+} (c)	250	Be^{2+}, Ni^{2+}	300
Bi^{3+}, Cr^{3+}, Hg^{2+} (d), La^{3+}, Pr^{3+}, Sc^{3+}, Sm^{3+}, Th^{4+}, V^{5+}, U^{6+}, Zr^{4+}	150	Bi^{3+}, Cr^{3+}, Fe^{3+}, La^{3+}, Mn^{2+}, Mo^{6+}, Pr^{3+}, Sm^{3+}, Th^{4+}, Ti^{4+}, V^{5+}, U^{6+}	200

* Masking agents: (a) 0.3 ml of 1 mol l^{-1} sodium fluoride; (b) 1.5 cm^3 of EDTA–citrate masking solution (prepared by mixing equal volumes of 0.1 mol dm^{-3} EDTA and 1.2 mol dm^{-3} sodium citrate); (c) 1 cm^3 of 0.25 mol dm^{-3} dimethylglyoxime; (d) 2 ml of 0.1 mol dm^{-3} sodium diethyldithiocarbamate.

solutions were added and the pH was re-adjusted to 10. Up to a 2000-fold molar excess of Ba^{II}, Ca^{II} and Sr^{II}, a 5000-fold molar excess of Cd^{II}, Cu^{II} and Zn^{II}, a 4000-fold molar excess of Mn^{II}, Ni^{II}, Pb^{II} and V^{V}, a 2000-fold molar excess of Be^{II}, Co^{II}, Fe^{III}, La^{III}, Mo^{VI}, Pr^{III} and Sm^{III}, a 1000-fold molar excess of Al^{III}, Bi^{III}, Sc^{III} and Th^{IV} and a 400-fold molar excess of Cr^{III}, U^{IV}, W^{VI} and Zr^{IV} did not interfere in the determination of 4.4×10^{-6} mol l^{-1} of gold(III).

However, Hg^{II}, Pd^{II} and Pt^{IV} seriously interfered. In the presence of 8 mmol l^{-1} sodium diethyldithiocarbamate, however, up to a 250-fold molar excess of Hg^{II} did not interfere, and 10 mmol l^{-1} dimethylglyoxime masked a 300-fold molar excess of Pd^{II} and Pt^{IV}.

Finally, the presence of reducing agents such as hydroxylamine hydrochloride and hydrazine sulfate did not alter the spectral characteristics of the ternary gold complex, whereas traces of an oxidizing agent (hydrogen peroxide) depressed the absorbance of the complex, indicating that excess of 2,4-DHBR reduces the metal ion to the M^{I} form before complexation. This is in agreement with the findings of Borissova *et al.*[16] for the reaction of gold(III) with dimethylaminobenzylidenerhodanine, which is a complex process involving the reduction of gold(III) to gold(I), followed by chelate formation.

Applications

The proposed methods were applied to the determination of silver and gold in a sulfide ore and for the determination of gold in silicate rocks. The ore was obtained from Um-Samuiki, in the south central eastern desert of Egypt, and the rocks from El-Daghbag, in the central eastern desert of Egypt.

The procedures of Jeffery and Hutchison[37] for sample decomposition were followed. Silver[38] and gold[39] were separated from matrix elements with a strong anion exchanger, using column and batch techniques, respectively. The results

Table 4 Comparison with other methods for silver determination

Reagent	pH	$\lambda_{max.}$/nm	$\varepsilon \times 10^{-4}$/ dm^3 mol^{-1} cm^{-1}	Sensitivity/ μg cm^{-2}	Remarks	Ref.
Dithizone	Up to 4 mol dm^{-3} H_2SO_4	462	3.1	0.003	Extraction with carbon tetrachloride	1
4-(2-Quinolylazo)phenol	9.2	530	8.3	0.001	Cu, Co, Fe, Ni and Pd interfere	2
2-[4-Amino-3-(1,2,4-triazolylazo)]naphthol-4-sulfonate	9–11	580	2.1	0.005		3
4,4′-Bis(dimethylamino)thiobenzophenone	3	520	9.3	0.001	Extraction with isoamyl alcohol; noble metals interfere	4
2-Cyano-3-iminodithiobutyrate	4–6	565	1.3	0.008	Hg interferes	5
2′,3′-Dihydroxypyridyl-4′-azobenzene-4-arsonate		535	3.0	0.004	Complex formation in strongly alkaline media	6
p-Diethylaminobenzylidenerhodanine	0.05 mol dm^{-3} HNO_3	490	2.2	0.005	Low solubility of complex	14
p-Dimethylaminobenzylidenerhodanine	0.05 mol dm^{-3} HNO_3	580	2.0	0.005	Long path length cuvettes are recommended	16
5-(4-Hydroxybenzylidene)rhodanine	Citrate buffer	490	1.5	0.007	Cu, Hg and noble metals interfere	17
5-[4-(2-methyl-3-hydroxy-5-hydroxymethyl)pyridylene]rhodanine	8.2	530	1.5	0.007	Pt metals interfere	18
5-(2,4-Dihydroxybenzylidene)rhodanine	10	547	7.1	0.002		This work

Table 5 Comparison with other methods for gold determination

Reagent	pH	$\lambda_{max.}$/nm	$\varepsilon \times 10^{-4}$/ l mol^{-1} cm^{-1}	Sensitivity/ μg cm^{-2}	Remarks	Ref.
Dithizone		420	2.8	0.007	Extraction with $CHCl_3$	7
Methiomeprazine hydrochloride	<6	630	1.3	0.015		8
Dithiodiantipyrylmethane		370	3.5	0.006	Absorbance independent of acidity of medium	9
2,2,2-Trifluoroethyl xanthate	2–11	452	0.1	1.97		10
4-(2-Pyridylazo)resorcinol	2.5	540	8.3	0.002	Extraction procedure; several metal ions interfere	12
4-(2-Thiazolylazo)resorcinol	1.5	520	1.5	0.013	Extraction with xylenol–butanol mixture	13
5-(4-Dimethylaminobenzylidene)rhodanine	0.12 mol dm^{-3} HCl	500	—	—	ε increases with pH but the solubility of the reagent decreases	22
5-(4-Dimethylaminobenzylidene)rhodanine	3	515	3.8	0.005	Mixed aqueous–pyridine system; Pt, Pd and Ag interfere	25
5-(4-Dimethylaminobenzylidene)rhodanine	0.12 mol dm^{-3}	515	3.9	0.005	Extraction with isoamyl acetate	40
5-(Phenyl)methylenerhodanine		422	0.9	0.022	Acetate buffer medium	41
5-(*o*-Hydroxyphenyl)methylenerhodanine		446	0.9	0.022	Acetate buffer medium	41
5-(2-Pyridyl)methylenerhodanine		418	1.1	0.018	Acetate buffer medium	41
5-(6-Methylpyridyl)methylenerhodanine		420	1.1	0.018	Acetate buffer medium	41
5-(2,4-Dihydroxybenzylidene)rhodanine–CPB	10	558	8.5	0.002		This work

obtained for silver and gold in the ore, as determined by the proposed procedures for ten replicates each, were 102.7 ± 0.25 and 1.06 ± 0.01 μg g^{-1}, respectively, whereas the corresponding values obtained using atomic absorption spectrometry were 102.3 and 1.06 μg g^{-1}.

For the determination of gold in two samples of silicate rocks, the results obtained by neutron activation analysis were 0.8 and 1.1 μg g^{-1} and the corresponding values obtained with the proposed procedure were 0.82 ± 0.02 and 1.14 ± 0.04 μg g^{-1} for ten replicates each.

Conclusion

Tables 4 and 5 compare the sensitivities, solubilities and other relevent properties of the proposed methods and some of the best reagents for silver and gold and some of the best rhodanine derivatives. The proposed methods have the advantage of being simple, reproducible, selective and more sensitive than many other methods. Procedures for silver determination with 4-(2-quinolylazo)phenol[2] and 4,4′-bis-(dimethylamino)thiobenzophenone[4] are slightly more sensitive. However, the selectivities of these methods are poorer than that of the proposed method (Table 4).

References

1 Schweitzer, G. K., and Dyer, F. F., *Anal. Chim. Acta*, 1960, **22**, 172.
2 Barua, S., Garg, B. S., Singh, R. P., and Singh, I., *Analyst*, 1980, **105**, 996.
3 Mukherjee, S., Garg, B. S., and Singh, R. P., *Chem. Anal. (Warsaw)*, 1984, **29**, 245.
4 Cheng, K. L., *Mikrochim. Acta*, 1967, 820.
5 Muraoka, M., Yamamoto, T., and Takeshima, T., *Analyst*, 1979, **104**, 87.
6 Verma, Y. S., Singh, I., Garg, B. S., and Singh, R. P., *Microchem. J.*, 1984, **29**, 326.
7 Titley, A. W., *Analyst*, 1962, **87**, 349.
8 Gowda, H. S., Padmaji, K. A., and Thimmaiah, K. N., *Analyst.*, 1981, **106**, 198.
9 Dolgorev, A. V., and Lysak, Ya. G., *Zh. Anal. Khim.*, 1974, **29**, 1766.
10 Hussain, M. F., Bansal, R. K., Puri, B. K., and Satake, M., *Analyst*, 1984, **109**, 1151.
11 Singh, I., Kadyan, P. S., Garg, B. S., and Barua, S., *Bull. Chem. Soc. Jpn.*, 1989, **62**, 1316.
12 Nagarkar, S. G., and Eshwar, M. C., *Anal. Chim. Acta*, 1976, **82**, 435.
13 Subrahmanyam, B., and Eshwar, M. C., *Anal. Chim. Acta*, 1976, **82**, 435.
14 Sandell, E. B., and Neumayer, J. J., *Anal. Chem.*, 1951, **23**, 1863.
15 Stephen, W. I., and Townshend, A., *J. Chem. Soc.*, 1965, 3738.
16 Borissova, R., Koeva, M., and Topalova, E., *Talanta*, 1975, **22**, 791.
17 Tanaka, Y., Daito, Y., Oda, J., and Omomri, M., *Bunseki Kagaku*, 1980, **29**, 381.
18 Godoy, R. E., and Guiram, P. A., *Analyst*, 1986, **111**, 1297.
19 Mizuike, A., *Talanta*, 1962, **9**, 948.
20 Weiss, H. V., and Lai, M. G., *Anal. Chim. Acta*, 1963, **28**, 242.
21 Mizuike, A., Iida, Y., Yamada, K., and Hirano, S., *Anal. Chim. Acta*, 1965, **32**, 428.
22 Borissova, R., *Talanta*, 1975, **22**, 797.
23 Gur'eva, R. F., Trutneva, L. M., and Savvin, S. B., *Zh. Anal. Khim.*, 1978, **33**, 632.
24 Stephen, W. I., and Townshend, A., *Anal. Chim. Acta*, 1965, **33**, 257.
25 Lichtenstein, I. E., *Anal. Chem.*, 1975, **47**, 465.
26 Hinze, W. L., in *Solution Chemistry of Surfactants*, ed. Mittal, K. L., Plenum Press, New York, 1979, p. 79.
27 Hinze, W. L., Singh, H. N., Baba, Y., and Harvey, N. G., *Trends Anal. Chem.*, 1984, **3**, 193.
28 Ohshita, K., Wada, H., and Nakagawa, G., *Anal. Chim. Acta*, 1986, **182**, 157.
29 Alvarez-Coque, M. C. G., Camanas, R. M. V., Vaya, M. C. M., Ramos, G. R., and Fernandez, C. M., *Talanta*, 1986, **33**, 697.
30 Matouskova, E., Nemcova, I., and Suk, V., *Chem. Zvesti*, 1981, **35**, 501.
31 Julian, P. L., and Strugis, B. M., *J. Am. Chem. Soc.*, 1935, **57**, 1126.
32 Rossotti, H., *The Study of Ionic Equilibria—An Introduction*, Longman, London, 1978.
33 Inczedy, J., *Analytical Applications of Complex Equilibria*, Ellis Horwood, Chichester, 1976, pp. 89–101.
34 Rosen, M. J., *Surfactants and Interfacial Phenomena*, Wiley, New York, 1978, p. 165.
35 Sanz-Medel, A., Alonso, J. I. G., and Gonzalez, E. B., *Anal. Chem.*, 1985, **57**, 1681.
36 Schwarzenbach, G., and Ackermann, H., *Helv. Chim. Acta*, 1948, **31**, 1029.
37 Jeffery, P. G., and Hutchison, D., in *Chemical Methods of Rock Analysis*, ed. Belcher, R., and Freiser, H., Pergamon Press, Oxford, 3rd edn., 1981, pp. 304–308.
38 Chanao, T. T., Fishman, M. J., and Ball, J. W., *Anal. Chim. Acta*, 1969, **47**, 89.
39 Mizuike, A., *Anal. Chim. Acta*, 1965, **32**, 428.
40 Cotton, T. M., and Woolf, A. A., *Anal. Chim. Acta*, 1960, **22**, 192.
41 Alfonso, G. G., and Ariza, J. L. G., *Microchem. J.*, 1981, **26**, 574.

Paper 4/03293D
Received June 3, 1994
Accepted June 23, 1994

Determination of Trace Amounts of Nickel by Chelating Ion Exchange and On-line Enrichment in Flow Injection Spectrophotometry

Rajesh Purohit* **and Surekha Devi†**

Department of Chemistry, Faculty of Science, M.S. University of Baroda, Baroda 390 002, India

Trace amounts of nickel were determined after preconcentration at batch levels and by flow injection using chelating resins. Various experimental conditions were optimized for the preconcentration procedure. The batch procedure for preconcentration was highly dependent on pH. In the continuous-flow method, nickel was eluted from the resin with 20 µl of 2 mol l^{-1} hydrochloric acid and was determined at 445 nm as the nickel–dimethylglyoxime complex. Column chromatographic separations of copper and nickel did not show any cross-contamination. The flow method was also used for the determination of nickel in various brands of chocolate and vegetable oil after preconcentration

Keywords: Nickel; preconcentration; separation; flow system; chocolate and vegetable oil

Introduction

The enrichment of metal ions by ion exchange continues to be the most popular method for the recovery of trace levels of metal ions. Flow injection (FI) has contributed to the development of several semi-automated methods for this purpose owing to its numerous advantages over conventional methods.[1–5] On-line preconcentration has mainly been carried out on activated alumina,[6] 8-hydroxyquinoline[3,7,8] and its derivatives[5] immobilized on silica gel or glass, Chelex 100,[1,2] resin 122[9] and tri(pyridylmethyl)ethylenediamine.[10]

Chelating resins containing 8-hydroxyquinoline have been known for the last 80 years but have limitations such as low exchange capacity, low chemical stability and slow exchange. Attempts have been made to overcome these limitations[11,12] and we have reported the general properties and synthetic routes for these resins in previous papers.[13,14] The potential of these chelating resins in the separation and determination of copper,[13] zinc[14] and lead[15] has already been reported.

The separation and determination of nickel, an essential trace element, by a continuous-flow method was first reported by Kuroda and Mochizuki[16] in 1981. To date, about 25 reports have appeared concerning the determination of nickel by FI methods but only a few involve determination after preconcentration.[17–20] In the present paper the use of novel ion exchangers for the determination of nickel at nanogram levels in chocolate and vegetable oil is described. The results obtained by both conventional batch and continuous-flow procedures are compared.

* Permanent address: Gujarat Jalseva Training Institute, Gandhinagar 382 015, India.

† To whom correspondence should be addressed.

Experimental

Analytical-reagent grade chemicals and high purity de-ionized water were used to prepare the metal ion solutions. Working solutions of nickel were prepared by appropriate dilution of a stock standard nickel solution. Acetate buffers of different pH were prepared from 0.2 mol l^{-1} sodium acetate and acetic acid. Dimethylglyoxime (DMG) solution (0.5% m/v) was prepared as required.

Synthesis of Chelating Resins

The synthesis and physico-chemical properties of resins containing 8-hydroxyquinoline (8HOQ), and resorcinol (R) or hydroquinone (HQ), and formaldehyde (F), 2-furaldehyde (Fu) and benzaldehyde (B) as cross-linking agents, have been described elsewhere.[13,14] The physico-chemical properties of the resins used are presented in Table 1.

Preconcentration of Nickel

The resins were used for batch and column chromatographic studies of nickel exchange. Optimization of the pH for preconcentration at the batch level was carried out according to a literature procedure,[21] using 0.2 mol l^{-1} acetate buffer of pH 2–8. Nickel was determined complexometrically in the supernatant solution and also by eluting the chelated metal from the resin with 0.1–2 mol l^{-1} hydrochloric acid. From the exchange kinetics, the value of $t_{1/2}$ (time required for 50% exchange of nickel) for the batch procedure was determined.[21]

The rate constant and activation energy for the exchange of nickel(II) were calculated by means of kinetic studies at 30, 35, 40 and 45 °C. The mode of diffusion of nickel through the solution towards the resin was determined by the interruption test[21,22] and by the method reported by Native *et al.*[23] During the interruption test, resin beads were interrupted by removing them from the solution for a short period of time (10 min) and then re-immersing them in the solution. From the nature of the graph of percentage exchange *versus* time, the mode of diffusion of the ions was determined as described by Helfferich.[21]

Various eluents such as acids, alkalis, electrolytes and complexing agents of different strengths were tested for the quantitative elution of nickel in batch experiments.

Chromatographic Separations

Chromatographic columns of 10–18 cm length and 0.7 cm id were prepared from the following resins: 8HOQFR (8-hydroxyquinoline–formaldehyde–resorcinol); 8HOQFHQ (8-hydroxyquinoline–formaldehyde–hydroquinone); 8HOQFuR (8-hydroxyquinoline–2-furaldehyde–resorcinol);

8HOQFuHQ (8-hydroxyquinoline–2-furaldehyde–hydroquinone); and 8HOQBR (8-hydroxyquinoline–benzaldehyde–resorcinol). The breakthrough and column capacities and interstitial volumes were determined according to literature methods.[21,24]

Binary mixtures of copper and nickel (1 + 1) were passed through the columns at the optimum pH, at a flow rate of 1 ml min^{-1} followed by washing of the columns with de-ionized water. The chelated metal was eluted with the appropriate eluting reagent and fractions of the column effluents were analysed for both metal ions.

On-line Preconcentration of Nickel

A continuous-flow manifold for the preconcentration of nickel at nanogram levels was constructed as shown in Fig. 1 using 4 × 0.2 cm microcolumns, a Tokyo Rikakikai microtube peristaltic pump, a Rheodyne RH 5020 injection valve, 0.5 mm id poly(tetrafluoroethylene) tubing and an ultraviolet–visible spectrophotometer with a 20 μl flow cell as the detector. The absorbance–time response was recorded on an *x–t* chart recorder at 445 nm. The conditions, such as variation in pH, column length, flow rate and metal and reagent concentration, were optimized for the preconcentration and determination of nickel. The chelated nickel was eluted from the column by injecting 20 μl of 2 mol l^{-1} hydrochloric acid followed by acetate buffer solution of pH 8 to avoid carryover of the sample to the next determination.

Determination of Nickel in Chocolate and Vegetable Oil

The determination of nickel in various chocolates and vegetable oils was carried out by using a dry digestion procedure. Samples (1, 5 and 10 g) of different brands of chocolate and vegetable oil were heated to 800 °C in a furnace. The residue was dissolved in 5 ml of 2 mol l^{-1} hydrochloric acid. The insoluble matter was filtered off and the filtrate was made up to 25 ml with de-ionized water.

A 5 ml aliquot of the solution was used for the preconcentration and determination of nickel as described earlier. The results obtained were compared with those obtained by atomic absorption spectrometry (AAS).

Results and Discussion

The physico-chemical properties of the resins under study are given in Table 1. The sodium exchange capacities and the rate of exchange were found to be lower and slower for resins with 2-furaldehyde and benzaldehyde as cross-linking agents. The exchange rate was faster for resins containing resorcinol than for those containing hydroquinone. This may be due to the difference in the complexing capacities of the two monomers. Maximum exchange of nickel was found to occur at pH 6–6.5, irrespective of the nature of the resin (Fig. 2). However, the exchange capacity and distribution coefficient were found to be functions of the type of resin. The selectivity order of the resins for nickel, based on the exchange capacity or distribution coefficient, is: 8HOQFHQ > 8HOQFR > 8HOQFuHQ > 8HOQFuR > 8HOQBR. Decreased selectivity was observed for resins containing cyclic cross-linking agents.

The results of the effect of the nickel ion concentration on the exchange capacity, presented in Fig. 3, indicate that the exchange of nickel is a concentration-dependent phenomenon. All the resins, irrespective of their structure, show saturation for exchange at a metal concentration of 0.1 mol l^{-1}.

In the study of the diffusion of nickel ions by means of the interruption test,[21,22] it was observed that the exchange of nickel is a particle diffusion process. In the interruption test, the interruption allows time for the concentration gradients in the beads to level out. Therefore, in a particle diffusion controlled process the exchange rate increases immediately after interruption. In film diffusion, no concentration gradient exists in the beads and the rate depends on the concentration difference across the film and, hence, interruption does not affect the exchange rate. The results obtained by the method of Native *et al.*[23] also support the particle diffusion process for the exchange of nickel.

Thermodynamics and Rate of Exchange

The exchange rates for the uptake of nickel by the resins were determined at 30, 35, 40 and 45 °C. The rate constant, k, for initial exchange was calculated using the equation for a first-order reaction

$$-\frac{dc}{dt} = kc \text{ and } -\log(a-f) = \frac{kt}{2.303}$$

where a is the initial concentration of nickel ion, c is the concentration of nickel at time t, and f is the fraction of ions exchanged on the resin. The plots of $-\log(a-f)$ *versus* time (t) were observed to be non-linear and did not pass through the origin. Hence, the rate constant was calculated from the initial rate of the reaction by using the mirror method,[25] in which a mirror, when oriented normal to the curve, shows a reflection which is a smooth continuation of the curve. A tangent is then drawn perpendicular to the normal and k is calculated from the slope of the line. The activation energy

Table 1 Physico-chemical properties of the resins*

Property	8HOQFR	8HOQFHQ	8HOQFuR	8HOQFuHQ	8HOQBR
Moisture content/g g^{-1}	0.03	0.08	0.64	1.98	1.51
True density/g ml^{-1}	1.40	1.50	1.25	1.16	1.18
Void volume/ml g^{-1}	0.78	0.66	0.53	0.49	0.63
Sodium exchange capacity/mmol g^{-1}	4.60	5.00	2.80	3.30	2.60
$t_{1/2}$ for sodium/min	7.00	4.00	10.00	12.00	24.00
Ni^{II} exchange capacity at pH 6/mmol g^{-1}	0.72	0.76	0.59	0.66	0.51
$t_{1/2}$ for nickel exchange/min	3.00	13.00	8.00	90.00	60.00
k_d (distribution coefficient for 0.1 mol l^{-1} nickel at pH 6)	7.33	8.25	6.01	6.84	5.40

* Abbreviations represent resins synthesized using 8-hydroxyquinoline (8HOQ), resorcinol (R), hydroquinone (HQ), formaldehyde (F), 2-furaldehyde (Fu) and benzaldehyde (B).

(ΔE) required for complex formation was determined using the Arrhenius equation

$$k = Ae^{-\Delta E/RT}$$

where R is the gas constant, A is the frequency factor and T is the temperature. From the slope of the plot of log k *versus* $1/T$, the value of ΔE was calculated and is given in Table 2. From the results it was observed that an increase in the exchange rate with temperature results in higher rate constants. It was also observed that the energy required for the formation of the nickel complex is higher than that required for copper,[13] zinc,[14] cadmium[14] and lead.[15]

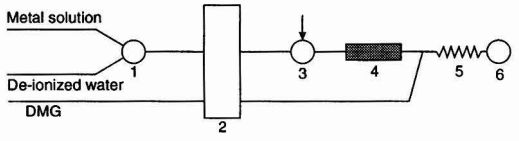

Fig. 1 FI manifold for on-line determination of Ni^{II} using DMG as reagent. 1, Two-way stopcock; 2, peristaltic pump; 3, injection valve; 4, microcolumn containing resin; 5, reaction coil; and 6, detector (ultraviolet–visible spectrophotometer).

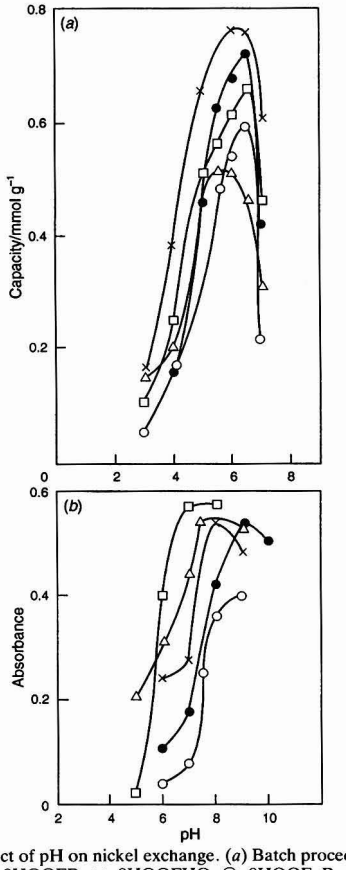

Fig. 2 Effect of pH on nickel exchange. (*a*) Batch procedure; (*b*) FI method. ●, 8HOQFR; ×, 8HOQFHQ; ○, 8HOQFuR; △, 8HOQFuHQ; and □, 8HOQBR.

Elution of Nickel From Resins

Elution of nickel from the resins was carried out with various eluting agents of different strengths. It was found that nickel can be quantitatively eluted with 0.5–1 mol l^{-1} hydrochloric acid; 0.2–1.0 mol l^{-1} sulfuric acid can elute nickel from 8HOQFR, 8HOFuR, 8HOQFHQ and 8HOQBR but not from 8HOQFuHq. Citrate and tartrate were unable to elute nickel from the resins.

Binary Separations

The separation of copper and nickel from binary mixtures containing 400 and 1000 μg ml^{-1} of each metal ion was carried out under the conditions given in Table 3, using columns of the resins under study. The flow rate of the solution through each column was maintained at 1 ml min^{-1}. Chelated nickel and copper were eluted with 0.1 and 3 mol l^{-1} hydrochloric acid, respectively. The column effluents were analysed for both metal ions by using appropriate masking reagents. The results obtained are given in Fig. 4 and Table 4. No cross-contamination was observed during separation.

FI System

A calibration graph for the determination of nickel was constructed by injecting a series of standard nickel ion solutions into the carrier stream of the flow manifold illustrated in Fig. 1, without the microcolumn. The percentage recovery after preconcentration was determined from the calibration graph.

The determination of nickel at nanogram levels was carried out by using the FI manifold shown in Fig. 1. Preconcentration of nickel was achieved by passing 5 ml of 1×10^{-7} mol l^{-1} (50 ng ml^{-1}) nickel solution at a flow rate of 3 ml min^{-1} through microcolumns containing the chelating resins 8HOQFR, 8HOQFHQ, 8HOQFuR, 8HOQFuHQ and 8HOQBR. Continuous monitoring of the column effluent showed quanti-

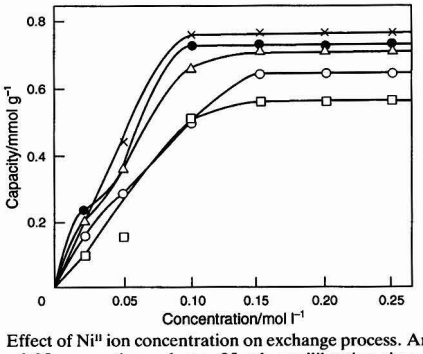

Fig. 3 Effect of Ni^{II} ion concentration on exchange process. Amount of resin, 0.25 g; reaction volume, 25 ml; equilibration time, 24 h. Symbols as in Fig. 2.

Table 2 Rate of exchange and activation energy for nickel

Resin	Rate constant, $k/10^2$ s^{-1} 30 °C	35 °C	40 °C	45 °C	Activation energy, ΔE/J mol^{-1}
8HOQFR	3.2	3.7	3.8	6.5	3699.3
8HOQFHQ	3.1	3.4	3.6	5.2	3578.1
8HOQFuR	1.6	2.3	2.5	3.6	4063.0
8HOQFuHQ	2.6	2.5	3.2	3.3	1354.3
8HOQBR	2.0	2.3	2.8	3.9	3941.7

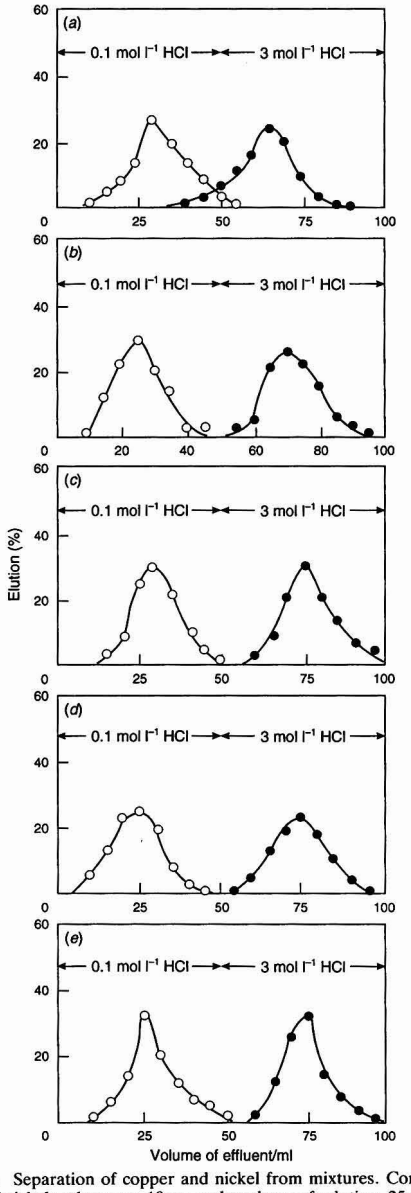

Fig. 4 Separation of copper and nickel from mixtures. Concentration of nickel and copper, 10 mg each; volume of solution, 25 ml; flow rate, 1 ml min^{-1}. ○, Nickel; and ●, copper. (*a*) 8HOQFR; (*b*) 8HOQFHQ; (*c*) 8HOQFuR; (*d*) 8HOQFuHQ; and (*e*) 8HOQBR.

tative uptake of nickel by the resin in the column. After washing the columns with acetate buffer of pH 7.5–9.0, the chelated nickel was eluted by injecting 20 μl of 2.0 mol l^{-1} hydrochloric acid. The dispersion was calculated by nebulizing 5 μg ml^{-1} of nickel solution and injecting 20 μl of the solution into the flow manifold, with and without the microcolumn. The introduction of the microcolumn did not affect the peak height. The FI peak height, in comparison with the steady-state response, gave a dispersion coefficient of 2.1 for the manifold. The dispersion of the system was observed to be dependent on the volume injected and increased with a decrease in the volume injected. On elution of nickel, sharp peaks were obtained indicating faster exchange kinetics.

In comparison with the conventional spectrophotometric analysis, the proposed FI method was observed to be highly sensitive, with detection limits at the ng ml^{-1} level.

Optimization of pH for the preconcentration of nickel was carried out by passing metal ion solutions of pH 2–10 through the microcolumns containing the synthesized resins. The chelated metal was eluted by injecting 20 μl of 2.0 mol l^{-1} hydrochloric acid. From the results presented in Fig. 2, it was found that preconcentration of nickel by the FI system mainly takes place in the alkaline region, unlike the batch procedure, and is less dependent on the pH.

Optimization of the column length for preconcentration was carried out by using microcolumns of 2, 3, 4 and 6 cm length and 0.2 cm id. A flow rate of 3 ml min^{-1} was maintained throughout. From the results obtained it was observed that 4

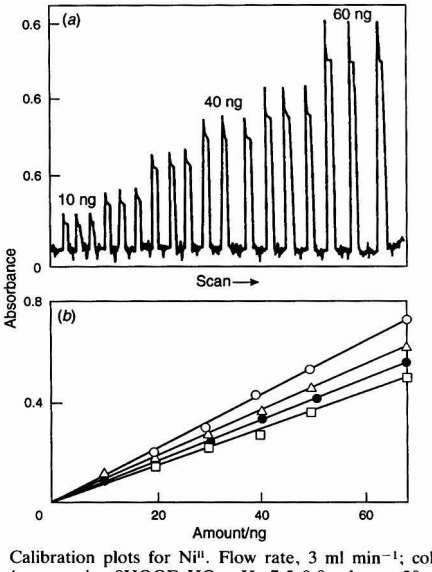

Fig. 5 Calibration plots for Ni^{II}. Flow rate, 3 ml min^{-1}; column length, 4 cm; resin, 8HOQFuHQ; pH, 7.5–9.0; eluent, 20 μl of 2 mol l^{-1} HCl. Symbols as in Fig. 2.

Table 3 Column characteristics

Property	8HOQFR	8HOQFHQ	8HOQFuR	8HOQFuHQ	8HOQBR
Column length/cm	17.50	17.50	9.00	10.50	9.30
Interstitial volume/ml	9.20	9.80	4.80	5.20	4.60
Breakthrough capacity/mequiv g^{-1}	0.10	0.09	0.09	0.08	0.09
Total capacity/mequiv g^{-1}	0.50	0.62	0.39	0.43	0.48
Degree of utilization*	0.20	0.14	0.23	0.19	0.19

* Breakthrough capacity/total capacity.

Table 4 Efficiency of recovery of nickel and copper from binary mixtures

	Amount of Ni^{2+}/mg			Amount of Cu^{2+}/mg		
Resin	Taken	Recovered*	Recovery (%)	Taken	Recovered*	Recovery (%)
8HOQFR	4.0	3.99 ± 0.021	99.8	4.0	4.01 ± 0.021	100.2
8HOQFHQ	4.0	4.03 ± 0.024	100.8	4.0	4.06 ± 0.028	101.5
8HOQFuR	4.0	4.01 ± 0.021	100.2	4.0	3.97 ± 0.025	99.2
8HOQFuHQ	4.0	3.97 ± 0.023	99.2	4.0	3.91 ± 0.031	97.8
8HOQBR	4.0	3.92 ± 0.028	98.0	4.0	3.99 ± 0.024	99.8
8HOQFR	10.0	9.98 ± 0.030	99.8	10.0	10.02 ± 0.026	100.2
8HOQFHQ	10.0	9.94 ± 0.031	99.4	10.0	9.99 ± 0.020	99.9
8HOQFuR	10.0	10.06 ± 0.030	100.6	10.0	9.99 ± 0.023	99.9
8HOQFuHQ	10.0	9.93 ± 0.029	99.3	10.0	9.93 ± 0.027	99.3
8HOQBR	10.0	9.99 ± 0.025	99.9	10.0	9.96 ± 0.022	99.6

* Values given are the means of five measurements ± standard deviations.

Table 5 Determination of nickel in chocolate and vegetable oil

Sample No.	Name of product	Nickel found by proposed method*/μg g^{-1}	Nickel found by AAS*/ μg g^{-1}
Chocolates—			
1	Cadbury, India	0.5 ± 0.02	0.45 ± 0.018
2	Nestlé, India	7.3 ± 0.02	8.0 ± 0.02
3	Amul, India	2.5 ± 0.03	2.1 ± 0.02
Vegetable oils (ghee)—			
1	Dalda, India	0.0	0.0
2	Sunflower, India	0.0	0.0
3	Madhuram, India	0.0	0.0

* Mean of nine determinations ± standard deviation.

cm long columns are efficient for preconcentration and that columns longer than 6 cm show a high degree of dispersion. The optimum flow rate was found to be 3.0 ml min^{-1}.

Elution of chelated nickel was carried out by injecting 20 μl of various acids of different strengths: 2 mol l^{-1} hydrochloric acid was found to give quantitative elution of nickel from all the resin columns studied. Elution of nickel using 2 mol l^{-1} hydrochloric acid gave a narrow peak of comparable height, indicating that the analyte concentration lies in a relatively narrow eluent range.

A calibration graph for the preconcentration of 5 ml of nickel solutions with concentrations of 10–70 μg ml^{-1} was obtained for each resin after elution of nickel with 20 μl of 2 mol l^{-1} hydrochloric acid. The results were recorded in triplicate as shown in Fig. 5. The regression coefficients were 0.9948, 0.9982, 0.9936, 0.9972 and 0.9926 for 8HOQFR, 8HOQFHQ, 8HOQFuR, 8HOQFuHQ and 8HOQBR, respectively. The lowest detection limit (based on twice the standard deviation of the blank signal) was found to be 10 μg ml^{-1} after preconcentration of 5 ml of solution. The relative standard deviations for $n = 5$ were in the range 0.4–2.8%.

Analysis of Chocolate and Vegetable Oil

The determination of nickel in different brands of chocolate and vegetable oil was carried out as described earlier. The results obtained are given in Table 5. Nickel was not detected in Dalda, Sunflower and Madhurum vegetable oil brands from India.

References

1 Olsen, S., Pessenda, L. C. R., Růžička, J., and Hansen, E. H., *Analyst*, 1983, **108**, 905.
2 Fang, Z., Růžička, J., and Hansen, E. H., *Anal. Chim. Acta*, 1984, **164**, 23.
3 Malamas, F., Bengtsson, M., and Johansson, G., *Anal. Chim. Acta*, 1984, **160**, 1.
4 Hirata, S., Umezaki, Y., and Ikeda, M., *Anal. Chem.*, 1986, **58**, 2602.
5 Devi, S., Khalil, A. J. H., and Townshend, A., *Quim. Anal.*, 1989, **8**, 159.
6 Zhang, Y., Riby, P., Cox, A. G., McLeod, C. W., Date, A. R., and Cheung, Y. Y., *Analyst*, 1988, **113**, 125.
7 Marshall, M. A., and Mottola, H. A., *Anal. Chem.*, 1985, **57**, 729.
8 Hartenstein, S. D., Růžička, J., and Christian, G. D., *Anal. Chem.*, 1985, **57**, 21.
9 Fang, Z., Xu, S., and Zhang, S., *Anal. Chim. Acta*, 1984, **164**, 41.
10 Bengtsson, M., Malamas, F., Torstensson, A., Regnell, O., and Johansson, G., *Mikrochim. Acta*, 1985, **III**, 209.
11 Pennington, L. D., and Williams, M. B., *Ind. Eng. Chem.*, 1956, **51**, 759.
12 Parrish, J. R., and Stevenson, R., *Anal. Chim. Acta*, 1974, **70**, 189.
13 Purohit, R., and Devi, S., *Talanta*, 1991, **38**, 753.
14 Purohit, R., and Devi, S., *Analyst*, 1991, **116**, 825.
15 Purohit, R., and Devi, S., *Anal. Chim. Acta*, 1992, **259**, 53.
16 Kuroda, R., and Mochizuki, T., *Talanta*, 1981, **28**, 389.
17 Chambaz, D., and Haerda, W., *J. Chromatogr.*, 1989, **482**, 335.
18 Cheng, C. J., Akagi, T., and Haraguchi, H., *Bull. Chem. Soc. Jpn.*, 1985, **58**, 3229.
19 Bengtsson, M., and Johansson, G., *Anal. Chim. Acta*, 1984, **158**, 147.
20 Sperling, M., Yin, X., and Welz, B., *J. Anal. At. Spectrom.*, 1991, **6**, 295.
21 Helfferich, F., *Ion Exchange*, McGraw-Hill, New York, 1962, p. 256.
22 Kressman, Y. R. E., and Kitchener, J. A., *Discuss. Faraday Soc.*, 1949, **7**, 90.
23 Native, M., Goldstein, S., and Schmuckler, G., *J. Inorg. Nucl. Chem.*, 1975, **37**, 1951.
24 Inczedy, J., *Analytical Applications of Ion Exchangers*, Pergamon Press, Oxford, 1966.
25 Forst, A. A., and Pearson, R. G., *Kinetics and Mechanism*, Wiley, New York, 1961, p. 46.

Paper 4/01908C
Received March 30, 1994
Accepted September 21, 1994

Use of the Sequential Injection Technique to Determine the Concentrations and Stoichiometries of Trimeprazine and Perphenazine Complexed With Palladium(II) in Hydrochloric Acid

Salah M. Sultan, Fakhr Eldin O. Suliman and Bahruddin B. Saad

Chemistry Department, King Fahd University of Petroleum and Minerals, KFUPM, Box 2026, Dhahran 31261, Saudi Arabia

An automated method for the determination of trimeprazine and perphenazine by complexation with palladium(II) in hydrochloric acid was developed. A sequential injection technique with a flow reversal of 29.4 μl s^{-1} and a measuring cycle of 73 s was used. Trimeprazine in the range 50–400 ppm was determined at pH 4.7 using 5.0×10^{-3} mol l^{-1} palladium(II) solution and monitoring the product spectrophotometrically at 515 nm. Perphenazine in the range 50–500 ppm was determined at pH 4.85 using 2.5×10^{-3} mol l^{-1} palladium(II) solution and monitoring the product at 560 nm. The technique was successfully applied to the determination of reaction stoichiometry. Interferences were studied and the method was found to be suitable for the determination of the two compounds in pharmaceutical preparations.

Keywords: Sequential injection analysis; stoichiometry; trimeprazine; perphenazine; palladium complexation

Introduction

Sequential injection (SI) is a versatile computer-controlled technique introduced recently by Růžička and Marshall[1] with so far only a limited number of publications. In the sequential injection (SI) technique, a selector valve equivalent to the injection valve in flow injection (FI) is used for precisely measured volumes of carrier, sample and reagent solution to be aspirated into a holding coil (HC), which are then propelled by flow reversal into a detector. By this technique, consumption of valuable reagents, drugs, *etc.*, could be minimized by injecting small amounts using the selector valve rather than being pumped continuously as in FI. With the SI technique a number of complicated operations such as dilution, injection of additional reagents, such as acids, and recalibration could all be executed easily and smoothly with the selection valve, which is controlled by a simple computer program. Other advantages of SI can be found elsewhere.[2–4]

In this paper, the SI technique was used for the determination of trimeprazine and perphenazine by spectrophotometry. A coloured complex was formed between the drug and palladium(II), which was monitored at 515 nm for trimeprazine and at 560 nm for perphenazine. It is interesting that both reagents, palladium and the sample (drug) were injected, thus consuming the minimum amount of reagent.

In this work, first, the SI technique was successfully used for the investigation of reaction stoichiometry utilizing the Job's plot method.[5] The SI method was applied by sequentially aspirating the drug solution followed by the palladium(II) solution. A volume of carrier solution was then aspirated. The carrier volume was selected to allow optimum mixing upon flow reversal towards the detector. The palladium(II)-to-drug mole ratio was varied, for the Job's plot analysis, by changing the aspiration timing of equimolar solutions of palladium(II) and the drug into the holding coil. The total volume of the two reagents was held at a constant value of 352.8 μl in each run. The ability of the SI apparatus to vary the volume of a reagent conveniently with millisecond precision is considered a great advantage and a revolution in FI methodology, having the potential to solve many research problems.

The determination of the drugs is based on the complexation reaction of palladium(II) with trimeprazine or perphenazine in hydrochloric acid media, which was extensively investigated and found to be feasible in a specific pH range. Other phenothiazine drugs have been reported to form complexes with palladium(II) of unusual stoichiometry, resulting in doubtful rationalization of the complex structures.[6–13] However, the stability of the complexes formed favoured this method and was found to be more advantageous than previous methods involving oxidation and in which a highly unstable radical product was monitored for quantification.[14–19]

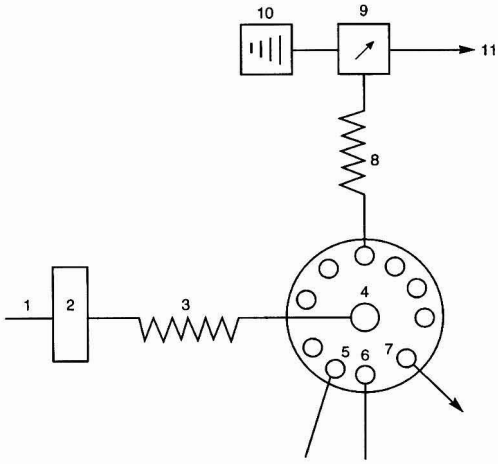

Fig. 1 Typical SI manifold; 1, carrier solution; 2, peristaltic pump; 3, holding coil; 4, selector valve; 5, palladium; 6, drug; 7, wash solution; 8, reaction coil; 9, spectrophotometer; 10, computer and/or recorder; 11, waste.

Experimental

Apparatus

The sequential injection manifold as shown in Fig. 1 was constructed from the following components. (a) Peristaltic pump (C4V, Alitea USA, Medina, WA, USA). (b) A Valco ten-port selector valve (Cheminert; Valco Instruments, Houston, TX, USA) was used to select the flows. Upchurch fittings (Upchurch, Oak Harbor, WA, USA) were used to lock unused ports. (c) The holding coil and the reaction coil tubing and also the tubing connecting the different units were made of PTFE (0.8 mm i.d.). PTFE nuts and ferrules (Upchurch) were used to fit these tubes into the different parts of the apparatus. Pump tubings were Phar Med 1.02 mm i.d. (Upchurch) held on the pump rollers by FI peristaltic pump tubing adapters (Upchurch). (d) A Spectronic Mini-20 spectrophotometer (Milton Roy, Rochester, NY, USA), equipped with a Uvonic Ultramicroflow cell of 20 μl and 1.0 mm pathlength was used. (e) A personal computer (Austin Computer Systems, Austin, TX, USA) working at 33 MHz, and equipped with a 120 Mb hard disk, 1 Mb RAM and VGA graphics, was used to monitor digitally the pump and the valve. The communication between the computer and the external devices was expanded by a general-purpose I/O board [Model ADA-110; Real Time Devices (RTD), State College, PA, USA]. The computer was also used to collect the data; alternatively, the data were recorded with a Model 0555 single-channel strip-chart recorder (Cole Parmer Instrument, Chicago, IL, USA).

A Perkin-Elmer Lambda 5 UV/VIS spectrophotometer equipped with 10.00 mm cells was used for preliminary investigations.

Stock standard solutions (1000 ppm) of the two phenothiazine drugs were prepared by dissolving the appropriate amount of the pure analytical-reagent grade products (May & Baker, supplied by Rhône-Poulenc) in water for trimeprazine tartrate and in dilute hydrochloric acid (1.0×10^{-3} mol l^{-1}) for perphenazine. The phenothiazine working solutions were then prepared by appropriate dilutions.

A stock standard palladium(II) solution of 0.025 mol l^{-1} was prepared by dissolving 0.4430 g of anhydrous palladium(II) chloride (Fluka) in 50 ml of 0.04 mol l^{-1} hydrochloric acid. The mixture was heated at 80 °C in a water-bath until all the palladium(II) chloride solid had dissolved, then cooled to room temperature and diluted to 100 ml with water.

Hydrochloric acid (0.1 mol l^{-1}) was prepared by diluting AnalaR concentrated acid.

Procedure

The steps of the procedure were fed into the computer, with a total analysis time of a single measuring cycle of 73 s. The procedure consists of the following steps. First, the carrier solution is pumped through valve 1, by setting the pump in the forward mode, for 25 s. Then 176.4 μl of 2.55×10^{-3} mol l^{-1} Pd^{II} solution was aspirated into the holding coil *via* valve 5 followed by aspiration of 176.4 μl of the appropriate drug solution into the holding coil *via* valve 6. The sequential aspiration of both the drug and Pd^{II} solutions was achieved by flow reversal. The volumes of the solutions were determined from the time of aspiration and the volumetric flow rate of the pump, which was 29.4 μl s^{-1} in this study. In the Job's plot method, aliquots of the metal (M) and the ligand (L) were mixed so that the total concentration of [M] + [L] remained constant. Therefore, the total volume aspirated was maintained constant at 352.8 μl by adjusting the aspiration times. The volume of each reagent was varied between 14.7 μl (0.5 s) and 338.1 μl (11.5 s). The total time of each measuring cycle was 73 s.

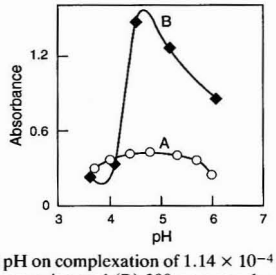

Fig. 2 Effect of pH on complexation of 1.14×10^{-4} mol l^{-1} Pd^{II} with (A) 160 ppm trimeprazine and (B) 300 ppm perphenazine.

Results and Discussion

The nature of the interaction between the palladium(II) and the drugs under investigation was believed to involve protonation of the drug followed by hydrogen bonding between the protonated nitrogen and one of the chlorine atoms on the palladium.[6,13] Complexes of the type ML_2X_2 and MLX_3 have also been reported.[13]

Preliminary investigations during this work revealed that at acidities higher than 1.0×10^{-4} mol l^{-1} HCl, another

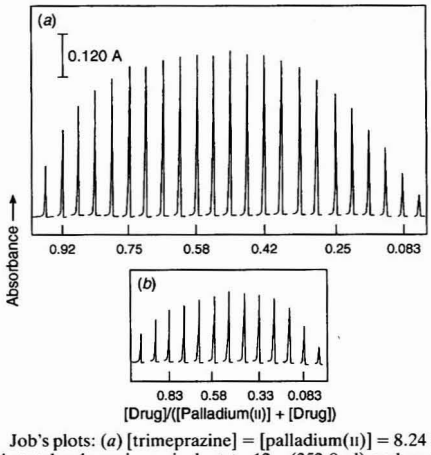

Fig. 3 Job's plots: (*a*) [trimeprazine] = [palladium(II)] = 8.24×10^{-4} mol l^{-1}; total volume is equivalent to 12 s (352.8 μl) and aspiration times were varied in 0.50 s steps; (*b*) [perphenazine] = [palladium(II)] = 5.70×10^{-4} mol l^{-1}; total volume is equivalent to 12 s and aspiration times were varied in 1.00 s steps.

Table 1 Results obtained by the SI method for the determination of 200 ppm of trimeprazine and perphenazine in the presence of some selected compounds

	Recovery ± standard deviation (%)*	
Compound added (ppm)	Trimeprazine	Perphenazine
Starch (2000)	100.14 ± 0.73	99.20 ± 0.52
Glucose (2000)	99.30 ± 0.86	101.50 ± 0.57
$MgSO_4$ (2000)	100.38 ± 0.70	99.80 ± 0.43
Citric acid (2000)	101.42 ± 0.91	99.5 ± 0.67
Sodium benzoate (400)	101.77 ± 0.84	99.8 ± 0.83
Ammonium acetate (400)	99.92 ± 0.96	101.6 ± 0.98

* $n = 6$.

absorbance maximum at a longer wavelength than that of the complex was observed. This could be attributed to dissociation of the complex and the appearance of the oxidized form of the phenothiazine. It was therefore necessary to optimize the chemical conditions prior to the quantitative measurements as outlined below.

Trimeprazine System

The purple complex formed was found to occur instantaneously with a peak maximum at 515 nm and remained stable for more than 2 d.

The effect of acidity on the complex was investigated for 160 ppm of trimeprazine and 1.14×10^{-3} mol l^{-1} palladium(II) between pH 3.51 and 6.0 as in Fig. 2, A. The complex was found to be stable over a wide range of HCl concentration, *i.e*, between pH 4 and 5.5.

The effect of palladium concentration on peak absorbance was studied for 50, 200 and 400 ppm of trimeprazine at pH 4.7 using palladium concentrations in the range 1.0×10^{-4}–6.0×10^{-3} mol l^{-1}. It was observed that the increase in absorbance was not significant beyond 5.5×10^{-3} mol l^{-1} palladium.

Job's plot for this system was studied at pH 4.70, with typical plots as in Fig. 3(*a*). A plot of absorbance *versus* molar fraction of palladium(II) using equimolar solutions of 8.24×10^{-4} mol l^{-1} for palladium(II) and trimeprazine resulted in a stoichiometry of 1 : 1.

A calibration equation of the form $A = 9.0583 \times 10^{-2} + 1.5905 \times 10^{-3} C$, where A is absorbance and C is concentration of trimeprazine in ppm, was obtained for the absorbance *versus* standard solutions of trimeprazine in the range 50–400 ppm, with a correlation coefficient (r^2) of 0.993.

Perphenazine System

The complex formation was fast with a peak maximum at 560 nm and the complex was found to be stable for more than 2 d.

The effect of acidity on peak absorbance was typically represented by Fig. 2, B. It is obvious that optimization to give the maximum peak absorbance might lead to erroneous results being obtained owing to the narrow stability range of pH, unless a suitable buffer is used for this system, in particular in the pH range of 4–6.

The effect of palladium concentration on the peak absorbance resembles that for the above system and has no significant effect beyond 2.5×10^{-3} mol l^{-1} at pH 4.85 for perphenazine in the range 50–400 ppm.

Fig. 3(*b*) is a typical Job's plot for this system, obtained at pH 4.85 using equimolar solutions of 5.70×10^{-4} mol l^{-1} for the drug and palladium. The stoichiometry was always 1 : 1.

The calibration equation $A = 8.5387 \times 10^{-2} + 1.5390 \times 10^{-3}$ C was obtained for the absorbance *versus* standard solutions of perphenazine in the range 50–500 ppm with $r^2 = 0.992$.

System Optimization

The instrument was operated at different flow rates but with a fixed holding coil length of 100 cm and a reaction coil length of 40 cm using 0.80 mm i.d. PTFE tubing. Considering a maximum total volume of palladium and the drug of about 353 μl required to be aspirated into the holding coil in the reversed mode of the pump for 6 s for each reagent, with a total measuring cycle of not much longer than 1 min, a flow rate of 29.4 μl s^{-1} was adjusted by the pump for all cycles.

Analytical Application

The method was applied to the determination of trimeprazine and perphenazine in synthetic samples containing some compounds usually added to pharmaceutical preparations as given in Table 1. From the percentage recovery, starch, glucose, magnesium sulfate and citric acid exhibited no interference even when added at a level ten times higher than the drug concentration. Sodium benzoate and ammonium acetate exhibited no interferences when added at levels up to twice the concentration of the drug.

The determination of trimeprazine and perphenazine in the same batch samples was carried out by the British Pharmacopoeia[20] and the US Pharmacopeia[21] methods. All these trials were deemed to have failed owing to high interferences from the above compounds and unsuitability of application to such low concentrations of the drugs using a titrimetric method. In this respect, the present method is far superior to the official methods. It is superior to the other reported methods[14–19] with respect to stability of the reaction product and specificity. Additionally, the SI technique can easily be automated, thus requiring consumption of considerably less reagents and minimum labour.

Dr. B. Saad is indebted to KFUPM for a post doctoral fellowship and also indebted to Universiti Sains Malaysia for leave of absence. Mr. F. O. Suliman is also indebted to KFUPM for offering a PhD Scholarship. The authors thank Rhône-Poulenc (Dagenham, Essex, UK) for the gift of the drugs.

References

1 Růžička, J., and Marshall, G. D., *Anal. Chim. Acta*, 1990, **237**, 329.
2 Guzman, M., Růžička, J., and Christian, G. D., *Talanta*, 1993, **40**, 81.
3 Růžička, J., *Anal. Chim. Acta*, 1992, **261**, 3.
4 Ivaska, A., and Růžička, J., *Analyst*, 1993, **118**, 885.
5 Job, P., *Ann. Chim.*, 1928, **9**, 113.
6 Pellizzetti, E., *J. Chem. Soc., Dalton Trans.*, 1980, 484.
7 Barbe, J., and Hurwic, J., *Ann. Pharm. Fr.*, 1973, **31**, 227.
8 Geary, W. J., Mason, N. J., Nowell, I. W., and Nixon, L. A., *J. Chem. Soc., Chem. Commun.*, 1980, 1064.
9 Ryan, J. A., *J. Am. Pharm. Assoc.*, 1959, **48**, 240.
10 Duddell, D. A., Goggin, P. L., Goodfellow, R. J., Norton, M. G., and Smith, J. G., *J. Chem. Soc. A*, 1970, 546.
11 Warren, R. J., *J. Pharm. Sci.*, 1966, **55**, 144.
12 Marsau, P., and Griffiths, A., *Acta Crystallogr., Sect. B*, 1973, **29**, 986.
13 Geary, W. J., Mason, N. J., Nowell, I. W., and Nixon, L. A., *J. Chem. Soc., Dalton Trans.*, 1982.
14 Sultan, S. M., *Analyst*, 1991, **116**, 177.
15 Sultan, S. M., *Microchem. J.*, 1991, **44**, 304.
16 Sultan, S. M., *Talanta*, 1993, **40**, 681.
17 Sultan, S. M., and Suliman, F. O., *Anal. Sci.*, 1992, **8**, 841.
18 Sultan, S. M., and Abdennabi, A., *Microchem. J.*, 1993, 48.
19 Sultan, S. M., and Suliman, F. O., *Talanta*, in the press.
20 *British Pharmacopoeia*, H.M. Stationery Office, London, 5th edn., 1980.
21 *US Pharmacopeia, 20th Revision*, US Pharmacopeial Convention, Rockville, MD, 15th edn., 1980, p. 601.

Paper 4/05099A
Received August 19, 1994
Accepted October 7, 1994

Simultaneous Determination of Molybdenum and Tungsten Using a Flow Injection System and without Pre-separation

Renmin Liu, Daojie Liu, Ailing Sun and Guihua Liu

Department of Chemistry, Liaocheng Teachers' College, Liaocheng, Shandong, China

A flow injection system is described for the determination of molybdenum and tungsten, based on their catalytic effects on the reaction of hydrogen peroxide and iodide. Two sample plugs are injected into the same carrier stream sequentially. One is for molybdenum determination and the other is for the sum of molybdenum and tungsten. For molybdenum determination, citric acid solution is simultaneously injected into a parallel carrier stream and merged with the sample plug by using the zone technique. The proposed method has been applied to the determination of molybdenum and tungsten in mineral samples.

Keywords: Flow injection; molybdenum determination; tungsten determination; hydrogen peroxide; iodide

Introduction

Flow injection (FI) has increasingly been recognized as an important tool in various fields such as clinical chemistry, food science, environmental pollution and industrial control, owing to its high reproducibility, flexibility, sample throughput, cost-effective performance and versatility. Much research on FI has been performed in recent years. A recent trend has been the design and optimization of measuring systems for two or more components.[1–5]

Molybdenum has properties similar to tungsten. It is difficult to separate and determine trace amount of Mo and W in the presence of each other. The simultaneous determination of Mo and W without separation is of great interest in mineralogical and geological analysis.

Mo^{VI} and W^{VI} have a catalytic effect on the reaction of hydrogen peroxide with potassium iodide.

$$H_2O_2 + 2KI + H_2SO_4 \rightleftharpoons I_2 + K_2SO_4 + 2H_2O \quad (1)$$

The iodine produced in the reaction is proportional to the concentrations of Mo^{VI} and W^{VI}. When citric acid is present in the solution, the catalytic effect of Mo^{VI} and W^{VI} decreases with increasing concentration of citric acid. The catalytic effect of Mo^{VI} decreases slightly, but that of W^{VI} decreases rapidly. In the present work, the reaction is employed in an FI system and a method for the determination of Mo^{VI} and W^{VI} without pre-separation is established. A three-loop injection valve is used to inject two sample plugs sequentially, one of which is merged with citric acid. In this manner, two FI peaks are sequentially recorded, one being the sum of Mo and W, and the other corresponding to Mo only.

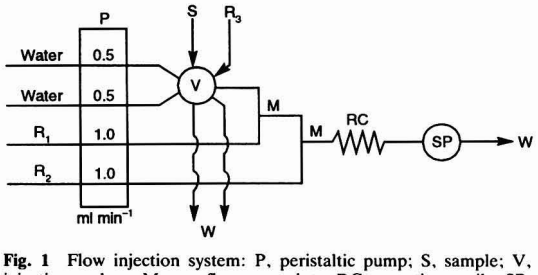

Fig. 1 Flow injection system: P, peristaltic pump; S, sample; V, injection valve; M, confluence point; RC, reaction coil; SP, spectrophotometer; R_1, hydrogen peroxide solution; R_2, starch–potassium iodide solution; R_3, citric acid; and W, waste.

Experimental

Reagents

Standard stock solution of Mo^{VI}, 1.0×10^{-3} mol dm^{-3}. This solution was prepared with use of ammonium molybdate. The working solutions were obtained by serial dilution with water.

Standard stock solution of W^{VI}, 1.0×10^{-3} mol dm^{-3}. This was prepared from sodium tungstate. The working solutions were obtained by serial dilution with water.

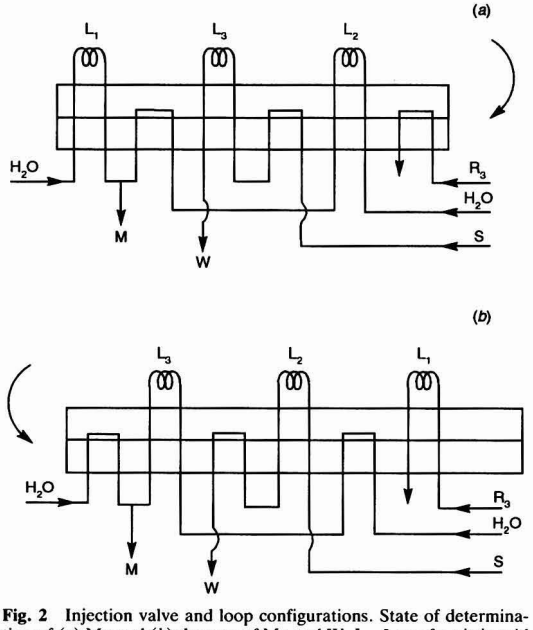

Fig. 2 Injection valve and loop configurations. State of determination of (*a*) Mo and (*b*) the sum of Mo and W. L_1, Loop for citric acid injection (200 μl); L_2, loop for sample injection in determination of Mo (120 μl); L_3, loop for sample injection in determination of the sum of Mo and W (120 μl). Other symbols are as for Fig. 1.

Starch–potassium iodide solution. This solution contained 0.20 mol dm^{-3} potassium iodide solution and 0.15% of starch and was freshly prepared before use.

Hydrogen peroxide solution. This contained 0.01 mol dm^{-3} hydrogen peroxide and 0.005 mol dm^{-3} sulfuric acid.

Citric acid aqueous solution, 5.0×10^{-3} mol dm^{-3}.

All solutions were prepared using analytical-reagent grade chemicals and doubly distilled water.

Apparatus

The FI manifold used is shown in Fig. 1. The peristaltic pump was supplied by Jiangsu Electroanalytical Instrument Plant. A Hitachi 220A spectrophotometer equipped with a flow cell was used as the detector. A dual six-way rotary valve (provided by Yellow Sea Fisheries Research Institute, Chinese Academy of Fisheries Sciences) with three loops was used for sample and citric acid injection. The connection of the valve is shown in Fig. 2.

Methods

General Procedure

The system was connected up with PTFE tubing (1.0 mm i.d.) as shown in Fig. 1. Three loops were mounted on the injection valve (Fig. 2). Two were for the samples and one was for citric acid. Two sample plugs were injected into the carrier (water) sequentially for separate spectrophotometric measurements. One was for Mo^{VI} determination and the other for the sum of Mo^{VI} and W^{VI}. For Mo^{VI} determination, the citric acid was simultaneously injected into another carrier (water) and merged with the sample plug by the merging zone technique. A 200 cm long reaction coil was used for the determination. The absorbance was recorded in the flow cell at 580 nm, the maximum absorption wavelength of a starch–iodine complex. Two peaks are observed for the two injections (Fig. 3). The first peak corresponds to the Mo^{VI} and the second to the sum of Mo^{VI} and W^{VI}. The first peak absorbance is the measure of Mo^{VI}. The absorbance of W^{VI} can be calculated by subtraction. The peak separation can be controlled by adjusting the interval of the injections. Good separation of the two peaks can be obtained when the injection interval is longer than 40 s. A series of standard solutions of Mo^{VI} and W^{VI} were prepared. The solutions were injected into the carrier as described for sample solutions.

Analysis of Mineral Samples

About 0.1–0.2 g of sample was weighed into an iron crucible and melted with sodium peroxide at 650–700 °C for 10 min in a muffle furnace. The fused salts were leached with hot water and diluted to 50 cm^3. Next, the solution was centrifuged at 3000 rpm. The pH of the supernatant was adjusted to about 3.0 and the liquid was analysed by the proposed method.

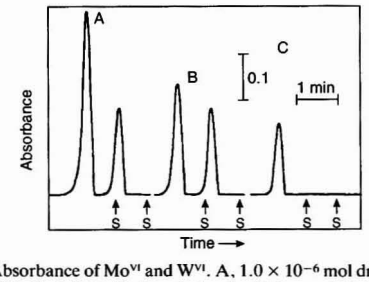

Fig. 3 Absorbance of Mo^{VI} and W^{VI}. A, 1.0×10^{-6} mol dm^{-3} each of Mo and W; B, 1.0×10^{-6} mol dm^{-3} of Mo; and C, 1.0×10^{-6} mol dm^{-3} of W. S indicates the time of injection for each sample plug.

Results and Discussion

Effect of Concentration of Reagents

Hydrogen peroxide can oxidize iodides in an acid medium. Sulfuric, nitric and hydrochloric acids were used to adjust the acidity of the hydrogen peroxide solution. No difference was found with the three acids. Sulfuric acid was used in the experiments. The effect of the concentration of sulfuric acid in hydrogen peroxide solution on the determination of 1.0×10^{-6} mol dm^{-3} Mo and W was studied. The results are shown in Fig. 4. The sensitivity to Mo and W is good and constant for 0.004–0.01 mol dm^{-3} sulfuric acid.

In the following experiments, the concentration of sulfuric acid in hydrogen peroxide solution was 0.005 mol dm^{-3}.

The influence of the concentration of hydrogen peroxide and potassium iodide was also studied. High sensitivity can be obtained when the potassium iodide to hydrogen peroxide molar ratio is >20 : 1 (Fig. 5). Under this condition, the effects of the concentrations of potassium iodide and hydrogen

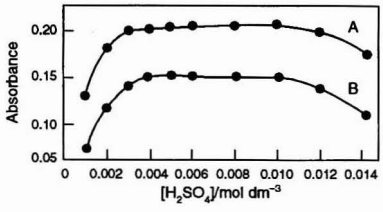

Fig. 4 Influence of sulfuric acid concentration on the determination of A, Mo^{VI} and B, W^{VI}.

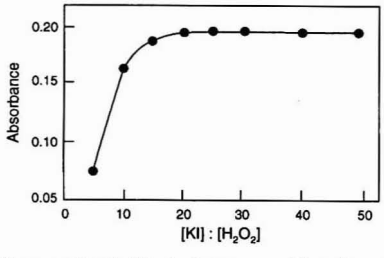

Fig. 5 Influence of the iodide: hydrogen peroxide molar ratio on the determination of 1.0×10^{-6} mol dm^{-3} Mo.

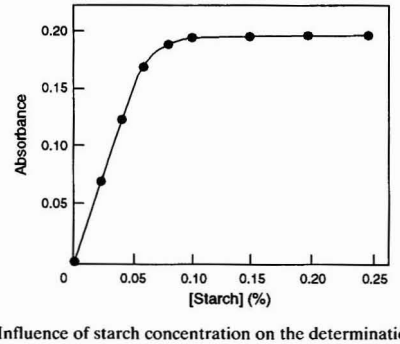

Fig. 6 Influence of starch concentration on the determination of 1.0×10^{-6} mol dm^{-3} Mo.

peroxide were examined. Good results were obtained for 0.20 mol dm^{-3} potassium iodide and 0.01 mol dm^{-3} hydrogen peroxide solutions.

The concentration of starch in the starch–potassium iodide solution was studied (Fig. 6). Good results can be obtained with 0.15% (m/m) of starch.

The influence of citric acid on the catalytic effect of Mo^{VI} and W^{VI} was studied by measuring 1.0×10^{-6} mol dm^{-3} Mo^{VI} and W^{VI} and a 1 : 1 mixture of Mo^{VI} and W^{VI}. The Mo signal was obtained separately in addition to the signal of the sum of Mo and W. Fig. 7 shows that the catalytic effect of W decreases to zero when the molar ratio between citric acid and W is >100. Citric acid of 1.5×10^{-3} mol dm^{-3} was used in this experiment. Under this condition, only one peak was obtained when the solution containing only W was injected (Fig. 3).

Calibration Graph

Mo^{VI} and W^{VI} both catalysed the oxidation reaction (1). At high concentrations of citric acid the catalytic effect of Mo^{VI} decreased slightly while that of W^{VI} disappeared. Thus, the absorbance corresponding to a similar concentration of Mo^{VI} in the first peak (for Mo determination only) is not the same as that in the second peak (for the sum of Mo and W). This should be taken into account in the determination.

A_1 and A_2 are the absorbances of the first and second peaks, respectively. The absorbance corresponding to Mo in first peak is A_1 and that in second peak is kA_1. Then the absorbance corresponding to W in the second peak is $(A_2 - kA_1)$. The coefficient k can be obtained from the Mo standard solution. When a series of mixed standard solutions of Mo and W are measured, the calibration graph for Mo can be obtained from A_1, and that of W from $(A_2 - kA_1)$.

Under the conditions described, mixed standard solutions of Mo^{VI} and W^{VI} (molar ratio 1 : 1) were measured. The calibration graph (Fig. 8) was linear in the range of 2×10^{-7}–3.2×10^{-6} mol dm^{-3} for the sum of Mo and W, and for the individual elements.

The detection limit, defined as three times the signal-to-noise ratio, is 4×10^{-8} mol dm^{-3} for Mo and 6×10^{-8} mol dm^{-9} for W.

Mixed standard solutions of different molar ratios of Mo and W, 10 : 1–1 : 10, were also measured. Recoveries of Mo and W for these solutions are given in Table 1. Good recoveries of Mo and W in mixtures can be obtained even at differing ratios.

The precisions ($n = 11$) for Mo and W were also studied by measuring the mixture of 1.0×10^{-6} mol dm^{-3} Mo^{VI} and 1.0×10^{-6} mol dm^{-3} W^{VI}. The relative standard deviations, s_r, for Mo and W were 0.67 and 0.88%, respectively.

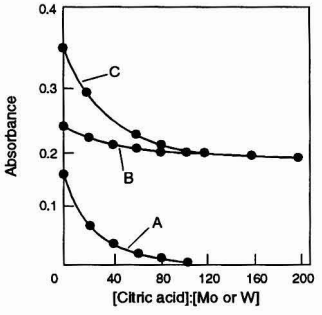

Fig. 7 Influence of citric acid concentration on the determination of Mo and W. A, W; B, Mo; and C, Mo and W.

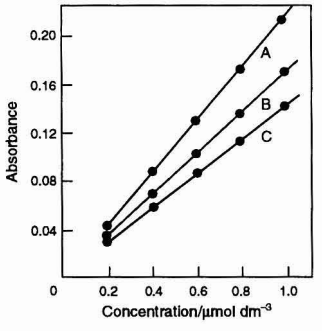

Fig. 8 Calibration graph for Mo and W. A, Mo, no citric acid present; B, Mo, citric acid present; and C, W, no citric acid present.

Table 2 Interference of foreign ions on the determination of 1.0×10^{-6} mol dm^{-3} Mo^{VI} and W^{VI}

Element or ion	(ion : Mo or W ratio)
K^+, Na^+, NH_4^+, Ca^{2+}, Mg^{2+}, Al^{3+}, Cl^-, SO_4^{2-} F^-, NO_3^-, SiO_3^{2-},	5000
Cd^{2+}, Zn^{2+}, Sr^{2+}, Mn^{2+} Ag^+, Ni^{2+}, Cr^{3+}, Ti^{IV},	2000
Br^-, Ac^-, CO_3^{2-}, PO_4^{3-}	1000
Ba^{2+}, Sb^{III}, Fe^{3+}	150
Pb^{2+}, Bi^{3+}	100

Table 3 Determination of Mo and W in mineral samples (μg g^{-1})

	Data obtained		Standard value		Relative error (%)	
Sample	Mo	W	Mo	W	Mo	W
GSR-1	3.43	8.04	3.5	8.4	−2.0	−4.3
GSD-3	92.72	4.78	92	4.9	0.8	−2.4
GSD-6	7.49	25.42	7.7	25.0	−2.7	1.7
GSD-12	8.23	37.9	8.4	37.4	−2.0	1.3
GRD-34	14.24	11.08	13.9	11.05	2.4	0.3
GRD-35	11.01	9.24	10.84	9.05	1.6	2.1
GRR-8	15.34	34.86	15.5	35.73	−1.0	−1.4

Table 1 Recovery of Mo and W in synthetic mixtures

Mo added/ μmol dm^{-3}	W added/ μmol dm^{-3}	Mo found/ μmol dm^{-3}	W found/ μmol dm^{-3}	Recovery (%)		s_r* (%)	
				Mo	W	Mo	W
2.00	0.20	1.97	0.21	98.5	105	0.62	1.98
1.00	0.50	1.01	0.52	101	104	0.71	1.26
0.50	1.00	0.48	0.98	96.0	98.0	0.82	0.94
0.20	2.00	0.20	2.02	100	101	0.97	0.82

* $n = 6$.

Interference

The interference of a number of foreign ions was studied by the addition of such ions to 1.0×10^{-6} mol dm^{-3} of Mo and W. The results are shown in Table 2 (relative error $\leqslant 5\%$).

Application

The proposed method has been applied to the determination of Mo and W in standard reference mineral samples (National Primary Standard Reference Samples, from the Physical and Chemical Survey Research Institute of China). The results are listed in Table 3.

References

1 Oguma, K., and Kuroda, R., *J. Flow Injection Anal.*, 1985, **2**, 98.
2 Motomizu, S., and Onoda, *Anal. Chim. Acta*, 1988, **214**, 298.
3 Cammann, K., *Z. Anal. Chem.*, 1988, **329**, 691.
4 Kozuka, S., Saito, K., Oguma, K., and Kuroda, R., *Analyst*, 1990, **115**, 431.
5 Yamane, T., and Goto, E., *Talanta*, 1991, **39**, 139.

Paper 4/02310B
Received April 19, 1994
Accepted July 14, 1994

Simultaneous Determination of Copper and Zinc in the Hair of Children by pH Gradient Construction in a Flow-injection System

Renmin Liu, Daojie Liu, Ailing Sun and Guihua Liu

Department of Chemistry, Liaocheng Teachers College, Liaocheng, Shandong, Peoples' Republic of China

A flow-injection method is described for the simultaneous determination of copper and zinc with a single detector using the pH gradient technique. Zincon is used as the colour reagent for the spectrophotometric determination. The linear range for the determination of zinc is 0.4–12 μg ml^{-1} and for copper is 0.1–3.0 μg ml^{-1}. About 20–30 samples can be determined in one hour. The proposed method has been applied to the determination of zinc and copper in childrens' hair.

Keywords: Simultaneous determination; copper and zinc; hair; flow injection; pH gradient construction

Introduction

Flow injection (FI) has been increasingly used in various fields, owing to its high sample throughput, cost effective performance and versatility. Initially the development of FI methods was focused on finding and optimizing measuring systems for selective detection. A recent trend has been the design and optimization of measuring systems for the simultaneous determination of two or more components, *i.e.*, multicomponent determination. Simultaneous determination in FI systems was reviewed in 1984 by Luque de Castro and Valcarcel.[1] Various techniques have been applied to multicomponent determinations in FI systems.[2–8]

Hair is an excretive organ of the human body. The content of microelements in hair can reflect the cumulative status of microelements in the body. Zinc and copper are two of these essential microelements and their determination in the hair of children is of great interest in the evaluation of nutrient status.

Zincon is a sensitive spectrophotometric reagent for copper and zinc. It reacts with copper at pH 5–9.5 and zinc at pH 8–9.5.[9] Hence, both copper and zinc react with zincon to form complexes at pH 8–9.5, and only copper reacts with zincon to form complexes at pH 5–7. In the present work, an FI method for the simultaneous determination of copper and zinc is established by the formation of a pH gradient in an FI system. The absorbance is measured at 606 nm. The proposed method is especially suitable for the determination of samples with zinc concentrations higher than those of copper, and has been applied successfully to the determination of copper and zinc in the hair of children.

Experimental

Reagents

Standard stock solution of copper: 1.0 mg ml^{-1}. (Shandong University).

Standard stock solution of zinc: 1.0 mg ml^{-1}. (Shandong University).

Carrier. A 6.2 g amount of boric acid and 7.5 g of potassium chloride were dissolved in 800 ml of water. The pH of the solution was adjusted to 9.5 and the solution diluted to 1000 ml.

Masking agent. To prepare sample solution and the standard working solutions of copper and zinc, 1.6 g of sodium citrate, 1.5 g of sodium triphosphate and 0.06 g of 1,10-phenanthroline were dissolved in 800 ml of water and the pH adjusted to 5.0 before dilution to 1000 ml.

Zincon solution. 0.03% aqueous solution (Beijing Chemical Plant) was used.

All solutions were prepared with analytical-reagent grade chemicals and doubly distilled, de-ionized water.

Apparatus

The FI manifold used is shown in Fig. 1. The peristaltic pump and injection valve were supplied by the Jiangsu Electroanalytical Instrument Plant. A Hitachi 220A spectrophotometer with a flow cell of 18 μl was used as the detector.

Procedure

The FI system was connected using PTFE tubing (0.8 mm i.d.) according to the arrangement shown in Fig. 1. The pH of the sample solutions was adjusted to 5.0 with masking agent, the samples were injected into the carrier stream and then the absorbance was recorded in the flow cell at 606 nm. When the sample injection volume is sufficiently large, a pH gradient of 9.5–5.0–9.5 can be formed in the carrier stream. Zinc and copper both react with zincon in the pH region 8.0–9.5, and only copper reacts with zincon in the pH region 8.0–5.0–8.0. Thus three peaks can be observed for one injection. The first and third peaks correspond to the sum of copper and zinc present, and the second to copper only. The peak height is used as a measure of absorbance.

A series of mixed standard solutions of copper and zinc were prepared by diluting standard stock solutions of copper and zinc with the masking agent solution. These solutions were then injected into the carrier stream before and after the sample runs.

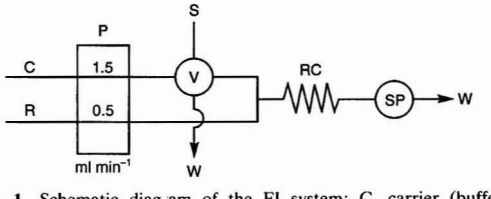

Fig. 1 Schematic diagram of the FI system: C, carrier (buffer solution); R, zincon solution; P, peristaltic pump; S, sample; V, injection valve; RC, reaction coil; SP, spectrophotometer; and W, waste.

Determination of Copper and Zinc in Hair

Hair samples were washed with acetone and de-ionized water to remove the surface contamination and dry-ashed in a muffle furnace at 450 °C. The residue was dissolved in nitric acid. The pH of the solution was adjusted to about 5.0 and the solution diluted to 50 ml with masking agent solution. The solution was then analysed by the proposed method and by atomic absorption spectrometry (AAS).

Results and Discussion

Determination of Copper and Zinc With Zincon

Zincon reacts with copper and zinc to form blue complexes. The absorption spectra of these complexes, as shown in Fig. 2, intersect at 606 nm. At this wavelength their absorption coefficients are equivalent and the sensitivities for copper and zinc are relatively high. Therefore, a wavelength of 606 nm was chosen for the determination.

Zincon reacts with copper at pH 5–9.5 and zinc at pH 8–9.5. This enables the simultaneous measurement of copper and zinc using the pH gradient method. When a pH 5.0 sample is injected into the carrier, a pH gradient is formed in the carrier. An idealized representation of the pH profile is given in Fig. 3. The pH of region I is between 8.0–9.5, and in region II is 8.0–5.0–8.0.

In region I, copper and zinc both react with zincon and the absorbance in this region can be described as:

$$A = A_{Cu} + A_{Zn}$$

In region II, only copper reacts with zincon and the absorbance can be described as:

$$A = A_{Cu}$$

The value of A_{Cu} in region I can be calculated with that in region II by measuring the standard solution of copper. Three peaks can be observed in one injection [Fig. 4 (*a*)–(*d*)]. The first and third peaks correspond to the sum of copper and zinc, and the second peak to copper only. The first peak is consistently higher than the third peak. The reason for this is not known. In the following experiments, the first peak is used for the determination of Cu and Zn, and the second peak for Cu only.

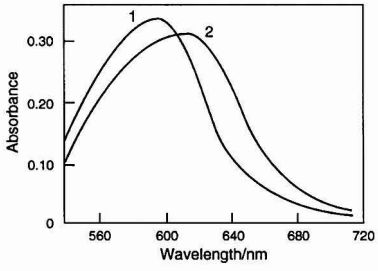

Fig. 2 Absorption spectra of Cu^{II}–zincon and Zn^{II}–zircon complexes. 1, 0.8 μg ml^{-1} of Cu; 2, 0.8 μg ml^{-1} of Zn.

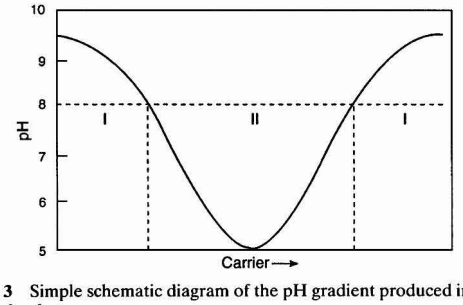

Fig. 3 Simple schematic diagram of the pH gradient produced in the sample plug.

Sample Injection Volume

In order to ensure the second peak corresponds only to copper, the pH gradient of 9.5–5.0–9.5 must be formed in the sample plug. The sample injection volume has a significant effect on the pH gradient when the pH of the sample solution remains constant. The influence of the sample injection volume on the determination was studied by injecting zinc solution into the carrier (Fig. 5). The results indicate that two separate peaks corresponding to zinc can be observed and the absorbance between the two peaks is equal to that of the baseline, when the sample injection volume is higher than 1.0 ml. In the following experiments, a 1.2 ml sample injection

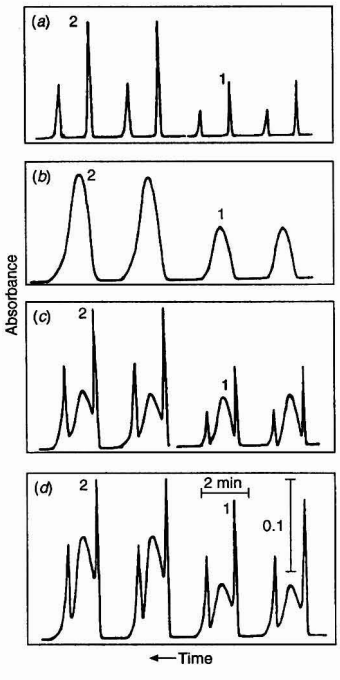

Fig. 4 Typical recording for Cu and Zn. (*a*) Zn only: 2.5 and 5.0 ppm; (*b*) Cu only: 0.5 and 1.0 ppm; (*c*) 2.5 ppm Zn and 0.5 ppm Cu, 5.0 ppm Zn and 0.5 ppm Cu; (*d*) 5.0 ppm Zn and 0.5 ppm Cu, 5.0 ppm Zn and 1.0 ppm copper.

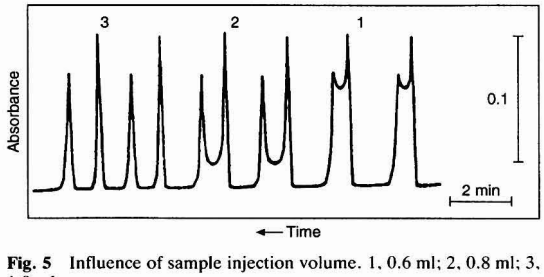

Fig. 5 Influence of sample injection volume. 1, 0.6 ml; 2, 0.8 ml; 3, 1.0 ml.

volume is employed. Under the given conditions, the dispersion, D, of the system is 2.2.

Calibration Graph

Under the conditions described, mixed standard solutions of zinc and copper were measured, the calibration graph was linear in the range 0.1–3.0 μg ml^{-1} for copper and 0.4–12 μg ml^{-1} for zinc. The detection limit, defined as three times the signal-to-noise ratio, is 0.02 μg ml^{-1} for Cu and 0.12 μg ml^{-1} for Zn.

Mixed standard solutions of different mass ratios of zinc and copper between 50:1 and 1:1 were also measured. Recoveries of zinc and copper in synthetic mixtures in de-ionized water at the pH 5.0 were determined. The results are shown in Table 1. Table 1 indicates that good recoveries of zinc and copper can be obtained from synthetic mixtures, even at differing ratios. The relative standard deviations (s_r) for the mixture of 2.0 μg ml^{-1} zinc and 0.5 μg ml^{-1} copper were 1.1 and 0.8%.

Synthetic mixtures of low Zn and high Cu concentrations were also measured. When the Cu:Zn mass ratio is higher than 8, the s_r for Zn is very large, and the precision for Zn is poor. Thus the proposed method is only suitable for samples with Cu:Zn mass ratios <8.

Table 1 Recovery of zinc and copper in synthetic mixtures

Zn added/ μg ml^{-1}	Cu added/ μg ml^{-1}	Zn found/ μg ml^{-1}	Cu found/ μg ml^{-1}	Recovery (%) Zn	Cu
10.0	2.0	9.94	1.92	99.4	99.0
10.0	0.2	9.92	0.21	99.2	105
5.0	2.0	5.08	2.04	102	102
5.0	0.2	5.05	0.19	101	95
2.0	2.0	1.92	2.06	96	103
2.0	0.2	0.94	0.18	97	90

Table 2 Recovery of zinc and copper in the presence of interfering ions

Ions	Amount added/ μg ml^{-1}	Zn found/ μg ml^{-1}	Cu found/ μg ml^{-1}	Recovery (%) Zn	Cu
Al^{III}	10.0	4.86	2.08	97.2	104
Fe^{III}	10.0	5.22	2.12	104	106
Mn^{II}	5.0	5.10	1.96	102	98.0
Ni^{II}	5.0	5.18	2.04	104	102
Co^{II}	5.0	5.26	2.06	106	103
Cd^{II}	5.0	4.92	1.94	98.4	97.0

Interferences

High concentrations of iron(III), manganese(II), nickel(II), cobalt(II), aluminium(III) and cadmium(II) interfere in the determination of copper and zinc with zincon as the chromogenic reagent. The interference of these elements at the levels present in hair samples can be masked by sodium citrate, sodium triphosphate and 1,10-phenanthroline.[10] Table 2 shows the recoveries of 2.0 μg ml^{-1} of Cu and 5.0 μg ml^{-1} of Zn in the presence of the interfering ions and the masking reagent.

Some hair samples were determined with and without the use of the masking agents. The results are given in Table 3. Table 3 shows that the masking agents used are effective.

Application

The proposed method has been applied to the determination of zinc and copper in the hair of children. All the samples were also analysed by AAS. The results are listed in Table 4.

Table 4 indicates that the amount of zinc in childrens hair increases with age but the amount of copper decreases. This is in accordance with the information given in ref. 11.

References

1 Luque de Castro, M. D., and Valcarcel, M., *Analyst*, 1984, **109**, 413.
2 Whitman, D. A., Christian, G. D., and Růžička, J., *Anal. Chim. Acta*, 1988, **214**, 197.

Table 3 Results of the comparison experiment with and without masking agents (MA)

	Data obtained with MA		Data obtained without MA		Data obtained AAS method		Relative error (%) With MA		Without MA	
Sample	Zn	Cu	Zn	Cu	Zn	Cu	Zn	Cu	Zn	Cu
1	81.4	11.3	76.2	12.6	83.6	11.1	−2.6	1.8	−8.9	14
2	76.8	12.2	70.4	11.8	78.2	12.0	−1.8	1.7	−10	−1.7
3	112.2	10.6	122.7	9.6	109.8	10.2	2.2	4.0	12	−5.9
4	106.4	9.48	104.4	8.94	106.8	9.68	−0.4	−2.1	−2.2	−7.6
5	68.7	12.6	71.2	12.8	66.6	13.2	3.2	−4.5	6.9	−3.0

Table 4 Determination of zinc and copper in the hair of children (boys)

Age of children	Number of children	Data obtained by proposed method/μg g^{-1} Zn	Cu	Data obtained by AAS method/μg g^{-1} Zn	Cu
1	68	79.2 ± 30.7	12.2 ± 1.43	78.7 ± 31.6	12.3 ± 1.26
2	60	84.3 ± 24.4	10.4 ± 0.68	84.7 ± 25.1	10.3 ± 0.52
3	76	91.8 ± 35.4	9.85 ± 0.57	90.2 ± 37.7	9.76 ± 0.42
4	68	97.5 ± 28.6	9.24 ± 0.48	98.8 ± 27.4	9.17 ± 0.44

3 Trojanowicz, M., and Szpunar-Lobinska, J., *Anal. Chim. Acta*, 1990, **230**, 125.
4 Canete, F., Rios, A., Luque de Castro, M. D., and Valcarcel, M., *Anal. Chim. Acta*, 1988, **214**, 375.
5 Lazaro, F., Luque de Castro, M. D., and Valcarcel, M., *Anal. Chim. Acta*, 1986, **185**, 57.
6 Betteridge, D., and Fields, B., *Anal. Chem.*, 1978, **50**, 654.
7 Rios, A., Luque de Castro, M. D., and Valcarcel, M., *Anal. Chem.*, 1986, **58**, 663.
8 Hildebrand, D. C., *Clin. Chem. (Winston-Salem, N.C.)*, 1974, **20**, 148.
9 Zeng, Y., Zhang, H., and Cheng, Z., *Handbook of Modern Chemical Reagents*, Chemical Industry Press, Beijing, 1989, p. 639.
10 Pan, Y., and Wang, J., *Lihua Jianyan, Huaxue Fence*, 1991, **27**, 235.
11 *Huazhong Ligong Daxue Kexu Jishu Xiehiu (Handbook of Data of Microelements)*, Dier Fence, 1988, p. 189.

Paper 4/04841E
Received August 8, 1994
Accepted September 14, 1994

Spectrophotometric Determination of 1,4-Dihydroxyanthraquinone

Kan Jin-qing

Department of Chemistry, Teachers College, Yangzhou University, Yangzhou 225002, People's Republic of China

Shi Yujun

Department of Chemistry, Nantong Teachers College, Nantong 226007, People's Republic of China

A spectrophotometric method for the determination of 1,4-dihydroxyanthraquinone in a mixed solvent system consisting of sulfuric acid and *N,N*-dimethylformamide is described. The effect of sodium carbonate, anthraquinone and mechanical impurities (dust) on the results is discussed. The accuracy of the measurements is better than 1%.

Keywords: 1,4-Dihydroxyanthraquinone determination; spectrophotometry; mixed solvent

Introduction

1,4-Dihydroxyanthraquinone is an intermediate in the synthesis of dyestuffs; its structure and properties have been widely studied[1–4] and methods for its determination have also been reported.[5–10] Techniques for the determination of 1,4-dihydroxyanthraquinone include chemical methods, polarography, spectral analysis and recrystallization gravimetric analysis; however, some of these techniques are time consuming (for example, it takes more than 24 h to analyse a sample using recrystallization gravimetric analysis), and some of the reagents used in the analysis are corrosive (*e.g.*, concentrated sulfuric acid, which is used as the solvent in spectral analysis). In other techniques, either the accuracy is poor or the conditions are difficult to control. In industrial production and scientific research, there is an increasing need for methods that allow the purity of the final product to be determined.

This paper describes a rapid and reliable spectrophotometric method for the determination of 1,4-dihydroxyanthraquinone in a mixed solvent system, which overcomes the acid electrodissociation of 1,4-dihydroxyanthraquinone and the effect of alkaline impurities on its determination.

Experimental

Apparatus and Chemicals

A Model 722 grating spectrophotometer with 1.00 cm silica and Corex cells (made in the Third Work of Analysis Instrument, Shanghai, China) was used. The spectrophotometric disc and wavelength were calibrated with a standard solution of 30 μg ml^{-1} of $K_2Cr_2O_7$ and a Pr–Nd filter disc assembly when necessary.

Two grades of 1,4-dihydroxyanthraquinone were used: a spectroscopically pure reagent (Tokyo Kasei Chemical, Tokyo, Japan) and an industrial product (Huaiyin, China).

Sulfuric acid and *N,N*-dimethyformamide (DMF), both of analytical-reagent grade, were also used.

Procedure

The mixed solvent was prepared by adding sulfuric acid to DMF so that the final concentration of sulfuric acid in the mixture was approximately 1.5 mol l^{-1}.

A 1.0 mg ml^{-1} standard solution of 1,4-dihydroxyanthraquinone was prepared by accurately weighing 25.0 ± 0.1 mg of 1,4-dihydroxyanthraquinone (spectroscopically pure) and allowing it to dissolve in the mixed solvent to give a final solution volume of 25 ml. An aliquot (50 μl) of the resulting solution was diluted to 10 ml with the mixed solvent. The absorbance of the diluted solution was measured at 480 nm using the Model 722 grating spectrophotometer.

For the analysis of an actual sample, the procedure described above was followed except that the standard solution was replaced by the sample solution.

As the absorbance was directly proportional to the sample percentage content over the range 75–100%, it was more convenient to calculate the percentage content of 1,4-dihydroxyanthraquinone from the following equation rather than from a calibration graph

$$x(\%) = \frac{A_d}{A_s} \times 100$$

where A_d is the absorbance of the sample and A_s is the absorbance of the standard solution.

Results and Discussion

Fig. 1 shows the absorption spectrum for the standard solution of 1,4-dihydroxyanthraquinone with a Model UV-24 spectrophotometer (Photological Instrument of Shimazu, Japan),

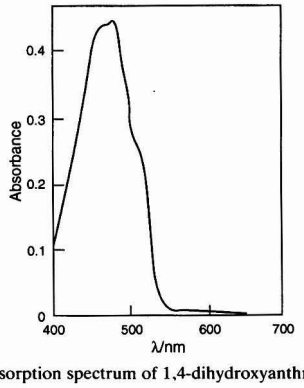

Fig. 1. Absorption spectrum of 1,4-dihydroxyanthraquinone.

from which it can be seen that the maximum absorbance for 1,4-dihydroxyanthraquinone in the mixed solvent is at 480 nm; this value differs by 40 nm from that given in the literature.[11] There may be two reasons for this difference: (1) the two spectrophotometers used were not of the same type and (2) the sample used in ref. 11 contained a small amount of alkali (*e.g.*, Na_2CO_3). It has been shown that the maximum absorbance for 1,4-dihydroxyanthraquinone dissolved in DMF is shifted to a longer wavelength when there is a small amount of alkali (*e.g.*, NaOH, Na_2CO_3) present.[1] The splitting and shoulder observed in the spectrum are due to an intramolecular tautomer of 1,4-dihydroxyanthraquinone.[3]

The standard and sample solutions can be stored for up to one year; measurement of the absorbance with the Model 722 grating spectrophotometer under the same conditions revealed that there was no change in the absorbance of fresh and aged solutions; in addition, the absorption spectra obtained with the Model UV-24 spectrophotometer were also unchanged. The results indicate that the use of the mixed solvent provides very stable solutions for the determination of 1,4-dihydroxyanthraquinone and, provided that the standard solution is stored in a sealed container, it can be used as a comparative standard for a prolonged period.

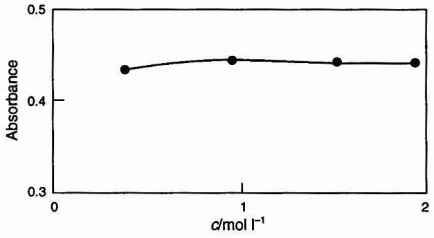

Fig. 2. Effect of sulfuric acid concentration on absorbance.

Fig. 2 shows the effect of the concentration of sulfuric acid on the absorbance when the concentration of the standard solution is fixed. The absorbance hardly changes with the concentration of sulfuric acid in the range 1.0–2.0 mol l^{-1}, but the absorbance changes slightly when the concentration of sulfuric acid is less than 0.40 mol l^{-1}. This is caused by the inhibition of the acid dissociation of 1,4-dihydroxyanthraquinone when the concentration of sulfuric acid is sufficiently high. The industrial 1,4-dihydroxyanthraquinone product often contains a small amount of alkali (*e.g.*, Na_2CO_3), and the electrodissociated state of 1,4-dihydroxyanthraquinone can be influenced by the alkaline impurity; hence the measured absorbance varies with the electrodissociated state of the system, and leads to poor reproducibility and accuracy. Considering the accuracy and reliability of the measurements obtained, we recommend that the mixed solvent system described here be selected, in which the concentration of sulfuric acid is about 1.5 mol l^{-1}; under these conditions, levels of Na_2CO_3 in the range 0–25% m/m do not influence the results of the measurements. It should be noted that the mixed solvent is not suitable when the concentration of sulfuric acid therein is less than 0.5 mol l^{-1}.

Table 1 Results of measurements when Na_2CO_3 acts as impurity*

A_s				0.444			
X_w (%)	75.6	80.0	85.9	89.8	92.0	95.2	98.7
A_d	0.333	0.355	0.378	0.396	0.409	0.426	0.436
x_d (%)	75.1	80.0	86.5	90.6	92.2	96.0	98.2
$(x_d - x_w)$ (%)	−0.5	0	0.6	0.8	0.2	0.8	−0.5

* A_s = Absorbance of standard solution; A_d = absorbance of sample; x_w = mass percentage content of 1,4-dihydroxyanthraquinone found by a weighing method; x_d = mass percentage content of 1,4-dihydroxyanthraquinone found by the proposed spectrophotometric method.

Table 2 Results of measurements when anthraquinone acts as impurity*

A_s				0.444			
x_w (%)	78.6	80.0	84.4	89.2	92.0	95.2	98.4
A_d	0.348	0.356	0.374	0.394	0.408	0.424	0.439
x_d (%)	78.4	80.1	84.2	88.8	91.8	95.6	98.9
$(x_d - x_w)$ (%)	−0.2	0.1	−0.2	−0.3	−0.2	0.4	0.5

* A_s, A_d, x_w and x_d as in Table 1.

Table 3 Results of measurements when dust acts as a mechanical impurity*

A_s				0.444			
x_w (%)	76.3	81.1	85.8	90.7	93.3	96.0	99.0
A_d	0.338	0.359	0.384	0.401	0.412	0.423	0.441
x_d (%)	76.1	80.9	86.5	90.3	92.9	95.2	99.3
$(x_d - x_w)$ (%)	−0.2	−0.2	0.7	−0.4	−0.4	−0.8	0.3

* A_s, A_d, x_w and x_d as in Table 1.

Table 4 Results of measurements on industrial products*

A_s					0.444				
No.	1	2	3	4	5	6	7	8	9
A_i	0.432	0.434	0.432	0.433	0.430	0.428	0.432	0.430	0.433
x (%)	96.1	96.3	96.1	96.2	96.0	95.9	96.1	96.0	96.2
$\bar{s}$					0.0012				

* A_s = Absorbance of standard solution; No. = sample number; A_i = absorbance of the industrial product; x = mass percentage content of 1,4-dihydroxyanthraquinone; $\bar{s}$ = standard deviation of the mass percentage content of the samples.

Tables 1–3 show the absorbance of solutions doped with various impurities, and the mass percentage content of 1,4-dihydroxyanthraquinone obtained by the proposed method by comparing the absorbance with that of the standard solution; the mass percentage content of solutions made up by a weighing method is also given. Both the mixed solvent method and the weighing method give satisfactory results with a tolerance of less than 1% when the content of 1,4-dihydroxyanthraquinone varies from 80 to 100% m/m. As the concentration of sulfuric acid is only about 1.5 mol l^{-1}, the mixed solvent method is superior to that reported by Yakobi *et al.*[7] in terms of the reliability and accuracy of the measurements.

The results of the analysis of industrial products are listed in Table 4; the results were coincident with the value (≥95%) given on the label by the Chemical Factory of Huaiyin, China; the proposed method also offers better reproducibility than recrystallization gravimetric analysis.

Conclusion

The spectrophotometric determination of 1,4-dihydroxyanthraquinone in a mixed solvent system has been described. The method is simple and reliable and avoids the need to use corrosive reagents such as concentrated sulfuric acid. Hence it is suitable for quality control purposes.

References

1 Gopalakrishnan, S., Neelakantan, S., and Raman, P. V., *J. Indian Chem. Soc.*, 1990, **67**, 390.
2 Issa, I. M., Issa, R. M., Idris, K. A., and Hammam, A. M., *Egypt. J. Chem.*, 1973, 67.
3 Morton, R. A., and Earlam, W. T., *J. Chem. Soc.*, 1941, 159.
4 Birkinshaw, S. H., *Biochem. J.*, 1955, **59**, 485.
5 Hoskins, E. C., *J. Assoc. Off. Anal. Chem.*, 1971, **54**, 1270.
6 Davis, R., Stockwell, P. B., and Pardue, H., *Lab. Pract.*, 1978, **27**, 957.
7 Yakobi, A. Ya., Ishchenko, L. L., and Promkina, V. A., *Khim. Prom-st., Ser: Metody Anal. Kontrolya Kach. Prod. Khim. Prom-sti*, 1980, **1**, 39.
8 Ruzicka, E., and Zajoncova, L., *Acta Univ. Palacki. Olomuc., Fac. Rerum Nat.*, 1984, **79** (Chem. 23), 119.
9 Pournaghi-Azar, M. H., and Golabi, S. M., *Talanta*, 1988, **35**, 959.
10 Thelen, B., Brandt, H. W., Auge, W., and Thiem, K. W., *Ger. Offen*, 2 637 689 (CL. C07C49), 1978.
11 *CRC Handbook of Chemistry and Physics*, ed. Grasselli, J. G., CRC Press, Cleveland, OH, 52nd edn., 1973, B-169.

Paper 4/03616F
Received June 14, 1994
Accepted September 7, 1994

Screening of Calf Urine for 19-Nortestosterone: Matrix Effect in Some Immunoassays*

Maurizio Paleologo Oriundi
Via di Sistiana 10/M, 34019 Duino-Aurisina, Trieste, Italy

Roberto Angeletti and E. Bastiani
Istituto Zooprofilattico Sperimentale delle Venezie, via Orus 2, Padova, Italy

Carlo Nachtmann
Istituto Zooprofilattico Sperimentale del Piemonte, Liguria e Valle d'Aosta, via Bologna 125, Torino, Italy

Kristina E. Vanoosthuyze and Carlos Van Peteghem
Laboratory of Food Analysis, Faculty of Pharmaceutical Sciences, University of Ghent, Ghent, Belgium

The performances of three enzyme linked immunosorbent assays (ELISAs) and one radioimmunoassay (RIA) in 17α-19-nortestosterone (17α-19-NT) analysis of bovine urine have been evaluated. Sample preparation was performed by enzymic deconjugation and solid-phase extraction. The main object of the study was the evaluation of the matrix effect, which is generally great in 19-NT immunoassays. Fifty-seven bovine urine samples have been analysed by immunoassay and by gas chromatography–mass spectrometry (GC–MS). The detection limit of GC–MS analysis was 1 μg l^{-1}. The mean sample blank values in urine analysis were close to 1.5 μg l^{-1} for one ELISA, and 0.4–0.8 μg l^{-1} for the other assays ($n = 55$, samples coming from several breeds in different geographic areas). The detection limits, calculated in compliance to the EEC criteria, were 2.67, 1.97, 2.05 and 5.01 μg l^{-1} for RIA, ELISAs 1, 2 and 3, respectively. The percentage of false positive results adopting this criteria were: 1.8, 3.6, 1.8 and 3.6%. The probability of the occurrence of false negative results was evaluated by adding 2 μg l^{-1} of 19-NT to a negative sample, was high in each assay. Two samples from experimentally treated animals gave positive results both in GC–MS and in immunoassays. The results obtained confirm that by employing immunoassay and solid-phase extraction as sample clean-up, it is not possible to apply the action level (2 ppb) suggested by the European Union (EU).

Keywords: 19-Nortestosterone; immunoassay; enzyme linked immunosorbent assay; bovine urine; matrix effect

Introduction

The screening of steroid hormones is generally performed by an immunoassay, either enzyme linked immunosorbent assay (ELISA) or radioimmunoassay (RIA). The positive results of screening analysis then have to be confirmed by gas chromatography–mass spectrometry (GC–MS) or high-performance liquid chromatography (HPLC). Most Italian control laboratories currently use RIA. A number of ELISA test kits for anabolic hormones are now available and some laboratories are using such kits for regulatory controls. By employing ELISA, the analysis can be performed in small laboratories (where RIA cannot be performed).

17β-19-nortestosterone (17β-19-NT) and its esters are quite often used as anabolic agents. Owing to its structure, closely related to natural compounds and metabolites, the detection of 19-nortestosterone (19-NT) by immunoassay is generally difficult. The matrix effect is great with liquid or solid-phase extraction (SPE) procedures. The aim of our study was to determine the detection limits of some available RIA and ELISA assays for 19-NT, and to verify whether the action level of 2 ppb, suggested in the Nationals Monitoring Plans of the European Union, can be applied in practice. As several studies demonstrated that the major part of 17β-19-NT is metabolized and excreted in bovine-urine samples as 17α-19-nortestosterone (17α-19-NT),[1,2] we decided to quantify this molecule instead of the parent compound. The spiking experiments have also been performed with 17α-19-NT.

Experimental

Reagents and Instrumentation

All organic solvents used were of analytical-reagent grade. SPE C_{18} columns were from Baker (Phillipsburgh, NJ, USA). *Helix pomatia* juice, 17 α-methyltestosterone and 17β-19-NT standards were from Sigma (St. Louis, MO, USA). 17α-19-NT was from Steraloids (Pawling, NJ, USA). For chromatographic analysis an HP-5890 II° gas chromatograph (Hewlett-Packard, Avondale, PA, USA) was used with a VG TS 250 mass spectrometer (VG Instruments, Stamford, CT, USA). Heptafluorobutyric acid anhydride from Pierce (Rockford, IL, USA) was used for derivatization.

Urine Samples

Bovine-urine samples were collected from regulatory control programs in Italy. Two samples from experimentally treated bovine were kindly supplied by Coop Italia (Bologna, Italy) and by Istituto Zooprofilattico Sperimentale of Teramo. Spiked samples were prepared by adding 2 and 4 ng of 17α-19-NT to a negative sample before the enzymic hydrolysis.

Antibodies and Standard Curves

The RIA and two ELISAs made use of antibodies arisen from 17-hemisuccinate-19-NT immunogen, and had a cross-reactivity of between 50 and 80% to the α-form of 19-NT.[3–5] The

* Presented at The Second International Symposium on Hormone and Veterinary Drug Residue Analysis, Oud St-Jan, Bruges, Belgium, May 31–June 3, 1994.

third ELISA antibody was raised in rabbits with a 17α-19-NT-3-carboxymethyloxime-bovine serum albumin, and was specific for the 17α-isomer of nortestosterone.[6] The standard curves were made with 17α-19-NT.

ELISA and RIA Sample Pre-treatment

Samples were purified by SPE procedure, according to the instructions of the ELISA kit manufacturers, with some modifications. Urine (1 ml) was diluted with 3 ml of 50 mmol l^{-1} sodium acetate buffer (pH 4.5) and 16 μl of *Helix pomatia* juice were added. The solution was incubated for 2 h at 37 °C. The hydrolysed samples were purified by C_{18} cartridges, previously rinsed with 3 ml methanol and 3 ml of a solution of 20 mmol l^{-1} TRIS HCl buffer (pH 8.5) containing 20% (v/v) methanol. Column washing was performed with 3 ml of TRIS–methanol solution and 3 ml of methanol–water (40 + 60, v/v). Samples were eluted with 2 ml of methanol, evaporated by nitrogen stream at 40 °C, then redissolved in 1 ml of distilled water. The dilution procedures following the different assay conditions were: 40% (v/v) methanol in two ELISAs (dilutions 1 + 1), distilled water in the third ELISA (dilution 1 + 9) and in RIA (undiluted extract). The assays were performed following kit instructions or, for RIA and the spare reagent ELISA, following literature recommendations.

GC–MS Analysis

Sample purification for GC–MS analysis was performed by extraction with $CHCl_3$ from basified urine samples after deconjugation by *Helix pomatia* juice. Urine (10 ml) diluted with water (1 + 1) were used. The extraction was performed with 3 × 20 ml of $CHCl_3$ on a Chem Elut column (Merck Italia, Milano). After evaporation of the eluate the sample was redissolved with 200 μl 20 mmol l^{-1} TRIS-HCl buffer (pH 8.5) 20% (v/v) methanol. In a similar manner to the immunoassay sample clean-up, the following SPE purification step was performed. The SPE eluate was evaporated and redissolved with 200 μl of methanol for derivatization with heptafluorobutyric acid anydride.[7] An internal standard of 17α-methyltestosterone was added. A DB-5 MS (J & W Scientific, Rancho Cordova, CA, USA) was used with the following temperature program: 70 °C for 1 min to 280 °C at 6 °C min^{-1}, and 10 min at 280 °C. Ions at *m/z* 666.3, 453.2 and 306.1 were monitored. Recovery of the method was greater than 80% (for both α- and β-19-NT).

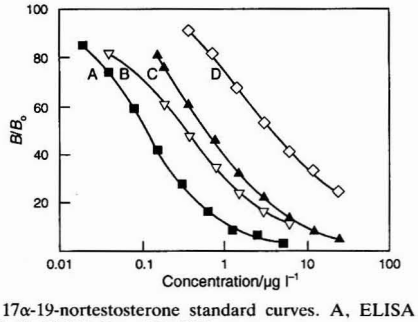

Fig. 1 17α-19-nortestosterone standard curves. A, ELISA 1; B, ELISA 3; C, ELISA 2; and D, RIA.

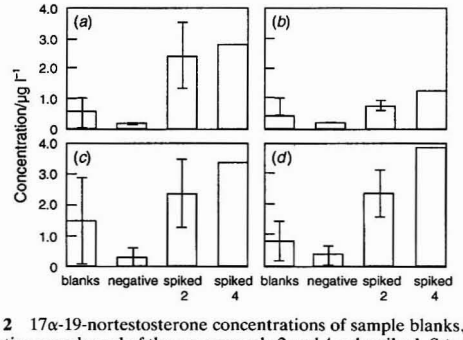

Fig. 2 17α-19-nortestosterone concentrations of sample blanks, of a negative sample and of the same sample 2 and 4 ppb spiked. Standard deviation is shown when available. (*a*) ELISA 1; (*b*) ELISA 2; (*c*) ELISA 3; and (*d*) RIA.

Results and Discussion

Fifty-seven bovine-urine samples were analysed by immunoassay and by GC–MS. Four samples derived from a group of experimentally treated calves: two from control animals and two from injected animals,[8] the remaining were from calves bred in different regions of Northern Italy. Apart from the two samples from the treated animals, the others gave negative results in GC–MS. The detection limit for GC–MS analysis was 1 μg l^{-1}. For the immunoassays, three different ELISAs and one RIA were employed. Out of three, two ELISAs were commercially available kits, and one was performed by spare reagents, developed in the Laboratory of Food Analysis, Faculty of Pharmaceutical Sciences, University of Ghent. Three assays were performed, running standard curves with 17α-19-NT, the main urinary metabolite of 19-NT, which was also used for spiking.

The standard curves obtained are shown in Fig. 1. The mean values of 80% B/B_0 were 0.8, 0.03, 0.2, 0.08 μg l^{-1} for RIA, ELISAs 1, 2 and 3, respectively. The values of 50% inhibition were 4.2, 0.11, 0.6, 0.35 μg l^{-1} for RIA, and ELISAs 1, 2 and 3, respectively. The reagent blanks gave undetectable values in all the assays.

The mean apparent 17α-19-NT concentration values of sample blanks were 0.78 ± 0.63, 0.53 ± 0.48, 0.43 ± 0.54 and 1.47 ± 1.58 μg l^{-1} (mean ± standard deviation, *s*), for RIA, ELISAs 1, 2 and 3, respectively (Fig. 2). Consequently, the respective detection limits were 2.67, 1.97, 2.05, and 5.61 μg l^{-1}. The percentage of false positive results calculated adopting the above mentioned detection limits as the doses of analyte above which the results are considered positive (cut-offs) were: 1.8, 3.6, 1.8 and 3.6%, respectively. The samples from 19-NT treated animals were positive (values always above the detection limits); the concentration values were in the range of 2–3 ppb for RIA and ELISAs 1 and 2, and, 5 and 9 ppb for ELISA 3.

Five samples made by spiking a negative urine sample with 2 μg l^{-1} of 17α-19-NT (low matrix effect) gave three negative and two positive results by RIA and by ELISA 1, and five negative results by ELISAs 2 and 3. Considering also the variability of the spiked samples' concentrations, neither RIA nor the evaluated ELISA assays seem be able to guarantee the detectability of 2 ppb of 17α-19-NT.

Note that the mean apparent concentrations and detection limits of 19-NT in bulls or cows could be quite higher (the matrix effect is often higher in older animals).

Note also that we did not follow completely the sample preparation procedure described by the kit manufacturers; moreover, owing to the different sensitivities of the various assays for 17α-19-NT, different dilution factors were applied in each assay.

Van Look[9] made a comparison between two of the three ELISAs employed here. The results obtained in that study are in agreement with ours: both assays gave a significant percentage of false (negative and positive) results.

Conclusions

By employing the materials and methods which are now available for 19-NT screening analysis and using as cut-off the detection limits, the percentage of false positive was acceptable. One the other hand, the analysis of a few spiked samples show that a higher action level should be fixed for this anabolic steroid. In any case a further study of the accuracy and reproducibility of 19-NT immunoassays is needed to determine a new action level.

The results of this study also show that a more specific extraction procedure should be adopted for 19-NT immunoassays. It is particularly advisable to implement internal and external quality control in 19-NT screening analysis.

References

1 Van Ginkel, L. A., Stephany, R. W., Van Rossum, H. J., Van Blitterswijk, H., Zoontjes, P. W., Hooijschuur, R. C. M., and Zuydendorp, J., *J. Chromatogr., Biomed. Appl.*, 1989, **489**, 95.
2 Haasnoot, W., Schilt, R., Hamers, A. R. M., and Huf, F. A., 1989, *J. Chromatogr., Biomed. Appl.*, **489**, 157.
3 Evrard, P., Gaspar, P., and Maghuin-Rogister, G., *J. Immunoassay*, 1986, **7**(4), 353.
4 Meyer, H. H. D. and Funke, P., in *Advances of Steroid Analysis, Proc. of the 3rd Symposium of the Analysis of Steroids, Sopron, Hungary, 1987*, ed. Gorog, S., Akademiai Kiado, Budapest, 1988, 225.
5 Haasnoot, W., van Bruchem, G. D., Paulussen, R. J. A., Schilt, R., Arts, J., Dijkstra, G., and Meijer, J. C., *Arch. Lebensmittelhyg.*, 1990, **41**, 131.
6 Van Look, L., Jansen, E. H. J. M., van den Berg, R. H., Zomer, B., Vanoosthuyze, K. E., and van Peteghem, C. H., *J. Chromatogr.*, 1991, **564** (2), 451.
7 Commission of the European Communities, *Veterinary Drug Residue*, 1992, ed. Heitzmann, R. J., 64.
8 Calvarese, S., Ramazza, V., Rubini, P., Urbani, G., Ferri, N., and Zucchi, M., *Analyst*, 1994, **119** (00), 000, 4/03403A.
9 Van Look, L. J., Meyer, H. H. D. and Van Peteghem, C. H., in *Food Safety and Quality Assurance: Applications of Immunoassay Systems*, ed. Morgan, M. R. A., Smith, C. J., and Williams, P. A., Elsevier, Amsterdam, 1991, pp. 231–235.

Paper 4/03831B
Received June 24, 1994
Accepted October 5, 1994

CUMULATIVE AUTHOR INDEX

JANUARY–FEBRUARY 1995

Abou-Shakra, Fadi R., 341
Abrigo, C., 47
Ala-Kleme, Timo, 367
Albero, Mª Isabel, 129
Analytical Methods Committee, 29
Andersson, Örjan, 423
Andrade, J. M., 249
Andrés, J. Verdú, 299
Angeletti, Roberto, 577
Antolovich, Michael, 1
Aoki, Nobumi, 135
Araujo, Pedro W., 295
Arias, J. J., 313
Astruc, A., 79
Astruc, M., 79
Augugliaro, Vincenzo, 237
Azani, R., 395
Baeyens, W. R. G., 463
Balazs, G. Bryan, 523
Baldin, C., 47
Barrero, J. M., 431
Bastiani, E., 577
Baumann, Wolfram, 243
Baxter, Douglas C., 69
Bekessy, Lambert K., 211
Berzas Nevado, J. J., 171
Bhilare, N. G., 391
Bissonnette, M. C., 395
Bjennes, Heidi, 367
Blais, J. S., 395
Blanchflower, W. J., 331
Bouropoulos, Nicolaos Ch., 347
Brereton, Richard G., 295
Brindle, Ian D., 183
Brunmark, Per, 41
Calokerinos, A. C., 463
Calos, Nicholas, 211
Cámara, C., 431
Cannavan, A., 331
Carbonell, Vicente, 231
Ceramelli, Giuseppe, 319
Chee, Kok Kay, 273, 281
Chi, Nai-Yuen, 511
Chromiak, Edward, 149
Chung, Mu-Jye, 511
Cirello-Egamino, Joanne, 183
Corti, Piero, 319
Dalene, Marianne, 41
Damiani, Patricia, 443
Danielsson, Bengt, 155
de la Fuente, Miguel Angel, 107
de la Guardia, Miguel, 231, 313
Dean, J. R., 355
del Barrio Martín, S., 85
Delgado Zamarreño, M. M., 139
Devi, Surekha, 555
Diaz-Garcia, Marta Elena, 457
Dowle, C. J., 355
Dreassi, Elena, 319
Dubest, Roger, 447
Edwards, Robert, 117
El-Shahat, M. F., 549
El-Zawawy, F. M., 549
Emteborg, Håkan, 69
Ersoy, Lale, 373
Falcó, P. Campíns, 299
Fernández, L., 431
Fernandez-Romero, J. M., 179
Fogg, Arnold G., 505
Frech, Wolfgang, 69
Fukasawa, Tsutomu, 543
Fukushima, Takeshi, 381
Furusawa, Motohisa, 437
Gao, De, 499
García, J. M., 313
García, Mª Soledad, 129
García Pinto, Carmelo, 53
Gennaro, M. C., 47
Głąb, Stanisław, 489
Glass, Robert S., 523
Godlewska, Beata, 143
Golimowski, Jerzy, 143
Gómez Laguna, M. A., 171
Gómez-Hens, Agustina, 125
Greenway, Gillian M., 477
Gu, Jun, 499
Güçer, Şeref, 101
Gupta, Vinod K., 495
Haapakka, Keijo, 367
Haas, Ulrich, 351
Hamano, Takashi, 135
Hasan, Berween A., 231
Hayakawa, Kazuichi, 377
Hernández Artiga, Maria Purificación, 485
Hernandez Mendez, J., 139
Hernández-Cassou, S., 305
Hill, Steve J., 413
Hitchen, S. M., 355
Hori, Yoshikazu, 187
Hsu, Fu-Shien, 511
Hulanicki, Adam, 143
Hunter, Thomas C., 161
Ibáñez, Gabriela, 443
Igarashi, Shukuro, 539
Imai, Kazuhiro, 381
Irons, Gordon P., 477
Ishiyama, Munetaka, 113
Ito, Yoshio, 135
Iwatsuki, Masaaki, 543
Jain, Suresh, 495
Jane, Yih-Song, 517
Jiménez, A. I., 313
Johansson, Karin, 423
Juárez, Manuela, 107
Kakehi, Kazuaki, 63
Kale, Uma, 325
Kan, Jin-qing, 573
Kane, M., 355
Kankare, Jouko, 367
Kato, Masaru, 381
Kavianpour, Keyhandokht, 295
Kawakami, Takanori, 539
Kennard, Colin H. L., 211
Kennedy, D. G., 331
Khalaf, Karim D., 231, 313
Koizumi, Yoshiyuki, 89
Kojima, Nobuaki, 135
Kolotyrkina, Irina Ya., 201
Koncki, Robert, 489
Kontoyannis, Christos G., 347
Koutsoukos, Petros G., 347
Lamble, Kathryn, 413
Lan, Wei Guang, 273, 281
Latva, Martti, 367
Lee, Hian Kee, 281
Leguille, F., 79
Levoir, Patrick, 447
Li, Ke, 361
Li, Sam F. Y., 361
Liang, Bing, 543
Liu, Daojie, 565, 569
Liu, Guihua, 565, 569
Liu, Renmin, 565, 569
Liu, Yi-Ming, 385
Lonardi, Silvano, 319
López, P., 249
Loukas, Yannis L., 533
Lowthian, Philip J., 271
Lu, Jianzhong, 453
Luque De Castro, M. D., 179
McCulloch, M. T., 35
Malahoff, Alexander, 201
Marengo, E., 47
Marina, M. L., 255
Martelletti, M. T., 47
Martínez-Lozano, Carmen, 471
Martins, Jorge L. S., 193
Masuda, Akimasa, 335
Matni, G., 395
Matsunaga, Akinobu, 377
Mattos, I. L., 179
Mecklenburg, Michael, 155
Meyer, Jean-Jacques, 447
Mikasa, Hiroshi, 187
Miki, Yasuyoshi, 63
Mishra, Rajendra Kumar, 197
Mitsuhashi, Yukimasa, 135
Miyake, Yasuko, 63
Miyazaki, Motoichi, 377
Mizukami, Eiichi, 377
Mohamed, A. A., 549
Morales-Rubio, Angel, 231, 313
Moreira, Josino C., 505
Moreno Cordero, Bernardo, 53
Motomizu, Shoji, 187
Muniategui, S., 249
Muñoz, Amalia, 529
Muñoz Leyva, Juan Antonio, 485
Murillo Pulgarín, J. A., 171
Nachtmann, Carlo, 577
Nakamura, Toshihiro, 89
Nashine, Neena, 197
Nishiyama, Katsuhiko, 113
Niwa, Tomoko, 167
Noike, Yuji, 89
Nomura, Satoshi, 503
Norlin, Peter, 155
Oguri, Shigeyuki, 63
Ohkura, Yosuke, 113
Öhman, Ove, 155
Ohto, Mikiya, 377
Oji, Yoshikiyo, 135
Olin, Åke, 423
Olivieri, Alejandro C., 443
Oshima, Mitsuko, 187
Paleologo Oriundi, Maurizio, 577
Palmisano, Leonardo, 237
Panadero, Sagrario, 125
Paulls, David A., 467
Pereiro-García, Rosario, 457
Pérez Pavón, José Luis, 53
Pérez-Bendito, Dolores, 125
Pérez-Conde, M. C., 431
Pérez-Ruiz, Tomás, 471
Perruccio, Piero Luigi, 319
Pinel, R., 79
Pires Valente, Antonio L., 419
Poole, Colin F., 289
Poole, Salwa K., 289
Prada, D., 249
Pramauro, Edmondo, 237
Prevot, Alessandra Bianco, 237
Price, Gareth J., 161
Purohit, Rajesh, 555
Ramsey, Michael H., 261
Rathore, Devendra P. S., 403
Reig, F. Bosch, 299
Ribone, María Elida, 443
Robards, Kevin, 1
Rodríguez, Adela Rosa, 529
Różańska, Barbara, 407
Saad, Bahruddin B., 561
Sahoo, Sarata K., 335
San Andres, M. P., 255
San José, C., 431
Sanchez Perez, A., 139
Sánchez-Pedreño, Concepción, 129
Santa, Tomofumi, 381
Saraswati, Rajananda, 95
Sarradin, P. M., 79
Sasamoto, Kazumi, 113
Sato, Jun, 89
Saurina, J., 305
Savini, Luisa, 319
Saxena, Reena, 403
Schiffrin, David J., 175
Schulman, S. G., 463
Semma, Masanori, 135
Sharp, Michael, 69
Shi, Yujun, 573
Shiga, Masanobu, 113
Shih, Jeng-Shong, 517
Shinde, V. M., 391
Shpigun, Lilija K., 201
Sievert, Ramón Cózar, 485
Sin, Yoke Min, 273, 281
Singh, Ajai K., 403
Skarping, Gunnar, 41
Smeller, Johanna M., 207
Srivastava, Suresh K., 495
Stoddart, Barry, 117
Suliman, Fakhr Eldin O., 561
Sultan, Salah M., 561
Summers, Leslie J., 523
Sun, Ailing, 565, 569
Susanto, Joko P., 187
Tachibana, Masaki, 437
Taniguchi, Isao, 113
Thompson, Michael, 261, 271
Tobal, Lorenzo, 129
Tomás, Virginia, 471
Tosunoğlu, Sedat, 373
Townshend, Alan, 117, 467
Toyo'oka, Toshimasa, 385
Tranter, R. L., 355
Turrion Nieves, M. B., 139
Uchida, Chikako, 63
Uden, Peter C., 419
Ueno, Keiyu, 113
Val, Otilia, 471
Valcárcel, M., 179
Valiraki, Aspasia P., 533
Valle Fuentes, F. J., 85
Van Calsteren, M. R., 395
van den Berg, Constant M. G., 143
Van den Borre, A., 463
Van der Weken, G., 463
Van Peteghem, Carlos, 577
Vanoosthuyze, Kristina E., 577
Velasco-García, Nieves, 457
Vera, S., 255
Vetter, Thomas W., 95
Vianna-Soares, Cristina D., 193
Vinha, Carlos A., 351
Voigtman, Edward, 325
Volker, F., 35
Vyza, Ekaterini A., 533
Wada, Hiroko, 167
Wang, Qiong-e, 121
Ward, Neil I., 341
Watters, Jr., Robert L., 95
Williams, Carl A., 341
Wilson, Robert, 175
Winquist, Fredrik, 155
Wong, Ming Keong, 273, 281
Woodhead, Jon D., 35
Xie, Bin, 155
Yamamoto, Atsushi, 377
Yaman, Mehmet, 101
Yang, Yu, 243
Yu, Ru-Qin, 499
Yuchi, Akio, 167
Zaki, M. T. M., 549
Zanoni, Maria Valnice B., 505
Zen, Jyh-Myng, 511
Zhang, Fan, 121
Zhang, X. R., 463
Zhang, Zhujun, 453
Zheng, Guo-Dong, 499
Zhuang, Hui-sheng, 121
Zolotov, Yury A., 201

INTERACTIVE CHEMISTRY TRAINING SOFTWARE

FROM THE ROYAL SOCIETY OF CHEMISTRY

Interactive Chemistry Training Software offers a first-class range of computer packages for analytical chemists, spectroscopists, and health and safety officers, produced by **Cognitive Solutions Ltd.,** a software house specialising in the development of packages for computer-based interactive training. There are currently five software packages available:

GC SoftBook **SoftCOSHH™ v2.0**

HPLC SoftBook **AAS SoftBook** **ICP SoftBook**

The visual, interactive nature of the product offers a much fuller and more effective method of training than conventional methods. The various principles and practical applications are presented in a colourful, animated form which is easy to use and requires minimal computer knowledge.

Each package is relatively inexpensive, representing a much more cost-effective training facility than more conventional techniques. Learning proceeds at the user's own pace, and any given section of the packages can be readily replayed, ensuring that principles can be grasped thoroughly before laboratory equipment is handled.

Full technical support is available to the purchaser, providing advice on content and usage of each package.

1995 Prices (VAT to be added)

All Packages are £295.00

SoftCOSHH™ v2.0 is £695.00

15% discount for educational users.
Multiple user discount prices available.

To order please contact:

The Royal Society of Chemistry, Turpin Distribution Services Limited, Blackhorse Road, Letchworth, Herts SG6 1HN, United Kingdom.
Telephone: +44 (0) 1462 672555. Fax: +44 (0) 1462 480947.
Please quote your credit card details. We can accept Access/Visa/Mastercard/EuroCard.

Turpin Distribution Services Limited is wholly owned by The Royal Society of Chemistry.

For information on RSC books and journals please contact:

Sales and Promotion Department, The Royal Society of Chemistry, Thomas Graham House, Science Park,
Milton Road, Cambridge CB4 4WF, United Kingdom.
Telephone: +44 (0) 1223 420066. Fax: +44 (0) 1223 423429. E-mail (Internet): RSC1@RSC.ORG.

RSC Members should order from the Membership Administration Department at the Cambridge address above.

THE ROYAL SOCIETY OF CHEMISTRY

Information Services

Book Reviews

Solid-State NMR I: Methods and II: Inorganic Matter
* Edited by P. Diehl, E. Fluck, H. Günther, R. Kosfeld and J. Seelig. *NMR Basic Principles and Progress. Volumes 30 and 31.* Pp. x + 282 (Volume I); x + 216 (Volume II). Springer-Verlag. 1994. Price DM248.00; sFr24.00; ÖS1934.00. ISBN 3-540-57189-2 (Volume I); 3-540-57190-6 (Volume II)

Nuclear magnetic resonance (NMR) spectra of solids cannot be measured in the same way as those from liquids and solutions. This is because the presence in solids of anisotropic interactions which in liquids are exactly averaged by the rapid thermal motion of the molecules. Chemical applications of NMR rely greatly on the fact that the precise value of the radiofrequency absorbed by the various nuclei in an organic molecule depends on the chemical environments giving rise to distinct 'chemically shifted' lines. The parameters derived from the spectrum of a liquid (positions, widths, intensities and multiplicities of lines, relaxation rates and mechanisms) provide information on the structure, conformation and molecular motion. By contrast, conventional NMR of solids, instead of sharp spectral lines, gives broad humps that conceal most of the information of interest to a chemist.

The development of magic-angle-spinning (MAS) NMR initiated a new era in the structural study of solids. The technique has greatly enhanced our knowledge of a wide range of materials used in the chemical, physical, biological and earth sciences and in the technology of glass and ceramics. However, it took nearly 20 years for MAS to become a routine tool for structural investigation. This is because of the difficulty in spinning the sample at the very high speeds required and insufficiently high magnetic fields. However, the introduction of Fourier-transform NMR, cross-polarization and superconducting magnets, during the 1960s and 1970s, greatly improved sensitivity. Many new techniques have appeared since Schaefer and Stejskal combined MAS and cross-polarization for the ^{13}C NMR of organics. For example, double-rotation (DOR) NMR, in which the sample is rotated around two different axes simultaneously, can monitor the nature of phase transitions, while spin-echo double resonance (SEDOR) determines the relative spatial disposition of spins.

Solid-state NMR is developing very rapidly and there is a constant need for up-to-date information about recent achievements. The general textbooks by Mehring and Fyfe were published more than 10 years ago, while the various monographs refer to specialized problems, and as such are of little interest to the general scientific audience. Volumes 30 and 31 of the series *NMR Basic Principles and Progress* remedy the problem. Not that they are addressed to beginners, but they need to be read, with great profit, by all those who work in solid-state chemistry or physics and are familiar with basic NMR techniques.

The 62-page opening chapter of NMR volume 30, entitled 'Introduction to Solid-State NMR', by Grimmer and Blümich is written in this spirit. The explanation of the fundamental techniques is very clear. Although the chapter necessarily covers mostly old ground, many modern examples are included. I note that the authors were able to dispense with the spherical tensor formalism, which chemists often find taxing. Lauprêtre's 'High-Resolution ^{13}C NMR Investigations of Local Dynamics in Bulk Polymers at Temperatures Below and Above the Glass Transition Temperature' is a useful monograph for everyone working with polymers. The chapter by Raftery and Chmelka on 'Xenon NMR Spectroscopy' is excellent. ^{129}Xe NMR has recently found a number of uses in various fields (particularly heterogeneous catalysis), and the authors themselves have greatly contributed to this development. I am particularly impressed by their ^{129}Xe 2D exchange spectrum (Fig. 19) and by the description of very exciting experiments that use optical pumping to probe the surfaces of solids.

In the chapter 'NMR as a Generalized Incoherent Scattering Experiment' Fleischer and Fujara draw on the analogy between stimulated echos in NMR and incoherent quasi-elastic neutron scattering. The chapter, which will have greater appeal to the physicist than to the chemist, is illustrated by some elegant experiments. The final contribution, 'NMR Imaging of Solids', by Blümler and Blümich is an up-to-date exposition of a rapidly growing field with applications mainly in chemical engineering. The various ideas described in this chapter will also be of interest to scientists working in medical imaging.

'these two volumes are certainly very welcome and will be indispensable to most solid-state NMR spectroscopists'.

NMR volume 31 opens with the chapter by Engelhardt and Koller '^{29}Si NMR of Inorganic Solids'. Engelhardt has been pursuing fundamental ^{29}Si and ^{27}Al studies of silicates and aluminosilicates, particularly zeolites since 1980, and in 1987 published an excellent monograph on the subject (in collaboration with Michel). This chapter is, of course, more up to date than that book. Clays and amorphous silicates are also discussed, and a good account is given of Fyfe's elegant two-dimensional ^{29}Si studies of purely siliceous zeolites, which led to an unambiguous assignment of ^{29}Si resonances to individual crystallographic sites for silicon in a number of materials.

Pfeifer's 'NMR of Solid Surfaces' is devoted to three topics: firstly, NMR studies of Brønsted acid sites in zeolites, carried out mainly by the author's group in Leipzig over the last 20 years are crucial to the understanding of the catalytic acidity of zeolites. No fewer than five different kinds of hydroxyls in zeolitic and $AlPO_4$ molecular sieves have been identified, and the NMR spectra correlated with infrared spectra; secondly, ^{27}Al NMR studies of extra-framework aluminium are closely related to Lewis acidity; and thirdly, molecular transport measurements, using the pulsed field gradient method, provide a direct measure of diffusion coefficients of adsorbed species, superior to that given by volumetric measurements.

Sebald's chapter deals with 'MAS and CP/MAS NMR of Less Common Spin-1/2 Nuclei'. ^{89}Y, ^{109}Ag, ^{183}W, ^{103}Rh and ^{57}Fe have low gyromagnetic ratios and are thus difficult to measure. However, they are important to a number of new materials, such as ceramics, high-temperature superconductors, homo- and heteropolytungstates and heterogeneous catalysts. Nuclei with large chemical-shift anisotropies (^{119}Sn, ^{199}Hg, ^{207}Pb, ^{195}Pt and ^{205}Tl) present spectroscopic problems of their own, but their study provides useful structural information, especially for organometallic chemistry. ^{113}Cd is also an interesting nucleus. The author, who did much of the work in this field, correlates solid-state and solution spectra and summarizes the results with admirable clarity.

Jäger's 'Satellite Transition Spectroscopy of Quadrupolar Nuclei' describes a useful method for deriving structural information on solids, particularly concerning quadrupolar parameters, from spinning sidebands which are often better resolved than the main resonance. A considerable gain in

resolution is also found, especially for high-spin nuclei, when observing satellite transitions rather than the central transition. Several applications to 'difficult' solids (such as glasses) are described. I wonder, however, whether the method really deserves the grand name of 'spectroscopy' (it is, after all, only one of many methods of NMR spectroscopy) or its own acronym (SATRAS).

In the timely review 'NMR-NQR Studies of High-Temperature Superconductors' Brinkmann and Mali summarize results in this field which involve mainly 'NMR-unfriendly' nuclei.

The advanced methods described in this book will soon be more widely employed to resolve many hitherto inaccessible problems in solid-state chemistry and physics. The field is certain to flourish in the years to come. I do not know whether the publishers plan further volumes on solid-state NMR to cover subjects (such as double rotation, dynamic angle spinning, spin-echo double resonance, cross-polarization to and from quadrupole nuclei and rotational resonance, to name but a few) which have been left out of volumes 30 and 31. In any case, these two volumes are certainly very welcome and will be indispensable to most solid-state NMR spectroscopists.

Jacek Klinowski
Department of Chemistry
University of Cambridge, UK

Efficiency in Research, Development and Production: The Statistical Design and Analysis of Chemical Experiments

By Leslie Davies. Royal Society of Chemistry. Pp. xii + 180. 1993. Price £19.50. ISBN 0-85186-137-7.

This book describes well some of the statistical techniques that have grown in the field of analytical chemistry. An easy to read book whose context covers the basics of error, accuracy and precision estimation, analysis of variance, experimental design and optimization procedures. The essentials of statistical analysis are dealt with in Chapter 2, which contains many worked examples and in-text exercises. Everything you would expect to find for the analytical chemist in terms of basic parametric testing can be found in this chapter. The main strength of this book and where it differs from other popular statistical texts is its in-depth approach to experimental design. Seven good chapters take the reader through the rationale of experimental design, factorial designs at two levels, fractional factorial designs at two levels, fractional factorial designs in sequence and factorial experiments at three levels. Again each chapter makes good use of worked examples and the fractional factorial approach is perhaps one of the best elucidations of the technique currently available to analytical chemists. In a more limited way, optimization forms the basis of chapters 4, 11 and 9 and although brief it was good to see a short chapter dedicated to Taguchi experimental design methodology. The book contains appendices of the necessary statistical tables and a valuable critique of current computer packages suitable for statistical data processing. Each chapter is augmented with a reference section and there is a very usable reference subject index at the rear of the book.

To one who read the book cover to cover the structure of the chapters seemed a little illogical with the Statistical Analysis chapter breaking up the Factorial Design chapters. In addition the optimization chapters have not been dealt with as a group. Nevertheless, to the reader who wants to access techniques and get going quickly with data analysis, there is a good contents list and one soon finds ones way around the chapters.

A compact book of 180 pages, this book is bursting with information on how to statistically process data. Its great strength for me was its approach to experimental design which is a subject of growing importance but for which few good practical texts exist. Strongly recommended for its experimental design, this book also offers a good readable source of basic statistical methods such as error and significance testing and deals suitably with optimization procedures. Reasonably priced and well produced by the RSC.

S. J. Haswell
School of Chemistry
University of Hull, UK

Computer-Enhanced Analytical Spectroscopy

Edited by Charles L. Wilkins. *Modern Analytical Chemistry. Volume 4.* Pp. xviii + 308. Plenum. 1993. Price US$89.50. ISBN 0-306-44456-9.

This is a collection of 12 papers presented at a symposium held in June 1992 on the application of chemometrics to analytical spectroscopy. They will probably be of more interest to people concerned with instrument and software design than to practising Analysts.

Most of the usual chemometric methods make an appearance (principal components, neural networks, Kalman filters, maximum entropy and others). Each paper discusses its authors' experience in applying such methods to a particular type of spectroscopy and a single or limited set of problems within that type. There are no general reviews covering all the possible methods for a problem or type of spectroscopy, nor all the applications of a chemometric method.

Except for one paper on UV/VIS spectroscopy most of the problems are either of structure determination or identification of 'unknowns' from a library. As is usual with chemometrics most of the work is empirical, with concentration on the statistics and computing rather than on the underlying chemistry or the assignment of the spectral features. Exceptions are a paper on computational chemistry which discusses the progress in *ab initio* calculation of vibrational spectra and the use of molecular mechanics to determine the conformation of adsorbed species in surface enhanced Raman spectroscopy and a paper on the prediction of fragmentation patterns in mass spectra.

'focuses on statistics and computing rather than on the underlying chemistry'

A theme that appears in several papers is the need for instruments that are sufficiently robust for 'field' examination of samples, *e.g.*, for identification of pollutants. Such instruments may have poorer resolution and calibration than laboratory instruments and the idea is to overcome this by chemometrics rather than by better engineering of the instruments. Analysts involved in these fields may be interested to review this work and consider whether this approach is acceptable. Particular attention needs to be given to the libraries and training sets to ensure that the question 'is this a controlled or forbidden substance?' is not confused with 'given that this is a forbidden substance, which forbidden substance is it?'.

Andrew Coutts
Rhone-Poulenc Rorer
Essex, UK

Conference Diary

Date	Conference	Location	Contact
1995			
March			
6–10	**PITTCON '95, Pittsburgh Conference On Analytical Chemistry and Applied Spectroscopy**	New Orleans, USA	**Pittsburgh Conference,** Suite 332, 300 Penn Centre Boulevard, Pittsburgh, PA 15235-9962, USA
9–10	**Advances in Genetic Screening and Diagnosis of Human Diseases**	San Fransisco, USA	**Ben Keddy,** Cambridge Healthtech Institute, Bay Colony Corporate Center, 1000, Wirter Street, Suite 3700, Waltham, MA 02154, USA **Tel:** +1 617 487 7989. **Fax:** +1 617 487 7937
13–16	**Trace Elements, Free Radicals, Cytokines, Chromosomal Analysis and Tumour Markers in Clinical Medicine and Biochemistry**	Kuwait City, Kuwait	**Hussain Dashti,** Department of Surgery, Faculty of Medicine, Kuwait University, P.O. Box 24923, Safat, Kuwait **Fax:** +965 531 8454
24	**The L.H. Sutcliffe Magnetic Resonance Symposium, covering ESR and NMR**	Guildford, UK	**Dr. D. G. Gillies,** Department of Chemistry, University of Surrey, Guildford, Surrey, UK GU2 5XH
28–31	**Scanning 95 Seventh Annual International Microscopy Meeting**	California, USA	**Mary K. Sullivan,** Foundation for Advances in Medicine and Science, P.O. Box 832, Mahwah, NJ 07430 0832, USA **Tel:** +1 201 818 1010. **Fax:** +1 201 818 0086
28–30	**3rd Symposium on Analytical Sciences**	Paris, France	**The Scientific Committee-3rd SAS,** 7 rue d'Argout, 75002 Paris, France **Tel:** +33 1 42 33 47 66
28–30	**Applications of Modern Mass Spectrometric Methods to Plant Science Research**	Swansea, UK	**Dr. R. P. Newton,** Biochemistry Group, School of Biological Sciences, University College, Swansea, Wales, UK SA2 8PP **Tel:** +44 (0)1792 295 377. **Fax:** +44 (0)1792 295 447
29–30	**Atomic Spectrometry Updates**	Bristol, UK	**J. R. Dean,** Department of Chemical and Life Sciences, University of Northumbria at Newcastle, Ellison Building, Newcastle upon Tyne, UK NE1 8ST **Tel:** +44 (0)191 227 3517. **Fax:** +44 (0)191 227 3519
April			
3–6	**7th Instrumental Analysis Symposium**	Madrid, Spain	**7as Jomadas de Analisis Instrumental (JAI) Expoanalitica & Biocienca,** Arda Reina Mª Cristina, Palacio no. 1, 08004-Barcelona, Spain **Tel:** +34 3 423 3101. **Fax:** +34 3 423 6348
10–13	**Annual Chemical Congress (with Analytical Session)**	Edinburgh, UK	**Dr. J. F. Gibson,** The Royal Society of Chemistry, Burlington House, Piccadilly, London, UK W1V 0BN **Tel:** +44 (0)171 437 8656. **Fax:** +44 (0)171 734 1227
23–25	**6th International Symposium on Pharmaceutical and Biomedical Analysis**	St. Louis, USA	**Shirley Schlessinger,** 400, East Randolph Street, Suite 1015, Chicago, Illinois 60601, USA **Tel:** +1 312 527 2011.
26–28	**6th International Symposium on Chiral Discrimination**	St. Louis, USA	**Shirley Schlessinger,** 400, East Randolph Street, Suite 1015, Chicago, Illinois 60601, USA **Tel:** +1 312 527 2011.
May			
3	**New Techniques in Bioanalysis**	Bradford, UK	**A. J. Crooks,** 'Cartref', 35 Queensbury Road, Salisbury, Wiltshire, UK SP1 3PH **Tel:** +44 (0)1722 334974.
7–10	**Handling of Environmental and Biological samples in Chromatography**	Lund, Sweden	**Mrs. M. Frei-Häusler,** Postfach 46, CH-4123 Allschwil 2, Switzerland **Fax:** +41 61 482 0805

Date	Conference	Location	Contact
7–11	**86th AOCS Annual Meeting & Expo**	Texas, USA	**AOCS Education/Meetings Department,** P.O. Box 3489, Champaign, IL 61826-3489, USA **Tel:** +1 217 359 2344. **Fax:** +1 217 351 8091
7–11	**Seventeenth International Symposium on Capillary Chromatography and Electrophoresis**	Virginia, USA	**Dr. Milton L. Lee,** Department of Chemistry, Brigham Young University, Provo, UT 84602-4672, USA **Tel:** +1 801 378 2135. **Fax:** +1 801 378 5474
9–12	**Metal Compounds in Environmental and Life 6—Analysis, Speciation and Specimen Banking**	Jülich, Germany	**H. W. Dürbeck,** Institute of Applied Physical Chemistry, Research Center Jülich (KFA), P.O. Box 1913, D-5170 Jülich, Germany
14–18	**EMAS 95 on Modern Developments and Applications in Microbeam Analysis**	St Malo, France	**EMAS Secretariat,** RIKILT-DLO, P.O. Box 230, 6700 AE Wageningen, The Netherlands
16–18	**Fourth International Conference on Progress in Analytical Chemistry in the Steel and Metals Industry**	Luxembourg	**R. Jowitt,** British Steel plc, Technical, Teesside Laboratories, P.O. Box 11, Grangetown, Middlesbrough, Cleveland, UK TS6 6UB **Fax:** +44 (0)1642 460321
21–26	**CLEO '95: Conference on Lasers and Electro-Optics**	Baltimore, USA	**Meetings Department,** Optical Society of America, 2010 Massachusetts Avenue, NW, Washington, DC 20036-1023, USA **Tel:** +1 202 223 9034. **Fax:** +1 202 416 6100
21–26	**QELS '95: Quantum Electronics and Laser Science Conference**	Baltimore, USA	**Meetings Department,** Optical Society of America, 2010 Massachusetts Avenue, NW, Washington, DC 20036-1023, USA. **Tel:** +1 202 223 9034. **Fax:** +1 202 416 6100
21–26	**ASMS Conference on Mass Spectrometry**	Atlanta, USA	**ASMS,** 815 Don Gaspar, Santa Fe, NM 87501, USA **Tel:** +1 505 989 4517.
22–24	**Eighth International Symposium on Polymer Analysis and Characterization (ISPAC-8)**	Sanibel Island, USA	**ISPAC Registration,** 815 Don Gaspar, Sante Fe, NM 87501 USA **Tel:** +1 505 989 4735. **Fax:** +1 505 989 1073
28–2/6	**19th International Symposium on Column Liquid Chromatography**	Innsbruck, Austria	**HPLC '95 Secretariat,** Tyrol Congress, Marktgraben 2, A-6020 Innsbruck, Austria **Tel:** +43 512 575600. **Fax:** +43 512 575607
June			
5–8	**5th Symposium on our Environment and 1st Asia–Pacific Workshop on Pesticides**	Convention City, Singapore	**The Secretariat,** 5th Symposium on our Environment, c/o Department of Chemistry, National University of Singapore, Kent Ridge, Republic of Singapore 0511 **Fax:** +65 779 1691
11–14	**1995 International Symposium, Exhibit and Workshops on Preparative Chromatography, Ion Exchange, and Adsorption/Desorption Processes**	Washington DC, USA	**Mrs. Janet Cunningham,** PREP '95 Symposium/ Exhibits Manager, Barr Enterprises, 10120 Kelly Road, P.O. Box 279, Walkersville, MD 21793, USA **Tel:** +1 301 898 3772. **Fax:** +1 301 898 5596
13–16	**ESIS 95—New Infrared Spectroscopy and Microspectroscopy: FTIR and Raman**	Lyon, France	**G. Lachenal,** Laboratoire des Materiaux Plastiques et Biomateriaux, Université Claude Bernard Lyon 1, 43 Boulevard du 11 Novembre, 69622 Villeurbanne Cedex, France
July			
2–6	**VII International Congress of Toxicology**	Seattle, USA	**Jada Hill,** The Sterling Group, 9393 W, 110th St., Suite, Overland Park, KS 66210, USA **Tel:** +1 913 345 2228. **Fax:** +1 913 345 0893
2–7	**12th International NMR Meeting**	Manchester, UK	**Dr. J. E. Gibson,** Royal Society of Chemistry, Burlington House, Piccadilly, London, UK W1V 0BN
9–13	**3rd International Symposium on Applied Mass Spectrometry in Health Sciences and 3rd European Tandem Mass Spectrometry Conference**	Barcelona, Spain	**Professor Emilio Gelpi,** Palau de Congressos, Departamento de Convencions, Avda, Reina Ma Christina, 08004 Barcelona, Spain

Date	Conference	Location	Contact
9–14	**13th Australian Symposium on Analytical Chemistry/4th Environmental Chemistry Conference**	Darwin, Australia	**13AC/4EC, Symposium Secretariat,** Convention Catalyst Int., GPO Box 2541, Darwin NT 0801, Australia **Tel:** +61 89 811 875. **Fax:** +61 89 411 639
9–15	**SAC 95**	Hull, UK	**Analytical Division,** The Royal Society of Chemistry, Burlington House, Piccadilly, London, UK W1V 0BN **Tel:** +44 (0)171 437 8656. **Fax:** +44 (0)171 734 1227
10–13	**Vth COMTOX Symposium on Toxicology and Clinical Chemistry of Metals**	Vancouver, Canada	**F. William Sunderman, Jr., M.D.,** Departments of Laboratory Medicine and Pharmacology, University of Connecticut Medical School, P.O. Box 1292, Farmington, CT 06034-1292, USA **Tel:** +1 203 679 2328. **Fax:** +1 203 679 2154
30–5/8	**XXIInd International Conference on Phenomena in Ionized Gases**	Hoboken, USA	**E. E. Kunhardt,** Physics Department, Stevens Institute of Technology, Hoboken, NJ 07030 USA **Tel:** +1 201 216 5099. **Fax:** +1 201 216 5638

August

5–10	**1995 International Symposium on Soil and Plant Analysis**	Wageningen, The Netherlands	**Soil and Plant Analysis Council,,** Georgia University Station, P.O. Box 2007, Athens, GA 30612-2007, USA **Tel:** +1 706 546 0425. **Fax:** +1 706 548 4891
13–17	**ICFIA '95, 7th International Conference on Flow Injection Analysis and JAFIA, Japanese Association for Flow Injection Analysis**	Seattle, USA	**Gary D. Christian,** Department of Chemistry, BG-10, University of Washington, Seattle, WA 98195, USA **Tel:** +1 206 685 3478. **Fax:** +1 206 543 5340. **E-Mail**: christia@chem.washington.edu
20–25	**12th International Symposium on Plasma Chemistry**	Minneapolis, USA	**L. Graven,** 315 Pillsbury Drive, SE, University of Minnesota, Minneapolis, MN 55455-0139, USA **Tel:** +1 612 625 9023. **Fax:** +1 612 626 1623
27–2/9	**CSI XXIX: Colloquium Spectroscopicum Internationale**	Leipzig, Germany	**GDCh-Geschäftsstelle, Abt. Tagungen,** Varrentrappestr. 40–42, Postfach 90 04 40, D-6000 Frankfurt am Main 90, Germany **Tel:** +49 69 791 7358. **Fax:** +49 69 791 7475
27–1/9	**46th Annual Meeting of the International Society of Electrochemistry (ISE46)**	Xiamen, China	**Secretariat,** XLVIth ISE Annual Meeting, P.O. Box 1995, Xiamen University, Xiamen 361005, China **Tel:** +86 592 208 5349. **Fax:** +86 592 208 8054
27–1/9	**Third International Conference on Magnetic Resonance Microscopy**	Würzburg, Germany	**Dr. A. Haas,** Physikalisches Institute, Universität Würzburg, Am Hubland, D-97074 Würzburg, Germany
27–30	**EUROTOX**	Prague, Czech Republic	**Czech Medical Association J. E. Purkyně,** EUROTOX '95, P.O. Box 88, Sokolská 31, 120 26 Prague 2, Czech Republic **Tel:** +42 2 24 915195. **Fax:** +42 2 24 216836

September

1–4	**CSI XXIX, Post-symposium ICP-MS and 11th German ICP-MS Users Meeting**	Wernigerode, Germany	**Professor Lieselotte Moenke,** Department of Chemistry, Martin-Luther University, Halle-Wittenberg, Institute of Analytical and Environmental Chemistry, Weinbergweg 16, D-06120 Halle, Germany
3–6	**Third International Meeting on Recent Advances in Magnetic Resonance Application to Porous Media**	Louvain la Neuve, Belgium	**Professor J. M. Dereppe,** Université de Louvain, Place L. Pasteur 1, B-1348, Louvain la Neuve, Belgium
3–8	**6th European Conference on the Spectroscopy of Biological Molecules**	Villeneuve d'Ascq, France	**Professor J. C. Merlin,** ECSBM '95, LASIR, UST Lille Bât. C5, 59655 Villeneuve d'Ascq Cedex, France

Date	Conference	Location	Contact
5–8	**RSC Autumn Meeting. Analytical and Faraday Symposium: Ions in Solution**	Sheffield, UK	**Dr. J. F. Gibson,** The Royal Society of Chemistry, Burlington House, Piccadilly, London, UK W1V 0BN **Tel:** +44 (0)171 437 8656. **Fax:** +44 (0)171 734 1227
10–14	**Ion-Ex '95, The Fourth International Conference and Industrial Exhibition on Ion Exchange Processes**	Wrexham, UK	**Ion-Ex '95 Conference Secretariat,** Faculty of Science, The North East Wales Institute, Connah's Quay, Deeside, Clwyd, UK CH5 4BR **Fax:** +44 (0)1244 814305
12–15	**5th [illegible]rnational Symposium on Drug Analysis**	Leuven, Belgium	**Professor J. Hoogmartens,** Institute of Pharmaceutical Sciences, Van Evenstraat 4, B-3000 Leuven, Belgium **Tel:** +32 16 32 34 40. **Fax:** +32 16 32 34 48
17–21	**30th Annual Meeting of the Federation of Analytical Chemistry and Spectroscopy Societies**	Philadelphia, USA	**FACSS, P.O. Box 278,** Manhattan, KS 66502-0003, USA **Tel:** +1 301 846 4797
24–28	**11th Asilomar Conference on Mass Spectrometry—Molecular Structure Determination: Activation, Mass Analysis and Detection**	Pacific Grove, USA	**Professor R. Graham Cooks,** Department of Chemistry, 1393 Brown Building, Purdue University, West Lafayette, IN 47907, USA
25–28	**5th Symposium on 'Kinetics in Analytical Chemistry' (KAC '95)**	Moscow, Russia	**Dr. I. F. Dolmanova,** Analytical Chemistry Division, Chemical Department, Lomonosov Moscow State University, 119899 Moscow, Russia **Tel:** +7 095 939 3346. **Fax:** +7 095 939 2579
October			
1–5	**21st World Congress of the International Society for Fat Research (ISF)**	The Hague, The Netherlands	**Mrs. J. Wills,** ISF Secretariat, P.O. Box 3489, Champaign, IL 61826–3489, USA **Tel:** +1 217 359 2344. **Fax:** +1 217 351 8091
9–13	**ECASIA '95**	Montreux, Switzerland	**EPEL-ECASIA 95,** Department des Materiaux/ LMCH, CH-1015 Lausanne, Switzerland **Fax:** +41 21 693 3946
15–20	**22nd Annual Conference of the Federation of Analytical Chemistry and Spectroscopy Societies**	Cincinnati, USA	**Joseph A. Caruso,** FACSS National Office, 198 Thomas Johnson Dr., Suite S-2, Frederick, MD 21702, USA **Tel:** +1 301 694 8122. **Fax:** +1 301 694 6860
24–27	**BCEIA '95—The International Sixth Beijing Conference and Exhibition on Instrumental Analysis**	Beijing, China	**General Service Office,** The International Sixth BCEIA, Room 585, Chinese Academy of Science Room, San Li He, Xi Jiao, P.O. Box 2143, Beijing 100045, China
November			
5–10	**1st Mediterranean Basin Conference on Analytical Chemistry**	Cordoba, Spain	**Professor Alfredo Sanz-Medel,** Department of Physical and Analytical Chemistry, Faculty of Chemistry, University of Oviedo, C/Julían Clavería, no. 8 33006 Oviedo, Spain **Tel:** +34 85 103474. **Fax:** +34 85 103480
5–10	**OPTCON '95**	San Jose, USA	**Meetings Department,** Optical Society of America, 2010 Massachusetts Avenue, NW, Washington, DC 20036-1023, USA **Tel:** +1 202 223 9034. **Fax:** +1 202 416 6100
14–15	**International Conference for Chemical Information Users**	Manchester, UK	**Dr. M. P. Coward,** Chemistry Department, UMIST, P.O. Box 88, Manchester, UK M60 1QD **Tel:** +44 (0)161 200 4491. **Fax:** +44 (0)161 228 1250
December			
17–22	**International Symposium on Environmental Biomonitoring and Specimen Banking**	Hawaii, USA	**K. S. Subraimanian,** Environmental Health Directorate, Health Canada, Tunney's Pasture, Ottawa, Ontario, Canada K1A OL2 **Tel:** +1 613 957 1874. **Fax:** +1 613 941 4545
20–21	**2nd LC/MS Symposium**	Cambridge, UK	**Dr. J. Oxford,** Glaxo Research and Development, Park Road, Ware, Hertfordshire, UK SG12 0DJ

Date	Conference	Location	Contact
1996			
January			
8–13	**1996 Winter Conference on Plasma Spectrometry**	Florida, USA	**R. Barnes,** Department of Chemistry, Lederle GRC Tower, University of Massachusettes, P.O. Box 34510, Amherst, MA 01003-4510, USA **Tel:** +1 413 545 2294. **Fax:** +1 413 545 4490
21–25	**VIth Latin American Congress on Chromatography**	Caracas, Venezuela	**Irene Romero,** Interep SA, P.O. Box 76343, Caracas 1070-A, Venezuela
February			
6–9	**Fourth International Symposium on Hyphenated Techniques in Chromatography (HTC 4); Hyphenated Chromatographic Analysers**	Bruges, Belgium	**Dr. R. Smits, Royal Flemish Chemical Society (KVCV), Working Party on Chromatography,** BASF Antwerpen N.V., Central Laboratory, Haven 725, Scheldelaan 600, B-2040 Antwerp, Belgium **Tel:** +32 3 561 2831. **Fax:** +32 3 561 3250
March			
17–21	**47th Pittsburgh Conference on Analytical Chemistry and Applied Spectroscopy**	Atlanta, USA	**The Pittsburgh Conference,** 300 Penn Center Boulevard, Suite 332, Pittsburgh, PA 15235-5503 USA **Tel:** +1 412 825 3220. **Fax:** +1 412 825 3224
31–4/4	**7th International Symposium on Supercritical Fluid Chromatography and Extraction**	Indianapolis, USA	**Janet Cunningham,** Barr Enterprises, 10120 Kelly Road, P.O. Box 279, Walkersville, MD 21793 USA **Tel:** +1 301 898 3772. **Fax:** +1 301 898 5598
April			
23–36	**Analytica Conference '96**	Münich, Germany	**Congress Center,** Messegelände, D-80325 München, Germany **Tel:** +49 89 5107 159. **Fax:** +49 89 5107 180
May			
7–9	**VIIth International Symposium on Luminescence Spectrometry in Biomedical Analysis—Detection Techniques and Applications in Chromatograph and Capillary Electrophoresis**	Monte-Carlo, Monaco	**Prof. Dr. Willy R. G. Baeyens,** University of Ghent, Pharmaceutical Institute, Department of Pharmaceutical Analysis, Harelbekestraat 72, B-9000 Ghent, Belgium **Tel:** +32 9 221 8951. **Fax:** +32 9 221 4175
June			
16–21	**HPLC '96: 20th International Symposium on High Performance Liquid Chromatography**	San Francisco, USA	**Mrs. Janet Cunningham,** Barr Enterprises, P.O. Box 279, Walkersville, MD 21793, USA **Tel:** +1 301 898 3772. **Fax:** +1 301 898 5596
July			
8–12	**XVI International Congress of Clinical Chemistry**	London, UK	**Mrs. Pat Nielsen,** XVIth International Congress of Clinical Chemistry, P.O. Box 227, Buckingham, UK MK18 5PN **Fax:** +44 (0)1280 6487
September			
1–7	**Euroanalysis IX**	Bologna, Italy	**Professor Luigia Sabbatini,** Euroanalysis IX, Dipartimento di Chimica, Università di Bari, Via Orabona, 4, 70126 Bari, Italy **Tel:** +39 80 242020. **Fax:** +39 80 242026
15–20	**21st International Symposium on Chromatography**	Stuttgart, Germany	**GDCh-Geschäftsstelle, Abt. Tagungen,** Varrentrappestr. 40–42, Postfach 90 04 40, D-6000 Frankfurt am Main 90, Germany **Tel:** +49 69 791 7358. **Fax:** +49 69 791 7475
30–4/11	**31st Annual Meeting of the Federation of Analytical Chemistry and Spectroscopy Societies**	Kansas City, USA	**FACSS,** P.O. Box 278, Manhattan, KS 66502-0003, USA **Tel:** +1 301 846 4797

Courses

Date	Conference	Location	Contact
April			
4–5	**Workshop in Chemical Information Retrieval**	Manchester, UK	**Dr. M. P. Coward,** Chemistry Department, UMIST, P.O. Box 88, Manchester, UK M60 1QD **Tel:** +44 (0)161 200 4491. **Fax:** +44 (0)161 228 1250
4–7	**Short Course on Chiral Resolution**	Rome, Italy	**Dr. S. Faniti,** CNR, Istituto di Cromatografia, C.P.10, I 00016, Monterotondo Scalo, Roma, Italy **Fax:** +39 6 906 25 849
5	**Nuclear Waste Disposal**	Loughborough, UK	**Dr. P. Warwick,** Department of Chemistry, Loughborough University of Technology, Loughborough, Leicestershire, UK LE11 3TU **Tel:** +44 (0)1509 222585
May			
10	**Education and Training of Chromatographers**	London, UK	**Dr. D. Simpson,** Analysis for Industry, Factories 2/3, Bosworth House, High Street, Thorpe-le-Soken, Essex, UK CO16 0EA **Tel:** +44 (0)1255 861714. **Fax:** +44 (0)1255 662111
18	**Meat Authenticity: Introduction to Immunoassay Test Kits**	Campden, UK	**Training Department,** Campden Food and Drink Research Association, Chipping Campden, Gloucester, UK GL55 6LD **Tel:** +44 (0)1386 840319. **Fax:** +44 (0)1386 841306
21	**Techniques for Polymer Analysis and Characterization**	Sanibel Island, USA	**Dr. Petr Munk,** Department of Chemistry, University of Texas at Austin, Austin, Texas 78712, USA **Tel:** +1 512 471 4179. **Fax:** +1 512 471 8696
22–25	**Modern Practice of Gas Chromatography**	Pensylvania, USA	**Sally Stafford,** Hewlett-Packard, Little Falls Site, 2850 Centerville Road, Wilmington, DE 19808-1610, USA **Tel:** +1 302 633 8444
30–1/6	**Sixteenth Annual Introductory HPLC Short Course**	Pensylvania, USA	**Bill Champion,** DuPont Merck Pharmaceutical Company, PRF Building, Chambers Works, Deepwater, NJ 08023, USA **Tel:** +1 609 540 4826
June			
7–12	**4th Annual Course on Practical Methods of Digestion for Trace Analysis**	Amherst, USA	**Nancy Teranto,** Questron Corporation, 4044 Quakerbridge Road, Mercerville, NJ08619 USA **Tel:** +1 609 587 6898. **Fax:** +1 609 587 0513
6–8	**5th Annual Flow Injection Atomic Spectrometry Short Course**	Amherst, USA	**J. Tyson,** Department of Chemistry, LGRC Tower, University of Massachusetts, Box 34510, Amherst, MA 01003-4510 USA **Tel:** +1 413 545 0195. **Fax:** +1 413 545 4846
16–20	**Capillary Electrophoresis, Routine Method for the Quality Control of Drugs: Practical Approach**	Montpellier, France	**Professor H. Fabre,** Laboratory of Analytical Chemistry, Faculty of Pharmacy, 15 Avenue Charles Flahault 34060 Montpellier, France **Tel:** +33 67 54 45 20. **Fax:** +33 67 52 89 15
26–30	**Radioisotope Techniques Short Course**	Loughborough, UK	**Dr. P. Warwick,** Department of Chemistry, Loughborough University of Technology, Loughborough, Leicestershire, UK LE11 3TU **Tel:** +44 (0)1509 222585
July			
17–19	**Techniques Workshop (Chemometrics)**	Hull, UK	**Dr. M. J. Adams,** School of Applied Sciences, University of Wolverhampton, Wulfruna Street, Wolverhampton, UK WV1 1SB **Tel:** +44 (0)1902 322141. **Fax:** +44 (0)1902 322680

Entries in the above listing are included at the discretion of the Editor and are free of charge. If you wish to publicize a forthcoming meeting please send full details to: *The Analyst* Editorial Office, Thomas Graham House, Science Park, Milton Road, Cambridge, UK CB4 4WF. Tel: +44 (0)223 420066. Fax: +44 (0)223 420247.

Future Issues will Include—

Near-infrared reflectance spectroscopy in the determination of the physical state of primary materials in pharmaceutical production—**Piero Corti, Elena Dreassi, Giuseppe Ceramelli, Luisa Savini and Piero Luigi Perruccio**

Sorption of yttrium hydroxyquinolinates by polyurethane foam and its use in analysis—**S. V. Beltyukova, Ninel A. Nazarenko and Svetlana V. Tsygankova**

Laser-induced fluorescence in the graphite furnace as a sensitive technique for the assessment of traces in North Arctic atmospheric aerosol samples—**Jonas Enger, Yvonne Malmsten, Peter Ljungberg and Ove Axner**

Generalized method for the simultaneous multicomponent determinations through a single catalyst kinetic run by using the rate spectrum—**Zhi-Cheng Gu and Xian-De Wang**

Determination of oligomer distribution of alkylphenol polyethoxylates and fatty alcohol polyethocylates by positive ion atmospheric pressure chemical ionization-mass spectrometry —**S. Pattanaargsorn, S. Sangvanich, P. Petsom and S. Roengsumran**

Studies on the voltammetric behaviour of puerarin and its application—**Hu Jingho and Li Qilong**

Copper, zinc and aluminium from dietary sources in the femur, brain and kidney of guinea pigs and a study of some elements in *in vivo* intestinal digesta by size exclusion chromatography–inductively coupled plasma-mass spectrometry—**Helen M. Crews, Linda M. W. Owen, Robert C. Massey and Nicholas J. Bishop**

Determination of ytterbium using europium modifier and graphite furnace atomic absorption spectrometry—**Zhang Jie and Sixuan Guo**

Neutron activation analysis of environmental objects—**G. M. Kolesov**

Inductively coupled plasma-atomic emission spectrometry analysis of low levels of selenium in natural waters—**Rob L. Adkins, Nick Walsh, Mike Edmunds and Janice M. Trafford**

Inductively coupled plasma-atomic emission spectroscopic determination of rare earth elements in granites and breisens using thin layer chromatography preconcentration—**Natalia S. Safronova, Svetlana S. Matveeve, Yury I. Fabelinsky and Valentin A. Ryabukhin**

Neutron activation analysis of platinum, palladium, iridium and gold in reference materials: A comparison between two methods—**Claudio A. Noguiera and Ana M. G. Figueiredo**

Cyanide detection using an amperometric biosensor of tyrosinase with catechol substrate—**Xiaoya Hu and Zongahou Leng**

Estimation of sampling bias between different sampling protocols on contaminated land—**M. H. Ramsey, Ariadni Argyraki and Michael Thompson**

Effects of acute exercise on urinary losses and serum concentrations of copper and zinc of moderately trained and untrained men consuming a controlled diet—**Richard A. Anderson, Noella A. Bryden, Marilyn M. Polansky and Patricia Deuster**

Ion probe measurements of trace elements in NIST SRM-610 Glass Standards—**Richard W. Hinton, G. Witt-Eickschen and B. Harte**

Flow injection of tetracyclines by electrocatalytic oxidation at a nickel-modified glassy carbon electrode—**P. Southwell-Keely, W. Oungpiptat and P. W. Alexander**

Voltammetric behaviour of vitamin B_1 (thiamine) at a glassy carbon electrode and its determination in multivitamin tablets using anion-exchange liquid chromatography with amperometric detection under basic conditions—**J. P. Hart, Michael D. Norman and Stephen Tsang**

Epithermal neutron activation analysis of mosses used to monitor heavy metal deposition around an iron smelter complex—**M. V. Frontasyeva and E. Steinnes**

Catalytic determination of iodide using the promethazine–hydrogen peroxide redox reaction—**Masaaki Iwatsuki, Ashraf A. Mohamed, M. F. El-Shahat and Tsutomu Fukasawa**

Two approaches to the study of radiocaesium partitioning and mobility in agricultural soils from the Chernobyl area—**Miquel Vidal, Maria Roig, Anna Rigol, Montserrat Llaurado, Gemma Rauret, Jan Wauters, Agnes Elsen and Adrien Cremers**

Gas chromatographic–mass spectrometric determination of chlorophenols in the urine of sawmill workers with past use of chlorophenol-containing anti-stain agents—**Helena Kontsas, Christina Roesenberg, Pirkko Pfaffli and Paavo Jappinen**

COPIES OF CITED ARTICLES

The Royal Society of Chemistry Library can usually supply copies of cited articles. For further details contact: The Library, Royal Society of Chemistry, Burlington House, Piccadilly, London W1V 0BN, UK. Tel: +44 (0)71-437 8656. Fax: +44 (0)71-287 9798. Telecom Gold 84: BUR210. Electronic Mailbox (Internet) LIBRARY@RSC.ORG.

If the material is not available from the Society's Library, the staff will be pleased to advise on its availability from other sources.

Please note that copies are not available from the RSC at Thomas Graham House, Cambridge.

JAASbase

An essential time-saving PC literature search tool for the analytical chemist

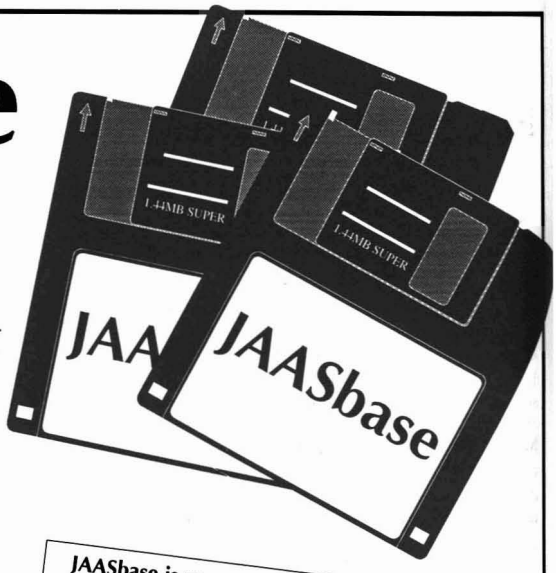

What JAASbase is ...

JAASbase is a unique database of atomic spectrometry reference information, containing full bibliographic references to journal articles and conference papers in the field of atomic spectrometry published since 1985. These references are selected by expert atomic spectroscopists, who add supplementary information that allows you to search for the references you require. The backfile (covering 1985 to 1994) contains over 28,000 references. Update disks add around another 4,000 references a year. JAASbase has been designed to work with the database manager Idealist, a fully indexed, free-text retrieval system.

How will JAASbase help you?

If you are an analytical scientist with a need for rapid access to information on techniques used in atomic spectrometry, JAASbase is the tool you need. Particularly if you work in an applications laboratory with a restricted budget for primary journals and little or no access to library facilities - JAASbase gives you instant access at your bench. Whether your area of analysis is food, the environment, quality control, geology, metallurgy, or whatever, JAASbase will quickly become an essential part of your working life.

JAASbase is your

- key to all atomic spectrometry literature
- user friendly guide to applications literature in many fields - geology, industrial analysis, the environment, food, clinical analysis ...
- easy way of keeping up with the growing volume of publications in your field
- convenient, time-saving, inexpensive searching facility on your PC
- own database - customize it to meet your specific requirements

1995 Subscription Price

JAASbase Backfile (1986-94)	£280.00/$490.00	Plus VAT in the UK
JAASbase Updates 1995	£ 99.00/$174.00	
Idealist Software	£210.00/$368.00	Available in disk size 3.5" or 5.25"

To order, please contact:

The Royal Society of Chemistry, Turpin Distribution Services Limited, Blackhorse Road, Letchworth, Herts SG6 1HN, United Kingdom. Telephone: +44 (0) 1462 672555. Fax: +44 (0) 1462 480947. Turpin Distribution Services Limited is wholly owned by The Royal Society of Chemistry.

RSC members' should order from:

The Royal Society of Chemistry, Membership Administration, Thomas Graham House, Science Park, Milton Road, Cambridge CB4 4WF, United Kingdom. Telephone: +44 (0) 1223 420066. Fax: +44 (0) 1223 423623. E-Mail: (Internet) RSC1@RSC.ORG.

THE ROYAL SOCIETY OF CHEMISTRY

Information Services

K:\ADS\JAASBASE.CDR

◆ N ◆ E ◆ W ◆

Focus on Diagnostics

... an important NEW monthly newsletter

Supplying crucial information drawn from both technical and commercial sources, this new publication brings together material that is otherwise difficult to access. Product, market and company information for diagnostics in the human health, animal health and agricultural sectors is covered quickly, worldwide. The newsletter is edited by an expert on the subject, who provides valuable analysis and comment. **Focus on Diagnostics** is a MUST for all those working in the sector.

With ***Focus on Diagnostics*** you can:

- scan ALL the relevant news in one place
- gain information vital to your business
- be alerted to news you would otherwise miss
- pinpoint potential competitor products whilst still at the r&d stage
- read about forthcoming conferences and key events

Subscribe to **Focus on Diagnostics** and keep one step ahead!

For a FREE sample please contact:

Alison Hey, Royal Society of Chemistry,
Thomas Graham House, Science Park,
Milton Road, Cambridge CB4 4WF, U.K.
Tel: +44 (0) 223 420066
Fax: +44 (0) 223 423429

ROYAL SOCIETY OF CHEMISTRY
Information Services

BAS

NEW Catalogue of BAS Certified Reference Materials

NEW Catalogue of Outside-Source Reference Materials

now available

For copies, please apply to:

BUREAU OF ANALYSED SAMPLES LTD
Newham Hall, Newby, Middlesbrough
Cleveland, England, TS8 9EA

Telephone: (01642) 300500
Fax: (01642) 315209

Circle 001 for further information

Gordon F. Kirkbright Bursary

In 1985, a fund was established as a memorial to Gordon F. Kirkbright for his contributions to analytical spectroscopy and to science in general. The fund is administered by the Committee of the Association of British Spectroscopists (ABS) and by the ABS Trust. The purpose of the fund is to enable promising young scientists (usually under the age of 30), such as postgraduate students or postdoctoral workers, of any nationality, to attend a recognized scientific meeting or to visit a place of learning. Application forms and full details may be obtained from:

Professor L. H. Sutcliffe,
Chemistry Department,
University of Surrey,
Guildford,
Surrey, GU2 5XH
United Kingdom

Phone: 0483 300800 ext. 9586 Fax: 0483 300803
E–mail: CHS1LS@SURREY.AC.UK

Completed application forms must be received no later than 28th February, 1995.

FIRST FOLD HERE

THE ANALYST READER ENQUIRY SERVICE

For further information about any of the products featured in the advertisements in this issue, write the appropriate number on the postcard, detach and post.

FOLD HERE

THE ANALYST READER ENQUIRY SERVICE

FEB'95

For further information about any of the products featured in the advertisements in this issue, please write the appropriate number in one of the boxes below.
Postage paid if posted in the British Isles but overseas readers must affix a stamp.

PLEASE USE BLOCK CAPITALS LEAVING A SPACE BETWEEN WORDS *Valid 12 months*

1 NAME

2 COMPANY

PLEASE GIVE YOUR BUSINESS ADDRESS IF POSSIBLE. IF NOT, PLEASE TICK HERE ☐

3 STREET

4 TOWN

5 COUNTY
POST CODE

6 COUNTRY

7 DEPARTMENT/
DIVISION

8 YOUR JOB TITLE/
POSITION

9 TELEPHONE NO

OFFICE USE ONLY REC'D PROC'D

FOLD HERE

Postage will be paid by Licensee

Do not affix Postage Stamps if posted in Gt. Britain, Channel Islands, N. Ireland or the Isle of Man

BUSINESS REPLY SERVICE
Licence No. WD 106

Reader Enquiry Service
The Analyst
The Royal Society of Chemistry
Burlington House, Piccadilly
LONDON
W1E 6WF
England

The unique source of information on analytical techniques

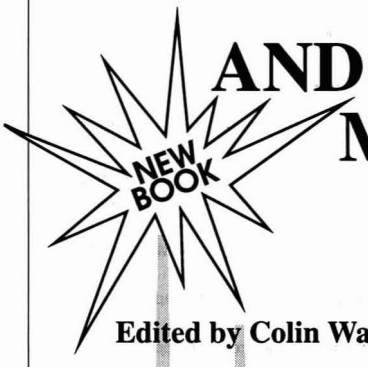

OFFICIAL AND STANDARDIZED METHODS OF ANALYSIS

Third Edition

Edited by Colin Watson, ***Atomic Spectrometry Consultancy, Ilford, Essex***

This important new book contains summaries of the analytical methods used in many areas, notably: health and safety; environmental monitoring; food analysis; quality control; water quality.

It enables analysts to assess all the options before committing to the particular technique that best suits their circumstances, whether performing only occasional analyses, analysing a wide variety of substances, or specializing in particular areas.

It provides details on development and evaluation of methods; the very latest techniques; detailed methods recommended by the Analytical Methods Committee of The Royal Society of Chemistry; food analysis methods approved by the Ministry of Agriculture, Fisheries and Food; water analysis; chromatographic and spectrometric methods; traditional 'wet' chemical tests.

It guarantees the analytical scientist certain benefits: informed purchasing and experimental decisions - saving time and money; confidence in achieving the most accurate, reliable results possible; and a sense of where given work and techniques fit in to the wider analytical picture.

Hardcover **xxiv + 778 pages** **ISBN 0 85186 441 4** **1994** **Price £110.00**

PLACE YOUR ORDER FOR THIS UNIQUE BOOK TODAY!

THE ROYAL SOCIETY OF CHEMISTRY
Information Services

To order, please contact:
The Royal Society of Chemistry, Turpin Distribution Services Limited, Blackhorse Road, Letchworth, Herts SG6 1HN, United Kingdom.
Telephone: +44 (0) 1462 672555. Fax: +44 (0) 1462 480947. Telex: 825372

RSC members wishing to purchase for personal use should contact:
The Royal Society of Chemistry, Membership Administration Department, Thomas Graham House, Science Park, Milton Road, Cambridge CB4 4WF, United Kingdom.
Telephone: +44 (0) 1223 420066. Fax: +44 (0) 1223 423623

485 **Determination of Total Base Number of Used Lubricating Oils From Marine Engines by Potentiometric Titration**—Maria Purificación Hernández Artiga, Juan Antonio Muñoz Leyva, Ramón Cózar Sievert

489 **Kinetic Model of pH-based Potentiometric Enzymic Sensors. Part 4. Enzyme Loading and Lifetime Factors**—Robert Koncki, Stanisław Głąb

495 **Determination of Lead Using a Poly(vinyl chloride)-based Crown Ether Membrane**—Suresh K. Srivastava, Vinod K. Gupta, Suresh Jain

499 **Nitrite-sensitive Liquid Membrane Electrodes Based on Metalloporphyrin Derivatives**—De Gao, Jun Gu, Ru-Qin Yu, Guo-Dong Zheng

503 **Incorporation of Dodecylbenzenesulfonic Acid in a Poly(vinyl chloride) Matrix Chloride Ion-selective Membrane Based on Tertiary Ammonium**—Satoshi Nomura

505 **Use of Solid-phase Extraction Cartridges With Differential-pulse Cathodic Stripping Voltammetry at a Hanging Mercury Drop Electrode: Determination of Nedocromil Sodium and Pentamidine Isethionate in Urine**—Maria Valnice B. Zanoni, Josino C. Moreira, Arnold G. Fogg

511 **Square-wave Voltammetric Determination of Copper(II) With a Nafion–Dimethylglyoxime Mercury-film Electrode**—Jyh-Myng Zen, Nai-Yuen Chi, Fu-Shien Hsu, Mu-Jye Chung

517 **Application of Crown Ether Coated Piezoelectric Crystal as a Detector for Ion Chromatography**—Yih-Song Jane, Jeng-Shong Shih

523 **'One-pot' Electrochemical Determination of Copper and Formaldehyde in Electroless Copper Plating Baths**—G. Bryan Balazs, Robert S. Glass, Leslie J. Summers

529 **Quantitative Determination of Cadmium, Zinc Thioneins Using Differential-pulse Polarography**—Amalia Muñoz, Adela Rosa Rodríguez

533 **Inclusion Complexes and Stability Studies of an Organophosphorous Insecticide With Cyclodextrins: Spectrophotometric and Kinetic Determination of Stability Constant**—Yannis L. Loukas, Ekaterini A. Vyza, Aspasia P. Valiraki

539 **Spectrophotometric Determination of Alkaline Phosphatase and α-Fetoprotein in Human Serum With 5,10,15,20-Tetrakis(4-phosphonooxyphenyl)porphine**—Takanori Kawakami, Shukuro Igarashi

543 **Mechanism of Nitrite-catalysed Oxidation of Chlorpromazine With Hydrogen Peroxide and/or Dissolved Oxygen Used for the Determination of Nitrite**—Bing Liang, Masaaki Iwatsuki, Tsutomu Fukasawa

549 **Spectrophotometric Determination of Silver and Gold with 5-(2,4-Dihydroxybenzylidene)rhodanine and Cationic Surfactants**—F. M. El-Zawawy, M. F. El-Shahat, A. A. Mohamed, M. T. M. Zaki

555 **Determination of Trace Amounts of Nickel by Chelating Ion Exchange and On-line Enrichment in Flow Injection Spectrophotometry**—Rajesh Purohit, Surekha Devi

561 **Use of the Sequential Injection Technique to Determine the Concentrations and Stoichiometries of Trimeprazine and Perphenazine Complexed With Palladium(II) in Hydrochloric Acid**—Salah M. Sultan, Fakhr Eldin O. Suliman, Bahruddin B. Saad

565 **Simultaneous Determination of Molybdenum and Tungsten Using a Flow Injection System and without Pre-separation**—Renmin Liu, Daojie Liu, Ailing Sun, Guihua Liu

569 **Simultaneous Determination of Copper and Zinc in the Hair of Children by pH Gradient Construction in a Flow Injection System**—Renmin Liu, Daojie Liu, Ailing Sun, Guihua Liu

573 **Spectrophotometric Determination of 1,4-Dihydroxyanthraquinone**—Kan Jin-qing, Shi Yujun

577 **Screening of Calf Urine for 19-Nortestosterone: Matrix Effect in Some Immunoassays**—Maurizio Paleologo Oriundi, Roberto Angeletti, E. Bastiani, Carlo Nachtmann, Kristina E. Vanoosthuyze, Carlos Van Peteghem

581 CUMULATIVE AUTHOR INDEX

NEWS AND VIEWS

19N **Book Reviews**

21N **Conference Diary**

26N **Courses**

27N **Papers in Future Issues**

Cover picture: Can analytical science be environmentally conscientious? (see Guest Editorial). Background photograph kindly supplied by The Building Research Establishment, Garston, Watford.

335 Simultaneous Measurement of Lithium and Boron Isotopes as Lithium Tetraborate Ion by Thermal Ionization Mass Spectrometry—Sarata K. Sahoo, Akimasa Masuda

341 Investigations Into the use of Inductively Coupled Plasma Mass Spectrometry for the Determination of Gold in Plant Materials—Carl A. Williams, Fadi R. Abou-Shakra, Neil I. Ward

347 Quantitative Analysis of Impurities in ε-Caprolactam by Raman Spectroscopy—Christos G. Kontoyannis, Nicolaos Ch. Bouropoulos, Petros G. Koutsoukos

351 Qualitative and Semiquantitative Analysis of Annatto and its Content in Food Additives by Photoacoustic Spectrometry—Ulrich Haas, Carlos A. Vinha

355 Extraction of Surfactants From Aqueous Media by Supercritical Fluid Extraction—M. Kane, J. R. Dean, S. M. Hitchen, C. J. Dowle, R. L. Tranter

361 Speciation of Selenium and Arsenic Compounds in Natural Waters by Capillary Zone Electrophoresis After On-column Preconcentration With Field-amplified Injection—Ke Li, Sam F. Y. Li

367 Time-resolved Luminescence Detection of Europium(III) Chelates in Capillary Electrophoresis—Martti Latva, Timo Ala-Kleme, Heidi Bjennes, Jouko Kankare, Keijo Haapakka

373 Determination of Baclofen in Human Plasma and Urine by High-performance liquid chromatography with Fluorescence Detection—Sedat Tosunoğlu, Lale Ersoy

377 Real-time Analysis of Multicomponent Chromatograms: Application to High-performance Liquid Chromatography—Atsushi Yamamoto, Akinobu Matsunaga, Mikiya Ohto, Eiichi Mizukami, Kazuichi Hayakawa, Motoichi Miyazaki

381 Enantiomeric Separation and Spectrofluorometric Detection of the Racemic Drugs, (±)-1-(2,6-Dimethylphenoxy)-2-propamine (Mexiletine) and (3*RS*)-4-Amino-3-hydroxybutanoic Acid (GABOB), Derivatized With 4-Fluoro-7-nitro-2,1,3-benzoxadiazole on a Phenylcarbamylated Cyclodextrin Bonded Stationary Phase—Takeshi Fukushima, Masaru Kato, Tomofumi Santa, Kazuhiro Imai

385 Development of Optically Active Fluorescent Edman-type Reagents—Toshimasa Toyo'oka, Yi-Ming Liu

391 Liquid–Liquid Extraction and Separation of Lanthanum(III) from Titanium(IV), Zirconium(IV), Hafnium(IV), Thorium(IV) and Uranium(VI)—N. G. Bhilare, V. M. Shinde

395 Determination of Free Selenomethionine in Nutritional Supplements by High-performance Liquid Chromatography Coupled with Thermochemical Hydride Generation Atomic Absorption Spectrometry—G. Matni, R. Azani, M. R. Van Calsteren, M. C. Bissonnette, J.-S. Blais

403 Salicylic Acid Functionalized Polystyrene Sorbent Amberlite XAD-2. Synthesis and Applications as a Preconcentrator in the Determination of Zinc(II) and Lead(II) by Using Atomic Absorption Spectrometry—Reena Saxena, Ajai K. Singh, Devendra P. S. Rathore

407 Atomic Absorption Spectrometric Determination of Platinum and Rhodium in Cobalt Oxide Catalyst—Barbara Rózańska

413 Determination of Trace Metals in Tea Using Both Microwave Digestion at Atmospheric Pressure and Inductively Coupled Plasma Atomic Emission Spectrometry—Kathryn Lamble, Steve J. Hill

419 Comparison of a Combined Helium–Argon Plasma With Pure Helium Plasmas for Gas Chromatography With Atomic Emission Detection—Antonio L. Pires Valente, Peter C. Uden

423 New Spectrofluorimetric Reagent, 2,3-Diamino-1,4-dibromonaphthalene, for the Determination of Selenium in Biological Materials—Karin Johansson, Örjan Andersson, Åke Olin

431 Pyoverdin-doped Sol–Gel Glass for the Spectrofluorimetric Determination of Iron(III)—J. M. Barrero, C. Cámara, M. C. Pérez-Conde, C. San José, L. Fernández

437 Solvent Extraction of Acenaphthene from Dodecane into Aqueous β-Cyclodextrin Medium and Application to Synchronous Spectrofluorimetric Determination in Kerosene—Masaki Tachibana, Motohisa Furusawa

443 Determination of Three Aspirin Metabolites in Human Urine by Derivative Synchronous Spectrofluorimetry—Patricia Damiani, María Élida Ribone, Gabriela Ibáñez, Alejandro C. Olivieri

447 Upgrading a Rapid-scanning Spectrometer With Microcomputerized Data Acquisition and Treatment to Measure Spectrokinetic Parameters of Photochromic Compounds—Jean-Jacques Meyer, Patrick Levoir, Roger Dubest

453 Optical Fibre Fluorosensor for Cadmium With Diethylaminoethyl-Sephadex as a Substrate—Jianzhong Lu, Zhujun Zhang

457 Optical Oxygen Sensing Materials Based on the Room-temperature Phosphorescence Intensity Quenching of Immobilized Erythrosin B—Marta Elena Diaz-Garcia, Rosario Pereiro-García, Nieves Velasco-García

463 Chemiluminescence Determination of Tetracyclines Based on Their Reaction With Hydrogen Peroxide Catalysed by the Copper Ion—X. R. Zhang, W. R. G. Baeyens, A. Van den Borre, G. Van der Weken, A. C. Calokerinos, S. G. Schulman

467 Sensitized Determination of Sulfite Using Flow Injection With Chemiluminescent Detection—David A. Paulls, Alan Townshend

471 Flow-injection Chemiluminometric Determination of Citrate Based on a Photochemical Reaction—Tomás Pérez-Ruiz, Carmen Martínez-Lozano, Virginia Tomás, Otilia Val

477 Investigation Into the Detection of Chlorine Species by Rhodamine 6G Chemiluminescence With Electrochemical Modification—Gordon P. Irons, Gillian M. Greenway

Continued on facing page—

ANALAO 120(2) 231–582, 17N–28N (1995) FEBRUARY 1995

The Analyst

The analytical journal of The Royal Society of Chemistry

CONTENTS

GUEST EDITORIAL

17N Towards Environmentally Conscientious Analytical Chemistry Through Miniaturization, Containment and Reagent Replacement—Miguel de la Guardia, Jaromir Ruzicka

PAPERS ON 'CLEAN' ANALYTICAL METHODS

231 In-line, Titanium Dioxide-catalysed, Ultraviolet Mineralization of Toxic Aromatic Compounds in the Waste Stream from a Flow Injection-based Resorcinol Analyser—Miguel de la Guardia, Karim D. Khalaf, Berween A. Hasan, Angel Morales-Rubio, Vicente Carbonell

237 Photocatalytic Treatment of Laboratory Wastes Containing Aromatic Amines—Edmondo Pramauro, Alessandra Bianco Prevot, Vincenzo Augugliaro, Leonardo Palmisano

243 Seasonal and Areal Variations of Polycyclic Aromatic Hydrocarbon Concentrations in Street Dust Determined by Supercritical Fluid Extraction and Gas Chromatography–Mass Spectrometry—Yu Yang, Wolfram Baumann

249 Costs, Laboratory Safety, Productivity and Faster Research Octane Number and Motor Octane Number Determinations in Industrial Chemistry Laboratories—J. M. Andrade, S. Muniategui, P. López, D. Prada

255 Spectrophotometric Determination of Copper(II), Nickel(II), and Cobalt(II) as Complexes with Sodium Diethyldithiocarbamate in the Anionic Micellar Media of Dodecylsulfate Salts—M. P. San Andres, M. L. Marina, S. Vera

261 Quality Concepts and Practices Applied to Sampling. An Exploratory Study—Michael Thompson, Michael H. Ramsey

271 A Horwitz-like Function Describes Precision in a Proficiency Test—Michael Thompson, Philip J. Lowthian

273 Orthogonal Array Design as a Chemometric Method for the Optimization of Analytical Procedures. Part 3. Five-level Design and its Application in a Polarographic Reaction System for Selenium Determination—Wei Guang Lan, Ming Keong Wong, Kok Kay Chee, Yoke Min Sin

281 Orthogonal Array Design as a Chemometric Method for the Optimization of Analytical Procedures. Part 4. Mixed-level Design and its Application to the High-performance Liquid Chromatographic Determination of Polycyclic Aromatic Hydrocarbons—Wei Guang Lan, Kok Kay Chee, Ming Keong Wong, Hian Kee Lee, Yoke Min Sin

289 Chemometric Evaluation of the Solvent Properties of Liquid Organic Salts—Salwa K. Poole, Colin F. Poole

295 Development of a Novel Methodology in the Determination of Magnesium from Chlorophyll *a* by Atomic Absorption Spectrometry Using Chemometric Experimental Design—Pedro W. Araujo, Keyhandokht Kavianpour, Richard G. Brereton

299 H-Point Standard Additions Method for Analyte Determination in Ternary Mixtures—J. Verdú Andrés, F. Bosch Reig, P. Campíns Falcó

305 Simultaneous Determination of Several Amino Acids With Multivariate Calibration Methods by Using a Continuous-flow System—J. Saurina, S. Hernández-Cassou

313 Application of the Partial Least-squares Calibration Method to the Simultaneous Kinetic Determination of Propoxur, Carbaryl, Ethiofencarb and Formetanate—J. M. Garcia, A. I. Jiménez, J. J. Arias, Karim D. Khalaf, Angel Morales-Rubio, Miguel de la Guardia

319 Application of Near-infrared Reflectance Analysis to the Integrated Control of Antibiotic Tablet Production—Elena Dreassi, Giuseppe Ceramelli, Luisa Savini, Piero Corti, Piero Luigi Perruccio, Silvano Lonardi

325 Signal and Noise Analysis of Non-modulated Polarimeters Using Mueller Calculus Simulations—Uma Kale, Edward Voigtman

331 Determination of Levamisole in Animal Tissues Using Liquid Chromatography–Thermospray Mass Spectrometry—A. Cannavan, W. J. Blanchflower, D. G. Kennedy

Continued on inside back cover—

Typeset and printed by Black Bear Press Limited, Cambridge, England

0003-2654(1995)2:1-0